

Complexity

# Finite-time Control of Complex Systems and Their Applications

Lead Guest Editor: Xiaodi Li

Guest Editors: Jianquan Lu, Oh-Min Kwon, and Sabri Arik





---

# **Finite-time Control of Complex Systems and Their Applications**

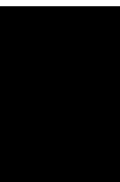
Complexity

---

## **Finite-time Control of Complex Systems and Their Applications**

Lead Guest Editor: Xiaodi Li

Guest Editors: Jianquan Lu, Oh-Min Kwon, and  
Sabri Arik




---

Copyright © 2021 Hindawi Limited. All rights reserved.

This is a special issue published in "Complexity." All articles are open access articles distributed under the Creative Commons Attribution License, which permits unrestricted use, distribution, and reproduction in any medium, provided the original work is properly cited.

# Chief Editor

Hiroki Sayama , USA

## Associate Editors

Albert Diaz-Guilera , Spain  
Carlos Gershenson , Mexico  
Sergio Gómez , Spain  
Sing Kiong Nguang , New Zealand  
Yongping Pan , Singapore  
Dimitrios Stamovlasis , Greece  
Christos Volos , Greece  
Yong Xu , China  
Xingang Yan , United Kingdom


## Academic Editors

Andrew Adamatzky, United Kingdom  
Marcus Aguiar , Brazil  
Tarek Ahmed-Ali, France  
Maia Angelova , Australia  
David Arroyo, Spain  
Tomaso Aste , United Kingdom  
Shonak Bansal , India  
George Bassel, United Kingdom  
Mohamed Boutayeb, France  
Dirk Brockmann, Germany  
Seth Bullock, United Kingdom  
Diyi Chen , China  
Alan Dorin , Australia  
Guilherme Ferraz de Arruda , Italy  
Harish Garg , India  
Sarangapani Jagannathan , USA  
Mahdi Jalili, Australia  
Jeffrey H. Johnson, United Kingdom  
Jurgen Kurths, Germany  
C. H. Lai , Singapore  
Fredrik Liljeros, Sweden  
Naoki Masuda, USA  
Jose F. Mendes , Portugal  
Christopher P. Monterola, Philippines  
Marcin Mrugalski , Poland  
Vincenzo Nicosia, United Kingdom  
Nicola Perra , United Kingdom  
Andrea Rapisarda, Italy  
Céline Rozenblat, Switzerland  
M. San Miguel, Spain  
Enzo Pasquale Scilingo , Italy  
Ana Teixeira de Melo, Portugal

Shahadat Uddin , Australia  
Jose C. Valverde , Spain  
Massimiliano Zanin , Spain





# Contents

## **Feedback Finite-Time Stabilization of Impulsive Linear Systems over Piecewise Quadratic Domains**

Jing Huang, Jianxing Li, Linshan Bu, and Honglei Xu 


Research Article (6 pages), Article ID 7651393, Volume 2021 (2021)

## **Second Zagreb and Sigma Indices of Semi and Total Transformations of Graphs**

Zhen Yang , Micheal Arockiaraj , Savari Prabhu , M. Arulperumjothi , and Jia-Bao Liu 

Research Article (15 pages), Article ID 6828424, Volume 2021 (2021)

## **Finite-Time Stability Analysis of Switched Genetic Regulatory Networks with Time-Varying Delays via Wirtinger's Integral Inequality**

Shanmugam Saravanan, M. Syed Ali, Grienggrai Rajchakit , Bussakorn Hammachukiattikul , Bandana Priya, and Ganesh Kumar Thakur

Research Article (21 pages), Article ID 9540548, Volume 2021 (2021)

## **Effectiveness of Price Limit on Stock Market Network: A Time-Migrated DCCA Approach**

Hongzeng He  and Shufen Dai 

Research Article (13 pages), Article ID 3265843, Volume 2021 (2021)

## **Stability and Stabilization of Delayed Neural Networks with Hybrid Impulses**

Kefa Zou , Xuechen Li , Nan Wang , Jungang Lou , and Jianquan Lu 

Research Article (9 pages), Article ID 8712027, Volume 2020 (2020)

## **Fractional-Order Iterative Learning Control with Initial State Learning for a Class of Multiagent Systems**

Xungen Li, Shuaishuai Lv , Mian Pan, Qi Ma, and Wenyu Cai


Research Article (14 pages), Article ID 9130875, Volume 2020 (2020)

## **Finite-Time Stability Analysis: A Tutorial Survey**

Honglei Xu 


Review Article (12 pages), Article ID 1941636, Volume 2020 (2020)

## **Fixed-Time Trajectory Tracking Control of Autonomous Surface Vehicle with Model Uncertainties and Disturbances**

Jiawen Cui and Haibin Sun 


Research Article (10 pages), Article ID 3281368, Volume 2020 (2020)

## **Finite-Time Stabilization and Destabilization Analysis of Quaternion-Valued Neural Networks with Discrete Delays**

Huiling Duan, Tao Peng, Zhengwen Tu, and Jianlong Qiu 

Research Article (12 pages), Article ID 8526030, Volume 2020 (2020)

## **Turing Instability of Brusselator in the Reaction-Diffusion Network**

Yansu Ji and Jianwei Shen 


Research Article (12 pages), Article ID 1572743, Volume 2020 (2020)

**Finite-Time Simultaneous Stabilization for Stochastic Port-Controlled Hamiltonian Systems over Delayed and Fading Channels**

Yaping Tang, Weiwei Sun , and Dongqing Liu


Research Article (12 pages), Article ID 6387025, Volume 2020 (2020)

**Adaptive Fuzzy Fast Finite-Time Tracking Control for Nonlinear Systems in Pure-Feedback Form with Unknown Disturbance**

Ke Xu, Huanqing Wang , Xiaoping Liu , and Ming Chen


Research Article (11 pages), Article ID 6347913, Volume 2020 (2020)

**Finite-Time Stability Criteria for a Class of High-Order Fractional Cohen–Grossberg Neural Networks with Delay**

Zhanying Yang, Jie Zhang, Junhao Hu, and Jun Mei 


Research Article (11 pages), Article ID 3604738, Volume 2020 (2020)

**Distributed Prescribed Finite Time Consensus Scheme for Economic Dispatch of Smart Grids with the Valve Point Effect**

Yingjiang Zhou , Shigao Zhu, and Qian Chen

Research Article (10 pages), Article ID 5476846, Volume 2020 (2020)

**Two-Player Location Game in a Closed-Loop Market with Quantity Competition**

Xiaofeng Chen , Qiankun Song, and Zhenjiang Zhao



Research Article (12 pages), Article ID 4325454, Volume 2020 (2020)

**A Polynomial Splines Identification Method Based on Control Nets**

Zhihua Wang  and Hongmei Kang


Research Article (12 pages), Article ID 7103963, Volume 2020 (2020)

**Finite-Time Adaptive Tracking Control for a Class of Pure-Feedback Nonlinear Systems with Disturbances via Decoupling Technique**

Qiangqiang Zhu, Ben Niu , Shengtao Li , Peiyong Duan, and Dong Yang

Research Article (11 pages), Article ID 1354340, Volume 2020 (2020)

**Finite-Time Stabilization for  $p$ -Norm Stochastic Nonlinear Systems with Output Constraints**

Shijun Guan and Liandi Fang 



Research Article (14 pages), Article ID 2486210, Volume 2020 (2020)

**Quadratic Filtering for Discrete-Time Systems with Measurement Delay and Packet Dropping**

Ling Li, Lei Tan, Xinmin Song , and Xuehua Yan

Research Article (9 pages), Article ID 1725121, Volume 2020 (2020)



**Synchronization Analysis for Stochastic Inertial Memristor-Based Neural Networks with Linear Coupling**

Lixia Ye, Yonghui Xia , Jin-liang Yan, and Haidong Liu 

Research Article (14 pages), Article ID 5430410, Volume 2020 (2020)

# Contents

## **Flocking Behavior of Cucker–Smale Model with Processing Delay**

Jianfei Cheng , Maoli Chen, and Xiao Wang 


Research Article (6 pages), Article ID 2724806, Volume 2020 (2020)

## **Semi-Supervised Cross-Modal Retrieval Based on Discriminative Comapping**

Li Liu , Xiao Dong , and Tianshi Wang 



Research Article (13 pages), Article ID 1462429, Volume 2020 (2020)

## **Finite-Time $H_2/H_\infty$ Control Design for Stochastic Poisson Systems with Applications to Clothing Hanging Device**

Yan Qi, Shiyu Zhong, and Zhiguo Yan 

Research Article (12 pages), Article ID 2463495, Volume 2020 (2020)

## **PWM-Based Finite-Time Tracking of Switched Buck Power Converters**

Hui Zhang  and Zhaojing Wu 


Research Article (9 pages), Article ID 5352306, Volume 2020 (2020)

## **The Optimal Pricing of Dual-Channel Supply Chain with the Third Party Product Recovery and Sales Effort**

Limin Wang, Qiankun Song , and Zhenjiang Zhao 




Research Article (18 pages), Article ID 4951341, Volume 2020 (2020)

## **New Results on Stability of Delayed Cohen–Grossberg Neural Networks of Neutral Type**

Ozlem Faydasicok 

Research Article (10 pages), Article ID 1973548, Volume 2020 (2020)

## **Upper and Lower Bounds for the Kirchhoff Index of the $n$ -Dimensional Hypercube Network**

Jia-Bao Liu , Jing Zhao, Zhi-Yu Shi, Jinde Cao , and Fuad E. Alsaadi 





Research Article (4 pages), Article ID 5307670, Volume 2020 (2020)

## **Periodic Averaging Principle for Neutral Stochastic Delay Differential Equations with Impulses**

Peiguang Wang  and Yan Xu 


Research Article (10 pages), Article ID 6731091, Volume 2020 (2020)

## **Fixed-Time Convergent Guidance Law with Impact Angle Control**

Zhongtao Cheng , Hao Wu, Bo Wang , Lei Liu , and Yongji Wang 






Research Article (9 pages), Article ID 5019689, Volume 2020 (2020)

## **Finite-Time Stability for a Class of Underactuated Systems Subject to Time-Varying Disturbance**

Jie Wu, Dan Yang, Xinyi He, and Xiaodi Li 

Research Article (7 pages), Article ID 8704505, Volume 2020 (2020)

## **Joint Character-Level Convolutional and Generative Adversarial Networks for Text Classification**

Tianshi Wang , Li Liu , Huaxiang Zhang , Long Zhang , and Xiuxiu Chen 

Research Article (11 pages), Article ID 8516216, Volume 2020 (2020)



## Research Article

# Feedback Finite-Time Stabilization of Impulsive Linear Systems over Piecewise Quadratic Domains

Jing Huang,<sup>1</sup> Jianxing Li,<sup>1</sup> Linshan Bu,<sup>2</sup> and Honglei Xu <sup>2</sup>

<sup>1</sup>School of Information Science and Engineering, Fujian University of Technology, Fuzhou, Fujian 350118, China

<sup>2</sup>School of Electrical Engineering, Computing and Mathematical Sciences, Curtin University, Perth, Western Australia 6845, Australia

Correspondence should be addressed to Honglei Xu; [h.xu@curtin.edu.au](mailto:h.xu@curtin.edu.au)

Received 17 July 2020; Accepted 17 August 2021; Published 7 September 2021

Academic Editor: Oh-Min Kwon

Copyright © 2021 Jing Huang et al. This is an open access article distributed under the Creative Commons Attribution License, which permits unrestricted use, distribution, and reproduction in any medium, provided the original work is properly cited.

This paper investigates the state feedback stabilization problem for a class of impulsive linear time-varying systems over specified time intervals and piecewise quadratic domains (PQDs). First, concepts related to finite-time stability and PQDs are given. Second, finite-time stability analysis over PQDs is implemented, and a variety of stability conditions involving differential linear matrix inequalities are investigated. Then, computationally tractable stability conditions are established for the control design. Finally, an illustrative example is presented to show the effectiveness of the designed state feedback control.

## 1. Introduction

Finite-time stability and stabilization are of importance in the applied mathematics and control fields and become a growing cross-disciplinary research area in the past decades. They can be found useful in a variety of applications; for example, when a rocket is launched, it should be controlled to stay in a specified region after a given time interval. Other practical applications include ATM networks [1], neural networks [2], and car suspension systems [3].

In this paper, we are interested in the finite-time stability and stabilization problems of impulsive linear systems in the quantitative sense. The system trajectory evolves in restrained regions during a specified interval of time. The concept of finite-time stability is different from that in the qualitative sense [4, 5], which emphasizes that the asymptotically stable system is capable to reach the equilibrium at the settling time. Lots of research results about Lyapunov stability for dynamical systems with impulsive effects have been developed (see, e.g., [6–9] and the references therein). Impulsive synchronization and control problems have attracted much research interest as well [10–16]. Furthermore, a variety of finite-time stability and stabilization problems are investigated for linear time-varying systems

and impulsive linear systems [3, 17, 18]. The initial domain  $\mathcal{X}_0$  and the trajectory domains  $\mathcal{X}_i$  are usually in the form of ellipsoids and polytopes [3, 19]. Recently, generalized piecewise quadratic domains are proposed for the initial and trajectory domains and stability conditions with less conservatism has been established in [20] and also reviewed in a recent review paper [21]. However, it should be worth noting that the existing stabilization and control methods such as those in [2, 3, 17, 18] are only suitable to ellipsoidal initial and trajectory domains and cannot be applied to the generalized piecewise quadratic domains, which motivates our research of this paper.

This paper investigates the state feedback finite-time stabilization problem for an impulsive linear system. Several sufficient conditions for finite-time stability are derived, and a state feedback control is designed. Comparing with previous work in [18, 19, 22], this paper has the following main contributions: (1) notions of piecewise quadratic functions and piecewise quadratic domains have been extended to impulsive linear time-varying systems; (2) computationally tractable sufficient conditions for finite-time stability with PQDs are established; and (3) efficient state feedback control to stabilize impulsive linear systems with respect to PQDs is designed.

The remainder of this paper is as follows. Section 2 presents the impulsive linear system model and preliminary concepts. Section 3 develops sufficient conditions for finite-time stability with PQDs. These stability results involve several computational efficient conditions to design state feedback control. In the next Section 4, a numerical example is given to demonstrate the obtained results. Finally, a conclusion is provided in Section 5.

*1.1. Notations.* Let  $\mathbb{R}^+$  denote a set of nonnegative real numbers and  $\mathbb{N}^+$  a set of positive integers. Let  $\mathbb{R}^n$  be the  $n$ -dimensional Euclidean space, and  $\Omega = [0, T], T > 0$ , be the time interval. Let  $A^T$  denote the transpose of  $A$  and  $I$  the identity matrix with an appropriate dimension. Let  $*$  be the symmetric component of a matrix. The matrix  $A \geq 0$  ( $A > 0$ ) is positive semidefinite (positive definite) if  $x^T A x \geq 0$  ( $x^T A x > 0$ ) for all  $x \in \mathbb{R}^n$ .  $A \geq B$  is equivalent to  $A - B \geq 0$ . For a set  $S_p = \{x_1, x_2, \dots, x_p\} \subseteq \mathbb{R}^n$ , let  $\text{cone}(S_p)$  denote its conical hull, i.e.,  $\text{cone}(S_p) = \{x | x = \sum_{i=1}^p \alpha_i x_i, \alpha_i \geq 0\}$ . Let  $\text{Ner}(S)$  denote the set of normalized extremal rays generating  $S_q$ , where  $\text{Ner}(S) = \{\bar{x}_1, \dots, \bar{x}_q\}$  with  $\|\bar{x}_i\|_2 = 1$ ,  $i = 1, \dots, q \leq p$ . For a piecewise continuous matrix-valued (or vector-valued) function  $F(\cdot)$  over  $\Omega$  and a positive real number  $\varepsilon$ , let us denote  $F^-(t) = \lim_{\varepsilon \rightarrow 0} F(t - \varepsilon)$  and  $F^+(t) = \lim_{\varepsilon \rightarrow 0} F(t + \varepsilon)$ .

## 2. Problem Statement

Consider the following impulsive linear system with time-dependent impulses:

$$\begin{cases} \dot{x}(t) = A(t)x(t) + B(t)u(t), & x(t_0) = x_0, \quad t \notin l = \{t_1, t_2, \dots\} \subset \Omega, \\ x(t^+) = C(t)x(t), & t \in l, \quad k = 1, 2, \dots, \end{cases} \quad (1)$$

where  $t \in \mathbb{R}^+$  is the time,  $x(t) \in \mathbb{R}^n$  is the state satisfying  $x(t^-) = \lim_{t \rightarrow 0} x(t) = x(t)$ , and  $u(t) \in \mathbb{R}^m$  is the control. Moreover,  $A(t)$ ,  $B(t)$ , and  $C(t)$  are given matrix-valued functions with appropriate dimensions. Without loss of generality, we assume that there exists a unique solution of equation (1).

Let  $U_i^0$  ( $i = 1, 2, \dots, v$ ) and  $U_j$  ( $j = 1, 2, \dots, u$ ) be the collections of cones satisfying the following conditions: (1) the dimensions of  $U_i^0$  and  $U_j$  are equal to  $n$ ; (2) both the union of  $U_i^0$ ,  $i = 1, \dots, v$ , and the union of  $U_j$ ,  $j = 1, \dots, u$ , can cover the state space  $\mathbb{R}^n$ , i.e.,  $\cup_{i=1}^v U_i^0 = \cup_{j=1}^u U_j = \mathbb{R}^n$ ; and (3)  $\text{In}\{U_p^0\} \cap \text{In}\{U_q^0\} = \emptyset$  and  $\text{In}\{U_p\} \cap \text{In}\{U_q\} = \emptyset$  for all  $p \neq q$ , where  $\text{In}\{\cdot\}$  is the interior operator. We denote by  $\Theta(U_p, U_q)$  the cone's intersection  $U_p \cap U_q$  and  $\text{Ner}(S) = \{\bar{x}_1, \dots, \bar{x}_q\}$  normalized extremal rays generating  $S$  where  $\bar{x}_{i2} = 1, i = 1, \dots, q$ . First, we need the following concepts on piecewise quadratic domains and finite-time stability over PQDs, which have been defined in [3, 20].

*Definition 1* (piecewise quadratic functions (PQFs)). A time-varying positive definite quadratic function

$$P_p(x, t) = x^T P_i(t)x, \quad \forall x \in U_i \text{ with } i = 1, \dots, v, \quad (2)$$

is said to be a piecewise quadratic function over a conical partition  $P = \{U_1, U_2, \dots, U_v\}$  of  $\mathbb{R}^n$ , where  $P_i \in \mathbb{R}^{n \times n}$ ,  $i = 1, \dots, v$ , are symmetric positive definite matrices in the cone  $U_i$ .

*Definition 2* (piecewise quadratic domains (PQDs)). A compact domain whose boundary is the unitary level curve of the piecewise quadratic function  $P_p(t, x)$  is said to be a piecewise quadratic domain (PQD) over a conical partition  $P = \{U_1, U_2, \dots, U_v\}$  of  $\mathbb{R}^n$ , i.e.,

$$\begin{aligned} \mathcal{X}_{P_p}(t) &:= \{x : P_p(t, x) \leq 1\}, \\ &= \{x : x^T P_i(t)x \leq 1, x \in U_i, i = 1, 2, \dots, v\}. \end{aligned} \quad (3)$$

*Remark 1.* Traditionally, both the initial domain and the trajectory domain are given in the form of the standard weighted quadratic norm (i.e., they are in ellipsoidal shapes). These restrictions will be much convenient to introduce quadratic Lyapunov functions to investigate the finite-time stability and stabilization problems. However, the obtained results are not suitable for polytopic domain cases. Piecewise quadratic domains not only are expressed as the class of ellipsoids but also are regarded as the generalization of polytopic domains. They can be applied to model initial and trajectory domains of different forms in many practical applications, such as those in mass-spring-friction systems and electrical circuits [3, 20].

*Definition 3* (finite-time stability with PQDs). Given two sets  $\mathcal{X}_0$  and  $\mathcal{X}(t)$ ,  $0 \in \mathcal{X}_0$ , the system equation (1) is said to be finite-time stable with respect to  $(\Omega, \mathcal{X}_0, \mathcal{X}(t))$  if

$$x_0 \in \mathcal{X}_0 \text{ implies } x(t) \in \mathcal{X}(t) \text{ for } t \in \Omega, \quad (4)$$

where the initial and trajectory domains are described as  $\mathcal{X}_0 = \{x \in \mathbb{R}^n | x_0^T R_i x_0 \leq 1, x_0 \in U_i^0, i = 1, 2, \dots, u\} \subseteq \mathcal{X}(t_0)$  and  $\mathcal{X}_t = \{x^T Q_j(t)x \leq 1, x \in U_j, j = 1, 2, \dots, v\}$  over conical partitions  $P_0 = \{U_1^0, U_2^0, \dots, U_u^0\}$  and  $P = \{U_1, U_2, \dots, U_v\}$ .

This paper aims to design a feedback controller  $u(t) = Fx(t)$ ,  $F \in \mathbb{R}^{m \times n}$  such that the controlled impulsive linear system equation (1) ensures the finite-time stability with PQDs. Now, we need to introduce the following lemma.

**Lemma 1** (see [20, 22]). *For a piecewise quadratic function  $P_p(t, x)$  over the given conical partition  $P$ , we denote by  $v_p = \{\bar{x}_1, \bar{x}_2, \dots, \bar{x}_q\}$  the set of generating rays. The piecewise quadratic function  $P_p(x, t)$  is continuous if and only if*

$$\begin{aligned} \bar{x}_h^T P_i(t) \bar{x}_h &= \bar{x}_h^T P_j(t) \bar{x}_h, \\ \bar{x}_h^T P_i(t) \bar{x}_l &= \bar{x}_h^T P_j(t) \bar{x}_l, \end{aligned} \quad (5)$$

for all  $\bar{x}_h, \bar{x}_l \in \text{Ner}\{\Theta(U_i, U_j)\}$ , where  $\Theta(U_i, U_j) = U_i \cap U_j$ .

## 3. Main Results

In this section, we establish several sufficient conditions of finite-time stability with PQDs for the impulsive linear system equation (1). For simplicity, we consider the initial

set  $\mathcal{X}_0$  and the time-varying set  $\mathcal{X}_t$  to be piecewise quadratic domains over the conical partition  $P = \{U_i\}, i = 1, 2, \dots, u$ . Then, when the control  $u(t) = 0$ , we have the following sufficient conditions for finite-time stability with PQDs.

**Theorem 1.** *The system equation (1) is finite-time stable with respect to  $(\Omega, \mathcal{X}_0, \mathcal{X}_t)$ , where the sets  $\mathcal{X}_0$  and  $\mathcal{X}_t$  are the given PQDs, if there exist a positive monotone increasing function  $\rho(\cdot)$  and a piecewise Lyapunov-like function  $V(t, x)$  such that*

$$\frac{\partial V(t, x)}{\partial t} + \frac{\partial V(t, x)}{\partial x} A(t)x(t) < 0, \quad t \notin l, \quad (6)$$

$$V(t^+, x) < V(t, x), \quad t \in l, \quad (7)$$

$$\begin{aligned} \rho(x^\top Q_i(t)x) &\leq V(t, x), \\ V(t_0, x_0) &< \rho(x_0^\top R_i x_0), \end{aligned} \quad (8)$$

for  $t \in \Omega$  and  $x \in U_i$  with  $i = 1, \dots, v$ .

*Proof.* We choose  $x_0$  satisfying  $x_0^\top R_i x_0 \leq 1$  and denote by  $x(t, x_0)$  the solution of the system equation (1). Next, we consider the case  $t \in (t_k, t_{k+1}]$ . Based on the condition equation (8), we have

$$x^\top Q_i(t)x \leq \rho^{-1}(V(t, x)). \quad (9)$$

Moreover, the condition equation (6) ensures that  $V(t, x)$  will decrease along the solution of the system equation (1), and hence we have  $V(t, x) \leq V(t_k^+, x(t_k^+))$ , for  $t \in (t_k, t_{k+1}]$ . In view of equation (7), we say  $V(t, x) \leq V(t_k, x(t_k))$  will be satisfied. Repeatedly using equations (6) and (7), we get

$$V(t, x) < V(t_0, x_0). \quad (10)$$

Hence, it follows from equations (9) and (10) and the fact that  $\rho(\cdot)$  is positive monotone increasing that

$$x^\top Q_i(t)x < \rho^{-1}(V(t_0, x_0)). \quad (11)$$

Finally, using equation (8) and the fact  $x_0^\top R_i x_0 \leq 1$ , we obtain  $x^\top Q_i(t)x < 1$ . It completes the proof.

We choose a positive definite monotone increasing function  $\rho(\eta) = \eta$  where  $\eta \in \mathbb{R}^+$  and a piecewise quadratic Lyapunov-like function over the above conical partition  $P$  as

$$V_{\mathcal{X}}(t, x) = x^\top P_i(t)x, \quad \forall x \in U_i, \text{ with } i = 1, \dots, v, \quad (12)$$

where  $P_i \in \mathbb{R}^{n \times n}, i = 1, \dots, v$ , are symmetric matrices. Then, a sufficient condition for the finite-time stability of impulsive linear system equation (1) can be given as follows.

**Theorem 2.** *The system equation (1) is finite-time stable with respect to  $(\Omega, \mathcal{X}_0, \mathcal{X}_t)$ , where the sets  $\mathcal{X}_0$  and  $\mathcal{X}_t$  are the given PQDs, if there exist piecewise continuously differentiable matrix-valued functions  $P_i(t) \in \mathbb{R}^{n \times n}$  such that*

$$x^\top (\dot{P}_i(t) + A(t)^\top P_i(t) + P_i(t)A(t))x < 0, \quad t \notin l, \quad (13)$$

$$x^\top C^\top(t)P_i^+(t)C(t)x < x^\top P_i(t)x, \quad t \in l, \quad (14)$$

$$x^\top (Q_i(t) - P_i)x \leq 0, \quad x_0^\top (P(t_0) - R_i)x_0 < 0, \quad (15)$$

for  $t \in \Omega$  and  $x \in U_i$  with  $i = 1, \dots, v$ .

*Proof.* By choosing  $V_{\mathcal{X}}(t, x) = x^\top P_i(t)x$ , it is straightforwardly derived that equations (11)–(13) can be guaranteed by equations (6)–(8). Then, by Theorem 1, we ensure that the system equation (1) is finite-time stable with respect to  $(\Omega, \mathcal{X}_0, \mathcal{X}_t)$ .

Sufficient conditions equations (11)–(13) in Theorem 2 are only theoretically useful because of the existence of the infinite number of differential linear matrix inequalities. Applying S-Procedure arguments and using the state feedback control  $u(t) = Fx(t)$ , we can derive the following computationally tractable sufficient conditions.

**Corollary 1.** *The system equation (1) is finite-time stabilizable with respect to  $(\Omega, \mathcal{X}_0, \mathcal{X}_t)$  under the feedback control law  $u(t) = Fx(t)$ , where the sets  $\mathcal{X}_0$  and  $\mathcal{X}_t$  are the given PQDs if there exist positive numbers  $b_{i,l}$ , positive real-valued functions  $c_{i,l}(t), z_{i,l}(t)$ , and matrices  $H_{i,l}$ , satisfying  $x^\top H_{i,l}x \leq 0, \forall x \in S_i, i = 1, \dots, v, l = 1, \dots, s$  such that there exist positive piecewise continuously differentiable matrix-valued functions  $P_i(t) \in \mathbb{R}^{n \times n}$ , such that the following conditions containing differential linear matrix inequalities are satisfied:*

$$\begin{aligned} \dot{P}_i(t) + (A(t) + B(t)F)^\top P_i(t) + P_i(t)(A(t) + B(t)F) \\ - \sum_{l=1}^s c_{i,l}(t)Q_{i,l} < 0, \quad t \notin l, \end{aligned} \quad (16)$$

$$C^\top(t)P_i^+(t)C(t) < P_i(t), \quad t \in l, \quad (17)$$

$$P_i(t) - Q_i(t) + \sum_{l=1}^s z_{i,l}(t)H_{i,l} \geq 0, \quad (18)$$

$$P_i(0) - R_i - \sum_{l=1}^s b_{i,l}H_{i,l} < 0, \quad (19)$$

$$\bar{x}_i^\top P_i(t)\bar{x}_i = \bar{x}_i^\top P_j(t)\bar{x}_i, \quad \forall \bar{x}_i \in \text{Ner}\{U_i \cap U_j\}, \quad (20)$$

$$\bar{x}_h^\top P_i(t)\bar{x}_i = \bar{x}_h^\top P_j(t)\bar{x}_i, \quad \forall \bar{x}_h, \bar{x}_i \in \text{Ner}\{U_i \cap U_j\}. \quad (21)$$

*Proof.* Using S-Procedure and Theorem 5 of [20], we obtain that the conditions equations (13)–(15) are derived if the conditions equations (16) and (19) are satisfied. Moreover, it follows from Lemma 1 and equations (20) and (21) that the piecewise quadratic Lyapunov function  $V_{\mathcal{X}}(t, x) = x^\top P_i(t)x$  is continuous. Thus, by Theorem 2, the conclusion of this theorem is obtained.

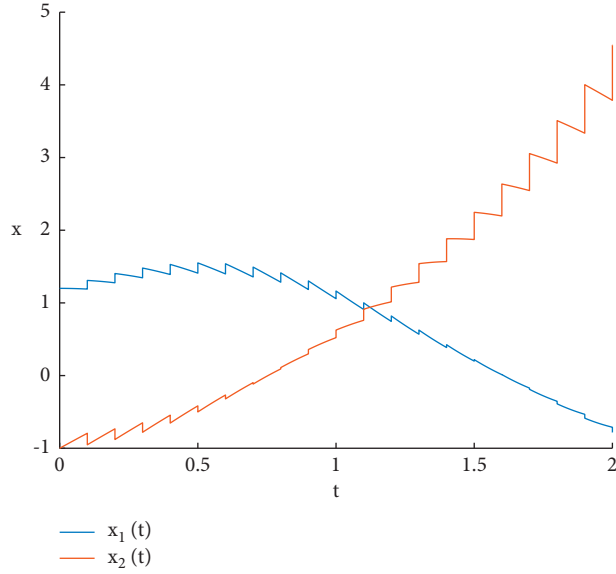


FIGURE 1: State trajectories  $x_1(t)$  and  $x_2(t)$  of the uncontrolled impulsive linear system equation (22) with 0.1 s equidistant impulsive intervals.

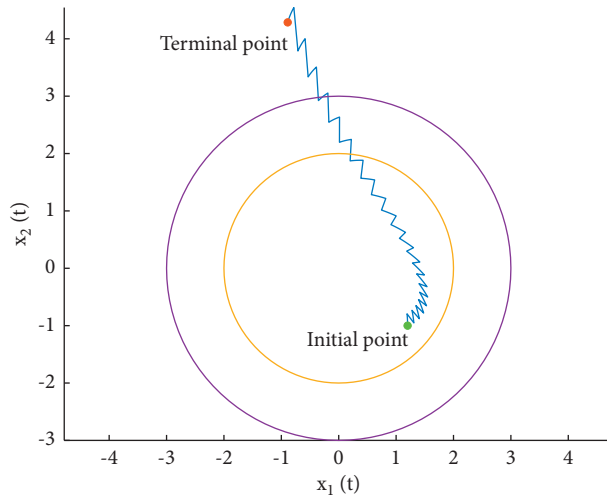


FIGURE 2: Phase portrait of the uncontrolled impulsive linear system equation (22) with 0.1 s equidistant impulsive intervals.

*Remark 2.* In Corollary 1, solving differential linear matrix inequalities and deciding the conical partitions are two main steps to influence the computational complexity. In the former step, more accurate approximation will increase the computational complexity, and in the later step, a greater number of the conical partitions will cause the computational burden as well.

#### 4. An Illustrative Example

In this section, we give an example to demonstrate the effectiveness of the proposed conditions. Let us consider the following impulsive linear control system:

$$\begin{cases} \dot{x}(t) = \begin{bmatrix} -3t & 1 \\ 1.5 & t \end{bmatrix} x(t) + \begin{bmatrix} 1.5 & 2 \\ 1.6 & 1 \end{bmatrix} u(t), & t \notin l = \{0.1, \dots, 0.1k, \dots\}, \\ x(t^+) = \begin{bmatrix} 1.1 & 0 \\ 0 & 1.2 \end{bmatrix} x(t^-), & t \in l, k \in \mathbb{N}^+, \end{cases} \quad (22)$$

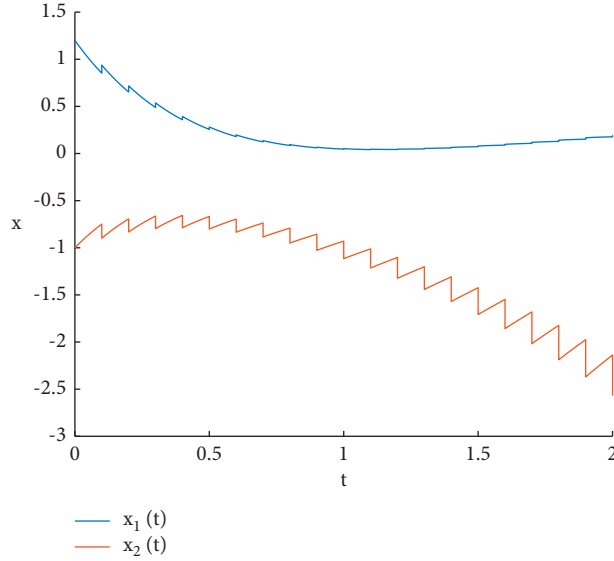


FIGURE 3: State trajectories  $x_1(t)$  and  $x_2(t)$  of the impulsive linear control system equation (22) with 0.1 s equidistant impulsive intervals.

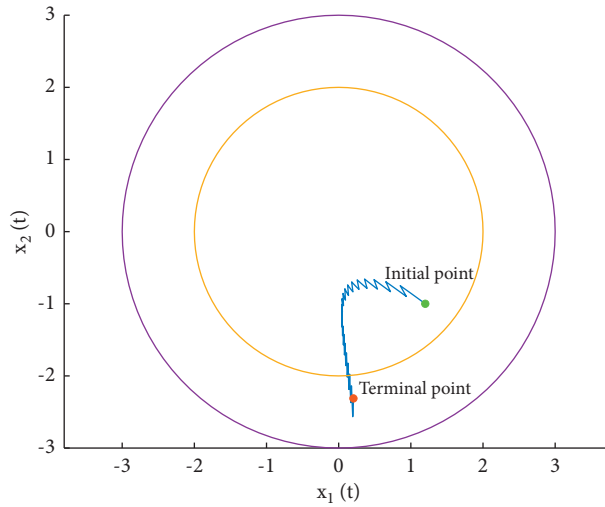


FIGURE 4: Phase portrait of the impulsive linear control system equation (22) with 0.1 s equidistant impulsive intervals.

with  $t \in \Omega = [0, 2]$  and the initial and trajectory domains

$$\mathcal{X}_0 = \{x: x^\top x < 4\}, \quad \text{and } \mathcal{X}_t = \{x: x^\top x < 9\}. \quad (23)$$

When the state feedback control  $u(t)$  is not implemented, the state trajectories and phase portrait of the impulsive linear system equation (10) with 0.1 s equidistant impulsive intervals are seen in Figures 1 and 2. From them, we can see that the state has been outside the set  $\mathcal{X}_t$  at  $T = 2$ , and hence the impulsive linear system equation (22) is not finite-time stable with respect to  $(\Omega, \mathcal{X}_0, \mathcal{X}_t)$ . Since in this example both initial and trajectory domains are ellipsoidal, the piecewise quadratic Lyapunov function will be continuous everywhere. Hence, equations (20) and (21) will be guaranteed straightforwardly. By using conditions equations (16)–(19), we can obtain a feasible solution for the state feedback matrix:

$$F = \begin{pmatrix} 3.1765 & -0.9412 \\ -3.8824 & 0.9059 \end{pmatrix}. \quad (24)$$

Then, applying  $u(t) = Fx(t)$  to equation (22), we simulate the state trajectories and phase portrait of the impulsive linear system equation (10) with 0.1 s equidistant impulsive interval in Figures 3 and 4, which show that the impulsive linear control system equation (22) is finite-time stable with respect to the given  $(\Omega, \mathcal{X}_0, \mathcal{X}_t)$ . So, the designed state feedback finite-time stabilizing controller is effective.

## 5. Conclusion

This paper has investigated the feedback finite-time stabilizing control problem for impulsive linear systems with respect to PQDs. First, the concepts of piecewise quadratic

functions and piecewise quadratic domains are provided. Finite-time stability in the quantitative sense is investigated. Then, sufficient conditions of finite-time stability with PQDs for impulsive linear systems are established. Based on these stability criteria, computationally tractable conditions to design state feedback control for the impulsive linear systems are derived. A numerical example is finally given to demonstrate the usefulness of the designed state feedback control.

## Data Availability

The data used to support the findings of this study are available from the corresponding author upon request.

## Conflicts of Interest

The authors declare that there are no conflicts of interest.

## Acknowledgments

This work was supported in part by the Australian Research Council (DP160102819), the Research Program of Fujian University of Technology (GY-Z18002), and the Open Fund Project of Key Scientific Research and Innovation Platform of Fujian University of Technology (2018).

## References

- [1] F. Amato, M. Ariola, C. T. Abdallah, and C. Cosentino, "Application of finite-time stability concepts to the control of ATM networks," in *Proceedings of the Annual Allerton Conference on Communication Control and Computing*, pp. 1071–1079, Monticello, IL, USA, October 2002.
- [2] P. Niamsup, K. Ratchagit, and V. N. Phat, "Novel criteria for finite-time stabilization and guaranteed cost control of delayed neural networks," *Neurocomputing*, vol. 160, pp. 281–286, 2015.
- [3] F. Amato, R. Ambrosino, M. Ariola, C. Cosentino, and G. De Tommasi, *Finite-Time Stability and Control*, Springer-Verlag, Berlin, Germany, 2014.
- [4] S. P. Bhat and D. S. Bernstein, "Finite-time stability of continuous autonomous systems," *SIAM Journal on Control and Optimization*, vol. 38, no. 3, pp. 751–766, 2000.
- [5] S. P. Bhat and D. S. Bernstein, "Geometric homogeneity with applications to finite-time stability," *Mathematics of Control, Signals, and Systems*, vol. 17, no. 2, pp. 101–127, 2005.
- [6] X. J. Ding and H. L. Xu, "Robust stability and stabilization of a class of impulsive switched systems," *Dynamics of Continuous Discrete and Impulsive Systems: Series B; Applications and Algorithms*, vol. 2, pp. 795–798, 2005.
- [7] X. Li and R. Rakkiyappan, "Impulsive controller design for exponential synchronization of chaotic neural networks with mixed delays," *Communications in Nonlinear Science and Numerical Simulation*, vol. 18, no. 6, pp. 1515–1523, 2013.
- [8] H. Xu and K. Lay Teo, " $H_\infty$  optimal stabilization of a class of uncertain impulsive systems: an LMI approach," *Journal of Industrial and Management Optimization*, vol. 5, no. 1, pp. 153–159, 2009.
- [9] H. Xu and K. L. Teo, "Stabilizability of discrete chaotic systems via unified impulsive control," *Physics Letters A*, vol. 374, no. 2, pp. 235–240, 2009.
- [10] B. Liu, X. Liu, G. Chen, and H. Wang, "Robust impulsive synchronization of uncertain dynamical networks," *IEEE Transactions on Circuits and Systems I: Regular Papers*, vol. 52, no. 7, pp. 1431–1441, 2005.
- [11] X. Liu, Y. Liu, and L. T. Kok, "Stability analysis of impulsive control systems," *Mathematical and Computer Modelling*, vol. 37, no. 12–13, pp. 1357–1370, 2003.
- [12] L. Li, X. Shi, and J. Liang, "Synchronization of impulsive coupled complex-valued neural networks with delay: the matrix measure method," *Neural Networks*, vol. 117, pp. 285–294, 2019.
- [13] M. Li, H. Chen, and X. Li, "Synchronization analysis of complex dynamical networks subject to delayed impulsive disturbances," *Complexity*, vol. 2020, Article ID 5285046, 12 pages, 2020.
- [14] G. Mu, L. Li, and X. Li, "Quasi-bipartite synchronization of signed delayed neural networks under impulsive effects," *Neural Networks*, vol. 129, pp. 31–42, 2020.
- [15] X. Xie, X. Liu, H. Xu, X. Luo, and G. Liu, "Synchronization of coupled reaction-diffusion neural networks: delay-dependent pinning impulsive control," *Communications in Nonlinear Science and Numerical Simulation*, vol. 79, Article ID 104905, 2019.
- [16] X. Xie, X. Liu, and H. Xu, "Synchronization of delayed coupled switched neural networks: mode-dependent average impulsive interval," *Neurocomputing*, vol. 365, pp. 261–272, 2019.
- [17] F. Amato, M. Ariola, M. Carbone, and C. Cosentino, "Finite-time control of linear systems: a survey," in *Current Trends in Nonlinear Systems and Control*, L. Menini, L. Zaccarian, and C. T. Abdallah, Eds., pp. 195–213, Springer, New York, NY, USA, 2006.
- [18] F. Amato, R. Ambrosino, M. Ariola, and G. De Tommasi, "Robust finite-time stability of impulsive dynamical linear systems subject to norm-bounded uncertainties," *International Journal of Robust and Nonlinear Control*, vol. 21, no. 10, pp. 1080–1092, 2011.
- [19] F. Amato, R. Ambrosino, M. Ariola, and C. Cosentino, "Finite-time stability of linear time-varying systems with jumps," *Automatica*, vol. 45, no. 5, pp. 1354–1358, 2009.
- [20] R. Ambrosino, E. Garone, M. Ariola, and F. Amato, "Piecewise quadratic functions for finite-time stability analysis," in *Proceedings of the 51st IEEE Conference on Decision and Control (CDC)*, pp. 6535–6540, IEEE, Maui, HI, USA, December 2012.
- [21] H. Xu, "Finite-time stability analysis: a tutorial survey," *Complexity*, vol. 2020, Article ID 1941636, 12 pages, 2020.
- [22] R. Ambrosino and E. Garone, "Robust stability of linear uncertain systems through piecewise quadratic lyapunov functions defined over conical partitions," in *Proceedings of the 51st IEEE Conference on Decision and Control (CDC)*, pp. 2872–2877, IEEE, Maui, HI, USA, December 2012.

## Research Article

# Second Zagreb and Sigma Indices of Semi and Total Transformations of Graphs

Zhen Yang <sup>1</sup>, Micheal Arockiaraj <sup>2</sup>, Savari Prabhu <sup>3</sup>, M. Arulperumjothi <sup>4</sup>,  
and Jia-Bao Liu <sup>5</sup>

<sup>1</sup>Chongqing Key Laboratory of Spatial Data Mining and Big Data Integration for Ecology and Environment  
Rongzhi College of Chongqing Technology and Business University, Chongqing 401320, China

<sup>2</sup>Department of Mathematics, Loyola College, Chennai 600034, India

<sup>3</sup>Department of Mathematics, Sri Venkateswara College of Engineering, Sriperumbudur 602117, India

<sup>4</sup>Department of Mathematics, Loyola College, University of Madras, Chennai 600034, India

<sup>5</sup>School of Mathematics and Physics, Anhui Jianzhu University, Hefei 230601, China

Correspondence should be addressed to Savari Prabhu; [drsavariprabhu@gmail.com](mailto:drsavariprabhu@gmail.com)

Received 5 July 2020; Revised 7 November 2020; Accepted 7 July 2021; Published 6 September 2021

Academic Editor: Oh-Min Kwon

Copyright © 2021 Zhen Yang et al. This is an open access article distributed under the Creative Commons Attribution License, which permits unrestricted use, distribution, and reproduction in any medium, provided the original work is properly cited.

The study of structure-property relations including the transformations of molecules is of utmost importance in correlations with corresponding physicochemical properties. The graph topological indices have been used effectively for such study and, in particular, bond-based indices play a vital role. The bond-additive topological indices of a molecular graph are defined as a sum of edge measures over all edges in which edge measures can be computed based on degrees, closeness, peripherality, and irregularity. In this study, we provide the mathematical characterization of the transformation of a structure that can be accomplished by the novel edge adjacency and incidence relations. We derive the exact expressions of bond type indices such as second Zagreb, sigma indices, and their coincides of total transformation and two types of semitransformations of the molecules which in turn can be used to characterize the topochemical and topostructural properties.

## 1. Introduction

Topological indices are graph invariants that play an important role in chemical and pharmaceutical sciences, since they can be used to predict physicochemical properties of organic compounds in view of successful applications in QSAR and QSPR techniques [1–5]. These indices are mainly classified into distance-based and degree-based. Development of such topological indices is of immense value in quantitative structure-activity relations. The first and second Zagreb indices were the oldest degree-based indices and found significant applications [6, 7]. The Zagreb indices have first appeared in the topological formula for the total  $\pi$ -energy of conjugated molecules and also useful in the study of anti-inflammatory activities of chemical instances. The generalization of the first Zagreb index is named as general sum-connectivity index [8] and there are many types

of generalization and reformulation on the Zagreb indices based on vertex and edge degrees [8–11], in particular, the forgotten index is recently revisited with important applications to drug molecular structures [12, 13].

It was known that most of the molecular structures are not regular and, hence, the quantitative measure based on irregularity is of great importance in mathematical chemistry. In the case of octane isomers, the application of various degree-based irregularity measures for the prediction of physicochemical properties such as boiling point, standard enthalpy of vaporization, acentric factor, enthalpy of vaporization, and entropy was tested and predicted with good accuracy [14]. As a result of which many topological indices of this kind have been discussed and a few of them are Col-latz–Sinogowitz, degree variance, discrepancy, Albertson, Bell, and total irregularity and sigma indices [14–17].

The Albertson index is the most commonly used irregularity measures that provide the structural perfection of chemical compounds. For this purpose, the imbalance of an edge is defined as the absolute difference between the degrees of end vertices and the summation is taken over all edges. In this paper, we focus our attention on the recently popular, sigma index, which is defined as the sum of squares of imbalance of every edge. Moreover, there is a nice relationship between second Zagreb, forgotten, and sigma indices which states that the difference between forgotten and sigma indices is twice the second Zagreb index [18] and some properties of the sigma index discussed in [19].

The structure of a molecular graph  $G$  can be transformed into another graph  $T(G)$  by imposing desired rules based on the original structure of  $G$  so that there is a one-to-one correspondence between original graph  $G$  and the transformation graph  $T(G)$ . Such a transformation of graphs and their characterization was attempted by many researchers in chemical graph theory [20–26] because the complex structure of transformation graph can be easily analyzed by the original graph. For instance, the first Zagreb index [21, 25], second Zagreb index [21, 27], forgotten index [20, 28] of transformation graphs, and Zagreb indices of transformation of line graph of subdivision graphs [29] were discussed. In this, we observe that the entire process of the second Zagreb index [27] was wrongly dealt and we will discuss with details in Section 3. Moreover, the forgotten index [20, 28] of transformation of graphs was considered with vertex  $a$ -Zagreb and  $(a, b)$ -Zagreb indices. In this study, we give the correct expressions for the second Zagreb index of transformation graphs and rewrite for the forgotten index via general sum-connectivity index. Finally, we derive the analytical expressions for the sigma index of two types of semitransformations and a total transformation.

Throughout this paper, we write  $G$  to denote a simple connected graph with vertex set  $V(G)$  and edge set  $E(G)$ . The number of elements in the vertex set and the edge set, respectively, is denoted by  $n$  (order) and  $m$  (size). The number of edges incident with a vertex  $s \in V(G)$  is called the degree of the vertex  $s$ , denoted by  $d_G(s)$ . The neighborhood of a vertex  $s$ , denoted by  $N_G(s)$ , is a set of all vertices which are adjacent to  $s$ . Two edges  $e, f \in E(G)$  are said to be adjacent if they share a common vertex and we write as  $e \sim f$  and in case they are not adjacent,  $e \not\sim f$ . In the same line of notation,  $s \in V(G)$ ,  $f \in E(G)$ , and  $s \sim f$  mean that  $s$  is an end vertex of  $f$  while  $s \not\sim f$  that  $s$  is not an end vertex of  $f$ . The degree of an edge  $e = st$ , denoted by  $d_G(e)$ , is the number of edges that are adjacent to  $e$ , i.e.,  $d_G(e) = d_G(s) + d_G(t) - 2$ . The complement of a graph  $G$ , represented by  $\overline{G}$ , is a graph obtained from  $G$  with the same vertex set of  $G$  such that  $s$  is adjacent to  $t$  in  $\overline{G}$  if and only if  $s$  is not adjacent to  $t$  in  $G$ . Hence, the size of  $\overline{G}$  is  $(1/2)[n^2 - n - 2m]$ , and the degree of each vertex  $s \in V(\overline{G})$  is  $d_{\overline{G}}(s) = n - d_G(s) - 1$ .

We close this section by listing down (in Table 1) certain bond-additive topological indices [7–13, 18, 28, 30, 31] and their coindices which are needed for our study.

## 2. Transformation Graphs

The concept of transformation graphs is to construct a new graph from the original graph  $G$  based on the structural connectivity. Generally, we can transform the original graph by imposing any combinations of the following:

For  $\alpha, \beta, \gamma \in \{+, -\}$ ,  $v_i \in V(G)$ ,  $1 \leq i \leq n$ , and  $e_j \in E(G)$ ,  $1 \leq j \leq m$ ,

- (1)  $v_i, v_j \in V(G)$ ,  $v_i$  is adjacent to  $v_j$  in  $G$  if  $\alpha = +$  and  $v_i$  is not adjacent to  $v_j$  in  $G$  if  $\alpha = -$
- (2)  $e_i, e_j \in E(G)$ ,  $e_i$  is adjacent to  $e_j$  in  $G$  if  $\beta = +$  and  $e_i$  is not adjacent to  $e_j$  in  $G$  if  $\beta = -$
- (3)  $v_i \in V(G)$  and  $e_j \in E(G)$ ,  $e_j$  is incident to  $v_i$  in  $G$  if  $\gamma = +$  and  $e_j$  is not incident to  $v_i$  in  $G$  if  $\gamma = -$

The type-I semitransformation of a graph  $G$ , denoted by  $T_{1\alpha\gamma}(G)$ , is a graph with the vertex set  $V(G) \cup E(G)$ , and for  $s, t \in V(T_{1\alpha\gamma}(G))$ ,  $s$  and  $t$  are adjacent in  $T_{1\alpha\gamma}(G)$  if and only if (#1) and (#3) hold [21]. Following this, it is natural to define another semitransformation, called type-II semitransformation and denoted by  $T_{2\beta\gamma}(G)$ , whose vertex set is  $V(G) \cup E(G)$ , and for  $s, t \in V(T_{2\beta\gamma}(G))$ ,  $s$  and  $t$  are adjacent in  $T_{2\beta\gamma}(G)$  if and only if (#2) and (#3) hold. The total transformation graph  $T_{\alpha\beta\gamma}(G)$  is a graph with the same vertex set as above  $V(G) \cup E(G)$ , and for  $s, t \in V(T_{\alpha\beta\gamma}(G))$ ,  $s$  and  $t$  are adjacent in  $T_{\alpha\beta\gamma}(G)$  if and only if (#1), (#2), and (#3) hold [32].

The concept of semitotal point, semitotal line, and total graphs came into the literature earlier [33, 34] and these three graphs are particular cases of our  $T_{1\alpha\gamma}(G)$ ,  $T_{2\beta\gamma}(G)$ , and  $T_{\alpha\beta\gamma}(G)$ , i.e.,  $T_{1++}(G)$  is the semitotal point graph,  $T_{2++}(G)$  is the semitotal line graph, and  $T_{+++}(G)$  is the total graph. Since there are four distinct 2-permutations of  $\{+, -\}$ , we can construct totally eight different graphs from two types of semitransformations. For a graph  $G$  depicted in Figure 1, the two types of semitransformation graphs are shown in Figure 2. In the same way, there are eight distinct 3-permutations of  $\{+, -\}$  and again totally eight graphs can be constructed from the total transformation in which  $T_{---}(G) \cong \overline{T_{+++}(G)}$ ,  $T_{--+}(G) \cong \overline{T_{+--}(G)}$ ,  $T_{-+-}(G) \cong \overline{T_{+-+}(G)}$ , and  $T_{-++}(G) \cong \overline{T_{+--}(G)}$ . For the same graph in Figure 1, the eight classes of total transformation graphs are given in Figure 3.

**Lemma 1** (see [21]). *Let  $G$  be graph with  $n$  and  $m$  as its order and size, respectively. Then, the order of  $T_{1\alpha\gamma}(G)$  is  $(m + n)$ , and the size is*

$$|ET_{1\alpha\gamma}(G)| = \begin{cases} 3m, & : \alpha = +, \gamma = +, \\ m(n - 1), & : \alpha = +, \gamma = -, \\ \frac{1}{2}n(n - 1) + m, & : \alpha = -, \gamma = +, \\ \frac{1}{2}n(n - 1) + m(n - 3), & : \alpha = -, \gamma = -. \end{cases} \quad (1)$$



TABLE 1: Bond-additive indices of  $G$ .

Item	Index	Coindex
First Zagreb	$M_1(G) = \sum_{st \in E(G)} [d_G(s) + d_G(t)]$	$\overline{M}_1(G) = \sum_{st \notin E(G)} [d_G(s) + d_G(t)]$
Second Zagreb	$M_2(G) = \sum_{st \in E(G)} d_G(s)d_G(t)$	$\overline{M}_2(G) = \sum_{st \notin E(G)} d_G(s)d_G(t)$
Forgotten	$F(G) = \sum_{st \in E(G)} [d_G(s)^2 + d_G(t)^2]$	$\overline{F}(G) = \sum_{st \notin E(G)} [d_G(s)^2 + d_G(t)^2]$
Sum-connectivity	$\chi_\alpha(G) = \sum_{st \in E(G)} [d_G(s) + d_G(t)]^\alpha$	$\overline{\chi}_\alpha(G) = \sum_{st \notin E(G)} [d_G(s) + d_G(t)]^\alpha$
Reformulated first Zagreb	$EM_1(G) = \sum_{e,f \in E(G)e \sim f} [d_G(e) + d_G(f)]$	$\overline{EM}_1(G) = \sum_{e,f \in E(G)e \not\sim f} [d_G(e) + d_G(f)]$
Reformulated second Zagreb	$EM_2(G) = \sum_{e,f \in E(G)e \sim f} d_G(e)d_G(f)$	$\overline{EM}_2(G) = \sum_{e,f \in E(G)e \not\sim f} d_G(e)d_G(f)$
Sigma	$\sigma(G) = \sum_{st \in E(G)} [d_G(s) - d_G(t)]^2$	$\overline{\sigma}(G) = \sum_{st \notin E(G)} [d_G(s) - d_G(t)]^2$

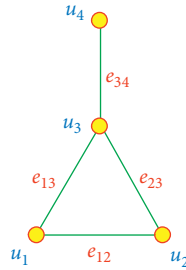


FIGURE 1: The graph  $G$ .

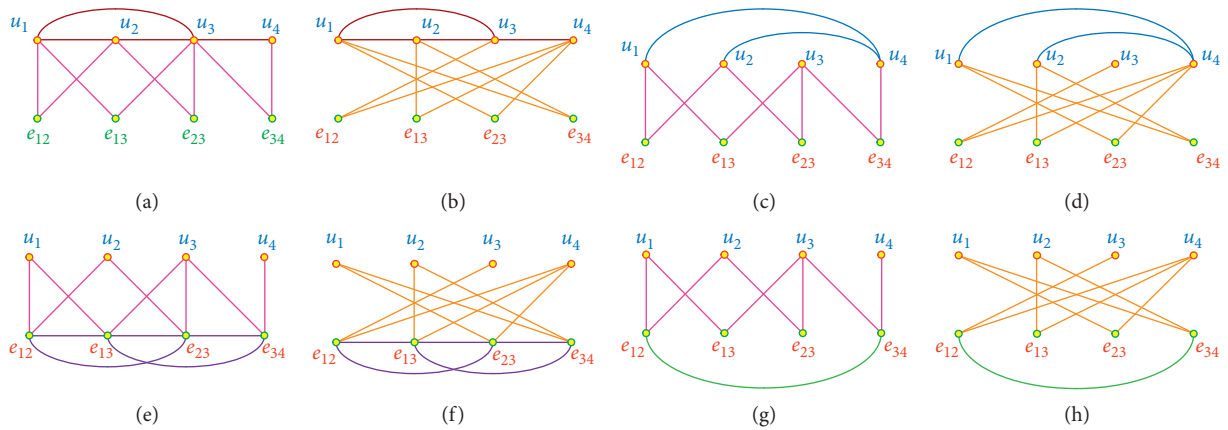


FIGURE 2: (a)  $T_{1++}(G)$ ; (b)  $T_{1+-}(G)$ ; (c)  $T_{1-+}(G)$ ; (d)  $T_{1--}(G)$ ; (e)  $T_{2++}(G)$ ; (f)  $T_{2+-}(G)$ ; (g)  $T_{2-+}(G)$ ; (h)  $T_{2--}(G)$ .

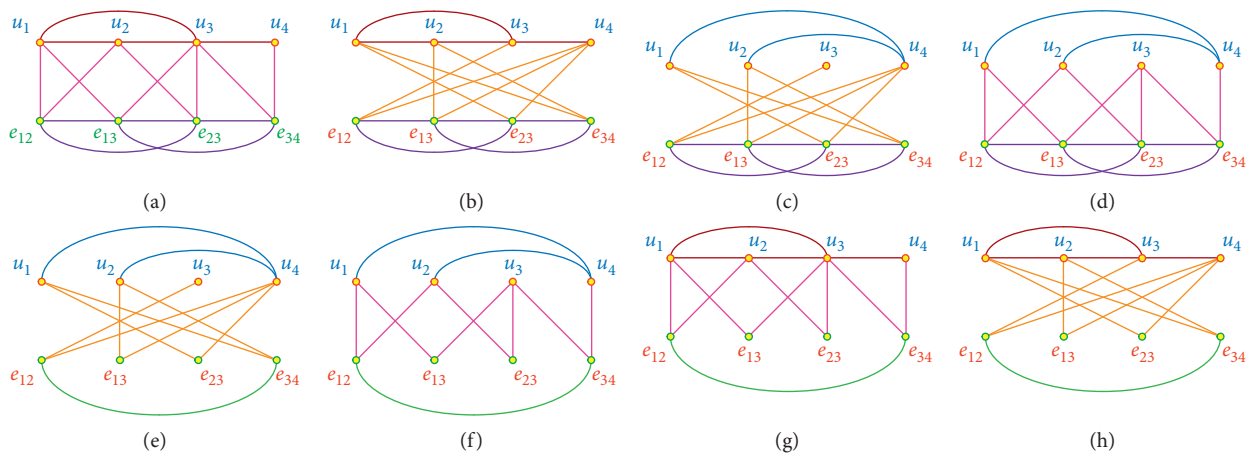


FIGURE 3: (a)  $T_{+++}(G)$ ; (b)  $T_{++-}(G)$ ; (c)  $T_{+-+}(G)$ ; (d)  $T_{+--}(G)$ ; (e)  $T_{---}(G)$ ; (f)  $T_{--+}(G)$ ; (g)  $T_{-+-}(G)$ ; (h)  $T_{-+-}(G)$ .

**Lemma 2.** Let  $G$  be graph with  $n$  and  $m$  as its order and size, respectively. Then, the order of  $T_{2\beta\gamma}(G)$  is  $(m+n)$ , and the size is

$$|E(T_{2\beta\gamma}(G))| = \begin{cases} \frac{1}{2}M_1(G) + m, & : \beta = +, \gamma = +, \\ \frac{1}{2}M_1(G) + mn - 3m, & : \beta = +, \gamma = -, \\ \frac{1}{2}[m^2 + 5m - M_1(G)], & : \beta = -, \gamma = +, \\ \frac{1}{2}[m^2 + 2mn - 3m - M_1(G)], & : \beta = -, \gamma = -. \end{cases} \quad (2)$$

**Lemma 3.** Let  $G$  be graph with  $n$  and  $m$  as its order and size, respectively. Then, the order of  $T_{\alpha\beta\gamma}(G)$  is  $(m+n)$ , and the size is

$$|E(T_{\alpha\beta\gamma}(G))| = \begin{cases} \frac{1}{2}[M_1(G) + 4m], & : \alpha = +, \beta = +, \gamma = +, \\ \frac{1}{2}[M_1(G) + 2m(n-2)], & : \alpha = +, \beta = +, \gamma = -, \\ \frac{1}{2}[m^2 + 7m - M_1(G)], & : \alpha = +, \beta = -, \gamma = +, \\ \frac{1}{2}[M_1(G) + n(n-1)], & : \alpha = -, \beta = +, \gamma = +, \\ \frac{1}{2}[(m+n)^2 - 5m - n - M_1(G)], & : \alpha = -, \beta = -, \gamma = -, \\ \frac{1}{2}[m^2 + n(n-1) + 3m - M_1(G)], & : \alpha = -, \beta = -, \gamma = +, \\ \frac{1}{2}[M_1(G) + 2m(n-4) + n(n-1)], & : \alpha = -, \beta = +, \gamma = -, \\ \frac{1}{2}[m^2 + 2mn - m - M_1(G)], & : \alpha = +, \beta = -, \gamma = -. \end{cases} \quad (3)$$

We now recall the results pertaining to the first and second Zagreb indices of type-I semitransformation graphs and the first Zagreb index of total transformation graph which are helpful for our study.

**Lemma 4** (see [21, 25]). Let  $G$  be a graph with order  $n$  and size  $m$ . Then,

- (i)  $M_1(T_{1++}(G)) = 4[m + M_1(G)]$
- (ii)  $M_1(T_{1+-}(G)) = nm^2 + m(n-2)^2$
- (iii)  $M_1(T_{1-+}(G)) = n(n-1)^2 + 4m$

$$(iv) M_1(T_{1--}(G)) = 4M_1(G) + m(n-2)^2 + (m+n-1)[n(m+n-1) - 8m]$$

**Lemma 5** (see [21]). Let  $G$  be a graph with order  $n$  and size  $m$ . Then,

- (i)  $M_2(T_{1++}(G)) = 4M_1(G) + 4M_2(G)$
- (ii)  $M_2(T_{1+-}(G)) = m^3 + m^2(n-2)^2$
- (iii)  $M_2(T_{1-+}(G)) = (1/2)[n(n-1)^3 - 2m(n-1)^2 + 8m(n-1)]$

$$(iv) \overline{M_2}(T_{1--}(G)) = (1/2)[4(n-2)M_1(G) - 4(m+n-1)\overline{M_1}(G) + 8\overline{M_2}(G) + (m+n-1)^2(n^2-n-2m) + 2m(m+n-1)(n-2)^2 - 8m^2(n-2)]$$

**Lemma 6** (see [25]). *Let  $G$  be a graph with order  $n$  and size  $m$ . Then,*

- (i)  $M_1(T_{+++}(G)) = 4M_1(G) + 2M_2(G) + F(G)$
- (ii)  $M_1(T_{++-}(G)) = mn(m+n-8) + 16m + 2(n-4)M_1(G) + 2M_2(G) + F(G)$
- (iii)  $M_1(T_{+-+}(G)) = m(m+3)^2 - 2(m+1)M_1(G) + 2M_2(G) + F(G)$
- (iv)  $M_1(T_{-++}(G)) = n(n-1)^2 + 2M_2(G) + F(G)$
- (v)  $M_1(T_{---}(G)) = (m+n)[(m+n)^2 - 10m - 2n + 1] + 8m - 2(m+n-3)M_1(G) + 2M_2(G) + F(G)$
- (vi)  $M_1(T_{--+}(G)) = n(n-1)^2 + m(m+3)^2 - (2m+6)M_1(G) + 2M_2(G) + F(G)$
- (vii)  $M_1(T_{-+-}(G)) = m(m+3)^2 + (m+n)(m+n-1)^2 - 2(m^2+7m)(m+n-1) + 2(n-2)M_1(G) + 2M_2(G) + F(G)$
- (viii)  $M_1(T_{+--}(G)) = m[(mn+1) + (m+n)(m+n-2)] - 2(m+n-1)M_1(G) + 2M_2(G) + F(G)$

### 3. Main Results

In this section, we derive the analytic expressions for the sigma index and coindex of semi and total transformations of graphs. Bearing the relation  $\sigma(G) = F(G) - 2M_2(G)$  in mind, we first study the second Zagreb index and then the forgotten index and finally deduce the results for the sigma index.

**3.1. Second Zagreb Index of Transformation Graphs.** The second Zagreb index of total transformation of graphs was expressed in [27], and by careful inspection, we notice that the entire process is vague and results in incorrect expressions. For instance, it was proved [27] that  $M_2(T_{+++}(G)) = 8M_1(G) + 6M_2(G) + F(G)$ . Suppose  $G = P_n$ , a path on  $n$  vertices. Then,  $T_{+++}(P_n)$  is a graph on  $2n-1$  vertices and  $4n-5$  edges in which 2 vertices of degrees 2 and 3 each and  $2n-5$  vertices of degree 4 while 2

edges with degrees of end vertices (2, 3) and (2, 4) each, and 4 edges with (3, 4) and  $4n-13$  edges with (4, 4). Hence,  $M_2(T_{+++}(G)) = 6 \times 2 + 8 \times 2 + 12 \times 4 + 16 \times (4n-13) = 64n - 132$ . However,  $M_1(P_n) = 4n - 6$ ,  $M_2(P_n) = 4n - 8$ , and  $F(P_n) = 8n - 14$ , resulting that  $8M_1(P_n) + 6M_2(P_n) + F(G) = 64n - 110$ . Hence, we now compute the correct analytic expressions of the second Zagreb index and coindex of total transformation graphs using reformulated Zagreb indices. Moreover, the type-II semitransformation is newly introduced in this paper, and hence we also obtain the exact expressions for first and second Zagreb indices. The following theorem gives the exact expression for second Zagreb indices of first four transformations in terms of edge version of first and second Zagreb indices of the arbitrary graph.

**Theorem 1.** *Let  $G$  be a graph with order  $n$  and size  $m$ . Then,*

- (i)  $M_2(T_{+++}(G)) = EM_2(G) + 2EM_1(G) + 8M_2(G) + 2M_1(G) + 2F(G) - 4m$
- (ii)  $M_2(T_{++-}(G)) = EM_2(G) + (n-2)EM_1(G) + (1/2)[(n-2)^2 + 2m(n-2)]M_1(G) + m^3 + m^2(n-2)(n-4) - m(n-2)^2$
- (iii)  $M_2(T_{+-+}(G)) = \overline{EM_2}(G) - (m+1)\overline{EM_1}(G) + (1/2)[m(m+1)^3] - (1/2)[(m^2-2m-11)M_1(G)] - 2F(G)$
- (iv)  $M_2(T_{-++}(G)) = EM_2(G) + 2EM_1(G) + 2nM_1(G) + (1/2)n(n-1)^3 - m[n^2-2n+5]$

*Proof.* The graph  $T_{+++}(G)$  has  $m+n$  vertices and  $(1/2)M_1(G) + 2m$  edges in which  $m$  edges are actual edges in  $G$  by condition (#1),  $(1/2)M_1(G) - m$  edges are produced by condition (#2) called edge adjacency relation edges (line graph edges), and  $2m$  edges are edges produced by condition (#3) called incidence relation edges. For any vertex  $s \in V(T_{+++}(G))$ ,

$$d_{T_{+++}(G)}(s) = \begin{cases} 2d_G(s), & \text{if } s \in V(G), \\ d_G(s) + 2, & \text{if } s \in E(G). \end{cases} \quad (4)$$

Therefore,

$$\begin{aligned} M_2(T_{+++}(G)) &= \sum_{st \in E(T_{+++}(G))} d_{T_{+++}(G)}(s)d_{T_{+++}(G)}(t) \\ &= \sum_{st \in E(T_{+++}(G)) \cap E(G)} d_{T_{+++}(G)}(s)d_{T_{+++}(G)}(t) + \sum_{st \in E(T_{+++}(G)) \cap E(L(G))} d_{T_{+++}(G)}(s)d_{T_{+++}(G)}(t) \\ &\quad + \sum_{st \in E(T_{+++}(G)) \setminus [E(G) \cup E(L(G))]} d_{T_{+++}(G)}(s)d_{T_{+++}(G)}(t) \\ &= \sum_{st \in E(G)} 2d_G(s)2d_G(t) + \sum_{s,t \in E(G), s \sim t} (d_G(s) + 2)(d_G(t) + 2) \end{aligned}$$

$$\begin{aligned}
& + \sum_{s \in V(G), t \in E(G) s \sim t} 2d_G(s)(d_G(t) + 2) \\
& = 4M_2(G) + \sum_{s, t \in E(G) s \sim t} d_G(s)d_G(t) \\
& \quad + \sum_{s, t \in E(G) s \sim t} 2[d_G(s) + d_G(t)] + 4|E(L(G))| \\
& \quad + \sum_{s \in V(G)} \sum_{x \in N_G(s)} 2d_G(s)[d_G(s) + d_G(x)] \\
& = 4M_2(G) + EM_2(G) + 2EM_1(G) + 4|E(L(G))| \\
& \quad + 2 \sum_{s \in V(G)} d_G(s)^3 + 2 \sum_{s \in V(G)} \sum_{x \in N_G(s)} d_G(s)d_G(x) \\
& = 4M_2(G) + EM_2(G) + 2EM_1(G) + 4\left(\frac{M_1(G)}{2} - m\right) + 2F(G) + 4M_2(G) \\
& = EM_2(G) + 2EM_1(G) + 8M_2(G) + 2M_1(G) + 2F(G) - 4m.
\end{aligned} \tag{5}$$

This completes the proof of assertion (i). Next, for any vertex  $s \in V(T_{+++}(G))$ ,

$$d_{T_{+++}(G)}(s) = \begin{cases} m, & \text{if } s \in V(G), \\ d_G(s) + n - 2, & \text{if } s \in E(G). \end{cases} \tag{6}$$

It can be seen that

$$\begin{aligned}
M_2(T_{+++}(G)) & = \sum_{st \in E(G)} d_G(s)d_G(t) + \sum_{s, t \in E(G) s \sim t} d_G(s)d_G(t) + \sum_{s \in V(G), t \in E(G) s \sim t} d_G(s)d_G(t) \\
& = \sum_{st \in E(G)} m \cdot m + \sum_{s, t \in E(G) s \sim t} (d_G(s) + n - 2)(d_G(t) + n - 2) + \sum_{s \in V(G), t \in E(G) s \sim t} m(d_G(t) + n - 2) \\
& = m^3 + EM_2(G) + (n - 2)EM_1(G) + (n - 2)^2|E(L(G))| \\
& \quad + \sum_{t \in E(G)} \sum_{s \in V(G) s \sim t} m(d_G(t) + n - 2) \\
& = m^3 + EM_2(G) + (n - 2)EM_1(G) + (n - 2)^2\left(\frac{M_1(G)}{2} - m\right) \\
& \quad + m \sum_{t \in E(G)} (n - 2)(d_G(t) + n - 2) \\
& = m^3 + EM_2(G) + (n - 2)EM_1(G) + \frac{1}{2}[(n - 2)^2M_1(G) - 2m(n - 2)^2] \\
& \quad + m(n - 2)\left(\sum_{t \in E(G)} d_G(t)\right) + m^2(n - 2)^2 \\
& = m^3 + EM_2(G) + (n - 2)EM_1(G) + \frac{1}{2}[(n - 2)^2M_1(G) - 2m(n - 2)^2] \\
& \quad + m(n - 2)[M_1(G) - 2m] + m^2(n - 2)^2 \\
& = EM_2(G) + (n - 2)EM_1(G) + \frac{1}{2}[(n - 2)^2 + 2m(n - 2)]M_1(G) \\
& \quad + m^3 + m^2(n - 2)(n - 4) - m(n - 2)^2.
\end{aligned} \tag{7}$$

To complete the proof of assertion (iii), we notice that for any vertex,  $s \in V(T_{+ \rightarrow}(G))$ ,

$$d_{T_{+ \rightarrow}(G)}(s) = \begin{cases} 2d_G(s), & \text{if } s \in V(G), \\ m+1-d_G(s), & \text{if } s \in E(G). \end{cases} \quad (8)$$

As before, we can easily write that

$$\begin{aligned} M_2(T_{+ \rightarrow}(G)) &= \sum_{st \in E(G)} 2d_G(s)2d_G(t) + \sum_{s,t \in E(G), s \sim t} (m+1-d_G(s))(m+1-d_G(t)) \\ &\quad + \sum_{s \in V(G), t \in E(G), s \sim t} 2d_G(s)(m+1-d_G(t)) \\ &= 4M_2(G) + (m+1)^2 \left[ \frac{m(m-1)}{2} - |E(L(G))| \right] - (m+1)\overline{EM}_1(G) + \overline{EM}_2(G) \\ &\quad + 2 \sum_{s \in V(G)} \sum_{x \in N_G(s)} d_G(s)(m+3-(d_G(s)+td_G(x))) \\ &= \overline{EM}_2(G) - (m+1)\overline{EM}_1(G) + 4M_2(G) + \frac{1}{2} [m(m+1)^3 - (m+1)^2 M_1(G)] \\ &\quad + 2(m+3)M_1(G) - 2F(G) - 4M_2(G) \\ &= \overline{EM}_2(G) - (m+1)\overline{EM}_1(G) + \frac{1}{2} [m(m+1)^3] - \frac{1}{2} [(m^2 - 2m - 11)M_1(G)] - 2F(G). \end{aligned} \quad (9)$$

The final assertion follows from the fact that for any vertex  $s \in V(T_{+ \rightarrow}(G))$ ,

$$d_{T_{+ \rightarrow}(G)}(s) = \begin{cases} n-1, & \text{if } s \in V(G), \\ d_G(s)+2, & \text{if } s \in E(G). \end{cases} \quad (10) \quad \square$$

**Theorem 2.** Let  $G$  be a graph with order  $n$  and size  $m$ . Then,

- (1)  $M_2(T_{---}(G)) = (1/2)[M_1^2(G) - (3(m+n-1)^2 - 8(2m+n-2))M_1(G) + (4m+4n-22)M_2(G) + (2m+2n-7)F(G) - 2EM_2(G) - 4EM_1(G) + (m+n)(m+n-1)^3 - 12m(m+n-1)^2 + 8m(2m+1)]$
- (2)  $M_2(T_{- \rightarrow}(G)) = (1/2)[M_1^2(G) - (3m^2 + 14m + 12n - 17)M_1(G) + (4m + 4n - 6)M_2(G) + (2m + 2n - 3)F(G) - 2EM_2(G) - 2(n-2)EM_1(G) + m^4 + 7m^3 + 4m^2n + 11m^2 - 2mn^2 + 24mn - 29m + n^4 - 3n^3 + 3n^2 - n]$
- (3)  $M_2(T_{+ \rightarrow}(G)) = (1/2)[M_1^2(G) + (3(m+n-1)^2 - 2(m^2 + 7m) - 2(m+1)(2m+2n-3) + m^2 - 2m - 11)M_1(G) + 2(2m+2n-3)M_2(G) + (2m+2n+1)F(G) - 2\overline{EM}_2(G) + 2(m+1)\overline{EM}_1(G) + (m+n)(m+n-1)^3 - 3(m+n-1)^2(m^2+7m) + (m^2+7m)^2 + m(m+3)^2(2m+2n-3) - m(m+1)^3]$
- (4)  $M_2(T_{+ \rightarrow}(G)) = (1/2)[M_1^2(G) + (2n(n-1) - 3(m+n-1)^2 - 4n)M_1(G) + 2(2m+2n-3)M_2(G) + (2m+2n-3)F(G) - 2EM_2(G) - 4EM_1(G) + (m+n)(m+n-1)^3 - 3n(n-1)(m+n-1)^2 + n^2(n-1)^2 + n(n-1)^2(2m+2n-3) - n(n-1)^3 + 2m(n^2 - 2n + 5)]$

*Proof.* It was proved [35] that

$$M_2(\overline{G}) = \frac{1}{2}n(n-1)^3 - 3m(n-1)^2 + 2m^2 + \frac{2n-3}{2}M_1(G) - M_2(G), \quad (11)$$

and known that  $\overline{T_{+++}(G)} \cong T_{---}(G)$ ,  $\overline{T_{+ \rightarrow}(G)} \cong T_{- \rightarrow}(G)$ ,  $\overline{T_{+ \rightarrow}(G)} \cong T_{+ \rightarrow}(G)$ , and  $\overline{T_{+ \rightarrow}(G)} \cong T_{+ \rightarrow}(G)$ . By Lemma 6 and Theorem 1, we can easily complete the proof.  $\square$

The Zagreb coindices are introduced in [36] with extensive applications in the field of chemical graph theory and widely discussed in [9, 10, 37–39]. Therefore, it will be worth finding the second Zagreb coindices of total transformations.

**Theorem 3.** Let  $G$  be a graph with order  $n$  and size  $m$ . Then,

- (1)  $\overline{M}_2(T_{+++}(G)) = (1/2)[M_1^2(G) + 8(m-1)M_1(G) - 18M_2(G) - 5F(G) - 2EM_2(G) - 4EM_1(G) + 8m(2m+1)]$
- (2)  $\overline{M}_2(T_{+ \rightarrow}(G)) = (1/2)[M_1^2(G) + (2mn - 4m - n^2 + 2n + 4)M_1(G) - 2M_2(G) - F(G) - 2EM_2(G) - 2(n-2)EM_1(G) + 2m^2n^2 - 2m^3 - 5m^2n + mn^2 - 8m]$
- (3)  $\overline{M}_2(T_{+ \rightarrow}(G)) = (1/2)[M_1^2(G) - (m^2 + 14m + 9)M_1(G) - 2M_2(G) + 3F(G) - 2\overline{EM}_2(G) + 2(m+1)\overline{EM}_1(G) + 10m^3 + 40m^2 - 10m]$
- (4)  $\overline{M}_2(T_{+ \rightarrow}(G)) = (1/2)[M_1^2(G) + 2n(n-3)M_1(G) - 2M_2(G) - F(G) - 2EM_2(G) - 4EM_1(G) + 2m(n^2 - 2n + 5)]$

- (5)  $\overline{M}_2(T_{---}(G)) = (1/2)[2EM_2(G) + 4EM_1(G) + (m^2 + n^2 + 2mn - 10m - 10n + 13)M_1(G) - 4(m + n - 5)M_2(G) - 2(m + n - 3)F(G) + 4m^3 + 8m^2n - 8m^2 + 4mn^2 - 8mn - 4m]$
- (6)  $\overline{M}_2(T_{--+}(G)) = (1/2)[2EM_2(G) + 2(n - 2)EM_1(G) + (m^2 - 2n^2 + 10m + 14n - 11)M_1(G) - 4(m + n - 1)M_2(G) - 2(m + n - 1)F(G) - 2m^3 + 2m^2n^2 - 6m^2n - 8m^2 + 8mn^2 - 30mn + 20m]$
- (7)  $\overline{M}_2(T_{-+-}(G)) = (1/2)[2\overline{EM}_2(G) - 2(m + 1)\overline{EM}_1(G) + (2m^2 - n^2 + 2mn + 4m + 6n + 6)M_1(G) - 4(m + n - 1)M_2(G) - 2(m + n + 1)F(G) + m^2n^2 + 7mn^2 - 32mn - 2m^3 - 16m^2 + 26m]$
- (8)  $\overline{M}_2(T_{+--}(G)) = (1/2)[2EM_2(G) + 4EM_1(G) + (m^2 + 2mn - 2m + n^2 + 2n + 1)M_1(G) - 4(m + n - 1)M_2(G) - 2(m + n - 1)F(G) + m^2n^2 - 2mn^2 - m^2n + 4mn - 10m]$

*Proof.* It was shown in [35] that

$$\overline{M}_2(G) = 2m^2 - \frac{1}{2}M_1(G) - M_2(G), \quad (12)$$

and combining the results of Lemma 6 and Theorem 1, we can finish the proof by simple mathematical calculations.  $\square$

The following theorem fills the gap in the literature with respect to the results found in [21, 25].

**Theorem 4.** *Let  $G$  be a graph with order  $n$  and size  $m$ . Then,*

- (1)  $M_1(T_{2++}(G)) = M_1(G) + F(G) + 2M_2(G)$  [25]
- (2)  $M_1(T_{2+-}(G)) = 2M_2(G) + F(G) + (2n - 7)M_1(G) + mn(m + n) - 4m(m + 2n - 4)$
- (3)  $M_1(T_{2-+}(G)) = 2M_2(G) + F(G) - (2m + 5)M_1(G) + m(m + 3)^2$
- (4)  $M_1(T_{2--}(G)) = 2M_2(G) + F(G) - (2m + 2n - 3)M_1(G) + m^2(n - 4) + m(m + n - 1)^2$
- (5)  $\overline{M}_1(T_{2++}(G)) = (m + n - 2)M_1(G) - 2M_2(G) - F(G) + 2mn + 2m(m - 1)$  [25]
- (6)  $\overline{M}_1(T_{2+-}(G)) = (m - n + 6)M_1(G) - 2M_2(G) - F(G) + mn(m + n) - 2m(m + 5)$
- (7)  $\overline{M}_1(T_{2-+}(G)) = (m - n + 6)M_1(G) - 2M_2(G) - F(G) + mn(m + 5) - 2m(m + 7)$
- (8)  $\overline{M}_1(T_{2--}(G)) = (m + n - 2)M_1(G) - 2M_2(G) - F(G) + mn(n - 3) + 2m(m + 1)$

*Proof.* From the construction of type-II semitransformation, it is easily seen that for any vertex  $s \in V(T_{2\beta\gamma}(G))$  such that  $s \in V(G)$ ,

$$d_{T_{2\beta\gamma}(G)}(s) = \begin{cases} d_G(s), & : \beta = +, \gamma = +, \\ d_G(s), & : \beta = -, \gamma = +, \\ m - d_G(s), & : \beta = +, \gamma = -, \\ m - d_G(s), & : \beta = -, \gamma = -. \end{cases} \quad (13)$$

In the same way, for any vertex  $s \in V(T_{2\beta\gamma}(G))$  such that  $s \in E(G)$ ,

$$d_{T_{2\beta\gamma}(G)}(s) = \begin{cases} d_G(s) + 2, & : \beta = +, \gamma = +, \\ m + 1 - d_G(s), & : \beta = -, \gamma = +, \\ n - 2 + d_G(s), & : \beta = +, \gamma = -, \\ m + n - 3 - d_G(s), & : \beta = -, \gamma = -. \end{cases} \quad (14)$$

The proof follows from routine mathematical simplifications and, in addition, using the relation  $\overline{M}_1(G) = 2m(n - 1) - M_1(G)$  [35].  $\square$

In [25], the authors have made an attempt to find the second Zagreb index of type-I semitransformation and left the calculations of type-II semitransformation due to its computational complexity. The following theorem gives the exact analytical expressions of the second Zagreb indices for type-II transformations of an arbitrary graph.

**Theorem 5.** *Let  $G$  be a graph with order  $n$  and size  $m$ . Then,*

- (1)  $M_2(T_{2++}(G)) = EM_2(G) + 2EM_1(G) + 2M_2(G) + M_1(G) + F(G) - 4m$
- (2)  $M_2(T_{2+-}(G)) = EM_2(G) + (n - 2)EM_1(G) + 2M_2(G) + (1/2)[n^2 + 2mn - 8m - 2n - 4]M_1(G) + F(G) + m^2(n - 4)^2 - m(n - 2)^2$
- (3)  $M_2(T_{2-+}(G)) = \overline{EM}_2(G) - (m + 1)\overline{EM}_1(G) - 2M_2(G) - (1/2)(m^2 - 5)M_1(G) - F(G) + (1/2)m(m + 1)^3$
- (4)  $M_2(T_{2--}(G)) = \overline{EM}_2(G) - (m + n - 3)\overline{EM}_1(G) - (1/2)[(m + n - 3)^2 + 2mn - 10m - 2n + 2]M_1(G) - 2M_2(G) - F(G) + (1/2)[m(m + 1)(m + n - 3)^2 + 2m^2(n - 4)(m + n - 1)]$
- (5)  $\overline{M}_2(T_{2++}(G)) = (1/2)[M_1^2(G) + (4m - 5)M_1(G) - 3F(G) - 2EM_2(G) - 4EM_1(G) - 6M_2(G) + 4m(m + 2)]$
- (6)  $\overline{M}_2(T_{2+-}(G)) = (1/2)[M_1^2(G) + (2mn - n^2 - 4m + 11)M_1(G) - 3F(G) - 2EM_2(G) - 2(n - 2)EM_1(G) - 6M_2(G) + mn(2mn - 9m + n) + 8m(m - 1)]$
- (7)  $\overline{M}_2(T_{2-+}(G)) = (1/2)[M_1^2(G) - m(m + 8)M_1(G) + 2M_2(G) - 2\overline{EM}_2(G) + 2(m + 1)\overline{EM}_1(G) + F(G) + 2m(3m^2 + 8m - 5)]$
- (8)  $\overline{M}_2(T_{2--}(G)) = (1/2)[M_1^2(G) - (m^2 - n^2 + 8m + 6n - 8)M_1(G) + 2M_2(G) + F(G) - 2\overline{EM}_2(G) + (m + n - 3)\overline{EM}_1(G) + mn(mn - m - 2n + 8) + 2m(3m^2 + 2m - 5)]$

*Proof.* The proof of (i)–(iv) is similar to Theorem 1, and for the sake the completeness, we give the proof of (i). The graph  $T_{2++}(G)$  has  $m + n$  vertices and  $(1/2)M_1(G) + m$  edges in which  $(1/2)M_1(G) - m$  edges are produced by condition (#2) called edge adjacency relation edges (line graph edges) and  $2m$  edges are edges produced by condition (#3) called

incidence relation edges. Also, for any vertex,  $s \in V(T_{2^{++}}(G))$ ,

$$d_{T_{2^{++}}(G)}(s) = \begin{cases} d_G(s), & \text{if } s \in V(G), \\ d_G(s) + 2, & \text{if } s \in E(G). \end{cases} \quad (15)$$

Hence,

$$\begin{aligned} M_2(T_{2^{++}}(G)) &= \sum_{st \in E(T_{2^{++}}(G))} d_{T_{2^{++}}(G)}(s)d_{T_{2^{++}}(G)}(t) \\ &= \sum_{st \in E(T_{2^{++}}(G)) \cap E(L(G))} d_{T_{2^{++}}(G)}(s)d_{T_{2^{++}}(G)}(t) + \sum_{st \in E(T_{2^{++}}(G)) \setminus E(L(G))} d_{T_{2^{++}}(G)}(s)d_{T_{2^{++}}(G)}(t) \\ &= \sum_{s,t \in E(G) s \sim t} (d_G(s) + 2)(d_G(t) + 2) + \sum_{s \in V(G), t \in E(G) s \sim t} d_G(s)[d_G(t) + 2] \\ &= \sum_{s,t \in E(G) s \sim t} d_G(s)d_G(t) + \sum_{s,t \in E(G) s \sim t} 2[d_G(s) + d_G(t)] + 4|E(L(G))| \\ &\quad + \sum_{s \in V(G)} \sum_{x \in N_G(s)} d_G(s)[d_G(s) + d_G(x)] \\ &= \sum_{s,t \in E(G) s \sim t} d_G(s)d_G(t) + \sum_{s,t \in E(G) s \sim t} 2[d_G(s) + d_G(t)] + 4|E(L(G))| + \sum_{s \in V(G)} d_G(s)^3 + \sum_{s \in V(G)} \sum_{x \in N_G(s)} d_G(s)d_G(x) \\ &= EM_2(G) + 2EM_1(G) + 4\left(\frac{M_1(G)}{2} - m\right) + F(G) + 2M_2(G) \\ &= EM_2(G) + 2EM_1(G) + 2M_2(G) + 2M_1(G) + F(G) - 4m. \end{aligned} \quad (16)$$

To complete the remaining parts, we apply equation (12) with the help of Theorem 4.  $\square$

**3.2. F-Index of Transformation Graphs.** The forgotten index and coindex of type-I semi and total transformations of graphs have been obtained [20, 28] in terms of first Zagreb, second Zagreb, vertex a-Zagreb, and (a, b)-Zagreb indices. In this section, we rewrite vertex a-Zagreb and (a, b)-Zagreb indices in terms of the sum-connectivity index. Before proceeding to this, we shall state a basic lemma.

**Lemma 7** (see [28]). *Let  $G$  be a connected graph of order  $n$  and size  $m$ . Then,*

- (i)  $F(\overline{G}) = n(n-1)^3 - F(G) - 6m(n-1)^2 + 3(n-1)M_1(G)$
- (ii)  $\overline{F}(G) = (n-1)M_1(G) - F(G)$

The following theorem is crucial for finding the sigma index of the transformation of an arbitrary graph.

**Theorem 6.** *Let  $G$  be a connected graph of order  $n$  and size  $m$ . Then,*

- (1)  $F(T_{+++}(G)) = 8F(G) + \chi_3(G)$
- (2)  $F(T_{++-}(G)) = \chi_3(G) + (3n-12)[F(G) + 2M_2(G)] + 3(n-4)^2M_1(G) + m(n-4)^3 + m^3n$
- (3)  $F(T_{+-+}(G)) = (3m+17)F(G) - \chi_3(G) + m(m+3)^3 - 3(m+3)^2M_1(G) + 6(m+3)M_2(G)$
- (4)  $F(T_{--+}(G)) = n(n-1)^3 + \chi_3(G)$
- (5)  $F(T_{---}(G)) = 6(m+n-1)M_2(G) - (3m^2 - 18m + 6mn - 18n + 3n^2 + 15)M_1(G) + (3m + 3n - 11)F(G) - \chi_3(G) + (m+n)(m+n-1)^3 - 12m(m+n-1)^2$
- (6)  $F(T_{-+-}(G)) = (3m+9)F(G) - \chi_3(G) - (3m^2 + 18m + 27)M_1(G) + (6m+18)M_2(G) + m^4 + 9m^3 + 27m^2 + 27m + n^4 - 3n^3 + 3n^2 - n$
- (7)  $F(T_{-+-(G)}) = \chi_3(G) + (3n-20)F(G) + (3n^2 - 12n + 12m + 36)M_1(G) + (6n-24)M_2(G) + (m+n)(m+n-1)^3 - m(m+3)^3 - 3(m+n-1)^2(m^2 + 7m) + 3m(m+3)^2(m+n-1)$

$$(8) F(T_{+--}(G)) = 3(m+n-1)F(G) + 6(m+n-1)M_2(G) - 3(m+n-1)^2M_1(G) - \chi_3(G) + (m+n)(m+n-1)^3 - n(n-1)^3 - 3mn(n-1)(m+n-1)$$

*Proof.* The proof of (i)–(iv) can be derived using the degrees of vertices from the proof of Theorem 1 and the remaining parts from Lemma 7.  $\square$

The following theorem is an easy consequence of combining Lemma 7 and Theorem 6, which will be used to compute the analytical expressions of the forgotten coincides of total transformations of an arbitrary graph.

**Theorem 7.** Let  $G$  be a connected graph of order  $n$  and size  $m$ . Then,

$$(1) \bar{F}(T_{+++}(G)) = 4(m+n-1)M_1(G) + 2(m+n-1)M_2(G) + (m+n-9)F(G) - \chi_3(G)$$

$$(2) \bar{F}(T_{++-}(G)) = (m-2n+11)F(G) - \chi_3(G) - (n^2-2mn+8m-14n+40)M_1(G) + (2m-4n+22)M_2(G) + 2m^2n^2 - 9m^2n + 16m^2 + 3mn^2 - 24mn + 48m$$

$$(3) \bar{F}(T_{+-+}(G)) = (n-2m-18)F(G) + \chi_3(G) + (m^2+18m-2mn-2n+29)M_1(G) + (2n-4m-20)M_2(G) + m^3n - 4m^3 + 6m^2n - 24m^2 + 9mn - 36m$$

$$(4) \bar{F}(T_{-++}(G)) = (m+n-1)F(G) + 2(m+n-1)M_2(G) - \chi_3(G) + mn^3 - 2mn^2 + mn$$

$$(5) \bar{F}(T_{---}(G)) = \chi_3(G) - (2m+2n-10)F(G) + (m^2+n^2+2mn-10m-10n+9)M_1(G) - 4(m+n-1)M_2(G) + 4m^3 + 8m^2n - 8m^2 + 4mn^2 - 8mn + 4m$$

$$(6) \bar{F}(T_{--+}(G)) = \chi_3(G) + (m^2+14m-2mn-6n+33)M_1(G) - (4m-2n+20)M_2(G) - (2m-n+10)F(G) + m^3n - 4m^3 + 6m^2n - 24m^2 + mn^3 - 2mn^2 + 10mn - 36$$

$$(7) \bar{F}(T_{-+-}(G)) = 2(m-2n+11)M_2(G) - \chi_3(G) - (n^2-2mn+16m-6n+32)M_1(G) + (m-2n+19)F(G) + 4m^3 + m^2n^2 + 8m^2 + 7mn^2 - 32mn + 52m$$

$$(8) \bar{F}(T_{+--}(G)) = \chi_3(G) - 4(m+n-1)M_2(G) - 2(m+n-1)F(G) + (m+n-1)^2M_1(G) + m^2n^2 - m^2n$$

**Theorem 8** (see [20]). Let  $G$  be a connected graph of order  $n$  and size  $m$ . Then,

$$(1) F(T_{1++}(G)) = 8F(G) + 8m$$

$$(2) F(T_{1+-}(G)) = nm^3 + m(n-2)^3$$

$$(3) F(T_{1-+}(G)) = n(n-1)^3 + 8m$$

$$(4) F(T_{1--}(G)) = 12(m+n-1)M_1(G) - 8F(G) + n(m+n-1)^3 - 12m(m+n-1)^2 + m(n-2)^3$$

$$(5) \bar{F}(T_{1++}(G)) = 4m(m+n-1) - 8m + 4(m+n-1)M_1(G) - 8F(G)$$

$$(6) \bar{F}(T_{1+-}(G)) = (m+n-1)(nm^2 + m(n-2)^2) - nm^3 - m(n-2)^3$$

$$(7) \bar{F}(T_{1-+}(G)) = (m+n-1)(4m+n(n-1)^2) - (n-1)^3 - 8m$$

$$(8) \bar{F}(T_{1--}(G)) = 8F(G) - 8(m+n-1)M_1(G) + m(m+n-1)(n-2)^2 + (m+n-1)^2(n(m+n-1) + 4m) - n(m+n-1)^3 - m(n-2)^3$$

**Theorem 9.** Let  $G$  be a connected graph of order  $n$  and size  $m$ . Then,

$$(1) F(T_{2++}(G)) = F(G) + \chi_3(G)$$

$$(2) F(T_{2+-}(G)) = m^3(n-6) + m(n-4)^3 + \chi_3(G) + (3n-13)F(G) + 6(n-4)M_2(G) + [3(n-4)^2 + 3m]M_1(G)$$

$$(3) F(T_{2-+}(G)) = F(G) + m(m+3)^3 - 3(m+3)^2M_1(G) + 3(m+3)[F(G) + 2M_2(G)] - \chi_3(G)$$

$$(4) F(T_{2--}(G)) = m^3(n-6) + m(m+n-1)^3 + (3m+3n-4)F(G) + 6(m+n-1)M_2(G) + [3m-3(m+n-1)^2]M_1(G) - \chi_3(G)$$

$$(5) \bar{F}(T_{2++}(G)) = (m+n-1)[M_1(G) + 2M_2(G)] + (m+n-2)F(G) - \chi_3(G)$$

$$(6) \bar{F}(T_{2+-}(G)) = (2m-4n+22)M_2(G) + (2mn-n^2+15n-10m-41)M_1(G) + (m-2n+12)F(G) - \chi_3(G) + (m+n-1)(mn(m+n) - 4m(m+2n-4)) - m^3(n-6) - m(n-4)^3$$

$$(7) \bar{F}(T_{2-+}(G)) = (2n-4m-20)M_2(G) + (n-2m-11)F(G) + (m^2+15m-2mn-5n+32)M_1(G) + \chi_3(G) + m(m+3)^2(n-4)$$

$$(8) \bar{F}(T_{2--}(G)) = \chi_3(G) - 4(m+n-1)M_2(G) + (m^2+2mn-4m-n+n^2)M_1(G) - (2m+2n-3)F(G) + 2m^3 + m^2n^2 - 5m^2n + 4m^2$$

*Proof.* The proof of the theorem follows from using the degrees of vertices as given in the proof of Theorem 4 and Lemma 7.  $\square$

**3.3.  $\sigma$ -Index of Transformation Graphs.** In this section, we first derive a relation between  $\sigma$ -index of a graph and its coindex. Following this, we derive another relation between  $\sigma$ -coindex of a graph and  $\sigma$ -index of the complement graph. Finally, we list down the  $\sigma$ -index and coindex of semi and total transformations of graphs from the above subsections. The following theorem gives the relationship between the sigma index and its coindex.

**Theorem 10.** Let  $G$  be any graph with  $n$  vertices and  $m$  edges. Then,



$$\sigma(G) + \bar{\sigma}(G) = nM_1(G) - 4m^2. \quad (17)$$

*Proof.* The proof is completed from the definitions of  $\sigma$ -index and coindex as explained in the following:

$$\begin{aligned} \sigma(G) + \bar{\sigma}(G) &= \sum_{st \in E(G)} [d_G(s) - d_G(t)]^2 + \sum_{st \notin E(G)} [d_G(s) - d_G(t)]^2 \\ &= \sum_{\{s,t\} \subseteq V(G)} [d_G(s) - d_G(t)]^2 \\ &= \sum_{\{s,t\} \subseteq V(G)} [d_G(s)^2 + d_G(t)^2 - 2d_G(s)d_G(t)] \\ &= \sum_{\{s,t\} \subseteq V(G)} [d_G(s)^2 + d_G(t)^2] - \sum_{\{s,t\} \subseteq V(G)} 2d_G(s)d_G(t) \\ &= F(G) + \bar{F}(G) - 2M_2(G) - 2\bar{M}_2(G) \\ &= (n-1)M_1(G) - 2M_2(G) - 2\left(2m^2 - M_2(G) - \frac{M_1(G)}{2}\right) \\ &= nM_1(G) - 4m^2. \end{aligned} \quad (18)$$

**Corollary 1.** Let  $G$  be any graph with  $n$  vertices and  $m$  edges. Then,

$$\bar{\sigma}(G) = nM_1(G) + 2M_2(G) - F(G) - 4m^2. \quad (19)$$

The following theorem establishes interesting result that the sigma index of the complement of a graph and sigma coindex of a graph is one and the same.

**Theorem 11.** Let  $G$  be any graph with  $n$  vertices and  $m$  edges. Then,

$$\sigma(\bar{G}) = \bar{\sigma}(G). \quad (20)$$

*Proof.* For any vertex  $s \in V(G)$ ,  $d_{\bar{G}}(s) = n - 1 - d_G(s)$ , and we have

$$\begin{aligned} \sigma(\bar{G}) &= \sum_{st \in E(\bar{G})} [d_{\bar{G}}(s) - d_{\bar{G}}(t)]^2 \\ &= \sum_{st \notin E(G)} [(n-1-d_G(s)) - (n-1-d_G(t))]^2 \\ &= \sum_{st \notin E(G)} [d_G(t) - d_G(s)]^2 \\ &= \bar{\sigma}(G). \end{aligned} \quad (21)$$

**Corollary 2.** Let  $G$  be any graph with  $n$  vertices and  $m$  edges. Then,

$$\bar{\sigma}(\bar{G}) = \sigma(G). \quad (22)$$

The main objective of this section is the following theorem.

**Theorem 12.** Let  $G$  be a connected graph of order  $n$  and size  $m$ . Then,

- (1)  $\sigma(T_{+++}(G)) = 4F(G) + \chi_3(G) - 2EM_2(G) - 4EM_1(G) - 16M_2(G) - 4M_1(G) + 8m$
- (2)  $\sigma(T_{++-}(G)) = \chi_3(G) + (3n-12)[F(G) + 2M_2(G)] - [(n-2)^2 + 2m(n-2) - 3(n-4)^2]M_1(G) - 2EM_2(G) - 2(n-2)EM_1(G) - 2m^3 - 2m^2(n-2)(n-4) + 2m(n-2)^2 + m(n-4)^3 + m^3n$
- (3)  $\sigma(T_{+-+}(G)) = 12F(G) - \chi_3(G) + 3(m+3)\chi_2(G) - 2\bar{EM}_2(G) + 2(m+1)\bar{EM}_1(G) + [m^2 - 2m - 11 - 3(m+3)^2]M_1(G) + m(m+3)^3 - m(m+1)^3$
- (4)  $\sigma(T_{--+}(G)) = \chi_3(G) - 2EM_2(G) - 4EM_1(G) - 4nM_1(G) + 2m(n^2 - 2n + 5)$
- (5)  $\sigma(T_{---}(G)) = 2EM_2(G) + 4EM_1(G) - M_1^2(G) + 4(n-m+1)M_1(G) + 2(m+n+8)M_2(G) + (m+n-4)F(G) - \chi_3(G) - 8m(2m+1)$
- (6)  $\sigma(T_{-+-}(G)) = 2EM_2(G) + 2(n-2)EM_1(G) - M_1^2(G) - \chi_3(G) + (12n-4m-44)M_1(G) + (2m-4n+24)M_2(G) + (m-2n+12)F(G) + 2m^3 + 16m^2 - 4m^2n + 2mn^2 - 24mn + 56m$

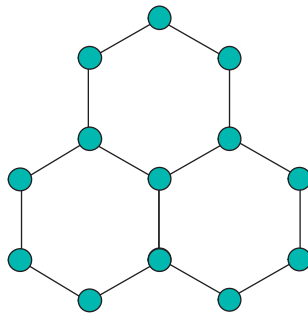


FIGURE 4: The molecular graph of perhydrophenalene G.

TABLE 2: Second Zagreb and sigma indices of total transformations of perhydrophenalene G.

S. no.	Total transformations of G	Second Zagreb index	Sigma index
1.	$T_{+++}(G)$	1587	48
2.	$T_{++-}(G)$	41652	342
3.	$T_{+-+}(G)$	16968	2334
4.	$T_{-++}(G)$	11331	1584
5.	$T_{---}(G)$	155358	504
6.	$T_{--+}(G)$	28560	534
7.	$T_{-+-}(G)$	86868	12582
8.	$T_{+--}(G)$	99894	8760

TABLE 3: Second Zagreb and sigma indices for semitransformations of perhydrophenalene G.

S. no.	Semitransformations of G	Second Zagreb index	Sigma index
1.	$T_{1++}(G)$	636	288
2.	$T_{1+-}(G)$	30600	2640
3.	$T_{1-+}(G)$	9792	3000
4.	$T_{1--}(G)$	72372	22608
5.	$T_{2++}(G)$	885	192
6.	$T_{2+-}(G)$	33069	318
7.	$T_{2-+}(G)$	15678	3654
8.	$T_{2--}(G)$	217794	15120

$$(7) \sigma(T_{--+}(G)) = 2\overline{EM}_2(G) - 2(m+1)\overline{EM}_1(G) - M_1^2(G) + \chi_3(G) + (2m^2 + 32m - 2mn + 38 - 2n)M_1(G) + (2n - 4m - 18)M_2(G) + (n - 2m - 21)F(G) + m^3n - 14m^3 + 6m^2n - 64m^2 + 9mn - 26m$$

$$(8) \sigma(T_{+--}(G)) = 2EM_2(G) + 4EM_1(G) - M_1^2(G) - \chi_3(G) - 2n(n-3)M_1(G) + (2m+2n)M_2(G) + (m+n)F(G) + n^3m - 4n^2m + 5nm - 10m$$

In sequence to Theorems 3 and 7, we have the following.

**Theorem 13.** Let G be a connected graph of order n and size m. Then,

$$(1) \overline{\sigma}(T_{+++}(G)) = 2EM_2(G) + 4EM_1(G) + 2(m+n+8)M_2(G) + 4(n-m+1)M_1(G) + (m+n-4)F(G) - \chi_3(G) - M_1^2(G) - 16m^2 - 8m$$

$$(2) \overline{\sigma}(T_{++-}(G)) = 2EM_2(G) + 2(n-2)EM_1(G) + 2(m-2n+12)M_2(G) + 4(3n-m-11)M_1(G) + (m-2n+12)F(G) - \chi_3(G) - M_1^2(G) + 2m^3 - 4m^2n + 16m^2 + 2mn^2 - 24mn + 56m$$

$$(3) \overline{\sigma}(T_{+-+}(G)) = 2\overline{EM}_2(G) - 2(m+1)\overline{EM}_1(G) + \chi_3(G) - M_1^2(G) + (2n - 4m - 18)M_2(G) + (2m^2 + 32m - 2mn + 38 - 2n)M_1(G) + (n - 2m - 21)F(G) + m^3n - 14m^3 + 6m^2n - 64m^2 + 9mn - 26m$$

$$(4) \overline{\sigma}(T_{-++}(G)) = 2EM_2(G) + 4EM_1(G) + 2(m+n)M_2(G) - 2n(n-3)M_1(G) + (m+n)F(G) - \chi_3(G) - M_1^2(G) + mn(n-1)^2 - 2m(n^2 - 2n + 5)$$

$$(5) \overline{\sigma}(T_{---}(G)) = \sigma(T_{+++}(G))$$

$$(6) \overline{\sigma}(T_{--+}(G)) = \sigma(T_{++-}(G))$$

$$(7) \overline{\sigma}(T_{-+-}(G)) = \sigma(T_{+-+}(G))$$

$$(8) \overline{\sigma}(T_{+--}(G)) = \sigma(T_{-++}(G))$$

The following theorems give the exact expressions of the sigma index of type-I and type-II semitransformations.

**Theorem 14.** Let G be graph with n and m as its order and size, respectively. Then,

$$(1) \sigma(T_{1++}(G)) = 8F(G) - 8M_1(G) - 8M_2(G) + 8m$$

$$(2) \sigma(T_{1+-}(G)) = nm^3 + m(n-2)^3 - 2m^3 - 2m^2(n-2)^2$$

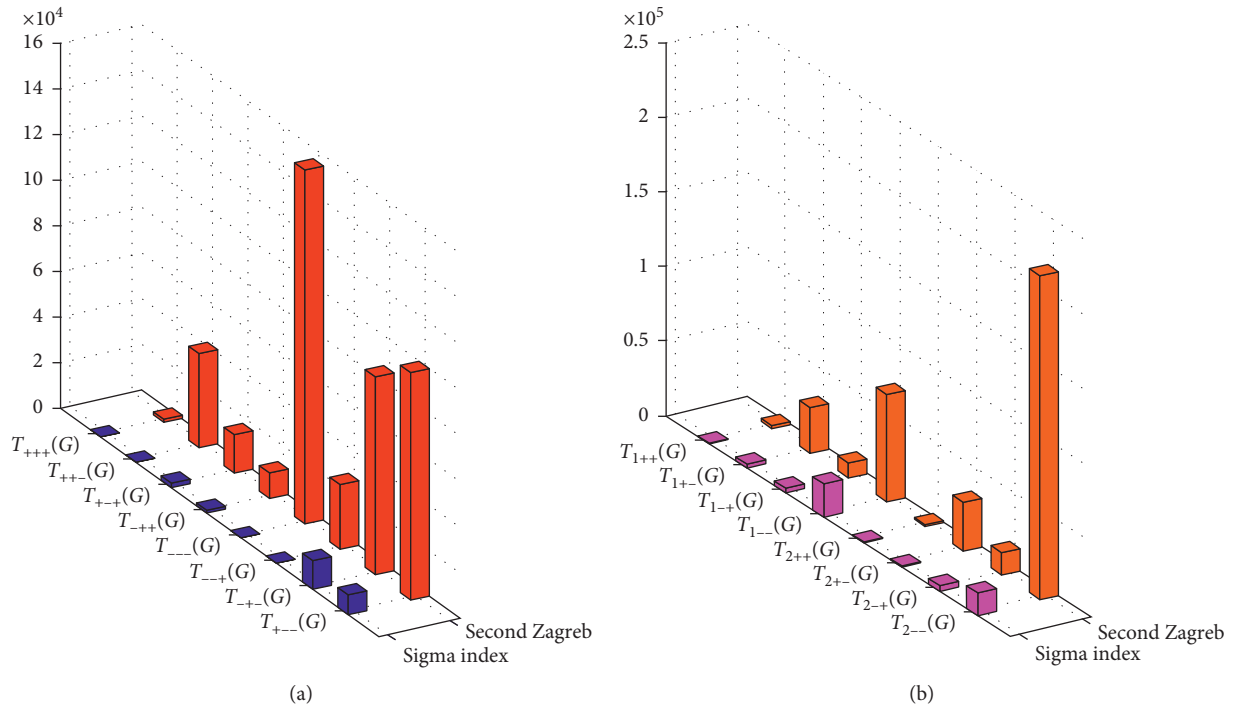


FIGURE 5: (a) Total transformation of the second Zagreb and sigma indices; (b) semitransformation of second the Zagreb and sigma indices.

$$(3) \sigma(T_{1_{++}}(G)) = 2m(n-1)^2 - 8m(n-1) + 8m$$

$$(4) \sigma(T_{1_{--}}(G)) = 4(m+n-1)\overline{M}_1(G) - 8F(G) + 4(3m+2n-1)M_1(G) - 8\overline{M}_2(G) + m^3n - 8mn^2 - 6m^2n + 17mn - 10m^3 - 4m^2 - 10m$$

$$(5) \overline{\sigma}(T_{1_{++}}(G)) = 4(m+n+2)M_1(G) + 8M_2(G) - 8F(G) - 4m(8m-n+2)$$

$$(6) \overline{\sigma}(T_{1_{+-}}(G)) = 2m^2(m-2n+4) + 2mn(n-4) + 8m$$

$$(7) \overline{\sigma}(T_{1_{-+}}(G)) = mn^3 - 8mn^2 + 21mn - 18m$$

$$(8) \overline{\sigma}(T_{1_{--}}(G)) = 8F(G) - 4(2m+n-1)M_1(G) - 4(m+n-1)\overline{M}_1(G) + 8\overline{M}_2(G) + 2m^2(m+4n-10) + 2m(4n^2 - 8n + 5)$$

$$(5) \overline{\sigma}(T_{2_{++}}(G)) = 2EM_2(G) + 4EM_1(G) - (3m-n-4)M_1(G) - M_1^2(G) + (m+n+1)F(G) + 2(m+n+2)M_2(G) - \chi_3(G) - 4m^2 - 8m$$

$$(6) \overline{\sigma}(T_{2_{+-}}(G)) = 2EM_2(G) + 2(n-2)EM_1(G) - M_1^2(G) - \chi_3(G) + (15n-6m-52)M_1(G) + (2m-4n+28)M_2(G) + (m-2n+15)F(G) + 2m^3 - 4m^2n + 12m^2 + 2mn^2 - 24mn + 56m$$

$$(7) \overline{\sigma}(T_{2_{-+}}(G)) = 2\overline{EM}_2(G) - 2(m+1)\overline{EM}_1(G) - M_1^2(G) + \chi_3(G) + (2m^2 - 2mn + 23m - 5n + 32)M_1(G) - 2(2m-n+11)M_2(G) - (2m-n+12)F(G) + m^3n - 10m^3 + 6m^2n - 40m^2 + 9mn - 26m$$

$$(8) \overline{\sigma}(T_{2_{--}}(G)) = 2\overline{EM}_2(G) - 2(m+n-3)\overline{EM}_1(G) + \chi_3(G) - M_1^2(G) + (2m^2 + 2mn + 4m + 5n - 8)M_1(G) - 2(2m+2n-1)M_2(G) - 2(m+n-1)F(G) - 4m^3 - 4m^2n + 2mn^2 - 8mn + 10m$$

**Theorem 15.** Let  $G$  be graph with  $n$  and  $m$  as its order and size, respectively. Then,

$$(1) \sigma(T_{2_{++}}(G)) = \chi_3(G) - 2EM_2(G) - 4EM_1(G) - 4M_2(G) - 4M_1(G) - F(G) + 8m$$

$$(2) \sigma(T_{2_{+-}}(G)) = \chi_3(G) + 3(n-5)F(G) + 2(3n-14)M_2(G) + (2n^2 - 2mn + 11m - 22n + 52)M_1(G) - 2EM_2(G) - 2(n-2)EM_1(G) + m^3n + mn^3 - 6m^3 - 2m^2n^2 + 16m^2n - 10mn^2 - 32m^2 + 40mn - 56m$$

$$(3) \sigma(T_{2_{-+}}(G)) = 2(m+1)\overline{EM}_1(G) - 2\overline{EM}_2(G) - (2m^2 + 18m + 32)M_1(G) + 3(m+4)F(G) + 2(3m+11)M_2(G) - \chi_3(G) + 6m^3 + 24m^2 + 26m$$

$$(4) \sigma(T_{2_{--}}(G)) = 2(m+n-3)\overline{EM}_1(G) - 2\overline{EM}_2(G) - (2m^2 + 2mn + 2n^2 + 7m + 2n - 8)M_1(G) + (3m+3n-2)F(G) + (6m+6n-2)M_2(G) - \chi_3(G) + 4m^3 + mn^3 - 4mn^2 + 8m^2n + 9mn - 8m^2 - 10m$$

## 4. Results and Discussion

The various expressions for the Zagreb and sigma topological indices computed here can be extremely useful in the thermodynamic properties such as the heat of formation and entropy for the structure-property predictions of the transformation of molecular materials when combined with total and semitype transformations. Since the enumeration and construction of different structures under given specific constraints have found potential applications in drug discovery via topological indices [40, 41], it can help the chemists by reducing the number of potential drug compounds that need to be experimentally considered. We computed expressions based on the degree measures of the given graph, and hence it can be con-

sidered as an efficient technique for vibrational spectroscopic chemical analysis through the vertex partitioning and providing significant simplifications in the vibrational mode analysis. Moreover, sigma indices obtained here offer the regularity perfection of the structure.

The semi and total transformation considered here provide 16 classes of new structures for the given graph based on the edge adjacency and incidence relations. Once we compute the topological indices such as Zagreb, reformulated Zagreb, forgotten, sum-connectivity, and sigma for the base graph and then using the results from Theorems 1–15, one can readily obtain the Zagreb and sigma indices for the new structures.

We now present the applications of our computed results for perhydrophenalene. The molecular graph of perhydrophenalene  $G$  is shown in Figure 4 and has 13 vertices and 15 edges. Moreover,  $G$  has 9 vertices of degree 2 and 4 vertices of degree 3. Clearly, the edge partition of  $G$  has three classes based on the degree of end vertices, namely,  $(2, 2)$ ,  $(2, 3)$ , and  $(3, 3)$  while the number of edges in the classes, respectively, are 6, 6, and 3.

From the above data, one can easily derive  $M_1(G) = 72$ ,  $M_2(G) = 87$ ,  $EM_1(G) = 126$ ,  $EM_2(G) = 195$ ,  $F(G) = 180$ ,  $\overline{EM}_1(G) = 462$ ,  $\overline{EM}_2(G) = 624$ ,  $\overline{M}_1(G) = 288$ ,  $\overline{M}_2(G) = 327$ ,  $\chi_2(G) = 354$ , and  $\chi_3(G) = 1782$ . Then, the calculations of second Zagreb and sigma indices of total and semitransformations of  $G$  are obtained from Theorems 1–15 and presented in Tables 2 and 3, respectively. These values are compared graphically and depicted in Figure 5.

In the case of the second Zagreb index of the molecular graph  $G$  of perhydrophenalene, we infer that  $M_2(T_{+++}(G)) \leq M_2(T_{++-}(G)) \leq M_2(T_{+-+}(G)) \leq M_2(T_{-++}(G)) \leq M_2(T_{+--}(G)) \leq M_2(T_{-+-}(G)) \leq M_2(T_{--+}(G)) \leq M_2(T_{-+-}(G))$  and  $M_2(T_{1++}(G)) \leq M_2(T_{2++}(G)) \leq M_2(T_{1+-}(G)) \leq M_2(T_{2+-}(G)) \leq M_2(T_{1--}(G)) \leq M_2(T_{2--}(G))$ .

On the other side, for the sigma index, we observe that  $\sigma(T_{+++}(G)) \leq \sigma(T_{++-}(G)) \leq \sigma(T_{+-+}(G)) \leq \sigma(T_{-++}(G)) \leq \sigma(T_{+--}(G)) \leq \sigma(T_{-+-}(G)) \leq \sigma(T_{--+}(G)) \leq \sigma(T_{-+-}(G))$  and  $\sigma(T_{2++}(G)) \leq \sigma(T_{1++}(G)) \leq \sigma(T_{2+-}(G)) \leq \sigma(T_{1+-}(G)) \leq \sigma(T_{1--}(G)) \leq \sigma(T_{2--}(G)) \leq \sigma(T_{1--}(G))$ .

## 5. Conclusion

The topological characterization of graphs and their transformations has been discussed in many research papers, in particular to Zagreb indices. Unfortunately, we have noticed the study on the second Zagreb index in total transformation graphs with some technical failures such as missing out edge degree-based indices and giving incorrect expressions. In this paper, we made a detailed study and derived the exact analytic expressions by incorporating reformulated Zagreb indices. As a byproduct, we have derived the sigma index of transformation graphs effectively using the forgotten index, and in addition, we have considered all possible semitransformations. The locus of this work will be definitely useful in computing other pending topological indices which are not computed for total transformation of graphs.

## Data Availability

The data used to support the findings of this study are included within paper.

## Conflicts of Interest

The authors declare that they have no conflicts of interest.

## Authors' Contributions

M.A., S.P., and M.A.J. conceptualized the study; M.A. and S.P. investigated the study; S.P. and M.A.J. prepared the original draft; M.A. and S.P. reviewed and edited the manuscript; Z.Y., M.A., and J.-B.L. supervised the study; and Z.Y. was responsible for funding acquisition.

## Acknowledgments

This work was supported by the Chongqing Nature Science Foundation (Grant No. CSTC2020jcyj-msxmX0546).

## References

- [1] S. C. Basak, D. Mills, and M. M. Mumtaz, "A quantitative structure-activity relationship (QSAR) study of dermal absorption using theoretical molecular descriptors," *SAR and QSAR in Environmental Research*, vol. 18, no. 1-2, pp. 45–55, 2007.
- [2] B. D. Gute, G. D. Grunwald, and S. C. Basak, "Prediction of the deral penetration of polycyclic aromatic hydrocarbons (PAHs): a hierarchical qsar approach," *SAR and QSAR in Environmental Research*, vol. 10, no. 1, pp. 1–15, 1999.
- [3] V. N. Viswanadhan, G. A. Mueller, S. C. Basak, and J. N. Weinstein, "Comparison of a neural net-based QSAR algorithm (PCANN) with hologram- and multiple linear regression-based QSAR approaches: application to 1, 4-dihydropyridine-based calcium channel antagonists," *Journal of Chemical Information and Computer Sciences*, vol. 41, no. 3, pp. 505–511, 2001.
- [4] J. Devillers and A. T. Balaban, *Topological Indices and Related Descriptors in QSAR and QSPR*, Gordon and Breach, Amsterdam, The Netherland, 1999.
- [5] M. Thakur, A. Thakur, and K. Balasubramanian, "QSAR and SAR studies on the reduction of some aromatic nitro compounds by xanthine oxidase," *Journal of Chemical Information and Modeling*, vol. 46, no. 1, pp. 103–110, 2006.
- [6] B. Furtula, I. Gutman, and M. Dehmer, "On structure-sensitivity of degree-based topological indices," *Applied Mathematics and Computation*, vol. 219, no. 17, pp. 8973–8978, 2013.
- [7] I. Gutman and N. Trinajstić, "Graph theory and molecular orbitals. Total  $\phi$ -electron energy of alternant hydrocarbons," *Chemical Physics Letters*, vol. 17, no. 4, pp. 535–538, 1972.
- [8] B. Zhou and N. Trinajstić, "On general sum-connectivity index," *Journal of Mathematical Chemistry*, vol. 47, no. 1, pp. 210–218, 2010.
- [9] A. R. Ashrafi, T. Doslic, and A. Hamzeh, "Extremal graphs with respect to the Zagreb coindices," *MATCH Communications in Mathematical and in Computer Chemistry*, vol. 65, no. 1, pp. 85–92, 2011.

- [10] S. Hossein-Zadeh, A. Hamzeh, and A. R. Ashrafi, "External properties of Zagreb coindices and degree distance of graphs," *Miskolc Mathematical Notes*, vol. 11, no. 2, pp. 129–138, 2010.
- [11] A. Miličević, S. Nikolić, and N. Trinajstić, "On reformulated Zagreb indices," *Molecular Diversity*, vol. 8, pp. 393–399, 2004.
- [12] B. Furtula and I. Gutman, "A forgotten topological index," *Journal of Mathematical Chemistry*, vol. 53, no. 4, pp. 1184–1190, 2015.
- [13] W. Gao, M. K. Siddiqui, M. Imran, M. K. Jamil, and M. R. Farahani, "Forgotten topological index of chemical structure in drugs," *Saudi Pharmaceutical Journal*, vol. 24, no. 3, pp. 258–264, 2016.
- [14] T. Réti, R. Sharafzadi, A. Drégelyi-Kiss, and H. Haghbin, "Graph irregularity indices used as molecular descriptors in QSPR Studies, MATCH Commun," *Mathematical and in Computer Chemistry*, vol. 79, pp. 509–524, 2018.
- [15] M. O. Albertson, "The irregularity of a graph," *Ars Combinatorica*, vol. 46, pp. 219–225, 1997.
- [16] F. K. Bell, "A note on the irregularity of graphs," *Linear Algebra and Its Applications*, vol. 161, pp. 45–54, 1992.
- [17] H. Abdo, D. Dimitrov, and I. Gutman, "Graph irregularity and its measures," *Applied Mathematics and Computation*, vol. 357, pp. 317–324, 2019.
- [18] I. Gutman, M. Togan, A. Yurtas, A. S. Cevik, and I. N. Cangul, "Inverse problem for sigma index," *MATCH Communications in Mathematical and in Computer Chemistry*, vol. 79, no. 2, pp. 491–508, 2018.
- [19] T. Reti, "On some properties of graph irregularity indices with a particular regard to the  $\sigma$ -index," *Applied Mathematics and Computation*, vol. 344, pp. 107–115, 2019.
- [20] K. Pattabiraman and M. Vijayaragavan, "Edge  $a$ -Zagreb indices and its coindices of transformation graphs," *Electronic Notes in Discrete Mathematics*, vol. 63, pp. 251–269, 2017.
- [21] B. Basavanagoud, I. Gutman, and V. R. Desai, "Zagreb indices of generalized transformation graphs and their complements," *Kragujevac Journal of Science*, vol. 37, pp. 99–112, 2015.
- [22] I. Gutman and Z. Tomovic, "On the application of line graphs in quantitative structure-property studies," *Journal of the Serbian Chemical Society*, vol. 65, no. 8, pp. 577–580, 2000.
- [23] I. Gutman and Z. Tomovic, "More on the line graph model for predicting physico-chemical properties of alkanes," *ACH - Models in Chemistry*, vol. 137, pp. 439–445, 2000.
- [24] I. Gutman, Z. Tomovic, B. K. Mishra, and M. Kuanar, "On the use of iterated line graphs in quantitative structure-property studies," *Indian Journal of Chemistry*, vol. 40A, pp. 4–11, 2001.
- [25] S. M. Hosamani and I. Gutman, "Zagreb indices of transformation graphs and total transformation graphs," *Applied Mathematics and Computation*, vol. 247, pp. 1156–1160, 2014.
- [26] Z. Tomovic and I. Gutman, "Modeling boiling points of cycloalkanes by means of iterated line graph sequences," *Journal of Chemical Information and Computer Sciences*, vol. 41, pp. 1041–1045, 2001.
- [27] P. V. Patil, G. G. Yattinahalli, and G. G. Yattinahalli, "Second Zagreb indices of transformation graphs and total transformation graphs," *Open Journal of Discrete Applied Mathematics*, vol. 3, no. 1, pp. 1–7, 2020.
- [28] K. Pattabiraman, "F-indices and its coindices of some classes of graphs," *Creative Mathematics and Informatics*, vol. 26, no. 2, pp. 201–210, 2017.
- [29] H. S. Ramane, S. Y. Talwar, and I. Gutman, "Zagreb indices and coindices of total graph, semi-total point graph and semi-total line graph of subdivision graphs," *Mathematics Interdisciplinary Research*, vol. 5, pp. 1–12, 2020.
- [30] B. Zhou and N. Trinajstić, "Some properties of the reformulated Zagreb indices," *Journal of Mathematical Chemistry*, vol. 48, no. 3, pp. 714–719, 2010.
- [31] H. Abdo and D. Dimitrov, "The total irregularity of graphs under graph operations," *Miskolc Mathematical Notes*, vol. 15, no. 1, pp. 3–17, 2014.
- [32] B. Wu and J. Meng, "Basic properties of total transformation graphs," *Journal of Mathematical Study*, vol. 34, pp. 109–116, 2001.
- [33] E. Sampathkumar and S. B. Chikkodimath, "The semi-total graphs of a graph-I," *Journal of the Karnatak University. Science*, vol. 18, pp. 274–280, 1973.
- [34] M. Behzad, "A criterion for the planarity of the total graph of a graph," *Mathematical Proceedings of the Cambridge Philosophical Society*, vol. 63, no. 3, pp. 679–681, 1967.
- [35] I. Gutman, B. Furtula, Z. Kovijanic Vukicevic, and G. Popivoda, "Zagreb indices and coindices," *MATCH Communications in Mathematical and in Computer Chemistry*, vol. 74, pp. 5–16, 2015.
- [36] T. Došlić, "Vertex-weighted Wiener polynomials for composite graphs," *Ars Mathematica Contemporanea*, vol. 1, pp. 66–80, 2008.
- [37] A. R. Ashrafi, T. Došlić, and A. Hamzeh, "The Zagreb coindices of graph operations," *Discrete Applied Mathematics*, vol. 158, no. 15, pp. 1571–1578, 2010.
- [38] H. Hua, A. Ashrafi, and L. Zhang, "More on Zagreb coindices of graphs," *Filomat*, vol. 26, pp. 1210–1220, 2012.
- [39] H. Hua and S. Zhang, "Relations between Zagreb coindices and some distance-based topological indices," *MATCH Communications in Mathematical and in Computer Chemistry*, vol. 68, pp. 199–208, 2012.
- [40] K. Balasubramanian, "Mathematical and computational techniques for drug discovery: promises and developments," *Current Topics in Medicinal Chemistry*, vol. 18, no. 32, pp. 2774–2799, 2018.
- [41] M. Arockiaraj, S. Klavžar, S. R. J. Kavitha, S. Mushtaq, and K. Balasubramanian, "Relativistic structural characterization of molybdenum and tungsten disulfide materials," *International Journal of Quantum Chemistry*, vol. 2020, Article ID e26492, , 2020.

## Research Article

# Finite-Time Stability Analysis of Switched Genetic Regulatory Networks with Time-Varying Delays via Wirtinger's Integral Inequality

Shanmugam Saravanan,<sup>1</sup> M. Syed Ali,<sup>2</sup> Grienggrai Rajchakit <sup>3,1</sup>  
Bussakorn Hammachukiattikul <sup>4,2</sup> Bandana Priya,<sup>5</sup> and Ganesh Kumar Thakur<sup>6</sup>

<sup>1</sup>School of Mechanical Engineering, Pusan National University, Busan 46241, Republic of Korea

<sup>2</sup>Department of Mathematics, Thiruvalluvar University, Vellore 632 115, Tamilnadu, India

<sup>3</sup>Department of Mathematics, Faculty of Science, Maejo University, Chiang Mai 50290, Sansai, Thailand

<sup>4</sup>Basic Sciences and Mathematics, Faculty of Engineering, Thai-Nichi Institute of Technology, Bangkok 10250, Thailand

<sup>5</sup>Department of Applied Sciences, Krishna Engineering College, Ghaziabad 201007, Uttar Pradesh, India

<sup>6</sup>Department of Applied Science, GL Bajaj Institute of Technology and Management, Greater Noida, Uttar Pradesh, India

Correspondence should be addressed to Grienggrai Rajchakit; griengkrai@yahoo.com and Bussakorn Hammachukiattikul; bussakorn@tni.ac.th

Received 23 June 2020; Revised 1 November 2020; Accepted 7 January 2021; Published 28 January 2021

Academic Editor: Jianquan Lu

Copyright © 2021 Shanmugam Saravanan et al. This is an open access article distributed under the Creative Commons Attribution License, which permits unrestricted use, distribution, and reproduction in any medium, provided the original work is properly cited.

The problem of finite-time stability of switched genetic regulatory networks (GRNs) with time-varying delays via Wirtinger's integral inequality is addressed in this study. A novel Lyapunov–Krasovskii functional is proposed to capture the dynamical characteristic of GRNs. Using Wirtinger's integral inequality, reciprocally convex combination technique and the average dwell time method conditions in the form of linear matrix inequalities (LMIs) are established for finite-time stability of switched GRNs. The applicability of the developed finite-time stability conditions is validated by numerical results.

## 1. Introduction

In recent years, GRNs have received much research attention, and many interesting results have been reported [1–8]. Generally, there are two types of gene network models, the Boolean model [9] and differential equation model [10]. In the Boolean model, the state converges to a terminal state via a series of state transitions that is determined by the Boolean rules. In this model, the activity of each gene is expressed in one of two states, ON or OFF, which is determined by a Boolean function by its own and by other related states. Whereas in the differential equation model, the variables describe the concentrations of gene products, such as mRNA and proteins as continuous values of the gene regulation system, and also, this model talks about the concentrations of gene products such as mRNA and proteins as variables in

GRNs [11–14]. There are many research results on the stability analysis for GRNs with time delay (e.g., [15–18]).

Time delays are ubiquitous in many fields because of finite propagation speeds of signals, finite processing times, finite reaction times, and finite switching speed of amplifiers. Since the biological system especially GRNs is a slow process of transcription, translation, and translocation [19–23], the time delay cannot be avoided. From the long term investigations, time delay will bring instability of the system, sustained oscillations such as bifurcation [24–26]. So, it is of great importance to deal delayed GRNs. For instance, in [27], authors presented a different equation model for GRNs with constant time delays and proposed stability analysis for GRNs with time delays. In [28], authors developed delay dependent criteria for stability of GRNs with delay and free-weighting matrices.

On the other hand, Markovian switching and switched systems have been studied extensively over the past decades, for its capacity in modeling practical systems and its potential applications. Including a variety of subsystems as constituent parts, switched systems are governed by a switching rule to coordinate the switching. Recently, the stability problem of Markovian jump GRNs and switched GRNs has been investigated in [29–34]. As we all know, most of gene networks contain some kinds of switching mechanisms. For instance, by increasing stimulation or by changing some regulatory mechanisms, a bistable system can switch from one steady state to the other. In [33, 35–39], authors investigated the stability for switched systems with time delays by utilizing an average dwell time approach.

Recently, many kinds of finite-time issues have attracted particular research interests, and there have been some results on finite-time stabilization and synchronization [40–47]. However, to the best of the authors knowledge, there have been very few results on the finite-time stability problem for delayed GRNs with time delays [48, 49], and the purpose of this study is therefore to shorten such a gap.

Motivated by the above discussion, in this study, we are concerned with the finite-time stability of switched GRNs, where the parameter values switch from one mode to another. By utilizing the average dwell time approach and by using a novel Lyapunov–Krasovskii functional, it is shown that the finite-time stability problem is solvable if a set of linear matrix inequalities (LMIs) is feasible. Finally, three examples are provided in the end of the study to show the effectiveness of the proposed criteria.

The rest of this study is organized as follows: in Section 2, preliminaries and problem formulation are given. In Section 3, some conditions are established to ensure the finite-time stability of the considered system. In Section 4, three examples are illustrated to show the effectiveness of the obtained theoretical results. And finally, conclusions are given in Section 5.

Notations: throughout this study,  $\mathbb{R}$ ,  $\mathbb{R}^n$ , and  $\mathbb{R}^{n \times m}$  denote, respectively, the set of all real numbers, real  $n$ -dimensional space, and real  $n \times m$ -dimensional space.  $\|\cdot\|$  denote the Euclidean norms in  $\mathbb{R}^n$ . For a vector or matrix  $P$ ,  $P^T$  denotes its transpose. For a square matrix  $P$ ,  $\lambda_{\max}(P)$  and  $\lambda_{\min}(P)$  denote the maximum eigenvalue and minimum eigenvalue of matrix  $P$ , respectively, and  $\text{sym}(P)$  is used to represent  $P + P^T$ . For simplicity, in symmetric block matrices, we often use  $*$  to represent the term that is induced by symmetry.

## 2. Problem Description and Preliminaries

Consider the following nonlinear GRNs with time-varying delays described by

$$\begin{cases} \dot{e}_1(t) = -Ae_1(t) + Bf(e_2(t - \tau(t))) + I, \\ \dot{e}_2(t) = -Ce_2(t) + D(e_1(t - \sigma(t))), \end{cases} \quad (1)$$

where  $e_1(t) = [e_{11}(t), e_{12}(t), \dots, e_{1n}(t)]^T \in \mathbb{R}^n$ ,  $e_2(t) = [e_{21}(t), e_{22}(t), \dots, e_{2n}(t)]^T \in \mathbb{R}^n$ ;  $e_{2i}(t) \in \mathbb{R}$  are the concentrations of mRNA and protein, respectively;  $f(\cdot) = [f_1(\cdot), \dots,$

$f_n(\cdot)]^T$  is the regulatory functions of mRNAs,  $A = \text{diag}(a_1, a_2, \dots, a_n)$  and  $C = \text{diag}(c_1, c_2, \dots, c_n)$  are the constant matrices, and they are the rates of degradation;  $D = \text{diag}(d_1, d_2, \dots, d_n)$  represents the translation rate;  $B = (b_{ij})$  is the regulative matrix, and  $\tau(t)$  and  $\sigma(t)$  are the time-varying delays.

For obtaining our conclusions, we make the following assumptions.

*Assumption 1.*  $f_s: \mathbb{R} \rightarrow \mathbb{R}$ ,  $s = 1, 2, \dots, n$  are monotonically increasing functions with saturation and satisfy

$$0 \leq \frac{f_s(a) - f_s(b)}{a - b} \leq u_s, \quad \forall a, b \in \mathbb{R}, s = 1, 2, \dots, n, \quad (2)$$

where  $u_s$ ,  $s = 1, 2, \dots, n$  are the nonnegative constants.

*Assumption 2.*  $\tau(t)$  and  $\sigma(t)$  are the time-varying delays satisfying

$$\begin{aligned} 0 &\leq \tau_1 \leq \tau(t) \leq \tau_2, \\ \dot{\tau}(t) &\leq \tau_d < \infty, \\ 0 &\leq \sigma_1 \leq \sigma(t) \leq \sigma_2, \\ \dot{\sigma}(t) &\leq \sigma_d < \infty, \\ \tau_{12} &= \tau_2 - \tau_1, \\ \sigma_{12} &= \sigma_2 - \sigma_1, \end{aligned} \quad (3)$$

where  $\tau_1, \tau_2, \sigma_1, \sigma_2$  are the constants. The initial condition of system (1) is assumed to be

$$-\rho \leq t \leq 0, \rho = \max\{\tau_2, \sigma_2\}. \quad (4)$$

Use the following transformation:

$$\begin{aligned} x(t) &= e_1(t) - e_1(t)^*, \\ y(t) &= e_2(t) - e_2(t)^*, \end{aligned} \quad (5)$$

where  $e_1^* = [e_{11}^*, e_{12}^*, \dots, e_{1n}^*]^T$  and  $e_2^* = [e_{21}^*, e_{22}^*, \dots, e_{2n}^*]^T$  constitute an equilibrium point of system (1) and then shift the intended equilibrium point to the origin. In this way, the system equation turns to be

$$\begin{cases} \dot{x}(t) = -Ax(t) + Bg(y(t - \tau(t))), \\ \dot{y}(t) = -Cy(t) + D(x(t - \sigma(t))), \end{cases} \quad (6)$$

where  $g(\cdot) = [g_1(\cdot), \dots, g_n(\cdot)]^T$ , and  $g_s(y(t)) = f_s(y(t) + e_2^*) - f_s(e_2^*)$ .

According to Assumption 1 and the definition of  $g_s(\cdot)$ , we know that  $g_s(\cdot)$  is bounded, that is,  $\exists F > 0$ , such that  $|g_s(\cdot)| \leq F$ ,  $s = 1, 2, \dots, n$  and satisfies the following sector condition:

$$0 \leq \frac{g_s(a)}{a} \leq u_s, \quad \forall a \in \mathbb{R} \setminus \{0\}, s = 1, 2, \dots, n. \quad (7)$$

Let  $U = \text{diag}\{u_1, u_2, \dots, u_n\}$ .

Sometimes, GRNs were described by the continuous time switched system, as in [33]; so system (6) can be described as the switching system with switching signal:

$$\begin{cases} \dot{x}(t) = -A_{p(t)}x(t) + B_{p(t)}g(y(t - \tau(t))), \\ \dot{y}(t) = -C_{p(t)}y(t) + D_{p(t)}(x(t - \sigma(t))), \end{cases} \quad (8)$$

where  $p(t): [0, \infty) \rightarrow \mathbb{N} = \{1, 2, \dots, N\}$  is the switching signal, which is a piece constant function depending on time  $t$ . For each  $i \in \mathbb{N}$ , the matrices are constant matrices of appropriate dimensions.

For the switching signal  $p(t)$ , we have the following switching sequence:  $\{(i_0, t_0), \dots, (i_k, t_k), \dots, | i_k \in \mathbb{N}, k = 0, 1, \dots\}$ ; in other words, when  $t \in [t_k, t_{k+1})$ ,  $i_k^{\text{th}}$  subsystem is activated. To assume  $x(t) = \phi(t)$ ,  $y(t) = \psi(t)$ .

For proving the theorem, we recall the following definition and lemmas.

**Definition 1** (See [50]). The system (8) is said to be finite-time stable with respect to positive real numbers  $(c_1, c_2, T)$ , if

$$\|\Phi(t)\|^2 + \|\Psi(t)\|^2 \leq c_1 \Rightarrow \|x(t)\|^2 + \|y(t)\|^2 \leq c_2, \quad t \in (0, T), \quad (9)$$

where

$$\begin{aligned} \left[ \int_{t-\eta_2}^{t-\eta_1} w(s) ds \right]^T M \left[ \int_{t-\eta_2}^{t-\eta_1} w(s) ds \right] &\leq (\eta_2 - \eta_1) \int_{t-\eta_2}^{t-\eta_1} w^T(s) M w(s) ds. \\ \left[ \int_{-\eta_2}^{-\eta_1} \int_{t+\theta}^t w(s) ds \right]^T M \left[ \int_{-\eta_2}^{-\eta_1} w(s) ds \right] &\leq \frac{(\eta_2^2 - \eta_1^2)}{2} \int_{-\eta_2}^{-\eta_1} \int_{t+\theta}^t w^T(s) M w(s) ds. \end{aligned} \quad (12)$$

**Lemma 2** (See [53]). Let  $f_1, f_2, \dots, f_N: \mathbb{R}^m \rightarrow \mathbb{R}$  have positive values in an open subset  $D$  of  $\mathbb{R}^m$ . Then, the reciprocally convex combination of  $f_i$  over  $D$  satisfies

$$\min_{\{\beta_i | \beta_i > 0, \sum_{i=1}^N \beta_i = 1\}} \sum_i \beta_i f_i(t) + \max_{g_{i,j}(t)} \sum_{i \neq j} g_{i,j}(t), \quad (13)$$

subjected to

$$\left\{ g_{ij}: \mathbb{R}^m \rightarrow \mathbb{R}, g_{j,i}(t) = g_{ij}(t), \begin{bmatrix} f_i(t) & g_{i,j}(t) \\ g_{i,j}(t) & f_j(t) \end{bmatrix} \geq 0 \right\}. \quad (14)$$

**Lemma 3** (See [54]). For a positive definite matrix  $M > 0$ , the following inequality holds for all continuously differentiable function  $x(t)$  in  $[a, b] \in \mathbb{R}^{n \times n}$ :

$$\begin{aligned} -(b-a) \int_a^b \dot{x}^T(s) M \dot{x}(s) ds &\leq -\Phi_1^T M \Phi_1 - 3 - \Phi_2^T M \Phi_2, \\ &= - \begin{bmatrix} \Phi_1 \\ \Phi_2 \end{bmatrix}^T \begin{bmatrix} M & 0 \\ 0 & 3M \end{bmatrix} \begin{bmatrix} \Phi_1 \\ \Phi_2 \end{bmatrix}, \end{aligned} \quad (15)$$

where  $\Phi_1 = x(b) - x(a)$ , and  $\Phi_2 = x(b) + x(a) - 2/(b-a) \int_a^b x(s) ds$ .

$$\begin{aligned} \|\Phi(t)\| &= \sup_{-p \leq t \leq 0} \{\|\phi(t)\|, \|\dot{\phi}(t)\|\}, \\ \|\Psi(t)\| &= \sup_{-p \leq t \leq 0} \{\|\psi(t)\|, \|\dot{\psi}(t)\|\}. \end{aligned} \quad (10)$$

**Definition 2** (See [51]). For any  $T_2 > T_1 \geq 0$ , let  $N_p(T_1, T_2)$  denote the switching number of  $p(t)$  on an interval  $(T_1, T_2)$ . If

$$N_p(T_1, T_2) \leq N_0 + \frac{T_2 - T_1}{\tau_a} \quad (11)$$

holds for given  $N_0 \geq 0$ ,  $\tau_a > 0$ , then the constant  $\tau_a$  is called the average dwell time and  $N_0$  is the chatter bound. Without loss of generality, we choose  $N_0 = 0$  throughout this study.

**Lemma 1** (See [52]). For any constant matrix  $M \in \mathbb{R}^{n \times n}$ ,  $M = M^T > 0$ , scalars  $\eta_2 > \eta_1 > 0$ , and vector function  $w: [\eta_1, \eta_2] \rightarrow \mathbb{R}^n$  such that the integrations concerned are well defined, and the following inequality holds

### 3. Main Results

In this section, we present a finite-time stability theorem for switching genetic regulatory networks with interval time-varying delays (8).

**Theorem 1.** The switched genetic networks (8) is finite-time stable with respect to positive real numbers  $(c_1, c_2, T_f)$  and constants  $\sigma_1, \sigma_2, \tau_1$ , and  $\tau_2$ ; if there exist symmetric positive definite matrices  $P_{1i}, P_{2i}, Q_{ni}$  ( $n = 1, 2, 3$ ),  $R_{ni}$  ( $n = 1, 2, \dots, 12$ ),  $S_{ni}$  ( $n = 1, 2, \dots, 4$ ) for all  $i \in \mathbb{N}$ , the diagonal matrix  $L_m = \text{diag}(l_{1m}, l_{2m}, \dots, l_{mm}) \geq 0$ ,  $m = 1, 2$ , and positive scalars  $\mu \geq 1$  and  $\alpha_i = \alpha > 0$  such that the following LMIs hold

$$\begin{aligned} \begin{bmatrix} R_{3i} & M_{1i} \\ * & R_{4i} \end{bmatrix} &> 0, \\ \begin{bmatrix} R_{6i} & \bar{R}_{6i} \\ * & R_{6i} \end{bmatrix} &\geq 0, \\ \begin{bmatrix} R_{8i} & \bar{R}_{8i} \\ * & R_{8i} \end{bmatrix} &\geq 0, \\ \begin{bmatrix} R_{10i} & \bar{R}_{10i} \\ * & R_{10i} \end{bmatrix} &> 0, \\ \begin{bmatrix} R_{12i} & M_{12i} \\ * & R_{12i} \end{bmatrix} &> 0, \end{aligned} \quad (16)$$

$$\Theta_{p(t)} = [\Theta_{ij}]_{22 \times 22} < 0, \quad (17)$$



$$\begin{aligned}
P_{li} &\leq \mu P_{lj}, \quad l = 1, 2, \\
Q_{li} &\leq \mu Q_{lj}, \quad l = 1, 2, 3, \\
R_{li} &\leq \mu R_{lj}, \quad l = 1, 2, \dots, 12, \\
M_{1i} &\leq \mu M_{1j}, S_{li} \leq \mu S_{lj}, \quad l = 1, 2, 3,
\end{aligned} \tag{18}$$

and the average dwell time of the switching signal  $p(t)$  satisfies

$$\tau_{ai} > \tau_{ai}^* = \frac{T \ln \mu_i}{\ln(c_2(\lambda_1 + \lambda_2)) - \ln(e^{\alpha_i T} dc_1)}, \tag{20}$$

where

$$e^{\{\sum_{i=1}^N \alpha_i T\}} dc_1 \leq c_2(\lambda_1 + \lambda_2), \tag{19}$$

---


$$\begin{aligned}
\Theta_{11} &= -P_{1i}A - A^T P_{1i}^T + Q_{1i} + Q_{3i} + \sigma_1^2 R_{5i} + \sigma_{12}^2 R_{6i} - 3e^{-\alpha\sigma_1} R_{7i} - e^{-\alpha\sigma_1} R_{7i} + \alpha P_{1i}, \\
\Theta_{13} &= e^{-\alpha\sigma_1} R_{7i} - 3e^{-\alpha\sigma_1} R_{7i}, \\
\Theta_{110} &= P_{1i}B, \Theta_{113} = \frac{6}{\sigma_1} e^{-\alpha\sigma_1} R_{7i}, \\
\Theta_{22} &= R_{1i} + R_{3i} - P_{2i}C - C^T P_{2i}^T + \tau_1^2 R_{9i} + \tau_{12}^2 R_{10i} - e^{-\alpha\tau_1} R_{11i} - 3e^{-\alpha\tau_1} R_{11i} + \alpha P_{2i}, \\
\Theta_{24} &= P_{2i}D, \\
\Theta_{26} &= e^{-\alpha\tau_1} R_{11i} - 3e^{-\alpha\tau_1} R_{11i}, \\
\Theta_{29} &= M_{1i} + U^T L_1^T, \\
\Theta_{218} &= \frac{6}{\tau_1} e^{-\alpha\tau_1} R_{11i}, \\
\Theta_{33} &= -e^{-\alpha\sigma_1} Q_{1i} + e^{-\alpha\sigma_1} Q_{2i} - e^{-\alpha\sigma_1} R_{7i} - 3e^{-\alpha\sigma_1} R_{7i} - e^{-\alpha\sigma_2} R_{8i}, \\
\Theta_{34} &= -e^{-\alpha\sigma_2} \bar{R}_{8i}^T + e^{-\alpha\sigma_2} R_{8i}, \\
\Theta_{35} &= e^{-\alpha\sigma_2} \bar{R}_{8i}^T, \Theta_{313} = \frac{6}{\sigma_1} e^{-\alpha\sigma_1} R_{7i}, \\
\Theta_{44} &= -(1 - \sigma_d) e^{-\alpha\sigma(t)} Q_{3i} + 2e^{-\alpha\sigma_2} \bar{R}_{8i} - 2e^{-\alpha\sigma_2} R_{8i}, \\
\Theta_{45} &= e^{-\alpha\sigma_2} \bar{R}_{8i}^T + e^{-\alpha\sigma_2} R_{8i}, \\
\Theta_{55} &= e^{-\alpha\sigma_2} Q_{2i}^T - e^{-\alpha\sigma_2} R_{8i}, \\
\Theta_{66} &= -e^{-\alpha\tau_1} R_{1i} + e^{-\alpha\tau_1} R_{2i} - e^{-\alpha\tau_1} R_{11i} - 3e^{-\alpha\tau_1} R_{11i} - e^{-\alpha\tau_2} R_{12i}, \\
\Theta_{67} &= -e^{-\alpha\tau_2} \bar{R}_{12i}^T + e^{-\alpha\tau_2} R_{12i}, \\
\Theta_{68} &= -e^{-\alpha\tau_2} \bar{R}_{12i}^T, \\
\Theta_{618} &= \frac{6}{\tau_1} e^{-\alpha\tau_1} R_{11i}, \\
\Theta_{77} &= -(1 - \tau_d) e^{-\alpha\tau(t)} R_{3i} + 2e^{-\alpha\tau_2} \bar{R}_{12i} - 2e^{-\alpha\tau_2} R_{12i}, \\
\Theta_{78} &= e^{-\alpha\tau_2} \bar{R}_{12i}^T + e^{-\alpha\tau_2} R_{12i}, \\
\Theta_{710} &= -(1 - \tau_d) e^{-\alpha\tau(t)} M_{1i} + UL_2,
\end{aligned}$$

$$\begin{aligned}
\Theta_{88} &= -e^{-\alpha\tau_2} R_{2i}^T - e^{-\alpha\tau_2} R_{12i}, \\
\Theta_{99} &= R_{4i} - 2L_1, \\
\Theta_{1010} &= -(1 - \tau_d) e^{-\alpha\tau_2} R_{4i} - 2L_2, \\
\Theta_{1111} &= \sigma_1^2 R_{7i} + \sigma_{12}^2 R_{8i} + e^{\alpha t} \frac{e^{\alpha\sigma_2} - \alpha\sigma_2 - 1}{\alpha^2} S_{1i} + e^{\alpha t} \frac{e^{\alpha\sigma_2} - e^{\alpha\sigma_1} - \alpha(\sigma_2 - \sigma_1)}{\alpha^2} S_{2i}, \\
\Theta_{1212} &= \tau_1^2 R_{11i} + \tau_{12}^2 R_{12i} + e^{\alpha t} \frac{e^{\alpha\tau_2} - \alpha\tau_2 - 1}{\alpha^2} S_{3i} + e^{\alpha t} \frac{e^{\alpha\tau_2} - e^{\alpha\tau_1} - \alpha(\tau_2 - \tau_1)}{\alpha^2} S_{4i}, \\
\Theta_{1313} &= -e^{\alpha\sigma_1} R_{5i} - \frac{12}{\sigma_1^2} e^{-\alpha\sigma_1} R_{7i}, \Theta_{1414} = -e^{\alpha\sigma_2} R_{6i}, \\
\Theta_{1415} &= -e^{\alpha\sigma_2} \bar{R}_{6i}, \Theta_{1515} = -e^{\alpha\sigma_2} R_{6i}, \\
\Theta_{1616} &= -e^{\alpha t} S_{1i}, \\
\Theta_{1717} &= -e^{\alpha t} S_{2i}, \\
\Theta_{1818} &= -e^{\alpha\tau_1} R_{9i} - \frac{12}{\tau_1^2} e^{-\alpha\tau_1} R_{11i}, \\
\Theta_{1919} &= -e^{\alpha\tau_2} R_{10i}, \Theta_{1920} = -e^{\alpha\tau_2} \bar{R}_{10i}, \\
\Theta_{2020} &= -e^{\alpha\tau_2} R_{10i}, \Theta_{2121} = -e^{\alpha t} S_{3i}, \\
\Theta_{2222} &= -e^{\alpha t} S_{4i}, \\
d &= \lambda_3 + \lambda_4 + \lambda_5 \sigma_1 e^{-\alpha\sigma_1} + \lambda_6 (\sigma_2 - \sigma_1) e^{-\alpha\sigma_2} + \lambda_7 \sigma_2 e^{-\alpha\sigma_2} + \lambda_8 \tau_1 e^{-\alpha\tau_1} \\
&\quad + \lambda_9 (\tau_2 - \tau_1) e^{-\alpha\tau_1} + \lambda_{10} \tau_2 e^{-\alpha\tau_2} + 2\lambda_{11} \tau_2 e^{-\alpha\tau_2} + \lambda_{12} \tau_2 e^{-\alpha\tau_2} + \lambda_{13} \frac{\sigma_1^3}{2} e^{-\alpha\sigma_1} \\
&\quad + \lambda_{14} \frac{(\sigma_2 - \sigma_1)^3}{2} e^{-\alpha\sigma_2} + \lambda_{15} \frac{\sigma_1^3}{2} e^{-\alpha\sigma_1} + \lambda_{16} \frac{(\tau_2 - \tau_1)^3}{2} e^{-\alpha\tau_2} + \lambda_{17} \frac{\tau_1^3}{2} e^{-\alpha\tau_1} \\
&\quad + \lambda_{18} \frac{(\tau_2 - \tau_1)^3}{2} e^{-\alpha\tau_2} + \lambda_{19} \frac{\tau_1^3}{2} e^{-\alpha\tau_1} + \lambda_{20} \frac{(\tau_2 - \tau_1)^3}{2} e^{-\alpha\tau_2} + \lambda_{21} \frac{\sigma_1^5}{4} e^{-\alpha\sigma_1} \\
&\quad + \lambda_{22} \frac{(\sigma_2^2 - \sigma_1^2)(\sigma_2 - \sigma_1)^3}{4} e^{-\alpha\sigma_2} + \lambda_{23} \frac{\tau_1^5}{4} e^{-\alpha\tau_1} + \lambda_{24} \frac{(\tau_2^2 - \tau_1^2)(\tau_2 - \tau_1)^3}{4} e^{-\alpha\tau_2}, \\
\lambda_1 &= \min_{i \in \mathbb{N}} \lambda_{\min}(P_{1i}), \lambda_2 = \min_{i \in \mathbb{N}} \lambda_{\min}(P_{2i}), \lambda_3 = \max_{i \in \mathbb{N}} \lambda_{\max}(P_{1i}), \\
\lambda_4 &= \max_{i \in \mathbb{N}} \lambda_{\max}(P_{2i}), \lambda_5 = \max_{i \in \mathbb{N}} \lambda_{\max}(Q_{1i}), \lambda_6 = \max_{i \in \mathbb{N}} \lambda_{\max}(Q_{2i}), \\
\lambda_7 &= \max_{i \in \mathbb{N}} \lambda_{\max}(Q_{3i}), \lambda_8 = \max_{i \in \mathbb{N}} \lambda_{\max}(R_{1i}), \lambda_{10} = \max_{i \in \mathbb{N}} \lambda_{\max}(R_{2i}), \\
\lambda_{11} &= \max_{i \in \mathbb{N}} \lambda_{\max}(R_{3i}), \lambda_{12} = \max_{i \in \mathbb{N}} \lambda_{\max}(R_{4i}), \lambda_{13} = \max_{i \in \mathbb{N}} \lambda_{\max}(R_{5i}), \\
\lambda_{14} &= \max_{i \in \mathbb{N}} \lambda_{\max}(R_{6i}), \lambda_{15} = \max_{i \in \mathbb{N}} \lambda_{\max}(R_{7i}), \lambda_{16} = \max_{i \in \mathbb{N}} \lambda_{\max}(R_{8i}), \\
\lambda_{17} &= \max_{i \in \mathbb{N}} \lambda_{\max}(R_{9i}), \lambda_{18} = \max_{i \in \mathbb{N}} \lambda_{\max}(R_{10i}), \lambda_{19} = \max_{i \in \mathbb{N}} \lambda_{\max}(R_{11i}), \\
\lambda_{20} &= \max_{i \in \mathbb{N}} \lambda_{\max}(R_{12i}), \lambda_{21} = \max_{i \in \mathbb{N}} \lambda_{\max}(S_{1i}), \lambda_{22} = \max_{i \in \mathbb{N}} \lambda_{\max}(S_{2i}), \\
\lambda_{23} &= \max_{i \in \mathbb{N}} \lambda_{\max}(S_{3i}), \lambda_{24} = \max_{i \in \mathbb{N}} \lambda_{\max}(S_{4i}).
\end{aligned} \tag{21}$$

*Proof.* Choose the Lyapunov functional candidate as where

$$V_{p(t)}(t) = V_{1p(t)} + V_{2p(t)} + V_{3p(t)} + V_{4p(t)} + V_{5p(t)} + V_{6p(t)}, \quad (22)$$

$$V_{1p(t)} = x^T(t)P_{1i}x(t) + y^T(t)P_{2i}y(t),$$

$$V_{2p(t)} = \int_{t-\sigma_1}^t e^{\alpha(s-t)} x^T(s)Q_{1i}x(s)ds + \int_{t-\sigma_2}^{t-\sigma_1} e^{\alpha(s-t)} x^T(s)Q_{2i}x(s)ds \\ + \int_{t-\sigma(t)}^t e^{\alpha(s-t)} x^T(s)Q_{3i}x(s)ds,$$

$$V_{3p(t)} = \int_{t-\tau_1}^t e^{\alpha(s-t)} y^T(s)R_{1i}y(s)ds + \int_{t-\tau_2}^{t-\tau_1} e^{\alpha(s-t)} y^T(s)R_{2i}y(s)ds \\ + \int_{t-\tau(t)}^t e^{\alpha(s-t)} \begin{bmatrix} y(s) \\ g(y(s)) \end{bmatrix}^T \begin{bmatrix} R_{3i} & M_{1i} \\ * & R_{4i} \end{bmatrix} \begin{bmatrix} y(s) \\ g(y(s)) \end{bmatrix} ds,$$

$$V_{4p(t)} = \int_{-\sigma_1}^0 \int_{t+\theta}^t \sigma_1 e^{\alpha(s-t)} x^T(s)R_{5i}x(s)dsd\theta + \int_{-\sigma_2}^{-\sigma_1} \int_{t+\theta}^t \sigma_{12} e^{\alpha(s-t)} x^T(s)R_{6i}x(s)dsd\theta \quad (23) \\ + \int_{-\sigma_1}^0 \int_{t+\theta}^t \sigma_1 e^{\alpha(s-t)} \dot{x}^T(s)R_{7i}\dot{x}(s)dsd\theta + \int_{-\sigma_2}^{-\sigma_1} \int_{t+\theta}^t \sigma_{12} e^{\alpha(s-t)} \dot{x}^T(s)R_{8i}\dot{x}(s)dsd\theta,$$

$$V_{5p(t)} = \int_{-\tau_1}^0 \int_{t+\theta}^t \tau_1 e^{\alpha(s-t)} y^T(s)R_{9i}y(s)dsd\theta + \int_{-\tau_2}^{-\tau_1} \int_{t+\theta}^t \tau_{12} e^{\alpha(s-t)} y^T(s)R_{10i}y(s)dsd\theta \\ + \int_{-\tau_1}^0 \int_{t+\theta}^t \tau_1 e^{\alpha(s-t)} \dot{y}^T(s)R_{11i}\dot{y}(s)dsd\theta + \int_{-\tau_2}^{-\tau_1} \int_{t+\theta}^t \tau_{12} e^{\alpha(s-t)} \dot{y}^T(s)R_{12i}\dot{y}(s)dsd\theta,$$

$$V_{6p(t)} = \int_{-\sigma_2}^0 \int_{\theta}^0 \int_{t+\gamma}^t \frac{\sigma_1^2}{2} e^{\alpha(s-\theta)} \dot{x}^T(s)S_{1i}\dot{x}(s)dsd\gamma d\theta + \int_{-\sigma_2}^{-\sigma_1} \int_{\theta}^0 \int_{t+\gamma}^t \frac{1}{2} (\sigma_2^2 - \sigma_1^2) e^{\alpha(s-\theta)} \dot{x}^T(s)S_{2i}\dot{x}(s)dsd\gamma d\theta \\ + \int_{-\tau_2}^0 \int_{\theta}^0 \int_{t+\gamma}^t \frac{\tau_1^2}{2} e^{\alpha(s-\theta)} \dot{y}^T(s)S_{3i}\dot{y}(s)dsd\gamma d\theta + \int_{-\tau_2}^{-\tau_1} \int_{\theta}^0 \int_{t+\gamma}^t \frac{1}{2} (\tau_2^2 - \tau_1^2) e^{\alpha(s-\theta)} \dot{y}^T(s)S_{4i}\dot{y}(s)dsd\gamma d\theta.$$

Taking the derivatives of  $V_{p(t)}$  along the trajectory of system (8), we have that

$$\dot{V}_{1p(t)} = 2x^T(t)P_{1i}\dot{x}(t) + 2y^T(t)P_{2i}\dot{y}(t), \quad (24)$$

$$\dot{V}_{2p(t)} = -\alpha V_{2p(t)} + x^T(t)Q_{1i}x(t) - e^{-\alpha\sigma_1} x^T(t-\sigma_1)Q_{1i}x(t-\sigma_1) \\ + e^{-\alpha\sigma_1} x^T(t-\sigma_1)Q_{2i}x(t-\sigma_1) - e^{-\alpha\sigma_2} x^T(t-\sigma_2)Q_{2i}x(t-\sigma_2) \\ + x^T(t)Q_{3i}x(t) - (1-\dot{\sigma}(t))e^{-\alpha\sigma(t)} x^T(t-\sigma(t))Q_{3i}x(t-\sigma(t)), \quad (25)$$

$$\begin{aligned}
\dot{V}_{3p(t)} &= -\alpha V_{3p(t)} + y^T(t)R_{1i}y(t) - e^{-\alpha\tau_1}y^T(t-\tau_1)R_{1i}y(t-\tau_1) + e^{-\alpha\tau_1}y^T(t-\tau_1)R_{2i}y(t-\tau_1) \\
&\quad - e^{-\alpha\tau_2}y^T(t-\tau_2)R_{2i}y(t-\tau_2) + \begin{bmatrix} y(t) \\ g(y(t)) \end{bmatrix}^T \begin{bmatrix} R_{3i} & M_{1i} \\ * & R_{4i} \end{bmatrix} \begin{bmatrix} y(t) \\ g(y(t)) \end{bmatrix} \\
&\quad - (1 - \dot{\tau}(t))e^{-\alpha\tau(t)} \begin{bmatrix} y(t-\tau(t)) \\ g(y(t-\tau(t))) \end{bmatrix}^T \begin{bmatrix} R_{3i} & M_{1i} \\ * & R_{4i} \end{bmatrix} \begin{bmatrix} y(t-\tau(t)) \\ g(y(t-\tau(t))) \end{bmatrix} \\
&\leq -\alpha V_{3p(t)} + y^T(t)R_{1i}y(t) - e^{-\alpha\tau_1}y^T(t-\tau_1)R_{1i}y(t-\tau_1) + e^{-\alpha\tau_1}y^T(t-\tau_1)R_{2i}y(t-\tau_1) \\
&\quad - e^{-\alpha\tau_2}y^T(t-\tau_2)R_{2i}y(t-\tau_2) + \begin{bmatrix} y(t) \\ g(y(t)) \end{bmatrix}^T \begin{bmatrix} R_{3i} & M_{1i} \\ * & R_{4i} \end{bmatrix} \begin{bmatrix} y(t) \\ g(y(t)) \end{bmatrix} \\
&\quad - (1 - \dot{\tau}(t))e^{-\alpha\tau_2} \begin{bmatrix} y(t-\tau(t)) \\ g(y(t-\tau(t))) \end{bmatrix}^T \begin{bmatrix} R_{3i} & M_{1i} \\ * & R_{4i} \end{bmatrix} \begin{bmatrix} y(t-\tau(t)) \\ g(y(t-\tau(t))) \end{bmatrix},
\end{aligned} \tag{26}$$

$$\begin{aligned}
\dot{V}_{4p(t)} &= -\alpha V_{4p(t)} + \sigma_1^2 x^T(t)R_{5i}x(t) - \int_{t-\sigma_1}^t \sigma_1 e^{\alpha(s-t)} x^T(s)R_{5i}x(s)ds \\
&\quad + \sigma_{12}^2 x^T(t)R_{6i}x(t) - \int_{t-\sigma_2}^{t-\sigma_1} \sigma_{12} e^{\alpha(s-t)} x^T(s)R_{6i}x(s)ds \\
&\quad + \sigma_1^2 \dot{x}^T(t)R_{7i}\dot{x}(t) - \int_{t-\sigma_1}^t \sigma_1 e^{\alpha(s-t)} \dot{x}^T(s)R_{7i}\dot{x}(s)ds \\
&\quad + \sigma_{12}^2 \dot{x}^T(t)R_{8i}\dot{x}(t) - \int_{t-\sigma_2}^{t-\sigma_1} \sigma_{12} e^{\alpha(s-t)} \dot{x}^T(s)R_{8i}\dot{x}(s)ds,
\end{aligned} \tag{27}$$

$$\begin{aligned}
\dot{V}_{5p(t)} &= -\alpha V_{5p(t)} + \tau_1^2 y^T(t)R_{9i}y(t) - \int_{t-\tau_1}^t \tau_1 e^{\alpha(s-t)} y^T(s)R_{9i}y(s)ds \\
&\quad + \tau_{12}^2 y^T(t)R_{10i}y(t) - \int_{t-\tau_2}^{t-\tau_1} \tau_{12} e^{\alpha(s-t)} y^T(s)R_{10i}y(s)ds \\
&\quad + \tau_1^2 \dot{y}^T(t)R_{11i}\dot{y}(t) - \int_{t-\tau_1}^t \tau_1 e^{\alpha(s-t)} \dot{y}^T(s)R_{11i}\dot{y}(s)ds \\
&\quad + \tau_{12}^2 \dot{y}^T(t)R_{12i}\dot{y}(t) - \int_{t-\tau_2}^{t-\tau_1} \tau_{12} e^{\alpha(s-t)} \dot{y}^T(s)R_{12i}\dot{y}(s)ds,
\end{aligned} \tag{28}$$

$$\begin{aligned}
\dot{V}_{6p(t)} &= -\alpha V_{6p(t)} + e^{\alpha t} \dot{x}^T(t) \frac{e^{\alpha\sigma_2} - \alpha\sigma_2 - 1}{\alpha^2} S_{1i} \dot{x}(t) - e^{\alpha t} \int_{-\sigma_2}^0 \int_{t+\theta}^t \dot{x}^T(s)S_{1i}\dot{x}(s)dsd\theta \\
&\quad + e^{\alpha t} \dot{x}^T(t) \frac{e^{\alpha\sigma_2} - e^{\alpha\sigma_1} - \alpha(\sigma_2 - \sigma_1)}{\alpha^2} S_{2i} \dot{x}(t) - e^{\alpha t} \int_{-\sigma_2}^{-\sigma_1} \int_{t+\theta}^t \dot{x}^T(s)S_{2i}\dot{x}(s)dsd\theta \\
&\quad + e^{\alpha t} \dot{x}^T(t) \frac{e^{\alpha\tau_2} - \alpha\tau_2 - 1}{\alpha^2} S_{3i} \dot{x}(t) - e^{\alpha t} \int_{-\tau_2}^0 \int_{t+\theta}^t \dot{x}^T(s)S_{3i}\dot{x}(s)dsd\theta \\
&\quad + e^{\alpha t} \dot{x}^T(t) \frac{e^{\alpha\tau_2} - e^{\alpha\tau_1} - \alpha(\tau_2 - \tau_1)}{\alpha^2} S_{4i} \dot{x}(t) - e^{\alpha t} \int_{-\tau_2}^{-\tau_1} \int_{t+\theta}^t \dot{x}^T(s)S_{4i}\dot{x}(s)dsd\theta.
\end{aligned} \tag{29}$$

From Lemmas 1 and 3, we have

$$\begin{aligned}
& -\sigma_1 \int_{t-\sigma_1}^t e^{\alpha(s-t)} x^T(s) R_{5i} x(s) ds \leq -e^{-\alpha\sigma_1} \left( \int_{t-\sigma_1}^t x(s) ds \right)^T R_{5i} \left( \int_{t-\sigma_1}^t x(s) ds \right), \\
& -\sigma_1 \int_{t-\sigma_1}^t e^{\alpha(s-t)} \dot{x}^T(s) R_{7i} \dot{x}(s) ds \leq -e^{-\alpha\sigma_1} \begin{bmatrix} \Phi_1(t) \\ \Phi_2(t) \end{bmatrix}^T \begin{bmatrix} R_{7i} & 0 \\ * & 3R_{7i} \end{bmatrix} \begin{bmatrix} \Phi_1(t) \\ \Phi_2(t) \end{bmatrix}, \\
& -\tau_1 \int_{t-\tau_1}^t e^{\alpha(s-t)} y^T(s) R_{9i} y(s) ds \leq -e^{-\alpha\tau_1} \left( \int_{t-\tau_1}^t y(s) ds \right)^T R_{9i} \left( \int_{t-\tau_1}^t y(s) ds \right), \\
& -\tau_1 \int_{t-\tau_1}^t e^{\alpha(s-t)} \dot{y}^T(s) R_{11i} \dot{y}(s) ds \leq e^{-\alpha\tau_1} \begin{bmatrix} \Phi_3(t) \\ \Phi_4(t) \end{bmatrix}^T \begin{bmatrix} R_{11i} & 0 \\ * & 3R_{11i} \end{bmatrix} \begin{bmatrix} \Phi_3(t) \\ \Phi_4(t) \end{bmatrix},
\end{aligned} \tag{30}$$

and from Lemma 2, we can obtain

$$\begin{aligned}
& -\sigma_{12} \int_{t-\sigma_2}^{t-\sigma_1} e^{\alpha(s-t)} x^T(s) R_{6i} x(s) ds = -\sigma_{12} e^{-\alpha\sigma_2} \int_{t-\sigma_2}^{t-\sigma(t)} x^T(s) R_{6i} x(s) ds \\
& -\sigma_{12} e^{-\alpha\sigma_2} \int_{t-\sigma(t)}^{t-\sigma_1} x^T(s) R_{6i} x(s) ds \leq e^{-\alpha\sigma_2} \begin{bmatrix} \psi_1 \\ \psi_2 \end{bmatrix}^T \begin{bmatrix} -R_{6i} & \bar{R}_{6i} \\ * & -R_{6i} \end{bmatrix} \begin{bmatrix} \psi_1 \\ \psi_2 \end{bmatrix}.
\end{aligned} \tag{31}$$

Similarly, we have

$$-\sigma_{12} \int_{t-\sigma_2}^{t-\sigma_1} e^{\alpha(s-t)} x^T(s) R_{8i} x(s) ds \leq e^{-\alpha\sigma_2} \begin{bmatrix} \psi_3 \\ \psi_4 \end{bmatrix}^T \begin{bmatrix} -R_{8i} & \bar{R}_{8i} \\ * & -R_{8i} \end{bmatrix} \begin{bmatrix} \psi_3 \\ \psi_4 \end{bmatrix}, \tag{32}$$

$$\begin{aligned}
& -\tau_{12} \int_{t-\tau_2}^{t-\tau_1} e^{\alpha(s-t)} x^T(s) R_{10i} x(s) ds = -\tau_{12} e^{-\alpha\tau_2} \int_{t-\tau_2}^{t-\tau(t)} x^T(s) R_{10i} x(s) ds \\
& -\tau_{12} e^{-\alpha\tau_2} \int_{t-\tau(t)}^{t-\tau_1} x^T(s) R_{10i} x(s) ds \leq e^{-\alpha\tau_2} \begin{bmatrix} \psi_5 \\ \psi_6 \end{bmatrix}^T \begin{bmatrix} -R_{10i} & \bar{R}_{10i} \\ * & -R_{10i} \end{bmatrix} \begin{bmatrix} \psi_5 \\ \psi_6 \end{bmatrix},
\end{aligned} \tag{33}$$

$$-\tau_{12} \int_{t-\tau_2}^{t-\tau_1} e^{\tau(s-t)} x^T(s) R_{12i} x(s) ds \leq e^{-\alpha\tau_2} \begin{bmatrix} \psi_7 \\ \psi_8 \end{bmatrix}^T \begin{bmatrix} -R_{12i} & \bar{R}_{12i} \\ * & -R_{12i} \end{bmatrix} \begin{bmatrix} \psi_7 \\ \psi_8 \end{bmatrix}, \tag{34}$$

where

$$\begin{aligned}
\psi_1 &= \int_{t-\sigma_2}^{t-\sigma(t)} x(s)ds, \\
\psi_2 &= \int_{t-\sigma(t)}^{t-\sigma_1} x(s)ds, \\
\psi_3 &= x(t-\sigma(t)) - x(t-\sigma_2), \\
\psi_4 &= x(t-\sigma_1) - x(t-\sigma(t)), \\
\psi_5 &= \int_{t-\tau_2}^{t-\tau(t)} y(s)ds, \\
\psi_6 &= \int_{t-\tau(t)}^{t-\tau_1} y(s)ds, \\
\psi_7 &= y(t-\tau(t)) - y(t-\tau_2), \\
\psi_8 &= y(t-\tau_1) - y(t-\tau(t)), \\
\Phi_1(t) &= x(t) - x(t-\sigma_1), \\
\Phi_2(t) &= x(t) + x(t-\sigma_1) - \frac{2}{\sigma_1} \int_{t-\sigma_1}^t x(s)ds, \\
\Phi_3(t) &= y(t) - y(t-\tau_1), \\
\Phi_4(t) &= y(t) + y(t-\tau_1) - \frac{2}{\tau_1} \int_{t-\tau_1}^t y(s)ds.
\end{aligned} \tag{35}$$

Meanwhile, for any  $L_m = \text{diag}(l_{1m}, l_{2m}, \dots, l_{nm}) \geq 0, m = 1, 2$ , the following inequality is true from Assumption 1.

$$\begin{aligned}
&-2 \sum_{i=1}^n l_{1i} g_i(y_i(t)) [g_i(y_i(t)) - u_i y_i(t)] \\
&-2 \sum_{i=1}^n l_{2i} g_i(y_i(t-\tau(t))) [g_i(y_i(t-\tau(t))) - u_i y_i(t-\tau(t))] \geq 0.
\end{aligned} \tag{36}$$

It can be written as

$$\begin{aligned}
&-2g^T(y(t))L_1g(y(t)) + 2y^T(t)UL_1g(y(t)) \\
&-2g^T(y(t-\tau(t)))L_2g(y(t-\tau(t))) \\
&+ 2y^T(t-\tau(t))UL_2g(y(t-\tau(t))) \geq 0.
\end{aligned} \tag{37}$$

What is more, the following equations are true for any matrices  $N_1, N_2$  with appropriate dimensions from system (8).

$$2\dot{x}^T(t)N_1[-Ax(t) + Bg(y(t-\tau(t))) - \dot{x}(t)] = 0, \tag{38}$$

$$2\dot{y}^T(t)N_2[-Cy(t) + Dx(t-\tau(t)) - \dot{y}(t)] = 0. \tag{39}$$

From (24) to (39), we have that

$$\dot{V}_{p(t)} - \alpha V_{p(t)} \leq \xi^T(t)\Theta_i\xi(t), \tag{40}$$

where

$$\begin{aligned}
\xi^T(t) &= \left[ x^T(t) \quad y^T(t) \quad x^T(t-\sigma_1) \quad x^T(t-\sigma(t)) \quad x^T(t-\sigma_2) \quad y^T(t-\tau_1) \right. \\
&\quad y^T(t-\tau(t)) \quad y^T(t-\tau_2) \quad g^T(y(t)) \quad g^T(y(t-\tau(t))) \quad \dot{x}^T(t) \quad \dot{y}^T(t) \quad \int_{t-\sigma_1}^t x^T(s)ds \\
&\quad \int_{t-\sigma_2}^{t-\sigma(t)} x^T(s)ds \quad \int_{t-\sigma(t)}^{t-\sigma_1} x^T(s)ds \quad \int_{t-\sigma_1}^0 \int_{t+\theta}^t \dot{x}^T(s)dsd\theta \quad \int_{-\sigma_2}^{-\sigma_1} \int_{t+\theta}^t \dot{x}^T(s)dsd\theta \\
&\quad \int_{t-\tau_1}^t y^T(s)ds \quad \int_{t-\tau_2}^{t-\tau(t)} y^T(s)ds \quad \int_{t-\tau(t)}^{t-\tau_1} y^T(s)ds \quad \int_{t-\tau_1}^0 \int_{t+\theta}^t \dot{y}^T(s)dsd\theta \\
&\quad \left. \int_{-\tau_2}^{-\tau_1} \int_{t+\theta}^t \dot{y}^T(s)dsd\theta \right].
\end{aligned} \tag{41}$$

By condition (17), we have

$$\dot{V}_{p(t)} + \alpha V_{p(t)} < 0. \tag{42}$$

Note that

$$\frac{d}{dt}(e^{-\alpha t}V_{p(t)}) < 0. \tag{43}$$

For any  $T > 0$ , let  $t_0 = 0$ , and we denote  $t_0, t_1, t_2, t_3, \dots, t_i, \dots, t_{N_p(0,T)}$  and  $t_1, t_2, \dots, t_i, \dots, t_{N_p(0,T)}$  as the switching times on the interval  $[0, 1]$ , where

$$N_p(0, T) = \sum_i^M N_{p_i}(0, T). \tag{44}$$

By integrating (43) for any  $t \in [t_i, t_{i+1}]$ , we find that

$$V_{p(t)} \leq e^{\alpha p(t_i)(t-t_i)} V_{p(t_i)}. \tag{45}$$

From (18), we can obtain

$$V_{p(t)} \leq \mu V(p_{t_i}, p(t_i^-)), \quad \forall (p(t_i) = i, p(t_i^-) = j) \in \mathbb{N} \times \mathbb{N}, i \neq j. \tag{46}$$

By substituting (46) into (45), we can obtain

$$\begin{aligned}
V_{p(t)} &\leq e^{\left\{ \alpha_{p(t_{N_p(t)(0,t)})} (t-t_{N_p(t)(0,t)}) \right\}} V(t_{N_p(0,t)}, p(t_{N_p(0,t)})) \\
&\leq \mu_{p(t_{N_p(0,t)})} e^{\left\{ \alpha_{p(t_{N_p(0,t)})} (t-t_{N_p(0,t)}) \right\}} V(x_{t_{N_p(0,t)}}, p(t_{N_p(0,t)-1})) \\
&\leq \mu_{p(t_{N_p(0,T)})} e^{\left\{ \alpha_{p(t_{N_p(0,T)})} (t-t_{N_p(0,T)}) + \alpha_{p(t_{N_p(0,T)-1})} (t_{N_p(0,T)} - t_{N_p(0,T)-1}) \right\}} \\
&V(x_{t_{N_p(0,T)-1}}, p(t_{N_p(0,T)-1})) + \mu_{p(t_{N_p(0,T)})} \\
&\int_{t_{N_p(0,T)-1}}^{t_{N_p(0,T)}} e^{\left\{ \alpha_{p(t_{N_p(0,T)})} (T-t_{N_p(0,T)}) \right\}} + \dots \\
&\leq \prod_{l=0}^{N_p(0,T)-1} \mu_{p(t_{l+1})} e^{\left\{ \sum_{i=0}^{N_p(0,T)-1} (\alpha_{p(t_{l+1})} + \alpha_{p(t_i)}) t_{l+1} + \alpha_{p(t_0)} T + \alpha_{p(t_0)} t_0 \right\}} V(x_{t_0}, p(t_0)) \\
&\leq e^{\left\{ \sum_{i=1}^N (T_i(0,T)/\tau_{ai}) \ln \mu_i + \sum_{i=1}^N \alpha_i T_i(0,T) \right\}} V(x_{t_0}, p(t_0)) \\
&\leq e^{\left\{ \sum_{i=1}^N ((\ln \mu_i / \tau_{ai}) + \alpha_i) T \right\}} V(x_{t_0}, p(t_0)).
\end{aligned} \tag{47}$$

On the other hand, it follows from (22) that

$$\begin{aligned}
V_{p(0)}(0) &= x^T(0)P_{1i}x(0) + y^T(0)P_{2i}y(0) + \int_{-\sigma_1}^0 e^{\alpha(s)} x^T(s)Q_{1i}x(s)ds + \int_{-\sigma_2}^{-\sigma_1} e^{\alpha(s)} x^T(s)Q_{2i}x(s)ds \\
&+ \int_{-\sigma(0)}^0 e^{\alpha(s)} x^T(s)Q_{3i}x(s)ds + \int_{-\tau_1}^0 e^{\alpha(s)} y^T(s)R_{1i}y(s)ds \\
&+ \int_{-\tau_2}^{-\tau_1} e^{\alpha(s)} y^T(s)R_{2i}y(s)ds + \int_{-\tau(0)}^0 e^{\alpha(s)} \begin{bmatrix} y(s) \\ g(y(s)) \end{bmatrix}^T \begin{bmatrix} R_{3i} & M_{1i} \\ * & R_{4i} \end{bmatrix} \begin{bmatrix} y(s) \\ g(y(s)) \end{bmatrix} ds \\
&+ \int_{-\sigma_1}^0 \int_{\theta}^0 \sigma_1 e^{\alpha(s)} x^T(s)R_{5i}x(s)dsd\theta + \int_{-\sigma_2}^{-\sigma_1} \int_{\theta}^0 \sigma_{12} e^{\alpha(s)} x^T(s)R_{6i}x(s)dsd\theta \\
&+ \int_{-\sigma_1}^0 \int_{\theta}^0 \sigma_1 e^{\alpha(s)} \dot{x}^T(s)R_{7i}\dot{x}(s)dsd\theta + \int_{-\sigma_2}^{-\sigma_1} \int_{\theta}^0 \sigma_{12} e^{\alpha(s)} \dot{x}^T(s)R_{8i}\dot{x}(s)dsd\theta \\
&+ \int_{-\tau_1}^0 \int_{\theta}^0 \tau_1 e^{\alpha(s)} y^T(s)R_{9i}y(s)dsd\theta + \int_{-\tau_2}^{-\tau_1} \int_{\theta}^0 \tau_{12} e^{\alpha(s)} y^T(s)R_{10i}y(s)dsd\theta \\
&+ \int_{-\tau_1}^0 \int_{\theta}^0 \tau_1 e^{\alpha(s)} \dot{y}^T(s)R_{11i}\dot{y}(s)dsd\theta + \int_{-\tau_2}^{-\tau_1} \int_{\theta}^0 \tau_{12} e^{\alpha(s)} \dot{y}^T(s)R_{12i}\dot{y}(s)dsd\theta
\end{aligned}$$

$$\begin{aligned}
& + \int_{-\sigma_2}^0 \int_{\theta}^0 \int_{\nu}^0 \frac{\sigma_1^2}{2} e^{\alpha(s-\theta)} \dot{x}^T(s) S_{1i} \dot{x}(s) ds d\nu d\theta + \int_{-\sigma_2}^{-\sigma_1} \int_{\theta}^0 \int_{\nu}^0 \sigma_{13} e^{\alpha(s-\theta)} \dot{x}^T(s) S_{2i} \dot{x}(s) ds d\nu d\theta \\
& + \int_{-\tau_2}^0 \int_{\theta}^0 \int_{\nu}^0 \frac{\tau_1^2}{2} e^{\alpha(s-\theta)} \dot{y}^T(s) S_{3i} \dot{y}(s) ds d\nu d\theta + \int_{-\tau_2}^{-\tau_1} \int_{\theta}^0 \int_{\nu}^0 \tau_{13} e^{\alpha(s-\theta)} \dot{y}^T(s) S_{4i} \dot{y}(s) ds d\nu d\theta, \\
V_{p(0)}(0) & \leq \left\{ \max_{i \in \mathbb{N}} \lambda_{\max}(P_{1i}) + \max_{i \in \mathbb{N}} \lambda_{\max}(P_{2i}) + \sigma_1 e^{-\alpha\sigma_1} \max_{i \in \mathbb{N}} \lambda_{\max}(Q_{1i}) + (\sigma_2 - \sigma_1) e^{-\alpha\sigma_2} \max_{i \in \mathbb{N}} \lambda_{\max}(Q_{2i}) \right. \\
& + \sigma_2 e^{-\alpha\sigma_2} \max_{i \in \mathbb{N}} \lambda_{\max}(Q_{3i}) + \tau_1 e^{-\alpha\tau_1} \max_{i \in \mathbb{N}} \lambda_{\max}(R_{1i}) + (\tau_2 - \tau_1) e^{-\alpha\tau_1} \max_{i \in \mathbb{N}} \lambda_{\max}(R_{2i}) \\
& + \tau_2 e^{-\alpha\tau_2} \max_{i \in \mathbb{N}} \lambda_{\max}(R_{3i}) + 2\tau_2 e^{-\alpha\tau_2} \max_{i \in \mathbb{N}} \lambda_{\max}(M_{1i}) + \tau_2 e^{-\alpha\tau_2} \max_{i \in \mathbb{N}} \lambda_{\max}(R_{4i}) \left[ \max(|L_i^-, L_i^+|) \right]^2 \\
& + \frac{\sigma_1^3}{2} e^{-\alpha\sigma_1} \max_{i \in \mathbb{N}} \lambda_{\max}(R_{5i}) + \frac{(\sigma_2 - \sigma_1)^3}{2} e^{-\alpha\sigma_2} \max_{i \in \mathbb{N}} \lambda_{\max}(R_{6i}) + \frac{\sigma_1^3}{2} e^{-\alpha\sigma_1} \max_{i \in \mathbb{N}} \lambda_{\max}(R_{7i}) \\
& + \frac{(\sigma_2 - \sigma_1)^3}{2} e^{-\alpha\sigma_2} \max_{i \in \mathbb{N}} \lambda_{\max}(R_{8i}) + \frac{\tau_1^3}{2} e^{-\alpha\tau_1} \max_{i \in \mathbb{N}} \lambda_{\max}(R_{9i}) + \frac{(\tau_2 - \tau_1)^3}{2} e^{-\alpha\tau_2} \max_{i \in \mathbb{N}} \lambda_{\max}(R_{10i}) \\
& + \frac{\tau_1^3}{2} e^{-\alpha\tau_1} \max_{i \in \mathbb{N}} \lambda_{\max}(R_{11i}) + \frac{(\tau_2 - \tau_1)^3}{2} e^{-\alpha\tau_2} \max_{i \in \mathbb{N}} \lambda_{\max}(R_{12i}) + \frac{\sigma_1^5}{4} e^{-\alpha\sigma_1} \max_{i \in \mathbb{N}} \lambda_{\max}(S_{1i}) \\
& + \frac{(\sigma_2^2 - \sigma_1^2)(\sigma_2 - \sigma_1)^3}{4} e^{-\alpha\sigma_2} \max_{i \in \mathbb{N}} \lambda_{\max}(S_{2i}) + \frac{\tau_1^5}{4} e^{-\alpha\tau_1} \max_{i \in \mathbb{N}} \lambda_{\max}(S_{3i}) \\
& + \left. \frac{(\tau_2^2 - \tau_1^2)(\tau_2 - \tau_1)^3}{4} e^{-\alpha\tau_2} \max_{i \in \mathbb{N}} \lambda_{\max}(S_{4i}) \right\} \\
& \times \sup_{-\rho \leq t \leq 0} \{ \|\Phi(t)\|^2, \|\Psi(t)\|^2 \}, \\
& \leq (\lambda_3 + \lambda_4 + \lambda_5 \sigma_1 e^{-\alpha\sigma_1} + \lambda_6 (\sigma_2 - \sigma_1) e^{-\alpha\sigma_2} + \lambda_7 \sigma_2 e^{-\alpha\sigma_2} + \lambda_8 \tau_1 e^{-\alpha\tau_1} \\
& + \lambda_9 (\tau_2 - \tau_1) e^{-\alpha\tau_1} + \lambda_{10} \tau_2 e^{-\alpha\tau_2} + 2\lambda_{11} \tau_2 e^{-\alpha\tau_2} + \lambda_{12} \tau_2 e^{-\alpha\tau_2} + \lambda_{13} \frac{\sigma_1^3}{2} e^{-\alpha\sigma_1} \\
& + \lambda_{14} \frac{(\sigma_2 - \sigma_1)^3}{2} e^{-\alpha\sigma_2} + \lambda_{15} \frac{\sigma_1^3}{2} e^{-\alpha\sigma_1} + \lambda_{16} \frac{(\tau_2 - \tau_1)^3}{2} e^{-\alpha\tau_2} + \lambda_{17} \frac{\tau_1^3}{2} e^{-\alpha\tau_1} \\
& + \lambda_{18} \frac{(\tau_2 - \tau_1)^3}{2} e^{-\alpha\tau_2} + \lambda_{19} \frac{\tau_1^3}{2} e^{-\alpha\tau_1} + \lambda_{20} \frac{(\tau_2 - \tau_1)^3}{2} e^{-\alpha\tau_2} + \lambda_{21} \frac{\sigma_1^5}{4} e^{-\alpha\sigma_1} \\
& + \lambda_{22} \frac{(\sigma_2^2 - \sigma_1^2)(\sigma_2 - \sigma_1)^3}{4} e^{-\alpha\sigma_2} + \lambda_{23} \frac{\tau_1^5}{4} e^{-\alpha\tau_1} + \lambda_{24} \frac{(\tau_2^2 - \tau_1^2)(\tau_2 - \tau_1)^3}{4} e^{-\alpha\tau_2} ) c_1, \\
& = dc_1.
\end{aligned} \tag{48}$$



Then, we can easily obtain

$$V_{p(t)}(t) = e^{\left\{\sum_{i=1}^N ((\ln \mu_i / \tau_{ai}) - \alpha_i) T\right\}} dc_1, \quad (49)$$

$$\begin{aligned} V_{p(t)}(t) &= x^T(t)P_{1i}x(t) + y^T(t)P_{2i}y(t) \\ &\geq \min_{i \in \mathbb{N}} \left[ \lambda_{\min}(P_{1i})\|x(t)\|^2 + \lambda_{\min}(P_{2i})\|y(t)\|^2 \right] \\ &= (\lambda_1 + \lambda_2) \left\{ \|x(t)\|^2 + \|y(t)\|^2 \right\}. \end{aligned} \quad (50)$$

From (49) and (50), we obtain

$$\|x(t)\|^2 + \|y(t)\|^2 \leq \frac{e^{\left\{\sum_{i=1}^N ((\ln \mu_i / \tau_{ai}) - \alpha_i) T\right\}} dc_1}{(\lambda_1 + \lambda_2)}. \quad (51)$$

Therefore, by Definition 1, we conclude that  $\|x(t)\|^2 + \|y(t)\|^2 < c_2$ . This completes the proof.

*Remark 1.* We introduce  $\int_{-\sigma_2}^0 \int_{\theta}^t \int_{t+\nu}^0 (\sigma_1^2/2) e^{\alpha(s-\theta)} \dot{x}^T(s)S_{1i}\dot{x}(s)dsd\nu d\theta + \int_{-\sigma_2}^{-\sigma_1} \int_{\theta}^0 \int_{t+\nu}^{-\sigma_2} \sigma_{13} e^{\alpha(s-\theta)} \dot{x}^T(s)S_{2i}\dot{x}(s)dsd\nu d\theta + \int_{-\tau_2}^0 \int_{\theta}^0 \int_{t+\nu}^t (\tau_1^2/2) e^{\alpha(s-\theta)} \dot{y}^T(s)S_{3i}\dot{y}(s)dsd\nu d\theta + \int_{-\tau_2}^{-\tau_1} \int_{\theta}^0 \int_{t+\nu}^t \tau_{13} e^{\alpha(s-\theta)} \dot{y}^T(s)S_{4i}\dot{y}(s)dsd\nu d\theta$  in our Lyapunov–Krasovskii functional. The novel Lyapunov–Krasovskii functional can make the stability criteria applicable to both fast and slow time-varying delays directly. Besides, by using the convex combination technique together with the Jensen inequality lemma, less conservative criteria are obtained.

Case: we consider the following genetic regulatory networks without switched term:

$$\begin{cases} \dot{x}(t) = -Ax(t) + Bg(y(t - \tau(t))), \\ \dot{y}(t) = -Cy(t) + D(x(t - \sigma(t))). \end{cases} \quad (52)$$

Based on Theorem 1, the next rate-independent corollary is derived.

**Corollary 1.** *The genetic regulatory network (52) is asymptotically stable with respect to positive real numbers  $\sigma_1, \sigma_2, \tau_1, \tau_2$ ; if there exist symmetric positive definite matrices  $P_1, P_2, Q_n (n = 1, 2, 3), R_n (n = 1, 2, \dots, 12), S_n (n = 1, 2, \dots, 4)$ , the diagonal matrix  $L_m = \text{diag}(l_{1m}, l_{2m}, \dots, l_{mm}) \geq 0, m = 1, 2$  such that the following LMIs hold*

$$\begin{aligned} \begin{bmatrix} R_3 & M_1 \\ * & R_4 \end{bmatrix} &\geq 0, \\ \begin{bmatrix} R_6 & \bar{R}_6 \\ * & R_6 \end{bmatrix} &\geq 0, \\ \begin{bmatrix} R_8 & \bar{R}_8 \\ * & R_8 \end{bmatrix} &\geq 0, \\ \begin{bmatrix} R_{10} & \bar{R}_{10} \\ * & R_{10} \end{bmatrix} &\geq 0, \\ \begin{bmatrix} R_{12} & \bar{R}_{12} \\ * & R_{12} \end{bmatrix} &\geq 0, \\ \bar{\Theta} &= [\bar{\Theta}_{ij}]_{22 \times 22} < 0, \end{aligned} \quad (53)$$

where,

$$\begin{aligned} \bar{\Theta}_{11} &= -P_1A - A^T P_1^T + Q_1 + Q_3 + \sigma_1^2 R_5 + \sigma_{12}^2 R_6 - 3e^{-\alpha\sigma_1} R_7 - e^{-\alpha\sigma_1} R_7 + \alpha P_1, \\ \bar{\Theta}_{13} &= e^{-\alpha\sigma_1} R_7 - 3e^{-\alpha\sigma_1} R_7, \\ \bar{\Theta}_{110} &= P_1 B, \bar{\Theta}_{113} = \frac{6}{\sigma_1} e^{-\alpha\sigma_1} R_7, \\ \bar{\Theta}_{22} &= R_1 + R_3 - P_2 C - C^T P_2^T + \tau_1^2 R_9 + \tau_{12}^2 R_{10} - e^{-\alpha\tau_1} R_{11} - 3e^{-\alpha\tau_1} R_{11} + \alpha P_2, \\ \bar{\Theta}_{24} &= P_2 D, \\ \bar{\Theta}_{26} &= e^{-\alpha\tau_1} R_{11} - 3e^{-\alpha\tau_1} R_{11}, \\ \bar{\Theta}_{29} &= M_1 + U^T L_1^T, \bar{\Theta}_{218} = \frac{6}{\tau_1} e^{-\alpha\tau_1} R_{11}, \\ \bar{\Theta}_{33} &= -e^{-\alpha\sigma_1} Q_1 + e^{-\alpha\sigma_1} Q_2 - e^{-\alpha\sigma_1} R_7 - 3e^{-\alpha\sigma_1} R_7 - e^{-\alpha\sigma_2} R_8, \\ \bar{\Theta}_{34} &= -e^{-\alpha\sigma_2} \bar{R}_8^T + e^{-\alpha\sigma_2} R_8, \\ \bar{\Theta}_{35} &= e^{-\alpha\sigma_2} \bar{R}_8^T, \\ \bar{\Theta}_{313} &= \frac{6}{\sigma_1} e^{-\alpha\sigma_1} R_7, \end{aligned}$$

$$\begin{aligned}
\bar{\Theta}_{44} &= -(1 - \sigma_d)e^{-\alpha\sigma(t)}Q_3 + 2e^{-\alpha\sigma_2}\bar{R}_8 - 2e^{-\alpha\sigma_2}R_8, \\
\bar{\Theta}_{45} &= e^{-\alpha\sigma_2}\bar{R}_8^T + e^{-\alpha\sigma_2}R_8, \\
\bar{\Theta}_{55} &= e^{-\alpha\sigma_2}Q_2^T - e^{-\alpha\sigma_2}R_8, \\
\bar{\Theta}_{66} &= -e^{-\alpha\tau_1}R_1 + e^{-\alpha\tau_1}R_2 - e^{-\alpha\tau_1}R_{11} - 3e^{-\alpha\tau_1}R_{11} - e^{-\alpha\tau_2}R_{12}, \\
\bar{\Theta}_{67} &= -e^{-\alpha\tau_2}\bar{R}_{12}^T + e^{-\alpha\tau_2}R_{12}, \\
\bar{\Theta}_{68} &= -e^{-\alpha\tau_2}\bar{R}_{12}^T, \\
\bar{\Theta}_{618} &= \frac{6}{\tau_1}e^{-\alpha\tau_1}R_{11}, \\
\bar{\Theta}_{77} &= -(1 - \tau_d)e^{-\alpha\tau(t)}R_3 + 2e^{-\alpha\tau_2}\bar{R}_{12} - 2e^{-\alpha\tau_2}R_{12}, \\
\bar{\Theta}_{78} &= e^{-\alpha\tau_2}\bar{R}_{12}^T + e^{-\alpha\tau_2}R_{12}, \\
\bar{\Theta}_{710} &= -(1 - \tau_d)e^{-\alpha\tau(t)}M_1 + UL_2, \\
\bar{\Theta}_{88} &= -e^{-\alpha\tau_2}R_2^T - e^{-\alpha\tau_2}R_{12}, \\
\bar{\Theta}_{99} &= R_4 - 2L_1, \\
\bar{\Theta}_{1010} &= -(1 - \tau_d)e^{-\alpha\tau_2}R_4 - 2L_2, \\
\bar{\Theta}_{1111} &= \sigma_1^2R_7 + \sigma_{12}^2R_8 + e^{\alpha t}\frac{e^{\alpha\sigma_2} - \alpha\sigma_2 - 1}{\alpha^2}S_1 + e^{\alpha t}\frac{e^{\alpha\sigma_2} - e^{\alpha\sigma_1} - \alpha(\sigma_2 - \sigma_1)}{\alpha^2}S_2, \\
\bar{\Theta}_{1212} &= \tau_1^2R_{11} + \tau_{12}^2R_{12} + e^{\alpha t}\frac{e^{\alpha\tau_2} - \alpha\tau_2 - 1}{\alpha^2}S_3 + e^{\alpha t}\frac{e^{\alpha\tau_2} - e^{\alpha\tau_1} - \alpha(\tau_2 - \tau_1)}{\alpha^2}S_4, \\
\bar{\Theta}_{1313} &= -e^{\alpha\sigma_1}R_5 - \frac{12}{\sigma_1^2}e^{-\alpha\sigma_1}R_7, \\
\bar{\Theta}_{1414} &= -e^{\alpha\sigma_2}R_6, \\
\bar{\Theta}_{1415} &= -e^{\alpha\sigma_2}\bar{R}_6, \\
\bar{\Theta}_{1515} &= -e^{\alpha\sigma_2}R_6, \\
\bar{\Theta}_{1616} &= -e^{\alpha t}S_1, \\
\bar{\Theta}_{1717} &= -e^{\alpha t}S_2, \\
\bar{\Theta}_{1818} &= -e^{\alpha\tau_1}R_9 - \frac{12}{\tau_1^2}e^{-\alpha\tau_1}R_{11}, \\
\bar{\Theta}_{1919} &= -e^{\alpha\tau_2}R_{10}, \\
\bar{\Theta}_{1920} &= -e^{\alpha\tau_2}\bar{R}_{10}, \\
\bar{\Theta}_{2020} &= -e^{\alpha\tau_2}R_{10}, \\
\bar{\Theta}_{2121} &= -e^{\alpha t}S_3, \\
\bar{\Theta}_{2222} &= -e^{\alpha t}S_4.
\end{aligned} \tag{54}$$

*Proof.* The corollary follows by a similar argument as that in proof of Theorem 1.

#### 4. Numerical Example

In this section, numerical examples are provided to illustrate the validity and the advantage of the proposed finite-time stability of switched GRNs with time-varying delays.

*Example 1.* Consider switched GRNs with time-varying delay (8) as

$$\begin{cases} \dot{x}(t) = -A_{p(t)}x(t) + B_{p(t)}g(y(t - \tau(t))), \\ \dot{y}(t) = -C_{p(t)}y(t) + D_{p(t)}(x(t - \sigma(t))), \end{cases} \quad (55)$$

with

$$\begin{aligned} A_1 &= \begin{bmatrix} 2 & 0 & 0 \\ 0 & 2 & 0 \\ 0 & 0 & 2 \end{bmatrix}, \\ B_1 &= \begin{bmatrix} 0 & 0 & -2 \\ -2 & 0 & 0 \\ 0 & -2 & 0 \end{bmatrix}, \\ C_1 &= \begin{bmatrix} 3 & 0 & 0 \\ 0 & 3 & 0 \\ 0 & 0 & 3 \end{bmatrix}, \\ D_1 &= \begin{bmatrix} 0.9 & 0 & 0 \\ 0 & 0.9 & 0 \\ 0 & 0 & 0.9 \end{bmatrix}, \\ A_2 &= \begin{bmatrix} 3 & 0 & 0 \\ 0 & 3 & 0 \\ 0 & 0 & 3 \end{bmatrix}, \\ B_2 &= \begin{bmatrix} 0 & -1.5 & 0 \\ -1.5 & 0 & 0 \\ 0 & -1.5 & 0 \end{bmatrix}, \\ C_2 &= \begin{bmatrix} 4 & 0 & 0 \\ 0 & 4 & 0 \\ 0 & 0 & 4 \end{bmatrix}, \\ D_2 &= \begin{bmatrix} 1.2 & 0 & 0 \\ 0 & 1.2 & 0 \\ 0 & 0 & 1.2 \end{bmatrix}. \end{aligned} \quad (56)$$

The activation function is chosen as  $U = \text{diag}\{0.65, 0.65, 0.65\}$ , and the values of  $c_1, c_2, T$  are given as follows:

$$\begin{aligned} \sigma_1 &= 0.7, \\ \sigma_2 &= 3.5, \\ \sigma_d &= 0.4, \\ \tau_1 &= 0.6, \\ \tau_2 &= 3.2, \\ \tau_d &= 0.2, \\ c_1 &= 1.5, \\ c_2 &= 4.5, \\ T &= 6, \\ \mu &= 1.5. \end{aligned} \quad (57)$$

We show the simulation result of the trajectories of the variables  $x(t)$  and  $y(t)$  in Figures 1 and 2. It should be point out that the condition is feasible when employing the LMI toolbox in MATLAB, solve LMIs (16)–(20), and then, we can reach feasible solution. Hence, the switched GRNs (8) is finite-time stable.

$$\begin{aligned} P_{11} &= \begin{bmatrix} 0.1837 & -0.0007 & -0.0007 \\ -0.0007 & 0.1837 & -0.0007 \\ -0.0007 & -0.0007 & 0.1837 \end{bmatrix}, \\ P_{21} &= \begin{bmatrix} 0.5336 & 0.0008 & 0.0008 \\ 0.0008 & 0.5336 & 0.0008 \\ 0.0008 & 0.0008 & 0.5336 \end{bmatrix}, \\ Q_{11} &= \begin{bmatrix} 0.0419 & -0.0000 & -0.0000 \\ -0.0000 & 0.0419 & -0.0000 \\ -0.0000 & -0.0000 & 0.0419 \end{bmatrix}, \\ Q_{21} &= \begin{bmatrix} 0.0225 & 0.0000 & 0.0000 \\ 0.0000 & 0.0225 & 0.0000 \\ 0.0000 & 0.0000 & 0.0225 \end{bmatrix}, \\ Q_{31} &= \begin{bmatrix} 0.1556 & 0.0003 & 0.0003 \\ 0.0003 & 0.1556 & 0.0003 \\ 0.0003 & 0.0003 & 0.1556 \end{bmatrix}, \\ R_{11} &= \begin{bmatrix} 0.0669 & 0.0001 & 0.0001 \\ 0.0001 & 0.0669 & 0.0001 \\ 0.0001 & 0.0001 & 0.0669 \end{bmatrix}, \\ R_{21} &= \begin{bmatrix} 0.0287 & 0.0000 & 0.0000 \\ 0.0000 & 0.0287 & 0.0000 \\ 0.0000 & 0.0000 & 0.0287 \end{bmatrix}, \\ R_{31} &= \begin{bmatrix} 0.1518 & -0.0001 & -0.0001 \\ -0.0001 & 0.1518 & -0.0001 \\ -0.0001 & -0.0001 & 0.1518 \end{bmatrix}, \end{aligned}$$

$$R_{41} = \begin{bmatrix} 0.0389 & 0.0000 & 0.0000 \\ 0.0000 & 0.0389 & 0.0000 \\ 0.0000 & 0.0000 & 0.0389 \end{bmatrix},$$

$$S_{11} = \begin{bmatrix} 0.0016 & -0.0000 & -0.0000 \\ -0.0000 & 0.0016 & -0.0000 \\ -0.0000 & -0.0000 & 0.0016 \end{bmatrix},$$

$$R_{51} = \begin{bmatrix} 0.0570 & -0.0000 & -0.0000 \\ -0.0000 & 0.0570 & -0.0000 \\ -0.0000 & -0.0000 & 0.0570 \end{bmatrix},$$

$$S_{21} = 10^{-3} \times \begin{bmatrix} 0.2915 & 0.0005 & 0.0005 \\ 0.0005 & 0.2915 & 0.0005 \\ 0.0005 & 0.0005 & 0.2915 \end{bmatrix},$$

$$R_{61} = \begin{bmatrix} 0.0053 & 0.0000 & 0.0000 \\ 0.0000 & 0.0053 & 0.0000 \\ 0.0000 & 0.0000 & 0.0053 \end{bmatrix},$$

$$S_{31} = \begin{bmatrix} 0.0023 & 0.0000 & 0.0000 \\ 0.0000 & 0.0023 & 0.0000 \\ 0.0000 & 0.0000 & 0.0023 \end{bmatrix},$$

$$R_{71} = \begin{bmatrix} 0.0562 & 0.0000 & 0.0000 \\ 0.0000 & 0.0562 & 0.0000 \\ 0.0000 & 0.0000 & 0.0562 \end{bmatrix},$$

$$S_{41} = 10^{-3} \times \begin{bmatrix} 0.4960 & 0.0007 & 0.0007 \\ 0.0007 & 0.4960 & 0.0007 \\ 0.0007 & 0.0007 & 0.4960 \end{bmatrix},$$

$$R_{81} = \begin{bmatrix} 0.0057 & -0.0000 & -0.0000 \\ -0.0000 & 0.0057 & -0.0000 \\ -0.0000 & -0.0000 & 0.0057 \end{bmatrix},$$

$$P_{12} = \begin{bmatrix} 0.1747 & 0.0001 & 0.0001 \\ 0.0001 & 0.1747 & 0.0001 \\ 0.0001 & 0.0001 & 0.1747 \end{bmatrix},$$

$$R_{91} = \begin{bmatrix} 0.1006 & 0.0000 & 0.0000 \\ 0.0000 & 0.1006 & 0.0000 \\ 0.0000 & 0.0000 & 0.1006 \end{bmatrix},$$

$$P_{22} = \begin{bmatrix} 0.1267 & 0.0003 & 0.0003 \\ 0.0003 & 0.1267 & 0.0003 \\ 0.0003 & 0.0003 & 0.1267 \end{bmatrix},$$

$$R_{101} = \begin{bmatrix} 0.0094 & 0.0000 & 0.0000 \\ 0.0000 & 0.0094 & 0.0000 \\ 0.0000 & 0.0000 & 0.0094 \end{bmatrix},$$

$$Q_{12} = \begin{bmatrix} 0.1265 & 0.0004 & 0.0004 \\ 0.0004 & 0.1265 & 0.0004 \\ 0.0004 & 0.0004 & 0.1265 \end{bmatrix},$$

$$R_{111} = \begin{bmatrix} 0.0627 & -0.0001 & -0.0001 \\ -0.0001 & 0.0627 & -0.0001 \\ -0.0001 & -0.0001 & 0.0627 \end{bmatrix},$$

$$Q_{22} = \begin{bmatrix} 0.1121 & -0.0004 & -0.0004 \\ -0.0004 & 0.1121 & -0.0004 \\ -0.0004 & -0.0004 & 0.1121 \end{bmatrix},$$

$$R_{121} = \begin{bmatrix} 0.0057 & -0.0000 & -0.0000 \\ -0.0000 & 0.0057 & -0.0000 \\ -0.0000 & -0.0000 & 0.0057 \end{bmatrix},$$

$$Q_{32} = \begin{bmatrix} 0.1745 & 0.0014 & 0.0014 \\ 0.0014 & 0.1745 & 0.0014 \\ 0.0014 & 0.0014 & 0.1745 \end{bmatrix},$$

$$\begin{aligned}
 R_{12} &= \begin{bmatrix} 0.1231 & 0.0008 & 0.0008 \\ 0.0008 & 0.1231 & 0.0008 \\ 0.0008 & 0.0008 & 0.1231 \end{bmatrix}, & R_{92} &= \begin{bmatrix} 0.1230 & -0.0001 & -0.0001 \\ -0.0001 & 0.1230 & -0.0001 \\ -0.0001 & -0.0001 & 0.1230 \end{bmatrix}, \\
 R_{22} &= \begin{bmatrix} 0.1145 & -0.0005 & -0.0005 \\ -0.0005 & 0.1145 & -0.0005 \\ -0.0005 & -0.0005 & 0.1145 \end{bmatrix}, & R_{102} &= \begin{bmatrix} 0.0675 & -0.0005 & -0.0005 \\ -0.0005 & 0.0675 & -0.0005 \\ -0.0005 & -0.0005 & 0.0675 \end{bmatrix}, \\
 R_{32} &= \begin{bmatrix} 0.1434 & 0.0020 & 0.0020 \\ 0.0020 & 0.1434 & 0.0020 \\ 0.0020 & 0.0020 & 0.1434 \end{bmatrix}, & R_{112} &= \begin{bmatrix} 0.0878 & -0.0006 & -0.0006 \\ -0.0006 & 0.0878 & -0.0006 \\ -0.0006 & -0.0006 & 0.0878 \end{bmatrix}, \\
 R_{42} &= \begin{bmatrix} 0.0863 & 0.0001 & 0.0001 \\ 0.0001 & 0.0863 & 0.0001 \\ 0.0001 & 0.0001 & 0.0863 \end{bmatrix}, & R_{122} &= \begin{bmatrix} 0.1055 & -0.0008 & -0.0008 \\ -0.0008 & 0.1055 & -0.0008 \\ -0.0008 & -0.0008 & 0.1055 \end{bmatrix}, \\
 R_{52} &= \begin{bmatrix} 0.1176 & -0.0002 & -0.0002 \\ -0.0002 & 0.1176 & -0.0002 \\ -0.0002 & -0.0002 & 0.1176 \end{bmatrix}, & S_{12} &= \begin{bmatrix} 0.1889 & -0.0000 & -0.0000 \\ -0.0000 & 0.1889 & -0.0000 \\ -0.0000 & -0.0000 & 0.1889 \end{bmatrix}, \\
 R_{62} &= \begin{bmatrix} 0.0641 & -0.0005 & -0.0005 \\ -0.0005 & 0.0641 & -0.0005 \\ -0.0005 & -0.0005 & 0.0641 \end{bmatrix}, & S_{22} &= \begin{bmatrix} 0.0736 & 0.0000 & 0.0000 \\ 0.0000 & 0.0736 & 0.0000 \\ 0.0000 & 0.0000 & 0.0736 \end{bmatrix}, \\
 R_{72} &= \begin{bmatrix} 0.0886 & -0.0005 & -0.0005 \\ -0.0005 & 0.0886 & -0.0005 \\ -0.0005 & -0.0005 & 0.0886 \end{bmatrix}, & S_{32} &= \begin{bmatrix} 0.1937 & -0.0000 & -0.0000 \\ -0.0000 & 0.1937 & -0.0000 \\ -0.0000 & -0.0000 & 0.1937 \end{bmatrix}, \\
 R_{82} &= \begin{bmatrix} 0.1177 & -0.0004 & -0.0004 \\ -0.0004 & 0.1177 & -0.0004 \\ -0.0004 & -0.0004 & 0.1177 \end{bmatrix}, & S_{42} &= \begin{bmatrix} 0.0685 & 0.0000 & 0.0000 \\ 0.0000 & 0.0685 & 0.0000 \\ 0.0000 & 0.0000 & 0.0685 \end{bmatrix}.
 \end{aligned}
 \tag{58}$$

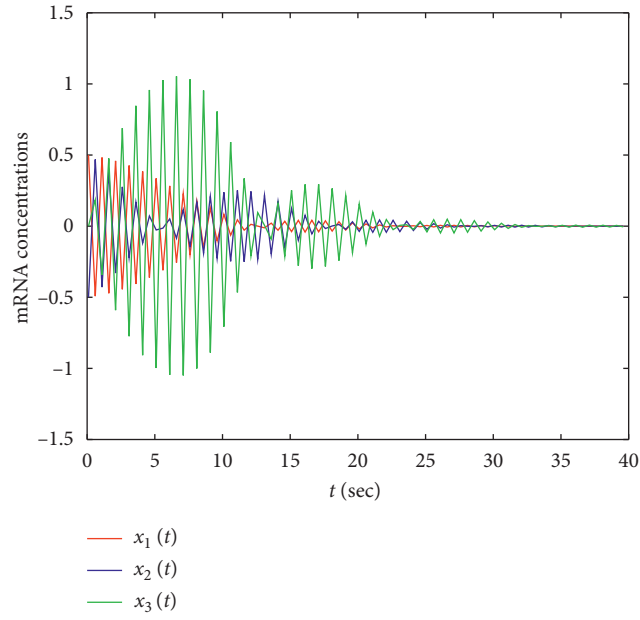


FIGURE 1: The mRNA concentrations  $x(t)$  in Example 1.

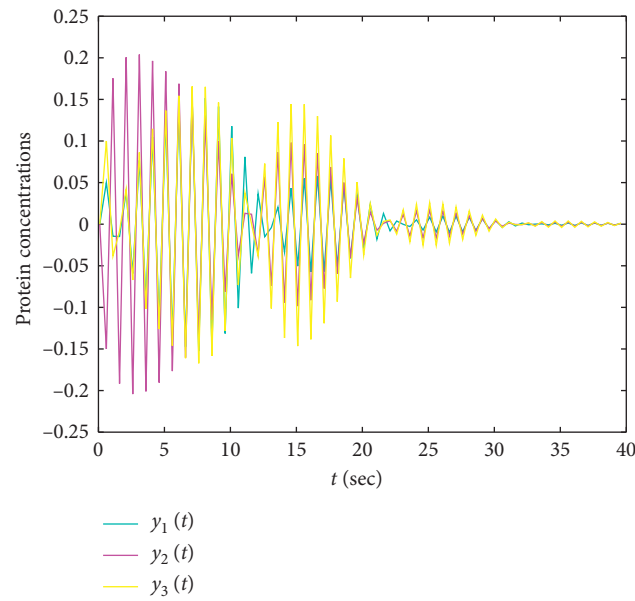
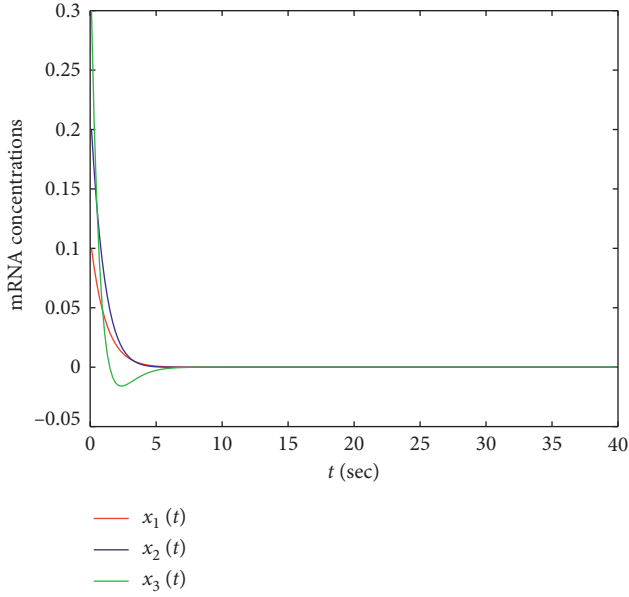
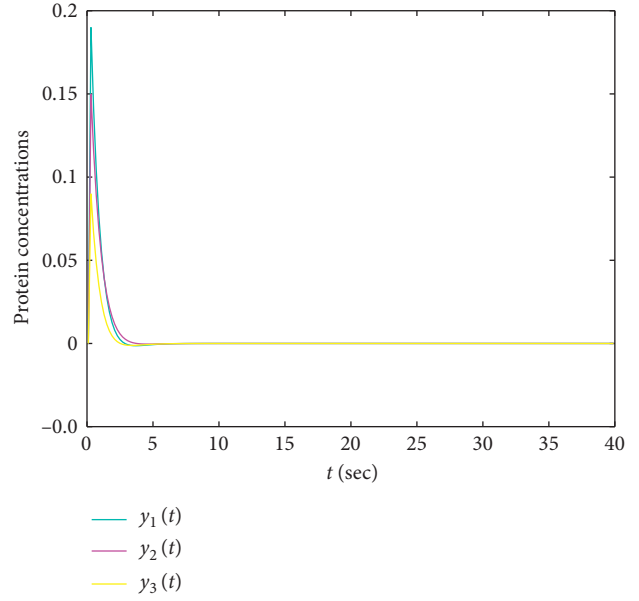


FIGURE 2: Protein concentrations  $y(t)$  in Example 2.

TABLE 1: The maximum allowable time delay upper bound for  $\tau_2$  with different values of  $\sigma_{12}$ .

$\sigma_{12}$	0.125	0.25	0.55	1.0	1.1
[15]	0.5	—	—	-8	—
[16]	—	—	1.0	—	—
[17]	2.8273	2.1661	1.1544	0.4904	0.3845
[18]	3.2957	3.1932	2.9455	2.5661	2.4799
Corollary 3.3	5.4924	5.0257	4.6412	4.4670	3.9249

FIGURE 3: The trajectories of  $x(t)$  in Example 2.FIGURE 4: The trajectories of  $y(t)$  in Example 2.*Example 2*

$$\begin{aligned}
 A &= \begin{bmatrix} 3 & 0 & 0 \\ 0 & 3 & 0 \\ 0 & 0 & 3 \end{bmatrix}, \\
 B &= \begin{bmatrix} 0 & 0 & -2.5 \\ -2.5 & 0 & 0 \\ 0 & -2.5 & 0 \end{bmatrix}, \\
 C &= \begin{bmatrix} 2.5 & 0 & 0 \\ 0 & 2.5 & 0 \\ 0 & 0 & 2.5 \end{bmatrix}, \\
 D &= \begin{bmatrix} 0.8 & 0 & 0 \\ 0 & 0.8 & 0 \\ 0 & 0 & 0.8 \end{bmatrix},
 \end{aligned} \tag{59}$$

$g(y) = y^2/1 + y^2$  and  $U = \text{diag}\{0.65, 0.65, 0.65\}$ .

Furthermore, for the parameters listed above, let  $\tau_d = 0.5$  and  $\sigma_d = 0.5$ .

In order to compare the results in [15–18], using Corollary 1, the comparison results are listed in Table 1 for  $\tau_2$ . Clearly, the results proposed in this study provide a larger admissible upper bound delay to guarantee the asymptotically stable system (52). In addition, the trajectories of the genetic regulatory network (52) are shown in Figures 3 and 4.

*Remark 2.* The discussion in Example 2 illustrates that the conditions in this study (Corollary 1) is less conservative than those in [15–18], which shows the superiority of our method compared with that in [15–18].

*Example 3.* Consider the following switched GRNs with time-varying delay:

$$\begin{cases} \dot{x}(t) = -A_{p(t)}x(t) + B_{p(t)}g(y(t - \tau(t))), \\ \dot{y}(t) = -C_{p(t)}y(t) + D_{p(t)}(x(t - \sigma(t))), \end{cases} \tag{60}$$

with

$$\begin{aligned}
 A_1 &= \begin{bmatrix} 3 & 0 \\ 0 & 3 \end{bmatrix}, \\
 B_1 &= \begin{bmatrix} 0.81 & -0.20 \\ 0.10 & 0.64 \end{bmatrix}, \\
 C_1 &= \begin{bmatrix} 3 & 0 \\ 0 & 3 \end{bmatrix}, \\
 D_1 &= \begin{bmatrix} 1 & 0 \\ 0 & 1 \end{bmatrix}, \\
 A_2 &= \begin{bmatrix} 4 & 0 \\ 0 & 4 \end{bmatrix}, \\
 B_2 &= \begin{bmatrix} 0.1 & -1 \\ -1 & 0.1 \end{bmatrix}, \\
 C_2 &= \begin{bmatrix} 4 & 0 \\ 0 & 4 \end{bmatrix}, \\
 D_2 &= \begin{bmatrix} 0.8 & 0 \\ 0 & 0.8 \end{bmatrix}.
 \end{aligned} \tag{61}$$

The activation function is chosen as  $U = \text{diag}\{0.2, 0.2\}$ , and the values of  $c_1, c_2, T$  are given as follows:

$$\begin{aligned}
\sigma_1 &= 0.2, \\
\sigma_2 &= 3.2, \\
\sigma_d &= 1, \\
\tau_1 &= 0.1, \\
\tau_2 &= 0.3, \\
\tau_d &= 0.1, \\
c_1 &= 1, \\
c_2 &= 3.2, \\
T &= 4, \\
\mu &= 0.9.
\end{aligned} \tag{62}$$

By employing the LMI toolbox in MATLAB, solve LMIs (16)–(20), and the feasible solutions are then reached.

## 5. Conclusion

In this study, a finite-time stability analysis for switched GRNs with time-varying delays has been investigated. We utilized the reciprocally convex combination method, Wirtinger’s integral inequality, and new triple integral with exponential function in Lyapunov–Krasovskii functionals; a less conservative LMI-based finite-time stability criterion is obtained with the switched ADT approach to reduce the conservatism of our results, compared with existing ones. A numerical example has been given to demonstrate the effectiveness and the advantage of our proposed methods. State estimation as well as other research topics such as switched lure systems and complex networks [55, 56] and stabilization of probabilistic Boolean networks [57, 58] of the time delay systems will be further investigated based on the methods proposed in this study.

## Data Availability

No data were used to support this study.

## Conflicts of Interest

The authors declare that there are no conflicts of interest.

## Authors’ Contributions

B.H. involved in funding acquisition; G.R. conceptualized the study, wrote the original draft, and validated; G.R., B.H., M.S.A., and S.S. developed software; G.R. and B.H. performed formal analysis, developed methodology, and reviewed and edited the manuscript; S.S., B.P., G.K.T., and M.S.A. supervised the study. All authors have read and agreed to the published version of the manuscript.

## Acknowledgments

This work was supported by the Basic Sciences and Mathematics, Faculty of Engineering, Thai-Nichi Institute of Technology, Bangkok, 10250, Thailand.

## References

- [1] V. Vembarasan, G. Nagamani, P. Balasubramaniam, and J. H. Park, “State estimation for delayed genetic regulatory networks based on passivity theory,” *Mathematical Biosciences*, vol. 244, no. 2, pp. 165–175, 2013.
- [2] M. S. Ali, N. Gunasekaran, C. K. Ahn, and P. Shi, “Sampled-data stabilization for fuzzy genetic regulatory networks with leakage delays,” *IEEE/ACM Transactions on Computational Biology and Bioinformatics*, vol. 15, no. 1, pp. 271–285, 2018.
- [3] X. Zhang, L. Wu, and J. Zou, “Globally asymptotic stability analysis for genetic regulatory networks with mixed delays: an m-matrix-based approach,” *IEEE/ACM Transactions on Computational Biology and Bioinformatics*, vol. 13, no. 1, pp. 135–147, 2016.
- [4] T. Liu, X. Zhang, and X. Gao, “Stability analysis for continuous-time and discrete-time genetic regulatory networks with delays,” *Applied Mathematics and Computation*, vol. 274, pp. 628–643, 2016.
- [5] K. Ratnavelu, M. Kalpana, and P. Balasubramaniam, “Asymptotic stability of Markovian switching genetic regulatory networks with leakage and mode-dependent time delays,” *Journal of the Franklin Institute*, vol. 353, no. 7, pp. 1615–1638, 2016.
- [6] L. Wang, Z.-P. Luo, H.-L. Yang, and J. Cao, “Stability of genetic regulatory networks based on switched systems and mixed time-delays,” *Mathematical Biosciences*, vol. 278, pp. 94–99, 2016.
- [7] L. Lu, Z. Xing, and B. He, “Non-uniform sampled-data control for stochastic passivity and passification of markov jump genetic regulatory networks with time-varying delays,” *Neurocomputing*, vol. 171, pp. 434–443, 2016.
- [8] F.-X. Wu, “Global and robust stability analysis of genetic regulatory networks with time-varying delays and parameter uncertainties,” *IEEE Transactions on Biomedical Circuits and Systems*, vol. 5, no. 4, pp. 391–398, 2011.
- [9] P. Smolen, D. A. Baxter, and J. H. Byrne, “Mathematical modeling of gene networks,” *Neuron*, vol. 26, no. 3, pp. 567–580, 2000.
- [10] H. Jong, “Modelling and simulation of genetic regulatory systems: a literature review,” *Journal of Computational Biology*, vol. 9, pp. 67–103, 2002.
- [11] A. Liu, L. Yu, W. Zhang, and B. Chen, “ $H_\infty$  filtering for discrete-time genetic regulatory networks with random delays,” *Mathematical Biosciences*, vol. 239, pp. 97–105, 2012.
- [12] W. Wang, S. Zhong, and F. Liu, “New delay-dependent stability criteria for uncertain genetic regulatory networks with time-varying delays,” *Neurocomputing*, vol. 93, pp. 19–26, 2012.
- [13] W. Yu, J. Lu, Z. D. Wang, J. Cao, and Q. Zhou, “Robust  $H_\infty$  control and uniformly bounded control for genetic regulatory network with stochastic disturbance,” *IET Control Theory & Applications*, vol. 4, pp. 1687–1706, 2014.
- [14] Y. He, J. Zeng, M. Wu, and C. Zhang, “Robust stabilization and  $H_\infty$  controllers design for stochastic genetic regulatory networks with time-varying delays and structured uncertainties,” *Mathematical Biosciences*, vol. 236, pp. 53–63, 2012.
- [15] F. Ren and J. Cao, “Asymptotic and robust stability of genetic regulatory networks with time-varying delays,” *Neurocomputing*, vol. 71, no. 4, pp. 834–842, 2008.
- [16] W. Zhang, J.-A. Fang, and Y. Tang, “Stochastic stability of markovian jumping genetic regulatory networks with mixed





- time delays,” *Applied Mathematics and Computation*, vol. 217, no. 17, pp. 7210–7225, 2011.
- [17] H. Wu, X. Liao, S. Guo, W. Feng, and Z. Wang, “Stochastic stability for uncertain genetic regulatory networks with interval time-varying delays,” *Neurocomputing*, vol. 72, no. 13, pp. 3263–3276, 2009.
- [18] W. Wang, Y. Wang, S. K. Nguang, S. Zhong, and F. Liu, “Delay partition method for the robust stability of uncertain genetic regulatory networks with time-varying delays,” *Neurocomputing*, vol. 173, pp. 899–911, 2016.
- [19] J. Liu, E. Tian, Z. Gu, and Y. Zhang, “State estimation for Markovian jumping genetic regulatory networks with random delays,” *Communications in Nonlinear Science and Numerical Simulation*, vol. 19, no. 7, pp. 2479–2492, 2014.
- [20] X. Lou, Q. Ye, and B. Cui, “Exponential stability of genetic regulatory networks with random delays,” *Neurocomputing*, vol. 73, no. 4, pp. 759–769, 2010.
- [21] K. Mathiyalagan and R. Sakthivel, “Robust stabilization and  $H_\infty$  control for discretetime stochastic genetic regulatory networks with time delays,” *Canadian Journal of Physics*, vol. 90, pp. 939–953, 2012.
- [22] X. Wan, L. Xu, H. Fang, and G. Ling, “Robust non-fragile  $H_\infty$  state estimation for discrete-time genetic regulatory networks with Markov jump delays and uncertain transition probabilities,” *Neurocomputing*, vol. 154, pp. 162–173, 2015.
- [23] G. Wang and J. Cao, “Robust exponential stability analysis for stochastic genetic networks with uncertain parameters,” *Communications in Nonlinear Science and Numerical Simulation*, vol. 14, no. 8, pp. 3369–3378, 2009.
- [24] X. Li, R. Rakkiyappan, and C. Pradeep, “Robust  $\mu$ -stability analysis of Markovian switching uncertain stochastic genetic regulatory networks with unbounded time-varying delays,” *Communications in Nonlinear Science and Numerical Simulation*, vol. 17, pp. 3894–3905, 2012.
- [25] Y. Li, Y. Zhu, N. Zeng, and M. Du, “Stability analysis of standard genetic regulatory networks with time-varying delays and stochastic perturbations,” *Neurocomputing*, vol. 74, no. 17, pp. 3235–3241, 2011.
- [26] A. Liu, L. Yu, D. Zhang, and W. Zhang, “Finite-time  $H_\infty$  control for discrete-time genetic regulatory networks with random delays and partly unknown transition probabilities,” *Journal of the Franklin Institute*, vol. 350, pp. 1944–1961, 2013.
- [27] J. H. Koo, D. H. Ji, S. C. Won, and J. H. Park, “An improved robust delay-dependent stability criterion for genetic regulatory networks with interval time delays,” *Communications in Nonlinear Science and Numerical Simulation*, vol. 17, no. 8, pp. 3399–3405, 2012.
- [28] P.-L. Liu, “Robust stability analysis of genetic regulatory network with time delays,” *ISA Transactions*, vol. 52, no. 3, pp. 326–334, 2013.
- [29] D. Zhang and L. Yu, “Passivity analysis for stochastic Markovian switching genetic regulatory networks with time-varying delays,” *Communications in Nonlinear Science and Numerical Simulation*, vol. 16, no. 8, pp. 2985–2992, 2011.
- [30] M. Mohammadian, A. H. Abolmasoumi, and H. R. Momeni, “ $H_\infty$  mode-independent filter design for Markovian jump genetic regulatory networks with time-varying delays,” *Neurocomputing*, vol. 87, pp. 10–18, 2012.
- [31] Y. Sun, G. Feng, and J. Cao, “Stochastic stability of Markovian switching genetic regulatory networks,” *Physics Letters A*, vol. 373, no. 18, pp. 1646–1652, 2009.
- [32] L. Yin, “Finite-time stability analysis of switched genetic regulatory networks,” *Journal Applied Mathematics*, vol. 2014, Article ID 730292, 11 pages, 2014.
- [33] Y. Yao, J. Liang, and J. Cao, “Stability analysis for switched genetic regulatory networks: an average dwell time approach,” *Journal of the Franklin Institute*, vol. 348, no. 10, pp. 2718–2733, 2011.
- [34] X. Wan, L. Xu, H. Fang, F. Yang, and X. Li, “Exponential synchronization of switched genetic oscillators with time-varying delays,” *Journal of the Franklin Institute*, vol. 351, no. 8, pp. 4395–4414, 2014.
- [35] X.-M. Sun, G.-P. Liu, W. Wang, and D. Rees, “Stability analysis for networked control systems based on average dwell time method,” *International Journal of Robust and Nonlinear Control*, vol. 20, no. 15, pp. 1774–1784, 2010.
- [36] Z. Xiang, Y. N. Sun, and M. S. Mahmoud, “Robust finite-time  $H_\infty$  control for a class of uncertain switched neutral systems,” *Communications in Nonlinear Science and Numerical Simulation*, vol. 17, pp. 1766–1778, 2012.
- [37] X. Liu, “Stabilization of switched linear systems with mode-dependent time-varying delays,” *Applied Mathematics and Computation*, vol. 216, no. 9, pp. 2581–2586, 2010.
- [38] J. Cheng, H. Zhu, S. Zhong, F. Zheng, and Y. Zeng, “Finite-time filtering for switched linear systems with a mode-dependent average dwell time,” *Nonlinear Analysis: Hybrid Systems*, vol. 15, pp. 145–156, 2015.
- [39] M. Syed Ali and S. Saravanan, “Robust finite-time  $H_\infty$  control for a class of uncertain switched neural networks of neutral-type with distributed time varying delays,” *Neurocomputing*, vol. 177, pp. 454–468, 2016.
- [40] N. Jiang, X. Liu, W. Yu, and J. Shen, “Finite-time stochastic synchronization of genetic regulatory networks,” *Neurocomputing*, vol. 167, pp. 314–321, 2015.
- [41] X. Lin, H. Du, S. Li, and Y. Zou, “Finite-time stability and finite-time weighted  $L_2$ -gain analysis for switched systems with time-varying delay,” *IET Control Theory*, vol. 7, pp. 1058–1069, 2013.
- [42] X. Fan, Y. Xue, X. Zhang, and J. Ma, “Finite-time state observer for delayed reaction-diffusion genetic regulatory networks,” *Neurocomputing*, vol. 227, pp. 18–28, 2017.
- [43] J. Qiu, K. Sun, C. Yang, X. Chen, X. Chen, and A. Zhang, “Finite-time stability of genetic regulatory networks with impulsive effects,” *Neurocomputing*, vol. 219, pp. 9–14, 2017.
- [44] M. Syed Ali and S. Saravanan, “Finite-time stability for memristor based uncertain neural networks with time-varying delays- via average dwell time approach,” *Chinese Journal of Physics*, vol. 55, no. 5, pp. 1953–1971, 2017.
- [45] M. Syed Ali and S. Saravanan, “Finite-time  $L_2$ -gain analysis for switched neural networks with time-varying delay,” *Neural Computing and Applications*, vol. 29, pp. 975–984, 2018.
- [46] S. Wang, T. Shi, M. Zeng, L. Zhang, F. E. Alsaadi, and T. Hayat, “New results on robust finite-time boundedness of uncertain switched neural networks with time-varying delays,” *Neurocomputing*, vol. 151, pp. 522–530, 2015.
- [47] X. Li, X. Lin, S. Li, and Y. Zou, “Finite-time stability of switched nonlinear systems with finite-time unstable subsystems,” *Journal of the Franklin Institute*, vol. 352, no. 3, pp. 1192–1214, 2015.
- [48] W. Wang, Y. Dong, S. Zhong, and F. Liu, “Finite-time robust stability of uncertain genetic regulatory networks with time-varying delays and reaction-diffusion terms,” *Complexity*, vol. 2019, Article ID 8565437, 18 pages, 2019.
- [49] Z. Wu, Z. Wang, and T. Zhou, “Finite-time stability of fractional-order time-varying delays gene regulatory networks with structured uncertainties and controllers,” *Complexity*, vol. 2020, Article ID 2315272, 19 pages, 2020.

- [50] J. Zhou, S. Xu, and H. Shen, "Finite-time robust stochastic stability of uncertain stochastic delayed reaction-diffusion genetic regulatory networks," *Neurocomputing*, vol. 74, no. 17, pp. 2790–2796, 2011.
- [51] X. M. Sun, J. Zhao, and D. J. Hill, "Stability and  $L_2$ -gain analysis for switched delay systems: a delay-dependent method," *Automatica*, vol. 42, pp. 1769–1774, 2006.
- [52] K. Gu, V. L. Kharitonov, and J. Chen, *Stability of Time Delay Systems*, Birkhuser, Boston, MA, USA, 2003.
- [53] P. Park, J. W. Ko, and C. Jeong, "Reciprocally convex approach to stability of systems with time-varying delays," *Automatica*, vol. 47, no. 1, pp. 235–238, 2011.
- [54] A. Seuret and F. Gouaisbaut, "Wirtinger-based integral inequality: application to time-delay systems," *Automatica*, vol. 49, no. 9, pp. 2860–2866, 2013.
- [55] W. Duan, Y. Li, J. Chen, and L. Jiang, "New results on stability analysis of uncertain neutral-type lure systems derived from a modified lyapunov-krasovskii functional," *Complexity*, vol. 2019, Article ID 1706264, 20 pages, 2019.
- [56] C. Huang, X. Zhang, H.-K. Lam, and S.-H. Tsai, "Synchronization analysis for nonlinear complex networks with reaction-diffusion terms using fuzzy-model-based approach," *IEEE Transactions on Fuzzy Systems*, vol. 1, 2020.
- [57] C. Huang, J. Lu, D. W. C. Ho, G. Zhai, and J. Cao, "Stabilization of probabilistic Boolean networks via pinning control strategy," *Information Sciences*, vol. 510, pp. 205–217, 2020.
- [58] C. Huang, J. Lu, G. Zhai, J. Cao, G. Lu, and M. Perc, "Stability and stabilization in probability of probabilistic boolean networks," *IEEE Transactions on Neural Networks and Learning Systems*, vol. 32, no. 1, p. 241, 2021.

## Research Article

# Effectiveness of Price Limit on Stock Market Network: A Time-Migrated DCCA Approach

Hongzeng He <sup>1,2</sup> and Shufen Dai <sup>1</sup>

<sup>1</sup>School of Economics and Management, University of Science and Technology Beijing, Beijing 100083, China

<sup>2</sup>Returned Overseas Talent and Expert Service Center, MOHRSS, Beijing 100083, China

Correspondence should be addressed to Hongzeng He; [hehongzeng@126.com](mailto:hehongzeng@126.com)

Received 5 July 2020; Accepted 21 July 2020; Published 18 January 2021

Guest Editor: Xiaodi Li

Copyright © 2021 Hongzeng He and Shufen Dai. This is an open access article distributed under the Creative Commons Attribution License, which permits unrestricted use, distribution, and reproduction in any medium, provided the original work is properly cited.

In this paper, we investigated the effectiveness of price limit on stock market with the correlation study and complex network technology. We proposed a time-migrated DCCA cross-correlation coefficient which is beneficial to detect the asynchronous correlations of nonstationary time series. The stock market network is constructed with the threshold method based on time-migrated DCCA. The effectiveness of the price limit during the stock market crash period is studied based on the time-migrated DCCA stock market network. The results indicate that the time-migrated DCCA ensures more relevant results than the equal-time DCCA method. An interesting finding is that the price limit has different effects on the stock market network at different stages of dynamic evolution. Market stabilization will be lowered and the systemic risk will be increased if the price limit is enhanced. Such studies are relevant for a better understanding of the stock market and have a significant contribution to the stock market in reality.

## 1. Introduction

It is believed that a number of systems could be described by complex networks, including traffic systems, ecological systems, and financial systems. The applications of complex networks have provided a new perspective for studying the mechanisms of these systems. In essence, the stock market is a typical complex network system since the vertices are stocks in the financial market and some vertices are connected by an edge if they have a relationship with each other. In the stock market, the price of stock fluctuates frequently with the dynamic evolution of the entire financial system. Previous studies suggest that a stock market network could be established based on the price correlations. From different angles, people provided many effective complex network construction methods such as minimum cost spanning tree (MST), planar maximally filtered graph (PMFG), and correlation threshold method. Huang and Tse used the correlation threshold method to construct a stock correlation network in order to analyze the information of stock markets

where the nodes are the stocks and the connections are determined by the threshold of Pearson correlation (PCC) [1, 2]. Originally, Mantegna used the Pearson correlation and MST method to build a stock network and revealed the general hierarchical structure of the market [3]. Bonanno et al. also used the method and found that stock market networks present different hierarchical structures as the time horizon changes [4]. Tumminello et al. also used the correlation coefficient between stock price dynamics time series and the PMFG method to generate stock networks [5].

Since the stock price correlations are widely used in the popular methods mentioned above, the studies of dynamic correlations and relationships become crucial for constructing the stock market complex network and analyzing the economic features of the stock market. In previous studies, there are some conventional methods to quantify the correlations of stock price time series, such as Pearson correlation, cross-correlation, and canonical correlation. But it is known that financial data are highly nonstationary and the conventional methods may not suited for it [6].

Accordingly, it is important to investigate the time-migrated or time-asynchronous correlations. To investigate the time characters of financial series, Grey Relational Analysis [7], Detrended Fluctuation Analysis (DFA), and Detrended Cross-correlation Analysis (DCCA) [8] were proposed to quantify the long-range power-law correlations of nonstationary time series.

Previous research has established that DCCA provides a proper approach to quantitatively measure the long-range cross-correlation of nonstationary time series. It inspires us to investigate the time series of stock market using these methods. To the best of our knowledge, there is still little research to gain the insights into time-migrated or time-asynchronous correlations of the stock market price series. Therefore, we present a time-migrated DCCA correlation coefficient in this paper. We not only calculate the DCCA correlation coefficients of the stock market but also investigate the time-migrated relationships. In the field of stock market regulation, price limit policy is widely used to prevent stock prices from rising or falling too violently, especially during the stock crash period. Once stock prices hit the limit, they are not allowed to move beyond the limit. The price limit is supposed to give frenzied traders time to cool off and save the price from “*falling off a cliff*” [9]. Many of the stock exchanges adopt price limit to maintain the stability and curb the overreaction of the stock market [10]. But there are other voices that the price limit is ineffective and imposes serious costs to the stock market [11]. Rare literature of price limit refers to the econometric analysis of the stock market model. In that case, we also evaluate the effectiveness of the price limit from the perspective of complex network in this paper. In this context, this research aims to address the following three questions:

- (1) How to mining the time-migrated correlations of the stock prices?
- (2) What are the properties and community structures of the stock market from the perspective of complex network.
- (3) How to evaluate the effectiveness of price limit reform on the stock market network.

To achieve this goal, we propose a time-migrated DCCA method and study the correlations of Chinese stock market. Lately, we apply the threshold method to construct stock market networks for analyzing the effectiveness of the price limit reform.

The paper is organized as follows. Section 2 presents dataset and methods employed in this study. Section 3 shows the properties and community structures of the stock market and provides effectiveness results of the price limit reform on stability and systemic risk. Section 4 concludes the paper. Finally, Data availability and References are also presented.

## 2. Materials and Methods

**2.1. Stock Market Dataset.** In this paper, we choose the CSI 300. The CSI 300 dataset contains the daily close prices of the 300 large-scale stocks with good liquidity. The CSI 300 index

usually covers about 60% of the Shanghai Composite and Shenzhen Component. The dataset of CSI 300 stock index is from Mar 28th, 2012 to Mar 29th, 2019 (data source: Choice Financial Terminal) which contains 1703 daily close prices of the CSI 300 companies, including the 2015 market crash period. The samples of the close price series are presented in Table 1.

To get a more stable price series, we calculate the return price of the dataset by

$$r_i(t) = \ln \left[ \frac{p_i(t+1)}{p_i(t)} \right], \quad (1)$$

where  $r_i(t)$  is the return price of stock  $i$  at the day  $t$ ,  $p_i(t+1)$  and  $p_i(t)$  are the close prices of stock  $i$  at the day  $t$  and the day  $t-1$ . Thus,  $i \in [1, 300]$  and  $t \in [1, 1702]$ . The daily return prices of the stock 000415 are presented in Figure 1. As is shown in Figure 1, the return price varies between  $[-1, 1]$  while the close price varies between  $[3.38, 28.28]$ . Thus, the return price has better properties to avoid the excessive influence and nonstationarity of the dataset.

In this paper, we obtain the DCCA cross-correlation coefficient and time-migrated DCCA cross-correlation coefficient with the return prices. For this purpose, we introduce a brief theoretical description of the two methods.

**2.2. DCCA Cross-Correlation Coefficient.** Traditionally, the DCCA cross-correlation coefficient is derived from DFA and DCCA [6, 12, 13]. The DFA method is a common method for investigating the long-range power-law self-correlations of single time series, and the DCCA method has demonstrated its usefulness to determine the long-range power-law cross-correlations of two nonstationary time series [14]. One step further, the DCCA cross-correlation coefficient is an effective method to quantify the level of cross-correlation between two nonstationary time series at different temporal scales [15–17]. The algorithm of DCCA correlation coefficient consists of five steps.

Step 1: Supposing that there are two stock price series  $\xi(t)$  and  $\eta(t)$ , we obtained two removing mean and accumulated time sequences:

$$\begin{aligned} \xi'(t) &= \sum_{i=1}^t [\xi(i) - \bar{\xi}], \\ \eta'(t) &= \sum_{i=1}^t [\eta(i) - \bar{\eta}]. \end{aligned} \quad (2)$$

Where  $\bar{\xi}$  and  $\bar{\eta}$  are the mean value of time series  $\xi(t)$  and  $\eta(t)$ ,  $t = 1, 2, \dots, T$ .

Step 2: We cut both time sequences  $\xi'(t)$  and  $\eta'(t)$  into  $(N-s)$  overlapping segments  $\xi'_k(t)$  and  $\eta'_k(t)$ , with  $k = 1, \dots, T-s$  and  $0 \leq s < T-1$ . The length of  $\xi'_k(t)$  and  $\eta'_k(t)$  is  $s+1$ .

Step 3: we calculate the local trend of each segment  $\xi'_k(t)$  and  $\eta'_k(t)$  by a least-squares fit method,  $\xi_k(t)$  and  $\eta_k(t)$ . Then we define the detrended time series for each

segment and calculate self-variance and covariance of each residual by:

$$F_{\xi\xi}^2(i) = \frac{1}{s+1} \sum_{t=1}^{s+1} [\tilde{\xi}_i(t) - \xi'_i(t)]^2, \quad (3)$$

$$F_{\eta\eta}^2(i) = \frac{1}{s+1} \sum_{t=1}^{s+1} [\tilde{\eta}_i(t) - \eta'_i(t)]^2,$$

$$F_{\xi\eta}^2(i) = \frac{1}{s+1} \sum_{t=1}^{s+1} [\tilde{\xi}_i(t) - \xi'_i(t)] [\tilde{\eta}_i(t) - \eta'_i(t)]. \quad (4)$$

Where  $\tilde{\xi}_k(t)$  and  $\tilde{\eta}_k(t)$  are the fitting polynomials of segment  $k$ . And  $\tilde{\xi}_i(t) - \xi'_i(t)$  and  $\tilde{\eta}_i(t) - \eta'_i(t)$  are the detrended time series of the segment  $i$ , respectively.

Step 4: We obtain the detrended covariance function of all segments by

$$F_{\text{DFA-}\xi}(s) = \left( \frac{1}{N-s} \sum_{i=1}^{N-s} F_{\xi\xi}^2(i) \right)^{(1/2)},$$

$$F_{\text{DFA-}\eta}(s) = \left( \frac{1}{N-s} \sum_{i=1}^{N-s} F_{\eta\eta}^2(i) \right)^{(1/2)}, \quad (5)$$

$$F_{\text{DCCA}}^2(s) = \frac{1}{N-s} \sum_{i=1}^{N-s} F_{\xi\eta}^2(i).$$

Step 5: Finally, we calculate the DCCA cross-correlation coefficient by

$$\rho_{\text{DCCA}}(s) = \frac{F_{\text{DCCA}}^2(s)}{F_{\text{DFA-}\xi}(s)F_{\text{DFA-}\eta}(s)}. \quad (6)$$

The DCCA cross-correlation coefficient is a function of the time segment length  $s$ . As we can see, the DCCA cross-correlation coefficient equals to Pearson cross-correlation coefficient when  $s = 0$ . According to the Cauchy-Schwarz inequality, the DCCA cross-correlation coefficient ranges  $[-1, 1]$ . Like the Pearson cross-correlation coefficient, the value of  $\rho_{\text{DCCA}}(s) = 0$  means there is no correlation between the two time series. The  $\rho_{\text{DCCA}}(s) = 1$  means a full positive correlation, whereas  $\rho_{\text{DCCA}}(s) = -1$  means a full negative correlation. A major advantage of  $\rho_{\text{DCCA}}(s)$  is to measure the cross-correlations between two nonstationary time series at the different segment length  $s$  [15]. It is more robust to contaminated noises and amplitude ratio than Pearson correlation [18]. There are a number of  $\rho_{\text{DCCA}}$  applications in meteorology [19, 20], physiology [21, 22], economy [13, 23], financial [14, 16, 24–26], and other research areas.

**2.3. Time-Migrated DCCA Cross-Correlation Coefficient.** Traditionally, the DCCA cross-correlation coefficient is implemented by measuring the correlations of each detrended segment synchronously. As is shown in equation (4), we use the equal-time segment  $i$  of  $\xi(t)$  and  $\eta(t)$  in Figure 2(a) when we calculate  $F_{\xi\eta}^2(i)$ . However, it should be further noticed that the price series have not only synchronous relationships but also asynchronous relationships in real-time stock markets. For example, there is a *lead-lag effect* on the stock market, which means that stock prices of some firms show a delayed or ahead temporal evolution pattern to other firms' stock prices [27–30]. Since a possible delay between the stocks could be accounted in the time series, we consider the following case in Figure 2(b): supposing two time series  $\xi(t)$  and  $\eta(t)$  in the stock market, we calculate the detrended correlations of each segment  $i$  in  $\xi(t)$  and  $\eta(t)$ , but in some cases, the segment  $i$  of  $\xi(t)$  may have a relationship with segment  $j$  of  $\eta(t)$  in some cases. So we consider these asynchronous relationships in the time-migrated DCCA cross-correlation coefficient.

The algorithm of time-migrated DCCA correlation coefficient consists of the following seven steps:

Step 1: We calculate removing mean and accumulated time sequences of  $\xi(t)$  and  $\eta(t)$ :

$$\xi'(t) = \sum_{i=1}^t [\xi(i) - \bar{\xi}],$$

$$\eta'(t) = \sum_{i=1}^t [\eta(i) - \bar{\eta}]. \quad (7)$$

Where  $\bar{\xi}$  and  $\bar{\eta}$  are the mean value of time series  $\xi(t)$  and  $\eta(t)$ ,  $t = 1, 2, \dots, T$ .

Step 2: We cut both two time sequences  $\xi'(t)$  and  $\eta'(t)$  into  $(N-s)$  overlapping segments  $\xi'_k(t)$  and  $\eta'_k(t)$ , with  $k = 1, \dots, T-s$  and  $0 \leq s < T-1$ . The length of  $\xi'_k(t)$  and  $\eta'_k(t)$  is  $s+1$ .

Step 3: For the detrended time series of the segment  $i$ , we calculate the time-migrated covariance of  $\xi'_i(t) - \xi'_i(t)$  and  $\tilde{\eta}_j(t) - \eta'_j(t)$ , where  $i, j = 1, \dots, T-s$ .

$$F_{\xi\eta}^2(i, j) = \frac{1}{s+1} \sum_{t=1}^{s+1} [\tilde{\xi}_i(t) - \xi'_i(t)] [\tilde{\eta}_j(t) - \eta'_j(t)]. \quad (8)$$

Step 4: We find the max value of  $F_{\xi\eta}^2(i, j)$  for  $\xi'(t)$  by

$$F_{\text{max-}\xi\eta}^2(i) = \max_{1 \leq j \leq N-s} F_{\xi\eta}^2(i, j). \quad (9)$$

Where  $i, j = 1, \dots, T-s$  and  $j^*$  is the argument that makes the equation (9) true:

$$j^*(i) = \operatorname{argmax}_{1 \leq j \leq N-s} F_{\xi\eta}^2(i, j). \quad (10)$$

Step 5: We calculate the detrended self-variance in each segment  $i$  of  $\xi(t)$  by

$$F_{\xi\xi}^2(i) = \frac{1}{s} \sum_{t=1}^{s+1} \left[ \tilde{\xi}_i(t) - \xi'_i(t) \right]^2. \quad (11)$$

According to the Cauchy-Schwarz inequality, we calculate detrended self-variance in the segment  $j^*(i)$  of  $\eta(t)$ :

$$F_{\eta^*\eta^*}^2(i) = \frac{1}{s} \sum_{t=1}^{s+1} \left[ \tilde{\eta}_{j^*(i)}(t) - \eta'_{j^*(i)}(t) \right]^2. \quad (12)$$

Step 6: We obtain the time-migrated detrended covariance function  $F_{tm-DCCA}^2(s)$ ,  $F_{DFA_\xi}(s)$  and  $F_{DFA_{\eta^*}}(s)$  by

$$\begin{aligned} F_{tm-DCCA}^2(s) &= \frac{1}{N-s} \sum_{i=1}^{N-s} F_{\max-\xi\eta}^2, \\ F_{DFA_\xi}(s) &= \left( \frac{1}{N-s} \sum_{i=1}^{N-s} F_{\xi\xi}^2(i) \right)^{(1/2)}, \\ F_{DFA_{\eta^*}}(s) &= \left( \frac{1}{N-s} \sum_{i=1}^{N-s} F_{\eta^*\eta^*}^2(i) \right)^{(1/2)}. \end{aligned} \quad (13)$$

Step 7: Finally, we calculate the time-migrated DCCA cross-correlation coefficient by

$$\rho_{tm-DCCA}(s) = \frac{F_{tm-DCCA}^2(s)}{F_{DFA_\xi}(s)F_{DFA_{\eta^*}}(s)}. \quad (14)$$

We calculate the relationships asynchronously in the time-migrated DCCA cross-correlation coefficient. We get the maximum of  $F_{\xi\eta}^2(i, j)$  to detect the time-migrated relationships of two stocks in order to maximize the correlation detection ability. According to the Cauchy-Schwarz inequality, the time-migrated DCCA cross-correlation coefficient is also a set of dimensionless coefficient ranging from  $-1$  to  $1$ . A higher value of DCCA cross-correlation coefficient means a closer relationship with each other.

The DCCA cross-correlation coefficient provides a proper approach to measure equal-time relationships between two nonstationary time series, but the time-migrated DCCA cross-correlation coefficient is also available for measuring relationships between two nonstationary time series with asynchronous relationships. They are both dimensionless coefficients that can be compared with other nondimensional methods, such as Pearson coefficients.

**2.4. Stock Market Network Model.** In the upper subsection, we studied the equal-time DCCA cross-correlation coefficient and the time-migrated DCCA cross-correlation coefficient. It is now well established from a variety of studies that a network could be constructed from the Pearson correlation coefficient matrix of the complex system

[1, 2, 4, 31–33]. In this section, we apply the threshold method to construct stock market networks with these two methods. Additionally, we compare the topology properties and community structures of the stock networks. First we calculate the equal-time DCCA cross-correlation coefficient  $\rho_{DCCA}^{ij}(s)$  and time-migrated DCCA cross-correlation coefficient  $\rho_{tm-DCCA}^{ij}(s)$  of the entire return price pairs in the dataset on a different time scale  $s$ . Then we obtain the maximum value when  $s = s^*$  by

$$\begin{aligned} \rho_{DCCA\_max}^{ij} &= \max_{s=s^*} \rho_{DCCA}^{ij}(s), \quad i, j \in [1, 300], \\ \rho_{tm-DCCA\_max}^{ij} &= \max_{s=s^*} \rho_{tm-DCCA}^{ij}(s), \quad i, j \in [1, 300], \end{aligned} \quad (15)$$

where  $\rho_{DCCA\_max}^{ij}$  and  $\rho_{tm-DCCA\_max}^{ij}$  are the max coefficients between stocks  $i$  and  $j$ .

Then a metric distance of stock  $i$  and  $j$  can be translated into connection weight by [3, 4, 32]

$$\begin{aligned} D_{DCCA}^{ij} &= \sqrt{2(1 - \rho_{DCCA\_max}^{ij})}, \\ w_{DCCA}^{ij} &= \frac{1}{D_{DCCA}^{ij}}, \\ D_{tm-DCCA}^{ij} &= \sqrt{2(1 - \rho_{tm-DCCA\_max}^{ij})}, \\ w_{tm-DCCA}^{ij} &= \frac{1}{D_{tm-DCCA}^{ij}}. \end{aligned} \quad (16)$$

In both cases, we get  $300 \times 300$  matrix of connection weights  $W_{DCCA}$  and  $W_{tm-DCCA}$ .

Finally, we set a certain threshold value  $\theta$  to construct the stock market network. Let the Graph  $G = (V, E)$  represents stock market network, where the node  $v_i \in V$  represents stock  $i$  and edge  $e_{ij} \in E$  represents the connections of the stock  $i$  and stock  $j$ . The set of connections is established by

$$E = \begin{cases} e_{ij} = 1, & i \neq j \text{ and } w_{ij} > \theta, \\ e_{ij} = 0, & i = j. \end{cases} \quad (17)$$

The complex network construction algorithm is given by Algorithm 1. We get different connection topologies with different values of threshold  $\theta$ .

### 3. Results and Discussion

In this study, we construct the stock market complex network based on the threshold method with two sets of coefficient matrices. Previous research has established certain applications of the complex network in economics: relationships [34], contagion [35–37], risk [38–41] and so on [42, 43], but few studies are based on the policy effect. So in order to quantify the effectiveness of price limit reform, we first analyze statistical characteristics of the coefficients and network properties; then we make an econometric analysis about the bailout strategy such as price limit reform base on the stock market network in this section.

TABLE 1: Close prices of three stocks in four trading days.

Stock code	Major business	May 13, 2016	May 16, 2016	May 17, 2016	May 18, 2016	May 19, 2016
000100	Electronic equipment	3.36	3.38	3.36	3.3	3.3
000157	Special equipment	4.12	4.13	4.11	4.06	4.05
000166	Securities service	8.06	8.08	8.06	8.07	8.03

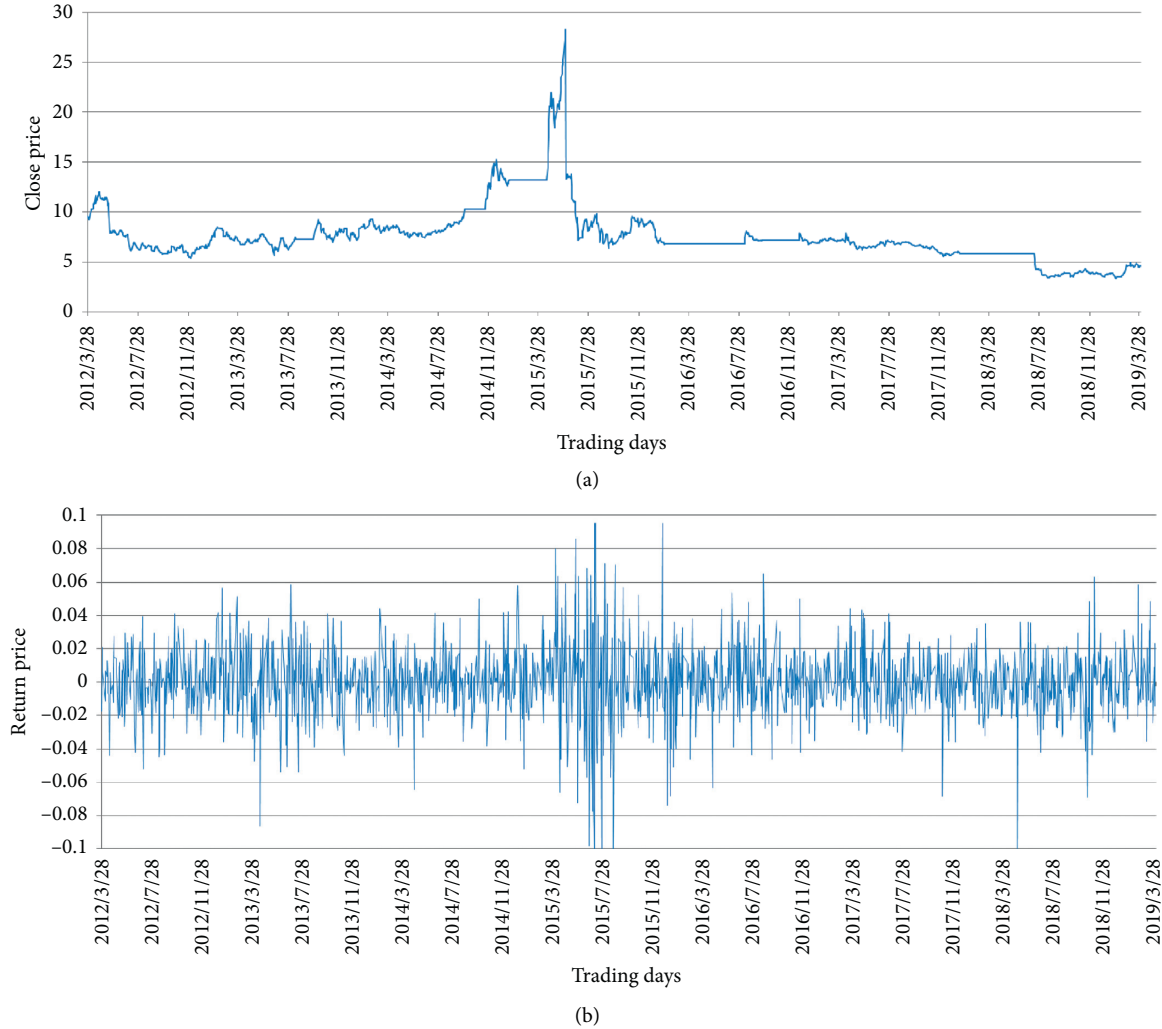


FIGURE 1: Closing prices and return prices of stock 000415.

**3.1. Statistical Analysis.** Based on the methods and dataset of Section 2, we calculate the correlation matrices with the two methods and examine the distributions of the empirical, respectively. It is crucial to  $\rho_{tm-DCCA_{max}}$  and  $\rho_{DCCA_{max}}$  with proper values of time segment length  $s$ . As is shown in Figure 3, a clear spike of  $\rho_{tm-DCCA_{max}}$  and  $\rho_{DCCA_{max}}$  appears with smaller value of  $s$  and the curves tend to flat as  $s$  increases. So we choose segment length  $1 \leq s \leq 15$  to analyze the relatively short term correlation coefficients.

We display the statistical results of DCCA and time-migrated DCCA in contrast to the PCC in Figure 4 and Table 2. The details of PCC coefficient could be obtained in

[1, 31]. It can be seen in Figure 4 that the  $\rho_{DCCA}$  distribution plot has a shape similar to the  $\rho_{PCC}$  distribution, and the time-migrated DCCA has a bigger mean value and kurtosis value than DCCA and PCC. It tells us we get a bigger correlation in most cases and the distribution is more concentrated. The time-migrated DCCA method could ensure more relevant results than the other two methods. In Figure 4, it is easy to see a more concentrated distribution of time-migrated DCCA which is more sensitive to the changing of threshold  $\theta$ . As a result, the constructed network based on the time-migrated DCCA is more representative with threshold  $\theta$ .

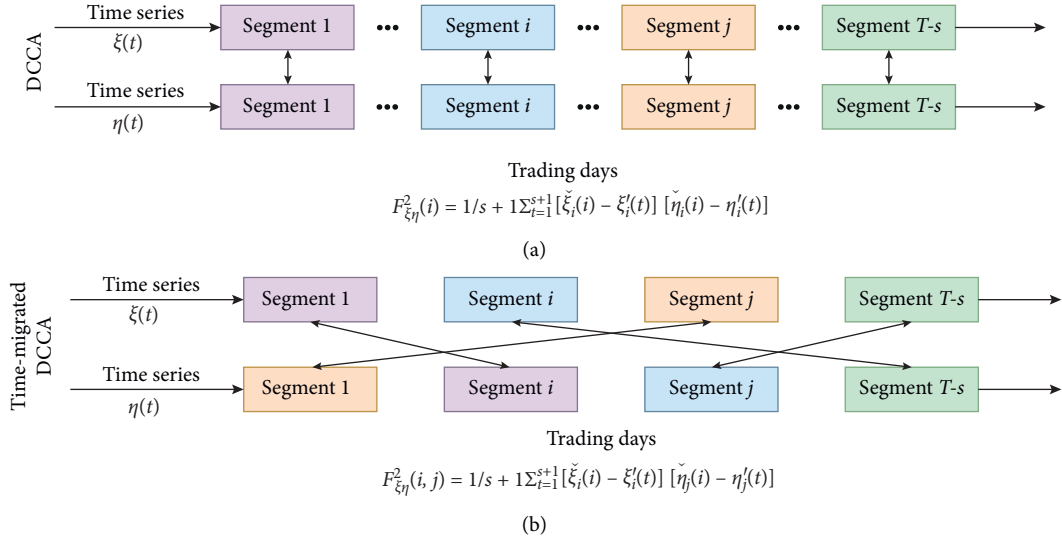


FIGURE 2: (a) Principles of DCCA cross-correlation coefficient (synchronous correlations). (b) The possible scenario of time-migrated DCCA cross-correlation coefficient (asynchronous correlations).

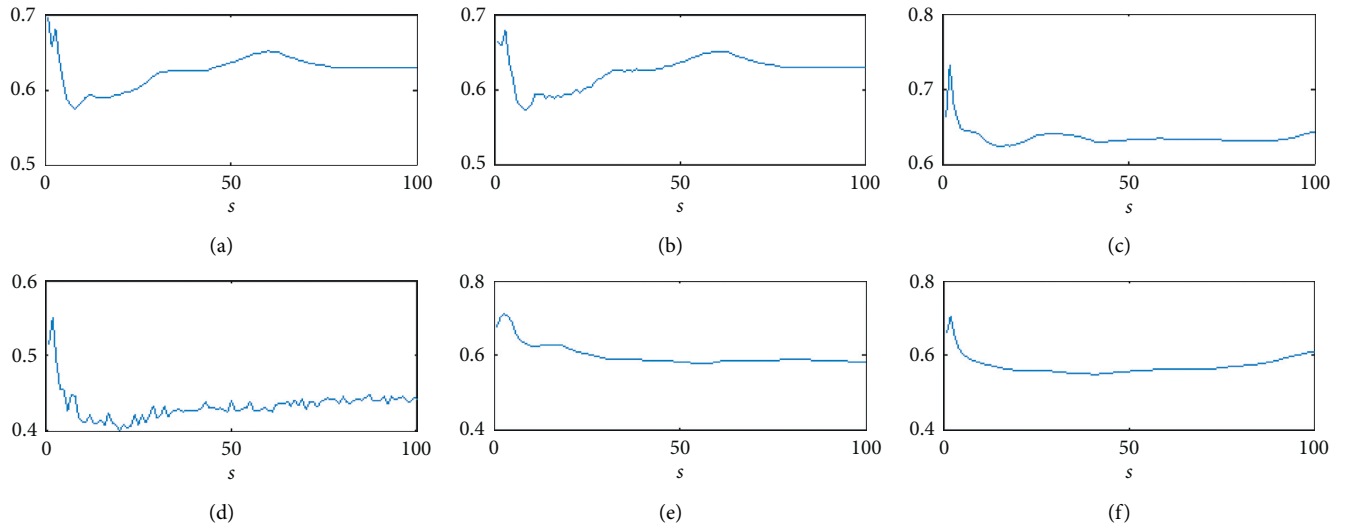


FIGURE 3: Some samples of  $\rho_{tm-DCCA_{max}}$  and  $\rho_{DCCA_{max}}$  at different time scales  $s$ .

Table 2 compares an overview of the three coefficients. It can be seen from Table 2 that statistics of DCCA and PCC are more similar to each other. The mean value of time-migrated DCCA is larger than DCCA and PCC, which means time-migrated DCCA detects more relationships of the dataset. The maximum of time-migrated DCCA is smaller than DCCA and PCC and the minimum is larger, which means the time-migrated DCCA has a smaller range. The smaller STD means a higher level data concentration of time-migrated DCCA and more sensitive to the threshold  $\theta$ .

### 3.2. Network Properties and Community Structure

**3.2.1. Evaluation of Coefficients.** The next section of the survey is concerned with network properties. First we analyze the giant component of the network with a different

threshold  $\theta$ . The giant component is an important quantity representing the largest fraction of the complex network, which is a measurement of the network effectiveness [44]. In Figure 5, we can see that the giant components of the DCCA stock network and time-migrated network decrease as the threshold  $\theta$  increases. Especially when threshold  $\theta$  increases from 1.32 to 2, the giant component of time-migrated DCCA network drops from 0.98 to 0.02 sharply. It is because most of the  $\rho_{TM-DCCA}$  are distributed in this range. As a result, the stock market networks are scale-free. In addition, we introduce the dataset of Shanghai and Shenzhen A-shares (2016–2018) to testify the applicability of the stock network model. We find that the stock market network is still scale-free and these statistics are also available for further research. We think that the network model remains robust across different periods and datasets.



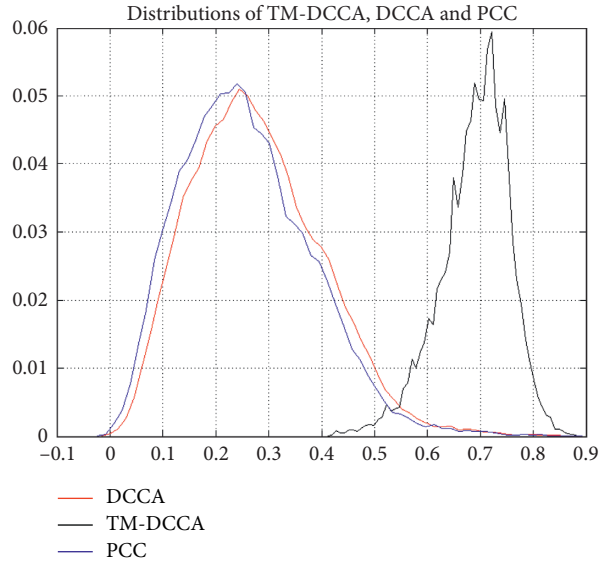


FIGURE 4: Distributions of time-migrated DCCA, DCCA and PCC coefficients.

**Input:** An empty complex network graph of stock market  $G = (V, E)$ , The sets of the stock market nodes  $v_i \in V$ , The weight matrix of the stock market  $w_{ij} \in W$ , The connection matrix of the stock market  $e_{ij} \in E$ , The threshold  $\theta$ , where  $i, j = 1, \dots, N$ ;

**Output:** The complex network graph of stock market

$G(V, E)$ ;

- (1) **for** each  $v_i \in V$  **do**
- (2)   add node  $v_i$  to  $V$  and update  $G = (V, E)$
- (3) **end**
- (4) **for** each  $e_{ij}$  and  $w_{ij}$  **do**
- (5)   **if**  $i \neq j$  and  $w_{ij} > \theta$  **then**
- (6)     set  $e_{ij} = 1$  and add edge  $e_{ij}$  to  $E$
- (7)     update  $G = (V, E)$ ;
- (8)   **end**
- (9) **end**

ALGORITHM 1: Complex network construction algorithm on stock market.

To construct the stock market network, we need a proper threshold  $\theta$  to determine the edge connectivity of the nodes. We divide all the  $\rho_{\text{TM-DCCA}}$  and  $\rho_{\text{DCCA}}$  into three conditions according to different thresholds by Table 3, suggested in [15]. In this paper, we consider that the pair of nodes have strong correlations if the  $\rho_{\text{TM-DCCA}}$  has a greater value (more than 1.62). Here we choose the threshold  $\theta_{\text{TM-DCCA}} = 1.62$  and  $\theta_{\text{DCCA}} = 1.25$  to construct the stock networks, which represents the stock network with connections. Therefore, about 33% of total nodes are included in the stock networks according to the threshold  $\theta_{\text{TM-DCCA}} = 1.62$  and  $\theta_{\text{DCCA}} = 1.25$ . Other isolated nodes are removed. Then, the connected nodes of the stock works are 106 and 101, the number of connections are 646 and 203. Finally, the average node degree is 12.189 and 4.02, average clustering coefficient is 0.066 and 0.77. With the threshold  $\theta$  defined, we describe

the network parameters in Table 4. The average degree of time-migrated DCCA network is much bigger than DCCA. In the time-migrated DCCA network, a smaller community has a bigger average degree which means that stocks in a smaller community have denser connections with each other.

**3.2.2. Evaluation of Coefficients.** In this section, we wish to compare the community structure of the stock market network. It helps us to analyze the relationships and network structure for further research. We apply the algorithm of Blondel to detect communities of the stock network which has been widely used in complex network analysis [45]. There are several advantages of the Blondel algorithm. The algorithm is a heuristic method that is fast and good for

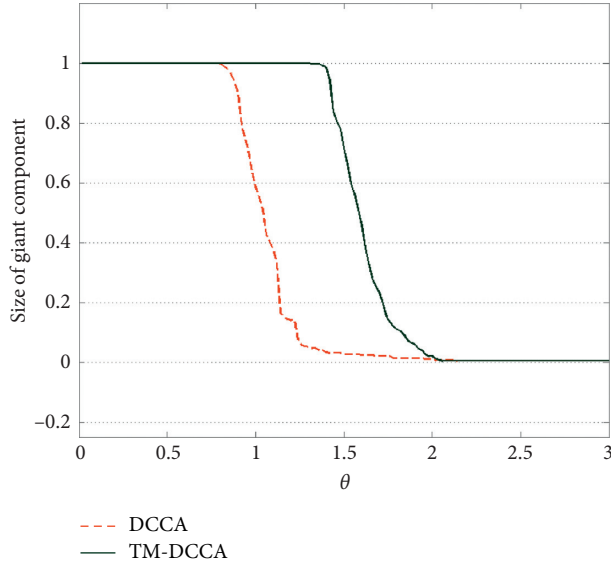


FIGURE 5: Giant components of time-migrated DCCA and DCCA coefficients.

TABLE 2: Statistical analysis of Time-migrated DCCA, DCCA, and PCC.

Statistics	Time-migrated DCCA	DCCA	PCC
Mean	0.6892	0.2769	0.2572
Max	0.8803	0.8900	0.8918
Min	0.4116	-0.0159	-0.0241
STD	0.0659	0.1234	0.1227
Skewness	-0.6612	0.5650	0.6173
Kurtosis	3.7184	3.4296	3.5463

TABLE 3: Correlation conditions of time-migrated DCCA and DCCA.

Correlation condition	Weak	Medium	Strong
Giant component	1.0-0.7	0.7-0.4	0.4-0.02
$\rho_{TM-DCCA}$	1.32-1.5	1.5-1.62	1.62-2.0
$\rho_{DCCA}$	0.78-0.96	0.96-1.08	1.08-1.76

large-scale networks. It is shown to outperform all other known community detection methods in terms of computation time in literature [45]. The algorithm is divided into two phases that are repeated iteratively. The first phase repeats the nodes allocation process until the maximum of the modularity is attained. The second phase consists in building a new network whose nodes are in the communities found during the first phase. A separating layout is used to reveal communities in stock market networks. As is shown in Figures 6-7, different node colors represent different communities and node label sizes reflect the node degree. Intuitively, nodes in the same community are stocks belonging to the same industry classification in the DCCA stock network in Figure 6. That matches our expectations. It is because the stock companies belonging to the same industry classification interact more frequently with each other and usually have closer relationships in reality. The

communities of time-migrated DCCA are density connected in comparison with DCCA.

The statistic details are shown in Table 5. We present 5 main communities in the DCCA network while 3 main communities in time-migrated DCCA in Table 5. We can see that the community sizes of time-migrated DCCA network are larger than DCCA. What stands out in the table is that the major business of DCCA network concentrated in one or two fields, but the major business of time-migrated DCCA network distributed in more than six fields. These findings suggest that the time-migrated DCCA network contains more relevant information than the DCCA network. Intuitively, the stock market networks can reflect important properties of the real stock market. This inspires us of a new idea: the stock network model could be helpful to analyze the effectiveness of the stock market policy according to the dynamic evolution process of the complex network system. Denser connections could give us more information about the relationships. Thus, we use the time-migrated DCCA stock network model to conduct our analysis on the effectiveness of price limit policy (Table 6).

3.3. *Simulation Results of Price Limit.* In this section, we attempt to provide some insight into the effectiveness of price limit by simulating the dynamic evolution of time-migrated DCCA stock network model. After evaluating the market stability and risk level under price limit and other situations, we find that the price limit has different effects at different stages of stock network evolution.

### 3.3.1. Experimental Indicators

*May-Wigner Stability Theorem.* May established a model for measuring the stability of a large complex ecosystem [46]. The theorem was approved and improved by researchers [47, 48]. The May-Wigner Stability theorem is used to investigate the stability of the financial system such as stock market complex systems [49, 50]. As a generalized stability indicator, the May-Wigner stability theorem is defined by 3 permanents: the size of the network  $N$ , the density of connections  $D$ , and the average interaction strength  $a$  [50].

$$NS = \sqrt{N} Da, \quad (18)$$

where  $NS$  represents the network stability. The system is considered stable when  $NS < 1$  and a smaller value of  $NS$  means the network is more stable. By definition, the density of connections  $D$  (graph density) and average interaction strength  $a$  (average node degree) in our research are given by

$$D = \frac{m}{C_N^2}, \quad (19)$$

$$a = \frac{m}{N},$$

where  $m$  is the number of connections and  $C_N^2$  is the maximum number of possible connections. The network stability factor has the following formula:

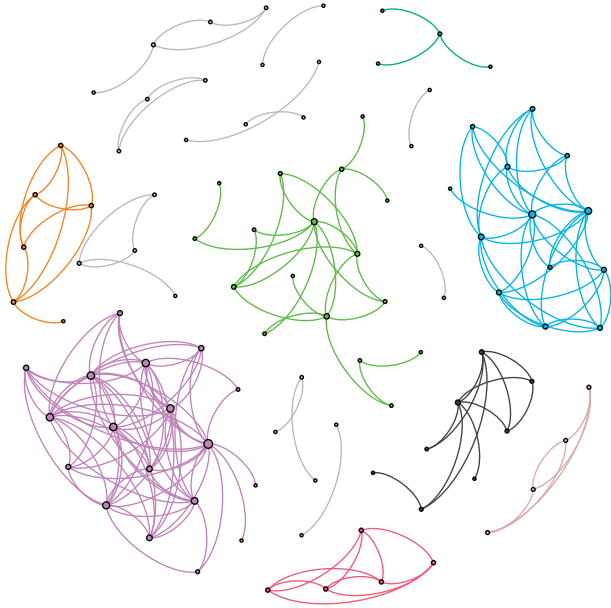


FIGURE 6: Topology graph of the DCCA stock network. Different node colors represent different communities and node and label sizes reflect the node degree.

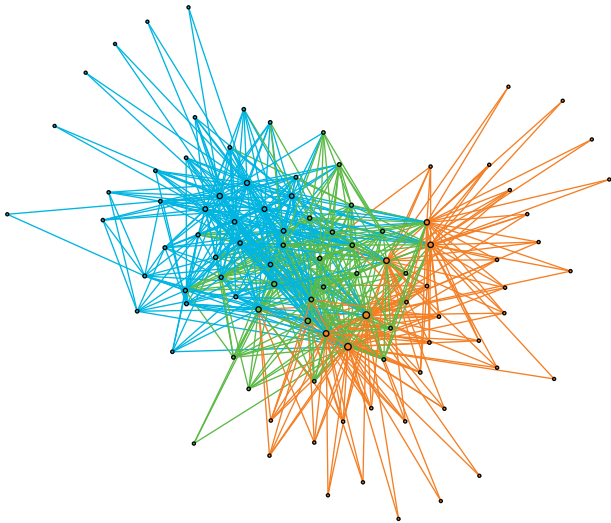


FIGURE 7: Topology graph of the time-migrated DCCA stock network. Different node colors represent different communities and node label sizes reflect the node degree.

TABLE 4: Network parameters of time-migrated DCCA and DCCA stock networks.

Parameters	$\theta_{\text{TM-DCCA}} = 1.62$	$\theta_{\text{DCCA}} = 1.25$
Number of nodes	300	300
Connected nodes	106	101
Number of connections	646	203
Average node degree	12.189	4.02
Graph density	0.116	0.04
Graph diameter	4	6
Average path length	2.283	1.796
Average clustering coefficient	0.066	0.77

$$NS = \sqrt{N Da} = \sqrt{N \frac{m}{c_N^2} \frac{m}{N}} = \frac{m^{(3/2)}}{N \sqrt{N-1}}. \quad (20)$$

So we can calculate the network stability  $NS(t)$  at time  $t$ .

In this study, we focus on the dynamic changes of the stock network. If the  $NS(t)$  changes rapidly, it means that the stability of the stock network varies dramatically, which represents a more volatile market. In order to measure the instability of the complex network, we define a dimensionless evaluation factor stability variation  $SV$  as follows:

$$SV = \frac{\sqrt{\left(\sum_{t=1}^n (NS(t) - \overline{NS(t)})/n\right)}}{\overline{NS(t)}}, \quad (21)$$

where  $NS(t)$  is the network stability of time  $t$  and a smaller value of  $SV$  means a milder stability fluctuation.

**Systemic Risk Evaluation.** An important area of risk management is the systemic risk evaluation. Studying the correlation coefficient matrix is an important topic of systemic risk evaluation [51]. We perform eigenvector technique on the stock network to measure the systemic risk. Using this approach, researchers have been able to evaluate the risk contributions of the stocks and calculate the systemic risk [44, 52, 53, 54, 55]. In this study, we evaluate risk contributions based on the eigenvector centrality:

$$R_i = \frac{1}{\lambda} \sum_{j=1}^N R_j g_{ij}, \quad i, j = 1, \dots, N, \quad (22)$$

where  $R_i$  is the risk contribution of stock  $i$ , which is defined to be proportional to the weighted sum of all the stocks connected to stock  $i$ .  $N$  is the total number of nodes in the stock network.  $g_{ij}$  is the element of correlation coefficient matrix  $G$ , which represents the  $\rho_{\text{TM-DCCA}}$  of stock  $i$  and stock  $j$ . It could be also expressed as in matrix form according to the eigenvector centrality theory:

$$G \vec{R} = \lambda \vec{R}, \quad (23)$$

where  $\lambda$  is the eigenvalue corresponding to the eigenvector. Then we compute the average of the risk contribution of all the stocks in the network and obtain the systemic risk of the whole stock market network at time  $t$ .

$$NR(t) = \frac{1}{N} \sum_{i=1}^N R_i, \quad i = 1, \dots, N. \quad (24)$$

And we evaluate the systemic risk under each conditions by

$$NR = \frac{1}{T} \sum_{t=1}^T NR_t, \quad t = 1, \dots, T. \quad (25)$$

**3.3.2. Simulation Results.** The fluctuations of the stock prices play an important role in the price discovery process, which provides crucial information on economic [56]. From

TABLE 5: Community Properties of DCCA stock market network.

DCCA communities ( $\theta_{DCCA} = 1.25$ )	Community A	Community B	Community C	Community D	Community E
Nodes	18	17	13	8	6
Major business	Securities service (17), pharmaceutical industry (1)	Mining industry (15), special equipment (2)	Banking (13)	Civil engineering (8)	Aerospace equipment (6)
Edges	77	26	39	12	11
Average node degree	8.56	3.059	6.000	3.000	3.667
Average path length	1.49	2.58	1.5	1.71	1.26
Graph density	0.503	0.191	0.500	0.429	0.733

TABLE 6: Community properties of the time-migrated DCCA stock market network.

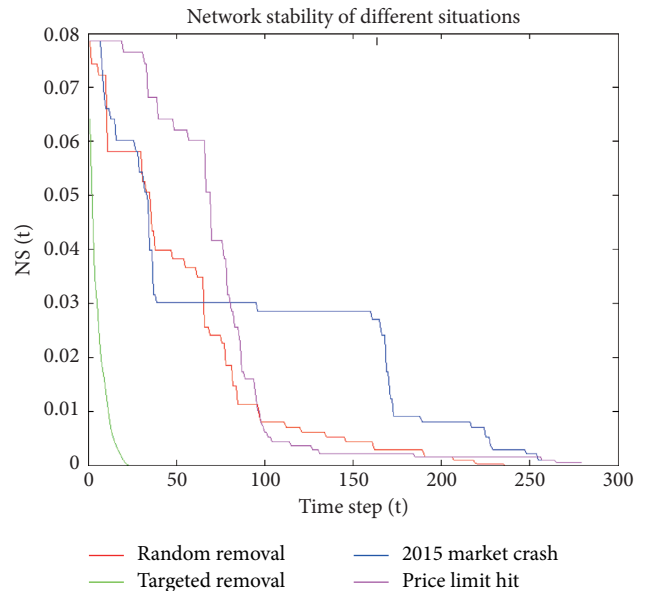
Time-migrated DCCA communities ( $\theta_{TM-DCCA} = 1.62$ )	Community A	Community B	Community C
Nodes	48	36	22
Major business	Securities service (9), banking (8), manufacturing (7), mining industry (4), pharmaceutical industry (3), real estate (3), energy industry (3), chemical industry (2), others (9)	Manufacturing (9), pharmaceutical industry (4), securities service (3), banking (2), real estate (2), transportation (2), information technology (2), civil engineering (2), others (10)	Mining industry (5), securities service (3), transportation (3), information technology (3), banking (2), others (6)
Edges	132	163	85
Average node degree	5.5	7.7	9.5
Average path length	2.24	1.72	1.97
Graph density	0.117	0.368	0.259

the perspective of price limit, the stock price is frenzied and the price discovery ability is weakened if a stock hits price limit [9, 11]. It leads to *market failure* somehow. At this point, we assume such an evaluation model: if the stock price  $i$  hits the price limit as it loses functionality, then node  $i$  will be removed from the network.

The simulation experiment is arranged as follows. First we calculate the stability factor and systemic risk factor  $NS(t)$  at time  $t$  ( $t = 1, \dots, T$ ). And we enhance price limit to analyze effectiveness of the time limit. Then we set the target removing and random removing strategy as the control group. Details of targeted removing and random removing strategy could be obtained in [57, 58]. Finally, we get the results of stability analysis and systemic risk analysis.

Figure 8 presents an overview of  $NS(t)$  of the time scale  $t$  for the four situations. Generally, we notice that all the stability factors exhibit a downward trend as evolution of the network because the number of nodes decreases faster than the edges. Especially we can see the following:

*Targeted Removal:* The nodes of the stock network are removed in accordance with the sequence from the biggest degree value to the smallest, which is called targeted removal of the most important nodes [58]. From Figure 8, we can see that the network stability of *targeted removal* curve (green line) drops off sharply at the beginning of the time step. Thus, this result indicates that the stock network is extremely vulnerable to targeted removal of the most important nodes.

FIGURE 8: Network stability  $NS(t)$  in different situations.

*Random Removal:* The nodes of the stock network are removed in a random order. Figure 8 shows that network stability factor of *random removal* (red line) has a relatively milder dynamic pattern compared to targeted removal. This indicates that the stock network is resistant to random removal.

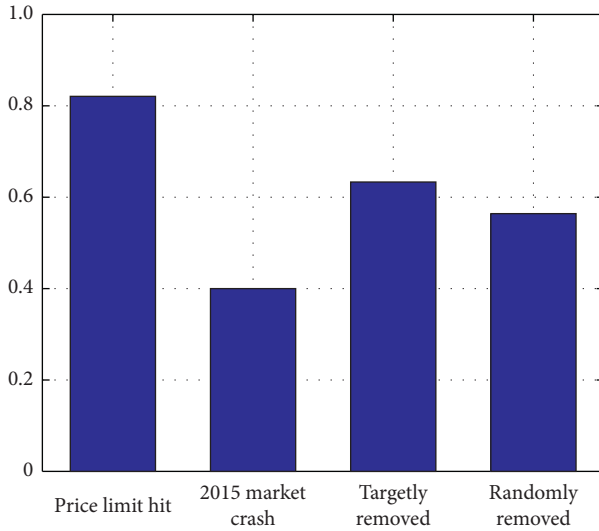


FIGURE 9: SV of different situations.

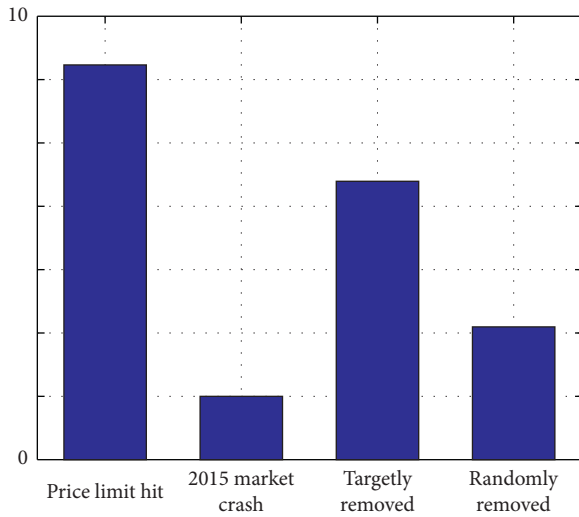


FIGURE 10: Systemic risk at different situations.

**2015 Market Crash:** The 2015 stock market began in June and lasted until August. About one thousand stocks hit the price limit. The stock market lost approximately 30 percent around the market crash. For the market crash simulation, we remove the node  $i$  if the stock  $i$  hits the price limit (10%) during the 2015 market crash. We can see that (blue line) the network factor of market crash drops at the beginning and a platform zone appears in the middle time, reflecting the actual situation of actual situation.

**Price Limit Hit:** In contrast to stock with 10% price limit, the price limit is set to 5% for investigating the network stability performance with an enhanced price limit level. In Figure 8, we find that the *price limit hit* (magenta line) drops more gently than market crash in the beginning, which means the network stability. Then the network stability factor of price limit hit presents a more precipitous drop than market crash afterward. It

means that the price limit hit could prevent violent variation, but also may lead to more violent variations afterwards.

In this case, it is possible to conclude that the *cooling-off effect* is significant when the price limit is first implemented, but the *magnet effect* also exists at the same time which takes the dominant in later time steps.

Figure 9 provides the normalized SV of different situations. Actually, price limit group indicates more the stability changes on average than the other three groups. It means that the price limit may cause stability changes in the stock market.

Figure 10 presents the systemic risk NR to compare the difference of the four situations. From Figure 10, we can see that systemic risk of *targeted removal* is higher than the *random removal*. And the price limit has the largest systemic risk. From the statistical results of systemic risk evaluation, we draw the conclusion that changing price limit has an effect on the market stabilization, and the systemic risk increases if the price limit is enhanced.

## 4. Conclusion

In this paper, we investigated the effectiveness of price limit on stock market based on the correlation study and complex network technology. Firstly, we proposed a time-migrated DCCA cross-correlation coefficient based on the DCCA cross-correlation coefficient. The time-migrated DCCA cross-correlation coefficient is suitable for nonstationary time series and detecting the time-migrated correlations, which ensure more relevant results than the DCCA method. Furthermore, we apply the threshold method to construct the stock networks and compare the topology properties and community structure of the stock network. We find that the time-migrated DCCA and DCCA stock network has different statistical properties and communities structures. And this fact has given us the opportunity to study the effectiveness of the price limit, especially during the stock market crash period. Finally, we simulated the dynamic evolution of the stock network under different situations. An interesting finding is that the price limit has different effects at different stages of evolution. We draw the conclusion that changing the price limit has an effect on market stabilization and the systemic risk, and the market stabilization will be lowered and the systemic risk will be increased if we enhance the price limit. We believe that such studies are relevant for a better understanding of the stock market and may lead to a better insight into the policy influence on the stock markets in further work. For example, the stock market network model could be helpful to evaluate the price limit performance in different situations. It may also contribute to risk management and stability regulation, which has a significant contribution to the stock market in reality.

## Data Availability

All data used in this study are available from the Choice Financial Terminal and <http://choice.eastmoney.com>.

## Conflicts of Interest

The authors declare that there are no conflicts of interest.

## Acknowledgments

This work was supported by National Natural Science Foundation of China (61673247), and the Research Fund for Distinguished Young Scholars and Excellent Young Scholars of Shandong Province (JQ201719).

## References

- [1] W.-Q. Huang, X.-T. Zhuang, and S. Yao, "A network analysis of the Chinese stock market," *Physica A: Statistical Mechanics and Its Applications*, vol. 388, no. 14, pp. 2956–2964, 2009.
- [2] C. K. Tse, J. Liu, and F. C. M. Lau, "A network perspective of the stock market," *Journal of Empirical Finance*, vol. 17, no. 4, pp. 659–667, 2010.
- [3] R. N. Mantegna, "Hierarchical structure in financial markets," *The European Physical Journal B*, vol. 11, no. 1, pp. 193–197, 1999.
- [4] G. Bonanno, F. Lillo, and R. N. Mantegna, "High-frequency cross-correlation in a set of stocks," *Quantitative Finance*, vol. 1, 2001.
- [5] M. Tumminello, T. Di Matteo, T. Aste, and R. N. Mantegna, "Correlation based networks of equity returns sampled at different time horizons," *The European Physical Journal B*, vol. 55, pp. 209–217, 2007.
- [6] G. F. Zebende, M. F. Da Silva, and A. Machado Filho, "DCCA cross-correlation coefficient differentiation: theoretical and practical approaches," *Physica A: Statistical Mechanics and Its Applications*, vol. 392, no. 8, pp. 1756–1761, 2013.
- [7] C. Hamzacebi and M. Pekkaya, "Determining of stock investments with grey relational analysis," *Expert Systems with Applications*, vol. 38, pp. 9186–9195, 2011.
- [8] G. F. Zebende, "DCCA cross-correlation coefficient: quantifying level of cross-correlation," *Physica A: Statistical Mechanics and Its Applications*, vol. 390, no. 4, pp. 614–618, 2011.
- [9] K. A. Kim and S. G. Rhee, "Price limit performance: evidence from the tokyo stock exchange," *The Journal of Finance*, vol. 52, no. 2, pp. 885–901, 1997.
- [10] X. Xiong, D. Nan, Y. Yang, and Z. Yongjie, "Study on market stability and price limit of Chinese stock index futures market: an agent-based modeling perspective," *PLoS One*, vol. 10, Article ID e0141605, 2015.
- [11] S. H. Chan, K. A. Kim, and S. G. Rhee, "Price limit performance: evidence from transactions data and the limit order book," *Journal of Empirical Finance*, vol. 12, no. 2, pp. 269–290, 2005.
- [12] L. Kristoufek, "Measuring correlations between non-stationary series with DCCA coefficient," *Physica A: Statistical Mechanics and Its Applications*, vol. 402, pp. 291–298, 2014.
- [13] L. Kristoufek, "Detrending moving-average cross-correlation coefficient: measuring cross-correlations between non-stationary series," *Physica A: Statistical Mechanics and Its Applications*, vol. 406, pp. 169–175, 2014.
- [14] Y. Yin and P. Shang, "Modified DFA and DCCA approach for quantifying the multiscale correlation structure of financial markets," *Physica A: Statistical Mechanics and Its Applications*, vol. 392, no. 24, pp. 6442–6457, 2013.
- [15] E. Guedes, A. Dionísio, P. J. Ferreira, and G. F. Zebende, "DCCA cross-correlation in blue-chips companies: a view of the 2008 financial crisis in the Eurozone," *Physica A: Statistical Mechanics and Its Applications*, vol. 479, pp. 38–47, 2017.
- [16] M. F. Da Silva, É. J. d. A. Leão Pereira, A. M. Da Silva Filho, A. P. Nunes De Castro, J. G. V. Miranda, and G. F. Zebende, "Quantifying cross-correlation between Ibovespa and Brazilian blue-chips: the DCCA approach," *Physica A: Statistical Mechanics and Its Applications*, vol. 424, pp. 124–129, 2015.
- [17] G. F. Zebende, A. A. Brito, and A. P. Castro, "DCCA cross-correlation analysis in time-series with removed parts," *Physica A: Statistical Mechanics and Its Applications*, vol. 545, p. 123472, 2020.
- [18] L. Piao and Z. Fu, "Quantifying distinct associations on different temporal scales: comparison of DCCA and Pearson methods," *Scientific Reports*, vol. 6, 2016.
- [19] R. T. Vassoler and G. F. Zebende, "DCCA cross-correlation coefficient apply in time series of air temperature and air relative humidity," *Physica A: Statistical Mechanics and Its Applications*, vol. 391, no. 7, pp. 2438–2443, 2012.
- [20] N. Yuan and Z. Fu, "Different spatial cross-correlation patterns of temperature records over China: a DCCA study on different time scales," *Physica A: Statistical Mechanics and Its Applications*, vol. 400, pp. 71–79, 2014.
- [21] Y. Chen, L. Cai, R. Wang et al., "DCCA cross-correlation coefficients reveals the change of both synchronization and oscillation in EEG of Alzheimer disease patients," *Physica A: Statistical Mechanics and Its Applications*, vol. 490, pp. 171–184, 2018.
- [22] B. Podobnik and H. E. Stanley, "Detrended cross-correlation analysis: a new method for analyzing two nonstationary time series," *Physical Review Letters*, vol. 100, 2008.
- [23] G.-J. Wang, C. Xie, Y.-J. Chen, and S. Chen, "Statistical properties of the foreign exchange network at different time scales: evidence from detrended cross-correlation coefficient and minimum spanning tree," *Entropy*, vol. 15, no. 12, pp. 1643–1662, 2013.
- [24] S. Li, X. Lu, and X. Liu, "Dynamic relationship between Chinese RMB exchange rate index and market anxiety: a new perspective based on MF-DCCA," *Physica A: Statistical Mechanics and Its Applications*, vol. 541, p. 123405, 2020.
- [25] Q. Ruan, S. Zhang, D. Lv, and X. Lu, "Financial liberalization and stock market cross-correlation: MF-DCCA analysis based on Shanghai-Hong Kong Stock Connect," *Physica A: Statistical Mechanics and Its Applications*, vol. 491, pp. 779–791, 2018.
- [26] X. Sun and Z. Liu, "Optimal portfolio strategy with cross-correlation matrix composed by DCCA coefficients: evidence from the Chinese stock market," *Physica A: Statistical Mechanics and Its Applications*, vol. 444, pp. 667–679, 2016.
- [27] T. M. Dao, F. McGroarty, and A. Urquhart, "Ultra-high-frequency lead-lag relationship and information arrival," *Quantitative Finance*, vol. 18, no. 5, pp. 725–735, 2018.
- [28] V. Arakelian and S. Qamhieh Hashem, "The leaders, the laggards, and the 'vulnerables'," *Risks*, vol. 8, p. 26, 2020.
- [29] K. Hou, "Industry information diffusion and the lead-lag effect in stock returns," *The Review of Financial Studies*, vol. 20, pp. 1113–1138, 2007.
- [30] A. W. Lo and A. C. MacKinlay, "When are contrarian profits due to stock market overreaction?," *The Review of Financial Studies*, vol. 3, pp. 175–205, 2015.
- [31] J.-P. Onnela, K. Kaski, and J. Kertész, "Clustering and information in correlation based financial networks," *The European Physical Journal B-Condensed Matter*, vol. 38, no. 2, pp. 353–362, 2004.

- [32] M. Ausloos and R. Lambiotte, "Clusters or networks of economies? A macroeconomy study through Gross Domestic Product," *Physica A: Statistical Mechanics and Its Applications*, vol. 382, no. 1, pp. 16–21, 2007.
- [33] S. Kumar and N. Deo, "Correlation and network analysis of global financial indices," *Physical Review E*, vol. 86, p. 026101, 2012.
- [34] H. Li, H. An, W. Fang, Y. Wang, W. Zhong, and L. Yan, "Global energy investment structure from the energy stock market perspective based on a heterogeneous complex network model," *Applied Energy*, vol. 194, 2017.
- [35] P. Gai and S. Kapadia, "Contagion in financial networks," *Proceedings of the Royal Society A: Mathematical, Physical and Engineering Sciences*, vol. 466, no. 2120, pp. 2401–2423, 2010.
- [36] R. Kali and J. Reyes, "Financial contagion on the international trade network," *Economic Inquiry*, vol. 48, no. 4, pp. 1072–1101, 2010.
- [37] L. Zhao, J. Wang, R. Huang, H. Cui, X. Qiu, and X. Wang, "Sentiment contagion in complex networks," *Physica A: Statistical Mechanics and Its Applications*, vol. 394, pp. 17–23, 2014.
- [38] J. Papenbrock and P. Schwendner, "Handling risk-on/risk-off dynamics with correlation regimes and correlation networks," *Financial Markets and Portfolio Management*, vol. 29, pp. 125–147, 2015.
- [39] N. Hautsch, J. Schaumburg, and M. Schienle, "Financial network systemic risk contributions," *Review of Finance*, vol. 19, no. 2, pp. 685–738, 2015.
- [40] M. Billio, M. Getmansky, A. W. Lo, and L. Pelizzon, "Econometric measures of connectedness and systemic risk in the finance and insurance sectors," *Journal of Financial Economics*, vol. 104, no. 3, pp. 535–559, 2012.
- [41] C. Liu and N. Arunkumar, "Risk prediction and evaluation of transnational transmission of financial crisis based on complex network," *Cluster Computing*, vol. 22, 2019.
- [42] D. A. Hsu, "A bayesian robust detection of shift in the risk structure of stock market returns," *Journal of the American Statistical Association*, vol. 77, no. 377, pp. 29–39, 1982.
- [43] U. Ayub, S. Z. A. Shah, and Q. Abbas, "Robust analysis for downside risk in portfolio management for a volatile stock market," *Economic Modelling*, vol. 44, pp. 86–96, 2015.
- [44] M. E. J. Newman, "The structure and function of complex networks," *SIAM Review*, vol. 45, no. 2, pp. 167–256, 2003.
- [45] V. D. Blondel, J. Guillaume, R. Lambiotte, and E. Lefebvre, "Fast unfolding of communities in large networks," *Journal of Statistical Mechanics: Theory and Experiment*, vol. 2008, 2008.
- [46] R. M. May, "Will a large complex system be stable?," *Nature*, vol. 238, no. 5364, pp. 413–414, 1972.
- [47] F. Juhász, *The May-Wigner Theorem For Block Random Matrices*, Computer and Automation Institute Hungarian Academy of Sciences, Budapest, Hungary, 1994.
- [48] Y. V. Fyodorov and B. A. Khoruzhenko, "Nonlinear analogue of the May–Wigner instability transition," *Proceedings of the National Academy of Sciences*, vol. 113, no. 25, pp. 6827–6832, 2016.
- [49] S. A. Levin, G. Sugihara, and R. M. May, "Complex systems Ecology for bankers," *Nature*, vol. 451, pp. 893–895, 2008.
- [50] R. H. Heiberger, "Stock network stability in times of crisis," *Physica A: Statistical Mechanics and Its Applications*, vol. 393, pp. 376–381, 2014.
- [51] A. Namaki, A. H. Shirazi, R. Raei, and G. R. Jafari, "Network analysis of a financial market based on genuine correlation and threshold method," *Physica A: Statistical Mechanics and Its Applications*, vol. 390, no. 21–22, pp. 3835–3841, 2011.
- [52] M. E. J. Newman and D. J. Watts, "Scaling and percolation in the small-world network model," *Physical Review E*, vol. 60, no. 6, pp. 7332–7342, 1999.
- [53] C. Fang and F. Marle, "Dealing with project complexity by matrix-based propagation modelling for project risk analysis," *Journal of Engineering Design*, vol. 24, no. 4, pp. 239–256, 2013.
- [54] M. Amiri, M. Zandieh, B. Vahdani, R. Soltani, and V. Roshanaei, "An integrated eigenvector-DEA-TOPSIS methodology for portfolio risk evaluation in the FOREX spot market," *Expert Systems With Applications*, vol. 37, no. 1, pp. 509–516, 2010.
- [55] P. Bonacich, "Factoring and weighting approaches to status scores and clique identification," *The Journal of Mathematical Sociology*, vol. 2, no. 1, pp. 113–120, 1972.
- [56] J. Hung, Y. Liu, I. Jiang, and S. Liang, "Price discovery and trading activity in Taiwan stock and futures markets," *Emerging Markets Finance and Trade*, vol. 56, pp. 963–976, 2020.
- [57] R. K. Albert, H. Jeong, and A. L. Barabasi, "Error and attack tolerance of complex networks," *Nature*, vol. 27, 2000.
- [58] P. Crucitti, V. Latora, M. Marchiori, and A. Rapisarda, "Error and attack tolerance of complex networks," *Nature*, vol. 340, pp. 378–382, 2000.

## Research Article

# Stability and Stabilization of Delayed Neural Networks with Hybrid Impulses

Kefa Zou <sup>1</sup>, Xuechen Li <sup>1</sup>, Nan Wang <sup>1</sup>, Jungang Lou <sup>2</sup>, and Jianquan Lu <sup>3,4</sup>

<sup>1</sup>School of Science, Xuchang University, Xuchang 461000, China

<sup>2</sup>Zhejiang Province Key Laboratory of Smart Management & Application of Modern Agricultural Resources, School of Information Engineering, Huzhou University, Huzhou 313000, China

<sup>3</sup>School of Mathematics, Southeast University, Nanjing 210096, China

<sup>4</sup>Key Laboratory of Complex Systems and Intelligent Computing in Universities of Shandong, School of Automation and Electrical Engineering, Linyi University, Linyi 276005, China

Correspondence should be addressed to Jianquan Lu; [jqluma@seu.edu.cn](mailto:jqluma@seu.edu.cn)

Received 16 July 2020; Revised 11 October 2020; Accepted 4 November 2020; Published 21 November 2020

Academic Editor: Giacomo Innocenti

Copyright © 2020 Kefa Zou et al. This is an open access article distributed under the Creative Commons Attribution License, which permits unrestricted use, distribution, and reproduction in any medium, provided the original work is properly cited.

In this paper, the stability and stabilization issues for a class of delayed neural networks with time-varying hybrid impulses are investigated. The hybrid effect of two types of impulses including both stabilizing and destabilizing impulses is considered simultaneously in the analysis of systems. To characterize the occurrence features of impulses, the concepts of average impulse interval and average impulse strength are employed. Based on the analysis of stability, a pinning impulsive controller which can ensure the global exponential stability of the studied neural networks is designed by pinning a small fraction of neurons. Finally, two numerical examples are given to illustrate the effectiveness of the proposed control schemes for delayed neural networks with hybrid impulses.

## 1. Introduction

During the past few decades, dynamic networks have been systematically studied due to their broad application background in different areas [1–9]. In recent years, in order to cater to the specific needs of modeling various practical systems, many kinds of dynamic networks with special structures have been developed, for example, [10–13] and the references therein. When networks encounter transient disturbance or abrupt dynamic variation in various instants, systems may display switching or impulsive behaviors [14, 15]. Consequently, impulsive neural networks, which can model various electronic or biological networks encountering instantaneous and abrupt changes frequently, have been extensively investigated in various fields of science and engineering [16–19]. On the contrary, time delays frequently appear in various dynamical systems [20, 21]. The existence of time delays in neural networks may induce more complex dynamical behaviors such as instability,

oscillations, and chaos [22–27]. Therefore, it is necessary to investigate effects of time delays and impulses on the stability of neural networks.

Generally, impulses can be divided into two categories according to their impact on systems. It is supposed that the impulses are destabilizing if the impulses can potentially destroy the stability of dynamical systems, while the impulses are considered to be stabilizing if they are potentially beneficial for the stabilization of dynamical systems. Stabilizing impulses can be considered as impulsive controllers, which can enhance the stabilization of dynamical systems. In the last several decades, stabilizing impulses and destabilizing impulses have been studied by a great many scholars [28–31]. At the same time, the impulsive control method has received many researchers' attention (see [32–36] and references therein). Particularly, stability or stabilization issue for dynamical systems with delays and impulses was investigated in [37–41] and references therein. In [42], a unified synchronization criterion for impulsive dynamical



networks subject to desynchronizing or synchronizing impulses was derived by using the average impulsive interval approach. In [43], some adequate conditions that can ensure the exponential synchronization of inertial memristor-based neural networks with time delay were given by utilizing the average impulsive interval approach. In [44], the pinning impulsive control strategy was proposed. By utilizing the Lyapunov method combined with the comparison principle, pinning stabilization of probabilistic Boolean networks subject to time delays was investigated in [45]. Synchronization problem for stochastic neural networks was studied by impulsively controlling partial states in [46]. Recently, networks with hybrid impulses were explored in [47, 48]. To reduce conservativeness, a novel piecewise Lyapunov–Krasovskii functional (LKF) was constructed by introducing a line-integral type Lyapunov function and some useful terms that take full advantage of the available information about the actual sampling pattern in [49].

In this paper, the concepts of average impulsive interval and average impulsive strength are introduced to characterize the features of hybrid impulses. Then, based on the Lyapunov method combined with the utilization of proper mathematical analysis techniques, the stability analysis for neural networks with time-varying delays and hybrid impulses is carried out. Under this circumstance, the classification of stabilizing and destabilizing impulses is not taken into account; just the overall effect of the impulses is taken into consideration. Furthermore, a pinning impulsive controller design procedure for the stabilization of the investigated neural networks is proposed based on the above analysis. In this controller, only a small fraction of variables is impulsively controlled to ensure the global and exponential stability of neural networks. The main contributions of this paper are summarized as follows: (1) a new concept of “average impulsive strength,” which can be used to characterize much wider range of impulsive sequences, is introduced to describe the hybrid impulses investigated in this paper. (2) By virtue of some proper disposing techniques relevant to average impulsive interval and average impulsive strength in the proof process of the main results, less conservative results can thereafter be obtained. (3) In consideration of the advantages of low cost and high efficiency of the pinning controller, the strategy that selects only a small fraction of neurons for impulsive control is adopted to achieve the stabilization of the delayed neural networks.

The remainder of this paper is arranged as follows: in Section 2, we propose the problem of stability and stabilization of delayed neural networks with hybrid impulses and give some necessary preliminaries. In Section 3, a criterion for determining the stability of delayed neural networks with hybrid impulses is established, and then a pinning impulsive controller is designed to stabilize delayed neural networks. In Section 4, numerical examples are given to illustrate our theoretical results. Finally, Section 5 presents the conclusion.

*Notation 1*. The standard notations are used in this paper.  $\mathbb{R}^+$  and  $\mathbb{R}^n$  denote the set of nonnegative real numbers and the  $n$ -dimensional Euclidean space.  $\mathbb{N}_+$  denotes the set of

positive integers. The superscript “T” represents the transpose of the matrix or vector. For  $x \in \mathbb{R}^n$ ,  $|x|$  denotes the Euclidean norm of  $x$ . For matrix  $A \in \mathbb{R}^n$ ,  $\|A\| = \sqrt{\lambda_{\max}(A^T A)}$ , where  $\lambda_{\max}(\cdot)$  represents the largest eigenvalue.  $\text{diag}(\dots)$  stands for a block-diagonal matrix. Given  $\tau > 0$ ,  $C([- \tau, 0], \mathbb{R}^n)$  denotes the family of continuous functions from  $[- \tau, 0]$  to  $\mathbb{R}^n$ .

## 2. Preliminaries

In this section, some preliminaries including model formulation, lemmas, and definitions are presented.

Consider the following neural network:

$$\dot{x}(t) = Cx(t) + Bg(x(t)) + Dg(x(t - \tau(t))) + I, \quad (1)$$

where  $x(t) = (x_1(t), x_2(t), \dots, x_n(t))^T \in \mathbb{R}^n$  is the state vector associated with the neurons;  $C = \text{diag}(c_1, c_2, \dots, c_n) < 0$  is the self-feedback matrix;  $B = (b_{ij})_{n \times n}$  and  $D = (d_{ij})_{n \times n}$  are the connection weight matrices;  $g(x(t)) = (g_1(x(t)), g_2(x(t)), \dots, g_n(x(t)))^T$  denotes the activation function of the neurons;  $I \in \mathbb{R}^n$  signifies constant external input; and  $\tau(t)$  represents the time-varying delays that satisfies  $0 \leq \tau(t) \leq \tau$ . For the nonlinear function  $g(\cdot)$ , we have the following assumption.

*Assumption 1.* Assume that  $g_i(\cdot)$  ( $i = 1, 2, \dots, n$ ) are globally Lipschitz continuous functions, i.e., there exist constants  $l_i > 0$  ( $i = 1, 2, \dots, n$ ) such that

$$|g_i(x_1) - g_i(x_2)| \leq l_i |x_1 - x_2|, \quad \text{for any } x_1, x_2 \in \mathbb{R}. \quad (2)$$

Denote  $L = \text{diag}(l_1, l_2, \dots, l_n)$ .

Let  $x^*$  be the equilibrium point of (1). For convenience, we can shift the intended equilibrium  $x^*$  to be original by letting  $y = x - x^*$ , and then system (1) can be transformed into

$$\dot{y}(t) = Cy(t) + Bf(y(t)) + Df(y(t - \tau(t))), \quad (3)$$

where  $y(t) = (y_1(t), y_2(t), \dots, y_n(t))^T \in \mathbb{R}^n$  is the state vector of the transformed system. It follows from (2) that the function  $f(y) = g(y + x^*) - g(x^*)$  satisfies

$$|f_i(x_1) - f_i(x_2)| \leq l_i |x_1 - x_2|, \quad \text{for any } x_1, x_2 \in \mathbb{R}. \quad (4)$$

In consideration of the time-varying impulse effects, the impulsive delayed neural network can be obtained in the following form:

$$\begin{cases} \dot{y}(t) = Cy(t) + Bf(y(t)) + Df(y(t - \tau(t))), & t \neq t_k, \\ y(t_k^+) = \alpha_k y(t_k^-), & k \in \mathbb{N}_+, \end{cases} \quad (5)$$

where  $\{t_1, t_2, t_3, \dots\}$  is a sequence of strictly increasing impulsive moments.  $\alpha_k \in \mathbb{R}$  represents the strength of impulses. We assume that  $y(t)$  is right-continuous at  $t = t_k$ , i.e.,  $y(t_k) = y(t_k^+)$ . Hence, the solutions of (5) are piecewise right-hand continuous functions which are discontinuous at  $t = t_k$  for  $k \in \mathbb{N}_+$ . The initial condition of (5) is given by  $y(t) = \phi(t) \in C([- \tau, 0], \mathbb{R}^n)$ .

**Definition 1.** (average impulsive interval; see [42]).  $T_a$  is called the average impulsive interval of the impulsive sequence  $\zeta = \{t_1, t_2, \dots\}$  if

$$\frac{T-t}{T_a} - N_0 \leq N_\zeta(T, t) \leq \frac{T-t}{T_a} + N_0, \quad \text{for all } T \geq t \geq 0, \quad (6)$$

where  $N_0$  is a positive integer and  $T_a$  is a positive number.  $N_\zeta(T, t)$  denotes the impulsive times of the impulsive sequence  $\zeta$  in the time interval  $(t, T)$ .

**Definition 2** (average impulsive strength).  $\alpha$  is called the average impulsive strength of the sequence  $\zeta(T, t) = \{t_1, t_{l+1}, \dots, t_{l+N_\zeta(T, t)-1}\}$  for all  $T \geq t \geq 0$  if

$$\begin{aligned} \alpha &= \frac{|\alpha_{N_\zeta(t, 0)}| + |\alpha_{N_\zeta(t, 0)+1}| + \dots + |\alpha_{N_\zeta(T, 0)-1}|}{\alpha} - N_1 \leq N_\zeta(T, t) \\ &\leq \frac{|\alpha_{N_\zeta(t, 0)}| + |\alpha_{N_\zeta(t, 0)+1}| + \dots + |\alpha_{N_\zeta(T, 0)-1}|}{\alpha} + N_1, \end{aligned} \quad (7)$$

where  $N_1$  is a positive integer and  $\alpha$  is a positive number.  $N_\zeta(T, t)$  denotes the impulsive times of the impulsive sequence  $\zeta$  in the time interval  $(t, T)$ .

Furthermore, inequality (7) implies that

$$\begin{aligned} \alpha \left(1 - \frac{N_1}{N_\zeta(T, t)}\right) &\leq \frac{|\alpha_{N_\zeta(t, 0)}| + |\alpha_{N_\zeta(t, 0)+1}| + \dots + |\alpha_{N_\zeta(T, 0)-1}|}{N_\zeta(T, t)} \\ &\leq \alpha \left(1 + \frac{N_1}{N_\zeta(T, t)}\right). \end{aligned} \quad (8)$$

**Remark 1.** The concept of average impulsive gain was proposed in [48], where the problem of the globally exponential synchronization of coupled neural networks with hybrid impulses was investigated. However, when the time-varying delays are taken into consideration simultaneously, this idea may fail to be applied to the analysis of the stability of delayed neural networks with hybrid impulses. To deal with the difficulties coming from time-varying delays, a new concept named ‘‘average impulsive strength’’ is introduced in this paper. The conditions of our concept are more strict, so it can ensure the establishment of the inequality in the comparison principle.

**Definition 3.** Impulsive neural networks (5) are said to be globally exponentially stable if there exist constants  $M > 0, \lambda > 0$ , and  $T_0 > 0$  such that, for any initial values,  $|y(t)|^2 \leq Me^{-\lambda t}$  holds for all  $t \geq T_0$ .

**Lemma 1** (see [42]). For any vectors  $x, y \in \mathbb{R}^n$ , scale  $\epsilon > 0$ , and positive definite matrix  $Q \in \mathbb{R}^{n \times n}$ , the following inequality holds:  $2x^T y \leq \epsilon x^T Q x + \epsilon^{-1} y^T Q^{-1} y$ .

**Lemma 2** (see [35]).  $\overline{m+1}$  Let  $0 \leq \tau_i(t) \leq \tau$ .  $F(t, u, \overline{u}_1, \overline{u}_2, \dots, \overline{u}_m): \mathbb{R}^+ \times \mathbb{R} \times \dots \times \mathbb{R} \rightarrow \mathbb{R}$  is nondecreasing in  $\overline{u}_i$  for each fixed  $(t, u, \overline{u}_1, \dots, \overline{u}_{i-1}, \overline{u}_{i+2}, \dots, \overline{u}_m)$ ,  $i = 1, 2, \dots, m$ , and  $I_k(u): \mathbb{R} \rightarrow \mathbb{R}$  is nondecreasing in  $u$ .

Suppose that

$$\begin{cases} D^+ u(t) \leq F(t, u(t), u(t - \tau_1(t)), \dots, u(t - \tau_m(t))), \\ u(t_k^+) \leq I_k(u(t_k^-)), \quad k \in \mathbb{N}_+, \\ D^+ v(t) > F(t, v(t), v(t - \tau_1(t)), \dots, v(t - \tau_m(t))), \\ v(t_k^+) \geq I_k(v(t_k^-)), \quad k \in \mathbb{N}_+. \end{cases} \quad (9)$$

Then,  $u(t) \leq v(t)$ , for  $-\tau \leq t \leq 0$ , implies that  $u(t) \leq v(t)$ , for  $t \geq 0$ .

### 3. Main Results

In this section, we will analyze the global exponential stability of delayed neural networks with hybrid impulses including both destabilizing and stabilizing impulses.

**Theorem 1.** Consider time-varying neural network (5) with hybrid impulses including both destabilizing and stabilizing impulses. Suppose that Assumption 1 holds and that the average impulsive interval of the impulsive sequence  $\zeta = \{t_1, t_2, \dots\}$  is  $T_a$ . Then, neural networks (5) with hybrid impulses are globally exponentially stable if the following inequality holds:

$$\eta_1 + M_0 q < 0, \quad (10)$$

where  $\eta_1 = p + 2 \ln \alpha / T_a$ ,  $p = \lambda_{\max}(C + C^T + BB^T + L^T L + DD^T)$ ,  $q = \lambda_{\max}(L^T L)$ , and  $M_0$  is a constant satisfying the following condition: when  $\alpha \geq 1$ ,  $M_0 = e^{2N_1} \alpha^{2N_0}$ ; otherwise,  $M_0 = e^{2N_1} \alpha^{-2N_0}$ .

**Proof.** Consider the Lyapunov function  $V(t) = y^T(t)y(t)$ . Then, the derivative of  $V(t)$  along the trajectories of system (5) can be obtained as follows:

$$\begin{aligned} D^+ V(t) &= y^T(t)(C + C^T)y(t) + 2y^T(t)Bf(y(t)) \\ &\quad + 2y^T(t)Df(y(t - \tau(t))), \quad t \in (t_{k-1}, t_k], k \in \mathbb{N}_+. \end{aligned} \quad (11)$$

By Lemma 1, one obtains

$$\begin{aligned} 2y^T(t)Bf(y(t)) &\leq y^T(t)BB^T y(t) + f^T(y(t))f(y(t)) \\ &\leq y^T(t)BB^T y(t) + y^T(t)L^T L y(t), \end{aligned} \quad (12)$$

$$\begin{aligned} 2y^T(t)Df(y(t - \tau(t))) &\leq y^T(t)DD^T y(t) + f^T(y(t - \tau(t))) \\ &\quad \cdot f(y(t - \tau(t))) \leq y^T(t)DD^T y(t) \\ &\quad + y^T(t - \tau(t))L^T L y(t - \tau(t)). \end{aligned} \quad (13)$$

From (11) to (13), it follows that

$$\begin{aligned}
D^+V(t) &\leq y^T(t)(C + C^T + BB^T + L^T L + DD^T)y(t) \\
&\quad + y^T(t - \tau(t))L^T L y(t - \tau(t)) \\
&\leq \lambda_{\max}(C + C^T + BB^T + L^T L + DD^T)V(t) \\
&\quad + \lambda_{\max}(L^T L)V(t - \tau(t)) = pV(t) + qV(t - \tau(t)), \\
&\quad t \in (t_{k-1}, t_k], k \in \mathbb{N}_+.
\end{aligned} \tag{14}$$

For  $t = t_k$ , one has

$$V(t_k^+) = y^T(t_k^+)y(t_k^+) = \alpha_k^2 y^T(t_k^-)y(t_k^-) = \alpha_k^2 V(t_k^-). \tag{15}$$

For any  $\varepsilon > 0$ , let  $v(t)$  be a unique solution of the following impulsive delay system:

$$\begin{cases} \dot{v}(t) = pv(t) + qv(t - \tau(t)) + \varepsilon, & t \neq t_k, \\ v(t_k^-) = \alpha_k^2 v(t_k^-), & t = t_k, k \in \mathbb{N}_+, \\ v(t) = |\phi(t)|^2, & -\tau \leq t \leq 0. \end{cases} \tag{16}$$

According to Lemma 2, one gets

$$v(t) \geq V(t), \quad t \geq 0. \tag{17}$$

By the formula for the variation of parameters, it follows from (16) that

$$v(t) = w(t, 0)v(0) + \int_0^t w(t, s)[qv(s - \tau(s)) + \varepsilon]ds, \tag{18}$$

where  $w(t, s), t > s \geq 0$ , is the Cauchy matrix of the linear system

$$\begin{cases} \dot{z}(t) = pz(t), & t \neq t_k, \\ z(t_k^+) = \alpha_k^2 z(t_k^-), & t = t_k, k \in \mathbb{N}_+. \end{cases} \tag{19}$$

According to the representation of the Cauchy matrix, we can obtain the following estimation: if  $N_\zeta(t, s) > 0$ , one has

$$\begin{aligned}
w(t, s) &= e^{p(t-s)} \prod_{s < t_k \leq t} \alpha_k^2 \\
&\leq e^{p(t-s)} \left( \frac{|\alpha_{N_\zeta(s, 0)}| + |\alpha_{N_\zeta(s, 0)+1}| + \cdots + |\alpha_{N_\zeta(t-s)-1}|}{N_\zeta(t-s)} \right)^{2N_\zeta(t-s)} \\
&\leq e^{p(t-s)} \left[ \alpha \left( 1 + \frac{N_1}{N_\zeta(t-s)} \right) \right]^{2N_\zeta(t-s)} \\
&\leq e^{2N_1} e^{p(t-s)} \alpha^{2N_\zeta(t-s)}.
\end{aligned} \tag{20}$$

Otherwise, when  $N_\zeta(t, s) > 0$ , one also has

$$w(t, s) = e^{p(t-s)} \leq e^{2N_1} e^{p(t-s)} \alpha^{2N_\zeta(t, s)}. \tag{21}$$

Since the average impulsive interval of the impulsive sequence  $\zeta = \{t_1, t_2, \dots\}$  is equal to  $T_a$ , we have

$$\frac{t-s}{T_a} - N_0 \leq N_\zeta(t, s) \leq \frac{t-s}{T_a} + N_0, \quad \text{for all } t \geq s \geq 0. \tag{22}$$

If  $\alpha \geq 1$ , it follows from (20) to (22) that

$$w(t, s) \leq e^{2N_1} e^{p(t-s)} \alpha^{2(t-s/T_a + N_0)} \leq \alpha^{2N_0} e^{2N_1} e^{(p+2\ln\alpha/T_a)(t-s)}. \tag{23}$$

Similarly, when  $\alpha < 1$ , it follows from (20) and (22) that

$$w(t, s) \leq e^{2N_1} e^{p(t-s)} \alpha^{2(t-s/T_a - N_0)} \leq \alpha^{-2N_0} e^{2N_1} e^{(p+2\ln\alpha/T_a)(t-s)}. \tag{24}$$

Letting  $\varepsilon \rightarrow 0$  and summarizing inequalities (23) and (24) give that there exists constant  $M_0 = \max\{\alpha^{2N_0} e^{2N_1}, \alpha^{-2N_0} e^{2N_1}\}$  such that

$$w(t, s) < M_0 e^{\eta_1(t-s)}, \tag{25}$$

where  $\eta_1 = p + 2\ln\alpha/T_a$ .

Let  $\eta = M_0 \sup_{-\tau \leq s \leq 0} |\phi(s)|^2$ . From (18) and (25), one obtains

$$v(t) \leq \eta e^{\eta_1 t} + \int_0^t M_0 e^{\eta_1(t-s)} [qv(s - \tau(s)) + \varepsilon] ds. \tag{26}$$

Define  $h(v) = v + \eta_1 + M_0 q e^{v\tau}$ . It follows from (10) that  $h(0) < 0$ . Since  $h(+\infty) = +\infty$  and  $\dot{h}(v) > 0$ , there exists a unique  $\lambda > 0$  such that

$$\lambda + \eta_1 + M_0 q e^{\lambda\tau} = 0. \tag{27}$$

On the contrary, it is obvious from (10) that  $M_0^{-1}\eta_1 + q < 0$ . Hence,

$$v(t) = |\phi(t)|^2 \leq \eta < \eta e^{-\lambda t} - \frac{\varepsilon}{M_0^{-1}\eta_1 + q}, \quad -\tau \leq t \leq 0. \tag{28}$$

Then, we claim

$$v(t) < \eta e^{-\lambda t} - \frac{\varepsilon}{M_0^{-1}\eta_1 + q}. \tag{29}$$

If inequality (29) is not true, there exists  $t^* > 0$  such that

$$v(t^*) \geq \eta e^{-\lambda t^*} - \frac{\varepsilon}{M_0^{-1}\eta_1 + q}, \tag{30}$$

$$v(t) < \eta e^{-\lambda t} - \frac{\varepsilon}{M_0^{-1}\eta_1 + q}, \quad t < t^*. \tag{31}$$

From (26) to (31), we have

$$\begin{aligned}
v(t^*) &\leq \eta e^{\eta_1 t^*} + \int_0^{t^*} M_0 e^{\eta_1(t^*-s)} [qv(s - \tau(s)) + \varepsilon] ds \\
&< e^{\eta_1 t^*} \left\{ \eta - \frac{\varepsilon}{M_0^{-1}\eta_1 + q} + \int_0^{t^*} M_0 e^{-\eta_1 s} \right. \\
&\quad \cdot \left[ q \left( \eta e^{-\lambda(s-\tau(s))} - \frac{\varepsilon}{M_0^{-1}\eta_1 + q} \right) + \varepsilon \right] ds \Big\}.
\end{aligned} \tag{32}$$

It is derived from (27) and (32) that

$$\begin{aligned}
v(t^*) &< e^{\eta_1 t^*} \left\{ \eta - \frac{\varepsilon}{M_0^{-1} \eta_1 + q} + \eta e^{-(\eta_1 + \lambda) t^*} \right. \\
&\quad \left. - \eta - \frac{\varepsilon}{M_0^{-1} \eta_1 + q} e^{-\eta_1 t^*} + \frac{\varepsilon}{M_0^{-1} \eta_1 + q} \right\} \\
&= \eta e^{-\lambda t^*} - \frac{\varepsilon}{M_0^{-1} \eta_1 + q},
\end{aligned} \tag{33}$$

which contradicts with (30), and so, (29) holds. Letting  $\varepsilon \rightarrow 0$ , one gets from (17) that

$$V(t) \leq v(t) \leq \eta e^{-\lambda t}. \tag{34}$$

By Definition 3, the solution  $y(t)$  of impulsive neural networks (5) is exponentially stable. The proof is hence completed.  $\square$

*Remark 2.* The concepts of average impulse interval [42, 43] and average impulsive strength are employed to characterize the features of hybrid impulses. The classification of stabilizing and destabilizing impulses is not taken into account; just the overall effect of the impulses is taken into consideration. By utilizing the comparison principle [35, 44], Lyapunov theory [35, 42–44], Young’s inequality technique [42, 43, 48], average impulsive interval approach [42, 43], and the concept of average impulsive strength, Theorem 1 presenting conditions of ensuring the global exponential stability of delayed neural networks (5) is derived.

In the following section, a pinning impulsive controller will be designed to globally and exponentially stabilize neural networks (5). In order to drive system (5) into the equilibrium point  $x^*$ , the following impulsive controller is constructed for  $l$  partial variables ( $l < n$ ):

$$u_i(t_k) = \begin{cases} 0, & i \notin \mathcal{D}(t_k), \\ \sum_{k=1}^{+\infty} \mu y_i(t) \delta(t - t_k), & i \in \mathcal{D}(t_k), \end{cases} \tag{35}$$

where  $\mu \in (-2, -1) \cup (-1, 0)$  is a constant, which means that the impulsive effects can be used to stabilize the delayed neural networks; the index set of  $l$  partial variables  $\mathcal{D}(t_k)$  which should be impulsively controlled is defined as follows: at time instant  $t_k$ , for the error of states of the partial variables  $y_1(t_k), y_2(t_k), \dots, y_n(t_k)$ , one can reorder the states such that  $|y_{p_1}(t_k)| \geq |y_{p_2}(t_k)| \geq \dots \geq |y_{p_n}(t_k)|$ .

Then, the index set of  $l$  controlled variables  $\mathcal{D}(t_k)$  is defined as  $\mathcal{D}(t_k) = \{p_1, p_2, \dots, p_l\}$ . After adding pinning impulsive controller (35) to the variables  $\mathcal{D}(t_k)$ , the controlled delayed neural networks can be rewritten as follows:

$$\begin{aligned}
\dot{y}(t) &= Cy(t) + Bf(y(t)) + Df(y(t - \tau(t))), \quad t \neq t_k, \\
y_i(t_k^+) &= \mu y_i(t_k^-) + y_i(t_k^-), \quad i \in \mathcal{D}(t_k), \\
y_i(t_k^+) &= y_i(t_k^-), \quad i \notin \mathcal{D}(t_k).
\end{aligned} \tag{36}$$

The initial conditions of delayed neural networks (36) are given by

$$y_i(t) = \phi_i(t) \quad -\tau \leq t \leq 0 \quad (i = 1, 2, \dots, n), \tag{37}$$

where  $\phi_i(t) \in C([- \tau, 0], \mathbb{R})$  with  $C([- \tau, 0], \mathbb{R})$  being the set of continuous functions from  $[- \tau, 0]$  to  $\mathbb{R}$ .

**Theorem 2.** Let  $\rho = n + l\mu(\mu + 2)/n \in (0, 1)$ . Suppose that Assumption 1 holds and that the average impulsive interval  $\zeta = \{t_1, t_2, \dots\}$  is  $T_a$ . Then, neural networks (36) are globally exponentially stabilized to the state  $x^*$  by pinning controller (35) if the following inequality holds:

$$\eta_2 + M_1 q < 0, \tag{38}$$

where  $\eta_2 = p + \ln \rho / T_a$ ,  $p = \lambda_{\max}(C + C^T + BB^T + L^T L + DD^T)$ ,  $q = \lambda_{\max}(L^T L)$ , and  $M_1 = \rho^{-N_0}$ .

*Proof.* Construct a Lyapunov function in the form of

$$V(t) = y^T(t)y(t) = \sum_{i=1}^n y_i^2(t). \tag{39}$$

By a similar analysis as Theorem 1, for any  $t \in [t_{k-1}, t_k]$ , taking the derivative of  $V(t)$  along the solution of (36) gives that

$$D^+V(t) \leq pV(t) + qV(t - \tau(t)). \tag{40}$$

For any  $k \in \mathbb{N}_+$ , we have

$$\begin{aligned}
V(t_k^+) &= \sum_{i=1}^n y_i^T(t_k^+) y_i(t_k^+) = \sum_{i \in \mathcal{D}(t_k)} (1 + \mu)^2 y_i^T(t_k^-) y_i(t_k^-) \\
&\quad + \sum_{i \notin \mathcal{D}(t_k)} y_i^T(t_k^-) y_i(t_k^-).
\end{aligned} \tag{41}$$

For any  $k \in \mathbb{N}_+$ , let  $\varphi(t_k^-) = \min\{|y_i(t_k^-)| : i \in \mathcal{D}(t_k)\}$  and  $\psi(t_k^-) = \max\{|y_i(t_k^-)| : i \notin \mathcal{D}(t_k)\}$ . According to the selection of parameters in set  $\mathcal{D}(t_k)$ , we have  $\varphi(t_k^-) \geq \psi(t_k^-)$ . Since  $\rho = 1 + l/n \cdot \mu(\mu + 2) \in (0, 1)$ , we get  $(1 - \rho)(n - l) = [\rho - (1 + \mu)^2]l$ . Hence, one has

$$\begin{aligned}
(1 - \rho) \sum_{i \notin \mathcal{D}(t_k)} y_i^T(t_k^-) y_i(t_k^-) &\leq (1 - \rho)(N - l)(\psi(t_k^-))^2 \\
&\leq (1 - \rho)(N - l)(\varphi(t_k^-))^2 \leq l[\rho - (1 + \mu)^2](\varphi(t_k^-))^2 \\
&\leq [\rho - (1 + \mu)^2] \sum_{i \in \mathcal{D}(t_k)} y_i^T(t_k^-) y_i(t_k^-),
\end{aligned} \tag{42}$$

which follows that

$$\begin{aligned}
(1 + \mu)^2 \sum_{i \in \mathcal{D}(t_k)} y_i^T(t_k^-) y_i(t_k^-) &+ \sum_{i \notin \mathcal{D}(t_k)} y_i^T(t_k^-) y_i(t_k^-) \\
&\leq \rho \sum_{i=1}^n y_i^T(t_k^-) y_i(t_k^-).
\end{aligned} \tag{43}$$

From (41) to (43), we have

$$V(t_k^+) \leq \rho V(t_k^-). \quad (44)$$

For any  $\varepsilon > 0$ , let  $v(t)$  be a unique solution of the following impulsive delayed system:

$$\begin{cases} \dot{v}(t) = p v(t) + q v(t - \tau_m(t)) + \varepsilon, & t \neq t_k, \\ v(t_k^+) = \rho v(t_k^-), & t = t_k, k \in \mathbb{N}_+, \\ v(t) = |\phi(t)|^2, & -\tau \leq t \leq 0. \end{cases} \quad (45)$$

According to Lemma 2, we can get

$$v(t) \geq V(t), \quad t \geq 0. \quad (46)$$

By the formula for the variation of parameters, it follows from (45) that

$$v(t) = w(t, 0)v(0) + \int_0^t w(t, s)[q v(s - \tau(s)) + \varepsilon] ds, \quad (47)$$

where  $w(t, s)$ ,  $t > s \geq 0$ , is the Cauchy matrix of the linear system

$$\begin{cases} \dot{z}(t) = p z(t), & t \neq t_k, \\ z(t_k^+) = \rho z(t_k^-), & t = t_k, k \in \mathbb{N}_+. \end{cases} \quad (48)$$

According to the representation of the Cauchy matrix, since  $0 < \rho < 1$  and  $t - s/T_a - N_0 \leq N_\zeta(t, s) \leq t - s/T_a + N_0$ , we can obtain the following estimation:

$$\begin{aligned} w(t, s) &= e^{p(t-s)} \prod_{s < t_k < t} \rho \leq e^{p(t-s)} \rho^{N_\zeta(t, s)} \leq e^{p(t-s)} \rho^{t-s/T_a - N_0} \\ &= M_1 e^{\eta_2(t-s)}, \end{aligned} \quad (49)$$

where  $M_1 = \rho^{-N_0}$  and  $\eta_2 = p + \ln \rho / T_a$ . Let  $M_2 = M_1 \sup_{-\tau \leq s \leq 0} |\phi(s)|^2$ . Then, it can be derived from (45) and (49) that

$$v(t) \leq M_2 e^{\eta_2 t} + \int_0^t M_1 e^{\eta_2(t-s)} [q v(s - \tau(s)) + \varepsilon] ds. \quad (50)$$

Define  $h(v) = v + \eta_2 + M_1 q e^{v\tau}$ . It follows from (38) that  $h(0) < 0$ . Since  $h(+\infty) = +\infty$  and  $\dot{h}(v) > 0$ , there exists unique  $\lambda > 0$  such that

$$\lambda + \eta_2 + M_1 q e^{\lambda\tau} = 0. \quad (51)$$

On the contrary, it is obvious from (38) that  $M_1^{-1} \eta_2 + q < 0$ . Hence,

$$v(t) = |\phi(t)|^2 < M_2 e^{-\lambda t} - \frac{\varepsilon M_1}{\eta_2 + M_1 q}, \quad -\tau \leq t \leq 0. \quad (52)$$

Then, we claim

$$v(t) < M_2 e^{-\lambda t} - \frac{\varepsilon M_1}{\eta_2 + M_1 q}. \quad (53)$$

If inequality (51) is not true, there exists  $t^* > 0$  such that

$$v(t^*) \geq M_2 e^{-\lambda t^*} - \frac{\varepsilon M_1}{\eta_2 + M_1 q}, \quad (54)$$

$$v(t) < M_2 e^{-\lambda t} - \frac{\varepsilon M_1}{\eta_2 + M_1 q}, \quad t < t^*. \quad (55)$$

From (50) and (55), we have

$$\begin{aligned} v(t^*) &\leq M_2 e^{\eta_2 t^*} + \int_0^{t^*} M_1 e^{\eta_2(t^*-s)} [q v(s - \tau(s)) + \varepsilon] ds \\ &< e^{\eta_2 t^*} \left\{ M_2 - \frac{\varepsilon M_1}{\eta_2 + M_1 q} + \int_0^{t^*} M_1 e^{-\eta_2 s} \right. \\ &\quad \cdot \left[ q \left( M_2 e^{-\lambda(s-\tau(s))} - \frac{\varepsilon M_1}{\eta_2 + M_1 q} \right) + \varepsilon \right] ds \Big\}. \end{aligned} \quad (56)$$

It is derived from (51) and (56) that

$$\begin{aligned} v(t^*) &< e^{\eta_2 t^*} \left\{ M_2 - \frac{\varepsilon M_1}{\eta_2 + M_1 q} + M_2 e^{-(\eta_2 + \lambda)t^*} - M_2 \right. \\ &\quad \left. + \frac{\varepsilon M_1}{\eta_2 + M_1 q} - \frac{\varepsilon M_1}{\eta_2 + M_1 q} e^{-\eta_2 t^*} \right\} = M_2 e^{-\lambda t^*} \\ &\quad - \frac{\varepsilon M_1}{\eta_2 + M_1 q}, \end{aligned} \quad (57)$$

which contradicts with (54), and so, (53) holds. Letting  $\varepsilon \rightarrow 0$ , one gets from (17) that

$$V(t) \leq v(t) \leq M_2 e^{-\lambda t}. \quad (58)$$

The proof is completed.  $\square$

## 4. Numerical Examples

Two numerical examples are presented to demonstrate the validity of the above results in this section.

*Example 1.* Consider neural networks (5) with the following parameters:

$$\begin{aligned} C &= \begin{bmatrix} -3 & 0 \\ 0 & -8 \end{bmatrix}, \\ B &= \begin{bmatrix} 0.3 & 0.1 \\ 0.2 & 0.2 \end{bmatrix}, \\ D &= \begin{bmatrix} 0.4 & 0.2 \\ 0 & 0.2 \end{bmatrix}, \\ L &= \begin{bmatrix} 0.1 & 0 \\ 0 & 0.2 \end{bmatrix}, \end{aligned} \quad (59)$$

and  $f(y(t)) = \tanh(0.8y(t))$ ,  $\tau(t) = e^t/1 + e^t$ , where  $y(t) = (y_1(t), y_2(t))^T$  is the state vector of the neural networks. By

calculation, we can easily know  $\eta_1 + M_0q = -3.5126$ . Figure 1 represents a hybrid impulsive sequence where  $T_a = 0.2, N_0 = 5, N_1 = 2$ , and  $\alpha = 1.2$ . The effect of the hybrid impulsive sequence is destabilizing.

According to Theorem 1, neural networks (5) with time-varying impulses will be globally exponentially stable if condition (10) is satisfied. Our numerical simulation draws the conclusion of Figure 2. From Figure 2, it can be observed that the state response of the neural networks tends to be stable quickly, which means the simulation results are consistent with the theory analysis.

*Example 2.* Consider neural networks (5) with

$$\begin{aligned}
 C &= \begin{bmatrix} 1 & 0 & 0 & 0 & 0 & 0 \\ 0 & -4 & 0 & 0 & 0 & 0 \\ 0 & 0 & -1 & 0 & 0 & 0 \\ 0 & 0 & 0 & -3 & 0 & 0 \\ 0 & 0 & 0 & 0 & -2 & 0 \\ 0 & 0 & 0 & 0 & 0 & -3 \end{bmatrix}, \\
 B &= \begin{bmatrix} 0.08 & 0 & -0.1 & 0 & 0 & 0 \\ 0 & 0.02 & 0 & 0.1 & -0.3 & 0 \\ -0.05 & 0 & -0.1 & 0.5 & 0 & 0.4 \\ 0.4 & 0.2 & -0.3 & 0.6 & -0.2 & 0.1 \\ 0 & 0 & 0 & 0.2 & -0.3 & 0 \\ 0.1 & -0.2 & 0 & 0 & 0.5 & -0.2 \end{bmatrix}, \\
 D &= \begin{bmatrix} 0.2 & 0.1 & 0 & 0 & 0 & 0 \\ 0 & 0.1 & 0.2 & 0.3 & 0 & 0 \\ 0.1 & 0 & -0.2 & 0 & 4 & 0.2 \\ 0 & 0.1 & 0 & 0.1 & 0.2 & 0.2 \\ 0 & 0.1 & 0.2 & 0.3 & 0 & 0 \\ 0.2 & 0.1 & 0.3 & 0 & 0 & 0.2 \end{bmatrix}, \\
 L &= \begin{bmatrix} 1 & 0 & 0 & 0 & 0 & 0 \\ 0 & 1 & 0 & 0 & 0 & 0 \\ 0 & 0 & 1 & 0 & 0 & 0 \\ 0 & 0 & 0 & 1 & 0 & 0 \\ 0 & 0 & 0 & 0 & 1 & 0 \\ 0 & 0 & 0 & 0 & 0 & 1 \end{bmatrix},
 \end{aligned} \tag{60}$$

and  $f(y(t)) = \tanh(0.8y(t))$ ,  $\tau(t) = e^t/1 + e^t$ , where  $y(t) = (y_1(t), y_2(t), \dots, y_6(t))^T$  is the state vector of the neural

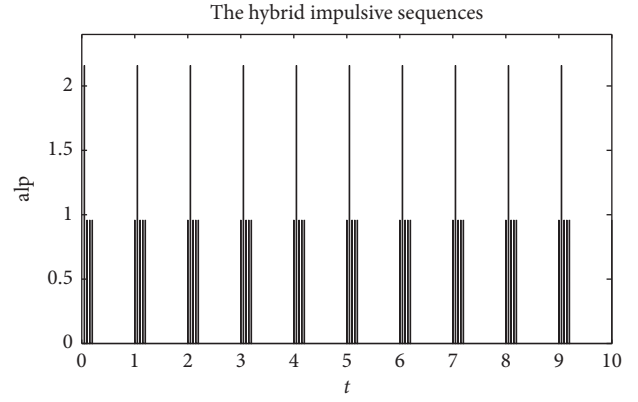


FIGURE 1: The hybrid impulsive sequence with  $T_a = 0.2, N_0 = 5, N_1 = 2$ , and  $\alpha = 1.2$ .

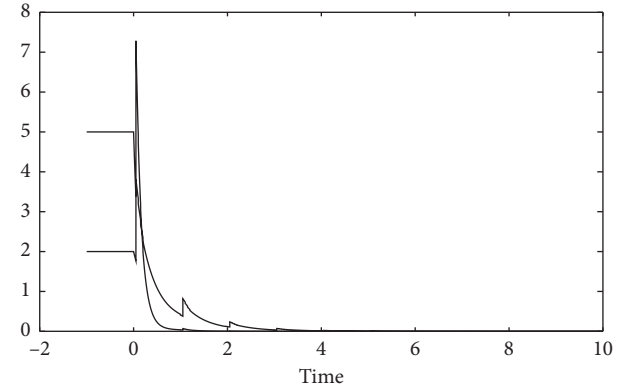


FIGURE 2: The state response of the neural networks in Theorem 1.

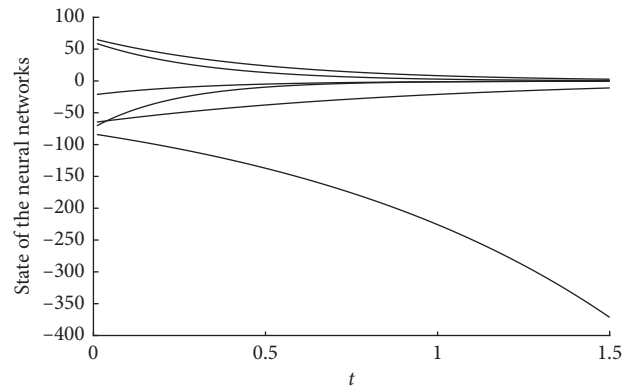


FIGURE 3: The state response of neural networks (5) without any controller in Theorem 2.

networks. The state response of neural networks (5) tends to be unstable without any controller, as is depicted in Figure 3. We select controller (35) with  $T_a = 0.25, N_0 = 3, \mu = -1.5, l = 3$ , and  $n = 6$ . By calculation, we can easily know  $\eta_2 + M_1q = -4.570469$ . According to Theorem 2, the

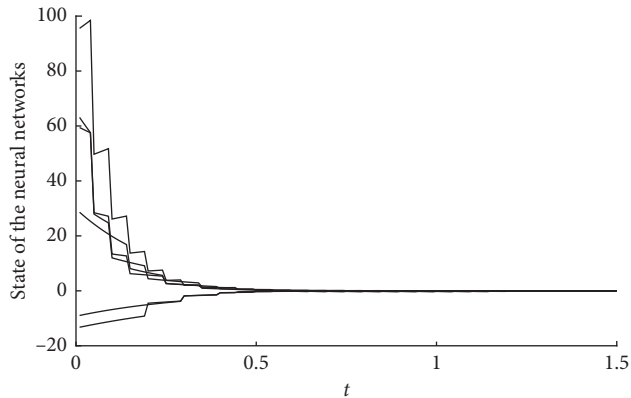


FIGURE 4: Simulation result for stabilization in Theorem 2.

pinning impulsive controller ensures global exponential stability of the considered neural networks. Simulation results approve the declared property (see Figure 4).

## 5. Conclusion

In this paper, the stability and stabilization problems of delayed neural networks with hybrid impulses have been studied. Based on Lyapunov stability theory combined with the comparison principle and the conception of average impulsive strength, a criterion for the exponential stability of delayed neural networks with hybrid impulses has been proposed. Then, a pinning impulsive controller has been designed to globally and exponentially stabilize the delayed neural networks with hybrid impulses. By revising the proof of the main results, some methods related to the concepts of average impulsive interval and average impulsive strength have been used to make the theoretical results less conservative. The derived stabilization criterion and the convergence rate are closely related with the proportion of the controlled neurons, time delay, impulsive strengths, and average impulsive interval of the neural networks. The validity of the theoretical results has been well explained by simulation results. In the future research, finite-time stabilization, persistent dwell-time, and state constraints will be included.

## Data Availability

This paper is a theoretical paper and does not need data analysis. The data used to support the findings of this study are cited at relevant places within the article.

## Conflicts of Interest

The authors declare that they have no conflicts of interest.

## Acknowledgments

This work was supported by the Zhejiang Provincial Natural Science Foundation of China (Grant no. LR20F020002) and the Fundamental Research Funds for the Central

Universities of Henan Province (Grant nos. 20B110018 and 19B110012).

## References

- [1] C. Huang, J. Lu, G. Zhai, J. Cao, G. Lu, and M. Perc, "Stability and stabilization in probability of probabilistic Boolean networks," *IEEE Transactions on Neural Networks and Learning Systems*, p. 1. In press, 2020.
- [2] C. Huang, X. Zhang, H.-K. Lam, and S.-H. Tsai, "Synchronization analysis for nonlinear complex networks with reaction-diffusion terms using fuzzy-model-based approach," *IEEE Transactions on Fuzzy Systems*, p. 1. In press, 2020.
- [3] K. Shi, J. Wang, Y. Tang, and S. Zhong, "Reliable asynchronous sampled-data filtering of T-S fuzzy uncertain delayed neural networks with stochastic switched topologies," *Fuzzy Sets and Systems*, vol. 381, no. 15, pp. 1–25, 2020.
- [4] C. Zhao, S. Zhong, X. Zhang, Q. Zhong, and K. Shi, "Novel results on nonfragile sampled-data exponential synchronization for delayed complex dynamical networks," *International Journal of Robust and Nonlinear Control*, vol. 30, no. 10, pp. 4022–4042, 2020.
- [5] R. Olfati-Saber and R. M. Murray, "Consensus problems in networks of agents with switching topology and time-delays," *IEEE Transactions on Automatic Control*, vol. 49, no. 9, pp. 1520–1533, 2004.
- [6] S. H. Strogatz, "Exploring complex networks," *Nature*, vol. 410, no. 6825, pp. 268–276, 2001.
- [7] M. E. J. Newman, "The structure and function of complex networks," *SIAM Review*, vol. 45, no. 2, pp. 167–256, 2003.
- [8] Y. Y. Wang, W. X. Zhou, J. Luo, H. C. Yan, H. Y. Pu, and Y. Peng, "Reliable intelligent path following control for a robotic airship against sensor faults," *IEEE/ASME Transactions on Mechatronics*, vol. 24, no. 6, pp. 2572–2582, 2020.
- [9] A. Chandrasekar, R. Rakkiyappan, J. Cao, and S. Lakshmanan, "Synchronization of memristor-based recurrent neural networks with two delay components based on second-order reciprocally convex approach," *Neural Networks*, vol. 57, pp. 79–93, 2014.
- [10] Y. Xia and J. Wang, "A general projection neural network for solving monotone variational inequalities and related optimization problems," *IEEE Transactions on Neural Networks*, vol. 15, no. 2, pp. 318–328, 2004.
- [11] Y. S. Xia and J. Wang, "A dual neural network for kinematic control of redundant robot manipulators," *IEEE Transactions on Systems Man & Cybernetics Part B Cybernetics A Publication of the IEEE Systems Man & Cybernetics Society*, vol. 31, no. 1, pp. 147–154, 2001.
- [12] S. Y. Zhu, J. G. Lou, Y. Liu, Y. Y. Li, and Z. Wang, "Event-triggered Control for the Stabilization of Probabilistic Boolean Control Networks," *Complexity*, vol. 2018, Article ID 9259348, 7 pages, 2018.
- [13] X. Yang, B. Chen, Y. Li, Y. Liu, and F. E. Alsaadi, "Stabilization of dynamic-algebraic Boolean control networks via state feedback control," *Journal of the Franklin Institute*, vol. 355, no. 13, pp. 5520–5533, 2018.
- [14] Y. Li, B. Li, Y. Liu, J. Lu, Z. Wang, and F. E. Alsaadi, "Set stability and stabilization of switched boolean networks with state-based switching," *IEEE Access*, vol. 6, pp. 35624–35630, 2018.
- [15] Y. Li, J. Lou, Z. Wang, and F. E. Alsaadi, "Synchronization of dynamical networks with nonlinearly coupling function under hybrid pinning impulsive controllers," *Journal of the Franklin Institute*, vol. 355, no. 14, pp. 6520–6530, 2018.

- [16] Z.-H. Guan and G. Chen, "On delayed impulsive Hopfield neural networks," *Neural Networks*, vol. 12, no. 2, pp. 273–280, 1999.
- [17] J. Lu, D. W. C. Ho, J. Cao, and J. Kurths, "Exponential synchronization of linearly coupled neural networks with impulsive disturbances," *IEEE Transactions on Neural Networks*, vol. 22, no. 2, pp. 329–336, 2011.
- [18] Y. Q. Wang, J. Q. Lu, and Y. J. Lou, "Halanay-type inequality with delayed impulses and its applications," *Science China*, vol. 62, no. 9, pp. 192–206, 2019.
- [19] J. Hu, G. Sui, X. Lv, and X. Li, "Fixed-time control of delayed neural networks with impulsive perturbations," *Nonlinear Analysis: Modelling and Control*, vol. 23, no. 6, pp. 904–920, 2018.
- [20] Z. G. Zeng, J. Wang, and X. X. Liao, "Global exponential stability of a general class of recurrent neural networks with time-varying delays," *IEEE Transactions on Circuits & Systems I: Fundamental Theory & Applications*, vol. 50, no. 10, pp. 1353–1358, 2003.
- [21] Z. Zeng and J. Wang, "Improved conditions for global exponential stability of recurrent neural networks with time-varying delays," *IEEE Transactions on Neural Networks*, vol. 17, no. 3, pp. 623–635, 2006.
- [22] J. Cao and D. W. C. Ho, "A general framework for global asymptotic stability analysis of delayed neural networks based on LMI approach," *Chaos, Solitons & Fractals*, vol. 24, no. 5, pp. 1317–1329, 2005.
- [23] S. Arik, "An analysis of exponential stability of delayed neural networks with time varying delays," *Neural Networks*, vol. 17, no. 7, pp. 1027–1031, 2004.
- [24] X. Li and J. Cao, "Adaptive synchronization for delayed neural networks with stochastic perturbation," *Journal of the Franklin Institute*, vol. 345, no. 7, pp. 779–791, 2008.
- [25] Y. Zhang and Q.-L. Han, "Network-based synchronization of delayed neural networks," *IEEE Transactions on Circuits and Systems I: Regular Papers*, vol. 60, no. 3, pp. 676–689, 2013.
- [26] Z. Wang, D. W. C. Ho, and X. Liu, "State estimation for delayed neural networks," *IEEE Transactions on Neural Networks*, vol. 16, no. 1, pp. 279–284, 2005.
- [27] K. Shi, Y. Tang, S. Zhong, C. Yin, X. Huang, and W. Wang, "Nonfragile asynchronous control for uncertain chaotic Lurie network systems with Bernoulli stochastic process," *International Journal of Robust and Nonlinear Control*, vol. 28, no. 5, pp. 1693–1714, 2018.
- [28] C. Li, Y. Y. Shen, and G. Feng, "Stabilizing effects of impulses in delayed BAM neural networks," *IEEE Transactions on Circuits and Systems II: Express Briefs*, vol. 55, no. 12, pp. 1284–1288, 2008.
- [29] C. Li, C. Li, and C. Liu, "Destabilizing effects of impulse in delayed BAM neural networks," *Modern Physics Letters B*, vol. 23, no. 29, pp. 3503–3513, 2009.
- [30] C. Li, S. Wu, G. G. Feng, and X. Liao, "Stabilizing effects of impulses in discrete-time delayed neural networks," *IEEE Transactions on Neural Networks*, vol. 22, no. 2, pp. 323–329, 2011.
- [31] L. Pan and J. Cao, "Robust stability for uncertain stochastic neural network with delay and impulses," *Neurocomputing*, vol. 94, no. 3, pp. 102–110, 2012.
- [32] T. Yang, L.-B. Yang, and C.-M. Yang, "Impulsive control of Lorenz system," *Physica D: Nonlinear Phenomena*, vol. 110, no. 1–2, pp. 18–24, 1997.
- [33] J. Cao, D. W. C. Ho, and Y. Yang, "Projective synchronization of a class of delayed chaotic systems via impulsive control," *Physics Letters A*, vol. 373, no. 35, pp. 3128–3133, 2009.
- [34] S. Chen, Q. Yang, and C. Wang, "Impulsive control and synchronization of unified chaotic system," *Chaos, Solitons & Fractals*, vol. 20, no. 4, pp. 751–758, 2004.
- [35] Z. Yang and D. Xu, "Stability analysis and design of impulsive control systems with time delay," *IEEE Transactions on Automatic Control*, vol. 52, no. 8, pp. 1448–1454, 2007.
- [36] K. Udhayakumar, R. Rakkiyappan, J.-d. Cao, and X.-g. Tan, "Mittag-Leffler stability analysis of multiple equilibrium points in impulsive fractional-order quaternion-valued neural networks," *Frontiers of Information Technology & Electronic Engineering*, vol. 21, no. 2, pp. 234–246, 2020.
- [37] X. Li, T. Caraballo, R. Rakkiyappan, and X. Han, "On the stability of impulsive functional differential equations with infinite delays," *Mathematical Methods in the Applied Sciences*, vol. 38, no. 14, pp. 3130–3140, 2015.
- [38] X. Li, J. Shen, and R. Rakkiyappan, "Persistent impulsive effects on stability of functional differential equations with finite or infinite delay," *Applied Mathematics and Computation*, vol. 329, pp. 14–22, 2018.
- [39] X. Yang, X. D. Li, X. Xi, and P. Duan, "Review of stability and stabilization for impulsive delayed systems," *Mathematical Biosciences & Engineering*, vol. 15, no. 6, pp. 1495–1515, 2018.
- [40] X. Li, X. Yang, and T. Huang, "Persistence of delayed cooperative models: impulsive control method," *Applied Mathematics and Computation*, vol. 342, pp. 130–146, 2019.
- [41] X. Li, D. O'Regan, and H. Akca, "Global exponential stabilization of impulsive neural networks with unbounded continuously distributed delays," *IMA Journal of Applied Mathematics*, vol. 80, no. 1, pp. 85–99, 2015.
- [42] J. Lu, D. W. C. Ho, and J. Cao, "A unified synchronization criterion for impulsive dynamical networks," *Automatica*, vol. 46, no. 7, pp. 1215–1221, 2010.
- [43] R. Rakkiyappan, D. Gayathri, G. Velmurugan, and J. Cao, "Exponential synchronization of inertial memristor-based neural networks with time delay using average impulsive interval approach," *Neural Processing Letters*, vol. 50, no. 3, pp. 2053–2071, 2019.
- [44] J. Lu, J. Kurths, J. Cao, N. Mahdavi, and C. Huang, "Synchronization control for nonlinear stochastic dynamical networks: pinning impulsive strategy," *IEEE Transactions on Neural Networks and Learning Systems*, vol. 23, no. 2, pp. 285–292, 2012.
- [45] P. Liu, L. Li, K. Shi, and J. Lu, "Pinning stabilization of probabilistic boolean networks with time delays," *IEEE Access*, vol. 8, pp. 154050–154059, 2020.
- [46] Y. Li, "Impulsive synchronization of stochastic neural networks via controlling partial states," *Neural Processing Letters*, vol. 46, no. 1, pp. 59–69, 2017.
- [47] X. Ji, J. Lu, J. Lou, J. Qiu, and K. Shi, "A unified criterion for global exponential stability of quaternion-valued neural networks with hybrid impulses," *International Journal of Robust and Nonlinear Control*, vol. 30, pp. 8098–8116, 2020, In press.
- [48] N. Wang, X. Li, J. Lu, and F. E. Alsaadi, "Unified synchronization criteria in an array of coupled neural networks with hybrid impulses," *Neural Networks*, vol. 101, pp. 25–32, 2018.
- [49] Y. Wang, H. Shen, and D. Duan, "On stabilization of quantized sampled-data neural-network-based control systems," *IEEE Transactions on Cybernetics*, vol. 47, no. 10, pp. 3124–3135, 2017.



## Research Article

# Fractional-Order Iterative Learning Control with Initial State Learning for a Class of Multiagent Systems

Xungen Li,<sup>1,2</sup> Shuaishuai Lv ,<sup>1,2</sup> Mian Pan,<sup>1</sup> Qi Ma,<sup>1</sup> and Wenyu Cai<sup>1</sup>

<sup>1</sup>The College of Electronics and Information, Hangzhou Dianzi University, Hangzhou 310018, China

<sup>2</sup>Pujiang Microelectronics and Intelligent Manufacturing Research Institute of Hangzhou Dianzi University, Jinhua 322200, China

Correspondence should be addressed to Shuaishuai Lv; lvshuai@hdu.edu.cn

Received 11 June 2020; Revised 19 September 2020; Accepted 1 October 2020; Published 28 October 2020

Academic Editor: Oh-Min Kwon

Copyright © 2020 Xungen Li et al. This is an open access article distributed under the Creative Commons Attribution License, which permits unrestricted use, distribution, and reproduction in any medium, provided the original work is properly cited.

To solve the consensus problem of fractional-order multiagent systems with nonzero initial states, both open- and closed-loop PD <sup>$\alpha$</sup> -type fractional-order iterative learning control are presented. Considering the nonzero states, an initial state learning mechanism is designed. The finite time convergences of the proposed methods are discussed in detail and strictly proved by using Lebesgue-p norm theory and fractional-order calculus. The convergence conditions of the proposed algorithms are presented. Finally, some simulations are applied to verify the effectiveness of the proposed methods.

## 1. Introduction

Fractional-order multiagent systems (FOMASs) is composed of multiple agents, which can coordinate with each other to perceive the external environment, and apply fractional-order calculus principle. Due to the autonomy, fault tolerance, flexibility, scalability, and collaboration capabilities of the FOMASs, it can be applied to the intelligent environment perception and intelligent operation, such as air formation control, traffic vehicle control, data convergence, sensor networks, and so on [1–4]. In order to realize the wide application of FOMASs, it is necessary to design the coordinated control effectively, including consensus control, formation control, coalescence control, and rendezvous control. And the consensus problem is the basic problem in FOMASs distributed coordination control. Its purpose is to design an appropriate distributed consensus control protocol based on the neighbor states of the agent and its own state information, so that the states of all the agents converge to the same value at a specific position or a certain moment.

The consensus problem of FOMASs was studied in [5] for the first time, in which the relationship between the consensus problem of FOMAS and the number of agents

and fractional orders was discussed, and some control strategies were given to improve the convergence speed of the FOMASs. In the same year, Cao and Ren [6] also applied the consensus theory to the formation control problem of FOMASs. Since then, the research and application of FOMASs consensus problems have been emerging, including linear fractional-order multiagents [7–10] and nonlinear fractional-order multiagents [11–14]. Song and Cao [7] used the stability theory of FOSSs and linear matrix inequality to study the consensus problem of linear FOMASs. And then they further considered the robust consensus problem of linear FOMASs when the fractional order satisfies  $\alpha \in (0, 2)$ [8]. Yu et al. [9] used the algebraic graph theory tool and the Lyapunov method to study the consensus problem of nonlinear FOMASs with a leader-following structure. Similarly, in [10, 11], the adaptive control and the sampling data control were designed to solve the consensus problem of nonlinear and linear FOMASs with and without leader-following structure, and some sufficient and necessary conditions related to fractional order, coupling gain, and Laplacian matrix spectrum were obtained to ensure that the system can achieve consensus. For the study of nonlinear FOMASs, there are also literatures [12–14].

However, most of the research just consider the asymptotic convergence problem of FOMASs, which means the tracking errors of the fractional-order agents gradually converge to zero as time increases. On some special occasions, such as industrial automatic production lines, the asymptotic convergence cannot meet the actual demands. As we all know, fractional-order iterative learning control (FOILC) methods for repetitive running systems can achieve complete tracking problems in finite time [15,16]. In [17,18], both distributed  $D^\alpha$ - and  $PD^\alpha$ -type FOILC were proposed and applied to linear FOMASs with fixed topology. Furthermore, for the linear time-varying integer-order system, Luo et al. proposed a FOILC framework with initial state learning and presented sufficient and necessary conditions for open-loop and closed-loop  $D^\alpha$ -type FOILC. But for FOMASs, it has not been researched using open and closed FOILC.

In the literature [17], the consensus problem of FOMASs is discussed using FOLIC. However, the authors just considered the zero initial states of FOMASs, which must ensure the strict positioning of the initial state during the iteration process. In this paper, for linear time-varying FOMASs with fixing the initial states over the directed graph, we design several fractional iterative learning controllers with the initial states learning algorithms. The contributions are summarized as follows. First, considering the nonzero initial state of FOMASs, we propose three different forms of fractional-order iterative learning updating laws. Second, an initial state learning algorithm together with the FOILC updating laws is designed. Finally, the convergences of the proposed algorithm are discussed and the convergence conditions are presented. The theoretical analysis and simulation experiments verify the effectiveness of the proposed method. The results show that both the tracking errors and the nonzero initial states can tend to zero in finite time as the iterative number increases.

The remainder of this paper is organized as follows. Section 2 overviews the related theories related to this article, including the graph theory, the definition of fractional calculus, and the problem formulation. The algorithm design and analysis employing FOILC with initial learning are discussed in Section 3. Section 4 demonstrates the simulation results to verify the effectiveness of the proposed methods. And briefly, conclusions are presented in Section 5.

## 2. Preliminaries

In this part, first, we introduce some basic definitions, lemmas, and properties, which will be used in the following sections.

**2.1. Graph Theory.** Consider  $N$  multiagents with the same dynamic. The direct graph  $\mathbb{G} = \{\mathbb{V}, \mathbb{E}, \mathbf{M}\}$  is used to describe the information transfer between multiagents, where  $\mathbb{V} = \{v_1, \dots, v_N\}$  is the node set,  $\mathbb{E} \subseteq \mathbb{V} \times \mathbb{V}$  is the edge set, and  $\mathbf{M} = (a_{ik})_{N \times N}$  is the adjacency matrix of the direct graph.  $(k, i) \in \mathbb{E} \subseteq \mathbb{V} \times \mathbb{V}$  is a direct edge of the agents  $k$  and  $i$ . The set

of neighbors of the  $i$ th agent is denoted by  $\mathbb{N}_i = \{k \in \mathbb{V}: (k, i) \in \mathbb{E}\}$ . The matrix element  $a_{ik} > 0$  represents node  $k$  passing information to node  $i$ ; otherwise,  $a_{ik} = 0$ . Here, the communication topology graph has no self-loop phenomenon, namely,  $a_{ii} = 0$ .  $\mathbf{D} = \text{diag}\{d_i, i \in \mathbb{S}_N\}$  is defined as the degree matrix, where  $d_i = \sum_{k=1}^N a_{ik}$ , and  $\mathbf{L} = \mathbf{D} - \mathbf{M}$  is the Laplacian matrix of the direct graph.

**2.2. The Norm.** In this paper, the vector Euclidian norm and its induced matrix norm is defined as  $\|\cdot\|$ .  $\mathbf{I}_m \in \mathbb{R}^{m \times m}$  is the identity matrix.  $\mathbb{C}^m[0, T]$  is defined as a function set and the  $m$ th derivative of  $\mathbb{C}^m[0, T]^{\wedge \#}$  is continuous over a finite time interval  $[0, T]$ .  $\mathbb{R}$  and  $\mathbb{N}$  are the sets of real and natural numbers.  $\mathbb{S}_N = \{0, 1, \dots, N\}$ . Denote the Kronecker product by  $\otimes$ , for some matrices  $\mathbf{A}, \mathbf{B}, \mathbf{C}$ , and  $\mathbf{D}$ , the following properties will be satisfied such that

$$k(\mathbf{A} \otimes \mathbf{B}) = k\mathbf{A} \otimes \mathbf{B} = \mathbf{A} \otimes k\mathbf{B}, \quad (1)$$

$$(\mathbf{A} + \mathbf{B}) \otimes \mathbf{C} = \mathbf{A} \otimes \mathbf{C} + \mathbf{B} \otimes \mathbf{C}, \quad (2)$$

$$(\mathbf{A} \otimes \mathbf{B})(\mathbf{C} \otimes \mathbf{D}) = \mathbf{AC} \otimes \mathbf{BD}, \quad (3)$$

$$\|\mathbf{A} \otimes \mathbf{B}\| = \|\mathbf{A}\| \cdot \|\mathbf{B}\|. \quad (4)$$

**Definition 1.** Assuming the continuous vector function  $\mathbf{f}: [0, T] \rightarrow \mathbb{R}^n \mathbf{f}(t) = [f^1(t), f^2(t), \dots, f^n(t)]^T$ , the Lebesgue- $p$  norm of  $\mathbf{f}(t)$  is defined as

$$\|\mathbf{f}(t)\|_p = \left[ \int_0^T \left( \max_{1 \leq i \leq n} |f^i(t)| \right)^p dt \right]^{(1/p)}, \quad 1 \leq p < \infty. \quad (5)$$

**Lemma 1** (see [19]). Assuming the functions  $\mathbf{g}(t) \in \mathbb{L}^q[0, T]$  and  $\mathbf{h}(t) \in \mathbb{L}^p[0, T]$ , then the convolution generalized Yong inequality of the functions  $\mathbf{g}(t)$  and  $\mathbf{h}(t)$  is

$$\|(\mathbf{g} * \mathbf{h})(t)\|_r \leq \|\mathbf{g}(t)\|_q \|\mathbf{h}(t)\|_p, \quad (6)$$

where  $1 \leq p, q, r \leq \infty$ ,  $(1/r) = (1/p) + (1/q) - 1$ , and  $(\mathbf{g} * \mathbf{h})(t) = \int_0^t \mathbf{g}(t - \tau) \mathbf{h}(\tau) d\tau$  is the convolution integral of  $\mathbf{g}(t)$  and  $\mathbf{h}(t)$ . In particular, if  $r = p$ , the inequality is converted to  $\|(\mathbf{g} * \mathbf{h})(t)\|_p \leq \|\mathbf{g}(t)\|_1 \|\mathbf{h}(t)\|_p$ .

### 2.3. Fractional Calculus

**Definition 2** (see [21]). The [21, 22] Riemann–Liouville fractional integrals of  $f(t)$  with order  $\alpha \in (0, 1)$  are defined as

$${}_t D_t^{-\alpha} f(t) = \frac{1}{\Gamma(\alpha)} \int_{t_0}^t (t - \tau)^{\alpha-1} f(\tau) d\tau, \quad (t > t_0), \quad (7)$$

$${}_t D_t^{-\alpha} f(t) = \frac{1}{\Gamma(\alpha)} \int_t^T (\tau - t)^{\alpha-1} f(\tau) d\tau, \quad (t < T),$$

where  $\Gamma(\cdot)$  is gamma function. The left- and right-sided Caputo derivatives are

$$\begin{aligned} {}_t^C D_t^\alpha f(t) &= {}_t^C D_t^{-(\lceil \alpha \rceil - \alpha + 1)} \left[ \frac{d^{\lceil \alpha \rceil + 1}}{dt^{\lceil \alpha \rceil + 1}} f(t) \right], \quad (t > t_0), \\ {}_t^C D_T^\alpha f(t) &= {}_t^C D_T^{-(\lceil \alpha \rceil - \alpha + 1)} \left[ \frac{d^{\lceil \alpha \rceil + 1}}{dt^{\lceil \alpha \rceil + 1}} f(t) \right], \quad (t < T), \end{aligned} \quad (8)$$

where  $\alpha \in \mathbf{R}^+$  and  $\lceil \alpha \rceil$  means the integral part of  $\alpha$ .

**Lemma 2** (see [20]). *Suppose the functions  $f(t), g(t)$  are continuous in  $[0, T]$ , and  ${}_t^C D_T^\alpha f(t), {}_0^C D_T^\alpha g(t) (t \in [0, T])$  exist, then the fractional integration by parts is*

$$\int_0^T ({}_t^C D_T^\alpha f(t)) g(t) dt = \int_0^T f(t) ({}_0^C D_T^\alpha g(t)) dt. \quad (9)$$

**Definition 3** (see [20, 23]). The Mittag-Leffler function can be described as

$$E_{\alpha, \beta}(z) = \sum_{k=0}^{\infty} \frac{z^k}{\Gamma(\alpha k + \beta)} \quad (\alpha > 0, \beta > 0, z \in \mathbf{C}^{n \times n}). \quad (10)$$

Particularly, when  $\beta = 1$ , we can obtain

$$E_{\alpha, 1}(z) = E_\alpha(z) = \sum_{k=0}^{\infty} \frac{z^k}{\Gamma(\alpha k + 1)}, \quad (\alpha > 0, z \in \mathbf{C}^{n \times n}). \quad (11)$$

**Lemma 3** (see [20]). *Let  $\Phi_{\alpha, \beta}(A, t) = t^{\beta-1} E_{\alpha, \beta}(At^\alpha) t \in [0, +\infty) \alpha > 0, \beta > 0, z \in \mathbf{C}^{n \times n}$ , then we have*

$$\begin{aligned} {}_t^C D_t^{1-\alpha} f(t) \Phi_{\alpha, 1}(A, t - \tau) &= \Phi_{\alpha, \alpha}(A, t - \tau), \quad 0 < \alpha < 1, \\ \frac{d}{d\tau} \Phi_{\alpha, 1}(A, t - \tau) &= -\Phi_{\alpha, \alpha}(A, t - \tau) A, \quad \alpha > 0, A \in \mathbf{C}^{n \times n}. \end{aligned} \quad (12)$$

**Lemma 4** (see [23]). *For the initial value problem*

$$\begin{cases} {}_t^C D_t^\alpha x(t) = Ax(t) + Bu(t), \\ x(t_0) = x_0. \end{cases}, \quad A \in \mathbf{C}^{n \times n}, B \in \mathbf{C}^{n \times p}, 0 < \alpha < 1. \quad (13)$$

The Volterra-type nonlinear integral equation can be obtained as

$$x(t) = \Phi_{\alpha, 1}(A, t)x_0 + \int_{t_0}^t \Phi_{\alpha, \alpha}(A, t - \tau)Bu(\tau)d\tau. \quad (14)$$

*Property 1.* If  $\mathbf{f}(t) \in \mathbf{C}(t_0, \infty)$ , then  $D^{1-\alpha} D^\alpha \mathbf{f}(t) = \mathbf{f}^{(1)}(t)$ ,  $\alpha \in (0, 1)$ , where  $\mathbf{f}^{(1)}(t) = (d/dt)\mathbf{f}(t)$ .

### 3. Problem Description

Considering  $N$  homogeneous fractional-order linear time-delay MASSs, it is assumed that each agent is completely nonregular and has repeated operational characteristics in a

finite time interval. At the  $i$ th iteration, the dynamics of the  $j$ th agent can be described as follows:

$$\begin{cases} {}_0^C D_t^\alpha \mathbf{x}_{i,j}(t) = \mathbf{A}\mathbf{x}_{i,j}(t) + \mathbf{B}\mathbf{u}_{i,j}(t), \\ \mathbf{y}_{i,j}(t) = \mathbf{C}\mathbf{x}_{i,j}(t), \end{cases} \quad (15)$$

where  $t \in [0, T]$ ,  ${}_0^C D_t^\alpha \mathbf{x}_{i,j}(t)$  is the left-sided  $\alpha$ -order derivative of  $\mathbf{x}_{i,j}(t)$ ,  $\alpha \in (0, 1)$ .  $\mathbf{x}_{i,j}(t) \in \mathbb{R}^m$  is the state vectors,  $\mathbf{u}_{i,j}(t) \in \mathbb{R}^{m_1}$  and  $\mathbf{y}_{i,j}(t) \in \mathbb{R}^{m_2}$  are the input and output vectors, respectively, and  $\mathbf{A}, \mathbf{B}, \mathbf{C}$  are constant matrices with  $m \times m$ ,  $m \times m_1$ , and  $m_2 \times m$ .

The expected trajectory  $\mathbf{y}_d(t)$  on the finite-time interval  $[0, T]$  is generated by the virtual leader and it is described as

$$\begin{cases} {}_0^C D_t^\alpha \mathbf{x}_d(t) = \mathbf{A}\mathbf{x}_d(t) + \mathbf{B}\mathbf{u}_d(t), \\ \mathbf{y}_d(t) = \mathbf{C}\mathbf{x}_d(t), \end{cases} \quad (16)$$

where  $\mathbf{u}_d(t)$  is the desired control input, and it is continuous and unique control input.

If the virtual leader is the agent 0, the new graph can be expressed as  $\overline{\mathbb{G}} = \{0 \cup \mathbb{V}, \overline{\mathbb{E}}, \overline{\mathbb{M}}\}$ , where  $\overline{\mathbb{E}}$  and  $\overline{\mathbb{M}}$  are the new edge set and the new adjacency matrix of  $\overline{\mathbb{G}}$ . The purpose is to design appropriate FOILC algorithms that enable each agent in the network topology to track the leader's trajectory over a finite time interval.

$\xi_{i,j}(t)$  is defined as the distributed information of the  $j$ th agent, which is measured or received from other agents at the  $i$ th iteration. Consider

$$\xi_{i,j}(t) = \sum_{k \in \mathbb{N}_j} a_{j,k} (\mathbf{y}_{i,k}(t) - \mathbf{y}_{i,j}(t)) + s_j (\mathbf{y}_d(t) - \mathbf{y}_{i,j}(t)), \quad (17)$$

where  $a_{j,k}$  is the entry of adjacency matrix  $\mathbf{M}$ ,  $s_j = 1$  if the  $j$ th agent can obtain the desired trajectory, and  $s_j = 0$  otherwise.

The tracking error of the  $j$ th agent is defined as  $\mathbf{e}_{i,j}(t) = \mathbf{y}_d(t) - \mathbf{y}_{i,j}(t)$ . Then, equation (17) can be reorganized as

$$\xi_{i,j}(t) = \sum_{k \in \mathbb{N}_j} a_{j,k} (\mathbf{e}_{i,j}(t) - \mathbf{e}_{i,k}(t)) + s_j \mathbf{e}_{i,j}(t). \quad (18)$$

Define column stack vectors in the  $i$ th iteration

$$\begin{cases} \mathbf{x}_i(t) = [\mathbf{x}_{i,1}(t)^T, \mathbf{x}_{i,2}(t)^T, \dots, \mathbf{x}_{i,N}(t)^T]^T, \\ \mathbf{e}_i(t) = [\mathbf{e}_{i,1}(t)^T, \mathbf{e}_{i,2}(t)^T, \dots, \mathbf{e}_{i,N}(t)^T]^T, \\ \mathbf{u}_i(t) = [\mathbf{u}_{i,1}(t)^T, \mathbf{u}_{i,2}(t)^T, \dots, \mathbf{u}_{i,N}(t)^T]^T, \\ \xi_i(t) = [\xi_{i,1}(t)^T, \xi_{i,2}(t)^T, \dots, \xi_{i,N}(t)^T]^T. \end{cases} \quad (19)$$

According to (19), (18) can be reorganized in a compact form

$$\xi_i(t) = ((\mathbf{L} + \mathbf{S}) \otimes \mathbf{I}_m) \mathbf{e}_i(t), \quad (20)$$

where  $L$  is the Laplacian matrix of graph  $\mathbb{G}$ ,  $\mathbf{I}_m$  is unit matrix, and  $\mathbf{S} = \text{diag}\{s_j, j \in \mathbb{S}_N\}$ .

Similarly, equation (15) can be rearranged as

$$\begin{cases} {}_0^C D_t^\alpha \mathbf{x}_i(t) = (\mathbf{I}_N \otimes \mathbf{A})\mathbf{x}_i(t) + (\mathbf{I}_N \otimes \mathbf{B})\mathbf{u}_i(t). \\ \mathbf{y}_i(t) = (\mathbf{I}_N \otimes \mathbf{C})\mathbf{x}_i(t). \end{cases} \quad (21)$$

**3.1. Open-Loop PD $^\alpha$ -type FOILC.** For FOMASs described by (15), considering the nonzero initial state, the open-loop PD $^\alpha$ -type FOILC algorithm with initial state learning is proposed as follows:

$$\begin{cases} \mathbf{u}_{i+1,j}(t) = \mathbf{u}_{i,j}(t) + \Gamma_{P1}\xi_{i,j}(t) + \Gamma_{D10} {}_0^C D_t^\alpha \xi_{i,j}(t), \\ \mathbf{x}_{i+1,j}(0) = \mathbf{x}_{i,j}(0) + \mathbf{B}\Gamma_{D1}\xi_{i,j}(0). \end{cases} \quad (22)$$

Similar to (20), the updating law (22) can be rewritten as

$$\begin{cases} \mathbf{u}_{i+1}(t) = \mathbf{u}_i(t) + ((\mathbf{L} + \mathbf{S}) \otimes \Gamma_{P1})\mathbf{e}_i(t) + ((\mathbf{L} + \mathbf{S}) \otimes \Gamma_{D1}) {}_0^C D_t^\alpha \mathbf{e}_i(t), \\ \mathbf{x}_{i+1}(0) = \mathbf{x}_i(0) + ((\mathbf{L} + \mathbf{S}) \otimes \mathbf{B}\Gamma_{D1})\mathbf{e}_i(0). \end{cases} \quad (23)$$

In order to facilitate the convergence analysis of the proposed methods, the following assumptions hold.

*Assumption 1.* CB is of full column rank.

*Remark 1.* In order to guarantee the flawless tracking performance, a typical supposition, i.e., identical initialization condition, is needed to be made in the ILC design. Remember that accurate tracking can only be accomplished with perfect initial conditions.

*Assumption 2* (see [17]). The graph  $\overline{\mathbb{G}}$  contains a spanning tree with the leader being the root.

*Remark 2.* This supposition is a prerequisite for the FOMASs consensus tracking problem, which means all followers can receive the leader's information directly or indirectly. Otherwise, due to the absence of data to make their control inputs accurate, the isolated agents cannot keep track of the leader's trajectory.

**Theorem 1.** Consider the FOMASs (15) and under the communication graph  $\overline{\mathbb{G}}$ , if Assumption 1 and 2 are satisfied. Distributed PD $^\alpha$ -type updating rule (23) is applied to the FOMASs (15). If the matrices  $\mathbf{A}, \mathbf{B}, \mathbf{C}$  and the learning gains  $\Gamma_{P1}$  and  $\Gamma_{D1}$  satisfy the following condition:

$$\rho_1 = \|\mathbf{I} - (\mathbf{L} + \mathbf{S}) \otimes \mathbf{C}\mathbf{B}\Gamma_{D1}\| + \beta < 1, \quad (24)$$

where  $\beta = \|\mathbf{I}_N \otimes \mathbf{C}\| \|(\mathbf{L} + \mathbf{S}) \otimes (\mathbf{B}\Gamma_{P1} + \mathbf{A}\mathbf{B}\Gamma_{D1})\| \|\Phi_{\alpha,\alpha}(\mathbf{I}_N \otimes \mathbf{A}, t)\|_1$ , then  $\lim_{i \rightarrow \infty} \|\mathbf{e}_{i+1}(t)\|_p = 0$ . Namely, the output  $\mathbf{y}_i(t)$  converges uniformly to the desired trajectory  $\mathbf{y}_d(t)$  as  $i \rightarrow \infty$ .

*Proof.* The convergence discussed is as follows.

Based on Lemma 4, we can write the FOMASs (15) as follows:

$$\begin{aligned} \mathbf{x}_i(t) &= \Phi_{\alpha,1}(\mathbf{I}_N \otimes \mathbf{A}, t)\mathbf{x}_i(0) \\ &+ \int_0^t \Phi_{\alpha,\alpha}(\mathbf{I}_N \otimes \mathbf{A}, t - \tau)(\mathbf{I}_N \otimes \mathbf{B})\mathbf{u}_i(\tau)d\tau. \end{aligned} \quad (25)$$

According to equalities (21), (23), and (25), we can obtain

$$\begin{aligned} \mathbf{e}_{i+1}(t) &= \mathbf{I}_N \otimes \mathbf{y}_d(t) - \mathbf{y}_{i+1}(t) \\ &= (\mathbf{I}_N \otimes \mathbf{y}_d(t) - \mathbf{y}_i(t)) - (\mathbf{y}_{i+1}(t) - \mathbf{y}_i(t)) \\ &= \mathbf{e}_i(t) - (\mathbf{I}_N \otimes \mathbf{C})(\mathbf{x}_{i+1}(t) - \mathbf{x}_i(t)) \\ &= \mathbf{e}_i(t) - (\mathbf{I}_N \otimes \mathbf{C})\Phi_{\alpha,1}(\mathbf{I}_N \otimes \mathbf{A}, t)(\mathbf{x}_{i+1}(0) - \mathbf{x}_i(0)) \\ &\quad - (\mathbf{I}_N \otimes \mathbf{C}) \int_0^t \Phi_{\alpha,\alpha}(\mathbf{I}_N \otimes \mathbf{A}, t - \tau)(\mathbf{I}_N \otimes \mathbf{B})(\mathbf{u}_{i+1}(\tau) - \mathbf{u}_i(\tau))d\tau \\ &= \mathbf{e}_i(t) - (\mathbf{I}_N \otimes \mathbf{C})\Phi_{\alpha,1}(\mathbf{I}_N \otimes \mathbf{A}, t)((\mathbf{L} + \mathbf{S}) \otimes \mathbf{B}\Gamma_{D1})\mathbf{e}_i(0) \\ &\quad - (\mathbf{I}_N \otimes \mathbf{C}) \int_0^t \Phi_{\alpha,\alpha}(\mathbf{I}_N \otimes \mathbf{A}, t - \tau)(\mathbf{I}_N \otimes \mathbf{B})((\mathbf{L} + \mathbf{S}) \otimes \Gamma_{P1})\mathbf{e}_i(\tau)d\tau \\ &\quad - (\mathbf{I}_N \otimes \mathbf{C}) \int_0^t \Phi_{\alpha,\alpha}(\mathbf{I}_N \otimes \mathbf{A}, t - \tau)(\mathbf{I}_N \otimes \mathbf{B})((\mathbf{L} + \mathbf{S}) \otimes \Gamma_{D1}) {}_0^C D_t^\alpha \mathbf{e}_i(\tau)d\tau \\ &= \mathbf{e}_i(t) - (\mathbf{I}_N \otimes \mathbf{C})\Phi_{\alpha,1}(\mathbf{I}_N \otimes \mathbf{A}, t)((\mathbf{L} + \mathbf{S}) \otimes \mathbf{B}\Gamma_{D1})\mathbf{e}_i(0) \\ &\quad - (\mathbf{I}_N \otimes \mathbf{C}) \int_0^t \Phi_{\alpha,\alpha}(\mathbf{I}_N \otimes \mathbf{A}, t - \tau)((\mathbf{L} + \mathbf{S}) \otimes \mathbf{B}\Gamma_{P1})\mathbf{e}_i(\tau)d\tau \\ &\quad - (\mathbf{I}_N \otimes \mathbf{C}) \int_0^t \Phi_{\alpha,\alpha}(\mathbf{I}_N \otimes \mathbf{A}, t - \tau)((\mathbf{L} + \mathbf{S}) \otimes \mathbf{B}\Gamma_{D1}) {}_0^C D_t^\alpha \mathbf{e}_i(\tau)d\tau \end{aligned} \quad (26)$$

where  $\mathbf{1}_{(\cdot)}$  is a vector in which all entries are 1.

From Lemma 2 and 3, we can see that

$$\begin{aligned}
& \int_0^t \Phi_{\alpha,\alpha}(\mathbf{I}_N \otimes \mathbf{A}, t - \tau) ((\mathbf{L} + \mathbf{S}) \otimes \mathbf{B}\Gamma_{D1})_0^C D_t^\alpha \mathbf{e}_i(t) d\tau \\
&= \int_0^t {}^C D_t^{1-\alpha} (\Phi_{\alpha,1}(\mathbf{I}_N \otimes \mathbf{A}, t - \tau)) ((\mathbf{L} + \mathbf{S}) \otimes \mathbf{B}\Gamma_{D1})_0^C D_t^\alpha \mathbf{e}_i(t) d\tau \\
&= \int_0^t \Phi_{\alpha,1}(\mathbf{I}_N \otimes \mathbf{A}, t - \tau) ((\mathbf{L} + \mathbf{S}) \otimes \mathbf{B}\Gamma_{D1})_0^C D_t^{1-\alpha} ({}^C D_t^\alpha \mathbf{e}_i(t)) d\tau \\
&= \int_0^t \Phi_{\alpha,1}(\mathbf{I}_N \otimes \mathbf{A}, t - \tau) ((\mathbf{L} + \mathbf{S}) \otimes \mathbf{B}\Gamma_{D1}) \mathbf{e}'_i(\tau) d\tau \\
&= \int_0^t \Phi_{\alpha,1}(\mathbf{I}_N \otimes \mathbf{A}, t - \tau) ((\mathbf{L} + \mathbf{S}) \otimes \mathbf{B}\Gamma_{D1}) d\mathbf{e}_i(\tau) \\
&= \Phi_{\alpha,1}(\mathbf{I}_N \otimes \mathbf{A}, t - \tau) ((\mathbf{L} + \mathbf{S}) \otimes \mathbf{B}\Gamma_{D1}) \mathbf{e}_i(\tau) \Big|_0^t \\
&\quad - \int_0^t \frac{d}{d\tau} (\Phi_{\alpha,1}(\mathbf{I}_N \otimes \mathbf{A}, t - \tau) ((\mathbf{L} + \mathbf{S}) \otimes \mathbf{B}\Gamma_{D1})) \mathbf{e}_i(\tau) d\tau \\
&= \Phi_{\alpha,1}(\mathbf{I}_N \otimes \mathbf{A}, 0) ((\mathbf{L} + \mathbf{S}) \otimes \mathbf{B}\Gamma_{D1}) \mathbf{e}_i(t) \\
&\quad - \Phi_{\alpha,1}(\mathbf{I}_N \otimes \mathbf{A}, t) ((\mathbf{L} + \mathbf{S}) \otimes \mathbf{B}\Gamma_{D1}) \mathbf{e}_i(0) \\
&\quad + \int_0^t \Phi_{\alpha,1}(\mathbf{I}_N \otimes \mathbf{A}, t - \tau) (\mathbf{I}_N \otimes \mathbf{A}) (\mathbf{I}_N \otimes \mathbf{B}) ((\mathbf{L} + \mathbf{S}) \otimes \Gamma_{D1}) \mathbf{e}_i(\tau) d\tau \\
&= ((\mathbf{L} + \mathbf{S}) \otimes \mathbf{B}\Gamma_{D1}) \mathbf{e}_i(t) - \Phi_{\alpha,1}(\mathbf{I}_N \otimes \mathbf{A}, t) ((\mathbf{L} + \mathbf{S}) \otimes \mathbf{B}\Gamma_{D1}) \mathbf{e}_i(0) \\
&\quad + \int_0^t \Phi_{\alpha,1}(\mathbf{I}_N \otimes \mathbf{A}, t - \tau) ((\mathbf{L} + \mathbf{S}) \otimes \mathbf{A}\mathbf{B}\Gamma_{D1}) \mathbf{e}_i(\tau) d\tau.
\end{aligned} \tag{27}$$

Taking (27) into (26), we further get

$$\begin{aligned}
\mathbf{e}_{i+1}(t) &= (\mathbf{I} - (\mathbf{I}_N \otimes \mathbf{C})) ((\mathbf{L} + \mathbf{S}) \otimes \mathbf{B}\Gamma_{D1}) \mathbf{e}_i(t) \\
&\quad - (\mathbf{I}_N \otimes \mathbf{C}) \int_0^t \Phi_{\alpha,\alpha}(\mathbf{I}_N \otimes \mathbf{A}, t - \tau) ((\mathbf{L} + \mathbf{S}) \otimes \mathbf{B}\Gamma_{P1}) \mathbf{e}_i(\tau) d\tau \\
&\quad - (\mathbf{I}_N \otimes \mathbf{C}) \int_0^t \Phi_{\alpha,1}(\mathbf{I}_N \otimes \mathbf{A}, t - \tau) ((\mathbf{L} + \mathbf{S}) \otimes \mathbf{A}\mathbf{B}\Gamma_{D1}) \mathbf{e}_i(\tau) d\tau \\
&= (\mathbf{I} - (\mathbf{L} + \mathbf{S}) \otimes \mathbf{C}\mathbf{B}\Gamma_{D1}) \mathbf{e}_i(t) - (\mathbf{I}_N \otimes \mathbf{C}) \int_0^t \Phi_{\alpha,\alpha}(\mathbf{I}_N \otimes \mathbf{A}, t - \tau) ((\mathbf{L} + \mathbf{S}) \otimes (\mathbf{B}\Gamma_{P1} + \mathbf{A}\mathbf{B}\Gamma_{D1})) \mathbf{e}_i(\tau) d\tau.
\end{aligned} \tag{28}$$

According to Lemma 1, taking Lebesgue-p norm on both sides of (28), we achieve

$$\|\mathbf{e}_{i+1}(t)\|_p \leq (\|\mathbf{I} - (\mathbf{L} + \mathbf{S}) \otimes \mathbf{C}\mathbf{B}\Gamma_{D1}\| + \beta) \|\mathbf{e}_i(t)\|_p = \rho_1 \|\mathbf{e}_i(t)\|_p, \tag{29}$$

where

$$\beta = \|\mathbf{I}_N \otimes \mathbf{C}\| \|(\mathbf{L} + \mathbf{S}) \otimes (\mathbf{B}\Gamma_{P1} + \mathbf{A}\mathbf{B}\Gamma_{D1})\| \|\Phi_{\alpha,\alpha}(\mathbf{I}_N \otimes \mathbf{A}, t)\|_1. \tag{30}$$

Recalling the condition of  $\rho < 1$ , it deduces that

$$\|\mathbf{e}_{i+1}(t)\|_p \leq \rho_1 \|\mathbf{e}_i(t)\|_p \leq \rho_1^i \|\mathbf{e}_1(t)\|_p. \tag{31}$$

So, as the iterations number increases, i.e.,  $i \rightarrow \infty$ , we obtain

$$\lim_{i \rightarrow \infty} \|\mathbf{e}_{i+1}(t)\|_p = 0. \tag{32}$$

It shows that the tracking errors of all the agents tend to reach zero in finite time when  $i \rightarrow \infty$ . The proof is completed. When  $\Gamma_{P1} = 0$ , the open-loop PD $^\alpha$ -type fractional-order algorithm degenerates into the  $D^\alpha$ -type fractional-order algorithm, which has the following form:

$$\mathbf{u}_{i+1}(t) = \mathbf{u}_i(t) + ((\mathbf{L} + \mathbf{S}) \otimes \Gamma_{D1}) \mathbf{e}_i^{(\alpha)}(t). \quad (33)$$

Thus, the following corollary can be obtained.  $\square$

**Corollary 1.** Consider the FOMASs (15) and under the communication graph  $\overline{\mathbb{G}}$ , if Assumptions 1 and 2 are satisfied. Distributed  $D\alpha$ -type updating rule (33) is applied to the FOMASs (15). Assuming that

$$\|\mathbf{I} - (\mathbf{L} + \mathbf{S}) \otimes \mathbf{C}\mathbf{B}\Gamma_{D1}\| + \beta_0 < 1 \quad (34)$$

holds for all  $[0, T]$ , where  $\beta_0 = \|\mathbf{I}_N \otimes \mathbf{C}\| \|(\mathbf{L} + \mathbf{S}) \otimes \mathbf{A}\mathbf{B}\Gamma_{D1}\| \|\Phi_{\alpha,\alpha}(\mathbf{I}_N \otimes \mathbf{A}, t)\|_1$ , then  $\lim_{i \rightarrow \infty} \|\mathbf{e}_{i+1}(t)\|_p = 0$ . Namely, the output  $\mathbf{y}_i(t)$  converges uniformly to the desired trajectory  $\mathbf{y}_d(t)$  as  $i \rightarrow \infty$ .

*Proof.* The process of proof is similar to Theorem 1.  $\square$

3.2. Closed-Loop  $PD^\alpha$ -Type FOILC. The closed-loop  $PD^\alpha$ -type FOILC updating law for the FOMASs (15) is designed as follows:

$$\begin{cases} \mathbf{u}_{i+1,j}(t) = \mathbf{u}_{i,j}(t) + \Gamma_{P2} \xi_{i+1,j}(t) + \Gamma_{D20}^C D_t^\alpha \xi_{i+1,j}(t), \\ \mathbf{x}_{i+1,j}(0) = \mathbf{x}_{i,j}(0) + \mathbf{B}\Gamma_{D2} \xi_{i+1,j}(0). \end{cases} \quad (35)$$

Similar to (23), the updating law (35) can be rewritten by the Kronecker product as

$$\begin{cases} \mathbf{u}_{i+1}(t) = \mathbf{u}_i(t) + ((\mathbf{L} + \mathbf{S}) \otimes \Gamma_{P2}) \mathbf{e}_{i+1}(t) + ((\mathbf{L} + \mathbf{S}) \otimes \Gamma_{D20})^C D_t^\alpha \mathbf{e}_{i+1}(t), \\ \mathbf{x}_{i+1}(0) = \mathbf{x}_i(0) + ((\mathbf{L} + \mathbf{S}) \otimes \mathbf{B}\Gamma_{D2}) \mathbf{e}_{i+1}(0), \end{cases} \quad (36)$$

where  $\mathbf{L}$  and  $\mathbf{S}$  are the same as defined in (20).

**Theorem 2.** Consider the FOMASs (15) under a directed graph  $\overline{\mathbb{G}}$ , if Assumptions 1 and 2 hold. The closed-loop  $PD^\alpha$ -type FOILC described in (36) is applied for the system (15). If learning gains  $\Gamma_{P2}$  and  $\Gamma_{D2}$  satisfy

$$0 < \rho_2 = \left( \frac{1}{\|(\mathbf{I} + (\mathbf{L} + \mathbf{S}) \otimes \mathbf{C}\mathbf{B}\Gamma_{D2})^{-1}\|} - \gamma \right)^{-1} < 1, \quad (37)$$

where

$$\gamma = \|\mathbf{I}_N \otimes \mathbf{C}\| \|(\mathbf{L} + \mathbf{S}) \otimes (\mathbf{B}\Gamma_{P2} + \mathbf{A}\mathbf{B}\Gamma_{D2})\| \|\Phi_{\alpha,\alpha}(\mathbf{I}_N \otimes \mathbf{A}, t)\|_1, \quad (38)$$

then  $\lim_{i \rightarrow \infty} \|\mathbf{e}_{i+1}(t)\|_p = 0$ . Hence, the system outputs  $\mathbf{y}_i(t)$  can fully track the desired trajectory  $\mathbf{y}_d(t)$  in a finite time when  $i \rightarrow \infty$  for all  $t \in [0, T]$ ; that is,  $\lim_{i \rightarrow \infty} \mathbf{y}_i(t) = \mathbf{y}_d(t)$ , ( $t \in [0, T]$ ).

*Proof.* From (15) and (36), we can get

$$\begin{aligned} \mathbf{e}_{i+1}(t) &= \mathbf{e}_i(t) - (\mathbf{I}_N \otimes \mathbf{C})(\mathbf{x}_{i+1}(t) - \mathbf{x}_i(t)) = \mathbf{e}_i(t) - (\mathbf{I}_N \otimes \mathbf{C})\Phi_{\alpha,1}(\mathbf{I}_N \otimes \mathbf{A}, t)(\mathbf{x}_{i+1}(0) - \mathbf{x}_i(0)) \\ &\quad - (\mathbf{I}_N \otimes \mathbf{C}) \int_0^t \Phi_{\alpha,\alpha}(\mathbf{I}_N \otimes \mathbf{A}, t - \tau) (\mathbf{I}_N \otimes \mathbf{B})(\mathbf{u}_{i+1}(\tau) - \mathbf{u}_i(\tau)) d\tau \\ &= \mathbf{e}_i(t) - (\mathbf{I}_N \otimes \mathbf{C})\Phi_{\alpha,1}(\mathbf{I}_N \otimes \mathbf{A}, t)((\mathbf{L} + \mathbf{S}) \otimes \mathbf{B}\Gamma_{D2}) \mathbf{e}_{i+1}(0) \\ &\quad - (\mathbf{I}_N \otimes \mathbf{C}) \int_0^t \Phi_{\alpha,\alpha}(\mathbf{I}_N \otimes \mathbf{A}, t - \tau) ((\mathbf{L} + \mathbf{S}) \otimes \mathbf{B}\Gamma_{P2}) \mathbf{e}_{i+1}(\tau) d\tau \\ &\quad - (\mathbf{I}_N \otimes \mathbf{C}) \int_0^t \Phi_{\alpha,\alpha}(\mathbf{I}_N \otimes \mathbf{A}, t - \tau) ((\mathbf{L} + \mathbf{S}) \otimes \mathbf{B}\Gamma_{D20})^C D_t^\alpha \mathbf{e}_{i+1}(t) d\tau, \end{aligned} \quad (39)$$

where  $\mathbf{1}_{(\cdot)}$  is a vector in which all entries are 1.

Similar to the derivation of (27), one can conclude that

$$\begin{aligned} \int_0^t \Phi_{\alpha,\alpha}(\mathbf{I}_N \otimes \mathbf{A}, t - \tau) ((\mathbf{L} + \mathbf{S}) \otimes \mathbf{B}\Gamma_{D20})^C D_t^\alpha \mathbf{e}_{i+1}(t) d\tau &= ((\mathbf{L} + \mathbf{S}) \otimes \mathbf{B}\Gamma_{D2}) \mathbf{e}_{i+1}(t) - \Phi_{\alpha,1}(\mathbf{I}_N \otimes \mathbf{A}, t) ((\mathbf{L} + \mathbf{S}) \otimes \mathbf{B}\Gamma_{D2}) \mathbf{e}_{i+1}(0) \\ &\quad + \int_0^t \Phi_{\alpha,1}(\mathbf{I}_N \otimes \mathbf{A}, t - \tau) ((\mathbf{L} + \mathbf{S}) \otimes \mathbf{A}\mathbf{B}\Gamma_{D2}) \mathbf{e}_{i+1}(\tau) d\tau. \end{aligned} \quad (40)$$

Substituting (40) into (39), it yields

$$\begin{aligned}
\mathbf{e}_{i+1}(t) &= \mathbf{e}_i(t) - (\mathbf{I}_N \otimes \mathbf{C})((\mathbf{L} + \mathbf{S}) \otimes \mathbf{B}\Gamma_{D2})\mathbf{e}_{i+1}(t) \\
&\quad - (\mathbf{I}_N \otimes \mathbf{C}) \int_0^t \Phi_{\alpha,\alpha}(\mathbf{I}_N \otimes \mathbf{A}, t - \tau)((\mathbf{L} + \mathbf{S}) \otimes \mathbf{B}\Gamma_{P2})\mathbf{e}_{i+1}(\tau)d\tau \\
&\quad - (\mathbf{I}_N \otimes \mathbf{C}) \int_0^t \Phi_{\alpha,1}(\mathbf{I}_N \otimes \mathbf{A}, t - \tau)((\mathbf{L} + \mathbf{S}) \otimes \mathbf{A}\mathbf{B}\Gamma_{D2})\mathbf{e}_{i+1}(\tau)d\tau \\
&= \mathbf{e}_i(t) - ((\mathbf{L} + \mathbf{S}) \otimes \mathbf{C}\mathbf{B}\Gamma_{D2})\mathbf{e}_{i+1}(t) - (\mathbf{I}_N \otimes \mathbf{C}) \\
&\quad \cdot \int_0^t \Phi_{\alpha,\alpha}(\mathbf{I}_N \otimes \mathbf{A}, t - \tau)((\mathbf{L} + \mathbf{S}) \otimes (\mathbf{B}\Gamma_{P2} + \mathbf{A}\mathbf{B}\Gamma_{D2}))\mathbf{e}_{i+1}(\tau)d\tau.
\end{aligned} \tag{41}$$

Therefore,

$$\begin{aligned}
&(\mathbf{I} + (\mathbf{L} + \mathbf{S}) \otimes \mathbf{C}\mathbf{B}\Gamma_{D2})\mathbf{e}_{i+1}(t) \\
&= \mathbf{e}_i(t) - (\mathbf{I}_N \otimes \mathbf{C}) \int_0^t \Phi_{\alpha,\alpha}(\mathbf{I}_N \otimes \mathbf{A}, t - \tau)((\mathbf{L} + \mathbf{S}) \\
&\quad \otimes (\mathbf{B}\Gamma_{P2} + \mathbf{A}\mathbf{B}\Gamma_{D2}))\mathbf{e}_{i+1}(\tau)d\tau.
\end{aligned} \tag{42}$$

According to Assumption 1, one can find a feedback gain matrix of differentiation  $\Gamma_{D2}$  such that  $\mathbf{I} + (\mathbf{L} + \mathbf{S}) \otimes \mathbf{C}\mathbf{B}\Gamma_{D2}$  is a nonsingular matrix. Therefore, premultiplying by  $(\mathbf{I} + (\mathbf{L} + \mathbf{S}) \otimes \mathbf{C}\mathbf{B}\Gamma_{D2})^{-1}$  on both sides of (42), taking Lebesgue- $p$  norm, and adopting the generalized Young inequality of convolution integral, it can be concluded that

$$\|\mathbf{e}_{i+1}(t)\|_p \leq \|(\mathbf{I} + (\mathbf{L} + \mathbf{S}) \otimes \mathbf{C}\mathbf{B}\Gamma_{D2})^{-1}\| \left( \|\mathbf{e}_i(t)\|_p + \lambda \|\mathbf{e}_{i+1}(t)\|_p \right), \tag{43}$$

where

$$\gamma = \|\mathbf{I}_N \otimes \mathbf{C}\| \|(\mathbf{L} + \mathbf{S}) \otimes (\mathbf{B}\Gamma_{P2} + \mathbf{A}\mathbf{B}\Gamma_{D2})\| \|\Phi_{\alpha,\alpha}(\mathbf{I}_N \otimes \mathbf{A}, t)\|_1. \tag{44}$$

Further

$$\begin{aligned}
\|\mathbf{e}_{i+1}(t)\|_p &\leq \left( \frac{1}{\|(\mathbf{I} + (\mathbf{L} + \mathbf{S}) \otimes \mathbf{C}\mathbf{B}\Gamma_{D2})^{-1}\|} - \gamma \right)^{-1} \|\mathbf{e}_i(t)\|_p \\
&= \rho_2 \|\mathbf{e}_i(t)\|_p.
\end{aligned} \tag{45}$$

Recalling the condition of  $\rho_2 < 1$ , according to inequality (43), it is deduced that

$$\|\mathbf{e}_{i+1}(t)\|_p \leq \rho_2 \|\mathbf{e}_i(t)\|_p \leq \rho_2^i \|\mathbf{e}_1(t)\|_p. \tag{46}$$

From (45), when the number of iterations is large enough, i.e.,  $i \rightarrow \infty$ , we obtain

$$\lim_{i \rightarrow \infty} \|\mathbf{e}_{i+1}(t)\|_p \rightarrow 0. \tag{47}$$

So, it can be proved that the errors of all the fractional-order agents tend to zero as  $i \rightarrow \infty$ . For the FOMASs (15), if  $\Gamma_{P2} = 0$  in (37), then the  $\text{PD}^\alpha$ -type FOILC will become  $D^\alpha$ -type FOILC.

$$\mathbf{u}_{i+1}(t) = \mathbf{u}_i(t) + ((\mathbf{L} + \mathbf{S}) \otimes \Gamma_{D2})\mathbf{e}_{i+1}^{(\alpha)}(t). \tag{48}$$

Thus, according to Theorem 2, we can obtain a corollary as follows.  $\square$

**Corollary 2.** For the FOMASs (15) under a directed graph  $\overline{\mathbb{G}}$ , suppose Assumptions 1 and 2 hold. If the learning gain  $\Gamma_{D2}$  in (48) is chosen such that

$$\left( \frac{1}{\|(\mathbf{I} + (\mathbf{L} + \mathbf{S}) \otimes \mathbf{C}\mathbf{B}\Gamma_{D2})^{-1}\|} - \gamma_0 \right)^{-1} < 1, \tag{49}$$

where

$$\gamma_0 = \|\mathbf{I}_N \otimes \mathbf{C}\| \|(\mathbf{L} + \mathbf{S}) \otimes \mathbf{A}\mathbf{B}\Gamma_{D2}\| \|\Phi_{\alpha,\alpha}(\mathbf{I}_N \otimes \mathbf{A}, t)\|_1. \tag{50}$$

Then the tracking error satisfies  $\lim_{i \rightarrow \infty} \|\mathbf{e}_{i+1}(t)\|_p = 0$ . Namely, the outputs  $\mathbf{y}_i(t)$  of the FOMASs (15) converge to the desired trajectory  $\mathbf{y}_d(t)$  uniformly in a finite time when  $i \rightarrow \infty$ , i.e.,  $\lim_{i \rightarrow \infty} \mathbf{y}_i(t) = \mathbf{y}_d(t)$ , ( $t \in [0, T]$ ).

*Proof.* The proof process of the corollary is similar to Theorem 2.  $\square$

**3.3. Open-Closed-Loop  $\text{PD}^\alpha$ -Type FOILC.** Considering the FOMASs (15), an open-closed-loop  $\text{PD}^\alpha$ -type FOILC is designed as

$$\begin{cases} \mathbf{u}_{i+1,j}(t) = \mathbf{u}_{i,j}(t) + \Gamma_{P1}\xi_{i,j}(t) + \Gamma_{D10} {}^C D_t^\alpha \xi_{i,j}(t) + \Gamma_{P2}\xi_{i+1,j}(t) + \Gamma_{D20} {}^C D_t^\alpha \xi_{i+1,j}(t), \\ \mathbf{x}_{i+1,j}(0) = \mathbf{x}_{i,j}(0) + \mathbf{B}(\Gamma_{D1}\xi_{i,j}(0) + \Gamma_{D2}\xi_{i+1,j}(0)). \end{cases} \tag{51}$$

Similar to (25), the updating law (51) can be rewritten by the Kronecker product as

$$\begin{cases} \mathbf{u}_{i+1}(t) = \mathbf{u}_i(t) + ((\mathbf{L} + \mathbf{S}) \otimes \Gamma_{P1})\mathbf{e}_i(t) + ((\mathbf{L} + \mathbf{S}) \otimes \Gamma_{D1})_0^C D_t^\alpha \mathbf{e}_i(t) + ((\mathbf{L} + \mathbf{S}) \otimes \Gamma_{P2})\mathbf{e}_{i+1}(t) + ((\mathbf{L} + \mathbf{S}) \otimes \Gamma_{D2})_0^C D_t^\alpha \mathbf{e}_{i+1}(t), \\ \mathbf{x}_{i+1}(0) = \mathbf{x}_i(0) + (\mathbf{L} + \mathbf{S}) \otimes \mathbf{B}(\Gamma_{D1}\mathbf{e}_i(0) + \Gamma_{D2}\mathbf{e}_{i+1}(0)), \end{cases} \quad (52)$$

where  $\mathbf{L}$  and  $\mathbf{S}$  are the same as defined in (20) and (36).

**Theorem 3.** Consider the FOMASs (15) under a directed graph  $\overline{\mathbb{G}}$ , if Assumptions 1 and 2 hold. Let the distributed closed-loop PD $^\alpha$ -type FOILC described in (52) be applied for the system with learning gains  $\Gamma_{P1}, \Gamma_{P2}, \Gamma_{D1}$ , and  $\Gamma_{D2}$  satisfying

$$\rho_2 \rho_1 < 1, \quad (53)$$

where

$$\rho_1 = \|\mathbf{I} - (\mathbf{L} + \mathbf{S}) \otimes \mathbf{C}\mathbf{B}\Gamma_{D1}\| + \beta,$$

$$\rho_2 = \left( \frac{1}{\|(\mathbf{I} + (\mathbf{L} + \mathbf{S}) \otimes \mathbf{C}\mathbf{B}\Gamma_{D2})^{-1}\|} - \gamma \right)^{-1} > 0,$$

$$\beta = \|\mathbf{I}_N \otimes \mathbf{C}\| \|(\mathbf{L} + \mathbf{S}) \otimes (\mathbf{B}\Gamma_{P1} + \mathbf{A}\mathbf{B}\Gamma_{D1})\| \|\Phi_{\alpha,\alpha}(\mathbf{I}_N \otimes \mathbf{A}, t)\|_1$$

$$\gamma = \|\mathbf{I}_N \otimes \mathbf{C}\| \|(\mathbf{L} + \mathbf{S}) \otimes (\mathbf{B}\Gamma_{P2} + \mathbf{A}\mathbf{B}\Gamma_{D2})\| \|\Phi_{\alpha,\alpha}(\mathbf{I}_N \otimes \mathbf{A}, t)\|_1. \quad (54)$$

Then  $\lim_{i \rightarrow \infty} \|\mathbf{e}_{i+1}(t)\|_p = 0$ . Thus, the system outputs  $\mathbf{y}_i(t)$  of the fractional-order agents converge to  $\mathbf{y}_d(t)$  when  $i \rightarrow \infty$  for all  $t \in [0, T]$ ; that is,  $\lim_{i \rightarrow \infty} \mathbf{y}_i(t) = \mathbf{y}_d(t)$ , ( $t \in [0, T]$ ).

*Remark 3.* According to the conditions of Theorems 1 and 2, in the sense of Lebesgue-p norm, the convergence conditions of the proposed algorithms are determined by the learning gain and the properties of the system.

## 4. Simulation

In this section, five fractional-order agents are considered, including a virtual leader and four followers. The directed fixed communication topology among agents is shown in Figure 1, where the fractional-order agents are labeled with 0, 1, 2, 3, and 4, respectively. The virtual leader has directed edges to agents 1 and 3.

From Figure 1, the Laplacian matrix  $\mathbf{L}$  and the information transfer matrix  $\mathbf{S}$  of the leader to the followers can be obtained as follows:

$$\mathbf{L} = \begin{bmatrix} 1 & -1 & 0 & 0 \\ -1 & 2 & 0 & -1 \\ 0 & 0 & 1 & -1 \\ 0 & -1 & -1 & 2 \end{bmatrix}, \quad (55)$$

$$\mathbf{S} = \text{diag}(1, 0, 1, 0).$$

The dynamic model of the  $j$ th agent is described as

$$\begin{cases} D^\alpha \mathbf{x}_j(t) = \begin{bmatrix} 0.4 & 2 \\ 5 & -6 \end{bmatrix} \mathbf{x}_j(t) + \begin{bmatrix} 1 & 0 \\ 0 & 1 \end{bmatrix} \mathbf{u}_j(t), \\ \mathbf{y}_j(t) = \begin{bmatrix} 0.85 & 0 \\ 0 & 1 \end{bmatrix} \mathbf{x}_j(t), \end{cases} \quad (56)$$

Here,  $t \in [0, 1]$ ,  $\alpha = 0.75$ .

Let the virtual leader be the given expected reference trajectory

$$\begin{cases} y_{d1} = t^2 + \sin(2\pi t), & (t \in [0, 1]), \\ y_{d2} = \sin(2\pi t), & (t \in [0, 1]). \end{cases} \quad (57)$$

In the following simulations, the initial states of the followers at first iteration are set as  $x_{0,1} = [0.1 \ 0.3]^T$ ,  $x_{0,2} = [-0.5 \ -0.7]^T$ ,  $x_{0,3} = [0.2 \ 0.4]^T$ , and  $x_{0,4} = [-0.6 \ 0.8]^T$ . The control objective of the initial state is  $x_d = [0 \ 0]^T$  and the initial control is set as  $\mathbf{u}_{0,j}(t) = 0$ ,  $j = 1, 2, 3, 4$  for all agents.

*Case 1.* Open-loop PD $^\alpha$ -type: the open-loop PD $^\alpha$ -type is applied to the multiagent system (1). Based on Theorem 1, the gains are selected as  $\Gamma_{P1} = \begin{bmatrix} 0.4 & 0 \\ 0 & 0.6 \end{bmatrix}$ ,  $\Gamma_{D1} = \begin{bmatrix} 0.2 & 0 \\ 0 & 0.3 \end{bmatrix}$ . Thus, we can calculate  $\rho_1 = \|\mathbf{I} - ((\mathbf{L} + \mathbf{D}) \otimes \Gamma_{D1})\mathbf{C}\mathbf{B}\| + \beta_1 = 0.9421 < 1$ , which satisfies the convergence condition (26).

The simulation results are shown in Figures 2–4. The initial states of the followers at the first iteration are  $x_{0,1} = [0.1 \ 0.3]^T$ ,  $x_{0,2} = [-0.5 \ -0.7]^T$ ,  $x_{0,3} = [0.2 \ 0.4]^T$ , and  $x_{0,4} = [-0.6 \ 0.8]^T$ . And the desired initial states of the four followers are zero; that is  $x_{0,j} = [0 \ 0]^T$  for  $j = 1, 2, 3, 4$ . Figure 2 shows the initial state learning process. It can be seen that the initial states  $x_1$  and  $x_2$  of the multiagent at time zero have a large error from the desired state at the beginning of the iteration, because the initial control is set as  $\mathbf{u}_{0,j}(t) = 0$ ,  $j = 1, 2, 3, 4$  for all agents. But as the number of iterations increases, the errors of the initial states gradually decrease. When the number of iterations reaches the 40th iteration, the initial state of  $x_2$  also converges to the desired initial state. And when the number of iterations reaches the 60th iteration, the initial state of  $x_1$  converges to the desired initial state. Figure 3 shows the output tracking results of  $y_1$  and  $y_2$ . It can be seen that each subsystem does not track the desired trajectory at the 5th iteration. With the increase of the number of iterations, when it reaches the 100th iteration, both the outputs  $y_1$  and  $y_2$  of all the agents fully track the



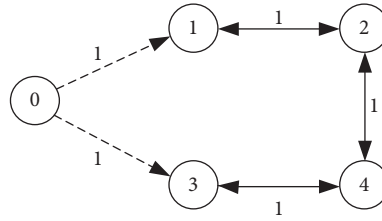


FIGURE 1: Communication graph among agents in the network.

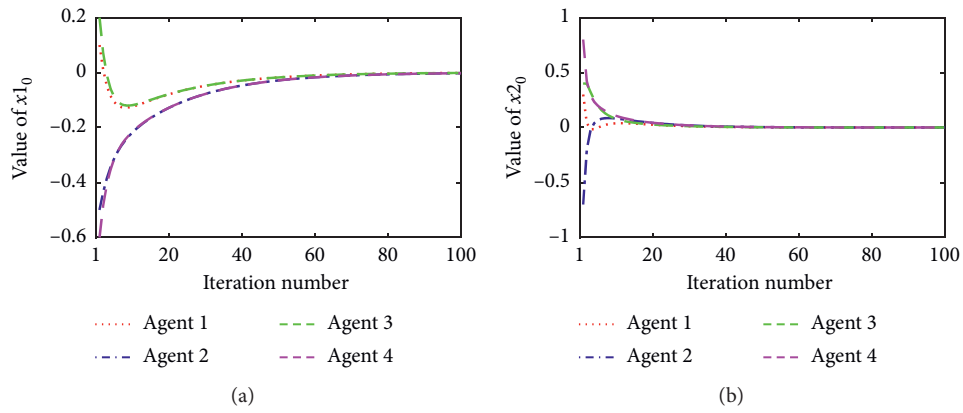


FIGURE 2: Initial state profile vs. iteration number by open-loop  $PD^\alpha$ -type. (a) Initial state learning of  $x_1$ . (b) Initial state learning of  $x_2$ .

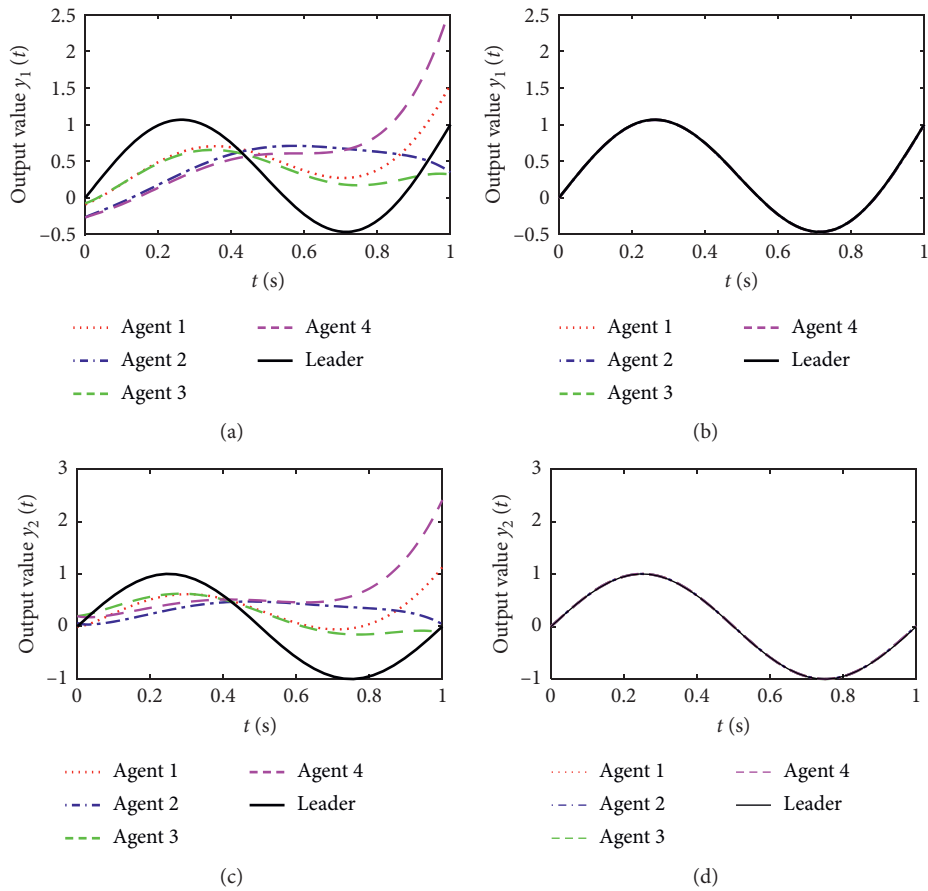


FIGURE 3: The tracking results of all agents at different iterations by open-loop  $PD^\alpha$ -type. (a) Output  $y_1$  at the 5th iteration. (b) Output  $y_1$  at the 100th iteration. (c) Output  $y_2$  at the 5th iteration. (d) Output  $y_2$  at the 100th iteration.

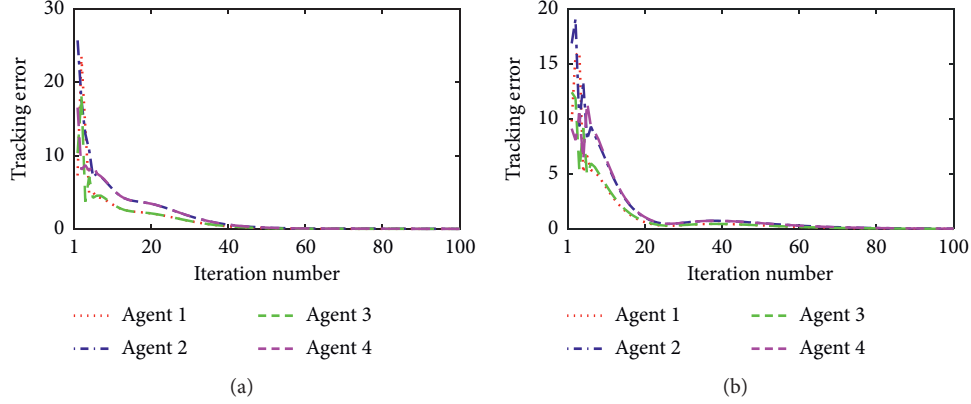


FIGURE 4: The 2-norm of tracking errors for all agents in each interaction by open-loop PD<sup>α</sup>-type. (a) Tracking errors of y1 with iterations. (b) Tracking errors of y2 with iterations.

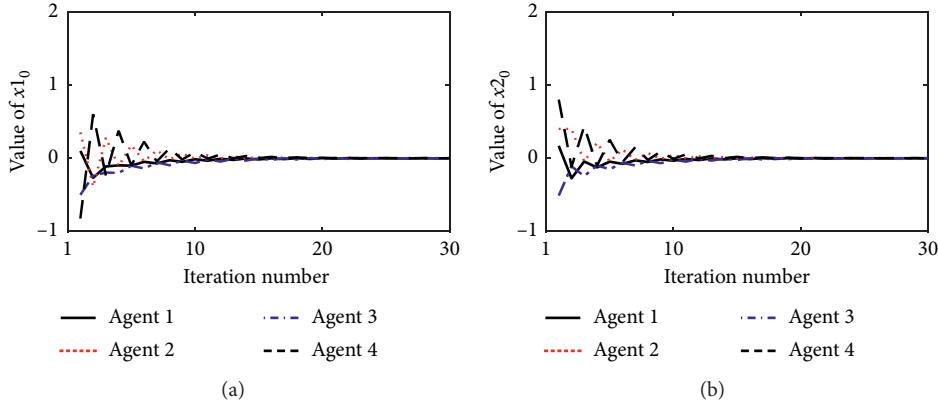


FIGURE 5: Initial state profile vs. iteration number by closed-loop PD<sup>α</sup>-type. (a) Initial state learning of x1. (b) Initial state learning of x2.

desired trajectory over the time period [0, 1]. We define the errors in the 2-norm sense at the *i*th iteration as  $\|y_{d,1} - y1_{i,j}\|_2$  and  $\|y_{d,2} - y2_{i,j}\|_2$  for  $j = 1, 2, 3, 4$ . Figure 4 depicts the tracking errors in each iteration; it shows that the tracking errors converge to zero as the iteration number increases. By the 60th iteration, the tracking errors of  $y1$  of the four followers in the 2-norm sense are 0.000456, 0.000862, 0.000351, and 0.000785, respectively. By the 80th iteration, the tracking errors of  $y2$  of the four followers in the 2-norm sense are 0.000648, 0.000978, 0.000596, and 0.000895, respectively.

*Case 2.* Closed-loop PD<sup>α</sup>-type: the initial inputs and initial state of the multiagents are the same as Case 1. Based on Theorem 2, we select the learning gains as  $\Gamma_{P2} = \begin{bmatrix} 0.504 & 0 \\ 0 & 0.396 \end{bmatrix}$ ,  $\Gamma_{D2} = \begin{bmatrix} 6 & 0 \\ 0 & 7 \end{bmatrix}$ . Clearly,  $\rho_2 = (1/\|\mathbf{I} + \mathbf{H} \otimes \Gamma_{D2} \mathbf{CB}\|) = 0.2146 < 1$ ; thus, the convergence condition can be satisfied.

Figures 5–7 show the trajectory tracking performances employing the closed-loop PD<sup>α</sup>-type ILC scheme. As it can be seen from Figure 5, similar to the simulation results of Case 1, the initial state of the agents tends to reach the

desired initial state as the iteration number increases. Figure 6 shows the outputs  $y1$  and  $y2$  with closed-loop PD<sup>α</sup>-type ILC at the 5th and 30th iterations. From Figure 6, the trajectories  $y1$  and  $y2$  of the followers can track the desired trajectory generated by the leader as the iteration number increases over the time period [0, 1]. Figure 7 shows the tracking errors of  $y1$  and  $y2$  of the four followers in 2-norm sense with the number of iterations. It can be seen that the errors gradually decrease and approach zero as the number of iteration increases. By the 30th iteration, the tracking errors of  $y1$  of the four followers in 2-norm sense are 0.000279, 0.000648, 0.000324, and 0.000472. The tracking errors of  $y2$  of the four followers in 2-norm sense are, respectively, 0.000187, 0.000547, 0.000298, and 0.000385. Besides, compared with the open-loop PD<sup>α</sup>-type, the closed-loop FOILC performs better and has faster convergence speed than the open-loop one.

*Case 3.* Open-closed-loop PD<sup>α</sup>-type

In this simulation, the initial states and inputs are the same as Case 1 and Case 2. According to Theorem 3, the learning gain matrix can be obtained as follows:

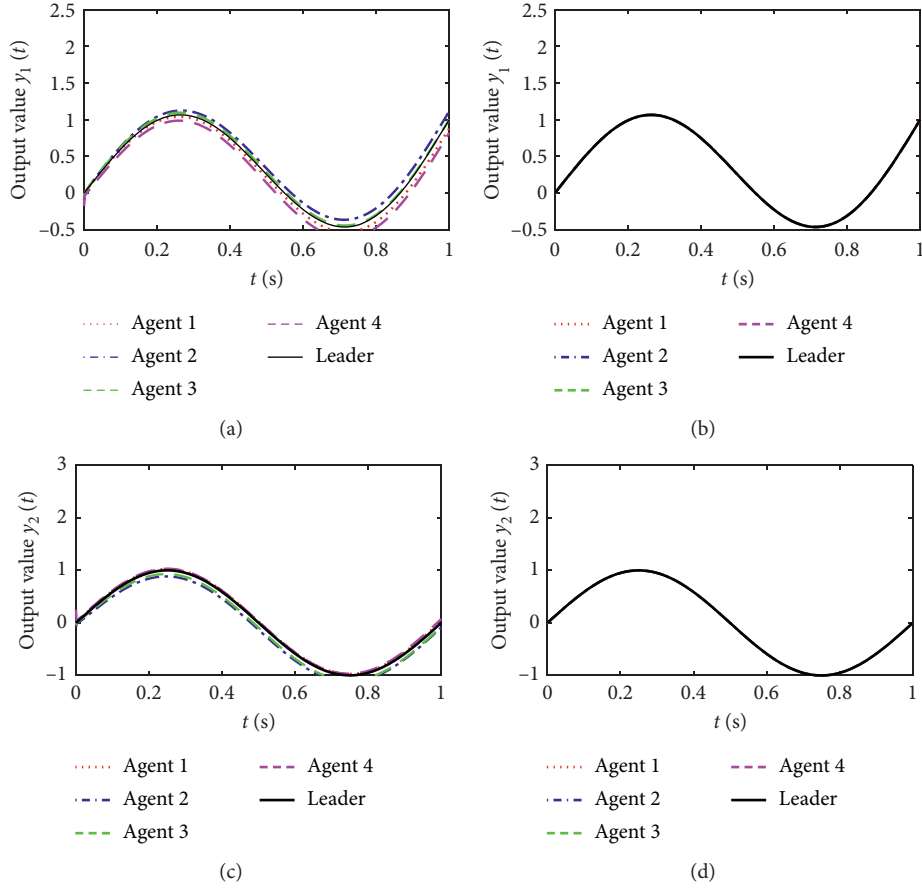


FIGURE 6: The tracking results of all agents at different iterations by closed-loop  $PD^\alpha$ -type. (a) Trajectories of  $y_1$  at the 5th iteration. (b) Trajectories of  $y_1$  at the 30th iteration. (c) Trajectories of  $y_2$  at the 5th iteration. (d) Trajectories of  $y_2$  at the 30th iteration.

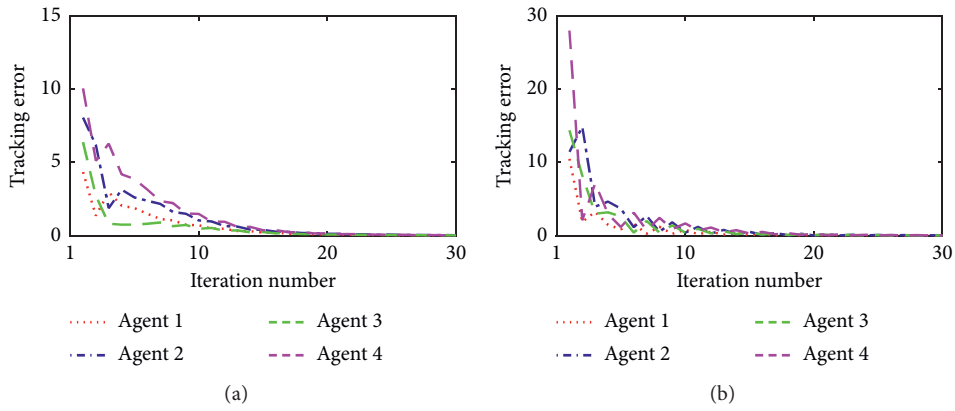


FIGURE 7: The 2-norm of tracking errors for all agents in each interaction by closed-loop  $PD^\alpha$ -type. (a) Tracking errors of  $y_1$  with iterations. (b) Tracking errors of  $y_2$  with iterations.

$$\Gamma_{P1} = \begin{bmatrix} 0.616 & 0 \\ 0 & 0.484 \end{bmatrix},$$

$$\Gamma_{D1} = \begin{bmatrix} 4.5 & 0 \\ 0 & 1.8 \end{bmatrix},$$

$$\Gamma_{P2} = \begin{bmatrix} 0.5 & 0 \\ 0 & 0.4 \end{bmatrix},$$

$$\Gamma_{D2} = \begin{bmatrix} 6 & 0 \\ 0 & 7 \end{bmatrix}.$$

(58)

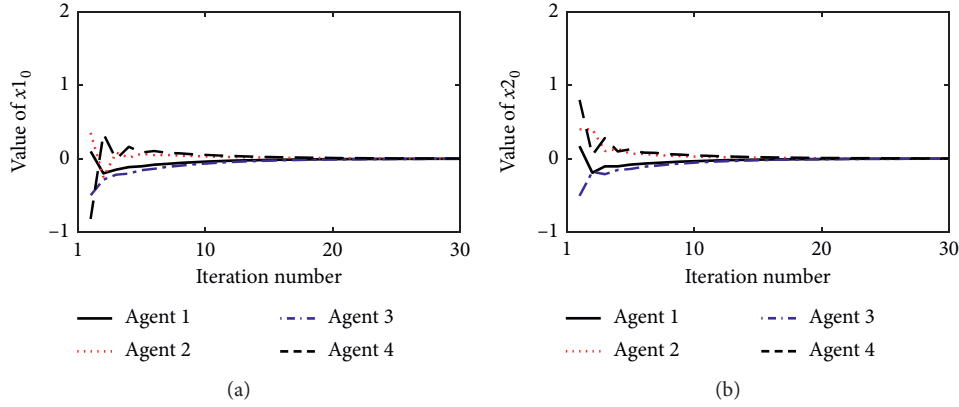


FIGURE 8: Initial state profile vs. iteration number by open-closed-loop PD $^\alpha$ -type. (a) Initial state learning of  $x_1$ . (b) Initial state learning of  $x_2$ .

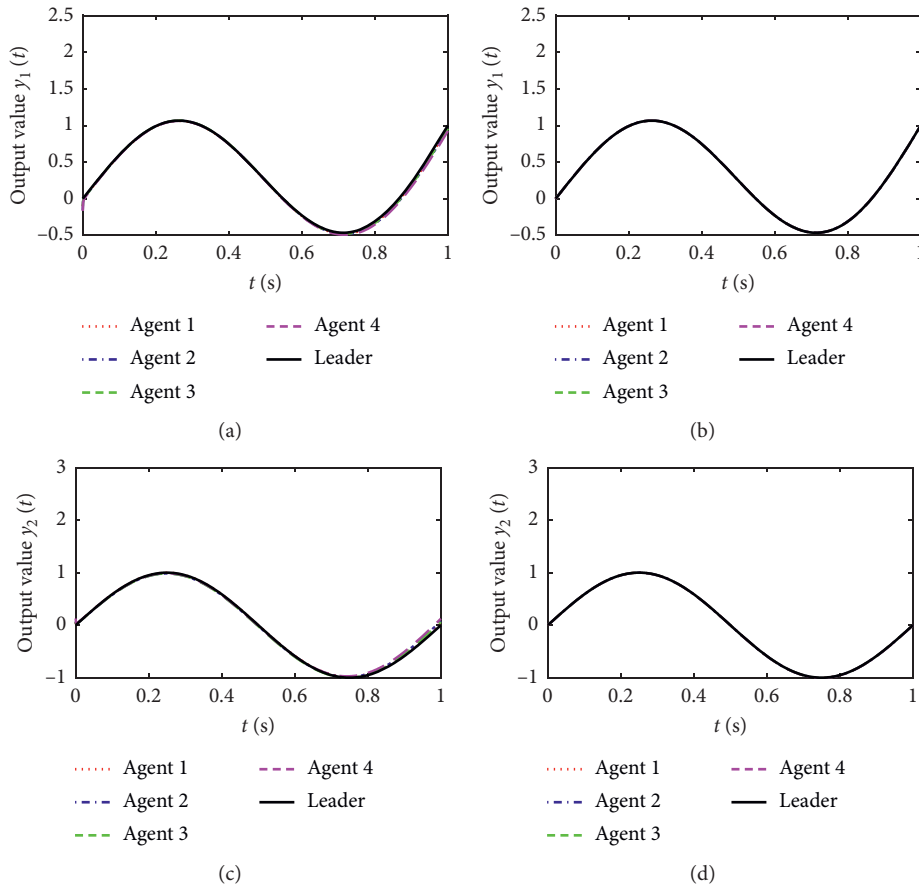


FIGURE 9: The tracking results of all agents at different iterations by open-closed-loop PD $^\alpha$ -type. (a) Trajectories of  $y_1$  at the 5th iteration. (b) Trajectories of  $y_1$  at the 30th iteration. (c) Trajectories of  $y_2$  at the 5th iteration. (d) Trajectories of  $y_2$  at the 30th iteration.

Clearly,  $\rho_2\rho_1 = 0.245 < 1$ ; thus, the convergence condition in Theorem 3 can be satisfied.

The simulation results with open-closed-loop PD $^\alpha$ -type FOILC are presented in Figures 8–10. The results are similar to those of the open-loop and closed-loop PD $^\alpha$ -type FOILC. From the results, both the initial states and the

outputs can converge to the desired values. And we can conclude that the proposed FOILC scheme with initial state learning works well as the iteration number increases. Figure 9 shows the output tracking results of  $y_1$  and  $y_2$ . It can be seen that the followers can fully track the desired trajectory as the iteration increases over the time

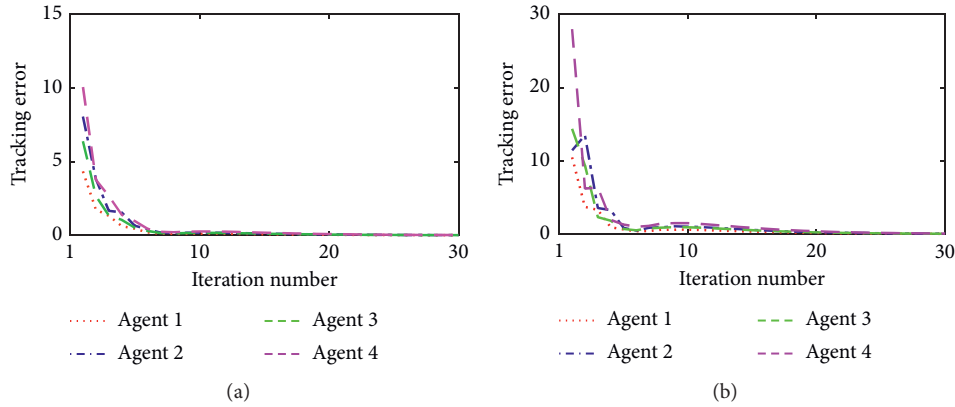


FIGURE 10: The 2-norm of tracking errors for all agents in each interaction by open-closed-loop  $PD^\alpha$ -type. (a) Tracking errors of  $y_1$  with iterations. (b) Tracking errors of  $y_2$  with iterations.

period  $[0, 1]$ . In addition, compared with open-loop  $PD^\alpha$ -type FOILC and closed-loop  $PD^\alpha$ -type, applying open-closed-loop  $PD^\alpha$ -type FOILC has better performance in the initial state and for the outputs.

## 5. Conclusion

In this paper, we have discussed the consensus problem with fixed communication graph, which has been addressed for fractional-order multiagent systems with initial state shift. Considering the initial state learning mechanism, open-loop  $PD^\alpha$  type, closed-loop  $PD^\alpha$  type, and open-closed-loop  $PD^\alpha$  type FOILC are proposed. The theoretical convergence of the proposed algorithm is analyzed and sufficient conditions are presented. Theoretical analysis shows that the proposed algorithms can guarantee the tracking errors of all the agents and the errors in the initial state tend to be zero in a finite time as the number of iterations increases. Finally, some simulation examples are used to validate the effectiveness. As a recommendation for the future, the convergence and robustness of fractional-order nonlinear systems can be studied by using the proposed method of this paper.

## Data Availability

The data used to support the findings of this study are available from the corresponding author upon request.

## Conflicts of Interest

The authors declare that there are no conflicts of interest regarding the publication of this paper.

## Acknowledgments

This study has been supported by the National Natural Science Foundation of China (no. 61871163), the Zhejiang Provincial Natural Science Foundation of China (no. LQ19E070003), and Zhejiang Provincial Key Lab of Equipment Electronics.

## References

- [1] J. Fu, G. Wen, W. Yu, and Z. Ding, "Finite-time consensus for second-order multi-agent systems with input saturation," *IEEE Transactions on Circuits and Systems II: Express Briefs*, vol. 65, no. 11, pp. 1758–1762, 2018.
- [2] Y. Cao, L. Zhang, C. Li, and M. Z. Q. Chen, "Observer-based consensus tracking of nonlinear agents in hybrid varying directed topology," *IEEE Transactions on Cybernetics*, vol. 47, no. 8, pp. 2212–2222, 2017.
- [3] Y. Tang and P. Yi, "Distributed coordination for a class of non-linear multi-agent systems with regulation constraints," *IET Control Theory & Applications*, vol. 12, no. 1, pp. 1–9, 2017.
- [4] X. Wang and G.-H. Yang, "Adaptive reliable coordination control for linear agent networks with intermittent communication constraints," *IEEE Transactions on Control of Network Systems*, vol. 5, no. 3, pp. 1120–1131, 2018.
- [5] Y. Cao, Y. Li, W. Ren, and Y. Chen, "Distributed coordination of networked fractional-order systems," *IEEE Transactions on Systems, Man, and Cybernetics, Part B: Cybernetics*, vol. 40, no. 2, pp. 362–370, 2010.
- [6] Y. Cao and W. Ren, "Distributed formation control for fractional-order systems: dynamic interaction and absolute/relative damping," *Systems & Control Letters*, vol. 59, no. 3–4, pp. 233–240, 2010.
- [7] C. Song and J. Cao, "Consensus of fractional-order linear systems," in *Proceedings of the 2013 9th Asian Control Conference (ASCC)*, Istanbul, Turkey, June 2013.
- [8] C. Song, J. Cao, and Y. Liu, "Robust consensus of fractional-order multi-agent systems with positive real uncertainty via second-order neighbors information," *Neurocomputing*, vol. 165, pp. 293–299, 2015.
- [9] Z. Yu, H. Jiang, and C. Hu, "Leader-following consensus of fractional-order multi-agent systems under fixed topology," *Neurocomputing*, vol. 149, no. PB, pp. 613–620, 2015.
- [10] Z. Yu, H. Jiang, C. Hu, and J. Yu, "Leader-following consensus of fractional-order multi-agent systems via adaptive pinning control," *International Journal of Control*, vol. 88, no. 9, pp. 1746–1756, 2015.
- [11] Z. Yu, H. Jiang, C. Hu, and J. Yu, "Necessary and sufficient conditions for consensus of fractional-order multiagent systems via sampled-data control," *IEEE Transactions on Cybernetics*, vol. 47, no. 8, pp. 1892–1901, 2017.
- [12] Z. Yaghoubi and H. A. Talebi, "Cluster consensus of general fractional-order nonlinear multi agent systems via adaptive

- sliding mode controller,” *Archives of Control Sciences*, vol. 29, no. 4, pp. 643–665, 2019.
- [13] F. Wang and Y. Yang, “On leaderless consensus of fractional-order nonlinear multi-agent systems via event-triggered control,” *Nonlinear Analysis: Modelling and Control*, vol. 24, no. 3, pp. 353–367, 2019.
- [14] D. Luo, J. Wang, and D. Shen, “P D  $\alpha$  type distributed learning control for nonlinear fractional order multiagent systems,” *Mathematical Methods in the Applied Sciences*, vol. 42, no. 13, pp. 4543–4553, 2019.
- [15] Y. Li, Y. Chen, and H.-S. Ahn, “Fractional-order iterative learning control for fractional-order linear systems,” *Asian Journal of Control*, vol. 13, no. 1, pp. 54–63, 2011.
- [16] Y. Li, Y. Chen, H.-S. Ahn, and G. Tian, “A survey on fractional-order iterative learning control,” *Journal of Optimization Theory and Applications*, vol. 156, no. 1, pp. 127–140, 2013.
- [17] S. Lv, M. Pan, X. Li et al., “Consensus tracking of fractional-order multiagent systems via fractional-order iterative learning control,” *Complexity*, vol. 2019, no. 8, 11 pages, Article ID 2192168, 2019.
- [18] D. Luo, J. Wang, and D. Shen, “Learning formation control for fractional-order multiagent systems,” *Mathematical Methods in the Applied Sciences*, vol. 41, no. 13, pp. 5003–5014, 2018.
- [19] J. Wang, T. Yang, G. Staskevich et al., “Approximately adaptive neural cooperative control for nonlinear multiagent systems with performance guarantee,” *International Journal of Systems Science*, vol. 48, no. 5-1, pp. 909–920, 2017.
- [20] X. H. Bu, Z. S. Hou, and F. S. Yu, “Iterative learning control for a class of linear continuous-time switched systems,” *Control Theory and Applications*, vol. 29, no. 8, pp. 1051–1056, 2012.
- [21] A. A. Kilbas, H. M. Srivastava, and J. J. Trujillo, *Theory and Applications of Fractional Differential Equations*, Elsevier, Amsterdam, The Netherlands, 2006.
- [22] S. Westerlund and L. Ekstam, “Capacitor theory,” *IEEE Transactions on Dielectrics and Electrical Insulation*, vol. 1, no. 5, pp. 826–839, 1994.
- [23] I. Podlubny, *Fractional Differential Equations*, Academic Press, Cambridge, MA, USA, 1999.

## Review Article

# Finite-Time Stability Analysis: A Tutorial Survey

Honglei Xu 

*School of Electrical Engineering, Computing and Mathematical Sciences, Curtin University, Perth, WA 6845, Australia*

Correspondence should be addressed to Honglei Xu; [h.xu@curtin.edu.au](mailto:h.xu@curtin.edu.au)

Received 16 July 2020; Revised 9 September 2020; Accepted 23 September 2020; Published 19 October 2020

Academic Editor: Jianquan Lu

Copyright © 2020 Honglei Xu. This is an open access article distributed under the Creative Commons Attribution License, which permits unrestricted use, distribution, and reproduction in any medium, provided the original work is properly cited.

In the past decades, there has been a growing research interest in the field of finite-time stability and stabilization. This paper aims to provide a self-contained tutorial review in the field. After a brief introduction to notations and two distinct finite-time stability concepts, dynamical system models, particularly in the form of linear time-varying systems and impulsive linear systems, are studied. The finite-time stability analysis in a quantitative sense is reviewed, and a variety of stability results including state transition matrix conditions, the piecewise continuous Lyapunov-like function theory, and the converse Lyapunov-like theorem are investigated. Then, robustness and time delay issues are studied. Finally, fundamental finite-time stability results in a qualitative sense are briefly reviewed.

## 1. Introduction

Finite-time stability was first introduced in a Russian journal [1] and later appeared in the western literature [2–4]. The term short-time stability is another name for it [5]. In the current literature, there are two different concepts of finite-time stability. The first is the traditional finite-time stability concept which concerns the restrained system behavior during a specified interval of time. The initial and trajectory domains and the time interval need to be specified in advance, so the traditional concept is a quantitative one. We call it finite-time stability in a quantitative sense. The second one characterizes an asymptotically stable system whose state reaches zero in a finite time, called a settling time. Similar to the Lyapunov stability, it is a qualitative concept, and hence, we call the second concept finite-time stability in the qualitative sense. The analysis and synthesis results of both finite-time stability concepts can be applied to many practical applications such as ATM networks [6], car suspension systems [7], and robot manipulators [8].

Finite-time stability in a quantitative sense emphasizes the following characteristics: the system restrains its trajectory to a predefined time-varying domain over a finite time interval for a bounded initial condition. Even though it

mimics the Lyapunov stability, it is quite different from the classical one due to its finite time interval and specified domains for initial conditions and system trajectories, i.e., a system is finite-time stable for some chosen initial and trajectory domains and time intervals but not finite-time stable for different ones. In the past few decades, many finite-time stability analysis and control design problems have been investigated and a variety of stability criteria have been obtained, see, for example, [3, 4, 9] and the references therein. Recently, computationally tractable finite-time stability criteria with less conservatism have been established under the help of new tools such as linear matrix inequalities [10], Lyapunov matrix equations [11], and differential linear matrix inequalities [12]. More recently, studies on the finite-time stability and stabilization have been extended from linear time-varying systems to complex dynamical systems such as switched systems [13–15] and stochastic systems [16].

On the other hand, finite-time stability in a qualitative sense has attracted much attention in recent years and become a growing interdisciplinary research area. It focuses on asymptotical stability analysis for dynamical systems whose trajectories reach an equilibrium point in a finite time. It is a stronger concept than asymptotical stability and has the settling-time characteristic. Relevant results on autonomous and nonautonomous nonlinear systems have been

discussed in [17–20]. Later, switched versions and time-delay versions appeared in the literature, e.g., [21–23]. Recently, relevant issues of underactuated systems with disturbance have been considered in [24]. In the context of this paper, the readers should be not hard to distinguish whether the concept of finite-time stability is quantitative or qualitative, so we can use the term “finite-time stability” in most places without causing confusion.

In this paper, we will summarize the results of finite-time stability from both quantitative and qualitative aspects. Several excellent surveys on finite-time stability have been found, see, for example, the review papers [25–27], the books [7, 28, 29], and the references therein. These publications report and survey finite-time stability on one aspect or another. This paper aims to provide a unified self-contained tutorial review of finite-time stability to introduce the recent discoveries in the field.

The remainder of this paper is as follows. Section 2 gives some basic mathematical preliminaries including two finite-time stability concepts. Section 3 reviews finite-time stability results in a quantitative sense, mostly for linear time-varying systems. Results involving time-dependent and state-dependent impulses, time delays, and uncertainty are also investigated. In Section 4, we briefly overview some results on finite-time stability in a qualitative sense. Finally, a conclusion is drawn in Section 5.

## 2. Mathematical Preliminaries

*2.1. Notations and Definitions.* Let  $\mathbb{R}^+$  denote a set of non-negative real numbers and  $\mathbb{R}^n$  the  $n$ -dimensional Euclidean space, and consider the time interval  $\Omega = [0, T]$ ,  $T > 0$ . Let  $A^T$  be the transpose of  $A$  and  $I$  be the identity matrix with an appropriate dimension. For a square matrix  $A$ , we denote by  $\lambda(A)$ ,  $\lambda_{\max}(A)$ , and  $\lambda_{\min}(A)$  the set of eigenvalues, the maximum eigenvalues, and the minimum eigenvalues of  $A$ , respectively. The symmetric components in a matrix are represented by  $*$ .  $A \geq 0$  ( $A > 0$ ), called to be positive semi-definite (positive definite), means  $x^T A x \geq 0$  ( $x^T A x > 0$ ) for all  $x \in \mathbb{R}^n$ .  $A \geq B$  is equivalent to  $A - B \geq 0$ . Let  $C([-h, 0], \mathbb{R}^n)$  denote the set of all vector-valued continuous functions on  $[-h, 0]$ . For  $x(t) \in C([-h, 0], \mathbb{R}^n)$ , it is represented by  $x_t = \{x(t+s) : s \in [-h, 0]\}$  with the norm  $\|x_t\| = \sup_{s \in [-h, 0]} \|x(t+s)\|$ . Let  $\mathcal{S}_\rho$  and  $\overline{\mathcal{S}}_\rho$  denote the open and closed sets of the allowable system states defined as  $\mathcal{S}_\rho = \{x \in \mathbb{R}^n \mid \|x(t)\|_Q^2 < \rho\}$  and  $\overline{\mathcal{S}}_\rho = \{x \in \mathbb{R}^n \mid \|x(t)\|_Q^2 \leq \rho\}$ , respectively, where  $\rho > 0$  and  $Q$  is a symmetric positive definite real matrix. We denote  $V_{\min}^\rho(t) = \min_{\|x\|=\rho} V(x, t)$  and  $V_{\max}^\rho(t) = \max_{\|x\|=\rho} V(x, t)$ . For a set  $S_p = \{x_1, x_2, \dots, x_p\} \subseteq \mathbb{R}^n$ , the conical hull of  $S_p$  is the set of all conical combinations, i.e.,  $\text{cone}(S_p) = \{x \mid x = \sum_{i=1}^p a_i x_i, a_i \geq 0\}$ . The set of normalized extremal rays generating  $S_q$ , denoted by  $\text{extr}(S) = \{\bar{x}_1, \dots, \bar{x}_q\}$  with  $\|\bar{x}_i\|_2 = 1$ ,  $i = 1, \dots, q \leq p$ , is the minimal set of unit vectors such that  $S = \text{cone}(\{\bar{x}_1, \dots, \bar{x}_q\})$ . Given a piecewise continuous matrix-valued (or vector-valued) function  $H(\cdot)$  over  $\Omega$  and a

positive real number  $\varepsilon$ , we denote  $H^-(t) = \lim_{\varepsilon \rightarrow 0} H(t - \varepsilon)$  and  $H^+(t) = \lim_{\varepsilon \rightarrow 0} H(t + \varepsilon)$ , i.e.,  $H^-(t)$  and  $H^+(t)$  are the left and right limits, respectively. Let the set  $\mathcal{C}$  be an open set having the origin and a boundary  $\partial\mathcal{C}$ .

We first look at the basic definition of finite-time stability for a dynamical system

$$\dot{x}(t) = f(t, x(t)), \quad (1)$$

where  $t \in \mathbb{R}^+$  is the time variable,  $x \in \mathbb{R}^n$  is the state variable, and  $f(\cdot)$  is a  $\mathbb{R}^n$ -valued function. Suppose that system (1) has a unique solution. We first introduce the concepts of “finite-time stability” in a quantitative sense and in a qualitative sense, respectively.

*Definition 1* (Finite-Time Stability in a Quantitative Sense). Given two sets  $\mathcal{X}_0$  and  $\mathcal{X}(t)$ ,  $0 \in \mathcal{X}_0$ , system (1) is said to be finite-time stable with respect to  $(\Omega, \mathcal{X}_0, \mathcal{X}(t))$  if

$$x_0 \in \mathcal{X}_0 \text{ implies } x(t) \in \mathcal{X}(t) \text{ for } t \in \Omega. \quad (2)$$

In Figure 1, we can see a graphical explanation of Definition 1, where the initial set  $\mathcal{X}_0$  and the time-varying set  $\mathcal{X}_t$  can be in various forms.

- (1) When they are ellipsoids, which are the most common forms existing in the literature (see, e.g., [7, 30–32]), they can be formulated as  $\mathcal{X}_0 = \{x_0 \in \mathbb{R}^n \mid x_0^T R x_0 \leq 1\}$  and  $\mathcal{X}_t = \{x \in \mathbb{R}^n \mid x^T Q(t) x \leq 1\}$ , where  $Q(t)$  is a bounded and piecewise continuous matrix-valued function of time and  $Q(0) < R$ . In many cases,  $\mathcal{X}_0$  and  $\mathcal{X}_t$  can also be expressed as  $\mathcal{X}_0 = \{x_0 \in \mathbb{R}^n \mid \|x_0\|_Q^2 < c_1\}$  and  $\mathcal{X}_t = \{x \in \mathbb{R}^n \mid \|x_t\|_Q^2 < c_2\}$  for  $c_2 > c_1 > 0$  [33].
- (2) When they are in the form of polytopes, they can be described by  $\mathcal{X}_0 = \text{conv}\{x_1^{(0)}, x_2^{(0)}, \dots, x_p^{(0)}\}$  and  $\mathcal{X}_t = \text{conv}\{x_1^{(t)}, x_2^{(t)}, \dots, x_q^{(t)}\} = \{x \in \mathbb{R}^n \mid a_i^T x \leq 1, i = 1, 2, \dots, q\}$ , where  $p$  and  $q$  are the number of vertices of the polytopes  $\mathcal{X}_0$  and  $\mathcal{X}_t$ , and  $x_i^{(0)}$  and  $x_j^{(t)}$  are the  $i$ -th vertex of the polytope  $\mathcal{X}_0$  and the  $j$ -th vertex of the polytope  $\mathcal{X}_t$  [34].
- (3) They can be formulated as much generalized piecewise quadratic domains over conical partitions  $\mathcal{P}_0 = \{U_1^0, U_2^0, \dots, U_u^0\}$  and  $\mathcal{P}_t = \{U_1^t, U_2^t, \dots, U_v^t\}$ . Then,  $\mathcal{X}_0 = \{x_0 \in \mathbb{R}^n \mid x_0^T R_i x_0 \leq 1, x_0 \in U_i^0, i = 1, 2, \dots, u\}$  and  $\mathcal{X}_t = \{x \in \mathbb{R}^n \mid x^T Q_i(t) x \leq 1, x \in U_i^t, i = 1, 2, \dots, v\}$ . It is obvious to see that the set of piecewise quadratic domains is a generalized set of ellipsoidal domains since an ellipsoidal domain is indeed a piecewise quadratic domain choosing  $Q_i = Q$  for all  $i = 1, 2, \dots, v$ . It can also represent the set of polytopical domains whose boundary is a polyhedral function’s level curve.

*Definition 2* (Finite-Time Stability in a Qualitative Sense). System (1) is said to be finite-time stable if for any  $x_0 \in \mathcal{C} \subset \mathbb{R}^n$ ,  $t \geq 0$  and  $\varepsilon > 0$ , there exist  $\delta(t, x_0) > 0$  and



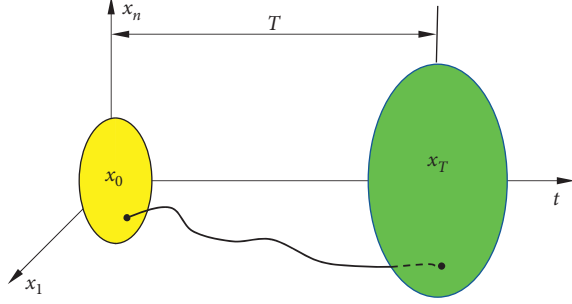


FIGURE 1: Schematic illustration of finite-time stability in a quantitative sense.

$T(x_0) > 0$  such that  $\|x_0\| \leq \delta$  implies  $\|x(t, x_0)\| \leq \varepsilon$ ,  $\lim_{t \rightarrow \infty} \|x(t, x_0)\| = 0$  and  $x(t) = 0$  for all  $t > T(x_0)$ . Here,  $T(x_0) = \inf\{T \geq 0 \mid x(t, x_0) = 0, \forall t \geq T\}$  is called the settling-time function of system (1), and the set  $\mathcal{C}$  is called the domain of attraction. Moreover, if  $\mathcal{C} = \mathbb{R}^n$ , system (1) is globally finite-time stable.

Similarly, a schematic illustration of Definition 2 is given in Figure 2.

**2.2. Mathematical Formulations.** System (1) is a general model for both linear and nonlinear systems depending on the choice of the function  $f(\cdot)$ . In the first part of this paper, we will focus on finite-time stability issues in a quantitative sense for continuous-time linear time-varying systems with and without finite jumps. In the second part of this paper, we will analyze finite-time stability in a qualitative sense for continuous-time nonlinear systems.

First, we introduce a linear time-varying system described as

$$\dot{x}(t) = A(t)x(t), \quad (3)$$

for a given initial condition  $x(0) = x_0$ , which has been considered in many papers, see, e.g., [7, 30]. Here,  $A(\cdot): \Omega \mapsto \mathbb{R}^{n \times n}$  is a continuous matrix-valued function.

In many practical scenarios, abrupt state changes and system jumping behaviors are commonly existing, and these finite jumps occur when the time points and/or the system states satisfy a certain triggering condition, say  $(t, x(t)) \in \mathcal{S} \subset \Omega \times \mathbb{R}^n$ . When the impulses are triggered, the impulsive mappings can be described by

$$x^+(t) = B(t)x^-(t) = B(t)x(t), \quad (t, x(t)) \in \mathcal{S}, \quad (4)$$

where  $B(\cdot): \Omega \mapsto \mathbb{R}^{n \times n}$  is a matrix-valued function, which describes the jumping behavior of system (3) with left continuity over the triggering set  $\mathcal{S} \subset \Omega \times \mathbb{R}^n$ . We call a dynamical system modeled by (3) and (4) to be an impulsive linear system. According to the triggering set  $\mathcal{S}$ , impulsive linear systems expressed by (3) and (4) can be categorized into two main types: the time-dependent impulsive linear systems and the state-dependent impulsive linear systems, which can be described by

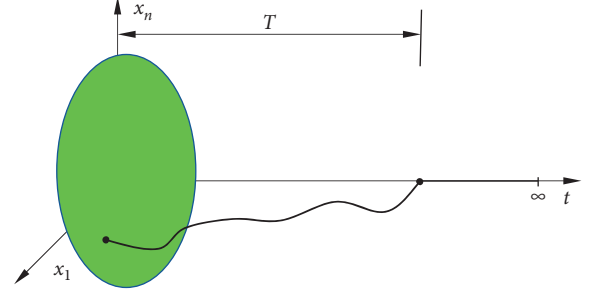


FIGURE 2: Schematic illustration of finite-time stability in a qualitative sense.

$$\begin{cases} \dot{x}(t) = A(t)x(t), & x(t_0) = x_0, & t \notin \mathcal{S} = \{t_1, t_2, \dots\} \subset \Omega, \\ x(t^+) = B(t)x(t), & t \in \mathcal{S}, & k = 1, 2, \dots, \end{cases} \quad (5)$$

$$\begin{cases} \dot{x}(t) = A(t)x(t), & x(t_0) = x_0, & x(t) \in \mathbb{R}^n \setminus \bigcup_{k=1}^N \mathcal{S}_k, \\ x(t^+) = B(t)x(t), & x(t) \in \mathcal{S}_k, & k = 1, 2, \dots, \end{cases} \quad (6)$$

respectively [31, 32, 35]. For a time-dependent impulsive linear system, the impulses occur at the given time points,  $t \in \mathcal{S} = \{t_1, t_2, \dots\} \subset \Omega$ , so the triggering set  $\mathcal{S}$  can be written as  $\mathcal{S} = \mathcal{S} \times \mathcal{D}(x_0, \mathcal{S})$ , where  $\mathcal{D}(x_0, \mathcal{S}) = \{x(t): t \in \mathcal{S}\} \subset \mathbb{R}^n$ . For a state-dependent impulsive linear system, the impulses happen when the system state reaches a preassigned set  $\mathcal{D} \subset \mathbb{R}^n$ , and then, the triggering set  $\mathcal{S}$  is written as  $\mathcal{S}(x_0, \mathcal{D}) = \{t \in \Omega: x(t) \in \mathcal{D}\} \subset \Omega$ . It is worth pointing out that the well-posedness of the triggering times should be guaranteed and the Zeno phenomena need to be avoided in this paper.

### 3. Finite-Time Stability in a Quantitative Sense

In this section, we will provide some results on finite-time stability in a quantitative sense for linear time-varying system (3) and its variants with impulses (4).

**3.1. State Transition Matrix.** In linear system theory, we know that the solution of (3) can be described as  $x(t) = \Phi(t, 0)x(0)$ , where the matrix-valued function  $\Phi(\cdot, \cdot)$  has the following basic properties:

$$\begin{aligned} \dot{\Phi}(t, 0) &= A(t)\Phi(t, 0), \\ \Phi(0, 0) &= I. \end{aligned} \quad (7)$$

This matrix-valued function  $\Phi(\cdot, \cdot)$  is called to be the state transition matrix, and an appropriate assumption on the nature of  $A(t)$  can ensure the existence and uniqueness of the state transition matrix. For system (3), it is stable in the sense of Lyapunov if there exists a positive constant  $M$  such that  $\|\Phi(t, 0)\| < M$  for all  $t \geq 0$ . Moreover, system (3) is asymptotically stable if it is stable and  $\lim_{t \rightarrow \infty} \Phi(t, 0) = 0$ .

As for finite-time stability of the system (3), a necessary and sufficient stability condition will be provided in the following theorem [30].

**Theorem 1.** *System (3) is finite-time stable with respect to  $(\Omega, \mathcal{X}_0, \mathcal{X}_t)$ , where  $\mathcal{X}_0 = \{x \in \mathbb{R}^n \mid x_0^\top R x_0 \leq 1\}$  and  $\mathcal{X}_t = \{x \in \mathbb{R}^n \mid x^\top Q(t)x \leq 1\}$  if and only if the state transition matrix of system (3) satisfies*

$$\Phi(t, 0)^\top Q(t) \Phi(t, 0) < R. \quad (8)$$

The state transition matrix approach has been extended to impulsive linear system (5) in [31, 32, 36]. Letting  $T \in [t_l, t_{l+1}]$ , the solution of the impulsive linear system (5) will be  $x(t) = \widehat{\Phi}(t, 0)x_0$ ,  $t \in \Omega$ , where  $\widehat{\Phi}(t, 0)$ , called the state transition matrix of (5), is a piecewise continuous matrix-valued function with discontinuous right-hand sides at the time instants  $t_k, k = 1, 2, \dots, l$ . In detail, when  $t \in (0, t_1]$ ,  $\widehat{\Phi}(t, 0)$  is the solution of the following matrix differential equation:

$$\frac{\partial}{\partial t} \widehat{\Phi}(t, 0) = A(t) \widehat{\Phi}(t, 0), \widehat{\Phi}(0, 0) = I, \quad (9)$$

$$\widehat{\Phi}(t_1^+, 0) = B(t_1) \widehat{\Phi}(t_1, 0).$$

In the sequel intervals for  $k = 1, 2, \dots, l-1$ ,  $\widehat{\Phi}(t, t_k)$  should satisfy

$$\frac{\partial}{\partial t} \widehat{\Phi}(t, t_k^+) = A(t) \widehat{\Phi}(t, t_k^+), \quad t \in (t_k, t_{k+1}], \quad (10)$$

$$\widehat{\Phi}(t_{k+1}^+, t_k^+) = B(t_{k+1}) \widehat{\Phi}(t_{k+1}, t_k^+).$$

In the end, when  $t \in (t_l, t_{l+1}]$ , we have

$$\frac{\partial}{\partial t} \widehat{\Phi}(t, t_l^+) = A(t) \widehat{\Phi}(t, t_l^+), \quad t \in (t_l, T]. \quad (11)$$

**Theorem 2.** *Impulsive linear system (5) is finite-time stable with respect to  $(\Omega, \mathcal{X}_0, \mathcal{X}_t)$ , where the sets  $\mathcal{X}_0$  and  $\mathcal{X}_t$  are the same with those in Theorem 1, if and only if for all  $t \in [0, T]$ , the following is satisfied:*

$$\widehat{\Phi}(t, 0)^\top Q(t) \widehat{\Phi}(t, 0) < R. \quad (12)$$

The conditions in the form of state transition matrices (8) and (12) in Theorems 1 and 2 are valuable for theoretical analysis but hard to apply due to the high computational difficulty, particularly for the time-varying case.

To obtain computational conditions for finite-time stability, some Lyapunov-like functions are needed to establish conditions in the form of linear matrix equalities or Lyapunov matrix inequalities. In some early work such as [3], it concludes that system (1) is finite-time stable with respect to  $(\Omega, \mathcal{S}_\alpha, \mathcal{S}_\beta)$  if and only if there exists a real-valued Lipschitz function  $V(t, x)$ , continuous on  $\Omega \times \overline{\mathcal{S}_\beta}$ , and a real-valued integrable function  $\varphi(t)$  such that, for  $t \in \Omega$ , we have  $\dot{V}_0(t, x) \leq \varphi(t)$  for all  $x \in [\mathcal{S}_\beta - \overline{\mathcal{S}_\alpha}]$  and  $\int_{t_1}^{t_2} \varphi(t) dt < V_{\min}^\beta(t_2) - V_{\max}^\alpha(t_1)$  for  $t_1 < t_2$  and  $t_1, t_2 \in \Omega$ . A

piecewise continuous Lyapunov-like function is the most common one in the literature, and relevant results will be presented in the following subsection.

**3.2. Piecewise Continuous Lyapunov-Like Functions.** To obtain computationally tractable finite-time stability conditions, we choose a quadratic piecewise continuous Lyapunov-like function  $V(t, x) = x^\top P(t)x$  and establish the following conditions containing coupled differential Lyapunov matrix equations and differential linear matrix inequalities.

**Theorem 3** (see [7, 30]). *System (3) is finite-time stable with respect to  $(\Omega, \mathcal{X}_0, \mathcal{X}_t)$ , where the sets  $\mathcal{X}_0$  and  $\mathcal{X}_t$  are the same with those in Theorem 1, if and only if for all  $t \in \Omega$ , there exists a symmetric piecewise differentiable matrix-valued function  $P(\cdot)$  such that the following conditions involving the differential matrix equation with boundary conditions are satisfied:*

$$\begin{aligned} \dot{P}(\tau) &= -A(\tau)^\top P(\tau) - P(\tau)A(\tau) - \varepsilon I, \quad \tau \in [0, t], \quad \varepsilon > 0, \\ P(t) &= Q(t), \quad P(0) < R. \end{aligned} \quad (13)$$

We see that Theorem 3 provides a necessary and sufficient condition for finite-stability of system (3). However, it is not practicable to verify the differential matrix equation in (13) for every  $\tau \in [0, t]$ , and hence, Theorem 3 is not suitable for the computational purpose. Using Theorem 3, we can obtain a sufficient condition with computational tractability for finite-stability of system (3).

**Theorem 4** (see [7, 30]). *System (3) is finite-time stable with respect to  $(\Omega, \mathcal{X}_0, \mathcal{X}_t)$ , where the sets  $\mathcal{X}_0$  and  $\mathcal{X}_t$  are the same as those in Theorem 1, if and only if for all  $t \in \Omega$  there exists a symmetric piecewise differentiable matrix-valued function  $P(\cdot)$  such that the following conditions involving the differential matrix equation with boundary conditions are satisfied:*

$$\begin{aligned} \dot{P}(t) &= -A(t)^\top P(t) - P(t)A(t) - \varepsilon I, \quad \varepsilon > 0, \\ P(t) &= Q(t), \quad P(0) < R. \end{aligned} \quad (14)$$

Nowadays, computational tools in the convex optimization framework such as linear matrix inequalities or differential linear matrix inequalities are very efficient, and we can obtain the following necessary and sufficient conditions including differential linear matrix inequalities, equivalent to (13):

$$\begin{aligned} \dot{P}(\tau) &< -A(\tau)^\top P(\tau) - P(\tau)A(\tau), \\ Q(t) &\leq P(t), \quad P(0) < R. \end{aligned} \quad (15)$$

The piecewise continuous Lyapunov-like function is also applied to the finite-time stability problem of impulsive linear systems. For linear time-varying systems with time-dependent impulses, we have the following finite-time stability results.

**Theorem 5** (see [36]). *System (5) is finite-time stable with respect to  $(\Omega, \mathcal{X}_0, \mathcal{X}_t)$ , where the sets  $\mathcal{X}_0$  and  $\mathcal{X}_t$  are the same with those in Theorem 1, if and only if for all  $t \in \Omega$  there exists a piecewise differentiable positive definite matrix-valued*

function  $P(\cdot)$  such that the following conditions involving differential linear matrix inequalities are satisfied:

$$\begin{aligned} \dot{P}(t) + A(t)^\top P(t) + P(t)A(t) &< 0, \quad t \notin \mathcal{J}, \\ P(t_k) &> B(t_k)^\top P(t_k^+) B(t_k), \quad k = 1, 2, \dots, \\ P(t) &\geq Q(t), \quad P(0) < R. \end{aligned} \quad (16)$$

Moreover, it is finite-time stable with respect to  $(\Omega, \mathcal{X}_0, \mathcal{X}_t)$  if and only if there exists a piecewise continuous positive definite matrix-valued solution  $Z(\cdot): \Omega \mapsto \mathbb{R}^{n \times n}$  such that the following conditions involving differential/difference Lyapunov equations are satisfied:

$$\begin{aligned} \dot{Z}(t) - A(t)Z(t) - Z(t)A(t)^\top &= 0, \quad t \notin \mathcal{J}, \\ Z^+(t_k) &= B(t_k)Z^-(t_k)B(t_k)^\top, \\ \&9; \quad t \in \mathcal{J}, \quad Z(0) &= R^{-1}, \\ G(t)W(t)G^\top(t) &< I, \quad \forall t \in \Omega, \end{aligned} \quad (17)$$

where  $G(\cdot)$  is a nonsingular matrix-valued function satisfying  $Q(t) = G^\top(t)G(t)$  in  $\Omega$ .

As for a linear time-varying system with state-dependent impulses (6), we have the following theorem to provide a sufficient condition for its finite-time stability.

**Theorem 6** (see [35]). *System (6) is finite-time stable with respect to  $(\Omega, \mathcal{X}_0, \mathcal{X}_t)$ , where the sets  $\mathcal{X}_0$  and  $\mathcal{X}_t$  are the same with those in Theorem 1, if and only if for all  $t \in \Omega$  there exists a piecewise differentiable positive definite matrix-valued function  $P(\cdot)$  such that the following conditions involving linear differential/difference matrix inequalities are satisfied:*

$$\begin{aligned} \dot{P}(t) + A(t)^\top P(t) + P(t)A(t) &< 0, \quad x(t) \in \mathbb{R}^n \setminus \bigcup_{k=1}^N \mathcal{S}_k, \\ x^\top (B(t)^\top P(t)B(t) - P(t))x &< 0, \quad x(t) \in \mathcal{S}_k, \quad k = 1, \dots, N, \\ P(t) &\geq G(t), \quad P(0) < R. \end{aligned} \quad (18)$$

When the initial set  $\mathcal{X}_0$  and the time-varying set  $\mathcal{X}_t$  are two given polytopes and a quadratic function  $V(x) = x^\top P x$  is chosen, we have following sufficient conditions of finite-time stability for a quadratic system:

$$\dot{x} = Ax + [x^\top C_1^\top x, x^\top C_2^\top x, \dots, x^\top C_n^\top x]^\top, \quad (19)$$

where  $C_i \in \mathbb{R}^{n \times n}$ ,  $i = 1, \dots, n$ .

**Theorem 7** (see [34]). *System (19) is finite-time stable with respect to  $(\Omega, \mathcal{X}_0, \mathcal{X}_t)$ , where the sets  $\mathcal{X}_0$  and  $\mathcal{X}_t$  are two given polytopes, if there exists a positive definite symmetric matrix  $P \in \mathbb{R}^{n \times n}$  such that*

$$\begin{aligned} \lambda_{\max}(P) \max_i \|x_{\mathcal{X}_0}^{(i)}\|^2 e^{\alpha T} \\ \begin{pmatrix} 1 & a_k^\top \\ a_k & P \end{pmatrix} \\ [A^\top + (B_1^\top x_{\mathcal{X}_t}^{(i)} B_2^\top x_{\mathcal{X}_t}^{(i)} \dots B_n^\top x_{\mathcal{X}_t}^{(i)})] P + P [A + (B_1^\top x_{\mathcal{X}_t}^{(i)} B_2^\top x_{\mathcal{X}_t}^{(i)} \dots B_n^\top x_{\mathcal{X}_t}^{(i)})^\top] - \alpha P \leq 0. \end{aligned} \quad (20)$$

The initial set  $\mathcal{X}_0$  and the time-varying set  $\mathcal{X}_t$  can also be piecewise quadratic domains over conical partitions  $\mathcal{P}_0 = \{U_1^0, U_2^0, \dots, U_u^0\}$  and  $\mathcal{P}_t = \{U_1^t, U_2^t, \dots, U_v^t\}$ , say  $\mathcal{X}_0 = \{x \in \mathbb{R}^n | x_0^\top R_i x_0 \leq 1, x_0 \in U_i^0, i = 1, 2, \dots, u\}$  and  $\mathcal{X}_t = \{x^\top Q_i(t)x \leq 1, x \in U_i^t, i = 1, 2, \dots, v\}$  [37, 38]. In such cases, we choose a time-varying piecewise quadratic Lyapunov-like function defined over the abovementioned conical partition as

$$V_{\mathcal{X}_t}(t, x) = x^\top P_i(t)x, \quad \forall x \in S_i \text{ with } i = 1, \dots, v, \quad (21)$$

where  $P_i \in \mathbb{R}^{n \times n}$ ,  $i = 1, \dots, v$ , are symmetric matrices. Then, a sufficient condition for the finite-time stability of linear-varying system (1) can be presented as follows.

**Theorem 8** (see [37]). *System (3) is finite-time stable with respect to  $(\Omega, \mathcal{X}_0, \mathcal{X}_t)$ , where the sets  $\mathcal{X}_0$  and  $\mathcal{X}_t$  are the given piecewise quadratic domains, if there exist positive definite symmetric matrices  $P_i \in \mathbb{R}^{n \times n}$  such that*

$$\begin{aligned} x^\top (\dot{P}_i(t) + A(t)^\top P_i(t) + P_i(t)A(t))x &< 0, \\ x^\top (P_i(t) - Q_i(t))x &\geq 0, \\ x^\top (P_i(0) - R_i)x &< 0. \end{aligned} \quad (22)$$

For  $t \in \Omega$  and  $x \in S_i$  with  $i = 1, \dots, v$ .

The sufficient conditions in (22) are not applicable due to the infinite number of matrix inequalities. Applying S-procedure arguments and considering the conical partition, a computationally tractable sufficient condition is also obtained in [37].

**Theorem 9** (see [37]). *System (3) is finite-time stable with respect to  $(\Omega, \mathcal{X}_0, \mathcal{X}_t)$ , where the sets  $\mathcal{X}_0$  and  $\mathcal{X}_t$  are the given piecewise quadratic domains, if there exist positive numbers  $b_{i,k}$ , positive real-valued functions  $c_{i,k}(t)$ ,  $z_{i,k}(t)$  and matrices  $H_{i,k}$ ,  $i = 1, \dots, v$  and  $k = 1, \dots, s$ , and positive definite symmetric matrices  $P_i \in \mathbb{R}^{n \times n}$  such that  $x^\top H_{i,k} x \leq 0$ ,  $\forall x \in S_i$  and there exist positive piecewise continuously differentiable matrix-valued functions  $P_i(t) \in \mathbb{R}^{n \times n}$ , such that the following*

conditions involving differential linear matrix inequalities and linear matrix inequalities are satisfied:

$$\begin{aligned} \dot{P}_i(t) + A(t)^\top P_i(t) + P_i(t)A(t) - \sum_{k=1}^s c_{i,k}(t)H_{i,k} &< 0, \\ P_i(t) - Q_i(t) + \sum_{k=1}^s z_{i,k}(t)H_{i,k} &\geq 0, \\ P_i(0) - R_i - \sum_{k=1}^s b_{i,k}H_{i,k} &< 0, \\ \widehat{x}_k^\top P_i(t)\widehat{x}_k = \widehat{x}_k^\top P_j(t)\widehat{x}_k, \forall \widehat{x}_k \in \text{extr}\{S_i \cap S_j\}, \\ \widehat{x}_h^\top P_i(t)\widehat{x}_k = \widehat{x}_h^\top P_j(t)\widehat{x}_k, \forall \widehat{x}_h, \widehat{x}_k \in \text{extr}\{S_i \cap S_j\}. \end{aligned} \quad (23)$$

**3.3. Converse Lyapunov-Like Theorem.** In [9], a converse Lyapunov-like theorem is established for finite-time uniformly stable continuous-time nonautonomous system (1). It provides the characterization of finite-time stability with regards to the existence of Lyapunov-like functions.

**Theorem 10** (see [9]). *If system (1) is uniformly stable with respect to  $(\Omega, \mathcal{S}_\alpha, \mathcal{S}_\beta)$ ,  $\alpha < \beta$ , then there exists a real-valued Lyapunov-like function  $V(t, x)$  satisfying*

$$\dot{V}_0(t, x) \leq \varphi(t), \quad (24)$$

for all  $x \in [\mathcal{S}_\beta - \overline{\mathcal{S}}_\alpha]$ , and

$$\int_{t_1}^{t_2} \varphi(t)dt < V_{\min}^\beta(t_2) - V_{\max}^\alpha(t_1), \quad (25)$$

for  $t_1 < t_2$  and  $t_1, t_2 \in \Omega$ .

Moreover, two necessary and sufficient conditions for the existence of a Lyapunov-like function  $V(t, x)$  for finite-time stability are given as follows.

**Theorem 11** (see [9]). *System (1) is finite-time stable with respect to  $(\Omega, \mathcal{S}_\alpha, \mathcal{S}_\beta)$ ,  $\alpha < \beta$ , if and only if there exist a Lipschitz continuous real-valued Lyapunov-like function  $V(t, x)$  and a continuous real-valued function  $\mu(\cdot)$  such that the following conditions are satisfied: (i)  $V(t, x) \geq \mu(\|x\|)$  for all, (ii)  $\dot{V}(t, x) \leq 0$  for all  $x \in [\mathcal{S}_\beta - \overline{\mathcal{S}}_\alpha]$ , and (iii)  $V_{\max}^\alpha(t) < \mu(\beta)$ .*

**Theorem 12** (see [39]). *System (1) is finite-time stable with respect to  $(\Omega, \mathcal{S}_\alpha, \mathcal{S}_\beta)$ ,  $\alpha < \beta$ , if and only if there exist a continuous real-valued Lyapunov-like function  $V(t, x)$  such that*

$$\dot{V}(t, x) \leq 0, \quad (26)$$

for all  $x \in \overline{\mathcal{S}}_\beta$ , and

$$V_{\min}^\beta(t_2) < V_{\max}^\alpha(t_1), \quad (27)$$

for all  $t_2 > t_1$  and  $\delta < \alpha$  with  $t_1, t_2 \in \Omega$ .

**3.4. Miscellaneous Issues.** Time delays are often encountered in many practical systems such as chemical processes, electric circuits, and networked systems, leading to

unsatisfactory system behaviours and even instability. So, various stability problems for delayed systems have attracted much attention to lots of researchers. Among them, finite-time stability analysis has been of particular interest bringing forth many papers such as [40–42].

A linear time-invariant delayed system can be represented by

$$\dot{x}(t) = A_0x(t) + A_1x(t-h), \quad h > 0, \quad (28)$$

with an associated initial state function

$$x(t) = \psi(t), \quad -h \leq t \leq 0. \quad (29)$$

To proceed, we need the following definitions.

**Definition 3.** System (28) associated with initial condition (29) is said to be finite-time stable with respect to  $(\zeta(\cdot), \beta, h)$  if  $\psi(t)^\top \psi(t) < \zeta(t)$ ,  $\forall t \in [-\tau, 0]$ , which implies  $x(t)^\top x(t) < \beta$ ,  $\forall t \in \Omega$ , where  $\zeta(\cdot)$  is a positive scalar-valued function satisfying  $\zeta(t) \leq \alpha$  for  $-h \leq t \leq 0$ , and  $\beta > \alpha > 0$ .

**Definition 4.** System (28) associated with initial condition (29) is said to be finite-time stable with respect to  $(\Omega, \alpha, \beta)$  if  $(\sup_{-h \leq \theta \leq 0} \|\psi(\theta)\|)^2 < \alpha$  implies  $\|x(t)\|^2 < \beta$ ,  $\forall t \in \Omega$ .

Next, we introduce two sufficient conditions for finite-time stability of linear delayed system (28) in the following two theorems.

**Theorem 13** (see [41]). *System (28) associated with the initial condition (29) is finite-time stable with respect to  $(\alpha, \beta, h)$  if for all  $t \in \Omega$ , we have*

$$\|\Phi(t)\| < \frac{\sqrt{(\beta/\alpha)}}{1 + \|A_1\|}, \quad (30)$$

where  $\Phi(t)$  is the fundamental matrix of linear delayed system (28).

**Theorem 14** (see [41]). *System (28) associated with initial condition (29) is finite-time stable with respect to  $(\Omega, \alpha, \beta)$  if*

$$(1 + \sigma_m t)^2 e^{2\sigma_m t} < \frac{\beta}{\alpha}, \quad (31)$$

where

$$\sigma_m = \sigma_{\max}(A_0) + \sigma_{\max}(A_1), \quad (32)$$

with  $\sigma_m(\cdot)$  being the largest singular value of the corresponding matrix.

In [40], the authors construct a delay-dependent Lyapunov-like function

$$V(t) = \left( x(t) + \int_0^h J(\theta)x(t-\theta)d\theta \right)^\top \left( x(t) + \int_0^h J(\theta)x(t-\theta)d\theta \right), \quad (33)$$

where  $J(t) \in \mathbb{R}^{n \times n}$  is a differentiable matrix-valued function on  $[0, h]$  such that the following differential matrix equation is satisfied:

$$\dot{J}(\theta) = (A_0 + J(0))J(\theta), \quad \theta \in [0, h], \quad (34)$$

with the initial condition  $J(h) = A_1$ . Then, the following result based on Lyapunov function (33) can be given.

**Theorem 15** (see [40]). *System (28) associated with initial condition (29) is finite-time stable with respect to  $(\alpha, \beta, h)$  if there exists a positive real number  $\gamma$  such that the following conditions are satisfied:*

$$\begin{aligned} & x(t - \theta)^\top x(t - \theta) \\ & \cdot (1 + h)(1 + \psi) \left(1 - \gamma\psi - \frac{ah}{\gamma}\right)^{-1} e^{\lambda_{\max}(R^\top + R)T} < \frac{\beta}{\alpha}, \\ & \gamma \in (\max\{\gamma_1, 0\}, \gamma_2), \gamma_{1,2} = \frac{1 \pm \sqrt{1 - 4\psi ha}}{2\psi}, \quad 4\psi ha < 1, \\ & \psi = \lambda_{\max}(J(0)J^\top(0)) \frac{e^{2\mu_1(\bar{A}_0)h} - 1}{2\mu_1(\bar{A}_0)}, \bar{A}_0 = A_0 + J(0), \end{aligned} \quad (35)$$

$$\begin{aligned} MA_0G &= \begin{pmatrix} A_{11} & A_{12} \\ A_{21} & A_{22} \end{pmatrix}, \begin{pmatrix} 0 \\ M_2 \end{pmatrix} A_0G = \begin{pmatrix} 0 & 0 \\ A_{21} & A_{22} \end{pmatrix}, MA_2G = \begin{pmatrix} D_{11} & D_{12} \\ D_{21} & D_{22} \end{pmatrix}, \\ W_1 &= PA_0 + A_0^\top P^\top + Q_1 + Q_2 \bar{M} A_0 + A_0^\top \bar{M}^\top Q_2^\top - \eta PE, W_2 = PA_1 + Q_2 \bar{M} A_1, \\ \bar{M} &= \begin{pmatrix} 0 \\ M_2 \end{pmatrix}, G^\top P M^{-1} = \begin{pmatrix} P_{11} & P_{12} \\ P_{21} & P_{22} \end{pmatrix}, M^{-1\top} M^{-1} = \begin{pmatrix} R_{11} & R_{12} \\ * & R_{22} \end{pmatrix}, \\ \alpha_1 &= \frac{\lambda_{\min}(P_{11})}{\lambda_{\max}(R_{11})}, \alpha_2 = \frac{\lambda_{\max}(P_{11})}{\lambda_{\min}(G^\top G)} + h\lambda_{\max}(Q_1), \alpha_3 = \frac{\alpha_2 \alpha}{\alpha_1}, \\ \alpha_4 &= \sum_{i=0}^{\lceil \tau/h \rceil - 1} \|A_{22}^{-1} D_{22}\|^i, \eta = \|A_{22}^{-1} D_{21} + A_{22}^{-1} D_{22}\|, \alpha_6 = \lambda_{\max}(G^\top G). \end{aligned} \quad (38)$$

Then, a sufficient condition for the finite-time stability of singular linear delayed system (37) was established in [42].

**Theorem 16** (see [42]). *System (37) associated with initial condition (29) is finite-time stable with respect to  $(\alpha, \beta, h)$  if there exists a positive number  $\gamma$ , a symmetric positive definite matrix  $Q_1 \in \mathbb{R}^{n \times n}$ , a nonsingular matrix  $P \in \mathbb{R}^{n \times n}$ , and a matrix  $Q_2 \in \mathbb{R}^{n \times n}$  such that*

$$\begin{aligned} PE &= E^\top P \geq 0, \begin{pmatrix} W_1 & W_2 \\ * & -Q_1 \end{pmatrix} < 0, \\ e^{\gamma T} \alpha_3 + \left(\alpha_5 + \eta \alpha_4 \sqrt{e^{\gamma T} \alpha_3}\right)^2 &\leq \frac{\beta}{\alpha_6}. \end{aligned} \quad (39)$$

where  $\mu_1(\cdot)$  is a matrix measure of the given matrix and  $J(0)$  is the solution of the following transcendental matrix equation:

$$e^{A_0 + J(0)h} J(0) = A_1. \quad (36)$$

Next, consider a singular linear delayed system

$$E\dot{x}(t) = A_0 x(t) + A_1 x(t - h), \quad h > 0, \quad (37)$$

where  $E \in \mathbb{R}^{n \times n}$  is a singular matrix with rank  $r < n$ . There exist two nonsingular matrices  $M = \begin{pmatrix} M_1 \\ M_2 \end{pmatrix}$  and  $G$  such that  $G$  such that  $\begin{pmatrix} I_r & 0 \\ 0 & 0 \end{pmatrix} = MEG$ . Let

More recently, the Lyapunov–Razumikhin approach is extended to finite-time stability for a nonlinear delayed system

$$\dot{x}(t) = f(t, x(t - h)), \quad (40)$$

in [43]. Sufficient conditions can be illustrated through the following theorem.

**Theorem 17** (see [43]). *System (40) associated with initial condition (29) is finite-time stable with respect to  $(\alpha, \beta, h)$  if there exists positive scalars  $\alpha, \beta, \eta, \sigma, T$  with  $\eta < \alpha < \beta$  and  $\sigma \in (0, T)$ , integrable real-valued function  $c(\cdot): \mathbb{R}^+ \mapsto \mathbb{R}$ , class  $\mathcal{K}$  functions  $\gamma_1, \gamma_2$ , and a differentiable function  $V: [-h, T] \times \mathbb{R}^n \mapsto \mathbb{R}^+$  such that (i)  $\gamma_1(|x|) \leq V(t, x) \leq \gamma_2(|x|), \forall (t, x) \in [-h, T] \times \mathbb{R}^n$ , (ii)  $\dot{V}(t, \psi(0)) \leq c(t)V(t,$*

$\psi(0)$ , whenever  $V(t+s, \psi(s)) \leq \Theta(t, s)V(t, \psi(0))$  for all  $t \in [0, T]$ ,  $s \in [-h, 0]$ , where

$$\Theta(t, s) = \exp\left(-\int_{\max\{t+s, 0\}}^t c(u)du\right), \quad (41)$$

and (iii)

$$\int_0^t c(u)du \leq \ln \frac{\gamma_1(\eta)}{\gamma_2(\sqrt{\alpha})}, \quad \forall t \in [0, T]. \quad (42)$$

Besides time delays, uncertainty is another important phenomenon commonly encountered in practical systems. The existence of uncertainty causes the poor performance and even instability. The finite-stability concept has been extended to uncertain linear systems [44–46]. The uncertainty can be expressed as norm-bounded uncertainty and structured uncertainty. Consider an uncertain linear system

$$\begin{pmatrix} \dot{P}(\tau) + A^\top(\tau)P(\tau) + P(\tau)A(\tau) + \gamma(\tau)F_2^\top(\tau)F_2(\tau) & P(\tau)F_1(\tau) + \gamma(\tau)F_2^\top(\tau)H(\tau) \\ F_1^\top(\tau)P(\tau) + \gamma(\tau)H(\tau)F_2(\tau) & -\gamma(\tau)(I - H^\top(\tau)H(\tau)) \end{pmatrix} < 0, \quad (44)$$

$$P(t) \geq Q(t), P(0) < R, \gamma(t) > 0, \quad \tau \in [0, t].$$

Similar to Theorem 3, necessary and sufficient conditions in Theorem 18 are not computationally tractable. For the computational purposes, we can see the following sufficient condition for finite-time stability of system (43).

**Theorem 19** (see [46]). *System (43) is finite-time stable with respect to  $(\Omega, \mathcal{X}_0, \mathcal{X}_t)$ , where the sets  $\mathcal{X}_0$  and  $\mathcal{X}_t$  are the same*

$$\begin{pmatrix} \dot{P}(t) + A^\top(t)P(t) + P(t)A(t) + \gamma(t)F_2^\top(t)F_2(t) & P(t)F_1(t) + \gamma(t)F_2^\top(t)H(t) \\ F_1^\top(t)P(t) + \gamma(t)H(t)F_2(t) & -\gamma(t)(I - H^\top(t)H(t)) \end{pmatrix} < 0, \quad (45)$$

$$P(t) \geq Q(t), P(0) < R, \gamma(t) > 0, \quad t \in \Omega.$$

Robustness analysis for a linear delayed system with structured uncertainty was conducted in [45], where the uncertain system is described by

$$\dot{x}(t) = (A_0 + D_0F(t)E_0)x(t) + (A_1 + D_1F(t)E_1)x(t-h), \quad (46)$$

$$\dot{x} = (A(t) + F_1(t)(I - \Delta(t)H(t))^{-1}\Delta(t)F_2(t))x(t), \quad (43)$$

where  $x(t) \in \mathbb{R}^n$ ,  $\Delta(\cdot)$  is a norm-bounded uncertainty function such as  $\|\Delta(t)\| \leq 1$  and  $F_1(\cdot), F_2(\cdot)$  are known matrices of appropriate dimensions. The following theorem will present a necessary and sufficient condition for finite-time stability of system (43).

**Theorem 18** (see [46]). *System (43) is finite-time stable with respect to  $(\Omega, \mathcal{X}_0, \mathcal{X}_t)$ , where the sets  $\mathcal{X}_0$  and  $\mathcal{X}_t$  are the same as those in Theorem 1, if and only if for all  $t \in \Omega$ , there exist a piecewise continuous function  $\gamma$  and a symmetric piecewise differentiable matrix-valued function  $P(\cdot)$  such that the following conditions involving differential linear matrix inequalities are satisfied:*

*as those in Theorem 1, if and only if for all  $t \in \Omega$ , there exist a piecewise continuous function  $\gamma$  and a symmetric piecewise differentiable matrix-valued function  $P(\cdot)$  such that the following conditions involving differential linear matrix inequalities are satisfied:*

where  $D_0, E_0, D_1, E_1$  are known matrices of appropriate dimension, and  $F(t)$  is the uncertain time-varying matrix with  $F(t)F(t)^\top \leq I, \forall t \in \Omega$ .

**Theorem 20.** (see [45]). *System (46) associated with initial condition (29) is finite-time stable with respect to  $(\alpha, \beta, h)$  if*

there exists positive real numbers  $\gamma, \delta, \beta_0, \beta_1, \beta_2, \beta_3$  and symmetric positive definite matrices  $P_1$  and  $P_2$  such that the following conditions are satisfied:

$$\begin{aligned} & \begin{bmatrix} \Omega_{11} & P_1 A_1 & P_1 D_0 & P_1 D_1 \\ * & -P_2 + \delta E_1^\top E_1 & 0 & 0 \\ * & * & -\gamma I & 0 \\ * & * & * & -\delta I \end{bmatrix} < 0, \\ & \Omega_{11} = A_0^\top P_1 + P_1 A_0 + P_2 - \beta_0 P_1 + \gamma E_0^\top E_0, \quad \beta_1 I < P_1 < \beta_2 I, \quad 0 < P_2 < \beta_3 I, \\ & \begin{bmatrix} -\beta e^{-\beta_0 t} \beta_1 & \sqrt{\alpha} \beta_2 & \sqrt{\alpha h} \beta_3 \\ * & -\beta_2 & 0 \\ * & * & -\beta_3 \end{bmatrix} < 0. \end{aligned} \quad (47)$$

If uncertain linear system (43) is affected by finite impulses (4), the system state will undergo abrupt changes at discrete time instants, which leads to more difficulty to analyze its stability performance. The following theorem from [46] gives a sufficient condition for finite-time stability of the linear time-varying system with both time-dependent impulses and uncertainty. More complex cases with a norm-bounded uncertainty on the impulsive matrix-valued

function and state-dependent impulses were also provided in [46] as well.

**Theorem 21** (see [44]). *System (3) is finite-time stable with respect to  $(\Omega, \mathcal{X}_0, \mathcal{X}_t)$ , where the sets  $\mathcal{X}_0$  and  $\mathcal{X}_t$  are the same as those in Theorem 1, if and only if for all  $t \in \Omega$ , there exists positive real number  $\gamma$  and a symmetric piecewise differentiable matrix-valued function  $P(\cdot)$  such that the following conditions are satisfied:*

$$\begin{aligned} & \begin{pmatrix} \dot{P}(t) + A^\top(t)P(t) + P(t)A(t) + \gamma F_2^\top F_2 & P(t)F_1 + \gamma F_2^\top H \\ F_1^\top P(t) + \gamma H^\top F_2 & -\gamma(I - H^\top H) \end{pmatrix} < 0, \quad t \notin \mathcal{J}, \\ & B(t)^\top P^+(t)B(t) - P(t) \leq 0, \quad t \in \mathcal{J}, \end{aligned} \quad (48)$$

All results mentioned above have illustrated the finite-time stability conditions in a quantitative sense, and we continue to introduce more results in a qualitative sense.

#### 4. Finite-Time Stability in a Qualitative Sense

It is well known that a radially unbounded positive definite function  $V: \mathcal{E} \subset \mathbb{R}^n \rightarrow \mathbb{R}^+$  with the property  $\dot{V}(x) < 0$  is a Lyapunov function. Lyapunov's second method demonstrates that the existence of the Lyapunov function is also equivalent to the asymptotical stability of system (1), which provides the foundation for the following necessary and sufficient conditions for finite-time stability results.

**Theorem 22** (see [27, 47]). *Consider an autonomous nonlinear system*

$$\dot{V}(x) \leq -cV(x)^\eta, \quad \text{for all } x \in \mathcal{E}. \quad (49)$$

*System (49) is finite-time stable if and only if there exists a smooth Lyapunov function (equivalently, all smooth Lyapunov functions)  $V: \mathcal{E} \rightarrow \mathbb{R}^+$  such that for all  $x \in \mathcal{E}$ ,*

$$T(x) = \int_{V(x)}^0 \frac{ds}{\dot{V}(x(\theta_x(s), x))} < +\infty, \quad (50)$$

where the map  $\theta_x$  is the inverse of  $t \mapsto V(x(t, x))$ .

**Theorem 23** (see [27, 47]). *System (49) is finite-time stable with a continuous settling-time function at the origin if and only if there exist a scalar  $\eta \in (0, 1)$ , a positive scalar  $c$ , and a smooth Lyapunov function  $V: \mathcal{E} \rightarrow \mathbb{R}^+$  such that*

$$\dot{V}(x) \leq -cV(x)^\eta, \quad \text{for all } x \in \mathcal{E}. \quad (51)$$

Moreover, the settling-time function  $T(x)$  should satisfy

$$T(x) \leq \frac{V(x)^{1-\eta}}{c(1-\eta)}. \quad (52)$$

A converse Lyapunov theorem was obtained for finite-time stability of nonlinear system (49) in [18]. As for the case that settling-time is continuous, we have the following converse theorem.

**Theorem 24** (see [18]). *If system (49) is finite-time stable with a continuous settling-time function at the origin and  $\eta \in (0, 1)$ , then there exists a continuous function  $V: \mathcal{C} \rightarrow \mathbb{R}^+$  such that*

$$\dot{V}(x) \leq -cV(x)^\eta, \quad \text{for all } x \in \mathcal{C}. \quad (53)$$

The abovementioned Lyapunov-based methods for analysis of finite-time stability may not be suitable for constructive design. Recently, an implicit Lyapunov function method to solve an algebraic equation was derived in [48], which provides a design method for a robust controller for the closed-loop systems to handle exogenous disturbances. The implicit Lyapunov function theorem only verifies stability conditions in an implicit way and does not need to solve the equation.

**Theorem 25** (see [48]). *System (1) is finite-time stable with a settling-time function  $T(x_0) \leq (V_0^\mu / (c\mu))$ , where  $Q(V_0, x_0) = 0$  if there exists a continuously differentiable function  $Z: \mathbb{R}_+ \times \mathbb{R}^n \rightarrow \mathbb{R}$  such that for any  $x \in \mathcal{C}$ , there exists a radially unbounded function  $V \in \mathbb{R}^+$  such that*

$$\begin{aligned} Z(V, x) = 0, \quad \frac{\partial Z(V, x)}{\partial V} < 0, \\ \sup_{t \in \mathbb{R}^+} \frac{\partial Z(V, x)}{\partial x} f < 0, \end{aligned} \quad (54)$$

for all  $(V, x) \in \Omega$ , where  $\Omega = \{(V, x) \in \mathbb{R}^+ \times \mathbb{R}^n: Z(V, x) = 0\}$  and  $\lim_{x \rightarrow 0} V = 0$ .

Recently, the notion of finite-time stability for nonlinear autonomous system (49) was extended to nonautonomous nonlinear system (1). These Lyapunov and converse Lyapunov results are derived and introduced in the following theorems.

**Theorem 26.** (see [17]). *System (1) is finite-time stable if there exist a scalar  $\eta \in (0, 1)$ , a positive function  $c(t)$ , a class  $\mathcal{K}$  function  $\gamma_1(\cdot)$ , and a continuously differentiable function  $V: \mathbb{R}^+ \times \mathcal{C} \rightarrow \mathbb{R}^+$  such that  $V(t, 0) = 0$ ,  $V(t, x) \geq \gamma_1(\cdot)$ , and*

$$\dot{V}(x) \leq -c(t)V(x)^\eta, \quad \text{for all } x \in \mathcal{C}. \quad (55)$$

Moreover, for the case  $\mathcal{C} = \mathbb{R}^n$ , then system (1) is globally finite-time stable. If there exists a class  $\mathcal{K}$  function  $\gamma_2(\cdot)$  such that  $V(t, x) \leq \gamma_2(\cdot)$ , then system (1) is uniformly finite-time stable.

**Theorem 27** (see [17]). *Let  $\eta \in (0, 1)$  and there exists a class  $\mathcal{K}$  function  $\varphi: [0, r] \rightarrow \mathbb{R}^+$ , where  $r > 0$  such that  $\mathcal{B}_r(0) \subseteq \mathcal{C}$  and*

$$\|f(t, x)\| \leq \varphi(\|x\|), \quad t \in [0, \infty), x \in \mathcal{B}_r(0). \quad (56)$$

If system (1) is uniformly finite-time stable and the settling-time function  $T(\cdot, \cdot)$  is jointly continuous at  $(t, 0)$ ,  $t \geq 0$ , then there exist a positive scalar  $c$ , a class  $\mathcal{K}$  function  $\gamma(\cdot)$ , and

a continuously differentiable function  $V: \mathbb{R}^+ \times \mathcal{C} \rightarrow \mathbb{R}^+$  such that  $V(t, 0) = 0$ ,  $V(t, x) \geq \gamma(\cdot)$ , and

$$\dot{V}(x) \leq -cV(x)^\eta, \quad \text{for all } x \in \mathcal{C}. \quad (57)$$

## 5. Conclusions

This paper has overviewed the fundamental results of the finite-time stability analysis of dynamical systems. The concepts of finite-time stability are classified into those in the quantitative and qualitative senses. Finite-time stability in a quantitative sense is firstly investigated. Then, finite-time stability results in a qualitative sense are outlined. This review paper is far from complete due to our limitations and nonawareness. We hope that this paper can be a useful resource for practitioners, researchers, and graduate students working in this field.

## Data Availability

The data used to support the findings of this study are available from the corresponding author upon request.

## Conflicts of Interest

The authors declare that they have no conflicts of interest.

## Acknowledgments

This work was supported in part by the Australian Research Council under Grant DP160102819.

## References

- [1] G. Kamenkov, "On stability of motion over a finite interval of time," *Journal of Applied Mathematics and Mechanics*, vol. 17, pp. 529–540, 2019, in Russian.
- [2] L. Weiss and E. Infante, "Finite time stability under perturbing forces and on product spaces," *IEEE Transactions on Automatic Control*, vol. 12, no. 1, pp. 54–59, 1967.
- [3] L. Weiss, "On uniform and nonuniform finite-time stability," *IEEE Transactions on Automatic Control*, vol. 14, no. 3, pp. 313–314, 1969.
- [4] A. A. Kayande and J. S W. Wong, "Finite time stability and comparison principles," in *Mathematical Proceedings of the Cambridge Philosophical Society*, vol. 64, pp. 749–756, Cambridge University Press, Cambridge, England, 1968.
- [5] P. Dorato, "Short-time stability in linear time-varying systems," Technical Report, Polytechnic Inst Of Brooklyn Ny Microwave Research Inst, New York City, NY, USA, 1961.
- [6] F. Amato, M. Ariola, C. Abdallah, and C. Cosentino, "Application of finite-time stability concepts to the control of ATM networks," in *Proceedings of the Annual Allerton Conference on Communication Control and Computing*, vol. 40, pp. 1071–1079, 2002.
- [7] F. Amato, R. Ambrosino, M. Ariola, C. Cosentino, G. De Tommasi et al., *Finite-time Stability and Control*, Springer, Berlin, Germany, 2014.
- [8] Y. Orlov, "Finite time stability and quasihomogeneous control synthesis of uncertain switched systems with application to underactuated manipulators," in *Proceedings of the 44th IEEE*



- Conference on Decision and Control*, pp. 4566–4571, Seville, Spain, December 2005.
- [9] L. Weiss, “Converse theorems for finite time stability,” *SIAM Journal on Applied Mathematics*, vol. 16, no. 6, pp. 1319–1324, 1968.
- [10] S. Boyd, L. El Ghaoui, E. Feron, and V. Balakrishnan, *Linear Matrix Inequalities in System and Control Theory*, SIAM, Lodhi, New Delhi, 1994.
- [11] Z. Gajic and M. T. J. Qureshi, *Lyapunov Matrix Equation in System Stability and Control*, Courier Corporation, Chelmsford, MA, USA, 2008.
- [12] A. Ohara and Y. Sasaki, “On solvability and numerical solutions of parameter-dependent differential matrix inequality,” vol. 4, pp. 3593–3594, in *Proceedings of the 40th IEEE Conference on Decision and Control*, vol. 4, IEEE, Orlando, FL, USA, December 2001.
- [13] H. Du, X. Lin, and S. Li, “Finite-time stability and stabilization of switched linear systems,” in *Proceedings of the 48th IEEE Conference on Decision and Control (CDC)*, pp. 1938–1943, Shanghai, China, 2009.
- [14] X. Li, X. Lin, S. Li, and Y. Zou, “Finite-time stability of switched nonlinear systems with finite-time unstable subsystems,” *Journal of the Franklin Institute*, vol. 352, no. 3, pp. 1192–1214, 2015.
- [15] R. Kuiava, B. K. Matos, and G. R. Razente, “Finite-time stability of a class of continuous-time non-homogeneous switched systems,” *Nonlinear Analysis: Hybrid Systems*, vol. 26, pp. 101–114, 2017.
- [16] Z. Yan, W. Zhang, and G. Zhang, “Finite-time stability and stabilization of Ito stochastic systems with Markovian switching: mode-dependent parameter approach,” *IEEE Transactions on Automatic Control*, vol. 60, no. 9, pp. 2428–2433, 2014.
- [17] W. M. Haddad, S. G. Nersesov, and L. Du, “Finite-time stability for time-varying nonlinear dynamical systems,” in *Proceedings of the American Control Conference*, pp. 4135–4139, Seattle, WA, USA, 2008.
- [18] S. P. Bhat and D. S. Bernstein, “Finite-time stability of continuous autonomous systems,” *SIAM Journal on Control and Optimization*, vol. 38, no. 3, pp. 751–766, 2000.
- [19] S. P. Bhat and D. S. Bernstein, “Geometric homogeneity with applications to finite-time stability,” *Mathematics of Control, Signals, and Systems*, vol. 17, no. 2, pp. 101–127, 2005.
- [20] E. Moulay and W. Perruquetti, “Finite time stability of nonlinear systems,” in *Proceedings of the 42nd IEEE International Conference on Decision and Control*, pp. 3641–3646, Lahaina, HI, USA, December 2003.
- [21] D. Liu and Q. Huang, “Research on finite-time stability of nonlinear switched systems,” in *Proceedings of the 25th Chinese Control and Decision Conference (CCDC)*, pp. 1314–1319, Guiyang, China, May 2013.
- [22] R. Yang and Y. Wang, “Finite-time stability and stabilization of a class of nonlinear time-delay systems,” *SIAM Journal on Control and Optimization*, vol. 50, no. 5, pp. 3113–3131, 2012.
- [23] H. Yang, B. Jiang, and J. Zhao, “On finite-time stability of cyclic switched nonlinear systems,” *IEEE Transactions on Automatic Control*, vol. 60, no. 8, pp. 2201–2206, 2014.
- [24] J. Wu, D. Yang, X. He, and X. Li, “Finite-time stability for a class of underactuated systems subject to time-varying disturbance,” *Complexity*, vol. 2020, pp. 1–7, Article ID 8704505, 2020.
- [25] F. Amato, M. Ariola, M. Carbone, and C. Cosentino, “Finite-time control of linear systems: A survey,” in *Current Trends in Nonlinear Systems and Control*, pp. 195–213, Springer, Berlin, Germany, 2006.
- [26] S.-H. Ding and S.-H. Li, “A survey for finite-time control problems,” *Control and Decision*, vol. 26, no. 2, pp. 161–169, 2011.
- [27] E. Moulay and W. Perruquetti, “Finite-time stability and stabilization: state of the art,” in *Advances in Variable Structure and Sliding Mode Control*, pp. 23–41, Springer, Berlin, Germany, 2006.
- [28] F. Amato, G. De Tommasi, and A. Pironti, *Finite-time Stability: An Input-Output Approach*, John Wiley & Sons, Hoboken, NJ, USA, 2018.
- [29] Y. Xia, J. Zhang, K. Lu, and N. Zhou, *Finite Time and Cooperative Control of Flight Vehicles*, Springer, Berlin, Germany, 2019.
- [30] F. Amato, M. Ariola, and C. Cosentino, “Finite-time stability of linear time-varying systems: Analysis and controller design,” *IEEE Transactions on Automatic Control*, vol. 55, no. 4, pp. 1003–1008, 2010.
- [31] F. Amato, R. Ambrosino, M. Ariola, F. Calabrese, and C. Cosentino, “Finite-time stability of linear time-varying systems with jumps: Analysis and controller design,” in *Proceedings of the American Control Conference*, pp. 1638–1643, Seattle, WA, USA, September 2008.
- [32] F. Amato, R. Ambrosino, M. Ariola, and C. Cosentino, “Finite-time stability of linear time-varying systems with jumps,” *Automatica*, vol. 45, no. 5, pp. 1354–1358, 2009.
- [33] S. Zhao, J. Sun, and L. Liu, “Finite-time stability of linear time-varying singular systems with impulsive effects,” *International Journal of Control*, vol. 81, no. 11, pp. 1824–1829, 2008.
- [34] F. Amato, C. Cosentino, and A. Merola, “Sufficient conditions for finite-time stability and stabilization of nonlinear quadratic systems,” *IEEE Transactions on Automatic Control*, vol. 55, no. 2, pp. 430–434, 2010.
- [35] R. Ambrosino, F. Calabrese, C. Cosentino, and G. De Tommasi, “Sufficient conditions for finite-time stability of impulsive dynamical systems,” *IEEE Transactions on Automatic Control*, vol. 54, no. 4, pp. 861–865, 2009.
- [36] F. Amato, G. De Tommasi, and A. Pironti, “Necessary and sufficient conditions for finite-time stability of impulsive dynamical linear systems,” *Automatica*, vol. 49, no. 8, pp. 2546–2550, 2013.
- [37] R. Ambrosino, E. Garone, M. Ariola, and F. Amato, “Piecewise quadratic functions for finite-time stability analysis,” in *Proceedings of the 51st IEEE Conference on Decision and Control (CDC)*, pp. 6535–6540, Wailea, HI, USA, December 2012.
- [38] J. Huang, J. Li, and H. Xu, “Feedback finite-time stabilization of impulsive linear systems over piecewise quadratic domains,” *Complexity*, vol. 2020, 2020.
- [39] J. Kaplan, “Converse theorems for finite-time stability and practical stability,” *IEEE Transactions on Circuit Theory*, vol. 20, no. 1, pp. 66–67, 1973.
- [40] D. L. Debeljkovic, S. B. Stojanovic, and A. M. Jovanovic, “Finite-time stability of continuous time delay systems: Lyapunov-like approach with Jensen’s and Coppel’s inequality,” *Acta Polytechnica Hungarica*, vol. 10, no. 7, pp. 135–150, 2013.
- [41] M. P. Lazarevic, D. L. Debeljkovic, Z. L. Nenadic, and S. A. Milinkovic, “Finite-time stability of delayed systems,” *IMA Journal of Mathematical Control and Information*, vol. 17, no. 2, pp. 101–109, 2000.
- [42] V. N. Phat, N. H. Muoi, and M. V. Bulatov, “Robust finite-time stability of linear differential-algebraic delay equations,”

- Linear Algebra and Its Applications*, vol. 487, pp. 146–157, 2015.
- [43] X. Li, X. Yang, and S. Song, “Lyapunov conditions for finite-time stability of time-varying time-delay systems,” *Automatica*, vol. 103, pp. 135–140, 2019.
  - [44] F. Amato, R. Ambrosino, M. Ariola, and G. De Tommasi, “Robust finite-time stability of impulsive dynamical linear systems subject to norm-bounded uncertainties,” *International Journal of Robust and Nonlinear Control*, vol. 21, no. 10, pp. 1080–1092, 2011.
  - [45] S. B. Stojanovic, D. L. Debeljkovic, and D. S. Antic, “Robust finite-time stability and stabilization of linear uncertain time-delay systems,” *Asian Journal of Control*, vol. 15, no. 5, pp. 1548–1554, 2013.
  - [46] F. Amato, M. Ariola, and C. Cosentino, “Robust finite-time stabilisation of uncertain linear systems,” *International Journal of Control*, vol. 84, no. 12, pp. 2117–2127, 2011.
  - [47] E. Moulay and W. Perruquetti, “Lyapunov-based approach for finite time stability and stabilization,” in *Proceedings of the 44th IEEE Conference on Decision and Control*, pp. 4742–4747, Seville, Spain, December 2005.
  - [48] A. Polyakov, D. Efimov, and W. Perruquetti, “Finite-time and fixed-time stabilization: implicit Lyapunov function approach,” *Automatica*, vol. 51, pp. 332–340, 2015.

## Research Article

# Fixed-Time Trajectory Tracking Control of Autonomous Surface Vehicle with Model Uncertainties and Disturbances

Jiawen Cui and Haibin Sun 

School of Engineering, Qufu Normal University, Rizhao 276826, China

Correspondence should be addressed to Haibin Sun; [fengyun198212@163.com](mailto:fengyun198212@163.com)

Received 26 May 2020; Revised 23 September 2020; Accepted 29 September 2020; Published 15 October 2020

Academic Editor: Jianquan Lu

Copyright © 2020 Jiawen Cui and Haibin Sun. This is an open access article distributed under the Creative Commons Attribution License, which permits unrestricted use, distribution, and reproduction in any medium, provided the original work is properly cited.

The issue of fixed-time trajectory tracking control for the autonomous surface vehicles (ASVs) system with model uncertainties and external disturbances is investigated in this paper. Particularly, convergence time does not depend on initial conditions. The major contributions include the following: (1) An integral sliding mode controller (ISMC) via integral sliding mode surface is first proposed, which can ensure that the system states can follow the desired trajectory within a fixed time. (2) Unknown external disturbances are absolutely estimated by means of designing a fixed-time disturbance observer (FTDO). By combining the FTDO and ISMC techniques, a new control scheme (FTDO-ISMC) is developed, which can achieve both disturbance compensation and chattering-free condition. (3) Aiming at reconstructing the unknown nonlinear dynamics and external disturbances, a fixed-time unknown observer (FTUO) is proposed, thus providing the FTUO-ISMC scheme that finally achieves trajectory tracking of ASVs with unknown parameters. Finally, simulation tests and detailed comparisons indicate the effectiveness of the proposed control scheme.

## 1. Introduction

With marine engineering operations developing and progressing, autonomous surface vehicles (ASVs) are instrumental in river and oil pipeline inspection, hull inspection, ocean survey, levee inspection, underwater archaeology, and underwater wreck inspection [1–5]. ASVs are usually perceived as a class of nonlinear dynamic systems equipped with complex external disturbances and model uncertainties [6]. It is an overwhelming matter to design a highly efficient controller for the ASV system.

Trajectory tracking is a basic problem for ASVs; however, as the system dynamics of ASV are highly nonlinear and there are unpredictable external disturbances in the marine environment, designing an effective controller for ASVs is a challenging issue. Many classical control algorithms such as feedback linearization [7], backstepping control [8], PID control [9], adaptive control [10], fuzzy control [11], and neural networks control [12] have been implemented to the trajectory tracking control of ASVs. The

system states generally realize either asymptotic convergence or exponential convergence. In addition, many scholars have proposed many compound control methods in combination with above different control theories that apply to actual control systems [13–18], especially ASV systems [5, 6, 9], etc.

The finite-time control scheme profits from short divergence span and strong robustness, which is applied to various nonlinear control systems. In this respect, continuous finite-time control schemes for robotic manipulators have already been designed utilizing terminal sliding mode control theory in [19], and a nonsingular terminal sliding mode control scheme for a marine vehicle with complex unknowns has been presented in [20]. Moreover, a finite-time integral sliding controller in [21] has been designed to realize the path following of the ASVs.

Although the finite-time tracking control problems are achieved in the above references, the convergence time is to depend on the original states. When the initial time tends to infinity, the convergence time also tends to infinity. However, compared with the finite-time control schemes, the

converge speed of the fixed-time control schemes is quite insensitive to initial condition [22, 23]. Recently, many fixed-time sliding mode control schemes have been proposed. For nonlinear systems with matched uncertainties and disturbances, a fixed-time nonsingular terminal sliding mode controller has been proposed in [24]. In [25], for the trajectory tracking control, a fixed-time nonsingular terminal sliding mode controller for a warship-launched submarine with multiple disturbances has been presented. In addition, a fixed-time sliding mode control for fault-tolerant trajectory tracking of an ASV has been designed in [26].

As known, chattering is an inherent phenomenon in sliding mode control. To reduce the chattering, a feasible solution is that disturbance observer-based control (DOBC) schemes are used to estimate external disturbances and model uncertainties and the disturbance estimation values are introduced into sliding mode control law. In order to improve the convergence speed and robustness, some finite-time disturbance observers were designed to estimate external disturbances and model uncertainties [27–32].

In this brief, the fixed-time trajectory tracking control scheme for ASVs with external disturbances and model uncertainties is explored. An integral sliding mode controller (ISMC) is firstly intended by using ISM surface for the ASV system without external disturbances, so that system states can attain the expected value in fixed time. Next, a fixed-time disturbance observer (FTDO) is designed to estimate the external disturbances and a new control scheme (FTDO-ISMC) is constructed to enable that the system states can accurately track the expected trajectory within fixed time even if there exist unexpected external disturbances. Furthermore, to guarantee good tracking performance against both disturbances and unknown system dynamics, a corresponding fixed-time unknown observer based on ISMC (FTUO-ISMC) control scheme is proposed. As a consequence, simulation results imply that the proposed control schemes can guarantee the system states to track the desired trajectory in a fixed time in spite of the ASV system subject to unknown disturbances and model uncertainties and the convergence speed is regardless of the origin states of the ASV system.

The remainder of this paper is structured as follows: In Section 2, some definitions and lemmas related to the trajectory tracking problem are formulated. The problem of the paper is described in Section 3. Section 4 describes the design of fixed-time controller and its stability analysis. Simulation results and discussion are mentioned in Section 5. And, Section 6 summarizes the main conclusions of this paper.

## 2. Preliminaries

**Lemma 1** (see [33]). *Consider the following double-integrator system:*

$$\begin{aligned} \dot{x}_1 &= x_2, \\ \dot{x}_2 &= u, \\ x(0) &= x_0, \end{aligned} \quad (1)$$

with the control law

$$\begin{aligned} u(t) &= -(k_1 [x_1]^{q_1} + k_1' [x_1] + k_2'' [x_1]^{q_1'}) \\ &\quad - (k_2 [x_2]^{q_2} + k_2' [x_2] + k_2'' [x_2]^{q_2'}), \end{aligned} \quad (2)$$

where parameters  $k_i > 0$ ,  $k_i' > 0$ ,  $k_i'' > 0$  ( $i = 1, 2$ ), and  $q_i, q_i'$  ( $i = 1, 2$ ) are chosen by

$$\begin{aligned} q_1 &= \frac{\varrho}{2 - \varrho}, \\ q_2 &= \varrho, \\ q_1' &= \frac{4 - 3\varrho}{2 - \varrho}, \\ q_2' &= \frac{4 - 3\varrho}{3 - 2\varrho}, \end{aligned} \quad (3)$$

with  $\varrho \in (0, 1)$  and  $[x]^\alpha = |x|^\alpha \text{sign}(x)$ ,  $\alpha \geq 0$ . Next, the state of the double-integrator system is fixed-time stability with convergence time  $t_f$ .

**Lemma 2** (see [34]). *Consider the following nonlinear system:*

$$\begin{aligned} \dot{x}(t) &= f(x, t), \\ f(0, t) &= 0, \\ x(0) &= x_0, \end{aligned} \quad (4)$$

where  $x \in \mathbb{R}^n$  and  $f: \mathbb{R}_+ \times \mathbb{R}^n \rightarrow \mathbb{R}^n$  is a nonlinear function. For the above system, suppose that there is a continuous radially unbounded function  $V: \mathbb{R}^n \rightarrow \mathbb{R}_+ \cup \{0\}$  which satisfies

- (1)  $V(x) = 0$ , when  $x = 0$
- (2)  $\dot{V}(x) \leq -\alpha V^p(x) - \beta V^q(x)$  for some  $\alpha, \beta, p, q > 0$ , with  $0 < p < 1$  and  $q > 1$

The considered nonlinear system is globally fixed-time stable within the settling time  $T$  satisfying

$$T \leq T_{\max} := \frac{1}{\alpha(1-p)} + \frac{1}{\beta(q-1)}. \quad (5)$$

## 3. System Modeling and Problem Formulation

The kinematics and dynamics of the ASV system regarded as rigid body with three degrees of freedom (3-DOF) are represented by [6]

$$\dot{\eta} = R(\varphi)v, \quad (6)$$

$$M\dot{v} = -C(v)v - D(v)v - g(\eta) + \tau + MR^T d_l(t), \quad (7)$$

where  $\eta = [x, y, \varphi]^T$  is the location  $(x, y)$  and course angle  $(\varphi)$  of ASVs in an earth-fixed inertial frame,  $v = [u, v, r]^T$  is the linear velocities  $(u, v)$  and angular rate  $(r)$  in the body-fixed frame,  $\tau = [F_u, F_v, F_r]^T$  stands for the actual control thrust, and  $d_l(t)$  denotes unsuspected external disturbances owing to complex surface environment including wind,

waves, and ocean current. The rotation matrix  $R(\varphi)$  is defined by

$$R(\varphi) = \begin{bmatrix} \cos \varphi & -\sin \varphi & 0 \\ \sin \varphi & \cos \varphi & 0 \\ 0 & 0 & 1 \end{bmatrix}, \quad (8)$$

being provided with the following characters:  $R^T(\varphi)R(\varphi) = I$ ,  $\dot{R}(\varphi) = R(\varphi)S(r)$ ,  $\forall \varphi \in [0, 2\pi]$ , and  $R^T(\varphi)S(r)R(\varphi) = R(\varphi)S(r)R^T(\varphi) = S(r)$ , where

$$S(r) = \begin{bmatrix} 0 & -r & 0 \\ r & 0 & 0 \\ 0 & 0 & 0 \end{bmatrix} \quad (9)$$

is the inertia matrix  $M = M^T > 0$  and

$$M = \begin{bmatrix} m - X_{\dot{u}} & 0 & 0 \\ 0 & m - Y_{\dot{v}} & mx_g - Y_{\dot{r}} \\ 0 & mx_g - N_{\dot{v}} & I_z - N_{\dot{r}} \end{bmatrix}, \quad (10)$$

where  $m$  is the mass of the system,  $I_z$  is the inertia matrix concerned with the yaw angle,  $Y_{\dot{r}} = N_{\dot{v}}$ , and  $X_{\dot{u}}$ ,  $Y_{\dot{v}}$ , and  $Z_{\dot{w}}$  denote the corresponding hydrodynamic derivatives. Coriolis and centripetal matrix  $C(v) = -C(v)^T$  have the following form:

$$C(v) = \begin{bmatrix} 0 & 0 & c_{13}(v) \\ 0 & 0 & c_{23}(v) \\ -c_{13}(v) & -c_{23}(v) & 0 \end{bmatrix}, \quad (11)$$

and the damping matrix  $D(v)$  is described by

$$D(v) = \begin{bmatrix} d_{11}(v) & 0 & 0 \\ 0 & d_{22}(v) & d_{23}(v) \\ 0 & d_{32}(v) & d_{33}(v) \end{bmatrix}, \quad (12)$$

where  $c_{13}(v) = -m(x_g r + v) + X_{\dot{u}}v + Y_{\dot{r}}r$ ,  $c_{23}(v) = mu - X_{\dot{u}}u$ , and  $d_{11}(v) = -X_{\dot{u}} - X_{|u|u}|u| - X_{|uu}u^2$ ,  $d_{22}(v) = -Y_{\dot{v}} - Y_{|v|v}|v|$ ,  $d_{23}(v) = -Y_{\dot{r}} - Y_{|v|r}|v| - Y_{|r|r}|r|$ ,  $d_{32}(v) = -N_{\dot{v}} - N_{|v|v}|v| - N_{|r|v}|r|$ , and  $d_{33}(v) = -N_{\dot{r}} - N_{|v|r}|v| - N_{|r|r}|r|$ . And  $g(\eta)$  is the gravity and buoyancy forces and moments, which is usually used as a constant in ASV.

Consider the desired trajectory as follows:

$$\dot{\eta}_d = R(\varphi_d)v_d, \quad (13)$$

$$M\dot{v}_d = -C(v_d)v_d - D(v_d)v_d + \tau_d, \quad (14)$$

where  $\eta_d = [x_d, y_d, \varphi_d]^T$  and  $v_d = [u_d, v_d, r_d]^T$  denote its desired position and velocity vectors, and the model contains no unknown nonlinear dynamics including external disturbances and model uncertainties.

*Assumption 1.* For disturbance vector  $d_l(t)$ , it is given that constants  $\kappa_i$  satisfies  $|\dot{d}_l(t)| \leq \kappa_i$ , where  $\kappa_i$  is an unknown nonnegative bounded constant.

The control purpose, in this paper, is to design fixed-time trajectory tracking control schemes so that the practical

position and velocity (6)-(7) can precisely pursuit the expected ones (13)-(14), respectively.

## 4. Controller Design and Stability Analysis

*4.1. Coordinate Transformation.* Consider coordinate transformations as follows:

$$\begin{aligned} \sigma &= Rv, \\ \sigma &\in \{\sigma, \sigma_d\}, \\ v &\in \{v, v_d\}, \\ R &\in \{R, R_d\}, \end{aligned} \quad (15)$$

where  $\sigma = [\sigma_1, \sigma_2, \sigma_3]^T$ ,  $\sigma_d = [\sigma_{d1}, \sigma_{d2}, \sigma_{d3}]^T$ ,  $R = R(\varphi)$ , and  $R_d = R(\varphi_d)$ .

By combining (6)-(7) and (15), we can obtain

$$\begin{aligned} \dot{\eta} &= \sigma, \\ \dot{\sigma} &= RM^{-1}\tau + \Theta(\eta, \sigma) + d_l(t), \end{aligned} \quad (16)$$

where

$$\begin{aligned} \Theta(\eta, \sigma) &= S(\sigma)\sigma - RM^{-1}(C(R^T\sigma) + D(R^T\sigma))R^T \\ &\quad \sigma - RM^{-1}g(\eta). \end{aligned} \quad (17)$$

Similarly, together with (13), (14), and (15), we obtain

$$\begin{aligned} \dot{\eta}_d &= \sigma_d, \\ \dot{\sigma}_d &= R_dM^{-1}\tau_d + \Theta_d(\eta_d, \sigma_d), \end{aligned} \quad (18)$$

where

$$\begin{aligned} \Theta_d(\eta_d, \sigma_d) &= S(\sigma_d)\sigma_d - R_dM^{-1}(C(R_d^T\sigma_d) \\ &\quad + D(R_d^T\sigma_d))R_d^T\sigma_d. \end{aligned} \quad (19)$$

Define the position and velocity error  $\eta_e = [\eta_{e1}, \eta_{e2}, \eta_{e3}]^T$  and  $\sigma_e = [\sigma_{e1}, \sigma_{e2}, \sigma_{e3}]^T$ . Then, we have

$$\begin{aligned} \dot{\eta}_e &= \sigma_e, \\ \dot{\sigma}_e &= RM^{-1}\tau - R_dM^{-1}\tau_d + d_l(t) + \Theta_e(\eta, \sigma, \eta_d, \sigma_d), \end{aligned} \quad (20)$$

where

$$\Theta_e(\eta, \sigma, \eta_d, \sigma_d) = \Theta(\eta, \sigma) - \Theta_d(\eta_d, \sigma_d). \quad (21)$$

*4.2. Design of the ISMC without External Disturbances.* In this section, an ISMC is firstly proposed for tracking error systems (20) and (21) without external disturbances, and the fixed-time stability is verified.

The ISM manifold is designed as follows:

$$s(\sigma_e(t)) = \sigma_e(t) + \int_{t_0}^t u_n(\sigma_e(\theta))d\theta, \quad (22)$$

where

$$u_n = k_1 [\eta_e]^{e_1} + k_1' [\eta_e] + k_1'' [\eta_e]^{e_1'} + k_2 [\sigma_e]^{e_2} + k_2' [\sigma_e] + k_2'' [\sigma_e]^{e_2'}. \quad (23)$$

and parameters are provided in Lemma 1.

The ISMC can be designed as

$$\tau_{\text{ISMC}} = MR^{-1} (R_d M^{-1} \tau_d - \Theta_e - u_n - \xi_1 [s]^\alpha - \xi_2 [s]^\beta), \quad (24)$$

where  $0 < \alpha < 1$ ,  $\beta > 1$ ,  $\xi_1 > 0$ , and  $\xi_2 > 0$ .

**Theorem 1** (ISMC). *Consider tracking error systems (20)-(21) without external disturbances, and an ISMC is designed by (24). Systems (6) and (7) can converge to desired trajectories (13) and (14) within a fixed time, i.e.,  $\eta \equiv \eta_d$  and  $v \equiv v_d$ , when  $t > T_{f1}$ .*

*Proof.* There are two processes in the whole verification: the reaching and the sliding phases:

- (i) Step 1: taking the derivative of ISM surfaces (22) and (23) along error systems (20) and (21) without external disturbances  $\hat{d}_i(t)$  and combining with the control law (24), we can obtain

$$\dot{s} = \dot{\sigma}_e + u_n = -\xi_1 [s]^\alpha - \xi_2 [s]^\beta. \quad (25)$$

Take the candidate Lyapunov function as follows:

$$V(s) = \frac{1}{2} s^2. \quad (26)$$

Differentiating it along the dynamics (25), we obtain

$$\begin{aligned} \dot{V}(s) &= s\dot{s} = s(-\xi_1 [s]^\alpha - \xi_2 [s]^\beta) = -\xi_1 |s|^{\alpha+1} - \xi_2 |s|^{\beta+1} \\ &= -2^{\alpha+1/2} \xi_1 V^{\alpha+1/2} - 2^{\beta+1/2} \xi_2 V^{\beta+1}. \end{aligned} \quad (27)$$

According to Lemma 2, it is claimed that the ISM control law will let the system states reach the ISM surface  $s = 0$  within a fixed time.

- (ii) Step 2: at that moment, error system (20) will reduce to the following system:

$$\begin{aligned} \dot{\eta}_e &= \sigma_e, \\ \dot{\sigma}_e &= -u_n(\eta_e, \sigma_e). \end{aligned} \quad (28)$$

By applying Lemma 1, we have that system (28) is globally fixed-time stable. Eventually, errors  $\eta_e$  and  $\sigma_e$  are converging to zero within a fixed time  $t_f$ , so this completes the proof. Under the ISMC scheme, the convergence time of the ASV system is  $T_{f1} = T_0 + t_f$ , where  $T_0 = 1/2^{(\alpha-1)/2} \xi_1 (1-\alpha) + 1/2^{(\beta-1)/2} \xi_2 (\beta-1)$ .

*Remark 1.* External disturbances are not considered in ISMC excogitation, but they are actually exist in the actual

environment. Therefore, controller design for the ASV system with external disturbances is essential.

**4.3. Design of FTDO-ISMC.** To achieve accurate tracking performance, in this section, a FTDO is built to estimate the external disturbances. Inspired by [35–37], a FTDO algorithm is established as

$$\begin{aligned} \chi_0 &= \sigma - \chi, \\ \dot{\chi} &= RM^{-1} \tau - R_d M^{-1} \tau_d + \Theta_e(\eta, \sigma, \eta_d, \sigma_d) + \hat{d}_1(t) + \psi_i, \\ \psi_i &= \lambda_{1i} |\chi_{0i}|^{1/2} \text{sign}(\chi_{0i}) + \lambda_{2i} |\chi_{0i}|^{\gamma_i} \text{sign}(\chi_{0i}), \\ \hat{d}_1(t) &= \beta_i \text{sign}(\chi_{0i}), \quad i = 1, 2, 3, \end{aligned} \quad (29)$$

where  $\chi_0 = [\chi_{01}, \chi_{02}, \chi_{03}]^T$  is an auxiliary variable,  $\psi = [\psi_1, \psi_2, \psi_3]^T$ ,  $\hat{d}_1(t) = [\hat{d}_{11}(t), \hat{d}_{12}(t), \hat{d}_{13}(t)]^T$  denotes the estimation of  $d_1(t)$ ,  $\lambda_{1i}$  and  $\lambda_{2i}$  are constants greater than zero,  $\beta_i > \kappa_i$ , and  $\gamma_i > 1$ .

The error dynamic of the observer is described as

$$\begin{aligned} \dot{\chi}_{0i} &= \chi_{1i} - \lambda_{1i} |\chi_{0i}|^{1/2} \text{sign}(\chi_{0i}) - \lambda_{2i} |\chi_{0i}|^{\gamma_i} \text{sign}(\chi_{0i}), \\ \dot{\chi}_{1i} &= -\beta_i \text{sign}(\chi_{0i}) + \dot{d}_{1i}(t), \end{aligned} \quad (30)$$

where  $\chi_{1i} = d_{1i}(t) - \hat{d}_{1i}(t)$  is the estimation error of external disturbance. It can be derived from [36, 37] that observer error system (18) is fixed-time stable according to Assumption 1, i.e., when  $t > t_1$ ,  $\chi_{0i} = \chi_{1i} = 0$ . And the  $t_1$  satisfies  $t_1 \leq (1/\lambda_2 (\gamma-1) \varepsilon^{\gamma-1} + 2\varepsilon^{1/2}/\lambda_1) (1 + 1/m((1/M) - (h(\lambda_1)/\lambda_1)))$  with  $\varepsilon > 0$ ,  $M = \alpha - \kappa$ ,  $m = \alpha + \kappa$ , and  $h(\lambda_1) = 1/\lambda_1 + (2 \exp(1)/m\lambda_1)^{1/3}$ .

**Theorem 2** (FTDO-ISMC). *Consider tracking error systems (20)-(21) with external disturbances satisfying Assumption 1; then, a FTDO-ISMC is designed as*

$$\tau_{\text{FTDO-ISMC}} = MR^{-1} (R_d M^{-1} \tau_d - \Theta_e - u_n - \hat{d}_1(t) - \xi_1 [s]^\alpha - \xi_2 [s]^\beta), \quad (31)$$

with  $\hat{d}_1$  estimated by FTDO (30). Systems (6) and (7) can converge to desired trajectories (13) and (14) within a fixed time, i.e.,  $\hat{d}_1(t) \equiv d_1(t)$ ,  $\eta \equiv \eta_d$ , and  $v \equiv v_d$ , when  $t > T_{f2}$ .

*Proof.* The derivative of ISM surface (13) is rewritten as

$$\dot{s} = \chi_1 - \xi_1 [s]^\alpha - \xi_2 [s]^\beta. \quad (32)$$

And derivative Lyapunov function  $V$  based on (32) obtains

$$\dot{V} = s\chi_1 - \xi_1 |s|^{\alpha+1} - \xi_2 |s|^{\beta+1}. \quad (33)$$

When the time  $t > t_1$ ,  $\hat{d}_1(t)$  equals  $d_1(t)$ , that is to say that the disturbance estimation error  $\chi_{1i}$  converges to zero within a fixed time. (33) is rewritten as

$$\dot{V} = -\xi_1 |s|^{\alpha+1} - \xi_2 |s|^{\beta+1}. \quad (34)$$

Based on Lemma 2, (34) is described by  $\dot{V} = -2^{\alpha+1/2} \xi_1 V^{\alpha+1/2} - 2^{\beta+1/2} \xi_2 V^{\beta+1/2}$  and we obtain that the

ISM manifold  $s = 0$  will be arrived within a fixed time  $T_1 = 1/2^{(\alpha-1)/2}\xi_1(1-\alpha) + 1/2^{(\beta-1)/2}\xi_2(\beta-1)$ . The system is still the same as (28) while  $s = 0$ . In other words, the tracking error system states  $\eta_e$  and  $v_e$  are still sufficient to ensure convergence along the sliding surface in a fixed time  $t_f$ . Under the FTDO-ISM scheme, the convergence time of the ASV system is  $T_{f2} \leq t_1 + T_1 + t_f$ . This concludes the proof.

*Remark 2.* Note that we do not testify that the proposed controller (31) can ensure the boundedness of errors  $\eta_e$  and  $\sigma_e$  in the time quantum  $[0, t_1]$  since the analysis of the dynamics of tracking error system is a difficult subject due to the complex nonlinear terms. In view of this reason, we have done a large number of simulations for ASV systems (6)-(7) under observer (29) and control laws (31), in which any divergence phenomenon is not observed. Practically, for the purpose of guaranteeing the boundedness of error system states in engineering, a bounded control rule can be applied in  $[0, t_1]$ . Therefore, it can assume that all states will not be divergent in fixed time in advance of the observer error dynamics converging.

*Remark 3.* Notice that it is difficult for  $\Theta_e$  to obtain the real value because  $C(v)$  and  $D(v)$  are unknown because of existing uncertainties in ASV uncertainties. The FTDO only estimates the external disturbances and the influence of nonlinear terms is not considered, which will be solved in this context.

**4.4. Design of FTUO-ISM.** In this section, the unknown nonlinear term consisting of  $C(v)$ ,  $D(v)$ , and  $g(\eta)$  together with the external disturbances  $d_i(t)$  are regarded as the lumped disturbances. Therefore, rewriting tracking error systems (20) and (21) yields

$$\begin{aligned} \dot{\eta}_e &= \sigma_e, \\ \dot{\sigma}_e &= RM^{-1}\tau - R_dM^{-1}\tau_d - \Theta_d + S(\sigma)\sigma + \Phi, \end{aligned} \quad (35)$$

where

$$\Phi = -RM^{-1}(C(R^T\sigma) + D(R^T\sigma))R^T\sigma - RM^{-1}g(\eta) + d_i(t), \quad (36)$$

is an unknown nonlinearity regarded as the lumped disturbances. According to [29], an assumption is presented as follows.

*Assumption 2.* There exists a bounded constant  $h_0$  such that  $|\dot{\Phi}| \leq h_0$ .

A FTUO is presented as

$$\begin{aligned} e_0 &= \sigma - e, \\ \dot{e} &= RM^{-1}\tau - R_dM^{-1}\tau_d - \Theta_d(\eta_d, \sigma_d) + S(\sigma)\sigma + \hat{\Phi} + \psi_i, \\ \psi_i &= \lambda_{1i}|e_{0i}|^{1/2}\text{sign}(e_{0i}) + \lambda_{2i}|e_{0i}|^{\gamma_i}\text{sign}(e_{0i}), \\ \dot{\hat{\Phi}}_i &= \beta_i\text{sign}(e_{0i}), \quad i = 1, 2, 3, \end{aligned} \quad (37)$$

where  $e_0 = [e_{01}, e_{02}, e_{03}]^T$  is an auxiliary variable,  $\psi = [\psi_1, \psi_2, \psi_3]^T$ ,  $\hat{\Phi} = [\hat{\Phi}_1, \hat{\Phi}_2, \hat{\Phi}_3]^T$  is the estimation of the unknown lumped disturbances  $\Phi$ ,  $\lambda_{1i}$  and  $\lambda_{2i}$  are positive constants,  $\beta_i > h_0$ , and  $\gamma_i > 1$ .

The error dynamic of the observer is described as

$$\begin{aligned} \dot{e}_{0i} &= e_{1i} - \lambda_{1i}|e_{0i}|^{1/2}\text{sign}(e_{0i}) - \lambda_{2i}|e_{0i}|^{\gamma_i}\text{sign}(e_{0i}), \\ \dot{e}_{1i} &= -\beta_i\text{sign}(e_{0i}) + \dot{\hat{\Phi}}_i(t), \end{aligned} \quad (38)$$

where the lumped disturbance estimation error is described as  $e_{1i} = \Phi_i - \hat{\Phi}_i$ . With the help of Assumption 2, observer error system (38) is found to be fixed-time stable according to [36, 37], i.e., when  $t > t_2$ ,  $e_{0i} = e_{1i} = 0$ . And, the  $t_2 \leq ((1/\lambda_2(\gamma-1)\epsilon^{\gamma-1}) + (2\epsilon^{1/2}/\lambda_1))(1 + (1/m(1/M - h(\lambda_1)/\lambda_1)))$  with  $M = \alpha - h_0$  and  $m = \alpha + h_0$  is different from the FTDO.

**Theorem 3 (FTUO-ISM).** Considering tracking error systems (35)-(36) with the unknown lumped disturbances satisfying Assumption 2, a FTUO-ISM is designed as

$$\tau_{\text{FTUO-ISM}} = MR^{-1}(R_dM^{-1}\tau_d + \Theta_d - S(\sigma)\sigma), \quad (39)$$

with  $\hat{\Phi}$  estimated by FTUO (40). Systems (6) and (7) can converge to desired ones (13) and (14) within a fixed time, i.e.,  $\hat{\Phi} \equiv \Phi$ ,  $\eta \equiv \eta_d$ , and  $v \equiv v_d$ , when  $t > T_{f3}$ .

*Proof.* The derivative of ISM surface (22) is redescribed as follows:

$$\dot{s} = e_1 - \xi_1|s|^\alpha - \xi_2|s|^\beta. \quad (40)$$

And the derivation of Lyapunov function (25) will be changed as

$$\dot{V} = se_1 - \xi_1|s|^{\alpha+1} - \xi_2|s|^{\beta+1}. \quad (41)$$

When the time  $t > t_2$ ,  $\hat{\Phi}$  equals  $\Phi$ ; to put it differently, the unknown lumped disturbance estimation error  $e_1$  converges to zero in a fixed time, which makes equation (41) become (27) such that system states arrive at  $s = 0$  within a fixed time  $T_2 = (1/2^{(\alpha-1)/2})\xi_1(1-\alpha) + (1/2^{(\beta-1)/2})\xi_2(\beta-1)$  based on Lemma 2. The tracking error system is the same as (28) after reaching the sliding surface, and it converges to origin along the sliding surface in a fixed time based on Lemma 1. Under the FTUO-ISM scheme, the convergence time of the ASV system is  $T_{f3} \leq t_2 + T_2 + t_f$ . The proof is absolutely accomplished.

*Remark 4.* Although the states of tracking error systems (35)-(36) under control law (40) are not proved to be bounded within  $[0, t_2]$  analogous to Remark 2, sufficient simulation results have been shown that any state does not diverge in  $[0, t_2]$ . Hence, we still suppose that the states of (35) are bounded within the time period  $[0, t_2]$ .

*Remark 5.* The ISMC scheme is designed based on integrated sliding mode surface for ASV systems without external disturbances. The FTDO-ISM scheme is designed when there are external disturbances in the ASV system. The

FTUO-ISM scheme is designed considering the model uncertainties and external disturbances of the ASV system. The similarity lies in that ISMC, FTDO-ISM, and FTUO-ISM schemes are all based on the state feedback to design the integral sliding mode controllers.

## 5. Simulation

For the sake of illustrating the efficiency and superiority of the developed ISMC, FTDO-ISM, and FTUO-ISM points at trajectory following of an ASV, simulation machine adopted the surface vehicle CyberShip II [38] whose main parameters can be found in [27].

In this section, simulation proposed three control laws verifying that the system states can track the trajectory given by (13) and (14) within a fixed time, where desired control input  $\tau_d$  is conducted by  $\tau_d = [5, 2 \cos^2(0.1\pi t), \sin^2(0.1\pi t)]^T$ . The origin condition is given by  $\eta(0) = [2, 1, \pi/2]^T$ ,  $v(0) = [0, 0, 0]^T$ ,  $\eta_d(0) = [1, 2, \pi/4]^T$ , and  $v_d(0) = [0, 0, 0]^T$ .

**5.1. Simulation on the ISMC.** The ISMC scheme is simulated without considering external disturbances, and the parameters of this scheme are chosen as follows:  $\rho = 0.7$ ,  $k_i = k'_i = k''_i = 5$ ,  $\xi_1 = \xi_2 = 3$ ,  $\alpha = 0.5$ , and  $\beta = 2$ . It is clearly expressed from Figures 1–3 that the desired system state is fully tracked by the system states within a fixed time.

In Figures 4 and 5, curves of tracking error are shown under two sets of initial conditions. The case one is as above and the case two is  $\eta(0) = [1, 1, \pi/3]^T$ ,  $v(0) = [1, 0, 0]^T$ ,  $\eta_d(0) = [1, 0, \pi/2]^T$ , and  $v_d(0) = [0, 1, 0]^T$ . The convergence time can be demonstrated to be similar in distinct initial states. The control input of ISMC is shown in Figure 6.

**5.2. Simulation on the FTDO-ISM.** In general, the external disturbances always exist in the ASV dynamics. The unknown external disturbances  $d_i(t)$  are chosen as

$$d_i(t) = \begin{bmatrix} 9\sin\left(0.1\pi t - \frac{\pi}{5}\right) \\ 6\sin\left(0.3\pi t + \frac{\pi}{6}\right) \\ 3\sin\left(0.2\pi t + \frac{\pi}{3}\right) \end{bmatrix}. \quad (42)$$

And the parameters of the proposed FTDO and corresponding controller  $\tau_{\text{FTDO-ISM}}$  are chosen as follows:

$\lambda_{1i} = \lambda_{2i} = 6$ ,  $\beta_1 = 9$ ,  $\beta_2 = 6$ ,  $\beta_3 = 3$ ;  $\gamma_1 = \gamma_2 = 0.3$ ,  $\gamma_3 = 0.8$ ;  $\rho = 0.7$ ,  $k_i = k'_i = k''_i = 5$ ,  $\xi_1 = \xi_2 = 4$ ,  $\alpha = 0.5$ , and  $\beta = 2$ .

Accordingly, simulation results of FTDO-ISM scheme are illustrated in Figures 7–13. From Figures 7–12, compared to the performance with ISMC, the FTDO-ISM scheme can also accurately control for tracking control of the ASV system among brief time in the presence of external disturbances. As can be seen from Figure 12, the FTDO can accurately estimate the external disturbances. The control

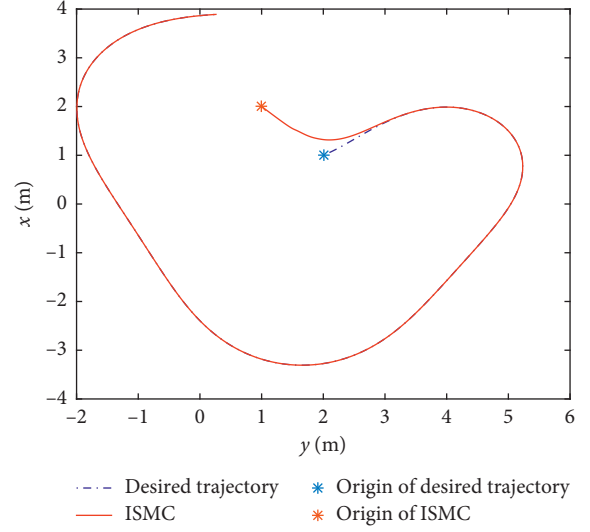


FIGURE 1: Planar trajectory tracking on ISMC.

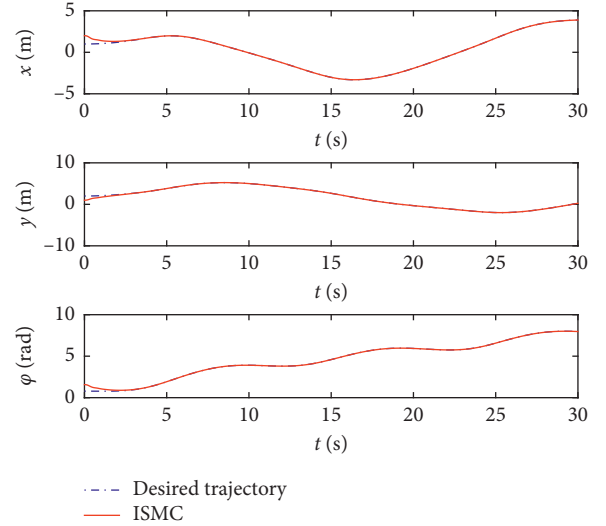


FIGURE 2: Position tracking on ISMC.

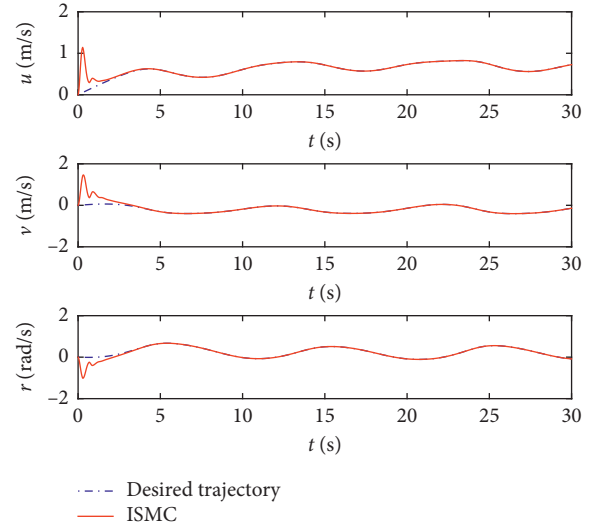


FIGURE 3: Velocity tracking on ISMC.



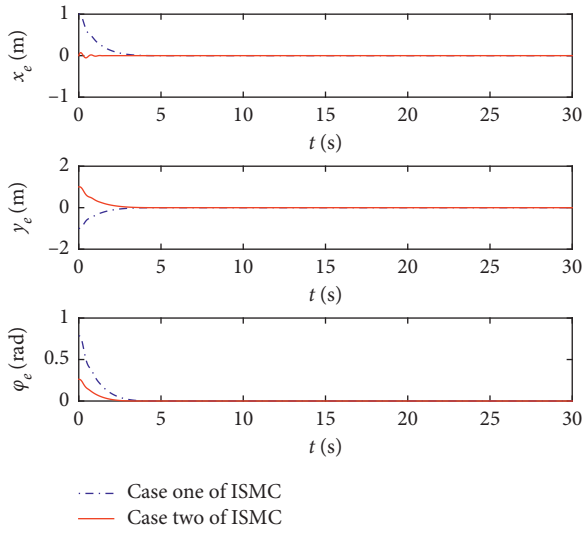


FIGURE 4: Position tracking errors on ISMC with different conditions.

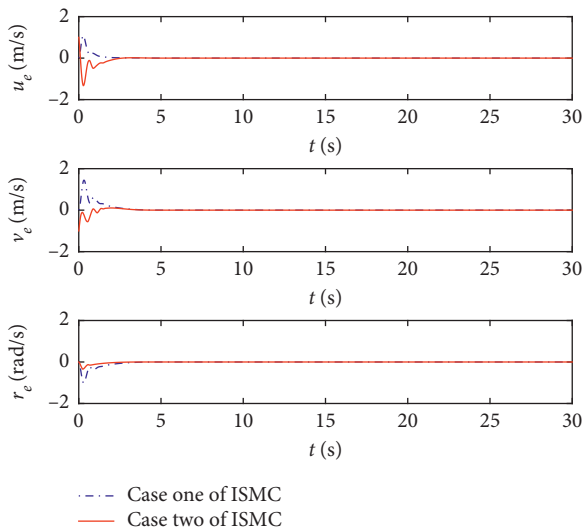


FIGURE 5: Velocity tracking errors on ISMC with different conditions.

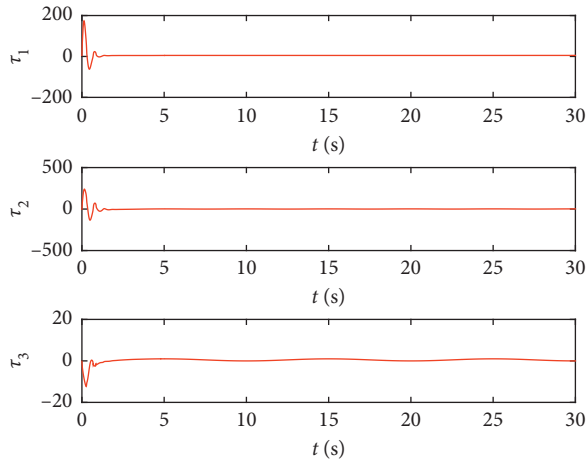


FIGURE 6: Control input on ISMC.

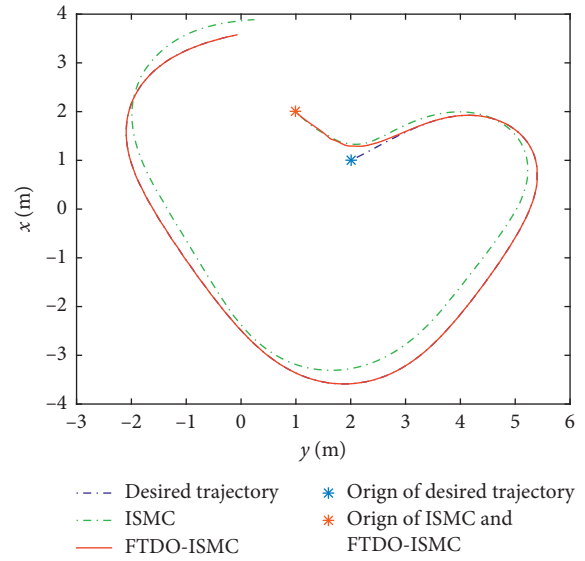


FIGURE 7: Planar trajectory tracking on ISMC and FTDO-ISM.

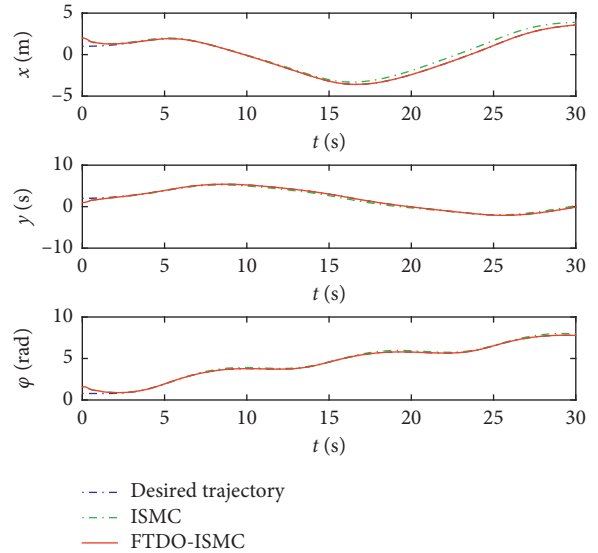


FIGURE 8: Position tracking on ISMC and FTDO-ISM.

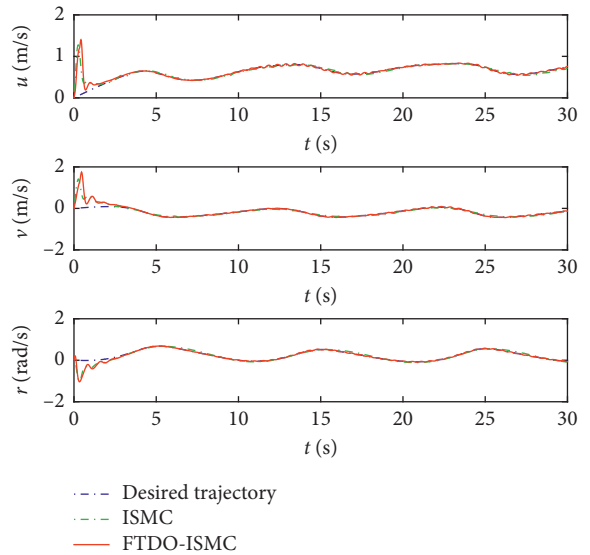


FIGURE 9: Velocity tracking on ISMC and FTDO-ISM.

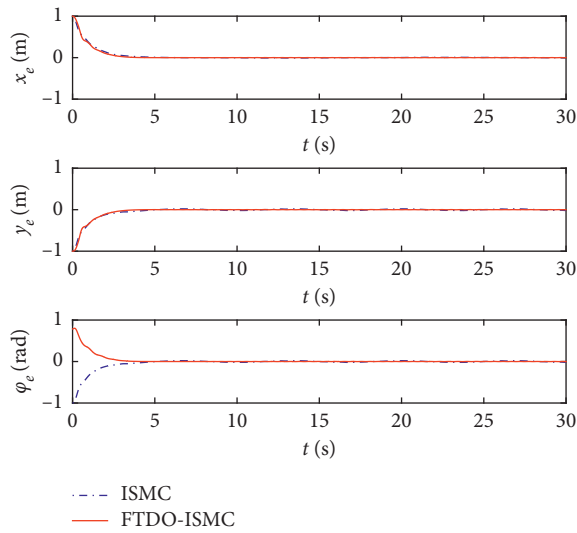


FIGURE 10: Position tracking errors on ISMC and FTDO-ISM.

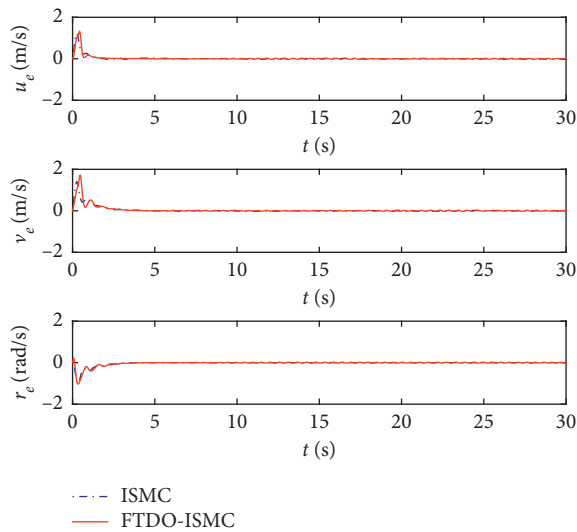


FIGURE 11: Velocity tracking errors on ISMC and FTDO-ISM.

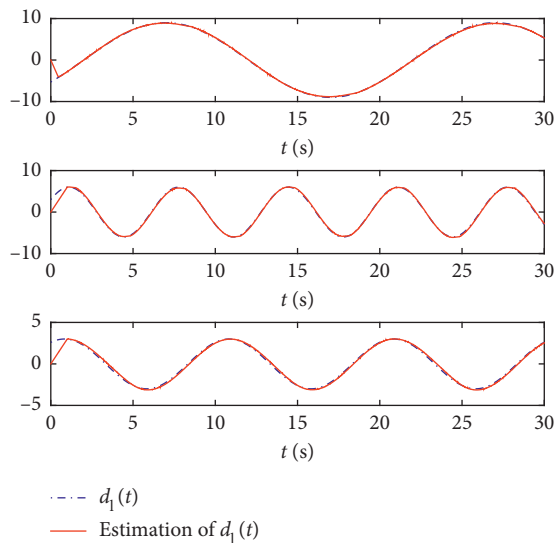


FIGURE 12: External disturbances and their estimations on FTDO-ISM.

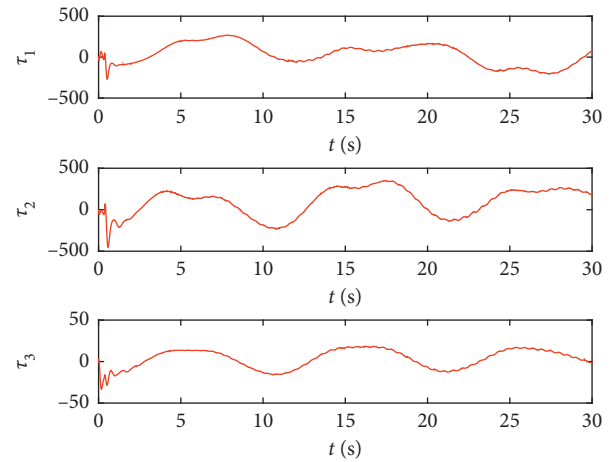


FIGURE 13: Control input under FTDO-ISM.

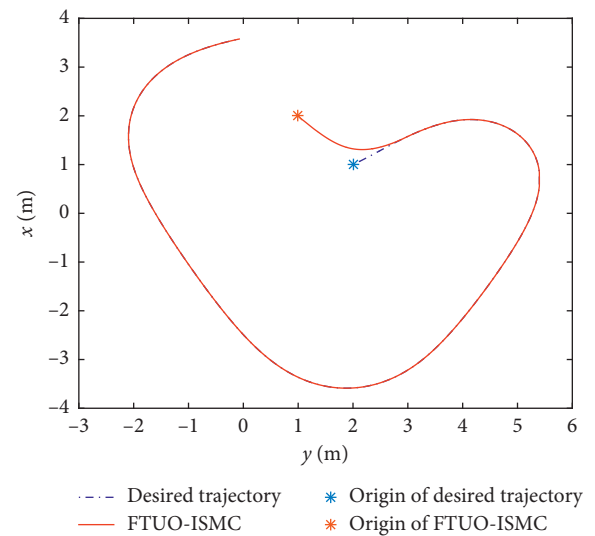


FIGURE 14: Planar trajectory tracking.

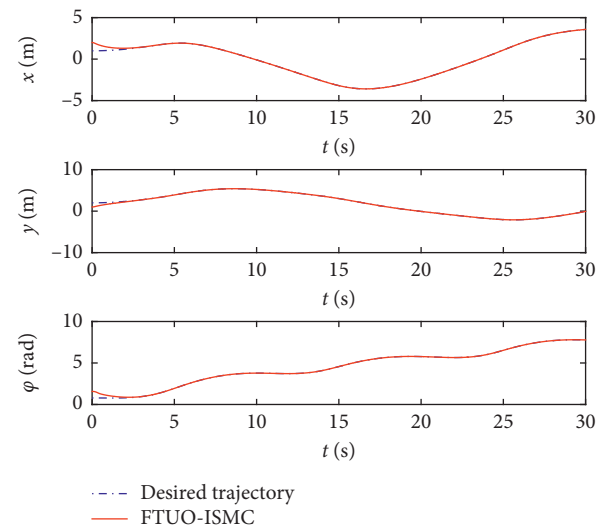


FIGURE 15: Position tracking on FTUO-ISM.

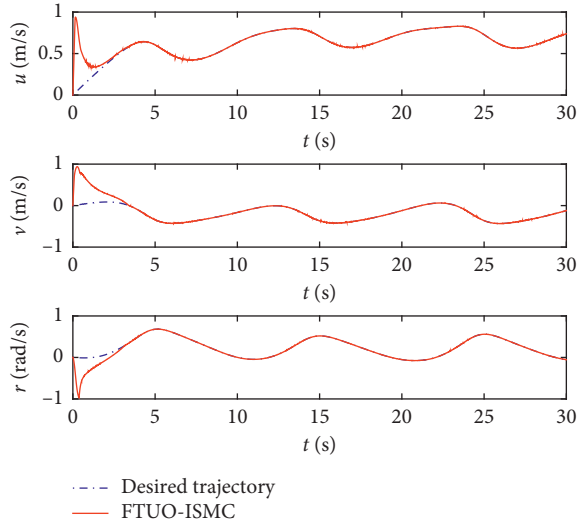


FIGURE 16: Velocity tracking on FTUO-ISM.

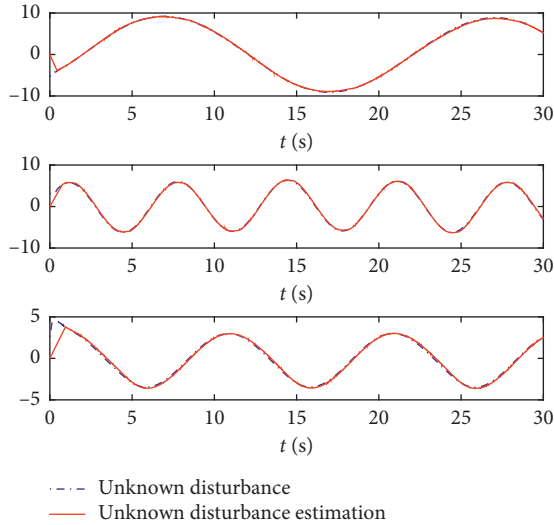


FIGURE 17: Unknown disturbance and its estimation on FTUO-ISM.

input of the ASV system under FTDO-ISM scheme is shown in Figure 13. Therefore, it can be concluded that the FTDO-ISM scheme can achieve good tracking performance while external disturbances are existing.

**5.3. Simulation on the FTUO-ISM.** The unknown lumped disturbances composed of the external disturbances and the model uncertainties of the ASV system are estimated together by the FTUO. The parameters of the proposed FTUO and corresponding controller  $\tau_{\text{FTUO-ISM}}$  are chosen as follows:  $\lambda_{1i} = \lambda_{2i} = 6$ ,  $\beta_1 = 9$ ,  $\beta_2 = 7$ , and  $\beta_3 = 4$ ;  $\gamma_1 = \gamma_2 = 0.3$  and  $\gamma_3 = 0.6$ ;  $\rho = 0.3$ ,  $k_i = k'_i = k''_i = 5$ ,  $\xi_1 = 4$ ,  $\xi_2 = 4$ ,  $\alpha = 0.1$ , and  $\beta = 2$ .

The simulation results of the ASV system under FTUO-ISM are all provided in Figures 14–17. It could be described from Figures 14–16 that the vehicle can follow the expected

trajectory accurately with the fixed time while the unknown lumped disturbances are presenting. In Figure 17, curves of unknown lumped disturbances and estimations are presented. From this figure, we can see that the proposed FTUO can effectively estimate the lumped disturbances. As a conclusion, the tracking performance of the FTUO-ISM is satisfied for the ASV system with external disturbances and parameter uncertainties.

## 6. Conclusion

In this paper, the problem of fixed-time trajectory tracking control has been investigated for ASVs with external disturbances and model uncertainties. By introducing integral sliding mode surface, an ISMC scheme has been proposed for ASVs, which can achieve position and velocity tracking in fixed time. Then, a fixed-time disturbance observer (FTDO) has been designed to estimate the external disturbances. The control scheme (FTDO-ISM) proposed by combining the ISM surface and the output of FTDO can accurately track the desired trajectory for ASVs with the external disturbances. A fixed-time unknown observer (FTUO) has been developed to calculate the unknown lumped disturbances, and a control law in the light of fixed-time unknown observer (FTUO-ISM) has been proposed to achieve accurate disturbances attenuation and trajectory tracking for the ASVs. Results on simulation have been used to illustrate the superiority and efficiency of the control schemes proposed.

## Data Availability

No data were used to support this study.

## Conflicts of Interest

The authors declares that there are no conflicts of interest.

## Acknowledgments

This work was partially supported by the National Natural Science Foundation of China under Grants 61773236, 61773235, 61703233, 61873331, and 61803225, partially by the Taishan Scholar Project of Shandong Province under Grants TSQN20161033 and ts201712040, partially by the Natural Science Foundation of Anhui Province (19080805MF219), partially by the Postdoctoral Science Foundation of China (2017M612236 and 2019T120574), and partially by the Interdisciplinary Scientific Research Projects of Qufu Normal University under Grant (xkjjc201905).

## References

- [1] A. P. Aguiar and J. P. Hespanha, "Trajectory-tracking and path-following of underactuated autonomous vehicles with parametric modeling uncertainty," *IEEE Transactions on Automatic Control*, vol. 52, no. 8, pp. 1362–1379, 2007.
- [2] Z. Zeng, L. Lian, K. Sammut, F. He, Y. Tang, and A. Lammas, "A survey on path planning for persistent autonomy of autonomous underwater vehicles," *Ocean Engineering*, vol. 110, no. Part A, pp. 303–313, 2015.

- [3] X. Xiang, C. Yu, and Q. Zhang, "On intelligent risk analysis and critical decision of underwater robotic vehicle," *Ocean Engineering*, vol. 140, pp. 453–465, 2017.
- [4] L. Perera, P. Oliveira, and C. Soares, "Maritime traffic monitoring based on vessel detection, tracking, state estimation, and trajectory prediction," *IEEE Transactions on Intelligent Transportation Systems*, vol. 13, no. 3, pp. 1188–1200, 2012.
- [5] A. Behal, D. M. Dawson, W. E. Dixon, and Y. Fang, "Tracking and regulation control of an underactuated surface vessel with nonintegrable dynamics," *IEEE Transactions on Automatic Control*, vol. 47, no. 3, pp. 495–500, 2002.
- [6] T. Fossen, *Marine Control Systems: Guidance, Navigation, and Control of Ships, Rigs and Underwater Vehicles* Marine Cybernetics AS, Trondheim, Norway, 2002.
- [7] L.-x. Pan, H.-z. Jin, and L.-l. Wang, "Robust control based on feedback linearization for roll stabilizing of autonomous underwater vehicle under wave disturbances," *China Ocean Engineering*, vol. 25, no. 2, pp. 251–263, 2011.
- [8] C. Shen, Y. Shi, and B. Buckham, "Trajectory tracking control of an autonomous underwater vehicle using lyapunov-based model predictive control," *IEEE Transactions on Industrial Electronics*, vol. 65, no. 7, pp. 5796–5805, 2018.
- [9] X. Xiang, C. Yu, and Q. Zhang, "Robust fuzzy 3D path following for autonomous underwater vehicle subject to uncertainties," *Computers & Operations Research*, vol. 84, pp. 165–177, 2017.
- [10] J.-H. Li and P.-M. Lee, "Design of an adaptive nonlinear controller for depth control of an autonomous underwater vehicle," *Ocean Engineering*, vol. 32, no. 17-18, pp. 2165–2181, 2005.
- [11] J. Guo, F.-C. Chiu, and C.-C. Huang, "Design of a sliding mode fuzzy controller for the guidance and control of an autonomous underwater vehicle," *Ocean Engineering*, vol. 30, no. 16, pp. 2137–2155, 2003.
- [12] M.-j. Zhang and Z.-z. Chu, "Adaptive sliding mode control based on local recurrent neural networks for underwater robot," *Ocean Engineering*, vol. 45, pp. 56–62, 2012.
- [13] C. Huang, J. Lu, D. W. Ho, G. Zhai, and J. Cao, "Stabilization of probabilistic boolean networks via pinning control strategy," *Information Sciences*, vol. 510, pp. 205–217, 2020.
- [14] C. Huang, X. Zhang, H. K. Lam, and S. H. Tsai, "Synchronization analysis for nonlinear complex networks with reaction-diffusion terms using fuzzy-model-based approach," *IEEE Transactions on Fuzzy Systems*, p. 1. In press, 2020.
- [15] C. Huang, J. Lu, G. Zhai, J. Cao, G. Lu, and M. Perc, "Stability and stabilization in probability of probabilistic boolean networks," *IEEE Transactions on Neural Networks and Learning Systems*, pp. 1–11. In press, 2020.
- [16] P. Liu, L. Li, K. Shi, and J. Lu, "Pinning stabilization of probabilistic boolean networks with time delays," *IEEE Access*, vol. 8, pp. 154050–154059, 2020.
- [17] X. Ji, J. Lu, J. Lou, J. Qiu, and K. Shi, "A unified criterion for global exponential stability of quaternion-valued neural networks with hybrid impulses," *International Journal of Robust and Nonlinear Control*, 2020, In press.
- [18] X. Li, X. Yang, and T. Huang, "Persistence of delayed cooperative models: impulsive control method," *Applied Mathematics and Computation*, vol. 342, pp. 130–146, 2019.
- [19] C. Yu, X. Yu, B. Shirnzadeh, and Z. Man, "Continuous finite-time control for robotic manipulators with terminal sliding mode," *Automatica*, vol. 44, no. 11, pp. 1957–1964, 2005.
- [20] N. Wang, S. Lv, W. Zhang, Z. Liu, and M. J. Er, "Finite-time observer based accurate tracking control of a marine vehicle with complex unknowns," *Ocean Engineering*, vol. 145, pp. 406–415, 2017.
- [21] S. Yu and X. Long, "Finite-time consensus for second-order multi-agent systems with disturbances by integral sliding mode," *Automatica*, vol. 54, pp. 158–165, 2015.
- [22] J. Hu, G. Sui, X. Lv, and X. Li, "Fixed-time control of delayed neural networks with impulsive perturbations," *Nonlinear Analysis: Modelling and Control*, vol. 23, no. 6, p. 904, 2018.
- [23] D. Yang, X. Li, and J. Qiu, "Output tracking control of delayed switched systems via state-dependent switching and dynamic output feedback," *Nonlinear Analysis: Hybrid Systems*, vol. 32, pp. 294–305, 2019.
- [24] L. Zhang, Y. Wang, Y. Hou, and H. Li, "Fixed-time sliding mode control for uncertain robot manipulators," *IEEE Access*, vol. 7, pp. 149750–149763, 2019.
- [25] Z. Zuo, "Non-singular fixed-time terminal sliding mode control of non-linear systems," *IET Control Theory & Applications*, vol. 9, no. 4, pp. 545–552, 2015.
- [26] L. Zhang, C. Wei, L. Jing, and N. Cui, "Fixed-time sliding mode attitude tracking control for a submarine-launched missile with multiple disturbances," *Nonlinear Dynamics*, vol. 93, no. 4, pp. 2543–2563, 2018.
- [27] N. Wang, X. Pan, and S. Su, "Finite-time fault-tolerant trajectory tracking control of an autonomous surface vehicle," *Journal of the Franklin Institute*, vol. 357, no. 16, pp. 11114–11135, 2019.
- [28] N. Wang, C. Qian, J.-C. Sun, and Y.-C. Liu, "Adaptive robust finite-time trajectory tracking control of fully actuated marine surface vehicles," *IEEE Transactions on Control Systems Technology*, vol. 24, no. 4, pp. 1454–1462, 2016.
- [29] X. Fang, F. Liu, and S. Zhao, "Trajectory tracking control for manned submersible system with disturbances via disturbance characterization index approach," *International Journal of Robust and Nonlinear Control*, vol. 29, no. 16, pp. 5641–5653, 2019.
- [30] J. Ni, L. Liu, M. Chen, and C. Liu, "Fixed-time disturbance observer design for brunovsky systems," *IEEE Transactions on Circuits and Systems. II-Express Briefs*, vol. 65, no. 3, pp. 341–345, 2018.
- [31] J. Sun, J. Yi, Z. Pu, and X. Tan, "Fixed-time sliding mode disturbance observer-based nonsmooth backstepping control for hypersonic vehicles," *IEEE Transactions on Systems, Man, and Cybernetics: Systems*, vol. 2, pp. 1–10. In press, 2018.
- [32] J. Zhang, S. Yu, and Y. Yan, "Fixed-time extended state observer-based trajectory tracking and point stabilization control for marine surface vessels with uncertainties and disturbances," *Ocean Engineering*, vol. 186, p. 106109, 2019.
- [33] B. Tian, Z. Zuo, X. Yan, and H. Wang, "A fixed-time output feedback control scheme for double integrator systems," *Automatica*, vol. 80, pp. 17–24, 2017.
- [34] A. Polyakov, "Nonlinear feedback design for fixed-time stabilization of linear control systems," *IEEE Transactions on Automatic Control*, vol. 57, no. 8, pp. 2106–2110, 2012.
- [35] H. Sun, L. Hou, G. Zong, and X. Yu, "Fixed-time attitude tracking control for spacecraft with input quantization," *IEEE Transactions on Aerospace and Electronic Systems*, vol. 55, no. 1, pp. 124–134, 2019.
- [36] M. Basin, C. Bharath Panathula, and Y. Shtessel, "Multivariable continuous fixed-time second-order sliding mode control: design and convergence time estimation," *IET Control Theory & Applications*, vol. 11, no. 8, pp. 1104–1111, 2017.
- [37] M. Basin, C. B. Panathula, and Y. Shtessel, "Adaptive uniform finite-/fixed-time convergent second-order sliding-mode control," *International Journal of Control*, vol. 89, no. 9, pp. 1777–1787, 2016.
- [38] R. Skjetne, T. I. Fossen, and P. V. Kokotović, "Adaptive maneuvering, with experiments, for a model ship in a marine control laboratory," *Automatica*, vol. 41, no. 2, pp. 289–298, 2005.

## Research Article

# Finite-Time Stabilization and Destabilization Analysis of Quaternion-Valued Neural Networks with Discrete Delays

Huiling Duan,<sup>1</sup> Tao Peng,<sup>1,2</sup> Zhengwen Tu,<sup>1</sup> and Jianlong Qiu <sup>3,4</sup>

<sup>1</sup>School of Mathematics and Statistics, Chongqing Three Gorges University, Wanzhou 404020, Chongqing, China

<sup>2</sup>Department of Systems Science, School of Mathematics, Southeast University, Nanjing 210096, China

<sup>3</sup>School of Automation and Electrical Engineering, Linyi University, Linyi 276005, China

<sup>4</sup>Key Laboratory of Complex Systems and Intelligent Computing in Universities of Shandong, Linyi University, Linyi 276005, China

Correspondence should be addressed to Jianlong Qiu; [qiu Jianlong@lyu.edu.cn](mailto:qiu Jianlong@lyu.edu.cn)

Received 18 July 2020; Revised 20 August 2020; Accepted 13 September 2020; Published 7 October 2020

Academic Editor: Sabri Arik

Copyright © 2020 Huiling Duan et al. This is an open access article distributed under the Creative Commons Attribution License, which permits unrestricted use, distribution, and reproduction in any medium, provided the original work is properly cited.

In this paper, the finite-time stabilization and destabilization of a class of quaternion-valued neural networks (QVNNs) with discrete delays are investigated. In order to surmount the difficulty of noncommutativity of quaternion, a new vector matrix differential equation (VMDE) is proposed by employing decomposition method. And then, a nonlinear controller is designed to stabilize the VMDE in a finite-time interval. Furthermore, under that controller, the finite-time stability and instability of the QVNNs are analyzed via Lyapunov function approach, and two criteria are derived, respectively; furthermore, the settling time is also estimated. At last, by two illustrative examples we verify the correctness of the conclusions.

## 1. Introduction

In 1961, in order to investigate the transient performance of the system, Perter Dorato gave a definition of short-time stability, which was also called finite-time stability later [1]. There are some differences between finite-time stability and classical stability theory, Lyapunov stability. Actually, the finite-time stability mainly reveals the transient dynamic characteristics of the system in a short and desired time interval; however, the Lyapunov stability mainly reveals dynamical behavior of the system in an infinite time interval [2–4]. For a long time, the research concerning the finite-time stability only focused on the stability analysis. However, very limited references considered the problem of controllability due to the difficulty in designing the control strategy [3,5–8]. In fact, many practical systems are required to reach their desired state quickly, such as flight control system, communication network system, and robot control [9–16]. Therefore, lots of scholars are devoted to the controllability of finite-time stability, and some interesting and meaningful results have been reported [2,4,9,17–28].

Nersesov et al. extended the finite-time stability theory and gave a control strategy to reach finite-time stability [2]. For the delayed complex-valued memristive neural networks, a new nonlinear delayed controller was designed to get the finite-time stabilization [4]. When discussing scalar linear systems, a finite-time controller was proposed in [22]. Based on state and output feedback, several especial finite-time controllers were firstly proposed for the stochastic system in [23]. On the other hand, it is also interesting to destabilize a stable system in a finite-time interval, such as preventing eavesdropping and signal encryption. Wang and Shen proposed some finite-time destabilization algebraic criteria for memristive neural networks, and a more general controller was designed to realize the finite-time destabilization for delayed complex-valued memristive neural networks [24]. However, the controllers designed in existing references are invalid to QVNNs because of the noncommutativity of quaternion. And many effective methods for studying the finite-time stability of QVNNs are yet to be discovered, which stimulates us to do this research.

Like  $x = c + di + ej + fk$ ,  $c, d, e, f \in \mathbb{R}$ , we call number  $x$  a quaternion proposed in 1843, and it satisfies the following rule:

$$\begin{aligned} i \times i = j \times j = k \times k = -1, i \times j = -j \times i = k, \\ j \times k = -k \times j = i, k \times i = -i \times k = j. \end{aligned} \quad (1)$$

Quaternion has been widely used in space control, computer 3D image processing, and attitude control of spacecraft [29]. Up to now, the neural network has obtained great development in many fields, such as signal processing, artificial intelligence, and optimization. Particularly, for the real-valued neural networks (RVNNs), many researchers have carried out a lot of work [30–33], as well as complex-valued neural networks (CVNNs) [3,4,34–37]. Since there are three imaginary parts of quaternion, combined with many advantages of neural network, QVNNs have many properties that RVNNs and CVNNs do not have and have been applied in many practical fields, such as high-dimensional data processing, image compression, pattern recognition, and optimization. While, much fewer attentions are given to the dynamical behavior of QVNNs [20,38–47]. Li and Zheng investigated the globally exponential passivity of quaternion-valued memristor-based neural networks with time delays [29]. Tu et al. investigated the globally asymptotical stability and exponential stability of a class of QVNNs with mixed delays via nonseparating technologies [42]. Based on fractional-order QVNNs, quasi-synchronization and bifurcation were also considered [43]. Nevertheless, according to our knowledge, it is still open and significant to study the finite-time stabilization of delayed QVNNs, such as how to carry out the finite-time stabilization of QVNNs and how to design the controller to stabilize the instable systems remain unresolvable. Some new theory and methods should be explored to resolve those problems. We mainly want to discuss the finite-time stability of QVNNs in this paper. By constructing a new vector Lyapunov candidate function and designing a nonlinear vector-matrix controller, both finite-time stabilization and destabilization of delayed QVNNs are analyzed. Furthermore, we only need to adjust the appropriate parameters, and the finite-time stabilization and destabilization can be realized. We sort out the chief contributions of this article as follows:

- (1) It is the first time that the finite-time stabilization and destabilization of QVNNs with discrete delays are studied. A new vector Lyapunov function is constructed and a new nonlinear vector-matrix controller is designed to investigate the aforementioned problem.
- (2) Based on the new developed method, some easily checked results for the finite-time stabilization and destabilization of QVNNs are provided, respectively. Compared to [4], the obtained criteria are more concise and natural.
- (3) The influence of initial condition of the system and parameter of the designed controller to the settling time is analyzed in detail.

The remaining sections of this article will be arranged as follows. In Section 2, an equivalent VMDE of QVNNs is

established and several correlative definitions, lemmas, and assumptions are presented. In Section 3, a new nonlinear vector-matrix controller is given, and both the finite-time destabilization and stabilization of QVNNs with discrete delays is analyzed. In Section 4, the validity of our proposed criteria is checked by two illustrative examples. In Section 5, a summary of the paper is given and some thoughts on the future work of finite-time problems are conceived.

*Notations.* The symbol  $\mathbb{R}$  expresses the real number set, the symbol  $\mathbb{C}$  expresses complex number set, and the symbol  $\mathbb{Q}$  expresses quaternion set. We call  $\mathbb{R}^{m \times l}$  and  $\mathbb{Q}^{m \times l}$  all  $m \times l$  real matrices set and quaternion matrices set, respectively.  $\mathbb{Q}^l$  is said to be  $l$ -dimensional quaternion space. A continuous mapping from  $[t_0 - \tau, t_0]$  to  $\mathbb{Q}^l$  is  $\phi \in C([t_0 - \tau, t_0]; \mathbb{Q}^l)$ . The transpose of  $B$  is noted by symbol  $B^T$ . We can use  $B > 0$  ( $B < 0$ ) to represent a positive definite (negative definite) matrix, respectively. A vector  $y = (y_1, y_2, \dots, y_l)^T \in \mathbb{R}^l < 0$  means that  $y_i < 0$ ,  $i = 1, \dots, l$ . The 1-norm of vector  $Q \in \mathbb{R}^l$  is written as  $\|Q\| = \sum_{i=1}^l |Q_i|$ . When  $b(t) = (b_1(t), b_2(t), \dots, b_l(t))^T \in \mathbb{R}^l$  and  $\gamma \in \mathbb{R}$ ,  $|b(t)|^\gamma = (|b_1(t)|^\gamma, |b_2(t)|^\gamma, \dots, |b_l(t)|^\gamma)^T$ ,  $\text{sgn}(b(t)) = (\text{sgn}(b_1(t)), \text{sgn}(b_2(t)), \dots, \text{sgn}(b_l(t)))^T$ .  $|B| = (|b_{ij}|) \in \mathbb{R}^{l \times l}$ , where  $B = (b_{ij}) \in \mathbb{R}^{l \times l}$ . A continuous function  $\alpha: [0, a] \rightarrow [0, +\infty)$  is a class  $\mathcal{X}$  function if it is strictly increasing and  $\alpha(0) = 0$ .  $I = (1, 1, \dots, 1)^T \in \mathbb{R}^l$ .  $E$  is an identity matrix.

## 2. Preliminaries

Based on the following QVNNs model with discrete time-varying delays, we will analyze how to stabilize and destabilize the QVNNs in a finite- and short-time interval:

$$\dot{x}(t) = -Cx(t) + Mg(x(t)) + Ng(x(t - \tau(t))) + I(t), \quad (2)$$

where  $x(t) = (x_1(t), x_2(t), \dots, x_l(t)) \in \mathbb{Q}^l$  is called a  $l$ -dimensional state variable at time  $t$ ,  $C = \text{diag}\{c_1, c_2, \dots, c_l\} \in \mathbb{R}^{l \times l}$  is called a self-feedback link weight matrix with  $c_i > 0$ ,  $i = 1, 2, \dots, l$ ,  $M, N \in \mathbb{Q}^{l \times l}$  denote link weight matrices,  $g(x(\cdot)) = (g_1(x_1(\cdot)), g_2(x_2(\cdot)), \dots, g_l(x_l(\cdot)))^T \in \mathbb{Q}^l$  is activation function,  $\tau(t)$  satisfies  $0 < \tau(t) < \tau$ ,  $0 < \tau < +\infty$ , which is the time-varying delay, and  $I(t) = (I_1(t), I_2(t), \dots, I_l(t))^T \in \mathbb{Q}^l$  denotes outer input vector which will be designed later. The initial condition is given by  $x(s) = \psi(s) \in \mathbb{Q}^l$ ,  $s \in [t_0 - \tau, t_0]$ , where  $\psi(s) = \psi^{(r)}(s) + \psi^{(i)}(s)i + \psi^{(j)}(s)j + \psi^{(k)}(s)k$ .

Let

$$\begin{aligned} x(t) &= x^{(r)}(t) + x^{(i)}(t)i + x^{(j)}(t)j + x^{(k)}(t)k, \\ M &= M^{(r)} + M^{(i)}i + M^{(j)}j + M^{(k)}k, \\ N &= N^{(r)} + N^{(i)}i + N^{(j)}j + N^{(k)}k, \\ g(x(t)) &= g^{(r)}(x^{(r)}(t)) + g^{(i)}(x^{(i)}(t))i \\ &\quad + g^{(j)}(x^{(j)}(t))j + g^{(k)}(x^{(k)}(t))k, \end{aligned} \quad (3)$$

where  $x^{(p)}(t)$ ,  $g^{(p)}(x^{(p)}(t)) \in \mathbb{R}^l$  and  $M^{(p)}, N^{(p)} \in \mathbb{R}^{l \times l}$ ,  $p = r, i, j, k$ .

*Remark 1.* In general, let  $x = x^{(r)} + x^{(i)}i + x^{(j)}j + x^{(k)}k$ , and the activation function  $g(x)$  should be written as follows:

$$\begin{aligned} g(x) &= g^{(r)}(x^{(r)}, x^{(i)}, x^{(j)}, x^{(k)}) + g^{(i)}(x^{(r)}, x^{(i)}, x^{(j)}, x^{(k)})i \\ &+ g^{(j)}(x^{(r)}, x^{(i)}, x^{(j)}, x^{(k)})j \\ &+ g^{(k)}(x^{(r)}, x^{(i)}, x^{(j)}, x^{(k)})k. \end{aligned} \quad (4)$$

However, in this paper, to reduce the difficulty of research and simplify the results of finite-time stability of

QVNNs, we employ a special activation function introduced above, such as the activation functions of illustrative examples later.

By means of decomposition methods as those used in [41,47], we decompose QVNNs (2) into four RVNNs equally and combine them into a equivalent VMDE as follows

$$\dot{Q}(t) = -\widehat{C}Q(t) + \widehat{A}\widehat{g}(Q(t)) + \widehat{B}\widehat{g}(Q(t - \tau(t))) + \widehat{I}(t), \quad (5)$$

$$Q(s) = \Psi(s), s \in [t_0 - \tau, t_0], \quad (6)$$

where

$$\begin{aligned} \widehat{C} &= \text{diag}\{C, C, C, C\} \in \mathbb{R}^{4l \times 4l}, \\ \widehat{A} &= \begin{pmatrix} M^{(r)} & -M^{(i)} & -M^{(j)} & -M^{(k)} \\ M^{(i)} & M^{(r)} & -M^{(k)} & M^{(j)} \\ M^{(j)} & M^{(k)} & M^{(r)} & -M^{(i)} \\ M^{(k)} & -M^{(j)} & M^{(i)} & M^{(r)} \end{pmatrix} \in \mathbb{R}^{4l \times 4l}, \widehat{B} = \begin{pmatrix} N^{(r)} & -N^{(i)} & -N^{(j)} & -N^{(k)} \\ N^{(i)} & N^{(r)} & -N^{(k)} & N^{(j)} \\ N^{(j)} & N^{(k)} & N^{(r)} & -N^{(i)} \\ N^{(k)} & -N^{(j)} & N^{(i)} & N^{(r)} \end{pmatrix} \in \mathbb{R}^{4l \times 4l}, \end{aligned} \quad (7)$$

$$Q(t) = (x^{(r)}(t)^T, x^{(i)}(t)^T, x^{(j)}(t)^T, x^{(k)}(t)^T)^T \in \mathbb{R}^{4l},$$

$$\Psi(s) = \Psi = (\psi^{(r)}(t)^T, \psi^{(i)}(t)^T, \psi^{(j)}(t)^T, \psi^{(k)}(t)^T)^T \in \mathbb{R}^{4l},$$

$$\widehat{I}(t) = \left( (I^{(r)}(t))^T, (I^{(i)}(t))^T, (I^{(j)}(t))^T, (I^{(k)}(t))^T \right)^T \in \mathbb{R}^{4l},$$

$$\widehat{g}(Q(t)) = \left( (g^{(r)}(x^{(r)}(t)))^T, (g^{(i)}(x^{(i)}(t)))^T, (g^{(j)}(x^{(j)}(t)))^T, (g^{(k)}(x^{(k)}(t)))^T \right)^T \in \mathbb{R}^{4l},$$

$$\widehat{g}(Q(t - \tau(t))) = \left( (g^{(r)}(x^{(r)}(t - \tau(t))))^T, (g^{(i)}(x^{(i)}(t - \tau(t))))^T, (g^{(j)}(x^{(j)}(t - \tau(t))))^T, \right.$$

$$\left. g^{(k)}(x^{(k)}(t - \tau(t))) \right)^T \in \mathbb{R}^{4l}.$$

*Remark 2.* In fact, system (5) is a real-valued system. Evidently, the dynamic characteristics of QVNNs (2) are in accord with those of system (5) by considering that  $x(t) = x^{(r)}(t) + x^{(i)}(t)i + x^{(j)}(t)j + x^{(k)}(t)k$  corresponds to  $Q(t)$ . Therefore, one only needs to analyze system (5)'s dynamical characteristics instead of system (2), and the difficulty of noncommutativity of quaternion can be overcome.

In order to explicitly present main results, some definitions, assumptions, and lemmas should be introduced firstly.

*Assumption 1.*  $g: \mathbb{R}^l \rightarrow \mathbb{R}^l$  (or  $g = (g_1, g_2, \dots, g_l)^T$ ), which is a continuous function, is called a function of class  $\Delta\{\alpha_1, \alpha_2, \dots, \alpha_l\}$ ; if  $g(x)$  satisfies  $g_i(0) = 0$  and for each  $a, b \in \mathbb{R}$ ,  $a \neq b$ , there exist  $\alpha_i > 0$  such that

$$0 \leq \frac{g_i(a) - g_i(b)}{a - b} \leq \alpha_i, \quad i = 1, 2, \dots, l, \quad (8)$$

and let  $\Delta = \text{diag}\{\alpha_1, \alpha_2, \dots, \alpha_l\}$ .

*Definition 1* (see [7]). System (5) can reach a stable state in a finite time if a initial condition  $\Psi$  is given such that the system (5) is Lyapunov stable and any solution  $Q(t, \Psi)$  of (5) satisfies  $Q(t, \Psi) = 0, \forall t \geq T(\Psi)$ , where  $T(\Psi): \mathbb{R}^{4l} \rightarrow \mathbb{R}^+ \cup \{0\}$  is the settling time function.

*Remark 3.* The convergence time interval of finite-time stability must be given in advance, but it is difficult to estimate the upper boundary of the time interval. In this paper, some new vector-matrix analysis techniques are developed to derive the upper boundary, and the vector-matrix techniques can be used to investigate the finite-time synchronization of QVNNs in future work.

*Assumption 2.* If Assumption 1 holds, one obtains  $\widehat{g} = ((g^{(r)})^T, (g^{(i)})^T, (g^{(j)})^T, (g^{(k)})^T)^T = (\widehat{g}_1, \widehat{g}_2, \dots, \widehat{g}_{4l})^T: \mathbb{R}^{4l} \rightarrow \mathbb{R}^{4l}$ ,  $\widehat{g} \in \widehat{\Delta}\{\alpha_1, \alpha_2, \dots, \alpha_l, \alpha_1, \alpha_2, \dots, \alpha_l, \alpha_1, \alpha_2, \dots, \alpha_l, \alpha_1, \alpha_2, \dots, \alpha_l\}$  and  $\widehat{\Delta} = \text{diag}\{\Delta, \Delta, \Delta, \Delta\}$ .

**Lemma 1** (see [48]). *The system VMDE (5) is called to be finite-time stable; if under Assumption 1 and the initial*

condition  $\psi \in \Omega$ , a continuous function  $V: [0, +\infty) \times \Omega \rightarrow \mathbb{R}^+$  ( $\alpha, r \in \mathcal{K}$ ) can satisfy:

- (1)  $V(t, 0) = 0, \alpha(\|\psi\|) \leq V(t, \psi), t \in [0, +\infty)$ .
- (2)  $D^+V(t, \psi) \leq -r(V(t, \psi))$  with  $\int_0^\varepsilon (dz/r(z)) < +\infty$ , for alle  $\varepsilon > 0, \psi \in \Omega$ .

And the settling time is estimated to be  $T \leq \int_0^{V(0, \psi)} (dz/r(z))$ . Moreover, when  $r(V) = kV^\sigma$  ( $k > 0, 0 < \sigma < 1$ ), the settling time can be estimated by the following inequality:

$$T \leq \int_0^{V(0, \psi)} \frac{dz}{r(z)} = \frac{V^{1-\sigma}(0, \psi)}{k(1-\sigma)}. \quad (9)$$

**Lemma 2** (see [49]). Let  $Q_j \geq 0$  for  $j = 1, 2, \dots, l$ , and  $0 < a \leq 1, b > 1$ ; then, the following inequalities hold:

$$\left( \sum_{j=1}^l Q_j \right)^a \leq \sum_{j=1}^l Q_j^a, l^{1-b} \left( \sum_{j=1}^l Q_j \right)^b \leq \sum_{j=1}^l Q_j^b. \quad (10)$$

**Lemma 3** (see [48]). If system (5) can reach a finite-time stable state, then we can find a function  $r \in \mathcal{K}$ , which is a

continuous and positive definite, such that, for all Lyapunov functions  $V(t, \psi)$  ( $V(t, \psi)$  is the same as  $V(t, \psi)$  in Lemma 1),

$$D^-V(t, \psi) \geq -r(V(t, \psi)), \quad (11)$$

$$\int_0^\varepsilon \frac{1}{r(z)} dz < +\infty, \quad (12)$$

always hold.

*Remark 4.* Lemma 1 is a sufficient condition for judging finite-time stability, and Lemma 3 is a necessary condition about finite-time stability. Lemma 3 can be used when we judge finite-time instability of that QVNN. Lemma 2 will be used to derive  $D^+V(t, \psi) \leq -r(V(t, \psi))$  and  $D^-V(t, \psi) \geq -r(V(t, \psi))$  in the proof of Theorems 1 and 2 later.

### 3. Main Results

In this section, by designing several suitable nonlinear controllers, some criteria are proposed to carry out stabilization and destabilization of system (5) in a finite time. The following controllers are designed:

$$\begin{aligned} I^{(r)}(t) &= -\lambda_1^{(r)} x^{(r)}(t) - \lambda_2^{(r)} \left( |x^{(r)}(t)|^{\sigma_1} \right)^T \text{sgn}(x^{(r)}(t)) - \theta^{(r)} \left( |x^{(r)}(t - \tau(t))| \right)^T \text{sgn}(x^{(r)}(t)), \\ I^{(i)}(t) &= -\lambda_1^{(i)} x^{(i)}(t) - \lambda_2^{(i)} \left( |x^{(i)}(t)|^{\sigma_1} \right)^T \text{sgn}(x^{(i)}(t)) - \theta^{(i)} \left( |x^{(i)}(t - \tau(t))| \right)^T \text{sgn}(x^{(i)}(t)), \\ I^{(j)}(t) &= -\lambda_1^{(j)} x^{(j)}(t) - \lambda_2^{(j)} \left( |x^{(j)}(t)|^{\sigma_1} \right)^T \text{sgn}(x^{(j)}(t)) - \theta^{(j)} \left( |x^{(j)}(t - \tau(t))| \right)^T \text{sgn}(x^{(j)}(t)), \\ I^{(k)}(t) &= -\lambda_1^{(k)} x^{(k)}(t) - \lambda_2^{(k)} \left( |x^{(k)}(t)|^{\sigma_1} \right)^T \text{sgn}(x^{(k)}(t)) - \theta^{(k)} \left( |x^{(k)}(t - \tau(t))| \right)^T \text{sgn}(x^{(k)}(t)), \end{aligned} \quad (13)$$

and the vector form

$$\hat{I}(t) = -\Lambda_1 Q(t) - \Lambda_2 Q_t^{\sigma_1} \text{sgn}(Q(t)) - \Theta Q_{t-\tau} \text{sgn}(Q(t)), \quad (14)$$

where  $\sigma_1 > 0$ , and  $\lambda_1^{(p)}, \lambda_2^{(p)}, \theta^{(p)} \in \mathbb{R}, p = r, i, j, k$ ,

$$\Lambda_1 = \text{diag}\{\lambda_1^{(r)}, \dots, \lambda_1^{(r)}, \lambda_1^{(i)}, \dots, \lambda_1^{(i)}, \lambda_1^{(j)}, \dots, \lambda_1^{(j)}, \lambda_1^{(k)}, \dots, \lambda_1^{(k)}\} \in \mathbb{Q}^{4l \times 4l},$$

$$\Lambda_2 = \text{diag}\{\lambda_2^{(r)}, \dots, \lambda_2^{(r)}, \lambda_2^{(i)}, \dots, \lambda_2^{(i)}, \lambda_2^{(j)}, \dots, \lambda_2^{(j)}, \lambda_2^{(k)}, \dots, \lambda_2^{(k)}\} \in \mathbb{Q}^{4l \times 4l},$$

$$\Theta = \text{diag}\{\theta^{(r)}, \dots, \theta^{(r)}, \theta^{(i)}, \dots, \theta^{(i)}, \theta^{(j)}, \dots, \theta^{(j)}, \theta^{(k)}, \dots, \theta^{(k)}\} \in \mathbb{Q}^{4l \times 4l},$$

$$Q_t = \text{diag}\{|x_1^{(r)}(t)|, \dots, |x_l^{(r)}(t)|, |x_1^{(i)}(t)|, \dots, |x_l^{(i)}(t)|, |x_1^{(j)}(t)|, \dots, |x_l^{(j)}(t)|, |x_1^{(k)}(t)|, \dots, |x_l^{(k)}(t)|\} \in \mathbb{Q}^{4l \times 4l},$$

$$Q_{t-\tau} = \text{diag}\{|x_1^{(r)}(t - \tau(t))|, \dots, |x_l^{(r)}(t - \tau(t))|, |x_1^{(i)}(t - \tau(t))|, \dots, |x_l^{(i)}(t - \tau(t))|, |x_1^{(j)}(t - \tau(t))|, \dots, |x_l^{(j)}(t - \tau(t))|, |x_1^{(k)}(t - \tau(t))|, \dots, |x_l^{(k)}(t - \tau(t))|\} \in \mathbb{Q}^{4l \times 4l},$$

$$\text{sgn}(Q(t)) = \left( \text{sgn}(x^{(r)}(t))^T, \text{sgn}(x^{(i)}(t))^T, \text{sgn}(x^{(j)}(t))^T, \text{sgn}(x^{(k)}(t))^T \right)^T \in \mathbb{Q}^{4l}.$$

(15)



**Theorem 1.** When Assumptions 1 and 2 hold,  $0 < \sigma_1 < 1$  and  $\Lambda_2 > 0$ , given positive diagonal matrices  $\Lambda_1$  and  $\Theta$  such that

$$\begin{aligned} I^T [-(\widehat{C} + \Lambda_1) + |\widehat{A}|\widehat{\Delta}] &< 0, \\ I^T (|\widehat{B}|\widehat{\Delta} - \Theta) &< 0, \end{aligned} \quad (16)$$

then under controller (14), the VMDE (5) will reach a stable state in a finite-time interval.  $T$  is the settling time and can be prescribed by  $T \leq (1/\lambda_{2\min}(1 - \sigma_1))V(0)^{1-\sigma_1}$ , where  $\lambda_{2\min} = \min\{\lambda_2^{(\mu)}\}$ ,  $\mu = r, i, j, k$ .

*Proof.* The following Lyapunov candidate functional will be considered by us:

$$V(t) = \|Q(t)\|. \quad (17)$$

Based on the solution trajectories of system (5) to calculate the upper-right Dini derivative of  $V(t)$ , one obtains

$$\begin{aligned} D^+V(t) &= \text{sgn}(Q(t))^T \dot{Q}(t) \\ &= \text{sgn}(Q(t))^T [-\widehat{C}Q(t) + \widehat{A}\widehat{g}(Q(t)) + \widehat{B}\widehat{g}(Q(t - \tau(t))) - \Lambda_1Q(t) - \Lambda_2Q_t^{\sigma_1} \text{sgn}(Q(t)) - \Theta Q_{t-\tau} \text{sgn}(Q(t))] \\ &\leq -I^T (\widehat{C} + \Lambda_1)|Q(t)| + I^T |\widehat{A}|\widehat{g}(Q(t)) + I^T |\widehat{B}|\widehat{g}(Q(t - \tau(t))) - I^T \Lambda_2 Q_t^{\sigma_1} I - I^T \Theta Q_{t-\tau} I \\ &\leq -I^T (\widehat{C} + \Lambda_1)|Q(t)| + I^T |\widehat{A}|\widehat{\Delta}|Q(t)| + I^T |\widehat{B}|\widehat{\Delta}|Q(t - \tau(t))| - I^T \Theta Q_{t-\tau} I - I^T \Lambda_2 Q_t^{\sigma_1} I \\ &\leq -I^T (\widehat{C} + \Lambda_1)|Q(t)| + I^T |\widehat{A}|\widehat{\Delta}|Q(t)| + I^T (|\widehat{B}|\widehat{\Delta} - \Theta)Q_{t-\tau} I - I^T \Lambda_2 Q_t^{\sigma_1} I \\ &= I^T [-(\widehat{C} + \Lambda_1) + |\widehat{A}|\widehat{\Delta}]|Q(t)| + I^T (|\widehat{B}|\widehat{\Delta} - \Theta)|Q(t - \tau(t))| - I^T \Lambda_2 Q_t^{\sigma_1} I, \end{aligned} \quad (18)$$

Here, by Assumption 2,  $|\widehat{g}_i(Q_i(t)) - \widehat{g}_i(0)| \leq \alpha_i |Q_i(t) - 0|$  ( $i = 1, \dots, 4l$ ) is used.

In view of  $I^T [-(\widehat{C} + \Lambda_1) + |\widehat{A}|\widehat{\Delta}] < 0$ ,  $I^T (|\widehat{B}|\widehat{\Delta} - \Theta) < 0$ , and Lemma 2, the following inequality can be established:

$$\begin{aligned} D^+V(t) &\leq -I^T \Lambda_2 Q_t^{\sigma_1} I \\ &\leq -\lambda_{2\min} (I^T Q_t I)^{\sigma_1} \\ &= -\lambda_{2\min} \|Q(t)\|^{\sigma_1} \\ &= -\lambda_{2\min} V^{\sigma_1}(t), \end{aligned} \quad (19)$$

where  $\lambda_{2\min} = \min\{\lambda_2^{(\mu)}\}$ ,  $\mu = r, i, j, k$ ,  $\Lambda_2 > 0$ .

And for all  $\varepsilon > 0$ , one has

$$\int_0^\varepsilon \frac{1}{\lambda_{2\min} z^\sigma} dz = \frac{1}{\lambda_{2\min}(1 - \sigma_1)} \varepsilon^{1-\sigma_1} < +\infty. \quad (20)$$

Hence, by Lemma 1, we obtain that system (5) is finite-time stable under controller (14). And the settling time is prescribed by

$$T \leq \int_0^{V(0)} \frac{1}{(\lambda_{2\min} z^{\sigma_1})} dz = \frac{1}{\lambda_{2\min}(1 - \sigma_1)} V(0)^{1-\sigma_1}. \quad (21) \quad \square$$

*Remark 5.* Obviously, the settling time is related to the parameters  $\lambda_{2\min}$  and  $V(0)$  under  $0 < \sigma_1 < 1$ . The results

obtained here is more general; let  $\sigma_1$  choose some special value, and the exponentially stable and power stable can be obtained. If  $\sigma_1 = 1$ , the VMDE (5) is exponentially stable. However, when  $\sigma_1 > 1$ ,  $t = \int_{V(t)}^{V(0)} 1/\lambda_{2\min} z^{\sigma_1} dz = V(t)^{1-\sigma_1} - V(0)^{1-\sigma_1}/\lambda_{2\min}(\sigma_1 - 1)$  or  $V(t) = [V(0)^{1-\sigma_1} + \lambda_{2\min}(\sigma_1 - 1)t]^{1/(1-\sigma_1)}$ ; then, we know VMDE (5) is power stable with power rate  $(1/1 - \sigma_1)$ .

**Theorem 2.** When Assumptions 1 and 2 hold,  $\sigma_1 > 1$  and  $\Lambda_2 > 0$ , given negative definite diagonal matrices  $\Lambda_1$  and  $\Theta$ , such that

$$I^T [\widehat{C} + \Lambda_1 + |\widehat{A}|\widehat{\Delta}] < 0, \quad (22)$$

$$I^T [|\widehat{B}|\widehat{\Delta} + \Theta] < 0, \quad (23)$$

then under controller (14), the VMDE (5) cannot reach a stable state in a finite time.

*Proof.* Choose the same Lyapunov candidate function as Theorem 1:

$$V(t) = \|Q(t)\|. \quad (24)$$

Computing the lower-right Dini derivative of  $V(t)$  based on the solution trajectories of system (5), one obtains

$$\begin{aligned}
D^-V(t) &= \text{sgn}(Q(t))^T \dot{Q}(t) \\
&= \text{sgn}(Q(t))^T [-\hat{C}Q(t) + \hat{A}\hat{g}(Q(t)) + \hat{B}\hat{g} \\
&\quad \cdot (-\Lambda_1 Q(t) - \Lambda_2 Q_t^{\sigma_1} \text{sgn}(Q(t)) - \Theta Q_{t-\tau} \text{sgn}(Q(t)))] \\
&\geq -I^T (\hat{C} + \Lambda_1) |Q(t)| - I^T |\hat{A}| \|\hat{g}(Q(t))\| - I^T \|\hat{B}\| \|\hat{g} \\
&\quad \cdot (Q(t - \tau(t))) - I^T \Lambda_2 Q_t^{\sigma_1} I - I^T \Theta Q_{t-\tau} I \\
&\geq -I^T (\hat{C} + \Lambda_1) |Q(t)| - I^T |\hat{A}| \|\hat{\Delta}|Q(t)| - I^T |\hat{B}| \|\hat{\Delta}|Q \\
&\quad \cdot (t - \tau(t)) - I^T \Theta Q_{t-\tau} I - I^T \Lambda_2 Q_t^{\sigma_1} I \\
&\geq -I^T (\hat{C} + \Lambda_1) |Q(t)| - I^T |\hat{A}| \|\hat{\Delta}|Q(t)| - I^T (|\hat{B}| \|\hat{\Delta} + \Theta) \\
&\quad \cdot Q_{t-\tau} I - I^T \Lambda_2 Q_t^{\sigma_1} I \\
&= -I^T [\hat{C} + \Lambda_1 + |\hat{A}| \|\hat{\Delta}|] |Q(t)| - I^T (|\hat{B}| \|\hat{\Delta} + \Theta) |Q \\
&\quad \cdot (t - \tau(t)) - I^T \Lambda_2 Q_t^{\sigma_1} I.
\end{aligned} \tag{25}$$

Here, by Assumption 2,  $|\hat{g}_i(Q_i(t)) - \hat{g}_i(0)| \leq \alpha_i |Q_i(t) - 0|$  ( $i = 1, \dots, 4l$ ) is employed.

And it follows from  $\hat{C} + \Lambda_1 + |\hat{A}| \|\hat{\Gamma}\| < 0$ ,  $|\hat{B}| t \|\hat{\Gamma}\| n + q \Theta h < 0$ , and Lemma 2 that

$$\begin{aligned}
D^-V(t) &\geq -I^T \Lambda_2 Q_t^{\sigma_1} I \\
&\geq -(4l)^{(1-\sigma_1)} \lambda_{2\max}(I^T Q_t I)^{\sigma_1} \\
&= -(4l)^{(1-\sigma_1)} \lambda_{2\max} \|Q(t)\|^{\sigma_1},
\end{aligned} \tag{26}$$

where  $\lambda_{2\max} = \max\{\lambda_2^{(p)}\}$ ,  $p = r, i, j, k$ ,  $\Lambda_2 > 0$ .  
Therefore,

$$D^-V(t) \geq -(4l)^{(1-\sigma_1)} \lambda_{2\max} V^{\sigma_1}(t). \tag{27}$$

However, by  $\sigma_1 > 1$ , for all  $\varepsilon > 0$ ,

$$\begin{aligned}
\int_0^\varepsilon \frac{1}{(4l)^{(1-\sigma_1)} \lambda_{2\max} z^{\sigma_1}} dz &= \frac{(4l)^{(\sigma_1-1)}}{\lambda_{2\max} (1-\sigma_1)} \\
&\cdot \left( \varepsilon^{1-\sigma_1} - \lim_{z \rightarrow 0^+} z^{1-\sigma_1} \right) = +\infty.
\end{aligned} \tag{28}$$

By Lemma 1, one obtains that system (5) under controller (14) cannot be finite-time stable.  $\square$

*Remark 6.* The time-varying delays of system (5) under controller (14) can be understood as follows. In fact, the third term  $-\Theta Q_{t-\tau} \text{sgn}(Q(t))$  in controller (14) and scaling techniques is employed to reduce its influence. And if the time delays are infinite, the system cannot achieve finite-time stabilization; therefore,  $\tau(t)$  is supposed to be finite. Furthermore, we cannot ignore time delays' influence when discussing the short-time stability of various dynamical systems. However, fewer literature utilized the time delays in their controllers;

hence, this paper attempts to design a nonlinear controller with time delays, which is a meaningful work.

*Remark 7.*  $I^T [-(\hat{C} + \Lambda_1) + |\hat{A}| \|\hat{\Delta}\|] < 0$ , as well as (16), (22), and (23), indicate the column summations of square matrices are negative. And they are algebraic expressions which can be easily checked.

*Remark 8.* Zhang et al. [4] considers stability and instability of a complex value neural network in a finite time. In this paper, the analysis method of [4] is generalized to the finite-time stability and instability of QVNNs. Compared to [4], though the derivation process of this paper is very brief, it can also explain the stability and instability of QVNNs well. Therefore, the vector-matrix analysis method can be widely used for the other stability analysis of neural networks. Furthermore, there is no result to discuss the finite-time stability and instability of QVNNs with discrete delays. This paper is one of the first to do this attempt.

## 4. Illustrative Examples

In this section, the validity and superiority of the proposed criteria will be checked via two illustrative examples. And we will show that our vector-matrix methods are more suitable for calculating some problems of high-dimension systems by computer programming.

*Example 1.* Consider the QVNNs model as follows:

$$\dot{x}(t) = -Cx(t) + Mg(x(t)) + Ng(x(t - \tau(t))) + I(t), \tag{29}$$

where

$$M = \begin{pmatrix} -6 + 5i + 5j + 5k & -4 + 2i - 3j + 1k \\ 4 - 2i + 3j + 1k & 9 + 5i + 1j + 6k \end{pmatrix},$$

$$N = \begin{pmatrix} 3 + 2i + 3j + 1.3k & 4 + 4i - 4j - 2k \\ -4 - 4i + 4j + 3k & 2 + 2i + 3j + 4k \end{pmatrix},$$

$$C = \text{diag}\{18, 7\}, \tau(t) = 0.45 \sin t + 0.35,$$

$$\begin{aligned}
g(x(t)) &= \frac{|x^{(r)}(t) + 1| - |x^{(r)}(t) - 1|}{2} \\
&\quad + \frac{|x^{(i)}(t) + 1| - |x^{(i)}(t) - 1|}{2} i \\
&\quad + \frac{|x^{(j)}(t) + 1| - |x^{(j)}(t) - 1|}{2} j \\
&\quad + \frac{|x^{(k)}(t) + 1| - |x^{(k)}(t) - 1|}{2} k.
\end{aligned} \tag{30}$$

Under  $I(t) = 0$  and initial condition  $x(s) = \begin{pmatrix} 2 \\ 3 \end{pmatrix} + \begin{pmatrix} -3 \\ 2.5 \end{pmatrix}i + \begin{pmatrix} -3 \\ -3.1 \end{pmatrix}j + \begin{pmatrix} 3 \\ 4 \end{pmatrix}k$ ,  $s \in [0.8, 0]$ , the state trajectories of system (29) are shown in Figure 1(a), which shows that system (29) is unstable. By Assumptions 1 and 2, choose  $\widehat{\Delta} = \text{diag}\{0.01, 0.01, 0.01, 0.01, 0.01, 0.01, 0.01, 0.01\}$ . To reach the finite-time stable conditions of Theorem 1, by (14), the following controller is designed:

$$\widehat{I}(t) = -\Lambda_1 Q(t) - \Lambda_2 Q_t^{\sigma_1} \text{sgn}(Q(t)) - \Theta Q_{t-\tau} \text{sgn}(Q(t)), \quad (31)$$

where

$$\begin{aligned} \sigma_1 &= 0.5, \\ \Lambda_2 &= \text{diag}\{20, 20, 20, 20, 20, 20, 20, 20\}. \end{aligned} \quad (32)$$

Then, when consider appropriate  $\widehat{\Delta}, \Lambda_1$  such that  $-\widehat{C} - \Lambda_1 + \widehat{A}\widehat{\Delta} < 0$ , the LMI toolbox in MATLAB is used, and then it is easy to check  $I^T(-\widehat{C} - \Lambda_1 + \widehat{A}\widehat{\Delta}) < 0$ . So, the following feasible solutions of  $\Lambda_1$  and  $\Theta$  can be obtained:

$$\begin{aligned} \Lambda_1 &= \text{diag}\{417.7830, 417.7830, 417.7830, 417.7830, 417.7830, 417.7830, 417.7830, 417.7830\}, \\ \Theta &= \text{diag}\{423.9499, 423.9499, 423.9499, 423.9499, 423.9499, 423.9499, 423.9499, 423.9499\}, \\ I^T(-\widehat{C} - \Lambda_1 + \widehat{A}\widehat{\Delta}) &= \{-434.5630, -423.9430, -434.4430, -423.9030, -434.5030, -423.8330, -434.2130, -423.2530\} < 0, \\ I^T(-\Theta + |\widehat{B}|\widehat{\Delta}) &= \{-423.3759, -422.9399, -422.9669, -422.8299, -423.1369, -422.8899, -422.9669, -422.8899\} < 0. \end{aligned} \quad (33)$$

Therefore, condition (16) of Theorem 1 can be verified. Hence, by Theorem 1, under controller (31), system (29) can reach the stable state in finite time, and one can estimate the settling time  $T \leq 0.9716$ . Furthermore, the state trajectories of  $x(t)$  of system (29) under controller (31) are shown in Figure 1(b), which shows that any solution of system (29) can converge to zero in a finite-time interval. Therefore, the correctness of Theorem 1 is verified.

Now, we analyze the effect of the parameter  $\Lambda_2$  and initial condition on the settling time  $T$ . When initial condition  $x(t) = 0$ , obviously,  $T = 0$ . Fix other values and increase the value  $\lambda_{2\min}$ ; the settling time will decrease, which can be shown in Figure 2. Therefore, the settling time in Theorem 1 is reasonable.

*Example 2.* Consider the QVNNs model as follows:

$$\dot{x}(t) = -Cx(t) + Mg(x(t)) + Ng(x(t - \tau(t))) + I(t), \quad (34)$$

where

$$\begin{aligned} M &= \begin{pmatrix} -3 + 2i + 2j - 4k & -0.4 - 2i - 3j + 1k \\ 0.4 + 2i + 3j - 1k & 3 + 0.5i + 1j + 1.9k \end{pmatrix}, \\ N &= \begin{pmatrix} 2 + 2i + 3j + 1.3k & -1.4 + 0.4i - 4j - 1.2k \\ 1.4 - 0.4i + 4j + 1.2k & 2 + 2i + 3j + 4k \end{pmatrix}, \\ C &= \text{diag}\{20, 20\}, \\ \tau(t) &= 0.45 \sin t + 0.1, \\ g(x(t)) &= \frac{|x^{(r)}(t) + 1| - |x^{(r)}(t) - 1|}{2} \\ &\quad + \frac{|x^{(i)}(t) + 1| - |x^{(i)}(t) - 1|}{2}i \\ &\quad + \frac{|x^{(j)}(t) + 1| - |x^{(j)}(t) - 1|}{2}j \\ &\quad + \frac{|x^{(k)}(t) + 1| - |x^{(k)}(t) - 1|}{2}k. \end{aligned} \quad (35)$$

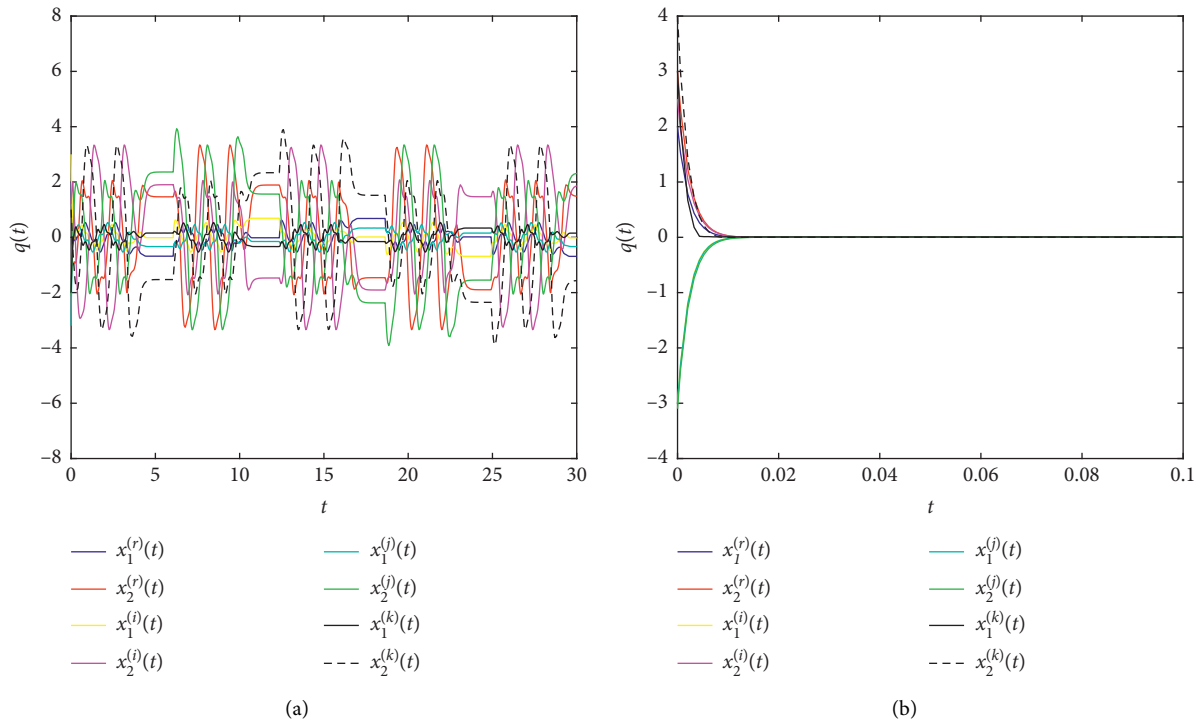


FIGURE 1: The state trajectories of  $x^r(t)$ ,  $x^i(t)$ ,  $x^j(t)$ ,  $x^k(t)$  of QVNs (29). (a) With  $I(t) = 0$ . (b) Under controller (31).

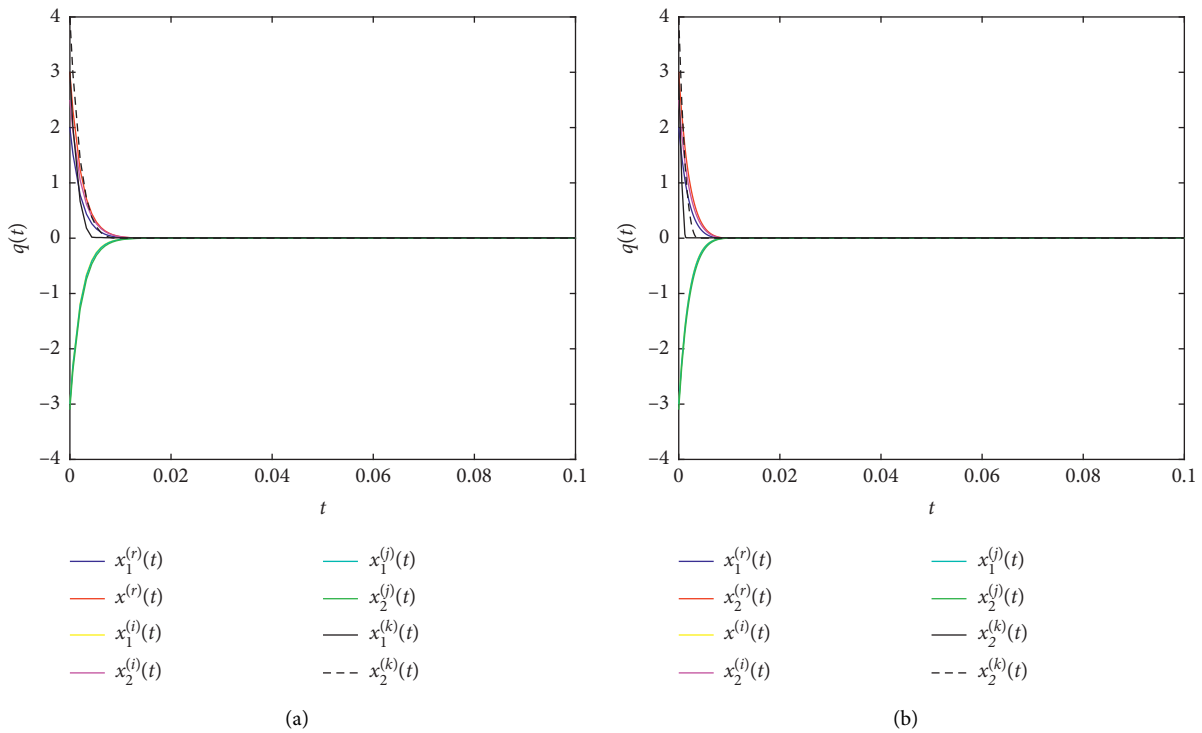


FIGURE 2: Continued.

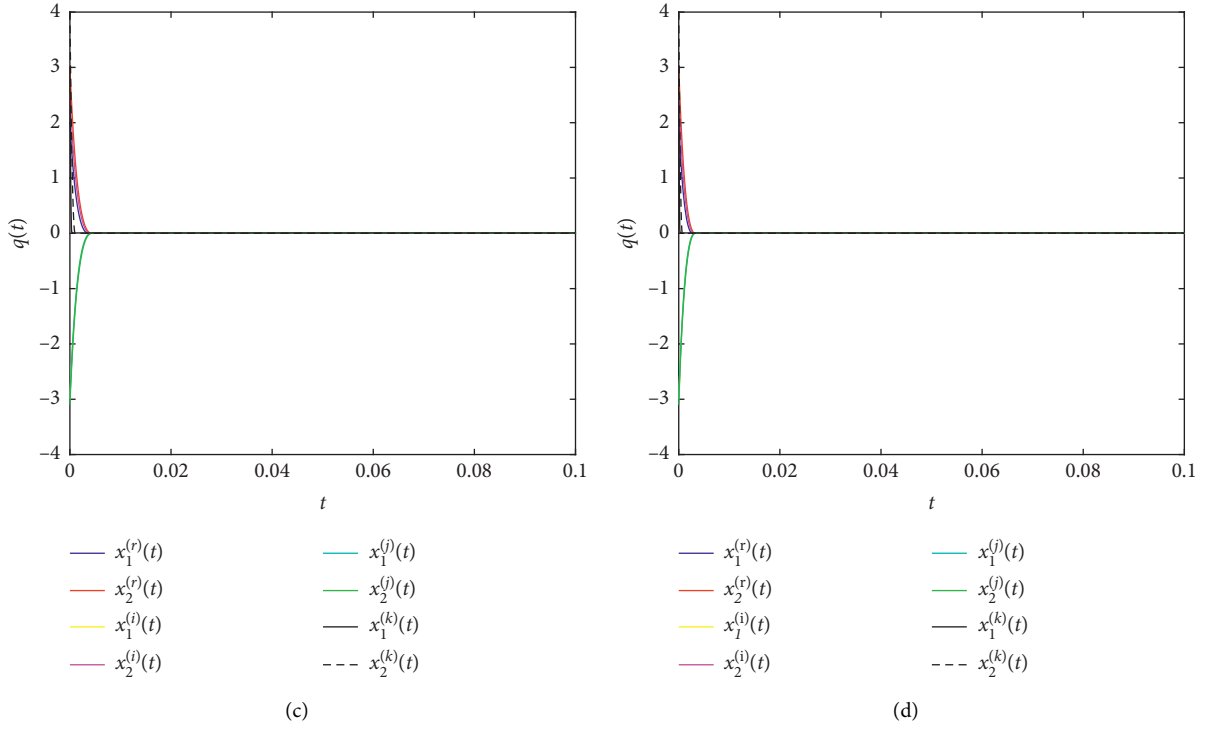


FIGURE 2: Effect of the change of  $\Lambda_2$  on the settling time of QVNNs model (29). (a)  $\Lambda_2 = 20 \times E$ , (b)  $\Lambda_2 = 100 \times E$ , (c)  $\Lambda_2 = 500 \times E$ , and (d)  $\Lambda_2 = 750 \times E$ .

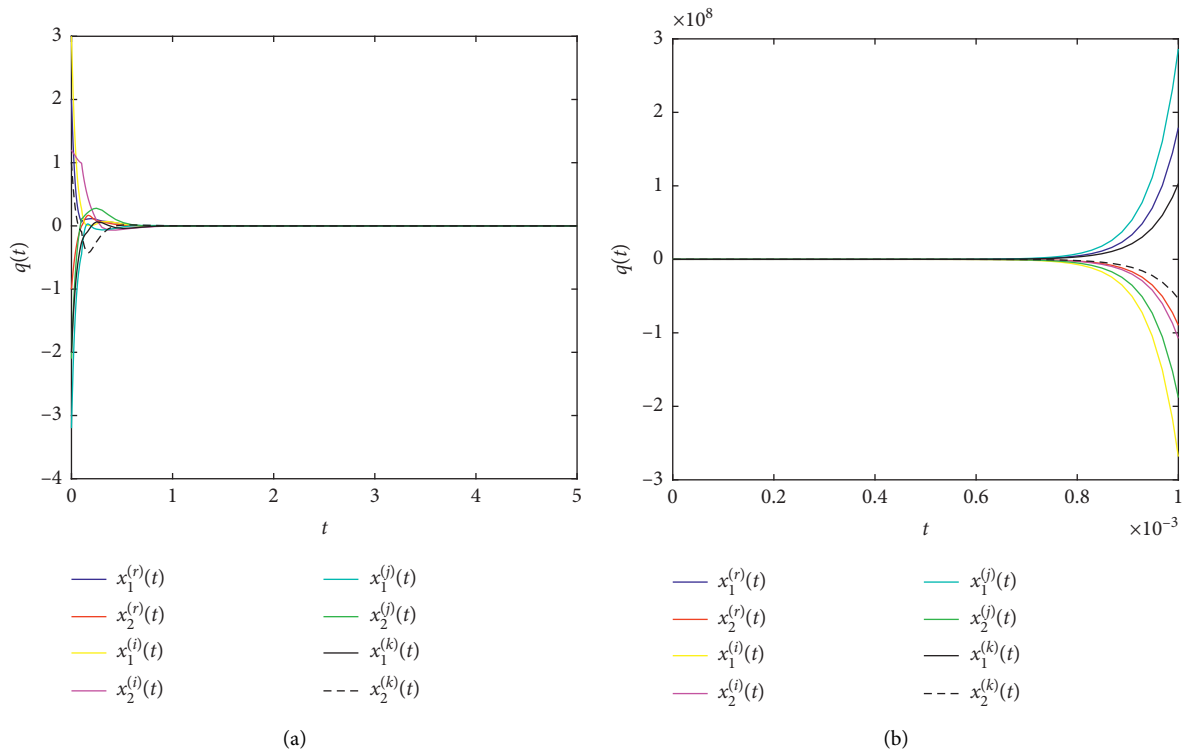


FIGURE 3: The state trajectories of  $x^{(r)}(t)$ ,  $x^{(i)}(t)$ ,  $x^{(j)}(t)$ , and  $x^{(k)}(t)$  of QVNNs model (34). (a) With  $I(t) = 0$ . (b) Under controller (31).

Under  $I(t) = 0$  and initial condition  $x(s) = \begin{pmatrix} 2 \\ -1 \end{pmatrix} + \begin{pmatrix} 3 \\ 1.2 \end{pmatrix}i + \begin{pmatrix} -3.2 \\ -2.1 \end{pmatrix}j + \begin{pmatrix} -2 \\ 1 \end{pmatrix}k$ ,  $s \in [0.55, 0]$ , the state trajectories of system (34) are shown in Figure 3(a), which shows that system (34) is stable. By Assumptions 1 and 2, we let  $\widehat{\Delta} = \text{diag}\{5, 5, 5, 5, 5, 5, 5, 5\}$ . To reach the finite-time instable conditions of Theorem 1, by (14), the following controller is designed:

$$\widehat{I}(t) = -\Lambda_1 Q(t) - \Lambda_2 Q_t^{\sigma_1} \text{sgn}(Q(t)) - \Theta Q_{t-\tau} \text{sgn}(Q(t)), \quad (36)$$

where

$$\begin{aligned} \sigma_1 &= 1.1, \\ \Lambda_2 &= \text{diag}\{10, 10, 10, 10, 10, 10, 10, 10\}. \end{aligned} \quad (37)$$

Then, similarly, to realize  $\widehat{C} + \Lambda_1 + |\widehat{A}|\widehat{\Delta} < 0$ ,  $\Theta + |\widehat{B}|\widehat{\Delta} < 0$ , the LMI toolbox in MATLAB is used and the following feasible solutions of  $\Lambda_1$  and  $\Theta$  can be obtained:

$$\begin{aligned} \Lambda_1 &= \text{diag}\{-18361, -18361, -18361, -18361, -18361, \\ &\quad -18361, -18361, -18361\}, \\ \Theta &= \text{diag}\{-18337, -18337, -18337, -18337, -18337, \\ &\quad -18337, -18337, -18337\}. \end{aligned} \quad (38)$$

And it so happened that

$$\begin{aligned} I^T(\widehat{C} + \Lambda_1 + |\widehat{A}|\widehat{\Delta}) &= 10^4 * \{-1.7779, -1.8002, -1.7779, \\ &\quad -1.7897, -1.7874, -1.8040, -1.7931, \\ &\quad -1.7954\} < 0, \\ I^T(\Theta + |\widehat{B}|\widehat{\Delta}) &= 10^4 * \{-1.8023, -1.7753, -1.7595, \\ &\quad -1.7582, -1.8032, -1.8019, -1.7937, \\ &\quad -1.7924\} < 0, \end{aligned} \quad (39)$$

Therefore, conditions (22) and (23) of Theorem 2 can be verified. The state trajectories of  $x(t)$  of system (34) are shown in Figure 3(b), which shows that the state variables of system (34) can become big enough from zero point in a finite time, i.e., system (34) can reach the instable state in a finite-time interval under (36). Hence, the correctness of Theorem 2 is verified.

*Remark 9.* Through the analysis of these two examples, the advantages of the vector-matrix method processing finite-time stabilization and destabilization of QVNNs are checked, which is easy to calculate by computer programming. Furthermore, this approach is applicable when discussing other high-dimensional systems.

## 5. Conclusion

In this paper, we analyze two interesting problems, the finite-time stabilization and destabilization of QVNNs with discrete delays, respectively. Utilizing the decomposition method, a new, vector-matrix and suitable nonlinear controller is constructed to carry out the finite-time stabilization and destabilization of the discussed QVNNs, which is used by fewer references. Furthermore, the obtained criteria are compact, effective, and easily checked. Through two numerical examples, the correctness, the convenience, and the applicability of the two criteria are all verified. In addition, the problems of fixed-time stabilization and preassigned-time control of QVNNs are also interesting and challenging, which we will consider in the near future. Moreover, in this paper, the activation functions in model (2) are special functions; hence, we will also discuss the finite-time stability of QVNNs with more general activation functions in future work.

## Data Availability

No data were used to support the findings of the study.

## Conflicts of Interest

The authors declare that they have no conflicts of interest.

## Acknowledgments

This work was supported in part by the National Natural Science Foundation of China under Grant no. 61877033, Natural Science Foundation of Shandong Province under Grant no. ZR2019MF021, Natural Science Foundation Project of Chongqing, China, under Grant no. cstc2018jcyjAX0588, and Scientific and Technological Research Program of Chongqing Municipal Education Commission under Grant no. KJQN201901206.

## References

- [1] P. Dorato, "Short time stability in linear time-varying systems," in *Proceedings of the IRE International Convention Record Part*, pp. 83–87, New York, NY, USA, January 1961.
- [2] S. G. Nersesov, C. Nataraj, and J. M. Avis, "Design of finite-time stabilizing controllers for nonlinear dynamical systems," *International Journal of Robust and Nonlinear Control*, vol. 19, no. 8, pp. 900–918, 2009.
- [3] R. Rakkiyappan, G. Velmurugan, and J. Cao, "Finite-time stability analysis of fractional-order complex-valued memristor-based neural networks with time delays," *Nonlinear Dynamics*, vol. 78, no. 4, pp. 2823–2836, 2014.
- [4] Z. Zhang, X. Liu, D. Zhou, C. Lin, J. Chen, and H. Wang, "Finite-time stabilizability and instabilizability for complex-valued memristive neural networks with time delays," *IEEE Transactions on Systems, Man, and Cybernetics: Systems*, vol. 48, no. 12, pp. 2371–2382, 2018.

- [5] L. Weiss, "On uniform and nonuniform finite-time stability," *IEEE Transactions on Automatic Control*, vol. 14, no. 3, pp. 313–314, 1969.
- [6] P. Dorato, L. Weiss, and E. Infante, "Comment on "Finite-time stability under perturbing forces and on product spaces"," *IEEE Transactions on Automatic Control*, vol. 12, no. 3, p. 340, 1967.
- [7] W. Lu, X. Liu, and T. Chen, "A note on finite-time and fixed-time stability," *Neural Networks*, vol. 81, pp. 11–15, 2016.
- [8] D. Yang, X. Li, J. Shen, and Z. Zhou, "State-dependent switching control of delayed switched systems with stable and unstable modes," *Mathematical Methods in The Applied Sciences*, vol. 41, no. 16, pp. 6968–6983, 2018.
- [9] F. Wang, J. Wang, K. Wang, C. Hua, and Q. Zong, "Finite-time control for uncertain systems and application to flight control," *Nonlinear Analysis-Modelling and Control*, vol. 25, no. 2, pp. 163–182, 2020.
- [10] Y. Hong, Y. Xu, and J. Huang, "Finite-time control for robot manipulators," *Systems & Control Letters*, vol. 46, no. 4, pp. 243–253, 2002.
- [11] X. Yu, Z. Liu, and Y. Zhang, "Fault-tolerant flight control design with finite-time adaptation under actuator stuck failures," *IEEE Transactions on Control Systems and Technology*, vol. 25, no. 4, pp. 1431–1440, 2017.
- [12] H. Gui and G. Vukovich, "Global finite-time attitude tracking via quaternion feedback," *Systems & Control Letters*, vol. 97, pp. 176–183, 2016.
- [13] C. Huang, J. Lu, G. Zhai, J. Cao, G. Lu, and M. Perc, "Stability and stabilization in probability of probabilistic boolean networks," *IEEE Transactions on Neural Networks and Learning Systems*, vol. 99, pp. 1–11, 2018.
- [14] J. Lu, L. Sun, Y. Liu, D. W. C. Ho, and J. Cao, "Stabilization of boolean control networks under aperiodic sampled-data control," *SIAM Journal on Control and Optimization*, vol. 56, no. 6, pp. 4385–4404, 2018.
- [15] S. Zhu, Y. Liu, Y. Lou, and J. Cao, "Stabilization of logical control networks: an event-triggered control approach," *Science in China Series F: Information Sciences*, vol. 63, no. 1, Article ID 112203, 2020.
- [16] S. Zhu, J. Lu, and Y. Liu, "Asymptotical stability of probabilistic boolean networks with state delays," *IEEE Transactions on Automatic Control*, vol. 65, no. 4, pp. 1779–1784, 2020.
- [17] R. Li and J. Cao, "Finite-time stability analysis for markovian jump memristive neural networks with partly unknown transition probabilities," *IEEE Transactions on Neural Networks*, vol. 28, no. 12, pp. 2924–2935, 2017.
- [18] P. Liu, L. Li, K. Shi, and J. Lu, "Pinning stabilization of probabilistic boolean networks with time delays," *IEEE Access*, vol. 8, pp. 154050–154059, 2020.
- [19] F. Amato, M. Darouach, and G. De Tommasi, "Finite-time stabilizability and detectability of linear systems. Part I: necessary and sufficient conditions for the existence of output feedback finite-time stabilizing controllers," in *Proceedings of the 2016 European Control Conference (ECC)*, pp. 1412–1417, Aalborg, Denmark, June, 2016.
- [20] X. Chen, Q. Song, Z. Li, Z. Zhao, and Y. Liu, "Stability analysis of continuous-time and discrete-time quaternion-valued neural networks with linear threshold neurons," *IEEE Transactions on Neural Networks and Learning Systems*, vol. 29, no. 7, pp. 2769–2781, 2018.
- [21] X. Fan, X. Zhang, L. Wu, and M. Shi, "Finite-time stability analysis of reaction-diffusion genetic regulatory networks with time-varying delays," *IEEE/ACM Transactions on Computational Biology and Bioinformatics*, vol. 14, no. 4, pp. 868–879, 2017.
- [22] E. Moulay, M. Dambrine, N. Yeganefar, and W. Perruquetti, "Finite-time stability and stabilization of time-delay systems," *Systems & Control Letters*, vol. 57, no. 7, pp. 561–566, 2008.
- [23] Z. Yan, G. Zhang, J. Wang, and W. Zhang, "State and output feedback finite-time guaranteed cost control of linear ito stochastic systems," *Journal of Systems Science and Complexity*, vol. 28, no. 4, pp. 813–829, 2015.
- [24] L. Wang and Y. Shen, "Finite-time stabilizability and instabilizability of delayed memristive neural networks with nonlinear discontinuous controller," *IEEE Transactions on Neural Networks and Learning Systems*, vol. 26, no. 11, pp. 2914–2924, 2015.
- [25] X. Li, J. Shen, and R. Rakkiyappan, "Persistent impulsive effects on stability of functional differential equations with finite or infinite delay," *Applied Mathematics and Computation*, vol. 329, pp. 14–22, 2018.
- [26] X. Yang, X. Li, Q. Xi, and P. Duan, "Review of stability and stabilization for impulsive delayed systems," *Mathematical Biosciences and Engineering*, vol. 15, no. 6, pp. 1495–1515, 2018.
- [27] X. Li, X. Yang, and T. Huang, "Persistence of delayed cooperative models: impulsive control method," *Applied Mathematics and Computation*, vol. 342, pp. 130–146, 2019.
- [28] Y. Wang, J. Lu, and Y. Lou, "Halanay-type inequality with delayed impulses and its applications," *Science in China Series F: Information Sciences*, vol. 62, no. 9, Article ID 192206, 2019.
- [29] N. Li and W. X. Zheng, "Passivity analysis for quaternion-valued memristor-based neural networks with time-varying delay," *IEEE Transactions on Neural Networks and Learning Systems*, vol. 31, no. 2, pp. 639–650, 2020.
- [30] W. Shen, X. Zhang, and Y. Wang, "Stability analysis of high order neural networks with proportional delays," *Neurocomputing*, vol. 372, pp. 33–39, 2020.
- [31] Z. Dong, X. Zhang, and X. Wang, "State estimation for discrete-time high-order neural networks with time-varying delays," *Neurocomputing*, vol. 411, pp. 282–290, 2020.
- [32] Z. Dong, X. Wang, and X. Zhang, "A nonsingular m-matrix-based global exponential stability analysis of higher-order delayed discrete-time cohen-rossberg neural networks," *Applied Mathematics and Computation*, vol. 385, p. 125401, 2020.
- [33] R. Yang, B. Wu, and Y. Liu, "A halanay-type inequality approach to the stability analysis of discrete-time neural networks with delays," *Applied Mathematics and Computation*, vol. 265, pp. 696–707, 2015.
- [34] X. Ji, J. Lu, J. Lou, J. Qiu, and K. Shi, "A unified criterion for global exponential stability of quaternion-valued neural networks with hybrid impulses," *International Journal of Robust and Nonlinear Control*, 2020.
- [35] Z. Wang and J. Cao, "Finite-time stabilization control of complex-valued neural networks with discontinuous activation functions and time delay," in *Proceedings of the 2019 Chinese Control Conference (CCC)*, pp. 1195–1200, Wuhan, China, July 2019.
- [36] X. Yang, J. Lam, D. W. C. Ho, and Z. Feng, "Fixed-time synchronization of complex networks with impulsive effects via nonchattering control," *IEEE Transactions on Automatic Control*, vol. 62, no. 11, pp. 5511–5521, 2017.
- [37] Y. Liu, P. Xu, J. Lu, and J. Liang, "Global stability of clifford-valued recurrent neural networks with time delays," *Nonlinear Dynamics*, vol. 84, no. 2, pp. 767–777, 2016.
- [38] S. Buchholz and N. Le Bihan, "Optimal separation of polarized signals by quaternionic neural networks," in

- Proceedings of the 2006 14th European Signal Processing Conference*, Florence, Italy, September 2006.
- [39] X. Qi, H. Bao, and J. Cao, "Synchronization criteria for quaternion-valued coupled neural networks with impulses," *Neural Networks*, vol. 128, pp. 150–157, 2020.
  - [40] X. Qi, H. Bao, and J. Cao, "Exponential input-to-state stability of quaternion-valued neural networks with time delay," *Applied Mathematics and Computation*, vol. 358, pp. 382–393, 2019.
  - [41] H. Duan, T. Peng, Z. Tu, J. Qiu, and J. Lu, "Globally exponential stability and globally power stability of quaternion-valued neural networks with discrete and distributed delays," *IEEE Access*, vol. 8, pp. 46837–46850, 2020.
  - [42] Z. Tu, Y. Zhao, N. Ding, Y. Feng, and W. Zhang, "Stability analysis of quaternion-valued neural networks with both discrete and distributed delays," *Applied Mathematics and Computation*, vol. 343, pp. 342–353, 2019.
  - [43] U. Kandasamy, X. Li, and R. Rajan, "Quasi-synchronization and bifurcation results on fractional-order quaternion-valued neural networks," *IEEE Transactions on Neural Networks and Learning Systems*, vol. 60, pp. 1–10, 2019.
  - [44] H. Deng and H. Bao, "Fixed-time synchronization of quaternion-valued neural networks," *Physica A: Statistical Mechanics and Its Applications*, vol. 527, Article ID 121351, 2019.
  - [45] Y. Liu, Y. Zheng, J. Lu, J. Cao, and L. Rutkowski, "Constrained quaternion-variable convex optimization: a quaternion-valued recurrent neural network approach," *IEEE Transactions on Neural Networks and Learning Systems*, vol. 3, no. 31, pp. 1022–1035, 2020.
  - [46] Y. Liu, D. Zhang, J. Lou, J. Lu, and J. Cao, "Stability analysis of quaternion-valued neural networks: decomposition and direct approaches," *IEEE Transactions on Neural Networks and Learning Systems*, vol. 29, no. 9, pp. 4201–4211, 2018.
  - [47] Y. Liu, D. Zhang, and J. Lu, "Global exponential stability for quaternion-valued recurrent neural networks with time-varying delays," *Nonlinear Dynamics*, vol. 87, pp. 553–565, 2017.
  - [48] E. Moulay and W. Perruquetti, "Finite time stability of differential inclusions," *Ima Journal of Mathematical Control and Information*, vol. 22, no. 4, pp. 465–475, 2005.
  - [49] H. K. Khalil and J. W. Grizzle, *Nonlinear Systems*, Prentice-Hall, Upper Saddle River, NJ, USA, 2002.



## Research Article

# Turing Instability of Brusselator in the Reaction-Diffusion Network

Yansu Ji<sup>1</sup> and Jianwei Shen<sup>2</sup> 

<sup>1</sup>School of Mathematics and Statistics, Zhengzhou University, Zhengzhou 450000, China

<sup>2</sup>School of Mathematics and Statistics, North China University of Water Resources and Electric Power, Zhengzhou 450046, Henan, China

Correspondence should be addressed to Jianwei Shen; [xcjwshen@gmail.com](mailto:xcjwshen@gmail.com)

Received 13 June 2020; Accepted 7 September 2020; Published 5 October 2020

Academic Editor: Xiaodi Li

Copyright © 2020 Yansu Ji and Jianwei Shen. This is an open access article distributed under the Creative Commons Attribution License, which permits unrestricted use, distribution, and reproduction in any medium, provided the original work is properly cited.

Turing instability constitutes a universal paradigm for the spontaneous generation of spatially organized patterns, especially in a chemical reaction. In this paper, we investigated the pattern dynamics of Brusselator from the view of complex networks and considered the interaction between diffusion and reaction in the random network. After a detailed theoretical analysis, we obtained the approximate instability region about the diffusion coefficient and the connection probability of the random network. In the meantime, we also obtained the critical condition of Turing instability in the network-organized system and found that how the network connection probability and diffusion coefficient affect the reaction-diffusion system of the Brusselator model. In the end, the reason for arising of Turing instability in the Brusselator with the random network was explained. Numerical simulation verified the theoretical results.

## 1. Introduction

Pattern formation, a kind of nonuniform macroscopic structure with some regularity in space or time, is ubiquitous. It was first proposed by Turing [1] for systems containing morphogens, although initially, they may be very uniform, a pattern or structure may later emerge due to the instability of the uniform equilibrium, which is triggered by random disturbances. A theoretical analysis of Turing instability in a semidiscrete Brusselator model has been investigated [2]. In [3], the authors proposed and discussed the Brusselator model in a random framework. The mean-field equation, which proved that an organized Turing pattern could be produced in a specific parameter region, was derived. To reveal the effect of external noise on the system, a detailed random analysis of the Brusselator scheme was conducted. The stochastic analysis revealed that such systems' structural stability would be disturbed even if the bifurcation parameters are subject to small external disturbances. There would be different space and

time structures in a certain range of noise intensity and correlation time [4]. It is well known that the Brusselator model is a typical model for studying patterns, so it has attracted the interest of many scholars in different fields. Firstly, the superdiffusion term on pattern formation and pattern selection in the Brusselator model has been well studied. They found that Turing instability can occur under superdiffusion even though the diffusing initiator is faster than the inhibitor [5]. And the model with superdiffusion has been well investigated in [6]. For the Brusselator model, the nonlinear diffusion term and the linear diffusion on the pattern patterns are compared. The process of pattern formation in one-dimensional and two-dimensional space domain was also studied in [7]. In addition, the Brusselator model also attracts interest from scholars studying chemistry and stochastic oscillations in [8, 9]. Then, from a basic point of equilibrium, the authors studied the regular Hopf bifurcation and the singular Hopf bifurcation of the Brusselator model under the reaction periodic force and obtained a method suitable for the study of the nonlinear

vibration of periodic forces in general [10]. Besides, the existence of the pattern formation of the Brusselator model under homogeneous Neumann boundary conditions and the prediction of pattern formation caused by Turing instability under certain assumptions have been well studied [11].

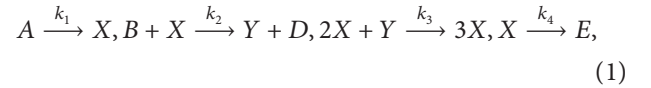
The study of random networks has become more and more popular among scholars in recent years. It is widely used in various fields such as biology, chemistry, and engineering, as discussed in [12–14]. In the study of chemical reactions, random networks can be used to describe the self-diffusion of molecules. In [15], the relationship between the eigenvalues of the Laplace matrix and the degree was pointed out. The localization properties of the Laplace eigenvectors in various random networks were explained. In particular, it provided a theoretical basis and method for further study of the dynamic characteristics of correlated stochastic networks. In [16], McCullen and Wagenknecht emphasized the importance of network structure, revealed the basic connection between small-scale activity patterns on the network and local pattern formation of the whole discipline, and investigated the reaction-diffusion system on the complex network topology. Regarding the analysis of self-organized systems on the network, Nakao and Mikhailov provided a new perspective on analyzing the pattern formation of activator-inhibitor systems on the network in [17]. The system instability caused by the diffusion term on an undirected random network with a certain probability was studied. The pattern theory of the directed network can be derived from [18]. Then, the Turing instability of the reaction-diffusion model defined on the complex network was studied in [19], and three types of models on the complex network were shown in the article. Numerical results showed that the uniform steady-state stability region depends on the network system's structure in the diffusion coefficient space. In [20], they inferred a general theoretical proof that the Turing system's three key features are directly determined by the topology. Recently, Mimar et al. [21] proved that the degree of Laplace can reflect the system's topological characteristics under different networks, which is related to the local characteristics of the diffusion coefficient.

Nowadays, Zheng and Shen [22] investigated the pattern formation in FitzHugh–Nagumo model with a random network, obtained the approximated Turing instability region about the diffusion coefficient and connection probability, and gave a feasible method for studying reaction-diffusion system with connection probability. Although it is known that connection probability plays an essential role in random networks, the influence of random networks on Brusselator cannot be ignored. Still, there are a few literature studies on the effects of network connection probability on Brusselator. In this paper, we explored the effect of random networks on the pattern formation of the reaction-diffusion system from node connection probability.

Next, we will combine the above methods to investigate the pattern dynamics behaviour of the Brusselator model in a random network with connection probability. For the network Laplacian matrix, the connection probability between network node pairs also plays an extremely significant role. Besides, the connection probability affects the diffusion term of the system by changing Laplacian eigenvalues and then affects the stability of the reaction-diffusion system. In Section 2, based on the positive equilibrium point, the Brusselator model's stability is analyzed. The critical condition of Turing instability for the reaction-diffusion system concerning the diffusion coefficient was obtained. In Section 3, the theoretical analysis of Turing instability for the reaction-diffusion system with diffusion term was introduced. In Section 4, the theoretical results obtained in the paper are summarized, and the results are verified by numerical simulation.

## 2. The Analysis of the Brusselator Model

*2.1. Linear Stability Analysis of Brusselator.* The reaction between molecules is described by the Brusselator model, which is a mathematical model proposed by the Brussels school to simulate self-organized phenomena. The Brusselator model studied in this paper is given by the following reaction formula [4]:



where  $k_i$  ( $i=1, 2, 3, 4$ ) is a positive parameter representing the reaction rate constant. According to the law of mass action, the differential equation of  $X$  and  $Y$  concentration can be written as follows:

$$\begin{cases} \frac{dc_X}{d\tau} = k_1c_A - (k_2c_B + k_4)c_X + k_3c_X^2c_Y, \\ \frac{dc_Y}{d\tau} = k_2c_Bc_X - k_3c_X^2c_Y, \end{cases} \quad (2)$$

where  $c_M$  is the constant variable representing the concentrations of  $M$  ( $M$  is the substance  $A, B, \dots$ ), and  $c_X$  and  $c_Y$  are the variables representing the concentrations of  $X$  and  $Y$ . To dimensionless, the differential equation (2) becomes the following:

$$\begin{cases} \frac{dx}{dt} = a - (b+1)x + x^2y = f(x, y), \\ \frac{dy}{dt} = bx - x^2y = g(x, y), \end{cases} \quad (3)$$

where  $x, y, t, a,$  and  $b$  are scale variables, and their expressions are as follows:

$$\begin{aligned}
t &= k_4 \tau, \\
a &= \sqrt{\frac{k_1^2 k_3}{k_4^3}} c_A, \\
b &= \frac{k_2}{k_4} c_B, \\
x &= \sqrt{\frac{k_3}{k_4}} c_X, \\
y &= \sqrt{\frac{k_3}{k_4}} c_Y.
\end{aligned} \tag{4}$$

It is well known that for chemical reaction systems, the positive equilibrium point has scientific significance. Therefore, we have a great deal of interest in the nonnegative equilibrium point and focus on the system's stability near the positive constant fixed points. Obviously, system (3) has the unique constant solution  $M(\bar{x}, \bar{y})$ , where  $\bar{x} = a$  and  $\bar{y} = (b/a)$ . According to the coordinate translation transformation, the equilibrium point  $M$  is translated to the origin  $O(0, 0)$ , that is, introducing  $X = x + \bar{x}$ ,  $Y = y + \bar{y}$  in the system. Then, the linearized system (3) can be expressed as follows:

$$\begin{cases} \frac{dX}{dt} = (b-1)X + a^2 Y, \\ \frac{dY}{dt} = -bX - a^2 Y. \end{cases} \tag{5}$$

To analyze the stability of the equilibrium point of system (5), we write the corresponding Jacobian matrix of the linearized system as follows:

$$J = \begin{pmatrix} b-1 & a^2 \\ -b & -a^2 \end{pmatrix}. \tag{6}$$

The characteristic equation of the system at point  $O$  is given by

$$\lambda_i^2 - P\lambda_i + Q = 0, \tag{7}$$

$$\begin{aligned}
P &= b-1-a^2, \\
Q &= a^2.
\end{aligned} \tag{8}$$

According to Weida's theorem and local equilibrium point stability theory, the equilibrium  $O$  is stable if and only if  $P < 0$  and  $Q > 0$  holds. From  $Q = a^2$  and the parameter domain, it is obvious that  $Q > 0$ , and from  $p = b-1-a^2$ , we can obtain parameters satisfying the condition

$$0 < b < 1 + a^2, \tag{9}$$

which is consistent with the condition that system (3) has a unique positive equilibrium point.

**Lemma 1.** *If the condition (9) holds, the unique positive equilibrium point  $M(\bar{x}, \bar{y})$  of system (3) is asymptotically stable.*

*Proof.* From the stability analysis of the above linearized system, it is clear that when condition (9) holds, the real part of the eigenvalues is negative, that is, the equilibrium point  $O$  is stable. Therefore, the equilibrium point  $M$  of nonlinear system (3) is the stable focus. When condition (9) holds, the unique positive constant solution  $M$  of the initial reaction system is asymptotically stable (Figure 1). The proof is completed.  $\square$

**2.2. Brusselator Model with Random Network.** The Brusselator model with the diffusion term can be described as the following equation set:

$$\begin{cases} \frac{\partial x}{\partial t} = f(x, y) + d_1 \nabla^2 x, \\ \frac{\partial y}{\partial t} = g(x, y) + d_2 \nabla^2 y. \end{cases} \tag{10}$$

Many scholars have well studied the system with the nonnetwork diffusion term. In this paper, the random network can describe the self-diffusion of molecules to investigate the stability change of the homogeneous state of system (3), where the connecting probability of a pair of network nodes is  $p$ . The following steps generate the random network and the adjacency matrix element:

Step 1: suppose the network consists of  $n$  nodes

Step 2: the value of the element  $A_{ij}$  of the adjacency matrix is generated as follows: there is an edge between  $i$  and  $j$  when the random number  $< p$ , which is  $A_{ij} = A_{ji} = 1$ , otherwise  $A_{ij} = A_{ji} = 0$ . For example, Figure 2 shows a random network structure with a connection probability of  $p = 0.05$ .

Then, the balance equation (3) corresponding to each network node can be rewritten as follows:

$$\begin{cases} \frac{dx_i}{dt} = f(x_i, y_i) + d_1 \sum_j L_{ij} x_i, \\ \frac{dy_i}{dt} = g(x_i, y_i) + d_2 \sum_j L_{ij} y_i, \end{cases} \tag{11}$$

where  $L_{ij} = A_{ij} - k_i \delta_{ij}$  is the Laplacian matrix,  $k_i$  is the degree of node  $i$ ,  $\delta_{ij} = 0$  if  $i \neq j$ , and  $\delta_{ij} = 1$  otherwise.

The general solution of equation (3) can be expressed as follows:

$$\begin{aligned}
x_i &= \sum_{m=1}^N c_m \beta_m e^{\lambda_m t} \phi_i^m, \\
y_i &= \sum_{m=1}^N c_m e^{\lambda_m t} \phi_i^m,
\end{aligned} \tag{12}$$

where  $\sum_j L_{ij} \phi_j^m = \Lambda_m \phi_i^m$ .

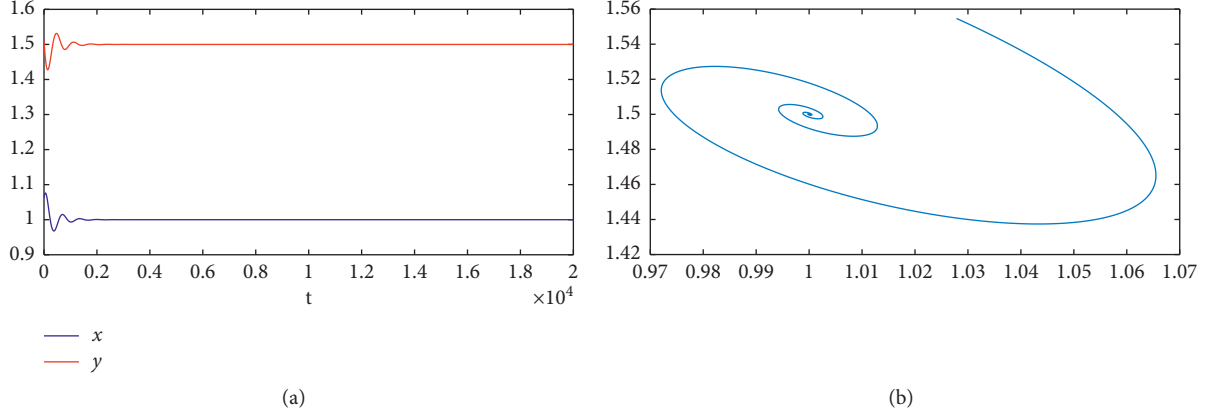


FIGURE 1: When the parameters  $a = 1$  and  $b = 1.5$ , the equilibrium of the Brusselator system (2) is asymptotically stable. (a) The time evolution diagram of the initial value around the equilibrium point. (b) The phase plane.

Firstly, we consider the system's unique positive equilibrium state  $M(\bar{x}, \bar{y})$  after joining the network diffusion, where  $f(\bar{x}, \bar{y}) = g(\bar{x}, \bar{y}) = 0$ . Suppose that the eigenvalues of the Laplacian matrix is  $\Lambda_i (i = 1, 2, \dots, n)$ , which is arranged in descending order, i.e.,  $0 = \Lambda_1 > \Lambda_2 > \dots > \Lambda_n$ . Then the Jacobian matrix of each node in the network diffusion system is expressed as follows:

$$J_i = \begin{pmatrix} b - 1 + d_1 \Lambda_i & a^2 \\ -b & -a^2 + d_2 \Lambda_i \end{pmatrix}. \quad (13)$$

Then the characteristic function of system (11) can be written as follows:

$$\lambda^2 - (b - 1 - a^2 + d_1 \Lambda_i + d_2 \Lambda_i) \lambda + d_1 d_2 \Lambda_i^2 + ((b - 1) d_2 - a^2 d_1) \Lambda_i + a^2 = 0. \quad (14)$$

From Section 2.1, we can know that  $b - 1 - a^2 + d_1 \Lambda_i + d_2 \Lambda_i < 0$ , so the necessary and sufficient condition for Turing instability is that there exists at least one  $\Lambda_i$  to satisfy  $w_{\Lambda_i} = d_1 d_2 \Lambda_i^2 + ((b - 1) d_2 - a^2 d_1) \Lambda_i + a^2 < 0$  or  $\text{Re}(\lambda) > 0$ . In addition, in order to obtain the Turing instability region of the system, we analyzed the stability of the reaction-diffusion system and obtained its critical value satisfies  $(4d_1 d_2 a^2 - ((b - 1) d_2 - a^2 d_1)^2 / 4d_1 d_2) = 0$  (Figure 3). It is obvious that this equation has two roots  $k_{1c}^2, k_{2c}^2$ , when  $\text{Re}(\lambda(k^2)) = 0$ . When the continuous system is unstable,  $\text{Re}(\lambda(k^2)) = 0$  is established in Figure 4, that is, the value range is  $k^2 \in D = \{\lambda | k_{1c}^2 < \lambda < k_{2c}^2\}$ . In addition, the relationship between the network node degree  $k_i$  and the local eigenvectors  $-\Lambda_i$  of the Laplacian matrix and the eigenvalues can be obtained in Figure 5.

**Lemma 2.** For the network Laplacian matrix  $L$ , generally  $k_{\max} = \max\{k_i\}, k_{\min} = \min\{k_i\}$  and  $\Lambda$  is the eigenvalue of  $L$ . Therefore,  $\Lambda \in C = \{\Lambda | -2k_{\max} < \Lambda < M_0 - k_{\min}\}$ .

**Lemma 3.** For a network-organized system, the system is always stable when all the eigenvalues of the network Laplacian matrix are not in the instability region  $\Lambda \cap D = \Phi$

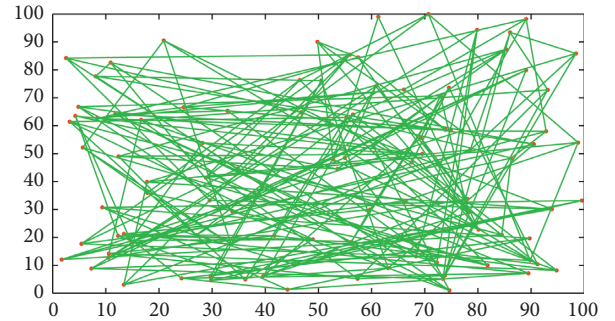


FIGURE 2: Network structure is displayed when connection probability  $p = 0.05$ .

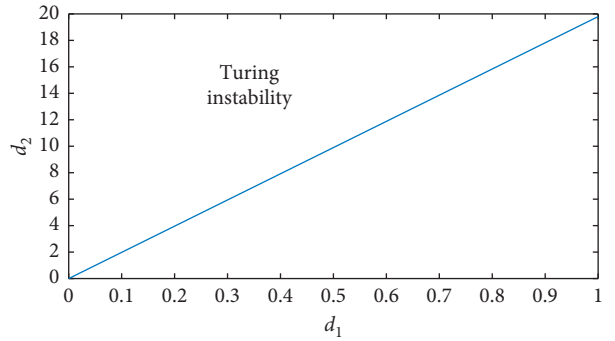


FIGURE 3: A region diagram of the occurrence of Turing instability for diffusion coefficient.

(empty set), the instability occurs when  $\Lambda \cap D \neq \Phi$ , and  $D \cap C \neq \Phi$ .

The detailed proofs of Lemmas 2 and 3 are given in reference [22].

**2.3. Application of Mean-Field Approximation.** Then, the mean-field approximation theory is applied to analyze further the reaction-diffusion system, which can explain the Turing instability mechanism induced by the network diffusion term. In the mean field, the reaction-diffusion system can be expressed as follows:

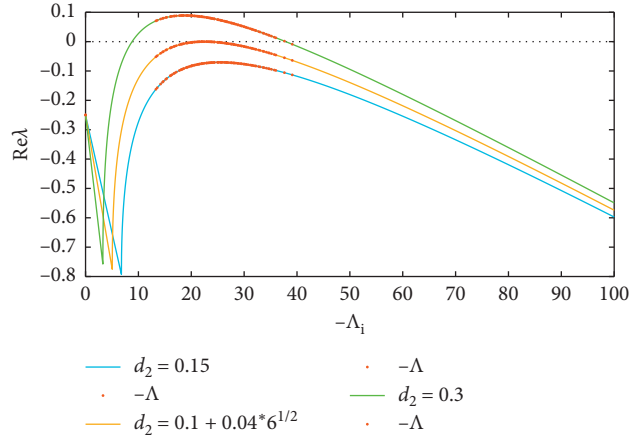


FIGURE 4: Linear stability analysis. The relationship graph between  $\text{Re}\lambda$  about  $\Lambda_i(k^2)$  when  $a = 1$ ,  $b = 1.5$ ,  $p = 0.1$ , and  $d_1 = 0.01$ . The critical values are  $\Lambda_c = -((2 + \sqrt{6})/(10 + 4\sqrt{6}))$  and  $d_{2c} = 0.1 + 0.04\sqrt{6}$ .

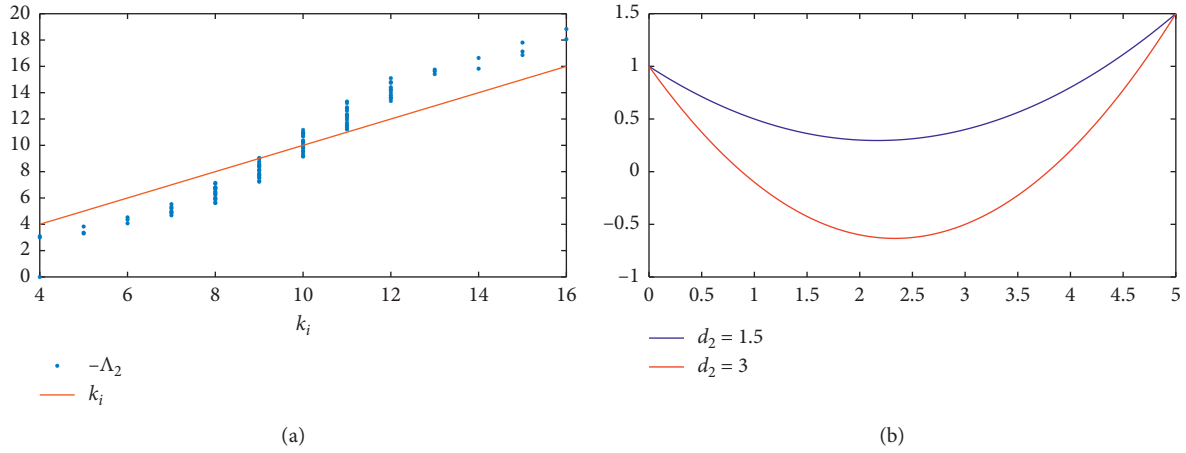


FIGURE 5: The role of  $k_i$ . (a) The relationship graph between degree  $k_i$  and eigenvalue  $-\Lambda_i$ . (b) About the dispersion relationship of  $k_i$  is shown.

$$\begin{cases} \frac{dx_i}{dt} = f(x_i, y_i) + d_1(C^x - k_i x_i), \\ \frac{dy_i}{dt} = g(x_i, y_i) + d_2(C^y - k_i y_i). \end{cases} \quad (15)$$

where  $C^x = \sum_{j=1}^N A_{ij} x_j$ ,  $C^y = \sum_{j=1}^N A_{ij} y_j$ , and  $k_i$  represents the degree of the network.

Mean-field approximation is a method to study complex multibody problems, turning multibody problems into monomer problems. For the Brusselator model, the interaction between a single molecule and other molecules is replaced by an external field effect on this molecule. Therefore, when the role of other molecules is fixed, and only the equilibrium state  $M(\bar{x}, \bar{y})$  of the system is considered, the corresponding single node system can be expressed as follows:

$$\begin{cases} \frac{dx_i}{dt} = f(x_i, y_i) + d_1(\bar{x} - k_i x_i), \\ \frac{dy_i}{dt} = g(x_i, y_i) + d_2(\bar{y} - k_i y_i). \end{cases} \quad (16)$$

From the linear analysis of system (16), the characteristic equation is given as follows:

$$\begin{aligned} \lambda^2 - (b - 1 - a^2 - d_1 k_i - d_2 k_i) \lambda + d_1 d_2 k_i^2 \\ + (a^2 d_1 - (b - 1) d_2) k_i + a^2 = 0. \end{aligned} \quad (17)$$

From the above analysis of the stability of Brusselator, system (16) without the diffusion effect is stable when  $0 < b < 1 + a^2$  holds. Assuming that  $\lambda_1$  and  $\lambda_2$  are the eigenvalues of equation (17), the stability of system (16) depends on the sign of  $w_{k_i}$ , where  $w_{k_i} = d_1 d_2 k_i^2 + (a^2 d_1 - (b - 1) d_2) k_i + a^2$ . If  $w_{k_i} > 0$ , system (16) is stable, otherwise unstable.

### 3. Results

In this section, we present an explanation of theoretical results based on chemical mechanisms. Firstly, the network adjacency matrix  $A$  is a symmetric matrix which is randomly generated based on a random network with probability  $p$ . The relationship between the Laplacian matrix and the

adjacency matrix of the network is  $L_{ij} = A_{ij} - k_i \delta_{ij}$ , where  $k_i$  is the degree of the node  $i$  and  $\delta_{ij}$  is a Dirac function, if  $i = j$ ,  $\delta_{ij} = 1$ , otherwise  $\delta_{ij} = 0$ .

We choose the parameters  $a = 1$  and  $b = 1.5$  and derive the relationship between the diffusion coefficients  $d_1$  and  $d_2$  when the Hopf bifurcation occurs from Figure 3, which shows the critical condition for  $d_1$  and  $d_2$  when Hopf instability occurs. When diffusion coefficients  $d_1$  and  $d_2$  meet the critical value, Hopf instability occurs after control parameters are set. And we can get that the system may be in an instability state when  $d_2 > (10 + 4\sqrt{6})d_1$ . When the ratio of  $d_2$  to  $d_1$  exceeds the critical value, the substance continues to interact to destroy the system's existing equilibrium state. However, when we consider the connection probability, not all values of the instability region can induce Turing instability in that the connection probability of network nodes will also affect the stability of the system. Next, we can give the numerical simulation to verify that Turing instability occurs which is not only related to the diffusion coefficients but also to the probability  $p$ . In addition, since the eigenvalues of the Laplacian matrix are discrete, it is a feasible method to study the effect of the distribution of eigenvalues on the system when we analyze continuous systems. From Lemma 2 and Figure 5, we can gain that the network Laplacian matrix eigenvalue  $-\Lambda_i$  is proportional to the node degree so that it can be approximated by the degree of the node.

The bifurcation diagram of the system concerning  $d_2$ , displayed in Figure 6, shows that the system remains stable when  $p = 0.0004$  and  $p = 0.69$ . And we perform some numerical simulations to certify the above analysis of the system's instability conditions, and the chemical mechanism of Turing instability in the system is given.

Firstly, we obtain the bifurcation diagram (Figures 7–11(a)) of the reaction-diffusion system with respect to  $d_2$  when  $d_1 = 0.01$  under different parameter  $p$ , which shows that the bifurcation point is consistent with the critical value for theoretical analysis.

In Figure 7, we can see that when  $p = 0.0005 > 0.0004$ ,  $d_2$  exceeds the critical value of instability; Turing instability will occur in the reaction-diffusion system. Figure 7(a) shows the bifurcation diagram of the system with respect to the diffusion coefficient, indicating that the system's stability will be destroyed with the increase of  $d_2$ . Figure 7(b) shows that the system will appear unstable when  $d_2 = 1.5$  and  $p = 0.0005$ .

Figure 8 demonstrates the stability of the network diffusion system with respect to the diffusion coefficient at  $p = 0.1$ . Figure 8(a) shows that the bifurcation diagram of system (11) on the diffusion coefficient can be obtained when the connection probability is given. When  $d_2 = 0.1$ , Figure 8(b) demonstrates that the system is stable. But when  $p = 0.1$  and  $d_2 = 0.3$ , the corresponding pattern formation (Figure 8(c)) is unstable. When  $p = 0.1$  and  $d_2 = 0.3$ , the real part of the eigenvalues of the system characteristic equation (17) changes with  $k_i$  and  $-\Lambda_i$  is shown in Figure 8(d), which shows that the system is unstable and Turing instability occurs.

When  $p = 0.2$ , the bifurcation diagram of  $x_i$  on  $d_2$  is shown in Figure 9(a), which illustrates that the system's equilibrium point is stable when  $d_2$  is lower than the critical bifurcation value. Still, Turing instability occurs when  $d_2$  is

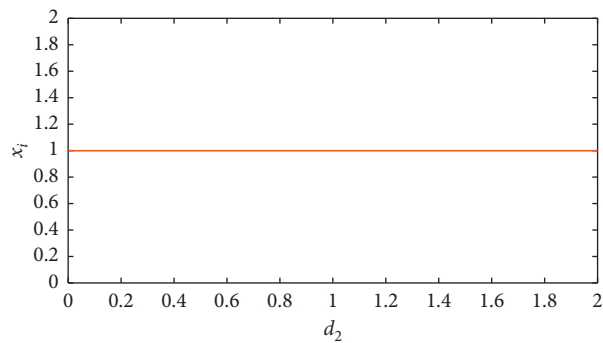


FIGURE 6: The bifurcation about  $d_2$  illustrates the system is stable when  $p = 0.0004$  and  $p = 0.69$ .

larger than the critical bifurcation value, and the substance will continue to react. From the pattern formation, which is shown in Figures 9(b) and 9(c), it can be seen that the Brusselator system is stable when  $p = 0.2$  and  $d_2 = 0.1$  and the system is unstable when  $d_2 = 0.3$ , which is consistent with the bifurcation diagram on  $d_2$ . From Figure 9(d), it can be concluded that when  $d_2 = 0.3$ , there exist some  $\text{Re}(\Lambda_i)$  falling into the unstable region, so the system is unstable.

When  $p = 0.33$ , the bifurcation diagram of  $x_i$  on  $d_2$  is shown in Figure 10(a), which illustrates that the system's equilibrium point is stable when  $d_2$  is lower than the critical bifurcation value. Still, Turing instability occurs when  $d_2$  is larger than the critical bifurcation value, and the substance will continue to react. From the pattern formation, which is shown in Figures 10(b) and 10(c), it can be seen that the Brusselator system is stable when  $p = 0.33$  and  $d_2 = 0.1$  and the system is unstable when  $d_2 = 0.3$ , which is consistent with the bifurcation diagram on  $d_2$ . Figure 10(d) shows that when  $d_2 = 0.3$ , there are some  $\text{Re}(\Lambda_i)$  falling into the unstable region, so the system is unstable.

For  $p = 0.43$ , the bifurcation diagram of concentration  $x_i$  with respect to  $d_2$  can be drawn as Figure 11, and the bifurcation point is consistent with the Turing instability threshold. The bifurcation diagram shows that when  $d_2$  is less than the critical value, the system is stable, otherwise unstable. As can be seen from Figures 11(b) and 11(c), the corresponding pattern information is stable when  $d_2 = 0.1$ , but unstable when  $d_2 = 0.3$ . In Figure 11(d), there exist some  $-\Lambda_i$  belonging to  $D$ , so Turing instability occurs when  $d_2 = 0.3$ .

When  $p = 0.53$ , we can give the bifurcation diagram of  $d_2$ , as shown in Figure 12(a), and the pattern formation when  $d_2 = 0.1$  is shown in Figure 12(b), which shows the system is stable. When the diffusion coefficient increases to a critical value, the uniform equilibrium point of the system begins to become unstable, and the current equilibrium state of the system is broken. So from Figure 12(c), when  $d_2 = 0.3$ , Turing instability occurs, and the system continues to interact. In Figure 12(d), there are some  $-\Lambda_i$  falling into the instability region, so the system appears the Turing bifurcation phenomenon when  $d_2 = 0.3$ .

But when  $p = 0.8$ , the bifurcation of  $d_2$  and the corresponding pattern formation of the system are exhibited in

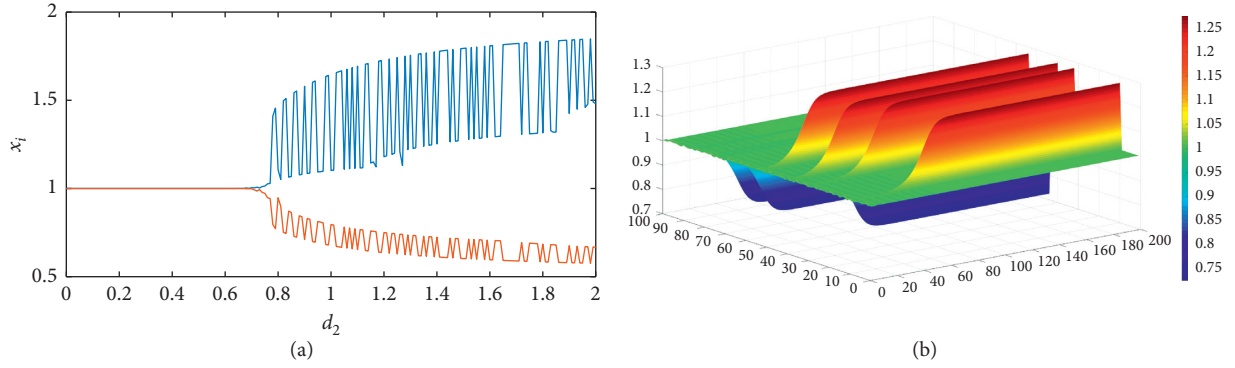


FIGURE 7: (a) The bifurcation diagram about  $d_2$  when  $p = 0.0005$  illustrates that the Turing instability occurs. (b) The pattern formation of the system when  $p = 0.0005$  and  $d_2 = 1.5$  illustrates the system is unstable.

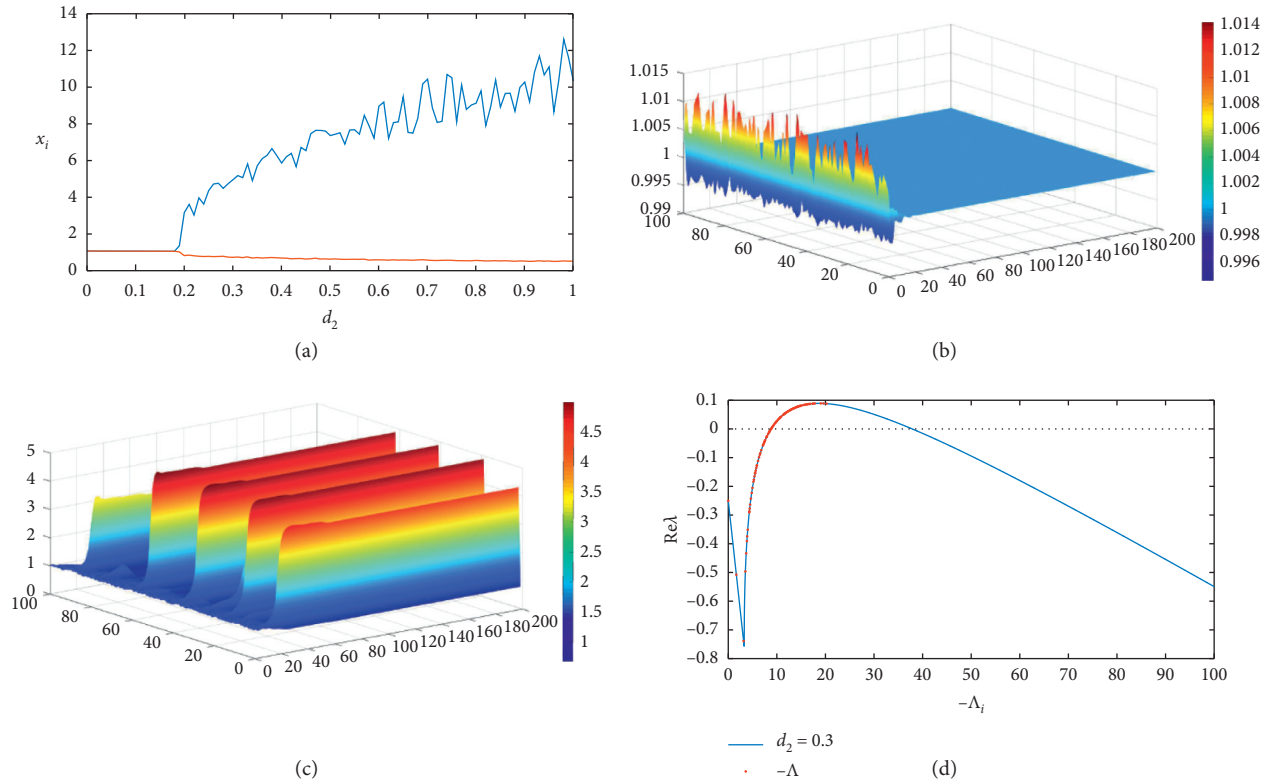


FIGURE 8: (a) The bifurcation diagram of  $d_2$  when  $p = 0.1$ . The pattern formation of the system when  $p = 0.1$ . (b) The system is stable when  $d_2 = 0.1$ . (c) Turing instability occurs when  $d_2 = 0.3$ . (d) When some  $-\lambda_i$  fall into the instability region, Turing instability occurs in the system.

Figure 13, demonstrating the system is stable. And the pattern formation, shown in Figures 13(b) and 13(c), indicates that when  $d_2 = 0.1$  and  $d_2 = 0.3$ , the system is stable. Figure 13(d) demonstrates that the system's eigenvalues do not fall in the Turing instability region  $\Lambda \cap D = \Phi$ , so when  $d_2 = 0.3$ , the system is stable. As the connection probability increases, the system's bifurcation threshold will be increased or even disappeared.

From Figure 4, we can conclude that Turing instability occurs when  $k_i \in [8, 39]$  by the mean-field theory. From Figure 14(a), we can obtain that when  $k_i = 7 < [8, 39]$  does

not belong to the instability region, the system will remain in a stable state. When  $k_i = 20$  (or  $30$ )  $\in [8, 39]$  falls into the unstable region, the stability of the equilibrium changes. Figures 14(b) and 14(c) mean that the molecular concentration does not reach a steady state, and the reaction continues. Figure 14(d) shows that the system is stable when  $k_i = 50 > [8, 39]$ .

In Figure 15, we give the bifurcation diagram of the deterministic system (16) with respect to the node degree. The figure shows that the system has a transcritical bifurcation about the parameter  $k_i$  near the equilibrium point,

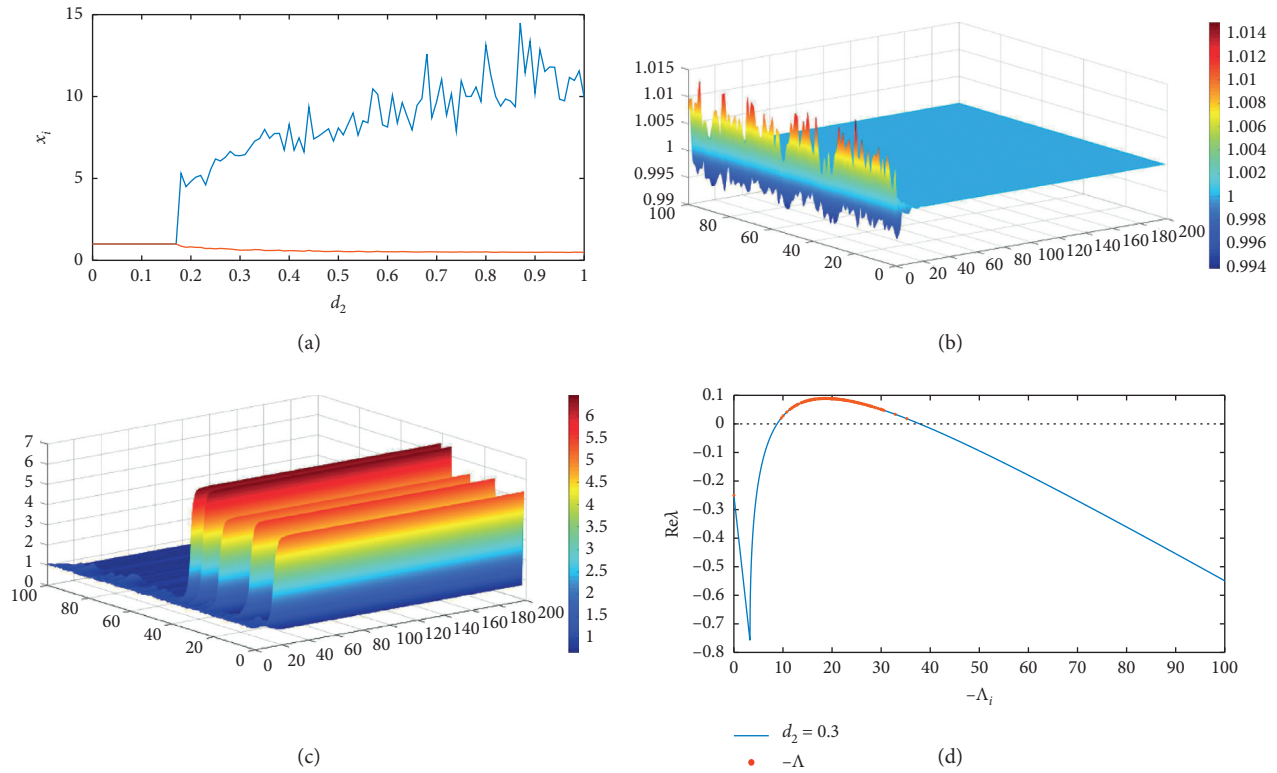


FIGURE 9: (a) The bifurcation diagram of  $d_2$  when  $p = 0.2$ . The pattern formation of the system when  $p = 0.2$ . (b) The system is stable when  $d_2 = 0.1$ . (c) Turing instability occurs when  $d_2 = 0.3$ . (d) When some  $- \Lambda_i$  fall into the instability region, Turing instability occurs in the system.

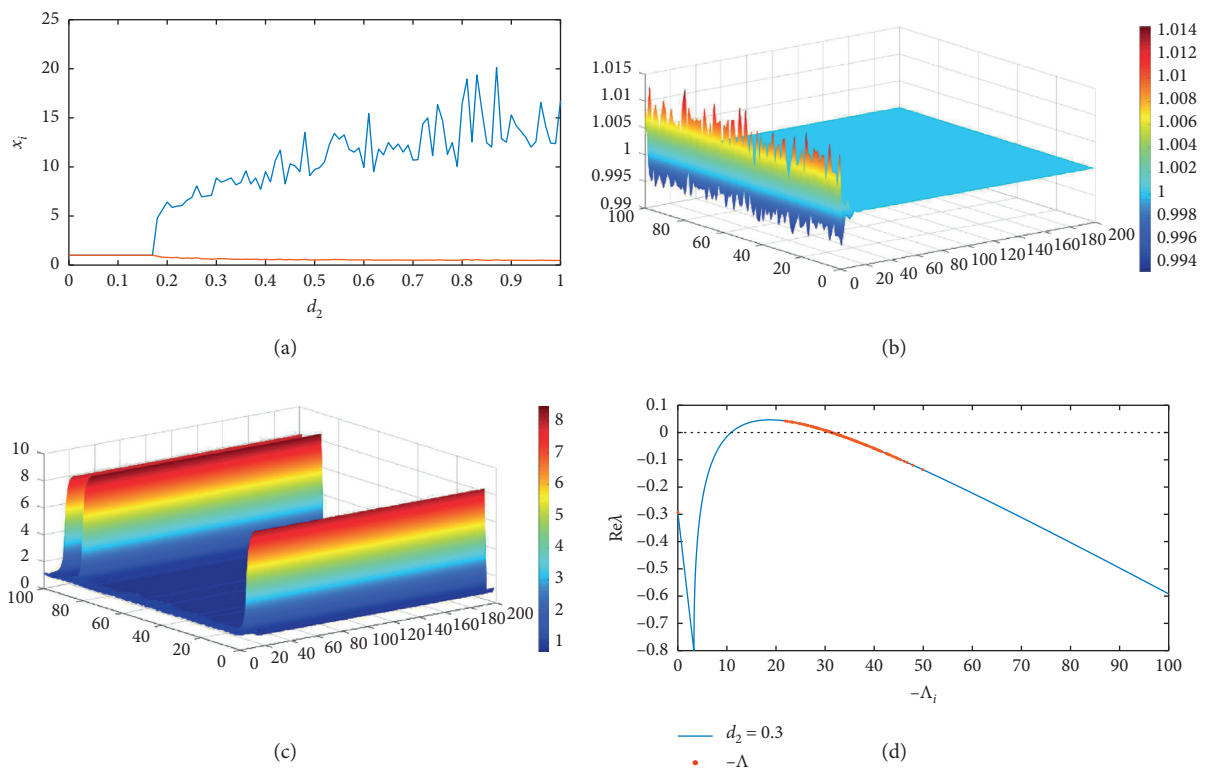


FIGURE 10: (a) The bifurcation diagram of  $d_2$  when  $p = 0.33$ . The pattern formation of the system when  $p = 0.33$ . (b) The system is stable when  $d_2 = 0.1$ . (c) Turing instability occurs when  $d_2 = 0.3$ . (d) When some  $- \Lambda_i$  fall into the instability region, Turing instability occurs in the system.



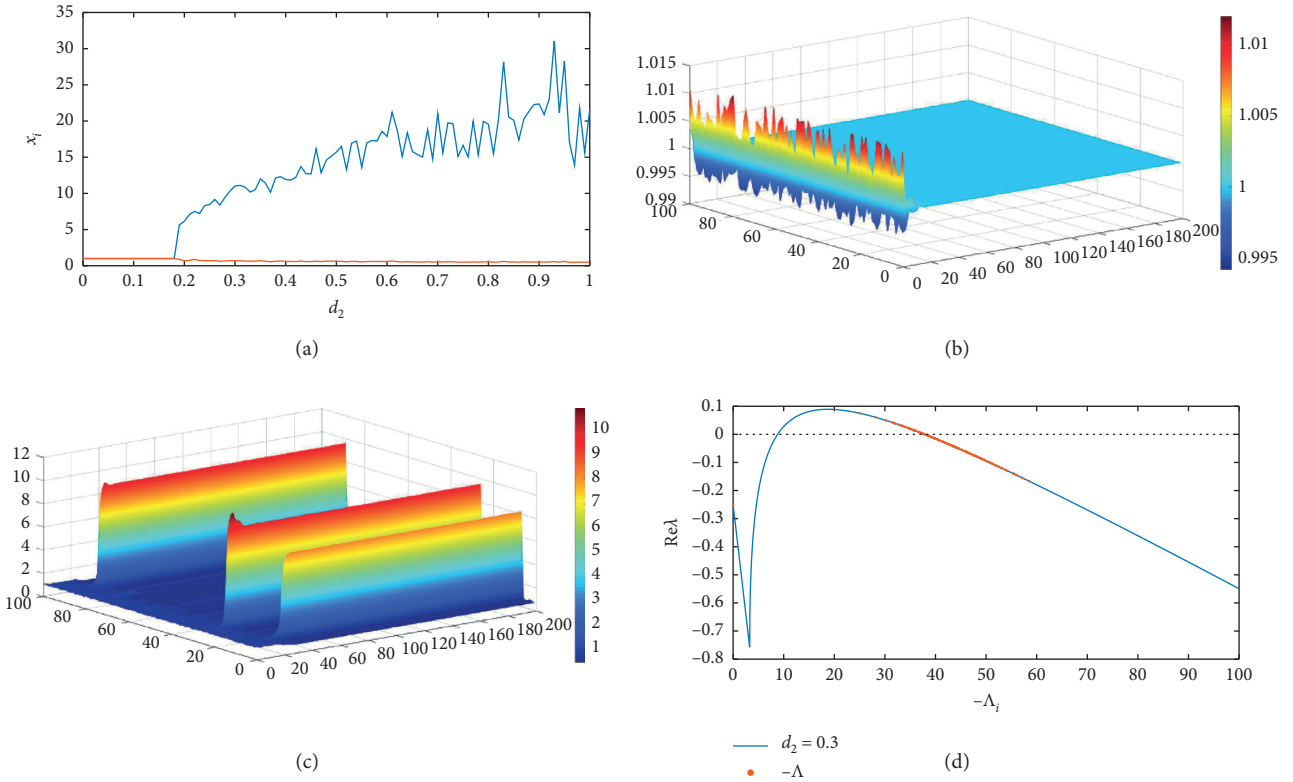


FIGURE 11: (a) The bifurcation diagram of  $d_2$  when  $p = 0.43$ . The pattern formation of the system when  $p = 0.43$ . The system is stable when  $d_2 = 0.1$  (b) and when  $d_2 = 0.3$  (c). (d) When some  $-\Lambda_i$  fall into the instability region, Turing instability occurs in the system.

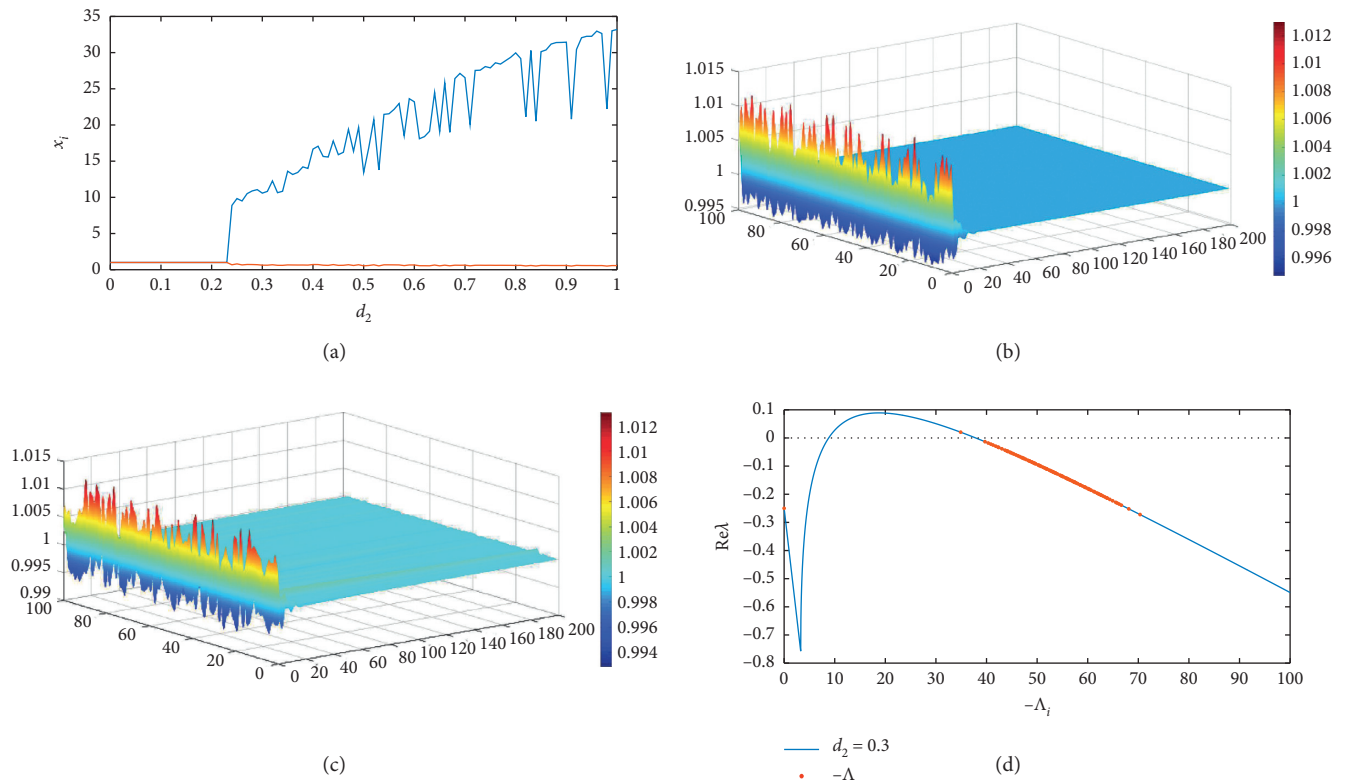


FIGURE 12: (a) The bifurcation diagram of  $d_2$  when  $p = 0.53$ . The pattern formation of the system when  $p = 0.53$ . (b) The system is stable when  $d_2 = 0.1$ . (c) Turing instability occurs when  $d_2 = 0.3$ . (d) When some  $-\Lambda_i$  fall into the instability region, Turing instability occurs in the system.

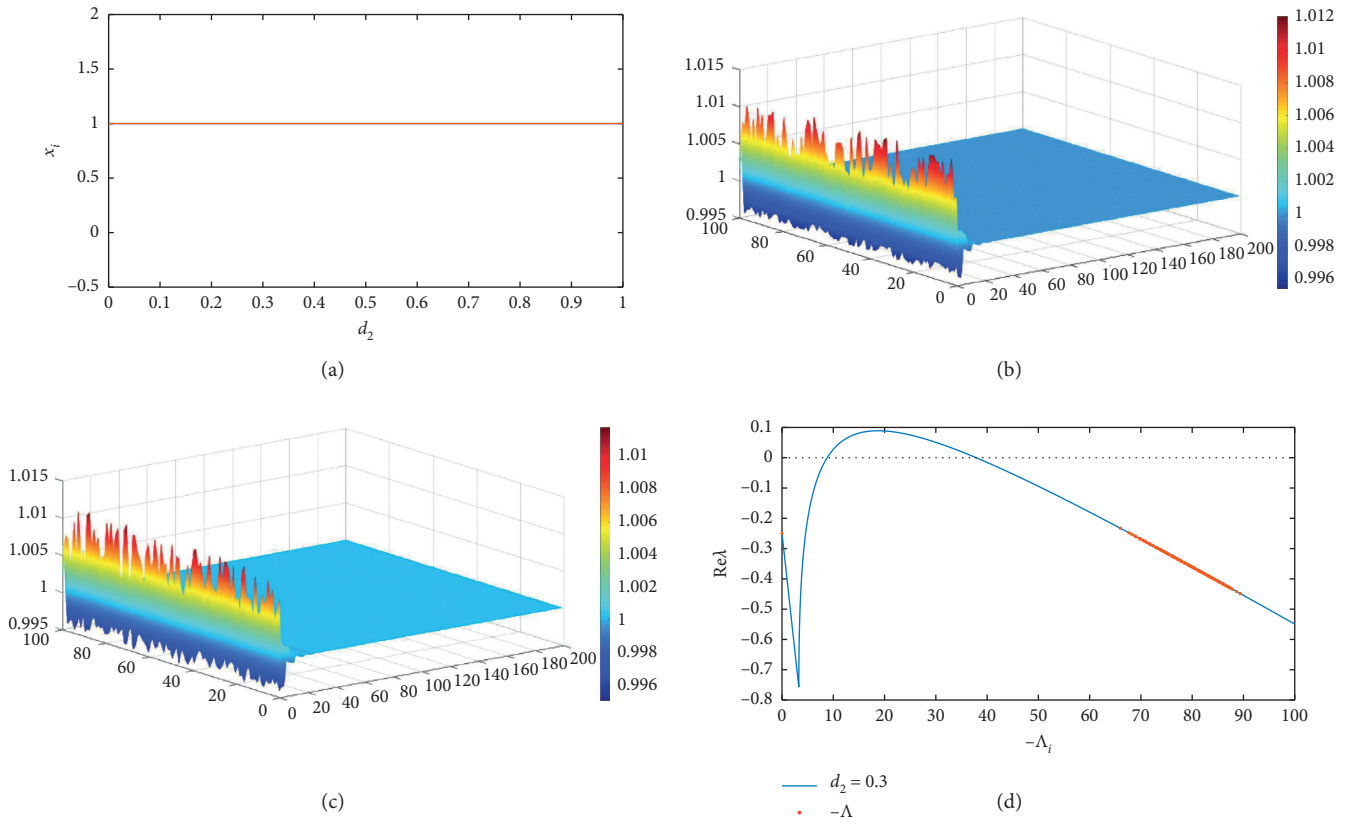


FIGURE 13: (a) The bifurcation diagram of  $d_2$  when  $p = 0.8$ . The pattern formation of the system when  $p = 0.8$ . The system is stable when  $d_2 = 0.1$  (b) and  $d_2 = 0.3$  (c). (d) When all  $-\Lambda_i$  do not fall into the instability region, the system is stable.

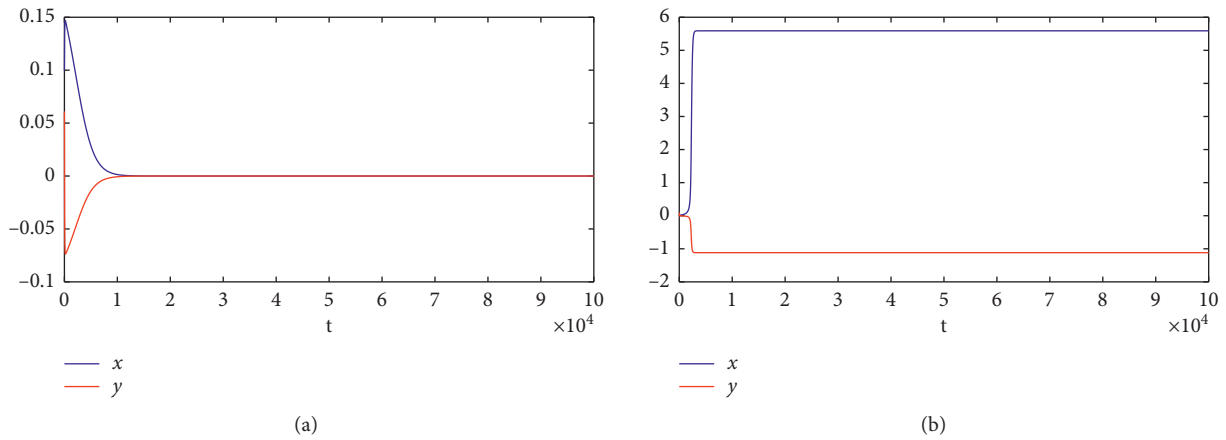


FIGURE 14: Continued.

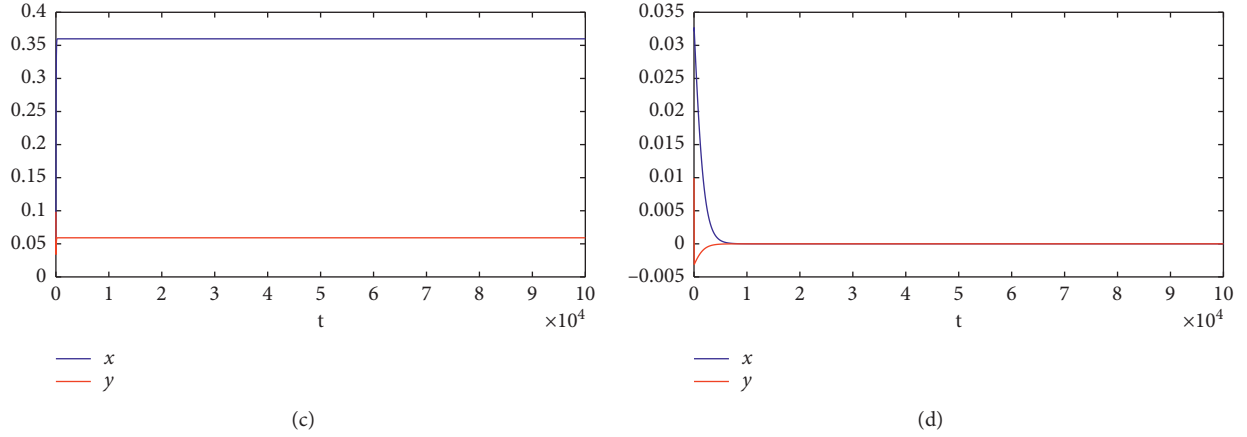


FIGURE 14: The mean-field approximation. (a) The system is stable when  $k_i = 7$  is not in instability region. The system is unstable when  $k_i = 20$  (b) and  $k_i = 30$  (c) are in instability region. (d) The system is stable when  $k_i = 50$  crosses instability region.

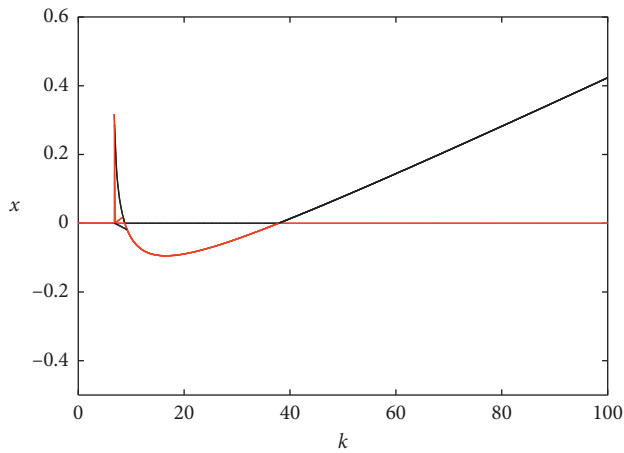


FIGURE 15: The bifurcation diagram of  $k_i$ . The black line indicates that the equilibrium point of the system is unstable, and the red line indicates that the equilibrium point is stable.

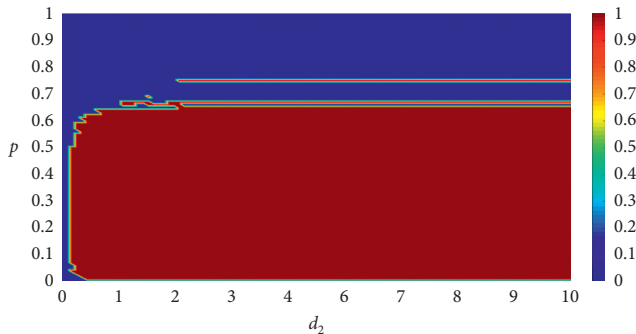


FIGURE 16: The instability region is related to the parameters  $d_2$  and  $p$ , where the red region is the instability region.

where the bifurcation points are, respectively,  $k_{1c} = 7.033$  and  $k_{2c} = 37.86$ , further confirming the system instability region about  $k_i$ .

For how the connection probability  $p$  affects the stability of the Brusselator system, the numerical simulation shows

that the Turing instability occurs when the connection probability is very large or very small. The approximate instability region of the reaction-diffusion system for the Brusselator model with respect to  $d_2$  and  $p$  is shown in Figure 16.

Therefore, from Lemma 3 and the above analysis when there is some  $\text{Re}(\lambda)$  in the Turing instability region  $\Lambda \cap D \neq \Phi$ , Turing instability occurs. It means that the introduction of a random network disrupts the equilibrium state of the reaction system.

Finally, through the above analysis and numerical simulation, we obtained the approximate region of Turing instability of  $d_2$  and  $p$ , which is given by Figure 16. In addition, we can also draw that the approximate instability region of the system on connection probability is  $(1/n^2) < p < (d_{2c}/d_1)(4/5)(\ln n/n)$ , where  $(1/n^2)$  means that the network node pairs are almost sparse. Here, we only give the approximate instability region for the connection probability. However, the more precise instability region and the derivation process for the Brusselator reaction-diffusion system still need further study.

## 4. Conclusion

In conclusion, firstly, the Turing instability critical value of the Brusselator model with a random network is obtained in Figure 3. In addition, for the connection probability, through numerical simulation and the eigenvalue characteristics of the network matrix, we can conclude that the critical value of Turing instability of the system about  $p$  is either very large or very small, that is, the approximate range of  $p$  is  $(1/n^2) < p < (d_{2c}/d_1)(4/5)(\ln n/n)$ . When the control parameters and  $d_1$  are given, the bifurcation of the reactant concentration on  $d_2$  under different connection probabilities verifies the approximate region of the system about  $p$ . It can be seen from the bifurcation graph that Turing instability will occur when  $p$  falls into the instability region from Figures 7–13(a). And we give the numerical simulation of the relation between the real part of the root of the characteristic equation and the eigenvalues of the network matrix. The

stability of the system near the equilibrium point is judged and verified by the real part of the eigenvalue exceeding the zero line in Figures 8–13(d) [18]. However, the upper bound of Turing instability on the connection probability is the best result of numerical simulation in this system, and its exact value needs to be explicitly derived. Therefore, we need to study the precise value of the upper bound on the Turing instability of the system concerning  $p$ .

Finally, we apply the mean-field theory to transform the problem of multimolecule interactions into a single-molecule problem. And the instability region of the reaction-diffusion system with respect to the network node degree is obtained. When  $k_i = 7 < [8, 39]$ , the system remains stable at the equilibrium point. When  $k_i = 20(30) \in [8, 39]$ , the system has Turing instability. When  $k_i = 50 > [8, 39]$ , the system is stable at the positive equilibrium point. And the bifurcation of  $k_i$  Figure 15 further verified this conclusion. In future research, we can further study the effect of random networks with specific characteristics on the reaction-diffusion system and work to determine the appropriate random networks for each system and the differences and connections between the effects of different random networks on the same reaction system.

## Data Availability

The data used to support the findings of the study are available from the corresponding author upon request.

## Conflicts of Interest

The authors declare that there are no conflicts of interest.

## Acknowledgments

This work was supported by the National Natural Science Foundation of China (11772291).

## References

- [1] A. Turing, "The chemical basis of morphogenesis," *Philosophical Transactions of the Royal Society B*, vol. 237, no. 641, pp. 37–72, 1952.
- [2] L. Xu, L. J. Zhao, Z. X. Chang et al., "Turing instability and pattern formation in a semi-discrete brusselator model," *Modern Physics Letters B*, vol. 27, no. 1, Article ID 1350006, 2013.
- [3] T. Biancalani, D. Fanelli, and F. Di Patti, "Stochastic turing patterns in the brusselator model," *Physical Review E*, vol. 81, no. 4, Article ID 046215, 2010.
- [4] S. S. Yerrapragada, J. K. Bandyopadhyay, V. K. Jayaraman, and B. D. Kulkarni, "Analysis of bifurcation patterns in reaction-diffusion systems: effect of external noise on the brusselator model," *Physical Review E*, vol. 55, no. 5, pp. 5248–5260, 1997.
- [5] A. A. Golovin, B. J. Matkowsky, and V. A. Volpert, "Turing pattern formation in the brusselator model with superdiffusion," *SIAM Journal on Applied Mathematics*, vol. 69, no. 1, pp. 251–272, 2008.
- [6] J. C. Tzou, B. J. Matkowsky, and V. A. Volpert, "Interaction of turing and hopf modes in the superdiffusive brusselator model," *Applied Mathematics Letters*, vol. 22, no. 9, pp. 1432–1437, 2009.
- [7] G. Gambino, M. C. Lombardo, M. Sammartino et al., "Turing pattern formation in the brusselator system with nonlinear diffusion," *Physical Review E*, vol. 88, no. 4, Article ID 042925, 2013.
- [8] Z. Hou and H. Xin, "Optimal system size for mesoscopic chemical oscillation," *ChemPhysChem*, vol. 5, no. 3, pp. 407–410, 2004.
- [9] V. V. Osipov and E. V. Ponziovskaia, "Stochastic resonance in the brusselator model," *Physical Review E*, vol. 61, no. 4, pp. 4603–4605, 2000.
- [10] Z. Jing, X. Zeng, and K. Y. Chan, "Harmonic and subharmonic bifurcation in the brussel model with periodic force," *Acta Mathematicae Applicatae Sinica*, vol. 13, no. 3, pp. 289–301, 1997.
- [11] R. Peng and M. Wang, "Pattern formation in the brusselator system," *Journal of Mathematical Analysis and Applications*, vol. 309, no. 1, pp. 151–166, 2005.
- [12] O. Mason and M. Verwoerd, "Graph theory and networks in biology," *IET Systems Biology*, vol. 1, no. 2, pp. 89–119, 2007.
- [13] W. Horsthemke, K. Lam, and P. K. Moore, "Network topology and turing instabilities in small arrays of diffusively coupled reactors," *Physics Letters A*, vol. 328, no. 6, pp. 444–451, 2004.
- [14] H. G. Othmer and L. E. Scriven, "Instability and dynamic pattern in cellular networks," *Journal of Theoretical Biology*, vol. 32, no. 3, pp. 507–537, 1971.
- [15] S. Hata and H. Nakao, "Localization of laplacian eigenvectors on random networks," *Scientific Reports*, vol. 7, no. 1, pp. 1–11, 2017.
- [16] N. McCullen and T. Wagenknecht, "Pattern formation on networks: from localised activity to turing patterns," *Scientific Reports*, vol. 6, no. 1, pp. 1–8, 2016.
- [17] H. Nakao and A. S. Mikhailov, "Turing patterns in network-organized activator-inhibitor systems," *Nature Physics*, vol. 6, no. 7, pp. 544–550, 2010.
- [18] M. Asllani, J. D. Challenger, F. S. Pavone et al., "The theory of pattern formation on directed networks," *Nature Communications*, vol. 5, no. 1, pp. 1–9, 2014.
- [19] Y. Ide, H. Izuhara, and T. Machida, "Turing instability in reaction-diffusion models on complex networks," *Physica A: Statistical Mechanics and Its Applications*, vol. 457, pp. 331–347, 2016.
- [20] X. Diego, L. Marcon, P. Muller et al., "Key features of turing systems are determined purely by network topology," *Physical Review X*, vol. 8, no. 2, Article ID 021071, 2018.
- [21] S. Mimar, M. M. Juane, J. Park et al., "Turing patterns mediated by network topology in homogeneous active systems," *Physical Review E*, vol. 99, no. 6, Article ID 062303, 2019.
- [22] Q. Zheng and J. Shen, "Turing instability induced by random network in fitzhugh-nagumo model," *Applied Mathematics and Computation*, vol. 381, Article ID 125304, 2020.

## Research Article

# Finite-Time Simultaneous Stabilization for Stochastic Port-Controlled Hamiltonian Systems over Delayed and Fading Channels

Yaping Tang, Weiwei Sun , and Dongqing Liu

*Institute of Automation, Qufu Normal University, Qufu, Shandong, China*

Correspondence should be addressed to Weiwei Sun; [wwsun@hotmail.com](mailto:wwsun@hotmail.com)

Received 17 June 2020; Accepted 31 July 2020; Published 29 September 2020

Guest Editor: Xiaodi Li

Copyright © 2020 Yaping Tang et al. This is an open access article distributed under the Creative Commons Attribution License, which permits unrestricted use, distribution, and reproduction in any medium, provided the original work is properly cited.

In this paper, a finite-time simultaneous stabilization problem is investigated for a set of stochastic port-controlled Hamiltonian (PCH) systems over delayed and fading noisy channels. The feedback control signals transmitted via a communication network suffer from both constant transmission delay and fading channels which are modeled as a time-varying stochastic model. First, on the basis of dissipative Hamiltonian structural properties, two stochastic PCH systems are combined to form an augmented system by a single output feedback controller and then sufficient conditions are developed for the semiglobally finite-time simultaneous stability in probability (SGFSSP) of the resulting closed-loop systems. The case of multiple stochastic PCH systems is also considered and a new control scheme is proposed for the systems to save costs and achieve computational simplification. Finally, an example is provided to verify the feasibility of the proposed simultaneous stabilization method.

## 1. Introduction

Port-controlled Hamiltonian (PCH) systems are known as an important class of nonlinear systems ([1, 2]). Compared to the general nonlinear systems, an excellent benefit of PCH systems is that the Hamiltonian function in the systems can be used as a Lyapunov function candidate in stability analysis (see, for instance, [3–5]). Thanks to the special system structure and clear physical meaning, applications of PCH systems can be found in a variety of engineering systems including power systems, robotic systems, and irreversible thermodynamic systems ([6–10]). In recent years, stabilization as well as simultaneous stabilization problem has been extensively studied for PCH systems ([11–14]). In terms of PCH systems with disturbances, the above stabilization problem has been resolved in [11, 13]. Taking actuator saturation into account, the study in [14] has proposed an adaptive control strategy to simultaneously stabilize PCH systems with parameter uncertainties.

On the other hand, there usually exist stochastic components and random disturbances in practical control

plants, which often result in performance degradation, as well as destabilization of the systems. In the last few decades, many researchers have made efforts to deal with the stabilization problem of stochastic systems ([15, 16]). For example, in [15], output feedback stabilization has been studied using the backstepping approach for Itô-type stochastic systems. As for stochastic PCH systems, the control problem has also captured public attentions ([17–20]). Exploiting an energy-based feedback control scheme, the authors of [17] have raised stochastic feedback stabilization results. In regard to time-varying stochastic PCH systems, the study in [18] has come up with a kind of stochastic generalized canonical transformations approach to stabilize stochastic PCH systems. In addition, the adaptive control topic for nonlinear stochastic Hamiltonian systems has been introduced in [19, 20]. Parameter uncertainty, randomness, and time delay are all considered in above references.

In many practical problems, the fast convergence within a fixed finite time interval plays an important role. Finite-time stabilization makes closed-loop systems enjoy fast convergence. In addition, disturbance rejection properties

and better robustness both can be reflected in the finite-time stabilization. Thus, many investigations about finite-time stabilization controller design have been carried out ([21–29]). For stochastic nonlinear systems which are written as Itô differential form, [23] has proposed a method to solve the finite-time stabilization problem. The finite-time stabilization of the Hamiltonian systems has been studied in [21, 25, 27, 28]. For instance, the finite-time feedback control manner is developed in [21] to deal with finite-time stabilization problem for PCH systems with nonvanishing disturbances.

Generally speaking, the phenomenon of fading channels as well as network-induced delay is very likely to occur in the networked control system, which can lead to various distortions and information constraints. By now, a considerable number of researches have been done for continuous and discrete systems over network-induced phenomenon ([30–38]). Under memoryless fading channels environment, the study in [33] has illustrated state feedback stabilization problem for linear continuous systems. This problem has been solved by realizing the balance between the demand of communication resource and the supply of that. Different from [33], an output feedback control scheme has been introduced in [35] to achieve mean-square stabilization over multiplicative fading channels for discrete systems. For continuous linear network control systems over delayed and fading channels, a necessary and sufficient condition has been established by algebraic Riccati equation method in [37], and mean-square stabilization problem has also been resolved. Recently, the problem of  $H_\infty$  filtering design has been solved in [36] for a class of nonlinear Hamiltonian systems considering fading channel and saturation.

Summarizing the above discussion, in this paper, we try to solve the finite-time simultaneous stabilization problem of stochastic PCH systems over delayed and fading channels and propose some new results that serve for the design of feedback controllers. The fading noisy channels modeled as multiple independent and memoryless forms exist between the controller and the plant. We try to design feedback controller to render closed-loop systems semiglobally finite-time simultaneous stable in probability (SGFSSP). To begin with, two stochastic PCH systems are considered. We will design a single output feedback controller which contributes to SGFSSP for the systems. Utilizing the structural properties of dissipative Hamiltonian systems, the two stochastic PCH systems form an augmented stochastic PCH system, which makes the problem solved easily. Through the Lyapunov function method and Itô differential formula, the closed-loop systems will be SGFSSP. Besides, we will extend our approach to the case of multiple stochastic PCH systems over delayed and fading channels. A feedback control strategy is proposed. At last, the feasibility of the above method is illustrated by the simulation.

The contributions of this paper mainly lie in the following two aspects: (1) taking network-induced delay and fading noisy channels environment into consideration, a new single output feedback controller design method is raised to deal with the SGFSSP problem for stochastic PCH systems. In this way, the controller implementation costs can

be greatly reduced, and the computational simplification of control can be achieved. (2) We make an in-depth study of the proposed method by extending the approach to the case of multiple PCH systems. SGFSSP result for multiple PCH systems over delayed and fading channels is given.

Notation:  $\mathbb{R}^n$  denotes the  $n$ -dimensional real column vectors and  $\mathbb{R}^{n \times m}$  is the real matrices with dimensions  $n \times m$ . A real-valued function  $f(x) \in \mathcal{C}^2$  represents that  $f(x)$  is a continuously twice differentiable function.  $\|\cdot\|$  represents the 2-norm.  $\text{diag}\{a_1, a_2, \dots, a_m\}$  represents diagonal matrix with  $a_1, a_2, \dots, a_m$  as its diagonal elements. We denote  $\lambda_{\min}(\cdot)$  as the smallest eigenvalue operator,  $\mathbb{E}\{\cdot\}$  as the expectation operator, and  $\text{Cov}(\cdot)$  as the covariance operator, respectively. For the probability space  $(\Omega, \mathcal{F}, \mathcal{P})$ ,  $\Omega$  denotes the sample space,  $\mathcal{F}$  denotes the  $\sigma$ -algebra of the observable random events, and  $\mathcal{P}$  is the probability measure on  $\Omega$ .

## 2. Problem Formulation and Preliminaries

Consider the following two stochastic PCH systems:

$$\begin{cases} dx(t) = [J(x(t)) - R(x(t))] \nabla H_1(x(t)) dt + g_1 u(t) dt + h_1 d\omega(t), \\ y(t) = g_1^T \nabla H_1(x(t)), \end{cases} \quad (1)$$

$$\begin{cases} d\xi(t) = [\hat{J}(\xi(t)) - \hat{R}(\xi(t))] \nabla H_2(\xi(t)) dt + g_2 u(t) dt + h_2 d\rho(t), \\ \eta(t) = g_2^T \nabla H_2(\xi(t)), \end{cases} \quad (2)$$

where  $x(t), \xi(t) \in \mathbb{R}^n$  are the system state vectors,  $u(t) \in \mathbb{R}^m$  is the control input which satisfies  $\mathbb{E}\{\int_0^t \|u(s)\|^2 ds\} < \infty$ , and  $y(t), \eta(t) \in \mathbb{R}^m$  are the outputs of systems. The signals  $\omega(t)$  and  $\rho(t)$  are both  $\kappa$ -dimensional independent standard Wiener process defined on probability space  $(\Omega, \mathcal{F}, \mathcal{P})$ . We assume  $\mathbb{E}\{d\omega(t)\} = 0$ ,  $\mathbb{E}\{d\rho(t)\} = 0$ ,  $\mathbb{E}\{[d\omega(t)]^2\} = dt$ , and  $\mathbb{E}\{[d\rho(t)]^2\} = dt$ .  $\nabla H_i(x) \in \mathbb{R}^{n \times 1}$  is the gradient of the Hamilton function  $H_i(x): \mathbb{R}^n \mapsto \mathbb{R}$ , which is defined as  $\nabla H_i(x) = (\partial H_i(x)/\partial x)$ , and  $H_i(x) \geq 0$ ,  $H_i(0) = 0$ , for all  $t \geq 0$ .  $J(x) \in \mathbb{R}^{n \times n}$  and  $\hat{J}(\xi) \in \mathbb{R}^{n \times n}$  are both skew-symmetric structure matrices;  $R(x) \in \mathbb{R}^{n \times n}$  and  $\hat{R}(\xi) \in \mathbb{R}^{n \times n}$  are positive definite strict dissipation matrices;  $g_1, g_2, h_1$ , and  $h_2$  are known real constant gain matrices. In addition, by setting  $f_1(x, u) = [J(x) - R(x)] \nabla H_1(x) + g_1 u$ ,  $f_2(\xi, u) = [\hat{J}(\xi) - \hat{R}(\xi)] \nabla H_2(\xi) + g_2 u$ . Suppose that there exist constants  $k_F > 0$  and  $k_G > 0$  such that

$$\begin{aligned} \|f_i(\theta_1, u) - f_i(\theta_2, u)\| &\leq k_F \|\theta_1 - \theta_2\|, \\ \|f_i(\theta_1, u)\| + \|h_i\| &\leq k_G (1 + \|\theta_1\| + \|u\|), \end{aligned} \quad (3)$$

hold for all  $\theta_1, \theta_2 \in \mathbb{R}^n$ ,  $u(t) \in \mathbb{R}^m$ ,  $t \geq 0$ , and  $i = 1, 2$ .

For generalized PCH systems, it is shown in [13] that the two PCH systems can be simultaneously stabilized by a controller  $u = -K(y(t) - \eta(t))$  over constraint conditions, where  $K$  is a gain matrix with appropriate dimension. Unfortunately, when it comes to the stochastic networked control system (NCS), the feedback control signals transmitted via a communication network may suffer from delayed and fading noisy channels.

Let us focus on the NCS as depicted in Figure 1. Suppose that the control signal  $u(t)$  suffers both constant transmission delay  $d > 0$  and signal attenuation in the closed-loop system. The transmission delay  $d$  is caused by the message delivery from the controller to the actuator. The transmission of signal  $u(t)$  is accomplished in a form of components through independent parallel channels. Then, the control signal  $u(t)$  arriving at the actuator is modeled by the following multiple independent and memoryless forms:

$$\varepsilon(t)u(t-d) + q(t), \quad (4)$$

where  $u(t) \in \mathbb{R}^m$  and  $(\varepsilon(t)u(t-d) + q(t)) \in \mathbb{R}^m$  are the input and output of channels, respectively.  $\varepsilon(t) \in \mathbb{R}^{m \times m}$  represents the multiplicative noise with the following form:

$$\varepsilon(t) = \text{diag}\{\varepsilon_1(t), \varepsilon_2(t), \dots, \varepsilon_m(t)\}. \quad (5)$$

$\mathbb{E}\{\varepsilon_i(t)\} = \mu_i$ ,  $\text{Cov}(\varepsilon_i(t), \varepsilon_i(s)) = \sigma_i^2 \delta(t-s)$ ,  $\mu_i \neq 0$ ,  $\sigma_i^2$  is known power spectral density.  $q(t) = [q_1(t), q_2(t), \dots, q_m(t)]^T \in \mathbb{R}^m$  is an additive white Gaussian process noise with  $\mathbb{E}\{q_i(t)\} = 0$  and known power spectral density  $\varrho_i^2$ , i.e.,  $\text{Cov}(q_i(t), q_i(s)) = \varrho_i^2 \delta(t-s)$ ,  $\delta$  denotes the Dirac delta function,  $i = 1, \dots, m$ . We make the following assumption for  $\varepsilon(t)$ .

#### Assumption 1

- (1)  $\varepsilon_i(t)$  and  $\varepsilon_j(t)$  are uncorrelated for  $i \neq j$ , i.e.,  $\mathbb{E}\{\varepsilon_i(t_1)\varepsilon_j(t_2)\} = 0$ ,  $\forall t_1, t_2 > 0$ , and  $i \neq j$
- (2)  $\varepsilon(t)$  is uncorrelated with  $\omega(t)$  and  $\rho(t)$

*Remark 1.* We consider interference channels noise in the systems and input channels noise. The conditions of Assumption 1 avoid the possible occurrence of noise coupling phenomenon.

Denote

$$\begin{aligned} M &:= \text{diag}\{\mu_1, \mu_2, \dots, \mu_m\}, \\ Q &:= \text{diag}\{\varrho_1^2, \varrho_2^2, \dots, \varrho_m^2\}. \end{aligned} \quad (6)$$

Obviously,  $M$  is nonsingular since  $\mu_i \neq 0$ . Without loss of generality, we assume  $\varrho_i^2 = 1$ , i.e.,  $Q = I_m \in \mathbb{R}^{m \times m}$  for simplicity hereinafter,  $i = 1, 2, \dots, m$ .

Substituting (4) into (1) and (2), we get

$$\begin{cases} dx(t) = [J(x(t)) - R(x(t))]\nabla H_1(x(t))dt \\ + g_1 \varepsilon(t)u(t-d)dt + g_1 d\omega(t) + h_1 d\omega(t), \\ y(t) = g_1^T \nabla H_1(x(t)), \end{cases} \quad (7)$$

$$\begin{cases} d\xi(t) = [\hat{J}(\xi(t)) - \hat{R}(\xi(t))]\nabla H_2(\xi(t))dt \\ + g_2 \varepsilon(t)u(t-d)dt + g_2 d\omega(t) + h_2 d\rho(t), \\ \eta(t) = g_2^T \nabla H_2(\xi(t)). \end{cases} \quad (8)$$

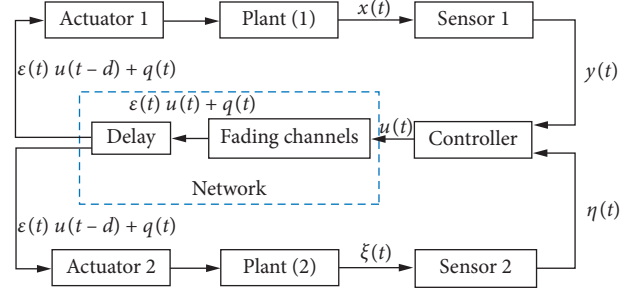


FIGURE 1: NCS over delayed and fading noisy channels.

*Remark 2.*  $q(t)$  is a white noise, which is formally regarded as the derivative of a Brownian motion  $\omega(t)$  (see [39]), i.e.,  $q(t) = (d\omega(t)/dt)$ , so we can further write that  $q(t)dt = d\omega(t)$ .

Before proceeding further, we need to put forward a definition as follows.

*Definition 1.* The stochastic PCH systems (7) and (8) are said to be semiglobally finite-time simultaneous stable in probability (SGFSSP) if

- (1) for any initial values  $\mathcal{X}_0 \in \mathbb{R}^{2n}$ , the solution  $\mathcal{X}(t)$  of systems (7) and (8) exists and is unique, where  $\mathcal{X}(t) = [x^T(t) \ \xi^T(t)]^T$
- (2) for every  $\mathcal{X}_0 \in \mathbb{R}^{2n} \setminus \{\Omega\}$  and  $\varepsilon > 0$ , the first hitting time  $T(\mathcal{X}_0, \varepsilon) = \inf\{t: \mathcal{X}(t; \mathcal{X}_0) \in \Omega\}$  is finite almost surely;  $T(\mathcal{X}_0, \varepsilon)$  and  $\Omega$  are called the settling time and the compact set, respectively
- (3) for all  $t \geq T(\mathcal{X}_0, \varepsilon)$ , the solution  $\mathcal{X}(t)$  of systems (7) and (8) satisfies  $\mathbb{E}(\|\mathcal{X}(t; \mathcal{X}_0)\|) < \varepsilon$

**Lemma 1.** Consider the following Itô form stochastic system:

$$dx(t) = f(x)dt + g(x)d\omega. \quad (9)$$

Suppose  $f(x)$  and  $g(x)$  are locally Lipschitz continuous in  $x$  and locally bounded,  $f(0) = 0$ , and  $g(0) = 0$ . If, for any  $x_0 \in \mathbb{R}^n$ , there exist class- $\mathcal{K}_\infty$  functions  $\gamma_1$  and  $\gamma_2$ , real numbers  $c > 0$ ,  $0 < \hbar < 1$ ,  $a > 0$  and a positive definite function  $V(x) \in \mathcal{C}^2$  such that

$$\gamma_1(\|x\|) \leq V(x) \leq \gamma_2(\|x\|), \quad (10)$$

$$\mathbb{E}\{\mathcal{L}V(x)\} \leq -cV^\hbar(x) + a, \quad (11)$$

then system (9) is SGFSSP. Furthermore, the compact set  $\Omega$  is expressed as

$$\Omega = \left\{ x \mid V^\hbar(x) \leq \frac{a}{c(1-b)} \right\}, \quad \forall 0 < b < 1, \quad (12)$$

and the settling time of system (9) with respect to  $x_0$  satisfies

$$T^* = \frac{1}{bc(1-h)} \left\{ V^{1-h}(x_0) - \left( \frac{a}{c(1-b)} \right)^{(1-h)/h} \right\}. \quad (13)$$

**Lemma 2.** For any real number  $z_i$ ,  $i = 1, \dots, n$ , and any positive real numbers  $\epsilon_1, \epsilon_2$  which satisfy  $0 < \epsilon_1 \leq \epsilon_2$ , it holds

$$\left( \sum_{i=1}^n |z_i|^{\epsilon_2} \right)^{(1/\epsilon_2)} \leq \left( \sum_{i=1}^n |z_i|^{\epsilon_1} \right)^{(1/\epsilon_1)}. \quad (14)$$

In Lemma 2, if  $\epsilon_1 = \beta \geq 1$  and  $\epsilon_2 = 1$ , then

$$\sum_{i=1}^n |z_i|^{1/\beta} \leq \left( \sum_{i=1}^n |z_i| \right)^{1/\beta}, \quad (15)$$

for any real number  $z_i$ ,  $i = 1, \dots, n$ .

In this paper, our main goal is to make the two systems (1) and (2) with the delayed and fading noisy channels SGFSSP. More specifically, based on Lemma 1, we have an interest in designing a suitable output feedback controller  $u(t-d)$  such that systems (7) and (8) satisfy (10) and (11). Besides, we extend our results to multiple stochastic PCH systems.

For the above purpose, the following assumptions and lemmas are essential in the sequel.

*Assumption 2.* The Hamilton functions  $H_1(x)$  and  $H_2(\xi)$  are given as

$$\begin{aligned} H_1(x) &= \sum_{i=1}^n (x_i^2)^{\alpha/(2\alpha-1)}, \\ H_2(\xi) &= \sum_{i=1}^n (\xi_i^2)^{\alpha/(2\alpha-1)}, \end{aligned} \quad (16)$$

where  $\alpha > 1$  is a real number.

*Assumption 3.* There exist constants  $c_1 > 0$  and  $c_2 > 0$  such that

$$\begin{aligned} c_1 &= \inf_{t \geq 0} \{ \lambda_{\min}(R(x(t))) \}, \\ c_2 &= \inf_{t \geq 0} \{ \lambda_{\min}(\widehat{R}(\xi(t))) \}. \end{aligned} \quad (17)$$

**Lemma 3.** For any matrices  $P_1, P_2 \in \mathbb{R}^{m \times n}$ , it follows that

$$P_1^T P_2 + P_2^T P_1 \leq P_1^T P_1 + P_2^T P_2. \quad (18)$$

### 3. SGFSSP of Two Stochastic PCH Systems and That of Multiple Stochastic PCH Systems

In this section, we will give the analysis result that serves for the SGFSSP of two stochastic PCH systems.

**Theorem 1.** Consider systems (7) and (8). Assumptions 2 and 3 are satisfied. If there exist matrices  $K = K^T$ ,  $L_1 = L_1^T$ ,

$L_2 = L_2^T$ , and  $L_3 = L_3^T$  such that the following matrix inequality

$$\Pi_1 = \begin{bmatrix} A_{11} & A_{12} & 0 & 0 & A_{15} & -g_1 K g_2^T \\ * & -L_2 & 0 & 0 & A_{25} & 0 \\ * & * & A_{33} & A_{34} & g_2 K g_1^T & A_{36} \\ * & * & * & \frac{1}{2} L_2 & 0 & A_{46} \\ * & * & * & * & -L_3 & 0 \\ * & * & * & * & * & -L_3 \end{bmatrix} < 0 \quad (19)$$

holds, where

$$\begin{aligned} A_{11} &= -2c_1 I_n - 2g_1 K g_1^T - L_1, \\ A_{12} &= \frac{1}{2}(L_1 + L_2), \\ A_{15} &= g_1 K g_1^T + \frac{1}{2}(L_1 + L_3), \\ A_{25} &= -\frac{1}{2}(L_2 + L_3), \\ A_{33} &= -2c_2 I_n + 2g_2 K g_2^T - L_1, \\ A_{34} &= \frac{1}{2}(L_1 + L_2), \\ A_{36} &= -g_2 K g_2^T + \frac{1}{2}(L_1 + L_3), \\ A_{46} &= -\frac{1}{2}(L_2 + L_3), \end{aligned} \quad (20)$$

then systems (7) and (8) are SGFSSP under the output feedback control law

$$u(t-d) = -M^{-1} K (y(t-d) - \eta(t-d)). \quad (21)$$

*Proof.* First of all, substituting (21) into (7) and (8), we obtain

$$\begin{aligned} dx(t) &= [J(x(t)) - R(x(t))] \nabla H_1(x(t)) dt \\ &\quad - g_1 \varepsilon(t) M^{-1} K g_1^T \nabla H_1(x(t-d)) dt \\ &\quad + g_1 \varepsilon(t) M^{-1} K g_2^T \nabla H_2(\xi(t-d)) dt \\ &\quad + g_1 d\bar{\omega}(t) + h_1 d\omega(t), \end{aligned} \quad (22)$$

$$\begin{aligned} d\xi(t) &= [\widehat{J}(\xi(t)) - \widehat{R}(\xi(t))] \nabla H_2(\xi(t)) dt \\ &\quad - g_2 \varepsilon(t) M^{-1} K g_1^T \nabla H_1(x(t-d)) dt \\ &\quad + g_2 \varepsilon(t) M^{-1} K g_2^T \nabla H_2(\xi(t-d)) dt \\ &\quad + g_2 d\bar{\omega}(t) + h_2 d\rho(t). \end{aligned} \quad (23)$$

Applying Newton–Leibnitz formula, we have



$$\begin{aligned} & \nabla H_1(x(t)) - \nabla H_1(x(t-d)) \\ &= \int_{t-d}^t (\nabla H_1(x(s)))' ds, \end{aligned} \quad (24)$$

$$\begin{aligned} & \nabla H_2(\xi(t)) - \nabla H_2(\xi(t-d)) \\ &= \int_{t-d}^t (\nabla H_2(\xi(s)))' ds. \end{aligned} \quad (25)$$

Then, systems (22) and (23) can be rewritten as

$$\begin{aligned} dx(t) &= [J(x(t)) - R(x(t))]\nabla H_1(x(t))dt \\ &\quad - g_1\varepsilon(t)M^{-1}Kg_1^T\nabla H_1(x)dt \\ &\quad + g_1\varepsilon(t)M^{-1}Kg_2^T\nabla H_2(\xi)dt \\ &\quad + g_1\varepsilon(t)M^{-1}Kg_1^T \int_{t-d}^t (\nabla H_1(x(s)))' dsdt \\ &\quad - g_1\varepsilon(t)M^{-1}Kg_2^T \int_{t-d}^t (\nabla H_2(\xi(s)))' dsdt \\ &\quad + g_1d\omega(t) + h_1d\omega(t), \end{aligned} \quad (26)$$

$$\begin{aligned} d\xi(t) &= -g_2\varepsilon(t)M^{-1}Kg_1^T\nabla H_1(x)dt \\ &\quad + [\hat{J}(\xi(t)) - \hat{R}(\xi(t))]\nabla H_2(\xi(t))dt \\ &\quad + g_2\varepsilon(t)M^{-1}Kg_2^T\nabla H_2(\xi)dt \\ &\quad + g_2\varepsilon(t)M^{-1}Kg_1^T \int_{t-d}^t (\nabla H_1(x(s)))' dsdt \\ &\quad - g_2\varepsilon(t)M^{-1}Kg_2^T \int_{t-d}^t (\nabla H_2(\xi(s)))' dsdt \\ &\quad + g_2d\omega(t) + h_2d\rho(t). \end{aligned} \quad (27)$$

Defining the vectors  $\mathcal{X}(t) = [x^T(t) \ \xi^T(t)]^T$ ,  $\zeta(t) = [\omega^T(t) \ \rho^T(t)]^T$ , the above equations can be further rewritten into an augmented Itô form stochastic PCH system described as

$$\begin{aligned} d\mathcal{X}(t) &= [J(\mathcal{X}(t)) - R(\mathcal{X}(t))]\nabla H(\mathcal{X}(t))dt \\ &\quad + G(t) \int_{t-d}^t \nabla H(\mathcal{X}(s))' dsdt \\ &\quad + g d\omega(t) + h d\zeta(t), \end{aligned} \quad (28)$$

where  $H(\mathcal{X}(t)) = H_1(x(t)) + H_2(\xi(t))$ ,  $R(\mathcal{X}(t)) = \text{diag}\{R(x(t)) + g_1\varepsilon(t)M^{-1}Kg_1^T, \hat{R}(\xi(t)) - g_2\varepsilon(t)M^{-1}Kg_2^T\}$ ,

$$\begin{aligned} J(\mathcal{X}(t)) &= \begin{bmatrix} J(x(t)) & g_1\varepsilon(t)M^{-1}Kg_2^T \\ -g_2\varepsilon(t)M^{-1}Kg_1^T & \hat{J}(\xi(t)) \end{bmatrix}, \\ G(t) &= \begin{bmatrix} g_1\varepsilon(t)M^{-1}Kg_1^T & -g_1\varepsilon(t)M^{-1}Kg_2^T \\ g_2\varepsilon(t)M^{-1}Kg_1^T & -g_2\varepsilon(t)M^{-1}Kg_2^T \end{bmatrix}, \\ \int_{t-d}^t (\nabla H(\mathcal{X}(s)))' ds &= \begin{bmatrix} \int_{t-d}^t (\nabla H_1(x(s)))' ds \\ \int_{t-d}^t (\nabla H_2(\xi(s)))' ds \end{bmatrix}, \\ g &= \begin{bmatrix} g_1 \\ g_2 \end{bmatrix}, \\ h &= \begin{bmatrix} h_1 & 0 \\ 0 & h_2 \end{bmatrix}. \end{aligned} \quad (29)$$

Next, choosing the following Lyapunov function candidate:

$$V(\mathcal{X}(t)) = 2H(\mathcal{X}(t)), \quad (30)$$

and according to Itô differential formula, we have

$$\begin{aligned} dV(\mathcal{X}(t)) &= \mathcal{L}V(\mathcal{X}(t))dt + \frac{\partial V(\mathcal{X}(t))}{\partial \mathcal{X}(t)} g d\omega(t) \\ &\quad + \frac{\partial V(\mathcal{X}(t))}{\partial \mathcal{X}(t)} h d\zeta(t), \end{aligned} \quad (31)$$

where

$$\begin{aligned} \mathcal{L}V(\mathcal{X}(t)) &= 2\nabla^T H(\mathcal{X}(t))[J(\mathcal{X}(t)) - R(\mathcal{X}(t))]\nabla H(\mathcal{X}(t)) \\ &\quad + 2\nabla^T H(\mathcal{X}(t))G(t) \int_{t-d}^t (\nabla H(\mathcal{X}(s)))' ds \\ &\quad + \text{tr}[g^T \text{Hess}(H(\mathcal{X}))g] \\ &\quad + \text{tr}[h^T \text{Hess}(H(\mathcal{X}))h]. \end{aligned} \quad (32)$$

Letting  $\lambda = \sup_{t \geq 0} \|\text{Hess}(H_1(x) + H_2(\xi))\|^2$  and based on Lemma 3, we conclude that

$$\begin{aligned} & \text{tr}[g^T \text{Hess}(H(\mathcal{X}))g] \\ & \leq \frac{1}{2} \text{tr}(g^T g) + \frac{1}{2} \text{tr}[g^T \text{Hess}(H(\mathcal{X}))\text{Hess}^T(H(\mathcal{X}))g] \\ & \leq \frac{1}{2} (\lambda + 1) \text{tr}(g^T g) \\ & = \frac{1}{2} (\lambda + 1) \sum_{j=1}^m \sum_{i=1}^n (\bar{g}_{ij}^2 + \hat{g}_{ij}^2), \end{aligned} \quad (33)$$

where  $\bar{g}_{ij}$  and  $\hat{g}_{ij}$  are the components of the matrices  $g_1 = (\bar{g}_{ij})_{n \times m}$  and  $g_2 = (\hat{g}_{ij})_{n \times m}$ , respectively. Similarly, we have

$$\begin{aligned} & \text{tr}[g^T \text{Hess}(H(\mathcal{X}))h] \\ & \leq \frac{1}{2} \text{tr}(h^T h) + \frac{1}{2} \text{tr}[h^T \text{Hess}(H(\mathcal{X}))\text{Hess}^T(H(\mathcal{X}))h] \\ & \leq \frac{1}{2} (\lambda + 1) \text{tr}(h^T h) \\ & = \frac{1}{2} (\lambda + 1) \sum_{k=1}^{\kappa} \sum_{i=1}^n (\bar{h}_{ik}^2 + \hat{h}_{ik}^2). \end{aligned} \quad (34)$$

Then, denoting

$$\tau := \sum_{j=1}^m \sum_{i=1}^n (\bar{g}_{ij}^2 + \hat{g}_{ij}^2) + \sum_{k=1}^{\kappa} \sum_{i=1}^n (\bar{h}_{ik}^2 + \hat{h}_{ik}^2), \quad (35)$$

we obtain that

$$\begin{aligned}
& \text{tr} \left[ g^T \text{Hess}(H(\mathcal{X}))g + h^T \text{Hess}(H(\mathcal{X}))h \right] \\
& \leq \frac{1}{2} (\lambda + 1) \left[ \sum_{j=1}^m \sum_{i=1}^n (\widehat{g}_{ij}^2 + \widehat{g}_{ij}^2) + \sum_{k=1}^{\kappa} \sum_{i=1}^n (\widehat{h}_{ik}^2 + \widehat{h}_{ik}^2) \right] \quad (36) \\
& = \frac{1}{2} (\lambda + 1) \tau.
\end{aligned}$$

Thus, taking expectations of both sides of (32), we have

$$\begin{aligned}
& \mathbb{E}\{\mathcal{L}V(\mathcal{X}(t))\} \\
& \leq 2\mathbb{E}\left\{ \nabla^T H(\mathcal{X}(t)) (J(\mathcal{X}(t)) - R(\mathcal{X}(t))) \nabla H(\mathcal{X}(t)) \right\} \\
& \quad + 2\mathbb{E}\left\{ \nabla^T H(\mathcal{X}(t)) G(t) \int_{t-d}^t (\nabla H(\mathcal{X}(s)))' ds \right\} \\
& \quad + \frac{1}{2} (\lambda + 1) \tau. \quad (37)
\end{aligned}$$

Due to the fact that

$$\begin{aligned}
& \mathbb{E}\left\{ \nabla^T H(\mathcal{X}(t)) J(\mathcal{X}(t)) \nabla H(\mathcal{X}(t)) \right\} \\
& = \nabla^T H(\mathcal{X}(t)) \bar{J}(\mathcal{X}(t)) \nabla H(\mathcal{X}(t)), \quad (38)
\end{aligned}$$

where

$$\begin{aligned}
\bar{J}(\mathcal{X}(t)) &= \begin{bmatrix} J(x(t)) & g_1 K g_2^T \\ -g_2 K g_1^T & \hat{J}(\xi(t)) \end{bmatrix} \\
&= \begin{bmatrix} J(x(t)) & g_1 K g_2^T \\ -(g_1 K g_2^T)^T & \hat{J}(\xi(t)) \end{bmatrix}, \quad (39)
\end{aligned}$$

and the fact that  $\bar{J}(\mathcal{X}(t)) = -\bar{J}^T(\mathcal{X}(t))$ , we get

$$\nabla^T H(\mathcal{X}(t)) \bar{J}(\mathcal{X}(t)) \nabla H(\mathcal{X}(t)) = 0. \quad (40)$$

Furthermore, the following inequality holds:

$$\begin{aligned}
& \mathbb{E}\{\mathcal{L}V(\mathcal{X}(t))\} \\
& \leq -\nabla^T H(\mathcal{X}(t)) \left( \bar{R}(\mathcal{X}(t)) + \bar{R}^T(\mathcal{X}(t)) \right) \nabla H(\mathcal{X}(t)) \\
& \quad + 2\nabla^T H(\mathcal{X}(t)) \bar{G} \int_{t-d}^t (\nabla H(\mathcal{X}(s)))' ds \quad (41) \\
& \quad + \frac{1}{2} (\lambda + 1) \tau,
\end{aligned}$$

where  $\bar{R}(\mathcal{X}(t)) = \text{diag}\{R(x(t)) + g_1 K g_1^T, \hat{R}(\xi(t)) - g_2 K g_2^T\}$ ,

$$\bar{G} = \begin{bmatrix} g_1 K g_1^T & -g_1 K g_2^T \\ g_2 K g_1^T & -g_2 K g_2^T \end{bmatrix}. \quad (42)$$

Since Assumption 3 holds, the following inequalities

$$\begin{aligned}
& -\nabla^T H_1(x(t)) R(x(t)) \nabla H_1(x(t)) \\
& \leq -\lambda_{\min}(R(x(t))) \nabla^T H_1(x(t)) \nabla H_1(x(t)) \quad (43) \\
& \leq -c_1 \nabla^T H_1(x(t)) \nabla H_1(x(t)) \\
& = -\nabla^T H_1(x(t)) (c_1 I_n) \nabla H_1(x(t)),
\end{aligned}$$

$$\begin{aligned}
& -\nabla^T H_2(\xi(t)) \hat{R}(\xi(t)) \nabla H_2(\xi(t)) \\
& \leq -\lambda_{\min}(\hat{R}(\xi(t))) \nabla^T H_2(\xi(t)) \nabla H_2(\xi(t)) \quad (44) \\
& \leq -c_2 \nabla^T H_2(\xi(t)) \nabla H_2(\xi(t)) \\
& = -\nabla^T H_2(\xi(t)) (c_2 I_n) \nabla H_2(\xi(t)),
\end{aligned}$$

are true. Then, (41) becomes

$$\begin{aligned}
& \mathbb{E}\{\mathcal{L}V(\mathcal{X}(t))\} \\
& \leq -\nabla^T H(\mathcal{X}(t)) \left( \bar{R} + \bar{R}^T \right) \nabla H(\mathcal{X}(t)) \\
& \quad + 2\nabla^T H(\mathcal{X}(t)) \bar{G} \int_{t-d}^t (\nabla H(\mathcal{X}(s)))' ds \quad (45) \\
& \quad + \frac{1}{2} (\lambda + 1) \tau,
\end{aligned}$$

where  $\bar{R} = \text{diag}\{c_1 I_n + g_1 K g_1^T, c_2 I_n - g_2 K g_2^T\}$ .

Assume that there exist matrices  $L_1 = L_1^T$ ,  $L_2 = L_2^T$ , and  $L_3 = L_3^T$  such that

$$\begin{aligned}
& (\nabla H(\mathcal{X}(t)) - \nabla H(\mathcal{X}(t-d))) \\
& \quad - \int_{t-d}^t (\nabla H(\mathcal{X}(s)))' ds \Big)^T \\
& \quad \cdot (-\text{diag}\{L_1, L_1\} \nabla H(\mathcal{X}(t)) \\
& \quad + \text{diag}\{L_2, L_2\} \nabla H(\mathcal{X}(t-d)) \\
& \quad + \text{diag}\{L_3, L_3\} \int_{t-d}^t (\nabla H(\mathcal{X}(s)))' ds) \equiv 0. \quad (46)
\end{aligned}$$

Combining (45) and (46), we deduce that

$$\begin{aligned}
& \mathbb{E}\{\mathcal{L}V(\mathcal{X}(t))\} \\
& \leq -\nabla^T H(\mathcal{X}(t)) \left( \bar{R} + \bar{R}^T \right) \nabla H(\mathcal{X}(t)) \\
& \quad + 2\nabla^T H(\mathcal{X}(t)) \bar{G} \int_{t-d}^t (\nabla H(\mathcal{X}(s)))' ds \\
& \quad + (\nabla H(\mathcal{X}(t)) - \nabla H(\mathcal{X}(t-d))) \\
& \quad - \int_{t-d}^t (\nabla H(\mathcal{X}(s)))' ds \Big)^T \\
& \quad \cdot (-\text{diag}\{L_1, L_1\} \nabla H(\mathcal{X}(t)) \\
& \quad + \text{diag}\{L_2, L_2\} \nabla H(\mathcal{X}(t-d)) \\
& \quad + \text{diag}\{L_3, L_3\} \int_{t-d}^t (\nabla H(\mathcal{X}(s)))' ds) \\
& \quad + \frac{1}{2} (\lambda + 1) \tau \\
& = v^T(t) \Pi_1 v(t) + \frac{1}{2} (\lambda + 1) \tau, \quad (47)
\end{aligned}$$

where

$$v(t) = \begin{bmatrix} \nabla H_1(x(t)) \\ \nabla H_1(x(t-d)) \\ \nabla H_2(\xi(t)) \\ \nabla H_2(\xi(t-d)) \\ \int_{t-d}^t (\nabla H_1(x(s)))' ds \\ \int_{t-d}^t (\nabla H_2(\xi(s)))' ds \end{bmatrix}. \quad (48)$$

Since  $\Pi_1 < 0$ , we further obtain

$$\begin{aligned} & \mathbb{E}\{\mathcal{L}V(\mathcal{X})\} \\ & \leq -\lambda_{\min}(-\Pi_1) \left( \nabla^T H_1(x(t)) \nabla H_1(x(t)) \right. \\ & \quad \left. + \nabla^T H_2(\xi(t)) \nabla H_2(\xi(t)) \right) \\ & \quad + \frac{1}{2}(\lambda + 1)\tau \\ & = -\lambda_{\min}(-\Pi_1) \nabla^T H(\mathcal{X}) \nabla H(\mathcal{X}) \\ & \quad + \frac{1}{2}(\lambda + 1)\tau. \end{aligned} \quad (49)$$

According to Assumption 2 and Lemma 2, we have

$$\begin{aligned} & \nabla^T H(\mathcal{X}) \nabla H(\mathcal{X}) \\ & = \left( \frac{2\alpha}{2\alpha-1} (x_1^2)^{(1-\alpha)/2\alpha-1} x_1, \dots, \frac{2\alpha}{2\alpha-1} (x_n^2)^{(1-\alpha)/2\alpha-1} x_n, \right. \\ & \quad \left. \frac{2\alpha}{2\alpha-1} (\xi_1^2)^{(1-\alpha)/2\alpha-1} \xi_1, \dots, \frac{2\alpha}{2\alpha-1} (\xi_n^2)^{(1-\alpha)/2\alpha-1} \xi_n \right) \\ & \quad \cdot \left( \frac{2\alpha}{2\alpha-1} (x_1^2)^{(1-\alpha)/2\alpha-1} x_1, \dots, \frac{2\alpha}{2\alpha-1} (x_n^2)^{(1-\alpha)/2\alpha-1} x_n, \right. \\ & \quad \left. \frac{2\alpha}{2\alpha-1} (\xi_1^2)^{(1-\alpha)/2\alpha-1} \xi_1, \dots, \frac{2\alpha}{2\alpha-1} (\xi_n^2)^{(1-\alpha)/2\alpha-1} \xi_n \right)^T \\ & = \left( \frac{2\alpha}{2\alpha-1} \right)^2 \left( \sum_{i=1}^n (x_i^2)^{1/(2\alpha-1)} + \sum_{i=1}^n (\xi_i^2)^{1/(2\alpha-1)} \right) \\ & = \left( \frac{2\alpha}{2\alpha-1} \right)^2 \sum_{i=1}^{2n} (\mathcal{X}_i^2)^{1/(2\alpha-1)} \\ & = \left( \frac{2\alpha}{2\alpha-1} \right)^2 \sum_{i=1}^{2n} \left[ (\mathcal{X}_i^2)^{\alpha/(2\alpha-1)} \right]^{1/\alpha} \\ & \geq \left( \frac{2\alpha}{2\alpha-1} \right)^2 \left[ \sum_{i=1}^{2n} (\mathcal{X}_i^2)^{\alpha/(2\alpha-1)} \right]^{1/\alpha} \\ & = \left( \frac{2\alpha}{2\alpha-1} \right)^2 V^{1/\alpha}(\mathcal{X}). \end{aligned} \quad (50)$$

Then inequality in (49) becomes

$$\begin{aligned} \mathbb{E}\{\mathcal{L}V(\mathcal{X})\} & \leq -\lambda_{\min}(-\Pi_1) \left( \frac{2\alpha}{2\alpha-1} \right)^2 V^{1/\alpha}(\mathcal{X}) \\ & \quad + \frac{1}{2}(\lambda + 1)\tau \\ & = -\bar{c}V^{\hbar_1}(\mathcal{X}) + a_1, \end{aligned} \quad (51)$$

where  $\bar{c} = \lambda_{\min}(-\Pi_1)(2\alpha/(2\alpha-1))^2 > 0$ ,  $0 < \hbar_1 = (1/\alpha) < 1$  and  $a_1 = (1/2)(\lambda + 1)\tau > 0$ . Thus, we obtain that inequality (51) satisfies (11) in Lemma 1. In addition, there exist two class- $\mathcal{K}_\infty$  functions  $\gamma_1(\|\mathcal{X}\|) = 2\|\mathcal{X}\|$  and  $\gamma_2(\|\mathcal{X}\|) = 2\|\mathcal{X}\|^2$  such that (10) in Lemma 1 holds.

Eventually, in view of Lemma 1, we arrive at a conclusion that systems (7) and (8) are SGFSSP under the output feedback controller (21). Furthermore, the settling time  $T_1^*$  is obtained and satisfies

$$\begin{aligned} T_1^* & = \frac{1}{b_1 \bar{c}(1-\hbar_1)} V^{1-\hbar_1}(\mathcal{X}_0) \\ & \quad - \frac{1}{b_1 \bar{c}(1-\hbar_1)} \left( \frac{a_1}{\bar{c}(1-b_1)} \right)^{(1-\hbar_1)/\hbar_1}, \end{aligned} \quad (52)$$

where  $0 < b_1 < 1$ . In addition, the compact set  $\Omega_1$  is expressed as

$$\Omega_1 = \left\{ x \mid V^{\hbar_1}(\mathcal{X}) \leq \frac{a_1}{\bar{c}(1-b_1)} \right\}. \quad (53)$$

The proof of this theorem is now completed.  $\square$

*Remark 3.* In [33], the channel is modeled as a cascade of a multiplicative noise and an additive white Gaussian noise. Based on this channel, we take the constant transmission delay into consideration. Thus, the channel model in this paper is more general. In addition, [33] proposes a state feedback controller design strategy to stabilize linear systems. Meanwhile, this paper deals with the output feedback simultaneous stabilization problem for stochastic PCH systems in finite time.

*Remark 4.* Under Lemma 1, how to choose a suitable Lyapunov function is an essential difficulty during the research. Accordingly, we have overcome this difficulty by taking  $H(x)$  as a Lyapunov function, and  $H(x)$  has a concrete form which is given in (19) in Assumption 2.

*Remark 5.* Through the proof of Theorem 1, we can see that even if the dimensions of  $x(t)$  are not the same as that of  $\xi(t)$ , the result of Theorem 1 still holds. Thus, the design strategy of controllers in Theorem 1 can be extended to multiple systems. Thus, we have the following analysis about SGFSSP of multiple stochastic PCH systems.

Next, consider the following multiple stochastic PCH systems:

$$\begin{cases} dx_j(t) = [J_j(x_j(t)) - R_j(x_j(t))] \nabla H_j(x_j(t)) dt \\ + g_j u(t) dt + h_j d\omega_j(t), \\ y_j(t) = g_j^T(x_j) \nabla H_j(x_j), \quad j = 1, 2, \dots, V, \end{cases} \quad (54)$$

where  $V$  is the number of stochastic systems,  $x_j(t) \in \mathbb{R}^{n_j}$  is the plant state vector,  $y_j(t) \in \mathbb{R}^m$  is the outputs of the plant, and the signal  $\omega_j(t) \in \mathbb{R}^{r_j}$  is the independent scalar Wiener process with  $\mathbb{E}\{d\omega_j(t)\} = 0$  and  $\mathbb{E}\{[d\omega_j(t)]^2\} = dt$ .  $\nabla H_j(x_j) \in \mathbb{R}^{n_j \times 1}$  is the gradient of the Hamilton function  $H_j(x_j): \mathbb{R}^{n_j} \rightarrow \mathbb{R}$ , which is defined as  $\nabla H_j(x_j) = (\partial H_j(x_j)/\partial x_j)$ , and  $H_j(x_j) \geq 0$ ,  $H_j(0) = 0$ , for all  $t \geq 0$ .  $J_j(x_j)$  is a skew-symmetric structure matrix;  $R_j(x_j) \in \mathbb{R}^{n_j \times n_j}$  is a positive definite strict dissipation matrix;  $g_j$  and  $h_j$  are known real constant gain matrices. In addition,  $J_j(x_j)$ ,  $R_j(x_j)$ ,  $g_j$ , and  $h_j$  satisfy locally Lipschitz condition.

*Assumption 4.* The Hamilton functions  $H_j(x_j)$  are given as

$$H_j(x_j) = \sum_{i=1}^{n_j} (x_{ji}^2)^{\alpha/(2\alpha-1)}. \quad (55)$$

*Assumption 5.* There exist constants  $c_3 > 0$  and  $c_4 > 0$  such that

$$\begin{aligned} c_3 &= \inf_{t \geq 0} \{\lambda_{\min}\{R_{j_1}(x_{j_1}(t)), \dots, R_{j_s}(x_{j_s}(t))\}\}, \\ c_4 &= \inf_{t \geq 0} \{\lambda_{\min}\{R_{j_{s+1}}(x_{j_{s+1}}(t)), \dots, R_{j_v}(x_{j_v}(t))\}\}. \end{aligned} \quad (56)$$

Assume that we can find out an arbitrary permutation  $(j_1, j_2, \dots, j_v)$  from the positive integer set  $\{1, 2, \dots, V\}$  and that  $S$  is a positive integer which satisfies  $1 \leq S \leq V - 1$ . In addition, taking  $V_1 = n_{j_1} + \dots + n_{j_s}$ ,  $V_2 = n_{j_{s+1}} + \dots + n_{j_v}$ ,  $\bar{r}_1 = r_{j_1} + \dots + r_{j_s}$ , and  $\bar{r}_2 = r_{j_{s+1}} + \dots + r_{j_v}$ , we divide the  $V$  stochastic PCH systems into two parts:  $\{j_1, \dots, j_s\}$  and  $\{j_{s+1}, \dots, j_v\}$ .

Defining the vectors  $\mathcal{X}_1(t) = [x_{j_1}^T(t), \dots, x_{j_s}^T(t)]^T \in \mathbb{R}^{V_1}$ ,  $W_1(t) = [\omega_{j_1}^T(t), \dots, \omega_{j_s}^T(t)]^T \in \mathbb{R}^{\bar{r}_1}$ ,  $\mathcal{X}_2(t) = [x_{j_{s+1}}^T(t), \dots, x_{j_v}^T(t)]^T \in \mathbb{R}^{V_2}$ ,  $W_2(t) = [\omega_{j_{s+1}}^T(t), \dots, \omega_{j_v}^T(t)]^T \in \mathbb{R}^{\bar{r}_2}$ , then system (54) becomes

$$\begin{cases} d\mathcal{X}_1(t) = [\bar{J}_1(\mathcal{X}_1(t)) - \bar{R}_1(\mathcal{X}_1(t))] \nabla \bar{H}_1(\mathcal{X}_1(t)) dt \\ + \bar{g}_1 u(t) dt + \bar{h}_1 dW_1(t), \\ Y_1(t) = \bar{g}_1^T \nabla \bar{H}_1(\mathcal{X}_1(t)), \end{cases} \quad (57)$$

$$\begin{cases} d\mathcal{X}_2(t) = [\bar{J}_2(\mathcal{X}_2(t)) - \bar{R}_2(\mathcal{X}_2(t))] \nabla \bar{H}_2(\mathcal{X}_2(t)) dt \\ + \bar{g}_2 u(t) dt + \bar{h}_2 dW_2(t), \\ Y_2(t) = \bar{g}_2^T \nabla \bar{H}_2(\mathcal{X}_2(t)), \end{cases} \quad (58)$$

where

$$\begin{aligned} \bar{J}_1(\mathcal{X}_1) &= -\bar{J}_1^T(\mathcal{X}_1) \\ &= \text{diag}\{J_{j_1}(x_{j_1}), \dots, J_{j_s}(x_{j_s})\} \in \mathbb{R}^{V_1 \times V_1}, \end{aligned}$$

$$\bar{R}_1(\mathcal{X}_1) = \text{diag}\{R_{j_1}(x_{j_1}), \dots, R_{j_s}(x_{j_s})\} > 0,$$

$$\bar{g}_1 = [g_{j_1}, \dots, g_{j_s}]^T \in \mathbb{R}^{V_1 \times m},$$

$$\bar{h}_1 = \text{diag}\{h_{j_1}, \dots, h_{j_s}\} \in \mathbb{R}^{V_1 \times \bar{r}_1},$$

$$\bar{J}_2(\mathcal{X}_2) = -\bar{J}_2^T(\mathcal{X}_2)$$

$$= \text{diag}\{J_{j_{s+1}}(x_{j_{s+1}}), \dots, J_{j_v}(x_{j_v})\} \in \mathbb{R}^{V_2 \times V_2},$$

$$\bar{R}_2(\mathcal{X}_2) = \text{diag}\{R_{j_{s+1}}(x_{j_{s+1}}), \dots, R_{j_v}(x_{j_v})\} > 0,$$

$$\bar{g}_2 = [g_{j_{s+1}}, \dots, g_{j_v}]^T \in \mathbb{R}^{V_2 \times m},$$

$$\bar{h}_2 = \text{diag}\{h_{j_{s+1}}, \dots, h_{j_v}\} \in \mathbb{R}^{V_2 \times \bar{r}_2},$$

$$\bar{H}_1(\mathcal{X}_1) = \sum_{k=1}^s H_{j_k}(x_{j_k}), \quad \bar{H}_2(\mathcal{X}_2)$$

$$Y_1 = y_{j_1} + \dots + y_{j_s},$$

$$Y_2 = y_{j_{s+1}} + \dots + y_{j_v}.$$

(59)

Substituting (4) into systems (57) and (58), we have

$$\begin{cases} d\mathcal{X}_1(t) = [\bar{J}_1(\mathcal{X}_1(t)) - \bar{R}_1(\mathcal{X}_1(t))] \nabla \bar{H}_1(\mathcal{X}_1(t)) dt \\ + \bar{g}_1 \varepsilon(t) u(t-d) dt + \bar{g}_1 d\omega(t) \\ + \bar{h}_1 dW_1(t), \\ Y_1(t) = \bar{g}_1^T \nabla \bar{H}_1(\mathcal{X}_1(t)), \end{cases} \quad (60)$$

$$\begin{cases} d\mathcal{X}_2(t) = [\bar{J}_2(\mathcal{X}_2(t)) - \bar{R}_2(\mathcal{X}_2(t))] \nabla \bar{H}_2(\mathcal{X}_2(t)) dt \\ + \bar{g}_2 \varepsilon(t) u(t-d) dt + \bar{g}_2 d\omega(t) \\ + \bar{h}_2 dW_2(t), \\ Y_2(t) = \bar{g}_2^T \nabla \bar{H}_2(\mathcal{X}_2(t)). \end{cases} \quad (61)$$

Furthermore, we can obtain the following corollary.

**Corollary 1.** Consider systems (60) and (61). Assumptions 4 and 5 are satisfied. If there exist matrices  $K = K^T$ ,  $N_1 = N_1^T$ ,  $N_2 = N_2^T$ ,  $N_3 = N_3^T$ , an arbitrary permutation  $(j_1, j_2, \dots, j_v)$  of  $\{1, 2, \dots, V\}$  and a positive integer  $S(1 \leq S \leq V)$  such that

$$\Pi_2 = \begin{bmatrix} B_{11} & B_{12} & 0 & 0 & B_{15} & -\tilde{g}_1 K \tilde{g}_2^T \\ * & -N_2 & 0 & 0 & B_{25} & 0 \\ * & * & B_{33} & B_{34} & \tilde{g}_2 K \tilde{g}_1^T & B_{36} \\ * & * & * & -\frac{1}{2}N_2 & 0 & B_{46} \\ * & * & * & * & -N_3 & 0 \\ * & * & * & * & * & -N_3 \end{bmatrix} < 0 \quad (62)$$

holds, where

$$\begin{aligned} B_{11} &= -2c_3 I_{V_1} - 2\tilde{g}_1 K \tilde{g}_1^T - N_1, \\ B_{12} &= \frac{1}{2}(N_1 + N_2), \\ B_{15} &= \tilde{g}_1 K \tilde{g}_1^T + \frac{1}{2}(N_1 + N_3), \\ B_{25} &= -\frac{1}{2}(N_2 + N_3), \\ B_{33} &= -2c_4 I_{V_2} + 2\tilde{g}_2 K \tilde{g}_2^T - N_1, \\ B_{34} &= \frac{1}{2}(N_1 + N_2), \\ B_{36} &= -\tilde{g}_2 K \tilde{g}_2^T + \frac{1}{2}(N_1 + N_3), \\ B_{46} &= -\frac{1}{2}(N_2 + N_3), \end{aligned} \quad (63)$$

then systems (60) and (61) are SGFSSP under the output feedback control law:

$$u(t-d) = -M^{-1}K(Y_1(t-d) - Y_2(t-d)). \quad (64)$$

*Proof:* the proof of this corollary is similar to the proof of Theorem 1, and we give some main analysis. First, similar to the proof of Theorem 1, we can obtain an augmented Itô form stochastic PCH system with state  $\bar{\mathcal{X}}(t) = [\mathcal{X}_1(t) \ \mathcal{X}_2(t)]^T$ . Next, choose the following Lyapunov function candidate:

$$V(\bar{\mathcal{X}}(t)) = 2(\tilde{H}_1(\mathcal{X}_1(t)) + \tilde{H}_2(\mathcal{X}_2(t))). \quad (65)$$

Let  $\lambda_1 = \sup_{t \geq 0} \|\text{Hess}(\sum_{j=1}^V H_j(x_j))\|^2$  and  $\tau_1 = \text{tr}(\sum_{j=1}^V g_j^T g_j + \sum_{j=1}^V h_j^T h_j)$ . Then, we have

$$\begin{aligned} \mathbb{E}\{\mathcal{L}V(\bar{\mathcal{X}})\} &\leq -\lambda_{\min}(-\Pi_2) \left(\frac{2\alpha}{2\alpha-1}\right)^2 V^{1/\alpha}(\bar{\mathcal{X}}) \\ &+ \frac{1}{2}(\lambda_1 + 1)\tau_1 \\ &= -\bar{c}V^{h_1}(\bar{\mathcal{X}}) + \bar{a}, \end{aligned} \quad (66)$$

where  $\bar{c} = \lambda_{\min}(-\Pi_2)(2\alpha/(2\alpha-1))^2 > 0$  and  $\bar{a} = (1/2)(\lambda_1 + 1)\tau_1 > 0$ . In the end, under Lemma 1, we can see that systems (60) and (61) are SGFSSP under the output feedback controller (64). Furthermore, the settling time  $T_2^*$  satisfies

$$T_2^* = \frac{1}{\bar{b}\bar{c}(1-h_1)} V^{1-h_1}(\bar{\mathcal{X}}_0) - \frac{1}{\bar{b}\bar{c}(1-h_1)} \left(\frac{\bar{a}}{\bar{c}(1-\bar{b})}\right)^{(1-h_1)/h_1}, \quad (67)$$

where  $0 < \bar{b} < 1$ . In addition, we have

$$\Omega_2 = \left\{ x \mid V^{h_1}(\bar{\mathcal{X}}) \leq \frac{\bar{a}}{\bar{c}(1-\bar{b})} \right\}. \quad (68)$$

The proof of this corollary is now completed.

#### 4. Illustrative Example

In this section, a numerical example is performed to illustrate the stabilization scheme for stochastic PCH systems subject to delayed and fading channels.

The considered systems are two stochastic PCH systems:

$$\begin{cases} dx(t) = [J(x) - R(x)]\nabla H_1(x)dt + g_1 u(t)dt \\ + h_1 d\omega(t), \\ y(t) = g_1^T \nabla H_1(x(t)), \end{cases} \quad (69)$$

$$\begin{cases} d\xi(t) = [\hat{J}(\xi)t - n\hat{R}q(\xi)]\nabla H_2(\xi)d + g_2 u(t)dt \\ + H_2 d\rho(t), \\ \eta(t) = g_2^T \nabla H_2(\xi(t)), \end{cases} \quad (70)$$

where  $x = [x_1 \ x_2]^T \in \mathbb{R}^2$ ,  $\xi = [\xi_1 \ \xi_2]^T \in \mathbb{R}^2$ ,  $H_1(x) = x_1^{4/3} + x_2^{4/3}$  ( $\alpha = 2$ ),  $H_2(\xi) = \xi_1^{4/3} + \xi_2^{4/3}$  ( $\alpha = 2$ ),

$$\begin{aligned} J(x) &= \begin{bmatrix} 0 & 1 \\ -1 & 0 \end{bmatrix}, \\ R(x) &= \begin{bmatrix} 1 & 0 \\ 0 & 2 \end{bmatrix}, \\ \hat{J}(\xi) &= \begin{bmatrix} 0 & 2 \\ -2 & 0 \end{bmatrix}, \\ \hat{R}(\xi) &= \begin{bmatrix} 2 & 0 \\ 0 & 3 \end{bmatrix}, \\ g_1 &= [0.025 \ 0.05]^T, \\ h_1 &= [0.05 \ 0.05]^T, \\ g_2 &= [0.05 \ 0.05]^T, \\ h_2 &= [0.05 \ 0.025]^T. \end{aligned} \quad (71)$$

We take the constant transmission delay  $d = 0.25$ . The control input signal  $u(t-d)$  is sent through the delayed and fading noisy channels to the actuator, so a single controller

for systems (69) and (70) is modeled as (4). Through statistical experiments, the probability density function of multiplicative noise  $\varepsilon(t)$  with mean  $\mu = 0.9$  and variance  $\sigma^2 = 0.065$  is listed as

$$p_t(\bar{s}) = \begin{cases} 0.05, & \bar{s} = 0, \\ 0.10, & \bar{s} = 0.5, \\ 0.85, & \bar{s} = 1. \end{cases} \quad (72)$$

Obviously,  $M = \mu = 0.9$ .

Substituting (4) into (69) and (70) leads to

$$\begin{aligned} dx(t) &= [J(x) - R(x)]\nabla H_1(x)dt \\ &\quad + g_1\varepsilon(t)u(t-0.25)dt + g_1d\omega(t) \\ &\quad + h_1d\omega(t), \end{aligned} \quad (73)$$

$$\begin{aligned} d\xi(t) &= [\hat{J}(\xi) - \hat{R}_2(\xi)]\nabla H_2(\xi)dt \\ &\quad + g_2\varepsilon(t)u(t-0.25)dt + g_2d\bar{\omega}(t) \\ &\quad + h_2d\rho(t). \end{aligned} \quad (74)$$

Choose  $L_1 = \begin{bmatrix} 2 & 1 \\ 1 & -1 \end{bmatrix}$ ,  $L_2 = \begin{bmatrix} 1 & 1 \\ 1 & 6 \end{bmatrix}$ , and  $L_3 = \begin{bmatrix} 3 & 1 \\ 1 & 1 \end{bmatrix}$ .

Then we can use the LMI toolbox of MATLAB to obtain

$$K = 4.447. \quad (75)$$

To sum up, all the conditions of Theorem 1 hold. Consequently, from Theorem 1, systems (73) and (74) are SGFSSP under the output feedback control law:

$$\begin{aligned} u(t-d) &= -0.16x_1^{1/3}(t-d) - 0.33x_2^{1/3}(t-d) \\ &\quad + 0.33\xi_1^{1/3}(t-d) + 0.33\xi_2^{1/3}(t-d). \end{aligned} \quad (76)$$

In the simulation, we choose the initial states of the systems as  $x(0) = [-0.3 \ 0.3]^T$ ,  $\xi(0) = [0.6 \ 0.4]^T$ , and set the parameter  $b_1 = 0.6$ . Then, considering (52) in Theorem 1, it is easy to obtain that the settling time  $T_1^* = 0.32s$ . The state trajectories of  $x$  and  $\xi$  are shown in Figures 2 and 3, respectively.

From Figures 2 and 3 in the simulation, we can see that a single controller (76) can simultaneously stabilize systems (69) and (70) in finite time. The settling time  $T_1^*$  is consistent with that of (52), and the states converge to the origin in 0.32 s. In summary, the output feedback controller proposed in Theorem 1 performs well in the SGFSSP of systems (69) and (70).

## 5. Conclusion

In this paper, the finite-time simultaneous stabilization in probability of stochastic PCH systems over delayed and fading channels has been investigated. On the basis of the dissipative Hamiltonian structural properties and Lyapunov functional technique, a single output feedback controller has been designed for two stochastic PCH systems, which guarantees the SGFSSP of the closed-loop Hamiltonian systems. The case of multiple stochastic PCH systems also has been studied. Sufficient conditions for the existence of the stabilization controllers have been derived in consideration of the

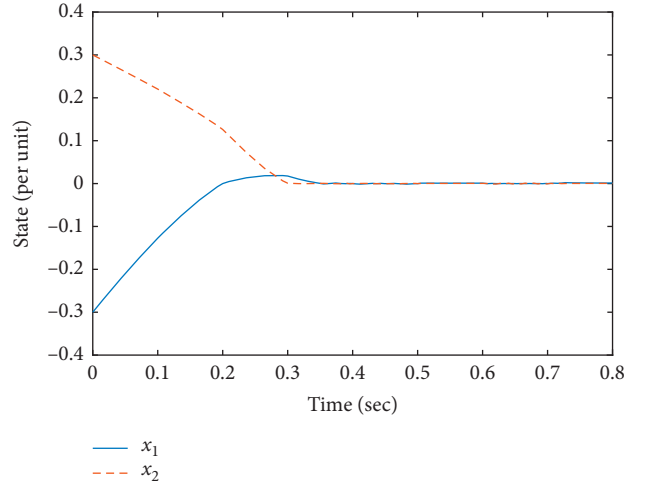


FIGURE 2: State trajectory of  $x_1$  and  $x_2$ .

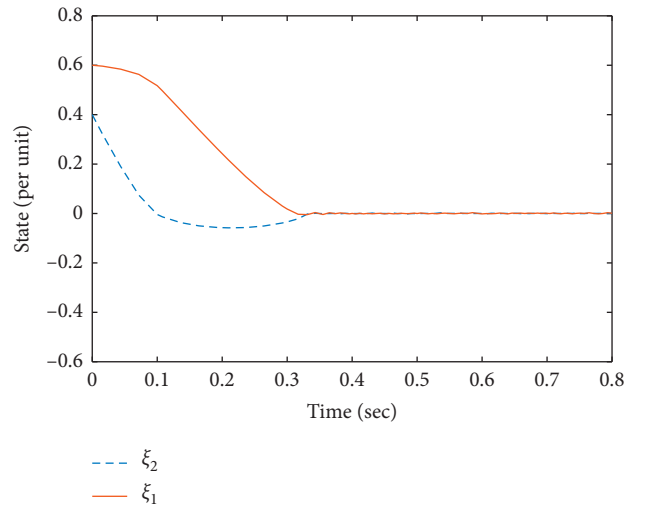


FIGURE 3: State trajectory of  $\xi_1$  and  $\xi_2$ .

phenomenon of delayed and fading channels. At last, a numerical example has highlighted the effectiveness of the stabilization technology proposed in this paper. As for network-based control, sometimes the states of systems are not fully measured, so a possible future research will be involved in observer-based simultaneous stabilization of a set of stochastic PCH systems over delayed and fading channels.

## Data Availability

No data were used to support this study.

## Conflicts of Interest

The authors declare that they have no conflicts of interest.

## Acknowledgments

This work was supported by the National Natural Science Foundation of China under grant 62073189.

## References

- [1] B. Maschke and A. J. Van der Schaft, "Port-controlled Hamiltonian systems: modeling origins and system theoretic properties," in *Proceedings of the IFAC Symposium Nonlinear Control Systems Design*, pp. 282–288, Bordeaux, France, 1992.
- [2] A. J. van der Schaft and B. Maschke, "The Hamiltonian formulation of energy conserving physical systems with external ports," *AEÜ International journal of electronics and communications*, vol. 49, pp. 362–371, 1995.
- [3] B. M. Afkham and J. S. Hesthaven, "Structure preserving model reduction of parametric Hamiltonian systems," *SIAM Journal on Scientific Computing*, vol. 36, no. 9, pp. 2616–2644, 2017.
- [4] T. Shen, S. Mei, Q. Lu, W. Hu, and K. Tamura, "Adaptive nonlinear excitation control with L2 disturbance attenuation for power systems," *Automatica*, vol. 39, no. 1, pp. 81–89, 2003.
- [5] W. Sun and X. Lv, "Practical finite-time fuzzy control for Hamiltonian systems via adaptive event-triggered approach," *International Journal of Fuzzy Systems*, vol. 22, no. 1, pp. 35–45, 2020.
- [6] P. Jagtap and M. Zamani, "Backstepping design for incremental stability of stochastic Hamiltonian systems with jumps," *IEEE Transactions on Automatic Control*, vol. 63, no. 1, pp. 255–261, 2018.
- [7] R. Ortega, M. Galaz, A. Astolfi et al., "Transient stabilization of multimachine power systems with nontrivial transfer conductances," *IEEE Transactions on Automatic Control*, vol. 50, no. 1, pp. 60–75, 2005.
- [8] H. Ramirez, Y. Le Gorrec, B. Maschke, and F. Couenne, "On the passivity based control of irreversible processes: a port-Hamiltonian approach," *Automatica*, vol. 64, pp. 105–111, 2016.
- [9] W. Sun, Y. Wu, and L. Wang, "Trajectory tracking of constrained robotic systems via a hybrid control strategy," *Neurocomputing*, vol. 330, pp. 188–195, 2019.
- [10] M. Zhang, P. Borja, R. Ortega et al., "PID passivity-based control of port-Hamiltonian systems," *IEEE Transactions on Automatic Control*, vol. 63, no. 4, pp. 1032–1044, 2018.
- [11] B. Fu, S. Li, X. Wang, and L. Guo, "Output feedback based simultaneous stabilization of two port-controlled Hamiltonian systems with disturbances," *Journal of the Franklin Institute*, vol. 356, no. 15, pp. 8154–8166, 2019.
- [12] W. W. Sun, "Stabilization analysis of time-delay Hamiltonian systems in the presence of saturation," *Applied Mathematics and Computation*, vol. 217, no. 23, pp. 9625–9634, 2011.
- [13] Y. Wang, G. Feng, and D. Cheng, "Simultaneous stabilization of a set of nonlinear port-controlled Hamiltonian systems," *Automatica*, vol. 43, no. 3, pp. 403–415, 2007.
- [14] A. Wei and Y. Wang, "Adaptive parallel simultaneous stabilization of a set of uncertain port-controlled Hamiltonian systems subject to actuator saturation," *International Journal of Adaptive Control and Signal Processing*, vol. 28, pp. 1128–1144, 2014.
- [15] X. Mu and H. Liu, "Stabilization for a class of stochastic nonlinear systems via output feedback," *IEEE Transactions on Automatic Control*, vol. 53, no. 1, pp. 360–367, 2008.
- [16] W. Ren and J. Xiong, "Stability analysis of impulsive stochastic nonlinear systems," *IEEE Transactions on Automatic Control*, vol. 62, no. 9, pp. 4791–4797, 2017.
- [17] W. M. Haddad, T. Rajpurohit, and X. Jin, "Energy-based feedback control for stochastic port-controlled Hamiltonian systems," *Automatica*, vol. 97, pp. 134–142, 2018.
- [18] S. Satoh and K. Fujimoto, "Passivity based control of stochastic port-Hamiltonian systems," *IEEE Transactions on Automatic Control*, vol. 58, no. 5, pp. 1139–1153, 2013.
- [19] W. Sun and L. Peng, "Observer-based robust adaptive control for uncertain stochastic Hamiltonian systems with state and input delays," *Nonlinear Analysis: Modelling and Control*, vol. 4, no. 19, pp. 626–645, 2014.
- [20] W. Sun and L. Peng, "Robust adaptive control of uncertain stochastic Hamiltonian systems with time varying delay," *Asian Journal of Control*, vol. 18, no. 2, pp. 642–651, 2016.
- [21] B. Fu, S. Li, L. Guo, J. Yang, and Q. Lan, "Finite-time stabilization of port-controlled Hamiltonian systems with nonvanishing disturbances," *Transactions of the Institute of Measurement and Control*, vol. 40, no. 10, pp. 2973–2981, 2018.
- [22] J. Hu, G. Sui, X. Lv, and X. Li, "Fixed-time control of delayed neural networks with impulsive perturbations," *Nonlinear Analysis: Modelling and Control*, vol. 23, no. 6, pp. 904–920, 2018.
- [23] M.-M. Jiang, X.-J. Xie, and K. Zhang, "Finite-time stabilization of stochastic high-order nonlinear systems with FT-SISS inverse dynamics," *IEEE Transactions on Automatic Control*, vol. 64, no. 1, pp. 313–320, 2019.
- [24] X. Li, X. Yang, and S. Song, "Lyapunov conditions for finite-time stability of time-varying time-delay systems," *Automatica*, vol. 103, pp. 135–140, 2019.
- [25] X. Lu, X. Zhang, and L. Sun, "Finite-time  $H_\infty$  control for nonlinear discrete Hamiltonian descriptor systems," *Journal of the Franklin Institute*, vol. 354, no. 14, pp. 6138–6151, 2017.
- [26] H. Ren, G. Zong, and T. Li, "Event-triggered finite-time control for networked switched linear systems with asynchronous switching," *IEEE Transactions on Systems, Man, and Cybernetics: Systems*, vol. 48, no. 11, pp. 1874–1884, 2018.
- [27] Z. Wang, A. Wei, G. Zong et al., "Finite-time stabilization and  $H_\infty$  control for a class of switched nonlinear port-controlled Hamiltonian systems subject to actuator saturation," *Journal of the Franklin Institute*, 2019.
- [28] R. Yang and Y. Wang, "Finite-time stability analysis and  $H_\infty$  control for a class of nonlinear time-delay Hamiltonian systems," *Automatica*, vol. 49, pp. 390–401, 2013.
- [29] G. Zong and H. Ren, "Guaranteed cost finite-time control for semi-Markov jump systems with event-triggered scheme and quantization input," *International Journal of Robust and Nonlinear Control*, vol. 29, no. 15, pp. 5251–5273, 2019.
- [30] Y. Chen, Z. Wang, Y. Yuan, and P. Date, "Distributed  $\mathcal{H}_\infty$  filtering for switched stochastic delayed systems over sensor networks with fading measurements," *IEEE Transactions on Cybernetics*, vol. 50, no. 1, pp. 2–14, 2020.
- [31] X. Li, D. O'Regan, and H. Akca, "Global exponential stabilization of impulsive neural networks with unbounded continuously distributed delays," *IMA Journal of Applied Mathematics*, vol. 80, no. 1, pp. 85–99, 2015.
- [32] Y. Li, H. Li, and W. Sun, "Event-triggered control for robust set stabilization of logical control networks," *Automatica*, vol. 95, pp. 556–560, 2018.
- [33] Q. Liu, W. Chen, Z. Wang, and L. Qiu, "Stabilization of MIMO systems over multiple independent and memoryless fading noisy channels," *IEEE Transactions on Automatic Control*, vol. 64, no. 4, pp. 1581–1594, 2019.
- [34] Q. Liu, Z. Wang, X. He, and D. H. Zhou, "Event-based distributed filtering with stochastic measurement fading," *IEEE Transactions on Industrial Informatics*, vol. 11, no. 6, pp. 1643–1652, 2015.
- [35] L. Su and G. Chesi, "On the design of output feedback controllers for LTI systems over fading channels," *IEEE Transactions on Automatic Control*, vol. 63, no. 5, pp. 1503–1508, 2018.

- [36] W. Sun, M. Qiu, M. Qiu, and X. Lv, "H  $\infty$  filter design for a class of delayed Hamiltonian systems with fading channel and sensor saturation," *AIMS Mathematics*, vol. 5, no. 4, pp. 2909–2922, 2020.
- [37] C. Tan, H. Zhang, and W. Wong, "Delay-dependent algebraic Riccati equation to stabilization of networked control systems: continuous-time case," *IEEE Transactions on Cybernetics*, vol. 48, no. 10, pp. 2783–2794, 2018.
- [38] Z. Yan, S. Zhong, and X. Liu, "Finite-time  $H_2/H_\infty$  control for linear Itô stochastic systems with  $(x, u, v)$  dependent noise," *Complexity*, vol. 2018, p. 13, Article ID 1936021, 2018.
- [39] X. Mao, *Stochastic Differential Equation and Applications*, Horwood Publishing, Chichester, UK, 2nd edition, 2007.



## Research Article

# Adaptive Fuzzy Fast Finite-Time Tracking Control for Nonlinear Systems in Pure-Feedback Form with Unknown Disturbance

Ke Xu,<sup>1</sup> Huanqing Wang ,<sup>1</sup> Xiaoping Liu ,<sup>2</sup> and Ming Chen<sup>3</sup>

<sup>1</sup>School of Mathematics and Physics, Bohai University, Jinzhou 121000, China

<sup>2</sup>Faculty of Engineering, Lakehead University, Thunder Bay, ON, Canada P7B 5E1

<sup>3</sup>School of Electronic and Information Engineering, University of Science and Technology Liaoning, Anshan, Liaoning, China

Correspondence should be addressed to Huanqing Wang; [ndwhq@163.com](mailto:ndwhq@163.com)

Received 15 June 2020; Accepted 1 August 2020; Published 25 September 2020

Guest Editor: Xiaodi Li

Copyright © 2020 Ke Xu et al. This is an open access article distributed under the Creative Commons Attribution License, which permits unrestricted use, distribution, and reproduction in any medium, provided the original work is properly cited.

In this paper, based on the fast finite-time stability theorem, an adaptive fuzzy control problem is considered for a class of nonlinear systems in pure-feedback form with unknown disturbance. In the controller design process, the mean value theorem is applied to address the nonaffine structure of the pure-feedback plant, the universal approximation capability of the fuzzy logic system (FLS) is utilized to compensate the unknown uncertainties, and the adaptive backstepping technique is used to design the controller model. Combined with the selection of the appropriate Lyapunov function at each step, a fuzzy-based adaptive tracking control scheme is proposed, which ensures that all signals in the closed-loop system are bounded and tracking error converges to a small neighborhood of the origin in fast finite-time. Finally, simulation results illustrate the validity of the proposed approach.

## 1. Introduction

During the recent years, the topics related to the field of nonlinear control have attracted a lot of attention [1–3]. Many approaches for controller design have been investigated, such as backstepping control, dynamic surface control, adaptive control, and so on. Among them, the adaptive control combined with the backstepping technique has provided a systematic framework model-based for control design. The adaptive backstepping control method solves the control design problem for nonlinear systems with unmatched conditions and uncertain parameters and ensures the stability of the closed-loop system successfully. Besides, it supplies an approach which can achieve the transient performance of the systems better by tuning design parameters. Until now, it has already become one of the popular control methods for nonlinear systems in [4–7]. In [8], an adaptive tracking control scheme was proposed for nonlinear strict-feedback systems with additive disturbances. In [9], the authors focused on the position control for a gear transmission servo system by using the backstepping technique. In [10], an adaptive controller was designed via backstepping

for nonlinear systems with quantized states. In [11], the adaptive backstepping control approach was developed for a class of stochastic cascade nonlinear time-delay systems.

Despite the adaptive backstepping control method having a few merits, there is a need for large-enough gains to suppress uncertainties, which will degrade control performances. It is not feasible for a controlled system with unknown nonlinear functions to use this method alone. Then, the fuzzy logic system (FLS) proposed by Wang and Mendel [12] and the neural network (NN) proposed by Polycarpou [13] have solved this problem well. Because of their universal approximation capabilities, they have become a set of powerful tools to compensate the unknown nonlinear functions of closed-loop systems. During the past decades, many scholars have obtained a lot of meaningful results by using FLSs and NNs combined with the adaptive backstepping technique in [14–26]. An adaptive NN-based fault-tolerant controller for the nonlinear system was investigated in [27]. Combining the adaptive backstepping technique with FLSs and NNs, several interesting control strategies were designed for uncertain stochastic nonlinear systems in [28, 29]. In [30], the authors presented a NNs-based robust

adaptive tracking control scheme for hexacopter UAVs. In [31], an adaptive fuzzy-based event-triggered controller was considered for strict-feedback nonlinear systems.

Although the fuzzy-based or NNs-based adaptive backstepping control approaches have made great progress, the existing literatures are restricted to the strict-feedback nonlinear systems, and only few results are available about the control of nonlinear systems in pure-feedback form. Different from the strict-feedback nonlinear systems, pure-feedback nonlinear systems possess nonaffine property. It means that there are not state variables to be used as virtual control signals and the actual control input in the pure-feedback form. Therefore, it is more hard and challenging to address the problems of controller design and stability analysis in the pure-feedback systems. In [32, 33], the authors presented the adaptive neural control for nonlinear pure-feedback systems. A fuzzy-based adaptive controller was designed for pure-feedback nonlinear systems in [34]. The control schemes were proposed for pure-feedback nonlinear systems with unknown uncertainties in [35, 36], which were designed by combining dynamic surface control with adaptive backstepping algorithm.

It is worth pointing out that the abovementioned literatures are developed on the basis of the Lyapunov asymptotically stability theorem. However, in practical applications, the finite-time control method has lots of advantages such as higher tracking precision, better robustness, and the ability to achieve systems transient performance faster. Recently, plenty of meaningful research results have been produced about the finite-time control problem in [37–42]. Based on the finite-time fault-tolerant control, a new control approach was introduced for robot manipulators by utilizing time-delay estimation in [43]. The adaptive finite-time control problem was addressed for a class of nonlinear systems with the actuator faults in [44]. In [45], the authors designed an adaptive decentralized controller for time-varying output-constrained nonlinear large-scale systems in finite-time. The Lyapunov theorem of finite-time stability was proposed for the first time in [46]. Then, in order to obtain the faster convergence rate, the fast finite-time stability was introduced in [47]. However, compared with the asymptotic control design process, the procedure of adaptive finite-time or fast finite-time controller design is more complex for the nonlinear strict-feedback systems. Furthermore, it is a difficult but meaningful unsolved issue to develop an adaptive fuzzy fast finite-time tracking control scheme for nonlinear systems in pure-feedback form. It is the main motivation of this paper.

Inspired by the aforementioned observations, in this paper, the problem of adaptive fuzzy fast finite-time tracking control is considered for a class of nonlinear systems in pure-feedback form with unknown disturbance. During the controller design, the mean value theorem is applied to deal with the nonaffine problem of the pure-feedback systems, FLSs are adopted to approximate packaged unknown nonlinearities, and an improved adaptive fuzzy fast finite-

time controller is designed via the backstepping technique. The stability of the closed-loop systems is guaranteed in fast finite-time. To sum up, the main contributions in this paper are listed below:

- (1) The fast finite-time theorem is extended to pure-feedback systems for the first time. Also, a fuzzy-based adaptive fast finite-time tracking control scheme for nonlinear systems in pure-feedback form with unknown disturbance is proposed for the first time, too.
- (2) Combined the traditional adaptive backstepping technique with the characteristics of the radial basis function of fuzzy logic systems, by applying the mean value theorem and the fast finite-time theory, the system structure is simplified so that reduces complexity of the controller design.

The remaining parts are organized as follows. Section 2 introduces problem formulation and preliminaries. Section 3 presents the controller design procedure in detail and stability analysis. Section 4 provides simulation results. Section 5 concludes this research.

## 2. Problem Formulation and Preliminaries

*2.1. System Descriptions and Control Problem.* Consider a class of nonlinear pure-feedback systems described as follows:

$$\begin{cases} \dot{x}_i(t) = f_i(\bar{x}_i, x_{i+1}), & 1 \leq i \leq n-1, \\ \dot{x}_n(t) = f_n(\bar{x}_n, u) + d(t), \\ y(t) = x_1(t), \end{cases} \quad (1)$$

in which  $\bar{x}_i(t) = [x_1(t), \dots, x_i(t)]^T \in R^i$ ,  $i = 1, \dots, n-1$  is the vector of the states and  $\bar{x}_n(t) = [x_n(t), \dots, x_n(t)]^T \in R^n$ ;  $y(t) \in R$  represents the system output;  $u \in R$  denotes input signal;  $d(t)$  is a bounded disturbance; and  $f_i(\cdot)$  and  $f_n(\cdot)$  represent unknown smooth functions.

Using the mean value theorem [48], we can express  $f_i(\cdot)$  and  $f_n(\cdot)$  in (1) as follows:

$$f_i(\bar{x}_i, x_{i+1}) = f_i(\bar{x}_i, x_{i+1}^0) + \frac{\partial f_i(\bar{x}_i, x_{i+1})}{\partial x_{i+1}} \Big|_{x_{i+1}=x_{i+1}^{\delta_i}} \times (x_{i+1} - x_{i+1}^0), \quad 1 \leq i \leq n-1, \quad (2)$$

$$f_n(\bar{x}_n, u) = f_n(\bar{x}_n, u^0) + \frac{\partial f_n(\bar{x}_n, u)}{\partial u} \Big|_{u=u^{\delta_n}} \times (u - u^0), \quad (3)$$

where  $x_{i+1}^{\delta_i} = \delta_i x_{i+1} + (1 - \delta_i) x_{i+1}^0$ , with  $0 < \delta_i < 1$ , and  $u^{\delta_n} = \delta_n u + (1 - \delta_n) u^0$ , with  $0 < \delta_n < 1$ .

For convenience of writing, we define  $h_i(\bar{x}_i, x_{i+1}^{\delta_i}) = (\partial f_i(\bar{x}_i, x_{i+1}) / (\partial x_{i+1}))|_{x_{i+1}=x_{i+1}^{\delta_i}}$  and  $h_n(\bar{x}_n, u^{\delta_n}) = (\partial f_n(\bar{x}_n, u) / (\partial u))|_{u=u^{\delta_n}}$ , which are unknown nonlinear functions. Then, substituting (2) with (3) into (4) and choosing  $x_{i+1}^0 = 0$ ,  $u^0 = 0$ , we get

$$\begin{cases} \dot{x}_i(t) = f_i(\bar{x}_i, 0) + h_i(\bar{x}_i, x_{i+1}^{\delta_i})x_{i+1}, \\ \dot{x}_n(t) = f_n(\bar{x}_n, 0) + h_n(\bar{x}_n, u^{\delta_n})u + d(t), \\ y(t) = x_1(t). \end{cases} \quad (4)$$

$$\left( \sum_{k=1}^n |x_k| \right)^\phi \leq \sum_{k=1}^n |x_k|^\phi. \quad (8)$$

The objective of this paper is to design a fuzzy-based fast finite-time tracking controller such that all signals in the closed-loop system are bounded and the output  $y$  can follow the specified desired trajectory  $y_d$ .

Throughout this paper, the following assumptions and lemmas are imposed on system (4).

*Assumption 1* (see [49]). The desired trajectory signal  $y_d$  and that up to the  $n$ th derivative are smooth and bounded.

*Assumption 2* (see [33]). There exists an unknown bounded constant  $d^*$  such that  $|d(t)| \leq d^*$ .

*Assumption 3* (see [50]). The function  $h_i(\bar{x}_i, x_{i+1}^{\delta_i})$  satisfies  $0 < \underline{h}_i \leq |h_i(\cdot)| \leq \bar{h}_i < \infty$ , for  $i = 1, \dots, n$ , where  $\underline{h}_i$  and  $\bar{h}_i$  are unknown constants.

*Remark 1.* According to Assumption 3, it is reasonable that the unknown smooth function  $h_i$  is strictly either positive or negative. Without losing generality, we assume that  $h_i > 0$ . For facilitating the actual controller design,  $\underline{h}_n$  is known.

**Lemma 1** (see [51]). Consider the system  $\dot{x} = f(x)$ , if there exists continuous function  $V(x)$ ,  $\mu_1 > 0, \mu_2 > 0, 0 < \gamma < 1$ , and  $0 < \eta < \infty$ , so that  $\dot{V}(x) \leq -\mu_1 V(x) - \mu_2 V^\gamma(x) + \eta$ , then the trajectory of system  $\dot{x} = f(x)$  is practical finite-time stable, and the residual set of the solution of system  $\dot{x} = f(x)$  is given by

$$\lim_{t \rightarrow T_r} V(x) \leq \min \left\{ \frac{\eta}{(1-\theta_0)\mu_1}, \left( \frac{\eta}{(1-\theta_0)\mu_2} \right)^{1/\gamma} \right\}, \quad (5)$$

where  $\theta_0$  satisfies  $0 < \theta_0 < 1$ . The settling time is bounded as

$$\begin{aligned} T_r \leq \max \left\{ t_0 + \frac{1}{\theta_0 \mu_1 (1-\gamma)} \ln \frac{\theta_0 \mu_1 V^{1-\gamma}(t_0) + \mu_2}{\mu_2}, t_0 \right. \\ \left. + \frac{1}{\mu_1 (1-\gamma)} \ln \frac{\mu_1 V^{1-\gamma}(t_0) + \theta_0 \mu_2}{\theta_0 \mu_2} \right\}. \end{aligned} \quad (6)$$

*Remark 2.* For the convenience of derivation and the proof of the process in this paper, the parameter in the aforementioned inequality is chosen as  $\gamma = 3/4$ .

**Lemma 2** (see [52]). For any constant  $\varepsilon > 0$  and variable  $z \in R$ , we have

$$0 \leq |z| - \frac{z^2}{\sqrt{z^2 + \varepsilon^2}} < \varepsilon. \quad (7)$$

**Lemma 3** (see [53]). For  $x_i \in R, i = 1, \dots, n$  and  $\phi \in [0, 1]$ , we have

**Lemma 4** (see [54]). For  $o_1 > 0, o_2 > 0, o_3 > 0, \gamma_1 \geq 0, \gamma_2 \geq 0, \gamma_3 \geq 0$ , the following inequality holds:

$$\begin{aligned} \gamma_1^{o_1} \gamma_2^{o_2} \gamma_3 \leq o_3 \gamma_1^{o_1+o_2} + \frac{o_2}{o_1 + o_2} \\ \times \left[ \frac{o_1}{o_3(o_1 + o_2)} \right]^{o_1/o_2} \gamma_2^{o_1+o_2} \gamma_3^{(o_1+o_2/o_2)}. \end{aligned} \quad (9)$$

**2.2. Fuzzy Logic Systems.** An FLS is composed of the knowledge base, the fuzzifier, the fuzzy inference engine, and the defuzzifier. The knowledge base comprises a collection of fuzzy If-Then rules of the following form:

$R^l$ : If  $Z_1$  is  $F_1^l, \dots$ , and  $Z_n$  is  $F_n^l$ , then  $\omega$  is  $G^l, l = 1, \dots, N$

Where  $Z = [Z_1, \dots, Z_n]^T \in R$  and  $\omega$  represent the FLS input and output,  $F_i^l$  and  $G^l$  are fuzzy sets, their fuzzy membership functions are  $\mu_{F_i^l}(Z_i)$  and  $\mu_{G^l}(\omega)$ , and  $N$  is rule number of If-Then.  $\omega$  can be expressed as

$$\omega(Z) = \sum_{l=1}^N \bar{W}_j \frac{\prod_{i=1}^n \mu_{F_i^l}(Z_i)}{\sum_{l=1}^N \left[ \prod_{i=1}^n \mu_{F_i^l}(Z_i) \right]}, \quad (10)$$

where  $\bar{W}_j = \max_{\omega \in R} \mu_{G^l}(\omega)$ .  
Let

$$S_j(Z) = \frac{\prod_{i=1}^n \mu_{F_i^l}(Z_i)}{\sum_{l=1}^N \left[ \prod_{i=1}^n \mu_{F_i^l}(Z_i) \right]}. \quad (11)$$

Denoting  $W = [\bar{W}_1, \dots, \bar{W}_N]^T$  and  $S(Z) = [S_1(Z), \dots, S_N(Z)]^T$ , the FLS can be reformulated as

$$\omega(Z) = W^T S(Z). \quad (12)$$

**Lemma 5** (see [12]). For a continuous function  $f(Z)$  defined on a compact set  $\Omega$  and  $\forall \varepsilon > 0$ , there exists an FLS (12) satisfying

$$\sup_{Z \in \Omega} |f(Z) - W^T S(Z)| \leq \varepsilon. \quad (13)$$

### 3. Adaptive Fuzzy Controller Design

In this section, a fuzzy-based adaptive control scheme is proposed by using the backstepping technique and FLSs for system (4). The design process of the controller contains  $n$  steps based on the following change of coordinates:

$$\begin{cases} z_1 = x_1 - y_d, \\ z_i = x_i - \alpha_{i-1}, \quad i = 2, \dots, n, \end{cases} \quad (14)$$

where  $\alpha_{i-1}$  is an intermediate control which will be developed for the corresponding  $i$ -subsystem combined with choosing the proper Lyapunov functions. The actual control law  $u$  will be constructed at Step  $n$  to cope with the stability problem of the closed-loop system and the unknown disturbance.

In each step, we apply an FLS  $W_i^T S_i(Z_i)$  to approximate the unknown nonlinearities and define an uncertain parameter  $\theta_i$ ,  $\hat{\theta}_i$  is the estimate of  $\theta_i$ , and  $\tilde{\theta}_i = \theta_i - \hat{\theta}_i$ . For the sake of simplicity,  $h_i(\bar{x}_i, x_{i+1}^{\delta_i})$  and  $h_n(\bar{x}_n, u^{\delta_n})$  will be abbreviated to  $h_i$  for  $i = 1, \dots, n-1$  and  $h_n$ .

Step 1: according to  $z_1 = x_1 - y_d$ , and  $x_2 = z_2 + \alpha_1$ , it follows from (14) that

$$\begin{aligned} \dot{z}_1 &= \dot{x}_1 - \dot{y}_d, \\ &= f_1 + h_1 x_2 - \dot{y}_d, \\ &= f_1 + h_1(z_2 + \alpha_1) - \dot{y}_d, \\ &= f_1 + h_1 z_2 + h_1 \alpha_1 - \dot{y}_d. \end{aligned} \quad (15)$$

Consider Lyapunov function  $V_1$  as

$$V_1 = \frac{1}{2} z_1^2 + \frac{h_1' \tilde{\theta}_1^2}{2r_1}, \quad (16)$$

where  $h_1' = \sqrt{h_1}$  and the design parameter  $r_1 > 0$ .

Then, we get

$$\begin{aligned} \dot{V}_1 &= z_1 \dot{z}_1 - \frac{h_1' \tilde{\theta}_1}{r_1} \dot{\tilde{\theta}}_1, \\ &= z_1 (h_1 z_2 + h_1 \alpha_1 + \Lambda_1) - \frac{z_1^2}{2} - \frac{h_1' \tilde{\theta}_1}{r_1} \dot{\tilde{\theta}}_1, \end{aligned} \quad (17)$$

where  $\Lambda_1 = f_1 - \dot{y}_d + (z_1/2)$  is an unknown smooth function, and it can be approximated by FLS such that

$$\Lambda_1(Z_1) = W_1^T S_1(Z_1) + \delta_1(Z_1), \quad |\delta_1(Z_1)| \leq \varepsilon_1, \quad (18)$$

where  $Z_1 = [x_1, y_d, \dot{y}_d]^T$ ,  $\delta_1(Z_1)$  is the estimate error. By using Lemma 5 and the completion of squares, one has

$$\begin{aligned} z_1 \Lambda_1(Z_1) &= z_1 (W_1^T S_1(Z_1) + \delta_1(Z_1)) \\ &\leq |z_1| (\|W_1\| \|S_1(Z_1)\| + \varepsilon_1) \\ &\leq \frac{h_1'}{2a_1^2} z_1^2 \theta_1 S_1^T S_1 + \frac{a_1^2}{2} + \frac{z_1^2}{2} + \frac{\varepsilon_1^2}{2}, \end{aligned} \quad (19)$$

where  $\theta_1 = \|W_1\|^2/h_1'$  and the constant  $a_1 > 0$ .

Substituting (19) into (17) yields

$$\dot{V}_1 \leq z_1 h_1 z_2 + z_1 h_1 \alpha_1 + \frac{a_1^2}{2} + \frac{\varepsilon_1^2}{2} + \frac{h_1'}{2a_1^2} z_1^2 \theta_1 S_1^T S_1 - \frac{h_1'}{r_1} \tilde{\theta}_1 \dot{\tilde{\theta}}_1. \quad (20)$$

The virtual control law  $\alpha_1$  is designed as follows:

$$\alpha_1 = -\frac{z_1 \check{\alpha}_1}{\sqrt{z_1^2 \check{\alpha}_1^2 + \varepsilon_1^2}}. \quad (21)$$

Combining with Lemma 2, one has

$$\begin{aligned} z_1 h_1 \alpha_1 &\leq -\frac{h_1 z_1^2 \check{\alpha}_1^2}{\sqrt{z_1^2 \check{\alpha}_1^2 + \varepsilon_1^2}} \\ &\leq \varepsilon_1 - z_1 \check{\alpha}_1 h_1' \end{aligned} \quad (22)$$

Then, choose  $\check{\alpha}_1$  and adaption law  $\dot{\tilde{\theta}}_1$  as

$$\check{\alpha}_1 = \frac{1}{2} K_{11} z_1 + K_{12} \left(\frac{1}{2}\right)^{3/4} (z_1^2)^{1/4} + \frac{1}{2a_1^2} z_1 \hat{\theta}_1 S_1^T S_1, \quad (23)$$

$$\dot{\tilde{\theta}}_1 = \frac{r_1}{2a_1^2} z_1^2 S_1^T S_1 - \varepsilon_1 \hat{\theta}_1, \quad (24)$$

where the design parameters  $a_1, K_{11}, K_{12} > 0$ .

Substituting (21)–(24) into (20) yields

$$\dot{V}_1 \leq -\bar{K}_{11} \left(\frac{z_1^2}{2}\right) - \bar{K}_{12} \left(\frac{z_1^2}{2}\right)^{3/4} + z_1 h_1 z_2 + \frac{h_1' \varepsilon_1 \tilde{\theta}_1 \hat{\theta}_1}{r_1} + \sigma_1, \quad (25)$$

where  $\bar{K}_{11} = K_{11} h_1'$ ,  $\bar{K}_{12} = K_{12} h_1'$ , and  $\sigma_1 = (a_1^2/2) + (\varepsilon_1^2/2) + \varepsilon_1 > 0$ .

Step  $i$  ( $2 \leq i \leq n-1$ ): utilizing the coordinate transformation in (14), the derivative of  $z_i$  is

$$\begin{aligned} \dot{z}_i &= \dot{x}_i - \dot{\alpha}_{i-1}, \\ &= f_i + h_i x_{i+1} - \dot{\alpha}_{i-1}, \\ &= f_i + h_i (z_{i+1} + \alpha_i) - \dot{\alpha}_{i-1}, \\ &= f_i + h_i z_{i+1} + h_i \alpha_i - \dot{\alpha}_{i-1}, \end{aligned} \quad (26)$$

where  $\dot{\alpha}_{i-1} = \sum_{j=1}^{i-1} (\partial \alpha_{i-1} / \partial x_j) (f_j + h_j x_{j+1}) + \sum_{j=1}^{i-1} (\partial \alpha_{i-1} / \partial \hat{\theta}_j) \dot{\hat{\theta}}_j + \sum_{j=0}^{i-1} (\partial \alpha_{i-1} / \partial y_d^{(j)}) y_d^{(j+1)}$ .

Select a Lyapunov function as

$$V_i = V_{i-1} + \frac{1}{2}z_i^2 + \frac{h'_i \tilde{\theta}_i^2}{2r_i}, \quad (27)$$

where  $h'_i = \sqrt{\tilde{h}_i}$  and the parameter  $r_i > 0$ .  
Next, the derivative of  $V_i$  is

$$\begin{aligned} \dot{V}_i &= \dot{V}_{i-1} + z_i \dot{z}_i - \frac{h'_i \tilde{\theta}_i \dot{\tilde{\theta}}_i}{r_i}, \\ &= - \sum_{j=1}^{i-1} \bar{K}_{j1} \left( \frac{z_j^2}{2} \right) - \sum_{j=1}^{i-1} \bar{K}_{j2} \left( \frac{z_j^2}{2} \right)^{3/4} \\ &\quad + \sum_{j=1}^{i-1} \frac{h'_j \varepsilon_j \tilde{\theta}_j \dot{\tilde{\theta}}_j}{r_j} + z_i (h_i z_{i+1} + h_i \alpha_i + \Lambda_i) \\ &\quad - \frac{z_i^2}{2} - \frac{h'_i \tilde{\theta}_i \dot{\tilde{\theta}}_i}{r_i} + \sigma_{i-1}, \end{aligned} \quad (28)$$

where  $\Lambda_i = f_i - \dot{\alpha}_{i-1} + z_{i-1} h_{i-1} + (z_i/2)$  is an unknown smooth function, and we adopt an FLS to approximate it such that

$$\Lambda_i(Z_i) = W_i^T S_i(Z_i) + \delta_i(Z_i), |\delta_i(Z_i)| \leq \varepsilon_i. \quad (29)$$

Combing Lemma 5 with the completion of squares, the following result holds:

$$\begin{aligned} z_i \Lambda_i(Z_i) &= z_i (W_i^T S_i(Z_i) + \delta_i(Z_i)) \\ &\leq |z_i| (\|W_i\| \|S_i(Z_i)\| + \varepsilon_i) \\ &\leq \frac{h'_i}{2a_i^2} z_i^2 \theta_i S_i^T S_i + \frac{a_i^2}{2} + \frac{z_i^2}{2} + \frac{\varepsilon_i^2}{2}, \end{aligned} \quad (30)$$

where  $\theta_i = \|W_i\|^2/h'_i$  and  $a_i > 0$  is a constant.  
Furthermore, substituting (30) into (28) yields

$$\begin{aligned} \dot{V}_i &\leq - \sum_{j=1}^{i-1} \bar{K}_{j1} \left( \frac{z_j^2}{2} \right) - \sum_{j=1}^{i-1} \bar{K}_{j2} \left( \frac{z_j^2}{2} \right)^{3/4} \\ &\quad + \sum_{j=1}^{i-1} \frac{h'_j \varepsilon_j \tilde{\theta}_j \dot{\tilde{\theta}}_j}{r_j} \\ &\quad - \frac{h'_i \tilde{\theta}_i \dot{\tilde{\theta}}_i}{r_i} + z_i h_i z_{i+1} + z_i h_i \alpha_i + \sigma_{i-1} \\ &\quad + \frac{h'_i}{2a_i^2} z_i^2 \theta_i S_i^T S_i + \frac{a_i^2}{2} + \frac{\varepsilon_i^2}{2}. \end{aligned} \quad (31)$$

The virtual control law  $\alpha_i$  is chosen as follows:

$$\alpha_i = - \frac{z_i \check{\alpha}_i^2}{\sqrt{z_i^2 \check{\alpha}_i^2 + \varepsilon_i^2}} \quad (32)$$

By using Lemma 2, we have

$$\begin{aligned} z_i h_i \alpha_i &\leq - \frac{h_i z_i^2 \check{\alpha}_i^2}{\sqrt{z_i^2 \check{\alpha}_i^2 + \varepsilon_i^2}} \\ &\leq \varepsilon_i - z_i \check{\alpha}_i h'_i \end{aligned} \quad (33)$$

Next,  $\check{\alpha}_i$  and  $\dot{\tilde{\theta}}_i$  are chosen as

$$\check{\alpha}_i = \frac{1}{2} K_{i1} z_i + K_{i2} \left( \frac{1}{2} \right)^{3/4} (z_i^2)^{1/4} + \frac{1}{2a_i^2} z_i \hat{\theta}_i S_i^T S_i, \quad (34)$$

$$\dot{\tilde{\theta}}_i = \frac{r_i}{2a_i^2} z_i^2 S_i^T S_i - \varepsilon_i \hat{\theta}_i, \quad (35)$$

where  $a_i, K_{i1}, K_{i2}$  are positive design parameters.

By substituting (33)–(35) into (31), the following result holds:

$$\begin{aligned} \dot{V}_i &\leq - \sum_{j=1}^i \bar{K}_{j1} \left( \frac{z_j^2}{2} \right) - \sum_{j=1}^i \bar{K}_{j2} \left( \frac{z_j^2}{2} \right)^{3/4} \\ &\quad + \sum_{j=1}^i \frac{h'_j \varepsilon_j \tilde{\theta}_j \dot{\tilde{\theta}}_j}{r_j} + z_i h_i z_{i+1} + \sigma_i, \end{aligned} \quad (36)$$

where  $\sum_{j=1}^i \bar{K}_{j1} = \sum_{j=1}^i K_{j1} h'_j$ ,  $\sum_{j=1}^i \bar{K}_{j2} = \sum_{j=1}^i K_{j2} h'_j$ , and  $\sigma_i = \sigma_{i-1} + (a_i^2/2) + (\varepsilon_i^2/2) + \varepsilon_i > 0$ .

Step  $n$ : the control input  $u$  will be designed in this step.  
Since  $z_n = x_n - \alpha_{n-1}$  in (14), the derivative of  $z_n$  is

$$\begin{aligned} \dot{z}_n &= \dot{x}_n - \dot{\alpha}_{n-1}, \\ &= f_n + h_n u + d(t) - \dot{\alpha}_{n-1}. \end{aligned} \quad (37)$$

Consider the following Lyapunov function:

$$V_n = V_{n-1} + \frac{1}{2} z_n^2 + \frac{h'_n \tilde{\theta}_n^2}{2r_n} + \frac{1}{2r_d} \tilde{d}^2, \quad (38)$$

where  $h'_n = \sqrt{\tilde{h}_n}$ ,  $\tilde{d} = d^* - \hat{d}$ ,  $\hat{d}$  is the estimate of the disturbance  $d^*$ , and  $r_n$  and  $r_d$  are positive design parameters.

Then, the time derivative of  $V_n$  is expressed as

$$\begin{aligned}
\dot{V}_n &= \dot{V}_{n-1} + z_n \dot{z}_n - \frac{h'_n \tilde{\theta}_n \dot{\hat{\theta}}_n}{r_n} - \frac{1}{r_d} \tilde{d} \dot{\hat{d}}, \\
&= - \sum_{j=1}^{n-1} \bar{K}_{j1} \left( \frac{z_j^2}{2} \right) - \sum_{j=1}^{n-1} \bar{K}_{j2} \left( \frac{z_j^2}{2} \right)^{3/4} + \sum_{j=1}^{n-1} \frac{h'_j \varepsilon_j \tilde{\theta}_j \hat{\theta}_j}{r_j} \\
&\quad + z_n (h_n u + \Lambda_n) - \frac{z_n^2}{2} + z_n d(t) \\
&\quad - \frac{h'_n \tilde{\theta}_n \dot{\hat{\theta}}_n}{r_n} + \frac{1}{r_d} \tilde{d} \dot{\hat{d}} + \sigma_{n-1},
\end{aligned} \tag{39}$$

where  $\Lambda_n = f_n - \dot{\alpha}_{n-1} + z_{n-1} h_{n-1} + (z_n/2)$  is an unknown smooth function, and it can be approximated by FLS such that

$$\Lambda_n(Z_n) = W_n^T S_n(Z_n) + \delta_n(Z_n), \quad |\delta_n(Z_n)| \leq \varepsilon_n. \tag{40}$$

With the help of the completion of squares and Lemma 5, one has

$$\begin{aligned}
z_n \Lambda_n(Z_n) &= z_n (W_n^T S_n(Z_n) + \delta_n(Z_n)) \\
&\leq |z_n| (\|W_n\| \|S_n(Z_n)\| + \varepsilon_n) \\
&\leq \frac{h'_n}{2a_n^2} z_n^2 \theta_n S_n^T S_n + \frac{a_n^2}{2} + \frac{z_n^2}{2} + \frac{\varepsilon_n^2}{2},
\end{aligned} \tag{41}$$

where  $\theta_n = \|W_n\|^2/h'_n$  and  $a_n > 0$  is a constant.

Furthermore, based on Assumption 2, (39) becomes

$$\begin{aligned}
\dot{V}_n &\leq - \sum_{j=1}^{n-1} \bar{K}_{j1} \left( \frac{z_j^2}{2} \right) - \sum_{j=1}^{n-1} \bar{K}_{j2} \left( \frac{z_j^2}{2} \right)^{3/4} + \sum_{j=1}^{n-1} \frac{h'_j \varepsilon_j \tilde{\theta}_j \hat{\theta}_j}{r_j} \\
&\quad - \frac{h'_n \tilde{\theta}_n \dot{\hat{\theta}}_n}{r_n} + z_n h_n u + \frac{h'_n}{2a_n^2} z_n^2 \theta_n S_n^T S_n \\
&\quad + \frac{a_n^2}{2} + \frac{\varepsilon_n^2}{2} + \sigma_{n-1} + |z_n| d^* - \frac{1}{r_d} \tilde{d} \dot{\hat{d}}.
\end{aligned} \tag{42}$$

Design the actual control signal  $u$

$$u = - \frac{z_n \tilde{\alpha}_n^2}{\sqrt{z_n^2 \tilde{\alpha}_n^2 + \varepsilon_n^2}} - \frac{\tanh(z_n/\omega) \hat{d}}{l_n}, \tag{43}$$

where  $\omega$  is a positive constant.

Combing (43) with Lemma 2, one has

$$\begin{aligned}
z_n h_n u &\leq - \frac{h_n z_n^2 \tilde{\alpha}_n^2}{\sqrt{z_n^2 \tilde{\alpha}_n^2 + \varepsilon_n^2}} - z_n \tanh\left(\frac{z_n}{\omega}\right) \hat{d} \\
&\leq \varepsilon_n - z_n \tilde{\alpha}_n h'_n - z_n \tanh\left(\frac{z_n}{\omega}\right) \hat{d}.
\end{aligned} \tag{44}$$

Then, choose  $\tilde{\alpha}_n$  and  $\dot{\hat{\theta}}_n$  as follows:

$$\tilde{\alpha}_n = \frac{1}{2} K_{n1} z_n + K_{n2} \left( \frac{1}{2} \right)^{3/4} (z_n^2)^{1/4} + \frac{1}{2a_n^2} z_n \hat{\theta}_n S_n^T S_n, \tag{45}$$

$$\dot{\hat{\theta}}_n = \frac{r_n}{2a_n^2} z_n^2 S_n^T S_n - \varepsilon_n \hat{\theta}_n, \tag{46}$$

where  $a_n, K_{n1}, K_{n2}$  are positive constants.

Combing (43)–(46),  $V_n$  can be rewritten as

$$\begin{aligned}
\dot{V}_n &\leq - \sum_{j=1}^{n-1} \bar{K}_{j1} \left( \frac{z_j^2}{2} \right) - \sum_{j=1}^{n-1} \bar{K}_{j2} \left( \frac{z_j^2}{2} \right)^{3/4} + \sum_{j=1}^{n-1} \frac{h'_j \varepsilon_j \tilde{\theta}_j \hat{\theta}_j}{r_j} \\
&\quad - \frac{1}{2} K_{n1} h'_n z_n^2 - K_{n2} h'_n \left( \frac{z_n^2}{2} \right)^{3/4} - z_n \tanh\left(\frac{z_n}{\omega}\right) (d^* - \tilde{d}) \\
&\quad + |z_n| d^* + \frac{a_n^2}{2} + \frac{\varepsilon_n^2}{2} + \sigma_{n-1} + \varepsilon_n - \frac{\tilde{d} \dot{\hat{d}}}{r_d}.
\end{aligned} \tag{47}$$

Utilizing the following property of the hyperbolic tangent function

$$0 \leq |z_n| - z_n \tanh\left(\frac{z_n}{\omega}\right) \leq 0.2785\omega, \tag{48}$$

we have

$$\begin{aligned}
\dot{V}_n &\leq - \sum_{j=1}^{n-1} \bar{K}_{j1} \left( \frac{z_j^2}{2} \right) - \sum_{j=1}^{n-1} \bar{K}_{j2} \left( \frac{z_j^2}{2} \right)^{3/4} + \sum_{j=1}^{n-1} \frac{h'_j \varepsilon_j \tilde{\theta}_j \hat{\theta}_j}{r_j} \\
&\quad - \frac{1}{2} K_{n1} h'_n z_n^2 - K_{n2} h'_n \left( \frac{z_n^2}{2} \right)^{3/4} + \tilde{d} \left( z_n \tanh\left(\frac{z_n}{\omega}\right) - \frac{\hat{d}}{r_d} \right) \\
&\quad + 0.2785\omega d^* + \frac{a_n^2}{2} + \frac{\varepsilon_n^2}{2} + \sigma_{n-1} + \varepsilon_n,
\end{aligned} \tag{49}$$

and  $\hat{d}$  can be constructed as

$$\dot{\hat{d}} = r_d \left[ z_n \tanh\left(\frac{z_n}{\omega}\right) - \sigma_d \hat{d} \right], \tag{50}$$

where  $\sigma_d$  is a positive constant.

By Young's inequality, the following inequality holds:

$$\begin{aligned}
\sigma_d \tilde{d} \hat{d} &= \sigma_d \tilde{d} (d^* - \tilde{d}) \\
&\leq - \frac{\sigma_d \tilde{d}^2}{2} + \frac{\sigma_d d^{*2}}{2}.
\end{aligned} \tag{51}$$

Substituting (50) and (51) into (49), it yields

$$\begin{aligned} \dot{V}_n \leq & - \sum_{j=1}^n \bar{K}_{j1} \left( \frac{z_j^2}{2} \right) - \sum_{j=1}^n \bar{K}_{j2} \left( \frac{z_j^2}{2} \right)^{3/4} \\ & + \sum_{j=1}^n \frac{h'_j \varepsilon_j \tilde{\theta}_j \hat{\theta}_j}{r_j} + 0.2785\omega d^* + \frac{\sigma_d d^{*2}}{2} - \frac{\sigma_d \tilde{d}^2}{2} + \sigma_n, \end{aligned} \quad (52)$$

where  $\sum_{j=1}^n \bar{K}_{j1} = \sum_{j=1}^n K_{j1} h'_j$ ,  $\sum_{j=1}^n \bar{K}_{j2} = \sum_{j=1}^n K_{j2} h'_j$ , and  $\sigma_n = \sigma_{n-1} + (a_n^2/2) + (\varepsilon_n^2/2) + \varepsilon_n > 0$ .

For  $\bar{\mu}_1 = \min(\bar{K}_{11}, \bar{K}_{21}, \dots, \bar{K}_{n1})$ ,  $\bar{\mu}_2 = \min(\bar{K}_{12}, \bar{K}_{22}, \dots, \bar{K}_{n2})$ , and Lemma 3, we have

$$- \sum_{j=1}^n \bar{K}_{j1} \left( \frac{z_j^2}{2} \right) \leq - \bar{\mu}_1 \sum_{j=1}^n \left( \frac{z_j^2}{2} \right) \leq - \bar{\mu}_1 \left( \sum_{j=1}^n \frac{z_j^2}{2} \right), \quad (53)$$

$$- \sum_{j=1}^n \bar{K}_{j2} \left( \frac{z_j^2}{2} \right)^{3/4} \leq - \bar{\mu}_2 \sum_{j=1}^n \left( \frac{z_j^2}{2} \right)^{3/4} \leq - \bar{\mu}_2 \left( \sum_{j=1}^n \frac{z_j^2}{2} \right)^{3/4}. \quad (54)$$

Furthermore, by applying Young's inequality, we obtain

$$\sum_{j=1}^n \frac{h'_j \varepsilon_j \tilde{\theta}_j \hat{\theta}_j}{r_j} \leq - \sum_{j=1}^n \frac{h'_j \varepsilon_j \tilde{\theta}_j^2}{2r_j} + \sum_{j=1}^n \frac{h'_j \varepsilon_j \theta_j^2}{2r_j}. \quad (55)$$

Substituting (53)–(55) into (52), one gets

$$\begin{aligned} \dot{V}_n \leq & - \bar{\mu}_1 \left( \sum_{j=1}^n \frac{z_j^2}{2} \right) - \bar{\mu}_2 \left( \sum_{j=1}^n \frac{z_j^2}{2} \right)^{3/4} - \sum_{j=1}^n \frac{h'_j \varepsilon_j \tilde{\theta}_j^2}{2r_j} \\ & + \sum_{j=1}^n \frac{h'_j \varepsilon_j \theta_j^2}{2r_j} - \left( \sum_{j=1}^n \frac{\tilde{\theta}_j^2}{2r_j} \right)^{3/4} + \left( \sum_{j=1}^n \frac{\tilde{\theta}_j^2}{2r_j} \right)^{3/4} \\ & - \left( \frac{\tilde{d}^2}{2r_d} \right)^{3/4} + \left( \frac{\tilde{d}^2}{2r_d} \right)^{3/4} - \frac{\sigma_d \tilde{d}^2}{2} \\ & + 0.2785\omega d^* + \frac{\sigma_d d^{*2}}{2} + \sigma_n. \end{aligned} \quad (56)$$

Using Lemma 4, for  $\alpha_1 = 1 - \alpha_2$ ,  $\alpha_2 = 3/4$ ,  $\alpha_3 = \alpha_1 \alpha_2^3$ ,  $\gamma_1 = 1$ ,  $\gamma_2 = \sum_{j=1}^n \tilde{\theta}_j^2 / 2r_j$ ,  $\gamma_3 = 1$ , the following inequality holds:

$$\left( \sum_{j=1}^n \frac{\tilde{\theta}_j^2}{2r_j} \right)^{3/4} \leq \alpha_3 + \sum_{j=1}^n \frac{\tilde{\theta}_j^2}{2r_j}. \quad (57)$$

Similarly, for  $\alpha_1 = 1 - \alpha_2$ ,  $\alpha_2 = 3/4$ ,  $\alpha_3 = \alpha_1 \alpha_2^3$ ,  $\gamma_1 = 1$ ,  $\gamma_2 = \tilde{d}^2 / 2r_d$ ,  $\gamma_3 = 1$ , one has

$$\left( \frac{\tilde{d}^2}{2r_d} \right)^{3/4} \leq \alpha_3 + \frac{\tilde{d}^2}{2r_d}. \quad (58)$$

Substituting (57) and (58) into (56), we get

$$\begin{aligned} \dot{V}_n \leq & - \bar{\mu}_1 \left( \sum_{j=1}^n \frac{z_j^2}{2} \right) - \bar{\mu}_2 \left( \sum_{j=1}^n \frac{z_j^2}{2} \right)^{3/4} - \left( \sum_{j=1}^n \frac{\tilde{\theta}_j^2}{2r_j} \right)^{3/4} \\ & - (h'_j \varepsilon_j - 1) \sum_{j=1}^n \frac{\tilde{\theta}_j^2}{2r_j} - \left( \frac{\tilde{d}^2}{2r_d} \right)^{3/4} - (r_d \sigma_d - 1) \frac{\tilde{d}^2}{2r_d} + \Xi, \end{aligned} \quad (59)$$

where

$\Xi = \sum_{j=1}^n h'_j \varepsilon_j \theta_j^2 / 2r_j + 0.2785\omega d^* + (\sigma_d d^{*2} / 2) + 2\alpha_3 + \sigma_n$ .  
Finally, for  $\mu_1 = \min\{\bar{\mu}_1, h'_j \varepsilon_j - 1, r_d \sigma_d - 1\}$ ,  $\mu_2 = \min\{\bar{\mu}_2, 1\}$ , according to Lemma 3, we obtain

$$\begin{aligned} \dot{V}_n \leq & - \mu_1 \left( \left( \sum_{j=1}^n \frac{z_j^2}{2} \right) + \left( \sum_{j=1}^n \frac{\tilde{\theta}_j^2}{2r_j} \right) + \left( \frac{\tilde{d}^2}{2r_d} \right) \right) \\ & - \mu_2 \left( \left( \sum_{j=1}^n \frac{z_j^2}{2} \right)^{3/4} + \left( \sum_{j=1}^n \frac{\tilde{\theta}_j^2}{2r_j} \right)^{3/4} + \left( \frac{\tilde{d}^2}{2r_d} \right)^{3/4} \right) + \Xi \\ \leq & - \mu_1 V_n - \mu_2 V_n^{3/4} + \Xi. \end{aligned} \quad (60)$$

In the present stage, the controller design has been finished and the following theorem concludes the main result of this research:

**Theorem 1.** *consider the closed-loop system consisting of the plant (1) and the control input (43) with the adaptive laws (24), (35), and (46). Under Assumptions 1–3 and the bounded initial conditions, all the signals defined in the closed-loop system are fast finite-time bounded and the tracking error  $z_1$  satisfies*

$$|z_1| \leq \sqrt{\frac{2\Xi}{\theta_0 \mu_1}}, \quad (61)$$

with assured settling time  $T_r$  as

$$\begin{aligned} T_r \leq & \max \left\{ t_0 + \frac{4}{\theta_0 \mu_1} \ln \frac{\theta_0 \mu_1 V^{1/4}(t_0) + \mu_2}{\mu_2}, t_0 \right. \\ & \left. + \frac{4}{\mu_1} \ln \frac{\mu_1 V^{1/4}(t_0) + \theta_0 \mu_2}{\theta_0 \mu_2} \right\}. \end{aligned} \quad (62)$$

*Proof.* According to (60), it can be concluded that  $V_n$  is bounded, since when  $V_n \geq \Xi / \mu_1$ ,  $\dot{V}_n \leq -\mu_2 V_n^{3/4} \leq 0$ . Also,  $z_j, \tilde{\theta}_j, \tilde{d}$  are bounded from the boundedness of  $V_n$ . The boundedness of  $\tilde{\theta}_j$  and  $\theta_j$  guarantee the boundedness of  $\hat{\theta}_j$ . Similarly,  $\tilde{d}$  is also bounded since  $\tilde{d} = \hat{d} - d^*$ . From (24),  $\alpha_1$  is bounded which is the result from the boundedness of  $z_1$  and  $\hat{\theta}_1$ . The boundedness of  $\alpha_1$  in (21) can be also inferred. As  $z_2 = x_2 - \alpha_1$ ,  $x_2$  is bounded because of the boundedness of  $\alpha_1$  and  $z_2$ . In an inductive manner, the boundedness of  $\hat{\theta}_2, \dots, \hat{\theta}_n, \alpha_2, \dots, \alpha_n$ , as well as  $x_3, \dots, x_n$ , can be

guaranteed. The boundedness of actual control signal  $u$  in (43) can also be inferred. Thus, the boundedness of all closed-loop signals can be explained.

Furthermore, we transform (60)  $\dot{V}_n \leq -\mu_1 V_n - \mu_2 V_n^{3/4} + \Xi$  into the following form  $\dot{V}_n \leq -(1-\theta_0)\mu_1 V_n - \theta_0\mu_1 V_n - \mu_2 V_n^{3/4} + \Xi$ , where  $0 < \theta_0 < 1$ . When  $V_n \geq \Xi/\theta_0\mu_1$ , namely,  $\Xi \leq \theta_0\mu_1 V_n$ , one has  $\dot{V}_n \leq -(1-\theta_0)\mu_1 V_n - \mu_2 V_n^{3/4}$ .

Based on (60) and Lemma 1, we obtain that  $V_n$  converges to the set  $\Omega_V = \{V_n: V_n < \Xi/\theta_0\mu_1\}$  in fast finite-time with the settling-time estimation

$$T_r \leq \max \left\{ t_0 + \frac{4}{\theta_0\mu_1} \ln \frac{\theta_0\mu_1 V^{1/4}(t_0) + \mu_2}{\mu_2}, t_0 + \frac{4}{\mu_1} \ln \frac{\mu_1 V^{1/4}(t_0) + \theta_0\mu_2}{\theta_0\mu_2} \right\}. \quad (63)$$

Combing with the definition of  $V_n$  in (38), it can be observed that  $1/2z_1^2 \leq V_n < \Xi/\theta_0\mu_1$ . Therefore, we have  $|z_1| \leq \sqrt{2\Xi/\theta_0\mu_1}$  in fast finite-time with guaranteed convergence time estimated as  $T_r$  in (63).

Through the abovementioned analysis, we have completed the proof.  $\square$

#### 4. Simulation

This part gives an example to prove that the proposed control scheme is valid. Consider the second-order pure-feedback nonlinear system with disturbance as follows:

$$\begin{cases} \dot{x}_1 = 0.5 \cos(x_1) + x_2 + 0.05 \sin(x_2), \\ \dot{x}_2 = \cos(x_2^2) + 2u + 0.5 \sin u + 0.1 \sin(t), \\ y = x_1, \end{cases} \quad (64)$$

where  $x_1$  and  $x_2$  represent the state variables and  $y$  and  $u$  denote the output and input signal, respectively.  $f_1(\bar{x}_1, x_2) = 0.5 \cos(x_1) + x_2 + 0.05 \sin(x_2)$ ,  $f_2(\bar{x}_2, u) = \cos(x_2^2) + 2u + 0.5 \sin u$ , and  $d(t) = 0.1 \sin(t)$ . The purpose is to establish a controller which can guarantee that all signals remain bounded in the closed-loop system, the system output  $y = x_1$  tracks the reference signal  $y_d = 0.4(\sin(t) + \sin(0.5t))$ , and the tracking error  $z_1 = x_1 - y_d$  is convergent.

By using Theorem 1, the virtual control signals and actual controller are expressed as follows:

$$\begin{aligned} \alpha_1 &= -\frac{z_1 \check{\alpha}_1^2}{\sqrt{z_1^2 \check{\alpha}_1^2 + \varepsilon_1^2}}, \\ \check{\alpha}_1 &= \frac{1}{2}K_{11}z_1 + K_{12} \left(\frac{1}{2}\right)^{3/4} (z_1^2)^{1/4} + \frac{1}{2a_1} z_1 \hat{\theta}_1 S_1^T S_1, \\ u &= -\frac{z_2 \check{\alpha}_2^2}{\sqrt{z_2^2 \check{\alpha}_2^2 + \varepsilon_2^2}} - \frac{\tanh(z_2/\omega) \hat{d}}{h_2}, \\ \check{\alpha}_2 &= \frac{1}{2}K_{21}z_2 + K_{22} \left(\frac{1}{2}\right)^{3/4} (z_2^2)^{1/4} + \frac{1}{2a_2} z_2 \hat{\theta}_2 S_2^T S_2, \end{aligned} \quad (65)$$

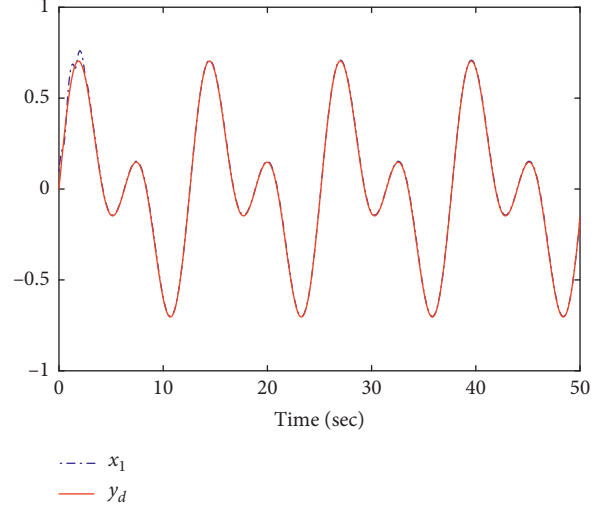


FIGURE 1: Reference signal  $y_d$  and system output  $x_1$ .

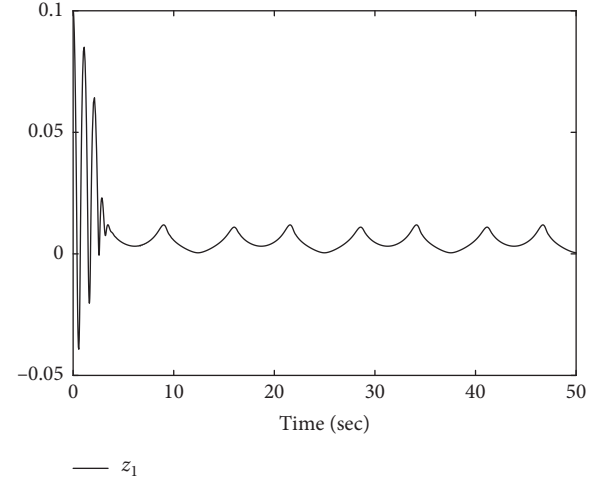


FIGURE 2: The tracking error  $z_1$ .

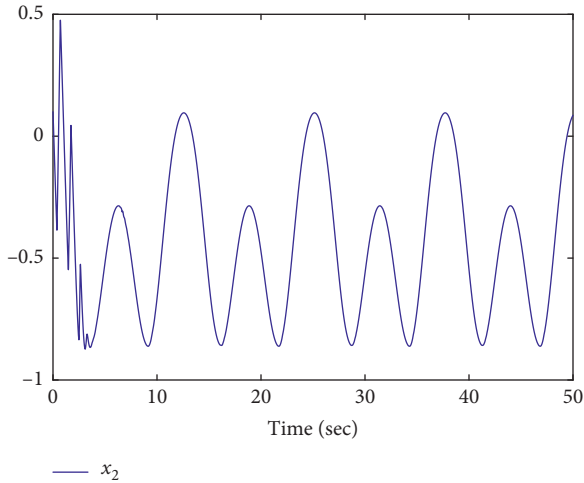
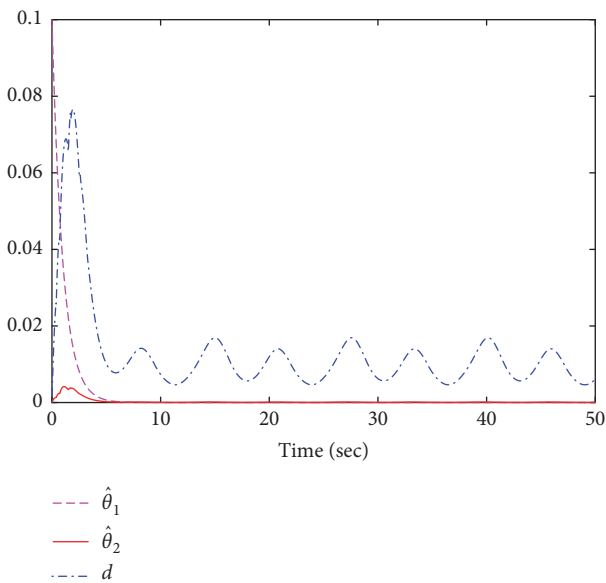
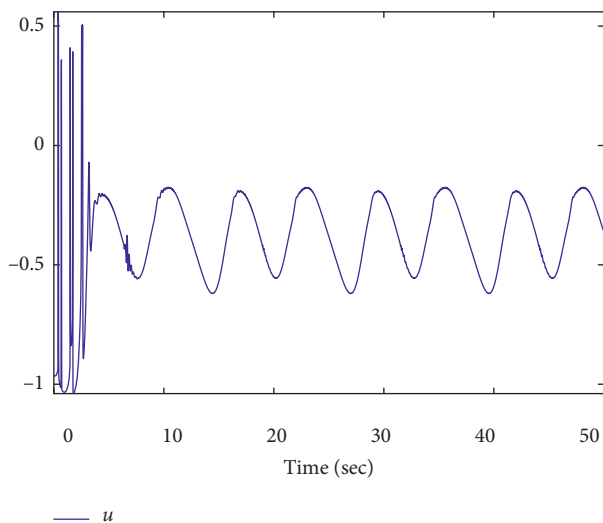
and the adaptive laws are constructed in the following forms:

$$\begin{aligned} \dot{\hat{\theta}}_1 &= \frac{r_1}{2a_1^2} z_1^2 S_1^T S_1 - \varepsilon_1 \hat{\theta}_1, \\ \dot{\hat{\theta}}_2 &= \frac{r_2}{2a_2^2} z_2^2 S_2^T S_2 - \varepsilon_2 \hat{\theta}_2, \\ \dot{\hat{d}} &= r_d \left[ z_2 \tanh\left(\frac{z_2}{\omega}\right) - \sigma_d \hat{d} \right]. \end{aligned} \quad (66)$$

In the simulation, the initial conditions are set as  $[x_1(0) \ x_2(0) \ \hat{d}(0) \ \hat{\theta}_1(0) \ \hat{\theta}_2(0)]^T = [0.1 \ 0.1 \ 0.0 \ 1.0 \ 1.0]^T$ . Also, the simulation is run by taking the design parameters as  $K_{11} = K_{12} = 40, K_{21} = K_{22} = 20, a_1 = a_2 = \varepsilon_1 = \varepsilon_2 = 1, r_1 = r_2 = \varepsilon_1 = 0.01, \omega = r_d = 0.1, \sigma_d = 10, h_2 = 1$ .

Figures 1–5 illustrate the simulation results. Figure 1 shows the desired signal  $y_d$  and the output  $y = x_1$ . Figure 2 depicts the trajectory of the tracking error  $z_1$ . Figure 3 shows the curve of the state  $x_2$ . From the abovementioned three



FIGURE 3: State variable  $x_2$ .FIGURE 4: The adaptive parameters  $\hat{\theta}_1, \hat{\theta}_2, \hat{d}$ .FIGURE 5: The input signal  $u$ .

figures, we can observe that the states  $x_1(t)$  and  $x_2(t)$  of (64) are bounded and  $x_1$  can tracks  $y_d$  under our design controller in Figures 1 and 3. Moreover, the tracking error  $z_1 - x_1 - y_d$  in Figure 2 is very small and converges into a small neighborhood of zero. Figure 4 displays that the adaptive laws  $\hat{\theta}_1, \hat{\theta}_2$ , and  $\hat{d}$  are bounded. The trajectory of  $u(t)$  is depicted in Figure 5, from which it can be seen that  $u(t)$  is bounded. Through the numerical simulation in Figures 1–5, the proposed control scheme achieves that  $y$  tracks  $y_d$  in a quick and precise way and desired convergence with the control performance.

## 5. Conclusions

The adaptive fuzzy-based fast finite-time tracking control via the backstepping technique has been developed for nonlinear systems in pure-feedback form with unknown disturbance. The mean value theorem was used to address the nonaffine problem of the pure-feedback systems, and FLSs were applied to approximate packaged unknown nonlinearities. All signals in the closed-loop system are bounded, and the reference signal can be tracked in fast finite-time. Simulation results have been given to prove the effectiveness of the suggested scheme. In this paper, the approximation error of the FLS is not taken into account. The future work will be concentrated on extending the results to more general nonlinear systems.

## Data Availability

The data used to support the findings of this study are available from the corresponding author upon request.

## Conflicts of Interest

The authors declare that they have no conflicts of interest.

## Acknowledgments

This work was supported by the National Natural Science Foundation of China (61773072, 61773073, and 61403177), Natural Science Foundation of Liaoning Province (20180550691 and 20180550590), and Education Department Project of Liaoning Province (2019LNJC09).

## References

- [1] X. Li, X. Fu, and R. Rakkiyappan, "Delay-dependent stability analysis for a class of dynamical systems with leakage delay and nonlinear perturbations," *Applied Mathematics and Computation*, vol. 226, pp. 10–19, 2014.
- [2] X. Li, J. Shen, H. Akca, and R. Rakkiyappan, "LMI-based stability for singularly perturbed nonlinear impulsive differential systems with delays of small parameter," *Applied Mathematics and Computation*, vol. 250, pp. 798–804, 2015.
- [3] X. Lv, R. Rakkiyappan, R. Rakkiyappan, and X. Li, " $\mu$ -stability criteria for nonlinear differential systems with additive leakage and transmission time-varying delays," *Nonlinear Analysis: Modelling and Control*, vol. 23, no. 3, pp. 380–400, 2018.

- [4] A. J. Koshkouei and A. S. I. Zinober, "Adaptive backstepping control of nonlinear systems with unmatched uncertainty," *Conference on Decision and Control*, vol. 5, pp. 4765–4770, 2000.
- [5] B. Xu, X. Liu, H. Wang, and Y. Zhou, "Event-triggered adaptive backstepping control for strict-feedback nonlinear systems with zero dynamics," *Complexity*, vol. 2019, Article ID 7890968, 13 pages, 2019.
- [6] J. Zhou, C. Wen, and Y. Zhang, "Adaptive backstepping control of a class of uncertain nonlinear systems with unknown backlash-like hysteresis," *IEEE Transactions on Automatic Control*, vol. 49, no. 10, pp. 1751–1757, 2004.
- [7] L. Sun, W. Huo, and Z. Jiao, "Adaptive backstepping control of spacecraft rendezvous and proximity operations with input saturation and full-state constraint," *IEEE Transactions on Industrial Electronics*, vol. 64, no. 1, pp. 480–492, 2017.
- [8] Z. Cai, M. S. deQueiroz, and D. M. Dawson, "Robust adaptive asymptotic tracking of nonlinear systems with additive disturbance," *IEEE Transactions on Automatic Control*, vol. 51, no. 3, pp. 524–529, 2006.
- [9] W. Wang, B. Xie, Z. Zuo, and H. Fan, "Adaptive backstepping control of uncertain gear transmission servosystems with asymmetric dead-zone nonlinearity," *IEEE Transactions on Industrial Electronics*, vol. 66, no. 5, pp. 3752–3762, 2019.
- [10] J. Zhou, C. Wen, W. Wang, and F. Yang, "Adaptive backstepping control of nonlinear uncertain systems with quantized states," *IEEE Transactions on Automatic Control*, vol. 64, no. 11, pp. 4756–4763, 2019.
- [11] X.-J. Xie and M. Jiang, "Dynamic state feedback stabilization of stochastic cascade nonlinear time-delay systems with SISS inverse dynamics," *IEEE Transactions on Automatic Control*, vol. 64, no. 12, pp. 5132–5139, 2019.
- [12] L.-X. Wang and J. M. Mendel, "Fuzzy basis functions, universal approximation, and orthogonal least-squares learning," *IEEE Transactions on Neural Networks*, vol. 3, no. 5, pp. 807–814, 1992.
- [13] M. M. Polycarpou, "Stable adaptive neural control scheme for nonlinear systems," *IEEE Transactions on Automatic Control*, vol. 41, no. 3, pp. 447–451, 1996.
- [14] H. Wang, X. Liu, and K. Liu, "Robust adaptive neural tracking control for a class of stochastic nonlinear interconnected systems," *IEEE Transactions on Neural Networks and Learning Systems*, vol. 27, no. 3, pp. 510–523, 2016.
- [15] B. Chen, H. Zhang, X. Liu, and C. Lin, "Neural observer and adaptive neural control design for a class of nonlinear systems," *IEEE Transactions on Neural Networks and Learning Systems*, vol. 29, no. 9, pp. 4261–4271, 2018.
- [16] W. Bai, T. Li, and S. Tong, "NN reinforcement learning adaptive control for a class of nonstrict-feedback discrete-time systems," *IEEE Transactions on Cybernetics*, 2020.
- [17] X. Zhao, X. Wang, S. Zhang, and G. Zong, "Adaptive neural backstepping control design for a class of nonsmooth nonlinear systems," *IEEE Transactions on Systems, Man, and Cybernetics: Systems*, vol. 49, no. 9, pp. 1820–1831, 2019.
- [18] X. Zhao, X. Wang, L. Ma, and G. Zong, "Fuzzy-approximation-based asymptotic tracking control for a class of uncertain switched nonlinear systems," *IEEE Transactions on Fuzzy Systems*, 2019.
- [19] W. He, Y. Chen, and Z. Yin, "Adaptive neural network control of an uncertain robot with full-state constraints," *IEEE Transactions on Cybernetics*, vol. 46, no. 3, pp. 620–629, 2016.
- [20] M. Chen, S.-Y. Shao, and B. Jiang, "Adaptive neural control of uncertain nonlinear systems using disturbance observer," *IEEE Transactions on Cybernetics*, vol. 47, no. 10, pp. 3110–3123, 2017.
- [21] S. Tong and Y. Li, "Robust adaptive fuzzy backstepping output feedback tracking control for nonlinear system with dynamic uncertainties," *Science China Information Sciences*, vol. 53, no. 2, pp. 307–324, 2010.
- [22] X. Li, D. O'Regan, and H. Akca, "Global exponential stabilization of impulsive neural networks with unbounded continuously distributed delays," *IMA Journal of Applied Mathematics*, vol. 80, no. 1, pp. 85–99, 2015.
- [23] M. Chen, H. Wang, and X. Liu, "Adaptive fuzzy practical fixed-time tracking control of nonlinear systems," *IEEE Transactions on Fuzzy Systems*, 2019.
- [24] M. Hamdy, S. Abd-Elhaleem, and M. A. Fkirin, "Time-varying delay compensation for a class of nonlinear control systems over network via  $H_\infty$  adaptive fuzzy controller," *IEEE Transactions on Systems, Man, and Cybernetics: Systems*, vol. 47, no. 8, pp. 2114–2124, 2017.
- [25] M. Hamdy, S. Abd-Elhaleem, and M. A. Fkirin, "Adaptive fuzzy predictive controller for a class of networked nonlinear systems with time-varying delay," *IEEE Transactions on Fuzzy Systems*, vol. 26, no. 4, pp. 2135–2144, 2018.
- [26] Y. Li, K. Li, and S. Tong, "Adaptive neural network finite-time control for multi-input and multi-output nonlinear systems with the powers of odd rational numbers," *IEEE Transactions on Neural Networks and Learning Systems*, vol. 31, no. 7, pp. 2532–2543, 2020.
- [27] M. Chen and G. Tao, "Adaptive fault-tolerant control of uncertain nonlinear large-scale systems with unknown dead zone," *IEEE Transactions on Cybernetics*, vol. 46, no. 8, pp. 1851–1862, 2016.
- [28] H. Wang, X. Liu, K. Liu, and H. R. Karimi, "Approximation-based adaptive fuzzy tracking control for a class of nonstrict-feedback stochastic nonlinear time-delay systems," *IEEE Transactions on Fuzzy Systems*, vol. 23, no. 5, pp. 1746–1760, 2015.
- [29] H. Li, L. Bai, L. Wang, Q. Zhou, and H. Wang, "Adaptive neural control of uncertain nonstrict-feedback stochastic nonlinear systems with output constraint and unknown dead zone," *IEEE Transactions on Systems, Man, and Cybernetics: Systems*, vol. 47, no. 8, pp. 2048–2059, 2017.
- [30] J. Zhang, D. Gu, C. Deng, and B. Wen, "Robust and adaptive backstepping control for hexacopter UAVs," *IEEE Access*, 2019.
- [31] X. Su, Z. Liu, G. Lai, Y. Zhang, and C. L. P. Chen, "Event-triggered adaptive fuzzy control for uncertain strict-feedback nonlinear systems with guaranteed transient performance," *IEEE Transactions on Fuzzy Systems*, vol. 27, no. 12, pp. 2327–2337, 2019.
- [32] S. S. Ge and C. Wang, "Adaptive NN control of uncertain nonlinear pure-feedback systems," *Automatica*, vol. 38, no. 4, pp. 671–682, 2002.
- [33] B. Ren, S. S. Ge, C. Su, and T. H. Lee, "Adaptive neural control for a class of uncertain nonlinear systems in pure-feedback form with hysteresis input," *IEEE Transactions on Systems, Man, and Cybernetics, Part B (Cybernetics)*, vol. 39, no. 2, pp. 431–443, 2009.
- [34] S. Tong and Y. Li, "Observer-based adaptive fuzzy backstepping control of uncertain nonlinear pure-feedback systems," *Science China Information Sciences*, vol. 57, no. 1, pp. 1–14, 2014.
- [35] T. P. Zhang and S. S. Ge, "Adaptive dynamic surface control of nonlinear systems with unknown dead zone in pure feedback form," *Automatica*, vol. 44, no. 7, pp. 1895–1903, 2008.

- [36] Y. Li, S. Tong, and T. Li, "Adaptive fuzzy output feedback dynamic surface control of interconnected nonlinear pure-feedback systems," *IEEE Transactions on Cybernetics*, vol. 45, no. 1, pp. 138–149, 2015.
- [37] F. Wang, B. Chen, Y. Sun, Y. Gao, and C. Lin, "Finite-time fuzzy control of stochastic nonlinear systems," *IEEE Transactions on Cybernetics*, 2019.
- [38] Y. Li, T. Yang, and S. Tong, "Adaptive neural networks finite-time optimal control for a class of nonlinear systems," *IEEE Transactions on Neural Networks and Learning Systems*, 2019.
- [39] X. Li, D. W. C. Ho, and J. Cao, "Finite-time stability and settling-time estimation of nonlinear impulsive systems," *Automatica*, vol. 99, no. 99, pp. 361–368, 2019.
- [40] X. Li, X. Yang, and S. Song, "Lyapunov conditions for finite-time stability of time-varying time-delay systems," *Automatica*, vol. 103, no. 103, pp. 135–140, 2019.
- [41] X. Lv and X. Li, "Finite time stability and controller design for nonlinear impulsive sampled-data systems with applications," *ISA Transactions*, vol. 70, pp. 30–36, 2017.
- [42] Y. Liu, X. Liu, Y. Jing, H. Wang, and X. Li, "Annular domain finite-time connective control for large-scale systems with expanding construction," *IEEE Transactions on Systems, Man, and Cybernetics: Systems*, 2020.
- [43] M. Van, S. S. Ge, and H. Ren, "Finite time fault tolerant control for robot manipulators using time delay estimation and continuous nonsingular fast terminal sliding mode control," *IEEE Transactions on Cybernetics*, vol. 47, no. 7, pp. 1681–1693, 2017.
- [44] F. Wang and X. Zhang, "Adaptive finite time control of nonlinear systems under time-varying actuator failures," *IEEE Transactions on Systems, Man, and Cybernetics: Systems*, vol. 49, no. 9, pp. 1845–1852, 2019.
- [45] P. Du, H. Liang, S. Zhao, and C. K. Ahn, "Neural-based decentralized adaptive finite-time control for nonlinear large-scale systems with time-varying output constraints," *IEEE Transactions on Systems, Man, and Cybernetics: Systems*, 2019.
- [46] L. Weiss and E. Infante, "Finite time stability under perturbing forces and on product spaces," *IEEE Transactions on Automatic Control*, vol. 12, no. 1, pp. 54–59, 1967.
- [47] Z.-Y. Sun, M.-M. Yun, and T. Li, "A new approach to fast global finite-time stabilization of high-order nonlinear system," *Automatica*, vol. 81, no. 81, pp. 455–463, 2017.
- [48] T. M. Apostol, *Mathematical Analysis*, Addison-Wesley, Reading, MA, USA, 1963.
- [49] B. Chen, X. Liu, K. Liu, and C. Lin, "Direct adaptive fuzzy control of nonlinear strict-feedback systems," *Automatica*, vol. 45, no. 6, pp. 1530–1535, 2009.
- [50] T. Wang, S. S. Ge, and C. C. Hang, "Stable adaptive control for a class of nonlinear systems using a modified Lyapunov function," *IEEE Transactions on Automatic Control*, vol. 45, no. 1, pp. 129–132, 2000.
- [51] J. Yu, P. Shi, and L. Zhao, "Finite-time command filtered backstepping control for a class of nonlinear systems," *Automatica*, vol. 92, no. 92, pp. 173–180, 2018.
- [52] C. Wang and Y. Lin, "Decentralized adaptive tracking control for a class of interconnected nonlinear time-varying systems," *Automatica*, vol. 54, no. 54, pp. 16–24, 2015.
- [53] Z. Zhu, Y. Xia, and M. Fu, "Attitude stabilization of rigid spacecraft with finite-time convergence," *International Journal of Robust and Nonlinear Control*, vol. 21, no. 6, pp. 686–702, 2011.
- [54] C. Qian and W. Lin, "Non-Lipschitz continuous stabilizers for nonlinear systems with uncontrollable unstable linearization," *Systems & Control Letters*, vol. 42, no. 3, pp. 185–200, 2001.

## Research Article

# Finite-Time Stability Criteria for a Class of High-Order Fractional Cohen–Grossberg Neural Networks with Delay

Zhanying Yang, Jie Zhang, Junhao Hu, and Jun Mei 

*School of Mathematics and Statistics, South-Central University for Nationalities, Wuhan 430074, Hubei, China*

Correspondence should be addressed to Jun Mei; [meij0000@163.com](mailto:meij0000@163.com)

Received 13 July 2020; Revised 10 August 2020; Accepted 18 August 2020; Published 9 September 2020

Academic Editor: Xiaodi Li

Copyright © 2020 Zhanying Yang et al. This is an open access article distributed under the Creative Commons Attribution License, which permits unrestricted use, distribution, and reproduction in any medium, provided the original work is properly cited.

This paper focuses on a class of delayed fractional Cohen–Grossberg neural networks with the fractional order between 1 and 2. Two kinds of criteria are developed to guarantee the finite-time stability of networks based on some analytical techniques. This method is different from those in some earlier works. Moreover, the obtained criteria are expressed as some algebraic inequalities independent of the Mittag–Leffler functions, and thus, the calculation is relatively simple in both theoretical analysis and practical applications. Finally, the feasibility and validity of obtained results are supported by the analysis of numerical simulations.

## 1. Introduction

Neural networks have been paid much attention owing to the powerful applications in diverse fields. With the increasing requirements in practical applications, many researchers have made great efforts to develop various types of neural networks, such as Cohen–Grossberg neural networks (CGNNs) [1], cellular neural networks, bidirectional associative memory neural networks, and recurrent neural networks. As a kind of special recurrent neural network, CGNNs were firstly proposed by Cohen and Grossberg in [1]. CGNN is quite general since it includes some well-known types of neural networks, such as Hopfield neural network, cellular neural network, and shunting neural network. Nowadays, CGNNs have gained more and more interests due to their promising applications in classification, parallel computation and optimization, etc. Many researchers have made great contribution to the research on CGNNs; see [2–11] and the references therein.

Nowadays, the fractional calculus has achieved significant progress in both theoretical research and practical applications. Compared with the integer-order derivative, the fractional-order derivative has some distinctive

features, such as infinite memory and great freedom. Consequently, the fractional-order derivative can better characterize many systems in the real world [12–14]. In order to more accurately model the dynamics of neurons, various fractional-order neural networks (FONNs) have been generated based on the integration of the fractional calculus and neural networks. In the recent decades, the research on FONNs has undergone a prosperous development, and there have been numerous works (see [10, 15–20] and the references therein). As we all know, the successful applications of FONNs are closely associated to the dynamics of networks, among which stability has been an active topic. There have been substantial works on various types of stability, such as asymptotical stability [10], finite-time stability [21], exponential stability [22], Mittag–Leffler stability [8], and Lagrange stability [11]. Many sufficient conditions have been established to achieve the stability of systems; see [16, 18–20, 23, 24] and the references therein.

Among various types of stability, finite-time stability (FTS) has aroused more interests in many fields, since many systems always operate over a limited period of time or it is necessary to focus on the behavior of systems within a limited period of time. In the existing works, there are

mainly two concepts of FTS. One means that the error of any two state variables tends to zero in a limited time interval, which is also regarded as a special case of Lyapunov asymptotic stability. The other is also called finite-time boundedness, which describes that the quantity related to state does not exceed a prescribed threshold in a limited time interval for a given bound on the initial value [25, 26]. It is obvious that “boundedness” is a distinctive feature of this FTS. As revealed in [25, 26], it is essentially different from the classical Lyapunov asymptotic stability. In practical applications, this kind of FTS can provide a quantitative bound related to the state, and it has made great contribution for describing the transient performance of system.

In the literature, there have been some interesting results [8–11, 23, 24, 27, 28] on fractional-order Cohen–Grossberg neural networks (FOCGNNs). For example, Ke and Miao [9] investigated the FTS for a class of delayed FOCGNNs by the generalized Bellman–Gronwall inequality. In [23], Zheng et al. studied the FTS and synchronization problem of a class of memristor-based FOCGNNs. Rajivganthi et al. [24] reported the FTS for a class of BAM FOCGNNs with time delays. In these works, the proofs are mainly based on some generalized Gronwall inequalities. In [8], Wan and Wu considered the Mittag–Leffler stability of fuzzy FOCGNNs with deviating argument. Recently, Pratap et al. [10] considered the asymptotic stability and pinning synchronization for a class of delayed FOCGNNs with discontinuous activations, and Huang et al. [11] investigated the Lagrange stability and the asymptotical stability for a class of delayed FOCGNNs. The proofs are mainly based on the Lyapunov theory and some properties related to the fractional calculus. For the FONNs in the aforementioned works, notice that the fractional order  $\alpha$  is between 0 and 1. In the real world, the fractional systems with high fractional order can appropriately describe many phenomena and have been successfully applied in physics, biology, and information science (see, for instance, [29–32]). On the other hand, some classical methods for the case  $\alpha \in (0, 1)$ , such as some Lyapunov methods [10] and LMI method [33], could not be directly extended to the high-order cases. Therefore, it is significant to follow through the problems on high-order FONNs.

For FONNs with the fractional order  $\alpha \in (1, 2)$ , there have been many excellent works on the finite-time stability or finite-time synchronization [15–17, 34–37]. The analysis is mainly based on the Laplace transform, the inverse Laplace transform, and the generalized Gronwall inequality related to the Mittag–Leffler functions. However, this method can not be directly used to deal with the FTS for FOCGNNs with  $\alpha \in (1, 2)$  owing to the technical reason. In order to solve this problem, it is desired to investigate a kind of different method.

In this paper, we are devoted to the FTS for a class of delayed FOCGNNs with  $\alpha \in (1, 2)$ . The main contributions are summarized as follows: (i) The fractional order of system considered in this paper is between 1 and 2. A

criterion is derived to achieve the FTS of system. Moreover, a criterion is established to ensure the FTS for the equilibrium point of system. (ii) The proofs are based on some analytical techniques, such as the Cauchy–Schwartz inequality, the generalized Gronwall inequality, and some properties of the Caputo derivative. This method is completely different from those in some earlier works [9, 15–17, 24, 34–37]. In particular, the obtained criteria are expressed as some algebraic inequalities and hence, the calculation is relatively easy in practical applications.

## 2. Preliminaries

This section starts with recalling some necessary definitions and properties related to the Caputo derivative.

*Definition 1* (see [38]). Let  $\mu \in \mathbb{R}^+$ ,  $m \in \mathbb{Z}^+$  and  $m - 1 < \mu < m$ . For  $\theta(t) \in C^m([t_0, +\infty), \mathbb{R}^n)$  The Caputo derivative with fractional order  $\mu$  of  $\theta$  is defined by

$${}^C D_t^\mu \theta(t) = \frac{1}{\Gamma(m - \mu)} \int_{t_0}^t (t - r)^{m - \mu - 1} \theta^{(m)}(r) dr, \quad t \geq t_0, \quad (1)$$

where  $\Gamma(\cdot)$  denotes the Gamma function, i.e.,

$$\Gamma(r) = \int_0^{+\infty} t^{r-1} e^{-t} dt. \quad (2)$$

*Definition 2* (see [38]). For  $\mu \in \mathbb{R}^+$  the fractional order integral with order  $\mu$  of a function  $\theta(t)$  is defined by

$$D_{t_0, t}^{-\mu} \theta(t) = \frac{1}{\Gamma(\mu)} \int_{t_0}^t (t - r)^{\mu - 1} \theta(r) dr. \quad (3)$$

**Proposition 1** (see [39]). Let  $\mu \in \mathbb{R}^+$ ,  $m \in \mathbb{Z}^+$ , and  $m - 1 < \mu < m$ . If  $\theta(t) \in C^m([t_0, +\infty), \mathbb{R})$ , then

$$D_{t_0, t}^{-\mu} ({}^C D_t^\mu \theta(t)) = \theta(t) - \sum_{k=0}^{m-1} \frac{\theta^{(k)}(t_0)}{k!} t^k. \quad (4)$$

Next, we list two inequalities, which will play a key role in the proofs of main results.

**Proposition 2** (generalized Gronwall inequality [40]). Let  $u(t)$ ,  $v(t)$  and  $w(t)$  be nonnegative  $L_q$  functions on the interval  $[0, T]$  For  $q \in [1, +\infty)$  if

$$u(t) \leq v(t) + w(t) \left( \int_0^t u^q(r) dr \right)^{1/q}, \quad t \in [0, T]. \quad (5)$$

Then,

$$\int_0^t u^q(r) dr \leq [1 - (1 - \Phi(t))^{1/q}]^{-q} \int_0^t v^q(r) \Phi(r) dr, \quad (6)$$

where  $\Phi(t) = \exp(-\int_0^t w^q(r) dr)$ .

**Proposition 3** (generalized Bernoulli inequality [41]). *Let  $t < 1$  and  $t \neq 0$ . For  $0 < d < 1$ , we have  $(1-t)^d < 1-dt$ . Moreover,  $(1-(1-t)^d)^{-1} < (dt)^{-1}$ .*

In what follows, we introduce a class of delayed FOCGNNs, which can be described as

$$\begin{aligned} {}_0^C D_t^\alpha x_i(t) = & -p_i(x_i(t)) \left[ q_i(x_i(t)) - \sum_{j=1}^n a_{ij} f_j(x_j(t)) \right. \\ & \left. - \sum_{j=1}^n b_{ij} g_j(x_j(t-\tau)) - I_i \right], \quad i = 1, 2, \dots, n, \end{aligned} \quad (7)$$

where  $1 < \alpha < 2$ ,  $x_i(t) \in \mathbb{R}$  is the state of the  $i$ -th neuron at time  $t$ .  $p_i(\cdot)$  stands for the amplification function and  $q_i(\cdot)$  corresponds to the behaved function. The constant  $\tau > 0$  denotes the time delay.  $a_{ij}$  and  $b_{ij}$  are the connection weights.  $f_j$  and  $g_j$  represent the activation functions.  $I_i$  stands for the constant external input.

For  $h(t) \in C([- \tau, 0], \mathbb{R}^m)$ , the norm is defined as  $\|h\| = \sup_{-\tau \leq r \leq 0} \sum_{i=1}^m |h_i(r)|$ . Let  $x(t)$  and  $y(t)$  stand for two arbitrary solutions for network (7), and let  $z(t) = x(t) - y(t)$ . The initial condition is given as follows:

$$\begin{aligned} z(t) &= \varphi(t), \\ z'(t) &= \psi(t), \\ t &\in [-\tau, 0], \end{aligned} \quad (8)$$

where  $\varphi(t), \psi(t) \in C([- \tau, 0], \mathbb{R}^n)$

**Definition 3.** Let  $0 < \delta < \varepsilon$ . For  $1 < \alpha < 2$ , if  $\{\|\varphi\|, \|\psi\|\} < \delta$  implies

$$\|z(t)\| < \varepsilon, \quad \forall t \in [0, T], \quad (9)$$

where  $\|z(t)\| = \sum_{i=1}^n |z_i(t)|$ , then network (7) can achieve the finite-time stability w.r.t.  $\{\delta, \varepsilon, T\}$ .

### 3. Main Results

In this section, we are devoted to two kinds of finite-time stability criteria for network (7) based on some properties related to the Caputo derivative and some inequalities.

**3.1. Stability Criterion I for Network (7).** Let us first introduce some further assumptions on the parameters of network (7) and some necessary notation.

(A1) The function  $p_i$  ( $i = 1, 2, \dots, n$ ) is a continuous and bounded function such that

$$\begin{aligned} 0 < \underline{p}_i \leq p_i(x) \leq \bar{p}_i, \\ |p_i(x) - p_i(y)| \leq p^* |x - y|, \end{aligned} \quad (10)$$

for  $x, y \in \mathbb{R}$ , where  $\underline{p}_i$ ,  $\bar{p}_i$ , and  $p^*$  are some positive constants.

(A2) For the functions  $p_i$  and  $q_i$  ( $i = 1, 2, \dots, n$ ), there exists  $\theta_i > 0$  such that

$$|p_i(x)q_i(x) - p_i(y)q_i(y)| \leq \theta_i |x - y|, \quad \forall x, y \in \mathbb{R}. \quad (11)$$

(A3) The functions  $f_j$  and  $g_j$  ( $j = 1, 2, \dots, n$ ) are bounded and satisfy the Lipschitz conditions, namely,

$$\begin{aligned} |f_j(x)| &\leq F_j, \\ |g_j(x)| &\leq G_j, \\ |f_j(x) - f_j(y)| &\leq \xi_j |x - y|, \\ |g_j(x) - g_j(y)| &\leq \eta_j |x - y|, \\ &\forall x, y \in \mathbb{R}, \end{aligned} \quad (12)$$

where  $F_j, G_j, \xi_j$  and  $\eta_j$  are positive constants.

Let

$$\begin{aligned} \lambda_1 &= \max_{1 \leq i \leq n} \left\{ \theta_i + p^* |I_i| + p^* \sum_{j=1}^n (|a_{ij}| F_j + |b_{ij}| G_j) \right\} \\ &\quad + \max_{1 \leq i \leq n} \left( \sum_{i=1}^n \xi_j \bar{p}_i |a_{ij}| \right), \\ \lambda_2 &= \max_{1 \leq j \leq n} \left( \sum_{i=1}^n \eta_j \bar{p}_i |b_{ij}| \right). \end{aligned} \quad (13)$$

**Theorem 1.** Let  $0 < \delta < \varepsilon$ . Under the assumptions (A1)–(A3), network (7) can achieve the FTS w.r.t.  $\{\delta, \varepsilon, T\}$  if  $\max\{\|\varphi\|, \|\psi\|\} < \delta$  and

$$(1+t) \left\{ 1 + 2e^{(\Lambda^2+1)t} \left( 1 - e^{-\Lambda^2 t} \right)^{1/2} \right\} < \frac{\varepsilon}{\delta}, \quad \forall t \in [0, T], \quad (14)$$

where  $\Lambda = (\lambda_1 + \lambda_2 e^{-t}) \sqrt{2\Gamma(2\alpha-1)/2^\alpha \Gamma(\alpha)}$ .

*Proof.* Let  $x(t)$ ,  $y(t)$ , and  $z(t)$  be defined as in Section 2. By Proposition 1, we obtain

$$\begin{aligned}
x_i(t) - y_i(t) &= x_i(0) - y_i(0) + (x'_i(0) - y'_i(0))t \\
&\quad - \frac{1}{\Gamma(\alpha)} \int_0^t (t-r)^{\alpha-1} (p_i(x_i(r))q_i(x_i(r)) - p_i(y_i(r))q_i(y_i(r)))dr \\
&\quad + \frac{1}{\Gamma(\alpha)} \int_0^t (t-r)^{\alpha-1} \left\{ p_i(x_i(r)) \sum_{j=1}^n a_{ij} f_j(x_j(r)) - p_i(y_i(r)) \sum_{j=1}^n a_{ij} f_j(y_j(r)) \right\} dr \\
&\quad + \frac{1}{\Gamma(\alpha)} \int_0^t (t-r)^{\alpha-1} \left\{ p_i(x_i(r)) \sum_{j=1}^n b_{ij} (g_j x_j(r-\tau)) - p_i(y_i(r)) \sum_{j=1}^n b_{ij} g_j(y_j(r-\tau)) \right\} dr \\
&\quad + \frac{1}{\Gamma(\alpha)} \int_0^t (t-r)^{\alpha-1} I_i [p_i(x_i(r)) - p_i(y_i(r))] dr.
\end{aligned} \tag{15}$$

Using the assumptions (A1)-(A2), we have

$$\begin{aligned}
|x_i(t) - y_i(t)| &\leq |x_i(0) - y_i(0)| + |x'_i(0) - y'_i(0)|t \\
&\quad + \frac{\theta_i + p^* |I_i|}{\Gamma(\alpha)} \int_0^t (t-r)^{\alpha-1} |x_i(r) - y_i(r)| dr \\
&\quad + \frac{1}{\Gamma(\alpha)} \int_0^t (t-r)^{\alpha-1} \left| p_i(x_i(r)) \sum_{j=1}^n a_{ij} f_j(x_j(r)) - p_i(y_i(r)) \sum_{j=1}^n a_{ij} f_j(y_j(r)) \right| dr \\
&\quad + \frac{1}{\Gamma(\alpha)} \int_0^t (t-r)^{\alpha-1} \left| p_i(x_i(r)) \sum_{j=1}^n b_{ij} (g_j x_j(r-\tau)) - p_i(y_i(r)) \sum_{j=1}^n b_{ij} g_j(y_j(r-\tau)) \right| dr.
\end{aligned} \tag{16}$$

For the term  $|p_i(x_i(r)) \sum_{j=1}^n a_{ij} f_j(x_j(r)) - p_i(y_i(r)) \sum_{j=1}^n a_{ij} f_j(y_j(r))|$ , the assumptions (A1) and (A3) lead to

$$\begin{aligned}
&\left| p_i(x_i(r)) \sum_{j=1}^n a_{ij} f_j(x_j(r)) - p_i(y_i(r)) \sum_{j=1}^n a_{ij} f_j(y_j(r)) \right| \\
&= \left| p_i(x_i(r)) \sum_{j=1}^n a_{ij} f_j(x_j(r)) - p_i(y_i(r)) \sum_{j=1}^n a_{ij} f_j(x_j(r)) \right| \\
&\quad + \left| p_i(y_i(r)) \sum_{j=1}^n a_{ij} f_j(x_j(r)) - p_i(y_i(r)) \sum_{j=1}^n a_{ij} f_j(y_j(r)) \right| \\
&\leq \sum_{j=1}^n p^* |a_{ij}| F_j |x_i(r) - y_i(r)| + \sum_{j=1}^n \bar{p}_i \xi_j |a_{ij}| |x_j(r) - y_j(r)|.
\end{aligned} \tag{17}$$

In the same way, we obtain

$$\begin{aligned}
&\left| p_i(x_i(r)) \sum_{j=1}^n b_{ij} (g_j x_j(r-\tau)) - p_i(y_i(r)) \sum_{j=1}^n b_{ij} (g_j y_j(r-\tau)) \right| \\
&\leq \sum_{j=1}^n p^* |b_{ij}| G_j |x_i(r) - y_i(r)| + \sum_{j=1}^n \bar{p}_i \eta_j |b_{ij}| |x_j(r-\tau) - y_j(r-\tau)|.
\end{aligned} \tag{18}$$

Substituting (17) and (18) into (16), we obtain

$$\begin{aligned}
|z_i(t)| &\leq |z_i(0)| + |z'_i(0)|t \\
&+ \frac{1}{\Gamma(\alpha)} \int_0^t (t-r)^{\alpha-1} [\theta_i + p^* |I_i| \\
&+ p^* \sum_{j=1}^n (|a_{ij}|F_j + |b_{ij}|G_j)] |z_i(r)| dr \\
&+ \frac{1}{\Gamma(\alpha)} \int_0^t (t-r)^{\alpha-1} \left( \sum_{j=1}^n \xi_j \bar{p}_i |a_{ij}| |z_j(r)| \right) dr \\
&+ \frac{1}{\Gamma(\alpha)} \int_0^t (t-r)^{\alpha-1} \left( \sum_{j=1}^n \eta_j \bar{p}_i |b_{ij}| |z_j(r-\tau)| \right) dr.
\end{aligned} \tag{19}$$

Consequently,

$$\begin{aligned}
\|z(t)\| &\leq \|z(0)\| + \|z'(0)\|t + \frac{\lambda_1}{\Gamma(\alpha)} \int_0^t (t-r)^{\alpha-1} \|z(r)\| dr \\
&+ \frac{\lambda_2}{\Gamma(\alpha)} \int_0^t (t-r)^{\alpha-1} \|z(r-\tau)\| dr.
\end{aligned} \tag{20}$$

With the Cauchy–Schwartz inequality, we obtain

$$\begin{aligned}
\|z(t)\| &\leq \|z(0)\| + \|z'(0)\|t \\
&+ \frac{\lambda_1}{\Gamma(\alpha)} \left( \int_0^t (t-r)^{2(\alpha-1)} e^{2r} dr \right)^{1/2} \left( \int_0^t e^{-2r} \|z(r)\|^2 dr \right)^{1/2} \\
&+ \frac{\lambda_2}{\Gamma(\alpha)} \left( \int_0^t (t-r)^{2(\alpha-1)} e^{2r} dr \right)^{1/2} \left( \int_0^t e^{-2r} \|z(r-\tau)\|^2 dr \right)^{1/2}.
\end{aligned} \tag{21}$$

In view of  $\int_0^t (t-r)^{2(\alpha-1)} e^{2r} dr < (2e^{2t}/4^\alpha)\Gamma(2\alpha-1)$ , we derive

$$\begin{aligned}
\|z(t)\| e^{-t} &\leq \|z(0)\| e^{-t} + \|z'(0)\| e^{-t} \\
&+ \frac{\sqrt{2\Gamma(2\alpha-1)}}{2^\alpha \Gamma(\alpha)} \left\{ \lambda_1 \left( \int_0^t e^{-2r} \|z(r)\|^2 dr \right)^{1/2} \right. \\
&\left. + \lambda_2 e^{-\tau} \left( \int_0^t e^{-2(r-\tau)} \|z(r-\tau)\|^2 dr \right)^{1/2} \right\}.
\end{aligned} \tag{22}$$

Let  $\omega(t) = \sup_{t-\tau \leq s \leq t} e^{-s} \|z(s)\|$ , then, for any  $r \in [0, t]$ , we have

$$\begin{aligned}
e^{-r} \|z(r)\| &\leq \omega(r), \\
e^{-(r-\tau)} \|z(r-\tau)\| &\leq \omega(r).
\end{aligned} \tag{23}$$

Thus, inequality (22) gives

$$\omega(t) \leq \delta e^{-t} (1+t) + \Lambda \left( \int_0^t \omega^2(r) dr \right)^{1/2}. \tag{24}$$

With Proposition 2, this yields

$$\begin{aligned}
\left( \int_0^t \omega^2(s) ds \right)^{1/2} &\leq \delta \left\{ 1 - \left( 1 - e^{-\Lambda^2 t} \right)^{1/2} \right\}^{-1} \\
&\cdot \left\{ \int_0^t (1+r)^2 e^{-2r} e^{-\Lambda r} dr \right\}^{1/2}.
\end{aligned} \tag{25}$$

Substituting this into inequality (24), we obtain

$$\begin{aligned}
\omega(t) &\leq \delta e^{-t} (1+t) + \delta \Lambda \left\{ 1 - \left( 1 - e^{-\Lambda^2 t} \right)^{1/2} \right\}^{-1} \\
&\cdot \left\{ \int_0^t (1+r)^2 e^{-2r} e^{-\Lambda^2 r} dr \right\}^{1/2}.
\end{aligned} \tag{26}$$

By virtue of Proposition 3, it follows that

$$\omega(t) \leq \delta (1+t) e^{-t} + 2\delta e^{\Lambda^2 t} (1+t) \left( 1 - e^{-\Lambda^2 t} \right)^{1/2}. \tag{27}$$

Thus,

$$\|z(t)\| \leq \delta (1+t) \left\{ 1 + 2e^{(\Lambda^2+1)t} \left( 1 - e^{-\Lambda^2 t} \right)^{1/2} \right\}. \tag{28}$$

With (14), this gives  $\|z(t)\| < \varepsilon$  for  $t \in [0, T]$ , which shows that network (7) achieves the FTS w.r.t.  $\{\delta, \varepsilon, T\}$ . The proof is finished.  $\square$

**3.2. Stability Criterion II for Network (7).** In this section, we discuss the finite-time stability of equilibrium point for network (7). For the parameters of network (7), some further hypotheses [9] are given as follows:

(H1) The function  $p_i(\cdot)$  ( $i = 1, 2, \dots, n$ ) is a continuous and bounded function such that  $0 < \underline{p}_i \leq p_i(\cdot) \leq \bar{p}_i$  on  $\mathbb{R}$ , where  $\underline{p}_i$  and  $\bar{p}_i$  are two positive constants.

(H2) The function  $q_i(\cdot)$  ( $i = 1, 2, \dots, n$ ) is a monotonic differentiable function such that  $0 < \underline{q}_i \leq q'_i(\cdot) \leq \bar{q}_i$  on  $\mathbb{R}$ , where  $\underline{q}_i$  and  $\bar{q}_i$  are two positive constants.

(H3) The functions  $f_j$  and  $g_j$  ( $j = 1, 2, \dots, n$ ) satisfy the Lipschitz conditions:

$$\begin{aligned}
|f_j(x) - f_j(y)| &\leq \xi_j |x - y|, \\
|g_j(x) - g_j(y)| &\leq \eta_j |x - y|, \\
&\forall x, y \in \mathbb{R},
\end{aligned} \tag{29}$$

where  $\xi_j$  and  $\eta_j$  are two positive constants.

(H4) For  $i, j = 1, 2, \dots, n$ ,  $a_{ij}, b_{ij}, \underline{q}_i, \xi_j$  and  $\eta_j$  satisfy the following condition:



$$\sum_{i=1}^n \frac{1}{q_i} \max_{1 \leq j \leq n} (a^* \xi_j + b^* \eta_j) < 1, \quad (30)$$

where  $a^* = \max_{1 \leq j \leq n} \sum_{i=1}^n |a_{ij}|$ ,  $b^* = \max_{1 \leq j \leq n} \sum_{i=1}^n |b_{ij}|$ .

By an argument similar to that in [9, 24], the assumptions (H1)–(H4) can guarantee the existence and uniqueness of equilibrium point for network (7). In what follows, we will concentrate on the finite-time stability for the equilibrium point  $x^*$ . Now, we introduce some notation. Let

$$\begin{aligned} \rho_1 &= \max_{1 \leq i \leq n} \{\bar{p}_i \bar{q}_i\} + \max_{1 \leq j \leq n} \left( a^* \xi_j \sum_{i=1}^n \bar{p}_i \right), \\ \rho_2 &= \max_{1 \leq j \leq n} \left( b^* \eta_j \sum_{i=1}^n \bar{p}_i \right), \\ \vartheta &= \frac{(\rho_1 + \rho_2 e^{-\tau}) \sqrt{2\Gamma(2\alpha - 1)}}{2^\alpha \Gamma(\alpha)}. \end{aligned} \quad (31)$$

For network (7), let  $x(t)$  represent an arbitrary solution with the initial conditions:  $x(t) = \phi^{(0)}(t)$ ,  $x'(t) = \phi^{(1)}(t)$  ( $t \in [-\tau, 0]$ ),

where  $\phi^{(0)}(t), \phi^{(1)}(t) \in C([-\tau, 0], \mathbb{R}^n)$ . Let  $\|\phi - x^*\| = \max\{\|\phi^{(0)}(t) - x^*\|, \|\phi^{(1)}(t) - (x^*)'\|\}$ .

**Theorem 2.** *Let  $0 < \delta < \varepsilon$ . Under the assumptions (H1)–(H4), the unique equilibrium point  $x^*$  of network (7) achieves the FTS w.r.t.  $\{\delta, \varepsilon, T\}$ , if  $\|\phi - x^*\| < \delta$  and*

$$(1+t) \left\{ 1 + 2e^{(\vartheta^2+1)t} \left( 1 - e^{-\vartheta^2 t} \right)^{1/2} \right\} < \frac{\varepsilon}{\delta}, \quad \forall t \in [0, T]. \quad (32)$$

*Proof.* Since  $x^*$  is the equilibrium point for system (7), we have

$$\begin{aligned} q_i(x_i^*) - \sum_{j=1}^n a_{ij} f_j(x_j^*) - \sum_{j=1}^n b_{ij} g_j(x_j^*) - I_i &= 0, \\ i &= 1, 2, \dots, n. \end{aligned} \quad (33)$$

Based on (7) and (33), we use Proposition 1 to obtain

$$\begin{aligned} x_i(t) - x_i^* &= x_i(0) - x_i^* + x_i'(0)t \\ &\quad - \frac{1}{\Gamma(\alpha)} \int_0^t (t-r)^{\alpha-1} (p_i(x_i) (q_i(x_i(r)) - q_i(x_i^*))) dr \\ &\quad + \frac{1}{\Gamma(\alpha)} \int_0^t (t-r)^{\alpha-1} \left( p_i(x_i) \sum_{j=1}^n a_{ij} (f_j(x_j(r)) - f_j(x_j^*)) \right) dr \\ &\quad + \frac{1}{\Gamma(\alpha)} \int_0^t (t-r)^{\alpha-1} \left( p_i(x_i) \sum_{j=1}^n b_{ij} (g_j(x_j(r-\tau)) - g_j(x_j^*)) \right) dr. \end{aligned} \quad (34)$$

For the term  $q_i(x_i(r)) - q_i(x_i^*)$ , applying Lagrange's mean value theorem, it follows that

$$|q_i(x_i(r)) - q_i(x_i^*)| \leq \bar{q}_i |x_i(r) - x_i^*|. \quad (35)$$

Let  $u_i(t) = x_i(t) - x_i^*$ . Obviously, equation (34) leads to

$$\begin{aligned} |u_i(t)| &\leq |u_i(0)| + |u_i'(0)|t + \frac{1}{\Gamma(\alpha)} \int_0^t (t-r)^{\alpha-1} \left( \bar{p}_i \bar{q}_i |u_i(r)| \right. \\ &\quad \left. + \sum_{j=1}^n \bar{p}_i |a_{ij}| \xi_j |u_j(r)| + \sum_{j=1}^n \bar{p}_i |b_{ij}| \eta_j |u_j(r-\tau)| \right) ds. \end{aligned} \quad (36)$$

Following the treatment similar to that of (20), we can obtain inequality (32).  $\square$

*Remark 1.* When  $p_i(x_i(t)) = 1$  and  $q_i(x_i(t)) = c_i x_i(t)$  ( $c_i > 0$ ), network (7) is reduced to that in [34]. The corresponding results can be easily derived from those in this paper.

*Remark 2.* When  $\alpha = 1$ , network (7) is reduced to an integer-order one. The corresponding finite-time criteria can be easily obtained by repeating the Proofs of Theorems 1 and 2.

*Remark 3.* For  $\alpha \in (0, 1)$ , Ke and Miao [9] studied the FTS of equilibrium point for a class of delayed FOCGNNs based on the generalized Bellman–Gronwall inequality; Rajivganthi et al. [24] considered the FTS for a class of BAM FOCGNNs with delay by resorting to some inequalities; Zheng et al. [23] reported the FTS for a class of memristor-based FOCGNNs with delay based on a kind of Gronwall's inequality. It seems to us that these methods can not be directly extended to the case of  $\alpha \in (1, 2)$ .

*Remark 4.* In the literature, there have been many works [15–17, 34–37] on the finite-time stability or finite-time synchronization for FONNs with  $\alpha \in (1, 2)$ . The obtained sufficient conditions are some inequalities involving the Mittag–Leffler functions. The proofs are mainly based on the

Laplace transform, the inverse Laplace transform, and the generalized Gronwall–Bellman inequalities related to the Mittag–Leffler functions. However, this method is not applicable to network (7) owing to the technical reason. In the present paper, a kind of different method was used to discuss the FTS of network (7). More precisely, two kinds of finite-time criteria were obtained based on some properties of the Caputo derivative and some inequalities. Especially, these two criteria are expressed as some algebraic inequalities independent of the Mittag–Leffler functions. Therefore, the verification is relatively easy in practical applications.

#### 4. Numerical Simulations

In this section, two examples are presented to illustrate the effectiveness of two criteria.

*Example 1.* Consider the following FOCGNN model:

$${}^C_0D_t^{1.8}x_i(t) = -p_i(x_i(t)) \left[ q_i(x_i(t)) - \sum_{j=1}^3 a_{ij}f_j(x_j(t)) - \sum_{j=1}^3 b_{ij}g_j(x_j(t-0.1)) - I_i \right], \quad i = 1, 2, 3. \quad (37)$$

Here,  $p_i(x_i(t)) = 0.2 \sin(x_i(t)) + 0.3$  and  $q_i(x_i(t)) = 0.8 \cos(x_i(t))$  for  $i = 1, 2, 3$ ,  $a_{11} = 0.027$ ,  $a_{12} = 0.008$ ,  $a_{13} = 0.029$ ,  $a_{21} = 0.018$ ,  $a_{22} = 0.017$ ,  $a_{23} = 0.005$ ,  $a_{31} = 0.003$ ,  $a_{32} = 0.029$ ,  $a_{33} = 0.029$ ,  $b_{11} = 0.029$ ,  $b_{12} = 0.004$ ,  $b_{13} = 0.024$ ,  $b_{21} = 0.015$ ,  $b_{22} = 0.013$ ,  $b_{23} = 0.029$ ,  $b_{31} = 0.024$ ,  $b_{32} = 0.028$ ,  $b_{33} = 0.02$ ,  $f_j(x_j(t)) = 0.05(|x_j(t) + 1| - |x_j(t) - 1|)$ ,  $g_j(x_j(t-0.1)) = 0.05(|x_j(t-0.1) + 1| - |x_j(t-0.1) - 1|)$ ,  $I_1 = 0.0478$ ,  $I_2 = -0.014$ , and  $I_3 = 0.081$ .

Obviously,  $0.1 \leq p_1(x_1) \leq 0.5$ ,  $0.1 \leq p_2(x_2) \leq 0.5$ ,  $0.1 \leq p_3(x_3) \leq 0.5$ ,  $p^* = 0.2$ ,  $\theta_1 = \theta_2 = \theta_3 = 0.56$ ,  $F_j = G_j = \xi_j = \eta_j = 0.1$ . Moreover, we obtain  $\lambda_1 = 0.5815$ ,  $\lambda_2 = 0.011$ , and  $\Lambda = 0.218$ .

Let  $x(t)$  and  $y(t)$  be two solutions of network (37) with the initial conditions:

$$\begin{aligned} x(t) &= (1.12 - 0.007t, 1.56 + 0.002t, -1.53 + 0.01t)^T, \\ x'(t) &= (-0.007, 0.002, 0.01)^T, \\ y(t) &= (1.125 - 0.001t, 1.566 + 0.006t, -1.525 + 0.02t)^T, \\ y'(t) &= (-0.001, 0.006, 0.02)^T, \end{aligned} \quad (38)$$

for  $t \in [-0.1, 0]$ . The time curves for  $x(t)$  and  $y(t)$  are shown in Figure 1.

Based on the initial conditions,  $\delta$  is taken as  $\delta = 0.02$ . Let  $\varepsilon = 1$ . Inequality (14) gives the settling time  $T_s = 2.7424$ . The time response of  $\|x(t) - y(t)\|$  is depicted in Figure 2. Obviously,  $\|x(t) - y(t)\| < 1$  holds for any  $t \in [0, 2.7424]$  which coincides with the result of Theorem 1.

*Example 2.* Consider the following FOCGNN model:

$${}^C_0D_t^{1.6}x_i(t) = -p_i(x_i(t)) \left[ q_i(x_i(t)) - \sum_{j=1}^3 a_{ij}f_j(x_j(t)) - \sum_{j=1}^3 b_{ij}g_j(x_j(t-0.1)) - I_i \right], \quad (39)$$

for  $i = 1, 2, 3$ , where  $p_i(x_i(t)) = 0.1 \cos(x_i(t)) + 0.2$  ( $i = 1, 2, 3$ ),  $q_1(x_1(t)) = 0.25x_1(t)$ ,  $q_2(x_2(t)) = 0.4x_2(t)$ ,  $q_3(x_3(t)) = 0.5x_3(t)$ ,  $a_{11} = 0.04$ ,  $a_{12} = 0.05$ ,  $a_{13} = -0.01$ ,  $a_{21} = 0.04$ ,  $a_{22} = -0.03$ ,  $a_{23} = -0.03$ ,  $a_{31} = -0.06$ ,  $a_{32} = 0.05$ ,  $a_{33} = 0.05$ ,  $b_{11} = -0.05$ ,  $b_{12} = 0.05$ ,  $b_{13} = 0.09$ ,  $b_{21} = 0.08$ ,  $b_{22} = -0.024$ ,  $b_{23} = -0.02$ ,  $b_{31} = 0.05$ ,  $b_{32} = -0.04$ ,  $b_{33} = 0.04$ ,  $f_j(x_j(t)) = 0.025(|x_j(t) + 1| - |x_j(t) - 1|)$ ,  $g_j(x_j(t-0.1)) = 0.025(|x_j(t-0.1) + 1| - |x_j(t-0.1) - 1|)$ ,  $I_1 = 0.042$ ,  $I_2 = 0.061$ , and  $I_3 = 0.039$ .

Obviously,

$$0.1 \leq p_1(x_1) \leq 0.3,$$

$$0.1 \leq p_2(x_2) \leq 0.3,$$

$$0.1 \leq p_3(x_3) \leq 0.3,$$

$$\frac{dq_1(x_1)}{dx_1} = 0.25, \quad (40)$$

$$\frac{dq_2(x_2)}{dx_2} = 0.4,$$

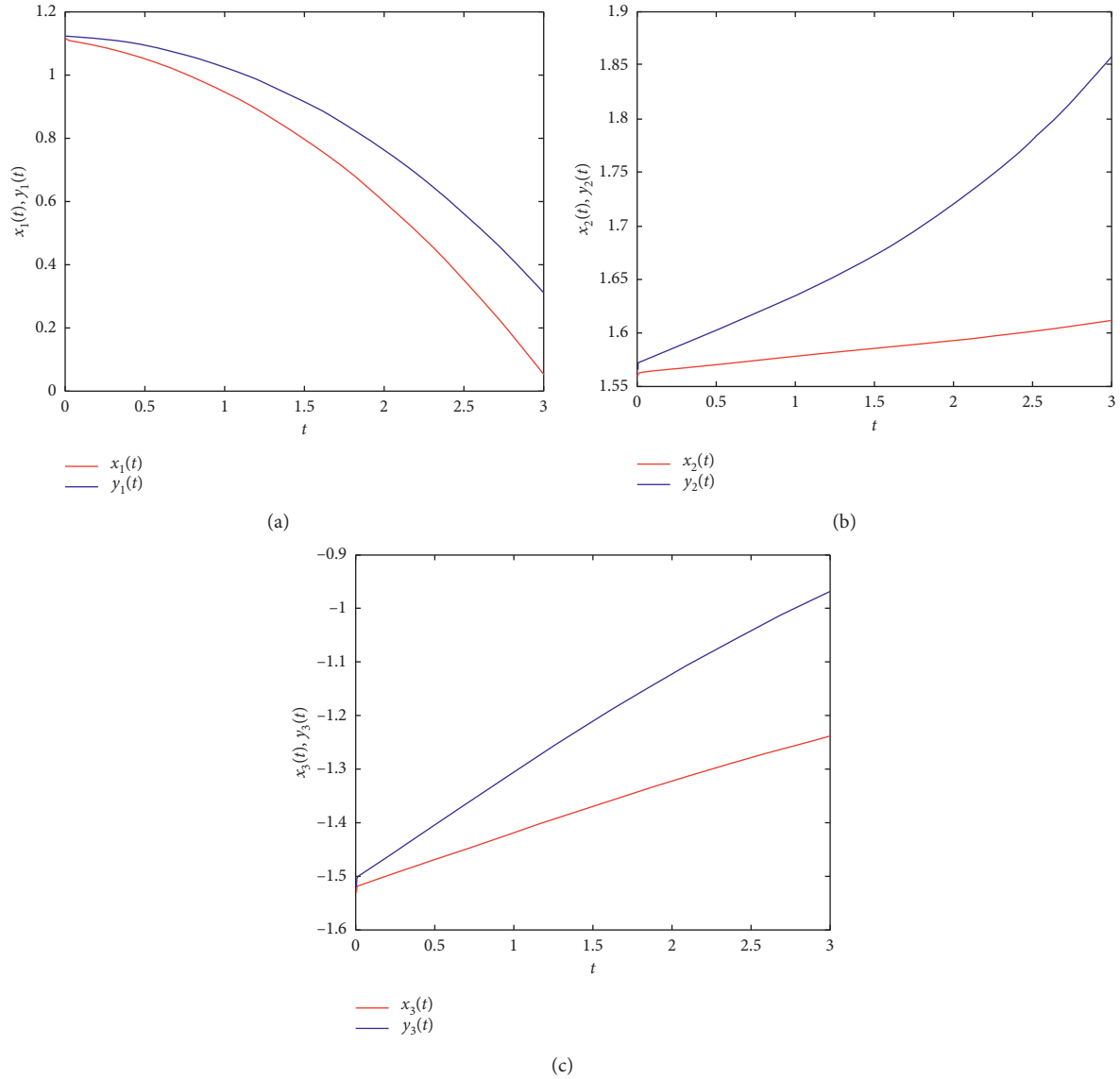
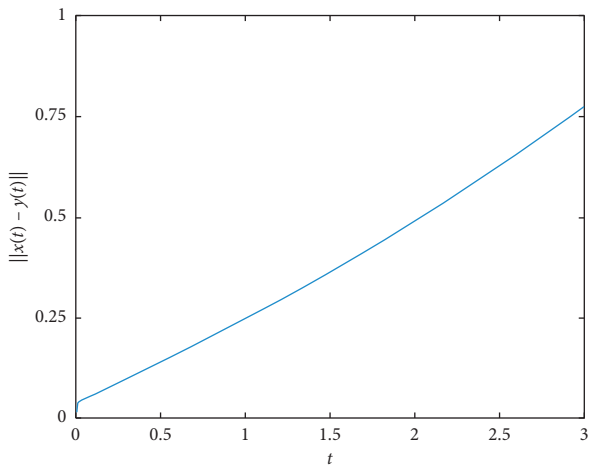
$$\frac{dq_3(x_3)}{dx_3} = 0.5.$$

From the above data, we take  $\xi_j = \eta_j = 0.05$  ( $j = 1, 2, 3$ ),  $a^* = 0.14$ , and  $b^* = 0.18$ . Moreover,

$$\sum_{i=1}^n \frac{1}{q_i} \max_{1 \leq j \leq n} (a^* \xi_j + b^* \eta_j) = 0.136 < 1. \quad (41)$$

This indicates that network (39) has a unique equilibrium point  $x^*$ . Based on (33), we have

$$\begin{cases} 0.25x_1^* + 0.01f_1(x_1^*) - 0.1f_2(x_2^*) - 0.08f_3(x_3^*) - 0.042 = 0, \\ 0.4x_2^* - 0.12f_1(x_1^*) + 0.054f_2(x_2^*) + 0.05f_3(x_3^*) - 0.061 = 0, \\ 0.5x_3^* + 0.01f_1(x_1^*) - 0.01f_2(x_2^*) - 0.09f_3(x_3^*) - 0.039 = 0. \end{cases} \quad (42)$$

FIGURE 1: The time response for  $x(t)$  and  $y(t)$ .FIGURE 2: The time response for the error between  $x(t)$  and  $y(t)$ .

This gives the equilibrium point  $x^* = (0.17, 0.15, 0.08)^T$ .

Let  $x(t)$  and  $y(t)$  be two solutions with the initial conditions:

$$x(t) = (0.15 + 0.0015t, 0.16 - 0.001t, 0.1 - 0.001t)^T,$$

$$x'(t) = (0.0015, -0.001, -0.001)^T,$$

$$y(t) = (0.18 - 0.001t, 0.13 + 0.0012t, 0.007 + 0.0012t)^T,$$

$$y'(t) = (-0.001, 0.0012, 0.0012)^T,$$

(43)

for any  $t \in [-0.1, 0]$ . The time curves are depicted in Figure 3. Moreover, the time evolution for  $\|x(t) - x^*\|$  and  $\|y(t) - x^*\|$  is shown in Figure 4.

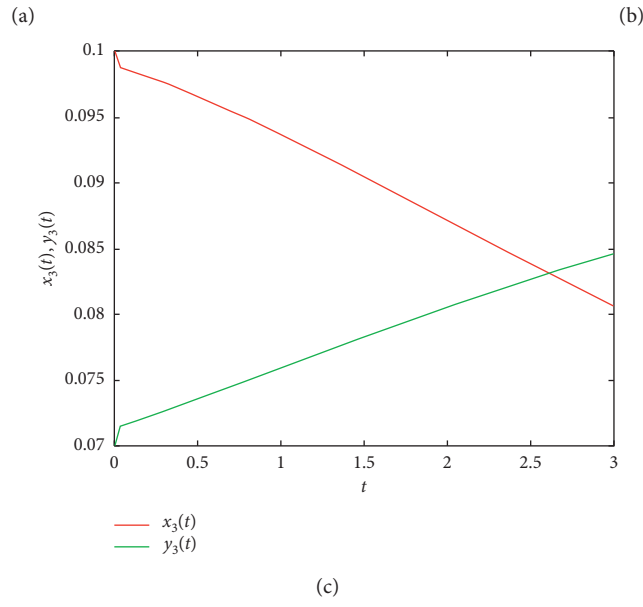
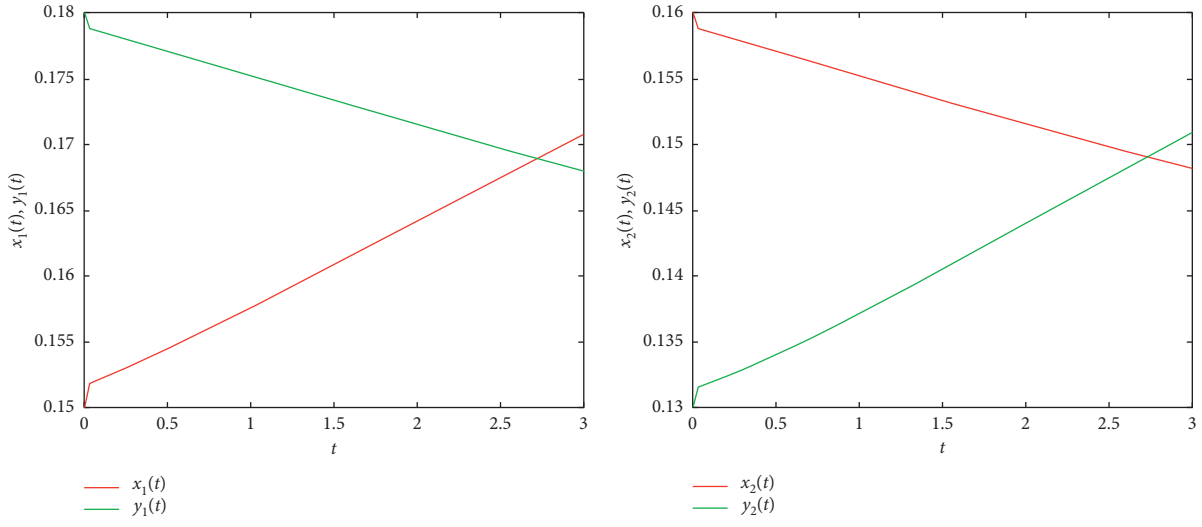


FIGURE 3: The time response for  $x(t)$  and  $y(t)$ .

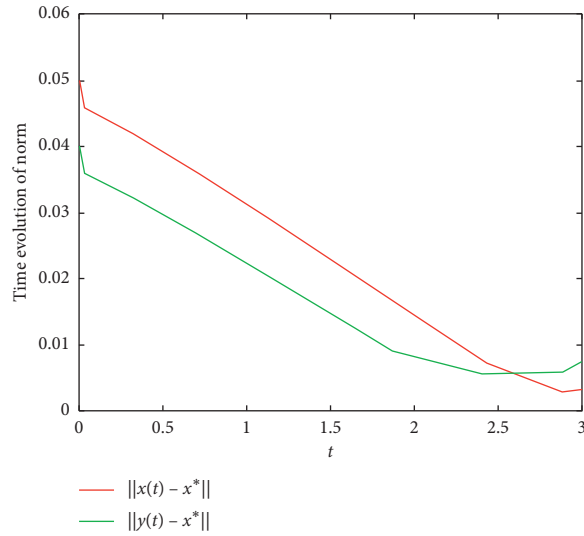


FIGURE 4: The time response for  $\|x(t) - x^*\|$  and  $\|y(t) - x^*\|$ .

Based on the above data, it follows that  $\rho_1 = 0.1563$ ,  $\rho_2 = 0.0081$  and  $\vartheta = 0.0897$ . We take  $\delta = 0.05$ . Let  $\varepsilon = 1$ . The condition (32) gives the settling time  $T_s = 2.694$ . From Figure 4, it can be checked that  $\|x(t) - x^*\| < 1$  and  $\|y(t) - x^*\| < 1$  hold for  $t \in [0, 2.694]$ . This fact is consistent with Theorem 2.

## 5. Conclusions

In the recent decade, many efforts have been made to the research on FONNs with the fractional order between 1 and 2. The methods are mainly based on the Laplace transform, the inverse Laplace transform, and the generalized Gronwall inequality related to the Mittag–Leffler functions. However, these methods do not work well for the considered FOCGNNs owing to the technical reason. In this paper, the finite-time stability criteria were derived based on the analytic techniques and some inequalities. This kind of method is completely different from the above ones. In particular, the obtained criteria are expressed as some algebraic inequalities independent of the Mittag–Leffler functions and thus, they can be easily verified in practical applications. In the future work, we will investigate the finite-time guaranteed cost control for FONNs with high fractional order. It seems to us that some new techniques would be developed to deal with this problem.

## Data Availability

The data used to support the findings of this study are included within the article.

## Conflicts of Interest

The authors declare that they have no conflicts of interest.

## Acknowledgments

This research was supported by the National Natural Science Foundation of China (Grant nos. 61773220, 61876192, and 61907021), the Natural Science Foundation of Hubei Province of China, the Fundamental Research Funds for the Central Universities of South-Central University for Nationalities (Grant nos. KTZ20051, CZT20020, and CZT20022), and School Talent Funds (No. YZZ19004).

## References

- [1] M. A. Cohen and S. Grossberg, "Absolute stability of global pattern formation and parallel memory storage by competitive neural networks," *IEEE Transactions on Systems, Man, and Cybernetics*, vol. SMC-13, no. 5, pp. 815–826, 1983.
- [2] Q. Zhu, J. Cao, and R. Rakkiyappan, "Exponential input-to-state stability of stochastic Cohen–Grossberg neural networks with mixed delays," *Nonlinear Dynamics*, vol. 79, no. 2, pp. 1085–1098, 2015.
- [3] X. Nie, W. X. Zheng, and J. Cao, "Multistability of memristive Cohen–Grossberg neural networks with non-monotonic piecewise linear activation functions and time-varying delays," *Neural Networks*, vol. 71, pp. 27–36, 2015.
- [4] M. Şayli and E. Yilmaz, "State-dependent impulsive Cohen–Grossberg neural networks with time-varying delays," *Neurocomputing*, vol. 171, pp. 1375–1386, 2016.
- [5] A. Abdurahman, H. Jiang, and K. Rahman, "Function projective synchronization of memristor-based Cohen–Grossberg neural networks with time-varying delays," *Cognitive Neurodynamics*, vol. 9, no. 6, pp. 603–613, 2015.
- [6] Z. Chen, D. Zhao, and J. Ruan, "Dynamic analysis of high-order Cohen–Grossberg neural networks with time delay," *Chaos, Solitons & Fractals*, vol. 32, no. 4, pp. 1538–1546, 2007.
- [7] Y. Shi and P. Zhu, "Asymptotic stability analysis of stochastic reaction-diffusion Cohen–Grossberg neural networks with mixed time delays," *Applied Mathematics and Computation*, vol. 242, pp. 159–167, 2014.
- [8] L. G. Wan and A. L. Wu, "Mittag–Leffler stability analysis of fractional-order fuzzy Cohen–Grossberg neural networks with deviating argument," *Advances in Difference Equations*, vol. 2017, no. 1, 2017.
- [9] Y. Ke and C. Miao, "Stability analysis of fractional-order Cohen–Grossberg neural networks with time delay," *International Journal of Computer Mathematics*, vol. 92, no. 6, pp. 1102–1113, 2015.
- [10] A. Pratap, R. Raja, J. Cao, C. P. Lim, and O. Bagdasar, "Stability and pinning synchronization analysis of fractional order delayed Cohen–Grossberg neural networks with discontinuous activations," *Applied Mathematics and Computation*, vol. 359, pp. 241–260, 2019.
- [11] Y.-J. Huang, X.-Y. Yuan, X.-H. Yang, H.-X. Long, and J. Xiao, "Multiple Lagrange stability and Lyapunov asymptotical stability of delayed fractional-order Cohen–Grossberg neural networks," *Chinese Physics B*, vol. 29, no. 2, Article ID 020703, 2020.
- [12] R. C. Koeller, "Application of fractional calculus to the theory of viscoelasticity," *Journal of Applied Mechanics*, vol. 51, no. 2, pp. 294–298, 1984.
- [13] R. L. Bagley and R. A. Calico, "Fractional order state equations for the control of viscoelastically damped structures," *Journal of Guidance, Control, and Dynamics*, vol. 14, no. 2, pp. 304–311, 1991.
- [14] T. T. Hartley and C. F. Lorenzo, "Dynamics and control of initialized fractional-order systems," *Nonlinear Dynamics*, vol. 29, no. 1–4, pp. 201–233, 2002.
- [15] C. Rajivganthi, F. A. Rihan, S. Lakshmanan, R. Rakkiyappan, and P. Muthukumar, "Synchronization of memristor-based delayed BAM neural networks with fractional-order derivatives," *Complexity*, vol. 21, no. 2, pp. 412–426, 2016.
- [16] R. Rakkiyappan, G. Velmurugan, and J. Cao, "Finite-time stability analysis of fractional-order complex-valued memristor-based neural networks with time delays," *Nonlinear Dynamics*, vol. 78, no. 4, pp. 2823–2836, 2014.
- [17] C. Y. Chen, S. Zhu, Y. C. Wei, and C. Y. Yang, "Finite-time stability of delayed memristor-based fractional-order neural networks," *IEEE Transactions on Cybernetics*, vol. 50, no. 4, pp. 1607–1616, 2018.
- [18] R. Wu, Y. Lu, and L. Chen, "Finite-time stability of fractional delayed neural networks," *Neurocomputing*, vol. 149, pp. 700–707, 2015.
- [19] L. Chen, J. Cao, R. Wu, J. A. Tenreiro Machado, A. M. Lopes, and H. Yang, "Stability and synchronization of fractional-order memristive neural networks with multiple delays," *Neural Networks*, vol. 94, pp. 76–85, 2017.
- [20] Z. Y. Yang and J. Zhang, "Stability analysis of fractional-order bidirectional associative memory neural networks with mixed

- time-varying delays,” *Complexity*, vol. 2019, Article ID 2363707, 22 pages, 2019.
- [21] J. Hu, G. Sui, X. Lv, and X. Li, “Fixed-time control of delayed neural networks with impulsive perturbations,” *Nonlinear Analysis: Modelling and Control*, vol. 23, no. 6, pp. 904–920, 2018.
- [22] X. Li, D. O’Regan, and H. Akca, “Global exponential stabilization of impulsive neural networks with unbounded continuously distributed delays,” *IMA Journal of Applied Mathematics*, vol. 80, no. 1, pp. 85–99, 2015.
- [23] M. Zheng, L. Li, H. Peng, J. Xiao, Y. Yang, and H. Zhao, “Finite-time stability and synchronization for memristor-based fractional-order Cohen-Grossberg neural network,” *The European Physical Journal B*, vol. 89, p. 204, 2016.
- [24] C. Rajivganthi, F. A. Rihan, S. Lakshmanan, and P. Muthukumar, “Finite-time stability analysis for fractional-order Cohen-Grossberg BAM neural networks with time delays,” *Neural Computing and Applications*, vol. 29, no. 12, pp. 1309–1320, 2016.
- [25] X. Yang, X. Li, and J. Cao, “Robust finite-time stability of singular nonlinear systems with interval time-varying delay,” *Journal of the Franklin Institute*, vol. 355, no. 3, pp. 1241–1258, 2018.
- [26] X. Li, X. Yang, and S. Song, “Lyapunov conditions for finite-time stability of time-varying time-delay systems,” *Automatica*, vol. 103, pp. 135–140, 2019.
- [27] M. Hui, C. Wei, J. Zhang et al., “Finite-time synchronization of memristor-based fractional order Cohen-Grossberg neural networks,” *IEEE Access*, vol. 8, pp. 73698–73713, 2020.
- [28] P. Wan and J. Jian, “Global mittag-leffler boundedness for fractional-order complex-valued cohen-grossberg neural networks,” *Neural Processing Letters*, vol. 49, no. 1, pp. 121–139, 2019.
- [29] F. Mainardi, “The fundamental solutions for the fractional diffusion-wave equation,” *Applied Mathematics Letters*, vol. 9, no. 6, pp. 23–28, 1996.
- [30] R. Gorenflo, F. Mainardi, D. Moretti, G. Pagnini, and P. Paradisi, “Fractional diffusion: probability distributions and random walk models,” *Physica A: Statistical Mechanics and Its Applications*, vol. 305, no. 1-2, pp. 106–112, 2002.
- [31] W. Zhang, X. Cai, and S. Holm, “Time-fractional heat equations and negative absolute temperatures,” *Computers & Mathematics with Applications*, vol. 67, no. 1, pp. 164–171, 2014.
- [32] W. Yu, Y. Li, G. Wen, X. Yu, and J. Cao, “Observer design for tracking consensus in second-order multi-agent systems: fractional order less than two,” *IEEE Transactions on Automatic Control*, vol. 62, no. 2, pp. 894–900, 2017.
- [33] X. Li, J. Shen, H. Akca, and R. Rakkiyappan, “LMI-based stability for singularly perturbed nonlinear impulsive differential systems with delays of small parameter,” *Applied Mathematics and Computation*, vol. 250, pp. 798–804, 2015.
- [34] R.-C. Wu, X.-D. Hei, and L.-P. Chen, “Finite-time stability of fractional-order neural networks with delay,” *Communications in Theoretical Physics*, vol. 60, no. 2, pp. 189–193, 2013.
- [35] R. Rakkiyappan, G. Velmurugan, and J. D. Cao, “Finite-time synchronization of fractional-order memristor-based neural networks with time delays,” *Neural Networks*, vol. 73, pp. 36–46, 2016.
- [36] J. Xiao, S. Zhong, Y. Li, and F. Xu, “Finite-time Mittag-Leffler synchronization of fractional-order memristive BAM neural networks with time delays,” *Neurocomputing*, vol. 219, pp. 431–439, 2017.
- [37] Y. P. Cao and C. Z. Bai, “Finite-time stability of fractional-order BAM neural networks with distributed delay,” *Abstract and Applied Analysis*, vol. 2014, Article ID 634803, 8 pages, 2014.
- [38] I. Podlubny, *Fractional Differential Equations*, Academic Press, New York, NY, USA, 1999.
- [39] C. Li and W. Deng, “Remarks on fractional derivatives,” *Applied Mathematics and Computation*, vol. 187, no. 2, pp. 777–784, 2007.
- [40] D. Willett, “Nonlinear vector integral equations as contraction mappings,” *Archive for Rational Mechanics and Analysis*, vol. 15, no. 1, pp. 79–86, 1964.
- [41] D. Mitrinovic, *Analytic Inequalities*, Springer, Berlin, Germany, 1970.

## Research Article

# Distributed Prescribed Finite Time Consensus Scheme for Economic Dispatch of Smart Grids with the Valve Point Effect

Yingjiang Zhou <sup>1,2</sup>, Shigao Zhu,<sup>1,2</sup> and Qian Chen<sup>1,2</sup>

<sup>1</sup>College of Automation and College of Artificial Intelligence, Nanjing University of Posts and Telecommunications, Nanjing 210023, China

<sup>2</sup>Jiangsu Engineering Lab for IOT Intelligent Robots (IOTRobot), Nanjing 210023, China

Correspondence should be addressed to Yingjiang Zhou; [zhouyj@njupt.edu.cn](mailto:zhouyj@njupt.edu.cn)

Received 11 July 2020; Revised 10 August 2020; Accepted 19 August 2020; Published 31 August 2020

Academic Editor: Jianquan Lu

Copyright © 2020 Yingjiang Zhou et al. This is an open access article distributed under the Creative Commons Attribution License, which permits unrestricted use, distribution, and reproduction in any medium, provided the original work is properly cited.

The distributed prescribed finite time consensus schemes for economic dispatch (ED) of smart grids with and without the valve point effect are researched in this paper. First, the optimization problem is transformed into a consensus of multiagent system problem, where both with and without the valve point effect are considered. Second, for the directed balance network, a prescribed finite time method has been arranged to solve the ED problem with and without the valve point effect. Third, with considering the constraints of generation units, the prescribed finite time result is also achieved. Finally, from the simulations, the efficiency of the proposed algorithms is validated.

## 1. Introduction

In the recent years, the research about the ED problem has attracted tremendous attentions, which is particularly important in the smart grid. The aim of the ED problem is to find the optimization of the minimum total generation cost. When there are certain practical constraints, the aim of the ED problem is to find the optimal outputs to minimum total generation cost while meeting the power demand. The traditional ways of solving the ED problem (e.g., genetic algorithm [1, 2], particle swarm optimization [3–6], and multiobjective collective decision optimization algorithm [7]) are centralized methods.

Recently, many research results focus on the distributed approach to resolve the ED problem [8–17], where the generation units only get the neighbor's information. The low communication cost, easy implementation and maintenance, and strong robustness against communication uncertainties are the benefits of distributed ED algorithms [8]. Many pioneering work about distributed ED were pointed in [8–10], but these results are not fully distributed. The fully distributed ED algorithms were first proposed in

[11], where the distributed consensus methods in multiagent systems (MASs) have been used. When there exist unknown communication uncertainties, the ED problem is developed by using the adaptive consensus-based robust strategy [12]. For sparse communication networks and time delay, a distributed scheme is provided based on consensus strategy [13]. In order to reduce the amount of communication of the smart grids, the event-triggered control solution was devised to achieve the distributed reactive power sharing control [14–16]. In the smart grids, the second-order consensus methods have been used to solve the ED problem [17]. Considering the complex networks with the reaction diffusion terms and the probabilistic Boolean networks, the synchronization and stabilization methods were investigated in [18–20], and we will focus on the ED algorithms in these kinds of networks.

The rate of convergence is a key factor of solving the ED problem [21–25], and fast convergence rate and strong robustness are the advantages of the finite time method [26, 27]. Considering the ED problem of generation, the distributed finite-step iterative strategy is arranged [21]. If the topology is jointly connected, distributed finite time ED

in smart grid is derived [22]. In [15, 22], the homogeneous method is applied to solve the finite time ED problem, but it is hard to estimate the convergence time. A novel fully distributed finite time algorithm is devised to address the ED problem in the smart grids [23]. The convergence time in the abovementioned algorithms is connected with the initial condition, if the initial condition is large, the convergence time will be very long. The prescribed finite time method was proposed for the first time in [24], where the convergence time can be set by the designer. Very recently, a distributed prescribed finite time method for the ED problem was proposed [25].

Another important topic is about the valve point effect [28–41]. Many meaningful works are focused on the valve point effect, such as evolutionary programming [28, 29], genetic algorithm [30–33], and particle swarm optimisation [34, 35]. The complicated, nonlinear, and nonconvex ED problem with the valve point effect has been settled by using the Maclaurin series-based Lagrangian algorithm [36]. In [37], the valve point loading effect and transmission losses are considered, where the ED problem has been resolved with the gradient and Newton methods. But, most algorithms are centralized, and relatively speaking, distributed methods are more consistent with the actual requirements. In [38], the ED problem with the valve point effect is resolved with a distributed pattern search scheme.

The contributions of this paper can be listed in the following three aspects. (1) For the directed balance network, a prescribed finite time approach has been pointed out to solve the ED problem. (2) The prescribed finite time method was also derived for solving the ED problem with considering the valve point effect in this paper. (3) With considering the constraints of generation units, the prescribed finite time result is still correct.

The remainder of this article is organized as follows. The graph theory and problem statement are introduced in Section 2. Section 3 proposes distributed prescribed finite time consensus algorithms of solving the optimization without and with the valve point effect and the generation constraints of generation units. Three simulation examples are proposed to validate our results in Section 4. In Section 5, the conclusion has been presented.

## 2. Graph Theory and Problem Statement

In this section, the graph theory and the problem statement are introduced.

**2.1. Graph Theory.** We define  $G = (V, E, A)$  as a weighted directed graph, where  $V = \{v_1, \dots, v_n\}$  represents the set of nodes,  $E \subseteq V \times V$  represents the set of edges,  $(v_i, v_j) \in E$  represents that nodes  $i$  can receive information from node  $j$ , and  $A = [a_{ij}] \in R^{n \times n}$  is the weighted adjacency matrix. If and only if there is a directed edge  $(v_i, v_j)$  in  $G$ , then the weight of the edge  $a_{ij} > 0$ ; otherwise,  $a_{ij} = 0$ , ( $i \neq j$ ,  $i, j = 1, \dots, n$ ). Assume that  $a_{ii} = 0$  for all  $i \in \{1, \dots, n\}$ . The Laplacian matrix of a directed graph  $G$  is  $L = [l_{ij}] \in R^{n \times n}$ , where  $l_{ii} = \sum_{j=1}^n a_{ij}$  and  $l_{ij} = -a_{ij}$ ,  $i \neq j$ ,  $i, j = 1, \dots, n$ .

The direct path from the node  $i_1$  to node  $i_m$  is  $(i_1, i_2), (i_2, i_3), \dots, (i_{m-1}, i_m)$ . If one node in a directed graph at least has a directed path to another node, the graph contains a directed spanning tree. If each node has a directed path to all other nodes in a directed graph, the directed graph is said to be strongly connected. If all the nodes satisfy  $d_{in}(i) = \sum_{j=1}^n a_{ij} = d_{out}(i) = \sum_{j=1}^n a_{ji}$ ,  $i, j = 1, \dots, n$  and the in-degree is equal to the out-degree, then the direct graph is said to be a balance graph.

Define an undirected mirror graph  $\widehat{G} = \{V, \widehat{E}, \widehat{A}\}$ , which has the same nodes  $V$  as  $G$ . The set of edges is  $\widehat{E} \subseteq V \times V$ , and the weighted symmetric adjacency matrix is  $\widehat{A} = [\widehat{a}_{ij}]$ , where

$$\widehat{a}_{ij} = \widehat{a}_{ji} = \frac{a_{ij} + a_{ji}}{2} \geq 0. \quad (1)$$

**2.2. Problem Statement.** Suppose the MASs consist of  $n$  agents. Also, we can describe the dynamics of the agent as follows:

$$\dot{x}_i = u_i, \quad (2)$$

where  $u_i$  is the control inputs,  $i = 1, \dots, n$ .

**Definition 1.** The MASs (2) is said to reach consensus in prescribed finite time, if for any preselected time  $T > 0$  such that  $\lim_{t \rightarrow T} x_i = x_j$  and for all  $t \geq T$ ,  $x_i = x_j$ ,  $i, j \in \{1, \dots, n\}$ .

**Lemma 1** (see [10]). *For the irreducible Laplacian matrix  $L$ , the algebraic connectivity  $a(L) > 0$ , where  $a(L) = \min_{x^T \xi = 0, x \neq 0} x^T \widehat{L} x / x^T \Xi x$ , with  $\widehat{L} = \Xi L + L^T \Xi / 2$ ,  $\xi = (\xi_1, \xi_2, \dots, \xi_n) > 0$ ,  $\Xi = \text{diag}(\xi_1, \dots, \xi_n)$ ,  $\sum_{i=1}^n \xi_i = 1$ , and  $\xi^T L = 0$ .*

In this paper, the ED problem with and without the valve point effect is considered. Suppose there are  $n$  generating units. The cost function of each generator is as follows:

$$C_i(P)_i = a_i P_i^2 + b_i P_i + c_i + d_i \left| \sin(e_i (P_i^{\min} - P_i)) \right|, \quad (3)$$

where  $C_i(P_i)$  is the cost of the  $i$ -th generator,  $P_i$  is the real power generation of the  $i$ -th unit,  $P_i^{\min}$  is the lower bound of the generation capacity, and  $a_i, b_i, c_i, d_i$ , and  $e_i$  are the positive cost function coefficients.  $d_i |\sin(e_i (P_i^{\min} - P_i))|$  is the valve point effect. If  $d_i = 0$ , it means that the valve point effect is not exist.

Our research objective is to minimize the total cost of  $n$  power generation systems in the case of power demand and supply balance.

The optimization problem can be summarized as follows:

$$\min \sum_{i=1}^n C_i(P_i). \quad (4)$$

Subjecting to the power balance constraint,

$$\sum_{i=1}^n P_i = P_D, \quad (5)$$

where  $P_D$  is the total load of the power system.



### 3. Main Theoretical Results

*3.1. Optimization by Consensus without the Valve Point Effect.*  
In this section, the distributed control method is devised to solve the optimization problem without the valve point effect.

*Definition 2.* The incremental cost of each generator  $i$  without valve point effect is defined as  $IC_i = \partial C_i(P_i)/\partial P_i = r_i P_i + b_i$ ,  $i = 1, 2, \dots, n$ , where  $r_i = 2a_i$ .

The Lagrange multiplier algorithm is applied to solve the optimization problem.

$$\begin{aligned} L(P_i, \lambda) &= \sum_{i=1}^n C_i(P_i) + \lambda \left( P_D - \sum_{i=1}^n P_i \right) \\ &= \sum_{i=1}^n (a_i P_i^2 + b_i P_i + c_i) + \lambda \left( P_D - \sum_{i=1}^n P_i \right), \end{aligned} \quad (6)$$

where  $\lambda$  is the Lagrange multiplier.

The minimum value of (6) can be obtained by differentiating the abovementioned equation.

$$\frac{\partial L}{\partial P_i} = \frac{\partial C_i(P_i)}{\partial P_i} - \lambda = r_i P_i + b_i - \lambda = 0. \quad (7)$$

So,  $\sum_{i=1}^n P_i = P_D$ . We have

$$\lambda = r_i P_i + b_i. \quad (8)$$

We define  $y_i(t) = \lambda_i = r_i P_i + b_i$ . Then, a distributed prescribed finite time protocol is designed for the optimization problem.

$$\dot{y}_i(t) = cr_i k(t) \sum_{j=1}^n \hat{a}_{ij} (y_j(t) - y_i(t)) = -cr_i k(t) \sum_{j=1}^n \hat{L}_{ij} y_j(t). \quad (9)$$

With initial conditions  $y_i(0) = r_i P_i(0) + b_i$ , the following equation is satisfied:

$$\sum_{i=1}^n P_i(0) = P_D. \quad (10)$$

$k(t) = k_1 + k_2/T - t \text{sign}[1 + \text{sign}(T - t)]$ ,  $k_1 > 0$ ,  $k_2 > 0$ , and  $c \geq 1/a(\Xi^{-1}\hat{L}) > 0$  are constants.  $T > 0$  is a prespecifiable convergence time.

From [10], condition (10) is satisfied.

**Theorem 1.** *If the topological graph is a strongly connected direct balance graph, the distributed prescribed finite time protocol (9) is designed to solve the prescribed finite time optimization problem without the valve point effect (4) via the initial conditions in (10).*

*Proof.* First, we will prove the balance between demand and supply of powers.

Let  $\xi_m = 1/rr_m$ , and  $y^*(t) = \sum_{m=1}^n \xi_m y_m(t) = (1/r) \sum_{m=1}^n (b_m/r_m + P_m(t))$  be the weighted average value of all the incremental costs, where  $r = \sum_{m=1}^n 1/r_m$ ,  $m = 1, 2, \dots, n$ . We know  $\hat{L}$  is zero row-sum and symmetric, so

$$\dot{y}^*(t) = -\frac{ck(t)}{r} \sum_{m=1}^n \sum_{j=1}^n \hat{L}_{mj} y_j(t) = 0 = \frac{1}{r} \sum_{m=1}^n \dot{P}_m(t). \quad (11)$$

This means

$$\sum_{m=1}^n P_m(t) = \sum_{m=1}^n P_m(0) = P_D. \quad (12)$$

From (12), we know the total output power of all the generators is a constant value, which means the balance between the demand and supply of powers is always true.

Then, we will prove the prescribed finite time consensus for the incremental cost of each generator.

We define  $\delta_i = y_i - y^*$  as the error states between the average value and the  $i$ -th generator,  $\delta = (\delta_1, \dots, \delta_n)^T$ . It is easy to see that  $\sum_{k=1}^n \xi_k = 1$  and  $\sum_{k=1}^n \xi_k \delta_k = 0$ . So, we can get the error system:

$$\dot{\delta}_i(t) = cr_i k(t) \sum_{j=1}^n \hat{a}_{ij} (\delta_j(t) - \delta_i(t)) = -cr_i k(t) \sum_{j=1}^n \hat{L}_{ij} \delta_j(t). \quad (13)$$

We choose the following Lyapunov function:

$$V(t) = \sum_{i=1}^n \frac{\delta_i^T \delta_i}{r_i}. \quad (14)$$

By using Lemma 1, the derivative of  $V(t)$  can be described as

$$\begin{aligned} \dot{V}(t) &= 2 \sum_{i=1}^n \frac{\delta_i^T \dot{\delta}_i}{r_i} = -2ck(t) \sum_{i=1}^n \sum_{j=1}^n \delta_i^T \hat{L}_{ij} \delta_j = -2ck(t) \delta^T \hat{L} \delta \\ &\leq -ck(t) a(\Xi^{-1}\hat{L}) \delta^T \Xi \delta \leq -ck(t) a(\Xi^{-1}\hat{L}) V(t). \end{aligned} \quad (15)$$

As  $k(t) = k_1 + k_2/T - t \text{sign}[1 + \text{sign}(T - t)]$ , we will prove the result in two intervals  $[0, T)$  and  $[T, \infty)$ .

For  $t \in [0, T)$ ,  $k(t) = k_1 + k_2/T - t$ . We have

$$\begin{aligned} \dot{V}(t) &\leq -c \left( k_1 + \frac{k_2}{T-t} \right) a(\Xi^{-1}\hat{L}) V = -ck_1 a(\Xi^{-1}\hat{L}) V \\ &\quad - c \frac{k_2}{T-t} a(\Xi^{-1}\hat{L}) V. \end{aligned} \quad (16)$$

We define  $z = (T - t)^{-k_2/2}$ ,  $t \in [0, T)$ . Then,  $\dot{z} = k_2/2 (T - t)^{-(k_2/2)-1}$ ,  $\dot{z}/z = k_2/2 (T - t)$ . As  $c \geq 1/a(\Xi^{-1}\hat{L}) > 0$ , we have

$$\dot{V}(t) \leq -k_1 V(t) - \frac{k_2}{T-t} V(t) = -k_1 V(t) - 2 \frac{\dot{z}}{z} V(t). \quad (17)$$

Then,

$$z^2 \dot{V}(t) \leq -k_1 z^2 V(t) - 2z \dot{z} V(t). \quad (18)$$

So,

$$\frac{d(z^2 V(t))}{dt} = z^2 \dot{V}(t) + 2z\dot{z}V(t) \leq -k_1 z^2 V(t). \quad (19)$$

Then,

$$z^2 V(t) \leq \exp^{-k_1 t} z(0)^2 V(0), \quad (20)$$

$$V(t) \leq z^{-2} \exp^{-k_1 t} z(0)^2 V(0) = \left(\frac{T-t}{T}\right)^2 \exp^{-k_1 t} V(0). \quad (21)$$

From (21), we know  $\lim_{t \rightarrow T^-} V(t) = 0$ .  
For  $t \in [T, \infty)$ ,  $k(t) = k_1$ . We have

$$\dot{V}(t) \leq -ck_1 a(\Xi^{-1} \hat{L})V < 0. \quad (22)$$

It means  $V$  will not rise anymore. So,  $\forall t \geq T$ ,  $V(t) = V(T) \equiv 0$ .

The prescribed finite time optimization problem without the valve point effect has been proved. The proof is completed.

Remark 1: the prescribed finite time fully distributed method is designed for solving the ED problem in Theorem 1. The result here is a fully distributed result, and it is different from the centralized algorithms.

Remark 2: note that the graph in Theorem 1 is a direct strongly connected balance graph, and it is an improvement over an undirected graph. The result here can also be used for any undirected connected graph. In the future work, we will focus on other direct graphs.

Remark 3: the prescribed finite time result has two advantages compared with the finite time result. Firstly, the convergence time can be preassigned as needed by the designer, as we know that the convergence time of the finite time results is connected with the initial condition. Secondly, the controller in the prescribed finite time result is continuous, while the controller in the finite time result is discontinuous. The continuous controller can make the system state change smoothly.

**3.2. Valve Point Effect.** In this section, the valve point effect is introduced. In the interval  $[0, \pi]$ , the piecewise linearization is employed. The effect of the valve point effect on the cost function is the type of the sine-wave function, as in Figure 1(a). The active real power generated can be obtained from the derivative of the sine-wave function, as in Figure 1(b). As the function in Figure 1(b) is periodic, the piecewise linearization is introduced to approximate the sine-wave function, as in Figure 1(c) [42].

Taking the derivative of formula (3),

$$\frac{dC_i(P_i)}{d(P_i)} = 2a_i P_i + b_i + d_i e_i \cos(\text{mod}(e_i(P_i^{\min} - P_i), \pi)), \quad (23)$$

where mod means the MOD function.

The piecewise linearization with different slopes is introduced:

$$d_i e_i \cos(\text{mod}(e_i(P_i^{\min} - P_i), \pi)) = g_i \left( P_i - q_i \left( \frac{\pi}{e_i} \right) \right) + k_i, \quad (24)$$

where  $g_i$  and  $k_i$  are constants and  $q_i = [(P_i - P_i^{\min})/(\pi/e_i)]$  is an integer number of intervals. From (23) and (24),

$$\begin{aligned} \frac{dC_i(P_i)}{d(P_i)} &= 2a_i P_i + b_i + g_i \left( P_i - q_i \left( \frac{\pi}{e_i} \right) \right) + k_i \\ &= (2a_i + g_i)P_i - g_i q_i \left( \frac{\pi}{e_i} \right) + b_i + k_i. \end{aligned} \quad (25)$$

**3.3. Optimization by Consensus with the Valve Point Effect.** Next, the distributed control approach is devised of solving the optimization problem with the valve point effect.

*Definition 3.* We define the incremental cost of each generator  $i$  as  $IC_i = \partial C_i(P_i)/\partial P_i = \bar{r}_i P_i + \eta_i$ , where  $\bar{r}_i = 2a_i + g_i$  and  $\eta_i = -g_i q_i (\pi/e_i) + b_i + k_i$ ,  $i = 1, 2, \dots, n$ .

The Lagrange multiplier algorithm is used to solve the optimization problem with the valve point effect.

$$\begin{aligned} L(P_i, \lambda) &= \sum_{i=1}^n C_i(P_i) + \lambda \left( P_D - \sum_{i=1}^n P_i \right) \\ &= \sum_{i=1}^n a_i P_i^2 + b_i P_i + c_i + d_i \left| \sin(e_i(P_i^{\min} - P_i)) \right| \\ &\quad + \lambda \left( P_D - \sum_{i=1}^n P_i \right). \end{aligned} \quad (26)$$

The minimum value of (26) can be obtained by differentiating equation (26).

$$\frac{\partial L}{\partial P_i} = \frac{\partial C_i(P_i)}{\partial P_i} - \lambda = \bar{r}_i P_i + \eta_i - \lambda = 0. \quad (27)$$

So,  $\sum_{i=1}^n P_i = P_D$ . We have

$$\lambda = \bar{r}_i P_i + \eta_i. \quad (28)$$

We define  $x_i(t) = \lambda_i = \bar{r}_i P_i + \eta_i$ ,  $i = 1, 2, \dots, n$ . Then, a distributed prescribed finite time protocol is designed for the optimization problem.

$$\dot{x}_i(t) = cr_i k(t) \sum_{j=1}^n \hat{a}_{ij} (x_j(t) - x_i(t)) = -cr_i k(t) \sum_{j=1}^n \hat{L}_{ij} x_j(t). \quad (29)$$

With initial conditions  $x_i(0) = \bar{r}_i P_i(0) + \eta_i$ , the following equation is satisfied:

$$\sum_{i=1}^n P_i(0) = P_D. \quad (30)$$

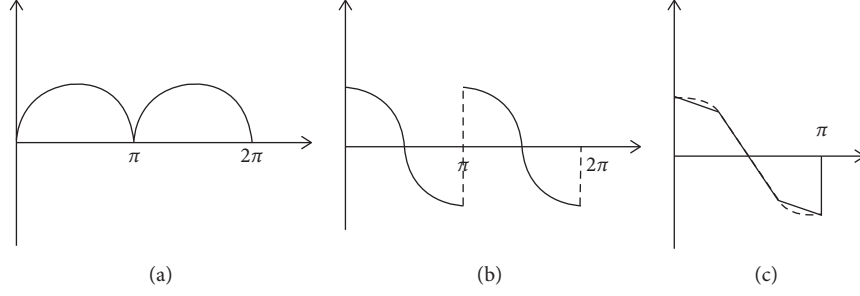


FIGURE 1: Piecewise linearization of the sine-wave part.

$k(t) = k_1 + k_2/T - t \text{sign}[1 + \text{sign}(T - t)]$ ,  $c \geq 1/a(\Xi^{-1}\hat{L}) > 0$ ,  $k_1 > 0$ ,  $k_2 > 0$  are constants.  $T > 0$  is a prespecifiable convergence time.

**Theorem 2.** *If the topological graph is a strongly connected direct balance graph, the distributed prescribed finite time protocol (29) is designed to solve the prescribed finite time optimization problem with the valve point effect (4) via the initial conditions in (30).*

The proof here is similar to the proof in Theorem 1. We omitted the proof here.

**3.4. Optimization by Consensus with the Power Generation Constraints.** Next, considering the power generation constraints of the generation-demand constraint, we need to further revise the distributed algorithms (9)-(10) to solve the ED problem.

The following three steps are derived to solve the constraints problem:

Step 1: by using the algorithm (9)-(10) in Theorem 1, we can get the optimal incremental cost  $\lambda^*$  and the optimal power generation value  $P_i^*$ .

Step 2: from Step 1, we get  $P_i^*$ . We check to see whether  $P_i^*$  is in the interval  $[P_{i,\min}, P_{i,\max}]$ . If  $P_i^* > P_{i,\max}$ , let  $P_i^* = P_{i,\max}$ . If  $P_i^* < P_{i,\min}$ , let  $P_i^* = P_{i,\min}$ .

We define  $\Omega_p$  as the generation units whose optimal values of power generation are  $P_i^* = P_{i,\max}$  or  $P_i^* = P_{i,\min}$ . Two auxiliary variables  $\hat{x}_i$ ,  $\hat{y}_i$  are introduced, and the initialize condition are

$$\hat{x}_i = \begin{cases} \frac{\lambda^* - b_i}{2a_i} - P_i^*, & i \in \Omega_p, \\ 0, & i \notin \Omega_p, \end{cases} \quad (31)$$

$$\hat{y}_i = \begin{cases} \frac{1}{2a_i}, & i \notin \Omega_p, \\ 0, & i \in \Omega_p. \end{cases}$$

The distributed average algorithms are introduced:

$$\dot{\hat{x}}_i(t) = cr_i k(t) \sum_{j=1}^n \hat{a}_{ij} (\hat{x}_j(t) - \hat{x}_i(t)), \quad (32)$$

$$\dot{\hat{y}}_i(t) = cr_i k(t) \sum_{j=1}^n \hat{a}_{ij} (\hat{y}_j(t) - \hat{y}_i(t)). \quad (33)$$

**Corollary 1.** *If the topological graph is a strongly connected direct balance graph, the distributed prescribed finite time algorithms (32) and (33) can solve the optimization problem with the power generation constraints in the preselected finite time  $T_1$ , i.e.,*

$$\lim_{t \rightarrow T_1} \hat{x}^*(t) = \sum_{i=1}^n \xi_i \hat{x}_i(0) = \sum_{i \in \Omega_p} \xi_i \left( \frac{\lambda^* - b_i}{2a_i} - P_i^* \right), \quad (34)$$

$$\lim_{t \rightarrow T_1} \hat{y}^*(t) = \sum_{i=1}^n \xi_i \hat{y}_i(0) = \sum_{i \in \Omega_p} \frac{\xi_i}{2a_i}. \quad (35)$$

*Proof.* When we set  $a_i = 0.5$ , it is easy to get the results (34) and (35), and the proof is similar to the proof in Theorem 1.

From (34) and (35), each generation unit obtains the average values of  $\hat{x}_i^*$  and  $\hat{y}_i^*$ . We can get the new incremental cost  $\lambda^{**}$  as follows:

$$\lambda^{**} = \lambda^* + \frac{\hat{x}_i^*}{\hat{y}_i^*}. \quad (36)$$

The new optimal value  $P_i^{**}$  can be obtained by

$$P_i^{**} = \begin{cases} \frac{\lambda^{**} - b_i}{2a_i} & i \notin \Omega_p \\ P_{i,\min} \text{ or } P_{i,\max} & i \in \Omega_p \end{cases}. \quad (37)$$

Step 3: check to see whether  $P_i^{**}$  is in the interval  $[P_{i,\min}, P_{i,\max}]$ . If  $P_i^{**}$  is not in the interval, set  $\lambda^* = \lambda^{**}$  and repeat Step 2. Otherwise,  $P_i^{**}$  is the final value.  $\square$

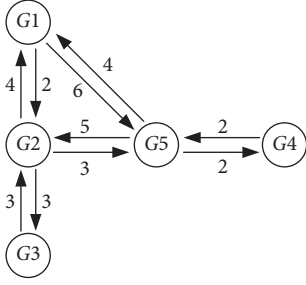
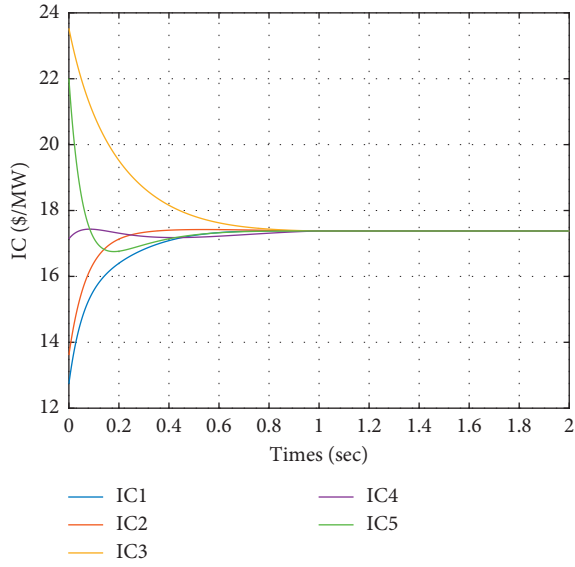


FIGURE 2: The topology graph of the generator model.

FIGURE 3: The incremental cost of generator  $\lambda_i$ .

#### 4. Numerical Examples

In this section, in order to verify the effectiveness of prescribed finite time algorithm for the ED problem of smart grids with the valve point effect, three numerical examples are listed, prescribed finite time optimization by consensus, prescribed finite time optimization by consensus with power generation constraints of generation units, and prescribed finite time optimization by consensus with the valve point effect. In this paper, a simulation model with 5 generators is selected, and the communication topology of the generator model can be seen in Figure 2.

The topology is balance directed, the adjacent matrix of

the graph can be written as  $A = \begin{bmatrix} 0 & 2 & 0 & 0 & 6 \\ 4 & 0 & 3 & 0 & 3 \\ 0 & 3 & 0 & 0 & 0 \\ 0 & 0 & 0 & 0 & 2 \\ 4 & 5 & 0 & 2 & 0 \end{bmatrix}$ , and the

Laplacian matrix of the MASs is  $L = \begin{bmatrix} 8 & -2 & 0 & 0 & -6 \\ -4 & 10 & -3 & 0 & -3 \\ 0 & -3 & 3 & 0 & 0 \\ 0 & 0 & 0 & 2 & -2 \\ -4 & -5 & 0 & -2 & 11 \end{bmatrix}$ .

The mirror diagram can be further obtained as

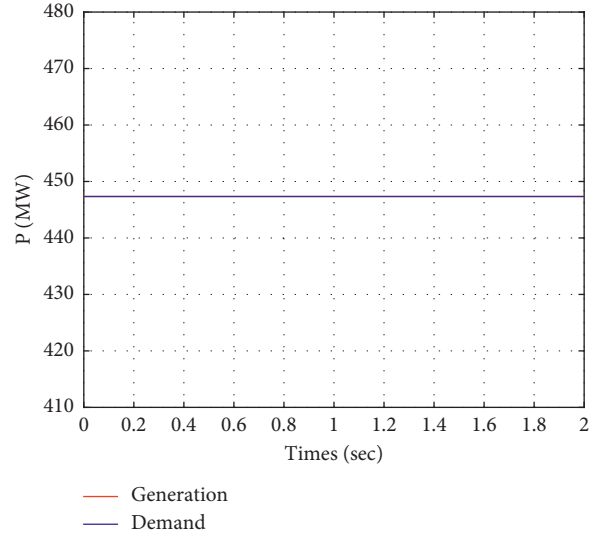
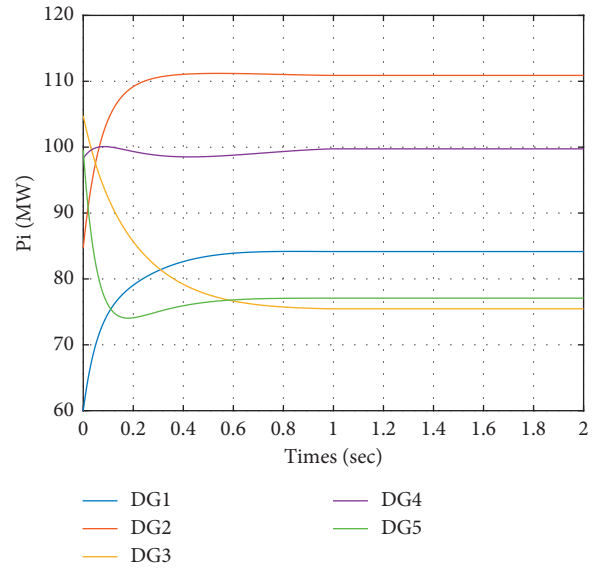


FIGURE 4: Total power demand of the generator.

FIGURE 5: The output power of generator  $P_i$ .

$\hat{A} = \begin{bmatrix} 0 & 3 & 0 & 0 & 5 \\ 3 & 0 & 3 & 0 & 4 \\ 0 & 3 & 0 & 0 & 0 \\ 0 & 0 & 0 & 0 & 2 \\ 5 & 4 & 0 & 2 & 0 \end{bmatrix}$ , and the Laplacian matrix of mirror

diagram is  $\hat{L} = \begin{bmatrix} 8 & -3 & 0 & 0 & -5 \\ -3 & 10 & -3 & 0 & -4 \\ 0 & -3 & 3 & 0 & 0 \\ 0 & 0 & 0 & 2 & -2 \\ -5 & -4 & 0 & -2 & 11 \end{bmatrix}$ .

For  $k(t) = k_1 + k_2/T - t \text{sign}[1 + \text{sign}(T - t)]$ , select  $k_1 = 1$ ,  $k_2 = 2$ ,  $c = 2$  in equation (9). Set  $a_1 = 0.096$ ,  $a_2 = 0.072$ ,  $a_3 = 0.105$ ,  $a_4 = 0.082$ ,  $a_5 = 0.103$ ,  $b_1 = 1.22$ ,  $b_2 = 1.41$ ,  $b_3 = 1.53$ ,  $b_4 = 1.02$ ,  $b_5 = 1.50$ ,  $c_1 = 51$ ,  $c_2 = 31$ ,  $c_3 = 78$ ,  $c_4 = 42$ , and  $c_5 = 81$ . The original values of  $\lambda_i(0)$  are

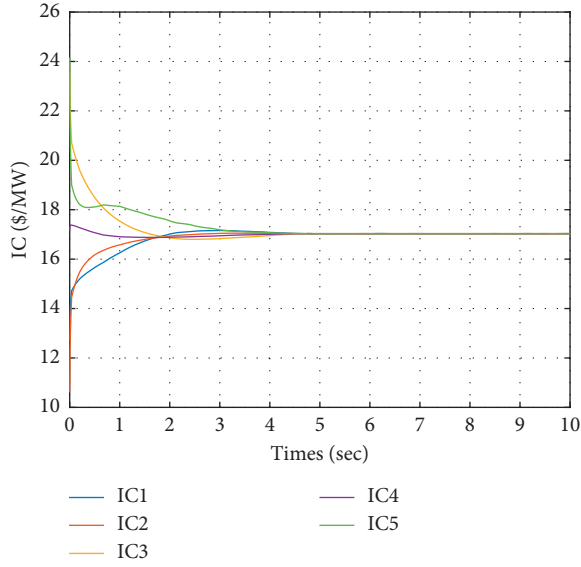


FIGURE 6: The incremental cost of generator  $\lambda_i$  with power generation constraints.

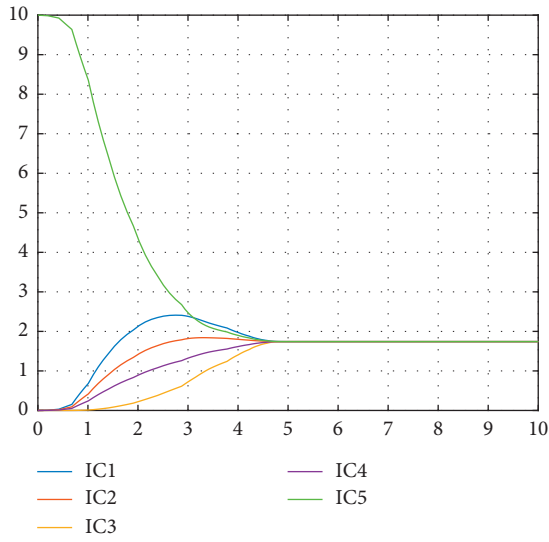


FIGURE 7: The incremental cost of generator  $x_i$  with power generation constraints.

$\lambda_1(0) = 12.74$ ,  $\lambda_2(0) = 13.61$ ,  $\lambda_3(0) = 23.53$ ,  $\lambda_4(0) = 17.14$ , and  $\lambda_5(0) = 22.01$ .

**4.1. Prescribed Finite Time Optimization by Consensus.** In this section, distributed ED algorithm (9) in a directed topology is used to solve the optimization problem without considering power generation constraints.

The convergence time can be set as 1 s. Figure 3 shows the incremental cost of the generator  $\lambda_i$ , and the stable consensus  $\lambda^* = 17.38$  after 1s. We can see that the generator power demand is about 447.34 MW from Figure 4, which satisfies the balance condition of power demand. It can be seen from Figure 5 that the optimal values of the generator

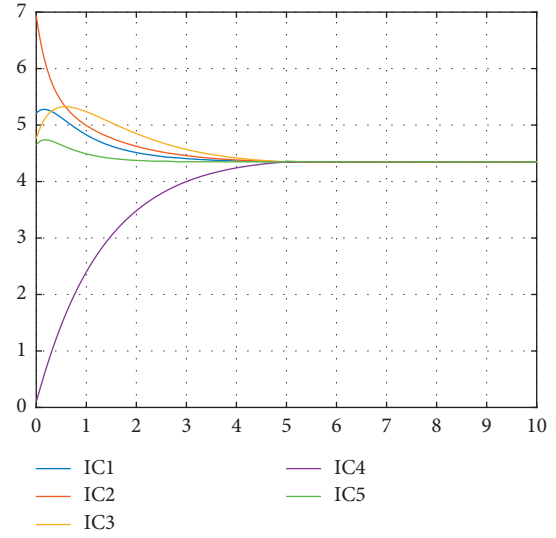


FIGURE 8: The incremental cost of generator  $y_i$  with power generation constraints.

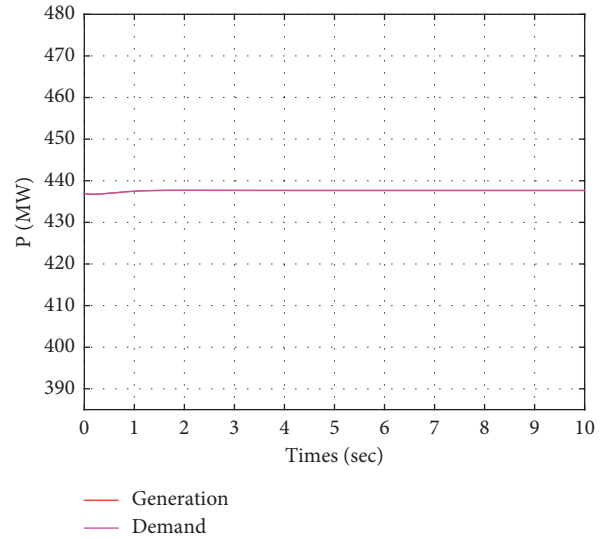


FIGURE 9: Total power demand of generator with power generation constraints.

power output are  $P_1 = 84.16$  MW,  $P_2 = 110.89$  MW,  $P_3 = 75.47$  MW,  $P_4 = 99.74$  MW, and  $P_5 = 77.08$  MW.

**4.2. Prescribed Finite Time Optimization by Consensus with Power Generation Constraints.** Power generation constraints of generator units are taken into account in this simulation. The maximum values of each generator constraints are  $P_{1H} = 200$ ,  $P_{2H} = 190$ ,  $P_{3H} = 180$ ,  $P_{4H} = 120$ , and  $P_{5H} = 180$ . The minimum power of each generators are  $P_{1L} = 60$ ,  $P_{2L} = 40$ ,  $P_{3L} = 50$ ,  $P_{4L} = 30$ , and  $P_{5L} = 20$ . The initial condition of the two auxiliary variables are  $\hat{x}_1(0) = 0$ ,  $\hat{x}_2(0) = 0$ ,  $\hat{x}_3(0) = 0$ ,  $\hat{x}_4(0) = 0$ ,  $\hat{x}_5(0) = 10$ ,  $\hat{y}_1(0) = 5.21$ ,  $\hat{y}_2(0) = 6.94$ ,  $\hat{y}_3(0) = 4.76$ ,  $\hat{y}_4(0) = 0.10$ , and  $\hat{y}_5(0) = 4.65$ . The convergence time is selected as 5 s. The incremental cost of the generator is  $\lambda^* = 17.03$ , as in Figure 6. According to

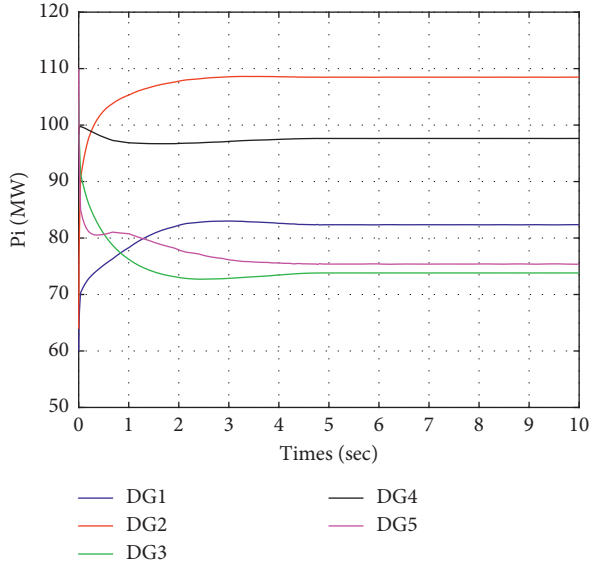


FIGURE 10: The output power of generator  $P_i$  with power generation constraints.

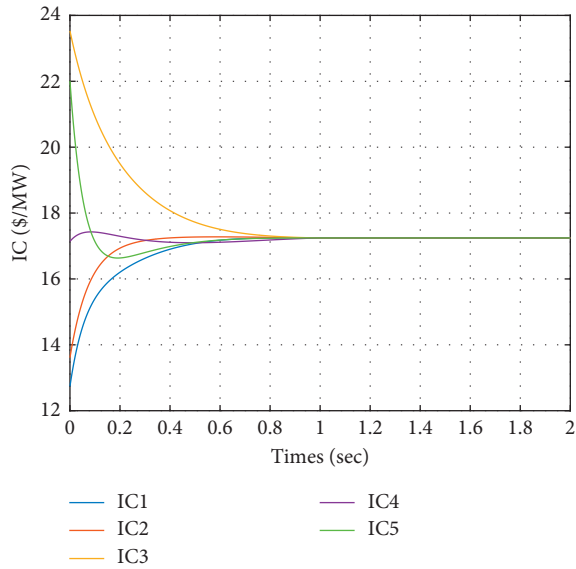


FIGURE 11: The incremental cost of generator  $\lambda_i$  with the valve point effect.

(33) and (34),  $\hat{x}_i^* = 1.74$  in Figure 7 and  $\hat{y}_i^* = 4.35$  in Figure 8 reach consensus in 5s. From (37), we can get the final incremental cost  $\lambda^* = 17.43$ . It can be seen from Figure 9 that the total generator demand is 437.67 MW, which satisfies the balance condition of power demand. From Figure 10, we found that each  $P_i$  will reach a value in prescribed finite time, that is,  $P_1^{**} = 82.35$  MW,  $P_2^{**} = 108.48$  MW,  $P_3^{**} = 73.81$  MW,  $P_4^{**} = 97.63$  MW, and  $P_5^{**} = 75.40$  MW.

**4.3. Prescribed Finite Time Consensus with the Valve Point Effect.** According to (23),  $d_1 = 0.45$ ,  $d_2 = 0.6$ ,  $d_3 = 0.32$ ,  $d_4 = 0.26$ ,  $d_5 = 0.33$ ,  $e_1 = 0.041$ ,  $e_2 = 0.036$ ,  $e_3 = 0.028$ ,

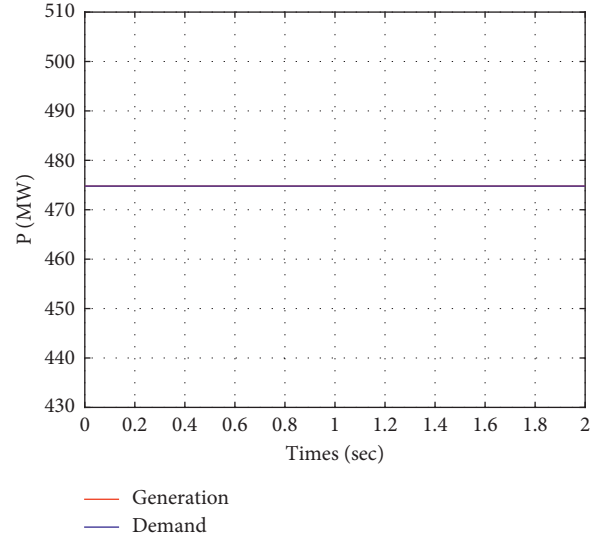


FIGURE 12: Total power demand of generator with the valve point effect.

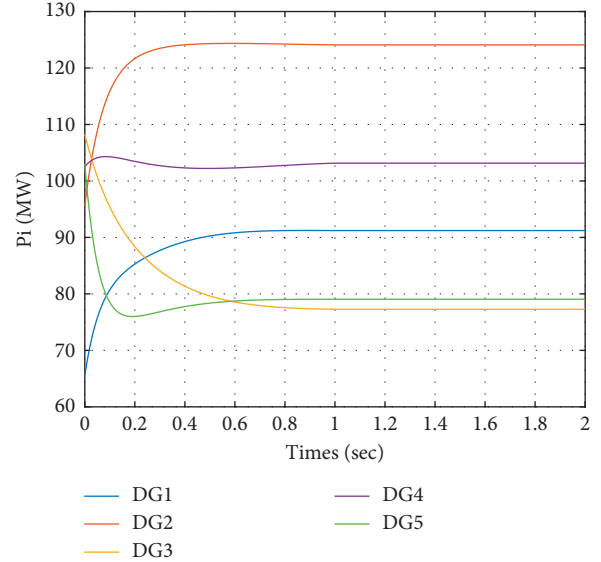


FIGURE 13: The output power of generator  $P_i$  with the valve point effect.

$e_4 = 0.052$ , and  $e_5 = 0.031$  are selected in this paper. In line with formula (28), we can set the convergence time as 1s. The incremental cost of the generator with the valve point effect is  $\lambda^* = 17.43$ , as shown in Figure 11. The total power requirement is 474.79 MW, as in Figure 12, which meets the balance of power demand and supply. From Figure 13, it is found that all  $P_i$  can reach consensus in prescribed finite time, where the steady states are  $P_1 = 91.22$  MW,  $P_2 = 124.10$  MW,  $P_3 = 77.28$  MW,  $P_4 = 103.14$  MW, and  $P_5 = 79.05$  MW.

## 5. Conclusions

This paper has solved the distributed prescribed finite time optimization ED problem with and without the valve point effect. The relationship between the consensus and

optimization problem of ED has been derived, and we can easily transform the optimization problem into a consensus problem. For both an undirected network and balance directed network, the prescribed finite time consensus schemes for ED of smart grids have been investigated. We found that if there exist constraints of generation units, the prescribed finite time optimization ED problem can also be solved.

## Data Availability

The authors pledge to provide all the codes and the data underlying the findings of the study.

## Conflicts of Interest

The authors declare that there are no conflicts of interest regarding the publication of this paper.

## Acknowledgments

The authors would like to thank the National Natural Science Foundation of China (grant nos. 61603196 and 61873326) for supporting this research work.

## References

- [1] A. Bakirtzis, V. Petridis, and S. Kazarlis, "Genetic algorithm solution to the economic dispatch problem," *IEEE Proceedings-Generation, Transmission and Distribution*, vol. 141, pp. 377–382, 2002.
- [2] P. Chen and H. Chang, "Large-scale economic dispatch by genetic algorithm," *IEEE Transactions on Power Systems*, vol. 10, no. 4, pp. 1919–1926, 1995.
- [3] Z.-L. Gaing, "Particle swarm optimization to solving the economic dispatch considering the generator constraints," *IEEE Transactions on Power Systems*, vol. 18, no. 3, pp. 1187–1195, 2003.
- [4] J. Park, Y. Jeong, J. Shin, and K. Lee, "An improved particle swarm optimization for nonconvex economic dispatch problems," *IEEE Transactions on Power Systems*, vol. 25, no. 1, pp. 156–166, 2010.
- [5] J.-B. Park, K.-S. Lee, J.-R. Shin, and K. Y. Lee, "A particle swarm optimization for economic dispatch with nonsmooth cost functions," *IEEE Transactions on Power Systems*, vol. 20, no. 1, pp. 34–42, 2005.
- [6] F. Yao, Z. Y. Dong, K. Meng, Z. Xu, H. H.-C. Iu, and K. P. Wong, "Quantum-inspired particle swarm optimization for power system operations considering wind power uncertainty and carbon tax in Australia," *IEEE Transactions on Industrial Informatics*, vol. 8, no. 4, pp. 880–888, 2012.
- [7] X. Xu, Z. Hu, Q. Su, and Z. Xiong, "Multiobjective collective decision optimization algorithm for economic emission dispatch problem," *Complexity*, vol. 2018, Article ID 1027193, 20 pages, 2018.
- [8] Z. Zhang and M. Chow, "Convergence analysis of the incremental cost consensus algorithm under different communication network topologies in a smart grid," *IEEE Transactions on Power Systems*, vol. 27, no. 4, pp. 761–1768, 2012.
- [9] Z. Zhang and M. Chow, "Decentralizing the economic dispatch problem using a two-level incremental cost consensus algorithm in a smart grid environment," in *Proceedings of the IEEE 2011 North American Power Symposium*, Boston, MA, USA, August 2011.
- [10] Z. Zhang and M. Chow, "The influence of time delays on decentralized economic dispatch by using incremental cost consensus algorithm," in *Control and Optimization Methods for Electric Smart Grids, Power Electronics and Power Systems*, A. Chakraborty and M. D. Ilic, Eds., pp. 313–326, Springer Science Business Media, Berlin, Germany, 2012.
- [11] W. Yu, C. Li, X. Yu, G. Wen, and J. Lü, "Distributed consensus strategy for economic power dispatch in a smart grid," in *Proceedings of the 10th Asian Control Conference*, Sabah, Malaysia, June 2015.
- [12] G. Wen, X. Yu, Z.-W. Liu, and W. Yu, "Adaptive consensus-based robust strategy for economic dispatch of smart grids subject to communication uncertainties," *IEEE Transactions on Industrial Informatics*, vol. 14, no. 6, pp. 2484–2496, 2018.
- [13] G. Chen and Z. Zhao, "Delay effects on consensus-based distributed economic dispatch algorithm in microgrid," *IEEE Transactions on Power Systems*, vol. 33, no. 1, pp. 602–612, 2018.
- [14] Y. Fan, G. Hu, and M. Egerstedt, "Distributed reactive power sharing control for microgrids with event-triggered communication," *IEEE Transactions on Control Systems Technology*, vol. 25, no. 1, pp. 118–128, 2017.
- [15] G. Chen, Z. Li, and Z. Zhao, "Event-triggered optimal active power control in islanded microgrid with variable demand and time-varying communication topology," *IEEE Transactions on Smart Grid*, vol. 10, no. 4, pp. 4015–4025, 2019.
- [16] C. Li, X. Yu, W. Yu, T. Huang, and Z.-W. Liu, "Distributed event-triggered scheme for economic dispatch in smart grids," *IEEE Transactions on Industrial Informatics*, vol. 12, no. 5, pp. 1775–1785, 2016.
- [17] X. He, D. W. C. Ho, T. Huang, J. Yu, H. Abu-Rub, and C. Li, "Second-order continuous-time algorithms for economic power dispatch in smart grids," *IEEE Transactions on Systems, Man, and Cybernetics: Systems*, vol. 48, no. 9, pp. 1482–1492, 2018.
- [18] C. Huang, X. Zhang, H. Lam, and S. Tsai, "Synchronization analysis for nonlinear complex networks with reaction-diffusion terms using fuzzy-model-based approach," *IEEE Transactions on Fuzzy Systems*, vol. 2020, Article ID 2974143, 13 pages, 2020.
- [19] C. Huang, J. Lu, G. Zhai, J. Cao, G. Lu, and M. Perc, "Stability and stabilization in probability of probabilistic boolean networks," *IEEE Transactions on Neural Networks and Learning Systems*, vol. 2020, Article ID 2978345, 11 pages, 2020.
- [20] C. Huang, J. Lu, D. W. C. Ho, G. Zhai, and J. Cao, "Stabilization of probabilistic boolean networks via pinning control strategy," *Information Sciences*, vol. 510, pp. 205–217, 2020.
- [21] G. Chen, Z. Zhao, and Z. Li, "Distributed finite-step iterative algorithm for economic dispatch of generation," *IEEE Transactions on Industrial Informatics*, vol. 14, no. 12, pp. 5221–5232, 2018.
- [22] G. Chen and Z. Li, "Consensus based distributed finite-time economic dispatch in smart grid with jointly connected topology," in *Proceedings of the 29th Chinese Control and Decision Conference*, Chongqing, China, May 2017.
- [23] G. Chen, J. Ren, and E. Feng, "Distributed finite-time economic dispatch of a network of energy resources," *IEEE Transactions on Smart Grid*, vol. 8, no. 2, pp. 822–832, 2017.
- [24] Y. Song, Y. Wang, J. Holloway, and M. Krstic, "Time-varying feedback for regulation of normal-form nonlinear systems in

- prescribed finite time,” *Automatica*, vol. 83, pp. 243–251, 2017.
- [25] H. Xiang, G. Chen, and Z. Zhao, “A distributed algorithm for economic dispatch in prescribed time,” *IFAC-PapersOnLine*, vol. 52, no. 24, pp. 184–189, 2019.
- [26] X. Li, D. W. C. Ho, and J. Cao, “Finite-time stability and settling-time estimation of nonlinear impulsive systems,” *Automatica*, vol. 99, pp. 361–368, 2019.
- [27] G. Mei, X. Wu, D. Ning, and J.-A. Lu, “Finite-time stabilization of complex dynamical networks via optimal control,” *Complexity*, vol. 21, no. S1, pp. 417–425, 2016.
- [28] H. Yang, P. Yang, and C. Huang, “Evolutionary programming based economic dispatch for units with nonsmooth fuel cost functions,” *IEEE Transactions on Power Systems*, vol. 11, no. 1, pp. 112–118, 1996.
- [29] N. Sinha, R. Chakrabarti, and P. Chattopadhyay, “Evolutionary programming techniques for economic load dispatch,” *IEEE Transactions on Evolutionary Computation*, vol. 7, no. 1, pp. 822–832, 2003.
- [30] D. Walters and G. Sheble, “Genetic algorithm solution of economic dispatch with valve point loading,” *IEEE Transactions on Power Systems*, vol. 8, no. 3, pp. 184–189, 1993.
- [31] S. Ling, H. Lam, F. Leung, and Y. LEE, “Improved genetic algorithm for economic load dispatch with valve-point loadings,” in *Proceedings of the 29th Annual Conference of the IEEE Industrial Electronics Society*, Roanoke, VA, USA, November 2003.
- [32] D. He, F. Wang, and Z. Mao, “A hybrid genetic algorithm approach based on differential evolution for economic dispatch with valve-point effect,” *International Journal of Electrical Power & Energy Systems*, vol. 30, no. 1, pp. 31–38, 2008.
- [33] C.-L. Chiang, “Improved genetic algorithm for power economic dispatch of units with valve-point effects and multiple fuels,” *IEEE Transactions on Power Systems*, vol. 20, no. 4, pp. 1690–1699, 2005.
- [34] T. Victorie and A. Jeyakumar, “Hybrid PSO-SQP for economic dispatch with valve-point effect,” *Electric Power Systems Research*, vol. 71, no. 1, pp. 51–59, 2004.
- [35] X. Chen, B. Xu, and W. Du, “An improved particle swarm optimization with biogeography-based learning strategy for economic dispatch problems,” *Complexity*, vol. 2018, Article ID 7289674, 15 pages, 2018.
- [36] S. Hemamalini and S. P. Simon, “Maclaurin series-based Lagrangian method for economic dispatch with valve-point effect,” *IET Generation, Transmission & Distribution*, vol. 3, no. 9, pp. 859–871, 2009.
- [37] M. Abouheaf, W. Lee, and F. Lewis, “Dynamic formulation and approximation methods to solve economic dispatch problems,” *IET Generation Transmission and Distribution*, vol. 7, no. 8, pp. 866–873, 2003.
- [38] F. Li, J. Qin, and Y. Kang, “Multi-agent system based distributed pattern search algorithm for non-convex economic load dispatch in smart grid,” *IEEE Transactions on Power Systems*, vol. 34, no. 3, pp. 2093–2102, 2019.
- [39] T. Nguyen, N. Quynh, and L. Dai, “Improved Firefly Algorithm: a novel method for optimal operation of thermal generating units,” *Complexity*, vol. 2018, Article ID 7267593, 23 pages, 2018.
- [40] R. Morsali, M. Mohammadi, I. Maleksaeedi, and N. Ghadimi, “A new multiobjective procedure for solving nonconvex environmental/economic power dispatch,” *Complexity*, vol. 20, no. 2, pp. 47–62, 2015.
- [41] L. Yang, D. He, and B. Li, “A selection hyper-heuristic algorithm for multiobjective dynamic economic and environmental load dispatch,” *Complexity*, vol. 2020, Article ID 4939268, 18 pages, 2020.
- [42] Y. Elsheakh, S. Zou, Z. Ma, and B. Zhang, “Decentralised gradient projection method for economic dispatch problem with valva point effect,” *IET Generation Transmission & Distribution*, vol. 34, no. 3, pp. 3844–3851, 2018.



## Research Article

# Two-Player Location Game in a Closed-Loop Market with Quantity Competition

Xiaofeng Chen <sup>1,2</sup>, Qiankun Song,<sup>2</sup> and Zhenjiang Zhao<sup>3</sup>

<sup>1</sup>School of Economics and Management, Chongqing Jiaotong University, Chongqing 400074, China

<sup>2</sup>Department of Mathematics, Chongqing Jiaotong University, Chongqing 400074, China

<sup>3</sup>Department of Mathematics, Huzhou University, Huzhou 313000, China

Correspondence should be addressed to Xiaofeng Chen; [xxffch@126.com](mailto:xxffch@126.com)

Received 7 July 2020; Revised 8 August 2020; Accepted 14 August 2020; Published 25 August 2020

Academic Editor: Sabri Arik

Copyright © 2020 Xiaofeng Chen et al. This is an open access article distributed under the Creative Commons Attribution License, which permits unrestricted use, distribution, and reproduction in any medium, provided the original work is properly cited.

This paper considers the two-player location game in a closed-loop market with quantity competition. Based on the Cournot and Hotelling models, a circle model is established for a closed-loop market in which two players (firms) play a location game under quantity competition. Using a two-stage (location-then-quantity) pattern and backward induction method, the existence of subgame-perfect Nash equilibria is proved for the location game in the circle model with a minimum distance transportation cost function. In addition, sales strategies are proposed for the two players for every local market on the circle when the players are in the equilibrium positions. Finally, an algorithm for simulating the competitive dynamics of the closed-loop market is designed, and two numerical simulations are provided to substantiate the effectiveness of the obtained results.

## 1. Introduction

Game theory, the science of strategy, was pioneered by John von Neumann when he proved the basic principles in 1928 [1]. As one of the main basic analysis tools for phenomena related to struggle or competition, game theory has been widely applied in politics, international relations, military strategy, biology, economics, computer science, and many other fields [2–7].

The location problem is an important topic in the fields of supply chain management and industrial organization. In 1929, Hotelling first introduced the game theory to the location problem and established the classic Hotelling model [8]. In this model, consumers are assumed to be evenly distributed on a linear street, and two companies of the same size that produce homogeneous goods determine their locations such that the profits are maximized. During the following decades, researchers investigated variations of the location problem based on the classic model and obtained a variety of results. In [9], the authors claimed that a price equilibrium solution exists everywhere in a modified version of the Hotelling

model and showed that both sellers tend to maximize their differentiation for this model. In [10], the authors studied Cournot competition in linear city model with a nonuniform consumer distribution and derived a necessary condition for an agglomeration equilibrium. In [11], the authors proved that a mixed strategy equilibrium exists for the Hotelling model if a pure strategy equilibrium does not exist. In [12], the authors extended the Hotelling spatial competition model in three aspects, namely, the number of firms, shape of the demand curve, and type of space. In [13], the author examined the Hotelling model for duopolistic competition with a class of utility functions and proved the existence of an equilibrium when the curvature of the utility functions is sufficiently high. In [14], the authors analyzed the relationship between consumer density and the equilibrium locations of the Hotelling model and noted that the equilibrium locations are closer if the density is higher. In [15], the author considered the problem of the existence of equilibrium states in the Hotelling model in the  $n$ -player case and analyzed the influence of the number of firms on the equilibrium outcome of Hotelling games. In

[16], the authors discussed the Hotelling duopoly model with network effects and brand loyalty and showed that a pure strategy price equilibrium exists if the transportation costs are linear functions. In [17], the authors considered the influence of production technology and labor inputs on spatial competition in Hotelling model and found that the production technology is the main influence on the equilibrium locations. It was proved that a pure strategy price-location Nash equilibrium exists in the Hotelling duopoly model under general conditions on the cost-of-location function in [18]. In [19], the authors developed a duopoly game using the Hotelling model to research the competition between brick-and-mortar retailers and online retailers.

In general, the real market cannot be described by a linear segment with evenly distributed customers such as Hotelling model and its extended versions. In actual situations, markets are distributed along complex transportation networks. Therefore, many researchers considered spatial competition in the pattern of circles and complex networks to more accurately represent actual markets. For example, the existence of an equilibrium in the circle model was proved by using a two-stage (location-then-price) method in [20]. It was shown that a unique price equilibrium exists on a circular road when the transportation cost function is quadratic in [21]. In [22], the authors studied the location game in a circular market and demonstrated that the equidistant location pattern is the unique equilibrium location for the players in this market. In [23], the authors investigated two shipping duopoly models in circular markets and proved the existence and nonexistence of the equilibrium in different models. In [24], the authors considered spatial competition among for a multiplant Cournot oligopoly in a circular city and proved the uniqueness of the equilibrium location if the number of plants is equal for the two firms. In [25], the authors derived some conditions for even spacing to be an equilibrium of a circular market based on a two-stage approach. In [26], the authors investigated spatial Cournot competition in a circular city and showed that nonmaximum dispersion is the unique location equilibrium when duopoly firms deliver products in different transportation modes.

Strongly motivated by the above discussion, in this paper, we investigate the two-player location game in a closed-loop market. In such a game, two players develop quantity competition in the market, whose shape can be viewed as a circle. The goal of each player is to choose the optimal point on the circle as its location such that its profit is maximized. The main contributions of this paper are highlighted as follows:

- (1) Not only is the optimal equilibrium state of the location game investigated, but also the optimal strategy, including the price and quantity plan for each player, is proposed.
- (2) A computer algorithm is designed to simulate the evolutionary process of the two-player game in a closed-loop market. The simulation examples demonstrate the effectiveness and feasibility of the algorithm.

- (3) It is shown that the two players follow the principle of maximum differentiation to choose their optimal locations in a closed-loop market model, which is strikingly different from Hotelling's minimum differentiation principle for a linear market model.

The remainder of this paper is organized as follows. In Section 2, some descriptions and assumptions for the two-player location game in a closed-loop market are introduced, and some important lemmas are provided. In Section 3, the two-player quantity competition in the closed-loop market is considered when the players' locations are fixed. The two-player location game in a closed-loop market is discussed in Section 4. An algorithm for simulating the dynamic evolution of the two players in the market is presented in Section 5. Finally, some conclusions are drawn in Section 6.

To end this section, we give some notations used in this paper.  $x \in [0, 1)$  stands for the position of the local market in a closed-loop market.  $x_1$  and  $x_2$  represent the positions of firms  $A$  and  $B$ , respectively.  $p$  is the price of the product, while  $q_1$  and  $q_2$  are the quantities produced by the two players. The function  $c_i$  represents the transportation cost per unit product from the position  $x_i$  to  $x$ , where  $i = 1, 2$ .

## 2. Basic Assumptions of the Closed-Loop Market

Consider two firms  $A$  and  $B$  in a closed-loop market. Without loss of generality, it is assumed that the closed loop is a circle with a circumference of 1. The points on the circle are arranged in the counterclockwise direction, and each point is called a local market. Consumers are evenly distributed on the circle with a density of 1. Firms  $A$  and  $B$  are distributed at two points on the circle (as shown in Figure 1(a)), and each firm produces homogeneous products with zero production cost.

For convenience of representation, the circle is disconnected at a certain point  $O$  in Figure 1(a), and the circle is straightened into a line segment  $OO'$  of length 1 (as shown in Figure 1(b)). Clearly, the line  $OO'$  in Figure 1(b) can be transformed into the circle in Figure 1(a). Therefore, the circle is equivalent to the segment  $OO'$ . Note that the two ends  $O$  and  $O'$  of the line segment correspond to the same point  $O$  on the circle. Take the left end  $O$  of line  $OO'$  as the origin, and take the  $OO'$  direction as the positive direction to establish a number axis. Then, the coordinate value  $x$  of a point on the right-half number axis represents the distance from the point to the origin  $O$ .

Suppose the locations of the firms  $A$  and  $B$  are, respectively,  $x_1$  and  $x_2$ , where  $x_1, x_2 \in [0, 1)$ . The firms are responsible for the distribution of goods to the local market  $x$ , and the transportation cost is 1 per unit product per unit distance. There are two ways to transport products from location  $x_i$  to the local market  $x$ , that is, counterclockwise and clockwise. We should choose the minimum distance for distribution. Therefore, the transportation cost per unit product from location  $x_i$  to the local market  $x$  is

$$c_i(x) = \min\{|x_i - x|, 1 - |x_i - x|\}, \quad i = 1, 2. \quad (1)$$

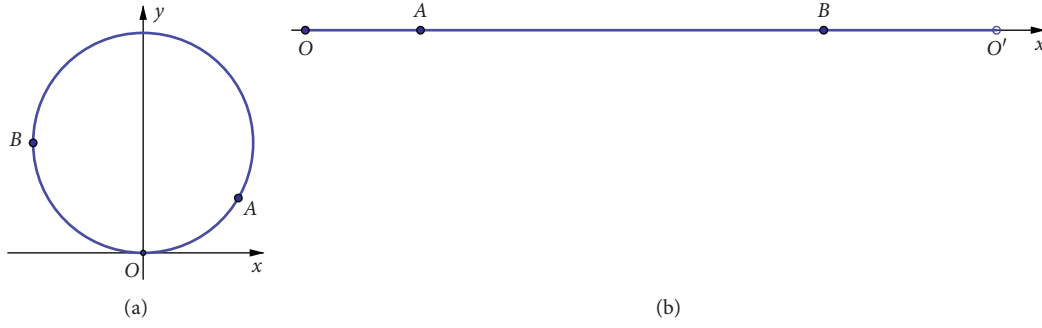


FIGURE 1: Circular market and its linearization. (a) Diagram of the circular market. (b) Linearization of the circle.

Clearly,  $c_1(x) = c_2(x)$  when  $x_1 = x_2$ , and  $c_1(x) + c_2(x) = 1/2$  when  $|x_1 - x_2| = 1/2$ . The transportation costs of the two firms from the same location to the local market  $x$  are equal if they are located at the same point, while the total transportation costs are  $1/2$  if they are located at opposite ends of a certain diameter in the circle.

In the following sections, the total costs of transportation on the circle and the total profit of the firms, which are related to some integrals of  $c_i(x)$ , will be calculated. Therefore, we present some conclusions on integrals of  $c_i(x)$ .

**Lemma 1.** For  $c_i(x)$  and  $c_i^2(x)$ , the following integrals hold:

$$\int_0^1 c_i(x) dx = \frac{1}{4} \quad (2)$$

$$\int_0^1 c_i^2(x) dx = \frac{1}{12}$$

**Lemma 2.** For the integral of the product of  $c_1(x)$  and  $c_2(x)$ , the following results are correct.

(i) When  $(x_1, x_2) \in [0, (1/2)) \times [0, (1/2))$ ,

$$\int_0^1 c_1(x)c_2(x) dx = \frac{2}{3}|x_1 - x_2|^3 - \frac{1}{2}(x_1 - x_2)^2 + \frac{1}{12}. \quad (3)$$

(ii) When  $(x_1, x_2) \in [0, (1/2)) \times [(1/2), 1)$ ,

$$\int_0^1 c_1(x)c_2(x) dx = -\frac{2}{3}|x_1 - x_2 + \frac{1}{2}|^3 + \frac{1}{2}(x_1 - x_2 + \frac{1}{2})^2 + \frac{1}{24}. \quad (4)$$

(iii) When  $(x_1, x_2) \in [(1/2), 1) \times [0, (1/2))$ ,

$$\int_0^1 c_1(x)c_2(x) dx = -\frac{2}{3}|x_2 - x_1 + \frac{1}{2}|^3 + \frac{1}{2}(x_2 - x_1 + \frac{1}{2})^2 + \frac{1}{24}. \quad (5)$$

(iv) When  $(x_1, x_2) \in [(1/2), 1) \times [(1/2), 1)$ ,

$$\int_0^1 c_1(x)c_2(x) dx = \frac{2}{3}|x_1 - x_2|^3 - \frac{1}{2}(x_1 - x_2)^2 + \frac{1}{12}. \quad (6)$$

Specifically,

$$\int_0^1 c_1(x)c_2(x) dx = \frac{1}{12}, \quad \text{if } x_1 = x_2, \quad (7)$$

$$\int_0^1 c_1(x)c_2(x) dx = \frac{1}{24}, \quad \text{if } |x_1 - x_2| = \frac{1}{2}.$$

The proofs of Lemmas 1 and 2 are presented in the appendix.

### 3. Quantity Competition in the Closed-Loop Market

In this section, we first recall the Cournot duopoly model proposed by Cournot in 1838 [27]. In this model, two players (firms) producing the same products compete by choosing their outputs independently under the assumption that their competitor does not change their output in response, which leads to a balanced result between competition and monopoly.

The basic assumptions of the Cournot model are that the market includes only two firms A and B that sell identical products; the production cost is zero (such as the acquisition of mineral water); the inverse demand function of the market is linear; firms A and B know the demand function of the market accurately; and both firms know each other's output. In this situation, each firm determines the output that can yield the maximum profit for them, which means that each firm passively adapts its output to the determined output of the other party. Next, we use the response function method to analyze the equilibrium state of production in the Cournot model.

Let the total market capacity be 1 and the inverse demand function be

$$p = f(q_1 + q_2) = 1 - q_1 - q_2, \quad (8)$$

where  $p$  is the price of the product and  $q_1$  and  $q_2$  are the quantities produced by firms A and B, respectively. Then, the profits of firms A and B are as follows:

$$\begin{aligned}\pi_1(q_1, q_2) &= pq_1 = q_1 - q_1^2 - q_1q_2, \\ \pi_2(q_1, q_2) &= pq_2 = q_2 - q_2^2 - q_1q_2.\end{aligned}\quad (9)$$

For firm A, the first-order condition maximizing its profit is that

$$\frac{\partial \pi_1}{\partial q_1} = 1 - 2q_1 - q_2 = 0, \quad (10)$$

$$\text{or } q_1 = \frac{1}{2}(1 - q_2).$$

Equation (10) is firm A's best response function, which represents the optimal output of firm A depending on the output of firm B. In other words, for each output of firm B, firm A will respond and determine the product that can maximize its profit.

Similarly, for firm B, the first-order profit-maximizing condition is

$$\frac{\partial \pi_2}{\partial q_2} = 1 - 2q_2 - q_1 = 0, \quad (11)$$

$$\text{or } q_2 = \frac{1}{2}(1 - q_1).$$

Equation (11) is firm B's best response function, which represents the relationship between the optimal output of firm B and the output of firm A.

By combining the best response functions (10) and (11), the equilibrium output solution of firms A and B can be obtained as follows:

$$q_1^* = q_2^* = \frac{1}{3}. \quad (12)$$

The equilibrium output of each firm is 1/3 of the market capacity. As shown in Figure 2, the response functions of firms A and B are linear since the demand function is linear. The intersection  $E$  of the two lines is the equilibrium solution of the Cournot model.

In the following, we consider the two-player game in a closed-loop market with quantity competition. Like demand function (8) in the Cournot model, for the closed-loop market, we assume that the demand function of the local market at  $x$  is

$$p(x) = 1 - q_1(x) - q_2(x), \quad \forall x \in [0, 1), \quad (13)$$

where  $p(x)$  is the price of the product for the local market  $x$  and  $q_1(x)$  and  $q_2(x)$  are the sales of firms A and B for the local market  $x$ , respectively. Therefore, the profits  $\pi_1$  and  $\pi_2$  of firms A and B in the local market  $x$  are, respectively,

$$\pi_1 = [1 - q_1(x) - q_2(x) - c_1(x)]q_1(x), \quad (14)$$

$$\pi_2 = [1 - q_1(x) - q_2(x) - c_2(x)]q_2(x), \quad (15)$$

where  $c_i(x)$ , defined in (1), represents the transportation cost per unit product from location  $x_i$  of the firm to the local market  $x$ . In a similar way to the response function approach for analyzing the Cournot model, we can extend the discussion. By calculating the partial derivatives of (14) and

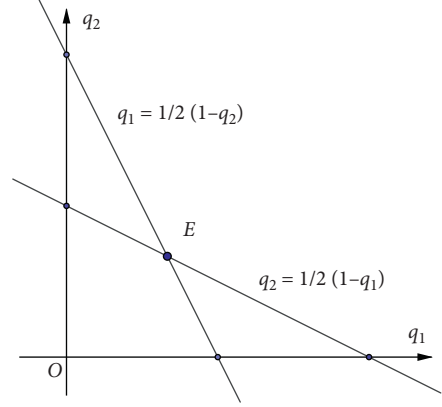


FIGURE 2: The response functions in the Cournot model.

(15), the first-order conditions for maximizing the profits of firms A and B in the local market  $x$  are obtained as follows:

$$\begin{cases} \frac{\partial \pi_1}{\partial q_1} = 1 - 2q_1(x) - q_2(x) - c_1(x) = 0, \\ \frac{\partial \pi_2}{\partial q_2} = 1 - q_1(x) - 2q_2(x) - c_2(x) = 0. \end{cases} \quad (16)$$

Then, the response functions of firms A and B in local market  $x$  are as follows:

$$q_1(x) = \frac{1}{2}[1 - q_2(x) - c_1(x)], \quad (17)$$

$$q_2(x) = \frac{1}{2}[1 - q_1(x) - c_2(x)]. \quad (18)$$

According to the above equations, in the equilibrium state of output competition, the quantities of products sold by the two firms in local market  $x$  are

$$q_1^*(x) = \frac{1}{3}[1 - 2c_1(x) + c_2(x)], \quad (19)$$

$$q_2^*(x) = \frac{1}{3}[1 + c_1(x) - 2c_2(x)].$$

Meanwhile, according to (14), (15), and (19), the profits of firms A and B in local market  $x$  are

$$\pi_1^*(x) = \frac{1}{9}[1 - 2c_1(x) + c_2(x)]^2, \quad (20)$$

$$\pi_2^*(x) = \frac{1}{9}[1 + c_1(x) - 2c_2(x)]^2.$$

By integrating (19) and employing Lemma 1, it can be obtained that the total outputs  $Q_1^*$  and  $Q_2^*$  of firms A and B are, respectively,

$$\begin{aligned} Q_1^* &= \int_0^1 q_1^*(x) dx = \frac{1}{4}, \\ Q_2^* &= \int_0^1 q_2^*(x) dx = \frac{1}{4}. \end{aligned} \quad (21)$$

which means that the equilibrium output of each firm is 1/4 of the market capacity.

Based on the above analysis, we can summarize the results in the following proposition.

**Proposition 1.** *In a closed-loop market with inverse demand function (8) and transportation cost function (1), if two players compete with the quantity of outputs, their equilibrium outputs are both 1/4, regardless of their locations  $x_1$  and  $x_2$ .*

*Remark 1.* Comparing the demand function (8) in the Cournot model with the demand function (13) in the closed-loop market discussed in this section, we find that the meaning of (13) is the same as that of (8) if  $x$  in (13) is fixed. Therefore, the output competition in each local market  $x$  on the circle can be regarded as a Cournot model with quantity competition, while the whole circle market can be regarded as being composed of an infinite number of Cournot models.

*Remark 2.* Comparing the response functions (10) and (11) in the Cournot model with the response functions (17) and (18) in the closed-loop market model, we find that the outputs  $q_i(x)$  in response functions (17) and (18) must deduce quantities whose values are equivalent to the transportation cost in the closed-loop market. As a result, the proportion of the equilibrium output of each firm to the total market capacity is reduced by 1/12.

#### 4. Location Game in the Closed-Loop Market

In the previous section, we assumed that positions  $x_1$  and  $x_2$  of firms  $A$  and  $B$  are fixed. In this section, we consider the locations of the firms as decision variables. Therefore, this section considers how firms  $A$  and  $B$  choose their optimal locations  $x_1$  and  $x_2$  to obtain the maximum profits through quantity competition.

In this situation, we can analyze the problem as a complete information dynamic game process composed of

two stages. In the first stage of the game, the two firms choose their locations in the circle market independently. Then, in the second stage, each firm launches the output competition after observing the location of the other firm. We adopt backward induction to solve the subgame-perfect Nash equilibria of this game.

In the second stage, each firm observes the position of the other firm and then competes for outputs. Therefore, the analysis approach in this stage is the same as that in the previous section. Since we still assume that the demand function  $p(x)$  is in the form of (13), the product quantities  $q_1^*(x)$  and  $q_2^*(x)$  sold by firms  $A$  and  $B$  in the local market  $x$  are still in the form of (19) when the output competition reaches the equilibrium state. Therefore, the profits  $\pi_1^*$  and  $\pi_2^*$  of firms  $A$  and  $B$  are still calculated according to (20) in the local market  $x$ .

In the first stage, each firm chooses its own optimal location to maximize its profit. The total profits  $\Pi_i$  of firms  $A$  and  $B$  in the whole closed-loop market are

$$\Pi_i(x_1, x_2) = \int_0^1 \pi_i^* dx, \quad i = 1, 2. \quad (22)$$

Substituting (20) into (22) and according to Lemma 1, it can be seen that

$$\Pi_i(x_1, x_2) = \frac{11}{108} - \frac{4}{9} \int_0^1 c_1(x)c_2(x)dx. \quad (23)$$

Then, the first-order conditions of profit maximization are that

$$\begin{cases} \frac{\partial \Pi_1}{\partial q_1} = 0, & \text{or } \frac{\partial \Pi_1}{\partial q_1} \text{ does not exist,} \\ \frac{\partial \Pi_2}{\partial q_2} = 0, & \text{or } \frac{\partial \Pi_2}{\partial q_2} \text{ does not exist,} \end{cases} \quad (24)$$

which are equivalent to

$$\begin{cases} \frac{\partial}{\partial x_1} \int_0^1 c_1(x)c_2(x)dx = 0, & \text{or } \frac{\partial}{\partial x_1} \int_0^1 c_1(x)c_2(x)dx \text{ does not exist,} \\ \frac{\partial}{\partial x_2} \int_0^1 c_1(x)c_2(x)dx = 0, & \text{or } \frac{\partial}{\partial x_2} \int_0^1 c_1(x)c_2(x)dx \text{ does not exist.} \end{cases} \quad (25)$$

We discuss  $(x_1, x_2)$  and whether they satisfy conditions (25) in four cases: (i)  $(x_1, x_2) \in [0, (1/2)) \times [0, (1/2))$ , (ii)  $(x_1, x_2) \in [0, (1/2)) \times [(1/2), 1)$ , (iii)  $(x_1, x_2) \in [(1/2), 1) \times [0, (1/2))$ , and (iv)  $(x_1, x_2) \in [(1/2), 1) \times [(1/2), 1)$ .

For cases (i) and (iv),  $\partial/\partial x_1 \int_0^1 c_1(x)c_2(x)dx$  does not exist if  $x_1 = x_2$  according to Lemma 2. Hence, conditions (25) are satisfied if  $x_1 = x_2$ . Similarly, for case (ii),

conditions (25) are satisfied if  $x_2 - x_1 = 1/2$ . For case (iii), conditions (25) are satisfied if  $x_1 - x_2 = 1/2$ . Therefore, the possible equilibrium positions of the two firms are at the same point or at opposite ends of a diameter of the circular market.

According to (23) and Lemma 2, we can calculate the profits of the two firms in the possible equilibrium locations as follows:

$$\Pi_i = \begin{cases} \frac{7}{108}, & x_1^* = x_2^* \text{ (at the same point),} \\ \frac{1}{12}, & |x_1^* - x_2^*| = \frac{1}{2}, \text{ (at opposite ends of a diameter).} \end{cases} \quad (26)$$

This result indicates that the maximum profit of the two firms at opposite ends of a diameter is larger than that at the same point. Next, we analyze the sales program, including sales volume and sales price, for the firms in the two possible equilibrium locations.

If the equilibrium location is at the same point, that is,  $x_1^* = x_2^*$ , according to (19) and (13), noting that  $c_1(x) = c_2(x)$ , each firm chooses a sales quantity  $q_i^*(x)$  and a corresponding sales price  $p^*(x)$  for the local market  $x$  as follows:

$$\begin{aligned} q_1^*(x) &= q_2^*(x) = \frac{1}{3}[1 - c_i(x)], \\ p^*(x) &= \frac{1}{3}[1 + 2c_i(x)]. \end{aligned} \quad (27)$$

Then, the total sales quantity  $Q_i^*$  of each firm in the whole market is

$$Q_1^* = Q_2^* = \int_0^1 q_i^*(x) dx = \frac{1}{4}. \quad (28)$$

In this situation, as shown in Figure 3, the sales price  $p^*(x)$  of the firms is positively correlated with the transportation cost  $c_i(x)$  and negatively correlated with the sales volume  $q_i^*(x)$ . Therefore, the price increases with an increase in the cost, while the sales volume decreases with an increase in the price.

If the equilibrium location is at opposite ends of a diameter, that is,  $|x_1^* - x_2^*| = 1/2$ , according to (19) and noting that  $c_1(x) + c_2(x) = 1/2$ , each manufacturer chooses a sales quantity  $q_i^*(x)$  and a corresponding sales price  $p^*(x)$  for the local market  $x$  as follows:

$$\begin{aligned} q_1^*(x) &= c_2(x), \\ q_2^*(x) &= c_1(x), \\ p^*(x) &= 1 - c_1(x) - c_2(x) = \frac{1}{2}. \end{aligned} \quad (29)$$

In this situation, as shown in Figure 4, the sales price  $p^*(x)$  of the two firms is a constant, while the sales volume  $q_i^*(x)$  is negatively related to the transportation cost  $c_i(x)$ . Thus, regardless of how the cost and sales volume change, the price is always constant, and the sales volume decreases as the cost increases.

Summarizing the above discussion, we obtain the conclusions shown in Table 1.

In fact, strategy 1 is not optimal. Based on (23) and Lemma 2, the second-order conditions can be calculated as

$$\lim_{x_1 \rightarrow x_2} \frac{\partial^2 \Pi_i}{\partial x_i^2} = \frac{4}{9} > 0. \quad (30)$$

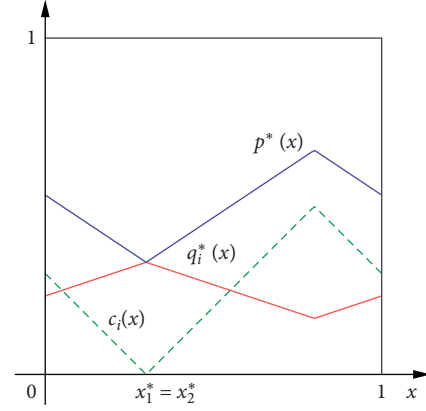


FIGURE 3: Price and quantity curves with the equilibrium positions at the same point.

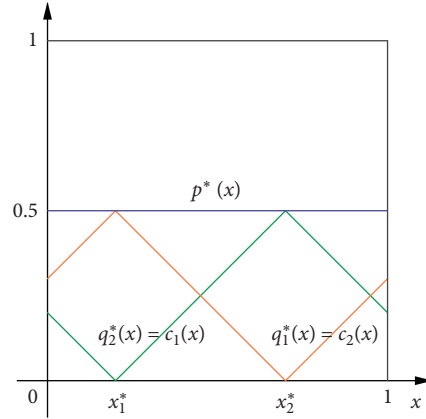


FIGURE 4: Price and quantity curves with equilibrium positions at opposite ends of a diameter.

Therefore, the second-order condition of maximizing  $\Pi_i(x_1, x_2)$  is not satisfied if  $x_1 = x_2$ . In addition, the profit  $\Pi_i(x_1, x_2)$  can also be Pareto improved. For example, the profit  $\Pi_i(x_1, x_2)$  of each firm is  $7/108$  if the firms are located at the same point; that is,  $x_1 = x_2$ . Now, assume that firm A's position is fixed at  $x_1$  and firm B's position  $x_2$  is changed slightly, that is,  $x_2 = x_1 + \delta$ , where  $\delta$  is a number close to but not zero. According to (23) and Lemma 2, the increment  $\Delta\Pi_i$  of the profit can be calculated as follows:

$$\Delta\Pi_i = \Pi_i(x_1, x_1 + \delta) - \Pi_i(x_1, x_2) = \frac{2}{9}\delta^2 - \frac{8}{27}|\delta|^3 > 0, \quad (31)$$

which shows that the profits of firms A and B have both increased.

Strategy 2 can be viewed as optimal because it cannot be Pareto improved. If the positions of firms A and B are changed from  $|x_1 - x_2| - (1/2) = 0$  to  $|x_1 - x_2| - (1/2) = \delta$ , where  $\delta$  represents a number close to but not equal to zero, then the increment  $\Delta\Pi_i$  of the profit can be calculated as

$$\Delta\Pi_i = \frac{8}{27}|\delta|^3 - \frac{2}{9}\delta^2 < 0. \quad (32)$$

TABLE 1: Location game strategies based on possible equilibrium positions.

Strategy	Equilibrium points	Cost	Sales program			Profit
			Price	Quantity	Total quantity	
1	$x_1^* = x_2^*$	$c_1(x) = c_2(x)$	$(1/3)[1 + 2c_i(x)]$	$(1/3)[1 - c_i(x)]$	$Q_1^* = Q_2^* = (1/4)$	7/108
2	$ x_1^* - x_2^*  = (1/2)$	$c_1(x) + c_2(x) = (1/2)$	1/2	$q_1^*(x) = c_2(x)$ $q_2^*(x) = c_1(x)$	$Q_1^* = Q_2^* = (1/4)$	1/12

Thus, the profit of each firm decreases.

Based on the above discussion, we summarize what we have demonstrated.

**Proposition 2.** *In the closed-loop market with inverse demand function (8) and transportation cost function (1), if the two players develop the location game with quantity competition, the equilibrium locations  $x_1^*$  and  $x_2^*$  satisfy  $|x_1^* - x_2^*| = (1/2)$ , which means that they are at opposite ends of a diameter of the market. Furthermore, when the firms are at their equilibrium locations, the sales strategies, including price and quantity, in the local market  $x$  are as follows:*

$$\begin{aligned}
 p^*(x) &= \frac{1}{2}, \\
 q_1^*(x) &= \min\{|x_2^* - x|, 1 - |x_2^* - x|\}, \\
 q_2^*(x) &= \min\{|x_1^* - x|, 1 - |x_1^* - x|\}.
 \end{aligned} \tag{33}$$

*Remark 3.* Proposition 2 indicates that when the two players are at the equilibrium locations, they should provide different quantities of products for different local markets. In the quantity strategy, a player provides greater quantities to the local market that is closest to its location. However, the player adopts the same price strategy for every local market, which means that the price is indiscriminately unified in the entire closed-loop market.

*Remark 4.* For a linear city model, H. Hotelling proposed the principle of minimum differentiation, according to which, two competing players will be located in the same location [8]. However, Proposition 2 describes the principle of maximum differentiation in this paper. In a closed-loop market, due to the nonlinearity of the transportation cost function (1), two players will keep the maximum dispersion between their locations, which is contrary to Hotelling's principle.

## 5. Numerical Simulations

To illustrate the competitive dynamics in the close-loop market and verify the validity of the results, we employ MATLAB to simulate the game process of players 1 and 2 (firms A and B). At the beginning of the simulation, each player randomly and independently chooses a point  $x_i$  on the circle as its position. Then, the two players start the first round of position adjustments based on their profits. Player 1 uses (23) to calculate its own profit  $\Pi_1(x_1, x_2)$  based on its

position  $x_1$  and player 2's position  $x_2$  and moves a small step around the circle in the appropriate direction such that its new position increases its profit. Then, player 2 computes its own profit  $\Pi_2(x_1, x_2)$  and moves a small step around the circle in the same manner as player 1. In this way, the two players adjust their positions in each round and move alternately around the circle until their profits no longer increase.

Therefore, the algorithm for simulating competitive dynamics in the close-loop market can be designed as follows.

Step 1: initialize the move step size  $h$  with a small number. Initialize the positions  $x_1$  and  $x_2$  of the two players with two random numbers in  $[0, 1]$ .

Step 2: use (23) to compute  $M_1 = \Pi_1(x_1, x_2)$ ,  $M_2 = \Pi_1(x_1 + h, x_2)$ , and  $M_3 = \Pi_1(x_1 - h, x_2)$ .

Step 3: if  $M_1 < M_2$ , assign the value  $x_1 + h$  to  $x_1$ . If  $M_1 < M_3$ , assign the value  $x_1 - h$  to  $x_1$ .

Step 4: use (23) to compute  $N_1 = \Pi_2(x_1, x_2)$ ,  $N_2 = \Pi_2(x_1, x_2 + h)$ , and  $N_3 = \Pi_2(x_1, x_2 - h)$ .

Step 5: if  $N_1 < N_2$ , assign the value  $x_2 + h$  to  $x_2$  and return to Step 2. If  $N_1 < N_3$ , assign the value  $x_2 - h$  to  $x_2$  and return to Step 2.

Based on this algorithm, two numerical simulations are performed for different pairs of initial positions, and the dynamic evolution of the players in the closed-loop market is shown in Figures 5 and 6. The initial positions of the two players are  $x_1 = 0.06$  and  $x_2 = 0.68$  for the first simulation in Figure 5 and  $x_1 = 0.66$  and  $x_2 = 0.52$  for the second simulation in Figure 6. The number of rounds from the initial state to the equilibrium state is 6 in the first simulation and 18 in the second simulation since the distance between the two positions in the initial state is shorter in the first simulation. It is seen that in the last round the positions  $x_1$  and  $x_2$  are not changed and satisfy  $|x_1 - x_2| = (1/2)$  in each simulation.

*Remark 5.* In [26], the authors investigated the location game in a circular market and derived some conditions for guaranteeing the existence and uniqueness of the location equilibrium. Compared with this previous work, we have not only shown that a maximum dispersion is the location equilibrium in a closed-loop market, but also proposed the sales strategies for the two players in the equilibrium position. Furthermore, an algorithm is designed for simulating the competitive dynamics of a closed-loop market. To the best of our knowledge, this algorithm has not been proposed in the literature on circular markets.

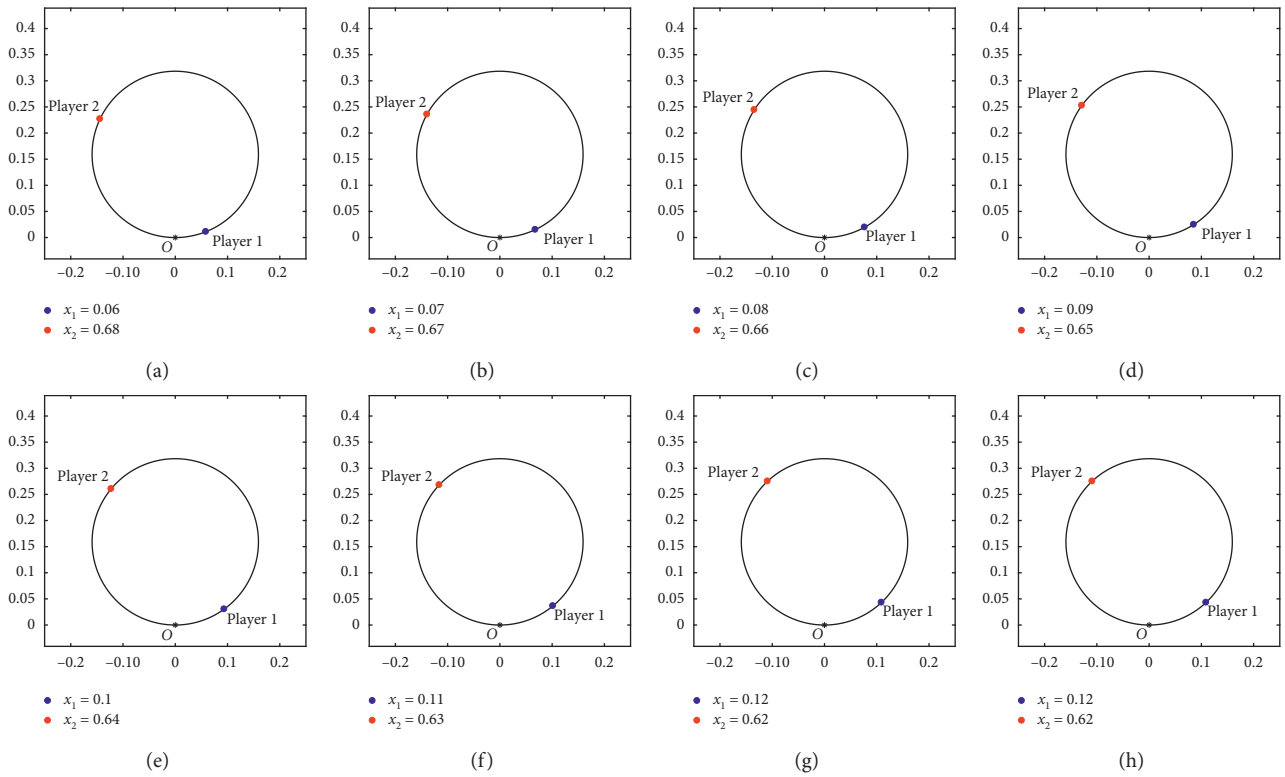


FIGURE 5: Dynamic evolution of the two-player location game in the closed-loop market with initial positions  $x_1 = 0.06$  and  $x_2 = 0.68$ .

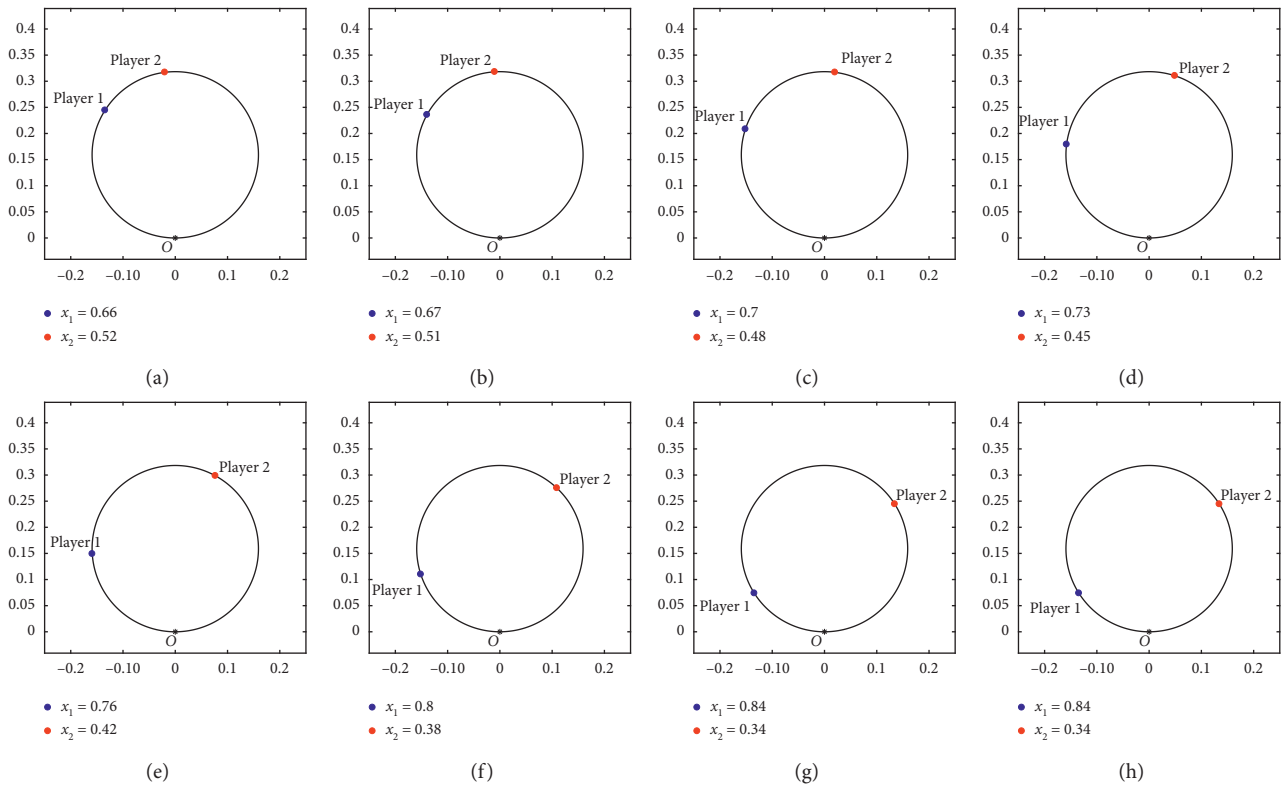


FIGURE 6: Dynamic evolution of the two-player location game in the closed-loop market with initial positions  $x_1 = 0.66$  and  $x_2 = 0.52$ .



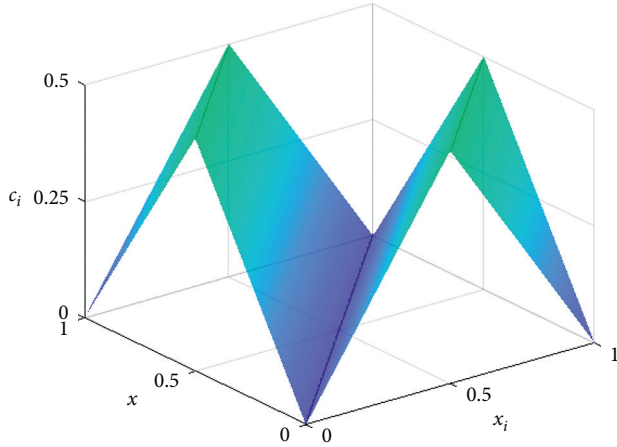


FIGURE 7: The graph of the function  $c_i$ .

## 6. Conclusion

To research the two-player location game in the closed-loop market, we consider the shape of the market as a circle. The location game with quantity competition between two players in a circular market is established. Using a two-stage approach, we solve the subgame-perfect Nash equilibria of the location game in the circular market. Moreover, we design an algorithm to simulate the dynamic evolution of the two-player location game in the closed-loop market and provide two numerical simulations to illustrate and validate the theoretical findings. The present research shows that the two players set their positions at opposite ends of a circle diameter in the optimal equilibrium state of the location game. At this point, they should adopt a differentiated quantity strategy and undifferentiated price strategy for the local markets. This paper considers the geometry of the market as a circle, which is a basic shape of the market. In fact, the geometry of the market could be very complex in the real world. Therefore, we will mainly focus on the research of multiplayer location game on complex networks in future.

*Remark 6.* Although the model in this paper is established under some ideal assumptions, the results have some positive reference value. In the real economic world, the whole Earth can be regarded as a circular market if observed along the Earth's latitude. There are two large countries, one in the east and the other in the west, at opposite ends of the diameter of the circular market. In theory, the competitive firms in the two countries are in an ideal equilibrium position. In fact, from the perspective of global geographical location, the firms in an equilibrium position have more location advantages than firms in other positions.

## Appendix

In this appendix, we prove Lemmas 1 and 2. Before proving them, we rewrite expression (1) of  $c_i(x)$ . Then, the relationship between  $|x_i - x|$  and  $1 - |x_i - x|$  in (1) needs to be discussed in the following six cases.

- (a)  $x_i - x > 0$  and  $|x_i - x| < 1 - |x_i - x|$ , if  $x_i \in [0, (1/2))$  and  $x \in [0, x_i)$
- (b)  $x_i - x \leq 0$  and  $|x_i - x| < 1 - |x_i - x|$ , if  $x_i \in [0, (1/2))$  and  $x \in [x_i, x_i + (1/2))$
- (c)  $x_i - x < 0$  and  $|x_i - x| \geq 1 - |x_i - x|$ , if  $x_i \in [0, (1/2))$  and  $x \in [x_i + (1/2), 1)$
- (d)  $x_i - x > 0$  and  $|x_i - x| > 1 - |x_i - x|$ , if  $x_i \in [(1/2), 1)$  and  $x \in [0, x_i - (1/2))$
- (e)  $x_i - x > 0$  and  $|x_i - x| \leq 1 - |x_i - x|$ , if  $x_i \in [(1/2), 1)$  and  $x \in [x_i - (1/2), x_i)$
- (f)  $x_i - x \leq 0$  and  $|x_i - x| < 1 - |x_i - x|$ , if  $x_i \in [(1/2), 1)$  and  $x \in [x_i, 1)$

Therefore,  $c_i$  can be regarded as a binary function with two variables  $x_i$  and  $x$ , which can be rewritten as

$$c_i = \begin{cases} x_i - x, & (x_i, x) \in \left[0, \frac{1}{2}\right) \times [0, x) \cup \left[\frac{1}{2}, 1\right) \times \left[x_i - \frac{1}{2}, x_i\right), \\ x - x_i, & (x_i, x) \in \left[0, \frac{1}{2}\right) \times \left[x_i, x_i + \frac{1}{2}\right) \cup \left[\frac{1}{2}, 1\right) \times [x_i, 1), \\ 1 - x + x_i, & (x_i, x) \in \left[0, \frac{1}{2}\right) \times \left[x_i + \frac{1}{2}, 1\right), \\ 1 - x_i + x, & (x_i, x) \in \left[\frac{1}{2}, 1\right) \times \left[0, x_i - \frac{1}{2}\right). \end{cases} \quad (\text{A.1})$$

Using MATLAB, the graph of the function  $c_i$  is plotted as shown in Figure 7. Obviously,  $c_i$  is a continuous function, but its partial derivatives do not exist at  $|x_i - x| = 0$  and  $|x_i - x| = (1/2)$ .

*The Proof of Lemma 1.* According to expression (A.1) of  $c_i$  and by the method of subsection integration, the lemma can be proved directly. The detailed calculation process is as follows.

For  $x_i \in [0, (1/2))$ , we can compute

$$\begin{aligned} \int_0^1 c_i(x) dx &= \int_0^{x_i} (x_i - x) dx + \int_{x_i}^{x_i+(1/2)} (x_i - x) dx \\ &\quad + \int_{x_i+(1/2)}^1 (1 - x + x_i) dx \\ &= \frac{1}{2}x_i^2 + \frac{1}{8} + \left(\frac{1}{8} - \frac{1}{2}x_i^2\right) = \frac{1}{4}. \end{aligned} \quad (\text{A.2})$$

For  $x_i \in [(1/2), 1)$ , we can compute

$$\begin{aligned} \int_0^1 c_i(x) dx &= \int_0^{x_i-(1/2)} (1 - x_i + x) dx + \int_{x_i-(1/2)}^{x_i} (x_i - x) dx \\ &\quad + \int_{x_i}^1 (x - x_i) dx \\ &= \left(-\frac{1}{2}x_i^2 + x_i - \frac{3}{8}\right) + \frac{1}{8} + \left(\frac{1}{2}x_i^2 - x_i + \frac{1}{2}\right) = \frac{1}{4}. \end{aligned} \quad (\text{A.3})$$

It follows from (A.2) and (A.3) that  $\int_0^1 c_i(x) dx = (1/4)$ .  
For  $x_i \in [0, (1/2))$ , we can compute

$$\begin{aligned} \int_0^1 c_i^2(x) dx &= \int_0^{x_i} (x_i - x)^2 dx + \int_{x_i}^{x_i+(1/2)} (x_i - x)^2 dx \\ &\quad + \int_{x_i+(1/2)}^1 (1 - x + x_i)^2 dx \\ &= \int_0^{x_i+(1/2)} (x_i - x)^2 dx + \int_{x_i+(1/2)}^1 (1 - x + x_i)^2 dx \\ &= \left(\frac{1}{3}x_i^3 + \frac{1}{24}\right) + \left(\frac{1}{24} - \frac{1}{3}x_i^3\right) = \frac{1}{12}. \end{aligned} \quad (\text{A.4})$$

For  $x_i \in [(1/2), 1)$ , we can compute

$$\begin{aligned} \int_0^1 c_i^2(x) dx &= \int_0^{x_i-(1/2)} (1 - x_i + x)^2 dx + \int_{x_i-(1/2)}^{x_i} (x_i - x)^2 dx \\ &\quad + \int_{x_i}^1 (x - x_i)^2 dx \\ &= \int_0^{x_i-(1/2)} (1 - x_i + x)^2 dx + \int_{x_i-(1/2)}^1 (x_i - x)^2 dx \\ &= \left(\frac{1}{3}x_i^3 - x_i^2 + x_i - \frac{7}{24}\right) + \left(-\frac{1}{3}x_i^3 + x_i^2 - x_i - \frac{3}{8}\right) = \frac{1}{12}. \end{aligned} \quad (\text{A.5})$$

It follows from (A.4) and (A.5) that  $\int_0^1 c_i^2(x) dx = (1/12)$ .

### The Proof of Lemma 2

(i) For  $(x_1, x_2) \in [0, (1/2)] \times [0, (1/2)]$ , it follows from (A.1) that

$$c_i(x) = \begin{cases} x_i - x, & x \in [0, x_i), \\ x - x_i, & x \in [x_i, x_i + \frac{1}{2}), \\ 1 - x + x_i, & x \in [x_i + \frac{1}{2}, 1). \end{cases} \quad (\text{A.6})$$

Consequently, for  $x_1 \leq x_2$ , we can compute

$$\begin{aligned} \int_0^1 c_1(x)c_2(x) dx &= \int_0^{x_1} (x_1 - x)(x_2 - x) dx + \int_{x_1}^{x_2} \\ &\quad \cdot (x - x_1)(x_2 - x) dx \\ &\quad + \int_{x_2}^{x_1+(1/2)} (x - x_1)(x_2 - x) dx + \int_{x_1+(1/2)}^{x_2+(1/2)} \\ &\quad \cdot (1 - x + x_1)(x_2 - x) dx \\ &\quad + \int_{x_2+(1/2)}^1 (1 - x + x_1)(1 - x + x_2) dx \\ &= -\frac{2}{3}(x_1 - x_2)^3 - \frac{1}{2}(x_1 - x_2)^2 + \frac{1}{12}. \end{aligned} \quad (\text{A.7})$$

Similarly, for  $x_1 > x_2$ , the following can be calculated:

$$\int_0^1 c_1(x)c_2(x) dx = \frac{2}{3}(x_1 - x_2)^3 - \frac{1}{2}(x_1 - x_2)^2 + \frac{1}{12}. \quad (\text{A.8})$$

Combining (A.7) and (A.8), we have

$$\int_0^1 c_1(x)c_2(x) dx = \frac{2}{3}|x_1 - x_2|^3 - \frac{1}{2}(x_1 - x_2)^2 + \frac{1}{12}, \quad (\text{A.9})$$

for  $(x_1, x_2) \in [0, (1/2)] \times [0, (1/2)]$ .

(ii) For  $(x_1, x_2) \in [0, (1/2)] \times [(1/2), 1)$ , it follows from (A.1) that

$$c_1(x) = \begin{cases} x_1 - x, & x \in [0, x_1), \\ x - x_1, & x \in [x_1, x_1 + \frac{1}{2}), \\ 1 - x + x_1, & x \in [x_1 + \frac{1}{2}, 1), \end{cases} \quad (\text{A.10})$$

$$c_2(x) = \begin{cases} 1 - x_2 + x, & x \in [0, x_2 - \frac{1}{2}), \\ x_2 - x, & x \in [x_2 - \frac{1}{2}, x_2), \\ x - x_2, & x \in [x_2, 1). \end{cases}$$

Consequently, for  $x_1 \leq x_2 - (1/2)$ , the following can be computed:

$$\begin{aligned}
\int_0^1 c_1(x)c_2(x)dx &= \int_0^{x_1} (x_1-x)(1-x_2+x)dx + \int_{x_1}^{x_2-(1/2)} \\
&\quad \cdot (x-x_1)(1-x_2+x)dx \\
&\quad + \int_{x_2-(1/2)}^{x_1+(1/2)} (x-x_1)(x_2-x)dx + \int_{x_1+(1/2)}^{x_2} \\
&\quad \cdot (1-x+x_1)(x_2-x)dx \\
&\quad + \int_{x_2}^1 (1-x+x_1)(x-x_2)dx \\
&= \frac{2}{3}\left(x_1-x_2+\frac{1}{2}\right)^3 + \frac{1}{2}\left(x_1-x_2+\frac{1}{2}\right)^2 + \frac{1}{24}.
\end{aligned} \tag{A.11}$$

Similarly, for  $x_1 > x_2 - (1/2)$ , we can compute

$$\int_0^1 c_1(x)c_2(x)dx = \frac{2}{3}\left(x_1-x_2+\frac{1}{2}\right)^3 + \frac{1}{2}\left(x_1-x_2+\frac{1}{2}\right)^2 + \frac{1}{24}. \tag{A.12}$$

It follows from (A.11) and (A.12) that

$$\int_0^1 c_1(x)c_2(x)dx = \frac{2}{3}\left|x_1-x_2+\frac{1}{2}\right|^3 + \frac{1}{2}\left(x_1-x_2+\frac{1}{2}\right)^2 + \frac{1}{24}, \tag{A.13}$$

if  $(x_1, x_2) \in [0, (1/2)] \times [(1/2), 1)$ .

(iii) For  $(x_1, x_2) \in [(1/2), 1) \times [0, (1/2))$ , as in (ii), we can compute

$$\int_0^1 c_1(x)c_2(x)dx = \frac{2}{3}\left|x_2-x_1+\frac{1}{2}\right|^3 + \frac{1}{2}\left(x_2-x_1+\frac{1}{2}\right)^2 + \frac{1}{24}. \tag{A.14}$$

(iv) For  $(x_1, x_2) \in [(1/2), 1) \times [(1/2), 1)$ , according to (A.1),  $c_i(x)$  can be reduced to

$$c_i(x) = \begin{cases} 1-x_i+x, & x \in \left[0, x_i-\frac{1}{2}\right), \\ x_i-x, & x \in \left[x_i-\frac{1}{2}, x_i\right), \\ x-x_i, & x \in [x_i, 1). \end{cases} \tag{A.15}$$

Consequently, for  $x_1 \leq x_2$ , we can compute

$$\begin{aligned}
\int_0^1 c_1(x)c_2(x)dx &= \int_0^{x_1-(1/2)} c_1(x)c_2(x)dx + \int_{x_1-(1/2)}^{x_2-(1/2)} c_1(x)c_2 \\
&\quad \cdot (x)dx + \int_{x_2-(1/2)}^{x_1} c_1(x)c_2(x)dx + \int_{x_1}^{x_2} c_1 \\
&\quad \cdot (x)c_2(x)dx + \int_{x_2}^1 c_1(x)c_2(x)dx \\
&= \frac{2}{3}(x_1-x_2)^3 - \frac{1}{2}(x_1-x_2)^2 + \frac{1}{24}.
\end{aligned} \tag{A.16}$$

Similarly, for  $x_1 > x_2$ , we can compute the following:

$$\int_0^1 c_1(x)c_2(x)dx = \frac{2}{3}(x_1-x_2)^3 - \frac{1}{2}(x_1-x_2)^2 + \frac{1}{24}. \tag{A.17}$$

It follows from (A.16) and (A.17) that

$$\int_0^1 c_1(x)c_2(x)dx = \frac{2}{3}|x_1-x_2|^3 - \frac{1}{2}(x_1-x_2)^2 + \frac{1}{24}, \tag{A.18}$$

for  $(x_1, x_2) \in [(1/2), 1) \times [(1/2), 1)$ .

Specifically, for  $x_1 = x_2$ , it follows from (A.13) and (A.18) that

$$\int_0^1 c_1(x)c_2(x)dx = \frac{1}{12}. \tag{A.19}$$

For  $|x_1 - x_2| = (1/2)$ , according to (A.13) and (A.14), we can obtain

$$\int_0^1 c_1(x)c_2(x)dx = \frac{1}{24}. \tag{A.20}$$

## Data Availability

The data used to support the findings of this study are available from the corresponding author upon request.

## Conflicts of Interest

The authors declare that there are no conflicts of interest regarding the publication of this paper.

## Acknowledgments

This work was supported in part by the National Natural Science Foundation of China under Grant 61773004, in part by the Natural Science Foundation Project of Chongqing under Grant cstc2018jcyjAX0606, and in part by the Science and Technology Research Program of Chongqing Municipal Education Commission under Grant KJQN201900701.

## References

- [1] J. von Neumann, "Zur theorie der gesellschaftsspiele," *Mathematische Annalen*, vol. 100, no. 1, pp. 295–320, 1928.
- [2] T. Ichiishi, A. Neyman, Y. Tauman, and K. Shell, *Game Theory and Applications*, Academic Press, Cambridge, MA, USA, 1990.
- [3] S. Lasaulce and H. Tembine, *Game Theory and Learning for Wireless Networks: Fundamentals and Applications*, Academic Press, Cambridge, MA, USA, 2011.
- [4] P. D. Giovanni and G. Zaccour, "A two-period game of a closed-loop supply chain," *European Journal of Operational Research*, vol. 232, pp. 22–40, 2014.
- [5] S. Goyal, H. Heidari, and M. Kearns, "Competitive contagion in networks," *Games and Economic Behavior*, vol. 113, pp. 58–79, 2019.
- [6] E. Talamàs, "Price dispersion in stationary networked markets," *Games and Economic Behavior*, vol. 115, pp. 247–264, 2019.
- [7] W.-C. Guo and F.-C. Lai, "Spatial cournot competition in two intersecting circular markets," *The Annals of Regional Science*, vol. 64, no. 1, pp. 37–56, 2020.
- [8] H. Hotelling, "Stability in competition," *The Economic Journal*, vol. 39, no. 153, pp. 41–57, 1929.
- [9] C. d'Aspremont, J. J. Gabszewicz, and J.-F. Thisse, "Computation of multi-facility location Nash equilibria on a network under quantity competition," *Econometrica*, vol. 47, no. 4, pp. 1145–1150, 1979.
- [10] B. Gupta, D. Pal, and J. Sarkar, "Spatial Cournot competition and agglomeration in a model of location choice," *Regional Science and Urban Economics*, vol. 27, no. 3, pp. 261–282, 1997.
- [11] E. Gal-or, "Hotelling's spatial competition as a model of sales," *Economics Letters*, vol. 9, no. 1, pp. 1–6, 1982.
- [12] D. Graitson, "Spatial competition a la Hotelling: a selective survey," *The Journal of Industrial Economics*, vol. 31, no. 1/2, pp. 11–25, 1982.
- [13] N. Economides, "Minimal and maximal product differentiation in Hotelling's duopoly," *Economics Letters*, vol. 21, no. 1, pp. 67–71, 1986.
- [14] S. P. Anderson, J. K. Goeree, and R. Ramer, "Location, location, location," *Journal of Economic Theory*, vol. 77, no. 1, pp. 102–127, 1997.
- [15] S. Brenner, "Hotelling games with three, four, and more players," *Journal of Regional Science*, vol. 45, no. 4, pp. 851–864, 2005.
- [16] L. Lambertini and R. Orsini, "On Hotelling's "stability in competition" with network externalities and switching costs," *Papers in Regional Science*, vol. 92, no. 4, pp. 873–883, 2013.
- [17] W.-C. Guo, F.-C. Lai, and D.-Z. Zeng, "A Hotelling model with production," *Mathematical Social Sciences*, vol. 73, pp. 40–49, 2015.
- [18] J. Hinlopen and S. Martin, "Costly location in Hotelling duopoly," *Research in Economics*, vol. 71, no. 1, pp. 118–128, 2017.
- [19] J. Chen and B. Chen, "When should the offline retailer implement price matching?" *European Journal of Operational Research*, vol. 277, no. 3, pp. 996–1009, 2019.
- [20] M. A. de Frutos, H. Hamoudi, and X. Jarque, "Equilibrium existence in the circle model with linear quadratic transport cost," *Regional Science and Urban Economics*, vol. 29, no. 5, pp. 605–615, 1999.
- [21] M. Peitz, "The circular road revisited: uniqueness and supermodularity," *Research in Economics*, vol. 53, no. 4, pp. 405–420, 1999.
- [22] B. Gupta, F.-C. Lai, D. Pal, J. Sarkar, and C.-M. Yu, "Where to locate in a circular city?" *International Journal of Industrial Organization*, vol. 22, no. 6, pp. 759–782, 2004.
- [23] T. Matsumura and D. Shimizu, "Cournot and Bertrand in shipping models with circular markets," *Papers in Regional Science*, vol. 85, no. 4, pp. 585–598, 2006.
- [24] D. Pal and J. Sarkar, "Spatial Cournot competition among multi-plant firms in a circular city," *Southern Economic Journal*, vol. 73, no. 1, pp. 246–258, 2006.
- [25] Q. Gong, Q. Liu, and Y. Zhang, "Optimal product differentiation in a circular model," *Journal of Economics*, vol. 119, no. 3, pp. 219–252, 2016.
- [26] C.-H. Sun, J.-F. Tsai, and F.-C. Lai, "Spatial Cournot competition in a circular city with more than two dispatches," *The Japanese Economic Review*, vol. 68, no. 4, pp. 413–442, 2017.
- [27] A. Cournot, *Recherches sur les Principes Mathématiques de la Théorie des Richesses*, Hachette, Paris, France, 1838.

## Research Article

# A Polynomial Splines Identification Method Based on Control Nets

Zhихua Wang<sup>1,2</sup> and Hongmei Kang<sup>3</sup>

<sup>1</sup>School of Mathematical Sciences, University of Science and Technology of China, Hefei 230026, China

<sup>2</sup>School of Mathematics and Computer Science, Anqing Normal University, Anqing 246011, China

<sup>3</sup>School of Mathematical Sciences, Soochow University, No. 1 Road Shizi, Suzhou, Jiangsu, China

Correspondence should be addressed to Zhихua Wang; 1208044765@qq.com

Received 22 April 2020; Revised 29 June 2020; Accepted 13 July 2020; Published 19 August 2020

Academic Editor: Oh-Min Kwon

Copyright © 2020 Zhихua Wang and Hongmei Kang. This is an open access article distributed under the Creative Commons Attribution License, which permits unrestricted use, distribution, and reproduction in any medium, provided the original work is properly cited.

In this study, based on Polynomial Splines with control nets, an identification method is investigated. We introduce polynomial splines with control nets defined over T-mesh. The basic idea is to extend T-vertices such that those T-vertices become interior cross vertices or boundary vertices. To this end, we introduce the design-suitable T-mesh for constructing polynomial splines with control net. In design-suitable T-meshes, there are no extra basis vertices produced by an appropriate extension of T-vertices. The basis functions are defined over each vertex in a design-suitable T-mesh by the means of constructing PHT-splines basis functions.

## 1. Introduction

T-splines [1, 2] are introduced to overcome the weakness of NURBS by allowing T-junctions. T-splines are considered as a generalization of NURBS surfaces and capable of local refinement, which makes T-splines a powerful modeling tool for advanced geometric modeling and adaptive isogeometric analysis (IGA) [3, 4]. Stimulated by the advent of T-splines and isogeometric analysis, locally refinable splines are born and now becoming flourishing. Currently, there are Hierarchical B-splines [5–7], truncated hierarchical B-splines (THB-splines) [8], truncated T-splines [9], truncated hierarchical tricubic  $C^0$  spline [10], blended B-spline based on unstructured quadrilateral and hexahedral meshes [11], analysis-suitable T-splines (AST-splines) [12], LR B-splines [13], modified T-splines [14], and polynomial splines over hierarchical T-meshes (PHT-splines) [15].

PHT-splines are introduced in [15] as bicubic  $C^1$  continuous polynomial splines spaces defined over hierarchical T-meshes. PHT-splines possess a set of nonnegative and linearly independent basis functions and allow for very efficient local refinement. PHT-splines have been widely applied in geometric processing and analysis. The finite

element discretization of elliptic equations based on PHT-splines was discussed in [16], where numerical solutions are refined adaptively and have the optimal convergence rate. PHT-splines are also favored in isogeometric analysis for solving elastic problems [3, 17, 18] and adaptive isogeometric analysis [19]. PHT-splines are also applied in reconstructing surface models efficiently. PHT-splines were used in stitching several surface patches to construct complex models in paper [20] and PHT-splines were also applied in surface reconstruction from a very large set of point clouds in implicit form [21]. IGA collocation approaches are introduced in paper [22], and PHT-splines have been used as basis functions for the adaptive collocation method [23].

In order to make PHT-splines better suited for analysis and geometric processing, some improvements and extensions have been made to PHT splines in recent years. In [24], the authors discussed the decay phenomenon of PHT-splines basis functions. They found some of the basis functions will tend to zero as the refinement level increases under certain types of refinement. Such a decay makes the stiffness matrix in isogeometric analysis be ill-conditioned, which is not expected by analysis. Thus a new basis

construction method is proposed for PHT-splines to avoid the decay. The extension of PHT-splines to general T-meshes is considered in [25], where the bicubic  $C^1$  continuous polynomial splines are defined over general T-meshes. The basis functions are constructed by computing the geometric information at basis vertices such that the resulting basis functions are nonnegative and linearly independent and form a partition of unity. PHT splines were defined over hierarchical T-meshes without irregular vertex in [15], and then the bicubic  $C^1$  continuous splines construction based on irregular quad layout were discussed in [26]. Current implementation of PHT-splines stores the basis functions in Bézier forms, which saves some computational costs but consumes a lot of memories. In [27], an algorithm to evaluate PHT-splines is provided where only the information about the control coefficients and the hierarchical mesh structure is given. The evaluation algorithm takes about the same computational costs while requiring much less amount of memory compared with the Bézier representations.

For PHT-splines, there is no one-to-one correspondence between the vertices in the underlying T-mesh and PHT-splines basis functions. The boundary vertices and interior cross vertices are called basis vertices. Each basis vertex is associated with four basis functions. The control net concept is essential in computer aided geometric design (CAGD), because the control net makes editing models easily and intuitively. In this paper, we introduce polynomial splines with control polygon to complement PHT-splines. The proposed splines defined over all the vertices of the underlying T-meshes, such that there is a one-to-one correspondence between control points and vertices in T-meshes. The basis idea is to extend T-vertices to be basis vertices. In order to avoid generating extra basis vertices when extending T-vertices, we introduce a subset of T-meshes, called design-suitable T-meshes. Over design-suitable T-meshes, the T-vertices can be extended appropriately without generating extra basis vertices. For a given T-mesh, it needs to connect some T-vertices to be a design-suitable T-mesh. We define polynomial splines basis functions over the design-suitable T-mesh. The resulting splines not only inherit the nice properties of PHT-splines, but also have control nets.

The paper is organized as follows. In Section 2, we review some preliminary knowledge about polynomial splines over T-meshes. In Section 3, we proposed a subset of T-mesh called design-suitable T-mesh and prove that there are no extra basis vertices produced by an appropriate extension. In Section 4, we present an algorithm of local refinement of the proposed splines. Finally, we give a conclusion of this paper in Section 5.

## 2. Preliminary Knowledge

**2.1. T-Meshes.** A T-mesh is a rectangular grid with T-junctions. The cells in a T-mesh must be rectangles. A grid point in a T-mesh is called a *vertex*. And the vertex on a boundary grid line is called a *boundary vertex*; otherwise, it is called an *interior vertex*. Interior vertices consist of cross

vertices and T-vertices. We adopt the notations  $\top$ ,  $\perp$ ,  $\vdash$ , and  $\dashv$  to indicate the four possible orientations of T-vertices. The T-vertices of type  $\vdash$  and  $\dashv$  are called horizontal T-vertices and the T-vertices of type  $\top$  and  $\perp$  are called vertical T-vertices.

**2.2. Bicubic  $C^1$  Continuous B-Splines.** Let

$$\begin{aligned} t_0, t_0 = t_1, t_1 < t_2, t_2 < \dots < t_j, t_j < \dots < t_{n-1}, \\ t_{n-1} = t_n, t_n \end{aligned} \quad (1)$$

be a knot vector with interior knots of multiplicity two. Then each knot  $t_j$  is associated with two cubic B-splines  $N_j^1(t) = N^3[t_{j-1}, t_{j-1}, t_j, t_j, t_{j+1}](t)$  and  $N_j^2(t) = N^3[t_{j-1}, t_j, t_j, t_{j+1}, t_{j+1}](t)$ . Both  $N_j^1(t)$  and  $N_j^2(t)$  together with their derivatives have the same support  $[t_{j-1}, t_{j+1}]$ . Except for  $N_j^1(t)$  and  $N_j^2(t)$ , all the other cubic B-splines and their derivatives vanish at  $t_j$ .

For given a tensor product mesh  $\mathcal{T}$ , the two associated global knot vectors in  $s$ -direction and  $t$ -direction are

$$\begin{aligned} U &= \{s_0, s_0 = s_1, s_1 < s_2, s_2 < \dots < s_j, s_j < \dots < s_{m-1}, s_{m-1} = s_m, s_m\}, \\ V &= \{t_0, t_0 = t_1, t_1 < t_2, t_2 < \dots < t_j, t_j < \dots < t_{n-1}, t_{n-1} = t_n, t_n\}, \end{aligned} \quad (2)$$

respectively. The bicubic  $C^1$  continuous B-splines surface defined over  $\mathcal{T}$  is spanned by the  $\{N_{i,j}^k\}_{i=0,j=0,k=0}^{i=m,j=n,k=3}$ , where  $N_{i,j}^k(s, t) = N_i^{k/2}(s)N_j^{[k/2]}(t)$ ,  $k = 0, 1, 2, 3$  are the four B-splines associated with the vertex  $(s_i, t_j)$ .

For a function  $f(x, y)$ , the function value, the first partial derivatives, and the mixed partial derivative are called the geometric information of  $f(x, y)$ , denoted by

$$\mathcal{E}f(x, y) = (f(x, y), f_x(x, y), f_y(x, y), f_{xy}(x, y)). \quad (3)$$

For the basis function  $N_{i,j}^k$  defined above, it has  $\mathcal{E}N_{i,j}^k(s_p, t_q) = \delta_{ip}\delta_{jq}$  and  $\delta_{ip} = 1$ , if  $i = p$ ; otherwise,  $\delta_{ip} = 0$ . That is the geometric information of  $N_{i,j}^k$  vanishes at other vertices in  $\mathcal{T}$  except its associated vertex  $(s_i, t_j)$ .

## 3. Polynomial Splines with Control Nets Defined over T-Meshes

PHT-splines span the polynomial splines space  $S(3, 3, 1, 1)$  over a T-mesh and are defined over cross interior vertices and boundary vertices (called basis vertices), resulting in PHT-splines lacking control net. Our aim is to equip PHT-splines with control net. For any given control mesh, we parameterize the control mesh into a T-mesh in 2D domain and then extend all T-vertices in the T-mesh such that they become basis vertices and no extra basis vertices is introduced, and finally construct basis functions of  $S(3, 3, 1, 1)$  over the extended T-mesh. Thus, there is a one-to-one correspondence between the control mesh and parameter T-mesh. For arbitrary T-mesh, it is inevitable that extra basis vertices are produced by directly extending T-vertices. Therefore, in order to avoid extra basis vertices, we introduce design-suitable T-meshes for defining basis functions.

3.1. *Design-Suitable T-Meshes.* For a given T-mesh  $\mathcal{T}$ , we shall adopt some definitions and notations (Figure 1).

- (i) *Extension of T-vertex.* The closed line segment created by extending a T-vertex in the missing direction until it intersects with an edge is called the extension of this T-vertex. Particularly, if the edge is an edge in  $\mathcal{T}$ , then the extension is called a full-extension. The extension of a horizontal (vertical) T-vertex is called the horizontal (vertical) extension, respectively. In Figure 1(b), the dotted line segments are full-extensions of T-vertices.
- (ii) *Full-Extension Mesh.* A T-mesh together with the full-extensions of all T-vertices in this T-mesh forms the full-extension mesh. Figure 1(b) shows the full-extension mesh of the T-mesh in Figure 1(a).
- (iii) *Edge-Type Intersections.* The intersection between two same type extensions and the intersection between an extension and a boundary edge is called an edge-type intersection (E-intersection for short). In Figure 1(b),  $v_0, v_1, \dots, v_7$  are all E-intersections.
- (iv) *Face-Type Intersections.* The intersection between a horizontal extension and a vertical extension is called a face-type intersection (F-intersection for short). In Figure 1(b),  $v_8, v_9, \dots, v_{13}$  are all F-intersections.
- (v) *Connectable Vertex.* Two vertices can be connected if the line segment formed by these two vertices splits the lying face into two subrectangles. If two T-vertices can be connected, then they are called connectable T-vertices (CT-vertex for short). The vertices are marked by blue solid circles in Figure 1(a).
- (vi) *E-Connectable T-Vertex.* For a T-vertex, if its extension intersects with the extension of another same type T-vertex or with a boundary edge, then the T-vertex is called an e-connectable T-vertex (ECT-vertex). The vertices marked by yellow solid circles in Figure 1(a) are ECT-vertices.
- (vii) *Normal T-Vertex.* For a T-vertex, if it is either a CT-vertex or an ECT-vertex, then it is called a normal T-vertex.
- (viii) *T-Element.* If there are T-vertices lying on the edges of an element, then the element is called a T-element.
- (ix) *C-Element.* For a T-element in  $\mathcal{T}$ , if there are ECT-vertices on the edges of this element, then the element is called a C-element. Those elements  $F_1, F_2, \dots, F_6$  in Figure 1(a) are connectable elements.
- (x) *S-Element.* For a C-element, if there exists a normal vertical (horizontal) T-vertex in the element such that its extension subdivides the element into two subelements and one subelement contains all the horizontal (vertical) ECT-vertices, then the

connectable element is called a S-element and the normal vertical (horizontal) T-vertex is called a ST-vertex. The element  $F_6$  is a S-element, while  $F_1, \dots, F_5$  are not S-elements.

*Definition 1.* For a given T-mesh  $\mathcal{T}$ , the corresponding full-extension T-mesh is denoted by  $\mathcal{T}_{ext}$ , if

- (i) there are no connectable T-vertices in  $\mathcal{T}$
- (ii) for each edge-type intersection in  $\mathcal{T}_{ext}$ , the underlying edge is attached to a S-element;

then  $\mathcal{T}$  is called a design-suitable T-mesh.

The diagonal T-mesh (the diagonal elements are refined in the diagonal direction) shown in Figure 2(a) is a design-suitable T-mesh. The T-mesh shown in Figure 1(b) is not a design-suitable T-mesh. But if we connect all the CT-vertices and ECT-vertices, then the resulting mesh is a design-suitable T-mesh which is shown in Figure 3(a).

For a design-suitable T-mesh, there are no extra basis vertices produced by extending T-vertices appropriately. The intuitive way is to extend a T-vertex in the missing direction, until it intersects with an edge in the underlying mesh instead of the original T-mesh. We call such a way of extending T-vertices as p-extending to distinguish from the extension mentioned above. For the design-suitable T-mesh shown in Figure 2(a), the new T-mesh produced by p-extending T-vertices is shown in Figure 2(b). We also plot the full-extension T-mesh in Figure 2(c) for comparison. This p-extending way is not enough for the T-meshes containing ECT-vertices. It still requires an order of extending T-vertices. Thus, we introduce the following algorithm to extend T-vertices in a given T-mesh, and the resulting T-mesh is denoted by  $\mathcal{T}_e$ .

- (i) Step one: p-extend T-vertices in S-elements and the adjacent elements of S-elements
  - (a) S-element: First p-extend the ST-vertices of an S-element; then p-extend the rest of T-vertices in the element
  - (b) Adjacent elements: First p-extend ECT-vertices; then p-extend the normal T-vertices
- (ii) Step two: p-extend T-vertices in the rest of T-elements
  - (a) First p-extend horizontal T-vertices; then p-extend vertical T-vertices

We take Figure 3 as an example to explain the above algorithm. In the T-mesh shown in Figure 3(a),  $F_1, F_2, \dots, F_6$  are T-elements. We need to extend the T-vertices in these elements. The element  $F_3$  is an S-element. We start from extending T-vertices in this element. The vertex  $v_5$  is a ST-vertex, and it is extended until it intersects with an existing edge. Then we extend the vertex  $v_4$ , and the first edge it intersects with is the extension of  $v_5$ . The element  $F_6$  is the adjacent element of  $F_3$ . The vertex  $v_8$  is p-extended. For the rest T-elements, if there are horizontal T-vertices, then extend them first. Thus, in  $F_3$ ,  $v_3$  is extended first and

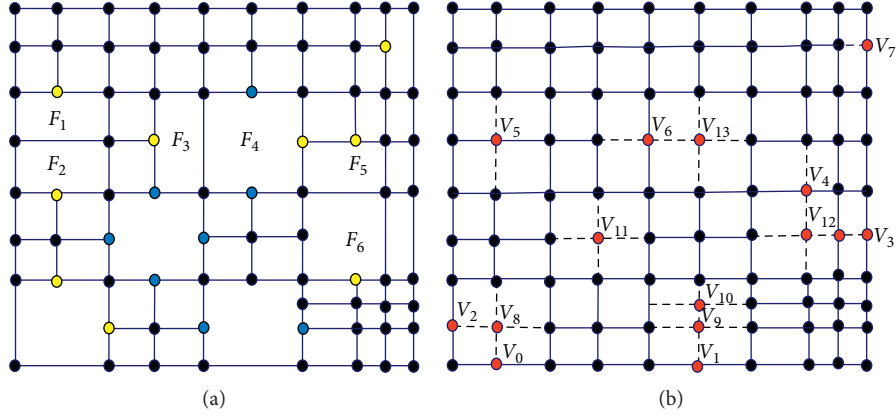


FIGURE 1: Full-extension T-mesh. (a) T-mesh; (b) full-extension T-mesh  $\mathcal{T}_{ext}$ .

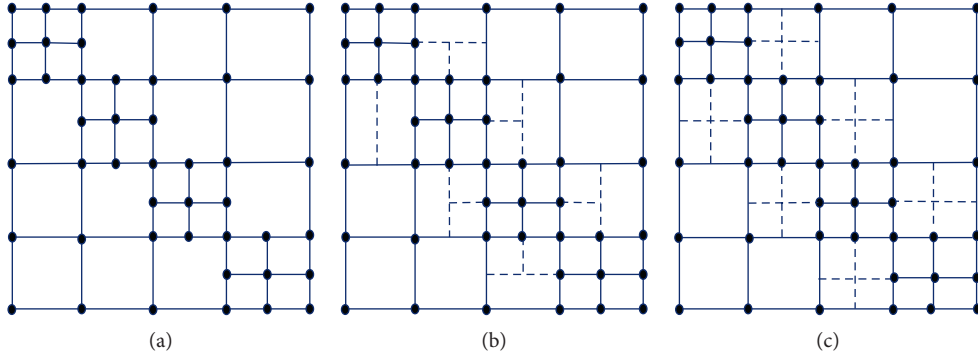


FIGURE 2: A design-suitable T-mesh and the p-extending. (a) Diagonal T-mesh, (b) p-extending, and (c) full-extension T-mesh.

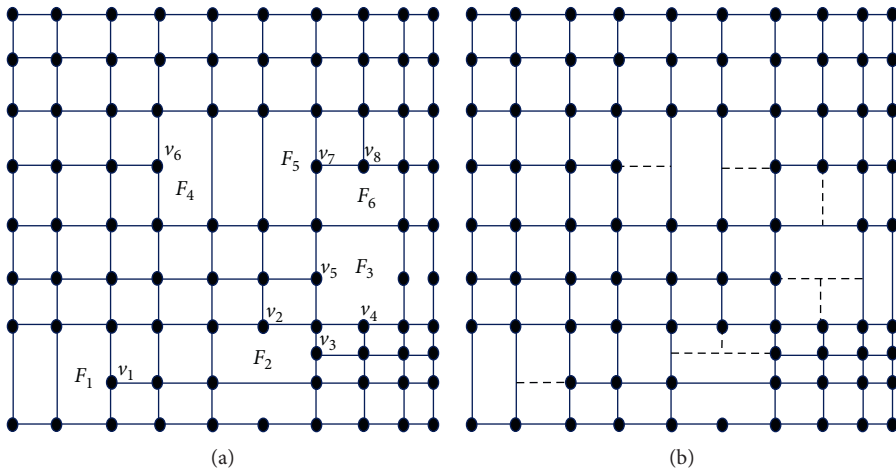


FIGURE 3: The proposed algorithm for extending T-vertices. (a) Design-suitable T-mesh; (b) extended T-mesh  $\mathcal{T}_e$ .

then  $v_2$  is extended. The resulting extended T-mesh is shown Figure 3(b).

**Theorem 1.** For a design-suitable T-mesh  $\mathcal{T}$ , extend the T-vertices in  $\mathcal{T}$  as above. Then there is a one-to-one correspondence between basis vertices in  $\mathcal{T}_e$  and vertices in  $\mathcal{T}$ ,

which means there are no extra basis vertices produced in  $\mathcal{T}_e$  by extending T-vertices in  $\mathcal{T}$  appropriately.

*Proof.* We only need to deal with T-elements. We extend T-vertices element by element. We need to prove there are no edge-type intersections and face-type intersections in  $\mathcal{T}_e$ . In a



design-suitable T-mesh, only extending ECT-vertices may produce edge-type intersections. Furthermore, there are no face-type intersections produced by p-extending. S-elements are extended first according to the above algorithm. Since ST-vertices are normal T-vertices, then their extensions intersect with existing edges and the intersections are T-vertices. According to the definition of ST-vertices, the extensions of ST-vertices prevent the intersection between ECT-vertices. Then extending T-vertices in the adjacent T-elements of S-elements will not produce new basis vertices. For the rest T-elements, there are no basis vertices produced by p-extending.  $\square$

**3.2. Construct Basis Functions over  $\mathcal{T}_e$ .** Let  $\mathbf{B}_i(s, t) = (B_i^1(s, t), B_i^2(s, t), B_i^3(s, t), B_i^4(s, t))$  be the basis functions associated with  $V_i$  needed to be constructed. There are mainly three steps for constructing  $\mathbf{B}_i(s, t)$  in [25]:

- (i) Find a rectangle containing all the vertices at which  $\mathbf{B}_i(s, t)$  which do not vanish in  $\mathcal{T}_e$
- (ii) Set the geometric information of bicubic  $C^1$  continuous B-splines associated with  $V_i$  over the rectangle as the geometric information of  $\mathbf{B}_i(s, t)$
- (iii) Set the geometric information at other basis vertices in the rectangle as zeros and represent  $\mathbf{B}_i(s, t)$  in the Bézier form or B-splines form

The method for finding a rectangle for each basis vertex in  $\mathcal{T}_e$  is stated as follows. For a basis vertex  $v_i = (s_{i_0}, t_{i_0})$  in  $\mathcal{T}_e$ , first put  $v_i$  into  $K_i$ , then check the neighboring vertices of the vertices in  $K_i$  and put the T-vertices into  $K_i$  recursively until there is no vertex added into  $K_i$ . The minimal rectangle containing all the vertices in  $K_i$  is denoted by  $R_V = [s_0, s_1] \times [t_0, t_1]$ , then  $R_V$  together with the knot lines  $s = s_{i_0}$  and  $t = t_{i_0}$  forms a  $2 \times 2$  tensor product mesh  $M_V = \{s_0, s_{i_0}, s_1\} \times \{t_0, t_{i_0}, t_1\}$ . For the sake of clearness, we call  $M_V$  as the support mesh of basis vertex  $v_i$ . Figure 4 shows the support meshes of four basis vertices  $v_{13}$ ,  $v_{17}$ , and  $v_4$  in the extended T-mesh, where the support meshes are shaded. In Figure 4(a),  $v_{13}$  is a basis vertex and among the neighbors of  $v_{13}$ ,  $v_{48}$  is a T-vertex; thus, it is put into  $K_i$ . Then we check the neighbors of  $v_{48}$ , and  $v_{49}$  is a T-vertex which is put into  $K_i$ . For  $v_{49}$ , there are no more vertices needed to be added into  $K_i$ . Thus, the set  $K_i = \{v_{13}, v_{48}, v_{49}\}$ . Similarly for  $v_{17}$  in Figure 4(b), now  $K_i = \{v_{17}, v_{50}, v_{51}\}$ . For the basis vertex  $v_4$  shown in Figure 4(c),  $K_i = \{v_4, v_{53}\}$ .

The four B-spline basis functions defined over  $M_V$  are denoted by  $N_k(s, t)$ ,  $k = 0, 1, 2, 3$ , and

$$N_k(s, t) = N^3[s_0, s_0, s_{i_0}, s_{i_0}, s_1, s_1](s) \times N^3[t_0, t_0, t_{i_0}, t_{i_0}, t_1, t_1](t). \quad (4)$$

Then the geometric information of four basis functions  $\mathbf{B}_i(s, t)$  at  $V_i$  is defined as the geometric information of  $N_k(s, t)$ ,  $k = 0, 1, 2, 3$ . The geometric information of  $\mathbf{B}_i(s, t)$  at the other basis vertices in  $M_V$  is set as zero. And the geometric information of  $\mathbf{B}_i(s, t)$  at T-vertices in  $M_V$  is computed by  $C^1$  constraints. According to the known geometric information of  $\mathbf{B}_i(s, t)$  at the vertices in  $M_V$ , then  $\mathbf{B}_i(s, t)$  can be easily represented in Bézier form or B-splines form.

**3.3. Polynomial Splines with Control Net Defined on T-Meshes.** With the help of index T-mesh, there is a one-to-one correspondence between vertices and basis functions. The index T-mesh is adopted in [3] for ease of constructing T-splines. It is constructed by plotting the knots at equally spaced intervals regardless of their actual spacing and labeling each knot line with integer values [3]. Figure 5(b) shows the index T-mesh of the mesh shown in Figure 5(a). Figure 5(c) shows a control net in  $\mathbb{R}^3$  corresponding to the T-mesh shown in Figure 5(a). Figure 5(d) shows the polynomial splines surface with control net Figure 5(c) defined on the design-suitable T-mesh Figure 5(a). Notice the knots in this paper are of multiplicity two; thus, if we view the T-mesh in index space, each vertex in T-meshes corresponds to four vertices in index T-mesh. In a design-suitable T-mesh, it happens that each vertex is associated with four basis functions. Thus, there is a one-to-one correspondence between vertices and basis functions exactly in a design-suitable T-mesh. For convenience, in this paper, we still use T-meshes for constructing T-meshes and local refinement. The index T-mesh is used only to explain the control net.

For a design-suitable T-mesh  $\mathcal{T}$ , we construct basis functions on the extended T-mesh  $\mathcal{T}_e$  as stated in section 3.2. The polynomial splines surface defined over  $\mathcal{T}$  is defined as follows:

$$S(u, v) = \sum_{i=1}^n \sum_{k=1}^4 \mathbf{P}_i^k B_i^k(u, v), \quad (u, v) \in [a, b] \times [c, d], \quad (5)$$

where  $B_i^k(u, v)$  are basis functions constructed in section 3.2 and  $\mathbf{P}_i^k \in \mathbb{R}^3$  are the corresponding control points. Figure 6 presents the polynomial splines model with control nets. The construction method is based on the above polynomial splines with control nets defined over T-meshes; we design a goblet model and a dolphin model; see Figures 7 and 8.

For a design-suitable T-mesh, we define four basis functions at each vertex. If we need to adjust the surface part corresponding to a T-vertex, we can adjust the control point corresponding to the basis functions defined at the T-vertex to modify the surface directly. But for PHT-spline surface, it can only be adjusted indirectly by adjusting the control points corresponding to the basis functions defined at other basis vertices. Figure 9 shows the modification of the surface by adjusting the position of the control points corresponding to the T-vertices and the normal basis vertices.

## 4. Local Refinement

Given a design-suitable T-mesh  $\mathcal{T}^1$ , denote the extended T-mesh as  $\mathcal{T}_e^1$ . The edge insertion is to insert edges into  $\mathcal{T}^1$ , the resulting T-mesh is denoted by  $\mathcal{T}^2$ . The local refinement is attributed to how to construct the extended T-mesh  $\mathcal{T}_e^2$  such that  $\mathcal{S}(3, 3, 1, 1, \mathcal{T}_e^1) \subseteq \mathcal{S}(3, 3, 1, 1, \mathcal{T}_e^2)$ , which is equivalent to  $\mathcal{T}_e^1 \subseteq \mathcal{T}_e^2$ .

Suppose a vertical edge  $e = \overline{v_0 v_1}$  is inserted into a element  $F$ , and the 2-neighboring elements of  $F$  in vertical direction are denoted by  $F_i$ ,  $i = 1, 2, \dots, l$  (if existing). The local refinement algorithm is described as follows:

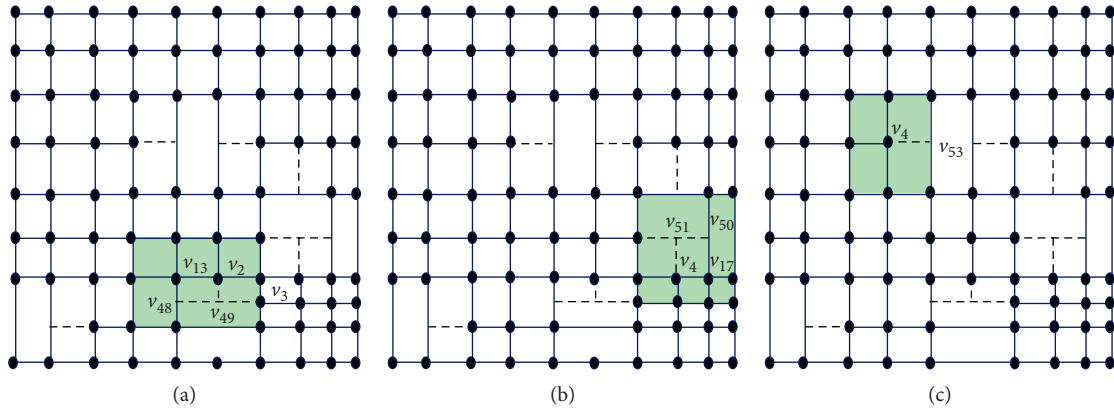


FIGURE 4: The support meshes of three basis vertices  $v_{13}$ ,  $v_{17}$  and  $v_4$ . (a) T-mesh, (b) extended T-mesh, and (c) extended T-mesh.

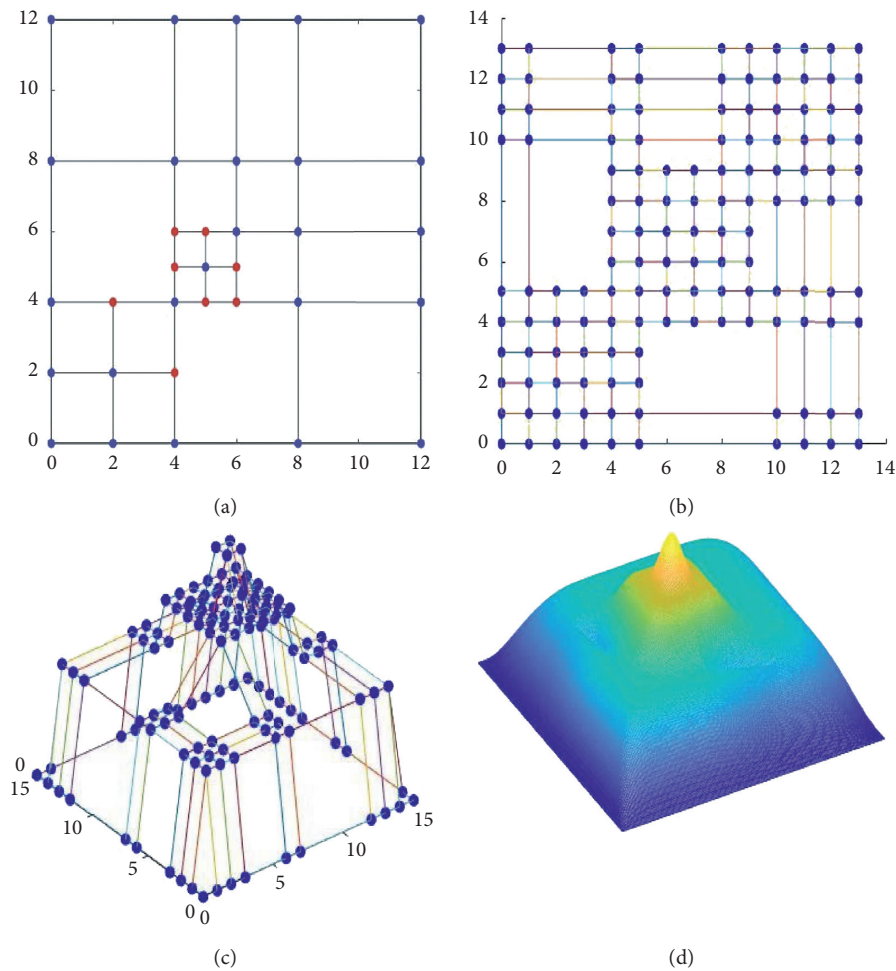


FIGURE 5: The index space and the control mesh. (a) A Design-suitable T-mesh. (b) The index mesh. (c) The control net. (d) The surface generated by the control net shown in (c).

- (1) If  $v_0$  ( $v_1$ ) is a CT-vertex or a ECT-vertex, then extend them until it is either a CT-vertex or ECT-vertex.
  - (2) Among the T-vertices in  $\{F_i\}_{i=1}^l$  and  $F$ , if the extension of a T-vertex in  $\mathcal{T}_e^1$  intersects with  $e$ , then p-extend the T-vertex. The resulting T-mesh is denoted by  $\mathcal{T}^2$ .
  - (3) Construct the extended T-mesh  $\mathcal{T}_e^2$ .
- (i) Update the new T-vertices which are in  $\mathcal{T}^2$  but not in  $\mathcal{T}^1$  by p-extending.
  - (ii) Keep the extensions in  $\mathcal{T}_e^1$  of the original T-vertices.

We use Figure 10 to demonstrate the local refinement algorithm as proposed above. A design-suitable T-mesh  $\mathcal{T}^1$  is shown in Figure 10(a) and the corresponding extended

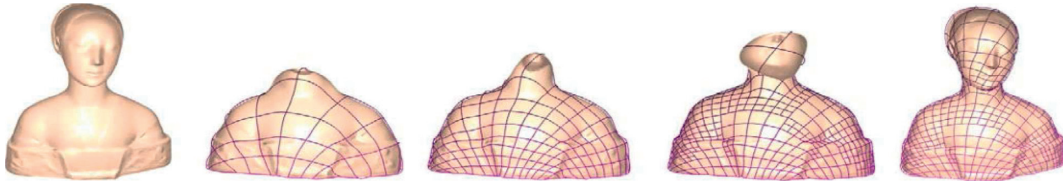


FIGURE 6: A model of the polynomial splines with control nets.

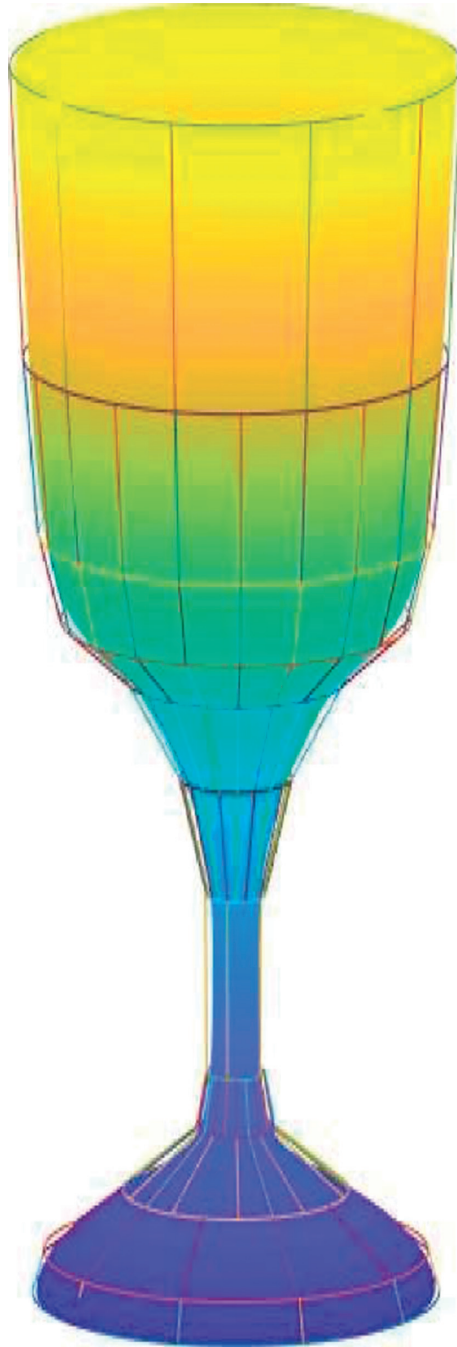


FIGURE 7: A goblet model designed by the polynomial splines with control nets.

T-mesh  $\mathcal{T}_e^1$  is shown in Figure 10(b). A vertical edge  $\overline{v_0 v_1}$  (marked by red line) is inserted in  $\mathcal{T}^1$ , which is shown in Figure 10(c). Now  $v_0$  is a CT-vertex and  $v_1$  is a ECT-vertex;

then they are extended as shown in Figure 10(d). For the horizontal T-vertices in  $F_1$  and  $F$ , their extensions with respect to  $\mathcal{T}_e^1$  intersect with  $e$ , extend them as shown in

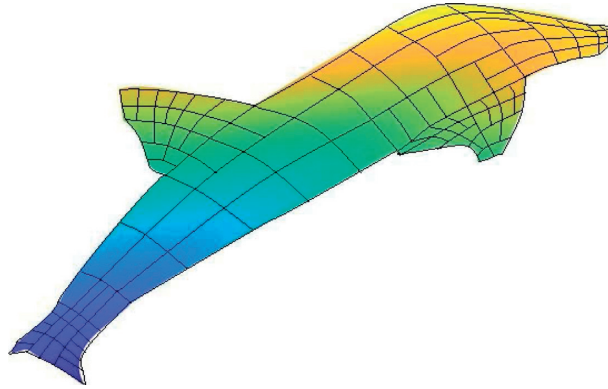


FIGURE 8: A dolphin model designed by the polynomial splines with control nets.

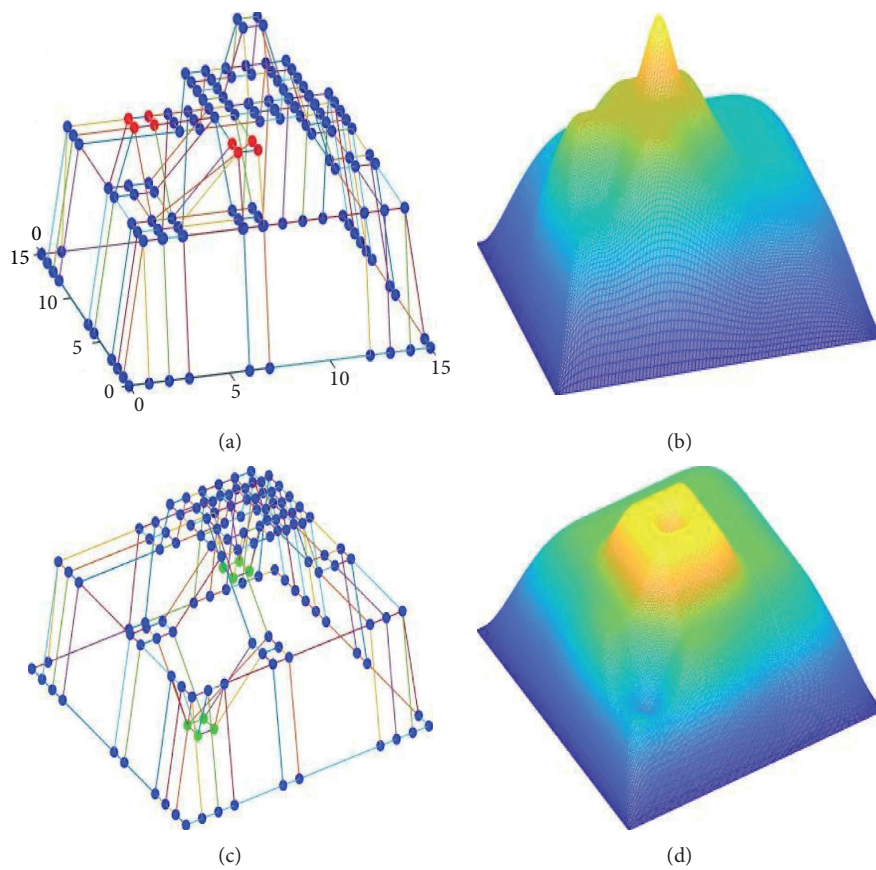


FIGURE 9: The index space and the control mesh. (a) Adjusting the position of the control points corresponding to the T-vertices in the Figure 5(c). (b) The surface figure obtained by adjusting the position of the control point corresponding to the T-vertices. (c) Adjusting the position of the control points corresponding to the basis vertices in the Figure 5(c). (d) The surface figure obtained by adjusting the position of the control point corresponding to the basis vertices.

Figure 10(e). The resulting T-mesh is a design-suitable T-mesh, denoted by  $\mathcal{T}^2$ . Finally, we construct the extended T-mesh corresponding to  $\mathcal{T}^2$ . We only need to update the extension of the new T-vertices. Figure 10(f) shows the extended T-mesh  $\mathcal{T}_e^2$ .

Figure 11 shows the local refinement of a diagonal T-mesh. The inserted edges are marked by red line segments and the additional inserted edges are marked by blue line

segments in Figures 11(c) and 11(e). Figures 10(d) and 10(f) show the extended T-meshes of Figures 11(c) and 11(e), respectively. Obviously, the extended T-mesh of the diagonal T-mesh shown in Figure 11(a) is contained in both the extended T-meshes shown in Figures 10(d) and 10(f). Notice there are at most 1 neighboring elements of the element  $F$  are need to be inserted into edges; thus, the refinement are local.

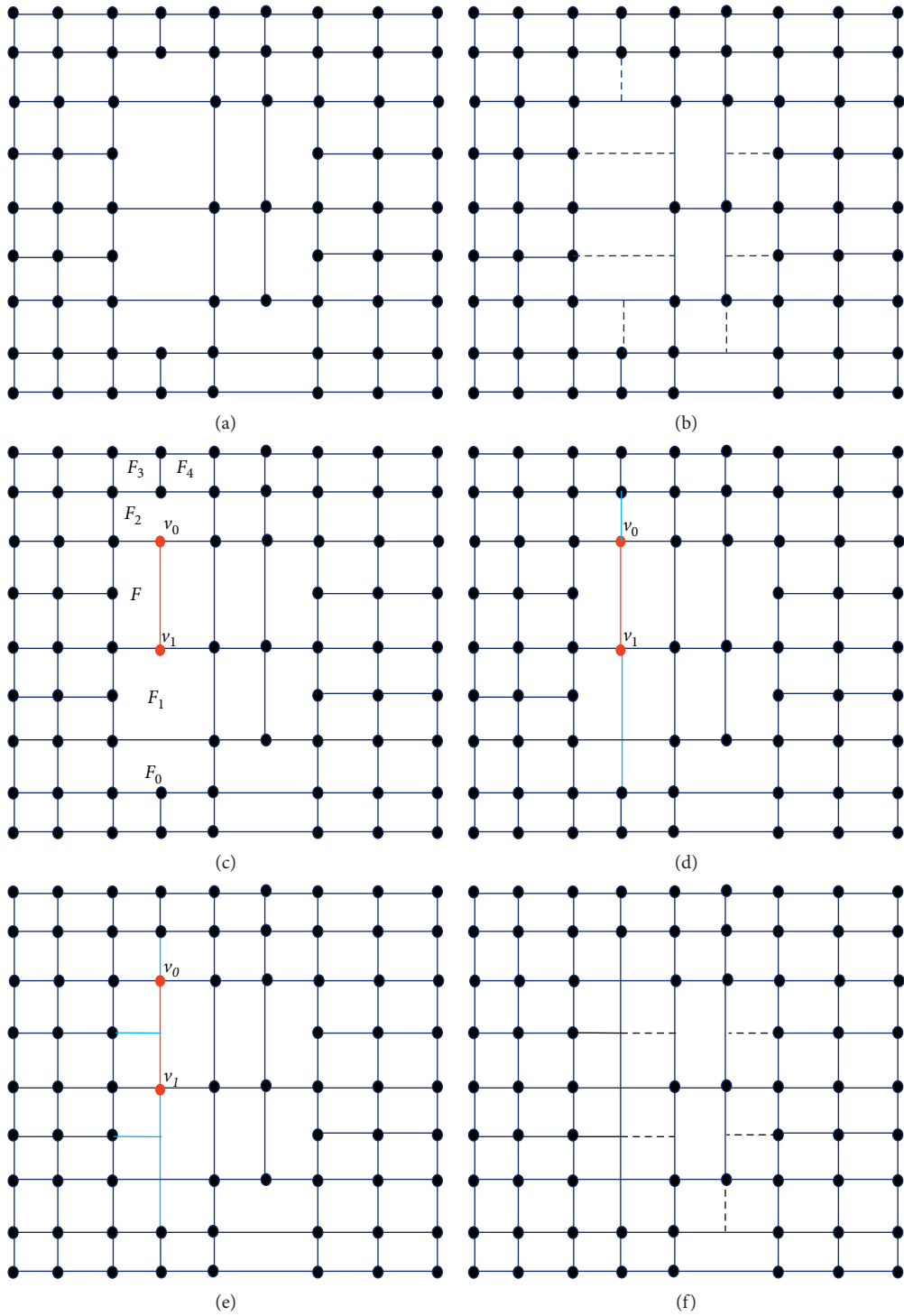


FIGURE 10: Steps of local refinement algorithm. (a) Design-suitable T-mesh  $\mathcal{T}^1$ , (b) extended T-mesh  $\mathcal{T}_e^1$ , (c) insert an edge (red line), (d) first step: extend  $v_0$  and  $v_1$ , (e) design-suitable T-mesh  $\mathcal{T}^2$ , (f) extended T-mesh  $\mathcal{T}_e^2$ .

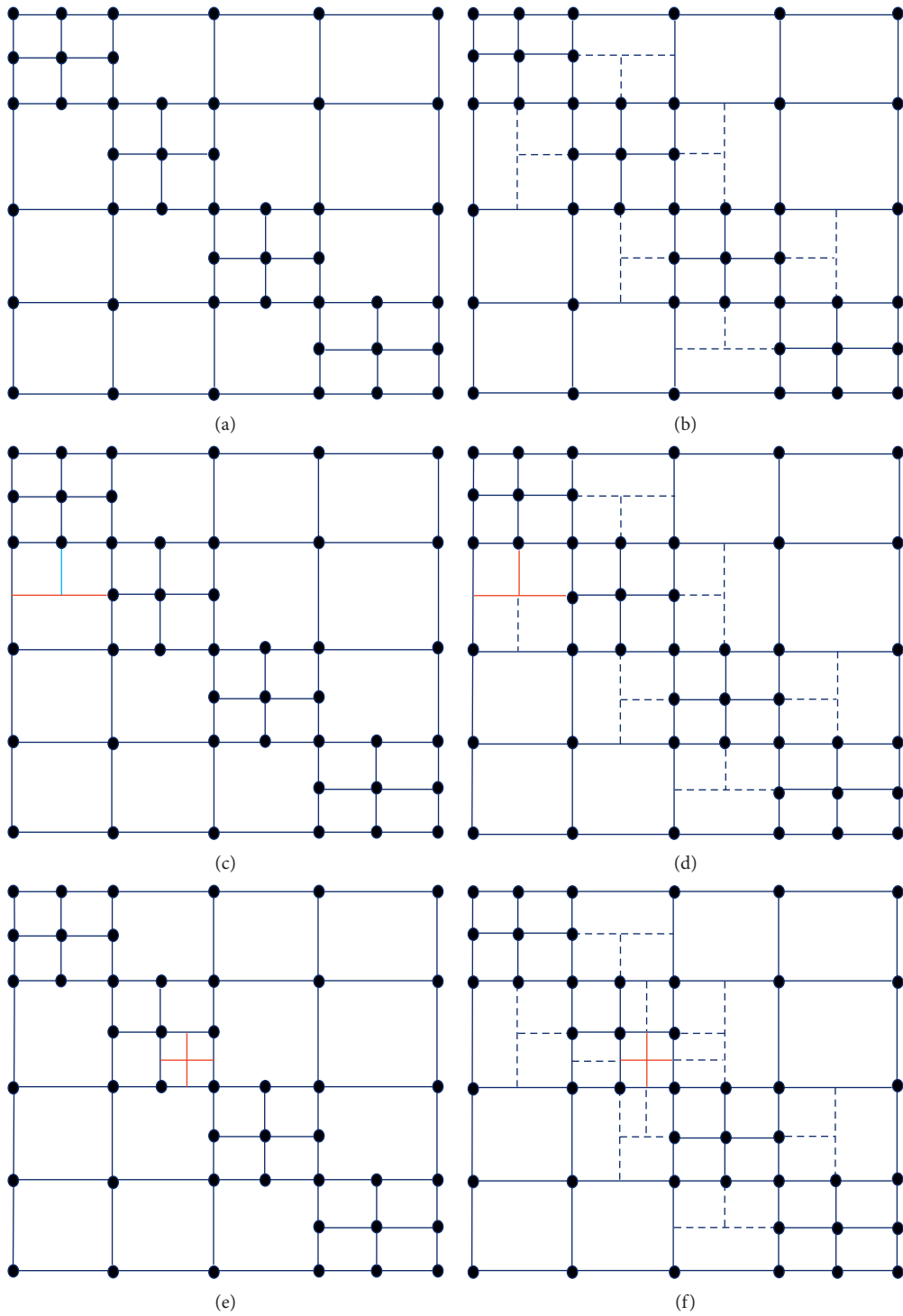


FIGURE 11: Local refinement of a diagonal T-mesh. (a) Design-suitable T-mesh  $\mathcal{T}^1$ . (b) Extended T-mesh  $\mathcal{T}_e^1$ . (c) Insert an edge (red line)  $\mathcal{T}^2$ . (d) Extended T-mesh  $\mathcal{T}_e^2$ . (e) Insert an edge (red line)  $\mathcal{T}^2$ . (f) Extended T-mesh  $\mathcal{T}_e^2$ .

## 5. Conclusions

In this paper, we present an algorithm for extending bicubic  $C^1$  polynomial spline spaces defined over any given T-meshes such that there is a one-to-one correspondence between basis functions and vertices in the T-meshes. The key idea is to extend the T-junctions such that the T-junctions become basis vertices. Thus how to extend these T-junctions to avoid extra basis vertices produced is the main challenge. In this paper, we proposed a subset of T-meshes called design-suitable T-meshes. For design-suitable T-meshes, we first extend T-vertices through an appropriate order and then construct basis functions on the extended T-meshes. There is a one-to-one correspondence between basis functions and vertices in the T-mesh. Furthermore, it is easy to modify a given T-mesh such that it becomes a design-suitable T-mesh.

## Data Availability

The data used to support the findings of this study are available from the corresponding author upon request.

## Conflicts of Interest

The authors declare that they have no conflicts of interest.

## Acknowledgments

The work was supported by the Natural Science Foundation of China (Nos. 11871447 and 11801393), the Natural Science Foundation of Jiangsu Province (No. BK20180831), and the Natural Science Foundation of the Education Department of Anhui Province (Grant nos. KJ2018A0363 and KJ2019A0580).

## References

- [1] T. W. Sederberg, J. Zheng, A. Bakenov, and A. Nasri, "T-splines and T-NURCCs," *ACM Transactions on Graphics*, vol. 22, no. 3, pp. 477–484, 2003.
- [2] T. W. Sederberg, D. L. Cardon, G. T. Finnigan, N. S. North, J. Zheng, and T. Lyche, "T-spline simplification and local refinement," *ACM Transactions on Graphics*, vol. 23, no. 3, pp. 276–283, 2004.
- [3] T. J. R. Hughes, J. A. Cottrell, and Y. Bazilevs, "Isogeometric analysis: CAD, finite elements, NURBS, exact geometry and mesh refinement," *Computer Methods in Applied Mechanics and Engineering*, vol. 194, no. 39–41, pp. 4135–4195, 2005.
- [4] J. A. Cottrell, T. J. R. Hughes, and Y. Bazilevs, *Isogeometric Analysis: Toward Integration of CAD and FEA*, Wiley, Hoboken, NJ, USA, 2009.
- [5] D. R. Forsey and R. H. Bartels, "Hierarchical B-spline refinement," *ACM SIGGRAPH Computer Graphics*, vol. 22, no. 4, pp. 205–212, 1988.
- [6] D. R. Forsey and R. H. Bartels, "Surface fitting with hierarchical splines," *ACM Transactions on Graphics (TOG)*, vol. 14, no. 2, pp. 134–161, 1995.
- [7] A. V. Vuong, C. Giannelli, B. Jüttler, and B. Simeon, "A hierarchical approach to adaptive local refinement in isogeometric analysis," *Computer Methods in Applied Mechanics and Engineering*, vol. 200, pp. 3554–3567, 2011.
- [8] C. Giannelli, B. Jüttler, and H. Speleers, "THB-splines: the truncated basis for hierarchical splines," *Computer Aided Geometric Design*, vol. 29, no. 7, pp. 485–498, 2012.
- [9] X. Wei, Y. Zhang, L. Liu, and T. J. R. Hughes, "Truncated T-splines: fundamentals and methods," *Computer Methods in Applied Mechanics and Engineering*, vol. 316, pp. 349–372, 2017.
- [10] X. Wei, Y. J. Zhang, and T. J. R. Hughes, "Truncated hierarchical tricubic  $C^0$  spline construction on unstructured hexahedral meshes for isogeometric analysis applications," *Computers & Mathematics with Applications*, vol. 74, no. 9, pp. 2203–2220, 2017.
- [11] X. Wei, Y. J. Zhang, D. Toshniwal et al., "Blended B-spline construction on unstructured quadrilateral and hexahedral meshes with optimal convergence rates in isogeometric analysis," *Computer Methods in Applied Mechanics and Engineering*, vol. 341, pp. 609–639, 2018.
- [12] M. A. Scott, X. Li, T. W. Sederberg, and T. J. R. Hughes, "Local refinement of analysis-suitable T-splines," *Computer Methods in Applied Mechanics and Engineering*, vol. 213–216, pp. 206–222, 2012.
- [13] T. Dokken, T. Lyche, and K. F. Pettersen, "Polynomial splines over locally refined box-partitions," *Computer Aided Geometric Design*, vol. 30, no. 3, pp. 331–356, 2013.
- [14] H. Kang, F. Chen, and J. Deng, "Modified T-splines," *Computer Aided Geometric Design*, vol. 30, no. 9, pp. 827–843, 2013.
- [15] J. Deng, F. Chen, X. Li et al., "Polynomial splines over hierarchical T-meshes," *Graphical Models*, vol. 70, no. 4, pp. 76–86, 2008.
- [16] L. Tian, F. Chen, and Q. Du, "Adaptive finite element methods for elliptic equations over hierarchical T-meshes," *Journal of Computational and Applied Mathematics*, vol. 236, no. 5, pp. 878–891, 2011.
- [17] N. Nguyen-Thanh, H. Nguyen-Xuan, S. P. A. Bordas, and T. Rabczuk, "Isogeometric analysis using polynomial splines over hierarchical T-meshes for two-dimensional elastic solids," *Computer Methods in Applied Mechanics and Engineering*, vol. 200, no. 21–22, pp. 1892–1908, 2011.
- [18] N. Nguyen-Thanh, J. Kiendl, H. Nguyen-Xuan et al., "Rotation free isogeometric thin shell analysis using PHT-splines," *Computer Methods in Applied Mechanics and Engineering*, vol. 200, no. 47–48, pp. 3410–3424, 2011.
- [19] P. Wang, J. Xu, J. Deng, and F. Chen, "Adaptive isogeometric analysis using rational PHT-splines," *Computer-Aided Design*, vol. 43, no. 11, pp. 1438–1448, 2011.
- [20] X. Li, J. Deng, and F. Chen, "Surface modeling with polynomial splines over hierarchical T-meshes," *The Visual Computer*, vol. 23, no. 12, pp. 1027–1033, 2007.
- [21] J. Wang, Z. Yang, L. Jin, J. Deng, and F. Chen, "Parallel and adaptive surface reconstruction based on implicit PHT-splines," *Computer Aided Geometric Design*, vol. 28, no. 8, pp. 463–474, 2011.
- [22] Y. Jia, C. Anitescu, Y. J. Zhang, and T. Rabczuk, "An adaptive isogeometric analysis collocation method with a recovery-based error estimator," *Computer Methods in Applied Mechanics and Engineering*, vol. 345, pp. 52–74, 2019.
- [23] Y. Jia, A. Cosmin, J. Z. Yongjie, G. Xu, C. Li, and R. Timon, "PHT-spline-based enhanced isogeometric collocation method," *Journal of Computer-Aided Design & Computer Graphics*, vol. 30, no. 4, pp. 702–706, 2018.
- [24] H. Kang, J. Xu, F. Chen, and J. Deng, "A new basis for PHT-splines," *Graphical Models*, vol. 82, pp. 149–159, 2015.

- [25] X. Li, J. Deng, and F. Chen, "Polynomial splines over general T-meshes," *The Visual Computer*, vol. 26, no. 4, pp. 277–286, 2010.
- [26] T. Nguyen and J. Peters, "Refinable  $C^1$  spline elements for irregular quad layout," *Computer Aided Geometric Design*, vol. 43, no. 8, pp. 123–130, 2016.
- [27] Z. Wang, F. Chen, and J. Deng, "Evaluation algorithm of PHT-spline surfaces," *Numerical Mathematics: Theory, Methods and Applications*, vol. 10, no. 4, pp. 760–774, 2017.



## Research Article

# Finite-Time Adaptive Tracking Control for a Class of Pure-Feedback Nonlinear Systems with Disturbances via Decoupling Technique

Qiangqiang Zhu,<sup>1</sup> Ben Niu ,<sup>1</sup> Shengtao Li ,<sup>1</sup> Peiyong Duan,<sup>1</sup> and Dong Yang<sup>2</sup>

<sup>1</sup>School of Information Science and Engineering, Shandong Normal University, Jinan 250014, China

<sup>2</sup>School of Engineering, Qufu Normal University, Rizhao 276826, China

Correspondence should be addressed to Ben Niu; niubensdu@163.com

Received 8 June 2020; Accepted 14 July 2020; Published 17 August 2020

Academic Editor: Jianquan Lu

Copyright © 2020 Qiangqiang Zhu et al. This is an open access article distributed under the Creative Commons Attribution License, which permits unrestricted use, distribution, and reproduction in any medium, provided the original work is properly cited.

This paper addresses the finite-time adaptive tracking control problem for a class of pure feedback nonlinear systems whose nonaffine functions may not be differentiable. By properly modeling the nonaffine function, the design difficulty of the pure feedback structure is overcome without using the median value theorem. In our design procedure, an finite-time adaptive controller is elaborately developed using the decoupling technology, which eliminates the limitation assumption on the partial derivatives of nonaffine functions. Furthermore, the constructed controller can stabilize the system within a finite-time so that all signals in the closed-loop system are semiglobally uniformly finite-time bounded (SGUFB), while ensuring the tracking performance. Finally, the simulation results prove the effectiveness of the proposed method.

## 1. Introduction

In the past few decades, there have been various research results on the nonfinite time stability of nonlinear systems [1–10], and these results are widely applied to practical systems. However, in actual engineering, the control goal is always expected to be achieved within a finite time. Nonfinite time stable schemes cannot accomplish such control objective because nonfinite time stable control often requires a long transient response. Therefore, the definition of finite-time stability was first proposed in [11, 12] and has received great attention. The finite-time stability can ensure that the system state variables quickly converge to equilibrium within a limited time. At present, the finite-time control of nonlinear systems has become a new research hot spot [13–15]. At the same time, there are many challenging problems which needs hard work to overcome.

On the contrary, the rapid development of computer technology has made great progress in the research of adaptive control [16–23]. It is worth mentioning that when

there exist completely unknown nonlinear functions in a nonlinear system with a strict feedback structure, radial basis function neural networks (RBF NNs) and fuzzy logic systems play an important role in its adaptive control [24–35]. Using the approximation ability of RBF NNs or fuzzy logic systems, there have been many meaningful research results on adaptive intelligent control for strict feedback nonlinear systems [36–39]. Despite great success in the research on adaptive intelligent control for strict feedback nonlinear systems have been achieved, the research on finite-time control for the nonlinear system is not fully considered [40–42].

In recent years, the finite-time adaptive control schemes for strict-feedback nonlinear systems have been developed in [43–47]. However, the finite-time control strategies in [43–47] are only applicable to the strict feedback nonlinear systems, but not applicable to the pure feedback nonlinear systems. It is worth noting that the study on the finite-time tracking control of pure feedback systems has achieved some results [48, 49], but almost all the results are obtained based

on the use of differential median theorem, which can convert the pure feedback structure into the strict feedback structure. This requires us to make restrictive assumptions for the partial derivatives of nonaffine functions. However, it is well known that nonsmooth nonlinearities, such as dead zones and hysteresis, exist in a wide range of practical control systems. Thus, not all system functions are differentiable in actual control, which requires exploring a new design technique to deal with the pure feedback structure.

In order to meet the actual requirements better, we consider the finite-time adaptive control problem for a class of nonlinear systems with the pure-feedback structure as well as external disturbances. A finite-time adaptive control method based on the decoupling technology is proposed to make the system have better transient response. By selecting the design parameters appropriately, the generated tracking error can converge to a smaller neighborhood of the origin so that the system output follows the desired trajectory within a limited time. The main contributions of this article are as follows. First, we consider a more general class of pure-feedback systems with nonaffine nonlinear functions that may not be differentiable. In order to make our method more practical in industrial control systems than the existing methods [50–59], the limitation of using the differential median theorem in the study of pure feedback systems is eliminated. Second, we construct a suitable controller to stabilize the system in a finite time, which not only ensures that the system state variables quickly converge to equilibrium within a limited time but also improves the robustness of the system and reduces the effects of approximation errors. Third, the appropriate scaling technique is applied to reduce the number of adaptive parameters in the process of designing the controller such that the developed result is more suitable for the actual operation process, which also reduces the complexity of the design procedure. In the end, even if the control direction of the system is unknown, our method can still make all signals in the closed-loop system which are SGUFB.

## 2. Mathematical Preliminaries

Consider a class of pure-feedback nonlinear systems given by

$$\begin{cases} \dot{\tau}_i = g_i(\bar{\tau}_i, \tau_{i+1}) + r_i(t), & 1 \leq i \leq n-1, \\ \dot{\tau}_n = g_n(\bar{\tau}_n, u) + r_n(t), \\ y = \tau_1, \end{cases} \quad (1)$$

where  $\bar{\tau}_i = [\tau_1, \tau_2, \dots, \tau_i]^T \in R^i$ ,  $y \in R$ , and  $u \in R$  are the system state, output, and control input, respectively,  $g_i(\bar{\tau}_i, \tau_{i+1}), 1 \leq i \leq n$  are unknown nonaffine nonlinear functions, and  $r_i(t)$  are the unknown external disturbances.

*Definition 1* (see [60]). *The equilibrium  $\zeta = 0$  of nonlinear system  $\dot{\zeta} = g(\zeta)$  is semiglobal practical finite-time stable (SGPFS) if for all  $\zeta(t_0) = \zeta_0$ , there exists  $\varepsilon > 0$  and a settling time  $T(\varepsilon, \zeta_0) < \infty$  to make  $\|\zeta(t)\| < \varepsilon$ , for all  $t \geq t_0 + T$ .*

**Lemma 1** (see [60]). *Consider the system  $\dot{\zeta} = f(\zeta)$ . If there is a smooth positive definite function  $V(\zeta)$  and scalars  $\kappa > 0$ ,  $0 < \eta < 1$ , and  $\rho > 0$  such that*

$$\dot{V}(\zeta) \leq -\kappa V^\eta(\zeta) + \rho, \quad t \geq 0, \quad (2)$$

*then this nonlinear system  $\dot{\zeta} = f(\zeta)$  is SGPFS.*

*Proof.* For  $\forall 0 < \theta \leq 1$ , from (2), one has

$$\dot{V}(\zeta) \leq -\theta \kappa V^\eta(\zeta) - (1-\theta)\kappa V^\eta(\zeta) + \rho. \quad (3)$$

Let  $\Omega_\zeta = \{\zeta \mid V^\eta(\zeta) \leq \rho/(1-\theta)\kappa\}$  and  $\bar{\Omega}_\zeta = \{\zeta \mid V^\eta(\zeta) > \rho/(1-\theta)\kappa\}$ , if  $\zeta(t) \in \bar{\Omega}_\zeta$ , one yields  $\dot{V}(\zeta) \leq -\theta \kappa V^\eta(\zeta)$ . By solving differential equations, we can obtain that

$$T_{\text{reach}} = \frac{1}{(1-\eta)\theta\kappa} \left[ V^{1-\eta}(\zeta(0)) - \left( \frac{\rho}{(1-\theta)\kappa} \right)^{(1-\eta)/\eta} \right]. \quad (4)$$

So,  $\zeta(t) \in \Omega_\zeta$  is held for  $\forall T \geq T_{\text{reach}}$ , otherwise, the trajectory of  $\zeta(t)$  does not exceed the set  $\Omega_\zeta$ . This means that the time to reach the set  $\Omega_\zeta$  is bounded as  $T_{\text{reach}}$ . In other words, the solution of  $\dot{\zeta} = f(\zeta)$  is bounded in a finite time.

**Lemma 2** (see [61]). *For real variables  $z$  and  $\varsigma$  and any positive constants  $\beta, \mu$ , and  $\iota$ , the following relation holds:*

$$|z|^\mu |\varsigma|^\beta \leq \frac{\mu}{\mu+\beta} \iota |z|^{\mu+\beta} + \frac{\beta}{\mu+\beta} \iota^{-\mu/\beta} |\varsigma|^{\mu+\beta}. \quad (5)$$

**Lemma 3** (see [62]). *For  $z_i \in R, i = 1, \dots, n, 0 \leq p \leq 1$ , the following inequality is true:*

$$\left( \sum_{i=1}^n |z_i| \right)^p \leq \sum_{i=1}^n |z_i|^p \leq n^{1-p} \left( \sum_{i=1}^n |z_i| \right)^p. \quad (6)$$

*Remark 1.* It is worth noting that system function  $g_i(\bar{\tau}_i, \tau_{i+1})$  is always assumed to satisfy  $0 \leq p_i \leq \partial g_i(\bar{\tau}_i, \tau_{i+1}) / \partial \tau_{i+1} \leq \bar{p}_i$ , ( $p_i, \bar{p}_i \in R$ ) in existing articles [52, 54, 55]. However, it is well known that not all system functions are differentiable in actual control, which requires exploring a new design technique to deal with the pure feedback structures. Next, we will introduce a decoupling technique to deal with the unknown nonaffine nonlinear functions of the pure feedback system (1) rather than the median theorem.

**Lemma 4** (see [63]). *In order to effectively design the control input of the system, the decoupling technology is utilized to deal with the nonaffine terms. After a series of processing, the following formula can be obtained:*

$$g_i(\bar{\tau}_i, \tau_{i+1}) = g_i(\bar{\tau}_i, 0) + P_i(\bar{\tau}_{i+1})\tau_{i+1} + \Gamma_i(\bar{\tau}_{i+1}), \quad (7)$$

where  $P_i(\bar{\tau}_{i+1})$  and  $\Gamma_i(\bar{\tau}_{i+1})$  are defined immediately below.

*Proof.* Define  $G_i(\bar{\tau}_i, \tau_{i+1}) = g_i(\bar{\tau}_i, \tau_{i+1}) - g_i(\bar{\tau}_i, 0)$ ,  $i = 1, 2, \dots, n$ , where  $\tau_{n+1} = u$  and  $\bar{\tau}_{n+1} = [\bar{\tau}_n^T, u]^T$ . We assume that the function  $G_i(\bar{\tau}_i, \tau_{i+1})$  satisfies

$$\begin{cases} \underline{G}_i \tau_{i+1} + \Delta_{1i} \leq G_i(\bar{\tau}_i, \tau_{i+1}) \leq \bar{G}_i \tau_{i+1} + \Delta_{2i}, & \tau_{i+1} \geq 0, \\ \underline{G}'_i \tau_{i+1} + \Delta_{3i} \leq G_i(\bar{\tau}_i, \tau_{i+1}) \leq \bar{G}'_i \tau_{i+1} + \Delta_{4i}, & \tau_{i+1} \leq 0, \end{cases} \quad (8)$$

where  $\underline{G}_i, \bar{G}_i, \underline{G}'_i$ , and  $\bar{G}'_i$  are unknown positive constants and  $\Delta_{1i}, \Delta_{2i}, \Delta_{3i}$ , and  $\Delta_{4i}$ ,  $i = 1, \dots, n$ , are unknown constants.

It can be shown that there exist functions  $\vartheta_{i1}(\bar{\tau}_{i+1})$  and  $\vartheta_{i2}(\bar{\tau}_{i+1})$ , taking values in the closed interval  $[0, 1]$  and satisfying

$$\begin{cases} G_i(\bar{\tau}_i, \tau_{i+1}) = (1 - \vartheta_{i1}(\bar{\tau}_{i+1}))(\underline{G}_i \tau_{i+1} + \Delta_{1i}) + \vartheta_{i1}(\bar{\tau}_{i+1})(\bar{G}_i \tau_{i+1} + \Delta_{2i}), & \tau_{i+1} \geq 0, \\ G_i(\bar{\tau}_i, \tau_{i+1}) = (1 - \vartheta_{i2}(\bar{\tau}_{i+1}))(\underline{G}'_i \tau_{i+1} + \Delta_{3i}) + \vartheta_{i2}(\bar{\tau}_{i+1})(\bar{G}'_i \tau_{i+1} + \Delta_{4i}), & \tau_{i+1} \leq 0. \end{cases} \quad (9)$$

To facilitate the controller design, we have defined the following simplified symbols  $P_i(\bar{\tau}_{i+1})$  and  $\Gamma_i(\bar{\tau}_{i+1})$  as

$$P_i(\bar{\tau}_{i+1}) = \begin{cases} (1 - \vartheta_{i1}(\bar{\tau}_{i+1}))\underline{G}_i + \vartheta_{i1}(\bar{\tau}_{i+1})\bar{G}_i, & \tau_{i+1} \geq 0, \\ \vartheta_{i2}(\bar{\tau}_{i+1})\bar{G}'_i + (1 - \vartheta_{i2}(\bar{\tau}_{i+1}))\underline{G}'_i, & \tau_{i+1} \leq 0, \end{cases} \quad (10)$$

$$\Gamma_i(\bar{\tau}_{i+1}) = \begin{cases} (1 - \vartheta_{i1}(\bar{\tau}_{i+1}))\Delta_{1i} + \vartheta_{i1}(\bar{\tau}_{i+1})\Delta_{2i}, & \tau_{i+1} \geq 0, \\ \vartheta_{i2}(\bar{\tau}_{i+1})\Delta_{4i} + (1 - \vartheta_{i2}(\bar{\tau}_{i+1}))\Delta_{3i}, & \tau_{i+1} \leq 0. \end{cases} \quad (11)$$

We can infer from the above definition that  $P_i(\bar{\tau}_{i+1})$  and  $\Gamma_i(\bar{\tau}_{i+1})$  are bounded. Then, we can model the nonaffine terms  $G_i(\bar{\tau}_i, \tau_i + 1)$  as

$$G_i(\bar{\tau}_i, \tau_i + 1) = P_i(\bar{\tau}_{i+1})\tau_{i+1} + \Gamma_i(\bar{\tau}_{i+1}). \quad (12)$$

Hence, (7) was established, and we can rewrite (1) as

$$\begin{cases} \dot{\tau}_i = g_i(\bar{\tau}_i, 0) + P_i(\bar{\tau}_{i+1})\tau_{i+1} + \Gamma_i(\bar{\tau}_{i+1}) + r_i(t), & 1 \leq i \leq n-1, \\ \dot{\tau}_n = g_n(\bar{\tau}_n, 0) + P_n(\bar{\tau}_{n+1})u + \Gamma_n(\bar{\tau}_{n+1}) + r_n(t), \\ y = \tau_1. \end{cases} \quad (13)$$

In backstepping design, the variable  $\tau_{i+1}$  is usually taken as the virtual control input for the  $i$ th subsystem. So, the virtual control coefficient function  $P_i(\bar{\tau}_{i+1})$  should not pass through the zero point. Therefore, the following assumption is pressed on the system (13).

*Assumption 1.* The desired trajectory  $y_d$  and its derivatives  $\dot{y}_d$  and  $\ddot{y}_d$  are continuous and bounded.

*Assumption 2.* Due to realistic considerations, for  $i = 1, \dots, n$ , there exist unknown positive constants  $r_i^*$  such that  $|r_i(t)| \leq r_i^*$ .

*Remark 2.* Define  $P_m = \min_{i=1,2,\dots,p} \{\underline{G}_i, \bar{G}_i, \underline{G}'_i, \bar{G}'_i\}$ ,  $P_M = \max_{i=1,2,\dots,p} \{\underline{G}_i, \bar{G}_i, \underline{G}'_i, \bar{G}'_i\}$ , and  $A_i^* = \max_{i=1,2,\dots,p} \{|\Delta_{1i}| +$

$|\Delta_{2i}|, |\Delta_{3i}| + |\Delta_{4i}|\}$ . It can be inferred from definitions (10) and (11) that the functions  $P_i(\bar{\tau}_{i+1})$  and  $\Gamma_i(\bar{\tau}_{i+1})$  satisfy

$$0 \leq P_m \leq P_i(\bar{\tau}_{i+1}) \leq P_M, \quad (14)$$

$$0 \leq |\Gamma_i(\bar{\tau}_{i+1})| \leq A_i^*. \quad (15)$$

RBFNNs: in the design of this article, the following radial basis function neural networks (RBF NNs) is used to approximate the continuous function  $h(Z): R^n \rightarrow R$ :

$$h_m(Z) = W^T \xi(Z), \quad (16)$$

where  $W = [W_1, W_2, \dots, W_l] \in R^l$  is the weight vector and the neural network node number  $l > 1$ .  $\xi(Z) = [\xi_1(Z), \dots, \xi_l(Z)]^T$  is the basic vector being chosen as the commonly used Gaussian functions, which has the form:

$$\xi_i(Z) = \exp\left[\frac{-(Z - \mu_i)^T (Z - \mu_i)}{\kappa^2}\right], \quad (17)$$

where  $Z \in \Omega_Z \subset R^n$  is the input vector,  $\mu_i = [\mu_{i1}, \dots, \mu_{in}]^T$  is the center of the respective field, and  $\kappa$  is the width of the Gaussian function.

As shown in [64], the neural network can approximate any continuous function on the compact set  $\Omega_Z \subset R^q$  to any desired accuracy  $\varepsilon^*$  as follows:

$$h_m(Z) = W^{*T} \xi(Z) + \varepsilon(Z), \quad Z \in \Omega_Z \subset R^q, \quad (18)$$

where  $W^*$  is the ideal constant weight vector and  $\varepsilon(Z)$  is the approximation error satisfying  $|\varepsilon(Z)| \leq \varepsilon^*$ ,  $\varepsilon^* > 0$  is a very small constant.

### 3. Adaptive State-Feedback Controller Design

In this section, the finite-time adaptive controller is proposed for the backstepping control of system (13). To start, consider the following change of coordinates:

$$\Xi_i = \tau_i - \alpha_{i-1}, \quad i = 1, 2, 3, \dots, n, \quad (19)$$

where  $\alpha_{i-1}$  is the virtual control signal constructed in step  $i-1$  and  $\alpha_0 = y_d$ .

Step 1: differentiating  $\Xi_1$  through the first system of (13), we have

$$\dot{\Xi}_1 = \dot{\tau}_1 - \dot{y}_d = g_1(\bar{\tau}_1, 0) + P_1(\bar{\tau}_2)\tau_2 + \Gamma_1(\bar{\tau}_2) + r_1(t) - \dot{y}_d. \quad (20)$$

Choose Lyapunov function candidate to construct the virtual control signal of this system as

$$V_1 = \frac{1}{2}\Xi_1^2 + \frac{P_m}{2\gamma_1}\tilde{\psi}_1^2. \quad (21)$$

By substituting (20), we can get the time derivative of  $V_1$  as

$$\begin{aligned} \dot{V}_1 = & \Xi_1 [g_1(\bar{\tau}_1, 0) + P_1(\bar{\tau}_2)(\Xi_2 + \alpha_1) + \Gamma_1(\bar{\tau}_2) \\ & + r_1(t) - \dot{y}_d] - \frac{P_m}{\gamma_1}\tilde{\psi}_1 \dot{\psi}_1, \end{aligned} \quad (22)$$

where  $\Xi_2 = \tau_2 - \alpha_1$ . Now, we define a new function as  $g'_1 = g_1(\bar{\tau}_1, 0) + (1/2)P_M\Xi_1 - \dot{y}_d + k_1\Xi_1^{2\eta-1} + (3/2)\Xi_1$  with  $\eta = (2n-1)/(2n+1)$ , where  $n$  is a natural number and  $k_1 > 0$  is a constant. Then, (22) can be rewritten as

$$\begin{aligned} \dot{V}_1 = & \Xi_1 \left[ g'_1 - k_1\Xi_1^{2\eta-1} - \frac{1}{2}P_M\Xi_1 - \frac{3}{2}\Xi_1 + P_1(\bar{\tau}_2)(\Xi_2 + \alpha_1) \right. \\ & \left. + \Gamma_1(\bar{\tau}_2) + r_1(t) \right] - \frac{P_m}{\gamma_1}\tilde{\psi}_1 \dot{\psi}_1 \\ = & \Xi_1 [g'_1 + P_1(\bar{\tau}_2)(\Xi_2 + \alpha_1)] + \Xi_1 (\Gamma_1(\bar{\tau}_2) \\ & + r_1(t)) - \frac{1}{2}P_M\Xi_1^2 - k_1\Xi_1^{2\eta} \\ & - \frac{3}{2}\Xi_1^2 - \frac{P_m}{\gamma_1}\tilde{\psi}_1 \dot{\psi}_1. \end{aligned} \quad (23)$$

Next, based on (15) and Assumption 2, we can obtain

$$\begin{aligned} \dot{V}_1 \leq & -\frac{P_M}{2}\Xi_1^2 - k_1\Xi_1^{2\eta} + \Xi_1(g'_1 + P_1(\bar{\tau}_2)(\Xi_2 + \alpha_1)) \\ & + |\Xi_1|(A_1^* + r_1^*) - \frac{3}{2}\Xi_1^2 - \frac{P_m}{\gamma_1}\tilde{\psi}_1 \dot{\psi}_1. \end{aligned} \quad (24)$$

Because the unknown function  $g'_1$  cannot be used for the controller design, we can infer from (18) that

$$g'_1 = W_1^{*T}\xi_1(\tau'_1) + \varepsilon_1(\tau'_1), \quad |\varepsilon_1(\tau'_1)| \leq \varepsilon_1^*, \quad (25)$$

where  $\tau'_1 = [\tau_1, y_d, \dot{y}_d]^T$ . For simplicity, we use  $\xi_1$  and  $\varepsilon_1$  instead of  $\xi_1(\tau'_1)$  and  $\varepsilon_1(\tau'_1)$ , respectively. Define  $\psi_1 = \|W_1^*\|^2/P_m$ , and  $\tilde{\psi}_1 = \psi_1 - \hat{\psi}_1$  is the parameter estimation error; then, using Yang's inequality and Remark 2, one yields

$$\Xi_1 P_1(\bar{\tau}_2)\Xi_2 \leq \frac{P_M}{2}\Xi_1^2 + \frac{P_M}{2}\Xi_2^2, \quad (26)$$

$$|\Xi_1|(A_1^* + r_1^*) \leq \Xi_1^2 + \frac{1}{2}A_1^{*2} + \frac{1}{2}r_1^{*2}, \quad (27)$$

$$\begin{aligned} \Xi_1 g'_1 = & \Xi_1 W_1^{*T}\xi_1 + \Xi_1 \varepsilon_1 \leq \frac{P_m}{2a_1^2}\Xi_1^2 \psi_1 \xi_1^T \xi_1 \\ & + \frac{1}{2}a_1^2 + \frac{1}{2}\Xi_1^2 + \frac{1}{2}\varepsilon_1^{*2}, \end{aligned} \quad (28)$$

where  $a_1 > 0$  is the design positive constant. Substituting (26) and (28) into (24) produces

$$\begin{aligned} \dot{V}_1 \leq & -\frac{c_1}{(1+P_m)}\Xi_1^{2\eta} + \Xi_1 \left( \frac{P_m}{2a_1^2}\Xi_1 \psi_1 \xi_1^T \xi_1 + P_1(\bar{\tau}_2)\alpha_1 \right) \\ & + \frac{1}{2}\delta_1^{*2} - \frac{P_m}{\gamma_1}\tilde{\psi}_1 \dot{\psi}_1 + \frac{P_M}{2}\Xi_2^2, \end{aligned} \quad (29)$$

where  $c_1 = k_1(1+P_m)$  and  $\delta_1^{*2} = a_1^2 + \varepsilon_1^{*2} + A_1^{*2} + r_1^{*2}$ . Next, we construct a virtual signal as

$$\alpha_1 = -k_1\Xi_1^{2\eta-1} - \frac{\hat{\psi}_1}{2a_1^2}\Xi_1 \xi_1^T \xi_1. \quad (30)$$

Substituting (30) into (29) yields

$$\dot{V}_1 \leq -c_1\Xi_1^{2\eta} + \frac{P_m}{\gamma_1}\tilde{\psi}_1 \left( \frac{\gamma_1}{2a_1^2}\Xi_1 \xi_1^T \xi_1 - \dot{\psi}_1 \right) + \frac{1}{2}\delta_1^{*2} + \frac{P_M}{2}\Xi_2^2. \quad (31)$$

Next, we construct the adaptive rate  $\dot{\hat{\psi}}_1$  as

$$\dot{\hat{\psi}}_1 = \frac{\gamma_1}{2a_1^2} \Xi_1^2 \xi_1^T \xi_1 - Y_1 \hat{\psi}_1, \quad \hat{\psi}_1(0) \geq 0, \quad (32)$$

where  $\gamma_1 > 0$  and  $Y_1 > 0$  are two design constants. As a result, one can obtain the following formula:

$$\dot{V}_1 \leq -c_1 \Xi_1^{2\eta} + \frac{P_m Y_1}{\gamma_1} \tilde{\psi}_1 \hat{\psi}_1 + \frac{1}{2} \delta_1^{*2} + \frac{P_M}{2} \Xi_2^2. \quad (33)$$

Step  $i$  ( $i = 2, \dots, n-1$ ): from (19), we can know that  $\Xi_i = \tau_i - \alpha_{i-1}$ . Next, we use  $P_i$  and  $\Gamma_i$  instead of  $P_i(\bar{\tau}_{i+1})$  and  $\Gamma_i(\bar{\tau}_{i+1})$  for simplicity. Then, the dynamic equation of  $\Xi_i$  is constructed as follows:

$$\dot{\Xi}_i = g_i(\bar{\tau}_i, 0) + P_i \tau_{i+1} + \Gamma_i + r_i(t) - \dot{\alpha}_{i-1}, \quad (34)$$

where

$$\begin{aligned} \dot{\alpha}_{i-1} = & \sum_{k=1}^{i-1} \frac{\partial \alpha_{i-1}}{\partial \tau_k} [g_k(\bar{\tau}_k, 0) + P_k \tau_{k+1} + \Gamma_k] + \sum_{k=1}^{i-1} \frac{\partial \alpha_{i-1}}{\partial \hat{\psi}_k} \dot{\hat{\psi}}_k \\ & + \sum_{k=0}^{i-1} \frac{\partial \alpha_{i-1}}{\partial y_d^{(k)}} y_d^{(k+1)}. \end{aligned} \quad (35)$$

Choose a Lyapunov function candidate as

$$V_i = V_{i-1} + \frac{1}{2} \Xi_i^2 + \frac{P_m}{2\gamma_i} \tilde{\psi}_i^2. \quad (36)$$

Differentiating  $V_i$  results in

$$\dot{V}_i = \dot{V}_{i-1} + \Xi_i [g_i(\bar{\tau}_i, 0) + P_i \tau_{i+1} + \Gamma_i + r_i(t) - \dot{\alpha}_{i-1}] - \frac{P_m}{\gamma_i} \tilde{\psi}_i \dot{\hat{\psi}}_i, \quad (37)$$

where  $\psi_i = \|W_i^{*2}\|/P_m$ ,  $\tilde{\psi}_i = \psi_i - \hat{\psi}_i$ , represents the parameter estimation error. Similar to the processing in the first step, we need to define a new function as  $g'_i = g_i(\bar{\tau}_i, 0) + P_M \Xi_i - \dot{\alpha}_{i-1} + k_i \Xi_i^{2\eta-1} + (3/2) \Xi_i$ , with  $k_i > 0$  is a design constant. Then, (37) can be rewritten as

$$\begin{aligned} \dot{V}_i = & \dot{V}_{i-1} + \Xi_i [g'_i + P_i (\Xi_{i+1} + \alpha_i)] + \Xi_i [\Gamma_i + r_i(t)] \\ & - P_M \Xi_i^2 - k_i \Xi_i^{2\eta} - \frac{3}{2} \Xi_i^2 - \frac{P_m}{\gamma_i} \tilde{\psi}_i \dot{\hat{\psi}}_i. \end{aligned} \quad (38)$$

Now, based on Assumptions 2 and Remark 2, one can obtain

$$\begin{aligned} \dot{V}_i \leq & \dot{V}_{i-1} + \Xi_i [g'_i + P_i (\Xi_{i+1} + \alpha_i)] + |\Xi_i| [A_i^* + r_i^*] \\ & - P_M \Xi_i^2 - k_i \Xi_i^{2\eta} - \frac{3}{2} \Xi_i^2 - \frac{P_m}{\gamma_i} \tilde{\psi}_i \dot{\hat{\psi}}_i. \end{aligned} \quad (39)$$

According to (18), we can choose the following neural network system:

$$g'_i = W_i^* \wedge \{\wedge^* T\} \xi_i(\tau'_i) + \varepsilon_i(\tau'_i), \quad |\varepsilon_i(\tau'_i)| \leq \varepsilon_i^*, \quad (40)$$

where  $\tau \leq \tau'_i = [\bar{\tau}_i^T, \hat{\psi}_{i-1}^T, \bar{y}_d^{(i)T}]^T \in \Omega_{\tau_i} \subset R^{3i}$  and  $\hat{\psi}_{i-1} = [\hat{\psi}_1, \hat{\psi}_2, \dots, \hat{\psi}_{i-1}]^T$ . For simplicity, we use  $\xi_i$  and  $\varepsilon_i$  to represent  $\xi_i(\tau'_i)$  and  $\varepsilon_i(\tau'_i)$ , respectively. Thus, we can obtain

$$\Xi_i P_i \Xi_{i+1} \leq \frac{P_M}{2} \Xi_i^2 + \frac{P_M}{2} \Xi_{i+1}^2, \quad (41)$$

$$|\Xi_i| (A_i^* + r_i^*) \leq \Xi_i^2 + \frac{1}{2} A_i^{*2} + \frac{1}{2} r_i^{*2}, \quad (42)$$

$$\Xi_i g'_i = \Xi_i W_i^{*T} \xi_i + \Xi_i \varepsilon_i \leq \frac{P_m}{2a_i^2} \psi_i \xi_i^T \xi_i + \frac{1}{2} a_i^2 + \frac{1}{2} \Xi_i^2 + \frac{1}{2} \varepsilon_i^{*2}, \quad (43)$$

where  $a_i > 0$  is the design positive constant. Like the first step, substituting (41)–(43) into (39), the following inequality holds:

$$\begin{aligned} \dot{V}_i \leq & -\frac{c_i}{(1+P_m)} \Xi_i^{2\eta} + \Xi_i \left[ \frac{P_m}{2a_i^2} \psi_i \xi_i^T \xi_i + P_i \alpha_i \right] + \frac{1}{2} \delta_i^{*2} \\ & - \frac{P_m}{\gamma_i} \tilde{\psi}_i \dot{\hat{\psi}}_i + \frac{P_M}{2} \Xi_{i+1}^2 - \frac{P_M}{2} \Xi_i^2 + \dot{V}_{i-1}, \end{aligned} \quad (44)$$

where  $c_i = k_i(1+P_m)$  and  $\delta_i^{*2} = a_i^2 + \varepsilon_i^{*2} + A_i^{*2} + r_i^{*2}$ . Next, we construct the virtual signal  $\alpha_i$  as well as the adaptive rate  $\psi_i$  as follows:

$$\alpha_i = -k_i \Xi_i^{2\eta-1} - \frac{\hat{\psi}_i}{2a_i^2} \Xi_i \xi_i^T \xi_i, \quad (45)$$

$$\dot{\hat{\psi}}_i = \frac{\gamma_i}{2a_i^2} \Xi_i^2 \xi_i^T \xi_i - Y_i \hat{\psi}_i, \quad \hat{\psi}_i(0) \geq 0, \quad (46)$$

where  $\gamma_i > 0$  and  $Y_i > 0$  are two design constants. As a result, substituting (45) and (46) into (44), one can get the following formula:

$$\dot{V}_i \leq \dot{V}_{i-1} - \frac{P_M \Xi_i^2}{2} - c_i \Xi_i^{2\eta} + \frac{P_m \Upsilon_i \hat{\tilde{\psi}}_i \hat{\psi}_i}{\gamma_i} + \frac{1}{2} \delta_i^{*2} + \frac{P_M \Xi_{i+1}^2}{2}. \quad (47)$$

Comparing (33) and (47), we can get the following formula by mathematical induction:

$$\dot{V}_i \leq - \sum_{k=1}^i c_k \Xi_k^{2\eta} + \sum_{k=1}^i \frac{P_m \Upsilon_k \hat{\tilde{\psi}}_k \hat{\psi}_k}{\gamma_k} + \sum_{k=1}^i \frac{1}{2} \delta_k^{*2} + \frac{P_M \Xi_{i+1}^2}{2}. \quad (48)$$

*Remark 3.* As can be seen from formulas (28) and (43), we used Yang's inequality to obtain  $\psi_i = \|W_i^{*2}\|/P_m$  in advance such that only one adaptive parameter should be estimated in each step of the controller design. However, multidimensional vectors (weight vectors) are directly estimated in some literatures such as  $W_i = \Gamma_i((1 - m(Z_i))z_i S_i(Z_i) - \sigma_i W_i)$  in [65], which makes the design of the adaptive rate more difficult. Therefore, the method we adopt can reduce the number of adaptive parameters compared to the previous method in [65].

Step  $n$ : define  $\psi_n = \|W_n^*\|^2/P_m \gamma_n$  where  $W_n^*$  is the ideal weight vector, and  $\tilde{\psi}_n = \psi_n - \hat{\psi}_n$  is the parameter estimation error. Choose the Lyapunov function candidate for system (13) as follows:

$$V_n = V_{n-1} + \frac{1}{2} \Xi_n^2 + \frac{P_m \tilde{\psi}_n^2}{2\gamma_n}, \quad (49)$$

where  $\gamma_n > 0$  is a design positive constant. It can be seen from the previous  $n-1$  step that the virtual control signal  $\alpha_{n-1}$  can be constructed such that the following inequality can be obtained:

$$\dot{V}_{n-1} \leq - \sum_{k=1}^{n-1} c_k \Xi_k^{2\eta} + \sum_{k=1}^{n-1} \frac{P_m \Upsilon_k \hat{\tilde{\psi}}_k \hat{\psi}_k}{\gamma_k} + \sum_{k=1}^{n-1} \frac{1}{2} \delta_k^{*2} + \frac{P_M \Xi_n^2}{2}. \quad (50)$$

As we all know, the dynamic equation of  $\Xi_n$  is as follows:

$$\dot{\Xi}_n = g_n(\bar{\tau}_n, 0) + P_n u + \Gamma_n + r_n(t) - \dot{\alpha}_{n-1}, \quad (51)$$

with

$$\begin{aligned} \dot{\alpha}_{n-1} = & \sum_{k=1}^{n-1} \frac{\partial \alpha_{n-1}}{\partial \tau_k} [g_k(\bar{\tau}_k, 0) + P_k \tau_{k+1} + \Gamma_k] + \sum_{k=1}^{n-1} \frac{\partial \alpha_{n-1}}{\partial \hat{\psi}_k} \dot{\hat{\psi}}_k \\ & + \sum_{k=0}^{n-1} \frac{\partial \alpha_{n-1}}{\partial y_d^{(k)}} y_d^{(k+1)}. \end{aligned} \quad (52)$$

From (49), one can get the time derivative of  $V_n$  along (51) as

$$\begin{aligned} \dot{V}_n = & \dot{V}_{n-1} + \Xi_n [g_n(\bar{\tau}_n, 0) + P_n u + \Gamma_n \\ & + r_n(t) - \dot{\alpha}_{n-1}] - \frac{P_m \tilde{\psi}_n \dot{\hat{\psi}}_n}{\gamma_n}. \end{aligned} \quad (53)$$

Similar to the processing in the above steps, we define a new function as  $g'_n = g_n + (1/2)P_M \Xi_n - \dot{\alpha}_{n-1} + k_n \Xi_n^{2\eta-1} + (3/2)\Xi_n$ , where  $k_n > 0$  is a design constant. Then, (53) can be rewritten as

$$\begin{aligned} \dot{V}_n = & \dot{V}_{n-1} + \Xi_n [g'_n + P_n u] + \Xi_n [\Gamma_n + r_n(t)] \\ & - \frac{1}{2} P_M \Xi_n^2 - k_n \Xi_n^{2\eta} - \frac{3}{2} \Xi_n^2 - \frac{P_m \tilde{\psi}_n \dot{\hat{\psi}}_n}{\gamma_n}. \end{aligned} \quad (54)$$

We designed the actual controller and the adaptation law as follows:

$$u = -k_n \Xi_n^{2\eta-1} - \frac{\hat{\psi}_n \Xi_n \xi_n^T \xi_n}{2a_n^2}, \quad (55)$$

$$\dot{\hat{\psi}}_n = \frac{\Upsilon_n \Xi_n^2 \xi_n^T \xi_n}{2a_n^2} - \Upsilon_n \hat{\psi}_n, \quad \hat{\psi}_n(0) \geq 0, \quad (56)$$

where  $\gamma_n > 0$  and  $\Upsilon_n > 0$  are two design constants. Like (38)–(48), it is easy to obtain

$$\dot{V}_n \leq - \sum_{j=1}^n c_j \Xi_j^{2\eta} + \sum_{j=1}^n \frac{P_m \Upsilon_j \hat{\tilde{\psi}}_j \hat{\psi}_j}{\gamma_j} + \sum_{j=1}^n \frac{\delta_j^{*2}}{2}, \quad (57)$$

where  $c_j = k_j(1 + P_m)$  and  $\delta_j^{*2} = a_j^2 + \varepsilon_j^{*2} + A_j^{*2} + r_j^{*2}$ .

## 4. Stability Analysis

In this section, the main result will be summarized in Theorem 1.

**Theorem 1.** Consider system (1) satisfying Assumptions 1–2, and suppose that the finite-time adaptive controller (55) and the adaptive law (46) as well as (56) are constructed based on the decoupling technology. As long as the design parameters  $\eta, k, a, \gamma$ , and  $\Upsilon$  are properly selected, it can be ensured that the system output  $y$  follows the desired trajectory  $y_d$ , and at the same time all the signals of the pure-feedback nonlinear systems (1) are SGUFB.

*Proof.* For the Lyapunov function candidate  $V = V_n$ , define  $c = \min\{c_j, \Upsilon_j, j = 1, 2, \dots, n\}$ . Then, it follows from (57) that

$$\dot{V} \leq -c \sum_{j=1}^n \Xi_j^{2\eta} + \sum_{j=1}^n \frac{P_m \Upsilon_j \hat{\tilde{\psi}}_j \hat{\psi}_j}{\gamma_j} + \sum_{k=1}^n \frac{\delta_j^{*2}}{2}. \quad (58)$$

From the definition of  $\tilde{\psi}$ , we can get  $\hat{\tilde{\psi}}_j \hat{\psi}_j \leq (1/2)\psi_j^2 - (1/2)\tilde{\psi}_j^2$ ; further rewrite (58) as

$$\dot{V} \leq -2^\eta c \sum_{j=1}^n \left( \frac{\Xi_j^2}{2} \right)^\eta - c \sum_{j=1}^n \frac{P_m \tilde{\psi}_j^2}{2\gamma_j} + \sum_{k=1}^n \frac{\delta_j^{*2}}{2} + \sum_{j=1}^n \frac{P_m \Upsilon_j}{2\gamma_j} \psi_j^2. \quad (59)$$

For Lemma 2, we choose the appropriate parameters for  $z = 1$ ,  $c = c^{1/\eta} \sum_{j=1}^n (P_m/2\gamma_j) \tilde{\psi}_j^2$ , and  $\mu = 1 - \eta$ ,  $\beta = \eta$ ,  $\iota = (c^\eta/\eta)^{-\eta/(1-\eta)}$ . Then, one can obtain

$$c \left( \sum_{j=1}^n \frac{P_m \tilde{\psi}_j^2}{2\gamma_j} \right)^\eta \leq (1 - \eta)\iota + c \sum_{j=1}^n \frac{P_m \tilde{\psi}_j^2}{2\gamma_j}. \quad (60)$$

Substituting (60) into (59) and using the zoom method of (6), the following inequality holds:

$$\begin{aligned} \dot{V} &\leq -2^\eta c \left( \sum_{j=1}^n \frac{\Xi_j^2}{2} \right)^\eta - c \left( \sum_{j=1}^n \frac{P_m \tilde{\psi}_j^2}{2\gamma_j} \right)^\eta + c \left( \sum_{j=1}^n \frac{P_m \tilde{\psi}_j^2}{2\gamma_j} \right)^\eta \\ &\quad - c \sum_{j=1}^n \frac{P_m \tilde{\psi}_j^2}{2\gamma_j} + \sum_{k=1}^n \frac{\delta_j^{*2}}{2} + \sum_{j=1}^n \frac{P_m \Upsilon_j}{2\gamma_j} \psi_j^2, \\ &\leq -2^\eta c \left( \sum_{j=1}^n \frac{\Xi_j^2}{2} \right)^\eta - c \left( \sum_{j=1}^n \frac{P_m \tilde{\psi}_j^2}{2\gamma_j} \right)^\eta + (1 - \eta)\iota \\ &\quad + \sum_{k=1}^n \frac{\delta_j^{*2}}{2} + \sum_{j=1}^n \frac{P_m \Upsilon_j}{2\gamma_j} \psi_j^2. \end{aligned} \quad (61)$$

Applying Lemma 3, we can further simplify the time derivative of  $V$  as

$$\dot{V} \leq -\kappa V^\eta + \rho, \quad (62)$$

where

$$\begin{aligned} \kappa &= \min\{2^\eta c, c\}, \\ \rho &= (1 - \eta)\iota + \sum_{k=1}^n \frac{\delta_j^{*2}}{2} + \sum_{j=1}^n \frac{P_m \Upsilon_j}{2\gamma_j} \psi_j^2. \end{aligned} \quad (63)$$

Now, define  $T^* = 1/((1 - \eta)\theta\kappa)[V^{1-\eta}(\Xi(0), \Phi(0)) - (\rho/(1 - \theta)\kappa)^{(1-\eta)/\eta}]$  with  $\Xi(0) = (\Xi_1(0), \Xi_2(0), \dots, \Xi_n(0))^T$ , and  $\Phi(0) = (\psi_1(0), \psi_2(0), \dots, \psi_n(0))^T$ . Based on Lemma 1, we can get  $V^\eta(\zeta) \leq \rho/((1 - \theta)\kappa)$  for  $\forall T \geq T^*$ . So, the solution of  $\dot{\zeta} = f(\zeta)$  is bounded in a finite time and all the signals in the nonlinear system (1) are SGUFB. To be more precise, the finite-time controller proposed by us can converge the tracking error to a small neighborhood of zero and remains there after the finite time  $T^*$ . In order to be more intuitive, we will confirm the research results through a simulation example.

## 5. A Simulation Example

In this section, we will demonstrate the effectiveness of the proposed scheme through the following simulation example.

Let us consider a two-dimensional nonaffine pure-feedback nonlinear system with disturbance as follows:

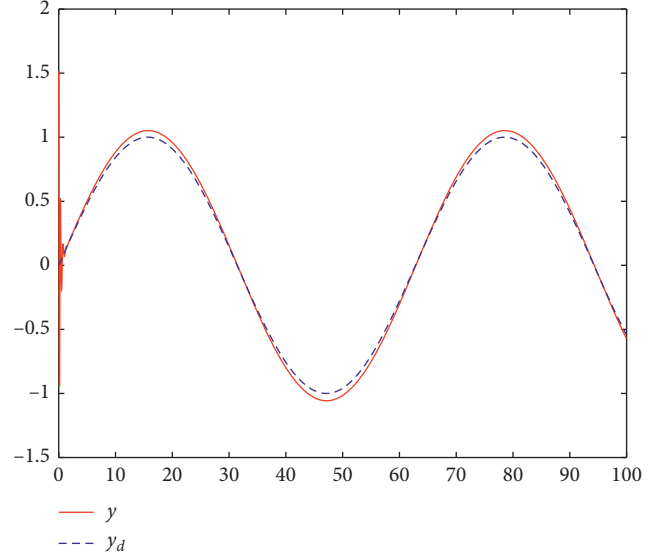


FIGURE 1: The responses of the system out  $y(t)$  and reference signal  $y_d$  of the example.

$$\begin{cases} \dot{\tau}_1 = \tau_1 + \tau_2 + \frac{\tau_2^3}{5} + 0.2 \sin^2(\tau_1 \tau_2), \\ \dot{\tau}_2 = \tau_1 \tau_2 + u + 0.1 \sin(\tau_1 \tau_2), \\ y = \tau_1, \end{cases} \quad (64)$$

where  $\bar{\tau}_i = [\tau_1, \tau_2, \dots, \tau_i]^T \in R^i$ ,  $i = 1, \dots, n$ ,  $y \in R$  are the system state and output and  $u \in R$  are the system control input, respectively. The reference signal of the system output is given as  $y_d = 0.1 \sin(t)$ . According Lemma 3, we construct virtual control signal and actual controller as well as the adaptation law for system (64) as follows:

$$\begin{aligned} \alpha_1 &= -k_1 \Xi_1^{2\eta-1} - \frac{\hat{\psi}_1}{2a_1^2} \Xi_1 \xi_1^T \xi_1, \\ \hat{\psi}_1 &= \frac{\gamma_1}{2a_1^2} \Xi_1^2 \xi_1^T \xi_1 - \Upsilon_1 \hat{\psi}_1, \quad \hat{\psi}_1(0) \geq 0, \\ u &= -k_2 \Xi_2^{2\eta-1} - \frac{\hat{\psi}_2}{2a_2^2} \Xi_2 \xi_2^T \xi_2, \\ \hat{\psi}_2 &= \frac{\gamma_2}{2a_2^2} \Xi_2^2 \xi_2^T \xi_2 - \Upsilon_2 \hat{\psi}_2, \quad \hat{\psi}_2(0) \geq 0. \end{aligned} \quad (65)$$

Then, the initial conditions are given as  $\tau_1(0) = 0$ ,  $\tau_2(0) = 0$ , and  $\hat{\psi}(0) = 0$ . We choose the design parameter in the simulation as follows:  $\eta = 99/101$ ,  $k_1 = 15$ ,  $k_2 = 8$ ,  $a_1 = 1$ ,  $a_2 = 1$ ,  $\gamma_1 = 10$ ,  $\gamma_2 = 10$ ,  $\Upsilon_1 = 0.5$ , and  $\Upsilon_2 = 0.5$ . Finally, we get Figures 1–6. Figure 1 denotes the responses of the system out  $y(t)$  and reference signal  $y_d$  of the example. The tracking error  $\Xi_1$  of the example between the output of the system and the reference signal converges to a small neighborhood, which can be observed intuitively in Figure 2. Figure 3 shows the response of the state  $\tau_2$  variable.

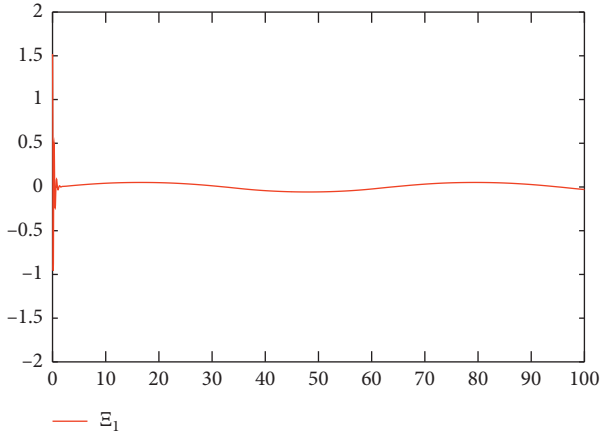


FIGURE 2: The response of the tracking error  $\Xi_1$  of the example.

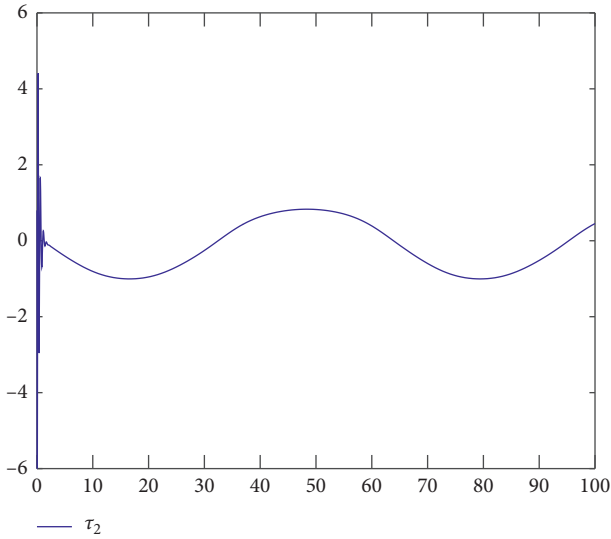


FIGURE 3: The response of the state variable  $\tau_2$  of the example.

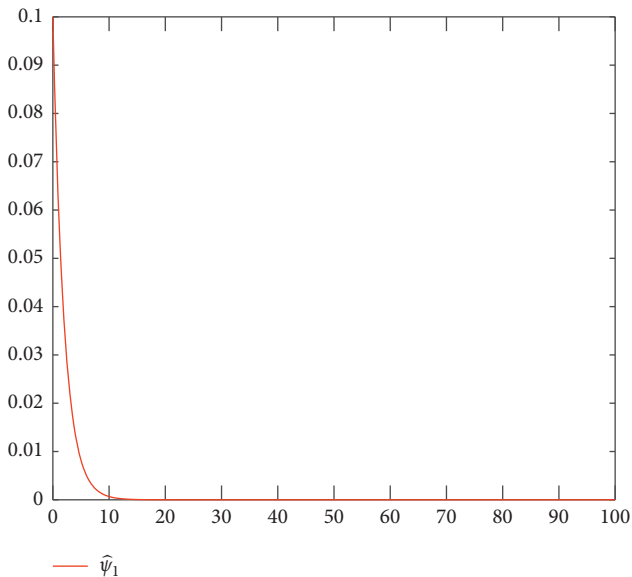


FIGURE 4: The response of the adaptive rate  $\hat{\psi}_1$  of the example.

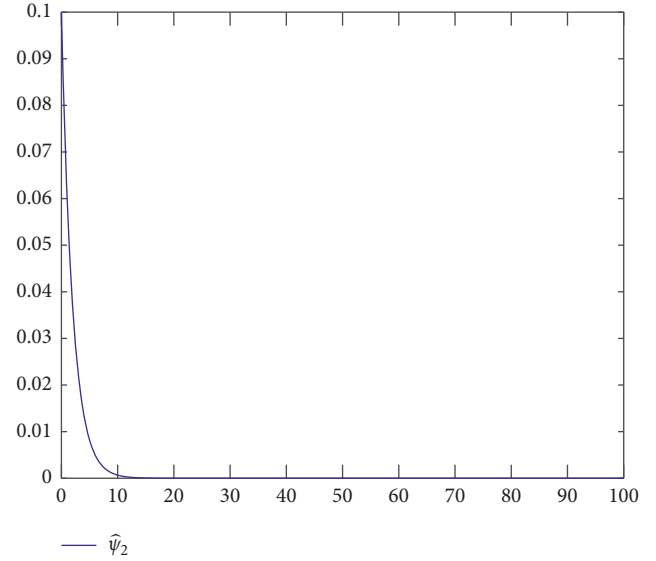


FIGURE 5: The response of the adaptive rate  $\hat{\psi}_2$  of the example.

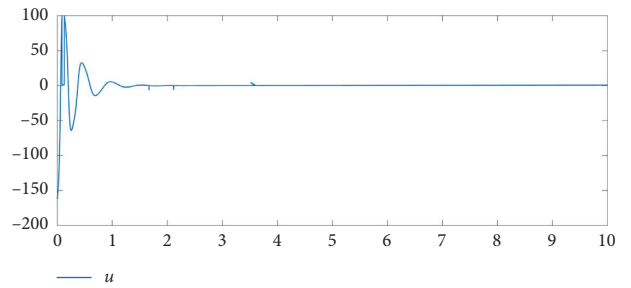


FIGURE 6: The response of the control law input  $u$ .

From the trends in Figures 4 and 5, it is clear to see that the boundedness of the adaptive rate  $\hat{\psi}_1$  and  $\hat{\psi}_2$ . It can be seen from these results that even though the nonaffine function of our simulation system is not differentiable, it has achieved excellent control performance. Finally, the response of the control law  $u_f$  is shown in Figure 6.

## 6. Conclusions

A novel finite-time adaptive controller has been presented for the considered pure-feedback nonlinear system in this paper. The first design difficulty in this paper is to decouple the pure feedback system without using the median value theorem. The second design difficulty is the extremely complicated formula derivation when designing the finite-time controller, in order to make the system variables converge to the equilibrium quickly in a limited time. Compared with the existing results, the developed method addressed the finite-time adaptive tracking control problem for the pure feedback system whose nonaffine functions may not be differentiable. Furthermore, the decoupling technology has been used in our design frame to eliminate the restrictive assumption of partial derivatives of nonaffine functions, which makes the method more widely used. It is worth noting that the finite-time controller constructed by



us can not only ensure that the system state variables quickly converge to equilibrium within a limited time but also improve the robustness of the closed-loop system. In the future, the finite-time adaptive control of various types of complex switched nonlinear systems can be further discussed, such as multiple input multiple output stochastic switched nonlower triangular systems and stochastic switched nonlower triangular pure feedback nonlinear systems.

## Data Availability

The data used to support the findings of this study are included within the article.

## Conflicts of Interest

The author declares that there are no conflicts of interest.

## Acknowledgments

This work was supported in part by the National Natural Science Foundation of China, under Grants 61873151, 61773192, 61773246, and 61803225, Shandong Provincial Natural Science Foundation, China, under Grant ZR2019MF009, Taishan Scholar Project of Shandong Province of China, under Grant tsqn20190-9078, and Major Program of Shandong Province Natural Science Foundation, under Grant ZR2018ZB0419.

## References

- [1] G. C. Walsh, O. Beldiman, and L. G. Bushnell, "Asymptotic behavior of nonlinear networked control systems," *IEEE Transactions on Automatic Control*, vol. 46, no. 7, pp. 1093–1097, 2001.
- [2] B. Niu, P. Zhao, J. D. Liu, H. J. Ma, and Y. J. Liu, "Global adaptive control of switched uncertain nonlinear systems: an improved MDADT method," *Automatica*, vol. 115, Article ID 108872, 2020.
- [3] B. Xian, D. M. Dawson, M. S. deQueiroz, and J. Chen, "A continuous asymptotic tracking control strategy for uncertain nonlinear systems," *IEEE Transactions on Automatic Control*, vol. 49, no. 7, p. 1206, 2004.
- [4] B. Niu, M. Liu, and A. Li, "Global adaptive stabilization of stochastic high-order switched nonlinear non-lower triangular systems," *Systems Control Letters*, vol. 136, Article ID 104596, 2020.
- [5] X. Li, J. Shen, H. Akca, and R. Rakkiyappan, "LMI-based stability for singularly perturbed nonlinear impulsive differential systems with delays of small parameter," *Applied Mathematics and Computation*, vol. 250, pp. 798–804, 2015.
- [6] A. R. Teel, J. Peuteman, and D. Aeyels, "Semi-global practical asymptotic stability and averaging," *Systems & Control Letters*, vol. 37, no. 5, pp. 329–334, 1999.
- [7] D. Angeli, "Intrinsic robustness of global asymptotic stability," *Systems & Control Letters*, vol. 38, no. 4-5, pp. 297–307, 1999.
- [8] E. Panteley and A. Loria, "On global uniform asymptotic stability of nonlinear time-varying systems in cascade," *Systems & Control Letters*, vol. 33, no. 2, pp. 131–138, 1998.
- [9] J. Sun, Y. Zhang, and Q. Wu, "Less conservative conditions for asymptotic stability of impulsive control systems," *IEEE Transactions on Automatic Control*, vol. 48, no. 5, pp. 829–831, 2003.
- [10] B. Niu, Y. Liu, W. Zhou, H. Li, P. Duan, and J. Li, "Multiple Lyapunov functions for adaptive neural tracking control of switched nonlinear nonlower-triangular systems," *IEEE Transactions on Cybernetics*, vol. 50, no. 5, pp. 1877–1886, 2020.
- [11] P. Dorato, "Short-time stability in linear time-varying systems," *Proceedings of IRE International Convention Record*, pp. 83–87, 1961.
- [12] L. Weiss and E. Infante, "Finite time stability under perturbing forces and on product spaces," *IEEE Transactions on Automatic Control*, vol. 12, no. 1, pp. 54–59, 1967.
- [13] J. Wu, D. Yang, X. Y. He, and X. D. Li, "Finite-time stability for a class of underactuated systems subject to time-varying disturbance," *Complexity*, vol. 2020, Article ID 8704505, 7 pages, 2020.
- [14] Y. P. Luo and Y. J. Yao, "Finite-time synchronization of uncertain complex dynamic networks with nonlinear coupling," *Complexity*, vol. 2019, Article ID 9821063, 14 pages, 2019.
- [15] J. Q. Lu, Y. Q. Wang, X. C. Shi, and J. D. Cao, "Finite-time bipartite consensus for multi-agent systems under detail-balanced antagonistic interactions," *IEEE Transactions on Systems, Man, and Cybernetics: Systems*, 2019.
- [16] Y. Li, S. Tong, and T. Li, "Hybrid fuzzy adaptive output feedback control design for uncertain MIMO nonlinear systems with time-varying delays and input saturation," *IEEE Transactions on Fuzzy Systems*, vol. 24, no. 4, pp. 841–853, 2015.
- [17] Y. H. Zhang, J. Sun, H. J. Liang, and H. Y. Li, "Event-triggered adaptive tracking control for multiagent systems with unknown disturbances," *IEEE Transactions on Cybernetics*, vol. 50, no. 3, pp. 890–901, 2020.
- [18] Y. Li, S. Tong, and S. C. Tong, "Adaptive fuzzy output-feedback stabilization control for a class of switched nonstrict-feedback nonlinear systems," *IEEE Transactions on Cybernetics*, vol. 47, no. 4, pp. 1007–1016, 2017.
- [19] B. Niu, D. Wang, N. D. Alotaibi, and F. E. Alsaadi, "Adaptive neural state-feedback tracking control of stochastic nonlinear switched systems: an average dwell-time method," *IEEE Transactions on Neural Networks and Learning Systems*, vol. 30, no. 4, pp. 1076–1087, 2019.
- [20] Z. L. Xiong, S. C. Qu, and J. Luo, "Adaptive multi-switching synchronization of high-order memristor-based hyperchaotic system with unknown parameters and its application in secure communication," *Complexity*, vol. 2019, Article ID 3827201, 18 pages, 2019.
- [21] Y. T. Wen and X. M. Ren, "Neural networks-based adaptive control for nonlinear time-varying delays systems with unknown control direction," *IEEE Press*, vol. 22, no. 10, pp. 1599–1612, 2011.
- [22] B. Niu, D. Wang, M. Liu, X. M. Song, H. Q. Wang, and P. Y. Duan, "Adaptive neural output feedback controller design of switched non-lower triangular nonlinear systems with time-delays," *IEEE Transactions on Neural Networks and Learning Systems*, 2019.
- [23] C. F. Hsu, C. M. Lin, and T. T. Lee, "Wavelet adaptive backstepping control for a class of nonlinear systems," *IEEE Transactions on Neural Networks*, vol. 17, no. 5, pp. 1175–1183, 2006.

- [24] L. Ma, X. Huo, X. Zhao, B. Niu, and G. Zong, "Adaptive neural control for switched nonlinear systems with unknown backlash-like hysteresis and output dead-zone," *Neurocomputing*, vol. 357, pp. 203–214, 2019.
- [25] S. Xing, F. a. Liu, Q. Wang, X. Zhao, and T. Li, "A hierarchical attention model for rating prediction by leveraging user and product reviews," *Neurocomputing*, vol. 332, pp. 417–427, 2019.
- [26] L. Zhu, Z. Huang, Z. Li, L. Xie, and H. T. Shen, "Exploring auxiliary context: discrete semantic transfer hashing for scalable image retrieval," *IEEE Transactions on Neural Networks and Learning Systems*, vol. 29, no. 11, pp. 5264–5276, 2018.
- [27] Y. Tan, M. Xiong, B. Niu, J. Liu, and S. Fei, "Distributed hybrid-triggered  $H_{\infty}$  filter design for sensor networked systems with output saturations," *Neurocomputing*, vol. 315, pp. 261–271, 2018.
- [28] Q. Wang, Y. Zheng, G. Yang, W. Jin, X. Chen, and Y. Yin, "Multiscale rotation-invariant convolutional neural networks for lung texture classification," *IEEE Journal of Biomedical and Health Informatics*, vol. 22, no. 1, pp. 184–195, 2018.
- [29] X. W. Zheng, B. Hu, D. J. Lu, and H. Liu, "A multi-objective virtual network embedding algorithm in cloud computing," *Journal of Internet Technology*, vol. 17, no. 4, pp. 633–642, 2016.
- [30] X. Li, D. O'Regan, and H. Akca, "Global exponential stabilization of impulsive neural networks with unbounded continuously distributed delays," *IMA Journal of Applied Mathematics*, vol. 80, no. 1, pp. 85–99, 2015.
- [31] B. Hu, H. Wang, X. Yu, W. Yuan, and T. He, "Sparse network embedding for community detection and sign prediction in signed social networks," *Journal of Ambient Intelligence and Humanized Computing*, vol. 10, no. 1, pp. 175–186, 2019.
- [32] C. Luo, C. Tan, X. Wang, and Y. Zheng, "An evolving recurrent interval type-2 intuitionistic fuzzy neural network for online learning and time series prediction," *Applied Soft Computing*, vol. 78, pp. 150–163, 2019.
- [33] X. Zheng, J. Tian, X. Xiao, X. Cui, and X. Yu, "A heuristic survivable virtual network mapping algorithm," *Soft Computing*, vol. 23, no. 5, pp. 1453–1463, 2019.
- [34] H. Zhang, H. Ji, and X. Wang, "Transfer learning from unlabeled data via neural networks," *Neural Processing Letters*, vol. 36, no. 2, pp. 173–187, 2012.
- [35] C. Huang, J. Q. Lu, G. S. Zhai, J. D. Cao, G. P. Lu, and M. Perc, "Stability and stabilization in probability of probabilistic boolean networks," *IEEE Transactions on Neural Networks and Learning Systems*, 2020.
- [36] B. Niu, D. Wang, N. D. Alotaibi, and F. E. Alsaadi, "Adaptive neural state-feedback tracking control of stochastic nonlinear switched systems: an average dwell-time method," *IEEE Transactions on Neural Networks and Learning Systems*, vol. 30, no. 4, pp. 1076–1087, 2018.
- [37] H. Ma, H. J. Liang, Q. Zhou, and C. K. Ahn, "Adaptive dynamic surface control design for uncertain nonlinear strict-feedback systems with unknown control direction and disturbances," *IEEE Transactions on Systems, Man, and Cybernetics: Systems*, vol. 49, no. 3, pp. 506–515, 2018.
- [38] S. Tong and Y. Li, "Observer-based fuzzy adaptive control for strict-feedback nonlinear systems," *Fuzzy Sets and Systems*, vol. 160, no. 12, pp. 1749–1764, 2009.
- [39] T. Zhang, S. S. Ge, and C. C. Hang, "Adaptive neural network control for strict-feedback nonlinear systems using backstepping design," *Automatica*, vol. 36, no. 12, pp. 1835–1846, 2000.
- [40] S. Tong, Y. Li, Y. M. Li, and Y. Liu, "Observer-based adaptive fuzzy backstepping control for a class of stochastic nonlinear strict-feedback systems," *IEEE Transactions on Systems, Man, and Cybernetics-Part B: Cybernetics*, vol. 41, no. 6, pp. 1693–1704, 2011.
- [41] D. Wang and J. Huang, "Neural network-based adaptive dynamic surface control for a class of uncertain nonlinear systems in strict-feedback form," *IEEE Transactions on Neural Networks*, vol. 16, no. 1, pp. 195–202, 2005.
- [42] B. Chen, X. Liu, K. Liu, and C. Lin, "Direct adaptive fuzzy control of nonlinear strict-feedback systems," *Automatica*, vol. 45, no. 6, pp. 1530–1535, 2009.
- [43] X. Peng, H. Q. Wu, and J. D. Cao, "Global nonfragile synchronization in finite time for fractional-order discontinuous neural networks with nonlinear growth activations," *IEEE Transactions on Neural Networks and Learning Systems*, vol. 30, no. 7, pp. 2123–2137, 2018.
- [44] Z. Wang and H. Wu, "Global synchronization in fixed time for semi-Markovian switching complex dynamical networks with hybrid couplings and time-varying delays," *Nonlinear Dynamics*, vol. 95, no. 3, pp. 2031–2062, 2019.
- [45] M. Liu and H. Wu, "Stochastic finite-time synchronization for discontinuous semi-Markovian switching neural networks with time delays and noise disturbance," *Neurocomputing*, vol. 310, pp. 246–264, 2018.
- [46] Z. Wang and H. Wu, "Projective synchronization in fixed time for complex dynamical networks with nonidentical nodes via second-order sliding mode control strategy," *Journal of the Franklin Institute*, vol. 355, no. 15, pp. 7306–7334, 2018.
- [47] X. Peng, H. Wu, K. Song, and J. Shi, "Global synchronization in finite time for fractional-order neural networks with discontinuous activations and time delays," *Neural Networks*, vol. 94, pp. 46–54, 2017.
- [48] Y. Wang and Y. Song, "Fraction dynamic-surface-based neuroadaptive finite-time containment control of multiagent systems in nonaffine pure-feedback form," *IEEE Transactions on Neural Networks and Learning Systems*, vol. 28, no. 3, pp. 678–689, 2017.
- [49] J. Zhang, Q. Zhu, Y. Li, and X. Wu, "Homeomorphism mapping based neural networks for finite time constraint control of a class of nonaffine pure-feedback nonlinear systems," *Complexity*, vol. 2019, Article ID 9053858, 11 pages, 2019.
- [50] A.-M. Zou, Z.-G. Hou, and M. Tan, "Adaptive control of a class of nonlinear pure-feedback systems using fuzzy backstepping approach," *IEEE Transactions on Fuzzy Systems*, vol. 16, no. 4, pp. 886–897, 2008.
- [51] G. Sun, D. Wang, and Z. Peng, "Adaptive control based on single neural network approximation for non-linear pure-feedback systems," *IET Control Theory and Applications*, vol. 6, no. 15, pp. 2387–2396, 2011.
- [52] J. Lian, S. Hou, X. Sui, F. Xu, and Y. Zheng, "Deblurring retinal optical coherence tomography via a convolutional neural network with anisotropic and double convolution layer," *IET Computer Vision*, vol. 12, no. 6, pp. 900–907, 2018.
- [53] S. S. Ge and C. Wang, "Adaptive NN control of uncertain nonlinear pure-feedback systems," *Automatica*, vol. 38, no. 4, pp. 671–682, 2002.
- [54] M. Wang, X. P. Liu, and P. Shi, "Adaptive neural control of pure-feedback nonlinear time-delay systems via dynamic surface technique," *IEEE Transactions on Systems, Man, and Cybernetics-Part B: Cybernetics*, vol. 41, no. 6, pp. 1681–1692, 2011.

- [55] T. P. Zhang, H. Wen, and Q. Zhu, "Adaptive fuzzy control of nonlinear systems in pure feedback form based on input-to-state stability," *IEEE Transactions on Fuzzy Systems*, vol. 18, no. 1, pp. 80–93, 2010.
- [56] C. Wang, D. J. Hill, S. S. Ge, and G. Chen, "An ISS-modular approach for adaptive neural control of pure-feedback systems," *Automatica*, vol. 42, no. 5, pp. 723–731, 2006.
- [57] Y. Li, "Impulsive synchronization of stochastic neural networks via controlling partial states," *Neural Processing Letters*, vol. 46, no. 1, pp. 59–69, 2017.
- [58] C. Huang, J. Q. Lu, D. W. C. Ho, G. S. Zhai, and J. D. Cao, "Stabilization of probabilistic boolean networks via pinning control strategy," *Information Sciences*, vol. 510, pp. 205–217, 2019.
- [59] C. Huang, X. Zhang, H. K. Lam, and S. H. Tsai, "Synchronization analysis for nonlinear complex networks with reaction-diffusion terms using fuzzy-model-based approach," *IEEE Transactions on Fuzzy Systems*, 2020.
- [60] F. Wang, B. Chen, X. Liu, and C. Lin, "Finite-time adaptive fuzzy tracking control design for nonlinear Systems," *IEEE Transactions on Fuzzy Systems*, vol. 26, no. 3, pp. 1207–1216, 2018.
- [61] C. Qian and W. Lin, "Non-Lipschitz continuous stabilizers for nonlinear systems with uncontrollable unstable linearization," *Systems & Control Letters*, vol. 42, no. 3, pp. 185–200, 2001.
- [62] G. H. Hardy, J. E. Littlewood, and G. Polya, "*Inequalities*," Cambridge University Press, Cambridge, UK, 1952.
- [63] Z. Liu, X. Dong, J. Xue, H. Li, and Y. Chen, "Adaptive neural control for a class of pure-feedback nonlinear systems via dynamic surface technique," *IEEE Transactions on Neural Networks and Learning Systems*, vol. 27, no. 9, pp. 1969–1975, 2016.
- [64] W. S. Chen, L. C. Jiao, J. Li, and R. H. Li, "Adaptive NN backstepping output-feedback control for stochastic nonlinear strict-feedback systems with time-varying delays," *IEEE Transactions on Systems, Man, and Cybernetics-Part B: Cybernetics*, vol. 40, no. 3, pp. 939–950, 2010.
- [65] J. Wu, W. S. Chen, D. Zhao, and J. Li, "Globally stable direct adaptive backstepping NN control for uncertain nonlinear strict-feedback systems," *Neurocomputing*, vol. 122, pp. 134–147, 2013.

## Research Article

# Finite-Time Stabilization for $p$ -Norm Stochastic Nonlinear Systems with Output Constraints

Shijun Guan<sup>1</sup> and Liandi Fang<sup>2,3</sup> 

<sup>1</sup>Department of Economic Management, Anhui Vocational College of Press and Publishing, Hefei 230601, China

<sup>2</sup>College of Mathematics and Computer Science, Tongling University, Tongling 244000, China

<sup>3</sup>School of Electrical and Information Engineering, Jiangsu University, Zhenjiang 212013, China

Correspondence should be addressed to Liandi Fang; fangld@tlu.edu.cn

Received 3 June 2020; Revised 7 July 2020; Accepted 10 July 2020; Published 12 August 2020

Guest Editor: Xiaodi Li

Copyright © 2020 Shijun Guan and Liandi Fang. This is an open access article distributed under the Creative Commons Attribution License, which permits unrestricted use, distribution, and reproduction in any medium, provided the original work is properly cited.

This paper investigates the finite-time stability problem of  $p$ -norm stochastic nonlinear systems subject to output constraint. To cope with the constraint on system output, a tan-type barrier Lyapunov function (BLF) is constructed. By using the constructed BLF and the backstepping technique, a new control algorithm is proposed with a continuous state-feedback controller being designed, which guarantees not only that the requirement of output constraint is always achieved but also that the origin of the system is finite-time stable. This result is demonstrated by both the rigorous analysis and the simulation example.

## 1. Introduction

During the past decades, the control problem of nonlinear systems has long been a hot topic, and many control design approaches have been proposed for various kinds of nonlinear systems, such as adaptive fuzzy control [1, 2], output tracking control [3, 4],  $H_\infty$  control [5, 6], and sliding mode control [7–10]. Due to their important roles in many science and industry applications, the stochastic nonlinear systems have attracted much interest in recent years. With the development of stochastic theory, various control design strategies have been developed for types of stochastic nonlinear systems by the backstepping technique, see [11–14], for examples. Especially, some works have considered  $p$ -norm stochastic nonlinear systems, which are inherently nonlinear due to the fractional powers of such systems being not identically equal to one. It should be noted that the inherent nonlinearities cause the stability and control design problems, which are not very easy to be solved [15]. Luckily, the issues have been well studied for  $p$ -norm stochastic nonlinear systems with different structures by the adding a power integrator technique in the existing literatures. For instance, Li et al. [16] have

considered the adaptive state-feedback stabilization for  $p$ -norm stochastic nonlinear systems; the output-feedback control has been addressed for  $p$ -norm stochastic nonlinear systems with time-varying delays in [17]; Zhao et al. [18] have proposed a neural tracking control algorithm for  $p$ -norm switched stochastic nonlinear systems. More latest studies can be found in [19–21] and the references within.

However, most of the abovementioned works about  $p$ -norm stochastic nonlinear systems did not take the output constraint into consideration. As it is well known, many actual systems are subject to output constraint due to the consideration of the system performance and operation safety [22, 23]. For this reason, the constrained control issue of nonlinear systems has drawn attention from many scholars. Tee et al. [24] have first proposed the notion of the barrier Lyapunov function (BLF) and consequently have developed a control design strategy for a class of strict-feedback deterministic nonlinear systems with output constraints. After then, with the aid of BLFs, control design schemes have been presented for many deterministic nonlinear systems with different types of constraints, including stability control for nonlinear systems with time-varying or asymmetric output constraints [25, 26], adaptive control for

nonlinear systems with full-state constrains [27], and sliding mode control for nonlinear systems with output constraints [28–30]. Moreover, since the finite-time control possesses some inherent advantages [31–33], techniques for the finite-time stabilization under output/state constraints have also been developed, respectively, for strict-feedback nonlinear systems [34], norm nonlinear systems [35–37], and switched nonlinear systems [38]. On the basis of these results, the constrained control schemes for some classes of stochastic nonlinear systems have also been proposed. Jin [39] has constructed an adaptive tracking controller for a class of output-constrained stochastic nonlinear systems in strict-feedback form. Later, the adaptive control problem and the finite-time control problem have been, respectively, addressed for stochastic nonlinear systems with full-state constraints in [40, 41]. Furthermore, the adaptive neural network or fuzzy constrained control problems have attracted some attention [42–46]. Nevertheless, the stochastic nonlinear systems with output constraints considered in most of the existing related works are in the strict-feedback form, rather than in  $p$ -normal form. On the contrary, the existing research has mainly focused on the adaptive control problem but did not take the finite-time stabilization into account.

Motivated by the above discussions, we will investigate the problem of the finite-time stabilization for a class of  $p$ -norm stochastic nonlinear systems with output constraints and unknown time-varying parameters. First of all, a BLF-based control strategy will be developed by the backstepping approach. Secondly, applying stochastic Lyapunov theorems and Itô's formula, the constructed state-feedback controller is rigorously proved to be able to ensure the achievement of the output constraint and the finite-time stability of the considered systems simultaneously. Finally, the main result of this paper will be further demonstrated by a simulation example.

## 2. Problem and Preliminaries

**2.1. Problem Statement.** The following class of stochastic nonlinear systems are considered:

$$\begin{aligned} dx_i &= \vartheta_i(t)x_{i+1}^{q_i}dt + f_i(\bar{x}_i)dt + g_i^T(\bar{x}_i)d\omega, \\ i &= 1, \dots, n-1, \\ dx_n &= \vartheta_n(t)u^{q_n}dt + f_n(\bar{x}_n)dt + g_n^T(\bar{x}_n)d\omega, \\ y &= x_1, \end{aligned} \quad (1)$$

where  $\omega$  is a  $N$ -dimension standard Wiener process;  $\bar{x}_i = (x_1, \dots, x_i)^T \in R^i$ ,  $u \in R$  and  $y \in R$  are system state, control input, and output, respectively;  $\vartheta_i(t)$  is the time-varying parameter; the nonlinear functions  $f_i: R^i \rightarrow R$  and  $g_i: R^i \rightarrow R^N$  are continuous and satisfy  $f_i(0) = g_i(0) = 0$ ; and the fractional powers  $q_i$ 's meet the requirement  $q_i \in R_{odd}^{\geq 1} = \{\tau \geq 1, \tau \text{ is the positive odd integers ratio}\}$ . The output  $y$  is required to satisfy

$$y \in \prod_1 = \{y(t) \in R, |y(t)| < b\} = \{x_1 \in R, |x_1(t)| < b\}, \quad (2)$$

where  $b$  is a known positive constant.

This paper aims to design a continuous state-feedback controller for system (1), which can ensure that the origin of the closed-loop system is finite-time stable in probability and the requirement of the output constraint is achieved.

### 2.2. Preliminaries

**Notations 1.** For  $k = 1, \dots, n$ , let  $g_k^{-T}(\bar{x}_k) = (g_1^T(x_1), \dots, g_i^T(\bar{x}_k))$  and  $\Pi_k = \{\bar{x}_k \in R^k, |x_1(t)| < b\}$ . For any  $\zeta \in R$  and  $\theta > 0$ , denote  $\varphi(\zeta) = [\zeta]^\theta = |\zeta|^\theta \text{sgn}(\zeta)$ .

Consider the following stochastic system:

$$dx = f(x)dt + g(x)d\omega, \quad (3)$$

where  $f(x)$  and  $g(x)$  are continuous satisfying  $f(0) = 0$  and  $g(0) = 0$ .

**Definition 1** (see [13]). For any given  $V(x) \in C^2(R^n)$ , associated with system (1), the second-order differential operator is defined as follows:

$$\mathcal{L}V = \frac{\partial V}{\partial x} f(x) + \frac{1}{2} \text{tr} \left\{ g^T(x) \frac{\partial^2 V}{\partial x^2} g(x) \right\}. \quad (4)$$

**Definition 2** (see [24]). Suppose that  $\Pi$  is an open set containing the origin and  $V: \Pi \rightarrow R$  is positive definite and continuously differentiable. Then, for system  $\dot{x} = g(x)$ ,  $V(x(t))$  is called a BLF if for each solution  $x(t)$  starting from  $x(t_0) \in \Pi$ ,  $V(x(t)) \rightarrow \infty$ , as  $x(t) \rightarrow \partial\Pi$ ,  $V(x(t)) \leq \tau$  for all  $t \geq t_0$  and for some  $\tau \in R^+$ .

**Assumption 1** (see [36]). For  $\forall i = 1, \dots, n$ , there exist known positive constants  $\underline{\vartheta}_i$  and  $\bar{\vartheta}_i$  such that  $\underline{\vartheta}_i \leq \vartheta_i(t) \leq \bar{\vartheta}_i$ .

**Assumption 2.** For  $i = 1, \dots, n$ , there are a constant  $\mu \in (-[1 + \sum_{j=2}^n q_1 \cdots q_{j-1}]^{-1}, 0)$  and known nonnegative smooth functions  $\psi_i(\bar{x}_i)$ ,  $\eta_i(\bar{x}_i)$  such that

$$\begin{aligned} |f_i(\bar{x}_i)| &\leq \psi_i(\bar{x}_i) \sum_{j=1}^i |x_j|^{(v_i + \mu/v_j)}, \\ \|g_i(\bar{x}_i)\| &\leq \eta_i(\bar{x}_i) \sum_{j=1}^i |x_j|^{(2v_i + \mu/2v_j)}, \end{aligned} \quad (5)$$

for all  $t \geq 0$ , where  $v_1 = 1$ ,  $v_{j+1} = ((v_j + \mu)/q_j) > 0$ ,  $j = 1, \dots, n$ .

**Remark 1.** Note that condition (4) is borrowed from [34]. However, the systems considered in [34] are  $p$ -norm deterministic nonlinear systems, while we consider  $p$ -norm stochastic nonlinear systems with drift terms  $f_i$ 's and

diffusion terms  $g_i$ 's in this paper. In light of  $\mu \in (-[1 + \sum_{j=2}^n q_1 \cdots q_{j-1}]^{-1}, 0)$ , the value of  $\mu$  is generally taken as  $\mu = -(m/p)$  for simplicity, where  $m$  and  $p$  represent even and odd integers, respectively. Then, the value of each  $v_j$  ( $j = 2, \dots, n$ ) can be obtained by applying  $v_1 = 1$  and  $v_{j+1} = ((v_j + \mu)/q_j) > 0$ . It can also be observed that both the denominator and numerator of each  $v_j$  are odd.

**Lemma 1** (see [13]). *Suppose that there exists a positive Lyapunov function  $V \in C^2(\mathbb{R}^n)$ , which satisfies  $\lim_{|x| \rightarrow \infty} V(x) = \infty$ . If  $\ell V$  is with respect to (3) and satisfies  $\ell V \leq 0, \forall x \in \mathbb{R}^n$ , then system (3) has a solution for any initial value.*

**Lemma 2** (see [13]). *Suppose that system (3) admits a solution for each initial value. If there are  $\kappa_\infty$  class functions  $\varrho_1(\cdot)$  and  $\varrho_2(\cdot)$ , a positive  $C^2$  Lyapunov function  $V$ , real numbers  $c > 0$ , and  $0 < \gamma < 1$ , such that*

$$\begin{aligned} \varrho_1(|x|) \leq V(x) \leq \varrho_2(|x|), x \in \mathbb{R}^n, \\ \ell V(x) \leq -cV^\gamma(x), x \in \mathbb{R}^n \setminus \{0\}. \end{aligned} \quad (6)$$

For all  $t \geq 0$ , then the origin of system (3) is finite-time stable in probability.

**Lemma 3** (see [37]). *Let  $a, b, \rho$ , and  $\varsigma$  be positive real numbers. For any  $z_1, z_2 \in \mathbb{R}$ , we have*

$$\rho |z_1|^a |z_2|^b \leq \varsigma \frac{a}{a+b} |z_1|^{a+b} + \frac{b}{a+b} \rho^{a+b/b} \varsigma^{-a/b} |z_2|^{a+b}. \quad (7)$$

**Lemma 4** (see [8]). *Let  $p \in (0, \infty)$ ; for any  $\varsigma_i \in \mathbb{R}, i = 1, \dots, n$ , one has*

$$\left(|\varsigma_1| + \dots + |\varsigma_n|\right)^p \leq d \left(|\varsigma_1|^p + \dots + |\varsigma_n|^p\right), \quad (8)$$

where  $d = n^{p-1}$  if  $p \geq 1$  and  $d = 1$  if  $0 < p < 1$ .

**Lemma 5** (see [10]). *Let  $a, d \in \mathbb{R}^+$  with  $a \geq 1$ . For any  $\varsigma_1, \varsigma_2 \in \mathbb{R}$ , we have*

- (i)  $|\varsigma_1^a - \varsigma_2^a| \leq a(2^{a-2} + 2)|\varsigma_1 - \varsigma_2|(|\varsigma_1 - \varsigma_2|^{a-1} + \varsigma_2^{a-1})$
- (ii)  $|\varsigma_1^{(d/a)} - \varsigma_2^{(d/a)}| \leq 2^{1-(1/a)} \left[|\varsigma_1|^d - |\varsigma_2|^d\right]^{(1/a)}$
- (iii)  $(|\varsigma_1| + |\varsigma_2|)^{1/a} \leq |\varsigma_1|^{1/a} + |\varsigma_2|^{1/a} \leq 2^{1-(1/a)} (|\varsigma_1| + |\varsigma_2|)^{1/a}$

### 3. Main Results

**3.1. A Tan-Type BLF.** Before carrying out the control design for system (1), we should handle the output constraint issue.

Firstly, we denote  $v_0 = \max_{1 \leq i \leq n} \{v_i\}$  and  $c_i = (v_0/v_i)$  ( $i = 1, \dots, n$ ). Let  $\sigma$  be a constant parameter satisfying  $\sigma \geq \sigma_0$ , where the value of  $\sigma_0$  is chosen as below:

- (i) If for all  $2 \leq i \leq n, 1 \leq c_i \leq 2$ , then  $\sigma_0 = 2v_0$
- (ii) If for all  $2 \leq i \leq n, c_i \geq 2$ , then  $\sigma_0 = v_0$

Consequently, it is clear that  $(\sigma/v_i) \geq 2$ .

Then, a tan-type BLF can be constructed on  $\Pi_1$  as follows:

$$V_b(x_1) = \frac{2b^{4\sigma-\mu}}{(4\sigma-\mu)\pi} \tan\left(\frac{\pi|x_1|^{4\sigma-\mu}}{2b^{4\sigma-\mu}}\right), \quad (9)$$

where  $\mu$  is given by Assumption 2 and  $\sigma$  is defined as above.

It is not hard to obtain from the expression of  $V_b(x_1)$  that

$$\begin{aligned} \frac{\partial V_b}{\partial x_1} &= \sec^2\left(\frac{\pi|x_1|^{4\sigma-\mu}}{2b^{4\sigma-\mu}}\right) [x_1]^{4\sigma-\mu-1} = G(x_1) [x_1]^{4\sigma-\mu-1}, \\ \frac{\partial^2 V_b}{\partial x_1^2} &= (4\sigma-\mu-1)G(x_1) |x_1|^{4\sigma-\mu-2} \\ &\quad + \frac{\pi(4\sigma-\mu)}{b^{4\sigma-\mu}} G(x_1) \tan\left(\frac{\pi|x_1|^{4\sigma-\mu}}{2b^{4\sigma-\mu}}\right) |x_1|^{2(4\sigma-\mu-1)}, \end{aligned} \quad (10)$$

where  $G(x_1) = \sec^2((\pi|x_1|^{4\sigma-\mu})/2b^{4\sigma-\mu})$ .

**Remark 2.** It should be noted that the BLF is modified from [34], which is constructed by fully taking the advantage of the given nonlinear growth conditions. As stated in [34], the control strategy based on  $V_b(x_1)$  is a universal method, which can handle stochastic systems with or without output constraints.

**3.2. Controller Design and Stability Analysis.** In what follows, a continuous state-feedback controller will be constructed, and the stability of system (1) under the designed controller will be rigorously analysed. To this end, a theorem is presented to describe the main result.

**Theorem 1.** *Suppose Assumptions 1-2 hold for system (1). For any constant  $b > 0$ , there is a continuous state-feedback controller such that*

- (i) *The output of system (1) is kept in a given constrained set in the sense of probability, i.e.,  $P\{|y(t)| < b\} = 1$*
- (ii) *The origin of the closed-loop system is finite-time stable in probability.*

*Proof.* The proof contains three parts. First of all, the design procedure of the controller is explicitly displayed. Then, the system output is proved to be kept in the given constrained set with probability one. In the last part, the finite-time stability of system (1) is rigorously analysed.  $\square$

#### 3.2.1. Part I: Design Procedure

**Step 1.** Let  $\varsigma_1 = [x_1]^\sigma$ , and choose the Lyapunov function  $V_1(x_1) = V_b(x_1)$ . Then, we can directly get from Definition 1 that

$$\begin{aligned}
\ell V_1 &\leq \vartheta_1(t)G(x_1)[x_1]^{4\sigma-\mu-1}x_2^{q_1} + \frac{4\sigma-\mu-1}{2} \\
&\quad \cdot G(x_1)|x_1|^{4\sigma-\mu-2}\eta_1^2|x_1|^{2+\mu} \\
&+ \bar{\vartheta}_1 G(x_1)|x_1|^{4\sigma-\mu-1}\psi_1|x_1|^{1+\mu} + \frac{\pi(4\sigma-\mu)}{2b^{4\sigma-\mu}} \\
&\quad \cdot |x_1|^{2(4\sigma-\mu-1)}G(x_1)\tan\left(\frac{\pi|x_1|^{4\sigma-\mu}}{2b^{4\sigma-\mu}}\right)\eta^2|x_1|^{2+\mu} \\
&\leq \vartheta_1(t)G(x_1)[\varsigma_1]^{((4\sigma-\mu-1)/\sigma)}\xi_2^{q_1} + \vartheta_1(t) \\
&\quad \cdot G(x_1)[\varsigma_1]^{((4\sigma-\mu-1)/\sigma)}(x_2^{q_1} - \xi_2^{q_1}) + H_1(x_1)G(x_1)\varsigma_1^4,
\end{aligned} \tag{11}$$

where  $H_1(x_1) \geq \bar{\vartheta}_1\psi_1 + (1/2)\eta_1^2(4\sigma-\mu-1) + (\pi(4\sigma-\mu)\eta_1^2/2b^{4\sigma-\mu})\tan(\pi|x_1|^{4\sigma-\mu}/2b^{4\sigma-\mu})|x_1|^{4\sigma-\mu}$  is a nonnegative  $C^2$  function and  $\xi_2$  is a virtual controller required to be design after later.

Then, we design

$$\xi_2 = -\lambda_1(x_1)[\varsigma_1]^{(v_2/\sigma)} \text{ with } \lambda_1(x_1) = \left(\frac{n+H_1(x_1)}{\vartheta_1}\right)^{(1/q_1)} > 0. \tag{12}$$

Substituting (12) into (13) yields

$$\begin{aligned}
\ell V_1(x_1) &\leq -nG(x_1)\varsigma_1^4 + \vartheta_1(t)G(x_1)[\varsigma_1]^{((4\sigma-\mu-1)/\sigma)} \\
&\quad \cdot (x_2^{q_1} - \xi_2^{q_1}) \\
&= \frac{1}{2}G(x_1)\varsigma_1^4 - \left(n - \frac{1}{2}\right)G(x_1)\varsigma_1^4 + \vartheta_1(t) \\
&\quad \cdot G(x_1)[\varsigma_1]^{((4\sigma-\mu-1)/\sigma)}(x_2^{q_1} - \xi_2^{q_1}) \\
&\leq -\frac{1}{2}G(x_1)\varsigma_1^4 - \left(n - \frac{1}{2}\right)\varsigma_1^4 + \vartheta_1(t) \\
&\quad \cdot G(x_1)[\varsigma_1]^{((4\sigma-\mu-1)/\sigma)}(x_2^{q_1} - \xi_2^{q_1}).
\end{aligned} \tag{13}$$

*Step 2.* We denote  $\varsigma_2 = [x_2]^{\sigma/v_2} - [\xi_2]^{\sigma/v_2}$  and define the positive Lyapunov function  $V_2$  on  $\Pi_2$  as  $V_2 = V_1 + \Psi_2$  with

$$\Psi_2 = \int_{\xi_2}^{x_2} \left[|r|^{(\sigma/v_2)} - [\xi_2]^{(\sigma/v_2)}\right]^{((4\sigma-\mu-1)/\sigma)} dr. \tag{14}$$

Since  $(\partial[\xi_2]^{(\sigma/v_2)}/\partial x_1) = -(\partial\lambda_1^{(\sigma/v_2)}(x_1)/[x_1]^\sigma - \sigma\lambda_1^{(\sigma/v_2)}(x_1)|x_1|^{(\sigma-1)})$  is valid, one can obtain

$$\begin{aligned}
\frac{\partial\Psi_2}{\partial x_2} &= [\varsigma_2]^{((4\sigma-\mu-1)/\sigma)}, \\
\frac{\partial\Psi_2}{\partial x_1} &= \frac{-4\sigma-\mu-v_2}{\sigma} \frac{\partial[\xi_2]^{(\sigma/v_2)}}{\partial x_1} \int_{\xi_2}^{x_2} \left| |r|^{(\sigma/v_2)} - [\xi_2]^{(\sigma/v_2)} \right|^{((3\sigma-\mu-v_2)/\sigma)} dr, \\
\frac{\partial^2\Psi_2}{\partial x_1\partial x_2} &= \frac{4\sigma-\mu-v_2}{\sigma} [\varsigma_2]^{((3\sigma-\mu-v_2)/\sigma)} \frac{\partial[\xi_2]^{(\sigma/v_2)}}{\partial x_1}, \\
\frac{\partial^2\Psi_2}{\partial x_2^2} &= \frac{4\sigma-\mu-v_2}{v_2} |x_2|^{(\sigma-v_2)/v_2} [\varsigma_2]^{((3\sigma-\mu-v_2)/\sigma)}, \\
\frac{\partial^2\Psi_2}{\partial x_1^2} &= \frac{-4\sigma-\mu-v_2}{\sigma} \frac{\partial^2[\xi_2]^{(\sigma/v_2)}}{\partial x_1^2} \int_{\xi_2}^{x_2} \left| |r|^{(\sigma/v_2)} - [\xi_2]^{(\sigma/v_2)} \right|^{((3\sigma-\mu-v_2)/\sigma)} dr \\
&\quad + \frac{4\sigma-\mu-v_2}{\sigma} \times \frac{3\sigma-\mu-v_2}{\sigma} \left(\frac{\partial[\xi_2]^{(\sigma/v_2)}}{\partial x_1}\right)^2 \int_{\xi_2}^{x_2} \left| |r|^{(\sigma/v_2)} - [\xi_2]^{(\sigma/v_2)} \right|^{((2\sigma-\mu-v_2)/\sigma)} dr.
\end{aligned} \tag{15}$$

Using Definition 1 again, we have

$$\begin{aligned}
\ell V_2 &\leq -\frac{1}{2}G(x_1)\varsigma_1^4 - \left(n - \frac{1}{2}\right)\varsigma_1^4 + \vartheta_1(t)G(x_1)[x_1]^{4\sigma-\mu-1}(x_2^{q_1} - \xi_2^{q_1}) + \frac{\partial\Psi_2}{\partial x_1}(\vartheta_1(t)x_2^{q_1} + f_1(x_1)) \\
&\quad + \frac{\partial\Psi_2}{\partial x_1}f_2(\bar{x}_2) + \frac{1}{2}tr\left\{\bar{g}_2^T \frac{\partial^2\Psi_2}{\partial \bar{x}_2^2} \bar{g}_2\right\} + \frac{\partial\Psi_2}{\partial x_2}\vartheta_2(t)\xi_3^{q_2} + \frac{\partial\Psi_2}{\partial x_2}\vartheta_2(t)(x_3^{q_2} - \xi_3^{q_2}),
\end{aligned} \tag{16}$$

where  $\xi_3$  is the virtual controller required to be designed later.

In the following, each term in the right hand of (16) will be estimated by its upper bound.

Firstly, applying  $0 < (v_2/\sigma) \leq 1$ ,  $0 < ((1 + \mu)/\sigma) \leq 1$  and Lemma 5, it is easily obtained that

$$|x_2 - \xi_2| \leq \left| [x_2]^{\sigma/v_2} - [\xi_2]^{\sigma/v_2} \right|^{v_2/\sigma} \times 2^{1-(v_2/\sigma)} \leq 2|\zeta_2|^{v_2/\sigma}, \quad (17)$$

$$|x_2|^{q_1} \leq \left| \zeta_2 + [\xi_2]^{\sigma/v_2} \right|^{(1+\mu)/\sigma} \leq |\zeta_2|^{(1+\mu)/\sigma} + \lambda_1^{(1+\mu)/v_2} |\zeta_2|^{(1+\mu)/\sigma}, \quad (18)$$

$$|x_2^{q_1} - \xi_2^{q_1}| \leq 2^{1-(1+\mu)/\sigma} \left| [x_2]^{\sigma/v_2} - [\xi_2]^{\sigma/v_2} \right|^{(1+\mu)/\sigma} \leq 2|\zeta_2|^{(1+\mu)/\sigma}. \quad (19)$$

It can be deduced from (19) and Lemma 3 that

$$\begin{aligned} \vartheta_1(t)G(x_1)[x_1]^{4\sigma-\mu-1} (x_2^{q_1} - \xi_2^{q_1}) &\leq 2\bar{\vartheta}_1 G(x_1) |\zeta_1|^{(4\sigma-\mu-1)/\sigma} \\ &\cdot |\zeta_2|^{(\mu+1)/\sigma} \leq \frac{1}{8}\gamma_1^4 + H_{21}(\bar{x}_2)\zeta_2^4, \end{aligned} \quad (20)$$

where  $H_{21}(\bar{x}_2) \geq ((\mu+1)/4\sigma)(2\bar{\vartheta}_1 G(x_1))^{4\sigma/(\mu+1)} (4\sigma/(8(4\sigma-\mu-1)))^{-(4\sigma-\mu-1)/(1+\mu)} \geq 0$  is a  $C^2$  function.

Secondly, one can obtain from Assumption 1 and Lemma 4 that

$$\begin{aligned} |f_2(\bar{x}_2)| &\leq \tilde{\psi}_2(\bar{x}_2) \left[ |x_1|^{(v_2+\mu)/v_1} + |x_2|^{(v_2+\mu)/v_2} \right] \\ &\leq \tilde{\psi}_2(\bar{x}_2) \left[ |\zeta_1|^{(v_2+\mu)/\sigma} + \lambda_1^{(v_2+\mu)/v_2} |\zeta_1|^{(v_2+\mu)/\sigma} \right. \\ &\quad \left. + |\zeta_2|^{(v_2+\mu)/\sigma} \right] \\ &\leq \tilde{\psi}_2(\bar{x}_2) \left[ |\zeta_1|^{(v_2+\mu)/\sigma} + \zeta_2^{(v_2+\mu)/\sigma} \right], \end{aligned} \quad (21)$$

$$\begin{aligned} \|g_2(\bar{x}_2)\| &\leq \eta_2(\bar{x}_2) \left[ |x_1|^{(2v_2+\mu)/2v_1} + |x_2|^{(2v_2+\mu)/2v_2} \right] \\ &\leq \eta_2(\bar{x}_2) \left[ |\zeta_1|^{(2v_2+\mu)/2\sigma} + \lambda_1^{(2v_2+\mu)/2v_2} |\zeta_1|^{(2v_2+\mu)/2\sigma} \right. \\ &\quad \left. + |\zeta_2|^{(2v_2+\mu)/2\sigma} \right] \leq \bar{\eta}_2(\bar{x}_2) \\ &\cdot \left[ |\zeta_1|^{(2v_2+\mu)/2\sigma} + |\zeta_2|^{(2v_2+\mu)/2\sigma} \right], \end{aligned} \quad (22)$$

where  $\tilde{\psi}_2(\bar{x}_2) \geq \psi_2(\bar{x}_2)(1 + \lambda_1^{(v_2+\mu)/v_2})$  and  $\bar{\eta}_2(\bar{x}_2) \geq \eta_2(\bar{x}_2)(1 + \lambda_1^{(2v_2+\mu)/2v_2})$  are nonnegative smooth functions.

Additionally, note that  $(\sigma/v_2) \geq 2$ . Then, as stated in [36], there exist  $C^2$  functions  $M_{21}(\bar{x}_2) \geq 0$ ,  $K_{21}(\bar{x}_2) \geq 0$ , and  $\tilde{M}_{21}(\bar{x}_2) \geq 0$ , such that

$$\left| \frac{\partial [\xi_2]^{\sigma/v_2}}{\partial x_1^2} \right| \leq \left| \frac{\partial \lambda_1^{\sigma/v_2}}{\partial x_1} \right| |x_1|^\sigma + \sigma \lambda_1^{\sigma/v_2} |x_1|^{\sigma-1} \leq M_{21}(\bar{x}_2) |\zeta_1|^{1-(1/\sigma)}, \quad (23)$$

$$\begin{aligned} \left| \frac{\partial^2 [\xi_2]^{\sigma/v_2}}{\partial x_1^2} \right| &\leq \left| \frac{\partial^2 \lambda_1^{\sigma/v_2}}{\partial x_1^2} \right| |x_1|^\sigma + 2\sigma \left| \frac{\partial \lambda_1^{\sigma/v_2}}{\partial x_1} \right| |x_1|^{\sigma-1} \\ &\quad + \sigma(\sigma-1) \lambda_1^{\sigma/v_2} |x_1|^{\sigma-2} \leq K_{21}(\bar{x}_2) |\zeta_1|^{1-(2/\sigma)}, \end{aligned} \quad (24)$$

$$\begin{aligned} \frac{\partial \Psi_2}{\partial x_1} &\leq \frac{4\sigma - \mu - v_2}{\sigma} \left| \frac{\partial [\xi_2]^{\sigma/v_2}}{\partial x_1} \right| \left| [x_2]^{\sigma/v_2} - [\xi_2]^{\sigma/v_2} \right|^{(3\sigma-\mu-v_2)/\sigma} \\ &\quad \cdot |x_2 - \xi_2| \leq \frac{4\sigma - \mu - v_2}{\sigma} \\ &\quad \times M_{21}(\bar{x}_2) |\zeta_1|^{1-(1/\sigma)} |\zeta_2|^{(3\sigma-\mu-v_2)/\sigma} \times 2|\zeta_2|^{v_2/\sigma} \\ &\leq \tilde{M}_{21}(\bar{x}_2) |\zeta_1|^{1-(1/\sigma)} |\zeta_2|^{(3\sigma-\mu)/\sigma}, \end{aligned} \quad (25)$$

$$\begin{aligned} \frac{1}{2} \frac{\partial^2 \Psi_2}{\partial x_1^2} &\leq \frac{4\sigma - \mu - v_2}{2\sigma} \left| \frac{\partial^2 [\xi_2]^{\sigma/v_2}}{\partial x_1^2} \right| \left| [x_2]^{\sigma/v_2} - [\xi_2]^{\sigma/v_2} \right|^{(3\sigma-\mu-v_2)/\sigma} \\ &\quad \cdot |x_2 - \xi_2| + \frac{(4\sigma - \mu - v_2)(3\sigma - \mu - v_2)}{2\sigma^2} \left( \frac{\partial [\xi_2]^{\sigma/v_2}}{\partial x_1} \right) \\ &\quad \cdot \left| [x_2]^{\sigma/v_2} - [\xi_2]^{\sigma/v_2} \right|^{(2\sigma-\mu-v_2)/\sigma} |x_2 - \xi_2| \\ &\leq \frac{4\sigma - \mu - v_2}{\sigma} K_{21}(\bar{x}_2) |\zeta_1|^{1-(2/\sigma)} |\zeta_2|^{(3\sigma-\mu)/\sigma} \\ &\quad + \frac{(4\sigma - \mu - v_2)(3\sigma - \mu - v_2)}{\sigma^2} \\ &\quad \cdot M_{21}^2(\bar{x}_2) |\zeta_1|^{2-(2/\sigma)} |\zeta_2|^{2\sigma-\mu/\sigma}. \end{aligned} \quad (26)$$

Then, using (18), (21), (25), Assumptions 1-2, and Lemma 3, we can infer

$$\begin{aligned} \frac{\partial \Psi_2}{\partial x_1} (\vartheta_1(t)x_2^{q_1} + f_1(x_1)) &\leq \tilde{M}_{21}(\bar{x}_2) \bar{\vartheta}_1 |\zeta_1|^{1-(1/\sigma)} |\zeta_2|^{(3\sigma-\mu)/\sigma} \\ &\quad \cdot \left( |\zeta_2|^{(1-\mu)/\sigma} + |\lambda_1|^{(1+\mu)/\sigma} \right) \\ &\quad + \tilde{M}_{21}(\bar{x}_2) |\zeta_1|^{1-(1/\sigma)} |\zeta_2|^{(3\sigma-\mu)/\sigma} \\ &\quad \cdot \tilde{\psi}_1 |\zeta_1|^{1-(1/\sigma)} \leq \frac{1}{8}\zeta_1^4 + H_{22}(\bar{x}_2)\zeta_2^4, \end{aligned} \quad (27)$$



where

$$\begin{aligned}
H_{22}(\bar{x}_2) \geq & \frac{3\sigma+1}{4\sigma} (\bar{\vartheta}_1 \tilde{M}_{21})^{(4\sigma/(3\sigma+1))} \left( \frac{4\sigma}{32(\sigma-1)} \right)^{-(\sigma-1)/3\sigma+1} \\
& + \frac{3\sigma-\mu}{4\sigma} (\bar{\vartheta}_1 \tilde{M}_{21} \lambda_1^{(1+\sigma)/v_2})^{(4\sigma/(3\sigma-\mu))} \\
& \cdot \left( \frac{4\sigma}{32(\sigma+\mu)} \right)^{((-\sigma+\mu)/3\sigma-\mu)} \\
& + \frac{3\sigma-\mu}{4\sigma} (\psi_1 \tilde{M}_{21})^{(4\sigma/(3\sigma-\mu))} \\
& \cdot \left( \frac{4\sigma}{16(\sigma+\mu)} \right)^{((-\sigma+\mu)/3\sigma-\mu)}, \tag{28}
\end{aligned}$$

is a nonnegative  $C^2$  function.

Moreover, from (19), Assumption 2, and Lemma 3, it can be deduced that

$$\begin{aligned}
\frac{\partial \Psi_2}{\partial x_2} f_2(\bar{x}_2) \leq & |\zeta_2|^{(4\sigma-\mu-v_2)/\sigma} \left[ \tilde{\psi}_2 \left( |\zeta_1|^{(v_2+\mu)/\sigma} + \zeta_2^{(v_2+\mu)/\sigma} \right) \right] \\
\leq & \frac{1}{8} \zeta_1^4 + H_{23}(\bar{x}_2) \zeta_2^4, \tag{29}
\end{aligned}$$

where  $H_{23}(\bar{x}_2) \geq \tilde{\psi}_2 + ((4\sigma-\mu-v_2)/4\sigma) (\tilde{\psi}_2)^{4\sigma/(4\sigma-\mu-v_2)} (4\sigma/(8(\mu+v_2)))^{-(\mu+v_2)/(4\sigma-\mu-v_2)} \geq 0$  is a  $C^2$  function.

On the contrary, it is noted that

$$\begin{aligned}
\frac{1}{2} \text{tr} \left\{ \bar{g}_2^T \frac{\partial^2 \Psi_2}{\partial \bar{x}_2^2} \bar{g}_2 \right\} = & \frac{1}{2} \frac{\partial^2 \Psi_2}{\partial x_1^2} \|g_1\|^2 + g_1^T \frac{\partial^2 \Psi_2}{\partial x_1 \partial x_2} g_2 \\
& + \frac{1}{2} \frac{\partial^2 \Psi_2}{\partial x_2^2} \|g_2\|^2. \tag{30}
\end{aligned}$$

Then, applying (22), (26), Assumption 2, and Lemma 3, there clearly exist nonnegative  $C^2$  functions  $H_{241}(\bar{x}_2)$ ,  $H_{242}(\bar{x}_2)$ , and  $H_{243}(\bar{x}_2)$  such that

$$\begin{aligned}
\frac{1}{2} \frac{\partial^2 \Psi_2}{\partial x_1^2} \|g_1\|^2 \leq & \frac{4\sigma-\mu-v_2}{\sigma} K_{21} |\zeta_1|^{1-(2/\sigma)} |\zeta_2|^{(3\sigma-\mu)/\sigma} \eta_1^2 |\zeta_1|^{(2+\mu)/\sigma} \\
& + \frac{(4\sigma-\mu-v_2)(3\sigma-\mu-v_2)}{2\sigma^2} \\
& \cdot M_{21}^2 |\zeta_1|^{2-(2/\sigma)} |\zeta_2|^{(2\sigma-\mu)/\sigma} \eta_1^2 |\zeta_1|^{(2+\mu)/\sigma} \\
\leq & \frac{1}{24} \zeta_1^4 + H_{241}(\bar{x}_2) \zeta_2^4, \tag{31}
\end{aligned}$$

$$\begin{aligned}
g_1^T \frac{\partial^2 \Psi_2}{\partial x_1 \partial x_2} g_2 \leq & \eta_1 |\zeta_1|^{(\mu+2)/2\sigma} \frac{4\sigma-\mu-v_2}{\sigma} |\zeta_2|^{(3\sigma-\mu-v_2)/\sigma} \\
& \times M_{21} |\zeta_1|^{(\sigma-1)/\sigma} \bar{\eta}_2 \left( |\zeta_1|^{(2v_2+\mu)/2\sigma} \right. \\
& \left. + |\zeta_2|^{(2v_2+\mu)/2\sigma} \right) \leq \frac{1}{24} \zeta_1^4 + H_{242}(\bar{x}_2) \zeta_2^4, \tag{32}
\end{aligned}$$

$$\begin{aligned}
\frac{1}{2} \frac{\partial^2 \Psi_2}{\partial x_2^2} \|g_2\|^2 \leq & \frac{4\sigma-\mu-v_2}{2v_2} |\zeta_2|^{(3\sigma-\mu-v_2)/\sigma} \\
& \cdot \left( |\zeta_2|^{((\sigma-v_2)/\sigma)} + \lambda_1^{((\sigma-v_2)/v_2)} |\zeta_1|^{((\sigma-v_2)/\sigma)} \right) \\
& \times 2\bar{\eta}_2^2 \left( |\zeta_1|^{(2v_2+\mu)/\sigma} + |\zeta_2|^{(2v_2+\mu)/\sigma} \right) \\
\leq & \frac{1}{24} \zeta_1^4 + H_{243}(\bar{x}_2) \zeta_2^4. \tag{33}
\end{aligned}$$

Substituting equations (31)–(33) into (30), one obtains

$$\frac{1}{2} \text{tr} \left\{ \bar{g}_2^T \frac{\partial^2 \Psi_2}{\partial \bar{x}_2^2} \bar{g}_2 \right\} \leq \frac{1}{8} \zeta_1^4 + H_{24}(\bar{x}_2) \zeta_2^4, \tag{34}$$

where  $H_{24}(\bar{x}_2) = H_{241}(\bar{x}_2) + H_{242}(\bar{x}_2) + H_{243}(\bar{x}_2) \geq 0$  is a  $C^2$  function.

Let  $H_2(\bar{x}_2) = H_{21}(\bar{x}_2) + H_{22}(\bar{x}_2) + H_{23}(\bar{x}_2) + H_{24}(\bar{x}_2) \geq 0$ . Design the virtual controller  $\xi_3$  as

$$\begin{aligned}
\xi_3 = & -\lambda_2(\bar{x}_2) [\zeta_2]^{(v_3/\sigma)} \text{ with } \lambda_2(\bar{x}_2) \\
= & \left( \frac{n-1+H_2(\bar{x}_2)}{\vartheta_2} \right)^{1/q_2} > 0. \tag{35}
\end{aligned}$$

Substituting (20), (27), (29), (34), and (35) into (16), one can obtain

$$\begin{aligned}
\mathcal{L}V_2 \leq & -\frac{1}{2} G(x_1) \zeta_1^4 - (n-1) (\zeta_1^4 + \zeta_2^4) + \vartheta_2(t) [\zeta_2]^{(4\sigma-\mu-v_2)/\sigma} \\
& \cdot (x_3^{q_2} - \xi_3^{q_2}). \tag{36}
\end{aligned}$$

*Inductive Step.* Suppose at step  $i-1$ , there exist a  $C^2$  Lyapunov function  $V_{i-1}: \Pi_{i-1} \rightarrow R^+$ , and a range of continuous virtual controllers  $\xi_1, \xi_2, \dots, \xi_i$  defined as

$$\begin{aligned}
\xi_1 = & 0, \\
\xi_1 = & [x_1]^{\sigma/v_1} - [\xi_1]^{\sigma/v_1}, \\
\xi_2 = & -\lambda(x_1) [\zeta_1]^{v_2/\sigma}, \\
\xi_2 = & [x_2]^{\sigma/v_2} - [\xi_2]^{\sigma/v_2}, \\
\xi_3 = & -\lambda_2(\bar{x}_2) [\zeta_2]^{v_3/\sigma}, \\
\xi_3 = & [x_3]^{\sigma/v_3} - [\xi_3]^{\sigma/v_3}, \\
& \vdots \\
\xi_i = & -\lambda_{i-1}(\bar{x}_{i-1}) [\zeta_{i-1}]^{v_i/\sigma}, \\
\xi_i = & [x_i]^{\sigma/v_i} - [\xi_i]^{\sigma/v_i}, \tag{37}
\end{aligned}$$

with  $\lambda_k(\bar{x}_k) > 0$ , for  $k = 1, \dots, i-1$ , such that

$$\begin{aligned} \ell V_{i-1} \leq & -\frac{1}{2}G(x_1)\zeta_1^4 - (n+2-i) \\ & \cdot \sum_{l=1}^{i-1} \zeta_l^4 + \vartheta_{i-1}(t)[\zeta_{i-1}]^{(4\sigma-\mu-v_i)/\sigma} (x_i^{q_{i-1}} - \xi_i^{q_{i-1}}). \end{aligned} \quad (38)$$

Then, the following property can be inferred.

**Proposition 1.** Choose the  $i$ th Lyapunov function  $V_i: \Pi_i \rightarrow R^+$  as  $V_i = V_{i-1} + \Psi_i$  with

$$\Psi_i = \int_{\xi_i}^{x_i} [[r]^{\sigma/v_i} - [\xi_i]^{\sigma/v_i}]^{(4\sigma-\mu-v_i)/\sigma} dr. \quad (39)$$

Then,  $V_i$  is  $C^2$  on  $\Pi_i$  and there exists a virtual controller  $\xi_{i+1}$  such that

$$\begin{aligned} \ell V_i \leq & -\frac{1}{2}G(x_1)\zeta_1^4 - (n+1-i) \sum_{l=1}^i \zeta_l^4 + \vartheta_{i-1}(t)[\zeta_i]^{(4\sigma-\mu-v_i)/\sigma} \\ & \cdot (x_{i+1}^{q_i} - \xi_{i+1}^{q_i}), \end{aligned} \quad (40)$$

where

$$\begin{aligned} \xi_{i+1} &= -\lambda_i(\bar{x}_i)[\zeta_i]^{v_{i+1}/\sigma} \text{ with } \lambda_i(\bar{x}_i) \\ &= \left[ \frac{n-i+1+H_i(\bar{x}_i)}{\underline{\vartheta}_i} \right]^{1/q_i} > 0. \end{aligned} \quad (41)$$

The proof of above Proposition 1 is provided in the Appendix.

*Step 3.* In light of the inductive step, when  $i = n$  and  $x_{n+1} = u$ , Proposition 1 holds. Thus, we choose the overall Lyapunov function  $V_n$  as  $V_n = V_{n-1} + \Psi_n$  with

$$\Psi_n = \int_{\xi_n}^{x_n} [[r]^{\sigma/v_n} - [\xi_n]^{\sigma/v_n}]^{(4\sigma-\mu-v_n)/\sigma} dr, \quad (42)$$

and define the virtual controller  $\xi_{n+1}$  as

$$\xi_{n+1} = -\lambda_n(x)[\zeta_n]^{v_{n+1}/\sigma} \text{ with } \lambda_n(x) = \left[ \frac{1+H_n(x)}{\underline{\vartheta}_n} \right]^{1/q_n} > 0. \quad (43)$$

Then,  $V_n(x)$  is clearly a  $C^2$  function on  $\Pi_n$ , and it is easy to obtain that

$$\ell V_n \leq -\frac{1}{2}G(x_1)\zeta_1^4 - \sum_{l=1}^n \zeta_l^4 + \vartheta_n(t)[\zeta_n]^{(4\sigma-\mu-v_n)/\sigma} (u^{q_n} - \xi_{n+1}^{q_n}). \quad (44)$$

Therefore, we can design

$$\begin{aligned} u = \xi_{n+1}(x) &= -\lambda_n(x)[x_n]^{\sigma/v_n} \\ &+ \lambda_{n-1}^{\sigma/v_n}[x_{n-1}]^{\sigma/v_{n-1}} + \lambda_{n-1}^{\sigma/v_n}\lambda_{n-2}^{\sigma/v_{n-2}}[x_{n-2}]^{\sigma/v_{n-2}} \\ &+ \dots + \lambda_{n-1}^{\sigma/v_n}\lambda_{n-2}^{\sigma/v_{n-2}} \dots \lambda_1^{\sigma/v_2}[x_1]^{\sigma/v_1}]^{v_n+\mu/\sigma q_n}, \end{aligned} \quad (45)$$

which results in

$$\ell V_n \leq -\frac{1}{2}G(x_1)\zeta_1^4 - \sum_{l=1}^n \zeta_l^4 \leq 0. \quad (46)$$

**3.2.2. Part II: Verification of Keeping the Output Constraint.** For any  $x(0) = (x_1(0))^T \in \Pi_n$ , by Ito's formula and (46), we can deduce

$$\begin{aligned} 0 \leq EV_n(x(t)) &= V_n(x(0)) + E \int_0^t \ell V_n(x(\tau)) dr \\ &\leq V_n(x(0)) < \infty. \end{aligned} \quad (47)$$

From  $V_n(x) = V_1(x_1) + \sum_{l=2}^n \Psi_l > 0$  and (47), it can be further verified that

$$0 \leq EV_1(x_1(t)) \leq V_n(x_0) < \infty, \quad (48)$$

which indicates

$$P\{V_1(x_1(t)) < \infty\} = 1. \quad (49)$$

Hence,  $P\{|y(t)| < b\} = P\{|x_1(t)| < b\} = 1$ . Then, Part I of Theorem 1 is proved.

**3.2.3. Part III: Stability Analysis.** Based on the definition of  $V_n$ , we easily obtain the fact that  $V_n$  is radially unbounded. Combining the fact with (40) and Lemma 1 directly infers that system (1) has a solution  $x(t, x(0))$  for any  $x(0) \in \Pi_n$ .

On the contrary, by a simple calculation, one obtains

$$\begin{aligned} V_n &= V_1 + \sum_{l=2}^n \Psi_l \\ &= V_1 + \sum_{l=2}^n \int_{\xi_l}^{x_l} [[r]^{\frac{\sigma}{v_l}} - [\xi_l]^{\frac{\sigma}{v_l}}]^{(4\sigma-\mu-v_l)/\sigma} dr \\ &\leq \frac{2b^{4\sigma-\mu}}{(4\sigma-\mu)\pi} \tan\left(\frac{\pi|x_1|^{4\sigma-\mu}}{2b^{4\sigma-\mu}}\right) + 2 \sum_{l=2}^n |\zeta_l|^{(4\sigma-\mu)/\sigma}. \end{aligned} \quad (50)$$

In addition, since  $4\sigma - \mu > 1$ , it is easy to get that  $0 \leq (\pi|x_1|^{4\sigma-\mu}/2b^{4\sigma-\mu}) < (\pi/2)$  for all  $x_1 \in \Pi_1$ . Then, applying the characteristics of tangent functions, it is not difficult to infer that

$$\begin{aligned} \tan\left(\frac{\pi|x_1|^{4\sigma-\mu}}{2b^{4\sigma-\mu}}\right) &\leq \frac{\pi}{2b^{4\sigma-\mu}}|x_1|^{4\sigma-\mu}G(x_1) \\ &\leq \frac{\pi(4\sigma-\mu)}{2b^{4\sigma-\mu}}|x_1|^{4\sigma-\mu}G(x_1). \end{aligned} \quad (51)$$

Now, let  $c = 2^{(\mu-8\sigma)/(4\sigma-\mu)^4} > 0$  and  $0 < \gamma = (4\sigma/(4\sigma-\mu)) < 1$ . According to (44), (45), and Lemma 4, we obtain

$$\begin{aligned} cV_n^\gamma &\leq 2^{(\mu-8\sigma)/(4\sigma-\mu)} \left[ \frac{2b^{4\sigma-\mu}}{(4\sigma-\mu)\pi} \tan\left(\frac{\pi|x_1|^{4\sigma-\mu}}{2b^{4\sigma-\mu}}\right) + 2 \sum_{l=1}^n |\zeta_1|^{\frac{4\sigma-\mu}{\sigma}} \right]^{4\sigma/(4\sigma-\mu)} \\ &\leq 2^{(\mu-8\sigma)/(4\sigma-\mu)} G(x_1)^{4\sigma/(4\sigma-\mu)} \zeta_1^4 \\ &\quad + \frac{1}{2} \sum_{l=1}^n \zeta_1^4 \leq \frac{1}{2} G(x_1) \zeta_1^4 + \frac{1}{2} \sum_{l=1}^n \zeta_1^4. \end{aligned} \quad (52)$$

So, one further obtains

$$\begin{aligned} \ell V_n + cV_n^\gamma &= \ell V_n + 2^{(\mu-8\sigma)/(4\sigma-\mu)} V_n^{4\sigma/(4\sigma-\mu)} \\ &\leq -\frac{1}{2} G(x_1) \zeta_1^4 - \sum_{l=1}^n \zeta_1^4 \\ &\quad + \frac{1}{2} G(x_1) \zeta_1^4 + \frac{1}{2} \sum_{l=1}^n \zeta_1^4 \leq -\frac{1}{2} \sum_{l=1}^n \zeta_1^4 \leq 0. \end{aligned} \quad (53)$$

In other words,  $\ell V_n \leq -cV_n^\gamma$ . Consequently, it is directly deduced from Lemma 2 that the origin of system (1) under controller (39) is finite-time stable in probability.

*Remark 3.* Comparing with the existing results in most of the literatures, the paper mainly focuses on the finite-time stabilization, instead of the boundness of tracking error. Moreover, the proposed approach can be extend to the tracking control by introducing a coordinate transformation before constructing the BLF.

#### 4. Simulation

In this section, we will provide the simulation results of the following example to illustrate the validity of the proposed strategy:

$$\begin{cases} dx_1 = x_2^{7/5} dt, \\ dx_2 = udt + \frac{1}{2}x_1^2 x_2^{1/5} dt + \frac{1}{8}(\sin x_2)^2 x_2^{3/5} d\omega, \\ y = x_1, \end{cases} \quad (54)$$

where  $q_1 = 7/5$ ,  $q_2 = 1$ , and  $\mu = -4/11 \in (-(5/12), 0)$ . Then,  $v_1 = 1$ ,  $v_2 = 5/11$ , and  $v_3 = 1/11$ . Since  $\vartheta_1(t) = \vartheta_2(t) = 1$ ,

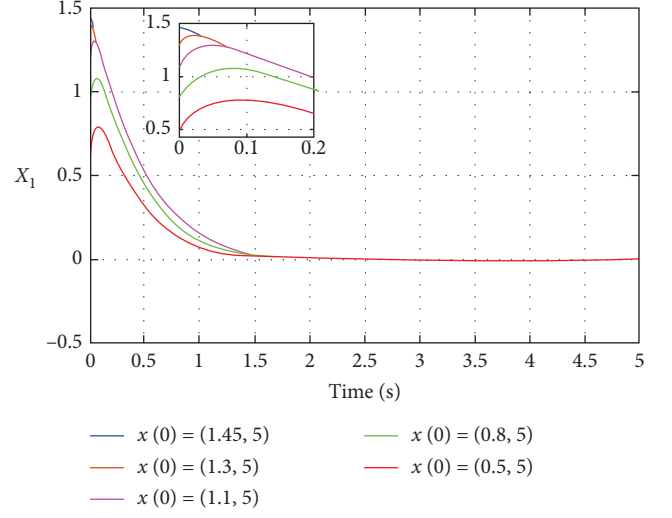


FIGURE 1: Trajectories of  $x_1(t)$ .

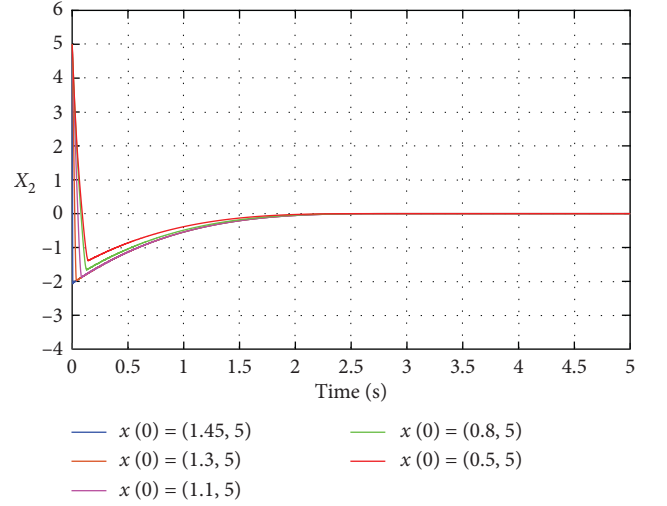


FIGURE 2: Trajectories of  $x_2(t)$ .

Assumption 1 is satisfied. And Assumption 2 is also satisfied with  $\psi_1 = \eta_1 = 0$ ,  $\psi_2 = (1/2)x_1^2$ , and  $\eta_2 = (1/8)(\sin x_2)^2$ . Furthermore, note that  $c_1 = 1, c_2 = 11/5 > 2$ , and  $\sigma_0 = 1$ . Thus, one can select  $\sigma = \sigma_0 = 1$ .

Now, let  $\zeta_1 = [x_1]$  and  $G(x_1) = \sec^2(\pi|x_1|^{48/11}/2b^{48/11})$ . In view of design procedure in Part I of the proof, we can design the virtual controller  $\xi_2$  as

$$\xi_2 = -2^{5/7} [\zeta_1]^{5/11} := -\lambda_1 [\zeta_1]^{5/11}. \quad (55)$$

Next, according to the design procedure, we denote  $\zeta_2 = [x_2]^{11/5} - [\xi_2]^{11/5}$  and further obtain that

$$\begin{aligned}
H_{21} &= \frac{7}{44}(2G(x_1))^{44/7} \left(\frac{44}{296}\right)^{-37/7}, \\
H_{22} &= \frac{86}{11}\lambda_1^{11/5} + \frac{37}{44} \left(\frac{86}{11}\lambda_1^{18/5}\right)^{44/37} \left(\frac{44}{56}\right)^{-7/37}, \\
H_{23} &= \frac{1}{2}x_1^2\lambda_1^{1/7} + \frac{43}{44} \left(\frac{1}{2}x_1^2\lambda_1^{1/7}\right)^{44/43} \left(\frac{44}{8}\right)^{-1/43}, \\
H_{24} &= \frac{37}{320}(\sin x_2)^4 + \frac{32}{44} \left(\frac{37}{320}(\sin x_2)^4\lambda_1^{12/5}\right)^{44/32} \left(\frac{44}{96}\right)^{-12/32}. \tag{56}
\end{aligned}$$

Let  $H_2 = H_{21} + H_{22} + H_{23} + H_{24}$  and  $\lambda_2 = 1 + H_2$ ; then, the controller  $u$  can be designed as

$$u = -\lambda_2[\zeta_2]^{1/11} = -\lambda_2[x_2]^{11/5} - [\zeta_2]^{11/5}]^{1/11}. \tag{57}$$

Finally, we suppose  $b = 1.5$  and select some different initial states  $x(0)$ 's with each  $x(0)$  satisfying  $x(0) \in \Pi_2$ . The simulation results of system (48) are shown in Figures 1 and 2. Figure 1 curves trajectories of  $x_1(t)$  under different initial values, which illustrate that the output constraint is always not violated. Meanwhile, the trajectories of  $x_2(t)$  is given in Figure 2. It can be observed from the two figures that system (48) under controller (51) is finite-time stable.

## 5. Conclusion

In this paper, the stability issue is addressed for a class of  $p$ -norm stochastic systems with output constraints and unknown time-varying parameters. Using a tan-type BLF, the finite-time control strategy is proposed by the adding a power integrator technique. On this basis, the designed controller has been proved to ensure that the origin of the closed-loop system is finite-time stable in probability and the system output is kept in a pre-given set. This conclusion has also been verified by the simulation results. It should be pointed out that the proposed approach is not applicable to the case of asymmetrical output constraints. In the future, we will try to modify the proposed method to be suitable for stochastic systems with asymmetrical output constraints or multi-input multi-output stochastic systems.

## Appendix

*Proof of Proposition 1.* For  $j, k = 1, \dots, i-1$ , one can get from the definition of  $\Psi_i$  that

$$\begin{aligned}
\frac{\partial \Psi_i}{\partial x_i} &= |\zeta_i|^{(4\sigma - \mu - v_i)/\sigma}, \\
\frac{\partial \Psi_i}{\partial x_j} &= \frac{-4\sigma + \mu + v_i}{\sigma} \frac{\partial [\xi_i]^{\sigma/v_i}}{\partial x_j} \int_{\xi_i}^{x_i} \left| [r]^{\sigma/v_i} - [\xi_i]^{\sigma/v_i} \right|^{(3\sigma - \mu - v_i)/\sigma} dr, \\
\frac{\partial^2 \Psi_i}{\partial x_j \partial x_i} &= \frac{-4\sigma + \mu + v_i}{\sigma} |\zeta_i|^{(3\sigma - \mu - v_i)/\sigma} \frac{\partial [\xi_i]^{\sigma/v_i}}{\partial x_j}, \\
\frac{\partial^2 \Psi_i}{\partial x_j \partial x_k} &= \frac{\partial^2 \Psi_i}{\partial x_k \partial x_j} = \frac{-4\sigma + \mu + v_i}{\sigma} \frac{\partial^2 [\xi_i]^{\sigma/v_i}}{\partial x_k \partial x_j} \int_{\xi_i}^{x_i} \left| [r]^{\sigma/v_i} - [\xi_i]^{\sigma/v_i} \right|^{(3\sigma - \mu - v_i)/\sigma} dr \\
&\quad + \frac{4\sigma - \mu - v_i}{\sigma} \frac{3\sigma - \mu - v_i}{\sigma} \frac{\partial [\xi_i]^{\sigma/v_i}}{\partial x_j} \frac{\partial [\xi_i]^{\sigma/v_i}}{\partial x_k} \int_{\xi_i}^{x_i} \left| [r]^{\sigma/v_i} - [\xi_i]^{\sigma/v_i} \right|^{(2\sigma - \mu - v_i)/\sigma} dr, \\
\frac{\partial^2 \Psi_i}{\partial x_i^2} &= \frac{4\sigma - \mu - v_i}{v_i} |x_i|^{(\sigma - v_i)/v_i} |\zeta_i|^{(3\sigma - \mu - v_i)/\sigma}. \tag{A.1}
\end{aligned}$$

Then, we have

$$\begin{aligned}
\ell V_i &= \ell V_{i-1} + \sum_{j=1}^{i-1} \frac{\partial \Psi_i}{\partial x_j} (\vartheta_j(t) x_{j+1}^{q_j} + f_j) + \frac{\partial \Psi_i}{\partial x_j} (\vartheta_i(t) x_{i+1}^{q_i} + f_i) \\
&\quad + \frac{1}{2} \text{tr} \left\{ \bar{g}_i^T \frac{\partial^2 \Psi_i}{\partial \bar{x}_i^2} \bar{g}_i \right\} \\
&\leq -\frac{1}{2} G(x_1) \zeta_1^4 - (n+2-i) \sum_{l=1}^{i-1} \zeta_l^4 + \vartheta_{i-1}(t) \\
&\quad \cdot [\zeta_{i-1}]^{(4\sigma - \mu - v_{i-1})/\sigma} (x_i^{q_{i-1}} - \xi_i^{q_{i-1}}) \\
&\quad + \sum_{j=1}^{i-1} \frac{\partial \Psi_i}{\partial x_j} (\vartheta_j(t) x_{j+1}^{q_j} + f_j) + \frac{\partial \Psi_i}{\partial x_i} \vartheta_i(t) x_{i+1}^{q_i} + \frac{\partial \Psi_i}{\partial x_i} f_i \\
&\quad + \frac{1}{2} \text{tr} \left\{ \bar{g}_i^T \frac{\partial^2 \Psi_i}{\partial \bar{x}_i^2} \bar{g}_i \right\}.
\end{aligned} \tag{A.2}$$

In the following, we introduce some sub-propositions to simplify the proof.  $\square$

**Proposition A.1.** For  $i = 3, \dots, n$ , there exist smooth non-negative functions  $\tilde{\psi}_i(\cdot)$  and  $\tilde{\eta}_i(\cdot)$  such that

$$\begin{aligned}
|f_i(\bar{x}_i)| &\leq \psi_i(\bar{x}_i) \left[ |\zeta_1|^{(v_i+\mu)/\sigma} + \sum_{j=2}^i \left( |\zeta_j|^{(v_i+\mu)/\sigma} + \lambda_{j-1}^{(v_i+\mu)/v_j} |\zeta_{j-1}|^{(v_i+\mu)/\sigma} \right) \right] \leq \tilde{\psi}_i(\bar{x}_i) \sum_{j=1}^i |\zeta_j|^{(v_i+\mu)/\sigma}, \\
\|g_i(\bar{x}_i)\| &\leq \eta_i(\bar{x}_i) \left[ |\zeta_1|^{(2v_i+\mu)/2\sigma} + \sum_{j=2}^i \left( |\zeta_j|^{(2v_i+\mu)/2\sigma} + \lambda_{j-1}^{(2v_i+\mu)/2v_j} |\zeta_{j-1}|^{(2v_i+\mu)/2\sigma} \right) \right] \leq \tilde{\eta}_i(\bar{x}_i) \sum_{j=1}^i |\zeta_j|^{(2v_i+\mu)/2\sigma},
\end{aligned} \tag{A.5}$$

where  $\tilde{\psi}_i(\cdot) \geq [\sum_{j=1}^i (1 + \lambda_{j-1}^{(v_i+\mu)/v_j})] \psi_i(\cdot)$ ,  $\tilde{\eta}_i(\cdot) \geq [\sum_{j=1}^i (1 + \lambda_{j-1}^{(2v_i+\mu)/2v_j})] \eta_i(\cdot)$  are nonnegative smooth functions.  $\square$

**Proposition A.2.** For  $i = 3, \dots, n$ , there exist nonnegative  $C^2$  functions  $H_{i1}(\cdot)$  such that

$$\vartheta_{i-1}(t) [\zeta_{i-1}]^{(4\sigma - \mu - v_{i-1})/\sigma} (x_i^{q_{i-1}} - \xi_i^{q_{i-1}}) \leq \frac{1}{8} \zeta_{i-1}^4 + H_{i1}(\bar{x}_i) \zeta_i^4. \tag{A.6}$$

*Proof.* Since  $(v_{i-1} + \mu)/\sigma \leq 1$ , it can be gotten from Lemma 5 that

$$\begin{aligned}
|x_i^{q_{i-1}} - \xi_i^{q_{i-1}}| &\leq 2^{1 - ((v_{i-1} + \mu)/\sigma)} \left| [x_i]^{\sigma/v_i} - [\xi_i]^{\sigma/v_i} \right|^{((v_{i-1} + \mu)/\sigma)} \\
&\leq 2 |\zeta_i|^{((v_{i-1} + \mu)/\sigma)}.
\end{aligned} \tag{A.7}$$

From (A.7) and Lemma 3, one can verify that

$$\begin{aligned}
|f_i(\bar{x}_i)| &\leq \tilde{\psi}_i(\bar{x}_i) \left( |\zeta_1|^{(v_i+\mu)/\sigma} + \dots + |\zeta_i|^{(v_i+\mu)/\sigma} \right), \\
\|g_i(\bar{x}_i)\| &\leq \tilde{\eta}_i(\bar{x}_i) \left( |\zeta_1|^{(2v_i+\mu)/2\sigma} + \dots + |\zeta_i|^{(2v_i+\mu)/2\sigma} \right).
\end{aligned} \tag{A.3}$$

*Proof.* For  $i = 3, \dots, n, j = 1, \dots, i$ , one has

$$\begin{aligned}
|x_j|^{(v_i+\mu)/v_j} &= \left| \zeta_j + [\xi_j]^{v_j} \right|^{(v_i+\mu)/\sigma} \leq |\zeta_j|^{(v_i+\mu)/\sigma} \\
&\quad + \left| \lambda_{j-1}^{\sigma/v_j} [\zeta_{j-1}] \right|^{(v_i+\mu)/\sigma} \leq |\zeta_j|^{(v_i+\mu)/\sigma} \\
&\quad + \lambda_{j-1}^{(v_i+\mu)/v_j} |\zeta_{j-1}|^{(v_i+\mu)/\sigma}, \\
|x_j|^{(2v_i+\mu)/2v_j} &= \left| \zeta_j + [\xi_j]^{v_j} \right|^{(2v_i+\mu)/2\sigma} \leq |\zeta_j|^{(2v_i+\mu)/2\sigma} \\
&\quad + \left| \lambda_{j-1}^{\sigma/v_j} [\zeta_{j-1}] \right|^{(2v_i+\mu)/2\sigma} \leq |\zeta_j|^{(2v_i+\mu)/2\sigma} \\
&\quad + \left| \lambda_{j-1}^{(2v_i+\mu)/2v_j} \zeta_{j-1} \right|^{(2v_i+\mu)/2\sigma},
\end{aligned} \tag{A.4}$$

which means

$$\begin{aligned}
&\vartheta_{i-1}(t) [\zeta_{i-1}]^{(4\sigma - \mu - v_{i-1})/\sigma} (x_i^{q_{i-1}} - \xi_i^{q_{i-1}}) \\
&\leq 2 \bar{\vartheta}_{i-1} |\zeta_{i-1}|^{(4\sigma - \mu - v_{i-1})/\sigma} |\zeta_i|^{(v_{i-1} + \mu)/\sigma} \leq \frac{1}{8} \zeta_{i-1}^4 + H_{i1}(\bar{x}_i) \zeta_i^4,
\end{aligned} \tag{A.8}$$

where  $H_{i1}(\cdot) \geq 0$  is a  $C^2$  function.  $\square$

**Proposition A.3.** For  $i = 3, \dots, n$ , there exist nonnegative  $C^2$  functions  $H_{i2}(\cdot)$  such that

$$\sum_{j=1}^{i-1} \frac{\partial \Psi}{\partial x_j} (\vartheta_j(t) x_{j+1}^{q_j} + f_j) \leq \frac{1}{8} \sum_{l=4}^{i-1} \zeta_l^4 + H_{i2}(\bar{x}_i) \zeta_i^4. \tag{A.9}$$

*Proof.* For  $i = 3, \dots, n, j = 1, \dots, i-1$ , there are nonnegative  $C^2$  functions  $\tilde{M}_{ij}(\cdot), M_{ij}(\cdot)$  such that

$$\begin{aligned}
\left| \frac{\partial [\xi_i]^{\sigma/v_i}}{\partial x_j} \right| &= \left| \frac{\partial \lambda_{i-1}^{\sigma/v_i}(\bar{x}_{i-1})}{\partial x_j} \right| |\zeta_{i-1}| + \lambda_{i-1}^{\sigma/v_i}(\bar{x}_{i-1}) \left| \frac{\partial \lambda_{i-2}^{\sigma/v_{i-1}}(\bar{x}_{i-2})}{\partial x_j} \right| |\zeta_{i-2}| + \dots + \lambda_{i-1}^{\sigma/\tau_i}(\bar{x}_{i-1}) \times \lambda_{i-2}^{\sigma/(\tau_{i-1})}(\bar{x}_{i-2}) \times \dots \\
&\quad \times \lambda_{j+1}^{\sigma/v_{j+2}}(\bar{x}_{j+1}) \left| \frac{\partial \lambda_j^{\sigma/v_{i+1}}(\bar{x}_j)}{\partial x_j} \right| |\zeta_j| + \lambda_{i-1}^{\sigma/v_i}(\bar{x}_{i-1}) \times \lambda_{i-2}^{\sigma/v_{i-1}}(\bar{x}_{i-2}) \times \dots \times \lambda_{j+1}^{\sigma/v_{j+2}}(\bar{x}_{j+1}) \lambda_j^{\sigma/v_{j+1}}(\bar{x}_j) \times \frac{\sigma}{v_j} |x_i|^{\sigma/v_j - 1} \\
&\leq \widehat{M}_{ij}(\bar{x}_i) \left[ \sum_{\tau=j}^{i-1} |\zeta_\tau| + |\zeta_j|^{1-(v_j/\sigma)} + |\zeta_{j-1}|^{1-(v_j/\sigma)} \lambda_{j-1}^{\sigma/v_{j-1}}(\bar{x}_{j-1}) \right] \leq M_{ij}(\bar{x}_i) \sum_{l=j-1}^{i-1} |\zeta_l|^{1-(v_j/\sigma)}.
\end{aligned} \tag{A.10}$$

Then, from (A.10), we can get

$$\begin{aligned}
\frac{\partial \Psi_i}{\partial x_i}(\vartheta_j(t)x_{j+1}^q + f_j) &\leq \frac{4\sigma - v_i - \mu \bar{\vartheta}_j}{\sigma} |\zeta_i|^{((4\sigma - v_i - \mu)/\sigma) - 1} \times M_{ij}(\bar{x}_i) \\
&\quad \times \left[ \sum_{\tau=j-1}^{i-1} |\zeta_\tau|^{1-(v_j/\sigma)} |x_i - \xi_i| \right] \left[ |x_{j+1}|^{(v_j+\mu)/(v_j+1)} + \tilde{\psi}_j \sum_{l=1}^j |\zeta_l|^{(v_j+\mu)/\sigma} \right] \leq \frac{1}{8(i-1)} \sum_{l=1}^{i-1} \zeta_l^4 + H_{i2j}(\bar{x}_i) \zeta_i^4,
\end{aligned} \tag{A.11}$$

where  $\tilde{M}_{ij}(\cdot)$ ,  $h_{il}(\cdot)$  and  $H_{i2j}(\cdot)$  are nonnegative  $C^2$  functions. Let  $H_{i2}(\cdot) = \sum_{j=1}^{i-1} H_{i2j}(\cdot)$ , which directly verify (A.9).  $\square$

**Proposition A.4.** For  $i = 3, \dots, n$ ,  $j = 1, \dots, i-1$ , there exist nonnegative  $C^2$  functions  $H_{i3}(\cdot)$  such that

$$\frac{\partial \Psi_i}{\partial x_i} f_i \leq \frac{1}{8} \sum_{l=1}^{i-1} \zeta_l^4 + H_{i3}(\bar{x}_i) \zeta_i^4. \tag{A.12}$$

*Proof.* For  $i = 3, \dots, n$ , according to Proposition A.1 and Lemma 3, there exist nonnegative  $C^2$  functions  $H_{i3}(\cdot)$  such that

$$\begin{aligned}
\frac{\partial \Psi_i}{\partial x_i} f_i &\leq |\zeta_i|^{(4\sigma - \mu - v_i)/\sigma} \times \tilde{\psi}_i(\bar{x}_i) \sum_{j=1}^i |\zeta_j|^{(v_i+\mu)/\sigma} \\
&\leq \frac{1}{8} \sum_{l=1}^{i-1} \zeta_l^4 + H_{i3}(\bar{x}_i) \zeta_i^4.
\end{aligned} \tag{A.13}$$

$\square$

**Proposition A.5.** For  $i = 3, \dots, n$ , there exist nonnegative  $C^2$  functions  $H_{i4}(\cdot)$  such that

$$\frac{1}{2} \text{tr} \left\{ \tilde{g}_i^T \frac{\partial^2 \Psi_i}{\partial \bar{x}_i^2} \tilde{g}_i \right\} \leq \frac{1}{8} \sum_{l=1}^{i-1} \zeta_l^4 + H_{i4}(\bar{x}_i) \zeta_i^4. \tag{A.14}$$

*Proof.* Note that

$$\begin{aligned}
\frac{1}{2} \text{tr} \left\{ \tilde{g}_i^T \frac{\partial^2 \Psi_i}{\partial \bar{x}_i^2} \tilde{g}_i \right\} &= \frac{1}{2} \left\{ \sum_{k,j=1, k \neq j}^{i-1} \frac{\partial^2 \Psi_i}{\partial x_k \partial x_j} g_k^T g_j + \sum_{k=1}^{i-1} \frac{\partial^2 \Psi_i}{\partial x_k^2} \|g_k\|^2 \right\} \\
&\quad + \left\{ 2 \sum_{j=1}^{i-1} \frac{\partial^2 \Psi_i}{\partial x_j \partial x_i} g_j^T g_i + \frac{\partial^2 \Psi_i}{\partial x_i^2} \|g_i\|^2 \right\}.
\end{aligned} \tag{A.15}$$

First of all, one gets from (A.10) that

$$\begin{aligned}
\left| \frac{\partial^2 [\xi_i]^{\sigma/v_i}}{\partial x_k^2} \right| &\leq \left| \frac{\partial M_{ik}(\bar{x}_i)}{\partial x_k} \right| \sum_{l=1}^{i-1} |\zeta_l|^{1-(v_k/\sigma)} \\
&\quad + M_{ik}(\bar{x}_i) \frac{\sigma - v_k}{\sigma} |\zeta_k|^{-(v_k/\sigma)} \frac{\sigma}{v_k} |x_k|^{\sigma/v_k - 1} \\
&\quad + M_{ik}(\bar{x}_i) \frac{\sigma - v_k}{\sigma} \sum_{l=k+1}^{i-1} |\zeta_l|^{-(v_k/\sigma)} M_{lk}(\bar{x}_i) \\
&\quad \cdot \sum_{q=k-1}^{l-1} |\zeta_q|^{1-(v_k/\sigma)} \leq K_{ik}(\bar{x}_i) \sum_{l=1}^{i-1} |\zeta_l|^{1-(2v_k/\sigma)},
\end{aligned} \tag{A.16}$$

where  $K_{ik}(\cdot) \geq 0$  is a  $C^2$  function.

From equation (A.10) and Proposition A.1, it can be inferred that

$$\frac{1}{2} \frac{\partial^2 \Psi_i}{\partial x_k^2} \|g_k\|^2 \leq \frac{1}{32(i-1)} \sum_{l=1}^{i-1} \zeta_l^4 + \tilde{H}_{i4k}(\bar{x}_i) \zeta_l^4, \tag{A.17}$$

where  $\tilde{H}_{i4k}(\cdot) \geq 0$  is a  $C^2$  function.

Then, one gets

$$\frac{1}{2} \sum_{k=1}^{i-1} \frac{\partial^2 \Psi_i}{\partial x_k^2} \|g_k\|^2 \leq \frac{1}{32} \sum_{l=1}^{i-1} \zeta_l^4 + H_{i41}(\bar{x}_i) \zeta_i^4, \quad (\text{A.18})$$

where  $H_{i41}(\cdot) = \sum_{k=1}^{i-1} \tilde{H}_{i4k}(\cdot)$ .

Besides, if  $k \neq j, k > j$ , there exist  $C^2$  functions  $\tilde{K}_{ikj}(\cdot) \geq 0$  such that

$$\begin{aligned} \left| \frac{\partial^2 [\xi_i]^{\sigma/v_i}}{\partial x_k \partial x_j} \right| &\leq \left| \frac{\partial \tilde{M}_{ij}(\bar{x}_i)}{\partial x_k} \right| \left[ \sum_{l=1}^{i-1} |\zeta_l| + |x_j|^{(\sigma/v_j)-1} \right] \\ &+ \tilde{M}_{ij}(\bar{x}_i) \sum_{l=k}^{i-1} \left| \frac{\partial \zeta_l}{\partial x_k} \right| \leq \tilde{K}_{ikj}(\bar{x}_i) \\ &\cdot \left[ \sum_{l=1}^{i-1} |\zeta_l| + |x_j|^{(\sigma/v_j)-1} + |x_k|^{(\sigma/v_k)-1} \right]. \end{aligned} \quad (\text{A.19})$$

Meanwhile, if  $k \neq j, k < j$ , we have

$$\begin{aligned} \left| \frac{\partial^2 [\xi_i]^{\sigma/v_i}}{\partial x_k \partial x_j} \right| &= \left| \frac{\partial^2 [\xi_i]^{\sigma/v_i}}{\partial x_j \partial x_k} \right| \leq \tilde{K}_{ijk}(\bar{x}_i) \\ &\cdot \left[ \sum_{l=1}^{i-1} |\zeta_l| + |x_k|^{(\sigma/v_k)-1} + |x_j|^{(\sigma/v_j)-1} \right]. \end{aligned} \quad (\text{A.20})$$

Hence, for  $\forall 1 \leq k \neq j \leq i-1$ , combining (A.19) with (A.20) yields

$$\left| \frac{\partial^2 [\xi_i]^{\sigma/v_i}}{\partial x_k \partial x_j} \right| \leq K_{ikl}(\bar{x}_i) \left[ \sum_{l=1}^{i-1} |\zeta_l| + |x_k|^{(\sigma/v_k)-1} + |x_j|^{(\sigma/v_j)-1} \right]. \quad (\text{A.21})$$

Then, for  $\forall 1 \leq k \neq j \leq i-1$ , it can be deduced from (A.21) and Lemma 3 that

$$\begin{aligned} \frac{1}{2} \frac{\partial^2 \Psi_i}{\partial x_k \partial x_j} g_k^T g_j &\leq \frac{4\sigma - \mu - v_i}{\sigma} K_{ikj}(\bar{x}_i) \left[ \sum_{l=1}^{i-1} |\zeta_l| + |x_k|^{(\sigma/v_k)-1} + |x_j|^{(\sigma/v_j)-1} \right] \times |\zeta_i|^{(3\sigma - \mu - v_i)/\sigma} |x_i - \xi_i| \times \tilde{\eta}_k \left( \sum_{m=1}^k |\zeta_m|^{(2v_k + \mu)/2\sigma} \right) \\ &\times \tilde{\eta}_j \left( \sum_{m=1}^j |\zeta_m|^{(2v_j + \mu)/2\sigma} \right) + \frac{(4\sigma - \mu - v_i)(3\sigma - \mu - v_i)}{\sigma^2} \times \left[ M_{ik}(\bar{x}_i) \sum_{l=1}^{i-1} |\zeta_l|^{1 - (v_k/\sigma)} \right] \times \left[ M_{ij}(\bar{x}_i) \sum_{l=1}^{i-1} |\zeta_l|^{1 - (v_j/\sigma)} \right] \\ &\times |\zeta_i|^{(2\sigma - \mu - v_i)/\sigma} |x_i - \xi_i| \times \tilde{\eta}_k \left( \sum_{m=1}^k |\zeta_m|^{(2v_k + \mu)/2\sigma} \right) \times \tilde{\eta}_j \left( \sum_{m=1}^j |\zeta_m|^{(2v_j + \mu)/2\sigma} \right) \\ &\leq \frac{1}{32(i-1)(i-2)} \sum_{l=1}^{i-1} \zeta_l^4 + \tilde{H}_{i4kj}(\bar{x}_i) \zeta_i^4, \end{aligned} \quad (\text{A.22})$$

where  $\tilde{H}_{i4kj}(\cdot) \geq 0$  are  $C^2$  functions. Hence, one has

$$\frac{1}{2} \sum_{k,j=1, k \neq j}^{i-1} \frac{\partial^2 \Psi_i}{\partial x_k \partial x_j} g_k^T g_j \leq \frac{1}{32} \sum_{l=1}^{i-1} |\zeta_l^4| + H_{i42}(\bar{x}_i) \zeta_i^4, \quad (\text{A.23})$$

where  $H_{i42}(\cdot) = \sum_{k,j=1, k \neq j}^{i-1} H_{i4kj}(\cdot)$ . Similarly, applying (A.10), Proposition A.1 and Lemma 3, we get

$$\sum_{j=1}^{i-1} \frac{\partial^2 \Psi_i}{\partial x_j \partial x_i} g_j^T g_i \leq \frac{1}{32} \sum_{l=1}^{i-1} |\zeta_l^4| + H_{i43}(\bar{x}_i) \zeta_i^4, \quad (\text{A.24})$$

$$\frac{\partial^2 \Psi_i}{\partial x_i^2} \|g_i\|^2 \leq \frac{1}{32} \sum_{l=1}^{i-1} |\zeta_l^4| + H_{i43}(\bar{x}_i) \zeta_i^4, \quad (\text{A.25})$$

where  $H_{i43}(\cdot)$  and  $H_{i44}(\cdot)$  are nonnegative  $C^2$  functions. Substituting (A.18), (A.23)–(A.25) into (A.15) directly infers (A.14). Till now, the proof of Proposition A.5 is finished.

Combining Propositions A.1–A.5 with (A.2) yields

$$\begin{aligned} \ell V_i &\leq -\frac{1}{2} G(x_1) \zeta_1^4 - (n+1-i) \sum_{l=1}^{i-1} \zeta_l^4 + H_i(\bar{x}_i) \zeta_i^4 \\ &+ \vartheta_i(t) [\zeta_i]^{(4\sigma - \mu - v_i)/\sigma} \xi_{i+1}^{q_i} + \vartheta_i(t) [\zeta_i]^{(4\sigma - \mu - v_i)/\sigma} \\ &\cdot (x_{i+1}^{q_i} - \xi_{i+1}^{q_i}), \end{aligned} \quad (\text{A.26})$$

where  $H_i(\cdot) = \sum_{t=1}^4 H_{it}(\cdot) \geq 0$  is a  $C^2$  functions.

Design

$$\begin{aligned} \xi_{i+1} &= -\lambda_i(\bar{x}_i) [\zeta_i]^{(v_i+1)/\sigma} \text{ with } \lambda_i(\bar{x}_i) \\ &= \left[ \frac{n-i+1 + H_i(\bar{x}_i)}{\underline{\vartheta}_i} \right]^{1/q_i} > 0. \end{aligned} \quad (\text{A.27})$$

Then, substituting the value of  $\xi_{i+1}$  into (A.27) yields that (40) holds.  $\square$

## Data Availability

No data were used to support this study.

## Conflicts of Interest

The authors declare that they have no conflicts of interest.

## Acknowledgments

This work was supported by the Project of Anhui Province Outstanding Young Talent Support Program with Grant no. gxyq2018089.

## References

- [1] S. C. Tong, X. Min, and Y. X. Li, "Observer-based adaptive fuzzy tracking control for strict-feedback nonlinear systems with unknown control gain functions," *IEEE Transactions on Cybernetics*, 2020.
- [2] S. Tong and Y. Li, "Robust adaptive fuzzy backstepping output feedback tracking control for nonlinear system with dynamic uncertainties," *Science China Information Sciences*, vol. 53, no. 2, pp. 307–324, 2010.
- [3] D. Yang, X. Li, and J. Qiu, "Output tracking control of delayed switched systems via state-dependent switching and dynamic output feedback," *Nonlinear Analysis: Hybrid Systems*, vol. 32, pp. 294–305, 2019.
- [4] X. Li, X. Yang, and T. Huang, "Persistence of delayed cooperative models: impulsive control method," *Applied Mathematics and Computation*, vol. 342, pp. 130–146, 2019.
- [5] H. Shen, F. Li, H. Yan, H. R. Karimi, and H.-K. Lam, "Finite-time event-triggered  $\mathcal{H}_\infty$  control for T-S fuzzy markov jump systems," *IEEE Transactions on Fuzzy Systems*, vol. 26, no. 5, pp. 3122–3135, 2018.
- [6] H. Shen, Z. G. Huang, J. D. Cao, and J. H. Park, "Exponential filtering for continuous-time switched neural networks under persistent Dwell-Time switching regularity," *IEEE Transactions on Cybernetics*, vol. 50, 2020.
- [7] S. Ding, A. Levant, and S. Li, "Simple homogeneous sliding-mode controller," *Automatica*, vol. 67, no. 5, pp. 22–32, 2016.
- [8] K. Q. Mei and S. H. Ding, "Second-order sliding mode controller design subject to an upper-triangular structure," *IEEE Transactions on Systems, Man, and Cybernetics: Systems*, 2019.
- [9] X. Liu, X. Su, P. Shi, and C. Shen, "Observer-based sliding mode control for uncertain fuzzy systems via event-triggered strategy," *IEEE Transactions on Fuzzy Systems*, vol. 27, no. 11, pp. 2190–2201, 2019.
- [10] S. Ding and S. Li, "Second-order sliding mode controller design subject to mismatched term," *Automatica*, vol. 77, pp. 388–392, 2017.
- [11] Z. F. Li, T. S. Li, G. Feng, R. Zhao, and Q. H. Shan, "Neural network-based adaptive control for pure-feedback stochastic nonlinear systems with time-varying delays and dead-zone input," *Systems, Man, and Cybernetics: Systems*, 2018.
- [12] T. S. Li, Z. F. Li, D. Wang, and C. L. P. Chen, "Output-feedback adaptive neural control for stochastic nonlinear time-varying delays systems with unknown control directions," *IEEE Transactions on Neural Networks and Learning Systems*, vol. 26, no. 6, pp. 1188–1201, 2015.
- [13] J. Yin and S. Khoo, "Continuous finite-time state feedback stabilizers for some nonlinear stochastic systems," *International Journal of Robust and Nonlinear Control*, vol. 25, no. 11, pp. 1581–1600, 2015.
- [14] Y. Li, K. Li, and S. Tong, "Finite-time adaptive fuzzy output feedback dynamic surface control for MIMO nonstrict feedback systems," *IEEE Transactions on Fuzzy Systems*, vol. 27, no. 1, pp. 96–110, 2019.
- [15] L. Fang, L. Ma, S. Ding, and D. Zhao, "Finite-time stabilization for a class of high-order stochastic nonlinear systems with an output constraint," *Applied Mathematics and Computation*, vol. 358, pp. 63–79, 2019.
- [16] W. Li, X. Liu, and S. Zhang, "Further results on adaptive state-feedback stabilization for stochastic high-order nonlinear systems," *Automatica*, vol. 48, no. 8, pp. 1667–1675, 2012.
- [17] W. T. Zha, J. Y. Zhai, and S. M. Fei, "Output feedback control for a class of stochastic high-order nonlinear systems with time-varying delays," *International Journal of Robust and Nonlinear Control*, vol. 24, no. 16, pp. 2243–2260, 2014.
- [18] X. Zhao, X. Wang, G. Zong, and X. Zheng, "Adaptive neural tracking control for switched high-order stochastic nonlinear systems," *IEEE Transactions on Cybernetics*, vol. 47, no. 10, pp. 3088–3099, 2017.
- [19] Z. Song and J. Zhai, "Decentralized output feedback stabilization for switched stochastic high-order nonlinear systems with time-varying state/input delays," *ISA Transactions*, vol. 90, pp. 64–73, 2019.
- [20] L. Liu, S. Xu, X.-J. Xie, and B. Xiao, "Observer-based decentralized control of large-scale stochastic high-order feedforward systems with multi time delays," *Journal of the Franklin Institute*, vol. 356, no. 16, pp. 9627–9645, 2019.
- [21] B. Niu, M. Liu, and A. Li, "Global adaptive stabilization of stochastic high-order switched nonlinear non-lower triangular systems," *Systems & Control Letters*, vol. 136, p. 104596, 2020.
- [22] J. H. Park, H. Shen, X. H. Chang, and T. H. Lee, *Recent Advances in Control and Filtering of Dynamic Systems with Constrained Signals*, Springer, Berlin, Germany, 2019.
- [23] L. Fang, L. Ma, S. Ding, and D. Zhao, "Robust finite-time stabilization of a class of high-order stochastic nonlinear systems subject to output constraint and disturbances," *International Journal of Robust and Nonlinear Control*, vol. 29, no. 16, pp. 5550–5573, 2019.
- [24] K. P. Tee, S. S. Ge, and E. H. Tay, "Barrier Lyapunov Functions for the control of output-constrained nonlinear systems," *Automatica*, vol. 45, no. 4, pp. 918–927, 2009.
- [25] K. P. Tee, B. Ren, and S. S. Ge, "Control of nonlinear systems with time-varying output constraints," *Automatica*, vol. 47, no. 11, pp. 2511–2516, 2011.
- [26] L. D. Fang, L. Ma, S. H. Ding, and J. H. Park, "Finite-time stabilization of high-order stochastic nonlinear systems with asymmetric output constraints," *IEEE Transactions on Systems, Man, and Cybernetics: Systems*, 2020.
- [27] Y.-J. Liu and S. Tong, "Barrier Lyapunov Functions-based adaptive control for a class of nonlinear pure-feedback systems with full state constraints," *Automatica*, vol. 64, pp. 70–75, 2016.
- [28] S. Ding, W.-H. Chen, K. Mei, and D. J. Murray-Smith, "Disturbance observer design for nonlinear systems represented by input-output models," *IEEE Transactions on Industrial Electronics*, vol. 67, no. 2, pp. 1222–1232, 2020.
- [29] S. H. Ding, J. H. Park, and C. C. Chen, "Second-order sliding mode controller design with output constraint," *Automatica*, vol. 112, Article ID 108704, 2020.
- [30] S. Ding, K. Mei, and S. Li, "A new second-order sliding mode and its application to nonlinear constrained systems," *IEEE Transactions on Automatic Control*, vol. 64, no. 6, pp. 2545–2552, 2019.



- [31] X. Yang, X. D. Li, X. Li, and Q. Xi, "Review of stability and stabilization for impulsive delayed systems," *Mathematical Biosciences & Engineering*, vol. 15, no. 6, pp. 1495–1515, 2018.
- [32] Q. K. Duan, S. H. Ding, and X. H. Yu, "Composite super-twisting sliding mode control design for PMSM speed regulation problem based on a novel disturbance observer," *IEEE Transactions on Energy Conversion*, 2020.
- [33] L. Liu, W. X. Zheng, and S. H. Ding, "An adaptive SOSM controller design by using a sliding-mode-based filter and its application to buck converter," *IEEE Transactions on Circuits and Systems I: Regular Papers*, vol. 67, no. 7, pp. 2409–2418, 2020.
- [34] R. Ma, Y. Liu, S. Zhao, and J. Fu, "Finite-time stabilization of a class of output-constrained nonlinear systems," *Journal of the Franklin Institute*, vol. 352, no. 12, pp. 5968–5984, 2015.
- [35] C. C. Chen, "A unified approach to finite-time stabilization of high-order nonlinear systems with and without an output constraint," *International Journal of Robust and Nonlinear Control*, vol. 29, no. 2, pp. 393–407, 2019.
- [36] C. C. Chen and G. S. Chen, "A new approach to stabilization of high-order nonlinear systems with an asymmetric output constraint," *International Journal of Robust and Nonlinear Control*, vol. 30, no. 2, pp. 756–775, 2020.
- [37] C. C. Chen and Z. Y. Sun, "A unified approach to finite-time stabilization of high-order nonlinear systems with an asymmetric output constraint," *Automatica*, vol. 111, Article ID 108581, 2020.
- [38] S. Huang and Z. Xiang, "Finite-time stabilisation of a class of switched nonlinear systems with state constraints," *International Journal of Control*, vol. 91, no. 6, pp. 1300–1313, 2018.
- [39] X. Jin, "Adaptive fault tolerant tracking control for a class of stochastic nonlinear systems with output constraint and actuator faults," *Systems & Control Letters*, vol. 107, pp. 100–109, 2017.
- [40] Y.-J. Liu, S. Lu, S. Tong, X. Chen, and C. L. P. Chen, "Adaptive control-based barrier Lyapunov functions for a class of stochastic nonlinear systems with full state constraints," *Automatica*, vol. 87, pp. 83–93, 2018.
- [41] J. Li, J. Xia, W. Sun, G. Zhuang, and Z. Wang, "Finite-time tracking control for stochastic nonlinear systems with full state constraints," *Applied Mathematics and Computation*, vol. 338, pp. 207–220, 2018.
- [42] L. D. Fang, H. S. Ding, J. H. Park, and L. Ma, "Adaptive fuzzy control for nontriangular stochastic high-order nonlinear systems subject to asymmetric output constraints," *IEEE Transactions on Cybernetics*, 2020.
- [43] Y. Liu, H. Ma, and H. Ma, "Adaptive fuzzy fault-tolerant control for uncertain nonlinear switched stochastic systems with time-varying output constraints," *IEEE Transactions on Fuzzy Systems*, vol. 26, no. 5, pp. 2487–2498, 2018.
- [44] B. Niu, W. Ding, H. Li, and X. Xie, "A novel neural-network-based adaptive control scheme for output-constrained stochastic switched nonlinear systems," *IEEE Transactions on Systems, Man, and Cybernetics: Systems*, vol. 49, no. 2, pp. 418–432, 2019.
- [45] L. D. Fang, S. H. Ding, J. H. Park, and L. Ma, "Adaptive fuzzy control for stochastic high-order nonlinear systems with output constraints," *IEEE Transactions on Fuzzy Systems*, 2020.
- [46] Y. Li and S. Tong, "Adaptive fuzzy output constrained control design for multi-input multioutput stochastic nonstrict-feedback nonlinear systems," *IEEE Transactions on Cybernetics*, vol. 47, no. 12, pp. 4086–4095, 2017.

## Research Article

# Quadratic Filtering for Discrete-Time Systems with Measurement Delay and Packet Dropping

Ling Li,<sup>1</sup> Lei Tan,<sup>1</sup> Xinmin Song ,<sup>1</sup> and Xuehua Yan<sup>2</sup>

<sup>1</sup>The School of Information Science and Engineering, Shandong Normal University, Jinan 250014, China

<sup>2</sup>School of Electrical Engineering, University of Jinan, Jinan, Shandong, China

Correspondence should be addressed to Xinmin Song; [xinminsong@sina.com](mailto:xinminsong@sina.com)

Received 11 May 2020; Accepted 19 June 2020; Published 5 August 2020

Academic Editor: Jianquan Lu

Copyright © 2020 Ling Li et al. This is an open access article distributed under the Creative Commons Attribution License, which permits unrestricted use, distribution, and reproduction in any medium, provided the original work is properly cited.

We consider the problem of remote estimation with time delay and multiplicative noise for multichannel systems. First, we apply the reorganized innovation analysis approach to construct the original delay system into a new delay-free system. Secondly, the delay-free system will be reconstructed by the quadratic filtering method to obtain an augmented system. Then, Kalman filtering theory and projection formula are used to solve two Riccati equations and one Lyapunov equation for the augmented system, and the quadratic filter for the measurement delay system on the packet loss network can be obtained. Finally, we use a numerical example to illustrate the effectiveness of the method.

## 1. Introduction

In recent years, the problem of missing measurements caused by unreliable channel transmission has been the focus of many scholars [1–3]. The research on the problem of packet loss can be roughly divided into two directions: one is to solve the linear estimator based on the minimum mean square error method and the other is to use the quadratic filtering method. Nahi [4] believes that the observation sequence may contain only noise when the packets are lost and derives a set of recursive formulas similar to Kalman filtering in the sense of the minimum mean square error. In [5], the Kalman filter is implemented by intermittent observation to solve the problem of information loss in large wireless sensor networks. Zhang et al. [6] propose an estimator that can be applied to an infinite horizon, and its iteration only includes solving a Riccati equation. This estimator avoids the convergence analysis problem caused by the calculation of the Lyapunov equation in traditional estimation methods. The authors in [7] apply the recombination innovation analysis method to obtain an optimal linear filter, which solves the remote estimation problem of the packet loss network with the measurement delay system obeying Bernoulli distribution.

However, with the development of engineering technology [8–10], the performance of the traditional linear estimator cannot meet the requirements of the real system. Therefore, people are paying more and more attention to the optimization design and implementation of the estimator. De Santis et al. [11] first propose a method called quadratic filtering, which uses a quadratic function of the measurement equation to improve the performance of the filter. Experiments show that this method is superior to the linear filtering method in estimating performance. This research has attracted great attention of many scholars. Caballero-Águila et al. [12] consider using innovative methods to solve the least square linear estimation problem and simplify the quadratic estimation problem into a linear estimation problem in a suitable augmented system. After that, Cacace et al. [13] add the packet loss factor to the measurement model and use the quadratic filtering method to obtain a filter iteration equation with a smaller estimation error. The Kronecker algebraic rules are used in [14] to discuss the stochastic properties of augmented noise in augmented systems. Then, the linear estimation of the discrete-time non-Gaussian system is obtained by the projection formula. Cacace et al. [15] propose a feedback quadratic filter that rewrites the system model by introducing an output

injection term and prove that the performance of the feedback quadratic filter depends on the gain parameter of the output term.

Meanwhile, researchers found that time delay is common due to uncertain factors such as bandwidth and network failures [16–21]. Especially, the state estimation problem has received much attention for time-delay systems in [22–26]. The emergence of time delay often leads to the instability and even worsens the overall performance of the system. Therefore, solving the time-delay problem in life is bound to be an important subject of our research. The emergence of time delay often leads to the instability of the system and even makes the overall performance of the system worse, so solving the problem of time delay in life is bound to be the most important research content [27]. By solving a partial differential equation, the solution of a continuous observation delay system is obtained. The authors in [28] transform the discrete system with observation delay into a nonobservation delay system estimation problem by expanding the dimensions and then obtain the filter based on the standard Kalman filtering theory. Zhang et al. [29] propose a new-information reorganization analysis theory, that is, keeping observation information unchanged and then rearranging and combining observation data from different channels and different time delays into a system without time delay. Finally, the new observation data are introduced into the innovation sequence, and the signal is designed by using the projection theory. Song et al. [7] extended the abovementioned innovation restructuring theory to the study of infinite time estimation and made a deeper demonstration of the estimation of multistable systems.

Inspired by the above studies, this paper considers the quadratic filter problem of time-delay systems with multi-channel multiplicative noise in discrete time. First of all, we assume that the measurement has a delay phenomenon, and the measurement is transmitted through multiple communication channels. The packet loss of each channel is described by the Bernoulli process of independent and identical distribution. Secondly, we use the innovation recombination theory to rearrange and combine the above observation data and obtain a new time-delay free observation system structure. Finally, we construct a quadratic filtering equation for the new time-delay free observation system and obtain a new filter by solving two Riccati equations and one Lyapunov equation. The main contribution of this paper is to effectively combine the quadratic filtering method with the innovation recombination theory; therefore, so as to obtain the quadratic filtering scheme of the discrete-time system with packet loss and measurement delay.

The rest of this article is organized as follows. First, Section 2 provides the question statement and preliminary. Section 3 provides quadratic filter solutions of the problem with detailed derivation processes. This part is the key result of this paper. Then, Section 4 is a simulation example to prove the effectiveness of the estimator algorithm in Section 3. Finally, the summary of this paper is given in Section 5.

*1.1. Notation.* Throughout this technical paper, the superscripts  ${}^T$  and  ${}^{-1}$  represent the transpose and inverse of a matrix,  $\mathcal{R}^n$  denotes the  $n$ -dimensional Euclidean space,  $\mathbb{E}\{\cdot\}$  stands for the mathematical expectation operator,  $\otimes$  and  $\odot$  are used to denote the Kronecker product and the Hadamard product, respectively,  $I$  represents an identity matrix of the appropriate dimension, and  $\delta_{ij} = 0$  for  $i \neq j$  and  $\delta_{ii} = 1$ . We use  $\text{diag}\{\lambda_1, \dots, \lambda_n\}$  to represent a diagonal matrix, where  $\lambda_1, \dots, \lambda_n$  are the diagonal elements of this diagonal matrix. If the dimensions are not explicitly stated, matrices are assumed to have compatible dimensions with algebraic operations.

## 2. Problem Statement and Preliminary

In this section, we consider a discrete time-delay system for which the state and measurement equations are as follows:

$$x(k+1) = A(k)x(k) + n(k), \quad (1)$$

$$y_0(k) = \xi(k)B_0(k)x(k) + v_0(k), \quad (2)$$

$$y_1(k) = \theta(k)B_1(k)x(k-d) + v_1(k), \quad k \geq d, \quad (3)$$

where  $k = 0, 1, 2, 3, \dots$  is the time instant,  $d$  is the measurement delay time,  $x(k) \in \mathcal{R}^n$ ,  $y_0(k) \in \mathcal{R}^{m_1}$ , and  $y_1(k) \in \mathcal{R}^{m_2}$  are, respectively, the system state and measurement, and  $n(k)$ ,  $v_0(k)$ , and  $v_1(k)$  are the system noise and measurement noise with zero mean and covariances  $\mathbb{E}\{n(k)n^T(j)\} = Q\delta_{k,j}$ ,  $\mathbb{E}\{v_0(k)v_0^T(j)\} = R_0\delta_{k,j}$ , and  $\mathbb{E}\{v_1(k)v_1^T(j)\} = R_1\delta_{k,j}$ , respectively. Here,  $\xi(k) = \text{diag}\{\xi_1(k), \dots, \xi_{m_1}(k)\}$  and  $\theta(k) = \text{diag}\{\theta_1(k), \dots, \theta_{m_2}(k)\}$ . The mutually uncorrelated and identically distributed (i.i.d.) Bernoulli random variables  $\xi_i(k)$  and  $\theta_i(k)$  are employed to describe, respectively. The packet loss phenomenon in the  $m_1$  channels and  $m_2$  channels is with  $P_r\{\xi_i(k) = 1\} = \alpha_i$ ,  $P_r\{\xi_i(k) = 0\} = 1 - \alpha_i$ ,  $P_r\{\theta_i(k) = 1\} = \beta_i$ , and  $P_r\{\theta_i(k) = 0\} = 1 - \beta_i$ . The initial state  $x(0)$  is a random vector with mean  $\mu_0$  and covariance matrix  $\mathbb{E}\{[x(0) - \mu_0][x(0) - \mu_0]^T\} = P_0$ . It should be noted that for simplicity, we assume that  $B_0(k)$  and  $B_1(k)$  are constant matrices with appropriate dimensions. The random processes  $n(k)$ ,  $v_0(k)$ ,  $v_1(k)$ ,  $\xi(k)$ , and  $\theta(k)$  are independent of the initial state  $x(0)$ .

For convenience, the measurement  $y(k)$  can be rewritten as the following:

$$y(k) = \begin{cases} y_0(k), & 0 \leq k < d, \\ \begin{bmatrix} y_0(k) \\ y_1(k) \end{bmatrix}, & k \geq d. \end{cases} \quad (4)$$

*2.1. Problem Statement.* For the given systems (1) and (4), we try to construct the quadratic state and measurement vector and then get the quadratic filter iteration equation of the new system through the projection method and the basic theory of the Kalman filter.

### 3. Main Results

Since there is a time delay  $d$  at instant  $k$ , state  $x(k-d)$  has an additional measurement  $y_1(k)$ . In addition, when  $k \geq d$ , the measurement  $y(k)$  contains the time delay. According to [29], the linear space  $\mathcal{L}\{\{y(s)\}_{s=0}^k\}$  contains the same information as  $\mathcal{L}\{\{Y_1(s)\}_{s=0}^{k-d}, \{Y_0(s)\}_{s=k-d+1}^k\}$ , where the new observations  $Y_1(s)$  and  $Y_0(s)$  are provided as follows:

$$\begin{aligned} Y_1(s) &= \begin{bmatrix} y_0(s) \\ y_1(s+d) \end{bmatrix}, \quad 0 \leq s \leq k-d, \\ Y_0(s) &= y_0(s), \quad k-d < s \leq k. \end{aligned} \quad (5)$$

For convenience,  $Y_0(s)$  and  $Y_1(s)$  can be rewritten as

$$\begin{aligned} Y_1(s) &= H_1 x(s) + V_1(s), \\ Y_0(s) &= H_0 x(s) + V_0(s), \end{aligned} \quad (6)$$

where

$$\begin{aligned} H_1 &= \begin{bmatrix} \xi(s)B_0 \\ \theta(s+d)B_1 \end{bmatrix}, \\ H_0 &= \xi(s)B_0, \\ V_1(s) &= \begin{bmatrix} v_0(s) \\ v_1(s+d) \end{bmatrix}, \\ V_0(s) &= v_0(s). \end{aligned} \quad (7)$$

Before introducing the quadratic filtering problem, we will construct the augmented state and measurement vectors by stacking the original vectors and obtaining their second-order Kronecker powers. Then, we can get the new state vector and the measurement vector as shown below:

$$x^{[2]}(s+1) = A^{[2]}x^{[2]}(s) + f(s) + m_{n(s)}^{(2)}, \quad (8)$$

where

$$f(s) = n^{[2]}(s) + Ax(s) \otimes n(s) + n(s) \otimes Ax(s) - m_{n(s)}^{(2)}, \quad (9)$$

with  $E\{f(s)\} = 0$ .

Similarly, it is not difficult to obtain the following measurement equation:

$$\begin{aligned} y_0^{[2]}(s) &= \phi^{[2]}B_0^{[2]}x^{[2]}(s) + l(s) + m_{V_0(s)}^{[2]}, \\ y_1^{[2]}(s) &= \begin{bmatrix} \phi & 0 \\ 0 & \varphi \end{bmatrix}^{[2]} \begin{bmatrix} B_0 \\ B_1 \end{bmatrix}^{[2]} x^{[2]}(s) + g(s) + m_{V_1(s)}^{[2]}, \end{aligned} \quad (10)$$

where

$$\begin{aligned} l(s) &= [\xi(s) - \phi]^{[2]}B_0^{[2]}x^{[2]}(s) + [\xi(s)B_0x(s)] \otimes V_0(s) + V_0(s) \otimes [\xi(s)B_0x(s)] + V_0^{[2]}(s) - m_{V_0(s)}^{(2)}, \\ g(s) &= \overline{H}_1^{[2]}x^{[2]}(s) + V_1^{[2]}(s) + H_1x(s) \otimes V_1(s) + V_1(s) \otimes H_1x(s) - m_{V_1(s)}^{(2)}, \\ \overline{H}_1 &= \begin{bmatrix} \xi(s) - \phi & 0 \\ 0 & \theta(s+d) - \varphi \end{bmatrix} \begin{bmatrix} B_0 \\ B_1 \end{bmatrix}, \end{aligned} \quad (11)$$

where

$$\begin{aligned} \phi^{[2]} &= \mathbb{E}\{\xi(s) \otimes \xi(s)\} = \begin{bmatrix} \phi_{11} & 0 & \cdots & 0 \\ 0 & \phi_{22} & \cdots & 0 \\ \vdots & \vdots & \ddots & \vdots \\ 0 & 0 & \cdots & \phi_{m_1 m_1} \end{bmatrix}, \\ \begin{bmatrix} \phi & 0 \\ 0 & \varphi \end{bmatrix}^{[2]} &= \mathbb{E}\left\{ \begin{bmatrix} \xi(s) & 0 \\ 0 & \theta(s) \end{bmatrix} \otimes \begin{bmatrix} \xi(s) & 0 \\ 0 & \theta(s) \end{bmatrix} \right\} \\ &= \begin{bmatrix} \text{diag}\{\phi_{11}, \varphi_{11}\} & 0 & \cdots & 0 \\ 0 & \text{diag}\{\phi_{22}, \varphi_{22}\} & \cdots & 0 \\ \vdots & \vdots & \ddots & \vdots \\ 0 & 0 & \cdots & \varphi_{m_2 m_2} \end{bmatrix}, \end{aligned} \quad (12)$$

in which

$$\begin{aligned} \phi_{11} &= \begin{bmatrix} \alpha_1 & 0 & \cdots & 0 \\ 0 & \alpha_1 \alpha_2 & \cdots & 0 \\ \vdots & \vdots & \ddots & \vdots \\ 0 & 0 & \cdots & \alpha_1 \alpha_{m_1} \end{bmatrix}, \\ \phi_{22} &= \begin{bmatrix} \alpha_2 \alpha_1 & 0 & \cdots & 0 \\ 0 & \alpha_2 & \cdots & 0 \\ \vdots & \vdots & \ddots & \vdots \\ 0 & 0 & \cdots & \alpha_2 \alpha_{m_1} \end{bmatrix}, \\ \phi_{m_1 m_1} &= \begin{bmatrix} \alpha_{m_1} \alpha_1 & 0 & \cdots & 0 \\ 0 & \alpha_{m_1} \alpha_2 & \cdots & 0 \\ \vdots & \vdots & \ddots & \vdots \\ 0 & 0 & \cdots & \alpha_{m_1} \end{bmatrix}, \end{aligned}$$

$$\begin{aligned}
\varphi_{11} &= \begin{bmatrix} \alpha_1\beta_1 & 0 & \cdots & 0 \\ 0 & \alpha_1\beta_1 & \cdots & 0 \\ \vdots & \vdots & \ddots & \vdots \\ 0 & 0 & \cdots & \alpha_1\beta_{m_2} \end{bmatrix}, \\
\varphi_{22} &= \begin{bmatrix} \alpha_2\beta_1 & 0 & \cdots & 0 \\ 0 & \alpha_2\beta_2 & \cdots & 0 \\ \vdots & \vdots & \ddots & \vdots \\ 0 & 0 & \cdots & \alpha_2\beta_{m_2} \end{bmatrix}, \\
\varphi_{m_2m_1} &= \begin{bmatrix} \beta_1\alpha_1 & 0 & \cdots & 0 \\ 0 & \beta_1\alpha_2 & \cdots & 0 \\ \vdots & \vdots & \ddots & \vdots \\ 0 & 0 & \cdots & \beta_1\beta_{m_2} \end{bmatrix}, \\
\varphi_{m_2m_2} &= \begin{bmatrix} \beta_{m_2}\alpha_1 & 0 & \cdots & 0 \\ 0 & \beta_{m_2}\alpha_2 & \cdots & 0 \\ \vdots & \vdots & \ddots & \vdots \\ 0 & 0 & \cdots & \beta_{m_2} \end{bmatrix},
\end{aligned} \tag{13}$$

with  $\phi = \text{diag}\{\alpha_1, \dots, \alpha_{m_1}\}$ ,  $\varphi = \text{diag}\{\beta_1, \dots, \beta_{m_2}\}$ ,  $E\{l(s)\} = 0$ , and  $E\{g(s)\} = 0$ .

Then, the new state vector and the measurement vector can be written as

$$\begin{aligned}
\mathbf{x}(s) &\triangleq \begin{bmatrix} x(s) \\ x^{[2]}(s) \end{bmatrix}, \\
\mathbf{y}(s) &\triangleq \begin{bmatrix} y(s) \\ y^{[2]}(s) \end{bmatrix}.
\end{aligned} \tag{14}$$

Finally, we can derive the augmented system as follows:

$$\mathbf{x}(s+1) = \mathbf{A}\mathbf{x}(s) + \mathbf{C}\mathbf{U}_0(s) + \mathbf{F}(s), \tag{15}$$

$$\mathbf{Y}_0(s) = \mathbf{H}_0\mathbf{x}(s) + \mathbf{E}_0\mathbf{U}_0(s) + \mathbf{L}(s), \tag{16}$$

$$\mathbf{Y}_1(s) = \mathbf{H}_1\mathbf{x}(s) + \mathbf{E}_1\mathbf{U}_1(s) + \mathbf{G}(s), \tag{17}$$

where

$$\begin{aligned}
\mathbf{A} &\triangleq \begin{bmatrix} A & 0 \\ 0 & A^{[2]} \end{bmatrix}, \\
\mathbf{C} &\triangleq \begin{bmatrix} 0 & 0 \\ I_{n^2 \times n^2} & 0 \end{bmatrix}, \\
\mathbf{F}(s) &\triangleq \begin{bmatrix} n(s) \\ f(s) \end{bmatrix}, \\
\mathbf{H}_0 &\triangleq \begin{bmatrix} \phi B_0 & 0 \\ 0 & \phi^{[2]} B_0^{[2]} \end{bmatrix}, \\
\mathbf{E}_0 &\triangleq \begin{bmatrix} 0 & 0 \\ 0 & I_{m_1^2 \times m_1^2} \end{bmatrix},
\end{aligned}$$

$$\begin{aligned}
\mathbf{U}_0(s) &\triangleq \begin{bmatrix} m_{n(s)}^{(2)} \\ m_{V_0}^{(2)}(s) \end{bmatrix}, \\
\mathbf{L}(s) &\triangleq \begin{bmatrix} (\xi(s) - \phi)B_0\mathbf{x}(s) + V_0(s) \\ l(s) \end{bmatrix}, \\
\mathbf{U}_1(s) &\triangleq \begin{bmatrix} m_{n(s)}^{(2)} \\ m_{V_1}^{(2)}(s) \end{bmatrix}, \\
\mathbf{E}_1 &\triangleq \begin{bmatrix} 0 & 0 \\ 0 & I_{m_2^2 \times m_2^2} \end{bmatrix}, \\
\mathbf{G}(s) &\triangleq \begin{bmatrix} \bar{H}_1\mathbf{x}(s) + V_1(s) \\ g(s) \end{bmatrix}, \\
\mathbf{H}_1 &\triangleq \begin{bmatrix} \begin{bmatrix} \phi & 0 \\ 0 & \varphi \end{bmatrix} \begin{bmatrix} B_0 \\ B_1 \end{bmatrix} & 0 \\ 0 & \begin{bmatrix} \phi & 0 \\ 0 & \varphi \end{bmatrix}^{[2]} \begin{bmatrix} B_0 \\ B_1 \end{bmatrix}^{[2]} \end{bmatrix}.
\end{aligned} \tag{18}$$

Note that the new measurements  $\mathbf{Y}_0(s)$  and  $\mathbf{Y}_1(s)$  are delay free.  $\{\mathbf{F}(s)\}$ ,  $\{\mathbf{L}(s)\}$ , and  $\{\mathbf{G}(s)\}$  for all  $s$  and the initial  $\mathbf{x}(0)$  are mutually independent. Moreover,  $\{\mathbf{F}(s)\}$ ,  $\{\mathbf{L}(s)\}$ , and  $\{\mathbf{G}(s)\}$  are zero mean such that  $\mathbb{E}\{\mathbf{F}(s)\mathbf{F}^T(j)\} = \mathbf{Q}_{F(s)}\delta_{s,j}$ ,  $\mathbb{E}\{\mathbf{L}(s)\mathbf{L}^T(j)\} = \mathbf{Q}_{L(s)}\delta_{s,j}$ , and  $\mathbb{E}\{\mathbf{G}(s)\mathbf{G}^T(j)\} = \mathbf{Q}_{G(s)}\delta_{s,j}$ , and the detailed calculation processes are given below:

$$\begin{aligned}
\mathbf{Q}_{F(s)} &= \begin{bmatrix} \mathbb{E}\{n(s)n^T(s)\} & \mathbb{E}\{n(s)f^T(s)\} \\ \mathbb{E}\{f(s)n^T(s)\} & \mathbb{E}\{f(s)f^T(s)\} \end{bmatrix} \\
&= \begin{bmatrix} \mathbb{E}\{n(s)n^T(s)\} & \mathbb{E}\{n(s)n^{[2]T}(s)\} \\ \mathbb{E}\{n^{[2]}(s)n^T(s)\} & *_{1} \end{bmatrix},
\end{aligned} \tag{19}$$

where

$$\begin{aligned}
*_{1} &= \mathbb{E}\left\{[n(s)n^T(s)] \otimes [n(s)n^T(s)]\right\} - m_{n(s)}^{(2)}m_{n(s)}^{(2)T} \\
&\quad + (I + \Pi)\left[(AD(s)^T) \otimes \mathbb{E}\{n(s)n^T(s)\}\right](I + \Pi).
\end{aligned} \tag{20}$$

It should be pointed out that the entries of  $\mathbb{E}\{n(s)n^{[2]T}(s)\}$ ,  $\mathbb{E}\{[n(s)n^T(s)] \otimes [n(s)n^T(s)]\}$ , and  $\mathbb{E}\{n(s)n^T(s)\}$  are known since they are the elements of  $m_{n(s)}^{(3)}$ ,  $m_{n(s)}^{(4)}$ , and  $m_{n(s)}^{(2)}$ , respectively.

For convenience, let us define

$$\begin{aligned}
D^{(0,2)}(s) &\triangleq \mathbb{E}\{x^{[2]}(s)\}, \\
D^{(1,2)}(s) &\triangleq \mathbb{E}\{x(s)x^{[2]T}(s)\}, \\
D^{(2,2)}(s) &\triangleq \mathbb{E}\{x^{[2]}(s)x^{[2]T}(s)\}.
\end{aligned} \tag{21}$$

Then, we can calculate that

$$\begin{aligned}
D^{(0,2)}(s+1) &= \mathbb{E}\{x^{[2]}(s+1)\} = \text{vec}^T(D(s+1)), \\
D^{(1,2)}(s+1) &= \mathbb{E}\{x(s+1)x^{[2]T}(s+1)\} \\
&= \mathbb{E}\{[Ax(s) + n(s)][A^{[2]}x^{[2]}(s) + f(s) + m_{n(s)}^{(2)}]\} \\
&= AD^{(1,2)}(s)A^{[2]T} + \mathbb{E}\{n(s)n^{[2]T}(s)\}, \\
D^{(2,2)}(s+1) &= \mathbb{E}\{x^{[2]}(s+1)x^{[2]T}(s+1)\} \\
&= \mathbb{E}\{[A^{[2]}x^{[2]}(s) + f(s) + m_{n(s)}^{(2)}] \times [A^{[2]}x^{[2]}(s) + f(s) + m_{n(s)}^{(2)}]\} \\
&= A^{[2]}D^{(2,2)}(s)A^{[2]T} + \mathbb{E}\{n^{[2]}(s)n^{[2]T}(s)\} + (I + \Pi) \times [(AD(s)A^T) \otimes \mathbb{E}\{n(s)n^T(s)\}](I + \Pi),
\end{aligned} \tag{22}$$

where  $\Pi$  is the matrix which guarantees that  $n(s) \otimes Ax(s) = \Pi(Ax(s) \otimes n(s))$ .

Following the similar way for  $\mathbf{Q}_{F(s)}$ , one has

$$\begin{aligned}
\mathbf{Q}_{L(s)} &= \mathbb{E}\{\mathbf{L}(s)\mathbf{L}^T(s)\} \\
&= \begin{bmatrix} \Gamma_1 \odot (B_0 D(s) B_0^T) + \mathbb{E}\{V_0(s) V_0^T(s)\} & *_2 \\ & *_{2^T} & *_3 \end{bmatrix}, \\
\mathbf{Q}_{G(s)} &= \mathbb{E}\{\mathbf{G}(s)\mathbf{G}^T(s)\} \\
&= \begin{bmatrix} \text{diag}\{\Gamma_1, \Lambda_1\} \odot (B_1 D(s) B_1^T) + \mathbb{E}\{V_1(s) V_1^T(s)\} & *_4 \\ & *_{4^T} & *_5 \end{bmatrix},
\end{aligned} \tag{23}$$

$$\begin{aligned}
*_2 &= \mathbb{E}\{V_0(s) V_0^{[2]T}(s)\} + \mathbb{E}\{[\xi(s) - \phi][\xi(s) - \phi]^{[2]T}\} B_0 D^{(1,2)}(s) B_0^{[2]T}, \\
*_3 &= (\Gamma_1 \otimes \Gamma_1) \odot (B_0^{[2]} D^{(2,2)}(s) B_0^{[2]T}) + \mathbb{E}\{V_0^{[2]}(s) V_0^{[2]T}(s)\} - m_{V_0(s)}^{(2)} m_{V_0(s)}^{(2)T} \\
&\quad + \mathbb{E}\{(\xi(s) - \phi)^{[2]} B_0^{[2]} D^{(0,2)}(s) m_{V_0(s)}^{(2)T} + m_{V_0(s)}^{(2)} D^{(0,2)T}(s) B_0^{[2]T} \mathbb{E}\{(\xi(s) - \phi)^{[2]T}\} \\
&\quad + (I + \Pi_1)[\Gamma_1 \odot (B_0 D(s) B_0^T) \otimes \mathbb{E}\{V_0(s) V_0^T(s)\}](I + \Pi_1), \\
*_4 &= \mathbb{E}\{\overline{H}_2 \overline{H}_2^{[2]T}\} (B D^{(1,2)}(s) B^{[2]T}) + \mathbb{E}\{V_1(s) V_1^{[2]T}(s)\}, \\
*_5 &= (\text{diag}\{\Gamma_1, \Lambda_1\} \otimes \text{diag}\{\Gamma_1, \Lambda_1\}) \odot (B_1^{[2]} D^{(2,2)}(s) B_1^{[2]T}) + \mathbb{E}\{V_1^{[2]}(s) V_1^{[2]T}(s)\} \\
&\quad + \mathbb{E}\{\overline{H}_2^{[2]}\} B^{[2]} D^{(0,2)}(s) m_{V_1(s)}^{(2)T} + m_{V_1(s)}^{(2)} D^{(0,2)T}(s) B^{[2]T} \mathbb{E}\{\overline{H}_2^{[2]T}\} - m_{V_1(s)}^{(2)} m_{V_1(s)}^{(2)T} \\
&\quad + (I + \Pi_2)[(\text{diag}\{\Gamma_1, \Lambda_1\}) \odot (B_1^{[2]} D^{(2,2)}(s) B_1^{[2]T}) \otimes \mathbb{E}\{V_1(s) V_1^T(s)\}](I + \Pi_2),
\end{aligned} \tag{24}$$

where

$$\begin{aligned}
\Gamma_1 &= \begin{bmatrix} \alpha_1(1 - \alpha_1) & 0 & \cdots & 0 \\ 0 & \alpha_2(1 - \alpha_2) & \cdots & 0 \\ \vdots & \vdots & \ddots & \vdots \\ 0 & 0 & \cdots & \alpha_{m_1}(1 - \alpha_{m_1}) \end{bmatrix}, \\
\Lambda_1 &= \begin{bmatrix} \beta_1(1 - \beta_1) & 0 & \cdots & 0 \\ 0 & \beta_2(1 - \beta_2) & \cdots & 0 \\ \vdots & \vdots & \ddots & \vdots \\ 0 & 0 & \cdots & \beta_{m_2}(1 - \beta_{m_2}) \end{bmatrix}, \\
\overline{H}_2 &= \begin{bmatrix} \xi(s) - \phi & 0 \\ 0 & \theta(s+d) - \varphi \end{bmatrix}, \\
B &= \begin{bmatrix} B_0 \\ B_1 \end{bmatrix}.
\end{aligned} \tag{25}$$

It should be noted that  $\Pi_1$  and  $\Pi_2$  are the matrices which ensure  $V_0(s) \otimes H_0 x(s) = \Pi_1(H_0 x(s) \otimes V_0(s))$  and  $V_1(s) \otimes H_1 x(s) = \Pi_2(H_1 x(s) \otimes V_1(s))$ . Then, notice that the entries of  $\mathbb{E}\{V_0(s) V_0^T(s)\}$ ,  $\mathbb{E}\{[V_0(s) V_0^T(s)] \otimes [V_0(s) V_0^T(s)]\}$ ,  $\mathbb{E}\{V_0^{[2]}(s) V_0^T(s)\}$ ,  $\mathbb{E}\{V_1(s) V_1^T(s)\}$ ,  $\mathbb{E}\{V_1^{[2]}(s) V_1^T(s)\}$ , and  $\mathbb{E}\{[V_1(s) V_1^T(s)] \otimes [V_1(s) V_1^T(s)]\}$  are known because they are the elements of  $m_{V_0(s)}^{(2)}$ ,  $m_{V_0(s)}^{(4)}$ ,  $m_{V_0(s)}^{(3)}$ ,  $m_{V_1(s)}^{(2)}$ ,  $m_{V_1(s)}^{(3)}$ , and  $m_{V_1(s)}^{(4)}$ , respectively.

We define the quadratic state estimator  $\widehat{\mathbf{x}}(s+1|s)$  as the projection of  $\mathbf{x}(s+1)$  onto the linear space  $\mathcal{L}\{\{\mathbf{Y}_1(i)\}_{i=0}^{k-d}, \{\mathbf{Y}_0(i)\}_{i=k-d+1}^k\}$ . In order to derive the projection, we give the following definitions of the innovation sequence:

$$\mathbf{w}(s, 0) = \mathbf{Y}_0(s) - \widehat{\mathbf{Y}}_0(s) = \mathbf{H}_0 \widetilde{\mathbf{x}}(s) + \mathbf{L}(s), \quad (26)$$

$$\mathbf{w}(s, 1) = \mathbf{Y}_1(s) - \widehat{\mathbf{Y}}_1(s) = \mathbf{H}_1 \widetilde{\mathbf{x}}(s) + \mathbf{G}(s), \quad (27)$$

where  $\widehat{\mathbf{Y}}_1(s, 1)$  is the projection of  $Y_1(s)$  onto the linear space of  $\mathcal{L}\{\{\mathbf{Y}_1(i)\}_{i=0}^{s-1}\}$  and  $\widehat{\mathbf{Y}}_0(s, 0)$  is the projection of  $\mathbf{Y}_0(s)$  onto the linear space of  $\mathcal{L}\{\{\mathbf{Y}_1(i)\}_{i=0}^{k-d}, \{\mathbf{Y}_0(i)\}_{i=k-d+1}^k\}$ . Then, we define  $\widetilde{\mathbf{x}}(s, 0) = \mathbf{x}(s) - \widehat{\mathbf{x}}(s, 0)$  and  $\widetilde{\mathbf{x}}(s, 1) = \mathbf{x}(s) - \widehat{\mathbf{x}}(s, 1)$ . It should be noted that the definitions of  $\widetilde{\mathbf{x}}(s, 0)$  and  $\widetilde{\mathbf{x}}(s, 1)$  are similar to  $\widehat{\mathbf{Y}}_0(s, 0)$  and  $\widehat{\mathbf{Y}}_1(s, 1)$ . In addition, we reckon that  $\{\{\mathbf{w}(i, 1)\}_{i=0}^{k-d}, \{\mathbf{w}(i, 0)\}_{i=k-d+1}^k\}$  is an independent white noise and spans the same linear space as  $\mathcal{L}\{\{\mathbf{Y}_1(i)\}_{i=0}^{k-d}, \{\mathbf{Y}_0(i)\}_{i=k-d+1}^k\}$ . Next, we derive the covariance  $\mathbf{R}_{w(s,0)}$  and  $\mathbf{R}_{w(s,1)}$  of the innovation sequence. For convenience, the following definitions are given:

$$\begin{aligned} \mathbf{P}_0(s) &\triangleq \mathbb{E}\{\widetilde{\mathbf{x}}(s, 0)\widetilde{\mathbf{x}}^T(s, 0)\}, \\ \mathbf{P}_1(s) &\triangleq \mathbb{E}\{\widetilde{\mathbf{x}}(s, 1)\widetilde{\mathbf{x}}^T(s, 1)\}, \\ \mathbf{D}(s) &\triangleq \mathbb{E}\{\mathbf{x}(s)\mathbf{x}^T(s)\}. \end{aligned} \quad (28)$$

Then, the covariance matrices of the innovation sequences (26) and (27) can be derived by the following formula:

$$\begin{aligned} \mathbf{R}_{w(s,0)} &= \mathbb{E}\{\mathbf{w}(s, 0)\mathbf{w}^T(s, 0)\} = \mathbf{H}_0 \mathbf{P}_0(s) \mathbf{H}_0^T + \mathbf{Q}_{L(s)}, \\ \mathbf{R}_{w(s,1)} &= \mathbb{E}\{\mathbf{w}(s, 1)\mathbf{w}^T(s, 1)\} = \mathbf{H}_1 \mathbf{P}_1(s) \mathbf{H}_1^T + \mathbf{Q}_{G(s)}. \end{aligned} \quad (29)$$

Finally, the covariance matrices  $\mathbf{P}_0(s+1)$  and  $\mathbf{P}_1(s+1)$  can be derived as

$$\mathbf{P}_1(s+1) = \mathbf{A} \mathbf{P}_1(s) \mathbf{A}^T + \mathbf{Q}_{F(s)} - \mathbf{A} \mathbf{P}_1(s) \mathbf{H}_1^T \mathbf{R}_{w(s,1)}^{-1} \mathbf{H}_1 \mathbf{P}_1(s) \mathbf{A}^T, \quad (30)$$

$$\mathbf{P}_1(0) = \mathbf{D}_1(0), \quad (31)$$

$$\mathbf{P}_0(s+1) = \mathbf{A} \mathbf{P}_0(s) \mathbf{A}^T + \mathbf{Q}_{F(s)} - \mathbf{A} \mathbf{P}_0(s) \mathbf{H}_0^T \mathbf{R}_{w(s,0)}^{-1} \mathbf{H}_0 \mathbf{P}_0(s) \mathbf{A}^T, \quad (32)$$

$$\mathbf{P}_0(k-d+1) = \mathbf{P}_1(k-d+1), \quad (33)$$

and the Lyapunov equation  $\mathbf{D}(s+1)$  can be calculated by

$$\mathbf{D}(s+1) = \mathbf{A} \mathbf{D}(s) \mathbf{A}^T + \mathbf{Q}_{F(s)}. \quad (34)$$

**Theorem 1.** For given systems (15)–(17), the quadratic filter  $\widehat{\mathbf{x}}(k|k)$  can be derived as

$$\begin{aligned} \widehat{\mathbf{x}}(k|k) &= \widehat{\mathbf{x}}(k, 0) + \mathbf{P}_0(k) \mathbf{H}_0^T \mathbf{R}_{w(k,0)}^{-1} [\mathbf{Y}_0(k) - \mathbf{H}_0 \widehat{\mathbf{x}}(k) \\ &\quad - \mathbf{E}_0 \mathbf{U}_0(k)], \end{aligned} \quad (35)$$

where the estimator  $\widehat{\mathbf{x}}(k|0)$  is computed by

$$\begin{aligned} \widehat{\mathbf{x}}(s+1, 0) &= \mathbf{A} \widehat{\mathbf{x}}(s, 0) + \mathbf{C} \mathbf{U}_0(s) + \mathbf{A} \mathbf{P}_0(s) \mathbf{H}_0^T \mathbf{R}_{w(s,0)}^{-1} [\mathbf{Y}_0(s) \\ &\quad - \mathbf{H}_0 \widehat{\mathbf{x}}(s) - \mathbf{E}_0 \mathbf{U}_0(s)], \end{aligned} \quad (36)$$

with the initial value  $\widehat{\mathbf{x}}(k-d+1, 0) = \widehat{\mathbf{x}}(k-d+1, 1)$ , and  $\widehat{\mathbf{x}}(k-d+1, 1)$  is obtained by

$$\begin{aligned} \widehat{\mathbf{x}}(s+1, 1) &= \mathbf{A} \widehat{\mathbf{x}}(s, 1) + \mathbf{C} \mathbf{U}_0(s) + \mathbf{A} \mathbf{P}_1(s) \mathbf{H}_1^T \mathbf{R}_{w(s,1)}^{-1} [\mathbf{Y}_1(s) \\ &\quad - \mathbf{H}_1 \widehat{\mathbf{x}}(s) - \mathbf{E}_1 \mathbf{U}_1(s)]. \end{aligned} \quad (37)$$

*Proof.* According to (15), we can directly prove (38) by the projection theorem:

$$\begin{aligned} \widehat{\mathbf{x}}(s+1, 0) &= \mathbf{A} \widehat{\mathbf{x}}(s, 0) + \mathbb{E}\{\mathbf{x}(s+1) \mathbf{w}^T(s, 0)\} \mathbf{R}_{w(s,0)}^{-1} \mathbf{w}(s, 0) \\ &= \mathbf{A} \widehat{\mathbf{x}}(s, 0) + \mathbf{C} \mathbf{U}_0(s) + \mathbf{A} \mathbf{P}_0(s) \mathbf{H}_0^T \mathbf{R}_{w(s,0)}^{-1} \\ &\quad \times [\mathbf{Y}_0(s) - \mathbf{H}_0 \widehat{\mathbf{x}}(s) - \mathbf{E}_0 \mathbf{U}_0(s)]. \end{aligned} \quad (38)$$

Then, we obtain the estimate error  $\widetilde{\mathbf{x}}(s+1, 0)$  by subtracting (38) from (15):

$$\widetilde{\mathbf{x}}(s+1, 0) = \mathbf{A} \widetilde{\mathbf{x}}(s, 0) + \mathbf{F}(s) - \mathbf{A} \mathbf{P}_0(s) \mathbf{H}_0^T \mathbf{R}_{w(s,0)}^{-1} \mathbf{w}(s, 0). \quad (39)$$

Therefore, the prediction error covariance  $\mathbf{P}_0(s+1)$  can be calculated from (39):

$$\begin{aligned} \mathbf{P}_0(s+1) &= \mathbb{E}\{\widetilde{\mathbf{x}}(s+1, 0)\widetilde{\mathbf{x}}^T(s+1, 0)\} \\ &= \mathbf{A} \mathbf{P}_0(s) \mathbf{A}^T + \mathbf{Q}_{F(s)} - \mathbf{A} \mathbf{P}_0(s) \mathbf{H}_0^T \mathbf{R}_{w(s,0)}^{-1} \mathbf{H}_0 \mathbf{P}_0(s) \mathbf{A}^T. \end{aligned} \quad (40)$$

Similar to formula (39), we can deduce (41) as follows:

$$\begin{aligned} \widehat{\mathbf{x}}(s+1, 1) &= \mathbf{A} \widehat{\mathbf{x}}(s, 1) + \mathbb{E}\{\mathbf{x}(s+1) \mathbf{w}^T(s, 1)\} \mathbf{R}_{w(s,1)}^{-1} \mathbf{w}(s, 1) \\ &= \mathbf{A} \widehat{\mathbf{x}}(s, 1) + \mathbf{C} \mathbf{U}_0(s) + \mathbf{A} \mathbf{P}_1(s) \mathbf{H}_1^T \mathbf{R}_{w(s,1)}^{-1} \\ &\quad \times [\mathbf{Y}_1(s) - \mathbf{H}_1 \widehat{\mathbf{x}}(s) - \mathbf{E}_1 \mathbf{U}_1(s)]. \end{aligned} \quad (41)$$

By combining (15) and (41), one has

$$\widetilde{\mathbf{x}}(s+1, 1) = \mathbf{A} \widetilde{\mathbf{x}}(s, 1) + \mathbf{F}(s) - \mathbf{A} \mathbf{P}_1(s) \mathbf{H}_1^T \mathbf{R}_{w(s,1)}^{-1} \mathbf{w}(s, 1). \quad (42)$$

As such, we get the Riccati equation:

$$\begin{aligned} \mathbf{P}_1(s+1) &= \mathbb{E}\{\widetilde{\mathbf{x}}(s+1, 1)\widetilde{\mathbf{x}}^T(s+1, 1)\} \\ &= \mathbf{A} \mathbf{P}_1(s) \mathbf{A}^T + \mathbf{Q}_{F(s)} - \mathbf{A} \mathbf{P}_1(s) \mathbf{H}_1^T \mathbf{R}_{w(s,1)}^{-1} \\ &\quad \times \mathbf{H}_1 \mathbf{P}_1(s) \mathbf{A}^T. \end{aligned} \quad (43)$$

By the definition of  $\widehat{\mathbf{x}}(k-d+1, 0)$  and  $\widehat{\mathbf{x}}(k-d+1, 1)$ , we can conclude that  $\widehat{\mathbf{x}}(k-d+1, 0) = \widehat{\mathbf{x}}(k-d+1, 1)$ . Therefore, formula (33) is proved.

The proof is finished.  $\square$

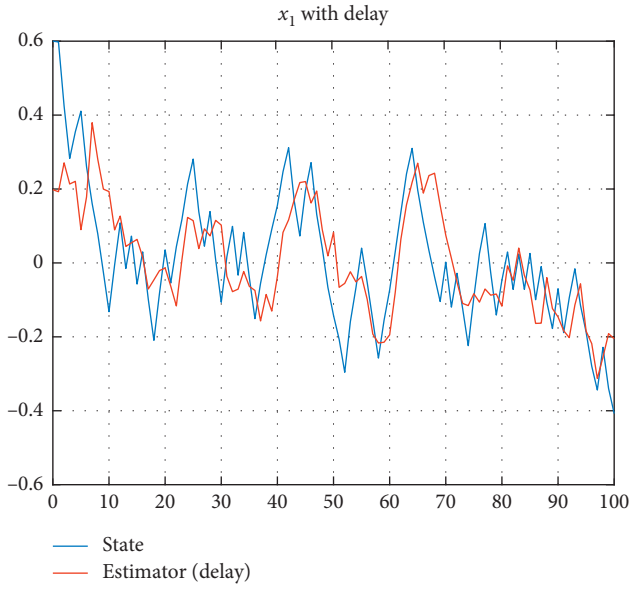


FIGURE 1: The first state component  $x_1(k)$  and the filter  $\hat{x}(k|k)$  (delay).

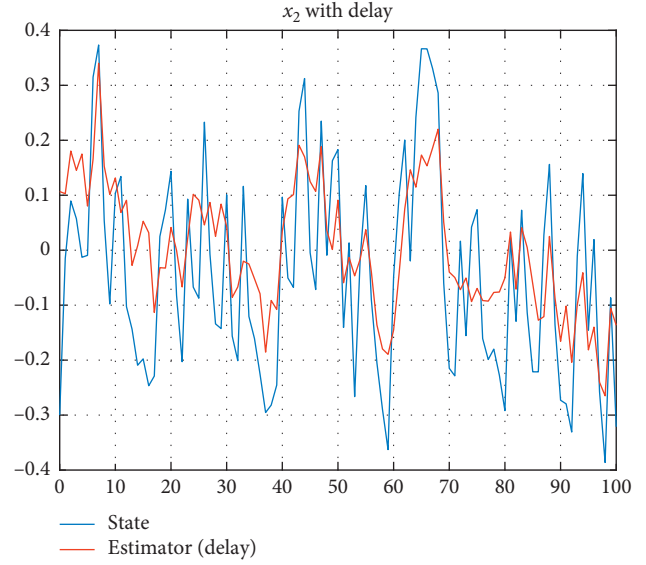


FIGURE 2: The second state component  $x_2(k)$  and the filter  $\hat{x}(k|k)$  (delay).

#### 4. Simulation Results

In this section, we demonstrate the effectiveness of the proposed algorithm by a simulation example. The linear discrete-time system can be written as follows:

$$\begin{aligned} x(k+1) &= \begin{bmatrix} 0.88 & 0.1 \\ 0.45 & 0.28 \end{bmatrix} x(k) + n(k), \\ y_0(k) &= \xi(k) \begin{bmatrix} 1 & 2 \\ 2 & 1 \end{bmatrix} x(k) + v_0(k), \\ y_1(k) &= \theta(k) \begin{bmatrix} 2 & 1 \\ 1 & 2 \end{bmatrix} x(k) + v_1(k), \end{aligned} \quad (44)$$

with initial values given as  $x(0) = \begin{bmatrix} 0.6 \\ -0.3 \end{bmatrix}$ ,  $\hat{x}(0) =$

$$\begin{bmatrix} 0 \\ 0 \end{bmatrix}, Q = \begin{bmatrix} 0.01 & 0 \\ 0 & 0.0225 \end{bmatrix}, D(0) = P(0) = \begin{bmatrix} 1.08 & 0 \\ 0 & 0.03 \end{bmatrix},$$

$$\phi = \text{diag}\{0.6, 0.7\}, \varphi = \text{diag}\{0.7, 0.9\}, R_0 = \begin{bmatrix} 0.0625 & 0 \\ 0 & 0.16 \end{bmatrix},$$

$$\text{and } R_1 = \begin{bmatrix} 0.04 & 0 \\ 0 & 0.09 \end{bmatrix}; n(k), v_0(k), \text{ and } v_1(k) \text{ are the}$$

white noises with zero mean and covariances  $Q, R_0$ , and  $R_1$ , respectively.

We use MATLAB to simulate the performance of the estimator in Theorem 1, and the numerical results are shown in Figures 1–4. First, it can be seen that Figures 1 and 2 represent quadratic estimators with measurement

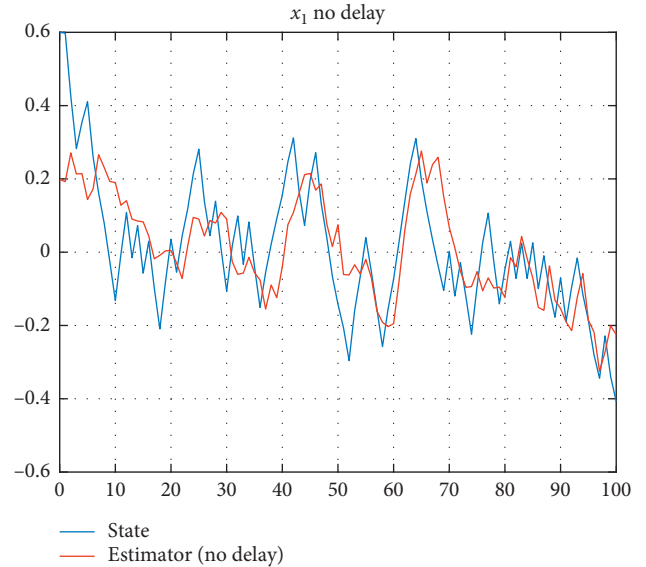


FIGURE 3: The first state component  $x_1(k)$  and the filter  $\hat{x}(k|k)$  (no delay).

delays, and Figures 3 and 4 reflect the quadratic estimation results without delays. Then, by comparing Figures 1 and 3 and Figures 2 and 4, it can be observed that the tracking effect of Figures 1 and 2 is better. Therefore, this experiment shows that the information from the measurement delay channel is really important in the design of the quadratic estimator.



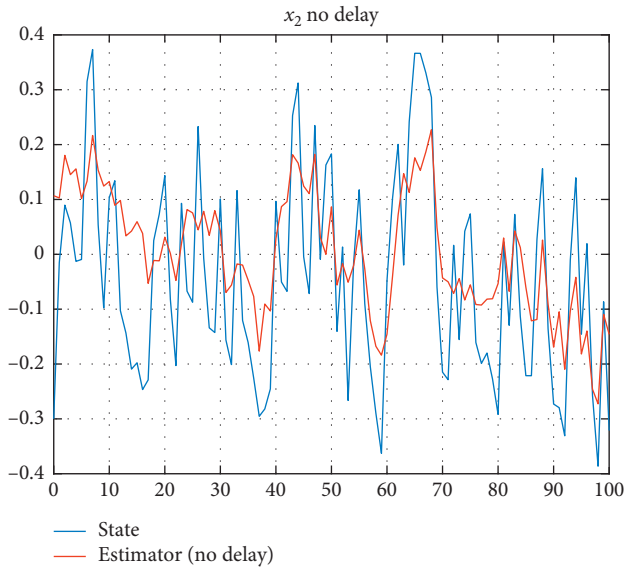


FIGURE 4: The second state component  $x_2(k)$  and the filter  $\hat{x}(k|k)$  (no delay).

## 5. Conclusion

We considered the problem of remote estimation with time delay and multiplicative noise for multichannel systems. At first, we applied the reorganized innovation analysis approach to construct the original delay system into a new delay-free system. Secondly, the delay-free system was reconstructed by the quadratic filtering method to obtain an augmented system. Then, the Kalman filtering theory and the projection formula were used to solve two Riccati equations and one Lyapunov equation for the augmented system, and the quadratic filter for the measurement delay system on the packet loss network was obtained. Finally, simulation experiments proved the effectiveness of the estimator algorithm.

## Data Availability

The simulation program data used to support the proposed approach in numerical example section is available from the corresponding author upon request. No data (except for the simulation program) were used to support this study.

## Conflicts of Interest

The authors express that there are no conflicts of interest concerning with the publication of this work.

## Authors' Contributions

The contribution of all the authors to the writing of this paper is identical. The final manuscript was read and approved by all of them.

## Acknowledgments

This work was supported in part by the National Science Foundation of China (61873152) and the Chinese

Postdoctoral Science Foundation (2019M652424 and 2017M612336).

## References

- [1] C. Pang and S. Sun, "Fusion predictors for multisensor stochastic uncertain systems with missing measurements and unknown measurement disturbances," *IEEE Sensors Journal*, vol. 15, no. 8, pp. 4346–4354, 2015.
- [2] X. Song and W. X. Zheng, "Linear estimation for discrete-time periodic systems with unknown measurement input and missing measurements," *ISA Transactions*, vol. 95, pp. 164–172, 2019.
- [3] L. Li, D. W. C. Ho, and J. Lu, "Event-based network consensus with communication delays," *Nonlinear Dynamics*, vol. 87, no. 3, pp. 1847–1858, 2016.
- [4] N. E. Nahi, "Optimal recursive estimation with uncertain observation," *IEEE Transactions on Information Theory*, vol. 15, no. 4, pp. 128–136, 1969.
- [5] B. Sinopoli, L. Schenato, M. Franceschetti, K. Poolla, M. I. Jordan, and S. S. Sastry, "Kalman filtering with intermittent observations," *IEEE Transactions on Automatic Control*, vol. 49, no. 9, pp. 1453–1464, 2004.
- [6] H. Zhang, X. Song, and L. Shi, "Convergence and mean square stability of suboptimal estimator for systems with measurement packet dropping," *IEEE Transactions on Automatic Control*, vol. 57, no. 5, pp. 1248–1253, 2012.
- [7] X. Song, Z. Duan, and J. H. Park, "Linear optimal estimation for discrete-time systems with measurement-delay and packet dropping," *Applied Mathematics and Computation*, vol. 284, pp. 115–124, 2016.
- [8] H. Liu, B. Xu, D. Lu, and G. Zhang, "A path planning approach for crowd evacuation in buildings based on improved artificial bee colony algorithm," *Applied Soft Computing*, vol. 68, pp. 360–376, 2018.
- [9] H. Liu, B. Liu, H. Zhang, L. Li, X. Qin, and G. Zhang, "Crowd evacuation simulation approach based on navigation knowledge and two-layer control mechanism," *Information Sciences*, vol. 436–437, pp. 247–267, 2018.
- [10] D. Yang, X. Li, and J. Qiu, "Output tracking control of delayed switched systems via state-dependent switching and dynamic output feedback," *Nonlinear Analysis: Hybrid Systems*, vol. 32, pp. 294–305, 2019.
- [11] A. De Santis, A. Germani, and M. Raimondi, "Optimal quadratic filtering of linear discrete-time non-Gaussian systems," *IEEE Transactions on Automatic Control*, vol. 40, no. 7, pp. 1274–1278, 1995.
- [12] R. Caballero-Águila, A. Hermoso-Carazo, and J. Linares-Pérez, "Linear and quadratic estimation using uncertain observations from multiple sensors with correlated uncertainty," *Signal Processing*, vol. 91, no. 2, pp. 330–337, 2011.
- [13] F. Cacace, A. Fasano, and A. Germani, "Quadratic filtering of non-Gaussian systems with intermittent observations," in *Proceedings of the 52nd IEEE Conference on Decision and Control*, Firenze, Italy, December 2013.
- [14] H. Zhao and C. Zhang, "Non-Gaussian noise quadratic estimation for linear discrete-time time-varying systems," *Neurocomputing*, vol. 174, pp. 921–927, 2016.
- [15] F. Cacace, F. Conte, A. Germani, and G. Palombo, "Feedback quadratic filtering," *Automatica*, vol. 82, pp. 158–164, 2017.
- [16] T. H. Lee, H. M. Trinh, and J. H. Park, "Stability analysis of neural networks with time-varying delay by constructing novel Lyapunov functionals," *IEEE Transactions on Neural*

- Networks and Learning Systems*, vol. 29, no. 9, pp. 4238–4247, 2018.
- [17] L. B. Wu and J. H. Park, “Adaptive fault-tolerant control of uncertain switched nonaffine nonlinear systems with actuator faults and time delays,” *IEEE Transactions on Systems, Man, and Cybernetics: Systems*, vol. 99, 2019.
  - [18] X. Li, J. Shen, H. Akca, and R. Rakkiyappan, “LMI-based stability for singularly perturbed nonlinear impulsive differential systems with delays of small parameter,” *Applied Mathematics and Computation*, vol. 250, pp. 798–804, 2015.
  - [19] B. Niu, D. Wang, M. Liu, X. Song, H. Wang, and P. Duan, “Adaptive neural output-feedback controller design of switched nonlinear triangular nonlinear systems with time delays,” in *Proceedings of the IEEE Transactions on Neural Networks and Learning Systems*, Piscataway, NJ, USA, December 2020.
  - [20] Z. Wang, J. Xu, X. Song, and H. Zhang, “Consensus problem in multi-agent systems under delayed information,” *Neurocomputing*, vol. 316, pp. 277–283, 2018.
  - [21] Z. Wang, H. Zhang, M. Fu, and H. Zhang, “Consensus for high-order multi-agent systems with communication delay,” *Science China-Information Science*, vol. 9, pp. 241–252, 2017.
  - [22] X. Song and J. H. Park, “Linear optimal estimation for discrete-time measurement delay systems with multichannel multiplicative noise,” *IEEE Transactions on Circuits and Systems II: Express Briefs*, vol. 64, no. 2, pp. 156–160, 2017.
  - [23] X. Yang, X. Li, X. Li, Q. Xi, and P. Duan, “Review of stability and stabilization for impulsive delayed systems,” *Mathematical Biosciences & Engineering*, vol. 15, no. 6, pp. 1495–1515, 2018.
  - [24] D. Yang, X. Li, J. Shen, and Z. Zhou, “State-dependent switching control of delayed switched systems with stable and unstable modes,” *Mathematical Methods in the Applied Sciences*, vol. 41, no. 16, pp. 6968–6983, 2018.
  - [25] T. H. Lee and J. H. Park, “New methods of fuzzy sampled-data control for stabilization of chaotic systems,” *IEEE Transactions on Systems, Man, and Cybernetics: Systems*, vol. 48, no. 12, pp. 2026–2034, 2018.
  - [26] L. B. Wu, J. H. Park, and N. N. Zhao, “Robust adaptive fault-tolerant tracking control for nonaffine stochastic nonlinear systems with full state constraints,” *IEEE Transactions on Cybernetics*, vol. 99, 2019.
  - [27] H. Kwakernaak, “Optimal filtering in linear systems with time delays,” *IEEE Transactions on Automatic Control*, vol. 12, no. 2, pp. 169–173, 1967.
  - [28] L. Xiao, A. Hassibi, and J. P. How, “Control with random communication delays via a discrete-time jump system approach,” in *Proceedings of the 2000 American Control Conference*, pp. 2199–2204, Chicago, IL, USA, June 2000.
  - [29] H. Zhang, X. Lu, and D. Cheng, “Optimal estimation for continuous-time systems with delayed measurements,” *IEEE Transactions on Automatic Control*, vol. 51, no. 5, pp. 823–827, 2006.

## Research Article

# Synchronization Analysis for Stochastic Inertial Memristor-Based Neural Networks with Linear Coupling

Lixia Ye,<sup>1</sup> Yonghui Xia ,<sup>2</sup> Jin-liang Yan,<sup>1</sup> and Haidong Liu <sup>3</sup>

<sup>1</sup>Department of Mathematics and Computer, Wuyi University, Wuyishan, Nanping 354300, China

<sup>2</sup>Department of Mathematics, Zhejiang Normal University, Jinhua 321004, China

<sup>3</sup>School of Mathematical Sciences, Qufu Normal University, Qufu 273165, China

Correspondence should be addressed to Yonghui Xia; xiadoc@163.com

Received 28 May 2020; Accepted 29 June 2020; Published 23 July 2020

Academic Editor: Jianquan Lu

Copyright © 2020 Lixia Ye et al. This is an open access article distributed under the Creative Commons Attribution License, which permits unrestricted use, distribution, and reproduction in any medium, provided the original work is properly cited.

This paper concerns the synchronization problem for a class of stochastic memristive neural networks with inertial term, linear coupling, and time-varying delay. Based on the interval parametric uncertainty theory, the stochastic inertial memristor-based neural networks (IMNNs for short) with linear coupling are transformed to a stochastic interval parametric uncertain system. Furthermore, by applying the Lyapunov stability theorem, the stochastic analysis approach, and the Halanay inequality, some sufficient conditions are obtained to realize synchronization in mean square. The established criteria show that stochastic perturbation is designed to ensure that the coupled IMNNs can be synchronized better by changing the state coefficients of stochastic perturbation. Finally, an illustrative example is presented to demonstrate the efficiency of the theoretical results.

## 1. Introduction

The memristor [1] is a kind of a nonlinear resistor with memory and nanoscale, which is widely applied in chaotic circuits, artificial neural networks, and so on. In [2], the relevant mechanisms of neural networks, such as long-term potentiation and spike time-dependent plasticity, are presented by applying basic electric circuits, and more complex mechanisms are constructed to mimic the synaptic connections in a (human) brain. During neuron transmission, synchronous resonance is a very important biological phenomenon. In recent years, a lot of systems have been investigated to realize synchronization such as time-varying switched systems, MNNs, and BAM neural networks [3–19]. In [8], a new switching pinning controller was designed to finite-time synchronization in nonlinear coupled neural networks by regulating a parameter. Therefore, it is necessary for synchronization to design a suitable controller, such as impulsive controller [11, 12, 20–22], nonchattering controller [19], and switching controller [6–8]. Based on parametric uncertainty and state dependency in the connection weight matrices of MNNs, the connection weight

matrices jump in certain intervals. Duan and Huang [23] proposed periodicity and dissipativity for memristor-based neural networks with mixed delays involving both time-varying delays and distributed delays via using Mawhin-like coincidence theorem, inclusion theory, and M-matrix properties. The authors established two different types of exponential synchronization criteria for the coupled MNNs based on the master-slave (drive response) concept and discontinuous state feedback controller, and simultaneously, an estimation of the exponential synchronization rate was estimated (see [24]). It is worth pointing out that, the authors in [25, 26] added the linear coupling and interval term into MNNs to achieve two different synchronization via applying the Halanay inequality [27] and the Lyapunov method. However, there were essential differences between the synchronization results established by these two literature studies. In [25], the differential inclusion method was applied to transform the coupled connection weight matrices; moreover, a discontinuous controller was designed to ensure that multiple IMMNNs can be synchronized. Li and Zheng [26] demonstrated that the coupled connection weight matrices can be decomposed by interval analysis [28],

which by weakening the matrices satisfies the conditions. Besides, the new synchronization criteria for IMMNs with linear coupling were established.

As we know, noise plays an important role in synchronization since it can stabilize an unstable system. In recent years, many scholars are very interested in synchronization of stochastic networks with time-varying delays [2, 29–38]. In 2013, the Jensen integral inequality was improved by the so-called Wirtinger-based integral inequality [33]. Furthermore, Gao et al. [29] showed that a state feedback controller and an adaptive updated law used to guarantee stochastic memristor-based neural networks with noise disturbance can be asymptotically synchronized. In [38], the authors investigated the synchronization of a stochastic multilayer dynamic network with time-varying delays and additive couplings by designing two pinning controllers. Therefore, taking stochastic perturbation into complex neural networks is very necessary and important.

Note that the stochastic systems were mainly first-order neural networks in previous works. In this paper, based on the model of [26], considering  $x_i(t), x_i(t - \tau(t)), f_i(x_i(t)), f_i(x_i(t - \tau(t)))$  will produce errors, the new model of the stochastic coupled inertial memristor-based neural networks is constructed. Meanwhile, new results on

synchronization in mean square are proposed. The main contributions of this paper are high-lighted as follows:

- (i) Stochastic perturbation is taken into account in the second-order [39] coupled memristor-based neural networks with inertial term. Synchronization analysis becomes more challenging for the system with higher order and higher dimension.
- (ii) The criterion for stochastic inertial memristor-based neural networks with linear coupling is proposed by applying the stochastic analysis techniques and the vector Lyapunov function method to realize synchronization in mean square.
- (iii) An illustrative example is given to illustrate that system (1) can be synchronized under the coupled network with five nodes. Besides, system (1) has strong anti-interference.

## 2. Model Formulation and Preliminaries

In this paper, we consider the model of stochastic coupled inertial memristor-based neural networks (IMMNs for short) with  $N$  coupled identical nodes described by the following equation:

$$\begin{aligned} d\left(\frac{dx_i(t)}{dt}\right) = & \left(-D\frac{dx_i(t)}{dt} - Cx_i(t) + A(x_i(t))f(x_i(t)) + B(x_i(t))f(x_i(t - \tau(t)))\right. \\ & \left.+ c \sum_{j=1}^N G_{ij}\Gamma\left(\frac{dx_i(t)}{dt} + x_j(t)\right)\right)dt + (\sigma_1 x_i(t) + \sigma_2 x_i(t - \tau(t))) \\ & + \sigma_3 f(x_i(t)) + \sigma_4 f(x_i(t - \tau(t)))dw_t, \quad i \in N, \end{aligned} \quad (1)$$

where  $x_i(t) = (x_{i1}(t), x_{i2}(t), \dots, x_{in}(t))^T \in R^n, i \in N$ ,  $D = \text{diag}(\beta_1, \beta_2, \dots, \beta_n)$ ,  $C = \text{diag}(c_1, c_2, \dots, c_n)$ , and  $\sigma_i = \text{diag}(\sigma_{i1}, \sigma_{i2}, \dots, \sigma_{in}), i = 1, 2, 3, 4$ , are the constant positive definite matrices and  $0 < \tau(t) < \tau$ ; the connection memristive weight matrix  $A(x_i(t)) = [a_{kj}(x_{ij}(t))]_{n \times n}$  and the delayed connection of the current voltage characteristics  $B(x_i(t)) = [b_{kj}(x_{ij}(t))]_{n \times n}$  satisfy the following conditions:

$$\begin{aligned} a_{kj}(x_{ij}(t)) = & \begin{cases} a_{kj}^*, & |x_{ij}| < T_j, \\ b_{kj}^{**}, & |x_{ij}| > T_j, \end{cases} \\ b_{kj}(x_{ij}(t)) = & \begin{cases} a_{kj}^*, & |x_{ij}| < T_j, \\ b_{kj}^{**}, & |x_{ij}| > T_j, \end{cases} \end{aligned} \quad (2)$$

where  $T > 0$  is the switching jump and  $a_{kj}^*, a_{kj}^{**}, b_{kj}^*$ , and  $b_{kj}^{**}$  are all constants,  $k, j \in n$ . The network coupling strength  $c > 0$  is a constant, and  $\Gamma = \text{diag}(\gamma_1, \gamma_2, \dots, \gamma_n) \in R^{n \times n}$  is the inner coupling matrix.  $G = (G_{ij})_{N \times N}$  is the constant coupling configuration matrix representing the topological structure of the system.  $G_{ij} > 0$  is defined as a link from node  $i$  to node  $j$ , otherwise,  $G_{ij} = 0$ . Besides,  $G$  satisfies

$$G_{ii} = - \sum_{j=1, j \neq i}^N G_{ij}, \quad i \in N. \quad (3)$$

The initial condition associated with system (1) is given as  $x_i(s) = \varphi_i(s) \in C^1([- \tau, 0], R^n), i \in N$ . And,  $f(x_i(t)) = (f_1(x_{i1}(t)), f_2(x_{i2}(t)), \dots, f_n(x_{in}(t)))^T$  denotes the output of the neuron unit, which satisfies the following assumption:

( $H_1$ ): for any two different  $u, v \in R$ , there exists a positive scalar  $l_i > 0 (i \in n)$  such that  $|f_i(u) - f_i(v)| \leq l_i |u - v|$ .

For stochastic systems, the Itô formula plays an important role in the synchronization. Consider a general stochastic system  $dx(t) = f(x(t), t)dt + g(x(t), t)dw_t$  on  $t > t_0$  with an initial value  $x(t_0) = x_0 \in R^n$ , where  $f: R^n \times R^+ \rightarrow R^{n \times m}$  and  $g: R^n \times R^+ \rightarrow R^{n \times m}$ . Denote a general nonnegative function  $V(x, t)$  on  $R^n \times R^+$  to be continuously twice differentiable in  $x$  and once differentiable in  $t$ , an stochastic differential operator  $t dV(x, t) = \mathcal{L}V(x, t)dt + V_x(x, t)g(x, t)dw_t$ ,

where  $\mathcal{L}V(x, t) = V_t(x, t) + V_x(x, t)f(x, t) + (1/2)\text{trac}[g^T(x, t)V_{xx}(x, t)g(x, t)]$ ,  $V_t(x, t) = \partial V(x, t)/\partial t$ ,  $V_x(x, t) = (\partial V(x, t)/\partial x_1, \partial V(x, t)/\partial x_2, \dots, \partial V(x, t)/\partial x_n)$ ,

$V_{xx}(x, t) = (\partial^2 V(x, t) / \partial x_i \partial x_j)_{n \times n}$ , and  $E[dV(x, t)] = E[\mathcal{L}V((x, t)dt)]$ .

Considering  $a_{kj}(x_{ij})$  and  $b_{kj}(x_{ij})$  are bounded, therefore,  $A(x_i(t)) \in [\underline{A}, \overline{A}]$ ,  $B(x_i(t)) \in [\underline{B}, \overline{B}]$ , where  $\underline{A} = (\underline{a}_{kj})_{n \times n}$ ,  $\overline{A} = (\overline{a}_{kj})_{n \times n}$ ,  $\underline{B} = (\underline{b}_{kj})_{n \times n}$ , and  $\overline{B} = (\overline{b}_{kj})_{n \times n}$  with  $\underline{a}_{kj} = \min\{a_{kj}^*, a_{kj}^{**}\}$ ,  $\overline{a}_{kj} = \max\{a_{kj}^*, a_{kj}^{**}\}$ ,  $\underline{b}_{kj} = \min\{b_{kj}^*, b_{kj}^{**}\}$ , and  $\overline{b}_{kj} = \max\{b_{kj}^*, b_{kj}^{**}\}$ .

By introducing the variable transformation,

$$r_i(t) = \frac{dx_i(t)}{dt} + x_i(t). \quad (4)$$

System (1) can be transformed into

$$\begin{cases} dx_i(t) = [-x_i(t) + r_i(t)]dt, \\ dr_i(t) = \left( -\Theta x_i(t) - \Lambda r_i(t) + [\underline{A}, \overline{A}]f(x_i(t)) + [\underline{B}, \overline{B}]f(x_i(t - \tau(t))) + c \sum_{j=1}^N G_{ij} \Gamma r_j(t) \right) dt \\ + (\sigma_1 x_i(t) + \sigma_2 x_i(t - \tau(t)) + \sigma_3 f(x_i(t)) + \sigma_4 f(x_i(t - \tau(t))))dw_t, \quad i \in N, \end{cases} \quad (5)$$

where  $\Theta = I + C - D$ ,  $\Lambda = D - I$ .

Based on interval uncertainty theory, the intervals  $[\underline{A}, \overline{A}]$  and  $[\underline{B}, \overline{B}]$  can be decomposed into  $[\underline{A}, \overline{A}] = A_0 + [-1, 1]H_A$  and  $[\underline{B}, \overline{B}] = B_0 + [-1, 1]H_B$ , where  $A_0 = (\underline{A} +$

$$\overline{A})/2, H_A = (1/2)(\overline{A} - \underline{A}) \text{ and } B_0 = (\underline{B} + \overline{B})/2, H_B = (1/2)(\overline{B} - \underline{B}).$$

Then, system (5) can be equivalently expressed as

$$\begin{cases} dx_i(t) = [-x_i(t) + r_i(t)]dt, \\ dr_i(t) = \left( -\Theta x_i(t) - \Lambda r_i(t) + A_0 f(x_i(t)) + B_0 f(x_i(t - \tau(t))) + E\Delta(t) + c \sum_{j=1}^N G_{ij} \Gamma r_j(t) \right) dt \\ + (\sigma_1 x_i(t) + \sigma_2 x_i(t - \tau(t)) + \sigma_3 f(x_i(t)) + \sigma_4 f(x_i(t - \tau(t))))dw_t, \quad i \in N, \end{cases} \quad (6)$$

where

$$\begin{aligned} E\Delta(t) &= \frac{1}{2}[-1, 1](\overline{A} - \underline{A})f(x_i(t)) + \frac{1}{2}[-1, 1](\overline{B} - \underline{B})f(x_i(t - \tau(t))) \\ &= [-1, 1](H_A f(x_i(t)) + H_B f(x_i(t - \tau(t)))) \end{aligned} \quad (7)$$

and  $E\Delta(t)$  is satisfied:

$$(E\Delta(t))^\top (E\Delta(t)) \leq (H_A f(x_i(t)))^\top (H_A f(x_i(t))) + (H_B f(x_i(t - \tau(t))))^\top (H_B f(x_i(t - \tau(t)))). \quad (8)$$

Let  $x(t) = (x_1(t)^\top, x_2(t)^\top, \dots, x_N(t)^\top)^\top$ ,  $r(t) = (r_1(t)^\top, r_2(t)^\top, \dots, r_N(t)^\top)^\top$ ,  $\mathbf{f}(x(t)) = (f(x_1(t))^\top, f(x_2(t))^\top, \dots, f(x_N(t))^\top)^\top$ ,  $\Theta = I_N \otimes \Theta$ ,  $\Lambda = I_N \otimes \Lambda$ ,  $\mathbf{G} = \mathbf{G} \otimes \Gamma$ ,  $\mathbf{A}_0 = I_N \otimes A_0$ ,  $\mathbf{B}_0 = I_N \otimes B_0$ ,  $E\Delta(t) = I_N \otimes E\Delta(t)$ ,  $\mathbf{H}_A = I_N \otimes H_A$ ,  $\mathbf{H}_B = I_N \otimes H_B$ , and  $\sigma_i = I_N \otimes \sigma_i$ ,  $i = 1, 2, 3, 4$ . For simplicity, we use  $x, r$ , and  $x_\tau$  instead of  $x(t), r(t)$ , and  $x(t - \tau(t))$  in the following sections. Then, system (6) can be written as

$$\begin{cases} dx = (-x + r)dt, \\ dr = (-\Theta x - \Lambda r + \mathbf{A}_0 \mathbf{f}(x) + \mathbf{B}_0 \mathbf{f}(x_\tau) + E\Delta(t) + c \mathbf{G} r)dt \\ + (\sigma_1 x + \sigma_2 x_\tau + \sigma_3 \mathbf{f}(x) + \sigma_4 \mathbf{f}(x_\tau))dw_t, \quad i \in N. \end{cases} \quad (9)$$

**Definition 1.** The stochastic coupled IMMNs (5) are said to be globally synchronized in the mean square sense if  $E[\|x_i(t) - x_j(t)\|^2] \rightarrow 0$  as  $t \rightarrow +\infty$  for any given initial conditions  $\psi_i(0)$ , where  $i, j = 1, 2, \dots, N$ .

**Lemma 1** (see [1]). Let  $G$  be an  $N \times N$  matrix in the set  $T(R; k)$ . Then, the  $(N-1) \times (N-1)$  matrix  $H$  defined by  $H = MGJ$  satisfies  $MG = HM$ , where  $G$  and  $J$  are given, respectively, by

$$M = \begin{bmatrix} 1 & -1 & 0 & \cdots & 0 & 0 \\ 0 & 1 & -1 & \cdots & 0 & 0 \\ \vdots & \vdots & \vdots & \ddots & \vdots & \vdots \\ 0 & 0 & 0 & \cdots & 1 & -1 \end{bmatrix}_{(N-1) \times N},$$

$$J = \begin{bmatrix} 1 & 1 & 1 & \cdots & 1 \\ 0 & 1 & 1 & \cdots & 1 \\ \vdots & \vdots & \ddots & \vdots & \vdots \\ 0 & 0 & \cdots & 1 & 1 \\ 0 & 0 & \cdots & 0 & 1 \\ 0 & 0 & \cdots & 0 & 0 \end{bmatrix}_{N \times (N-1)}, \quad (10)$$

and  $T(\tilde{R}, K)$  is the set of matrices with entries in  $R$  such that the sum of the entries in each row is equal to  $R$ .

**Lemma 2.** For any positive definite symmetric constant matrix  $M \in R^{n \times n}$ , if there exist the scalars  $r_1 < r_2$  and vector function  $w: [r_1, r_2] \rightarrow R^n$  such that the concerned integrations are well defined, then the following inequality holds:

$$\left( \int_{r_1}^{r_2} w(s) ds \right)^\top M \int_{r_1}^{r_2} w(s) ds \leq r_{12} \int_{r_1}^{r_2} w^\top(s) M w(s) ds, \quad (11)$$

where  $r_{12} = r_2 - r_1$ .

**Lemma 3.** Given any real matrices  $X$  and  $Y$  and  $Q > 0$  with appropriate dimensions, then the following matrix inequality holds:

$$X^\top Y + Y^\top X \leq X^\top Q X + Y^\top Q^{-1} Y. \quad (12)$$

**Lemma 4** (see [40]). The LMI  $\begin{bmatrix} S_{11}(x) & S_{12}(x) \\ S_{12}^\top(x) & S_{22}(x) \end{bmatrix} > 0$ , where  $S_{11}(x) = S_{11}^\top(x)$ ,  $S_{22}(x) = F^\top(x)$ , and  $S_{12}(x)$  depend on  $x$ , is equivalent to each of the following conditions:

- (i)  $S_{11}(x) > 0, S_{22}(x) - S_{12}^\top(x) S_{11}^{-1}(x) S_{12}(x) > 0$
- (ii)  $S_{22}(x) > 0, S_{11}(x) - S_{12}^\top(x) S_{22}^{-1}(x) S_{12}(x) > 0$

### 3. Main Results

**Theorem 1.** Under the assumption  $(H_1)$ ,  $0 < \tau(t) < \tau$ , and  $\dot{\tau}(t) \leq \mu$  ( $\mu > 0$ ), the stochastic coupled IMMNs (1) are globally synchronized in mean square sense if there exist positive definite symmetric matrices  $P, Q, V_i \in R^{n \times n}$ ,  $i = 1, 2, 3, 4, 5, 6$ , and positive diagonal matrices  $R, S, T, \tilde{R}, S_1, S_2, S_3, S_4, S_5 \in R^{n \times n}$ , such that the following matrix inequalities hold:  $\Phi < 0$  and  $\Pi - \Psi \Phi^{-1} \Psi > 0$ , where

$$\Phi = \begin{bmatrix} \Phi_{11} & \Phi_{12} & \Phi_{13} \\ * & \Phi_{22} & \Phi_{23} \\ * & * & \Phi_{33} \end{bmatrix},$$

$$\Psi = \begin{bmatrix} P - Q\Theta_1 - \tau^2 R - V_1 + \frac{1}{\tau} V_1 S^{-1} V_4 & V_1 + \frac{1}{\tau} V_1 S^{-1} V_5 & V_1 + \frac{1}{\tau} V_1 S^{-1} V_6 \\ -V_2 + \frac{1}{\tau} V_2 S^{-1} V_4 & V_2 + \frac{1}{\tau} V_2 S^{-1} V_5 & V_2 + \frac{1}{\tau} V_2 S^{-1} V_6 \\ -V_3 + \frac{1}{\tau} V_3 S^{-1} V_4 & V_3 + \frac{1}{\tau} V_3 S^{-1} V_5 & V_3 + \frac{1}{\tau} V_3 S^{-1} V_6 \end{bmatrix}, \quad (13)$$

$$\Pi = \begin{bmatrix} \Pi_{44} + \gamma_{44} & V_4 + \frac{1}{\tau} V_4 S^{-1} V_5 & V_4 + \frac{1}{\tau} V_4 S^{-1} V_6 \\ * & 2V_5 + \frac{1}{\tau} V_5 S^{-1} V_5 & V_5 + \frac{1}{\tau} V_5 S^{-1} V_6 \\ * & * & 2V_6 - \tilde{R} + \frac{1}{\tau} V_6 S^{-1} V_6 \end{bmatrix},$$

with

$$\begin{aligned}
\Phi_{11} &= -2P + (\tau^2 - 1)R + H_1^\top(Q + \tau^2 S)H_1 + \frac{1}{\tau}V_1 S^{-1}V_1 + \tau^2 \Theta_1^\top \tilde{R} \Theta_1 + \gamma_{11}, \\
\Phi_{12} &= H_1^\top(Q + \tau^2 S)H_2 + \frac{1}{\tau}V_1 S^{-1}V_2, \\
\Phi_{13} &= R + \frac{1}{\tau}V_1 S^{-1}V_3, \\
\Phi_{22} &= H_2^\top(Q + \tau^2 S)H_2 + \frac{1}{\tau}V_2 S^{-1}V_2 + \gamma_{22}, \\
\Phi_{23} &= \frac{1}{\tau}V_2 S^{-1}V_3, \\
\Pi_{44} &= \tau^2 (cH - \Lambda_1)^\top \tilde{R} (cH - \Lambda_1) + \tau^2 R + 2Q(cH - \Lambda_1) - 2V_4 + \frac{1}{\tau}V_4 S^{-1}V_4, \\
\gamma_{44} &= (Q + \tau^2 (cH^\top - \Lambda_1^\top) \tilde{R})(A_0^{N-1} + H_A^{N-1})S_1(A_0^{N-1\top} + H_A^{N-1\top})(Q + \tau^2 \tilde{R}(cH - \Lambda_1)) \\
&\quad + (Q + \tau^2 (cH^\top - \Lambda_1^\top) \tilde{R})(B_0^{N-1\top} + H_B^{N-1\top})S_2(B_0^{N-1} + H_B^{N-1})(Q + \tau^2 \tilde{R}(cH - \Lambda_1)), \\
\gamma_{11} &= 2(H_1^\top(Q + \tau^2 S)H_3 + \tau^2 \Theta_1^\top \tilde{R}(A_0^{N-1} + H_A^{N-1}))L + L^\top(S_1^{-1} + S_4^{-1} + T)L \\
&\quad + L^\top(H_3^\top(Q + \tau^2 S)H_3 + \tau^2(A_0^{N-1\top} + H_A^{N-1\top})\tilde{R}(A_0^{N-1} + H_A^{N-1}))L \\
&\quad + L^\top(H_3^\top(Q + \tau^2 S)H_4 + \tau^2(A_0^{N-1\top} + H_A^{N-1\top})\tilde{R}(B_0^{N-1} + H_B^{N-1})) \\
&\quad \times S_5(H_4^\top(Q + \tau^2 S)H_3 + \tau^2(B_0^{N-1\top} + H_B^{N-1\top})\tilde{R}(A_0^{N-1} + H_A^{N-1}))L \\
&\quad + (H_1^\top(Q + \tau^2 S)H_4 + \tau^2 \Theta_1^\top \tilde{R}(B_0^{N-1} + H_B^{N-1}))S_3 \\
&\quad \times (H_4^\top(Q + \tau^2 S)H_1 + \tau^2(B_0^{N-1\top} + H_B^{N-1\top})\tilde{R}\Theta_1), \\
\gamma_{22} &= L^\top(S_2^{-1} + S_3^{-1} + S_5^{-1} + H_4^\top(Q + \tau^2 S)H_4 - (1 - \mu)T)L + 2H_2^\top(Q + \tau^2 S)H_4 L \\
&\quad + \tau^2 L^\top(B_0^{N-1\top} + H_B^{N-1\top})\tilde{R}(B_0^{N-1} + H_B^{N-1})L + H_2^\top(Q + \tau^2 S)H_3 S_4 H_3^\top(Q + \tau^2 S)H_2.
\end{aligned} \tag{14}$$

*Proof.* For convenience, we set

$$\begin{aligned}
g(t) &= -\Theta x - \Lambda r + \mathbf{A}_0 \mathbf{f}(x) + \mathbf{B}_0 \mathbf{f}(x_\tau) + \mathbf{E} \Delta(t) + c \mathbf{G} r(t), \\
y(t) &= \sigma_1 x + \sigma_2 x_\tau + \sigma_3 \mathbf{f}(x) + \sigma_4 \mathbf{f}(x_\tau).
\end{aligned} \tag{15}$$

Consider the following Lyapunov–Krasovskii functional:

$$V(t, x) = \sum_{i=1}^6 V_i(t, x), \tag{16}$$

where

$$\begin{aligned}
V_1(t, x) &= x(t)^\top M^\top P M x(t), \\
V_2(t, x) &= r(t)^\top M^\top Q M r(t), \\
V_3(t, x) &= \int_{t-\tau(t)}^t \mathbf{f}(x(s))^\top M^\top T M \mathbf{f}(x(s)) ds, \\
V_4(t, x) &= \tau \int_{-\tau}^0 \int_{t+\theta}^t \dot{x}(s)^\top M^\top R M \dot{x}(s) ds d\theta, \\
V_5(t, x) &= \tau \int_{-\tau}^0 \int_{t+\theta}^t y(s)^\top M^\top S M y(s) ds d\theta, \\
V_6(t, x) &= \tau \int_{-\tau}^0 \int_{t+\theta}^t g(s)^\top M^\top \tilde{R} M g(s) ds d\theta,
\end{aligned} \tag{17}$$

for simplicity, we use  $\dot{x}(t)$  instead of  $dx(t)/dt$  in the paper.

By the It  $\hat{\delta}$  formula, we can calculate  $\mathcal{L}V(t, x)$  along system (9), and then we have

$$\mathcal{L}V(t, x) = \sum_{i=1}^6 \mathcal{L}V_i(t, x), \quad (18)$$

and  $\mathcal{L}V_i(t, x), i = 1, 2, 3, 4, 5, 6$  are calculated along system (9) as follows:

$$\mathcal{L}V_1(t) = 2x^\top M^\top P(-x + r) \triangleq \xi(t)^\top \Omega_1 \xi(t), \quad (19)$$

where

$$\xi(t)^\top = \left( x(t)^\top M^\top, x(t - \tau(t))^\top M^\top, x(t - \tau)^\top M^\top, r(t)^\top M^\top, r(t - \tau)^\top M^\top, \left( \int_{t-\tau}^t Mg(s)ds \right)^\top \right),$$

$$\Omega_1 = \begin{bmatrix} -2P & 0 & 0 & P & 0 & 0 \\ 0 & 0 & 0 & 0 & 0 & 0 \\ 0 & 0 & 0 & 0 & 0 & 0 \\ P & 0 & 0 & 0 & 0 & 0 \\ 0 & 0 & 0 & 0 & 0 & 0 \\ 0 & 0 & 0 & 0 & 0 & 0 \end{bmatrix}, \quad (20)$$

$$\begin{aligned} \mathcal{L}V_2(t) &= 2r^\top M^\top QMg(t) + y(t)^\top M^\top QMy(t) \\ &\leq \xi(t)^\top \Omega_2 \xi(t) + 2x^\top M^\top H_1^\top QH_3 Mf(x) + 2x^\top M^\top H_1^\top QH_4 Mf(x_\tau) \\ &\quad + 2r^\top M^\top Q(\mathbf{A}_0^{N-1} + \mathbf{H}_A^{N-1})Mf(x) + 2r^\top M^\top Q(\mathbf{B}_0^{N-1} + \mathbf{H}_B^{N-1})Mf(x_\tau) \\ &\quad + 2x_\tau^\top M^\top H_2^\top QH_3 Mf(x) + 2x_\tau^\top M^\top H_2^\top QH_4 Mf(x_\tau) + f(x)^\top M^\top H_3^\top QH_3 Mf(x) \\ &\quad + 2f(x)^\top M^\top H_3^\top QH_4 Mf(x_\tau) + f(x_\tau)^\top M^\top H_4^\top QH_4 Mf(x_\tau), \end{aligned} \quad (21)$$

where

$$\begin{aligned} M\sigma_i &= H_i M, (i = 1, 2, 3, 4), M\Theta = \Theta_1 M, M\Lambda = \Lambda_1 M, M\mathbf{A}_0 = \mathbf{A}_0^{N-1} M, \\ M\mathbf{B}_0 &= \mathbf{B}_0^{N-1} M, M\mathbf{H}_A = \mathbf{H}_A^{N-1} M, M\mathbf{H}_B = \mathbf{H}_B^{N-1} M, \\ \Omega_2 &= \begin{bmatrix} H_1^\top QH_1 & H_1^\top QH_2 & 0 & -Q\Theta_1 & 0 & 0 \\ H_1^\top QH_2 & H_2^\top QH_2 & 0 & 0 & 0 & 0 \\ 0 & 0 & 0 & 0 & 0 & 0 \\ -Q\Theta_1 & 0 & 0 & 2Q(cH - \Lambda_1) & 0 & 0 \\ 0 & 0 & 0 & 0 & 0 & 0 \\ 0 & 0 & 0 & 0 & 0 & 0 \end{bmatrix}, \end{aligned} \quad (22)$$

$$\begin{aligned} \mathcal{L}V_3(t) &= f((x)^\top)^\top TMf(x) - (1 - \dot{\tau}(t))f(x_\tau)^\top M^\top TMf(x_\tau) \\ &\leq f(x)^\top M^\top TMf(x) - (1 - \mu)f(x_\tau)^\top M^\top TMf(x_\tau), \end{aligned} \quad (23)$$

$$\mathcal{L}V_4(t) = \tau^2 x(t)^\top M^\top RMx(t) - \tau \int_{t-\tau}^t \dot{x}(s)^\top M^\top RM\dot{x}(s)ds, \quad (24)$$

where  $\dot{\tau}(t)$  is the derivative of  $\tau(t)$ .

By applying Lemma 2, one has



$$-\tau \int_{t-\tau}^t \dot{x}(s)^\top M^\top R M \dot{x}(s) ds \leq - \left( \int_{t-\tau}^t M \dot{x}(s) ds \right)^\top R \left( \int_{t-\tau}^t M \dot{x}(s) ds \right), \quad (25)$$

then  $\mathcal{L}V_4(t) \leq \xi(t)^\top \Omega_3 \xi(t)$ , where

$$\Omega_3 = \begin{bmatrix} (\tau^2 - 1)R & 0 & R & -\tau^2 R & 0 & 0 \\ 0 & 0 & 0 & 0 & 0 & 0 \\ R & 0 & -R & 0 & 0 & 0 \\ -\tau^2 R & 0 & 0 & \tau^2 R & 0 & 0 \\ 0 & 0 & 0 & 0 & 0 & 0 \\ 0 & 0 & 0 & 0 & 0 & 0 \end{bmatrix},$$

$$\mathcal{L}V_5(t) = \tau^2 y(t)^\top M^\top S M y(t) - \tau \int_{t-\tau}^t y(s)^\top M^\top S M y(s) ds. \quad (26)$$

Recalling (9) and (15), it is easy to see that the following equalities hold:

$$0 = 2\xi(t)^\top V \left( r(t) - r(t-\tau) - \int_{t-\tau}^t g(s) ds - \int_{t-\tau}^t y(s) dw_s \right), \quad (27)$$

where

$$V = (V_1(t)^\top \ V_2(t)^\top \ V_3(t)^\top \ V_4(t)^\top \ V_5(t)^\top \ V_6(t)^\top)^\top.$$

By Lemma 3, we have

$$2\xi(t)^\top V \int_{t-\tau}^t y(s) dw_s \leq \frac{1}{\tau} \xi(t)^\top V S^{-1} V^\top \xi(t) + \tau \left( \int_{t-\tau}^t y(s) dw_s \right)^\top S \left( \int_{t-\tau}^t y(s) dw_s \right). \quad (28)$$

Then,

$$\begin{aligned} \mathcal{L}V_5(t) &\leq \xi(t)^\top \Omega_4 \xi(t) + \tau \left( \int_{t-\tau}^t M y(s) dw_s \right)^\top \left( \int_{t-\tau}^t M y(s) dw_s \right) \\ &\quad - \tau \int_{t-\tau}^t y(s)^\top M^\top S M y(s) ds + 2\tau^2 x^\top M^\top H_1^\top S H_3 M f(x) \\ &\quad + 2\tau^2 x^\top M^\top H_1^\top S H_4 M f(x_\tau) + 2\tau^2 x_\tau^\top M^\top H_2^\top S H_3 M f(x) \\ &\quad + 2\tau^2 x_\tau^\top M^\top H_2^\top S H_4 M f(x_\tau) + \tau^2 f(x)^\top M^\top H_3^\top S H_3 M f(x) \\ &\quad + 2\tau^2 f(x)^\top M^\top H_3^\top S H_4 M f(x_\tau) + \tau^2 f(x_\tau)^\top M^\top H_4^\top S H_4 M f(x_\tau), \end{aligned} \quad (29)$$

where

$$\Omega_4 = \begin{bmatrix} \tau^2 H_1^\top S H_1 & \tau^2 H_1^\top S H_2 & 0 & -V_1 & V_1 & V_1 \\ * & \tau^2 H_2^\top S H_2 & 0 & -V_2 & V_2 & V_2 \\ * & * & 0 & -V_3 & V_3 & V_3 \\ * & * & * & -2V_4 & V_4 & V_4 \\ * & * & * & * & 2V_5 & V_5 \\ * & * & * & * & * & 2V_6 \end{bmatrix} + \frac{1}{\tau} V S^{-1} V^\top. \quad (30)$$

Using the property of the Itô isometry, we have

$$E \left( \left( \int_{t-\tau}^t M y(s) dw_s \right)^\top S \left( \int_{t-\tau}^t M y(s) dw_s \right) \right) = E \left( \int_{t-\tau}^t y(s)^\top M^\top S M y(s) ds \right). \quad (31)$$

Based on Lemma 2 and (15), we have

$$\begin{aligned}
\mathcal{L}V_6(t) &= \tau^2 g(t)^\top M^\top \tilde{R} M g(t) - \tau \int_{t-\tau}^t g(s)^\top M^\top \tilde{R} M g(s) ds \\
&\leq \tau^2 g(t)^\top M^\top \tilde{R} M g(t) - \left( \int_{t-\tau}^t M g(s) ds \right)^\top \tilde{R} \left( \int_{t-\tau}^t M g(s) ds \right) \\
&\leq \xi(t)^\top \Omega_5 \xi(t) + 2\tau^2 x^\top M^\top \Theta_1^\top \tilde{R} (\mathbf{A}_0^{N-1} + \mathbf{H}_A^{N-1}) M \mathbf{f}(x) \\
&\quad + 2\tau^2 x^\top M^\top \Theta_1^\top \tilde{R} (\mathbf{B}_0^{N-1} + \mathbf{H}_B^{N-1}) M \mathbf{f}(x_\tau) \\
&\quad + 2\tau^2 r^\top M^\top (cH^\top - \Lambda_1^\top) \tilde{R} (\mathbf{A}_0^{N-1} + \mathbf{H}_A^{N-1}) M \mathbf{f}(x) \\
&\quad + 2\tau^2 r^\top M^\top (cH^\top - \Lambda_1^\top) \tilde{R} (\mathbf{B}_0^{N-1} + \mathbf{H}_B^{N-1}) M \mathbf{f}(x_\tau) \\
&\quad + \tau^2 \mathbf{f}(x)^\top M^\top (\mathbf{A}_0^{N-1\top} + \mathbf{H}_A^{N-1\top}) \tilde{R} (\mathbf{A}_0^{N-1} + \mathbf{H}_A^{N-1}) M \mathbf{f}(x) \\
&\quad + 2\tau^2 \mathbf{f}(x)^\top M^\top (\mathbf{A}_0^{N-1\top} + \mathbf{H}_B^{N-1\top}) \tilde{R} (\mathbf{B}_0^{N-1} + \mathbf{H}_B^{N-1}) M \mathbf{f}(x_\tau) \\
&\quad + \tau^2 \mathbf{f}(x_\tau)^\top M^\top (\mathbf{B}_0^{N-1\top} + \mathbf{H}_B^{N-1\top}) \tilde{R} (\mathbf{B}_0^{N-1} + \mathbf{H}_B^{N-1}) M \mathbf{f}(x_\tau),
\end{aligned} \tag{32}$$

where

$$M\mathbf{G} = H\mathbf{M},$$

$$\Omega_5 = \begin{bmatrix} \tau^2 \Theta_1^\top \tilde{R} \Theta_1 & 0 & 0 & -\tau^2 \Theta_1^\top \tilde{R} (cH - \Lambda_1) & 0 & 0 \\ 0 & 0 & 0 & 0 & 0 & 0 \\ 0 & 0 & 0 & 0 & 0 & 0 \\ -\tau^2 \Theta_1^\top \tilde{R} (cH - \Lambda_1) & 0 & 0 & \tau^2 (cH^\top - \Lambda_1^\top) \tilde{R} (cH - \Lambda_1) & 0 & 0 \\ 0 & 0 & 0 & 0 & 0 & 0 \\ 0 & 0 & 0 & 0 & 0 & -\tilde{R} \end{bmatrix}. \tag{33}$$

Under assumption  $(H_1)$  and Lemma 3, we obtain

$$\begin{aligned}
&2r^\top M^\top (Q + \tau^2 (cH^\top - \Lambda_1^\top) \tilde{R}) (\mathbf{A}_0^{N-1} + \mathbf{H}_A^{N-1}) M \mathbf{f}(x) \\
&= 2 \sum_{i=1}^{N-1} (r_i - r_{i+1})^\top (Q + \tau^2 (cH^\top - \Lambda_1^\top) \tilde{R}) (\mathbf{A}_0^{N-1} + \mathbf{H}_A^{N-1\top}) (f(x_i) - f(x_{i+1})) \\
&\leq 2 \sum_{i=1}^{N-1} (r_i - r_{i-1})^\top (Q + \tau^2 (cH^\top - \Lambda_1^\top) \tilde{R}) (\mathbf{A}_0^{N-1} + \mathbf{H}_A^{N-1}) L(x_i - x_{i+1}) \\
&\leq \sum_{i=1}^{N-1} (r_i - r_{i+1})^\top (Q + \tau^2 (cH^\top - \Lambda_1^\top) \tilde{R}) (\mathbf{A}_0^{N-1} + \mathbf{H}_A^{N-1}) S_1 (\mathbf{A}_0^{N-1\top} + \mathbf{H}_A^{N-1\top}) \\
&\quad \times (Q + \tau^2 \tilde{R} (cH - \Lambda_1)) (r_i - r_{i+1}) + \sum_{i=1}^{N-1} (x_i - x_{i+1})^\top L^\top S_1^{-1} L (x_i - x_{i+1}) \\
&= r^\top M^\top (Q + \tau^2 (cH^\top - \Lambda_1^\top) \tilde{R}) (\mathbf{A}_0^{N-1} + \mathbf{H}_A^{N-1}) S_1 (\mathbf{A}_0^{N-1\top} + \mathbf{H}_A^{N-1\top}) \\
&\quad \times (Q + \tau^2 \tilde{R} (cH - \Lambda_1)) M r + x^\top M^\top L^\top S_1^{-1} L M x.
\end{aligned} \tag{34}$$

Similarly, we have

$$\begin{aligned}
& 2r^\top M^\top (Q + \tau^2 (cH^\top - \Lambda_1^\top) \tilde{R}) (\mathbf{B}_0^{N-1} + \mathbf{H}_B^{N-1}) \mathbf{M}f(x_\tau) \\
& \leq \sum_{i=1}^{N-1} (r_i - r_{i+1})^\top (Q + \tau^2 (cH^\top - \Lambda_1^\top) \tilde{R}) (\mathbf{B}_0^{N-1} + \mathbf{H}_B^{N-1}) S_2 \\
& \quad \times (\mathbf{B}_0^{N-1\top} + \mathbf{H}_B^{N-1\top}) (Q + \tau^2 \tilde{R} (cH - \Lambda_1)) (r_i - r_{i+1}) \\
& \quad + \sum_{i=1}^{N-1} (x_i(t - \tau(t)) - x_{i+1}(t - \tau(t)))^\top L^\top S_2^{-1} L (x_i(t - \tau(t)) - x_{i+1}(t - \tau(t))) \\
& = r^\top M^\top (Q + \tau^2 (cH^\top - \Lambda_1^\top) \tilde{R}) (\mathbf{B}_0^{N-1} + \mathbf{H}_B^{N-1}) S_2 (\mathbf{B}_0^{N-1\top} + \mathbf{H}_0^{N-1\top}) \\
& \quad \times (Q + \tau^2 \tilde{R} (cH - \Lambda_1)) M r + x_\tau^\top M^\top L^\top S_2^{-1} L M x_\tau.
\end{aligned} \tag{35}$$

Next, it is easy to verify that

$$\begin{aligned}
& 2x^\top M^\top (H_1(Q + \tau^2 S)H_3 + \tau^2 \Theta_1^\top \tilde{R}(\mathbf{A}_0^{N-1} + \mathbf{H}_A^{N-1})) \mathbf{M}f(x) \\
& \leq x^\top M^\top (2H_1^\top(Q + \tau^2 S)H_3 + 2\tau^2 \Theta_1^\top \tilde{R}(\mathbf{A}_0^{N-1} + \mathbf{H}_A^{N-1})) L M x,
\end{aligned} \tag{36}$$

$$\begin{aligned}
& 2x^\top M^\top (H_1(Q + \tau^2 S)H_4 + \tau^2 \Theta_1^\top \tilde{R}(\mathbf{B}_0^{N-1} + \mathbf{H}_B^{N-1})) \mathbf{M}f(x_\tau) \\
& \leq x^\top M^\top (H_1^\top(Q + \tau^2 S)H_4 + \tau^2 \Theta_1^\top \tilde{R}(\mathbf{B}_0^{N-1} + \mathbf{H}_B^{N-1})) S_3 \\
& \quad \times (H_4^\top(Q + \tau^2 S)H_1 + \tau^2 (\mathbf{B}_0^{N-1\top} + \mathbf{H}_B^{N-1\top}) \tilde{R} \Theta_1) M x + x_\tau^\top M^\top L^\top S_3^{-1} L M x_\tau,
\end{aligned} \tag{37}$$

$$\begin{aligned}
& 2x_\tau^\top M^\top H_2^\top (Q + \tau^2 S) H_3 \mathbf{M}f(x) \\
& \leq x^\top M^\top L^\top S_4^{-1} L M x + x_\tau^\top M^\top H_2^\top (Q + \tau^2 S) H_3 S_4 H_3^\top (Q + \tau^2 S) H_2 M x_\tau,
\end{aligned} \tag{38}$$

$$2x_\tau^\top M^\top H_2^\top (Q + \tau^2 S) H_4 \mathbf{M}f(x_\tau) \leq 2x_\tau^\top M^\top H_2^\top (Q + \tau^2 S) H_4 L M x_\tau, \tag{39}$$

$$\begin{aligned}
& \mathbf{f}((x)^\top M^\top (\tau^2 (\mathbf{A}_0^{N-1\top} + \mathbf{H}_A^{N-1\top}) \tilde{R} (\mathbf{A}_0^{N-1} + \mathbf{H}_A^{N-1}) + H_3^\top (Q + \tau^2 S) H_3 + T) \mathbf{M}f(x) \\
& \leq x^\top M^\top L^\top (T + H_3^\top (Q + \tau^2 S) H_3 + \tau^2 (\mathbf{A}_0^{N-1\top} + \mathbf{H}_A^{N-1\top}) \tilde{R} (\mathbf{A}_0^{N-1} + \mathbf{H}_A^{N-1})) L M x,
\end{aligned} \tag{40}$$

$$\begin{aligned}
& 2\mathbf{f}(x)^\top M^\top (\tau^2 (\mathbf{A}_0^{N-1\top} + \mathbf{H}_A^{N-1\top}) \tilde{R} (\mathbf{B}_0^{N-1} + \mathbf{H}_B^{N-1}) + H_3^\top (Q + \tau^2 S) H_4) \mathbf{M}f(x_\tau) \\
& \leq x^\top M^\top L^\top (H_3^\top (Q + \tau^2 S) H_4 + \tau^2 (\mathbf{A}_0^{N-1\top} + \mathbf{H}_A^{N-1\top}) \tilde{R} (\mathbf{B}_0^{N-1} + \mathbf{H}_B^{N-1})) \\
& \quad \times S_5 (H_4^\top (Q + \tau^2 S) H_3 + \tau^2 (\mathbf{B}_0^{N-1\top} + \mathbf{H}_B^{N-1\top}) \tilde{R} (\mathbf{A}_0^{N-1} + \mathbf{H}_A^{N-1})) L M x \\
& \quad + x_\tau^\top M^\top L^\top S_5^{-1} L M x_\tau,
\end{aligned} \tag{41}$$

$$\begin{aligned}
& \mathbf{f}(x_\tau)^\top M^\top (\tau^2 (\mathbf{B}_0^{N-1\top} + \mathbf{H}_B^{N-1\top}) \tilde{R} (\mathbf{B}_0^{N-1} + \mathbf{H}_B^{N-1})) \mathbf{M}f(x_\tau) \\
& \quad + \mathbf{f}(x_\tau)^\top M^\top (H_4^\top (Q + \tau^2 S) H_4 - (1 - \mu) T) \mathbf{M}f(x_\tau) \\
& \leq x_\tau^\top M^\top L^\top (H_4^\top (Q + \tau^2 S) H_4 - (1 - \mu) T) L M x_\tau \\
& \quad + x_\tau^\top M^\top L^\top (\tau^2 (\mathbf{B}_0^{N-1\top} + \mathbf{H}_B^{N-1\top}) \tilde{R} (\mathbf{B}_0^{N-1} + \mathbf{H}_B^{N-1})) L M x_\tau.
\end{aligned} \tag{42}$$

Substituting (19)–(42) into (18), we arrive at

$$E[\mathcal{L}V(t)] \leq E[\xi(t)^\top \Xi \xi(t)] \leq \lambda_{\max}(\Xi) E[\|\xi(t)\|^2], \tag{43}$$

where

$$\Xi = \begin{bmatrix} \Xi_{11} & \Xi_{12} & \Xi_{13} & \Xi_{14} & \Xi_{15} & \Xi_{16} \\ * & \Xi_{22} & \Xi_{23} & \Xi_{24} & \Xi_{25} & \Xi_{26} \\ * & * & \Xi_{33} & \Xi_{34} & \Xi_{35} & \Xi_{36} \\ * & * & * & \Xi_{44} & \Xi_{45} & \Xi_{46} \\ * & * & * & * & \Xi_{55} & \Xi_{56} \\ * & * & * & * & * & \Xi_{66} \end{bmatrix}, \quad (44)$$

with

$$\Xi_{11} = -2P + (\tau^2 - 1)R + H_1^\top (Q + \tau^2 S) H_1 + \frac{1}{\tau} V_1 S^{-1} V_1 + \tau^2 \Theta_1^\top \bar{R} \Theta_1 + \gamma_{11},$$

$$\Xi_{12} = H_1^\top (Q + \tau^2 S) H_2 + \frac{1}{\tau} V_1 S^{-1} V_2,$$

$$\Xi_{13} = R + \frac{1}{\tau} V_1 S^{-1} V_3,$$

$$\Xi_{14} = P - Q \Theta_1 - \tau^2 R + \frac{1}{\tau} V_1 S^{-1} V_4 - V_1,$$

$$\Xi_{15} = V_1 + \frac{1}{\tau} V_1 S^{-1} V_5,$$

$$\Xi_{16} = V_1 + \frac{1}{\tau} V_1 S^{-1} V_6,$$

$$\Xi_{22} = H_2^\top (Q + \tau^2 S) H_2 + \frac{1}{\tau} V_2 S^{-1} V_2 + \gamma_{22},$$

$$\Xi_{23} = \frac{1}{\tau} V_2 S^{-1} V_3,$$

$$\Xi_{24} = -V_2 + \frac{1}{\tau} V_2 S^{-1} V_4,$$

$$\Xi_{25} = V_2 + \frac{1}{\tau} V_2 S^{-1} V_5,$$

$$\Xi_{26} = V_2 + \frac{1}{\tau} V_2 S^{-1} V_6,$$

$$\Xi_{33} = -R + \frac{1}{\tau} V_3 S^{-1} V_3,$$

$$\Xi_{34} = -V_3 + \frac{1}{\tau} V_3 S^{-1} V_4,$$

$$\Xi_{35} = V_3 + \frac{1}{\tau} V_3 S^{-1} V_5,$$

$$\begin{aligned}
\Xi_{36} &= V_3 + \frac{1}{\tau}V_3S^{-1}V_6, \\
\Xi_{44} &= \tau^2(cH - \Lambda_1)^\top \bar{R}(cH - \Lambda_1) + \tau^2R + 2Q(cH - \Lambda_1) - 2V_4 + \frac{1}{\tau}V_4S^{-1}V_4 + \gamma_{44}, \\
\Xi_{45} &= V_4 + \frac{1}{\tau}V_4S^{-1}V_5, \\
\Xi_{46} &= V_4 + \frac{1}{\tau}V_4S^{-1}V_6, \\
\Xi_{55} &= 2V_5 + \frac{1}{\tau}V_5S^{-1}V_5, \\
\Xi_{56} &= V_5 - \bar{R} + \frac{1}{\tau}V_5S^{-1}V_6, \\
\Xi_{66} &= 2V_6 - \bar{R} + \frac{1}{\tau}V_6S^{-1}V_6, \\
\gamma_{11} &= 2(H_1^\top(Q + \tau^2S)H_3 + \tau^2\Theta_1^\top \bar{R}(A_0^{N-1} + H_A^{N-1}))L + L^\top(S_1^{-1} + S_4^{-1} + T)L \\
&\quad + L^\top(H_3^\top(Q + \tau^2S)H_3 + \tau^2(A_0^{N-1\top} + H_A^{N-1\top})\bar{R}(A_0^{N-1} + H_A^{N-1}))L \\
&\quad + L^\top(H_3^\top(Q + \tau^2S)H_4 + \tau^2(A_0^{N-1\top} + H_A^{N-1\top})\bar{R}(B_0^{N-1} + H_B^{N-1})) \\
&\quad \times S_5(H_4^\top(Q + \tau^2S)H_3 + \tau^2(B_0^{N-1\top} + H_A^{N-1\top})\bar{R}(A_0^{N-1} + H_A^{N-1}))L \\
&\quad + (H_1^\top(Q + \tau^2S)H_4 + \tau^2\Theta_1^\top \bar{R}(B_0^{N-1} + H_B^{N-1}))S_3 \\
&\quad \times (H_4^\top(Q + \tau^2S)H_1 + \tau^2(B_0^{N-1\top} + H_B^{N-1\top})\bar{R}\Theta_1), \\
\gamma_{22} &= L^\top(S_2^{-1} + S_3^{-1} + S_5^{-1} + H_4^\top(Q + \tau^2S)H_4 - (1 - \mu)T)L + 2H_2^\top(Q + \tau^2S)H_4L \\
&\quad + \tau^2L^\top(B_0^{N-1\top} + H_B^{N-1\top})\bar{R}(B_0^{N-1} + H_B^{N-1})L + H_2^\top(Q + \tau^2S)H_3S_4H_3^\top(Q + \tau^2S)H_2, \\
\gamma_{44} &= (Q + \tau^2(cH^\top - \Lambda_1^\top)\bar{R})(A_0^{N-1} + H_A^{N-1})S_1(A_0^{N-1\top} + H_A^{N-1\top})(Q + \tau^2\bar{R}(cH - \Lambda_1)) \\
&\quad + (Q + \tau^2(cH^\top - \Lambda_1^\top)\bar{R})(B_0^{N-1\top} + H_B^{N-1\top})S_2(B_0^{N-1} + H_B^{N-1})(Q + \tau^2\bar{R}(cH - \Lambda_1)).
\end{aligned} \tag{45}$$

Based on Lemma 4 and the conditions of Theorem 1, we have the matrix  $\Xi < 0$ ; then,  $\lambda_{\max}(\Xi) < 0$ .

Obviously, we obtain  $E[\mathcal{L}V(t)] < 0$ . Hence, it follows the stochastic stability theory that the stochastic coupled IMMNs (1) are globally synchronized in mean square sense.  $\square$

#### 4. Conclusion

Based on interval uncertainty theory, the stochastic analysis techniques and the vector Lyapunov function method are applied to realize the global synchronization in mean square sense. Nevertheless, the criterion given in Theorem 1 is different from the results in the existing literature. Moreover, the time delay is dependent, and the upper bound of the delayed derivative is 0 or less than 1. Hence, Theorem 1

would be feasible and less conservative. It is worth noting that the upper bound of the random factor can be calculated when the state parameter of the system is selected based on Theorem 1. Similarly, the stochastic coupled IMMNs (1) have strong anti-interference. In addition, the coupling of various neural nodes can be described. The example in Section 5 fully illustrates these two points.

#### 5. Numerical Simulations

Now, we perform some numerical simulations to illustrate our analysis.

*Example 1.* Consider the following stochastic inertial memristor-based neural networks with five coupled identical nodes:

$$\begin{aligned}
d\left(\frac{dx_i(t)}{dt}\right) &= \left(-D\frac{dx_i(t)}{dt} - Cx_i(t) + A(x_i(t))f(x_i(t)) + B(x_i(t))f(x_i(t-\tau(t)))\right) \\
&+ c \sum_{j=1}^N G_{ij}\Gamma\left(\left(\frac{dx_j(t)}{dt} + x_j(t)\right)\right)dt + (\sigma_1x_i(t) + \sigma_2x_i(t-\tau(t))) \\
&+ \sigma_3f(x_i(t)) + \sigma_4f(x_i(t-\tau(t)))d\omega_i, \quad i = 1, 2, 3, 4, 5,
\end{aligned} \tag{46}$$

where the activation function  $f(x_i(t)) = 0.6 \tanh(x_i)$ , the time delay  $\tau(t) = e^t/(e^t + 1)$ , and the coupling strength  $c = 0.5$ . The system parameters are taken as

$$\begin{aligned}
D &= \begin{bmatrix} 6 & 0 \\ 0 & 6 \end{bmatrix}, \\
C &= \begin{bmatrix} 2 & 0 \\ 0 & 2 \end{bmatrix}, \\
\Gamma &= \begin{bmatrix} 1 & 0 \\ 0 & 1 \end{bmatrix}, \\
G &= \begin{bmatrix} -2.2 & 1 & 0 & 0 & 0.2 \\ 1 & -3.2 & 1.2 & 0 & 0 \\ 0 & 2 & -3.5 & 0.5 & 0 \\ 0 & 0 & 2 & -4.4 & 1.4 \\ 0.2 & 0 & 0 & 3 & -4.2 \end{bmatrix}, \\
\sigma_1 &= \begin{bmatrix} 2 & 0 \\ 0 & 2 \end{bmatrix}, \\
\sigma_2 &= \begin{bmatrix} 1.8 & 0 \\ 0 & 1.8 \end{bmatrix}, \\
\sigma_3 &= \begin{bmatrix} 1.6 & 0 \\ 0 & 1.6 \end{bmatrix}, \\
\sigma_4 &= \begin{bmatrix} 1.4 & 0 \\ 0 & 1.4 \end{bmatrix},
\end{aligned} \tag{47}$$

$$A(x_i(t)) = \begin{bmatrix} a_{11}(x_{i1}(t)) & a_{12}(x_{i2}(t)) \\ a_{21}(x_{i1}(t)) & a_{22}(x_{i2}(t)) \end{bmatrix},$$

$$B(x_i(t)) = \begin{bmatrix} b_{11}(x_{i1}(t)) & b_{12}(x_{i2}(t)) \\ b_{21}(x_{i1}(t)) & b_{22}(x_{i2}(t)) \end{bmatrix},$$

with the memristor connection weights:

$$\begin{aligned}
a_{11}(x) &= \begin{cases} 0.2, & |x| \leq 0.1, \\ -0.2, & |x| > 0.1, \end{cases} \\
a_{12}(x) &= \begin{cases} 0.6, & |x| \leq 0.1, \\ -0.6, & |x| > 0.1, \end{cases} \\
a_{21}(x) &= \begin{cases} 0.4, & |x| \leq 0.1, \\ -0.4, & |x| > 0.1, \end{cases} \\
a_{22}(x) &= \begin{cases} 0.4, & |x| \leq 0.1, \\ -0.4, & |x| > 0.1, \end{cases} \\
b_{11}(x) &= \begin{cases} 0.2, & |x| \leq 0.1, \\ -0.2, & |x| > 0.1, \end{cases} \\
a_{12}(x) &= \begin{cases} 0.4, & |x| \leq 0.1, \\ -0.4, & |x| > 0.1, \end{cases} \\
b_{21}(x) &= \begin{cases} 0.3, & |x| \leq 0.1, \\ -0.3, & |x| > 0.1, \end{cases} \\
b_{22}(x) &= \begin{cases} 0.3, & |x| \leq 0.1, \\ -0.3, & |x| > 0.1. \end{cases}
\end{aligned} \tag{48}$$

Obviously, by calculation, we can get the Lipschitz constants  $L = 0.6 * I_2$ , and the upper bound of the delay  $\tau = 1$ .

In order to show the effectiveness of Theorem 1, we display the synchronization of each node  $x_{ij}(t)$  ( $i = 1, 2, 3, 4, 5; j = 1, 2$ ) in Figure 1. Moreover, Figures 2 and 3 depict the synchronization error trajectories of  $x_{i1}(t) - x_{11}(t)$  and  $x_{i2}(t) - x_{12}(t)$ ,  $i = 1, 2, 3, 4$ .

## Data Availability

No data were used to support this study.

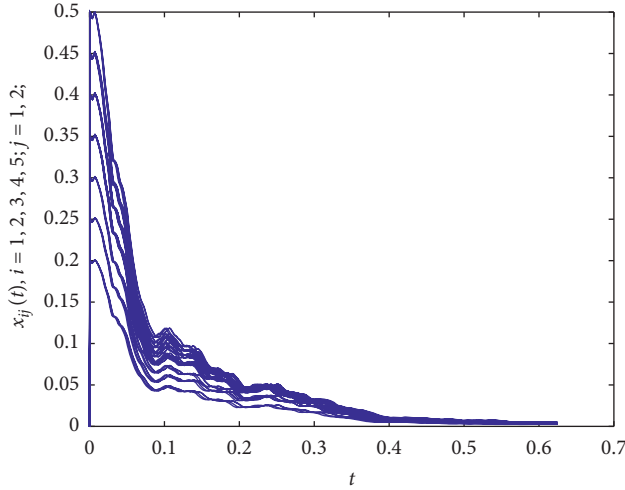


FIGURE 1: The synchronization of each node  $x_{ij}(t)$  in Example 1.

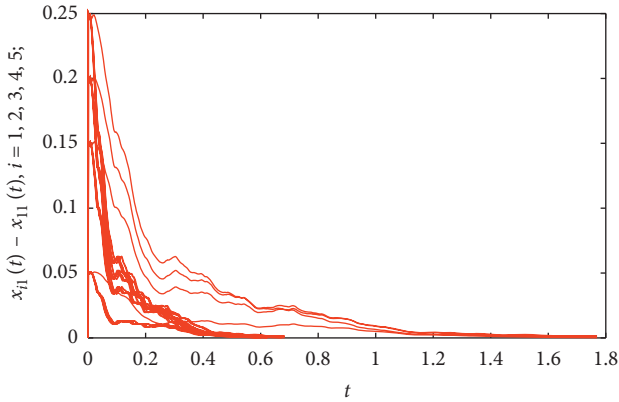


FIGURE 2: The synchronization error trajectories of  $x_{i1}(t) - x_{11}(t)$  in Example 1.

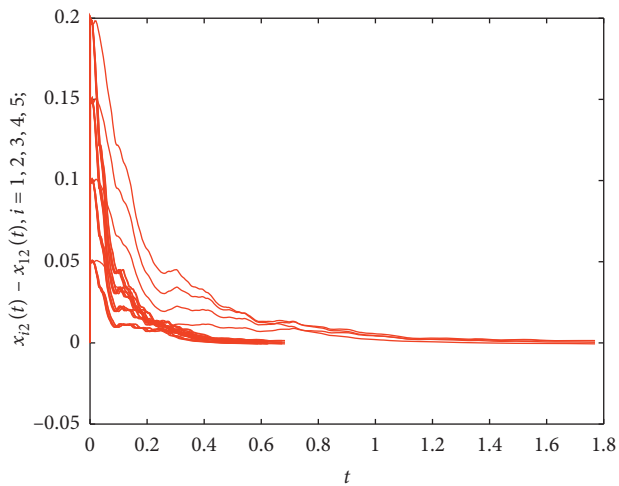


FIGURE 3: The synchronization error trajectories of  $x_{i2}(t) - x_{12}(t)$  in Example 1.

## Conflicts of Interest

The authors declare that there are no conflicts of interest regarding the publication of this article.

## Acknowledgments

This work was jointly supported by the Natural Science Foundation of Zhejiang Province under Grant (no. LY20A010016), National Natural Science Foundation of China under Grant (no. 11931016), the Scientific Research Foundation for the Introduced Senior Talents, Wuyi University (Grant no. YJ201802), Department of Education Foundation of Jiangsu Province (no. 201804), and the Natural Science Foundation of Shandong Province (China) (no. ZR2018MA018).

## References

- [1] Chua, "Memristor—the missing circuit element," *Trans Circuit Theory*, vol. 18, pp. 507–519, 1978.
- [2] A. Thomas, "Memristor-based neural networks," *Applied Physics*, vol. 46, pp. 1–12, 2013.
- [3] L. Chen, C. Huang, H. Liu, and Y. Xia, "Anti-synchronization of a class of chaotic systems with application to Lorenz system: a unified analysis of the integer order and fractional order," *Mathematics*, vol. 7, no. 6, p. 559, 2019.
- [4] C. Huang, J. Q. Lu, G. S. Zhai, J. D. Cao, G. P. Lu, and M. Perc, "Stability and stabilization in probability of probabilistic boolean networks," *IEEE Transactions on Neural Networks and Learning Systems*, 2020.
- [5] C. Huang, X. Zhang, H. K. Lam, and S.-H. Tsa, "Synchronization analysis for nonlinear complex networks with reaction-diffusion terms using fuzzy-model-based approach," *IEEE Transactions on Fuzzy Systems*, 2020.
- [6] Y. Liu, J. D. Cao, L. Q. Wang, and Z. G. Wu, "On pinning reachability of probabilistic Boolean control networks," *Science China Information Sciences*, vol. 63, no. 6, pp. 169–201, 2020.
- [7] Y. Liu, L. Sun, J. Lu, and J. Liang, "Feedback controller design for the synchronization of Boolean control networks," *IEEE Transactions on Neural Networks and Learning Systems*, vol. 27, no. 9, pp. 1991–1996, 2016.
- [8] X. Liu, H. Su, and M. Z. Q. Chen, "A switching approach to designing finite-time synchronization controllers of coupled neural networks," *IEEE Transactions on Neural Networks and Learning Systems*, vol. 27, no. 2, pp. 471–482, 2016.
- [9] X. Liu, J. Lam, W. Yu, and G. Chen, "Finite-time consensus of multiagent systems with a switching protocol," *IEEE Transactions on Neural Networks and Learning Systems*, vol. 27, no. 4, pp. 853–862, 2016.
- [10] X. Liu, D. W. C. Ho, J. Cao, and W. Xu, "Discontinuous observers design for finite-time consensus of multiagent systems with external disturbances," *IEEE Transactions on Neural Networks and Learning Systems*, vol. 28, no. 11, pp. 2826–2830, 2017.
- [11] X. Li, D. W. C. Ho, and J. Cao, "Finite-time stability and settling-time estimation of nonlinear impulsive systems," *Automatica*, vol. 99, pp. 361–368, 2019.

- [12] X. Li and S. Song, "Stabilization of delay systems: delay-dependent impulsive control," *IEEE Transactions on Automatic Control*, vol. 62, no. 1, pp. 406–411, 2017.
- [13] X. Li and J. Wu, "Sufficient stability conditions of nonlinear differential systems under impulsive control with state-dependent delay," *IEEE Transactions on Automatic Control*, vol. 63, no. 1, pp. 306–311, 2018.
- [14] J. Q. Lu, Y. Q. Wang, X. C. Shi, and J. D. Cao, "Finite-time bipartite consensus for multi-agent systems under detail-balanced antagonistic interactions," *IEEE Transactions on Systems, Man and Cybernetics: Systems (Regular Paper)*, 2019, In press.
- [15] H. Li and X. Ding, "A control Lyapunov function approach to feedback stabilization of logical control networks," *SIAM Journal on Control and Optimization*, vol. 57, no. 2, pp. 810–831, 2019.
- [16] Y. Li, H. Li, and X. Ding, "Set stability of switched delayed logical networks with application to finite-field consensus," *Automatica*, vol. 113, p. 108768, 2020.
- [17] D. Wang, L. Huang, and L. Tang, "Synchronization criteria for discontinuous neural networks with mixed delays via functional differential inclusions," *IEEE Transactions on Neural Networks and Learning Systems*, vol. 29, no. 5, pp. 1809–1821, 2018.
- [18] D. S. Wang, L. H. Huang, and L. K. Tang, "Dissipativity and synchronization for generalized BAM neural networks with multivariate discontinuous activations," *IEEE Transactions on Neural Networks and Learning Systems*, vol. 29, no. 8, pp. 3815–3827, 2018.
- [19] X. Yang, J. Lam, D. W. C. Ho, and Z. Feng, "Fixed-time synchronization of complex networks with impulsive effects via nonchattering control," *IEEE Transactions on Automatic Control*, vol. 62, no. 11, pp. 5511–5521, 2017.
- [20] J. Lu, C. Ding, J. Lou, and J. Cao, "Outer synchronization of partially coupled dynamical networks via pinning impulsive controllers," *Journal of the Franklin Institute*, vol. 352, no. 11, pp. 5024–5041, 2015.
- [21] B. Zhang, Y. Xia, L. Zhu, H. Liu, and L. Gu, "Global stability of fractional order coupled systems with impulses via a graphic approach," *Mathematics*, vol. 7, no. 8, p. 744, 2019.
- [22] Y. Zhang, J. Zhuang, Y. Xia, Y. Bai, J. Cao, and L. Gu, "Fixed-time synchronization of the impulsive memristor-based neural networks," *Communications in Nonlinear Science and Numerical Simulation*, vol. 77, pp. 40–53, 2019.
- [23] L. Duan and L. Huang, "Periodicity and dissipativity for memristor-based mixed time-varying delayed neural networks via differential inclusions," *Neural Networks*, vol. 57, pp. 12–22, 2014.
- [24] Z. Cai, L. Huang, and L. Zhang, "New conditions on synchronization of memristor-based neural networks via differential inclusions," *Neurocomputing*, vol. 186, pp. 235–250, 2016.
- [25] J. Lu, X. Guo, T. Huang, and Z. Wang, "Consensus of signed networked multi-agent systems with nonlinear coupling and communication delays," *Applied Mathematics and Computation*, vol. 350, pp. 153–162, 2019.
- [26] N. Li and W. X. Zheng, "Synchronization criteria for inertial memristor-based neural networks with linear coupling," *Neural Networks*, vol. 106, pp. 260–270, 2018.
- [27] A. Halanay, *Differential Equations: Stability, Oscillations, Time Lags*, Academic Press, New York, NY, USA, 1966.
- [28] R. E. Moore, *Interval Analysis*, Prentice-Hall, Englewood, NJ, USA, 1996.
- [29] J. Gao, P. Zhu, W. Xiong, J. Cao, and L. Zhang, "Asymptotic synchronization for stochastic memristor-based neural networks with noise disturbance," *Journal of the Franklin Institute*, vol. 353, no. 13, pp. 3271–3289, 2016.
- [30] Y. Li, "Impulsive synchronization of stochastic neural networks via controlling partial states," *Neural Processing Letters*, vol. 46, no. 1, pp. 59–69, 2017.
- [31] J. Liang, Z. Wang, T. Hayat, and A. Alsaedi, "Distributed  $H_\infty$  state estimation for stochastic delayed 2-D systems with randomly varying nonlinearities over saturated sensor networks," *Information Sciences*, vol. 370–371, no. 20, pp. 708–724, 2016.
- [32] H. Li, X. Xu, and X. Ding, "Finite-time stability analysis of stochastic switched Boolean networks with impulsive effect," *Applied Mathematics and Computation*, vol. 347, pp. 557–565, 2019.
- [33] A. Seurer and F. Couaisbaue, "The Wirtinger-based inequality: application to time-delay systems," *Automatica*, vol. 49, pp. 2860–2866, 2013.
- [34] S. Xu and J. Lam, "A new approach to exponential stability analysis of neural networks with time-varying delays," *Neural Networks*, vol. 19, no. 1, pp. 76–83, 2006.
- [35] W. Yu and J. Cao, "Synchronization control of stochastic delayed neural networks," *Physica A: Statistical Mechanics and Its Applications*, vol. 373, pp. 252–260, 2007.
- [36] Q. Zhu and H. Wang, "Output feedback stabilization of stochastic feedforward systems with unknown control coefficients and unknown output function," *Automatica*, vol. 87, no. 2, pp. 166–175, 2018.
- [37] J. Zhuang, Y. Zhou, and Y. Xia, "Intra-layer synchronization in duplex networks with time-varying delays and stochastic perturbations under impulsive control," *Neural Processing Letters*, 2020.
- [38] J. Zhuang, Y. Zhou, Y. Zhou, and Y. Xia, "Synchronization analysis of drive-response multi-layer dynamical networks with additive couplings and stochastic perturbations," *Discrete & Continuous Dynamical Systems-S*, 2018.
- [39] W. Yu, W. Ren, W. X. Zheng, G. Chen, and J. Lü, "Distributed control gains design for consensus in multi-agent systems with second-order nonlinear dynamics," *Automatica*, vol. 49, no. 7, pp. 2107–2115, 2013.
- [40] S. Bod, L. Ei Ghaoui, E. Feron, and V. Balarkrishnan, *Linear Matrix Inequalities in System and Control Theory*, SIAM, Philadelphia, PA, USA, 1994.



## Research Article

# Flocking Behavior of Cucker–Smale Model with Processing Delay

Jianfei Cheng , Maoli Chen, and Xiao Wang 

Department of Mathematics, College of Liberal Arts and Sciences, National University of Defense Technology, Changsha 410073, China

Correspondence should be addressed to Xiao Wang; wxiao\_98@nudt.edu.cn

Received 5 May 2020; Accepted 23 June 2020; Published 23 July 2020

Guest Editor: Xiaodi Li

Copyright © 2020 Jianfei Cheng et al. This is an open access article distributed under the Creative Commons Attribution License, which permits unrestricted use, distribution, and reproduction in any medium, provided the original work is properly cited.

The dynamics of a delay multiparticle swarm, which contains symmetric and asymmetric pairwise influence functions, are analyzed. Two different sufficient conditions to achieve conditional flocking are obtained. One does not have a clear relationship with this delay, and the other proposes a range of processing delays that affect the emergence of a flock. It is also pointed out that if the interparticle communication function has tail dissipation, unconditional flocking can be guaranteed. Compared with the previous results, the range of the communication rate  $\beta$  that allows a flock to emerge has been expanded from 1/4 to 1/2.

## 1. Introduction

There are many survival-oriented clusters in nature, such as ant colonies that coordinate food transportation, birds that increase the success rate of foraging, and fish that unite against danger, and so on. The research on the colony of biological groups should be traced back to Reynolds' simulation experiments on birds in [1]; further some scholars have proposed many motion models to mathematically characterize them. Among them, a second-order model proposed by Cucker and Smale in [2, 3] to explain self-organizing behavior in complex adaptive systems has been favored by researchers and continuously improved. For example, Motsch and Tadmor in [4] modified the symmetry of the influence intensity between particles to be asymmetric to explore the aggregation behavior of nonuniformly distributed particle swarms. Some scholars have carried out the impact of the time delay on flocking or consensus of the system in [5–7] and the references therein.

Liu and Wu in [5] proposed a model with processing delay, which is described as

$$\begin{cases} \dot{x}_i(t) = v_i(t), & i = 1, 2, \dots, N, \\ \dot{v}_i(t) = \alpha \sum_{j=1}^N I(\|x_i(t-\tau) - x_j(t-\tau)\|) (v_j(t-\tau) - v_i(t)), \end{cases} \quad (1)$$

where  $x_i, v_i \in R^d$  and  $d$  is a positive integer,  $\alpha > 0$  indicates the intensity of the influence between particles, and  $\tau > 0$  represents the time lag, which includes the response time of the particle  $i$  and the communication time between particles  $i$  and  $j$ . The communication function can be defined as

$$\begin{aligned} I(r_{ij}) &= I^{\text{CS}}(r_{ij}) := \frac{\psi(r_{ij})}{N} \text{ or } I(r_{ij}) \\ &= I^{\text{MT}}(r_{ij}) := \frac{\psi(r_{ij})}{\sum_{k=1}^N \psi(r_{ik})}, \end{aligned} \quad (2)$$

which further satisfies  $\sum_{l=1}^N I(r_{kl}) = 1$  for all  $k \in \Gamma$ , where  $\psi(r) = (1 + r^2)^{-\beta}$ ,  $\beta \geq 0$ ,  $r_{ij}(t) = \|x_i(t) - x_j(t)\|$ ,  $i, j \in \Gamma$ . Further, system (1) can be simplified to

$$\begin{cases} \dot{x}_i(t) = v_i(t), & i \in \Gamma, \\ \dot{v}_i(t) = \alpha (\bar{v}_i(t) - v_i(t)), \end{cases} \quad (3)$$

where  $\bar{v}_i(t) = \sum_{j=1}^N I(r_{ij}(t-\tau))v_j(t-\tau)$ . The initial conditions are

$$\begin{aligned} x_i(\theta) &= \varphi_i(\theta), \\ v_i(\theta) &= \phi_i(\theta), \\ \theta &\in [-\tau, 0], \end{aligned} \quad (4)$$

where  $(\varphi_i, \phi_i) \in C^2 = C \times C$  and  $C := C([- \tau, 0], \mathbb{R}^2)$  is the Banach space of all continuous functions.

In this study, we further consider the flocking conditions of the delayed model proposed in [5]. The significant contributions of our results are reflected in the following three aspects. (1) Compared with Theorem 3.1 in [5], the unconditional flocking condition  $\int_{-\infty}^{\infty} \psi^2(r) dr = \infty$  is improved to  $\int_{-\infty}^{\infty} \psi(r) dr = \infty$ , that is, the communication rate  $\beta$  is expanded from 1/4 to 1/2. (2) Note that with  $\tau = 0$  in (1), the communication rate  $\beta$  of unconditional flocking in [4] has also been expanded from 1/4 to 1/2. (3) It is clearly pointed out that processing delay can affect the occurrence of aggregation behavior, which is specifically manifested in the controllable range of the delay in flocking conditions.

The following two variables ( $D_x$  and  $D_v$ ) are used to analyze the evolution of the aggregation behavior of systems (3) and (4), for  $t \geq -\tau$ :

$$\begin{aligned} D_x(t) &= \max_{i,j \in \Gamma} \left\{ \|x_i(t) - x_j(t)\| \right\}, \\ D_v(t) &= \max_{i,j \in \Gamma} \left\{ \|v_i(t) - v_j(t)\| \right\}. \end{aligned} \quad (5)$$

Thus, for both  $I^{\text{CS}}(r)$  and  $I^{\text{MT}}(r)$ , it follows from a few simple calculations that a uniform result can be directly verified about the estimation of influence function  $I(r)$  as

$$I(r_{ij}(t-\tau)) \geq \frac{\psi(D_x(t-\tau))}{N}, \quad \text{for all } i, j \in \Gamma. \quad (6)$$

We still adopt the definition of time-asymptotic flocking proposed in [4].

**Definition 1.** Let  $\{x_i(t), v_i(t)\}_{i=1}^N$  be a solution to systems (3) and (4); a time-asymptotic flocking can be achieved if and only if the solution satisfies  $\sup_{t>0} D_x(t) < +\infty$  and  $\lim_{t \rightarrow +\infty} D_v(t) = 0$ , where  $D_x(t)$  and  $D_v(t)$  are given in (5).

## 2. Main Results

This section proposes two different sufficient conditions for systems (3) and (4) with  $I^{\text{CS}}$  or  $I^{\text{MT}}$  to achieve the conditional flocking in Theorem 1 and Theorem 2. We have also established certain conditions for the completion of unconditional flocking in Theorem 3.

**2.1. Conditional Flocking.** To establish the flocking solution of systems (3) and (4), the following important auxiliary lemmas are introduced first.

**Lemma 1** (see [8]). *Let  $x(t)$  be the solution of the linear functional differential equation,  $\dot{x}(t) = \lambda - \delta_1 x(t) + \delta_2 x(t-\tau)$ . If  $|\delta_2| < \delta_1$ , then*

$$\lim_{t \rightarrow +\infty} x(t) = x^* = \frac{\lambda}{\delta_1 - \delta_2}. \quad (7)$$

**Lemma 2.** *Let  $\{x_i(t), v_i(t)\}_{i=1}^N$  be a solution to systems (3) and (4); then, we have*

$$\begin{aligned} &\langle v_i(t) - v_j(t), \bar{v}_i(t) - \bar{v}_j(t) \rangle \\ &\leq \left( 1 - \frac{\psi(D_x(t-\tau))}{N} \right) D_v(t) D_v(t-\tau), \end{aligned} \quad (8)$$

where  $D_x$  and  $D_v$  are defined in (5).

*Proof.* Making use of system (3) yields

$$\begin{aligned} &\langle v_i(t) - v_j(t), \bar{v}_i(t) - \bar{v}_j(t) \rangle \\ &= \sum_{p=1}^N I(r_{ip}(t-\tau)) \sum_{q \neq p} I(r_{jq}(t-\tau)) \\ &\quad \cdot \langle v_i(t) - v_j(t), v_p(t-\tau) - v_q(t-\tau) \rangle \\ &\leq \sum_{p=1}^N I(r_{ip}(t-\tau)) \sum_{q \neq p} I(r_{jq}(t-\tau)) D_v(t) D_v(t-\tau). \end{aligned} \quad (9)$$

Using inequality (6) and the normalization assumptions for communication functions, that is,  $\sum_{j=1}^N I(r_{ij}(t-\tau)) = 1$ , we get

$$\begin{aligned} &\langle v_i(t) - v_j(t), \bar{v}_i(t) - \bar{v}_j(t) \rangle \\ &\leq \sum_{p=1}^N I(r_{ip}(t-\tau)) \sum_{q \neq p} I(r_{jq}(t-\tau)) D_v(t) D_v(t-\tau) \\ &= \sum_{p=1}^N I(r_{ip}(t-\tau)) (1 - I(r_{jp}(t-\tau))) D_v(t) D_v(t-\tau) \\ &\leq \left( 1 - \frac{\psi(D_x(t-\tau))}{N} \right) D_v(t) D_v(t-\tau), \end{aligned} \quad (10)$$

and this proof is completed.  $\square$

**Lemma 3.** *Let  $\{x_i(t), v_i(t)\}_{i=1}^N$  be a solution of systems (3) and (4); then, the upper Dini derivative of  $D_x(t)$  and  $D_v(t)$  satisfies*

$$\begin{aligned} D^+ D_x(t) &\leq D_v(t), \text{ a.e. } t \geq -\tau, \\ D^+ D_v(t) &\leq \alpha \left( 1 - \frac{\psi(D_x(t-\tau))}{N} \right) D_v(t-\tau) - \alpha D_v(t). \end{aligned} \quad (11)$$

*Proof.* Without loss of generality, let  $D_x(t) = \|x_p(t) - x_q(t)\|$  at time  $t$ , where  $p, q \in \Gamma$ . One can obtain

$$D^+ D_x(t) \leq \|\dot{x}_p(t) - \dot{x}_q(t)\| = \|v_p(t) - v_q(t)\| \leq D_v(t). \quad (12)$$

Similarly, without loss of generality, let  $D_v(t)$  satisfy  $D_v(t) = \|v_p(t) - v_q(t)\|$  at time  $t$ , where  $p, q \in 1, 2, \dots, N$ ; it follows from Lemma 2 that

$$\begin{aligned}
D^+ D_v^2(t) &= 2\alpha \langle v_p(t) - v_q(t), \dot{v}_p(t) - \dot{v}_q(t) \rangle \\
&= 2\alpha \langle v_p(t) - v_q(t), \bar{v}_p(t) - \bar{v}_q(t) \rangle - 2\alpha D_v^2(t) \\
&\leq 2\alpha \left( 1 - \frac{\psi(D_x(t-\tau))}{N} \right) D_v(t) D_v(t-\tau) - 2\alpha D_v^2(t).
\end{aligned} \tag{13}$$

Therefore, (11) is proven.

To establish the flocking conditions, we define a set containing all the initial configurations of asymptotic flocking allowed, that is,

$$\mathcal{S} := \left\{ \begin{array}{l} (x_i(\theta), v_i(\theta)), \\ \theta \in [-\tau, 0], \\ i = 1, 2, \dots, N. \end{array} \right. \tag{14}$$

$$D_v(0) + \alpha \int_{-\tau}^0 D_v(s) ds < \frac{\alpha}{N} \int_{D_x(-\tau)}^{\infty} \psi(r) dr \Big\},$$

where  $D_x$  and  $D_v$  are shown in (5) and  $\psi(r) = (1+r^2)^{-\beta}$ ,  $\beta \geq 0$  is defined in [2, 3].  $\square$

**Theorem 1.** For  $\beta > (1/2)$ , suppose that the initial conditions (4) are selected from the set  $\mathcal{S}$ ; then systems (3) and (4) with  $I^{MT}(r)$  or  $I^{CS}(r)$  can complete the conditional flocking.

*Proof.* Inspired by the work in [5, 9], we take the following Lyapunov function:

$$\begin{aligned}
E(D_x, D_v)(t) &= D_v(t) + \frac{\alpha}{N} \int_{D_x(-\tau)}^{D_x(t-\tau)} \psi(r) dr \\
&\quad + \alpha \int_{-\tau}^0 D_v(t+s) ds.
\end{aligned} \tag{15}$$

Thus, the upper Dini derivative of  $E(D_x, D_v)(t)$  along  $(D_x, D_v)$  with respect to  $t$  is shown below.

$$\begin{aligned}
D^+ E(D_x(t), D_v(t)) \\
= D^+ D_v(t) + \frac{\alpha}{N} D^+ \int_{D_x(-\tau)}^{D_x(t-\tau)} \psi(r) dr + \alpha D^+ \int_{-\tau}^0 D_v(t+s) ds.
\end{aligned} \tag{16}$$

Furthermore, combining with Lemma 3, we have  $D^+ E(D_x(t), D_v(t)) \leq 0$ , which means that  $E(D_x, D_v)(t)$  is nonincreasing and then  $E(D_x, D_v)(t) \leq E(D_x, D_v)(0)$  for all  $t > 0$ . Thus,

$$\frac{\alpha}{N} \int_{D_x(-\tau)}^{D_x(t-\tau)} \psi(r) dr \leq D_v(0) + \alpha \int_{-\tau}^0 D_v(s) ds. \tag{17}$$

Since the initial conditions (4) are selected from the set  $\mathcal{S}$ , it follows from (16) that

$$\frac{\alpha}{N} \int_{D_x(-\tau)}^{D_x(t-\tau)} \psi(r) dr < \frac{\alpha}{N} \int_{D_x(-\tau)}^{\infty} \psi(r) dr. \tag{18}$$

Due to the fact that  $\psi$  has a divergent tail, there must be a constant  $D^* < \infty$  such that  $D_x(t-\tau) \leq D^*$  for  $t \geq 0$ . Considering inequality (6) yields

$$I(r_{ij}(t-\tau)) \geq \frac{\psi(D_x(t-\tau))}{N} \geq \frac{\psi(D^*)}{N}, \quad \text{for all } j \in \Gamma. \tag{19}$$

Using the second inequality in (11) in Lemma 3, we can further derive that

$$D^+ D_v(t) \leq \alpha \left( 1 - \frac{\psi(D^*)}{N} \right) D_v(t-\tau) - \alpha D_v(t). \tag{20}$$

Making use of Lemma 1, we can show that  $D_v(t) \rightarrow 0$  as  $t \rightarrow \infty$  and systems (3) and (4) converge to a flock as shown in Definition 1. The proof is completed.

Another flocking condition closely related to processing delay is proposed in the following theorem.  $\square$

**Theorem 2.** For  $\beta > (1/2)$ , suppose that the initial configurations (4) are met as follows:

$$0 < D_v(0) < \frac{\alpha}{N} \int_{D_x(-\tau)}^{\infty} \psi(r) dr, \tag{21}$$

and the processing delay  $\tau$  satisfies

$$0 < \tau < \tau_0 := \frac{1}{\alpha R_\tau} \left( \frac{\alpha}{N} \int_{D_x(-\tau)}^{\infty} \psi(r) dr - D_v(0) \right), \tag{22}$$

where  $R_\tau := \max_{\theta \in [-\tau, 0]} D_v(\theta) > 0$  and  $D_x, D_v$  are defined in (5); then, systems (3) and (4) with  $I^{MT}(r)$  or  $I^{CS}(r)$  converge to a flock.

*Proof.* We only need to prove that the initial conditions which satisfy (22) all exist in the set  $\mathcal{S}$  defined in (8). Note that

$$\frac{\alpha}{N} \int_{D_x(-\tau)}^{\infty} \psi(r) dr > D_v(0) + \alpha \tau R_\tau > D_v(0) + \alpha \int_{-\tau}^0 D_v(s) ds, \tag{23}$$

which means that the initial conditions which satisfy (22) all exist in set  $\mathcal{S}$ . Consequently, systems (3) and (4) converge to a flock.  $\square$

*Remark 1.* The following notes are listed for the above two different results of conditional flocking.

- (1) Note that with  $\tau = 0$ , Theorem 1 and Theorem 2 will degenerate into  $D_v(0) < (\alpha/N) \int_{D_x(-\tau)}^{\infty} \psi(r) dr$ . If  $\alpha = N$ , then the flocking condition is further written as  $D_v(0) < \int_{D_x(-\tau)}^{\infty} \psi(r) dr$ , thereby improving Theorem 3.1 in [4].
- (2) Comparing Theorem 1 and Theorem 2, we can get the following two points worthy of attention. First, it is clear from the set of allowed initial conditions that the former is larger than the latter. Second, the latter helps us realize that the occurrence of aggregation behavior is indeed affected by the size of  $\tau$ .

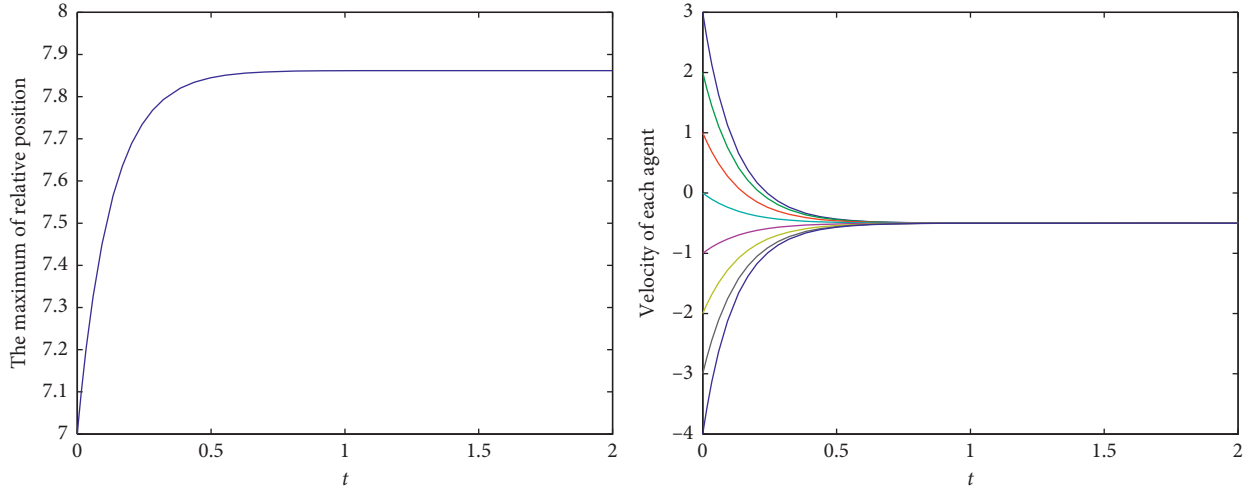


FIGURE 1:  $\alpha = 15, \beta = 0.51 > 0.5, \tau = 0$ . Systems (3) and (4) converge to a flock.

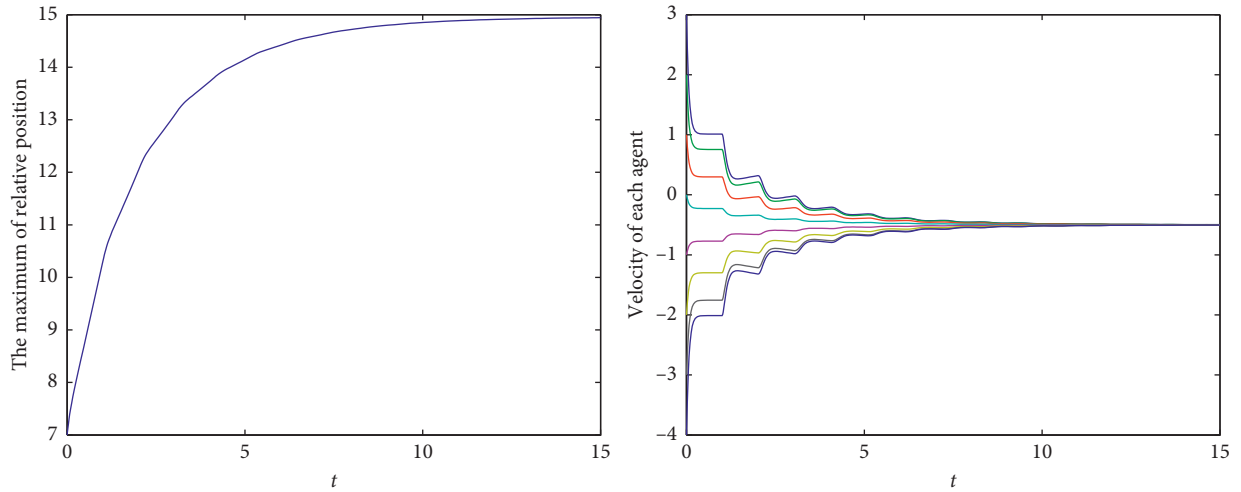


FIGURE 2:  $\alpha = 15, \beta = 0.51, \tau = 1 < \tau_0$ . Systems (3) and (4) converge asymptotically to form a flock. The convergence rate is slower than that in Example 1 due to processing delays. The diameter of the population is larger than that in Example 1, which means that the cohesion and aggregation density between particles are not as good as the case in Example 1.

**2.2. Unconditional Flocking.** The following theorem describes the implementation of unconditional flocking for systems (3) and (4).

**Theorem 3.** For  $\beta \in [0, (1/2)]$ , systems (3) and (4) with  $I^{MT}(r)$  or  $I^{CS}(r)$  converge unconditionally to a flock.

*Proof.* If  $\beta \in [0, (1/2)]$ , then the interparticle communication function has a tail dissipation  $\int_{-\infty}^{\infty} \psi(r) dr = \infty$ . Similar to the proof of Theorem 1, it can directly verify the unconditional flocking result. It will be omitted here.  $\square$

*Remark 2.* The two annotations for Theorem 3 are described below.

- (1) The fundamental reason for the unconditional flocking of systems (3) and (4) is that the following condition always holds for any initial configuration:

$$D_v(0) + \alpha \int_{-\tau}^0 D_v(s) ds < \frac{\alpha}{N} \int_{D_x(-\tau)}^{\infty} \psi(r) dr = \infty. \quad (24)$$

- (2) Note that with  $\tau = 0$ , the unconditional flocking result in [4] is improved to  $\int_{-\infty}^{\infty} \psi(r) dr = \infty$ , which means that the communication rate  $\beta$  is expanded from 1/4 to 1/2.
- (3) Compared with Theorem 3.1 in [5], the range of communication rate  $\beta$  has been expanded. Specifically, we promote the results from  $\int_{-\infty}^{\infty} \psi^2(r) dr = \infty$  to  $\int_{-\infty}^{\infty} \psi(r) dr = \infty$ , that is, we extend the communication rate  $\beta$  from 1/4 to 1/2. Thus, the results in [5] have been improved.

### 3. Numerical Simulations

Some numerical simulations will be enumerated to illustrate the effect of processing delay on the aggregation behavior of systems (3) and (4). For the convenience of calculation,

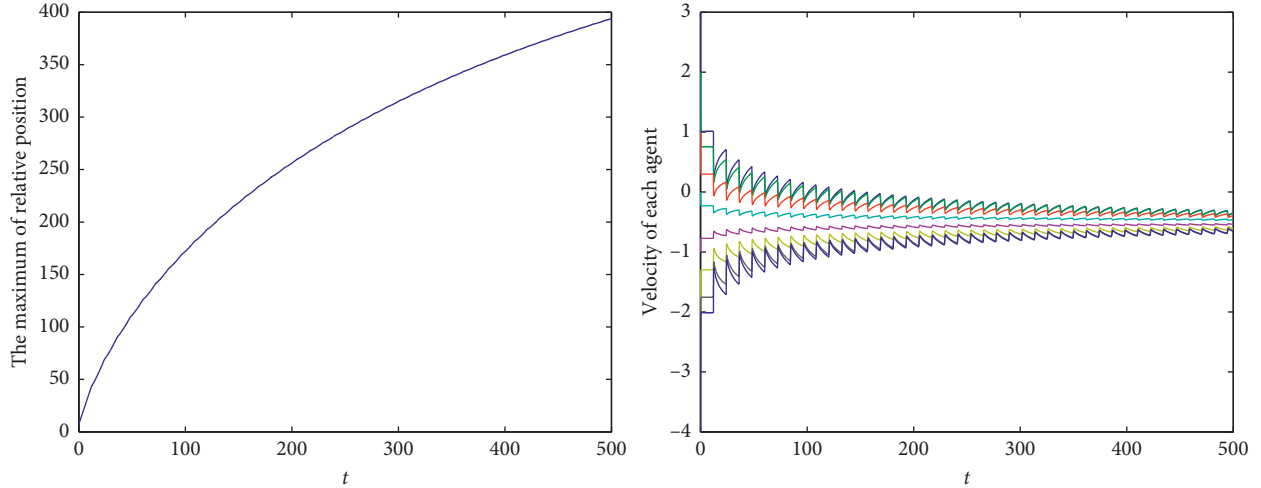


FIGURE 3:  $\alpha = 15, \beta = 0.51, \tau = 12 > \tau_0$ . Systems (3) and (4) fail to the emergence of flocking due to the destruction of (22) in Theorem 2.

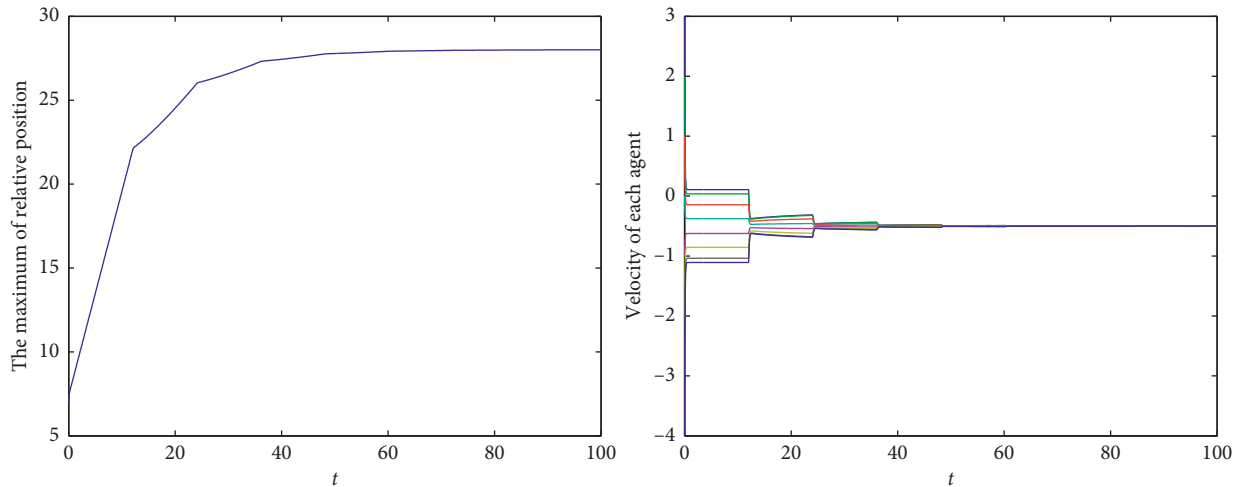


FIGURE 4:  $\alpha = 15, \beta = 0.2 < 0.5, \tau = 12$ . Systems (3) and (4) form a flock unconditionally.

consider a particle swarm composed of 8 particles and its initial conditions are set as  $(\varphi_i(\theta), \phi_i(\theta)) = (8 - i, 4 - i)$ ,  $i = 1, \dots, 8, \theta \in [-\tau, 0]$ . The parameters in (3) are fixed as  $\alpha = 15$ ,  $\beta = 0.51 > 0.5$ , and further we have  $\tau_0 = 1.0116$  from (22). To understand the aggregation behavior of the groups (3) and (4) intuitively and conveniently, we used two features in all experiments, namely, the velocity of each particle and the maximum of the relative position between particles.

*Example 1.*  $\alpha = 15, \beta = 0.51, \tau = 0$  (see Figure 1).

It can be seen from Figure 1 that without a time delay, the particle swarm can converge asymptotically to form a flock under the fixed initial configurations and the above parameters.

*Example 2.*  $\alpha = 15, \beta = 0.51, \tau = 1 < \tau_0$  (see Figure 2).

Considering the delay range (22) established in Theorem 2, we can claim that the flocking of the particle population (3) and (4) with  $\tau = 1 < \tau_0$  can be maintained. As we can see in Figure 2, systems (3) and (4) can still aggregate and form a

flock after introducing processing time lag  $\tau$ , which satisfies (22).

*Example 3.*  $\alpha = 15, \beta = 0.51, \tau = 12 > \tau_0$  (see Figure 3).

As shown in Figure 3, under the same initial condition with Example 2, this group cannot converge to a flock, and its fatal factor is that  $\tau = 12 > \tau_0$ , that is, (22) in Theorem 2 is broken.

To realize the emergence of flocking in this group, the following method can be adopted, that is, to appropriately adjust the communication rate between particles so that  $\beta < 0.5$ . It may be selected as  $\beta = 0.2 < 0.5$  and then combined with the discussion in Theorem 3; the system unconditionally converges to a flock. The simulation results are shown in Figure 4.

## 4. Conclusions

We study the emergence conditions of flocking of multiple particle swarms with processing delays, establish two

sufficient conditions for conditional flocking in Theorem 1 and Theorem 2, and give an unconditional flocking result in Theorem 3. In particular, Theorem 2 intuitively explains the fact that processing delays affect the emergence of flocking, which is reflected in the time-lag range (22) that affects the emergence of flocking. For  $0 \leq \beta \leq 1/2$ , we note that  $\tau = 0$ , which is obtained from the analysis in Remark 1 and Remark 2, and the flocking results in [4] have been improved from  $D_v(0) < \int_0^\infty \psi^2(r)dr$  to  $D_v(0) < \int_0^\infty \psi(r)dr$ . It means that the communication rate  $\beta$  has been expanded from 1/4 to 1/2. Compared with the work on the flocking results in [5], we have also expanded  $\beta$  from 1/4 to 1/2.

### Data Availability

The data used to support the findings of this study are included within the article.

### Conflicts of Interest

The authors declare that they have no conflicts of interest.

### Acknowledgments

This study was supported by the National Natural Science Foundation of China (11401577 and 11671011).

### References

- [1] C. W. Reynolds, "Flocks, herds and schools: a distributed behavioral model," *ACM SIGGRAPH Computer Graphics*, vol. 21, no. 4, pp. 25–34, 1987.
- [2] F. Cucker and S. Smale, "On the mathematics of emergence," *Japanese Journal of Mathematics*, vol. 2, no. 1, pp. 197–227, 2007.
- [3] F. Cucker and S. Smale, "Emergent behavior in flocks," *IEEE Transactions on Automatic Control*, vol. 52, no. 5, pp. 852–862, 2007.
- [4] S. Motsch and E. Tadmor, "A new model for self-organized dynamics and its flocking behavior," *Journal of Statistical Physics*, vol. 144, no. 5, pp. 923–947, 2011.
- [5] Y. Liu and J. Wu, "Flocking and asymptotic velocity of the Cucker-Smale model with processing delay," *Journal of Mathematical Analysis and Applications*, vol. 415, no. 1, pp. 53–61, 2014.
- [6] X. Wang, L. Wang, and J. Wu, "Impacts of time delay on flocking dynamics of a two-agent flock model," *Communications in Nonlinear Science and Numerical Simulation*, vol. 70, pp. 80–88, 2019.
- [7] M. Chen and X. Wang, "Flocking dynamics for multi-agent system with measurement delay," *Mathematics and Computers in Simulation*, vol. 171, pp. 187–200, 2020.
- [8] J. K. Hale and S. M. V. Lunel, *Introduction to Functional Differential Equations*, Springer-Verlag, Berlin, Germany, 1993.
- [9] S.-Y. Ha and J.-G. Liu, "A simple proof of the Cucker-Smale flocking dynamics and mean-field limit," *Communications in Mathematical Sciences*, vol. 7, no. 2, pp. 297–325, 2009.

## Research Article

# Semi-Supervised Cross-Modal Retrieval Based on Discriminative Comapping

Li Liu , Xiao Dong , and Tianshi Wang 

*School of Information Science and Engineering, Shandong Normal University, Jinan 250014, China*

Correspondence should be addressed to Li Liu; [liuli\\_790209@163.com](mailto:liuli_790209@163.com)

Received 8 May 2020; Revised 7 June 2020; Accepted 13 June 2020; Published 18 July 2020

Academic Editor: Jianquan Lu

Copyright © 2020 Li Liu et al. This is an open access article distributed under the Creative Commons Attribution License, which permits unrestricted use, distribution, and reproduction in any medium, provided the original work is properly cited.

Most cross-modal retrieval methods based on subspace learning just focus on learning the projection matrices that map different modalities to a common subspace and pay less attention to the retrieval task specificity and class information. To address the two limitations and make full use of unlabelled data, we propose a novel semi-supervised method for cross-modal retrieval named modal-related retrieval based on discriminative comapping (MRRDC). The projection matrices are obtained to map multimodal data into a common subspace for different tasks. In the process of projection matrix learning, a linear discriminant constraint is introduced to preserve the original class information in different modal spaces. An iterative optimization algorithm based on label propagation is presented to solve the proposed joint learning formulations. The experimental results on several datasets demonstrate the superiority of our method compared with state-of-the-art subspace methods.

## 1. Introduction

In real applications, data are often represented in different ways or obtained from various domains. As a consequence, the data with the same semantic may exist in different modalities or exhibit heterogeneous properties. With the rapid growth of multimodal data, there is an urgent need for effectively analyzing the data obtained from different modalities [1–5]. Although there is much attention to the multimodal analysis, the most common method is to ensemble the multimodal data to improve the performance [6–9]. Cross-modal retrieval is an efficient way to achieve data from different modal data. The typical example is to take the image as a query to retrieve related texts (I2T) or to search images by utilizing the textual description (T2I). Figure 1 shows the detailed process for I2T and T2I tasks. The results obtained by cross-modal retrieval are more comprehensive compared with the results of traditional single-modality.

Generally, semantic gap and relevant measure impede the development of cross-modal retrieval. Although there are many approaches to solve this problem, the performance of these approaches still cannot achieve a satisfactory level.

Therefore, the methods [10–16] are proposed to learn a common subspace by minimizing the pairwise differences to make different modalities comparable. However, task specificity and class information are often ignored, which leads to low-level retrieval performance.

To solve these problems mentioned above, this paper proposes a novel semi-supervised joint learning framework for cross-modal retrieval by integrating the common subspace learning, task-related learning, and class discriminative learning. Firstly, inspired by canonical correlation analysis (CCA) [7] and linear least squares, a couple of projection matrices are learnt by coupled linear regression to map original multimodal data to the common subspace. At the same time, linear discriminant analysis (LDA) and task-related learning (TRL) are used to keep the data structure in different modalities and the semantic relationship in the projection space. Furthermore, to mine the category information of unlabelled data, a semi-supervised strategy is utilized to propagate the semantic information from labelled data to unlabelled data. Experimental results on three public datasets show that the proposed method outperforms the previous state-of-the-art subspace approaches.

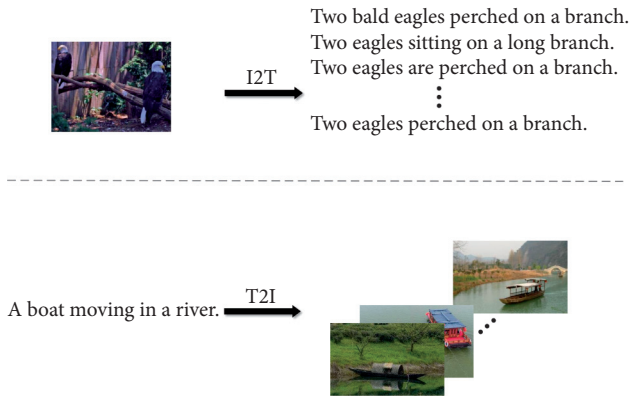


FIGURE 1: Using an image to retrieve texts and a text to retrieve images.

The main contributions of this paper can be summarized as follows:

- (1) The proposed joint formulation seamlessly combines semi-supervised learning, task-related learning, and linear discriminative analysis into a unified framework for cross-modal retrieval
- (2) The class information of labelled data is propagated to unlabelled data, and the linear discriminative constraint is introduced to preserve the interclass and intraclass similarity among different modalities

The remainder of the paper is organized as follows. In Section 2, we briefly overview the related work on the cross-modal retrieval problem. The details of the proposed methodology and the iterative optimization method are introduced in Section 3. Section 4 reports the experimental results and analysis. Conclusions are finally given in Section 5.

## 2. Related Work

Because cross-modal retrieval plays an important role in various applications, many subspace-based methods have been proposed by establishing the intermodal and intramodal correlation. Rasiwasia et al. [7] investigated the retrieval performance of various combinations of image features and textual representations, which cover all possibilities in terms of the two guiding hypotheses. Later, partial least squares (PLS) [17] has also been used for the cross-modal matching problem. Sharma and Jacobs [18] used PLS to linearly map images from different views into a common linear subspace, where the images have a high correlation. Chen et al. [19] solved the problem of cross-modal document retrieval by using PLS to transform image features into the text space, and the method easily achieved the similarity measure between two modalities. In [20, 21], the bilinear model and generalized multiview analysis (GMA) have been proposed and performed well in the field of cross-modal retrieval.

In addition to CCA, PLS, and GMA, Mahadevan et al. [22] proposed a manifold learning algorithm that can simultaneously reduce the dimension of data from different modalities. Mao et al. [23] introduced a cross-media retrieval method named parallel field alignment retrieval, which

integrates a manifold alignment framework from the perspective of vector fields. Lin and Tang [24] proposed a common discriminant feature extraction (CDFE) method to learn the difference within each scattering matrix and between scattering matrices. Sharma et al. [21] improved LDA and marginal Fisher analysis (MFA) to generalized multiview LDA (GMLDA) and generalized multiview MFA (GMMFA) by extending from single-modality to multimodalities. Inspired by the semantic information, Gong et al. [25] proposed a three-view CCA to deeply explore the correlation between features and their corresponding semantics in different modalities.

Furthermore, other methods, such as dictionary learning, graph-based learning, and multiview embedding, are proposed for the cross-modal problem [26–29]. Zhuang et al. [30] proposed Slim2 by adding a group sparse representation to the pairwise relation learning to project different modalities into a common space. Xu et al. [31] proposed that dictionary learning and feature learning should be combined to learn the projection matrix adaptively. Deng et al. [32] proposed a discriminative dictionary learning method with the common label alignment by learning the coefficients of different modalities. Wei et al. [33] proposed a modal-related method named MDCR to solve the modal semantic problem. Wu et al. [34] utilized spectral regression and a graph model to jointly learn the minimum error regression and latent space. Wang et al. [35] proposed an adversarial learning framework, which can learn modality-invariant and discriminative representations of different modalities. And in this framework, the modality classifier and the feature projector compete with each other to obtain a better pair of feature representations. Cao et al. [36] used multiview embedding to obtain latent representations for visual object recognition and cross-modal retrieval. Zhang et al. [37] utilized a graph model to learn a common space for cross-modal by adding the relationship of intraclass and interclass in the projection process.

The main purpose of these methods is to solve the correlation of distance measure, but the class information and task specificity are not well solved. Therefore, how to solve the two problems at the same time for different tasks is particularly important. Based on the idea, we learn two couples of projections for different retrieval tasks and apply a linear discriminative constraint to the projection matrices. To achieve this goal, we combine task-related learning with linear discriminative analysis through semi-supervised label propagation. Figure 2 shows the flowchart of our method. Experimental results on three open cross-modal datasets demonstrate that our cross-modal retrieval method outperforms the latest methods.

## 3. Methodology

To improve the retrieval performance, we introduce the discriminative comapping and pay more attention to different retrieval tasks and class information preservation. Here, we focus on the retrieval of I2T and I2T, and it is easy to expand our method to the retrieval of other modalities.



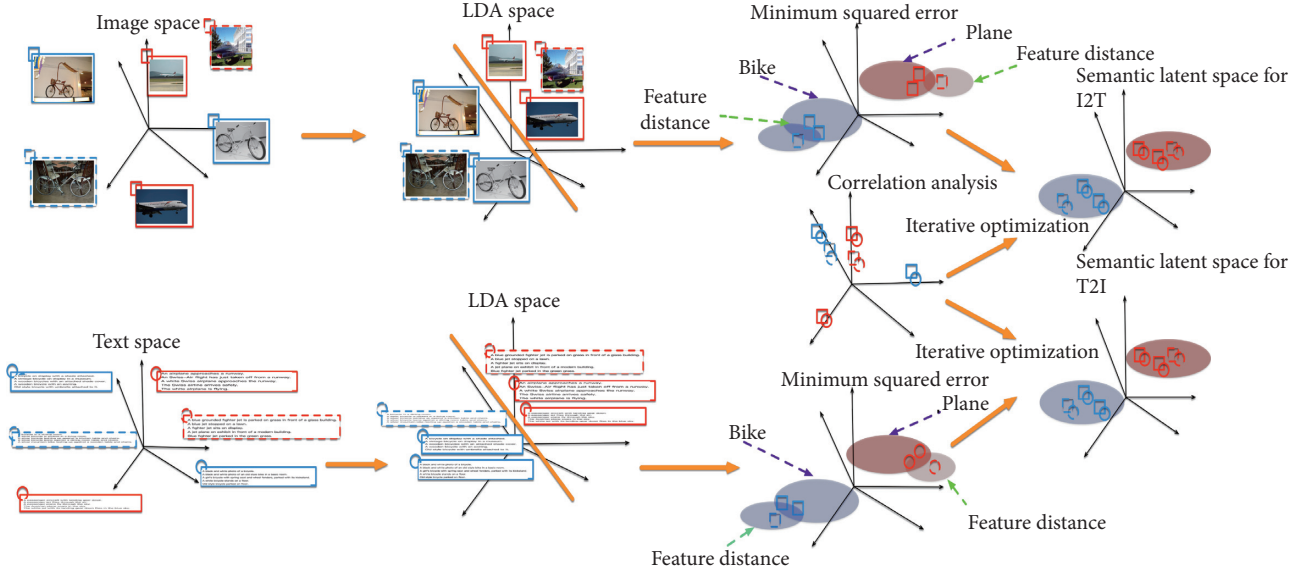


Figure 2: The flowchart of the proposed method. Images are represented by square icons, and the texts are represented by round icons. The images and texts with full lines are labelled data, and the rest are unlabelled data. Different colours indicate different categories. Our method adopts LDA to make different classes separate and make full use of the semi-supervised strategy to maximize the correlation between different modalities simultaneously.

**3.1. The Objective Function.** Define image data as  $I = [I_l; I_u] \in \mathbb{R}^{n \times p}$  and text data as  $T = [T_l; T_u] \in \mathbb{R}^{n \times q}$  separately, where  $I_l \in \mathbb{R}^{n_l \times p}$  and  $T_l \in \mathbb{R}^{n_l \times q}$  denote the labelled image  $n_l$  and its text with  $p$  dimensions, and  $I_u \in \mathbb{R}^{n_u \times p}$  and  $T_u \in \mathbb{R}^{n_u \times q}$  represent the unlabelled image  $n_u$  and its text with  $q$  dimensions. Let  $D = \{I_i, T_i\}_{i=1}^n$  be  $n$  pairs of image and text documents, where  $D_l = \{I_l, T_l\}_{i=1}^{n_l}$  and  $D_u = \{I_u, T_u\}_{i=1}^{n_u}$  denote the labelled and unlabelled documents, respectively.  $S = [S_l; S_u] \in \mathbb{R}^{n \times c}$  is the semantic matrix, where  $c$  is the category number,  $S_l$  is the label of labelled data with one-hot coding, and  $S_u$  is the pseudo-label of unlabelled data. The goal of our method is to learn two couples of projection matrices that project data from different modalities into a common space for different tasks. Then, the cross-modal retrieval can be performed in the common space.

We propose a novel modal-related projection strategy based on semi-supervised learning for task specificity. Here, the pairwise closeness of multimodal data and the semantic projection are combined into a unified formulation. For I2T and T2I, the minimization forms are obtained as follows:

$$f_1(V, W) = \min_{V, W} \|IV^T - TW^T\|_F^2 + \|IV^T - S\|_F^2, \quad (1)$$

$$f_2(V, W) = \min_{V, W} \|IV^T - TW^T\|_F^2 + \|TW^T - S\|_F^2, \quad (2)$$

where  $V$  and  $W$  stand for the projection matrices for modalities  $I$  and  $T$  separately.

The linear discriminant constraint to equations (1) and (2) is introduced to preserve the class information in the latent projection subspace. We denote  $m_i$  as the mean of the labelled samples in the  $i$ th class and  $m$  as the mean of all labelled samples. The intraclass scatter matrix can be defined

as  $S_w = \sum_{i=1}^c (P(i)/n_i) \sum_{x_k \in \text{class } i} (x_k - m_i)(x_k - m_i)^T$ , and the total scatter matrix can be represented as  $S_t = \sum_{i=1}^c P(i) (\bar{m}_i - m)(\bar{m}_i - m)^T$ . The objective function is represented as follows:

$$\min_{W, W^T = I_k} \frac{\text{tr}(W^T S_w W)}{\text{tr}(W^T S_t W)}, \quad (3)$$

where  $W \in \mathbb{R}^{d \times k}$  is the projection matrix and  $d$  is the dimension of the basic vector.

According to equation (3), the linear discriminant constraint can be transformed into  $W S_{w-t} W^T$ , where  $S_{w-t}$  is  $S_w - \gamma S_t$ . The intraclass scatter of  $I$  is represented as  $S_w I$ , and the interclass scatter of  $I$  is  $S_t$ . Under the multimodal condition, our method utilizes LDA projections to preserve class information of each modal. The corresponding formula is as follows:

$$\min_{V, W} V^T A V + W^T B W, \quad (4)$$

where  $A$  and  $B$  denote  $S_w I - \gamma_1 S_t I$  and  $S_w T - \gamma_2 S_t T$  separately.

We add equation (4) to equations (1) and (2), respectively, and then get the objective functions of I2T and T2I in the following:

$$F_1(V, W) = \min_{V, W} \lambda \|IV^T - TW^T\|_F^2 + (1 - \lambda) \|IV^T - S\|_F^2 + \mu_1 \text{tr}(V^T A V) + \mu_2 \text{tr}(W^T B W), \quad (5)$$

$$F_2(V, W) = \min_{V, W} \lambda \|IV^T - TW^T\|_F^2 + (1 - \lambda) \|TW^T - S\|_F^2 + \mu_1 \text{tr}(V^T A V) + \mu_2 \text{tr}(W^T B W), \quad (6)$$

where  $\lambda$  is a tradeoff coefficient to balance pairwise information and semantic information and  $\mu_1$  and  $\mu_2$  are regularization parameters to balance the structure information of the image and text. According to equations (1) and (2), the structure projection of  $I$  and  $T$  is the same as the semantic projection. Consequently, our method can bridge the feature and semantic spaces. This can decrease the loss of projection and improve the performance of cross-modal retrieval.

We introduce the semi-supervised learning strategy. To propagate the label information from the labelled data, we utilize the radial basis function (RBF) kernel to evaluate the pairwise similarities between the unlabelled data after projection, and then the similarities are regarded as the label information to be updated in the optimization process until the results converge. For any data  $x_i$  and  $x_j$ , the kernel function is defined as follows:

$$k(x_i, x_j) = \exp\left(-\frac{\|X_i - X_j\|^2}{2\beta^2}\right), \quad (7)$$

where  $\beta$  is the kernel parameter.

**3.2. Algorithm Optimization.** The objective functions of equations (5) and (6) are nonconvex, so the iteration method is used to update each variant when other variants are fixed alternatively.

For any matrix  $M \in \mathbb{R}^{N \times d}$ , the partial derivative of equation (5) is represented as follows:

$$\begin{aligned} \frac{\partial F_1}{\partial V} &= 2(\lambda(VI^T I - WT^T I) + (1 - \lambda)(VI^T I - S^T I)) \\ &\quad + \mu_1(VA + VA^T), \end{aligned} \quad (8)$$

$$\frac{\partial F_1}{\partial W} = 2\lambda(WT^T T - VI^T T) + \mu_2(WB + WB^T). \quad (9)$$

Similarly, the partial derivative of equation (6) is given as follows:

$$\begin{aligned} \frac{\partial F_2}{\partial W} &= 2(\lambda(WT^T T - VI^T T) + (1 - \lambda)(WT^T T - S^T T)) \\ &\quad + \mu_2(WB + WB^T), \end{aligned} \quad (10)$$

$$\frac{\partial F_2}{\partial V} = 2\lambda(VI^T I - WT^T I) + \mu_1(VA + VA^T). \quad (11)$$

According to equations (8)–(11), our method can be solved by gradient descent. Algorithm 1 describes the optimization of cross-modal learning. After the projection matrices for the I2T and T2I tasks are obtained,  $I$  and  $T$  can be mapped to the common space where cross-modal retrieval is achieved.

## 4. Experiments

To evaluate the performance of the proposed method (MRRDC), we do comparison experiments with several other methods on three public datasets.

### 4.1. Datasets

**4.1.1. Wikipedia Dataset.** This dataset consists of 2,866 image-text pairs labelled with one of 10 semantic classes. In this dataset, 2,173 pairs of data are selected as the training set, and the rest are the testing set. In our experiments, we use the public dataset [7] provided by Rasiwasia et al. (wiki-R), where images are represented by 128-dimensional SIFT description histograms [38], and the representation of the texts with 10 dimensions is derived from an LDA model [39]. At the same time, we also use the dataset provided by Wei et al. (wiki-W) [40], where 4,096-dimensional CNN features [41] are used to present images and 100-dimensional LDA features are utilized to denote the texts.

**4.1.2. Pascal Sentence Dataset [40].** This dataset consists of 1,000 image-text pairs with 20 categories. We randomly choose 30 pairs from each category as training samples and the rest as test samples. The image features are 4,096-dimensional CNN features, and the text features are 100-dimensional LDA features.

**4.1.3. INRIA-Websearch [42].** This dataset contains 71,478 pairs of image and text annotations from 353 classes. We remove some pairs which are marked as irrelevant and select the pairs that belong to any one of the 100 largest categories. Then, we get a subset of 14,698 pairs for evaluation. We randomly select 70% of pairs from each category as the training set (10,332 pairs), and the rest are treated as the testing set (4,366 pairs). Similarly, images are represented with 4,096-dimensional CNN features, and the textual tags are represented with 100-dimensional LDA features.

**4.2. Evaluation Metrics.** To evaluate the performance of the proposed method, two typical cross-modal retrieval tasks are conducted: I2T and T2I. In the test phase, the projection matrices are used to map the multimodal data into the common subspace. Then, the data of different modalities can be retrieved. In all experiments, the cosine distance is adopted to measure the feature similarities. Given a query, the aim of each cross-modal task is to find the top- $k$  nearest neighbors from the retrieval results.

The performance of the algorithms is evaluated by mean average precision (mAP), which is one of the standard information retrieval metrics. To obtain mAP, average precision (AP) is calculated by

$$AP = \frac{1}{R} \sum_{i=1}^R P(i)\sigma(i), \quad (12)$$

where  $R$  is the number of correlation data in the test dataset,  $P(i)$  is the precision of top  $r$  retrieval data, and if  $\sigma(i) = 1$ , the top  $r$  retrieval data are relevant; otherwise,  $\sigma(i) = 0$ . Then, the value of mAP can be obtained by averaging AP for all queries. The larger the mAP, the better the retrieval performance. Besides the mAP, the precision-recall curves and mAP performance for each class are used to evaluate the effectiveness of different methods.

Input: all image feature matrices  $I \in \mathbb{R}^{n \times q}$ , all text feature matrices  $T \in \mathbb{R}^{n \times p}$ , and the corresponding semantic matrix  $S = [S_l; S_u]$ .  
Initial:  $V_i, W_j, i = 0, j = 0$ , and set the parameters  $\lambda, \mu_1, \mu_2, \epsilon_1, \epsilon_2, \sigma$  and maximum iteration time.  $\sigma$  is the step size in the alternating updating process,  $\epsilon_1$  and  $\epsilon_2$  is the convergence condition.  
Repeat:  
value1 =  $F_1(V_i, W_j)$   
=  $\min_{V_i, W_j} \lambda \|IV_i^T - TW_j^T\|_F^2 + (1 - \lambda) \|IV_i^T - S_l\|_F^2 + \mu_1 \text{tr}(V^T AV) + \mu_2 \text{tr}(W^T BW)$ ;  
 $V_{i+1} = V_i - \sigma ((\partial f_1 t(V_i, W_j)) / \partial V_i)$ ;  
value2 =  $F_1(V_{i+1}, W_j)$   
=  $\min_{V_{i+1}, W_j} \lambda \|IV_{i+1}^T - TW_j^T\|_F^2 + (1 - \lambda) \|IV_{i+1}^T - S_l\|_F^2 + \mu_1 \text{tr}(V^T AV) + \mu_2 \text{tr}(W^T BW)$ ;  
 $i = i + 1$ ;  
Until value1 - value2  $< \epsilon_1$ ;  
Repeat:  
value3 =  $F_1(V_i, W_j)$   
=  $\min_{V_i, W_j} \lambda \|IV_i^T - TW_j^T\|_F^2 + (1 - \lambda) \|IV_i^T - S_l\|_F^2 + \mu_1 \text{tr}(V^T AV) + \mu_2 \text{tr}(W^T BW)$ ;  
 $W_{j+1} = W_j - \sigma ((\partial f_1 t(V_i, W_j)) / \partial W_j)$ ;  
value4 =  $F_1(V_i, W_{j+1})$   
=  $\min_{V_i, W_{j+1}} \lambda \|IV_i^T - TW_{j+1}^T\|_F^2 + (1 - \lambda) \|IV_i^T - S_l\|_F^2 + \mu_1 \text{tr}(V^T AV) + \mu_2 \text{tr}(W^T BW)$ ;  
 $j = j + 1$ ;  
Until value3 - value4  $< \epsilon_2$ ;  
 $S_u = k(I_u V^T, T_u W^T)$ ;  
 $t = t + 1$ ;  
 $S_t = (S_l, S_u)$ ;  
Until  $t >$  maximum iteration number  
Output:  $V_i, W_j$

ALGORITHM 1: Optimization for MRRDC.

**4.3. Comparison Methods.** To verify that our method has good performance, we compare our method with seven state-of-the-art methods, such as PLS [18], CCA [7], SM [7], SCM [7], GMLDA [21], GMMFA [21], MDCR [33], JLSLR [34], ACMR [35], and SGRCR [37].

PLS, CCA, SM, and SCM are typical methods that utilize pairwise information to learn a common latent subspace, where the similarity between different multimodals can be measured by metric methods directly. These kinds of approaches make the pairwise data in the multimodal dataset closer in the learned common subspace. GMLDA, GMMFA, and MDCR are based on the semantic category information via supervised learning. Due to the use of label information, these methods can easily learn a more discriminative subspace.

**4.4. Experimental Setup.** The parameters of the proposed MRRDC in Algorithm 1 for the retrieval tasks of I2T and T2I are set as follows:  $\lambda = 0.5$ ,  $\gamma_1 = 0.3$ ,  $\gamma_2 = 0.3$ ,  $\mu_1 = 0.5$ ,  $\mu_2 = 0.5$ ,  $\gamma_1 = 0.5$ ,  $\gamma_2 = 0.5$ ,  $\epsilon_1 = 10^{-5}$ , and  $\epsilon_2 = 0.001$  on Wikipedia provided by Rasiwasia and INRIA-Websearch. On Wikipedia provided by Wei and Pascal,  $\lambda = 0.3$ , and the rest are the same with the above. In our experiment, learning rate  $\sigma$  is set  $10^{-4}$ .

**4.5. Results and Analysis.** Table 1 shows all the mAP scores achieved by PLS, CCA, SM, SCM, GMMFA, GMLDA, MDCR, and our method on wiki-R, wiki-W, Pascal Sentence, and INRIA-Websearch. We observe that our method outperforms its counterparts. This may be because the

projection matrices preserve more discriminative class information via semi-supervised learning. The common subspace of our method is more discriminative and effective by further exploiting the class semantic of intramodality and intermodality similarity simultaneously. From Table 1, we also find that, in most cases, GMMFA, GMLDA, MDCR, and MRRDC always perform better than PLS, CCA, SM, and SCM, and images with CNN features have superiority compared with the shallow features. For the first result, this is because PLS, CCA, SM, and SCM only use pairwise information, but the other approaches add class information to their objective functions, which provides better separation between different categories in the latent common subspace. For the second result, this is due to the powerful semantic representation of CNN.

The precision-recall curves on wiki-R, wiki-W, Pascal Sentence, and INRIA-Websearch are plotted in Figure 3. Figure 4 shows the mAP scores of comparison approaches and our method, and the rightmost bar of each figure shows the average mAP scores. For most categories, the mAP of our method outperforms that of comparison methods. From these experimental results, we can draw the following conclusions:

- (1) Compared with the current state-of-the-art methods, our method improves the average mAP greatly. Our method consistently outperforms compared methods, which is due to the factor that MRRDC learns projection matrices in task-related and linear discrimination ways for different modalities, where different modalities can preserve semantic and original class information. Besides, both labelled data

TABLE 1: Retrieval performance (mAP) on three public datasets.

Methods	wiki-R			wiki-W		
	I2T (%)	T2I (%)	Average (%)	I2T (%)	T2I (%)	Average (%)
PLS	23.75	17.23	20.49	35.95	35.10	35.53
CCA	24.14	19.71	21.93	33.16	31.66	32.41
SM	22.64	21.84	22.24	36.85	38.67	37.76
SCM	26.62	22.57	24.59	37.48	39.26	38.37
GMMFA	23.09	20.34	21.72	28.41	24.87	26.64
GMLDA	24.64	19.52	22.08	30.03	28.06	29.05
JLSLR	23.60	21.22	22.41	39.42	36.91	38.17
MDCR	26.19	21.03	23.61	41.07	37.75	39.41
ACMR	<b>33.22</b>	24.50	<b>28.86</b>	50.61	42.82	46.72
SGRCR	28.42	22.71	25.57	43.65	40.60	42.10
MRRDC	28.93	<b>26.29</b>	27.61	<b>62.34</b>	<b>53.00</b>	<b>57.67</b>

Methods	Pascal sentence			INRIA-Websearch		
	I2T (%)	T2I (%)	Average (%)	I2T (%)	T2I (%)	Average (%)
PLS	36.53	37.63	37.08	19.38	26.03	22.71
CCA	37.99	37.20	37.59	26.03	27.95	26.99
SM	44.98	43.39	44.19	37.83	35.31	36.57
SCM	40.71	39.35	40.03	35.44	30.87	33.16
GMMFA	37.32	34.70	36.01	28.09	30.37	29.23
GMLDA	40.80	38.77	39.79	47.59	54.07	50.83
JLSLR	45.42	45.56	45.49	52.51	54.53	53.52
MDCR	43.22	46.22	44.72	47.09	45.99	46.54
ACMR	46.81	56.23	51.52	55.85	66.92	61.39
SGRCR	49.23	50.00	49.60	54.10	55.40	54.78
MRRDC	<b>66.49</b>	<b>58.54</b>	<b>62.52</b>	<b>56.70</b>	<b>68.81</b>	<b>62.76</b>

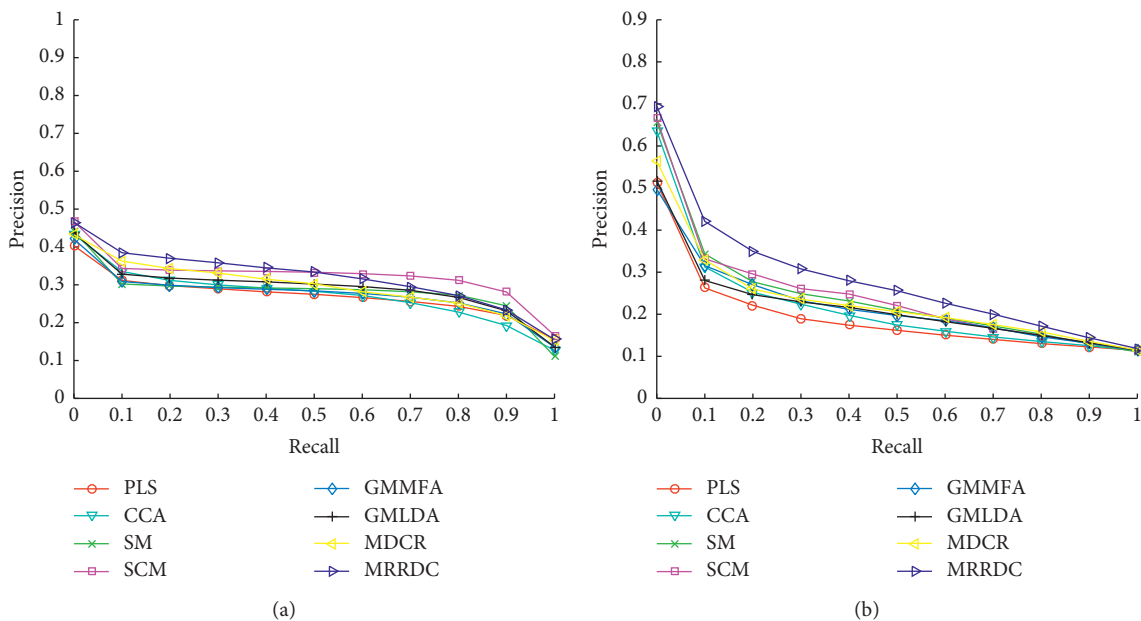
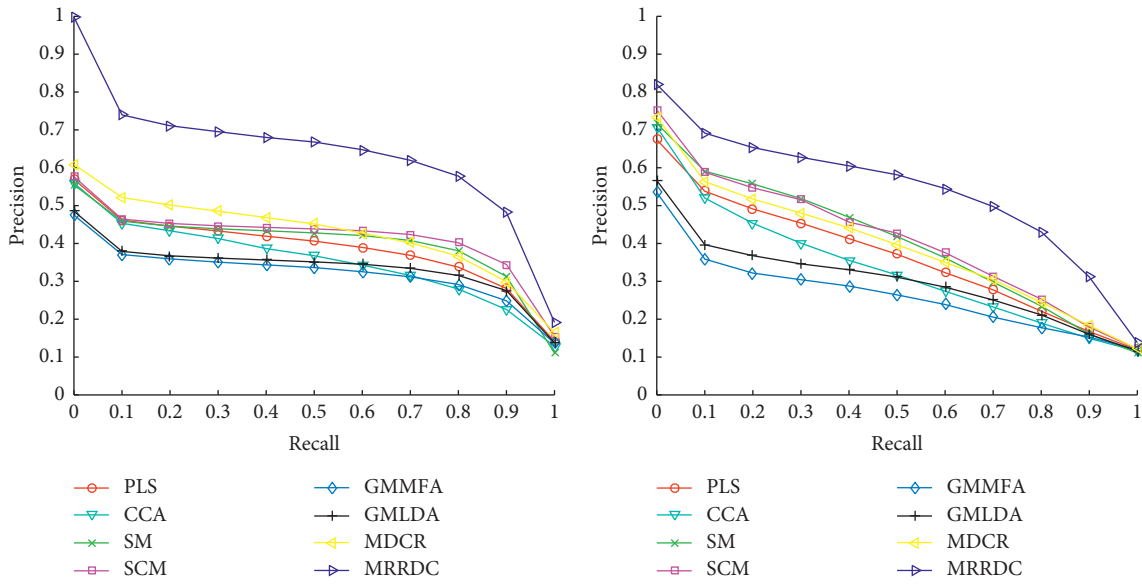
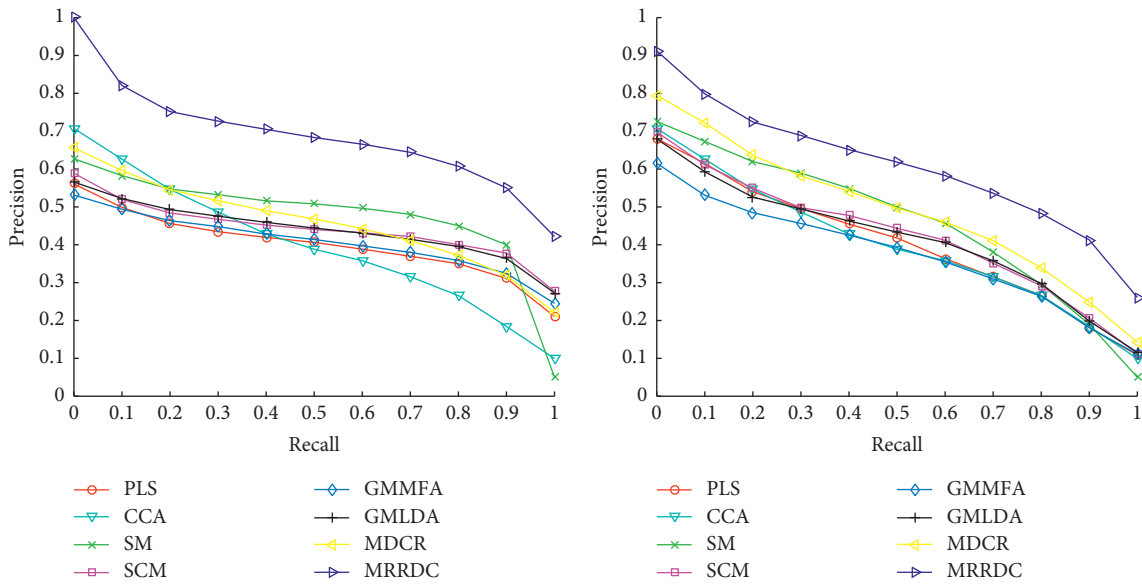


FIGURE 3: Continued.



(c)

(d)



(e)

(f)

FIGURE 3: Continued.

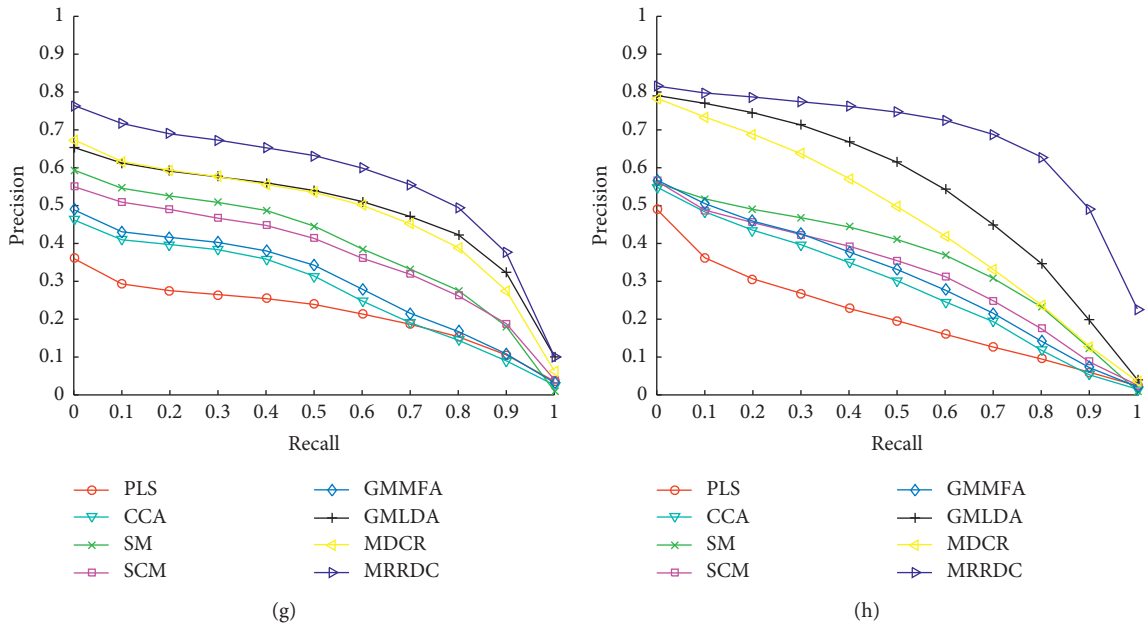


FIGURE 3: Precision-recall curves of the proposed MRRDC and compared methods. (a) I2T on wiki-R. (b) T2I on wiki-R. (c) I2T on wiki-W. (d) T2I on wiki-W. (e) I2T on Pascal. (f) T2I on Pascal. (g) I2T on INRIA-Websearch. (h) T2I on INRIA-Websearch.

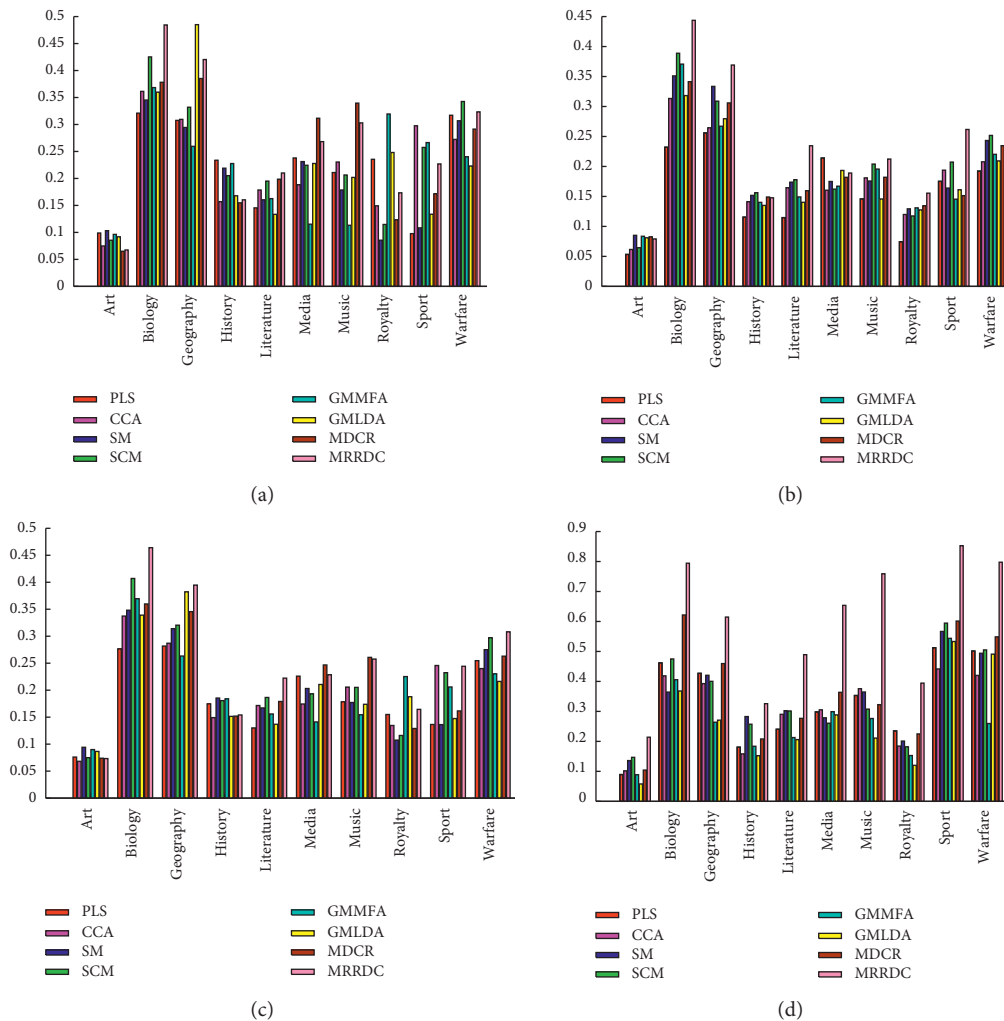


FIGURE 4: Continued.

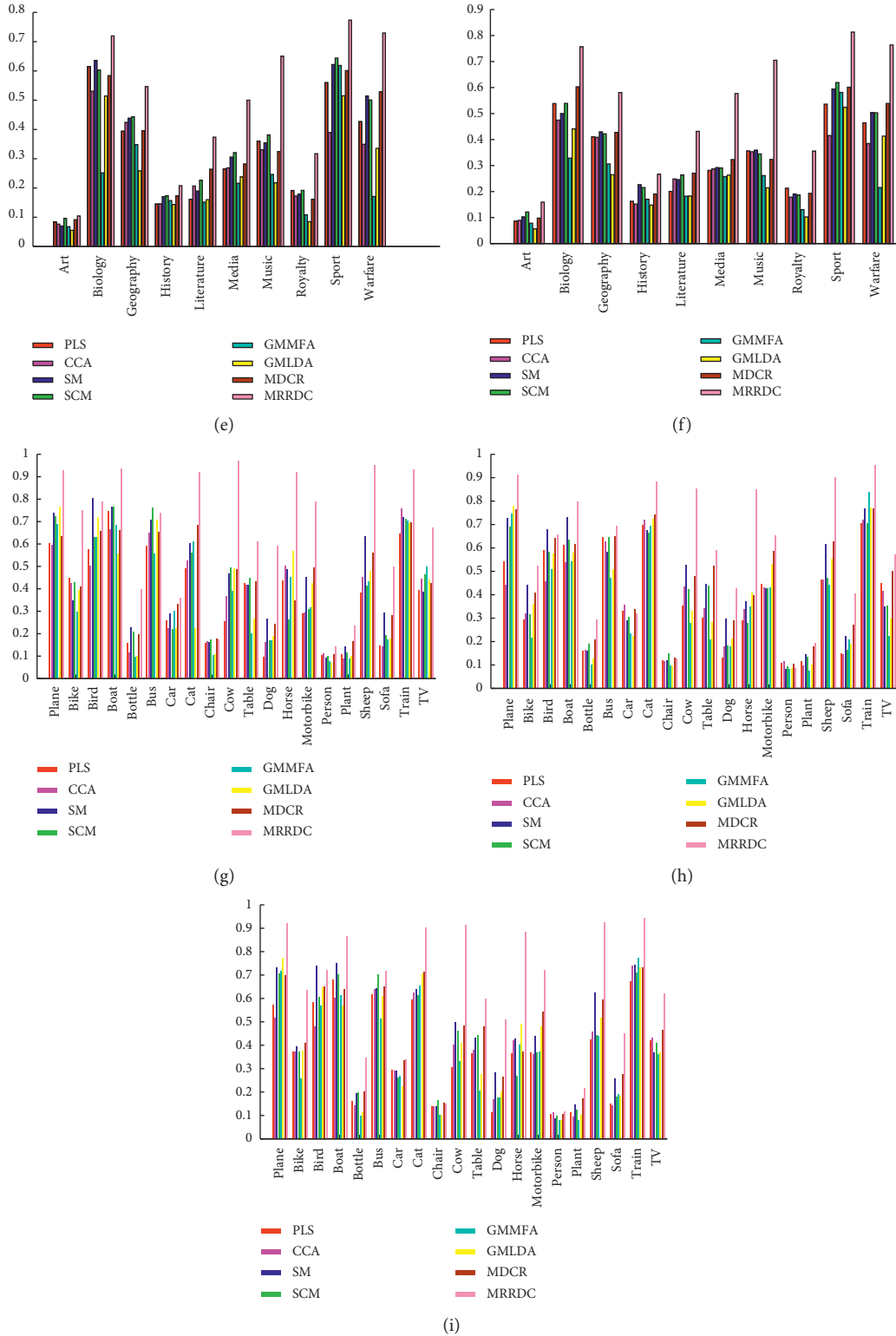


FIGURE 4: The mAP performance for each class on Wikipedia datasets and Pascal Sentence dataset. (a) I2T on wiki-R. (b) T2I on wiki-R. (c) Average on wiki-R. (d) I2T on wiki-W. (e) T2I on wiki-W. (f) Average on wiki-W. (g) I2T on Pascal. (h) T2I on Pascal. (i) Average on Pascal.

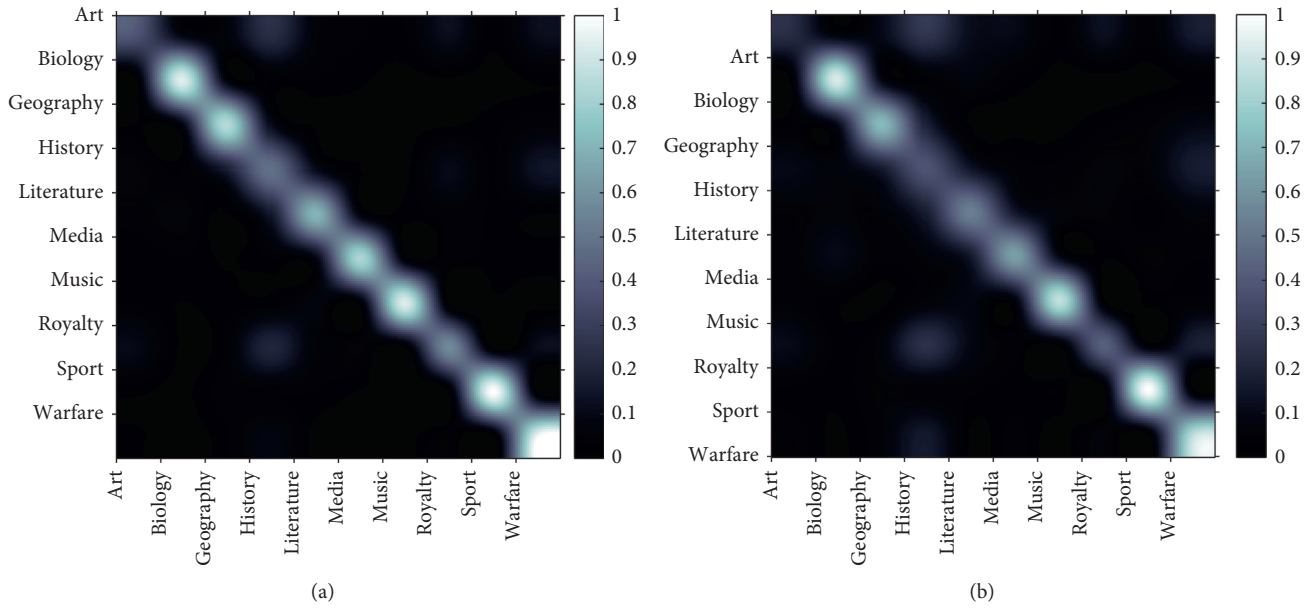


FIGURE 5: Class-level confusion matrices computed by the (a) image query and (b) text query on wiki-W.

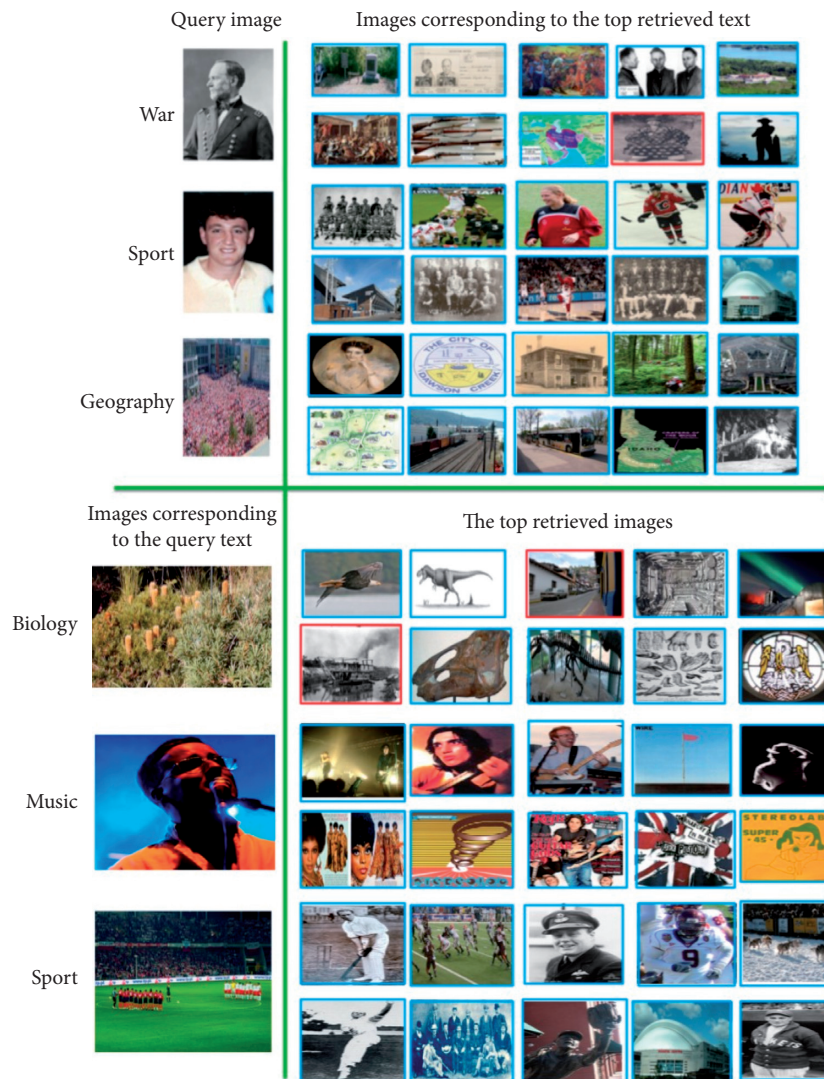


FIGURE 6: Image queries and the corresponding top retrieved images, and text queries and the corresponding top retrieved images.



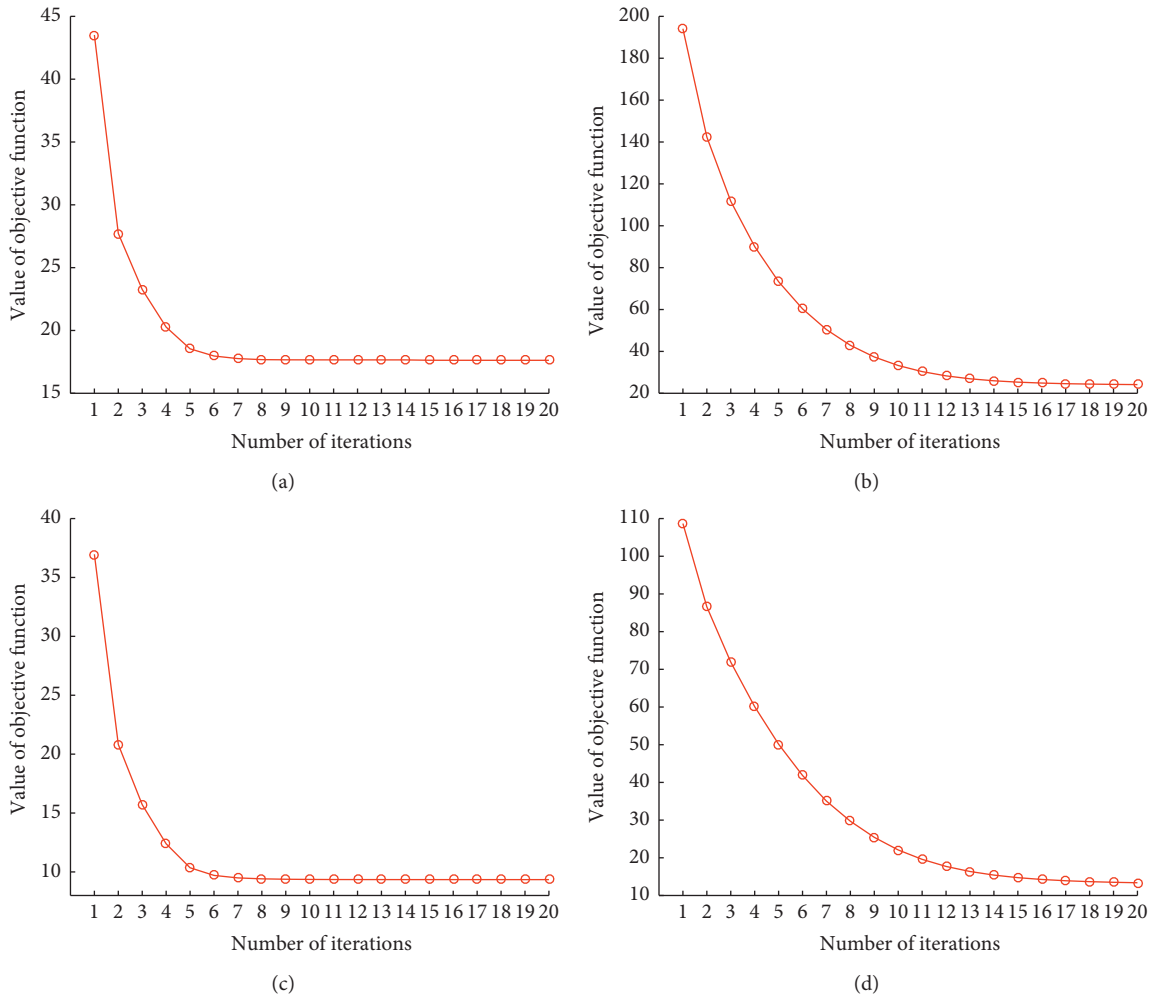


FIGURE 7: Convergence curves of the objective function value using Algorithm 1 on Wikipedia and Pascal datasets. The figure shows that the objective function value monotonically decreases until convergence by applying the iterative algorithm. (a) Image query on wiki-W. (b) Text query on wiki-W. (c) Image query on Pascal. (d) Text query on Pascal.

and unlabelled data of all the different modalities are explored. The labelled information can be propagated to the unlabelled data during the training process.

- (2) In most cases, GMLDA and GMMFA outperform CCA since GMLDA and GMMFA add category information to their formulation, which makes the common projection subspace more suitable for cross-modal retrieval.
- (3) Compared with the shallow features, CNN features have great advantages for the I2T task, which is because CNN features can easily obtain the semantic information from original images directly.

To further verify the effectiveness of our proposed MRRDC, we also provide the confusion matrices on single-modal retrieval and the query examples for I2T and T2I in Figures 5 and 6 separately. Intuitively, from Figure 5, our method can achieve high precision in each category, which proves that the projection space is discriminative. We also observe from Figure 6 that, in many categories, our proposed

method always successfully obtains the best retrieval results from query samples.

**4.6. Convergence.** Our objective formulation is solved by an iterative optimization algorithm. In a practical application, a fast retrieval speed is necessary. In Figure 7, we plot the convergence curves of our optimization algorithm as to the objective function value of equations (5) and (6) at each iteration on wiki-W and Pascal Sentence datasets separately. In this figure, the curve is monotonic at each iteration, and the algorithm generally converges within about 20 iterations for these datasets. The fast speed can ensure the high efficiency of our method.

## 5. Conclusion

In this paper, we propose an effective semi-supervised cross-modal retrieval approach based on discriminative comapping. Our approach uses different couples of discriminative projection matrices to map different modalities to the

common space where the correlation between different modalities can be maximum for different retrieval tasks. In particular, we use labelled samples to propagate the category information to unlabelled samples, and the original class information is preserved by using linear discriminant analysis. Therefore, the proposed method not only uses the relationship of different retrieval tasks but also keeps the structure information for different modalities. In the future, we will mine the correlation between different modalities and focus on the unsupervised cross-modal retrieval method for unlabelled data.

## Data Availability

The data supporting this paper are from the reported studies and datasets in the cited references.

## Conflicts of Interest

The authors declare that there are no conflicts of interest regarding the publication of this paper.

## Acknowledgments

This work was partially supported by the National Natural Science Foundation of China (no. 61702310), the Major Fundamental Research Project of Shandong, China (no. ZR2019ZD03), and the Taishan Scholar Project of Shandong, China (no. ts20190924).


## References

- [1] R. Bekkerman and J. Jeon, "Multi-modal clustering for multimedia collections," in *Proceedings of the IEEE Conference on Computer Vision and Pattern Recognition*, pp. 1–8, Minneapolis, MN, USA, July 2007.
- [2] D. Eynard, A. Kovnatsky, M. M. Bronstein, K. Glashoff, and A. M. Bronstein, "Multimodal manifold analysis by simultaneous diagonalization of laplacians," *IEEE Transactions on Pattern Analysis and Machine Intelligence*, vol. 37, no. 12, pp. 2505–2517, 2015.
- [3] S. Escalera, J. Gonzalez, X. Baro, and J. Shotton, "Guest editors' introduction to the special issue on multimodal human pose recovery and behavior analysis," *IEEE Transactions on Pattern Analysis and Machine Intelligence*, vol. 38, no. 8, pp. 1489–1491, 2016.
- [4] L. Liu, B. Zhang, H. Zhang, and N. Zhang, "Graph steered discriminative projections based on collaborative representation for Image recognition," *Multimedia Tools and Applications*, vol. 78, no. 17, pp. 24501–24518, 2019.
- [5] Z. Cheng, X. Chang, L. Zhu, R. C. Kanjirathinkal, and M. Kankanhalli, "MMALFM," *ACM Transactions on Information Systems*, vol. 37, no. 2, pp. 1–28, 2019.
- [6] K. Wang, R. He, L. Wang, W. Wang, and T. Tan, "Joint feature selection and subspace learning for cross-modal retrieval," *IEEE Transactions on Pattern Analysis and Machine Intelligence*, vol. 38, no. 10, pp. 2010–2023, 2016.
- [7] N. Rasiwasia, J. C. Pereira, E. Coviello et al., "A new approach to cross-modal multimedia retrieval," in *Proceedings of the International Conference on Multimedia-MM'10*, pp. 251–260, Firenze, Italy, October 2010.
- [8] L. Liu, S. Chen, X. Chen, T. Wang, and L. Zhang, "Fuzzy weighted sparse reconstruction error-steered semi-supervised learning for face recognition," *The Visual Computer*, vol. 3, pp. 1–14, 2019.
- [9] L. Zhu, Z. Huang, Z. Li, L. Xie, and H. T. Shen, "Exploring auxiliary context: discrete semantic transfer hashing for scalable image retrieval," *IEEE Transactions on Neural Networks and Learning Systems*, vol. 29, no. 11, pp. 5264–5276, 2018.
- [10] L. Zhu, Z. Huang, X. Liu, X. He, J. Sun, and X. Zhou, "Discrete multimodal hashing with canonical views for robust mobile landmark search," *IEEE Transactions on Multimedia*, vol. 19, no. 9, pp. 2066–2079, 2017.
- [11] L. Zhu, X. Lu, Z. Cheng, J. Li, and H. Zhang, "Flexible multimodal hashing for scalable multimedia retrieval," *ACM Transactions on Intelligent Systems and Technology*, vol. 11, no. 2, pp. 1–20, 2020.
- [12] X. Lu, L. Zhu, Z. Cheng, X. Song, and H. Zhang, "Efficient discrete latent semantic hashing for scalable cross-modal retrieval," *Signal Processing*, vol. 154, pp. 217–231, 2019.
- [13] Y. Fang, H. Zhang, and Y. Ren, "Unsupervised cross-modal retrieval via multi-modal graph regularized smooth matrix factorization hashing," *Knowledge-Based Systems*, vol. 171, pp. 69–80, 2019.
- [14] F. Shang, H. Zhang, L. J. Sun, and H. Zhang, "Adversarial cross-modal retrieval based on dictionary learning," *Neurocomputing*, vol. 355, pp. 93–104, 2019.
- [15] F. Shang, H. Zhang, J. Liu, and H. Zhang, "Semantic consistency cross-modal dictionary learning with rank constraint," *Journal of Visual Communication and Image Representation*, vol. 62, pp. 259–266, 2019.
- [16] M. Zhang, J. Li, H. Zhang, and L. Liu, "Deep semantic cross modal hashing with correlation alignment," *Neurocomputing*, vol. 381, pp. 240–251, 2020.
- [17] R. Rosipal and N. Kramer, "Overview and recent advances in partial least squares," in *Subspace, Latent Structure and Feature Selection, Statistical and Optimization*, pp. 34–51, Springer, Berlin, Germany, 2005.
- [18] A. Sharma and D. W. Jacobs, "Bypassing synthesis: PLS for face recognition with pose, low-resolution and sketch," in *Proceedings of the IEEE Conference on Computer Vision and Pattern Recognition*, pp. 593–600, Providence, RI, USA, June 2011.
- [19] Y. Chen, L. Wang, W. Wang, and Z. Zhang, "Continuum regression for cross-modal multimedia retrieval," in *Proceedings of the IEEE International Conference on Image Processing*, pp. 1949–1952, Orlando, FL, USA, September 2012.
- [20] J. B. Tenenbaum and W. T. Freeman, "Separating style and content with bilinear models," *Neural Computation*, vol. 12, no. 6, pp. 1247–1283, 2000.
- [21] A. Sharma, A. Kumar, H. Daume III, and D. W. Jacobs, "Generalized multiview analysis: a discriminative latent space," in *Proceedings of the IEEE Conference on Computer Vision and Pattern Recognition*, pp. 2160–2167, Providence, RI, USA, June 2012.
- [22] V. Mahadevan, C. W. Wong, J. C. Pereira et al., "Maximum covariance unfolding: manifold learning for bimodal data," in *Advances in Neural Information Processing Systems*, , pp. 918–926, 2011.
- [23] X. Mao, B. Lin, D. Cai, X. He, and J. Pei, "Parallel field alignment for cross media retrieval," in *Proceedings of the ACM Multimedia Conference*, pp. 897–906, Dallas, Texas, USA, April 2013.

- [24] D. Lin and X. Tang, "Inter-modality face recognition," in *European Conference on Computer Vision*, pp. 13–26, Springer, Berlin, Germany, 2006.
- [25] Y. Gong, Q. Ke, M. Isard, and S. Lazebnik, "A multi-view embedding space for modeling internet images, tags, and their semantics," *International Journal of Computer Vision*, vol. 106, no. 2, pp. 210–233, 2014.
- [26] X. Xu, L. He, H. Lu, L. Gao, and Y. Ji, "Deep adversarial metric learning for cross-modal retrieval," *World Wide Web*, vol. 22, no. 2, pp. 657–672, 2019.
- [27] X. Xu, H. Lu, J. Song, Y. Yang, H. T. Shen, and X. Li, "Ternary adversarial networks with self-supervision for zero-shot cross-modal retrieval," *IEEE Transactions on Cybernetics*, vol. 50, no. 6, pp. 2400–2413, 2020.
- [28] Y. Peng, J. Qi, X. Huang, and Y. Yuan, "CCL: cross-modal correlation learning with multigrained fusion by hierarchical network," *IEEE Transactions on Multimedia*, vol. 20, no. 2, pp. 405–420, 2018.
- [29] Y. Peng and J. Qi, "CM-GANs: Cross-modal generative adversarial networks for common representation learning," *ACM Transactions on Multimedia Computing, Communications, and Applications*, vol. 15, no. 1, pp. 1–24, 2019.
- [30] Y. Zhuang, Y. Wang, F. Wu, Y. Zhang, and W. Lu, "Supervised coupled dictionary learning with group structures for multi-modal retrieval," in *Proceedings of the AAAI Conference on Artificial Intelligence*, pp. 1070–1076, Bellevue, WA, USA, July 2013.
- [31] X. Xu, A. Shimada, R. Taniguchi, and L. He, "Coupled dictionary learning and feature mapping for cross-modal retrieval," in *Proceedings of the IEEE International Conference on Multimedia and Expo*, pp. 1–6, Turin, Italy, June 2015.
- [32] C. Deng, X. Tang, J. Yan, W. Liu, and X. Gao, "Discriminative dictionary learning with common label alignment for cross-modal retrieval," *IEEE Transactions on Multimedia*, vol. 18, no. 2, pp. 208–218, 2016.
- [33] Y. Wei, Y. Zhao, Z. Zhu et al., "Modality-dependent cross-media retrieval," *ACM Transactions on Intelligent Systems and Technology*, vol. 7, no. 4, pp. 1–13, 2016.
- [34] J. Wu, Z. Lin, and H. Zha, "Joint latent subspace learning and regression for cross-modal retrieval," in *Proceedings of the 40th International ACM SIGIR Conference on Research and Development in Information Retrieval*, pp. 917–920, Tokyo, Japan, August 2017.
- [35] B. Wang, Y. Yang, X. Xu, A. Hanjalic, and H. T. Shen, "Adversarial cross-modal retrieval," in *Proceedings of the 2017 ACM on Multimedia Conference-MM'17*, pp. 154–162, Mountain View, CA, USA, October 2017.
- [36] G. Cao, A. Iosifidis, K. Chen, and M. Gabbouj, "Generalized multi-view embedding for visual recognition and cross-modal retrieval," *IEEE Transactions on Cybernetics*, vol. 48, no. 9, pp. 2542–2555, 2018.
- [37] M. Zhang, H. Zhang, J. Li, L. Wang, Y. Fang, and J. Sun, "Supervised graph regularization based cross media retrieval with intra and inter-class correlation," *Journal of Visual Communication and Image Representation*, vol. 58, pp. 1–11, 2019.
- [38] Y. Ke and R. Sukthankar, "PCA-SIFT: a more distinctive representation for local image descriptors," in *Proceedings of the 2004 IEEE Computer Society Conference on Computer Vision and Pattern Recognition*, pp. 506–513, Washington, DC, USA, July 2004.
- [39] D. M. Blei, A. Y. Ng, and M. I. Jordan, "Latent dirichlet allocation," *Journal of Machine Learning Research*, vol. 3, pp. 993–1022, 2003.
- [40] Y. Wei, Y. Zhao, C. Lu et al., "Cross-modal retrieval with CNN visual features: a new baseline," *IEEE Transactions on Cybernetics*, vol. 47, no. 2, pp. 449–460, 2016.
- [41] A. Krizhevsky, I. Sutskever, and G. E. Hinton, "ImageNet classification with deep convolutional neural networks," *Communications of the ACM*, vol. 60, no. 6, pp. 84–90, 2017.
- [42] J. Krapac, M. Allan, J. J. Verbeek, and F. Jurie, "Improving web image search results using query-relative classifiers," in *Proceedings of the IEEE Conference on Computer Vision and Pattern Recognition*, pp. 1094–1101, San Francisco, CA, USA, August 2010.

## Research Article

# Finite-Time $H_2/H_\infty$ Control Design for Stochastic Poisson Systems with Applications to Clothing Hanging Device

Yan Qi,<sup>1</sup> Shiyu Zhong,<sup>2,3</sup> and Zhiguo Yan <sup>2,4</sup>

<sup>1</sup>School of Fine Arts and Design, University of Jinan, Jinan 250022, China

<sup>2</sup>School of Electrical Engineering and Automation, Qilu University of Technology (Shandong Academy of Sciences), Jinan 250353, China

<sup>3</sup>College of Electrical Engineering and Automation, Shandong University of Science and Technology, Qingdao 266590, China

<sup>4</sup>School of Control Science and Engineering, Shandong University, Jinan 250061, China

Correspondence should be addressed to Zhiguo Yan; [yanzg500@sina.com](mailto:yanzg500@sina.com)

Received 11 April 2020; Accepted 2 June 2020; Published 14 July 2020

Guest Editor: Xiaodi Li

Copyright © 2020 Yan Qi et al. This is an open access article distributed under the Creative Commons Attribution License, which permits unrestricted use, distribution, and reproduction in any medium, provided the original work is properly cited.

In this paper, the design of finite-time  $H_2/H_\infty$  controller for linear Itô stochastic Poisson systems is considered. First, the definition of finite-time  $H_2/H_\infty$  control is proposed, which considers the transient performance,  $H_2$  index, and  $H_\infty$  index simultaneously in a predetermined finite-time interval. Then, the state feedback and observer-based finite-time  $H_2/H_\infty$  controllers are presented and some new sufficient conditions are obtained. Moreover, an algorithm is given to optimize  $H_2$  and  $H_\infty$  index, simultaneously. Finally, a simulation example indicates the effectiveness of the results.

## 1. Introduction

It is known to all that stochastic systems have been studied extensively and applied to biological network [1], power systems [2], financial systems [3, 4], and other fields. There are also many other applications of stochastic systems (see, e.g., [5–7]). In the past few decades, stochastic systems driven by Wiener noise have been widely investigated. For example, Shaikin [8] solved the optimization problem for multiplicative stochastic systems with several external disturbances and vector Wiener processes. Xiang et al. [9] introduced the finite-time properties and state feedback  $H_\infty$  control problem for switched stochastic systems with Wiener noise. Yan et al. [10] were concerned with finite-time  $H_2$  control of the Markovian stochastic systems with Wiener noise. However, in the real world, an actual physical system is inevitably affected by Wiener noise and Poisson jump noise. At present, some achievements have been made in the research of stochastic Poisson systems (see, e.g., [11–14]).

On the other hand,  $H_2/H_\infty$  optimization control is one of the most important problems in the controlled system.

The  $H_2$  optimal control system has good system performance, while the  $H_\infty$  control theory can deal with the system robustness problem well. In view of this, Bernstein and Haddad [15] proposed the  $H_2/H_\infty$  mixed control problem, which can solve both the problems of system performance and robustness. Since then, the  $H_2/H_\infty$  control has been developed and used extensively (see, e.g., [16–19]). Besides, in some engineering research, such as communication system [20–23], robotic operating system [24], and industrial production system [25], more attention should be paid to the system transient performance. In order to describe system transient performance clearly, the concepts of finite-time stability (FTS) and finite-time boundedness (FTB) are proposed, which reflect the specific system behavior in a relatively short time interval. Nowadays, the problems of FTS and FTB have been deeply investigated (see, e.g., [26–36]). In consideration of the merits of FTB and  $H_2/H_\infty$  control, the finite-time  $H_2/H_\infty$  control for stochastic systems with Wiener noise is first presented in [37], which satisfies both FTB and  $H_2/H_\infty$  performance index. However, in many practical systems, it is not only disturbed

by Wiener noise, but also by Poisson noise. So far, there are few literature studies to investigate this problem of stochastic Poisson systems affected by both Wiener and Poisson noises.

Motivated by aforementioned discussions, the problems of finite-time  $H_2/H_\infty$  control for stochastic Poisson systems with both Wiener noise and Poisson noise are considered in this paper. The main work of this paper consists of the following three aspects:

- (i) Unlike the model considered in [37], this paper studies the model of stochastic Poisson systems with Wiener and Poisson noises. The former considers only Wiener noise, and the latter considers both Wiener and Poisson noises. Moreover, in the former model, the measurement output  $y(t)$  is composed of only the state, but the measurement output considered in the latter model is composed of both the state and external interference. The latter model is more general than the former model in [37], which is used to model many real systems.

- (ii) The two theorems (Theorems 2 and 4) are obtained to guarantee the existence of state feedback finite-time (SFFT) and observer-based finite-time (OBFT)  $H_2/H_\infty$  controllers, respectively. The two theorems (Theorems 2 and 4) contain the parameters both  $\alpha$  and Poisson jump intensity  $\lambda$ , which are complex than the corresponding conditions in [37]. By adjusting the two parameters, the most satisfying finite-time  $H_2/H_\infty$  controllers will be designed.
- (iii) A new optimization algorithm constrained by matrix inequality is proposed to demonstrate the relationships among  $\alpha$ ,  $\lambda$ , and optimal  $H_2/H_\infty$  index, which is more complex than that in [37].

Notations: the notations presented in this work are standard. For specific contents, one can refer to [37].

## 2. Preliminaries

Consider a continuous-time stochastic Poisson system

$$\begin{cases} dx(t) = [A_{11}x(t) + B_{11}v(t) + F_1r(t)]dt + [A_{12}x(t) + B_{12}v(t) + F_2r(t)]d\mathcal{W}(t) \\ \quad + [A_{13}x(t) + B_{13}v(t) + F_3r(t)]d\mathcal{N}(t), \\ y(t) = C_{11}x(t) + D_{11}r(t), \\ z(t) = C_{12}x(t) + D_{12}v(t), \\ x(0) = x_0 \in \mathbb{R}^n, \end{cases} \quad (1)$$

where  $A_{11}, A_{12}, A_{13}, B_{11}, B_{12}, B_{13}, C_{11}, C_{12}, D_{11}, D_{12}, F_1, F_2,$  and  $F_3$  are known constant matrices.  $x(t) \in \mathbb{R}^l$ ,  $y(t) \in \mathbb{R}^q$ ,  $z(t) \in \mathbb{R}^s$ , and  $v(t) \in \mathbb{R}^n$  are the state vector, measurement output, control output, and control input, respectively.  $x_0$  is the initial condition of the system.  $\mathcal{W}(t)$  presents one-dimensional standard Wiener process and  $\mathcal{N}(t)$  is the marked Poisson process with Poisson jump intensity  $\lambda$ .  $r(t) \in \mathbb{R}^p$  is the disturbance input which satisfies the following equation:

$$\mathcal{E} \int_0^t r'(s)r(s)ds < f, \quad (f > 0). \quad (2)$$

Next, the definition of mean-square FTB of system (1) is introduced.

*Definition 1.* Given some scalars  $b_2 > b_1 > 0$  and  $T > 0$  and a matrix  $R > 0$ , the above stochastic system (1) with  $v(t) \equiv 0$  is mean-square FTB w.r.t.  $(b_1, b_2, T, R, f)$ , if

$$\mathcal{E}[x'(0)Rx(0)] \leq b_1 \implies \mathcal{E}[x'(t)Rx(t)] < b_2, \quad \forall t \in [0, T]. \quad (3)$$

*Remark 1.* From Definition 1, we can know that the concept of FTB describes the specific behavior of the stochastic system (1) in a prescribed time interval.

**Lemma 1** (see [38]). Let  $\overline{\mathcal{V}}(t, x) \in C^2(\mathbb{R}^1, \mathbb{R}^n)$  and  $\overline{\mathcal{V}}(t, x) > 0$ . Consider the following system

$$dx(t) = A_1(x)dt + A_2(x)d\mathcal{W}(t) + A_3(x)d\mathcal{N}(t), \quad (4)$$

its stochastic differential of  $\overline{\mathcal{V}}(t, x)$  is given by

$$d\overline{\mathcal{V}}(t, x) = \mathcal{L}\overline{\mathcal{V}}(t, x)dt + \frac{\partial \overline{\mathcal{V}}(t, x)}{\partial x} A_2(x)d\mathcal{W}(t) + [\overline{\mathcal{V}}(t, x + A_3(x)) - \overline{\mathcal{V}}(t, x)]d\mathcal{N}(t), \quad (5)$$

where

$$\mathcal{L}\overline{\mathcal{V}}(t, x) = \frac{\partial \overline{\mathcal{V}}(t, x)}{\partial t} + \frac{\partial \overline{\mathcal{V}}(t, x)}{\partial x} A_1(x) + \frac{1}{2} A_2'(x) \frac{\partial^2 \overline{\mathcal{V}}(t, x)}{\partial x^2} A_2(x) + \lambda [\overline{\mathcal{V}}(t, x + A_3(x)) - \overline{\mathcal{V}}(t, x)]. \quad (6)$$

### 3. Design of SFFT $H_2/H_\infty$ Controller

In this section, a SFFT  $H_2/H_\infty$  controller for system (1) is designed. Consider a linear SF controller

$$v(t) = Kx(t), \quad (7)$$

$$\begin{cases} dx(t) = [\tilde{A}_{11}x(t) + F_1r(t)]dt + [\tilde{A}_{12}x(t) + F_2r(t)]d\mathcal{W}(t) + [\tilde{A}_{13}x(t) + F_3r(t)]d\mathcal{N}(t), \\ y(t) = C_{11}x(t) + D_{11}r(t), \\ z(t) = \tilde{C}x(t), \\ x(0) = x_0 \in R^n, \end{cases} \quad (8)$$

where  $\tilde{A}_{11} = A_{11} + B_{11}K$ ,  $\tilde{A}_{12} = A_{12} + B_{12}K$ ,  $\tilde{A}_{13} = A_{13} + B_{13}K$ , and  $\tilde{C} = C_{12} + D_{12}K$ .

Next, we choose the following  $H_2$  cost function:

$$J_1(x(t), v(t)) = \mathcal{E} \int_0^T [x'(t)G_1x(t) + v'(t)G_2v(t)]dt, \quad (9)$$

where  $G_1 > 0$  and  $G_2 > 0$  are known weighting scalars or positive matrices.

Similarly, substituting the SF controller (7) into (9), the following formula is obtained:

$$J_1(x(t)) = \mathcal{E} \int_0^T [x'(t)G_1x(t) + x'(t)K'G_2Kx(t)]dt. \quad (10)$$

Given  $\gamma > 0$  and assuming zero initial condition, the control output  $z(t)$  and the disturbance input  $r(t)$  satisfy the following equation:

$$\mathcal{E} \int_0^T z'(t)z(t)dt < \gamma^2 \mathcal{E} \int_0^T r'(t)r(t)dt. \quad (11)$$

Based on the above preparations, the definition of the SFFT  $H_2/H_\infty$  controller is introduced.

*Definition 2.* Given positive scalars  $b_1, b_2, T$ , and  $f$  and a matrix  $R > 0$ . If a positive scalar  $J_1^*$  exists, a SF controller (7) can be designed to make the following conditions hold:

- (i) The closed-loop system (8) is mean-square FTB w.r.t.  $(b_1, b_2, T, R, f)$
- (ii) The  $H_2$  cost function (10) meets  $J_1(x(t)) \leq J_1^*$  under  $r(t) = 0$  condition
- (iii) Assuming that the initial state is zero and the nonzero disturbance input and the control output satisfy inequality (11); then (7) is the SFFT  $H_2/H_\infty$  controller for system (1)

*Remark 2.* Definition 3 implies that a SFFT  $H_2/H_\infty$  controller not only makes the closed-loop system FTB, but also gets minimum performance cost and better interference suppression capability. In actual systems, these three aspects really need to be considered. For example, in industrial steel

where  $K$  is the required SF gain matrix.

Substituting (7) into (1), the following closed-loop system is obtained:

rolling heating furnace, excessive instantaneous furnace temperature cannot be permitted. Moreover, it is hoped that the fuel consumption is less and the anti-interference ability is stronger in the rolling furnace.

Next, the following theorem is given for obtaining the SFFT  $H_2/H_\infty$  controller.

**Theorem 1.** Given positive scalars  $b_1, b_2, T$ , and  $f$  and a matrix  $R > 0$ , if there exist a nonnegative scalar  $\alpha$  and two matrices  $N > 0$  and  $K$  such that

$$\begin{bmatrix} \mathcal{T}_1 & F_1 & \tilde{N}\tilde{A}'_{12} & \sqrt{\lambda}\tilde{N}(\tilde{A}_{13} + I)' \\ * & -\gamma^2 I & F'_2 & \sqrt{\lambda}F'_3 \\ * & * & -\tilde{N} & 0 \\ * & * & * & -\tilde{N} \end{bmatrix} < 0, \quad (12)$$

$$\begin{bmatrix} \mathcal{T}_2 & \tilde{N}\tilde{A}'_{12} & \sqrt{\lambda}\tilde{N}(\tilde{A}_{13} + I)' \\ * & -\tilde{N} & 0 \\ * & * & -\tilde{N} \end{bmatrix} < 0, \quad (13)$$

$$\frac{b_1}{\lambda_{\min}(N)} + f\gamma^2 < \frac{b_2}{\lambda_{\max}(N)}e^{-\alpha T}, \quad (14)$$

hold, where  $\tilde{N} = R^{-1/2}NR^{-1/2}$ ,  $\mathcal{T}_1 = \tilde{A}_{11}\tilde{N} + \tilde{N}\tilde{A}'_{11} - \lambda\tilde{N} - \alpha\tilde{N} + \tilde{N}'\tilde{C}'\tilde{C}\tilde{N}$ , and  $\mathcal{T}_2 = \tilde{A}_{11}\tilde{N} + \tilde{N}\tilde{A}'_{11} - \lambda\tilde{N} - \alpha\tilde{N} + \tilde{N}G_1\tilde{N} + \tilde{N}K'G_2K\tilde{N}$ , then  $v(t) = Kx(t)$  is said to be a SFFT  $H_2/H_\infty$  controller and we can get the upper bound of  $H_2$  index, that is,  $J_{state}^* = \lambda_{\max}(N^{-1})b_1e^{\alpha T}$ .

*Proof.* Here are three steps to prove Theorem 1.

Step 1: prove that system (3) is mean-square FTB.

Obviously,

$$\begin{bmatrix} \tilde{N}\tilde{C}'\tilde{C}\tilde{N} & 0 & 0 & 0 \\ 0 & 0 & 0 & 0 \\ 0 & 0 & 0 & 0 \\ 0 & 0 & 0 & 0 \end{bmatrix} = \begin{bmatrix} \tilde{N}\tilde{C}' \\ 0 \\ 0 \\ 0 \end{bmatrix} \begin{bmatrix} \tilde{N}\tilde{C}' \\ 0 \\ 0 \\ 0 \end{bmatrix}' \geq 0. \quad (15)$$

Therefore, condition (12) means

$$\begin{bmatrix} \widetilde{\mathcal{F}}_1 & F_1 & \widetilde{N}\widetilde{A}'_{12} & \sqrt{\lambda}\widetilde{N}(\widetilde{A}_{13}+I)' \\ * & -\gamma^2 I & F_2' & \sqrt{\lambda}F_3' \\ * & * & -\widetilde{N} & 0 \\ * & * & * & -\widetilde{N} \end{bmatrix} < 0, \quad (16)$$

where  $\widetilde{\mathcal{F}}_1 = \widetilde{A}_{11}\widetilde{N} + \widetilde{N}\widetilde{A}'_{11} - \lambda\widetilde{N} - \alpha\widetilde{N}$ .

Let  $\overline{\mathcal{V}}(x(t)) = x'(t)\widetilde{N}^{-1}x(t)$ , and applying Lemma 1 for  $\overline{\mathcal{V}}(x(t))$ , the  $\mathcal{L}_1\overline{\mathcal{V}}(x(t))$  of system (8) is given by

$$\mathcal{L}_1\overline{\mathcal{V}}(x(t)) = \begin{bmatrix} x(t) \\ r(t) \end{bmatrix}' \begin{bmatrix} \overline{Z}_1 & \overline{Z}_2 \\ * & \overline{Z}_3 \end{bmatrix} \begin{bmatrix} x(t) \\ r(t) \end{bmatrix}, \quad (17)$$

where  $\overline{Z}_1 = \widetilde{A}_{11}'\widetilde{N}^{-1} + \widetilde{N}^{-1}\widetilde{A}_{11} + \widetilde{A}_{12}'\widetilde{N}^{-1}\widetilde{A}_{12} + \lambda(\widetilde{A}_{13} + I)'\widetilde{N}^{-1}(\widetilde{A}_{13} + I) - \lambda\widetilde{N}^{-1}$ ,  $\overline{Z}_2 = \lambda(\widetilde{A}_{13} + I)'\widetilde{N}^{-1}F_3 + \widetilde{A}_{12}'\widetilde{N}^{-1}F_2 + \widetilde{N}^{-1}F_1$ , and  $\overline{Z}_3 = \lambda F_3'\widetilde{N}^{-1}F_3 + F_2'\widetilde{N}^{-1}F_2$ .

Pre- and postmultiplying (16) by  $\text{diag}\{\widetilde{N}^{-1}, I, \widetilde{N}^{-1}, \widetilde{N}^{-1}\}$ , we can get the following inequality:

$$\begin{bmatrix} \mathcal{J}_1 & \widetilde{N}^{-1}F_1 & \widetilde{A}'_{12}\widetilde{N}^{-1} & \mathcal{J}_2 \\ * & -\gamma^2 I & F_2'\widetilde{N}^{-1} & \sqrt{\lambda}F_3'\widetilde{N}^{-1} \\ * & * & -\widetilde{N}^{-1} & 0 \\ * & * & * & -\widetilde{N}^{-1} \end{bmatrix} < 0, \quad (18)$$

where  $\mathcal{J}_1 = \widetilde{A}_{11}'\widetilde{N}^{-1} + \widetilde{N}^{-1}\widetilde{A}_{11} - \lambda\widetilde{N}^{-1} - \alpha\widetilde{N}^{-1}$  and  $\mathcal{J}_2 = \sqrt{\lambda}(\widetilde{A}_{13} + I)'\widetilde{N}^{-1}$ .

By utilizing Schur complement, (18) is equivalent to

$$\begin{bmatrix} \overline{Z}_1 - \alpha\widetilde{N}^{-1} & \overline{Z}_2 \\ * & \overline{Z}_3 - \gamma^2 I \end{bmatrix} < 0. \quad (19)$$

Taking conditions (17) and (19) into consideration, it follows

$$\mathcal{L}_1\overline{\mathcal{V}}(x(t)) < \alpha\overline{\mathcal{V}}(x(t)) + \gamma^2 r'(t)r(t). \quad (20)$$

Integrating from 0 to  $t$  on both sides of (20), then taking mathematical expectation, one has

$$\mathcal{E}\overline{\mathcal{V}}(x(t)) < \mathcal{E}\overline{\mathcal{V}}(x(0)) + \alpha \int_0^t \mathcal{E}\overline{\mathcal{V}}(x(s))ds + \gamma^2 \int_0^t \mathcal{E}r'(s)r(s)ds. \quad (21)$$

Utilizing Gronwall inequality in [26], it follows

$$\mathcal{E}\overline{\mathcal{V}}(x(t)) < \mathcal{E}\overline{\mathcal{V}}(x(0))e^{\alpha t} + \gamma^2 e^{\alpha t} \int_0^t \mathcal{E}r'(s)r(s)ds. \quad (22)$$

On the basis of above conditions, we have

$$\begin{aligned} \mathcal{E}\overline{\mathcal{V}}(x(t)) &= \mathcal{E}[x'(t)R^{1/2}N^{-1}R^{1/2}x(t)] \geq \lambda_{\min} \\ &\cdot (N^{-1})E[x'(t)Rx(t)], \end{aligned} \quad (23)$$

$$\begin{aligned} \mathcal{E}\overline{\mathcal{V}}(x(0))e^{\alpha t} &= \mathcal{E}[x'(0)R^{1/2}N^{-1}R^{1/2}x(0)]e^{\alpha t} \\ &\leq \lambda_{\max}(N^{-1})E[x'(0)Rx(0)]e^{\alpha t} \\ &\leq \lambda_{\max}(N^{-1})b_1 e^{\alpha T}, \end{aligned} \quad (24)$$

$$\gamma^2 e^{\alpha t} \int_0^t \mathcal{E}r'(s)r(s)ds < e^{\alpha T} f \gamma^2. \quad (25)$$

From (22) to (25), the following inequality is obtained:

$$\mathcal{E}[x'(t)Rx(t)] < \lambda_{\max}(N)e^{\alpha T} \left[ \frac{b_1}{\lambda_{\min}(N)} + f \gamma^2 \right]. \quad (26)$$

According to condition (14), we get that (26) leads to  $\mathcal{E}[x'(t)Rx(t)] < b_2$  for all  $t \in [0, T]$ . So, system (8) is mean-square FTB w.r.t.  $(b_1, b_2, T, R, f)$ .

Step 2: prove that the  $H_2$  cost function (10) satisfies  $J_1(x(t)) \leq J_1^*$  under  $r(t) = 0$  condition.

When  $r(t) = 0$ , we get that the  $\mathcal{L}_2\overline{\mathcal{V}}(x(t))$  of system (8) is given by

$$\begin{aligned} \mathcal{L}_2\overline{\mathcal{V}}(x(t)) &= x'(t) \left[ \widetilde{A}_{11}'\widetilde{N}^{-1} + \widetilde{N}^{-1}\widetilde{A}_{11} + \widetilde{A}_{12}'\widetilde{N}^{-1}\widetilde{A}_{12} \right. \\ &\quad \left. + \lambda(\widetilde{A}_{13} + I)'\widetilde{N}^{-1}(\widetilde{A}_{13} + I) - \lambda\widetilde{N}^{-1} \right] x(t). \end{aligned} \quad (27)$$

By Schur complement, the equivalent condition of (13) is given by

$$\begin{aligned} &\widetilde{N}\widetilde{A}_{11} + \widetilde{A}_{11}\widetilde{N} + \widetilde{N}\widetilde{A}'_{12}\widetilde{N}^{-1}\widetilde{A}_{12}\widetilde{N} \\ &+ \lambda\widetilde{N}(\widetilde{A}_{13} + I)'\widetilde{N}^{-1}(\widetilde{A}_{13} + I)\widetilde{N} + \widetilde{N}G_1\widetilde{N} \\ &+ \widetilde{N}K'G_2K\widetilde{N} - \lambda\widetilde{N} - \alpha\widetilde{N} < 0. \end{aligned} \quad (28)$$

Pre- and postmultiplying (28) by  $\widetilde{N}^{-1}$ , it yields

$$\begin{aligned} &\widetilde{A}_{11}'\widetilde{N}^{-1} + \widetilde{N}^{-1}\widetilde{A}_{11} + \widetilde{A}_{12}'\widetilde{N}^{-1}\widetilde{A}_{12} + G_1 + K'G_2K \\ &+ \lambda(\widetilde{A}_{13} + I)'\widetilde{N}^{-1}(\widetilde{A}_{13} + I) - \lambda\widetilde{N}^{-1} - \alpha\widetilde{N}^{-1} < 0. \end{aligned} \quad (29)$$

According to (27) and (29), we get

$$\mathcal{L}_2\overline{\mathcal{V}}(x(t)) + x'(t)(G_1 + K'G_2K)x(t) - \alpha\overline{\mathcal{V}}(x(t)) < 0. \quad (30)$$

Integrating from 0 to  $t$  on both sides of (30), then taking mathematical expectation, the following inequality is obtained:

$$\begin{aligned} & \mathcal{E} \int_0^t x'(t)(G_1 + K'G_2K)x(t)dt + \mathcal{E}\overline{\mathcal{V}}(x(t)) \\ & < \mathcal{E}\overline{\mathcal{V}}(x(0)) + \alpha \mathcal{E} \int_0^t \overline{\mathcal{V}}(x(t))dt. \end{aligned} \quad (31)$$

From (31), we get

$$\mathcal{E}\overline{\mathcal{V}}(x(t)) < \mathcal{E}[\overline{\mathcal{V}}(x(0))] + \alpha \mathcal{E} \int_0^t \overline{\mathcal{V}}(x(t))dt, \quad (32)$$

$$J_1(x(t)) < \alpha \mathcal{E} \int_0^t \overline{\mathcal{V}}(x(t))dt + \mathcal{E}[\overline{\mathcal{V}}(x(0))]. \quad (33)$$

From (32), by Gronwall inequality, one has

$$\mathcal{E}\overline{\mathcal{V}}(x(t)) < \mathcal{E}\overline{\mathcal{V}}(x(0))e^{\alpha t}. \quad (34)$$

Combining (33) and (34), it is obtained that

$$\begin{aligned} J_1(x(t)) & < \alpha \mathcal{E} \int_0^t x'(0)R^{1/2}N^{-1}R^{1/2}x(0)e^{\alpha t} dt \\ & \quad + \mathcal{E} \left[ x'(0)\tilde{N}^{-1}x(0) \right] \\ & = \mathcal{E} \left[ x'(0)R^{1/2}N^{-1}R^{1/2}x(0)e^{\alpha t} \right] \\ & < \lambda_{\max}(N^{-1})b_1e^{\alpha T} = J_1^*. \end{aligned} \quad (35)$$

Step 3: prove that the nonzero disturbance and the control output satisfy inequality (11).

Pre- and postmultiplying (12) respectively by  $\text{diag}\{\tilde{N}^{-1}, I, \tilde{N}^{-1}, \tilde{N}^{-1}\}$ , and then using Schur complement, we have

$$\begin{bmatrix} \mathcal{T}_3 & \overline{Z}_2 \\ * & -\gamma^2 I + \overline{Z}_2 \end{bmatrix} < 0, \quad (36)$$

where  $\mathcal{T}_3 = \tilde{A}_{11}'\tilde{N}^{-1} + \tilde{N}^{-1}\tilde{A}_{11} + \tilde{A}_{12}'\tilde{N}^{-1}\tilde{A}_{12} + \lambda(\tilde{A}_{13} + I)'\tilde{N}^{-1}(\tilde{A}_{13} + I) + \tilde{C}'\tilde{C} - \lambda\tilde{N}^{-1} - \alpha\tilde{N}^{-1}$ .

Combining (17), (36), we get

$$\mathcal{L}_1 \overline{\mathcal{V}}(x(t)) < \alpha \overline{\mathcal{V}}(x(t)) + \gamma^2 r'(t)r(t) - z'(t)z(t). \quad (37)$$

Pre- and postmultiplying (37) by  $e^{-\alpha t}$ , one has

$$e^{-\alpha t} \mathcal{L}_1 \overline{\mathcal{V}}(x(t)) < \alpha e^{-\alpha t} \overline{\mathcal{V}}(x(t)) + e^{-\alpha t} [\gamma^2 r'(t)r(t) - z'(t)z(t)]. \quad (38)$$

By applying Lemma 1, we obtain

$$\mathcal{L}_1 [e^{-\alpha t} \overline{\mathcal{V}}(x(t))] = -\alpha e^{-\alpha t} \overline{\mathcal{V}}(x(t)) + e^{-\alpha t} \mathcal{L}_1 \overline{\mathcal{V}}(x(t)). \quad (39)$$

According to (38) and (39), it yields

$$\mathcal{L}_1 [e^{-\alpha t} \overline{\mathcal{V}}(x(t))] < e^{-\alpha t} [\gamma^2 r'(t)r(t) - z'(t)z(t)]. \quad (40)$$

Because  $e^{-\alpha t}$  is between 0 and 1, for (40), we have

$$\mathcal{L}_1 [e^{-\alpha t} \overline{\mathcal{V}}(x(t))] < \gamma^2 r'(t)r(t) - z'(t)z(t). \quad (41)$$

Integrating from 0 to  $t$  on both sides of (41), then taking mathematical expectation, the following inequality can be obtained under zero initial condition:

$$e^{-\alpha t} \mathcal{E} \overline{\mathcal{V}}(x(t)) < \gamma^2 \mathcal{E} \int_0^t r'(s)r(s)ds - \mathcal{E} \int_0^t z'(s)z(s)ds. \quad (42)$$

We know that  $e^{-\alpha t} \mathcal{E} \overline{\mathcal{V}}(x(t)) > 0$ , so it yields

$$\mathcal{E} \int_0^t z'(s)z(s)ds < \gamma^2 \mathcal{E} \int_0^t r'(s)r(s)ds. \quad (43)$$

This completes the proof.

It is obvious that conditions (12)–(14) are not linear matrix inequalities. In order to simplify the solving process, the following theorem is given.

**Theorem 2.** Given positive scalars  $b_1, b_2, T$ , and  $f$  and a matrix  $R > 0$ , if there exist two scalars  $m > 0$  and  $\alpha \geq 0$  and two matrices  $N > 0$  and  $Y$  such that

$$\begin{bmatrix} \mathcal{T}_4 & F_1 & \mathcal{T}_5 & \mathcal{T}_6 & \mathcal{T}_7 \\ * & -\gamma^2 I & F_2' & F_3' & 0 \\ * & * & -\tilde{N} & 0 & 0 \\ * & * & * & -\tilde{N} & 0 \\ * & * & * & * & -I \end{bmatrix} < 0, \quad (44)$$

$$\begin{bmatrix} \mathcal{T}_4 & \mathcal{T}_5 & \mathcal{T}_6 & \tilde{N} & Y' \\ * & -\tilde{N} & 0 & 0 & 0 \\ * & * & -\tilde{N} & 0 & 0 \\ * & * & * & -G_1^{-1} & 0 \\ * & * & * & * & -G_2^{-1} \end{bmatrix} < 0, \quad (45)$$

$$\begin{bmatrix} f\gamma^2 - b_2e^{-\alpha T} & \sqrt{b_1} \\ * & -m \end{bmatrix} < 0, \quad (46)$$

$$mI < N < I, \quad (47)$$

hold, where  $\mathcal{T}_4 = A_{11}\tilde{N} + \tilde{N}A_{11}' - \lambda\tilde{N} - \alpha\tilde{N} + B_{11}Y + Y'B_{11}'$ ,  $\mathcal{T}_5 = \tilde{N}A_{12}' + Y'B_{12}'$ ,  $\mathcal{T}_6 = \sqrt{\lambda}(\tilde{N}A_{13}' + Y'B_{13}' + \tilde{N})$ , and  $\mathcal{T}_7 = \tilde{N}C_{12}' + Y'D_{12}'$ , then  $v(t) = Kx(t) = Y\tilde{N}^{-1}x(t)$  is said to be a SFFT  $H_2/H_\infty$  controller and we can get the upper bound of  $H_2$  index, that is,  $J_1^* = m^{-1}b_1e^{\alpha T}$ .

*Proof.* Let  $Y = K\tilde{N}$ , inequalities (12) and (13) can be obtained from (44) and (45), respectively, and (14) in Theorem 1 can be obtained from (46) and (47) easily. This ends the proof.  $\square$

*Remark 3.* In Theorem 2, when  $\alpha$  is fixed, (44)–(47) can be treated as LMIs which are easy to solve.



#### 4. Design of OBFT $H_2/H_\infty$ Controller

In some practical cases, not all states can be measured directly. Therefore, the design of OBFT  $H_2/H_\infty$  controller is necessary. Typically, an OB dynamic controller is given by

$$\begin{cases} d\hat{x}(t) = [A_{11}\hat{x}(t) + B_{11}v(t) + L(y(t) - C_{11}\hat{x}(t))]dt, \\ v(t) = K\hat{x}(t), \\ \hat{x}(0) = 0, \end{cases} \quad (48)$$

$$\begin{cases} d\tilde{x}(t) = [\bar{A}_{11}\tilde{x}(t) + W_1r(t)]dt + [\bar{A}_{12}\tilde{x}(t) + W_2r(t)]d\mathcal{W}(t) + [\bar{A}_{13}\tilde{x}(t) + W_3r(t)]d\mathcal{N}(t), \\ \tilde{z}(t) = H\tilde{x}(t), \end{cases} \quad (49)$$

and then we get the closed-loop cost function

$$J_2(\tilde{x}(t)) = \mathcal{E} \int_0^T \tilde{x}'(t)\Xi\tilde{x}(t)dt, \quad (50)$$

where

$$\begin{aligned} \tilde{x}(t) &= \begin{bmatrix} x(t) \\ \hat{x}(t) \end{bmatrix}, \\ \bar{A}_{11} &= \begin{bmatrix} A_{11} & B_{11}K \\ LC_{11} & A_{11} + B_{11}K - LC_{11} \end{bmatrix}, \\ W_1 &= \begin{bmatrix} F_1 \\ LD_{11} \end{bmatrix}, \\ \bar{A}_2 &= \begin{bmatrix} A_{12} & B_{12}K \\ 0 & 0 \end{bmatrix}, \\ W_2 &= \begin{bmatrix} F_2 \\ 0 \end{bmatrix}, \\ \bar{A}_{13} &= \begin{bmatrix} A_{13} & B_{13}K \\ 0 & 0 \end{bmatrix}, \\ W_3 &= \begin{bmatrix} F_3 \\ 0 \end{bmatrix}, \\ H &= [C'_{12} K' D'_{12}]', \\ \Xi &= \begin{bmatrix} G_1 & 0 \\ 0 & K'G_2K \end{bmatrix}. \end{aligned} \quad (51)$$

Assuming that the initial state is zero, the control output  $\tilde{z}(t)$  and the arbitrary nonzero disturbance input  $r(t)$  satisfy the following equation:

$$\mathcal{E} \int_0^T \tilde{z}'(t)\tilde{z}(t)dt < \gamma^2 \mathcal{E} \int_0^T r'(t)r(t)dt. \quad (53)$$

Then, we give the definition of OBFT  $H_2/H_\infty$  control.

*Definition 3.* Given positive scalars  $b_1, b_2, T$ , and  $f$  and a matrix  $\bar{R} > 0$ . If a positive scalar  $J_2^*$  exists, an OBFT controller (48) can be designed to make the following conditions hold:

where  $\hat{x}(t) \in R^n$  is the estimation of  $x(t)$  and  $L$  is the desired estimator gain.

Substituting the OB controller (48) into system (1), we will obtain the following closed-loop system:

(i) System (49) is mean-square FTB w.r.t.  $(b_1, b_2, T, \bar{R}, f)$ , that is,  $\mathcal{E}[x'(0)\bar{R}x(0)] \leq b_1 \implies \mathcal{E}[x'(t)\bar{R}x(t)] < b_2$ , where  $0 < b_1 < b_2$ ,  $T > 0$  and  $\bar{R} = \begin{bmatrix} R & 0 \\ 0 & R \end{bmatrix}$

(ii) The  $H_2$  cost function (50) meets  $J_2(\tilde{x}(t)) \leq J_2^*$  under  $r(t) = 0$  condition

(iii) Assuming that the initial state is zero, the nonzero disturbance input and the control output satisfy inequality (53); then (48) is an OBFT  $H_2/H_\infty$  controller for system (1)

Next, the following theorem is given for obtaining the OBFT  $H_2/H_\infty$  controller for system (1).

**Theorem 3.** Given positive scalars  $b_1, b_2, T$ , and  $f$  and a matrix  $\bar{R} > 0$ , if there exist a nonnegative scalar  $\beta$  and a positive matrix  $P$  such that

$$\begin{bmatrix} \mathcal{H}_1 & \bar{P}W_1 & \bar{A}'_{12}\bar{P} & \sqrt{\lambda}(\bar{A}_{13} + I)'\bar{P} \\ * & -\gamma^2 I & W_2'\bar{P} & \sqrt{\lambda}W_3'\bar{P} \\ * & * & -\bar{P} & 0 \\ * & * & * & -\bar{P} \end{bmatrix} < 0, \quad (54)$$

$$\begin{aligned} &\bar{A}'_{11}\bar{P} + \bar{P}\bar{A}_{11} + \bar{A}'_{12}\bar{P}\bar{A}_{12} + \lambda(\bar{A}_{13} + I)'\bar{P}(\bar{A}_{13} + I) \\ &- \lambda\bar{P} - \beta\bar{P} + \Xi < 0, \end{aligned} \quad (55)$$

$$\lambda_{\max}(P)b_1 + f\gamma^2 < \lambda_{\min}(P)b_2e^{-\beta T}, \quad (56)$$

hold, where  $\bar{P} = \bar{R}^{1/2}P\bar{R}^{1/2}$  and  $\mathcal{H}_1 = \bar{A}'_{11}\bar{P} + \bar{P}\bar{A}_{11} + H'H - \beta\bar{P} - \lambda\bar{P}$ , then (48) is said to be an OBFT  $H_2/H_\infty$  controller and we can get the upper bound of  $H_2$  index, that is,  $J_2^* = \lambda_{\max}(P)b_1e^{\beta T}$ .

*Proof.* Here are three steps to prove the theorem.

Step 1: prove that system (49) is mean-square FTB.

Let  $\overline{\mathcal{V}}(\tilde{x}(t)) = \tilde{x}'(t)\tilde{P}\tilde{x}(t)$  where  $\tilde{P} > 0$ . Applying generalized Itô formula for  $\overline{\mathcal{V}}(\tilde{x}(t))$ , the  $\mathcal{L}_3\overline{\mathcal{V}}(\tilde{x}(t))$  of system (49) is given by

$$\mathcal{L}_3\overline{\mathcal{V}}(\tilde{x}(t)) = \begin{bmatrix} \tilde{x}(t) \\ r(t) \end{bmatrix}' \begin{bmatrix} \tilde{Z}_1 & \tilde{Z}_2 \\ * & \tilde{Z}_3 \end{bmatrix} \begin{bmatrix} \tilde{x}(t) \\ r(t) \end{bmatrix}, \quad (57)$$

where  $\tilde{Z}_1 = \overline{A}'_1\tilde{P} + \tilde{P}\overline{A}_{11} + \overline{A}'_{12}\tilde{P}\overline{A}_{12} + \lambda(\overline{A}_{13} + I)'\tilde{P}(\overline{A}_{13} + I) - \lambda\tilde{P}$ ,  $\tilde{Z}_2 = \tilde{P}W_1 + \overline{A}'_{12}\tilde{P}W_2 + \lambda(\overline{A}_{13} + I)'\tilde{P}W_3$ , and  $\tilde{Z}_3 = W_2'\tilde{P}W_2 + \lambda W_3'\tilde{P}W_3$ .

Note that

$$\begin{bmatrix} H'H & 0 & 0 & 0 \\ 0 & 0 & 0 & 0 \\ 0 & 0 & 0 & 0 \\ 0 & 0 & 0 & 0 \end{bmatrix} = \begin{bmatrix} H' \\ 0 \\ 0 \\ 0 \end{bmatrix} \begin{bmatrix} H' \\ 0 \\ 0 \\ 0 \end{bmatrix}' \geq 0. \quad (58)$$

Therefore, inequality (54) means

$$\begin{bmatrix} \mathcal{H}_2 & \tilde{P}W_1 & \overline{A}'_{12}\tilde{P} & \sqrt{\lambda}(\overline{A}_{13} + I)'\tilde{P} \\ * & -\gamma^2 I & W_2'\tilde{P} & \sqrt{\lambda}W_3'\tilde{P} \\ * & * & -\tilde{P} & 0 \\ * & * & * & -\tilde{P} \end{bmatrix} < 0, \quad (59)$$

where  $\mathcal{H}_2 = \overline{A}'_1\tilde{P} + \tilde{P}\overline{A}_{11} - \beta\tilde{P} - \lambda\tilde{P}$ .

By utilizing Schur complement, (59) can be converted into

$$\begin{bmatrix} \tilde{Z}_1 - \beta\tilde{P} & \tilde{Z}_2 \\ * & -\gamma^2 I + \tilde{Z}_3 \end{bmatrix} < 0. \quad (60)$$

Combining (57) and (60), we get

$$\mathcal{L}_3\overline{\mathcal{V}}(\tilde{x}(t)) < \beta\overline{\mathcal{V}}(\tilde{x}(t)) + \gamma^2 r'(t)r(t). \quad (61)$$

Integrating from 0 to  $t$  on both sides of (61), then taking mathematical expectation, the following inequality is obtained:

$$\begin{aligned} \mathcal{E}\overline{\mathcal{V}}(\tilde{x}(t)) &< \mathcal{E}\overline{\mathcal{V}}(\tilde{x}(0)) + \beta \int_0^t \mathcal{E}\overline{\mathcal{V}}(\tilde{x}(s))ds \\ &+ \gamma^2 \int_0^t \mathcal{E}r'(s)r(s)ds. \end{aligned} \quad (62)$$

According to Gronwall inequality, it yields

$$\mathcal{E}\overline{\mathcal{V}}(\tilde{x}(t)) < \mathcal{E}\overline{\mathcal{V}}(\tilde{x}(0))e^{\beta t} + \gamma^2 e^{\beta t} \int_0^t \mathcal{E}r'(s)r(s)ds. \quad (63)$$

According to known conditions, it yields

$$\begin{aligned} \mathcal{E}\overline{\mathcal{V}}(\tilde{x}(t)) &= \mathcal{E}\left[\tilde{x}'(t)\tilde{R}^{1/2}P\tilde{R}^{1/2}\tilde{x}(t)\right] \\ &\geq \lambda_{\min}(P)\mathcal{E}[\tilde{x}'(t)\tilde{R}\tilde{x}(t)], \end{aligned} \quad (64)$$

$$\begin{aligned} \mathcal{E}\overline{\mathcal{V}}(\tilde{x}(0))e^{\beta t} &= \mathcal{E}\left[\tilde{x}'(0)\tilde{R}^{1/2}P\tilde{R}^{1/2}\tilde{x}(0)\right]e^{\beta t} \\ &\leq \lambda_{\max}(P)\mathcal{E}[\tilde{x}'(0)\tilde{R}\tilde{x}(0)]e^{\beta t} \\ &\leq \lambda_{\max}(P)b_1e^{\beta T}, \end{aligned} \quad (65)$$

$$\gamma^2 e^{\beta t} \int_0^t \mathcal{E}r'(s)r(s)ds < e^{\beta T} f\gamma^2. \quad (66)$$

From (63) to (66), we obtain

$$\mathcal{E}[\tilde{x}'(t)\tilde{R}\tilde{x}(t)] < \frac{\lambda_{\max}(P)b_1e^{\beta T} + f\gamma^2e^{\beta T}}{\lambda_{\min}(P)}. \quad (67)$$

According to (56) and (67), we get  $\mathcal{E}[\tilde{x}'(t)\tilde{R}\tilde{x}(t)] < b_2$  for all  $t \in [0, T]$ . So, system (49) is FTB w.r.t.  $(b_1, b_2, T, \tilde{R}, f)$ .

Step 2: prove that the  $H_2$  cost function (50) satisfies  $J_2(\tilde{x}(t)) \leq J_2^*$  under  $r(t) = 0$  condition.

When  $r(t) = 0$ , we get that the  $\mathcal{L}_4\overline{\mathcal{V}}(\tilde{x}(t))$  of system (49) is given by

$$\begin{aligned} \mathcal{L}_4\overline{\mathcal{V}}(\tilde{x}(t)) &= \tilde{x}'(t) \left[ \overline{A}'_{11}\tilde{P} + \tilde{P}\overline{A}_{11} + \overline{A}'_{12}\tilde{P}\overline{A}_{12} \right. \\ &\quad \left. + \lambda(\overline{A}_{13} + I)'\tilde{P}(\overline{A}_{13} + I) - \lambda\tilde{P} \right] \tilde{x}(t). \end{aligned} \quad (68)$$

According to (55), we have

$$\mathcal{L}_4\overline{\mathcal{V}}(\tilde{x}(t)) - \beta\overline{\mathcal{V}}(\tilde{x}(t)) + \tilde{x}'(t)\Xi\tilde{x}(t) < 0. \quad (69)$$

Integrating from 0 to  $t$  on both sides of (69), then taking mathematical expectation, it yields

$$\begin{aligned} \mathcal{E}\overline{\mathcal{V}}(\tilde{x}(t)) + \mathcal{E} \int_0^t \tilde{x}'(t)\Xi\tilde{x}(t)dt \\ < \mathcal{E}\overline{\mathcal{V}}(\tilde{x}(0)) + \beta\mathcal{E} \int_0^t \overline{\mathcal{V}}(\tilde{x}(t))dt. \end{aligned} \quad (70)$$

From (70), we have

$$\mathcal{E}\overline{\mathcal{V}}(\tilde{x}(t)) < \mathcal{E}\overline{\mathcal{V}}(\tilde{x}(0)) + \beta\mathcal{E} \int_0^t \overline{\mathcal{V}}(\tilde{x}(t))dt, \quad (71)$$

$$\mathcal{E} \int_0^t \tilde{x}'(t)\Xi\tilde{x}(t)dt < \mathcal{E}\overline{\mathcal{V}}(\tilde{x}(0)) + \beta\mathcal{E} \int_0^t \overline{\mathcal{V}}(\tilde{x}(t))dt. \quad (72)$$

Using Gronwall inequality for (71), one has

$$\mathcal{E}\overline{\mathcal{V}}(\tilde{x}(t)) < \mathcal{E}\overline{\mathcal{V}}(\tilde{x}(0))e^{\beta t}. \quad (73)$$

From (72) and (73), we have

$$\begin{aligned}
J_2(\tilde{x}(t)) &< \beta \mathcal{E} \int_0^t \overline{\mathcal{V}}(\tilde{x}(t)) dt + \mathcal{E} \overline{\mathcal{V}}(\tilde{x}(0)) \\
&< \beta \mathcal{E} \int_0^t \overline{\mathcal{V}}(\tilde{x}(0)) e^{\beta t} dt + \mathcal{E} \overline{\mathcal{V}}(\tilde{x}(0)) \quad (74) \\
&= \mathcal{E} \overline{\mathcal{V}}(\tilde{x}(0)) e^{\beta t} < \lambda_{\max}(P) b_1 e^{\beta T} = J_2^*.
\end{aligned}$$

Step 3: prove that the nonzero disturbance and the control output satisfy the inequality (53).

By using Schur complement, we can obtain the following equivalent conditions of (54):

$$\begin{bmatrix} \tilde{Z}_1 + H'H - \beta \tilde{P} & \tilde{Z}_2 \\ * & \tilde{Z}_3 - \gamma^2 I \end{bmatrix} < 0. \quad (75)$$

According to (57) and (75), we get

$$\mathcal{L}_3 \overline{\mathcal{V}}(\tilde{x}(t)) < \beta \overline{\mathcal{V}}(\tilde{x}(t)) + \gamma^2 r'(t)r(t) - z'(t)z(t). \quad (76)$$

Repeating the proof process of Step 3 in Theorem 1, it yields

$$\mathcal{E} \int_0^t z'(s)z(s) ds < \gamma^2 \mathcal{E} \int_0^t r'(s)r(s) ds. \quad (77)$$

This completes the proof.

Because the nonlinear problem of inequalities (54)–(56) in Theorem 3 is difficult to solve, we transform the inequalities (54)–(56) into LMIs.  $\square$

**Theorem 4.** Given positive scalars  $b_1, b_2, T$ , and  $f$ , if there exist two positive scalars  $\beta$  and  $\zeta$  and three matrices  $\tilde{P}_{11} > 0$ ,  $\tilde{P}_{22} > 0$ , and  $M$  such that

$$\begin{bmatrix} \Sigma_{11} & \Sigma_{12} & \Sigma_{13} \\ * & \Sigma_{22} & \Sigma_{23} \\ * & * & \Sigma_{33} \end{bmatrix} < 0, \quad (78)$$

$$\begin{bmatrix} Y_{11} - (\beta + \lambda)\tilde{P}_{11} & Y_{12} \\ * & Y_{22} - (\beta + \lambda)\tilde{P}_{22} \end{bmatrix} < 0, \quad (79)$$

$$e^{\beta T}(\zeta b_1 + f\gamma^2) - b_2 < 0, \quad (80)$$

$$I < \text{diag}\{\tilde{P}_{11}, \tilde{P}_{22}\} < \zeta I, \quad (81)$$

hold, where  $\Sigma_{11} = A'_{11}\tilde{P}_{11} + \tilde{P}_{11}A_{11} + A'_{12}\tilde{P}_{11}A_{12} + C'_{12}C_{12} + \lambda(A'_{13} + I)\tilde{P}_{11}(A_{13} + I) - (\beta + \lambda)\tilde{P}_{11}$ ,  $\Sigma_{12} = C'_{11}M' + \tilde{P}_{11}B_{11}K + A'_{12}\tilde{P}_{11}B_{12}K + C'_{12}D_{12}K + \lambda(A'_{13} + I)\tilde{P}_{11}B_{13}K$ ,  $\Sigma_{22} = (A_{11} + B_{11}K)' \tilde{P}_{22} + \tilde{P}_{22}(A_{11} + B_{11}K) + K' B'_{12} \tilde{P}_{11} B_{12} K + \lambda K' B'_{13} \tilde{P}_{11} B_{13} K + \lambda \tilde{P}_{22} - MC_{11} - C'_{11}M' + K'D'_{12}D_{12}K - (\beta + \lambda)\tilde{P}_{22}$ ,  $\Sigma_{13} = \tilde{P}_{11}F_1 + A'_{12}\tilde{P}_{11}F_2 + \lambda(A'_{13} + I)\tilde{P}_{11}F_3$ ,  $\Sigma_{23} = MD_{11} + K'B'_{12}\tilde{P}_{11}F_2 + \lambda K'B'_{13}\tilde{P}_{11}F_3$ ,  $\Sigma_{33} = F_2\tilde{P}_{11}F_2 + \lambda F_3\tilde{P}_{11}F_3 - \gamma^2 I$ ,  $Y_{11} = A'_{11}\tilde{P}_{11} + \tilde{P}_{11}A_{11} + A'_{12}\tilde{P}_{11}A_{12} + \lambda(A'_{13} + I)\tilde{P}_{11}(A_{13} + I) + G_1$ ,  $Y_{12} = C'_{11}M' + \tilde{P}_{11}B_{11}K + A'_{12}\tilde{P}_{11}B_{12}K + \lambda(A'_{13} + I)\tilde{P}_{11}B_{13}K$ ,  $Y_{22} = (A_{11} + B_{11}K)' \tilde{P}_{22} + \tilde{P}_{22}(A_{11} + B_{11}K) + K' B'_{12} \tilde{P}_{11} B_{12} K - MC_{11} - C'_{11}M' + \lambda K' B'_{13} \tilde{P}_{11} B_{13} K + \lambda \tilde{P}_{22} + K' G_2 K$ , then (48) is said to be an OBFT  $H_2/H_\infty$  controller and we can get the upper bound of  $H_2$

index, that is,  $J_2^* = \zeta b_1 e^{\beta T}$ . Furthermore, the estimator gain matrix  $L = \tilde{P}_{22}^{-1}M$  is obtained.

*Proof.* Let  $\tilde{P} = \text{diag}\{\tilde{P}_{11}, \tilde{P}_{22}\}$  and  $M = \tilde{P}_{22}L$ , by substituting (51) and (52) into (54) and (55), (78) and (79) can be easily derived, respectively. From (80) and (81), we can deduce that (49) holds. This ends the proof.  $\square$

## 5. Algorithm

In this section, we propose an algorithm to optimize  $H_2$  index and  $H_\infty$  index.

Analysis: in Theorem 2, let  $J_1^* < \xi$ , the following inequality is derived:

$$\frac{Ne^{-\alpha T}}{b_1} - \xi^{-1}I > 0, \quad (82)$$

where  $0 < b_1 < b_2$ ,  $T > 0$ ,  $\alpha \geq 0$ , and  $m > 0$ .

The main purpose of the algorithm is to check whether inequalities (44)–(47) in Theorem 2 have feasible solutions by changing the value of  $\alpha$ . If there exist feasible solutions, then  $\xi$  and  $\gamma^2$  are optimized to get the minimum values. The detailed algorithm will be given as follows (Algorithm 1).

## 6. Examples

In this section, system (8) can be used to simulate a clothing hanging device and the parameters are as follows:

$$\begin{aligned}
A_{11} &= \begin{bmatrix} -15 & -9 \\ 8 & -12 \end{bmatrix}, \\
A_{12} &= \begin{bmatrix} -0.6 & 1 \\ 1.3 & -1.2 \end{bmatrix}, \\
A_{13} &= \begin{bmatrix} -1.8 & 1 \\ 1.4 & -1.5 \end{bmatrix}, \\
B_{11} &= [-9 \ 5]', \\
B_{12} &= [8.7 \ 2.3]', \\
B_{13} &= [-2.8 \ 1]', \\
F_1 &= [-0.6 \ 0.5]', \\
F_2 &= [0.3 \ -0.2]', \\
F_3 &= [0.4 \ -0.2]', \\
C_{11} &= [-0.9 \ -1.5], \\
C_{12} &= [-1.8 \ -2.5], \\
x(0) &= [-0.7 \ 0.7]',
\end{aligned} \quad (83)$$

and  $G_1 = 5$ ,  $G_2 = 4$ ,  $D_{11} = 8$ ,  $D_{12} = 10$ ,  $b_1 = 1$ ,  $b_2 = 4$ ,  $T = 1$ ,  $R = I$ ,  $f = 0.4$ , and  $\lambda = 2.5$ .

**6.1. Design of SFFT  $H_2/H_\infty$  Controller.** By using the above algorithm in Section 5, the relationships of  $\alpha$  and  $\xi$  (Figure 1),  $\alpha$  and  $\gamma$  (Figure 2), and  $\xi$  and  $\gamma$  (Figure 3) are derived, respectively. It can be seen from Figure 1 that the value of  $\xi$  increases with the increase of  $\alpha$ . Besides, it is obvious that

Step 1: given  $b_1, b_2, R, T, f$ , and  $\lambda$ .

Step 2: take an appropriate step size  $d_\alpha$  for  $\alpha$ , and then the values of  $\alpha$  are expressed as  $\alpha_i$ .

Step 3: let  $i = 1$ .

Step 4: if  $\alpha_i$  makes the following problems  $\min_{s.t. (37)-(40), (74), N>0} \xi$  and  $\min_{s.t. (37)-(40), (74), N>0} \gamma^2$  feasible, then store  $\alpha_i$  into  $U(i)$ ,  $\xi_{\min}$  into  $V(i)$ , and  $\gamma_{\min}$  into  $W(i)$ , and let  $\alpha_{i+1} = \alpha_i + d_\alpha$ , loop. Otherwise, go to Step 5.

Step 5: exit.

ALGORITHM 1: Optimization algorithm.

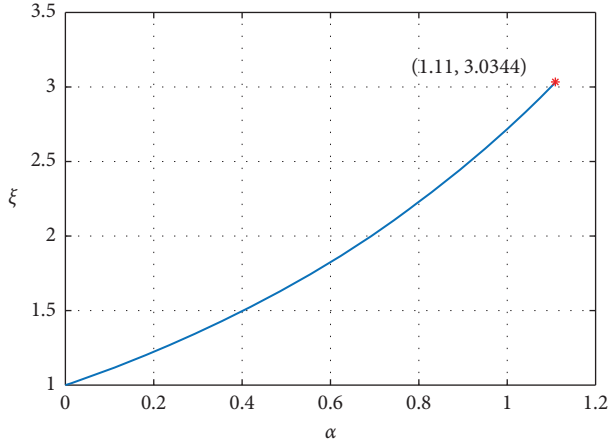


FIGURE 1:  $\xi$  versus  $\alpha$ .

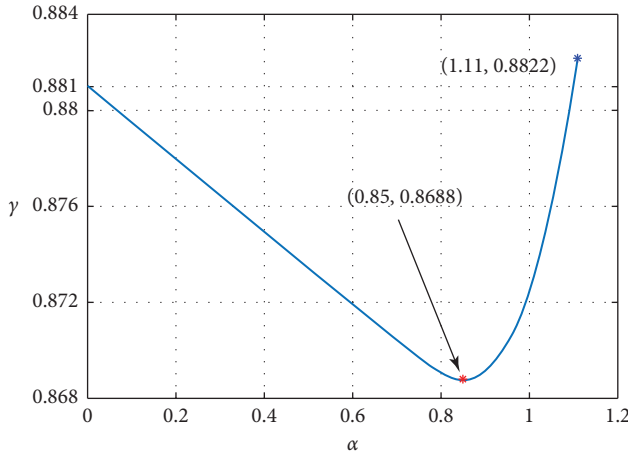


FIGURE 2:  $\gamma$  versus  $\alpha$ .

$\xi = 1$  when  $\alpha = 0$  and  $\xi = 3.0344$  when  $\alpha = 1.11$ , that is, the minimum and maximum values of  $H_2$  performance index are 1 and 3.0344, respectively. Also, the range of  $\alpha$  is  $[0, 1.11]$ .

As you can see from Figure 2, the value of  $\gamma$  decreases first and then increases with the increase of  $\alpha$ . When  $\alpha = 0.85$ ,  $\gamma$  can take the minimum value of 0.8688; at this point, we can get the optimal value of  $H_\infty$  performance index. When  $\alpha = 1.11$ ,  $\gamma$  can take the minimum value of 0.8822. Also,  $\alpha$  can be taken within  $[0, 1.11]$ .

In fact, Figure 3 reflects the relation between  $\xi$  and  $\gamma$ . As shown in Figure 3, with the increase of  $\xi$ , the value of  $\gamma$  decreases first, and at the point of  $\xi = 2.3397$ , the value of  $\gamma$

begins to increase. From Figures 1 to 3, we can see how to choose the right state feedback finite-time  $H_2/H_\infty$  controller. If the cost problem is mainly considered, a smaller  $\alpha$  can be selected. If the ability to suppress interference is mainly considered, we need to refer to Figure 2 to select the appropriate  $\alpha$ .

Next, substituting  $\alpha = 0$  into Theorem 2, we get

$$N = \begin{bmatrix} 0.8673 & -0.0135 \\ -0.0135 & 0.8946 \end{bmatrix}, Y = [-0.0366 \quad 0.0770], \quad (84)$$

$$m = 0.5237.$$

Then, we get the controller gain matrix as follows:

$$K = [-0.0409 \quad 0.0854]. \quad (85)$$

Because the state  $x(t)$  in this example is two-dimensional, we make  $x(t) = [x_1(t) \ x_2(t)]^T$ . Figure 4 describes the trajectories of  $x_1(t)$ ,  $x_2(t)$ , and  $E[x'(t)Rx(t)]$  with stochastic fluctuation driven by both Wiener and Poisson noises in Figures 5 and 6 versus the dimensionless time  $\lambda t$ . From Figure 4, we can see that the trajectory of  $E[x'(t)Rx(t)]$  does not exceed  $b_2 = 4$  in the time interval  $\lambda T = 2.5$ . Obviously, when the time interval is  $T = 1$ , the trajectory does not exceed the given range, so we conclude that system (8) is mean-square FTB w.r.t.  $(1, 4, 1, I, 0.4)$ . Among them, we assume that  $r(t) = \sin t (\int_0^1 \sin^2 t dt < f = 0.4)$ .

**6.2. Design of OBFT  $H_2/H_\infty$  Controller.** As in the case of state feedback, similar results can be obtained in the case of observer-based finite-time  $H_2/H_\infty$  control. The relationships of  $\beta$  and  $\xi$  (Figure 7),  $\beta$  and  $\gamma$  (Figure 8), and  $\xi$  and  $\gamma$  (Figure 9) are derived, respectively. It can be seen from Figure 7 that the value of  $\xi$  increases with the increase of  $\beta$ . Besides, it is obvious that  $\xi = 1$  when  $\beta = 0$  and  $\xi = 2.5857$  when  $\beta = 0.95$ , that is, the minimum and maximum values of  $H_2$  performance index are 1 and 2.5857, respectively. Also, the range of  $\beta$  is  $[0, 0.95]$ .

As you can see from Figure 8, the value of  $\gamma$  decreases first and then increases with the increase of  $\beta$ . When  $\beta = 0.72$ ,  $\gamma$  can take the minimum value of 1.1456, and at this point, we can get the optimal value of  $H_\infty$  performance index. Besides, the maximum value of  $H_\infty$  performance index is 1.1650 when  $\beta = 0.95$ . Also, the range of  $\beta$  is  $[0, 0.95]$ .

In fact, Figure 9 reflects the relation between  $\xi$  and  $\gamma$ . As shown in Figure 9, with the increase of  $\xi$ , the value of  $\gamma$  decreases first, and at the point of  $\xi = 2.0544$ , the value of  $\gamma$  begins to increase. From Figures 7 to 9, we can see how to

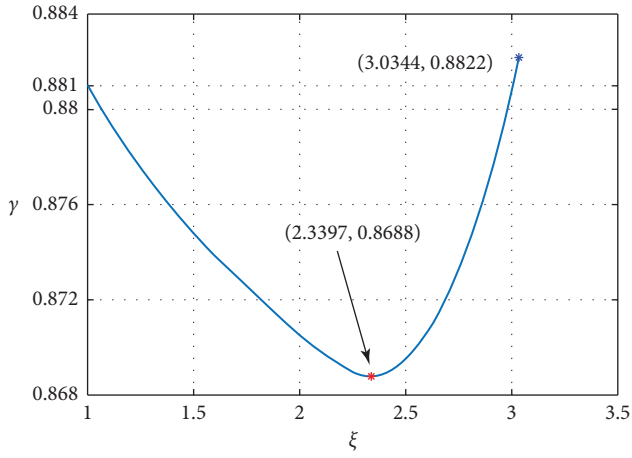


FIGURE 3:  $\gamma$  versus  $\xi$ .

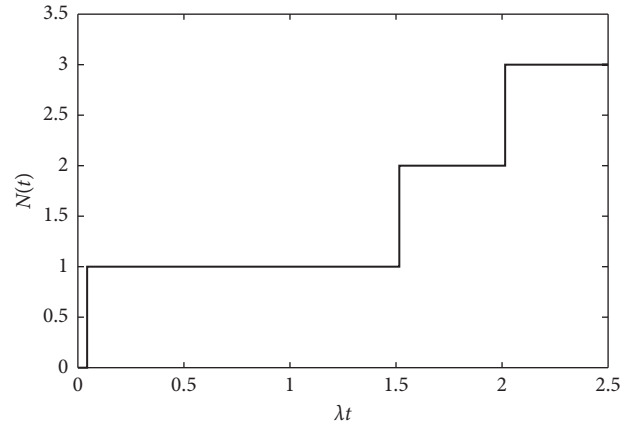


FIGURE 6: The time evolution of Poisson counting process.

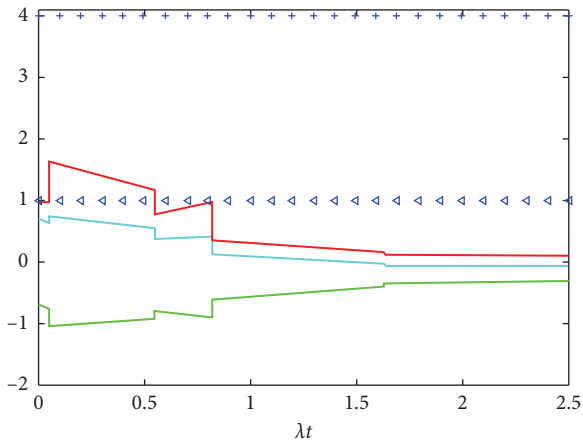


FIGURE 4: The trajectory for  $E[x'(t)Rx(t)]$ .

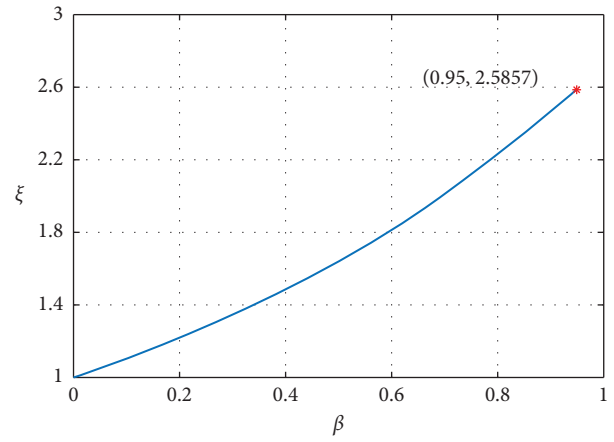


FIGURE 7:  $\xi$  versus  $\beta$ .

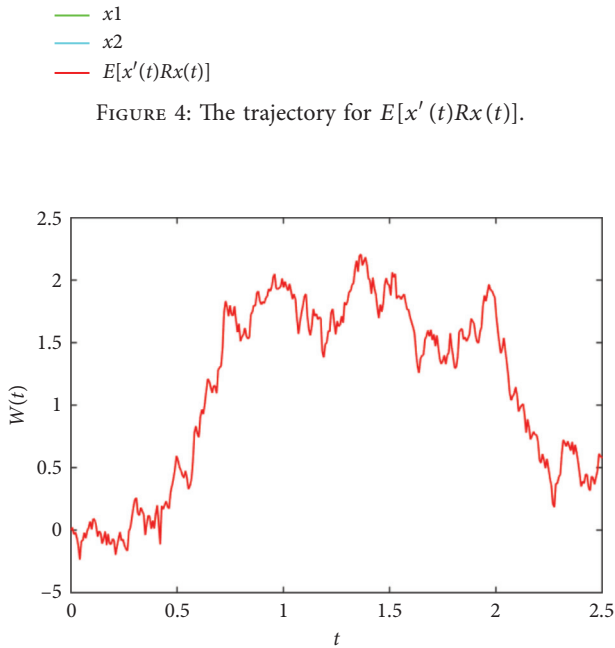


FIGURE 5: The time evolution of Wiener process.

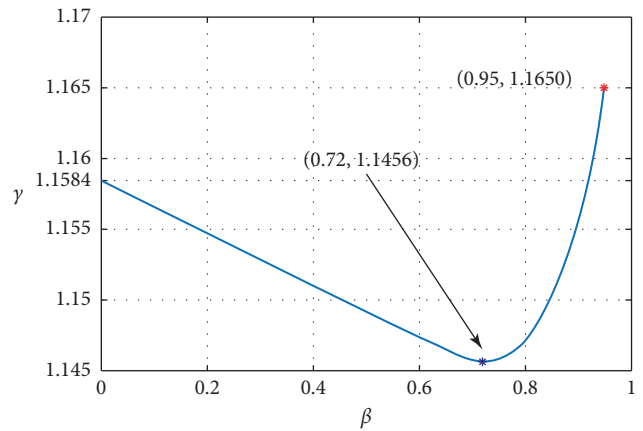
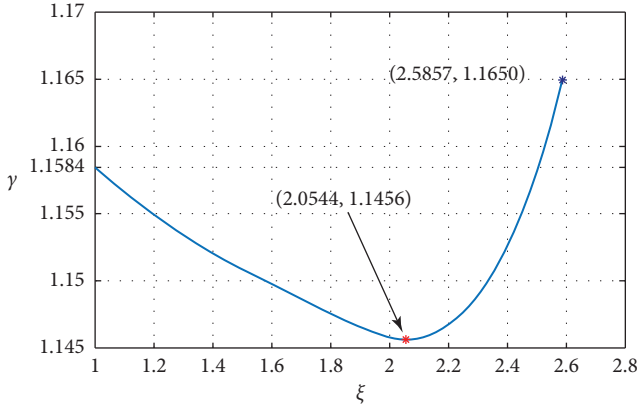
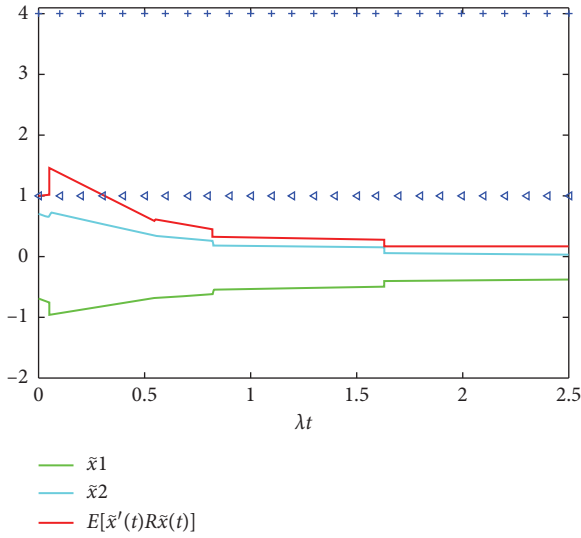


FIGURE 8:  $\gamma$  versus  $\beta$ .

choose the right OBFT  $H_2/H_\infty$  controller. If the cost problem is mainly considered, select the smaller  $\beta$  with reference to Figure 7. If the ability to suppress interference is mainly considered, we need to refer to Figure 8 to select the appropriate  $\beta$ .

FIGURE 9:  $\gamma$  versus  $\xi$ .FIGURE 10: The trajectory for  $E[x'(t)R\tilde{x}(t)]$ .

Substituting  $\beta = 0$  into Theorem 4, we have

$$\begin{aligned}
 P_{11} &= \begin{bmatrix} 1.3326 & 0.0458 \\ 0.0458 & 1.5739 \end{bmatrix}, \\
 P_{22} &= \begin{bmatrix} 1.4821 & -0.0298 \\ -0.0298 & 1.7362 \end{bmatrix}, \\
 M &= \begin{bmatrix} -0.0326 \\ 0.1348 \end{bmatrix}, \\
 \zeta &= 2.7271.
 \end{aligned} \tag{86}$$

Then, we obtain the following observer gain matrix:

$$L = \begin{bmatrix} -0.0205 \\ 0.0773 \end{bmatrix}. \tag{87}$$

Because the state  $\tilde{x}$  in this example is two-dimensional, we make  $\tilde{x} = [\tilde{x}_1 \tilde{x}_2]'$ . Figure 10 describes the trajectories of  $\tilde{x}_1$ ,  $\tilde{x}_2$ , and  $E[x'(t)R\tilde{x}(t)]$  with stochastic fluctuation driven by both Wiener and Poisson noises in Figures 5 and 6

versus the dimensionless time  $\lambda t$ . From Figure 10, it is obvious that the trajectory of  $E[x'(t)R\tilde{x}(t)]$  does not exceed  $b_2 = 4$  in the time interval  $\lambda T = 2.5$ . Obviously, when the time interval is  $T = 1$ , the trajectory does not exceed the given range, so we draw a conclusion that system (8) is mean-square FTB w.r.t. (1, 4, 1, I, 0.4). Among them, we assume that  $r(t) = \sin t (\int_0^1 \sin^2 t dt < f = 0.4)$ .

## 7. Conclusions

In this paper, state feedback and observer-based finite-time  $H_2/H_\infty$  controllers for stochastic Poisson systems have been designed, respectively. Two sufficient conditions for guaranteeing the existence of controllers have been proposed and converted to matrix inequality constrained optimization problems, and an algorithm for all Theorems has been provided to derive the optimal  $H_2$  index and  $H_\infty$  index under the condition of the finite-time boundedness.

## Data Availability

The data used to support the findings of this study are included within the article.

## Conflicts of Interest

The authors declare that there are no conflicts of interest regarding the publication of this paper.

## Acknowledgments

This work was supported by the National Natural Science Foundation of China (Grant nos. 61877062 and 61977043), China Postdoctoral Science Foundation (Grant no. 2017M610425), and Open Foundation of Key Laboratory of Pulp and Paper Science and Technology of Ministry of Education of China (Grant no. KF201419).

## References

- [1] B. Chen, S. Wong, and C. Li, "On the calculation of system entropy in nonlinear stochastic biological networks," *Entropy*, vol. 17, no. 10, pp. 6801–6833, 2015.
- [2] S. Mei, W. Wei, and F. Liu, "On engineering game theory with its application in power systems," *Control Theory and Technology*, vol. 15, no. 1, pp. 1–12, 2017.
- [3] Y. Yang, J. Xia, J. Zhao, X. Li, and Z. Wang, "Multiobjective nonfragile fuzzy control for nonlinear stochastic financial systems with mixed time delays," *Nonlinear Analysis: Modelling and Control*, vol. 24, no. 5, 2019.
- [4] C.-F. Wu, B.-S. Chen, and W. Zhang, "Multiobjective investment policy for a nonlinear stochastic financial system: a fuzzy approach," *IEEE Transactions on Fuzzy Systems*, vol. 25, no. 2, pp. 460–474, 2017.
- [5] Y. Tang, X. Wu, P. Shi, and F. Qian, "Input-to-state stability for nonlinear systems with stochastic impulses," *Automatica*, vol. 113, no. 3, Article ID 108766, 2020.
- [6] X. Wu, Y. Tang, and J. Cao, "Input-to-state stability of time-varying switched systems with time delays," *IEEE*

- Transactions on Automatic Control*, vol. 64, no. 6, pp. 2537–2544, 2019.
- [7] X. Wu, Y. Tang, J. Cao, and X. Mao, “Stability analysis for continuous-time switched systems with stochastic switching signals,” *IEEE Transactions on Automatic Control*, vol. 63, no. 9, pp. 3083–3090, 2018.
- [8] M. E. Shaikin, “Multiplicative stochastic systems with multiple external disturbances,” *Automation and Remote Control*, vol. 79, no. 2, pp. 300–310, 2018.
- [9] Z. Xiang, C. Qiao, and M. S. Mahmoud, “Finite-time analysis and  $H_\infty$  control for switched stochastic systems,” *Journal of the Franklin Institute*, vol. 349, no. 3, pp. 915–927, 2012.
- [10] Z. Yan, J. H. Park, and W. Zhang, “Finite-time guaranteed cost control for Itô Stochastic Markovian jump systems with incomplete transition rates,” *International Journal of Robust and Nonlinear Control*, vol. 27, no. 1, pp. 66–83, 2017.
- [11] M. Hafayed, A. Abba, and S. Abbas, “On mean-field stochastic maximum principle for near-optimal controls for Poisson jump diffusion with applications,” *International Journal of Dynamics and Control*, vol. 2, no. 3, pp. 262–284, 2014.
- [12] X. Yang and Q. Zhu, “ $p$ th moment exponential stability of stochastic partial differential equations with Poisson jumps,” *Asian Journal of Control*, vol. 16, no. 5, pp. 1482–1491, 2014.
- [13] X. Lin and R. Zhang, “ $H_\infty$  control for stochastic systems with Poisson jumps,” *Journal of Systems Science and Complexity*, vol. 24, no. 4, pp. 683–700, 2011.
- [14] A. Anguraj, K. Ravikumar, and D. Baleanu, “Approximate controllability of a semilinear impulsive stochastic system with nonlocal conditions and Poisson jumps,” *Advances in Difference Equations*, vol. 2020, no. 1, 2020.
- [15] D. S. Bernstein and W. M. Haddad, “LQG control with an  $H_\infty$  performance bound: a Riccati equation approach,” *IEEE Transactions on Automatic Control*, vol. 34, no. 3, pp. 293–305, 1989.
- [16] B.-S. Chen and W. Zhang, “Stochastic  $H_2/H_\infty$  control with state-depend noise,” *IEEE Transactions on Automatic Control*, vol. 49, no. 1, pp. 45–57, 2004.
- [17] H. Ma, W. Zhang, and T. Hou, “Infinite horizon  $H_2/H_\infty$  control for discrete-time time-varying Markov jump systems with multiplicative noise,” *Automatica*, vol. 48, no. 7, pp. 1447–1454, 2012.
- [18] Y. Huang, W. Zhang, and G. Feng, “Infinite horizon  $H_2/H_\infty$  control for stochastic systems with Markovian jumps,” *Automatica*, vol. 44, no. 3, pp. 857–863, 2008.
- [19] W. Zhang, L. Xie, and B. Chen, *Stochastic  $H_2/H_\infty$  Control: A Nash Game Approach*, CRC Press, Boca Raton, FL, USA, 2017.
- [20] X. Yang, Q. Song, Y. Liu, and Z. Zhao, “Finite-time stability analysis of fractional-order neural networks with delay,” *Neurocomputing*, vol. 152, pp. 19–26, 2015.
- [21] A. Elahi and A. Alfi, “Finite-time  $H_\infty$  control of uncertain networked control systems with randomly varying communication delays,” *ISA Transactions*, vol. 69, pp. 65–88, 2017.
- [22] X. Li, J. Shen, and R. Rakkiyappan, “Persistent impulsive effects on stability of functional differential equations with finite or infinite delay,” *Applied Mathematics and Computation*, vol. 329, pp. 14–22, 2018.
- [23] X. Li and M. Bohner, “An impulsive delay differential inequality and applications,” *Computers & Mathematics with Applications*, vol. 64, no. 6, pp. 1875–1881, 2012.
- [24] M. Galicki, “Finite-time trajectory tracking control in a task space of robotic manipulators,” *Automatica*, vol. 67, pp. 165–170, 2016.
- [25] H. Garg and S. P. Sharma, “Stochastic behavior analysis of complex repairable industrial systems utilizing uncertain data,” *ISA Transactions*, vol. 51, no. 6, pp. 752–762, 2012.
- [26] Z. Yan, G. Zhang, and W. Zhang, “Finite-time stability and stabilization of linear Itô stochastic systems with state and control-dependent noise,” *Asian Journal of Control*, vol. 15, no. 1, pp. 270–281, 2013.
- [27] Z. Yan, W. Zhang, and G. Zhang, “Finite-time stability and stabilization of Itô stochastic systems with markovian switching: mode-dependent parameter approach,” *IEEE Transactions on Automatic Control*, vol. 60, no. 9, pp. 2428–2433, 2015.
- [28] Y.-j. Ma, B.-w. Wu, and Y.-E. Wang, “Finite-time stability and finite-time boundedness of fractional order linear systems,” *Neurocomputing*, vol. 173, no. 3, pp. 2076–2082, 2016.
- [29] M. Li and J. Wang, “Finite time stability of fractional delay differential equations,” *Applied Mathematics Letters*, vol. 64, pp. 170–176, 2017.
- [30] Z. Yan, Y. Song, and X. Liu, “Finite-time stability and stabilization for Itô-type stochastic Markovian jump systems with generally uncertain transition rates,” *Applied Mathematics and Computation*, vol. 321, pp. 512–525, 2017.
- [31] X. Yang, X. Li, X. Xi, and P. Duan, “Review of stability and stabilization for impulsive delayed systems,” *Mathematical Biosciences & Engineering*, vol. 15, no. 6, pp. 1495–1515, 2018.
- [32] X. Li, X. Yang, and T. Huang, “Persistence of delayed cooperative models: impulsive control method,” *Applied Mathematics and Computation*, vol. 342, pp. 130–146, 2019.
- [33] D. Yang, X. Li, and J. Qiu, “Output tracking control of delayed switched systems via state-dependent switching and dynamic output feedback,” *Nonlinear Analysis: Hybrid Systems*, vol. 32, pp. 294–305, 2019.
- [34] Z. Yan, M. Zhang, Y. Song, and S. Zhong, “Finite-time  $H_\infty$  control for Itô-type nonlinear time-delay stochastic systems,” *IEEE Access*, vol. 8, pp. 83622–83632, 2020.
- [35] R. Nie, Q. Ai, S. He, Z. Yan, X. Luan, and F. Liu, “Robust finite-time control and estimation for uncertain time-delayed switched systems by observer-based sliding mode technique,” *Optimal Control Applications and Methods*, 2020.
- [36] R. Wang, J. Xing, and Z. Xiang, “Finite-time stability and stabilization of switched nonlinear systems with asynchronous switching,” *Applied Mathematics and Computation*, vol. 316, pp. 229–244, 2018.
- [37] Z. Yan, S. Zhong, and X. Liu, “Finite-time  $H_2/H_\infty$  control for linear Itô stochastic systems with  $x$ ,  $u$ ,  $v$ -dependent noise,” *Complexity*, vol. 2018, Article ID 1936021, 13 pages, 2018.
- [38] F. Hanson, *Applied Stochastic Processes and Control for Jump-Diffusions: Modeling, Analysis and Computation*, SIAM, Philadelphia, PA, USA, 2007.

## Research Article

# PWM-Based Finite-Time Tracking of Switched Buck Power Converters

Hui Zhang  and Zhaojing Wu 

*School of Mathematics and Informational Sciences, Yantai University, Yantai 264005, Shandong Province, China*

Correspondence should be addressed to Zhaojing Wu; wuzhaojing00@188.com

Received 27 April 2020; Accepted 11 June 2020; Published 30 June 2020

Guest Editor: Xiaodi Li

Copyright © 2020 Hui Zhang and Zhaojing Wu. This is an open access article distributed under the Creative Commons Attribution License, which permits unrestricted use, distribution, and reproduction in any medium, provided the original work is properly cited.

In this paper, the problem of finite-time tracking is investigated for switched buck power converters based on the pulse width modulation (PWM) technique. For the continuous model, an equivalent continuous controller is solved by the backstepping technique, such that all signals are finite-time stable. PWM-based finite-time tracking with the equivalent control input is proposed for the switched buck converter, such that the tracking error converges to an arbitrarily small neighborhood of the origin in finite time, and the origin of the closed-loop system is practically finite-time stable. Simulation results are given to demonstrate the effectiveness of the proposed schemes.

## 1. Introduction

Electrical systems described by the multiple circuit topologies associated with the regulating switch are switched DC-DC power converters [1], which have widespread applications in power systems, photovoltaic systems, communication equipment, computers, and industrial electronics. The three basic topologies of switched DC-DC power converters are buck, boost, and buck-boost. The research of these power converters has drawn a great deal of attention for the development in both power electronics and control theory [2–4]. A good deal of results on point stabilization and trajectory tracking has been obtained under the switching method [5] and PWM technique [6]. Some switching methods have been investigated for stabilization of power converters, i.e., optimal switching instants based on a numerical optimization approach [7], state-dependent switching with the aid of variable-structure control [8], and switching law by combining sliding mode control with an equivalent control input [9–12]. The references mentioned above regard the switching signal as the control input directly based on switched systems theory.

The output voltage regulation of PWM-based DC-DC power converters has already been an extremely active research. The output voltage tracking was discussed by selecting

passivity-based control [13–15], energy shaping control [16, 17], and state feedback indirect control with non-minimum phase [18, 19]. In order to estimate the uncertain load resistances and enhance output performance, the adaptive backstepping controllers were proposed with better robustness and adaptability [20–23]. Most of the results focused on asymptotical convergence rate for DC-DC power converters. Compared with asymptotical stability, finite-time stability has a faster convergence performance in terms of time optimization. Finite-time control has aroused a great deal of interest in recent years. For DC-DC buck converters, finite-time tracking control via integral terminal sliding modes was presented in [24]. The output voltage regulation control is investigated to guarantee the finite-time convergence rate based on finite-time convergent observer [25, 26] or via adaptive saturated finite-time control algorithm [27]. However, all these references above only considered point stabilization for continuous average models with the continuous control as a control input.

Little work has been done on PWM control to achieve the trajectory tracking problem of switched power converters so far. In this paper, we consider PWM-based finite-time tracking of switched buck power converters, where the system input is a digital control. The main work consists of the following aspects.



- (1) Finite-time stability of a nonlinear system with continuous control is given as a priori information, and it is firstly proved that the closed-loop digital system is practically finite-time stable in the condition of the continuous control replaced by physical PWM control.
- (2) For the corresponding continuous system, an equivalent continuous controller is designed using the backstepping method, such that the tracking error tends to zero in a finite time, and the closed-loop error system is finite-time stable in terms of time optimization compared with [22, 23].
- (3) For the switched buck converter, PWM-based finite-time tracking with the equivalent control input is proposed such that the tracking error converges to an arbitrarily small neighborhood of the origin in finite time, and the origin of the closed-loop system is practically finite-time stable.

The paper is organized as follows. Problem formulation is given in Section 2. PWM and its implementation are presented in Section 3. PWM-based finite-time tracking is researched in Section 4. Simulation results for buck converters are presented in Section 5. The paper is concluded in Section 6.

Notations: For a vector  $x$ ,  $|x|$  denotes its usual Euclidean norm and  $x^T$  denotes its transpose;  $|X|$  denotes the Frobenius norm of a matrix  $X$  defined by  $|X| = (\text{Tr}\{XX^T\})^{(1/2)}$ , where  $\text{Tr}(\cdot)$  denotes the trace of a square matrix;  $\mathbb{R}_+$  denotes the set of all nonnegative real numbers;  $\mathbb{R}^n$  denotes the real  $n$ -dimensional space;  $\mathbb{R}^{n \times r}$  denotes the real  $n \times r$  matrix space;  $\mathcal{C}^i$  denotes the set of all functions with continuous  $i$ -th partial derivative;  $AB$  denotes the distance between  $A$  and  $B$ ;  $S_{ABCD}$  denotes the area of a rectangle  $ABCD$ .

## 2. Problem Formulation

Consider the switch-regulated buck converter circuit as shown in Figure 1.  $E$  is the voltage parameter of the supply voltage,  $R$  is the resistance of the resistor,  $C$  is the capacitance of the capacitor,  $L$  is the inductance of the inductor,  $VD$  is the diode, and  $VT$  is a PWM gate drive controlled switch. The control variable  $\sigma$  is introduced to denote the switch state,  $\sigma = 1$  when  $VT = \text{ON}$ , and  $\sigma = 0$  when  $VT = \text{OFF}$ . That is, such a control input takes values in the discrete set  $\{0, 1\}$ . It is assumed that there is no noise in the circuit; Figure 2 is the equivalent circuit of Figure 1.

In order to establish the circuit model associated with the regulating switch position, we need to make an explanation for those physical symbols. The inductive current  $\dot{q}_L$  respects the derivative of the circulating electric charge  $q_L$ ;  $q_C$  is the electrical charge stored in the capacitor, and  $(q_C/C)$  is the capacitor voltage. The switch-regulated buck converter circuit is presented as

$$\begin{aligned} \frac{q_C}{C} &= -R(\dot{q}_C - \dot{q}_L), \\ L\dot{q}_L &= -R(\dot{q}_L - \dot{q}_C) + \sigma E. \end{aligned} \quad (1)$$

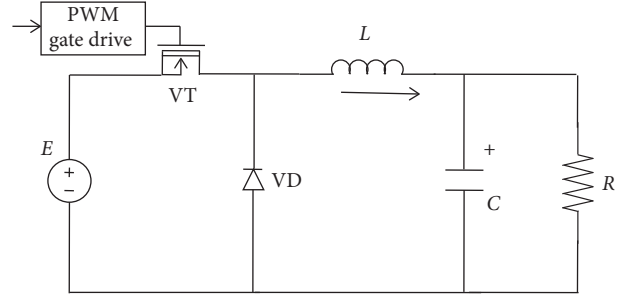


FIGURE 1: The buck converter circuit.

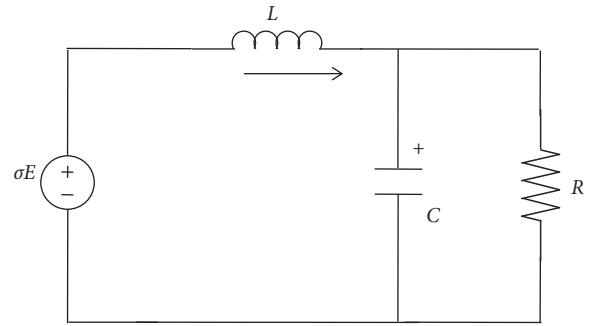


FIGURE 2: Equivalent circuit of Figure 1.

Substituting the second equation into the first, it can be rewritten as

$$\begin{aligned} \dot{q}_C &= \dot{q}_L - \frac{q_C}{RC}, \\ \dot{q}_L &= -\frac{q_C}{LC} + \frac{E}{L}\sigma. \end{aligned} \quad (2)$$

Let  $x_1 = (q_C/C)$ ,  $x_2 = \dot{q}_L$ ; the dynamic equation is derived as

$$\begin{aligned} \dot{x}_1 &= -\frac{1}{RC}x_1 + \frac{1}{C}x_2, \\ \dot{x}_2 &= -\frac{1}{L}x_1 + \frac{1}{L}E\sigma, \end{aligned} \quad (3)$$

where  $x_1$  and  $x_2$  represent the capacitor voltage and the inductor current, respectively, and the variable  $\sigma$  is the digital control which represents time series produced by servo amplifiers and only take values from binary set  $\{0, 1\}$ . Let  $y = x_1$ , that is, the output is the capacitor voltage, which is also the resistor voltage.

Given a smooth reference signal  $y_r(t) \in \mathcal{C}^2(\mathbb{R})$ , where  $y_r(t)$ ,  $\dot{y}_r(t)$ ,  $\ddot{y}_r(t)$  are bounded with known constants. The aim of this paper is to design a switching signal  $\sigma$  for the switched buck converter (3), such that the capacitor voltage  $y = x_1$  can be driven to track a given reference signal  $y_r(t)$  in a finite time; simultaneously, all signals in the resulting system are required to be practically finite-time stable.

To study finite-time tracking, we introduce some basic concepts and lemmas that will serve as the basis for the development of our digital switching control.

*Definition 1* (see [29, 28]). Consider a nonlinear system

$$\dot{x} = f(x), \quad x(0) = x_0, \quad x \in \mathcal{D} \subseteq \mathbb{R}^n, \quad (4)$$

where  $f: \mathcal{D} \rightarrow \mathbb{R}^n$  is continuous,  $f(0) = 0$ , and  $\mathcal{D}$  is an open neighborhood of the origin. The origin of system (4) is finite-time stable (FS), if it is Lyapunov stable and finite-time convergent in a neighborhood  $\mathcal{D}_0 \subseteq \mathcal{D}$  of the origin. By “finite-time convergence,” we mean that there is a settling time  $T^* \in (0, \infty)$ , such that for  $(\forall x_0 \in \mathcal{D}_0 \setminus \{0\})$ ,  $(x(t) \in \mathcal{D}_0 \setminus \{0\})$  for  $t \in [0, T^*)$ ,  $\lim_{t \rightarrow T^*} x(t) = 0$ , that is,

$$x(t) = 0, \quad \forall t > T^*. \quad (5)$$

When  $\mathcal{D}_0 = \mathcal{D} = \mathbb{R}^n$ , the origin is a globally finite-time stable equilibrium.

*Definition 2* (see [30]). The origin of system (4) is said to be practical finite-time stable (PFS), if for all initial conditions  $x_0$ , there exist a constant  $\varepsilon_T > 0$  and a settling time  $T^*$  ( $\varepsilon_T, x_0 < \infty$ ), such that

$$|x(t)| \leq \varepsilon_T, \quad \forall t > T^*. \quad (6)$$

*Remark 1.* For PFS, if  $\varepsilon_T$  depends on  $T$  and  $T \rightarrow 0$ ,  $\varepsilon_T \rightarrow 0$ , then the effect of PFS is the same as FS. As  $T$  gets smaller, the bound  $\varepsilon_T$  of PFS here becomes smaller and even tends to zero compared with boundedness of [30].

**Lemma 1** (see [31]). *For any real number  $x_i$ ,  $i = 1, \dots, n$ , and  $0 < p \leq 1$ , the following inequality holds:*

$$(|x_1| + \dots + |x_n|)^p \leq |x_1|^p + \dots + |x_n|^p. \quad (7)$$

**Lemma 2** (see [28]). *For system (4), suppose there exist constants  $a > 0$ ,  $0 < \beta < 1$ , and a positive definite function  $V(x) \in \mathcal{C}^1: \overline{\mathcal{D}} \rightarrow \mathbb{R}$  ( $\overline{\mathcal{D}} \subset \mathcal{D} \subset \mathbb{R}^n$  is a neighborhood of the origin), such that*

$$\dot{V}(x) \leq -aV^\beta(x), \quad \forall x \in \overline{\mathcal{D}}, \quad (8)$$

*then, the origin of system (4) is finite-time stable, and the settling time  $T^*$  satisfies*

$$T^* \leq \frac{1}{a(1-\beta)} V(x_0)^{1-\beta}. \quad (9)$$

If  $\overline{\mathcal{D}} = \mathbb{R}^n$  and  $V(x)$  is radially unbounded, the origin of system (4) is globally finite-time stable.

### 3. PWM and Its Implementation

For a nonlinear system

$$\dot{x} = f(x) + Bu, \quad x(0) = x_0, \quad (10)$$

where  $x \in \mathbb{R}^n$ ,  $f \in \mathbb{R}^{n \times 1}$  is a locally Lipschitz continuous function,  $B \in \mathbb{R}^n$  is a constant vector, and  $u \in \mathbb{R}$  is the digital

control produced by servo amplifiers; it can only take values from binary set  $\{0, 1\}$ .

In order to design such digital control, we first give a priori hypothesis for system (10).

*Assumption 1.* There exists a continuous static control

$$u = \mu(x) \in [0, 1], \quad (11)$$

such that the origin of the closed-loop system (10) with continuous static control (11) is finite-time stable.

To achieve digitization, regarding  $\mu(t) = \mu(x(t))$  as a duty ratio, from the viewpoint of mathematics, a PWM control is a strategy defined as [32]

$$u = \overline{\sigma}_T(t) = \begin{cases} 1, & t_k \leq t < t_k + \mu(t_k)T, \\ 0, & t_k + \mu(t_k)T \leq t < t_k + T, \end{cases} \quad (12)$$

$$t_{k+1} = t_k + T, \quad t_0 = 0, \quad k = 0, 1, 2, \dots,$$

where  $t_k$  is a sampling instant and  $T$  represents the sampling period, where  $T$  is parameter-tuning. However, it is very difficult to implement the PWM control (12). The one is how to get exact  $\mu(t_k)$  at  $t_k$  with variable-step resolution, the other one comes from the fact that PWM control should be a physical signal produced by a servo circuit instead of numerical signal directly.

*Remark 2.* By [1], systems (10) and (11) are the average models of the PWM controlled system (10) with (12). As  $T \rightarrow 0$ , the duty ratio  $\mu(t)$  as the equivalent control replaces the PWM control  $\overline{\sigma}_T(t)$  in (12). The duty ratio  $\mu(t)$  may be designed in the form of a state feedback function, and thus it is easy to achieve some performance index of the closed-loop PWM switched system. In practice, the PWM control is generated as a discrete gate pulse signal [33], comparing a desired analog control signal with a fixed-frequency ramp.

One approximate implementation of PWM control (12) is presented as

$$u = \sigma_T(t) = \begin{cases} 1, & \mu(t) > u_0(t), \\ 0, & \mu(t) < u_0(t), \end{cases} \quad (13)$$

where  $\mu(t)$  is the function as (11) and  $u_0(t)$  is a triangular wave with magnitude  $A = 1$  and same period  $T$  as (12) (see Figure 3).

If continuous control (11) is changed to PWM implementation (13), the stability analysis of system (10) will be given as follows.

For PWM implementation (13), we will discuss the relationship between  $\sigma_T(t)$  and  $\mu(t)$  on the interval  $[0, t]$ .

(1) If  $\mu(t) = a$  ( $a \in (0, 1)$  is a constant), we have (see Figure 4)

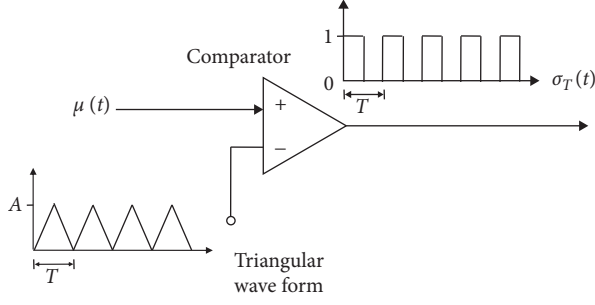


FIGURE 3: Producing pulse using comparator.

$$\begin{aligned}
 \int_0^{(T/2)} \mu(s) ds &= S_{\text{OFGE}} \\
 &= \frac{aT}{2} \\
 &= \frac{\text{OF}}{\text{OA}} \frac{T}{2} \\
 &= \frac{\text{OH}}{\text{OC}} \frac{T}{2} \\
 &= \frac{\text{OD}}{\text{OE}} S_{\text{OACE}} = S_{\text{OABD}} \\
 &= \int_0^{(T/2)} \sigma_T(s) ds.
 \end{aligned} \tag{14}$$

Case (1):  $\exists n \in \mathbb{N}^+, t = nT$ ; from (14),

$$\int_0^t \sigma_T(s) ds = \int_0^{nT} \sigma_T(s) ds = \int_0^{nT} \mu(s) ds = \int_0^t \mu(s) ds. \tag{15}$$

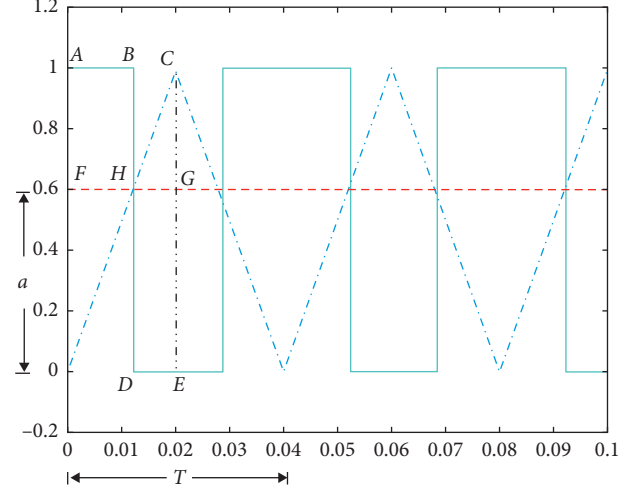
Case (2):  $\exists n \in \mathbb{N}^+, t \in (nT, (n+1)T)$ ; from (15) and the values of  $\mu(t)$  and  $\sigma_T(t)$ ,

$$\begin{aligned}
 \lim_{T \rightarrow 0} \int_0^t \sigma_T(s) ds &= \lim_{T \rightarrow 0} \int_0^t \mu(s) ds - \lim_{T \rightarrow 0} \int_{nT}^t \mu(s) ds \\
 &\quad + \lim_{T \rightarrow 0} \int_{nT}^t \sigma_T(s) ds \\
 &= \int_0^t \mu(s) ds.
 \end{aligned} \tag{16}$$

From two cases above, if  $\mu(t) = a$ , one gets that

$$\lim_{T \rightarrow 0} \int_0^t \sigma_T(s) ds = \int_0^t \mu(s) ds, \quad \forall t \geq 0. \tag{17}$$

(2) If  $\mu(t)$  is a continuous function, there exists simple function series  $\sum_{i=1}^n a_i I_{E_i}(t)$ , such that

FIGURE 4: The pulse generated comparing  $\mu = a$  with a triangular wave.

$$\mu(t) = \lim_{n \rightarrow \infty} \sum_{i=1}^n a_i I_{E_i}(t), \tag{18}$$

where  $E_1, \dots, E_n$  are  $n$  disjoint closed sets of  $[0, \infty)$ . Let the length of  $E_i$  be less than that of  $T$ ; then,  $T \rightarrow 0$  leads to  $n \rightarrow \infty$ .

$$\begin{aligned}
 \int_0^t \mu(s) ds &= \lim_{n \rightarrow \infty} \sum_{i=1}^n \int_0^t a_i I_{E_i}(s) ds \\
 &= \lim_{n \rightarrow \infty} \sum_{i=1}^n \lim_{T \rightarrow 0} \int_0^t \sigma_T(s) I_{E_i}(s) ds \\
 &= \lim_{T \rightarrow 0} \int_0^t \sigma_T(s) ds, \quad \forall t \geq 0.
 \end{aligned} \tag{19}$$

The solution of system (10) with (11) is denoted as  $x_\mu$ , and the solution of system (10) and PWM implementation (13) is denoted as  $x_{\sigma_T}$ ; by formula (19), the following relationship holds

$$\begin{aligned}
 \lim_{T \rightarrow 0} x_{\sigma_T}(t) &= x_0 + \int_0^t f(x(s)) ds + B \lim_{T \rightarrow 0} \int_0^t \sigma_T(s) ds \\
 &= x_0 + \int_0^t f(x(s)) ds + B \int_0^t \mu(s) ds \\
 &= x_\mu(t), \quad \forall t \geq 0.
 \end{aligned} \tag{20}$$

which implies that

$$x_{\sigma_T}(t) = x_\mu(t) + D_T, \quad \lim_{T \rightarrow 0} D_T = 0, \quad \forall t \geq 0. \tag{21}$$

According to Assumption 1, the origin of system (10) with (11) is finite-time stable. By Definition 1, there exists a settling time  $T^* \in (0, \infty)$ , such that

$$x_\mu(t) = 0, \quad \forall t > T^*. \tag{22}$$

From (22) and 21, we have that

$$|x_{\sigma_T}(t)| \leq |D_T|, \quad \lim_{T \rightarrow 0} D_T = 0, \quad \forall t \geq 0. \quad (23)$$

As a consequence, there exists  $e_T$ , such that  $|D_T| \leq e_T$ , and

$$|x_{\sigma_T}(t)| \leq e_T, \quad \lim_{T \rightarrow 0} e_T = 0, \quad \forall t \geq 0. \quad (24)$$

According to Definition 2, the origin of closed-loop digital system (10) and (13) is practically finite-time stable. From the above analysis, we can get the result.

**Theorem 1.** *For system (10) under Assumption 1, if continuous static control  $\mu(t)$  (11) is replaced by PWM control  $\sigma_T(t)$  (13), then the origin of closed-loop digital system (10) with (13) is practically finite-time stable.*

*Remark 3.* According to Theorem 1, system (10) with (13) is practically finite-time stable. From (24), as  $T \rightarrow 0$ ,  $e_T \rightarrow 0$ . This implies that the sampling period  $T$  can be tuned smaller, and system (10) with (13) is closer to be finite-time stable. Moreover, all signals can be made arbitrarily small for small enough  $T$ .

#### 4. PWM-Based Finite-Time Tracking

For the switched buck converter (3), in order to achieve the tracking target, we give the ideas for design as follows:

- (1) Design the equivalent continuous control by the backstepping method
- (2) The digital control is produced using the equivalent continuous control based on the PWM technique

*4.1. Design of a Finite-Time State Feedback Controller.* System (3) with equivalent continuous control  $\mu$  is presented as

$$\dot{x}_1 = -\frac{1}{RC}x_1 + \frac{1}{C}x_2, \quad (25)$$

$$\dot{x}_2 = -\frac{1}{L}x_1 + \frac{1}{L}E\mu.$$

For the continuous system (25), the backstepping method is adopted to design a finite-time state feedback controller  $\mu$ , such that the capacitor voltage  $x_1$  tracks the given reference voltage  $y_r(t)$  in a finite time.

Introduce the track error

$$z_1 = x_1 - y_r. \quad (26)$$

*Step 1.* From (25) and (26), the derivative of  $z_1$  with respect to time turns out to be

$$\dot{z}_1 = -\frac{1}{RC}x_1 + \frac{1}{C}x_2 - \dot{y}_r. \quad (27)$$

Choosing the Lyapunov function  $V_1 = (1/2)z_1^2$ , the derivative of  $V_1$  along the system (27) is given by

$$\dot{V}_1 = z_1 \left( -\frac{1}{RC}x_1 + \frac{1}{C}x_2 - \dot{y}_r \right). \quad (28)$$

As  $(1/C)x_2$  is just a variable and not an effective control input, (27) cannot be enforced for all  $t \geq 0$ . Nevertheless, it shows that the desired value for the variable  $(1/C)x_2$  is

$$\alpha_1 = -c_1 z_1^{2\beta-1} + \frac{1}{RC}x_1 + \dot{y}_r, \quad (29)$$

where  $c_1 > 0$  and  $\beta \in ((1/2), 1)$  are design parameters. Substituting (29) into (28), we have

$$\dot{V}_1 = -c_1 z_1^{2\beta} + z_1 \left( \frac{1}{C}x_2 - \alpha_1 \right). \quad (30)$$

*Step 2.* Indeed, design the error

$$z_2 = \frac{1}{C}x_2 - \alpha_1. \quad (31)$$

From (25) and (31), deriving  $z_2$  with respect to time yields

$$\dot{z}_2 = -\frac{1}{LC}x_1 + \frac{1}{LC}E\mu - \dot{\alpha}_1. \quad (32)$$

For the second Lyapunov-like function  $V = V_2 = V_1 + (1/2)z_2^2$ , the derivative of  $V$  along the system (32) satisfies

$$\begin{aligned} \dot{V} &= -c_1 z_1^{2\beta} + z_1 z_2 + z_1 \dot{z}_2 \\ &= -c_1 z_1^{2\beta} - c_2 z_2^{2\beta} + z_2 \left[ c_2 z_2^{2\beta-1} + z_1 - \frac{1}{LC}x_1 + \frac{1}{LC}E\mu - \dot{\alpha}_1 \right], \end{aligned} \quad (33)$$

where  $c_2 > 0$  is a design parameter. The finite-time state feedback controller is designed as

$$\mu = \frac{LC}{E} \left[ -z_1 - c_2 z_2^{2\beta-1} + \frac{1}{LC}x_1 + \dot{\alpha}_1 \right]. \quad (34)$$

Substituting (34) into (33) results in

$$\dot{V} = -c_1 z_1^{2\beta} - c_2 z_2^{2\beta}. \quad (35)$$

In view of the above control analysis, we give the stability result of the continuous system in the following.

**Theorem 2.** *For system (3) with continuous control  $\mu$  (34), all the signals of the closed-loop error systems (27), (32), and (34) are finite-time stable, and the tracking error converges to the origin in a finite time. Moreover, the equivalent continuous control (34) is bounded, and by choosing design parameters appropriately,  $\mu$  can be obtained such that*

$$\mu(t) \in [0, 1], \quad t \geq 0. \quad (36)$$

*Proof.* By defining  $z = (z_1^T, z_2^T)^T$  and  $V(z) = (1/2)z_1^2 + (1/2)z_2^2$ ,  $V(z)$  is a positive definite function. From (35) and Lemma 1,

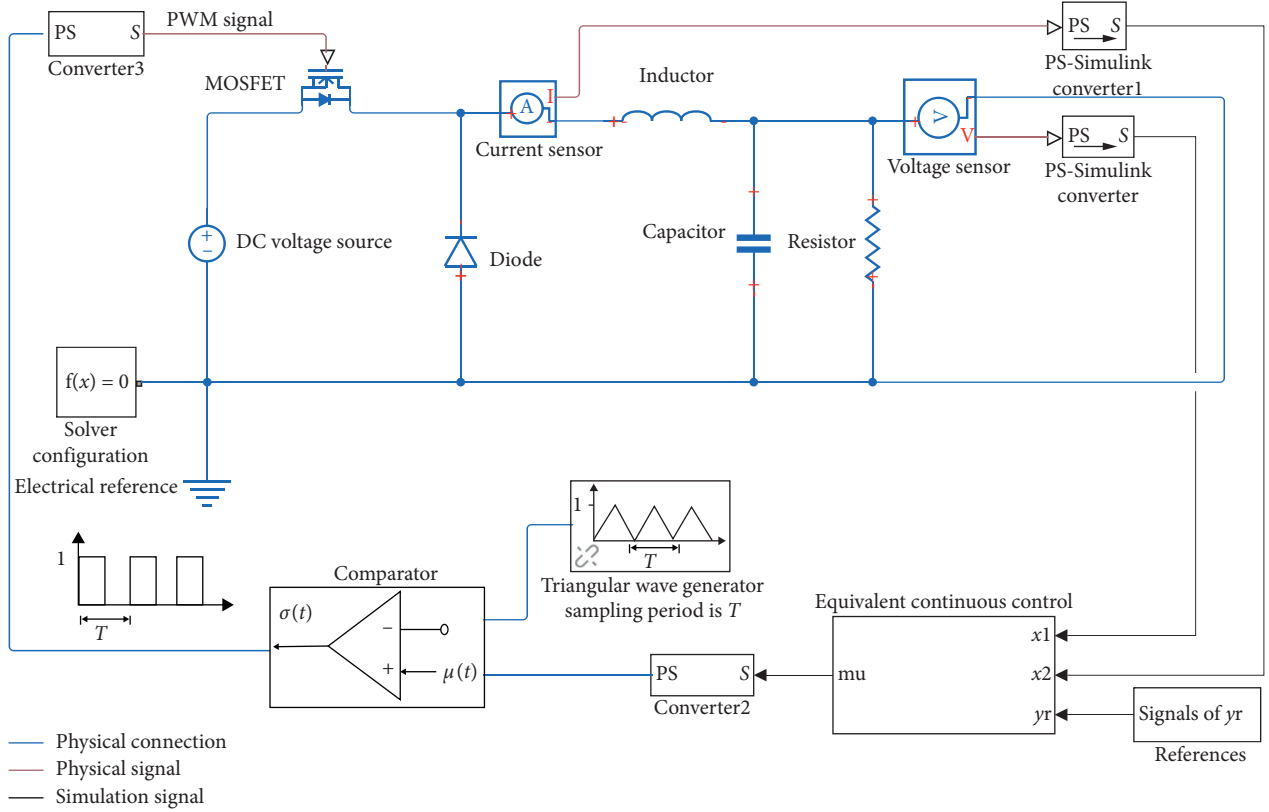


FIGURE 5: The control framework of buck converters under PWM-based finite-time tracking control.

$$\begin{aligned}
 \dot{V} &= -c_1 z_1^{2\beta} - c_2 z_2^{2\beta} \\
 &\leq -2c_1 \left(\frac{z_1^2}{2}\right)^\beta - 2c_2 \left(\frac{z_2^2}{2}\right)^\beta \\
 &\leq -c \left(\frac{1}{2}z_1^2 + \frac{1}{2}z_2^2\right)^\beta \\
 &\leq -cV^\beta,
 \end{aligned} \tag{37}$$

where  $c = \min\{2c_1, 2c_2\}$  and  $\beta \in ((1/2), 1)$ . According to Lemma 2, the closed-loop error system is finite-time stable. Besides, based on Definition 1, we can obtain that

$$z(t) = 0, \forall t \geq T^* \text{ with } T^* \leq \frac{1}{c(1-\beta)} V^{1-\beta}(z_0), \quad z(t) = 0, \forall t \geq T^*. \tag{38}$$

By the definition of  $z$ ,

$$x_1 - y_r = 0, \quad \forall t > T^*, \tag{39}$$

that is, the tracking error converges to the origin in a finite time. Furthermore, from (38), this implies that  $z$  is bounded. For the boundedness of  $y_r$ ,  $\dot{y}_r$ , and  $\ddot{y}_r$ , it can be obtained that  $\alpha_1$  and states  $x_1, x_2$  are bounded. After that,  $v(t) := LC[-z_1 - c_2 z_2^{2\beta-1} + (1/LC)x_1 + \dot{\alpha}_1]$  is bounded, that is, there exists a positive constant  $E > 0$ , such that  $|v(t)| \leq E$ . Then,  $\mu = (v(t)/E) \in [-1, 1]$ . Let the beginning values of inductor current  $x_1$  and capacitor voltage  $x_2$  of circuits be zero, and

choose design parameters  $c_1, c_2$  appropriately; we can get  $\mu(t) \in [0, 1], t \geq 0$ .  $\square$

**4.2. Design of PWM-Based Finite-Time Tracking Controller.** For the switched buck converter (3), there exists an equivalent continuous finite-time state feedback control (34), that is,

$$\mu = \frac{LC}{E} \left[ -z_1 - c_2 z_2^{2\beta-1} + \frac{1}{LC} x_1 + \dot{\alpha}_1 \right] \in [0, 1], t \geq 0, \tag{40}$$

by choosing positive parameters  $E, c_1, c_2$  appropriately. Based on PWM implementation (13) and continuous signal (40), the binary PWM control is designed as

$$\sigma = \sigma_T(t) = \begin{cases} 1, & \mu(t) > u_0(t), \\ 0, & \mu(t) < u_0(t), \end{cases} \tag{41}$$

where  $\sigma$  is the digital switch in the buck converter (3) and  $u_0(t)$  is the triangular wave with period  $T$ .

In order to indicate the proposed PWM-based finite-time tracking control approach more clearly, the control block diagram is shown in Figure 5, where the switching signal  $\sigma(t)$  is generated by the PWM technique comparing equivalent continuous control  $\mu(t)$  with fixed-frequency triangle wave by comparator.

**Theorem 3.** For the switched buck converter (3), if continuous control  $\mu$  (40) is replaced by binary PWM control  $\sigma$  (41), then the closed-loop error systems (27) and (32) with (41) are

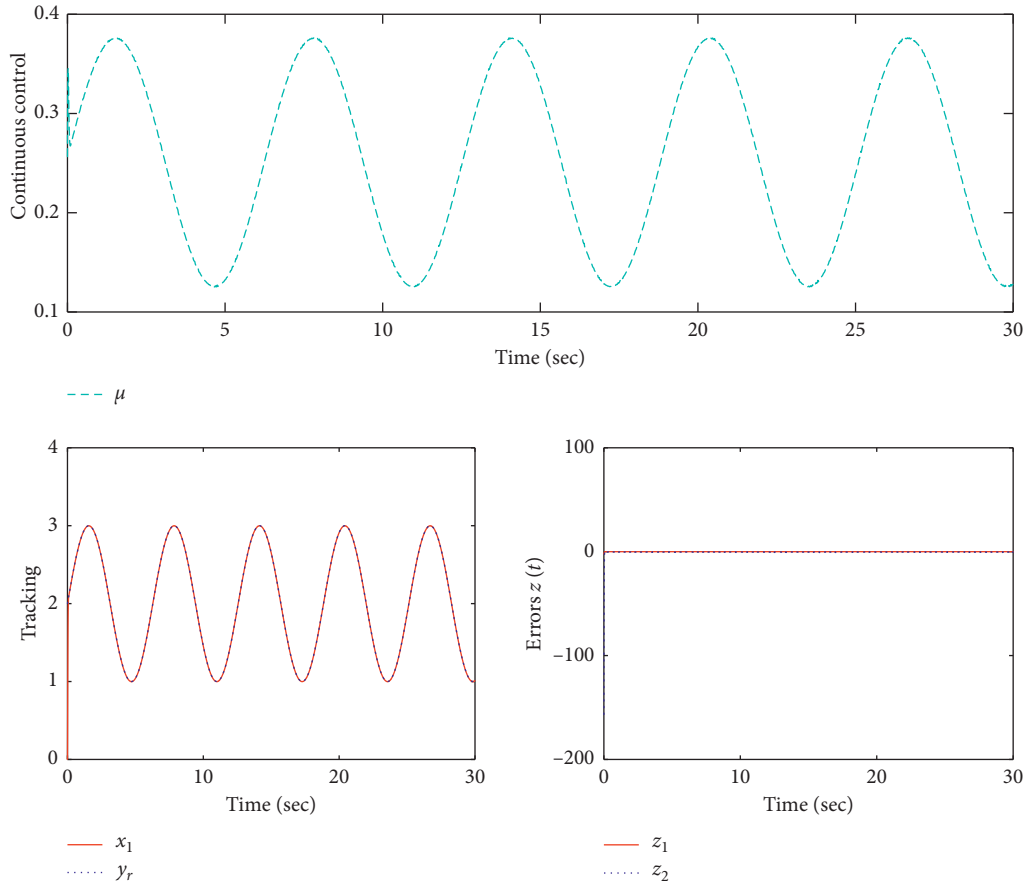


FIGURE 6: The response of closed-loop continuous model (25) with equivalent continuous control (40).

practically finite-time stable. Furthermore, the tracking error can be made arbitrarily small for small enough  $T$ .

*Proof.* According to Theorem 2, the closed-loop error systems (27) and (32) with (40) are finite-time stable. Based on Theorem 1, the closed-loop error systems (27) and (32) with (41) are practically finite-time stable.

Furthermore,  $z_1 = x_1 - y_r$  is a component of states  $z$  of the closed-loop error system; based on Remark 3, when  $T$  is small enough, the tracking error  $x_1 - y_r$  can be made arbitrarily small.  $\square$

*Remark 4.* Finite-time point regulation problem was discussed for continuous average models in [25–27] with the continuous control as a control input. Compared with [25–27], PWM control based on the equivalent control input (i.e., the duty ratio function) is considered for finite-time trajectory tracking of switched power converters in this paper, and here the digital control is the system input.

## 5. Simulation Results

*Example 1.* To investigate the effectiveness of the proposed control method, we give the simulation results as follows.

The corresponding closed-loop systems are considered with two different cases:

- (i) The continuous model (25) based on finite-time state feedback controller (40)
- (ii) The switched buck converter (3) based on PWM-based finite-time tracking (41)

In the simulation, suppose that the output voltage reference for tracking is  $y_r(t) = 2 + \sin t$ ; the circuit parameters are  $E = 8$  V,  $L = 0.2$  H,  $C = 0.001$  F, and  $R = 5$   $\Omega$ ; the initial values are  $x_1(0) = (q_C(0)/C) = 0$  and  $x_2(0) = \dot{q}_L(0) = 0$ ; and the design parameters are  $c_1 = 80$ ,  $c_2 = 80$ ,  $\beta = (99/101)$ , and  $T = 0.001$ .

To make comparisons of simulation results, the two system cases are discussed keeping other parameters intact, respectively. Figures 6 and 7 show the responses of the corresponding closed-loop system with the different cases. Figure 6 implies that the tracking error tends to the origin in a finite time. From Figure 7, it can be learned that the tracking error converges to a small neighborhood of the origin in a finite time. Compared with Figure 6, Figure 7 illustrates the validity of PWM-based finite-time tracking control of the closed-loop system.

## 6. Conclusions

The problem of finite-time tracking for switched buck converters is considered in this paper. PWM-based

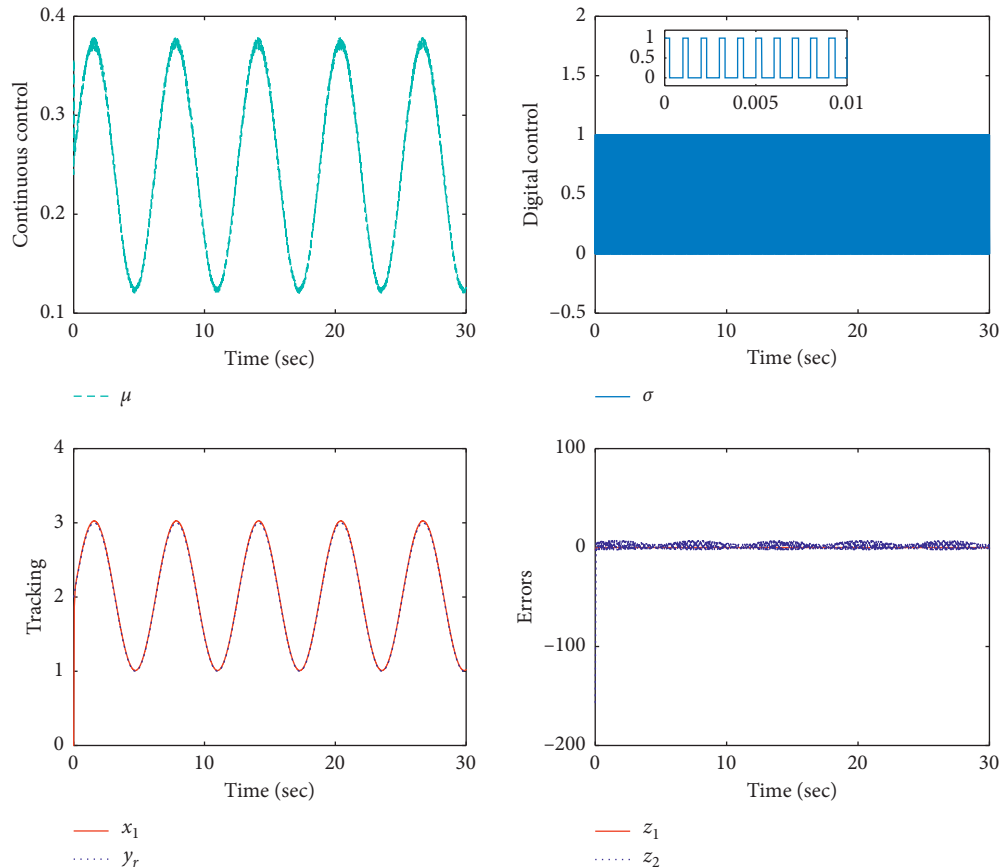


FIGURE 7: The response of closed-loop switched buck converter (3) with PWM control (41).

tracking control with the equivalent control input is proposed for the switched buck converter, such that the tracking error converges to an arbitrarily small neighborhood of the origin in finite time, and the origin of the closed-loop system is practically finite-time stable. Simulation results are given to demonstrate the effectiveness of the proposed schemes.

It is an interesting and challenging direction under current research. The finite-time control method can be further generalized to solve other converters, such as boost converter, buck-boost converter, and Čuk converters; another future research is regarding stochastic PWM control of systems based on random theory [34, 35].

### Data Availability

The data used to support the findings of this study are included within the article.

### Conflicts of Interest

The authors declare that they have no conflicts of interest.

### Acknowledgments

This study was supported by the National Natural Science Foundation of China (61703359, 61773332, and 61673332).

### References

- [1] R. Ortega, A. Loria, P. J. Nicklasson, and H. Sira-Ramirez, *Passivity-based Control of Euler-Lagrange Systems: Mechanical, Electrical and Electromechanical Applications*, Springer-Verlag, Berlin, Germany, 1998.
- [2] J. Alvarez-Ramirez and G. Espinosa-Pérez, "Stability of current-mode control for DC-DC power converters," *Systems & Control Letters*, vol. 45, no. 2, pp. 113–119, 2002.
- [3] W. L. D. Koning, "Digital optimal reduced-order control of pulse-width-modulated switched linear systems," *Automatica*, vol. 39, no. 11, pp. 1997–2003, 2003.
- [4] Y. He and F. L. Luo, "Sliding-mode control for DC-DC converters with constant switching frequency," *Control Theory and Applications*, vol. 153, no. 1, pp. 37–45, 2006.
- [5] G. S. Deaecto, F. S. Garcia, J. A. Pomilio, and J. C. Geromel, "Switched affine systems control design with application to DC-DC converters," *Control Theory & Applications*, vol. 4, no. 7, pp. 1201–1210, 2010.
- [6] H. Rodriguez, R. Ortega, G. Escobar, and N. Barabanov, "A robustly stable output feedback saturated controller for the boost dc-to-dc converter," *Systems & Control Letters*, vol. 40, no. 1, pp. 1–8, 2000.
- [7] R. C. Loxton, K. L. Teo, V. Rehbock, and W. K. Ling, "Optimal switching instants for a switched-capacitor DC/DC power converter," *Automatica*, vol. 45, no. 4, pp. 973–980, 2009.
- [8] R. Cardim, M. C. M. Teixeira, E. Assuncao, and M. R. Covacic, "Variable-structure control design of switched systems with an application to a DC-DC power converter," *IEEE*

- Transactions on Industrial Electronics*, vol. 56, no. 9, pp. 3505–3513, 2009.
- [9] S. C. Tan, Y. M. Lai, and C. K. Tse, “General design issues of sliding mode controllers in DC-DC converters,” *IEEE Transactions on Industrial Electronics*, vol. 55, no. 3, pp. 1160–1174, 2008.
- [10] S. C. Tan, Y. M. Lai, and C. K. Tse, *Sliding Mode Control of Switching Power Converters: Techniques and Implementation*, CRC Press, Boca Raton, FL, USA, 2011.
- [11] G. Liu and C. Zhang, “Sliding mode control of reaction flywheel-based brushless DC motor with buck converter,” *Chinese Journal of Aeronautics*, vol. 26, no. 4, pp. 967–975, 2013.
- [12] V. Utkin, “Sliding mode control of DC/DC converters,” *Journal of the Franklin Institute*, vol. 350, no. 8, pp. 2146–2165, 2013.
- [13] D. Jeltsema and J. M. A. Scherpen, “Tuning of passivity-preserving controllers for switched-mode power converters,” *IEEE Transactions on Automatic Control*, vol. 49, no. 8, pp. 1333–1344, 2004.
- [14] S. Almér, U. Jonsson, C. Chung-Yao Kao, and J. Mari, “Stability analysis of a class of PWM systems,” *IEEE Transactions on Automatic Control*, vol. 52, no. 6, pp. 1072–1078, 2007.
- [15] C.-Y. Chan, “Simplified parallel-damped passivity-based controllers for dc-dc power converters,” *Automatica*, vol. 44, no. 11, pp. 2977–2980, 2008.
- [16] H. Sira-Ramirez, R. A. Perez-moreno, R. Ortega, and M. Garcia-Esteban, “Passivity-based controllers for the stabilization of DC-to-DC power converters,” *Automatica*, vol. 33, no. 4, pp. 499–513, 1997.
- [17] W. He, C. A. Soriano-Rangel, R. Ortega, A. Astolfi, F. Mancilla-David, and S. Li, “Energy shaping control for buck-boost converters with unknown constant power load,” *Control Engineering Practice*, vol. 74, pp. 33–43, 2018.
- [18] J. M. Olm, X. Ros-Oton, and Y. B. Shtessel, “Stable inversion of Abel equations: application to tracking control in DC-DC nonminimum phase boost converters,” *Automatica*, vol. 47, no. 1, pp. 221–226, 2011.
- [19] K. Sundareswaran, V. Devi, S. Peddapati, P. S. R. Nayak, and S. Sankar, “Feedback controller design for a boost converter through evolutionary algorithms,” *IET Power Electronics*, vol. 7, no. 4, pp. 903–913, 2014.
- [20] L. K. Yi, J. Zhao, and D. Ma, “Adaptive backstepping sliding mode nonlinear control for Buck DC/DC switched power converter,” in *Proceedings of the IEEE International Conference on Control and Automation*, Hokkaido, Japan, July 2007.
- [21] L. Fan, Y. Yu, and K. Boshnakov, “Adaptive backstepping based terminal sliding mode control for DC-DC convertor,” in *Proceedings of the International Conference on Computer Application and System Modeling*, Taiyuan, China, October 2010.
- [22] T. K. Nizami and C. Mahanta, “An intelligent adaptive control of DC-DC buck converters,” *Journal of the Franklin Institute*, vol. 353, no. 12, pp. 2588–2613, 2016.
- [23] Z. Wang, S. Li, J. Wang, and Q. Li, “Robust control for disturbed buck converters based on two GPI observers,” *Control Engineering Practice*, vol. 66, pp. 13–22, 2017.
- [24] C.-S. Chiu and C.-T. Shen, “Finite-time control of DC-DC buck converters via integral terminal sliding modes,” *International Journal of Electronics*, vol. 99, no. 5, pp. 643–655, 2012.
- [25] H. Du, Y. Cheng, Y. He, and R. Jia, “Finite-time output feedback control for a class of second-order nonlinear systems with application to DC-DC buck converters,” *Nonlinear Dynamics*, vol. 78, no. 3, pp. 2021–2030, 2014.
- [26] J. Wang, C. Zhang, S. Li, J. Yang, and Q. Li, “Finite-time output feedback control for PWM-based DC-DC Buck power converters of current sensorless mode,” *IEEE Transactions on Control Systems Technology*, vol. 25, no. 4, pp. 1359–1371, 2017.
- [27] Y. Chen, C. Yang, G. Wen, and Y. He, “Adaptive saturated finite-time control algorithm for buck-type DC-DC converter systems,” *International Journal of Adaptive Control and Signal Processing*, vol. 31, no. 10, pp. 1428–1436, 2017.
- [28] S. P. Bhat and D. S. Bernstein, “Finite-time stability of continuous autonomous systems,” *SIAM Journal on Control and Optimization*, vol. 38, no. 5, pp. 751–766, 2000.
- [29] X. Zhang, G. Feng, and Y. Sun, “Finite-time stabilization by state feedback control for a class of time-varying nonlinear systems,” *Automatica*, vol. 48, no. 3, pp. 499–504, 2012.
- [30] Z. Zhu, Y. Xia, and M. Fu, “Attitude stabilization of rigid spacecraft with finite-time convergence,” *International Journal of Robust and Nonlinear Control*, vol. 21, no. 6, pp. 686–702, 2011.
- [31] G. H. Hardy, J. E. Littlewood, and G. Polya, *Inequalities*, Cambridge University Press, Cambridge, UK, 1952.
- [32] H. Sira-Ramirez, “A geometric approach to pulse-width modulated control in nonlinear dynamical systems,” *IEEE Transactions on Automatic Control*, vol. 34, no. 2, pp. 184–187, 1989.
- [33] D. M. Mitchell, *Switching Regulator Analysis*, McGraw-Hill, New York, NY, USA, 1998.
- [34] T. Jiao, G. Zong, and C. K. Ahn, “Noise-to-state practical stability and stabilization of random neural networks,” *Nonlinear Dynamics*, vol. 100, no. 3, pp. 2469–2481, 2020.
- [35] T. C. Jiao, W. X. Zheng, and S. Y. Xu, “Unified stability criteria of random nonlinear time-varying impulsive switched systems,” *IEEE Transactions on Circuits and Systems I: Regular Papers*, Piscataway, NJ, USA, April 2020.



## Research Article

# The Optimal Pricing of Dual-Channel Supply Chain with the Third Party Product Recovery and Sales Effort

Limin Wang <sup>1</sup>, Qiankun Song <sup>2</sup>, and Zhenjiang Zhao <sup>3</sup>

<sup>1</sup>School of Economic and Management, Chongqing Jiaotong University, Chongqing 400074, China

<sup>2</sup>Department of Mathematics, Chongqing Jiaotong University, Chongqing 400074, China

<sup>3</sup>Department of Mathematics, Huzhou University, Huzhou 313000, China

Correspondence should be addressed to Qiankun Song; [qiankunsong@163.com](mailto:qiankunsong@163.com)

Received 25 April 2020; Accepted 9 June 2020; Published 25 June 2020

Guest Editor: Xiaodi Li

Copyright © 2020 Limin Wang et al. This is an open access article distributed under the Creative Commons Attribution License, which permits unrestricted use, distribution, and reproduction in any medium, provided the original work is properly cited.

The optimal pricing of dual-channel supply chain with the third party product recovery and sales effort is considered in this paper. The optimal selling pricing of direct channel and retail channel in the forward supply chain and the optimal collection pricing of retail channel and the third party in the backward supply chain are given for the general case under the centralized and decentralized model. Then, the effect of sales effort of the retailer and the optimal pricing strategy with sales effort under the centralized and decentralized model are provided and analyzed. Finally, the comparative analysis of four situations is carried out by numerical results.

## 1. introduction

In order to improve the utilization rate of resources and reduce environmental pollution, many enterprises are engaged in remanufacturing [1–4]. With the development of science and technology, products could be used for recycling and restoring their original function. Remanufacturing products could meet expectations of consumers on new products, at the same time, the process of remanufacturing could reduce resource consumption and emissions. Research has shown that, by implementing product remanufacturing strategy, enterprises can save the cost of 40%–65%. This not only saves the raw materials of the new parts but also avoids the waste of the resource [5]. The China Daily reported on January 4, 2018, since China adopted the global ban on the import of waste, the European and American countries faced a garbage crisis. Therefore, recycling and remanufacturing becomes even more important. In addition, due to changes in consumer shopping habits and the environmental protection consciousness enhancement, more and more enterprises would see the remanufacturing as a strategy to expand market share, and many companies have established a remanufacturing system [6–12].

Companies such as Caterpillar, GE Aviation, and Mercedes-Benz have built remanufacturing plants in Shanghai.

Because the remanufacturing has very potent prospect, many independent manufacturers have focused on this area [13–20]. Many of construction equipment retailers are gradually implementing the remanufacturing strategy, as a result the remanufacturing has lower production cost. Therefore, it is one available strategy through discounts to attract consumers when facing competitive threat on the market [21]. It is widely believed that the remanufacturing market activities are more complex than the traditional production and the sales process. For many different characteristics of remanufacturing goods, such as the uncertain sources of the product of supply chain, the process involves the forward and reverse logistics [22]. Therefore, for those who are engaged in remanufacturing enterprise, how to build a profitable closed-loop supply chain to effectively recycle used products should be considered. On the contrary, the distribution of new products and remanufactured products is one of the pressing problems.

Results on remanufacturing recycling dual-channel are less researched in the existing literature. In [23], the presence of competing retailers is considered in the reverse channel.

Recovery system on the management of manufacturers and retailers was modeled and studied. Huang et al. studied the optimal decision of dual recycling channels of the closed-loop supply chain and put forward the macroeconomic regulation and control policy based on the numerical analysis. The authors discussed that the dual recycling channel is more effective than the single recycling channel for more manufacturers [24]. In [25], the authors studied the manufacturer-oriented three reverse-mixed recycling channels of the closed-loop supply chain structure, namely, the manufacturer and retailer mix recycling channels, manufacturer and third-party recycling channels, and retailer and third-party mix recycling channels, coming to a conclusion that the mixture of manufacturers and retailers is the most effective recycling channels.

In real life, the sales effort on the market has become a key factor in determining the selling price [26]. There are many approaches to improve the market demand for products through sales effort, such as providing the bigger shelf space, promotion, and advertising. Many research results about the effect of sales effort on achieving supply chain coordination. Ma et al. discussed the profits of retailer and manufacturer characteristics under different channel strategies and sales effort levels [27]. In [28], the authors predicted a supplier-retailer of agricultural supply chain, including market demand which depends on the sales effort, and provided service.

Based on the above analysis, this paper aims to study the optimal pricing of the dual-channel supply chain with the third-party product recovery and sales effort. First of all, for the general case under the centralized and decentralized model, discuss the optimal selling pricing of the direct channel and retail channel in the forward supply chain and the optimal collection pricing of the retail channel and the third party in the backward supply chain. Then, the optimal pricing strategy with sales effort under the centralized and decentralized model is provided and analyzed. Finally, the comparative analysis of four situations is carried out by numerical results.

The organizational structure of this paper is given as follows. Section 1 is the introduction of this paper; Section 2 is the model description of this paper; Section 3 studies the optimal selling pricing of the direct channel and retail channel in the forward supply chain and the optimal collection pricing of the retail channel and the third party in the backward supply chain; Section 4 discusses the centralized model and decentralized model with sales effort; Section 5 carries out the comparative analysis of four situations by numerical results; Section 6 summarizes the research of this paper.

## 2. Model Description

In this paper, we consider a kind of closed-loop supply chain with a dual channel which consists of three members: one manufacturer, one retailer, and one third party. As shown in Figure 1, in the forward supply chain, the manufacturer produces products at cost  $c_r$  and sells products to consumer by direct channel at price  $p_d$ . The manufacturer sells

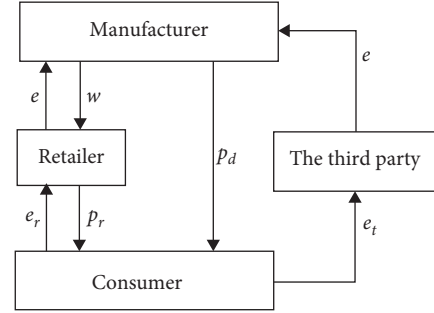


FIGURE 1: The structure of the whole supply chain system.

products to the retailer at wholesale price  $w$  and the retailer sells products to the consumer by the retail channel at price  $p_r$ . In the reverse supply chain, the retailer and the third party collect the used products from the consumer at recycling prices  $e_r$  and  $e_t$ , respectively. The manufacturer recycles the used products for remanufacturing from the retailer and the third party at recycling price of  $e$ .

The manufacturer should make a decision about the price of the direct channel and the wholesale price to the retailer, the retailer makes a decision about the price of the retail channel and the recycling price  $e_r$ , and the third party needs to consider the recycling price  $e_t$  to maximize their own profits, respectively. Throughout this paper, the notations are given as Table 1.

To obtain the main results, we give the following assumptions.

*Assumption 1.* As mentioned in [29], the demand function is considered as one linear function on the direct selling price and retail selling price. Since the influence of the self-price on demand should be larger than the influence of cross price, we assume that  $b_1 > b_2$ .

*Assumption 2.* For the significance of remanufacturing, the unit produce cost of producing new products  $c_n$  and unit produce cost of remanufacturing products  $c_r$  should satisfy that  $c_r + e \leq c_n$ .

*Assumption 3.* Since that the profit of collecting products must be nonnegative for the retailer and third party to guarantee the effectiveness of recycle, there exists  $e_r \leq e$  and  $e_t \leq e$ .

*Assumption 4.* Assume that the collection rate  $\tau$  is a constant number, which means that, for the whole demand function  $D$ ,  $\tau D$  would be remanufactured products and  $(1 - \tau)D$  would be new manufactured products.

*Assumption 5.* In this paper, similar with the market demand functions, the collection functions for the retailer and the third party are considered as linear functions on their collection price. We assume that  $\tau_r = (1 - \alpha)\tau D + \beta_1 e_r - \beta_2 e_t$  and  $\tau_t = \alpha\tau D + \beta_1 e_t - \beta_2 e_r$ , where  $\alpha$  represents the basic market share to the third party,  $\alpha\tau D$  stands for the proportion of consumers' preference for the third party, and

TABLE 1: Table of notations.

Notation	Meaning
$i$	$i = r, d, t$ stands for the retail channel, direct channel, and third party, respectively
$p_i$	Unit selling price of channel $i$ , $i = r, d$
$e$	The collection price from the retailer and third party
$e_i$	The collection price from the consumer through channel $i$ , $i = r, t$
$w$	The wholesale of nongreen product to the retailer
$s$	Sales effort
$b_1$	Self-price demand elasticity coefficient
$b_2$	Cross-price demand elasticity coefficient
$\tau$	Collection rate of products
$\tau_i$	Collection demand of channel $i$ , $i = r, t$
$\beta_i$	Collection demand elasticity coefficient, $i = 1, 2$
$c_n$	Unit produce cost of producing new products
$c_r$	Unit produce cost of remanufacturing products

$(1 - \alpha)\tau$   $D$  stands for the proportion of consumers' preference for the retail channel so that  $\tau_r + \tau_t = \tau$   $D + (\beta_1 - \beta_2)(e_r + e_t)$ .

*Assumption 6.* According to [30], we assume that the collection cost is considered as the quadratic function of the collection rate, which is considered as  $(1/2)k\tau_i^2$  for  $i = r, t$ .

Based on Assumption 1, the demand functions of the retail channel and direct channel are expressed as linear functions of self-price, cross price, and market scale, which are, respectively, shown as follows:

$$\begin{aligned} D_r &= D_1 - b_1 p_r + b_2 p_d, \\ D_d &= D_2 - b_1 p_d + b_2 p_r, \end{aligned} \quad (1)$$

where  $D_1$  stands for the proportion of consumers' preference for the retail channel and  $D_2$  stands for the proportion of consumers' preference for the direct channel.

According to Assumption 5, the collection demand functions of the retail channel and third party channel are expressed as linear functions of self-collecting price, cross-

collecting price, and collecting rate, which are, respectively, shown as follows:

$$\begin{aligned} \tau_r &= (1 - \alpha)\tau \quad D + \beta_1 e_r - \beta_2 e_t, \\ \tau_t &= \alpha\tau \quad D + \beta_1 e_t - \beta_2 e_r, \end{aligned} \quad (2)$$

where  $D = D_1 + D_2$  stands for the potential whole market demand.

Accordingly, based on the above assumptions and demand functions, the profit function of the retailer is considered as follows:

$$\pi_r(p_r, e_r) = D_r(p_r - w) + \tau_r(e - e_r) - \frac{1}{2}k\tau_r^2, \quad (3)$$

where  $D_r(p_r - w)$  stands for the profit of selling products to the consumer by the retail channel and  $\tau_r(e - e_r)$  represents the profit of collecting products from the manufacturer. The collection cost is considered as  $(1/2)k\tau_r^2$ .

Denote that the unit produce cost of remanufacturing products is  $c_r$ ; then, the profit function of the manufacturer is given by

$$\pi_d(w, p_d) = D_r w + D_d p_d - [(1 - \tau)D - (\beta_1 - \beta_2)(e_r + e_t)]c_n - [\tau \quad D + (\beta_1 - \beta_2)(e_r + e_t)](c_r + e), \quad (4)$$

where the  $D_r w$  and  $D_d p_d$  represents the profit of selling products to the consumer by the retail channel and direct channel, respectively.  $[(1 - \tau)D - (\beta_1 - \beta_2)(e_r + e_t)]c_n$  denotes the producing cost for new products and  $[\tau \quad D + (\beta_1 - \beta_2)(e_r + e_t)](c_r + e)$  stands for the recycling and remanufacturing cost for the collected products.

The collection cost of the third party is considered as  $(1/2)k\tau_t^2$  so that the profit function of the third party is presented as

$$\pi_t(e_t) = \tau_t(e - e_t) - \frac{1}{2}k\tau_t^2. \quad (5)$$

### 3. Equilibrium Analysis

*3.1. Centralized Model.* In the centralized model, all members of the supply chain system cooperatively make a decision on the unit selling price of the retail channel and direct channel and the collection price from the consumer. The profit of the whole supply chain is expressed as

$$\begin{aligned}
\pi_{sc}(p_r, p_d, e_r, e_t) &= D_r p_r + D_d p_d + (\beta_1 - \beta_2)(e_r + e_t)(c_n - c_r) - (1 - \tau) D c_n \\
&\quad - \tau D c_r - \tau_r e_r - \tau_t e_t - \frac{1}{2} k \tau_r^2 - \frac{1}{2} k \tau_t^2 \\
&= (D_1 - b_1 p_r + b_2 p_d) p_r + (D_2 - b_1 p_d + b_2 p_r) p_d + (\beta_1 - \beta_2)(e_r + e_t)(c_n - c_r) \\
&\quad - (1 - \tau) D c_n - \tau D c_r - [(1 - \alpha) \tau D + \beta_1 e_r - \beta_2 e_t] e_r - (\alpha \tau D + \beta_1 e_t - \beta_2 e_r) e_t \\
&\quad - \frac{1}{2} k [(1 - \alpha) \tau D + \beta_1 e_r - \beta_2 e_t]^2 - \frac{1}{2} k (\alpha \tau D + \beta_1 e_t - \beta_2 e_r)^2.
\end{aligned} \tag{6}$$

**Proposition 1.** When the market is under centralized situation, if the parameters satisfy that

$(2\beta_1 + k\beta_1^2 + k\beta_2^2) - 2\beta_2(1 + k\beta_1) > 0$ , then there exists the unique optimal solution:

$$\begin{aligned}
p_r^{c1*} &= \frac{b_1 D_1 + b_2 D_2}{2(b_1^2 - b_2^2)}, \\
p_d^{c1*} &= \frac{b_2 D_1 + b_1 D_2}{2(b_1^2 - b_2^2)}, \\
e_r^{c1*} &= \frac{(2\beta_1 + k\beta_1^2 + k\beta_2^2)[(\beta_1 - \beta_2)(c_n - c_r) + k\beta_2 \alpha \tau D - (1 + k\beta_1)(1 - \alpha) \tau D] + 2\beta_2(1 + k\beta_1)[(\beta_1 - \beta_2)(c_n - c_r) + k\beta_2(1 - \alpha) \tau D - (1 + k\beta_1) \alpha \tau D]}{(2\beta_1 + k\beta_1^2 + k\beta_2^2)^2 - 4\beta_2^2(1 + k\beta_1)^2}, \\
e_t^{c1*} &= \frac{(2\beta_1 + k\beta_1^2 + k\beta_2^2)[(\beta_1 - \beta_2)(c_n - c_r) + k\beta_2(1 - \alpha) \tau D - (1 + k\beta_1) \alpha \tau D] + 2\beta_2(1 + k\beta_1)[(\beta_1 - \beta_2)(c_n - c_r) + k\beta_2 \alpha \tau D - (1 + k\beta_1)(1 - \alpha) \tau D]}{(2\beta_1 + k\beta_1^2 + k\beta_2^2)^2 - 4\beta_2^2(1 + k\beta_1)^2}.
\end{aligned} \tag{7}$$

*Proof.* According to the profit function of whole supply chain (6), taking the first-order derivatives of  $\pi_{sc}(p_r, p_d, e_r, e_t)$  along the retail price  $p_r$ , the direct price  $p_d$ ,

the collecting price of retailer  $e_r$ , and the collecting price of the third party  $e_t$ , we could obtain

$$\begin{aligned}
\frac{\partial \pi_{sc}(p_r, p_d, e_r, e_t)}{\partial p_r} &= -2b_1 p_r + 2b_2 p_d + D_1, \\
\frac{\partial \pi_{sc}(p_r, p_d, e_r, e_t)}{\partial p_d} &= 2b_2 p_r - 2b_1 p_d + D_2, \\
\frac{\partial \pi_{sc}(p_r, p_d, e_r, e_t)}{\partial e_r} &= -(2\beta_1 + k\beta_1^2 + k\beta_2^2) + 2\beta_2(1 + k\beta_1)e_t + (\beta_1 - \beta_2)(c_n - c_r) + k\beta_2 \alpha \tau D - (1 + k\beta_1)(1 - \alpha) \tau D, \\
\frac{\partial \pi_{sc}(p_r, p_d, e_r, e_t)}{\partial e_t} &= 2\beta_2(1 + k\beta_1)e_r - (2\beta_1 + k\beta_1^2 + k\beta_2^2)e_t + (\beta_1 - \beta_2)(c_n - c_r) + k\beta_2(1 - \alpha) \tau D - (1 + k\beta_1) \alpha \tau D.
\end{aligned} \tag{8}$$

Hence, the Hessian matrix is given as

$$H^{c1} = \begin{pmatrix} -2b_1 & 2b_2 & 0 & 0 \\ 2b_2 & -2b_1 & 0 & 0 \\ 0 & 0 & -2\beta_1 - k\beta_1^2 - k\beta_2^2 & 2\beta_2(1 + k\beta_1) \\ 0 & 0 & 2\beta_2(1 + k\beta_1) & -2\beta_1 - k\beta_1^2 - k\beta_2^2 \end{pmatrix}. \tag{9}$$

Obviously, the second derivative satisfies that  $\partial^2 \pi_{sc}(p_r, p_d, e_r, e_t) / \partial p_r^2 = \partial^2 \pi_{sc}(p_r, p_d, e_r, e_t) / \partial p_d^2 = -2b_1 < 0$ . Based on the condition of proposition,  $(2\beta_1 + k\beta_1^2 + k\beta_2^2) - 2\beta_2(1 + k\beta_1) > 0$ , it could be obtained that  $(2\beta_1 + k\beta_1^2 + k\beta_2^2)^2 - 4\beta_2^2(1 + k\beta_1)^2 > 0$ . Therefore, the profit function  $\pi_{sc}(p_r, p_d, e_r, e_t)$  is joint concave on  $p_r, p_d, e_r$ , and  $e_t$ . The optimal solution could be obtained by solving the first-order condition. The proof is completed.

*Remark 1.* Proposition 1 shows the optimal solution under centralized situation. According to the result of Proposition 1, it could be concluded that the retail selling price and direct selling price are related with the values of  $D_1$  and  $D_2$ . Under the assumption that  $D_1 = (1 - \rho)a$  and  $D_2 = \rho a$ , we could find  $p_r^c > p_d^c$  if  $0 < \rho < 0.5$  and  $p_r^c < p_d^c$  if  $0.5 < \rho < 1$ . It demonstrates that the channel has higher selling price when the channel occupies higher market share. Furthermore, if  $\alpha = 0.5$ , then  $e_r^{c1*} = e_t^{c1*} = ((2\beta_1 + k\beta_1^2 + k\beta_2^2 + 2\beta_2$

$(1 + k\beta_1)) [(\beta_1 - \beta_2)(c_n - c_r) + 0.5k\beta_2\tau - D - 0.5(1 + k\beta_1)\tau - D] / (2\beta_1 + k\beta_1^2 + k\beta_2^2)^2 - 4\beta_2^2(1 + k\beta_1)^2$ ). It shows that, under the centralized decision model, if the potential demand of the retailer and the third party for the recycled products was equal, there is no competitive relationship on the behavior of the recycled products, and the price of the recycled products is consistent.

*3.2. Decentralized Model.* This section considers that manufacturers, retailers, and third parties, respectively, make sales pricing decisions and collection pricing decisions to maximize their respective profits. Consider the supply chain under the manufacturer-led Stackelberg model. According to the profit function of retailer (3), profit function of manufacturer (4), and profit function of third party (5), it has

$$\pi_r(p_r, e_r) = (D_1 - b_1 p_r + b_2 p_d)(p_r - w) + [(1 - \alpha)\tau - D + \beta_1 e_r - \beta_2 e_t](e - e_r) - \frac{1}{2}k[(1 - \alpha)\tau - D + \beta_1 e_r - \beta_2 e_t]^2, \quad (10)$$

$$\pi_d(p_d, w) = (D_1 - b_1 p_r + b_2 p_d)w + (D_2 - b_1 p_r + b_2 p_d)p_d + (\beta_1 - \beta_2)(c_n - c_r - e)(e_r + e_t) - (1 - \tau)Dc_n - \tau - D(c_r + e), \quad (11)$$

$$\pi_t(e_t) = (\alpha\tau - D + \beta_1 e_t - \beta_2 e_r)(e - e_t) - \frac{1}{2}k(\alpha\tau - D + \beta_1 e_t - \beta_2 e_r)^2. \quad (12)$$

**Proposition 2.** When the market is under decentralized situation, if the parameters of supply chain (10)–(12) satisfy

the condition of  $\beta_1^2(2 + k\beta_1)^2 - \beta_2^2(1 + k\beta_1)^2 > 0$ , then there exists the unique optimal solution:

$$\begin{aligned} p_r^{d1*} &= \frac{3b_1^2 D_1 - b_2^2 D_1 + 2b_1 b_2 D_2}{4b_1 D_1 (b_1^2 - b_2^2)}, \\ p_d^{d1*} &= \frac{b_2 D_1 + b_1 D_2}{2(b_1^2 - b_2^2)}, \\ e_r^{d1*} &= \frac{\beta_1(2 + k\beta_1)[\beta_1 e - (1 + k\beta_1)(1 - \alpha)\tau - D] + \beta_2(1 + k\beta_1)[\beta_1 e - (1 + k\beta_1)\alpha\tau - D]}{\beta_1^2(2 + k\beta_1)^2 - \beta_2^2(1 + k\beta_1)^2}, \\ e_t^{d1*} &= \frac{\beta_1(2 + k\beta_1)[\beta_1 e - (1 + k\beta_1)\alpha\tau - D] + \beta_2(1 + k\beta_1)[\beta_1 e - (1 + k\beta_1)(1 - \alpha)\tau - D]}{\beta_1^2(2 + k\beta_1)^2 - \beta_2^2(1 + k\beta_1)^2}. \end{aligned} \quad (13)$$

*Proof.* For the retailer and the third party, according to the profit functions of the retailer and the third party (10) and (12), taking the first-order derivatives of  $\pi_r(p_r, e_r)$  and

$\pi_t(e_t)$  along the retail price  $p_r$ , the collecting price of retailer  $e_r$ , and the collecting price of the third party  $e_t$ , respectively, we could obtain

$$\begin{aligned}\frac{\partial \pi_r(p_r, e_r)}{\partial p_r} &= -2b_1 p_r + b_2 p_d + b_1 w + D_1, \\ \frac{\partial \pi_r(p_r, e_r)}{\partial e_r} &= -\beta_1(2 + k\beta_1)e_r + \beta_2(1 + k\beta_1)e_t + \beta_1 e - (1 + k\beta_1)(1 - \alpha)\tau \quad D, \\ \frac{\partial \pi_t(e_t)}{\partial e_t} &= \beta_2(1 + k\beta_1)e_r - \beta_1(2 + k\beta_1)e_t + \beta_1 e - (1 + k\beta_1)\alpha\tau \quad D.\end{aligned}\tag{14}$$

Hence, the Hessian matrix is given as

$$H^{d1} = \begin{pmatrix} -2b_1 & 0 & 0 \\ 0 & -\beta_1(2 + k\beta_1) & \beta_2(1 + k\beta_1) \\ 0 & \beta_2(1 + k\beta_1) & -\beta_1(2 + k\beta_1) \end{pmatrix}.\tag{15}$$

Obviously, the second derivative satisfies that  $(\partial^2 \pi_r(p_r, e_r)/\partial p_r^2) = -2b_1 < 0$  and  $(\partial^2 \pi_t(e_t)/\partial e_t^2) = (\partial^2 \pi_r$

$(p_r, e_r)/\partial e_r^2) = -\beta_1(2 + k\beta_1) < 0$ . Based on the condition of proposition,  $\beta_1^2(2 + k\beta_1)^2 - \beta_2^2(1 + k\beta_1)^2 > 0$ . Therefore, the profit functions  $\pi_r(p_r, e_r)$  and  $\pi_t(e_t)$  are joint concave on  $p_r$ ,  $e_r$ , and  $e_t$ . The optimal solution could be obtained by solving the first-order condition as follows:

$$\begin{aligned}p_r^{d1*} &= \frac{1}{2b_1}(b_2 p_d + b_1 w + D_1), \\ e_r^{d1*} &= \frac{\beta_1(2 + k\beta_1)[\beta_1 e - (1 + k\beta_1)(1 - \alpha)\tau \quad D] + \beta_2(1 + k\beta_1)[\beta_1 e - (1 + k\beta_1)\alpha\tau \quad D]}{\beta_1^2(2 + k\beta_1)^2 - \beta_2^2(1 + k\beta_1)^2}, \\ e_t^{d1*} &= \frac{\beta_1(2 + k\beta_1)[\beta_1 e - (1 + k\beta_1)\alpha\tau \quad D] + \beta_2(1 + k\beta_1)[\beta_1 e - (1 + k\beta_1)(1 - \alpha)\tau \quad D]}{\beta_1^2(2 + k\beta_1)^2 - \beta_2^2(1 + k\beta_1)^2}.\end{aligned}\tag{16}$$

Substitute the  $p_r^{d1*}$ ,  $e_r^{d1*}$ , and  $e_t^{d1*}$  into profit function (10), and it obtains

$$\begin{aligned}\pi_d(p_d, w) &= \left[ D_2 - b_1 p_d + \frac{b_2}{2b_1}(b_2 p_d + b_1 w + D_1) \right] p_d + \frac{1}{2}(b_2 p_d + b_1 w + D_1)w \\ &\quad + (\beta_1 - \beta_2)(c_n - c_r - e)(e_r + e_t) - (1 - \tau)Dc_n - \tau \quad D(c_r + e).\end{aligned}\tag{17}$$

For the manufacturer, taking the first-order derivatives of  $\pi_d(p_d, w)$  along the direct price  $p_d$  and wholesale price  $w$ , we could obtain

$$\frac{\partial \pi_d(p_d, w)}{\partial p_d} = \left( -2b_1 + \frac{b_2^2}{b_1} \right) p_d + b_2 w + D_2 + \frac{b_2 D_1}{2b_1},\tag{18}$$

$$\frac{\partial \pi_d(p_d, w)}{\partial w} = b_2 p_d - b_1 w + \frac{D_1}{2}.$$

The Hessian matrix is given as

$$H_1^{d1} = \begin{pmatrix} -2b_1 + \frac{b_2^2}{b_1} & b_2 \\ b_2 & -b_1 \end{pmatrix}.\tag{19}$$

Obviously, the second derivative satisfies that  $(\partial^2 \pi_d(p_d, w)/\partial p_d^2) = -2b_1 + (b_2^2/b_1) < 0$ ,  $(\partial^2 \pi_d(p_d, w)/\partial w^2) = -b_1 < 0$ , and  $|H_1^{d1}| = 2(b_1^2 - b_2^2) > 0$ . Therefore, the profit function  $\pi_d(p_d, w)$  is joint concave on  $p_d$  and  $w$ . The optimal solution could be obtained by solving the first-order condition as follows:

$$p_d^{d1*} = \frac{b_2 D_1 + b_1 D_2}{2(b_1^2 - b_2^2)},\tag{20}$$

$$w^{1*} = \frac{b_2^2 D_1 + b_1 b_2 D_2}{2b_1(b_1^2 - b_2^2)} + \frac{D_1}{2b_1}.$$

The proof is completed.

According to the conclusion of Proposition 2, in the decentralized model, the wholesale price of the

manufacturer to retailers is the same as the retail selling price of traditional channels in the centralized model, that is,  $w^{2*} = p_r^{c1*}$ , which leads to higher selling prices for retailers under the decentralized model. As for the collection price, the result shows the collection price under the centralized model is higher than the collection price under decentralized model for  $e_r^{c1*} > e_r^{d1*}$  and  $e_t^{c1*} > e_t^{d1*}$ .  $\square$

#### 4. The Optimization on Sales Effort

The decision on sales effort of the retailer is considered in this section. In practical application, the sales effort on the market has become a key factor of the retail price. More examples show that the demand function depends on sales effort. Taylor points out that the retailer's sales effort service (mainly sales work, includes providing space or shelf space, promotion, and advertising) increases the demand for products, and the results demonstrated how to realize supply chain coordination through the sales and service effect [26]. Therefore, this section discusses and compares

the optimal pricing and optimal profit with sales effort of the retailer.

Denote the sales effort of the retailer as  $s$ ; then, the demand functions of dual channels are expressed as follows:

$$\begin{aligned}\widehat{D}_r &= D_1 - b_1 p_r + b_2 p_d + g_1 s, \\ \widehat{D}_d &= D_2 - b_1 p_d + b_2 p_r + g_2 s.\end{aligned}\quad (21)$$

Based on the demand functions, the profit function of the retailer is

$$\widehat{\pi}_r(p_r, e_r) = \widehat{D}_r(p_r - w) + \widehat{\tau}_r(e - e_r) - \frac{1}{2}k\widehat{\tau}^2 - \frac{1}{2}\eta s^2, \quad (22)$$

where  $\widehat{D}_r(p_r - w)$  is the profit of selling products by the retail channel and  $\widehat{\tau}_r(e - e_r)$  is the profit of collection products from consumers,  $(1/2)k\widehat{\tau}^2$  is the cost of collection products, and  $(1/2)\eta s^2$  is the cost of sales effort.

The profit function of the manufacturer is

$$\widehat{\pi}_d(w, p_d) = \widehat{D}_r w + \widehat{D}_d p_d + (\beta_1 - \beta_2)(c_n - c_r - e)(e_r + e_t) - (1 - \tau)Dc_n - \tau D(c_r + e), \quad (23)$$

where  $\widehat{D}_r w$  is the profit of the retail channel,  $\widehat{D}_d p_d$  is the profit of the direct channel,  $(1 - \tau)Dc_n$  is the production cost of the new product, and  $\tau D(c_r + e)$  is the production cost of the remanufactured product. The profit function of the third party is

$$\pi_t(e_t) = \tau_t(e - e_t) - \frac{1}{2}k\tau_t^2. \quad (24)$$

*4.1. Centralized Model with Sales Effort.* According to the profit functions of the retailer, manufacturer, and third party (22)–(24), the profit of the whole supply chain is expressed as

$$\begin{aligned}\widehat{\pi}_{sc}(p_r, p_d, e_r, e_t) &= D_r p_r + D_d p_d + (\beta_1 - \beta_2)(c_n - c_r)(e_r + e_t) - (1 - \tau)Dc_n \\ &\quad - \tau Dc_r - \tau_r e_r - \tau_t e_t - \frac{1}{2}k\tau_r^2 - \frac{1}{2}k\tau_t^2 \\ &= (D_1 - b_1 p_r + b_2 p_d + g_1 s)p_r + (D_2 - b_1 p_d + b_2 p_r + g_2 s)p_d \\ &\quad - (1 - \tau)Dc_n - \tau Dc_r - [(1 - \alpha)\tau D + \beta_1 e_r - \beta_2 e_t]e_r \\ &\quad - [\alpha\tau D + \beta_1 e_t - \beta_2 e_r]e_t - \frac{1}{2}k[(1 - \alpha)\tau D + \beta_1 e_r - \beta_2 e_t]^2 \\ &\quad - \frac{1}{2}k[\alpha\tau D + \beta_1 e_t - \beta_2 e_r]^2 - \frac{1}{2}\eta s^2.\end{aligned}\quad (25)$$

**Proposition 3.** When the market is under centralized situation with sales effort, if the parameters of (25) satisfy that  $2b_1^2\eta - 2b_2g_1g_2 - b_1(g_1^2 + g_2^2) - 2b_2^2\eta > 0$ , then there exists the unique optimal solution under the centralized model with sales effort:

$$\begin{aligned}
p_r^{c2*} &= \frac{b_1D_1 + b_2D_2}{2(b_1^2 - b_2^2)} + \frac{(b_1g_1 + b_2g_2)[(b_1D_1 + b_2D_2)g_1 + (b_1D_2 + b_2D_1)g_2]}{2(b_1^2 - b_2^2)[2\eta(b_1^2 - b_2^2) - (b_1g_1 + b_2g_2)g_1 - (b_1g_2 + b_2g_1)g_2]}, \\
p_d^{c2*} &= \frac{b_1D_2 + b_2D_1}{2(b_1^2 - b_2^2)} + \frac{(b_1g_2 + b_2g_1)[(b_1D_1 + b_2D_2)g_1 + (b_1D_2 + b_2D_1)g_2]}{2(b_1^2 - b_2^2)[2\eta(b_1^2 - b_2^2) - (b_1g_1 + b_2g_2)g_1 - (b_1g_2 + b_2g_1)g_2]}, \\
e_r^{c2*} &= \frac{(2\beta_1 + k\beta_1^2 + k\beta_2^2)[(\beta_1 - \beta_2)(c_n - c_r) + k\beta_2\alpha\tau \quad D - (1 + k\beta_1)(1 - \alpha)\tau \quad D] + 2\beta_2(1 + k\beta_1)[(\beta_1 - \beta_2)(c_n - c_r) + k\beta_2(1 - \alpha)\tau \quad D - (1 + k\beta_1)\alpha\tau \quad D]}{(2\beta_1 + k\beta_1^2 + k\beta_2^2)^2 - 4\beta_2^2(1 + k\beta_1)^2}, \\
e_t^{c2*} &= \frac{(2\beta_1 + k\beta_1^2 + k\beta_2^2)[[(\beta_1 - \beta_2)(c_n - c_r) + k\beta_2(1 - \alpha)\tau \quad D - (1 + k\beta_1)\alpha\tau \quad D]] + 2\beta_2(1 + k\beta_1)[(\beta_1 - \beta_2)(c_n - c_r) + k\beta_2\alpha\tau \quad D - (1 + k\beta_1)(1 - \alpha)\tau \quad D]}{(2\beta_1 + k\beta_1^2 + k\beta_2^2)^2 - 4\beta_2^2(1 + k\beta_1)^2}, \\
s^{c2*} &= \frac{(b_1D_1 + b_2D_2)g_1 + (b_1D_2 + b_2D_1)g_2}{2\eta(b_1^2 - b_2^2) - (b_1g_1 + b_2g_2)g_1 - (b_1g_2 + b_2g_1)g_2}.
\end{aligned} \tag{26}$$

*Proof.* According to the profit function of the whole supply chain with sales effort (25), taking the first-order derivatives of  $\hat{\pi}_{sc}(p_r, p_d, e_r, e_t, s)$  along the retail price  $p_r$ , the direct

price  $p_d$ , the collecting price of retailer  $e_r$ , the collecting price of the third party  $e_t$ , and the sales effort  $s$ , we could obtain

$$\frac{\partial \hat{\pi}_{sc}(p_r, p_d, e_r, e_t, s)}{\partial p_r} = -2b_1p_r + 2b_2p_d + d_1 + g_1s,$$

$$\frac{\partial \hat{\pi}_{sc}(p_r, p_d, e_r, e_t, s)}{\partial p_d} = 2b_2p_r - 2b_1p_d + d_2 + g_2s,$$

$$\frac{\partial \hat{\pi}_{sc}(p_r, p_d, e_r, e_t, s)}{\partial s} = g_1p_r + g_2p_d - \eta s,$$

$$\frac{\partial \hat{\pi}_{sc}(p_r, p_d, e_r, e_t, s)}{\partial e_r} = -(2\beta_1 + k\beta_1^2 + k\beta_2^2)e_r + 2\beta_2(1 + k\beta_1)e_t + (\beta_1 - \beta_2)(c_n - c_r) + k\beta_2\alpha\tau \quad D - (1 + k\beta_1)(1 - \alpha)\tau \quad D,$$

$$\frac{\partial \hat{\pi}_{sc}(p_r, p_d, e_r, e_t, s)}{\partial e_t} = 2\beta_2(1 + k\beta_1)e_r - (2\beta_1 + k\beta_1^2 + k\beta_2^2)e_t + (\beta_1 - \beta_2)(c_n - c_r) + k\beta_2(1 - \alpha)\tau \quad D - (1 + k\beta_1)\alpha\tau \quad D.$$

(27)

Hence, the Hessian matrix is given as

$$H^{c2} = \begin{pmatrix} -2b_1 & 2b_2 & g_1 \\ 2b_2 & -2b_1 & g_2 \\ g_1 & g_2 & -\eta \end{pmatrix}. \tag{28}$$

Obviously, the second derivative satisfies that  $(\partial^2 \hat{\pi}_{sc}(p_r, p_d, e_r, e_t, s)/\partial p_r^2) = (\partial^2 \hat{\pi}_{sc}(p_r, p_d, e_r, e_t, s)/\partial p_d^2) = -2b_1 < 0$  and  $(\partial^2 \hat{\pi}_{sc}(p_r, p_d, e_r, e_t, s)/\partial s^2) = -\eta < 0$ . Based on the condition of proposition,  $4b_2(2\beta_1 + k\beta_1^2 + k\beta_2^2) - 2\beta_2(1 + k\beta_1) > 0$ , it could be obtained that  $|H^{c2}| = -4b_1^2\eta + 4b_2g_1g_2 + 2b_1(g_1^2 + g_2^2) + 4b_2^2\eta < 0$ . Therefore, the profit function  $\hat{\pi}_{sc}(p_r, p_d, e_r, e_t, s)$  is joint concave on  $p_r, p_d, e_r, e_t$ , and  $s$ . The optimal solution could be obtained by solving the first-order condition:

$$p_r^{c2*} = \frac{b_1D_1 + b_2D_2}{2(b_1^2 - b_2^2)} + \frac{b_1g_1 + b_2g_2}{2(b_1^2 - b_2^2)} s^{c2*},$$

$$p_d^{c2*} = \frac{b_1D_2 + b_2D_1}{2(b_1^2 - b_2^2)} + \frac{b_1g_2 + b_2g_1}{2(b_1^2 - b_2^2)} s^{c2*},$$

$$s^{c2*} = \frac{(b_1D_1 + b_2D_2)g_1 + (b_1D_2 + b_2D_1)g_2}{2\eta(b_1^2 - b_2^2) - (b_1g_1 + b_2g_2)g_1 - (b_1g_2 + b_2g_1)g_2}. \tag{29}$$

The proof is completed.

According to Propositions 1 and 3, the optimal solution of the centralized model with and without sales effort could be obtained:



$$p_r^{c2*} - p_r^{c1*} = \frac{(b_1g_1 + b_2g_2)[(b_1D_1 + b_2D_2)g_1 + (b_1D_2 + b_2D_1)g_2]}{2(b_1^2 - b_2^2)[2\eta(b_1^2 - b_2^2) - (b_1g_1 + b_2g_2)g_1 - (b_1g_2 + b_2g_1)g_2]} > 0, \quad (30)$$

$$p_d^{c2*} - p_d^{c1*} = \frac{(b_1g_2 + b_2g_1)[(b_1D_1 + b_2D_2)g_1 + (b_1D_2 + b_2D_1)g_2]}{2(b_1^2 - b_2^2)[2\eta(b_1^2 - b_2^2) - (b_1g_1 + b_2g_2)g_1 - (b_1g_2 + b_2g_1)g_2]} 0.$$

It indicates that the cost of sales effort brings higher selling price, and the increased part is proportional to the sales effort:  $p_r^{c2*} - p_r^{c1*} = (b_1g_1 + b_2g_2/2(b_1^2 - b_2^2))s^{c2*}$  and  $p_d^{c2*} - p_d^{c1*} = (b_1g_2 + b_2g_1/2(b_1^2 - b_2^2))s^{c2*}$ .  $\square$

**4.2. Decentralized Model with Sales Effort.** This section considers that manufacturers, retailers, and third parties,

respectively, make sales pricing decisions and collection pricing decisions to maximize their respective profits under the decentralized model with sales effort. Consider the supply chain under the manufacturer-led Stackelberg model. According to the profit function of retailer (22), profit function of manufacturer (23), and profit function of the third party (24), it has

$$\begin{aligned} \hat{\pi}_r(p_r, e_r, s) &= (D_1 - b_1p_r + b_2p_d + g_1s)(p_r - w) + [(1 - \alpha)\tau D + \beta_1e_r - \beta_2e_t] \\ &\quad \cdot (e - e_r) - \frac{1}{2}k[(1 - \alpha)\tau D + \beta_1e_r - \beta_2e_t]^2 - \frac{1}{2}\eta s^2, \end{aligned} \quad (31)$$

$$\begin{aligned} \hat{\pi}_d(w, p_d) &= (D_1 - b_1p_r + b_2p_d + g_1s)w + (D_2 - b_1p_d + b_2p_r + g_2s)p_d \\ &\quad + (\beta_1 - \beta_2)(c_n - c_r - e)(e_r + e_t) - (1 - \tau)Dc_n - \tau D(c_r + e), \end{aligned} \quad (32)$$

$$\hat{\pi}_t(e_t) = (\alpha\tau D + \beta_1e_t - \beta_2e_r)(e - e_t) - \frac{1}{2}k(\alpha\tau D + \beta_1e_t - \beta_2e_r)^2. \quad (33)$$

**Proposition 4.** When the market is under the decentralized model with sales effort, if the parameters of supply chain (31)–(33) satisfy the condition of  $2b_1\eta - g_1^2 > 0$  and

$4b_1^2\eta[(2b_1^2 - b_2^2)\eta - b_1g_1^2 - b_2g_1g_2] - (2b_1b_2\eta - b_2g_1^2 - b_1g_1g_2)^2 > 0$ , then there exists the unique optimal solution:

$$\begin{aligned} p_r^{d2*} &= \frac{b_2\eta(2b_1^2\eta\phi + D_1b_1\eta\phi) + (b_1\eta w - g_1^2)(2D_1b_1\eta\kappa + \phi\phi)}{(2b_1\eta - g_1^2)(4b_1^2\eta\kappa - \phi^2)} + \frac{D_1\eta}{2b_1\eta - g_1^2}, \\ s^{d2*} &= \frac{b_2g_1(2b_1^2\eta\phi + D_1b_1\eta\phi) - b_1g_1(2D_1b_1\eta\kappa + \phi\phi)}{(2b_1\eta - g_1^2)(4b_1^2\eta\kappa - \phi^2)} + \frac{D_1g_1}{2b_1\eta - g_1^2}, \\ p_d^{d2*} &= \frac{2b_1^2\eta\phi + D_1b_1\eta\phi}{4b_1^2\eta\kappa - \phi^2}, \\ w^{d2*} &= \frac{2D_1b_1\eta\kappa + \phi\phi}{4b_1^2\eta\kappa - \phi^2}, \\ w^{d2*} &= \frac{2D_1b_1\eta\kappa + \phi\phi}{4b_1^2\eta\kappa - \phi^2}, \\ e_r^{d2*} &= \frac{\beta_1(2 + k\beta_1)[\beta_1e - (1 + k\beta_1)(1 - \alpha)\tau D] + \beta_2(1 + k\beta_1)[\beta_1e - (1 + k\beta_1)\alpha\tau D]}{\beta_1^2(2 + k\beta_1)^2 - \beta_2^2(1 + k\beta_1)^2}, \\ e_t^{d2*} &= \frac{\beta_1(2 + k\beta_1)[\beta_1e - (1 + k\beta_1)\alpha\tau D] + \beta_2(1 + k\beta_1)[\beta_1e - (1 + k\beta_1)(1 - \alpha)\tau D]}{\beta_1^2(2 + k\beta_1)^2 - \beta_2^2(1 + k\beta_1)^2}, \end{aligned} \quad (34)$$

where  $\phi = D_1(b_2\eta + g_1g_2) + D_2(2b_1\eta - g_1^2)$ ,  $\kappa = (2b_1^2 - b_2^2)\eta - b_1g_1^2 - b_2g_1g_2$ , and  $\phi = 2b_1b_2\eta - b_2g_1^2 - b_1g_1g_2$ .

*Proof.* For the retailer and the third party, according to the profit functions of the retailer and the third party (31) and

(33), taking the first-order derivatives of  $\hat{\pi}_r(p_r, e_r, s)$  and  $\hat{\pi}_t(e_t)$  along the retail price  $p_r$ , the collecting price of retailer

$e_r$ , sales effort  $s$ , and the collecting price of the third party  $e_t$ , respectively, we could obtain

$$\begin{aligned}\frac{\partial \hat{\pi}_r(p_r, e_r, s)}{\partial p_r} &= -2b_1 p_r + b_2 p_d + b_1 w + g_1 s + D_1, \\ \frac{\partial \hat{\pi}_r(p_r, e_r, s)}{\partial s} &= g_1 p_r - g_1 w - \eta s, \\ \frac{\partial \hat{\pi}_r(p_r, e_r, s)}{\partial e_r} &= -\beta_1(2 + k\beta_1)e_r + \beta_2(1 + k\beta_1)e_t + \beta_1 e - (1 + k\beta_1)(1 - \alpha)\tau - D, \\ \frac{\partial \hat{\pi}_t(e_t)}{\partial e_t} &= \beta_2(1 + k\beta_1)e_r - \beta_1(2 + k\beta_1)e_t + \beta_1 e - (1 + k\beta_1)\alpha\tau - D.\end{aligned}\tag{35}$$

Based on the condition of proposition  $2b_1\eta - g_1^2 > 0$ , it obtains that

$$\begin{aligned}p_r^{d2*} &= \frac{b_2\eta p_d + (b_1\eta w - g_1^2)w + D_1\eta}{2b_1\eta - g_1^2}, \\ s^{d2*} &= \frac{b_2g_1 p_d - b_1g_1 w + D_1g_1}{2b_1\eta - g_1^2}, \\ e_r^{d2*} &= \frac{\beta_1(2 + k\beta_1)[\beta_1 e - (1 + k\beta_1)(1 - \alpha)\tau - D] + \beta_2(1 + k\beta_1)[\beta_1 e - (1 + k\beta_1)\alpha\tau - D]}{\beta_1^2(2 + k\beta_1)^2 - \beta_2^2(1 + k\beta_1)^2}, \\ e_t^{d2*} &= \frac{\beta_1(2 + k\beta_1)[\beta_1 e - (1 + k\beta_1)\alpha\tau - D] + \beta_2(1 + k\beta_1)[\beta_1 e - (1 + k\beta_1)(1 - \alpha)\tau - D]}{\beta_1^2(2 + k\beta_1)^2 - \beta_2^2(1 + k\beta_1)^2}.\end{aligned}\tag{36}$$

Substitute the  $p_r^{d2*}$ ,  $s^{d2*}$ ,  $e_r^{d2*}$ , and  $e_t^{d2*}$  into profit function (32), for the manufacturer, taking the first-order

derivatives of  $\hat{\pi}_d(p_d, w)$  along the direct price  $p_d$  and wholesale price  $w$ , and we could obtain

$$\begin{aligned}\frac{\partial \pi_d(p_d, w)}{\partial p_d} &= \frac{-2[(2b_1^2 - b_2^2)\eta - b_1g_1^2 - b_2g_1g_2]}{2b_1\eta - g_1^2} p_d + \frac{2b_1b_2\eta - b_2g_1^2 - b_1g_1g_2}{2b_1\eta - g_1^2} w + \frac{D_1(b_2\eta + g_1g_2) + D_2(2b_1\eta - g_1^2)}{2b_1\eta - g_1^2}, \\ \frac{\partial \pi_d(p_d, w)}{\partial w} &= \frac{2b_1b_2\eta - b_2g_1^2 - b_1g_1g_2}{2b_1\eta - g_1^2} p_d - \frac{2b_1^2\eta}{2b_1\eta - g_1^2} w + \frac{D_1b_1\eta}{2b_1\eta - g_1^2}.\end{aligned}\tag{37}$$

The Hessian matrix is given as

$$H^{d2} = \begin{pmatrix} -2[(2b_1^2 - b_2^2)\eta - b_1g_1^2 - b_2g_1g_2] & 2b_1b_2\eta - b_2g_1^2 - b_1g_1g_2 \\ 2b_1b_2\eta - b_2g_1^2 - b_1g_1g_2 & -2b_1^2\eta \end{pmatrix}.\tag{38}$$

TABLE 2: Table of basic data.

Parameter	$b_1$	$b_2$	$\tau$	$c_n$	$c_r$	$\eta$	$\alpha$	$\beta_1$	$\beta_2$	$k$	$e$	$g_1$	$g_2$
Value	0.7	0.2	0.9	50	1	1	0.51	0.9	0.2	0.1	5	0.8	0.5

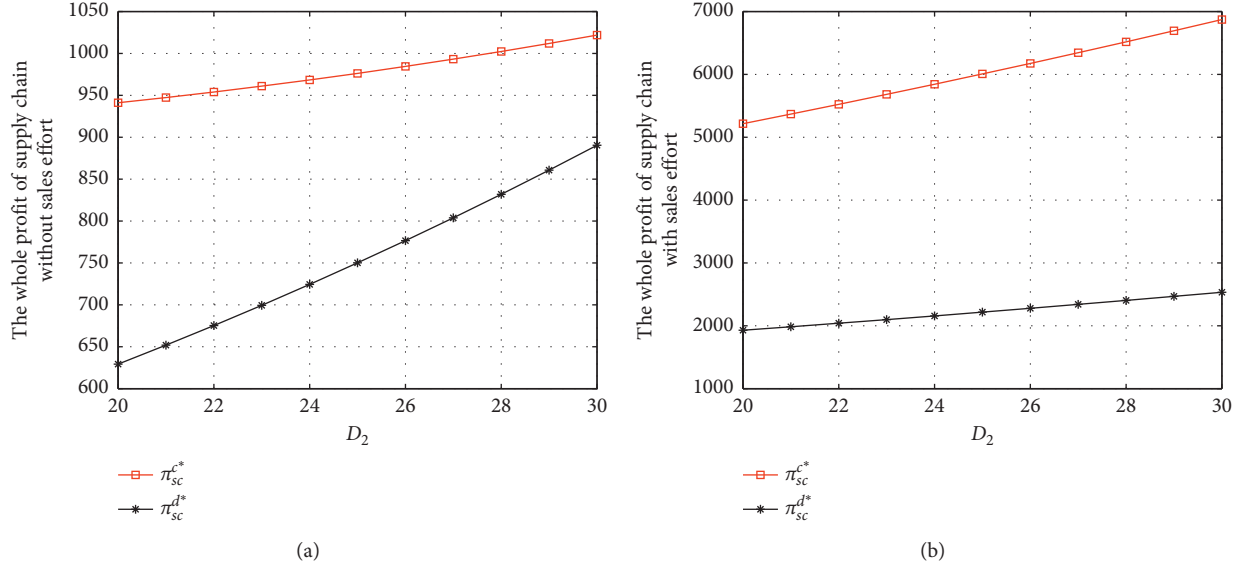


FIGURE 2: The optimal profit of whole supply chain under the centralized and decentralized model.

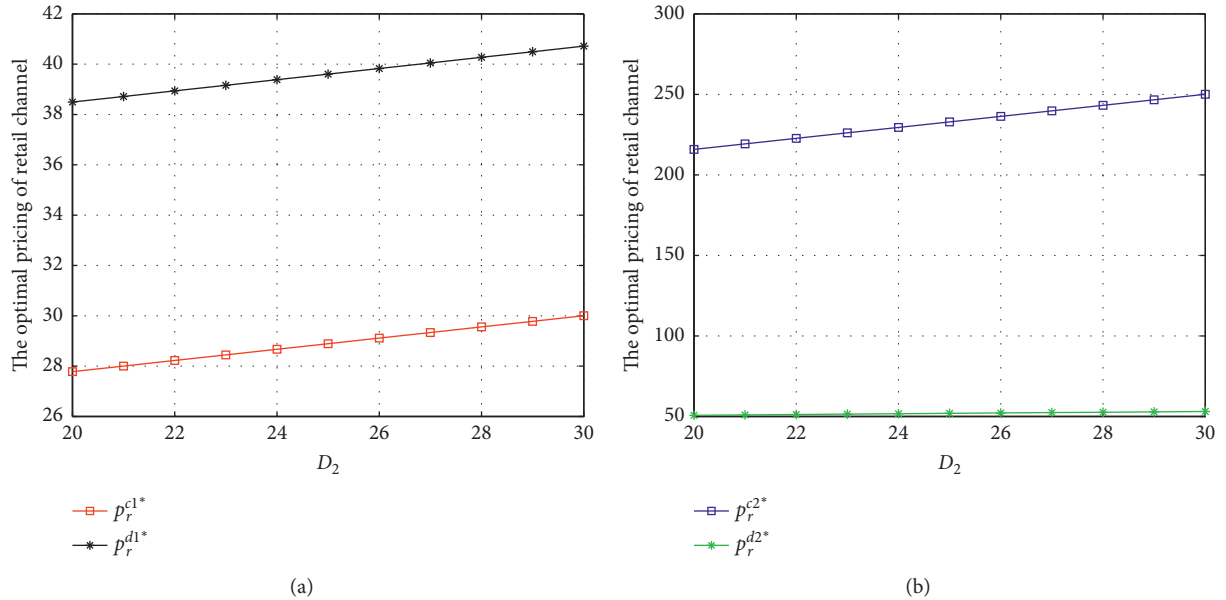


FIGURE 3: The optimal retail selling price under the centralized and decentralized model.

According to the condition of Proposition 4,  $4b_1^2\eta[(2b_1^2 - b_2^2)\eta - b_1g_1^2 - b_2g_1g_2] - (2b_1b_2\eta - b_2g_1^2 - b_1g_1g_2)^2 > 0$ , we know  $|H^{d2}| = 4b_1^2\eta[(2b_1^2 - b_2^2)\eta - b_1g_1^2 - b_2g_1g_2] - (2b_1$

$b_2\eta - b_2g_1^2 - b_1g_1g_2)^2 > 0$ . Therefore, the profit function  $\hat{\pi}_D(p_d, w)$  is joint concave on  $p_d$  and  $w$ . The optimal solution could be obtained by solving the first-order condition as follows:

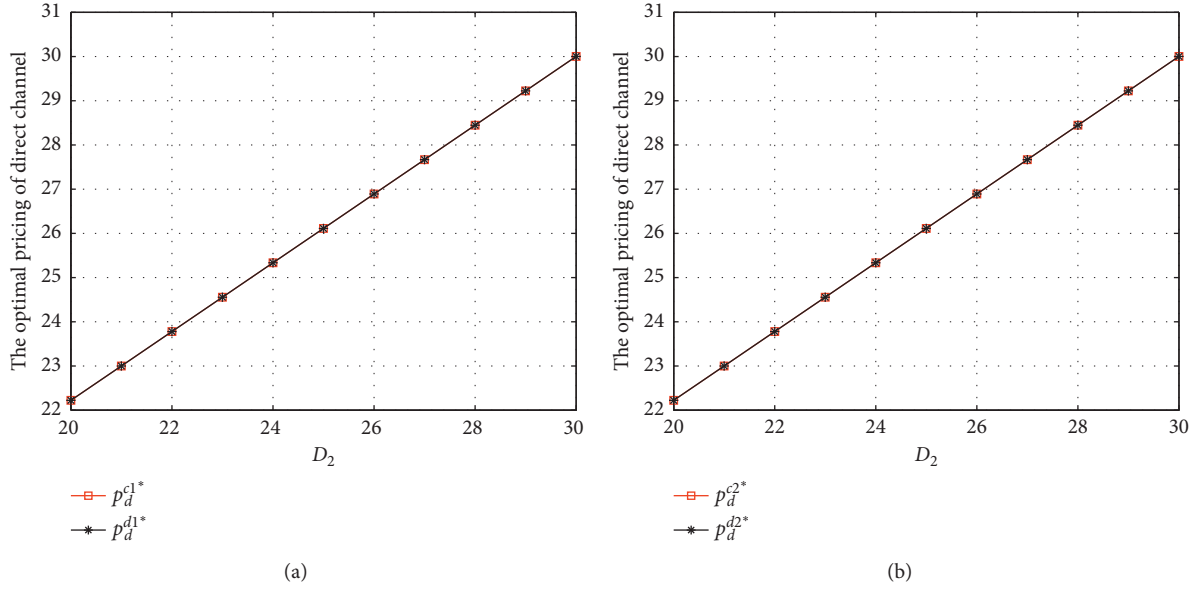


FIGURE 4: The optimal direct selling price under the centralized and decentralized model.

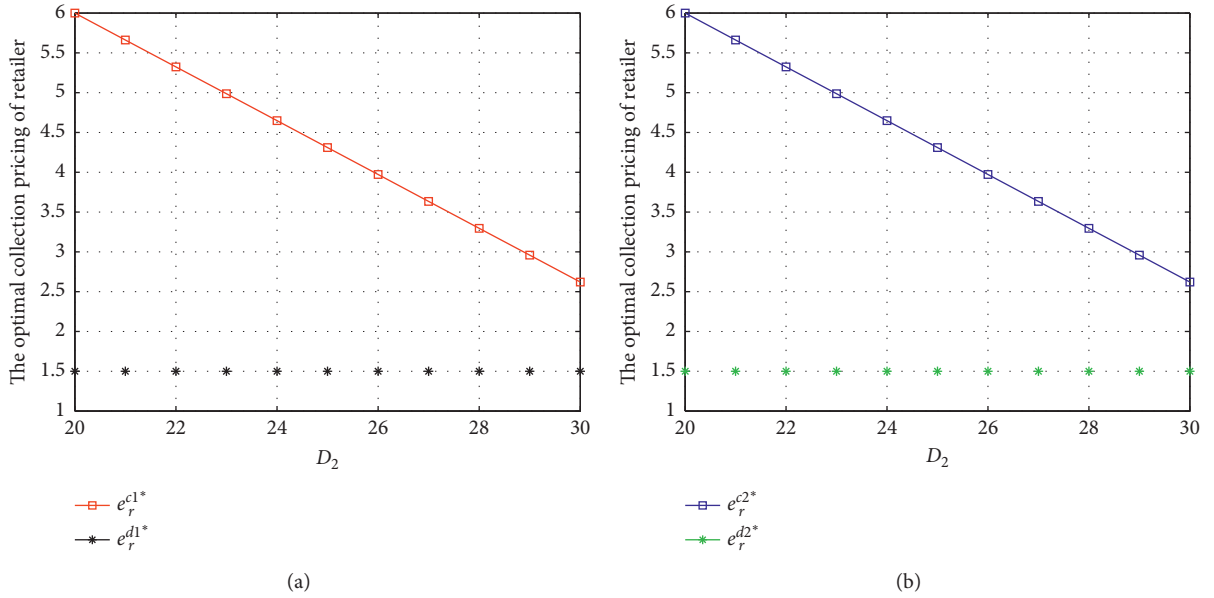


FIGURE 5: The optimal collection price of the retailer under the centralized and decentralized model.

$$\begin{aligned}
 P_d^{d2*} &= \frac{2b_1^2\eta[D_1(b_2\eta + g_1g_2) + D_2(2b_1\eta - g_1^2)] + D_1b_1\eta(2b_1b_2\eta - b_2g_1^2 - b_1g_1g_2)}{4b_1^2\eta[(2b_1^2 - b_2^2)\eta - b_1g_1^2 - b_2g_1g_2] - (2b_1b_2\eta - b_2g_1^2 - b_1g_1g_2)^2}, \\
 w^{d2*} &= \frac{2D_1b_1\eta[(2b_1^2 - b_2^2)\eta - b_1g_1^2 - b_2g_1g_2]}{4b_1^2\eta[(2b_1^2 - b_2^2)\eta - b_1g_1^2 - b_2g_1g_2] - (2b_1b_2\eta - b_2g_1^2 - b_1g_1g_2)^2} \\
 &\quad + \frac{(2b_1b_2\eta - b_2g_1^2 - b_1g_1g_2)[D_1(b_2\eta + g_1g_2) + D_2(2b_1\eta - g_1^2)]}{4b_1^2\eta[(2b_1^2 - b_2^2)\eta - b_1g_1^2 - b_2g_1g_2] - (2b_1b_2\eta - b_2g_1^2 - b_1g_1g_2)^2}.
 \end{aligned} \tag{39}$$

The proof is completed.  $\square$

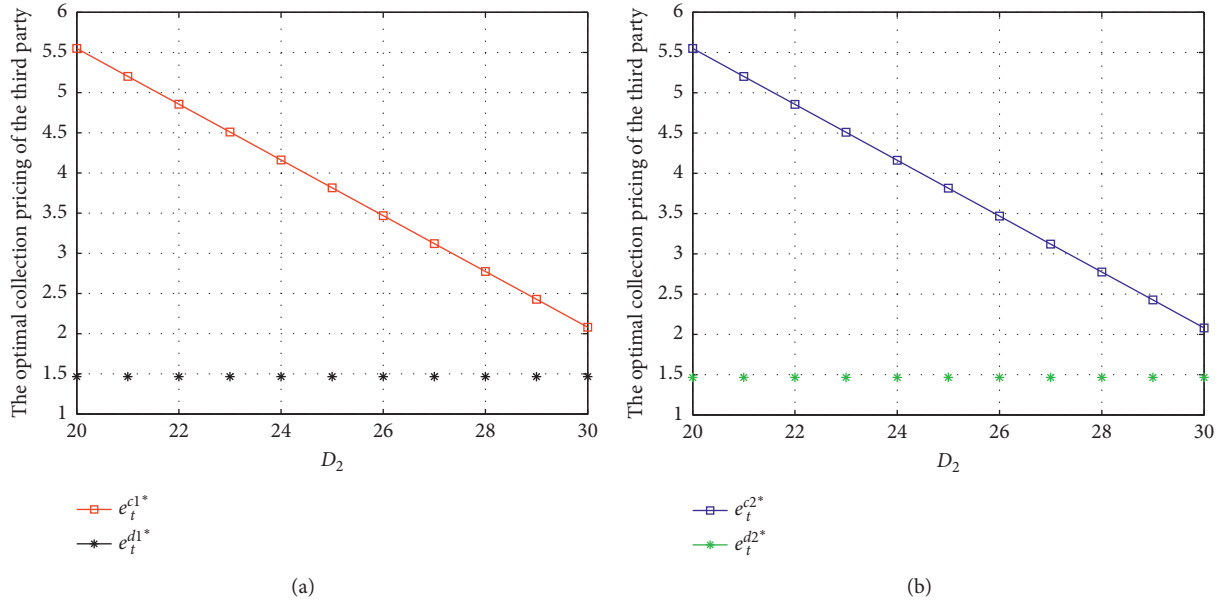


FIGURE 6: The optimal collection price of the third party under the centralized and decentralized model.

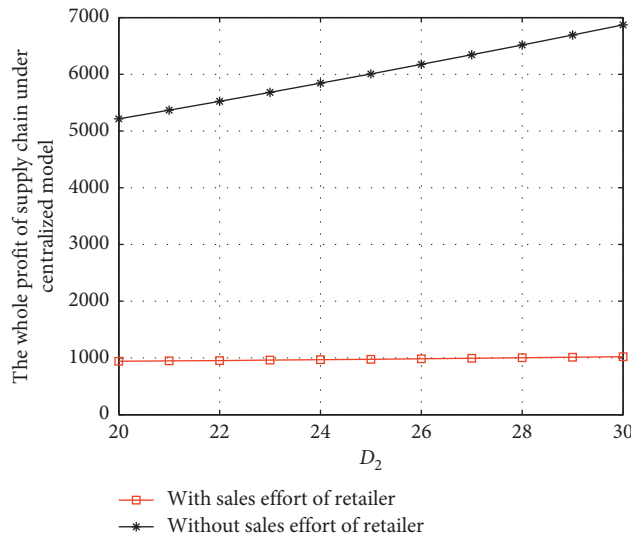


FIGURE 7: The optimal profit of whole supply chain with sales effort under the centralized model.

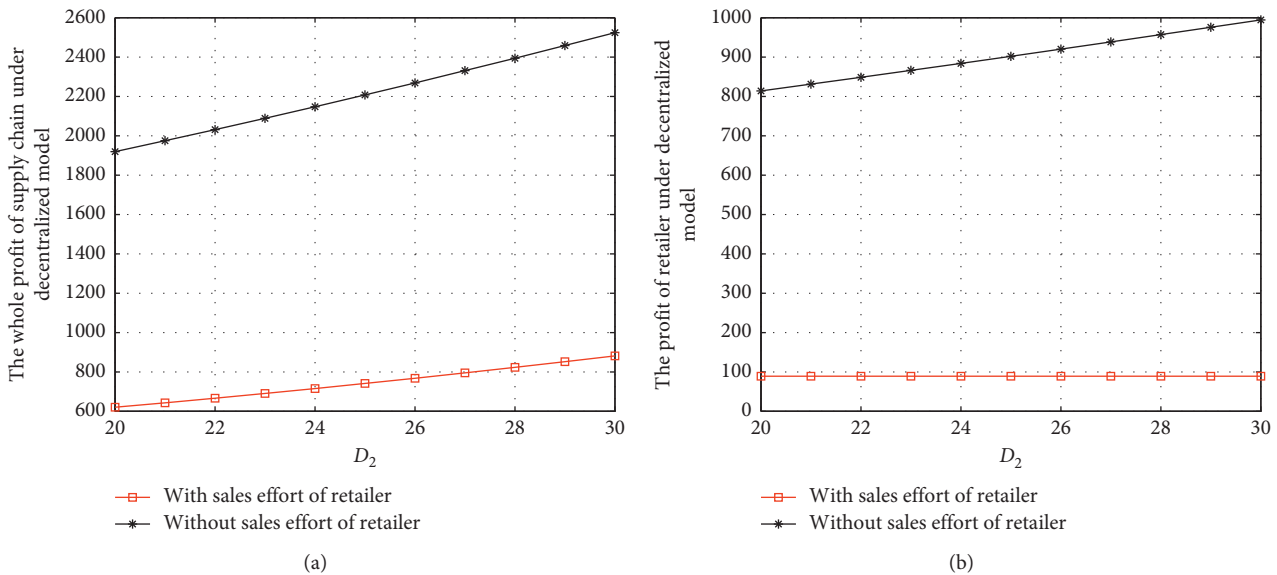
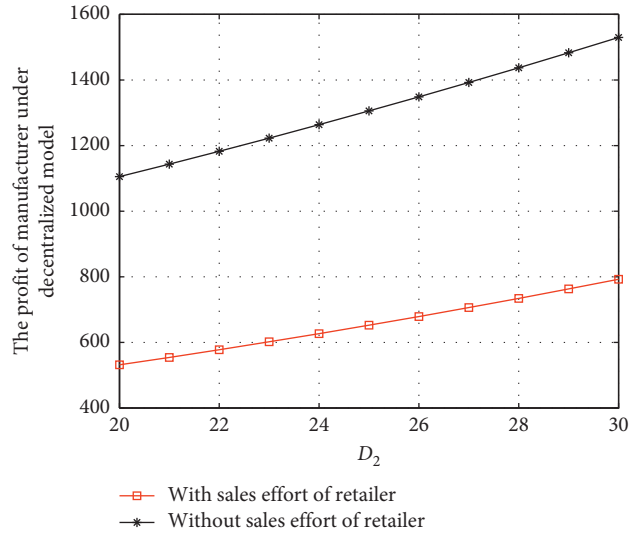
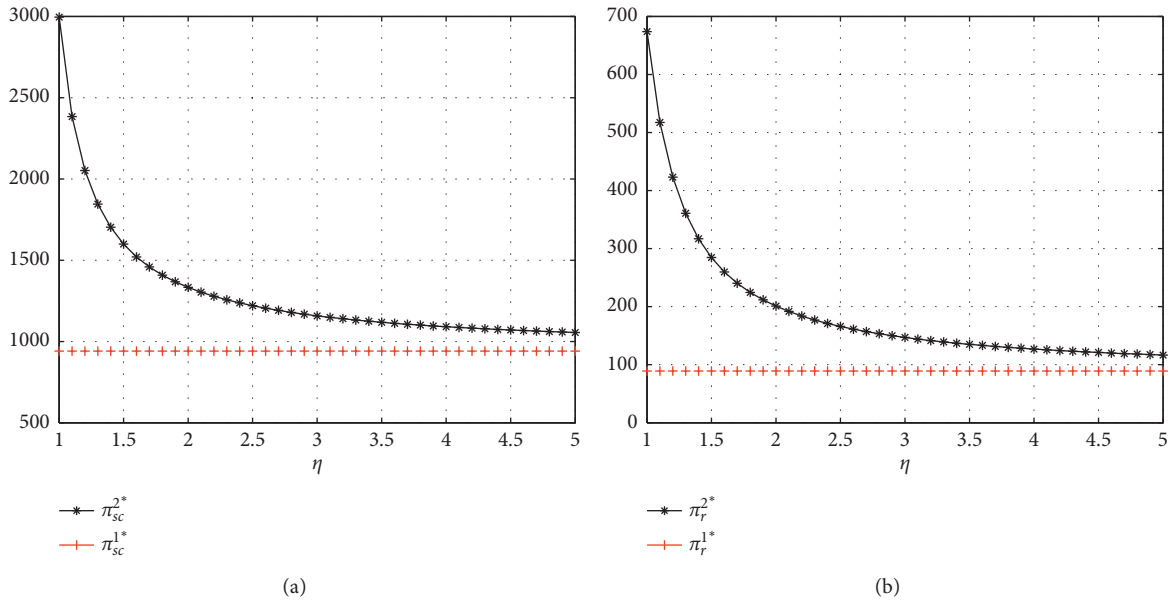


FIGURE 8: Continued.



(c)

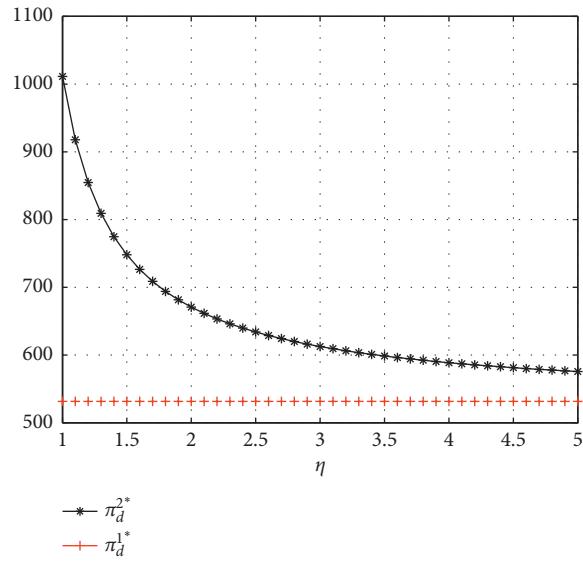
FIGURE 8: The optimal profit with and without sales effort under the decentralized model.



(a)

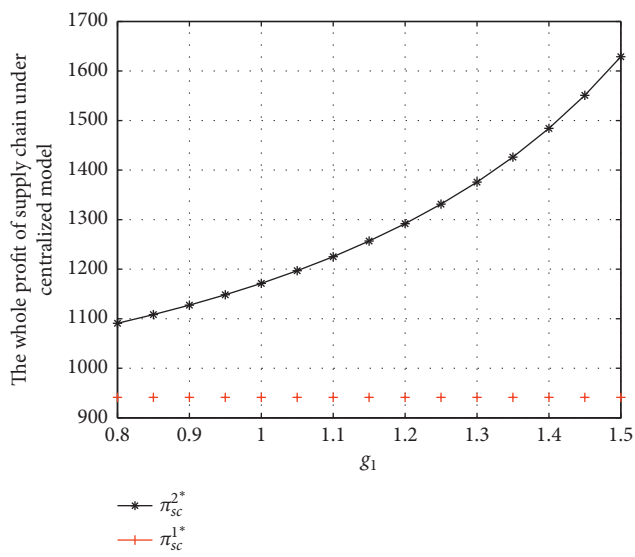
(b)

FIGURE 9: Continued.

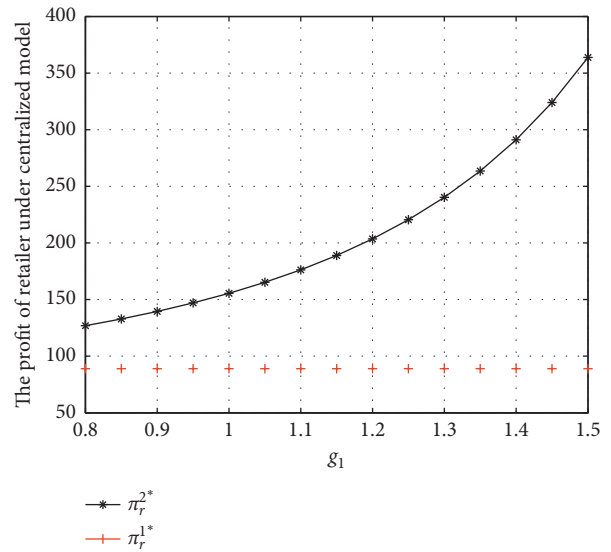


(c)

FIGURE 9: The effect of the value of  $\eta$  on profit under the centralized model and decentralized model.

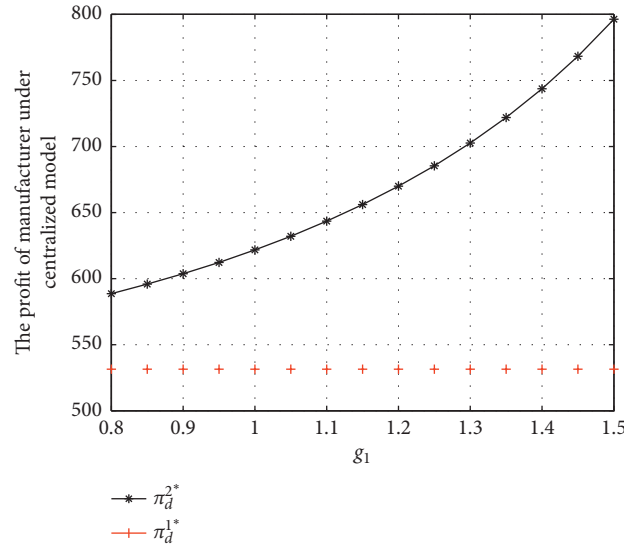


(a)



(b)

FIGURE 10: Continued.



(c)

FIGURE 10: The effect of the value of  $g_1$  on profit under the centralized model and decentralized model.

*Remark 2.* In the study of [19], analysis for strategy of the closed-loop supply chain with dual recycling channel was carried out. Based on game theory, the authors characterized the supply chain performance in terms of the pricing decisions and the recycling strategies for both the decentralized and the centralized channel scenarios. On the contrary, the supply chain channel strategy with quality and marketing effort-dependent demand was considered in [22]. Different from the existing results, this paper provides four scenarios for different decision models and with or without sales effort. The optimal solution is derived and comparison for four scenarios is given in this paper.

## 5. Numerical Illustrations

This section carries on numerical example analysis of the proposed propositions by comparing the optimal decision of four propositions. Sensitivity analysis are provided to illustrate the impact of supply chain parameters on system performance. Table 2 shows the basic data.

*5.1. Centralized Model and Decentralized Model.* By comparing the optimal solution under the centralized model and decentralized model with and without sales effort, it could be concluded from Figure 2 that the profit under the centralized model is always higher than the profit under the decentralized model. Therefore, Pareto improvement could be achieved by the revenue sharing contract.

Figures 3 and 4 show that, with the increase of the market scale, retail selling price and direct selling price will increase. It is easy to understand that the increase of the market scale leads to higher demand. Under the decentralized model, the retail selling price is higher than the retail selling price under the centralized model. The existence of wholesale price brings this result under the decentralized model. Figure 4 shows that the direct selling price of the

manufacturer is independent of the decentralized model or centralized model. Figures 5 and 6 are the collection price of the retailer and the third party, respectively. With the increase of the market scale, the collection price would decrease.

### 5.2. The Effect of Sales Effort on Optimal Pricing and Profit.

The demand for different channels depends on the choice of consumers, and the sales effort of the retailer has an important influence on the market. In the process of operation and management, managers should pay attention to the channel preference of customers. As shown in Figure 7, sales effort of the retailer under the centralized model could increase the whole profit of supply chain.

It can be seen from Figure 8 that the sales effort of the retailer under the decentralized model could increase the whole profit of the supply chain and the profit of the manufacturer and retailer, respectively.

*5.3. Sensitivity Analysis.* This section discusses the effect of the marginal cost coefficient of sales effort on profit. It can be found from Figure 9 that when  $\eta$  increases, each member's profit decreases and the rate of change decreases.

It can be found from Figure 10 that when  $g_1$  increases, the profits of each supply chain members all increase and the rate of change increases.

## 6. Conclusions

This paper studies the optimal pricing of the dual-channel supply chain with the third-party product recovery and sales effort. First of all, for the general case under the centralized and decentralized model, the optimal selling pricing of the direct channel and retail channel in the forward supply chain and the optimal collection pricing of the retail channel and the third party in the backward supply chain are discussed.



Then, the optimal pricing strategy with sales effort under the centralized and decentralized model is provided and analyzed. Finally, the comparative analysis of four situations is carried out by numerical results. The effect of sales effort and decision-making model on the optimal pricing, demand, and profit is demonstrated.

## Data Availability

The data used to support the findings of this study are available from the corresponding author upon request.

## Conflicts of Interest

The authors declare that they have no conflicts of interest.

## Acknowledgments

This work was supported by the National Natural Science Foundation of China under Grants 61773004 and 61803056 and in part by the Natural Science Foundation Project of Chongqing under Grant cstc2018jcyjAX0365 and Program of Chongqing Innovation Team Project in University under Grant CXTDX201601022.

## References

- [1] V. V. Agrawal, A. Atasu, and K. Van Ittersum, "Remanufacturing, third-party competition, and consumers' perceived value of new products," *Management Science*, vol. 61, no. 1, pp. 60–72, 2015.
- [2] G. Ferrer and J. M. Swaminathan, "Managing new and remanufactured products," *Management Science*, vol. 52, no. 1, pp. 15–26, 2006.
- [3] J. Ding, W. Chen, and W. Wang, "Production and carbon emission reduction decisions for remanufacturing firms under carbon tax and take-back legislation," *Computers & Industrial Engineering*, vol. 143, Article ID 106419, 2020.
- [4] M. Pazoki and G. Zaccour, "A mechanism to promote product recovery and environmental performance," *European Journal of Operational Research*, vol. 274, no. 2, pp. 601–614, 2019.
- [5] W. Kerr and C. Ryan, "Eco-efficiency gains from remanufacturing," *Journal of Cleaner Production*, vol. 9, no. 1, pp. 75–81, 2001.
- [6] L. Wu, L. Liu, and Z. Wang, "Competitive remanufacturing and pricing strategy with contrast effect and assimilation effect," *Journal of Cleaner Production*, vol. 257, Article ID 120333, 2020.
- [7] A. Yenipazarli, "Managing new and remanufactured products to mitigate environmental damage under emissions regulation," *European Journal of Operational Research*, vol. 249, no. 1, pp. 117–130, 2016.
- [8] T.-M. Choi, Y. Chen, and S. H. Chung, "Online-offline fashion franchising supply chains without channel conflicts: choices on postponement and contracts," *International Journal of Production Economics*, vol. 215, pp. 174–184, 2019.
- [9] C.-H. Wu, "OEM product design in a price competition with remanufactured product," *Omega*, vol. 41, no. 2, pp. 287–298, 2013.
- [10] D. Krass, T. Nedorezov, and A. Ovchinnikov, "Environmental taxes and the choice of green technology," *Production and Operations Management*, vol. 22, no. 5, pp. 1035–1055, 2013.
- [11] D. Hammond and P. Beullens, "Closed-loop supply chain network equilibrium under legislation," *European Journal of Operational Research*, vol. 183, no. 2, pp. 895–908, 2007.
- [12] X. Chang, H. Xia, H. Zhu, T. Fan, and H. Zhao, "Production decisions in a hybrid manufacturing-remanufacturing system with carbon cap and trade mechanism," *International Journal of Production Economics*, vol. 162, pp. 160–173, 2015.
- [13] M. E. Ferguson and L. B. Toktay, "The effect of competition on recovery strategies," *Production and Operations Management*, vol. 15, no. 3, pp. 351–368, 2006.
- [14] L. Liu, Z. Wang, L. Xu, X. Hong, and K. Govindan, "Collection effort and reverse channel choices in a closed-loop supply chain," *Journal of Cleaner Production*, vol. 144, pp. 492–500, 2017.
- [15] R. Kleber, M. Reimann, G. C. Souza, and W. Zhang, "Two-sided competition with vertical differentiation in both acquisition and sales in remanufacturing," *European Journal of Operational Research*, vol. 284, no. 2, pp. 572–587, 2020.
- [16] N. M. Modak, N. Modak, S. Panda, and S. S. Sana, "Analyzing structure of two-echelon closed-loop supply chain for pricing, quality and recycling management," *Journal of Cleaner Production*, vol. 171, pp. 512–528, 2018.
- [17] S. Panda, N. M. Modak, and L. E. Cárdenas-Barrón, "Coordinating a socially responsible closed-loop supply chain with product recycling," *International Journal of Production Economics*, vol. 188, pp. 11–21, 2017.
- [18] N. M. Modak and P. Kelle, "Managing a dual-channel supply chain under price and delivery-time dependent stochastic demand," *European Journal of Operational Research*, vol. 272, no. 1, pp. 147–161, 2019.
- [19] S. He, D. Zhu, Y. Chen, X. Liu, Y. Chen, and X. Wang, "Application and problems of emergy evaluation: a systemic review based on bibliometric and content analysis methods," *Ecological Indicators*, vol. 114, Article ID 106304, 2020.
- [20] Y. Zhou, F. Hu, and Z. Zhou, "Pricing decisions and social welfare in a supply chain with multiple competing retailers and carbon tax policy," *Journal of Cleaner Production*, vol. 190, pp. 752–777, 2018.
- [21] A. Atasu, M. Sarvary, and L. N. Van Wassenhove, "Remanufacturing as a marketing strategy," *Management Science*, vol. 54, no. 10, pp. 1731–1746, 2008.
- [22] S. Agrawal, R. K. Singh, and Q. Murtaza, "A literature review and perspectives in reverse logistics," *Resources, Conservation and Recycling*, vol. 97, pp. 76–92, 2015.
- [23] R. C. Savaskan and L. N. Van Wassenhove, "Reverse channel design: the case of competing retailers," *Management Science*, vol. 52, no. 1, pp. 1–14, 2006.
- [24] M. Huang, M. Song, L. H. Lee, and W. K. Ching, "Analysis for strategy of closed-loop supply chain with dual recycling channel," *International Journal of Production Economics*, vol. 144, no. 2, pp. 510–520, 2013.
- [25] X. Hong, Z. Wang, D. Wang, and H. Zhang, "Decision models of closed-loop supply chain with remanufacturing under hybrid dual-channel collection," *The International Journal of Advanced Manufacturing Technology*, vol. 68, no. 5–8, pp. 1851–1865, 2013.
- [26] T. A. Taylor, "Supply chain coordination under channel rebates with sales effort effects," *Management Science*, vol. 48, no. 8, pp. 992–1007, 2002.
- [27] P. Ma, H. Wang, and J. Shang, "Supply chain channel strategies with quality and marketing effort-dependent demand," *International Journal of Production Economics*, vol. 144, no. 2, pp. 572–581, 2013.

- [28] H. Yang, J. Chen, X. Chen, and B. Chen, "The impact of customer returns in a supply chain with a common retailer," *European Journal of Operational Research*, vol. 256, no. 1, pp. 139–150, 2017.
- [29] G. Hua, S. Wang, and T. C. E. Cheng, "Price and lead time decisions in dual-channel supply chains," *European Journal of Operational Research*, vol. 205, no. 1, pp. 113–126, 2010.
- [30] D. Ghosh and J. Shah, "A comparative analysis of greening policies across supply chain structures," *International Journal of Production Economics*, vol. 135, no. 2, pp. 568–583, 2012.

## Research Article

# New Results on Stability of Delayed Cohen–Grossberg Neural Networks of Neutral Type

Ozlem Faydasicok 

*Department of Mathematics, Faculty of Science Istanbul University, Vezneciler, Istanbul, Turkey*

Correspondence should be addressed to Ozlem Faydasicok; [kozlem@istanbul.edu.tr](mailto:kozlem@istanbul.edu.tr)

Received 15 May 2020; Accepted 27 May 2020; Published 16 June 2020

Guest Editor: Xiaodi Li

Copyright © 2020 Ozlem Faydasicok. This is an open access article distributed under the Creative Commons Attribution License, which permits unrestricted use, distribution, and reproduction in any medium, provided the original work is properly cited.

This research work conducts an investigation of the stability issues of neutral-type Cohen–Grossberg neural network models possessing discrete time delays in states and discrete neutral delays in time derivatives of neuron states. By setting a new generalized appropriate Lyapunov functional candidate, some novel sufficient conditions are proposed for global asymptotic stability for the considered neural networks of neutral type. This paper exploits some basic properties of matrices in the derivation of the results that establish a set of algebraic mathematical relationships between network parameters of this neural system. A key feature of the obtained stability criteria is to be independent from time and neutral delays. Therefore, the derived results can be easily tested. Moreover, a constructive numerical example is studied to check the verification of presented global stability conditions.

## 1. Introduction

In the past few decades, a variety of neural network models including Hopfield neural networks (HNNs), cellular neural networks (CNNs), Cohen–Grossberg neural networks (CGNNs), and bidirectional associative memory neural networks (BAMNNs) have been utilized for solving some typical engineering problems associated with pattern recognitions, signal processing, associative memories, and optimization related problems [1–9]. In these typical engineering applications, it is usually desired that the dynamics of the employed neural network must exhibit some certain behaviors depending on the characteristics of the problem to be solved. For instance, if one needs to solve an optimization problem, then the aimed designed neural network may require to possess a unique and globally asymptotically stable equilibrium point for every fixed input value. In this aspect, it becomes an important requirement to analyze stability behaviors of dynamical neural systems. On the contrary, neural networks have also been electronically implemented for real time applications of various classes of engineering problems. It is known that, in the process of electronically implementing a neural network, because of the

finite switching speed of operational amplifiers and signal transmission times of neurons due to the communications of neurons, delay parameters encounter. The presence of the time delay parameters may lead to various complex non-linear dynamics including instability, periodic solutions, and chaos. Therefore, one needs to consider the possible effects of these time delays on the stability properties of neural systems. In the recent literature, the stability issues for delayed neural networks have been addressed by a variety of researchers, and various sets of novel sufficient results on global asymptotic stability of the equilibrium point for different neural network models have been published [10–25]. It should mention that stability analysis of neural networks whose mathematical model with only time delays may not be appropriate to address the complete characteristics of dynamics for these types of neural network models. The reason for this fact is that, in many cases, beside the states involving time delays, the time derivative of the states may also have some different types of delays. In this sense, we need to consider the neural networks having delays both in states and in time derivative of states. A neural network that is modelled in this way is called neutral-type neural network. A widely studied neural network of this class

is that of Cohen–Grossberg neural networks possessing discrete time and neutral delay parameters. This neural network model is defined by the nonlinear dynamical equations:

$$\begin{aligned} \dot{x}_i(t) = & d_i(x_i(t)) \left( -c_i(x_i(t)) + \sum_{j=1}^n a_{ij} f_j(x_j(t)) \right. \\ & \left. + \sum_{j=1}^n b_{ij} f_j(x_j(t - \tau_j)) + u_i \right) + \sum_{j=1}^n e_{ij} \dot{x}_j(t - \zeta_j). \end{aligned} \quad (1)$$

where  $x_i(t)$  is representing states for the neurons,  $c_i(x_i(t))$  is some behaved functions, and  $d_i(x_i(t))$  is representing the amplification functions. The constant elements  $a_{ij}$  and  $b_{ij}$  are representing interconnection weights among the neurons.  $\tau_j (1 \leq j \leq n)$  is representing time delays and  $\zeta_j (1 \leq j \leq n)$  is representing neutral delays. The element  $e_{ij}$  is denoting the weights of time derivative of states including delays.  $f_j(\cdot)$  is denoting neuronal activation functions, and  $u_i$  is constant input of  $i$ th neuron. In system (1), we state some general assumptions. Let  $\tau = \max\{\tau_j\}$ ,  $\zeta = \max\{\zeta_j\}$ ,  $1 \leq j \leq n$ , and  $\delta = \max\{\tau, \zeta\}$ . Under these assumptions, neural network model (1) keeps the initial values stated by  $x_i(t) = \varphi_i(t)$  and  $\dot{x}_i(t) = \vartheta_i(t) \in C([-\delta, 0], R)$ . We note that

$C([-\delta, 0], R)$  represents real-valued functions that are described on the interval  $[-\delta, 0]$  to  $R$ .

We can make some remarks on system (1) to address the role of this system. If we make some simple changes in the mathematical model of system (1), we can easily have some other forms of neural network models. If we let  $e_{ij} = 0, \forall i, j$ , then system (5) becomes a delayed Cohen–Grossberg network. If we let  $e_{ij} = 0, \forall i, j$  and  $d_i(x_i(t)) = 1$  and  $c_i(x_i(t)) = x_i(t)$ , then, system (1) will define the class of Hopfield neural networks. If we let  $e_{ij} = 0, \forall i, j$ ,  $d_i(x_i(t)) = 1c_i$ ,  $c_i(x_i(t)) = x_i(t)$ , and  $f_j(\cdot)$  be a specific activation function with the binary output values, then neural network (1) turns into the cellular neural network. Thus, the stability analysis of (1) will also address the stability of many different neural network models.

In stability analysis of the neutral-type network system whose dynamical activities are governed by (1), the primary question to be addressed is the determination of mathematical relationships in the neuron states and the functions  $d_i(x_i(t))$ ,  $c_i(x_i(t))$ , and  $f_i(x_i(t))$ . The well-known basic assumptions on these nonlinear functions are given below.

$A_1$ : the function  $d_i(x_i(t))$  has the following property:

$$0 < \mu_i \leq d_i(x_i(t)) \leq \rho_i, \quad \forall i, \forall x_i(t) \in R, \quad (2)$$

where  $\mu_i$  and  $\rho_i$  are positive valued real constants.

$A_2$ :  $c_i(x_i(t))$  have the following property:

$$0 < \gamma_i \leq \frac{c_i(x_i(t)) - c_i(y_i(t))}{x_i(t) - y_i(t)} = \frac{|c_i(x_i(t)) - c_i(y_i(t))|}{|x_i(t) - y_i(t)|} \leq \psi_i, \quad \forall i, \forall x_i(t), y_i(t) \in R, x_i(t) \neq y_i(t), \quad (3)$$

where  $\gamma_i$  and  $\psi_i$  are positive valued real constants.

$A_3$ : the function  $d_i(x_i(t))$  has the following property:

$$|f_i(x_i(t)) - f_i(y_i(t))| \leq \ell_i |x_i(t) - y_i(t)|, \quad \forall i, \forall x_i(t), y_i(t) \in R, x_i(t) \neq y_i(t), \quad (4)$$

where  $\ell_i$  is positive-valued real constant.

If neutral-type neural networks possess discrete delays, then the mathematical models of such neural systems can be stated in the forms of vectors and matrices. Then, we can study the stability of such neural networks by exploiting the linear matrix inequality approach using the other appropriate mathematical methods. In [26–34], the stability of neutral-type neural networks have been studied, and by constructing some classes of suitable Lyapunov functionals together with setting some useful lemmas and new mathematical techniques, different novel stability results on the considered neutral-type neural networks of various types of linear matrix inequalities have been presented. In [35–40], novel global stability conditions for neutral-type neural networks in the forms of different linear matrix inequality formulations have been proposed by employing various proper Lyapunov functionals with the triple or four integral terms. In [41, 42] various stability problems for neutral-type neural networks have been analyzed, and by setting the

semifree weighting matrix techniques and an augmented Lyapunov functional, some less conservative and restrictive global stability conditions of linear matrix inequalities have been proposed. In [42], the stability for neural networks of neutral-type possessing discrete delays has been suitable conducted, and by employing a proper Lyapunov functional that makes a combination of the descriptor model transformation, a novel stability criterion has been formulated in linear matrix inequalities. In [16], stability of neural systems has been addressed, and by proposing an appropriate Lyapunov functionals utilizing auxiliary function-type integral inequalities and reciprocally convex method, various sets of stability results via linear matrix inequalities have been obtained. In [43], the Lagrange stability issue of neutral-type neural systems having mixed delays has been analyzed, and by using the suitable Lyapunov functionals and applying some appropriate linear matrix inequality techniques, various sufficient criteria have been obtained to ensure Lagrange stability of neural networks of neutral type.

In [44], the issues associated with stability of neutral-type singular neural systems involving different delay parameters have been studied, and by setting a novel adequate Lyapunov functional and some rarely integral inequalities, a new global asymptotic stability condition via linear matrix inequality has been derived. In [45], dynamical issues of neural networks of neutral-type possessing some various delay parameters have been analyzed, and different stability results have been derived employing linear matrix inequality combining with Razumikhin-like approaches.

We should point out that the results of [16, 26–45] employ some various classes of linear matrix inequality techniques to obtain different sets of stability conditions for neutral-type neural networks. However, the stability results derived via the linear matrix inequality method are required to test some negative definite properties of high-dimensional matrices whose elements are formed by the system parameters of neural networks. Due to these complex calculation problems, it becomes a necessity to propose different stability conditions for neutral-type neural networks, which are not stated in linear matrix inequality forms. In this concept, the current paper will focus on the dynamical analysis of neural system (1) to derive some easily verifiable algebraic stability conditions.

## 2. Stability Analysis

The basic contribution of this section will be deriving some stability conditions implying the stability of neutral-type Cohen–Grossberg neural system whose model is given by (1). We now proceed with a first step to provide a simpler procedure with the proofs of the stability conditions. This step needs to transform the equilibrium points  $\hat{x} = (\hat{x}_1, \hat{x}_2, \dots, \hat{x}_n)^T$  of Cohen–Grossberg neural system represented by equation (1) to the origin. This will be achieved by utilizing the simple formula  $z_i(t) = x_i(t) - \hat{x}_i$ , which turns neutral-type neural network (1) to an equivalent neutral-type neural network which has a set of differential equations that govern the dynamics of this system:

$$\begin{aligned} \dot{z}_i(t) = \alpha_i(z_i(t)) & \left( -\beta_i(z_i(t)) + \sum_{j=1}^n a_{ij} g_j(z_j(t)) \right. \\ & \left. + \sum_{j=1}^n b_{ij} g_j(z_j(t - \tau_j)) \right) + \sum_{j=1}^n e_{ij} \dot{z}_j(t - \zeta_j). \end{aligned} \quad (5)$$

(5) can be represented in the vectors and matrices forms as given below:

$$\begin{aligned} \dot{z}(t) = \alpha(z(t)) & (-\beta(z(t)) + Ag(z(t)) \\ & + Bg(z(t - \tau))) + E\dot{z}(t - \zeta), \end{aligned} \quad (6)$$

where the system matrices are  $A = (a_{ij})_{n \times n}$ ,  $B = (b_{ij})_{n \times n}$ ,  $E = (e_{ij})_{n \times n}$  and

$$\begin{aligned} z(t) &= (z_1(t), z_2(t), \dots, z_n(t))^T, \\ z(t - \tau) &= ((z_1(t - \tau_1), z_2(t - \tau_2), \dots, z_n(t - \tau_n))^T, \\ g(z(t)) &= (g_1(z_1(t)), g_2(z_2(t)), \dots, g_n(z_n(t)))^T, \\ \alpha(z(t)) &= \text{diag}(\alpha_1(z_1(t)), \alpha_2(z_2(t)), \dots, \alpha_n(z_n(t))), \\ \beta(z(t)) &= (\beta_1(z_1(t)), \beta_2(z_2(t)), \dots, \beta_n(z_n(t)))^T, \\ g(z(t - \tau)) &= (g_1(z_1(t - \tau_1)), g_2(z_2(t - \tau_2)), \dots, g_n(z_n(t - \tau_n)))^T, \\ \dot{z}(t - \zeta) &= (\dot{z}_1(t - \zeta_1), \dot{z}_2(t - \zeta_2), \dots, \dot{z}_n(t - \zeta_n))^T. \end{aligned} \quad (7)$$

After transforming neutral system (1) into neutral system (5), we have new transformed functions in system (5). The function  $\alpha_i(z_i(t))$  are of the form

$$\alpha_i(z_i(t)) = d_i(z_i(t) + \hat{x}_i). \quad (8)$$

The function  $\beta_i(z_i(t))$  are of the form

$$\beta_i(z_i(t)) = c_i(z_i(t) + \hat{x}_i) - c_i(\hat{x}_i). \quad (9)$$

The function  $g_i(z_i(t))$  are of the form

$$g_i(z_i(t)) = f_i(z_i(t) + \hat{x}_i) - f_i(\hat{x}_i). \quad (10)$$

According the properties by  $A_1$ ,  $A_2$ , and  $A_3$ , these new transformed functions possess the following properties:

$$\begin{aligned} 0 < \mu_i \leq \alpha_i(z_i(t)) \leq \rho_i, \quad \forall i, \\ \gamma_i z_i^2(t) \leq z_i(t) \beta_i(z_i(t)) \leq \psi_i z_i^2(t), \quad \forall i, \\ |g_i(z_i(t))| \leq \ell_i |z_i(t)|, \quad \forall i. \end{aligned} \quad (11)$$

*Fact 1.* Consider a real matrix  $A = (a_{ij})_{n \times n}$  and a real vector  $x = (x_1, x_2, \dots, x_n)^T$ . We can state the following inequality:

$$x^T A^T A x \leq \sum_{i=1}^n \sum_{j=1}^n \left| \sum_{k=1}^n a_{ki} a_{kj} \right| x_i^2. \quad (12)$$

*Fact 2.* Consider a real matrix  $A = (a_{ij})_{n \times n}$  and a real vector  $x = (x_1, x_2, \dots, x_n)^T$ . We can state the following inequality:

$$x^T A^T A x \leq \|A\|_2^2 \|x\|_2^2. \quad (13)$$

A combination of facts 1 and 2 can be expressed by the following fact.

*Fact 3.* Consider a real matrix  $A = (a_{ij})_{n \times n}$  and a real vector  $x = (x_1, x_2, \dots, x_n)^T$ . We can state the following inequality:

$$x^T A^T A x \leq k_1 \sum_{i=1}^n \sum_{j=1}^n \left| \sum_{k=1}^n a_{ki} a_{kj} \right| x_i^2 + k_2 \|A\|_2^2 \sum_{i=1}^n x_i^2, \quad (14)$$

where  $k_1$  and  $k_2$  are the binary constants such that  $k_1 + k_2 = 1$  and  $k_1 k_2 = 0$ .

*Fact 4.* Let  $A = (a_{ij})_{n \times n}$  be a real matrix,  $D = \text{diag}(d_i > 0)$  be a positive diagonal matrix, and  $x = (x_1, x_2, \dots, x_n)^T$  be a real vector. The following inequality can be stated:

$$x^T A^T D D A x \leq \sum_{i=1}^n \sum_{j=1}^n \sum_{k=1}^n d_k^2 |a_{kj}| |a_{ki}| x_i^2. \quad (15)$$

*Fact 5.* Consider any two real vectors  $x = (x_1, x_2, \dots, x_n)^T$  and  $y = (y_1, y_2, \dots, y_n)^T$ . The following inequality can be stated:

$$2x^T y \leq kx^T x + \frac{1}{k}y^T y, \quad (16)$$

where  $k$  can be chosen as any arbitrary positive real number.

The key contribution of this paper can now be presented by the theorem stated below.

**Theorem 1.** *Suppose the conditions given by  $A_1$ ,  $A_2$ , and  $A_3$  hold. Let  $\kappa$  and  $\xi$  be positive real-valued numbers. Then, the origin of Cohen–Grossberg neural system of neutral type expressed by (5) is globally asymptotically stable if the system parameters of (5) satisfy the conditions:*

$$\varepsilon_i = \frac{\gamma_i^2}{\ell_i^2} - (2 + \kappa) \left( p_1 \sum_{j=1}^n \left| \sum_{k=1}^n a_{ki} a_{kj} \right| + p_2 \|A\|_2^2 \right) - (2 + \xi) \left( q_1 \sum_{j=1}^n \left| \sum_{k=1}^n b_{ki} b_{kj} \right| + q_2 \|B\|_2^2 \right) > 0, \quad (17)$$

$$\varepsilon_i = r_1 \left( \frac{1}{\rho_i^2} - \left( 1 + \frac{1}{\kappa} + \frac{1}{\xi} \right) \sum_{j=1}^n \sum_{k=1}^n \frac{1}{\mu_k^2} |e_{ki}| |e_{kj}| \right) + r_2 \left( \frac{1}{\rho_M^2} - \left( 1 + \frac{1}{\kappa} + \frac{1}{\xi} \right) \frac{1}{\mu_m^2} \|E\|_2^2 \right) > 0,$$

where  $\mu_m = \min_{1 \leq i \leq n} (\mu_i)$ ,  $\rho_M = \max_{1 \leq i \leq n} (\rho_i)$ ,  $p_1, p_2, q_1, q_2, r_1$ , and  $r_2$  are the binary constants such that  $p_1 + p_2 = 1$ ,  $p_1 p_2 = 0$ ,  $q_1 + q_2 = 1$ ,  $q_1 q_2 = 0$ ,  $r_1 + r_2 = 1$ , and  $r_1 r_2 = 0$ .

*Proof.* Construct a suitable Lyapunov functional candidate given by

$$\begin{aligned} V(t) = & \sum_{i=1}^n \int_0^{z_i(t)} 2 \frac{\beta_i(s)}{\alpha_i(s)} ds + \sum_{i=1}^n \int_{t-\zeta_i}^t \frac{1}{\alpha_i^2(z_i(s))} \frac{1}{z_i^2(s)} ds + k \sum_{i=1}^n \int_{t-\tau_i}^t z_i^2(s) ds, \\ & + (2 + \xi) \sum_{i=1}^n \int_{t-\tau_i}^t \ell_i^2 \left( q_1 \sum_{j=1}^n \left| \sum_{k=1}^n b_{ki} b_{kj} \right| + q_2 \|B\|_2^2 \right) z_i^2(s) ds, \end{aligned} \quad (18)$$

where  $k$  is a real-valued positive number whose appropriate value will be specified in the process of the proof. If we take the time derivative of the Lyapunov functional  $V(t)$  along the trajectories of Cohen–Grossberg neural network model defined by (5), we will derive the equation:

$$\begin{aligned} \dot{V}(t) = & \sum_{i=1}^n 2 \frac{\beta_i(z_i(t))}{\alpha_i(z_i(t))} \dot{z}_i(t) + (2 + \xi) \sum_{i=1}^n \ell_i^2 \left( q_1 \sum_{j=1}^n \left| \sum_{k=1}^n b_{ki} b_{kj} \right| + q_2 \|B\|_2^2 \right) z_i^2(t) \\ & - (2 + \xi) \sum_{i=1}^n \ell_i^2 \left( q_1 \sum_{j=1}^n \left| \sum_{k=1}^n b_{ki} b_{kj} \right| + q_2 \|B\|_2^2 \right) z_i^2(t - \tau_i) \\ & + \sum_{i=1}^n \left( \frac{1}{\alpha_i^2(z_i(t))} \dot{z}_i^2(t) - \frac{1}{\alpha_i^2(z_i(t - \zeta_i))} \dot{z}_i^2(t - \zeta_i) \right) \\ & + k \sum_{i=1}^n z_i^2(t) - k \sum_{i=1}^n z_i^2(t - \tau_i). \end{aligned} \quad (19)$$

(19) may be rearranged as

$$\begin{aligned} \dot{V}(t) = & 2\beta^T(z(t))\alpha^{-1}(z(t))\dot{z}(t) \\ & + \sum_{i=1}^n \left( -\frac{1}{\alpha_i^2(z_i(t - \zeta_i))} \dot{z}_i^2(t - \zeta_i) + k z_i^2(t) - k z_i^2(t - \tau_i) \right) \\ & + (\alpha^{-1}(z(t))\dot{z}(t))^T \alpha^{-1}(z(t))\dot{z}(t) \\ & + (2 + \xi) \sum_{i=1}^n \int_{t-\tau_i}^t \ell_i^2 \left( q_1 \sum_{j=1}^n \left| \sum_{k=1}^n b_{ki} b_{kj} \right| + q_2 \|B\|_2^2 \right) z_i^2(t) \\ & - (2 + \xi) \sum_{i=1}^n \int_{t-\tau_i}^t \ell_i^2 \left( q_1 \sum_{j=1}^n \left| \sum_{k=1}^n b_{ki} b_{kj} \right| + q_2 \|B\|_2^2 \right) z_i^2(t - \tau_i). \end{aligned} \quad (20)$$

Note the inequalities

$$\begin{aligned} 2\beta^T(z(t))\alpha^{-1}(z(t))\dot{z}(t) = & 2\beta^T(z(t))(-\beta(z(t))) \\ & + Ag(z(t)) + Bg(z(t - \tau)) \\ & + 2\beta^T(z(t))\alpha^{-1}(z(t))E\dot{z}(t - \zeta) \end{aligned} \quad (21)$$

$$\begin{aligned} & (\alpha^{-1}(z(t))\dot{z}(t))^T \alpha^{-1}(z(t))\dot{z}(t) \\ = & (-\beta(z(t)) + Ag(z(t)) + Bg(z(t - \tau)) + \alpha^{-1}(z(t))E\dot{z}(t - \zeta))^T \cdot \\ & (-\beta(z(t)) + Ag(z(t)) + Bg(z(t - \tau)) + \alpha^{-1}(z(t))E\dot{z}(t - \zeta)) \end{aligned} \quad (22)$$

Combining (22) with (23) leads to

$$\begin{aligned}
& \left( 2\beta^T(z(t)) + (\alpha^{-1}(z(t))\dot{z}(t))^T \right) \alpha^{-1}(z(t)) \dot{z}(t) \\
& - \beta^T(z(t))\beta(z(t)) + g^T(z(t))A^T Ag(z(t)) + g^T(z(t-\tau))B^T Bg(z(t-\tau)) \\
& + 2g^T(z(t))A^T Bg(z(t-\tau)) + 2g^T(z(t))A^T \alpha^{-1}(z(t))E\dot{z}(t-\zeta) \\
& + 2g^T(z(t-\tau))B^T \alpha^{-1}(z(t))E\dot{z}(t-\zeta) \\
& + \dot{z}^T(t-\zeta)E^T \alpha^{-1}(z(t))\alpha^{-1}(z(t))E\dot{z}(t-\zeta).
\end{aligned} \tag{23}$$

By the virtue of fact 5, the following inequalities can be written as

$$2g^T(z(t))A^T Bg(z(t-\tau)) \leq g^T(z(t))A^T Ag(z(t)) + g^T(z(t-\tau))B^T Bg(z(t-\tau)), \tag{24}$$

$$\begin{aligned}
2g^T(z(t))A^T \alpha^{-1}(z(t))E\dot{z}(t-\zeta) & \leq \kappa g^T(z(t))A^T Ag(z(t)) \\
& + \frac{1}{\kappa} \dot{z}^T(t-\zeta)E^T \alpha^{-2}(z(t))E\dot{z}(t-\zeta),
\end{aligned} \tag{25}$$

$$\begin{aligned}
2g^T(z(t-\tau))B^T \alpha^{-1}(z(t))E\dot{z}(t-\zeta) & \leq \xi g^T(z(t-\tau))B^T Bg(z(t-\tau)) \\
& + \frac{1}{\xi} \dot{z}^T(t-\zeta)E^T \alpha^{-2}(z(t))E\dot{z}(t-\zeta).
\end{aligned} \tag{26}$$

Using (24)–(26) in (23) results in

$$\begin{aligned}
& \left( 2\beta^T(z(t)) + (\alpha^{-1}(z(t))\dot{z}(t))^T \right) \alpha^{-1}(z(t)) \dot{z}(t) \\
& - \beta^T(z(t))\beta(z(t)) + (2 + \kappa)g^T(z(t))A^T Ag(z(t)) \\
& + (2 + \xi)g^T(z(t-\tau))B^T Bg(z(t-\tau)) + \left( 1 + \frac{1}{\kappa} + \frac{1}{\xi} \right) \dot{z}^T(t-\zeta)E^T \alpha^{-2}(z(t))E\dot{z}(t-\zeta)
\end{aligned} \tag{27}$$

We first note the following equality:

$$-\beta^T(z(t))\beta(z(t)) = -\sum_{i=1}^n \beta_i^2(z_i(t)). \tag{28}$$

By fact 3, we express the inequalities:

$$\begin{aligned}
g^T(z(t))A^T Ag(z(t)) & \leq \sum_{i=1}^n \left( p_1 \sum_{j=1}^n \left| \sum_{k=1}^n a_{ki} a_{kj} \right| g_i^2(z_i(t)) + p_2 \|A\|_2^2 g_i^2(z(t)) \right), \\
g^T(z(t-\tau))B^T Bg(z(t-\tau)) & \leq q_1 \sum_{i=1}^n \sum_{j=1}^n \left| \sum_{k=1}^n b_{ki} b_{kj} \right| g_i^2(z_i(t-\tau_i)) \\
& + q_2 \|B\|_2^2 \sum_{i=1}^n g_i^2(z_i(t-\tau_i)).
\end{aligned} \tag{29}$$

Using the property of fact 4, we express the inequality:

$$\begin{aligned} \dot{z}^T(t-\zeta)E^T\alpha^{-2}(z(t))E\dot{z}(t-\zeta) &\leq \sum_{i=1}^n \left( r_1 \sum_{j=1}^n \sum_{k=1}^n \frac{1}{\alpha_k^2(z_k(t))} |e_{ki}| |e_{kj}| z_i^2(t-\zeta_i) \right. \\ &\left. + r_2 \|\alpha^{-2}(z(t))\|_2^2 \|E\|_2^2 \dot{z}_i^2(t-\zeta_i) \right). \end{aligned} \quad (30)$$

Using (28)–(30) in (27) yields

$$\begin{aligned} &(2\beta^T(z(t)) + (\alpha^{-1}(z(t))\dot{z}(t))^T)\alpha^{-1}(z(t))\dot{z}(t) \\ &+ (2 + \xi) \sum_{i=1}^n \left( \left( q_1 \sum_{j=1}^n \left| \sum_{k=1}^n b_{ki} b_{kj} \right| g_i^2(z_i(t-\tau_i)) + q_2 \|B\|_2^2 g_i^2(z_i(t-\tau_i)) \right) \right) \\ &\leq - \sum_{i=1}^n \left( \beta_i^2(z_i(t)) + (2 + \kappa) \left( p_1 \sum_{j=1}^n \left| \sum_{k=1}^n a_{ki} a_{kj} \right| g_i^2(z_i(t)) + p_2 \|A\|_2^2 g_i^2(z_i(t)) \right) \right) \quad (31) \\ &+ \left( 1 + \frac{1}{\kappa} + \frac{1}{\xi} \right) \left( r_1 \sum_{i=1}^n \sum_{j=1}^n \sum_{k=1}^n \frac{1}{\alpha_k^2(z_k(t))} |e_{ki}| |e_{kj}| z_i^2(t-\zeta_i) \right. \\ &\left. + r_2 \|\alpha^{-2}(z(t))\|_2^2 \|E\|_2^2 \sum_{i=1}^n \dot{z}_i^2(t-\zeta_i) \right). \end{aligned}$$

$A_1$  implies the following inequalities:

$$\frac{1}{\alpha_k^2(z_k(t))} \leq \frac{1}{\mu_k^2} \quad (32)$$

$$\|\alpha^{-2}(z(t))\|_2^2 \leq \frac{1}{\mu_m^2}. \quad (33)$$

$A_2$  implies that

$$\gamma_i^2 z_i^2(t) \leq \beta_i^2(z_i(t)). \quad (34)$$

$A_3$  implies that

$$g_i^2(z_i(t)) \leq \ell_i^2 z_i^2(t) \quad (35)$$

$$g_i^2(z_i(t-\tau_i)) \leq \ell_i^2 z_i^2(t-\tau_i). \quad (36)$$

Using (32)–(36) in (37) leads to

$$\begin{aligned} &(2\beta^T(z(t)) + (\alpha^{-1}(z(t))\dot{z}(t))^T)\alpha^{-1}(z(t))\dot{z}(t) \\ &- \sum_{i=1}^n \gamma_i^2 z_i^2(t) + (2 + \kappa) \sum_{i=1}^n \ell_i^2 \left( p_1 \sum_{j=1}^n \left| \sum_{k=1}^n a_{ki} a_{kj} \right| + p_2 \|A\|_2^2 \right) z_i^2(t) \\ &\leq \\ &+ (2 + \xi) \sum_{i=1}^n \ell_i^2 \left( q_1 \sum_{j=1}^n \left| \sum_{k=1}^n b_{ki} b_{kj} \right| + q_2 \|B\|_2^2 \right) z_i^2(t-\tau_i) \\ &+ \left( 1 + \frac{1}{\kappa} + \frac{1}{\xi} \right) \sum_{i=1}^n \left( r_1 \sum_{j=1}^n \sum_{k=1}^n \frac{1}{\mu_k^2} |e_{ki}| |e_{kj}| + r_2 \frac{1}{\mu_m^2} \|E\|_2^2 \right) z_i^2(t-\zeta_i). \end{aligned} \quad (37)$$

$A_1$  implies the following inequality:

$$\frac{1}{\rho_M^2} \leq \frac{1}{\rho_i^2} \leq \frac{1}{\alpha_i^2(z_i(t-\zeta_i))}. \quad (38)$$

Then, by (38), we can write



$$\begin{aligned}
-\sum_{i=1}^n \frac{1}{\alpha_i^2(z_i(t-\zeta_i))} \dot{z}_i^2(t-\zeta_i) &\leq -r_1 \sum_{i=1}^n \frac{1}{\rho_i^2} \dot{z}_i^2(t-\zeta_i) \\
&\quad - r_2 \frac{1}{\rho_M^2} \sum_{i=1}^n \dot{z}_i^2(t-\zeta_i).
\end{aligned} \tag{39}$$

Using (37) and (39) in (20) results in

$$\begin{aligned}
\dot{V}(t) &\leq \sum_{i=1}^n \left( -\gamma_i^2 z_i^2(t) + (2+\kappa) \ell_i^2 \left( p_1 \sum_{j=1}^n \left| \sum_{k=1}^n a_{ki} a_{kj} \right| + p_2 \|A\|_2^2 \right) z_i^2(t) \right. \\
&\quad \left. + (2+\xi) \sum_{i=1}^n \ell_i^2 \left( q_1 \sum_{j=1}^n \left| \sum_{k=1}^n b_{ki} b_{kj} \right| + q_2 \|B\|_2^2 \right) z_i^2(t) \right. \\
&\quad \left. + \left( 1 + \frac{1}{\kappa} + \frac{1}{\xi} \right) \sum_{i=1}^n \left( r_1 \sum_{j=1}^n \sum_{k=1}^n \frac{1}{\mu_k^2} |e_{ki}| |e_{kj}| + r_2 \frac{1}{\mu_m^2} \|E\|_2^2 \right) z_i^2(t-\zeta_i) \right. \\
&\quad \left. - r_1 \sum_{i=1}^n \frac{1}{\rho_i^2} \dot{z}_i^2(t-\zeta_i) - r_2 \frac{1}{\rho_M^2} \sum_{i=1}^n \dot{z}_i^2(t-\zeta_i) + k \sum_{i=1}^n (z_i^2(t) - z_i^2(t-\tau_i)) \right) \\
&= -\sum_{i=1}^n \ell_i^2 \left( \frac{\gamma_i^2}{\rho_i^2} - (2+\kappa) \left( p_1 \sum_{j=1}^n \left| \sum_{k=1}^n a_{ki} a_{kj} \right| + p_2 \|A\|_2^2 \right) \right. \\
&\quad \left. - (2+\xi) \left( q_1 \sum_{j=1}^n \left| \sum_{k=1}^n b_{ki} b_{kj} \right| + q_2 \|B\|_2^2 \right) \right) z_i^2(t) \\
&\quad - \sum_{i=1}^n r_1 \left( \frac{1}{\rho_i^2} - \left( 1 + \frac{1}{\kappa} + \frac{1}{\xi} \right) \sum_{j=1}^n \sum_{k=1}^n \frac{1}{\mu_k^2} |e_{ki}| |e_{kj}| \right) z_i^2(t-\zeta_i) \\
&\quad - \sum_{i=1}^n r_2 \left( \frac{1}{\rho_M^2} - \left( 1 + \frac{1}{\kappa} + \frac{1}{\xi} \right) \frac{1}{\mu_m^2} \|E\|_2^2 \right) z_i^2(t-\zeta_i) + k \sum_{i=1}^n (z_i^2(t) - z_i^2(t-\tau_i)) \\
&= \sum_{i=1}^n (-\varepsilon_i \ell_i^2 z_i^2(t) - \varepsilon_i \dot{z}_i^2(t-\zeta_i)) + k \sum_{i=1}^n (z_i^2(t) - z_i^2(t-\tau_i)) \\
&\leq \sum_{i=1}^n (-\varepsilon_m \ell_m^2 z_i^2(t) - \varepsilon_m \dot{z}_i^2(t-\zeta_i)) + k \sum_{i=1}^n (z_i^2(t) - z_i^2(t-\tau_i)) \\
&= -(\varepsilon_m \ell_m^2 - k) \|z(t)\|_2^2 - \varepsilon_m \|\dot{z}(t-\zeta)\|_2^2 - k \|z(t-\tau)\|_2^2,
\end{aligned} \tag{40}$$

where  $\varepsilon_m = \min_{1 \leq i \leq n} (\varepsilon_i)$ ,  $\ell_m = \min_{1 \leq i \leq n} (\ell_i)$ , and  $\ell_m = \min_{1 \leq i \leq n} (\ell_i)$ .

From (40), one can obtain the inequality:

$$\dot{V}(t) \leq -(\varepsilon_m \ell_m^2 - k) \|z(t)\|_2^2. \tag{41}$$

In (41), the choice  $k < \varepsilon_m \ell_m^2$  will make it possible for  $\dot{V}(t)$  to be negative definite and every transformed states  $z(t) \neq 0$ .

In (40), taking  $z(t) \neq 0$  will directly yield the result:

$$\dot{V}(t) \leq -k \|z(t-\tau)\|_2^2. \tag{42}$$

(42) directly implies that  $\dot{V}(t)$  will have negative values for every transformed delayed state  $z(t-\tau) \neq 0$ .

Let the transformed state  $z(t) = 0$  together with delayed transformed state  $z(t-\tau) = 0$ . Then, we immediately get from (40) that

$$\dot{V}(t) \leq -\varepsilon_m \|\dot{z}(t-\zeta)\|_2^2. \tag{43}$$

(43) directly yields that time derivative of this studied Lyapunov functional  $\dot{V}(t)$  will be negative for every  $\dot{z}(t - \zeta) \neq 0$ .

Let  $z(t) = 0$ ,  $z(t - \tau) = 0$ , and  $\dot{z}(t - \zeta) = 0$ . This case leads to the fact that  $\dot{z}(t) = 0$ . Hence, from (19), we get that  $\dot{V}(t) = 0$ . Hence, we note that  $\dot{V}(t) = 0$  at the equilibrium point which is the origin of system (5) and  $\dot{V}(t) < 0$  except for the equilibrium point. Hence, this Lyapunov functional analysis ensures that the origin of system (5) is asymptotically stable. In addition, the Lyapunov functional given by (18) is radially bounded, meaning that  $V(t) \rightarrow \infty$  when  $\|z(t)\| \rightarrow \infty$ . The radially unboundedness of this Lyapunov functional guarantees that the origin of neutral-type Cohen–Grossberg neural network (5) is globally asymptotically stable. Q.E.D.  $\square$

### 3. An Instructive Example

This section gives an instructive example for the sake of indicating the applicability of results expressed by the conditions of Theorem 1.

Example: consider a case of neutral-type neural system (1) of four neurons, which has the system matrices given as follows:

$$\begin{aligned}
 A &= \frac{1}{2} \begin{bmatrix} a & a & a & a \\ -a & -a & a & a \\ -a & a & -a & a \\ a & -a & -a & a \end{bmatrix}, \\
 B &= \frac{1}{2} \begin{bmatrix} b & b & b & b \\ -b & -b & b & b \\ -b & b & -b & b \\ b & -b & -b & b \end{bmatrix}, \\
 E &= \frac{1}{2} \begin{bmatrix} e & e & e & e \\ e & e & e & e \\ e & e & e & e \\ e & e & e & e \end{bmatrix},
 \end{aligned} \tag{44}$$

where  $a$ ,  $b$ , and  $e$  are being some positive constants. For this example, we also make the choices for the parameters  $\mu_1 = \mu_2 = \mu_3 = \mu_4 = 1$ ,  $\rho_1 = \rho_2 = \rho_3 = \rho_4 = 1$ ,  $\gamma_1 = \gamma_2 = \gamma_3 = \gamma_4 = 2$ ,  $\psi_1 = \psi_2 = \psi_3 = \psi_4 = 2$ , and  $\ell_1 = \ell_2 = \ell_3 = \ell_4 = 1$ . For the system matrices  $A$ ,  $B$ , and  $E$ , one may calculate

$$\begin{aligned}
 A^T A &= \begin{bmatrix} a^2 & 0 & 0 & 0 \\ 0 & a^2 & 0 & 0 \\ 0 & 0 & a^2 & 0 \\ 0 & 0 & 0 & a^2 \end{bmatrix}, \\
 B^T B &= \begin{bmatrix} b^2 & 0 & 0 & 0 \\ 0 & b^2 & 0 & 0 \\ 0 & 0 & b^2 & 0 \\ 0 & 0 & 0 & b^2 \end{bmatrix}, \\
 E^T E &= \begin{bmatrix} e^2 & e^2 & e^2 & e^2 \\ e^2 & e^2 & e^2 & e^2 \\ e^2 & e^2 & e^2 & e^2 \\ e^2 & e^2 & e^2 & e^2 \end{bmatrix}.
 \end{aligned} \tag{45}$$

Then, we can obtain the following:  $\|A\|_2^2 = a^2$ ,  $\|B\|_2^2 = b^2$ ,  $\|E\|_2^2 = 4e^2$ , and

$$\begin{aligned}
 \sum_{j=1}^4 \left| \sum_{k=1}^4 a_{ki} a_{kj} \right| &= a^2, \quad \sum_{j=1}^4 \left| \sum_{k=1}^4 b_{ki} b_{kj} \right| = b^2, \\
 \sum_{j=1}^4 \sum_{k=1}^4 |e_{ki}| |e_{kj}| &= 4e^2, \quad i = 1, 2, 3, 4.
 \end{aligned} \tag{46}$$

According to Theorem 1, this example establishes the following conditions:

$$\begin{aligned}
 \varepsilon_i &= 4 - (2 + \kappa)(p_1 + p_2)a^2 - (2 + \xi)(q_1 + q_2)b^2 \\
 &= 4 - (2 + \kappa)a^2 - (2 + \xi)b^2, \\
 \varepsilon_i &= r_1 \left( 1 - \left( 1 + \frac{1}{\kappa} + \frac{1}{\xi} \right) 4e^2 \right) + r_2 \left( 1 - \left( 1 + \frac{1}{\kappa} + \frac{1}{\xi} \right) 4e^2 \right) \\
 &= \left( 1 - \left( 1 + \frac{1}{\kappa} + \frac{1}{\xi} \right) 4e^2 \right).
 \end{aligned} \tag{47}$$

Let  $\kappa = 2$  and  $\xi = 2$ . Then,  $\varepsilon_i = 4(1 - a^2 - b^2)$  and  $\varepsilon_i = 1 - 8e^2$ ,  $i = 1, 2, 3, 4$ . Clearly, the conditions  $a^2 + b^2 < 1$  and  $e < (1/2\sqrt{2})$  establish the global stability of system (5).

### 4. Conclusions

This research work has been conducted as an investigation of the stability issues for neutral-type Cohen–Grossberg neural network models possessing discrete time delays in states and discrete neutral delays in time derivatives of neuron states. By setting a novel generalized appropriate Lyapunov

functional candidate, some new sufficient conditions have been proposed for global asymptotic stability for the considered delayed neural networks of neutral type. This paper has exploited some basic properties of matrices in the derivation of the results that established a set of algebraic mathematical relationships between network parameters of the neural system. The obtained stability criteria proved to be independent from the time and neutral delays. Therefore, the proposed results can be easily verified. A constructive numerical example has also been presented to check the applicability of the presented global stability conditions.

## Data Availability

No data were used to support this study.

## Conflicts of Interest

The author declares that there are no conflicts of interest.

## References

- [1] M. A. Cohen and S. Grossberg, "Absolute stability of global pattern formation and parallel memory storage by competitive neural networks," *IEEE Transactions on Systems, Man, and Cybernetics*, vol. SMC-13, no. 5, pp. 815–826, 1983.
- [2] L. Wang and X. Zou, "Exponential stability of Cohen-Grossberg neural networks," *Neural Networks*, vol. 15, no. 3, pp. 415–422, 2002.
- [3] S. Mohamad and K. Gopalsamy, "Exponential stability of continuous-time and discrete-time cellular neural networks with delays," *Applied Mathematics and Computation*, vol. 135, no. 1, pp. 17–38, 2003.
- [4] J. J. Hopfield, "Neural networks and physical systems with emergent collective computational abilities," *Proceedings of the National Academy of Sciences*, vol. 79, no. 8, pp. 2554–2558, 1982.
- [5] L. O. Chua and L. Yang, "Cellular neural networks: theory," *IEEE Transactions on Circuits and Systems*, vol. 35, no. 10, pp. 1257–1272, 1988.
- [6] A. Guez, V. Protopopescu, and J. Barhen, "On the stability, and design of nonlinear continuous neural networks," *IEEE Transactions on Systems, Man and Cybernetics*, vol. 18, no. 1, pp. 80–87, 1998.
- [7] S. C. Tong, Y. M. Li, and H. G. Zhang, "Adaptive neural network decentralized backstepping output-feedback control for nonlinear large-scale systems with time delays," *IEEE Transactions on Neural Networks*, vol. 22, no. 7, pp. 1073–1086, 2011.
- [8] M. Galicki, H. Witte, J. Dörschel, M. Eiselt, and G. Griessbach, "Common optimization of adaptive preprocessing units and a neural network during the learning period. Application in EEG pattern recognition," *Neural Networks*, vol. 10, no. 6, pp. 1153–1163, 1997.
- [9] B. Kosko, "Bidirectional associative memories," *IEEE Transactions on Systems, Man, and Cybernetics*, vol. 18, no. 1, pp. 49–60, 1988.
- [10] H. Zhu, R. Rakkiyappan, and X. Li, "Delayed state-feedback control for stabilization of neural networks with leakage delay," *Neural Networks*, vol. 105, pp. 249–255, 2018.
- [11] Q. Song, Q. Yu, Z. Zhao, Y. Liu, and F. E. Alsaadi, "Boundedness and global robust stability analysis of delayed complex-valued neural networks with interval parameter uncertainties," *Neural Networks*, vol. 103, pp. 55–62, 2018.
- [12] J. Wang, H. Jiang, T. Ma, and C. Hu, "Delay-dependent dynamical analysis of complex-valued memristive neural networks: continuous-time and discrete-time cases," *Neural Networks*, vol. 101, pp. 33–46, 2018.
- [13] W. Xie and Q. Zhu, "Mean square exponential stability of stochastic fuzzy delayed Cohen-Grossberg neural networks with expectations in the coefficients," *Neurocomputing*, vol. 166, pp. 133–139, 2015.
- [14] Q. Zhu and J. Cao, "Robust exponential stability of Markovian jump impulsive stochastic Cohen-Grossberg neural networks with mixed time delays," *IEEE Transactions on Neural Networks*, vol. 21, no. 8, pp. 1314–1325, 2010.
- [15] H. Liu, Z. Wang, B. Shen, T. Huang, and F. E. Alsaadi, "Stability analysis for discrete-time stochastic memristive neural networks with both leakage and probabilistic delays," *Neural Networks*, vol. 102, pp. 1–9, 2018.
- [16] R. Manivannan, R. Samidurai, J. Cao, A. Alsaadi, and F. E. Alsaadi, "Stability analysis of interval time-varying delayed neural networks including neutral time-delay and leakage delay," *Chaos, Solitons & Fractals*, vol. 114, pp. 433–445, 2018.
- [17] J. Zhou, Y. Liu, J. Xia, Z. Wang, and S. Arik, "Resilient fault-tolerant anti-synchronization for stochastic delayed reaction-diffusion neural networks with semi-Markov jump parameters," *Neural Networks*, vol. 125, pp. 194–204, 2020.
- [18] Z. Xu, X. Li, and P. Duan, "Synchronization of complex networks with time-varying delay of unknown bound via delayed impulsive control," *Neural Networks*, vol. 125, pp. 224–232, 2020.
- [19] X. Song, J. Man, S. Song, and Z. Wang, "Finite-time nonfragile time-varying proportional retarded synchronization for Markovian Inertial Memristive NNs with reaction-diffusion items," *Neural Networks*, vol. 123, pp. 317–330, 2020.
- [20] X. You, Q. Song, and Z. Zhao, "Existence and finite-time stability of discrete fractional-order complex-valued neural networks with time delays," *Neural Networks*, vol. 123, pp. 248–260, 2020.
- [21] J. Xiao, S. Wen, X. Yang, and S. Zhong, "New approach to global Mittag-Leffler synchronization problem of fractional-order quaternion-valued BAM neural networks based on a new inequality," *Neural Networks*, vol. 122, pp. 320–337, 2020.
- [22] X. Huang, J. Jia, Y. Fan, Z. Wang, and J. Xia, "Interval matrix method based synchronization criteria for fractional-order memristive neural networks with multiple time-varying delays," *Journal of the Franklin Institute*, vol. 357, no. 3, pp. 1707–1733, 2020.
- [23] M. S. Ali, G. Narayanan, S. Sevgen, V. Shekher, and S. Arik, "Global stability analysis of fractional-order fuzzy BAM neural networks with time delay and impulsive effects," *Communications in Nonlinear Science and Numerical Simulation*, vol. 78, Article ID 104853, 2019.
- [24] Y. Cao, S. Wang, Z. Guo, T. Huang, and S. Wen, "Synchronization of memristive neural networks with leakage delay and parameters mismatch via event-triggered control," *Neural Networks*, vol. 119, pp. 178–189, 2019.
- [25] T. Wei, P. Lin, Y. Wang, and L. Wang, "Stability of stochastic impulsive reaction-diffusion neural networks with S-type distributed delays and its application to image encryption," *Neural Networks*, vol. 116, pp. 35–45, 2019.
- [26] M. S. Mahmoud and A. Ismail, "Improved results on robust exponential stability criteria for neutral-type delayed neural

- networks," *Applied Mathematics and Computation*, vol. 217, no. 7, pp. 3011–3019, 2010.
- [27] J. H. Park, O. M. Kwon, and S. M. Lee, "LMI optimization approach on stability for delayed neural networks of neutral-type," *Applied Mathematics and Computation*, vol. 196, no. 1, pp. 236–244, 2008.
- [28] R. Rakkiyappan and P. Balasubramaniam, "LMI conditions for global asymptotic stability results for neutral-type neural networks with distributed time delays," *Applied Mathematics and Computation*, vol. 204, no. 1, pp. 317–324, 2008.
- [29] S. M. Lee, O. M. Kwon, and J. H. Park, "A novel delay-dependent criterion for delayed neural networks of neutral type," *Physics Letters A*, vol. 374, no. 17–18, pp. 1843–1848, 2010.
- [30] S. Xu, J. Lam, D. W. C. Ho, and Y. Zou, "Delay-dependent exponential stability for a class of neural networks with time delays," *Journal of Computational and Applied Mathematics*, vol. 183, no. 1, pp. 16–28, 2005.
- [31] R. Rakkiyappan and P. Balasubramaniam, "New global exponential stability results for neutral type neural networks with distributed time delays," *Neurocomputing*, vol. 71, no. 4–6, pp. 1039–1045, 2008.
- [32] W. Weera and P. Niamsup, "Novel delay-dependent exponential stability criteria for neutral-type neural networks with non-differentiable time-varying discrete and neutral delays," *Neurocomputing*, vol. 173, pp. 886–898, 2016.
- [33] M. Zheng, L. Li, H. Peng, J. Xiao, Y. Yang, and H. Zhao, "Finite-time stability analysis for neutral-type neural networks with hybrid time-varying delays without using Lyapunov method," *Neurocomputing*, vol. 238, pp. 67–75, 2017.
- [34] Y. Dong, L. Guo, and J. Hao, "Robust exponential stabilization for uncertain neutral neural networks with interval time-varying delays by periodically intermittent control," *Neural Computing and Applications*, vol. 32, no. 7, pp. 2651–2664, 2020.
- [35] K. Shi, H. Zhu, S. Zhong, Y. Zeng, and Y. Zhang, "New stability analysis for neutral type neural networks with discrete and distributed delays using a multiple integral approach," *Journal of the Franklin Institute*, vol. 352, no. 1, pp. 155–176, 2015.
- [36] K. Shi, S. Zhong, H. Zhu, X. Liu, and Y. Zeng, "New delay-dependent stability criteria for neutral-type neural networks with mixed random time-varying delays," *Neurocomputing*, vol. 168, pp. 896–907, 2015.
- [37] D. Liu and Y. Du, "New results of stability analysis for a class of neutral-type neural network with mixed time delays," *International Journal of Machine Learning and Cybernetics*, vol. 6, no. 4, pp. 555–566, 2015.
- [38] R. Samidurai, S. Rajavel, R. Sriraman, J. Cao, A. Alsaedi, and F. E. Alsaadi, "Novel results on stability analysis of neutral-type neural networks with additive time-varying delay components and leakage delay," *International Journal of Control, Automation and Systems*, vol. 15, no. 4, pp. 1888–1900, 2017.
- [39] K. Shi, H. Zhu, S. Zhong, Y. Zhang, and W. Wang, "Stability analysis of neutral type neural networks with mixed time-varying delays using triple-integral and delay-partitioning methods," *ISA Transactions*, vol. 58, pp. 85–95, 2015.
- [40] P. Balasubramaniam, G. Nagamani, and R. Rakkiyappan, "Global passivity analysis of interval neural networks with discrete and distributed delays of neutral type," *Neural Processing Letters*, vol. 32, no. 2, pp. 109–130, 2010.
- [41] H. Mai, X. Liao, and C. Li, "A semi-free weighting matrices approach for neutral-type delayed neural networks," *Journal of Computational and Applied Mathematics*, vol. 225, no. 1, pp. 44–55, 2009.
- [42] S. Lakshmanan, C. P. Lim, M. Prakash, S. Nahavandi, and P. Balasubramaniam, "Neutral-type of delayed inertial neural networks and their stability analysis using the LMI Approach," *Neurocomputing*, vol. 230, pp. 243–250, 2017.
- [43] Z. Tu and L. Wang, "Global Lagrange stability for neutral type neural networks with mixed time-varying delays," *International Journal of Machine Learning and Cybernetics*, vol. 9, no. 4, pp. 599–609, 2018.
- [44] Y. Ma, N. Ma, L. Chen, Y. Zheng, and Y. Han, "Exponential stability for the neutral-type singular neural network with time-varying delays," *International Journal of Machine Learning and Cybernetics*, vol. 10, no. 5, pp. 853–858, 2019.
- [45] H. Zhang, Z. Liu, and G. B. Huang, "Novel delay-dependent robust stability analysis for switched neutral-type neural networks with time-varying delays via SC technique," *IEEE Transactions on Systems, Man, and Cybernetics-Part B: Cybernetics*, vol. 40, pp. 1480–1491, 2010.

## Research Article

# Upper and Lower Bounds for the Kirchhoff Index of the $n$ -Dimensional Hypercube Network

Jia-Bao Liu <sup>1,2</sup>, Jing Zhao,<sup>2</sup> Zhi-Yu Shi,<sup>2</sup> Jinde Cao <sup>1</sup> and Fuad E. Alsaadi <sup>3</sup>

<sup>1</sup>School of Mathematics, Southeast University, Nanjing 210096, China

<sup>2</sup>School of Mathematics and Physics, Anhui Jianzhu University, Hefei 230601, China

<sup>3</sup>Department of Electrical and Computer Engineering, Faculty of Engineering, King Abdulaziz University, Jeddah 21589, Saudi Arabia

Correspondence should be addressed to Jinde Cao; [jdcao@seu.edu.cn](mailto:jdcao@seu.edu.cn)

Received 17 March 2020; Revised 15 May 2020; Accepted 26 May 2020; Published 16 June 2020

Academic Editor: Eric Campos

Copyright © 2020 Jia-Bao Liu et al. This is an open access article distributed under the Creative Commons Attribution License, which permits unrestricted use, distribution, and reproduction in any medium, provided the original work is properly cited.

The hypercube  $Q_n$  is one of the most admirable and efficient interconnection network due to its excellent performance for some practical applications. The Kirchhoff index  $Kf(G)$  is equal to the sum of resistance distances between any pairs of vertices in networks. In this paper, we deduce some bounds with respect to Kirchhoff index of hypercube network  $Q_n$ .

## 1. Introduction

Network is usually modelled by a connected graph  $G = (V_G, E_G)$  with order  $n$ , labeled as  $V_G = \{v_1, v_2, \dots, v_n\}$  and  $E_G = \{e_1, e_2, \dots, e_m\}$ . The adjacency matrix  $A(G)$  of  $G$  is a square matrix with  $n$  vertices, in which elements  $a_{ij}$  are 1 or 0, depending on whether there is an edge or not between vertices  $i$  and  $j$ . The degree diagonal matrix of  $G$  is denoted by  $D(G) = \text{diag}\{d_1, d_2, \dots, d_n\}$ , where  $d_1, d_2, \dots, d_n$  are the degree of vertices  $v_1, v_2, \dots, v_n$ , respectively. Together with the adjacency and degree matrix, one arrives at the Laplacian matrix, whose expression can be written as  $L(G) = D(G) - A(G)$ . For other notations and graph theoretical terminologies that not state here, we follow [1].

Various parameters are always used to characterize and describe the complex networks of which the fundamental one is named as the distance  $d_{ij}$ , concerned as the shortest path between the vertices  $i$  and  $j$  in networks. Similarly considering the distance  $d_{ij}$ , Klein and Randić in 1993 presented a novel distance function, named as resistance distance [2]. Denote  $r_{ij}$  the resistance distance between two arbitrary vertices  $i$  and  $j$  in electrical networks by replacing every edge by a unit resistor [3–7]. The Kirchhoff index  $Kf(G)$  of networks is defined as

$$Kf(G) = \sum_{i < j} r_{ij}(G). \quad (1)$$

The Kirchhoff index has attracted more and more attentions due to its practical applications in the fields of physical interpretations, electric circuit, and so on [8–11]. The Kirchhoff index of some product graphs, join graphs, and corona graphs were studied [5, 7]. The more results of the applications on the Kirchhoff index were explored in [12–14].

In what follows, the rest of the context is summarized. Section 2 proposes the main definition and preliminaries in our discussion. Some bounds on the Kirchhoff index of hypercubes  $Q_n$  are deduced in Section 3. We conclude the paper in Section 4.

## 2. Definition and Preliminaries

In this section, we recall some basic definition in graph theory. The hypercube network  $Q_n$  may be constructed from the family of subsets of a set with a binary string of length  $n$ , by making a vertex for each possible subset and joining two vertices by an edge whenever the corresponding subsets differ in a single binary string. The hypercube network  $Q_n$  admits several definitions of which one is stated as below [15].

The hypercube network  $Q_n$  is repeatedly constructed by making two copies of  $Q_{n-1}$ , written as  $Q_{n-1}^0$  and  $Q_{n-1}^1$ , respectively. Meanwhile, adding repeatedly  $2^{n-1}$  edges as below, let  $V(Q_{n-1}^0) = \{0U = 0u_2u_3 \dots u_n; u_i = 0 \text{ or } 1\}$  and  $V(Q_{n-1}^1) = \{1V = 1v_2v_3 \dots v_n; v_i = 0 \text{ or } 1\}$ . A node  $0U = 0u_2u_3 \dots u_n$  of

$Q_{n-1}^0$  is linked to another node  $1V = 1v_2v_3 \dots v_n$  of  $Q_{n-1}^1$  if and only if  $u_i = v_i$  for each  $i, 2 \leq i \leq n$ .

The hypercube network  $Q_n$  obtained more and more admirable concentrations due to its surprising properties, for instance, symmetry, regular structure, strong connectivity, small diameter, and so on [16, 17]. For more results on the hypercube network and its applications, see [18–21].

Next, we recall the formula for the Kirchhoff index in the hypercube  $Q_n$  with  $n \geq 2$ .

**Theorem 1** (see [3]). *For the hypercube network  $Q_n$  with  $n \geq 2$ ,*

$$\text{Kf}(Q_n) = 2^n \sum_{i=1}^n \binom{n}{i} \frac{1}{2i}, \quad (2)$$

where  $2i (i = 1, \dots, n)$  is the eigenvalue of the Laplacian matrix of the hypercube network and the binomial coefficients  $\binom{n}{i}$  are the multiplicities of the eigenvalues  $2i$ .

**Theorem 2** (see [22]).

$$\lim_{n \rightarrow \infty} \sum_{i=0}^{n-1} \frac{n}{2^i(n-i)} = 2. \quad (3)$$

The authors of [23] obtained a closed-form formula for the Kirchhoff index of the  $d$ -dimensional hypercube and found the asymptotic value  $2^{2^d}/d$  by using probabilistic tools. The result of Theorem 3 is obtained by directly calculating the eigenvalues of the Laplacian matrix of the hypercube network, which is different from the technique in [23].

### 3. Main Results

In this section, one will estimate the Kirchhoff index of  $n$ -dimensional hypercube, i.e., our goal is to estimate the quantity:

$$2^n \sum_{i=1}^n \binom{n}{i} \frac{1}{2i}. \quad (4)$$

**Theorem 3.** *For the hypercube network  $Q_n$  with  $n \geq 2$ , then*

$$\frac{4^n}{n} \left( \frac{n}{n+1} - \frac{n(n+2)}{2^{n+1}(n+1)} \right) \leq \text{Kf}(Q_n). \quad (5)$$

Consider that

$$\begin{aligned} \sum_{i=1}^n \binom{n}{i} \frac{1}{i} &\geq \sum_{i=1}^n \binom{n}{i} \frac{1}{i+1} \\ &= \binom{n}{1} \frac{1}{2} + \binom{n}{2} \frac{1}{3} + \dots + \binom{n}{n} \frac{1}{n+1} \\ &= \frac{1}{2} \frac{n!}{1!(n-1)!} + \frac{1}{3} \frac{n!}{2!(n-2)!} + \dots + \frac{1}{n+1} \\ &= \frac{1}{n+1} \frac{(n+1)!}{2!(n-1)!} + \frac{1}{n+1} \frac{(n+1)!}{3!(n-2)!} + \dots + \frac{1}{n+1} \\ &= \sum_{i=1}^n \binom{n+1}{i+1} \frac{1}{n+1}. \end{aligned} \quad (6)$$

By virtue of

$$\sum_{i=1}^n \binom{n+1}{i+1} = 2^{n+1} - n - 2. \quad (7)$$

By means of calculating the right of equation (6), one can establish the following identity:

$$\sum_{i=1}^n \binom{n+1}{i+1} \frac{1}{n+1} = \frac{2^{n+1} - n - 2}{n+1}. \quad (8)$$

Since

$$\frac{2^{n+1} - n - 2}{n+1} \leq \sum_{i=1}^n \binom{n}{i} \frac{1}{i} = 2 \sum_{i=1}^n \binom{n}{i} \frac{1}{2i}, \quad (9)$$

$$\frac{2^{n+1} - n - 2}{n+1} \leq 2 \sum_{i=1}^n \binom{n}{i} \frac{1}{2i}.$$

Hence,

$$\frac{2^n 2^n}{n+1} - \frac{2^{n-1}(n+2)}{n+1} = 2^{n-1} \frac{2^{n+1} - n - 2}{n+1} \leq \text{Kf}(Q_n) = 2^n \sum_{i=1}^n \binom{n}{i} \frac{1}{2i} \quad (10)$$

Simply, from the left of the above inequality, we obtain

$$\frac{4^n}{n} \left( \frac{n}{n+1} - \frac{n(n+2)}{2^{n+1}(n+1)} \right) \leq \text{Kf}(Q_n). \quad (11)$$

Apparently, the left of the above inequality converges to the asymptotic value  $2^{2^d}/d$  for large enough  $n$ . The proof of lower bound is completed.

For the upper bound, we have similar theorem to consider as follows.

**Theorem 4.** *For the hypercube networks  $Q_n$  with  $n \geq 2$ , then*

$$\text{Kf}(Q_n) \leq \frac{4^n}{n} \left( \frac{2n}{n+1} - \frac{n+2}{2^n(n+1)} \right), \quad (12)$$

$$\begin{aligned} \sum_{i=1}^n \frac{1}{2i} C_n^i &\leq \sum_{i=1}^n \frac{1}{i+1} C_n^i \\ &= \frac{1}{2} C_n^1 + \frac{1}{3} C_n^2 + \dots + \frac{1}{n+1} C_n^n \\ &= \frac{1}{2} \frac{n!}{1!(n-1)!} + \frac{1}{3} \frac{n!}{2!(n-2)!} + \dots + \frac{1}{n+1} \\ &= \frac{1}{n+1} \frac{(n+1)!}{2!(n-1)!} + \frac{1}{n+1} \frac{(n+1)!}{3!(n-2)!} + \dots + \frac{1}{n+1} \\ &= \sum_{i=1}^n \frac{1}{n+1} C_{n+1}^{i+1}. \end{aligned} \quad (13)$$

Based on equation (8), we can obtain that

$$2^n \sum_{i=1}^n \frac{C_n^i}{2i} = \text{Kf}(Q_n) \leq 2^n \frac{2^{n+1} - n - 2}{n+1}. \quad (14)$$

Hence,

$$\text{Kf}(Q_n) \leq 2^n \frac{2^{n+1} - n - 2}{n+1} = \frac{4^n}{n} \left( \frac{2n}{n+1} - \frac{n+2}{2^n(n+1)} \right). \quad (15)$$

The above estimate looks a little complicated. The upper bound is roughly twice the asymptotic value. Hence, a new upper bound is explored as follows.

**Theorem 5.** For the hypercube network  $Q_n$  with  $n \geq 2$ ,

$$\text{Kf}(Q_n) \leq \frac{4^n}{n}. \quad (16)$$

Following the identity which is obtained in [24],

$$\sum_{i=1}^n \frac{x^i}{i} = \left( \frac{1}{n} + \frac{1}{n-1} + \dots + 1 \right) + \sum_{i=1}^n \binom{n}{i} \frac{(x-1)^i}{i}. \quad (17)$$

Fixing  $x = 2$ , one arrives at

$$\sum_{i=1}^n \binom{n}{i} \frac{1}{i} = \sum_{i=1}^n \frac{2^i}{i} - \left( \frac{1}{n} + \frac{1}{n-1} + \dots + 1 \right). \quad (18)$$

Namely,

$$\sum_{i=1}^n \binom{n}{i} \frac{1}{i} = \sum_{i=1}^n \frac{2^i - 1}{i}. \quad (19)$$

According to equation (19) and Theorem 2, one obtains

$$\text{Kf}(Q_n) = 2^{n-1} \cdot \sum_{i=1}^n \frac{2^i - 1}{i}. \quad (20)$$

Using equation (20), one has

$$\text{Kf}(Q_n) \leq 2^{n-1} \cdot \sum_{i=1}^n \frac{2^i}{i}. \quad (21)$$

On the contrary,

$$2^{n-1} \cdot \sum_{i=1}^n \frac{2^i}{i} = \frac{1}{n} \cdot 2^{2n-1} \cdot \sum_{i=0}^{n-1} \frac{n}{2^i(n-i)}. \quad (22)$$

Using Theorem 2 and substituting equations (22) to (21), one obtains the desired result:

$$\text{Kf}(Q_n) \leq \frac{4^n}{n}. \quad (23)$$

This has completed the proof.

#### 4. Further Discussion

We, at this place, try another way to estimate the Kirchhoff index of  $n$ -dimensional hypercubes.

**Theorem 6.** For the hypercube networks  $Q_n$  with  $n \geq 2$ , then

$$\text{Kf}(Q_n) = 2^{n-1} \sum_{i=1}^n \frac{2^i - 1}{i}. \quad (24)$$

Let  $S_n = \sum_{i=1}^n C_n^i / i$ , then

$$\begin{aligned} S_n - S_{n-1} &= \sum_{i=1}^n \frac{C_n^i}{i} - \sum_{i=1}^{n-1} \frac{C_{n-1}^i}{i} \\ &= \left[ \frac{1}{n} + \sum_{i=1}^{n-1} \frac{C_n^i}{i} \right] - \sum_{i=1}^{n-1} \frac{C_{n-1}^i}{i} \\ &= \frac{1}{n} + \sum_{i=1}^{n-1} \frac{1}{i} [C_n^i - C_{n-1}^i] \\ &= \frac{1}{n} + \sum_{i=1}^{n-1} \frac{1}{i} C_{n-1}^{i-1}. \end{aligned} \quad (25)$$

Consequently,

$$n \cdot (S_n - S_{n-1}) = 1 + \sum_{i=1}^{n-1} \frac{n!}{i!(n-i)!} = 1 + \sum_{i=1}^{n-1} C_n^i = 2^n - 1. \quad (26)$$

One can easily check that  $S_1 = 1$ . Hence,  $S_n - S_{n-1} = (2^n/n) - (1/n)$ .

By virtue of the above equality, we obtain

$$S_n = \sum_{i=1}^n \frac{2^i}{i} - \sum_{i=1}^n \frac{1}{i}. \quad (27)$$

Therefore,

$$\text{Kf}(Q_n) = 2^{n-1} \sum_{i=1}^n \frac{2^i - 1}{i}. \quad (28)$$

The proof of Theorem 6 is completed.

#### Data Availability

The data used to support the findings of this study are available within paper.

#### Conflicts of Interest

The authors declare no conflicts of interest.

#### Authors' Contributions

Data curation was carried out by J-B.L.; J-B.L. and J.Cao helped with the methodology; J.Z., Z-Y.S., and F.E. Alsaadi wrote the original draft. All authors read and approved the final manuscript.

#### Acknowledgments

The work of was partly supported by the China Postdoctoral Science Foundation under Grant no. 2017M621579, Postdoctoral Science Foundation of Jiangsu Province under Grant no. 1701081B, and Project of Anhui Jianzhu University under Grant nos. 2016QD116 and 2017dc03.

#### References

- [1] J. M. Xu, *Topological Structure and Analysis of Interconnection Networks*, Kluwer Academic Publishers, London, UK, 2001.

- [2] D. J. Klein and M. Randić, "Resistance distances," *Journal of Mathematical Chemistry*, vol. 12, no. 1, pp. 81–95, 1993.
- [3] J. -B. Liu, J. Cao, X.-F. Pan, and A. Elaiw, "The Kirchhoff index of hypercubes and related complex networks," *Discrete Dynamics in Nature and Society*, vol. 2013, Article ID 543189, 7 pages, 2013.
- [4] E. Estrada and N. Hatano, "Topological atomic displacements Kirchhoff and Wiener indices of molecules," *Chemical Physics Letters*, vol. 486, no. 4–6, pp. 166–170, 2010.
- [5] P. W. Fowler, "Resistance distance in fullerene graphs," *Croatica Chemica Acta*, vol. 75, no. 2, pp. 401–408, 2002.
- [6] H. P. Zhang, X. Y. Jiang, and Y. Yang, "Bicyclic graphs with extremal Kirchhoff index," *Match Communications in Mathematical and in Computer Chemistry*, vol. 61, no. 3, pp. 697–712, 2009.
- [7] C. Arauz, "The Kirchhoff indexes of some composite networks," *Discrete Applied Mathematics*, vol. 160, no. 10, pp. 1429–1440, 2009.
- [8] H. Zhang and Y. Yang, "Kirchhoff index of composite graphs," *Discrete Applied Mathematics*, vol. 157, no. 11, pp. 2918–2927, 2009.
- [9] M. Bianchi, A. Cornaro, J. L. Palacios, and A. Torriero, "Bounds for the Kirchhoff index via majorization techniques," *Journal of Mathematical Chemistry*, vol. 51, no. 2, pp. 569–587, 2013.
- [10] H. H. Wang, H. Hua, and D. Wang, "Cacti with minimum, second-minimum, and third-minimum Kirchhoff indices," *Mathematical Communications*, vol. 15, no. 2, pp. 347–358, 2010.
- [11] M. Hong, W. Sun, S. Liu, and T. Xuan, "Coherence analysis and Laplacian energy of recursive trees with controlled initial states," *Frontiers of Information Technology Electronic Engineering*, vol. 21, pp. 931–938, 2020.
- [12] J.-B. Liu, X.-F. Pan, J. Cao, and J. Cao, "Some properties on Estrada index of folded hypercubes networks," *Abstract and Applied Analysis*, vol. 2014, Article ID 380874, 6 pages, 2014.
- [13] J.-B. Liu and X.-F. Pan, "Minimizing Kirchhoff index among graphs with a given vertex bipartiteness," *Applied Mathematics and Computation*, vol. 291, pp. 84–88, 2016.
- [14] J.-B. Liu, X.-F. Pan, L. Yu, and D. Li, "Complete characterization of bicyclic graphs with minimal Kirchhoff index," *Discrete Applied Mathematics*, vol. 200, pp. 95–107, 2016.
- [15] I. Raman and S. A. Choudum, "Embedding certain height-balanced trees and complete  $P^m$ -ary trees into hypercubes," *Journal of Discrete Algorithms*, vol. 22, no. 1, pp. 53–65, 2013.
- [16] J. Fink, "Perfect matchings extend to Hamilton cycles in hypercubes," *Journal of Combinatorial Theory, Series B*, vol. 97, no. 6, pp. 1074–1076, 2007.
- [17] A. Bossard and K. Kaneko, "k-pairwise disjoint paths routing in perfect hierarchical hypercubes," *The Journal of Supercomputing*, vol. 14, no. 3, pp. 1–11, 2013.
- [18] J.-H. Park, H.-S. Lim, and H.-C. Kim, "Panconnectivity and pancyclicity of hypercube-like interconnection networks with faulty elements," *Theoretical Computer Science*, vol. 377, no. 1–3, pp. 170–180, 2007.
- [19] D. Wang and M. Lu, "Edge fault tolerance of super edge connectivity for three families of interconnection networks," *Information Sciences*, vol. 188, no. 3, pp. 260–268, 2012.
- [20] J. M. Xu, J. W. Wang, and W. W. Wang, "On super and restricted connectivity of some interconnection networks," *Ars Combinatoria*, vol. 94, no. 6, pp. 25–32, 2010.
- [21] X. J. Li and M. Xu, "Edge fault tolerance of hypercube-like networks," *Information Processing Letters*, vol. 113, no. 19–21, pp. 760–763, 2013.
- [22] J. Zhang, Y. Xiang, and W. Sun, "A discrete random walk on the hypercube," *Physica A: Statistical Mechanics and Its Applications*, vol. 494, pp. 1–7, 2018.
- [23] J. L. Palacios and J. M. Renom, "Bounds for the Kirchhoff index of regular graphs via the spectra of their random walks," *International Journal of Quantum Chemistry*, vol. 110, no. 9, pp. 1637–1641, 2010.
- [24] D. E. Knuth, "The art of computer programming," *Fundamental Algorithms*, vol. 1, Addison-Wesley, Boston, MA, USA, 3rd edition, 1997.



## Research Article

# Periodic Averaging Principle for Neutral Stochastic Delay Differential Equations with Impulses

Peiguang Wang  and Yan Xu 

*College of Mathematics and Information Science, Hebei University, Baoding 071002, Hebei, China*

Correspondence should be addressed to Yan Xu; [xuyanbd@hbu.edu.cn](mailto:xuyanbd@hbu.edu.cn)

Received 30 March 2020; Revised 9 May 2020; Accepted 29 May 2020; Published 15 June 2020

Guest Editor: Xiaodi Li

Copyright © 2020 Peiguang Wang and Yan Xu. This is an open access article distributed under the Creative Commons Attribution License, which permits unrestricted use, distribution, and reproduction in any medium, provided the original work is properly cited.

In this paper, we study the periodic averaging principle for neutral stochastic delay differential equations with impulses under non-Lipschitz condition. By using the linear operator theory, we deal with the difficulty brought by delay term of the neutral system and obtain the conclusion that the solutions of neutral stochastic delay differential equations with impulses converge to the solutions of the corresponding averaged stochastic delay differential equations without impulses in the sense of mean square and in probability. At last, an example is presented to show the validity of the proposed theories.

## 1. Introduction

Delay, impulse, and noise are natural phenomena in most practical issues and those phenomena are generally modeled by stochastic delay differential equations with impulses, and noise can be described by Brownian motion. Recent theoretical and computational advancements indicate that stochastic delay differential equations with impulses tend to generate rich and complex dynamics. However, because of the complexity of the system, it is difficult to obtain the exact solution of the vast majority of stochastic delay differential equations with impulses. In this background, it is very important to look for an approximate system which is more amenable for analysis and simulation, and it governs the evolution of the original system over a long time scale.

The averaging principle is an effective method to understand the main part of the behavior of dynamical systems. It allows to avoid the detailed analysis of complex original systems and consider the simplified equations. The first analysis for averaging principle for stochastic differential equations was deeply addressed by Khasminskij [1]. And then the averaging principle has been applied for various types of stochastic differential equations. Generally speaking, the results of averaging principle in standard form mainly fall into two categories. The first one is considered in slow-

fast systems or two-time-scale systems. It approximates coupled slow component equation in two-time-scale systems by a noncoupled equation often called an averaged equation. Many important results for averaging principle for two-time-scale stochastic differential equations have been carried out, see, for example, [2–6]. The second is approximating a nonautonomous stochastic differential equation by an autonomous stochastic differential equation. The results obtained by this method can be referred to the papers [7–9] and the references therein. However, there are few results on average principle for neutral stochastic delay differential equations. Recently, averaging principle for stochastic delay differential equations of the neutral type driven by G-Brownian motion was studied [10], in which the impulses are not considered in the system.

Motivated by the previous discussion, in this paper, we study the average principle for the neutral stochastic delay differential equations with impulses. We overcome the difficulties caused by the delay term which is included under the differentiation at the left-hand side, and the impulse appears in neutral stochastic differential equations.

The structure of the paper is the following. In Section 2, we introduce some basic concepts, notations, and necessary hypotheses. In Section 3, under several sufficient conditions, we obtain the main results that the solutions of neutral

stochastic delay differential equations with impulses converge to the solutions of the corresponding averaged stochastic delay differential equations without impulses in the sense of mean square and in probability. In Section 4, we offer an example to illustrate the effectiveness of the obtained results.

## 2. Model Description and Preliminaries

In this section, we will introduce the basic concepts, the model, and some preliminary lemmas.

Let  $(\Omega, \mathcal{F}, \{\mathcal{F}_t\}_{t \geq 0}, P)$  be a complete probability space with a filtration  $\{\mathcal{F}_t\}_{t \geq 0}$  satisfying the usual conditions (i.e.,

$$\begin{cases} d[x(t) + c(t)x(t - \tau)] = f(t, x(t), x(t - \tau))dt + g(t, x(t), x(t - \tau))dB(t), & t \neq t_j, j = 1, 2, \dots, l, \\ x(t_j^+) - x(t_j^-) = I_j(x(t_j)), & t = t_j, j = 1, 2, \dots, l, \end{cases} \quad (1)$$

where  $c \in C((-\infty, U], [0, 1])$  is a  $T$ -periodic function,  $0 < U < \infty$ . The mappings  $f: [0, U] \times \mathbb{R}^d \times \mathbb{R}^d \rightarrow \mathbb{R}^d$  and  $g: [0, U] \times \mathbb{R}^d \times \mathbb{R}^d \rightarrow \mathbb{R}^{d \times m}$  are Borel measurable and  $T$ -periodic in the first argument.  $I_j: \mathbb{R}^d \rightarrow \mathbb{R}^d$ ,  $x(t_j^+)$  and  $x(t_j^-)$  represent the right and the left limits of  $x(t_j)$ ,  $j \in \{1, 2, \dots, l\}$ . We assume that there exists a positive constant  $l$  such that  $t_{j+l} = t_j + T$ ,  $I_{j+l}(x(t_{j+l})) = I_j(x(t_j))$ ,  $j \in \mathbb{Z}^+$ , and  $[0, T] \cap \{t_j, j \in \mathbb{Z}^+\} = \{t_1, t_2, \dots, t_l\}$ . The initial condition  $x_0$  is defined by

$$x_0 = \xi = \{\xi(t): -\infty < t \leq 0\} \in C_{\mathcal{F}_t}^2((-\infty, 0]; \mathbb{R}^d). \quad (2)$$

The following lemmas are important to obtain our results.

**Lemma 1** (see [11]). *Suppose  $H$  is a bounded linear operator on Banach space  $X$ ; if  $\|H\| < 1$ , then  $I - H$  has bounded inverse operator  $(I - H)^{-1}$  and  $\|(I - H)^{-1}\| \leq (1 / (1 - \|H\|))$ .*

**Lemma 2** (see [11]). *Suppose  $H$  is a bounded linear operator on Banach space  $X$  and has an inverse bounded operator, for arbitrary  $\Delta H: X \rightarrow X$ , if  $\|\Delta H\| < (1 / \|H^{-1}\|)$ , then  $S = H + \Delta H$  has a bounded inverse and  $S^{-1} = \sum_{j=0}^{\infty} (-1)^j H^{-1} (H^{-1} \Delta H)^j$ .*

Let

$$\begin{cases} du(t) = f(t, (\Phi^{-1}u)(t), (\Phi^{-1}u)(t - \tau))dt + g(t, (\Phi^{-1}u)(t), (\Phi^{-1}u)(t - \tau))dB(t), & t \neq t_j, j = 1, 2, \dots, l, \\ u(t_j^+) - u(t_j^-) = (\Phi I_j \Phi^{-1})(u(t_j)), & t = t_j, j = 1, 2, \dots, l, \\ u(0) = (\Phi^{-1}x)(0) = u_0. \end{cases} \quad (7)$$

Hence,  $u(t)$  is an  $T$ -periodic solution of system (2) if and only if  $(\Phi^{-1}u)(t)$  is an  $T$ -periodic solution of system (1).

it is right continuous and  $\mathcal{F}_0$  contains all  $P$ -null sets) and  $B(t)$  is  $m$ -dimensional Brownian motion defined on the space.  $\mathcal{K}$  denotes the family of all concave continuous nondecreasing functions  $\alpha: \mathbb{R}^+ \rightarrow \mathbb{R}^+$  such that  $\alpha(0) = 0$ ,  $\int_{0^+} (\alpha(s))^{-1} ds = \infty$ . Let  $C((-\infty, 0]; \mathbb{R}^d)$  denote the family of all continuous functions  $\xi: (-\infty, 0] \rightarrow \mathbb{R}^d$  with the norm  $\|\xi\| = \sup_{-\infty < \theta \leq 0} |\xi(\theta)|$  and  $|\cdot|$  denote any norm in  $\mathbb{R}^d$ . Let  $C_{\mathcal{F}_t}^2((-\infty, 0]; \mathbb{R}^d)$  denote the family of all  $\mathcal{F}_t$ -measurable,  $C((-\infty, 0]; \mathbb{R}^d)$ -valued random variables  $\xi = \{\xi(\theta): (-\infty < \theta \leq 0)\}$  such that  $E\|\xi\|^2 < \infty$ .

In this paper, we will discuss the following neutral stochastic delay differential equations with impulses:

$$\begin{aligned} PC((-\infty, U]) = & \left\{ x: x|_{(t_j, t_{j+1})_{(-\infty, U]}} \in C((-\infty, 0]; \mathbb{R}^d), x(t_j^+) \right. \\ & \left. = x(t_j), j = 1, 2, \dots, l \right\}, \end{aligned} \quad (3)$$

and consider the Banach space

$$W = \{x: x \in PC((-\infty, U]), x(t) = x(t + T)\}. \quad (4)$$

Let  $\Phi: W \rightarrow W$  be defined by

$$(\Phi x)(t) = x(t) + c(t)x(t - \tau). \quad (5)$$

**Lemma 3** (see [12]). *Let  $c^M = \max_{t \in (-\infty, U]} c(t)$ . If  $0 \leq c(t) < 1$ , then  $\Phi$  has a bounded inverse  $\Phi^{-1}$  on  $W$ , and for all  $x \in W$ ,*

$$(\Phi^{-1}x)(t) = \sum_{j \geq 0} \prod_{0 \leq i \leq j-1} (-1)^i c(t - i\tau)x(t - j\tau) \quad (6)$$

and  $\|\Phi^{-1}x\| \leq (\|x\| / (1 - c^M))$ .

Since  $\Phi$  and  $\Phi^{-1}$  are both linear operators, we can change system (1) by using the inverse transformation of  $\Phi$  into the following form:

To study the averaging principle of system (1), we impose the following hypotheses on the coefficients.

( $H_1$ ) For all  $x_1, y_1, x_2, y_2 \in \mathbb{R}^d$  and  $t \in [0, U]$ , there exist  $\alpha \in \mathcal{X}$  such that

$$\begin{aligned} & |f(t, x_1, y_1) - f(t, x_2, y_2)|^2 \vee |g(t, x_1, y_1) - g(t, x_2, y_2)|^2 \\ & \leq \alpha(|x_1 - x_2|^2 + |y_1 - y_2|^2), \end{aligned} \quad (8)$$

where  $a \vee b := \max\{a, b\}$ .

Furthermore, by the definition of  $\alpha$ , there must exist positive constants  $k_1$  and  $k_2$  such that

$$\alpha(r) \leq k_1 r + k_2, \quad \text{for all } r \geq 0. \quad (9)$$

( $H_2$ ) For every  $x \in \mathbb{R}^d$ , there exists a positive constant  $N_1$  such that  $|I_j(x)| \leq N_1$ .

Consider the standard form of system (2)

$$\begin{cases} du_\varepsilon(t) = \varepsilon f(t, (\Phi^{-1}u_\varepsilon)(t), (\Phi^{-1}u_\varepsilon)(t-\tau))dt + \sqrt{\varepsilon} g(t, (\Phi^{-1}u_\varepsilon)(t), (\Phi^{-1}u_\varepsilon)(t-\tau))dB(t), & t \neq t_j, j = 1, 2, \dots, l, \\ u_\varepsilon(t_j^+) - u_\varepsilon(t_j^-) = \varepsilon(\Phi I_j \Phi^{-1})(u_\varepsilon(t_j)), & t = t_j, j = 1, 2, \dots, l, \\ u_\varepsilon(0) = u_0. \end{cases} \quad (10)$$

Accordingly, the standard form of system (1) is

$$\begin{cases} d[x_\varepsilon(t) + c(t)x_\varepsilon(t-\tau)] = \varepsilon f(t, x_\varepsilon(t), x_\varepsilon(t-\tau))dt + \sqrt{\varepsilon} g(t, x_\varepsilon(t), x_\varepsilon(t-\tau))dB(t), & t \neq t_j, j = 1, 2, \dots, l, \\ x_\varepsilon(t_j^+) - x_\varepsilon(t_j^-) = \varepsilon I_j(x_\varepsilon(t_j)), & t = t_j, j = 1, 2, \dots, l, \\ x_\varepsilon(0) = x_0, \end{cases} \quad (11)$$

where the functions  $f, g, I_j, j \in \{1, 2, \dots, l\}$  have the same conditions as in ( $H_1$ ) and ( $H_2$ ), and  $\varepsilon \in [0, \varepsilon_0]$  is a positive small parameter with  $\varepsilon_0$  is a fixed number.

Let  $\bar{f}(x, y): \mathbb{R}^d \times \mathbb{R}^d \rightarrow \mathbb{R}^d$ ,  $\bar{g}(x, y): \mathbb{R}^d \times \mathbb{R}^d \rightarrow \mathbb{R}^{d \times m}$ , and  $\overline{\Phi I \Phi^{-1}}(x): \mathbb{R}^d \rightarrow \mathbb{R}^d$  be measurable functions and satisfy the conditions in ( $H_1$ ) – ( $H_2$ ) and the following definitions:

$$\begin{aligned} \bar{f}(x, y) &= \frac{1}{T} \int_0^T f(s, x, y) ds, \\ \bar{g}(x, y) &= \frac{1}{T} \int_0^T g(s, x, y) ds, \end{aligned} \quad (12)$$

$$\overline{\Phi I \Phi^{-1}}(x) = \frac{1}{T} \sum_{j=1}^l (\Phi I_j \Phi^{-1})(x).$$

We also assume that the following hypothesis is satisfied.

( $H_3$ ) There exists a constant  $M > 0$  such that  $|f(t, x, y)|^2 < M$ ,  $|g(t, x, y)|^2 < M$ ,  $|\bar{f}(x, y)|^2 < M$ , and  $|\bar{g}(x, y)|^2 < M$  for every  $t \in [0, U]$ .

Now, we consider the following averaged stochastic delay differential equations which correspond to the original standard form (10):

$$\begin{cases} dv_\varepsilon(t) = \varepsilon \left( \bar{f}((\Phi^{-1}v_\varepsilon)(t), (\Phi^{-1}v_\varepsilon)(t-\tau)) + \overline{\Phi I \Phi^{-1}}(v_\varepsilon(t)) \right) dt \\ + \sqrt{\varepsilon} \bar{g}((\Phi^{-1}v_\varepsilon)(t), (\Phi^{-1}v_\varepsilon)(t-\tau)) dB(t), \\ v_\varepsilon(0) = u_0. \end{cases} \quad (13)$$

Let  $(\Phi^{-1}v_\varepsilon)(t) = y_\varepsilon(t)$ , for system (11), we consider averaged stochastic delay differential equations:

$$\begin{cases} dy_\varepsilon(t) = \varepsilon \left( \bar{f}((\Phi^{-1}y_\varepsilon)(t), (\Phi^{-1}y_\varepsilon)(t-\tau)) + \overline{\Phi I \Phi^{-1}}(y_\varepsilon(t)) \right) dt \\ + \sqrt{\varepsilon} \bar{g}((\Phi^{-1}y_\varepsilon)(t), (\Phi^{-1}y_\varepsilon)(t-\tau)) dB(t), \\ y_\varepsilon(0) = x_0. \end{cases} \quad (14)$$

Obviously, under hypotheses ( $H_1$ ) – ( $H_2$ ), one can follow [13, 14] to prove the existence and uniqueness of the periodic probability solutions on  $(-\infty, U]$  of the standard form (10) and (11) and the averaged form (13) and (14), respectively. Now, we offer the proof for the relationship between  $x_\varepsilon(t)$  and  $y_\varepsilon(t)$ .

### 3. Main Results and Proofs

In this section, we will use the periodic averaging principle to investigate the neutral stochastic delay differential equations with impulses.

In the rest of the paper,  $C_i$  and  $O_i, i = 1, 2, 3$ , and  $P_j, j = 1, 2, 3, 4$  are all constants. Our main results are the following.

**Theorem 1.** *Suppose hypotheses  $(H_1) - (H_3)$  are satisfied and systems (10) and (13)–(11) and (14) have solutions  $u_\varepsilon, v_\varepsilon, x_\varepsilon$ , and  $y_\varepsilon$ , respectively, where  $\varepsilon \in (0, \varepsilon_0]$  is a positive small parameter with  $\varepsilon_0$  a constant, then there exist constants  $\varepsilon_1 \in (0, \varepsilon_0]$ ,  $\mu_1 > 0$ , and  $\mu_2 > 0$  such that, for any  $\varepsilon \in (0, \varepsilon_1], t \in [0, \mu_2 \varepsilon^{-1}]$ ,*

$$E \sup_{t \in [0, \mu_2 \varepsilon^{-1}]} |u_\varepsilon(t) - v_\varepsilon(t)|^2 \leq \mu_1 \varepsilon, \quad (15)$$

and then, we obtain

$$E \sup_{t \in [0, \mu_2 \varepsilon^{-1}]} |x_\varepsilon(t) - y_\varepsilon(t)|^2 \leq \|\Phi^{-1}\|^2 \mu_1 \varepsilon. \quad (16)$$

*Proof.* By using the elementary inequality, for any  $t \in [0, U]$ , we have

$$\begin{aligned} & |u_\varepsilon(t) - v_\varepsilon(t)|^2 \\ & \leq 3\varepsilon^2 \left| \int_0^t [f(s, (\Phi^{-1}u_\varepsilon)(s), (\Phi^{-1}u_\varepsilon)(s-\tau)) \right. \\ & \quad \left. - \bar{f}((\Phi^{-1}v_\varepsilon)(s), (\Phi^{-1}v_\varepsilon)(s-\tau))] ds \right|^2 \\ & \quad + 3\varepsilon \left| \int_0^t [g(s, (\Phi^{-1}u_\varepsilon)(s), (\Phi^{-1}u_\varepsilon)(s-\tau)) \right. \\ & \quad \left. - \bar{g}((\Phi^{-1}v_\varepsilon)(s), (\Phi^{-1}v_\varepsilon)(s-\tau))] dB(s) \right|^2 \\ & \quad + 3\varepsilon^2 \left| \sum_{j=1}^{\infty} (\Phi I_j \Phi^{-1})(u_\varepsilon(t_j)) - \int_0^t \overline{\Phi I \Phi^{-1}}(v_\varepsilon(t)) ds \right|^2 \\ & := J_1 + J_2 + J_3. \end{aligned} \quad (17)$$

For the first term  $J_1$ , thanks again to the elementary inequality yields:

$$\begin{aligned} & E \sup_{0 \leq s \leq t} J_1 \\ & \leq 6\varepsilon^2 E \sup_{0 \leq s \leq t} \left| \int_0^s [f(\theta, (\Phi^{-1}u_\varepsilon)(\theta), (\Phi^{-1}u_\varepsilon)(\theta-\tau)) - f(\theta, (\Phi^{-1}v_\varepsilon)(\theta), (\Phi^{-1}v_\varepsilon)(\theta-\tau))] d\theta \right|^2 \\ & \quad + 6\varepsilon^2 E \sup_{0 \leq s \leq t} \left| \int_0^s [f(\theta, (\Phi^{-1}v_\varepsilon)(\theta), (\Phi^{-1}v_\varepsilon)(\theta-\tau)) - \bar{f}((\Phi^{-1}v_\varepsilon)(\theta), (\Phi^{-1}v_\varepsilon)(\theta-\tau))] d\theta \right|^2. \end{aligned} \quad (18)$$

According Hölder's inequality and hypothesis  $(H_1)$ , we arrive at

$$\begin{aligned} & 6\varepsilon^2 E \sup_{0 \leq s \leq t} \left| \int_0^s [f(\theta, (\Phi^{-1}u_\varepsilon)(\theta), (\Phi^{-1}u_\varepsilon)(\theta-\tau)) - f(\theta, (\Phi^{-1}v_\varepsilon)(\theta), (\Phi^{-1}v_\varepsilon)(\theta-\tau))] d\theta \right|^2 \\ & \leq 6\varepsilon^2 t k_1 \int_0^t E \sup_{0 \leq \theta \leq s} \left[ |(\Phi^{-1}u_\varepsilon)(\theta) - (\Phi^{-1}v_\varepsilon)(\theta)|^2 + |(\Phi^{-1}u_\varepsilon)(\theta-\tau) - (\Phi^{-1}v_\varepsilon)(\theta-\tau)|^2 \right] ds + 6\varepsilon^2 t^2 k_2 \\ & \leq 6\varepsilon^2 t k_1 \int_0^t \|\Phi^{-1}\|^2 E \sup_{0 \leq \theta \leq s} [|u_\varepsilon(\theta) - v_\varepsilon(\theta)|^2 + |u_\varepsilon(\theta-\tau) - v_\varepsilon(\theta-\tau)|^2] ds + 6\varepsilon^2 t^2 k_2 \\ & \leq 12\varepsilon^2 t k_1 \|\Phi^{-1}\|^2 \int_0^t E \sup_{0 \leq \theta \leq s} |u_\varepsilon(\theta) - v_\varepsilon(\theta)|^2 ds + 6\varepsilon^2 t^2 k_2. \end{aligned} \quad (19)$$

Let  $n$  be the largest integer such that  $nT \leq t$ . Then, for every  $i = \{1, \dots, n\}$ , we obtain

$$\begin{aligned}
& 6\varepsilon^2 E \sup_{0 \leq s \leq t} \left| \int_0^s [f(\theta, (\Phi^{-1}v_\varepsilon)(\theta), (\Phi^{-1}v_\varepsilon)(\theta - \tau)) - \bar{f}((\Phi^{-1}v_\varepsilon)(\theta), (\Phi^{-1}v_\varepsilon)(\theta - \tau))] d\theta \right|^2 \\
& \leq 12\varepsilon^2 E \sup_{0 \leq s \leq t} \left| \sum_{i=1}^n \int_{(i-1)T}^{iT} [f(\theta, (\Phi^{-1}v_\varepsilon)(\theta), (\Phi^{-1}v_\varepsilon)(\theta - \tau)) - \bar{f}((\Phi^{-1}v_\varepsilon)(\theta), (\Phi^{-1}v_\varepsilon)(\theta - \tau))] d\theta \right|^2 \\
& \quad + 12\varepsilon^2 E \sup_{0 \leq s \leq t} \left| \int_{nT}^s [f(\theta, (\Phi^{-1}v_\varepsilon)(\theta), (\Phi^{-1}v_\varepsilon)(\theta - \tau)) - \bar{f}((\Phi^{-1}v_\varepsilon)(\theta), (\Phi^{-1}v_\varepsilon)(\theta - \tau))] d\theta \right|^2 \\
& \leq 72\varepsilon^2 nT \int_0^T E \sup_{0 \leq \theta \leq s} \alpha \left( \left| (\Phi^{-1}v_\varepsilon)(\theta) - (\Phi^{-1}v_\varepsilon)(iT) \right|^2 + \left| (\Phi^{-1}v_\varepsilon)(\theta - \tau) - (\Phi^{-1}v_\varepsilon)(iT - \tau) \right|^2 \right) ds \\
& \quad + 36\varepsilon^2 E \sup_{0 \leq s \leq t} \left| \sum_{i=1}^n \int_{(i-1)T}^{iT} [f(\theta, (\Phi^{-1}v_\varepsilon)(iT), (\Phi^{-1}v_\varepsilon)(iT - \tau)) - \bar{f}((\Phi^{-1}v_\varepsilon)(iT), (\Phi^{-1}v_\varepsilon)(iT - \tau))] d\theta \right|^2 \\
& \quad + 12\varepsilon^2 E \sup_{0 \leq s \leq t} \left| \int_{nT}^s [f(\theta, (\Phi^{-1}v_\varepsilon)(\theta), (\Phi^{-1}v_\varepsilon)(\theta - \tau)) - \bar{f}((\Phi^{-1}v_\varepsilon)(\theta), (\Phi^{-1}v_\varepsilon)(\theta - \tau))] d\theta \right|^2.
\end{aligned} \tag{20}$$

By the Hölder's inequality, Burkholder–Davis–Gundy's inequality, and hypotheses  $(H_1)$  and  $(H_3)$ , it follows that

$$\begin{aligned}
& E \sup_{0 \leq s \leq t} \left| (\Phi^{-1}v_\varepsilon)(s) - (\Phi^{-1}v_\varepsilon)(iT) \right|^2 + E \sup_{0 \leq s \leq t} \left| (\Phi^{-1}v_\varepsilon)(s - \tau) - (\Phi^{-1}v_\varepsilon)(iT - \tau) \right|^2 \\
& \leq \|\Phi^{-1}\|^2 E \sup_{0 \leq s \leq t} |v_\varepsilon(iT) - v_\varepsilon(iT - \tau)|^2 + 2\|\Phi^{-1}\|^2 E \sup_{0 \leq s \leq t} |v_\varepsilon(s) - v_\varepsilon(iT)|^2 \\
& \leq C_1 + C_2 \varepsilon^2 E \sup_{0 \leq s \leq t} \int_{iT}^s |\bar{f}((\Phi^{-1}v_\varepsilon)(\theta), (\Phi^{-1}v_\varepsilon)(\theta - \tau))|^2 d\theta \\
& \quad + C_2 \varepsilon E \sup_{0 \leq s \leq t} \int_{iT}^s |\bar{g}((\Phi^{-1}v_\varepsilon)(\theta), (\Phi^{-1}v_\varepsilon)(\theta - \tau))|^2 d\theta \\
& \leq C_1 + C_2 \varepsilon^2 MT + C_2 \varepsilon MT, \\
& \quad t \in [(i-1)T, iT].
\end{aligned} \tag{21}$$

The definition of  $\bar{f}$  implies that

$$\begin{aligned}
& E \sup_{0 \leq s \leq t} \left| \sum_{i=1}^n \int_{(i-1)T}^{iT} [f(\theta, (\Phi^{-1}v_\varepsilon)(iT), (\Phi^{-1}v_\varepsilon)(iT - \tau)) - \bar{f}((\Phi^{-1}v_\varepsilon)(iT), (\Phi^{-1}v_\varepsilon)(iT - \tau))] d\theta \right|^2 \\
& \leq n \sum_{i=1}^n E \sup_{0 \leq s \leq t} \left| \int_0^T f(\theta, (\Phi^{-1}v_\varepsilon)(iT), (\Phi^{-1}v_\varepsilon)(iT - \tau)) d\theta - T \bar{f}((\Phi^{-1}v_\varepsilon)(iT), (\Phi^{-1}v_\varepsilon)(iT - \tau)) \right|^2 \\
& = 0.
\end{aligned} \tag{22}$$

Thus, we have

$$\begin{aligned}
E \sup_{0 \leq s \leq t} J_1 &\leq 12\varepsilon^2 t k_1 \|\Phi^{-1}\|^2 \int_0^t E \sup_{0 \leq \theta \leq s} |u_\varepsilon(\theta) - v_\varepsilon(\theta)|^2 ds + 6\varepsilon^2 t^2 k_2 \\
&\quad + 72\varepsilon^2 n T \int_0^T E \sup_{0 \leq \theta \leq s} \left[ k_1 \left( \left| (\Phi^{-1} v_\varepsilon)(\theta) - (\Phi^{-1} v_\varepsilon)(iT) \right|^2 + \left| (\Phi^{-1} v_\varepsilon)(\theta - \tau) - (\Phi^{-1} v_\varepsilon)(iT - \tau) \right|^2 \right) + k_2 \right] ds + 48\varepsilon^2 t MT \\
&\leq 12\varepsilon^2 t k_1 \|\Phi^{-1}\|^2 \int_0^t E \sup_{0 \leq \theta \leq s} |u_\varepsilon(\theta) - v_\varepsilon(\theta)|^2 ds + 6\varepsilon^2 t^2 k_2 \\
&\quad + 72\varepsilon^2 n k_1 T^2 (C_1 + C_2 \varepsilon^2 MT + C_2 \varepsilon MT) + 72\varepsilon^2 n k_2 T^2 + 48\varepsilon^2 t MT \\
&:= \varepsilon O_1 \int_0^t E \sup_{0 \leq \theta \leq s} |u_\varepsilon(\theta) - v_\varepsilon(\theta)|^2 ds + \varepsilon P_1.
\end{aligned} \tag{23}$$

For the second term  $J_2$ , apply Burkholder–Davis–Gundy’s inequality to deduce

$$\begin{aligned}
E \sup_{0 \leq s \leq t} J_2 &\leq 3\varepsilon C_3 E \sup_{0 \leq s \leq t} \int_0^s \left| g(\theta, (\Phi^{-1} u_\varepsilon)(\theta), (\Phi^{-1} u_\varepsilon)(\theta - \tau)) - \bar{g}((\Phi^{-1} v_\varepsilon)(\theta), (\Phi^{-1} v_\varepsilon)(\theta - \tau)) \right|^2 d\theta \\
&\leq 6\varepsilon C_3 E \sup_{0 \leq s \leq t} \int_0^s \left| g(\theta, (\Phi^{-1} u_\varepsilon)(\theta), (\Phi^{-1} u_\varepsilon)(\theta - \tau)) - g(\theta, (\Phi^{-1} v_\varepsilon)(\theta), (\Phi^{-1} v_\varepsilon)(\theta - \tau)) \right|^2 d\theta \\
&\quad + 6\varepsilon C_3 E \sup_{0 \leq s \leq t} \int_0^s \left| g(\theta, (\Phi^{-1} v_\varepsilon)(\theta), (\Phi^{-1} v_\varepsilon)(\theta - \tau)) - \bar{g}((\Phi^{-1} v_\varepsilon)(\theta), (\Phi^{-1} v_\varepsilon)(\theta - \tau)) \right|^2 d\theta.
\end{aligned} \tag{24}$$

Furthermore, on account of hypothesis  $(H_1)$ , we have

$$\begin{aligned}
E \sup_{0 \leq s \leq t} \int_0^s &\left| g(\theta, (\Phi^{-1} v_\varepsilon)(\theta), (\Phi^{-1} v_\varepsilon)(\theta - \tau)) - \bar{g}((\Phi^{-1} v_\varepsilon)(\theta), (\Phi^{-1} v_\varepsilon)(\theta - \tau)) \right|^2 d\theta \\
&\leq E \sup_{0 \leq s \leq t} \sum_{i=1}^n \int_{(i-1)T}^{iT} \left| g(\theta, (\Phi^{-1} v_\varepsilon)(\theta), (\Phi^{-1} v_\varepsilon)(\theta - \tau)) - \bar{g}((\Phi^{-1} v_\varepsilon)(\theta), (\Phi^{-1} v_\varepsilon)(\theta - \tau)) \right|^2 d\theta \\
&\quad + E \sup_{0 \leq s \leq t} \int_{nT}^s \left| g(\theta, (\Phi^{-1} v_\varepsilon)(\theta), (\Phi^{-1} v_\varepsilon)(\theta - \tau)) - \bar{g}((\Phi^{-1} v_\varepsilon)(\theta), (\Phi^{-1} v_\varepsilon)(\theta - \tau)) \right|^2 d\theta \\
&\leq 3E \sup_{0 \leq s \leq t} \sum_{i=1}^n \int_{(i-1)T}^{iT} \left| g(\theta, (\Phi^{-1} v_\varepsilon)(\theta), (\Phi^{-1} v_\varepsilon)(\theta - \tau)) - g(\theta, (\Phi^{-1} v_\varepsilon)(iT), (\Phi^{-1} v_\varepsilon)(iT - \tau)) \right|^2 d\theta \\
&\quad + 3E \sup_{0 \leq s \leq t} \sum_{i=1}^n \int_{(i-1)T}^{iT} \left| g(\theta, (\Phi^{-1} v_\varepsilon)(iT), (\Phi^{-1} v_\varepsilon)(iT - \tau)) - \bar{g}((\Phi^{-1} v_\varepsilon)(iT), (\Phi^{-1} v_\varepsilon)(iT - \tau)) \right|^2 d\theta \\
&\quad + 3E \sup_{0 \leq s \leq t} \sum_{i=1}^n \int_{(i-1)T}^{iT} \left| \bar{g}((\Phi^{-1} v_\varepsilon)(iT), (\Phi^{-1} v_\varepsilon)(iT - \tau)) - \bar{g}((\Phi^{-1} v_\varepsilon)(\theta), (\Phi^{-1} v_\varepsilon)(\theta - \tau)) \right|^2 d\theta + 4MT \\
&\leq 3n \int_0^T E \sup_{0 \leq \theta \leq s} \alpha \left( \left| (\Phi^{-1} v_\varepsilon)(\theta) - (\Phi^{-1} v_\varepsilon)(iT) \right|^2 + \left| (\Phi^{-1} v_\varepsilon)(\theta - \tau) - (\Phi^{-1} v_\varepsilon)(iT - \tau) \right|^2 \right) ds \\
&\quad + 12nMT + 4MT.
\end{aligned} \tag{25}$$

Hence, we obtain

$$\begin{aligned}
E \sup_{0 \leq s \leq t} J_2 &\leq 12\varepsilon C_3 k_1 \|\Phi^{-1}\|^2 \int_0^t E \sup_{0 \leq \theta \leq s} |u_\varepsilon(\theta) - v_\varepsilon(\theta)|^2 ds + 6\varepsilon C_3 k_2 t + 18\varepsilon C_3 n k_2 T \\
&\quad + 18\varepsilon C_3 n k_1 T (C_1 + \varepsilon^2 C_2 M T + \varepsilon C_2 M T) + 72\varepsilon C_3 n M T + 24\varepsilon C_3 M T \\
&:= \varepsilon O_2 \int_0^t E \sup_{0 \leq \theta \leq s} |u_\varepsilon(\theta) - v_\varepsilon(\theta)|^2 ds + \varepsilon P_2.
\end{aligned} \tag{26}$$

For the third term  $J_3$ , utilizing hypothesis  $(H_2)$ , we deduce

$$\begin{aligned}
E \sup_{0 \leq s \leq t} J_3 &\leq 6\varepsilon^2 l (n+1) E \sup_{0 \leq s \leq t} \sum_{j=1}^l \left| (\Phi I_j \Phi^{-1})(u_\varepsilon(t_j)) \right|^2 \\
&\quad + 6\varepsilon^2 \frac{1}{T^2} l t E \sup_{0 \leq s \leq t} \sum_{j=1}^l \int_0^s |\Phi I_j \Phi^{-1}(v_\varepsilon(\theta))|^2 d\theta \\
&\leq 6\varepsilon^2 l^2 (n+1) N_1 + 6\varepsilon^2 l^2 (n+1)^2 N_1 \\
&:= \varepsilon P_3,
\end{aligned} \tag{27}$$

Combining (23), (23), and (27), we conclude that

$$\begin{aligned}
E \sup_{0 \leq s \leq t} |u_\varepsilon(s) - v_\varepsilon(s)|^2 &\leq \varepsilon (O_1 + O_2) \int_0^t E \sup_{0 \leq \theta \leq s} |u_\varepsilon(\theta) - v_\varepsilon(\theta)|^2 ds + \varepsilon (P_1 + P_2 + P_3) \\
&:= \varepsilon O_3 \int_0^t E \sup_{0 \leq \theta \leq s} |u_\varepsilon(\theta) - v_\varepsilon(\theta)|^2 ds + \varepsilon P_4,
\end{aligned} \tag{28}$$

and in addition, using Gronwall's inequality, we have

$$E \sup_{0 \leq s \leq t} |u_\varepsilon(s) - v_\varepsilon(s)|^2 \leq \varepsilon P_4 e^{\varepsilon O_3 t}. \tag{29}$$

Therefore, selecting  $\mu_2 > 0$  such that, for every  $t \in [0, \mu_2 \varepsilon^{-1}] \subseteq [0, U]$ , setting  $\mu_1 = P_4 e^{O_3 \mu_2}$ , we can choose  $\varepsilon_1 \in (0, \varepsilon_0]$  such that, for each  $\varepsilon \in (0, \varepsilon_1]$  and  $t \in [0, \mu_2 \varepsilon^{-1}]$ ,

$$E \sup_{t \in [0, \mu_2 \varepsilon^{-1}]} |u_\varepsilon(t) - v_\varepsilon(t)|^2 \leq \mu_1 \varepsilon, \tag{30}$$

and then, we obtain

$$\begin{aligned}
E \sup_{t \in [0, \mu_2 \varepsilon^{-1}]} |x_\varepsilon(t) - y_\varepsilon(t)|^2 &= E \sup_{t \in [0, \mu_2 \varepsilon^{-1}]} \left| (\Phi^{-1} u_\varepsilon)(t) - (\Phi^{-1} v_\varepsilon)(t) \right|^2 \leq \|\Phi^{-1}\|^2 \mu_1 \varepsilon.
\end{aligned} \tag{31}$$

**Corollary 1.** Suppose hypotheses  $(H_1) - (H_3)$  are satisfied. Then, for any parameter  $\gamma > 0$ , we have

$$\lim_{\varepsilon \rightarrow 0} P(|x_\varepsilon(t) - y_\varepsilon(t)| > \gamma) = 0. \tag{32}$$

*Proof.* In fact, under the consequence of Theorem 1, by using Chebyshev–Markov inequality, for any given number  $\gamma > 0$ , we can derive

$$P(|x_\varepsilon(t) - y_\varepsilon(t)| > \gamma) \leq \frac{1}{\gamma^2} E |x_\varepsilon(t) - y_\varepsilon(t)|^2 \leq \frac{\|\Phi^{-1}\|^2 \mu_1 \varepsilon}{\gamma^2}. \tag{33}$$

The conclusion follows by letting  $\varepsilon \rightarrow 0$ .

The proof is complete.  $\square$

#### 4. Illustrative Example

*Example 1.* Consider the following neutral stochastic delay differential equations with impulses:

$$\begin{cases} d \left[ x_\varepsilon(t) + \frac{1}{4} x_\varepsilon(t - \tau) \right] = \varepsilon (x_\varepsilon(t) + x_\varepsilon(t - \tau)) dt + 2\sqrt{\varepsilon} \cos^2 t x_\varepsilon(t - \tau) dB(t), & t \neq t_j, j = 1, 2, \dots, l, \\ x_\varepsilon(t_j^+) - x_\varepsilon(t_j^-) = -0.04 x_\varepsilon(t_j), & t = t_j, j = 1, 2, \dots, l, \end{cases} \tag{34}$$

where  $x_\varepsilon(t) = \xi(t), t \in (-\infty, 0]$ .

Let  $(\Phi x)(t) = x(t) + (1/4)x(t - \tau) = u(t)$  and consider the following stochastic delay differential equations with impulses:

$$\left\{ \begin{array}{l} d[u_\varepsilon(t)] = \varepsilon \left( \sum_{i \geq 0} \left(-\frac{1}{4}\right)^i u_\varepsilon(t - i\tau) + \sum_{i \geq 0} \left(-\frac{1}{4}\right)^i u_\varepsilon(t - (i+1)\tau) \right) dt \\ + 2\sqrt{\varepsilon} \cos^2 t \sum_{i \geq 0} \left(-\frac{1}{4}\right)^i u_\varepsilon(t - (i+1)\tau) dB(t), \quad t \neq t_j, j = 1, 2, \dots, l, \\ u_\varepsilon(t_j^+) - u_\varepsilon(t_j^-) = -0.04u_\varepsilon(t_j), \quad t = t_j, j = 1, 2, \dots, l, \end{array} \right. \quad (35)$$

$$f(t, (\Phi^{-1}u_\varepsilon)(t), (\Phi^{-1}u_\varepsilon)(t - \tau)) = \sum_{i \geq 0} \left(-\frac{1}{4}\right)^i u_\varepsilon(t - i\tau) + \sum_{i \geq 0} \left(-\frac{1}{4}\right)^i u_\varepsilon(t - (i+1)\tau),$$

$$g(t, (\Phi^{-1}u_\varepsilon)(t), (\Phi^{-1}u_\varepsilon)(t - \tau)) = 2\cos^2 t \sum_{i \geq 0} \left(-\frac{1}{4}\right)^i u_\varepsilon(t - (i+1)\tau),$$

$$(\Phi I_j \Phi^{-1})(u_\varepsilon(t_j)) = -0.04u_\varepsilon(t_j).$$

Then,

$$\begin{aligned} \overline{f}((\Phi^{-1}v_\varepsilon)(t), (\Phi^{-1}v_\varepsilon)(t - \tau)) &= \frac{1}{\pi} \int_0^\pi f(t, (\Phi^{-1}v_\varepsilon)(t), (\Phi^{-1}v_\varepsilon)(t - \tau)) dt \\ &= \sum_{i \geq 0} \left(-\frac{1}{4}\right)^i v_\varepsilon(t - i\tau) + \sum_{i \geq 0} \left(-\frac{1}{4}\right)^i v_\varepsilon(t - (i+1)\tau), \\ \overline{g}((\Phi^{-1}v_\varepsilon)(t), (\Phi^{-1}v_\varepsilon)(t - \tau)) &= \frac{1}{\pi} \int_0^\pi g(t, (\Phi^{-1}v_\varepsilon)(t), (\Phi^{-1}v_\varepsilon)(t - \tau)) dt \\ &= \sum_{i \geq 0} \left(-\frac{1}{4}\right)^i v_\varepsilon(t - (i+1)\tau), \\ \overline{\Phi I \Phi^{-1}}(v_\varepsilon(t)) &= \frac{1}{\pi} \sum_{j=1}^q (\Phi I_j \Phi^{-1})(v_\varepsilon(t_j)), \end{aligned} \quad (36)$$

and define a new averaged stochastic delay differential equations:

$$\begin{aligned} dv_\varepsilon(t) &= \varepsilon \left( \overline{f}((\Phi^{-1}v_\varepsilon)(t), (\Phi^{-1}v_\varepsilon)(t - \tau)) + \overline{\Phi I \Phi^{-1}}(v_\varepsilon(t)) \right) dt \\ &\quad + \sqrt{\varepsilon} \overline{g}((\Phi^{-1}v_\varepsilon)(t), (\Phi^{-1}v_\varepsilon)(t - \tau)) dB(t), \end{aligned} \quad (37)$$



namely,

$$\begin{aligned} dy_\varepsilon(t) = & \varepsilon \left( \sum_{i \geq 0} \left(-\frac{1}{4}\right)^i v_\varepsilon(t - i\tau) + \sum_{i \geq 0} \left(-\frac{1}{4}\right)^i v_\varepsilon(t - (i+1)\tau) + \frac{1}{\pi} \sum_{j=1}^q (-0.04)v_\varepsilon(t_j) \right) dt \\ & + \sqrt{\varepsilon} \sum_{i \geq 0} \left(-\frac{1}{4}\right)^i v_\varepsilon(t - (i+1)\tau) dB(t). \end{aligned} \quad (38)$$

Let  $(\Phi^{-1}v_\varepsilon)(t) = y_\varepsilon(t)$ , we have

$$\begin{aligned} dy_\varepsilon(t) = & \varepsilon \left( \sum_{i \geq 0} \left(-\frac{1}{4}\right)^i y_\varepsilon(t - i\tau) + \sum_{i \geq 0} \left(-\frac{1}{4}\right)^i y_\varepsilon(t - (i+1)\tau) + \frac{1}{\pi} \sum_{j=1}^q (-0.04)y_\varepsilon(t_j) \right) dt \\ & + \sqrt{\varepsilon} \sum_{i \geq 0} \left(-\frac{1}{4}\right)^i y_\varepsilon(t - (i+1)\tau) dB(t). \end{aligned} \quad (39)$$

When  $t \in [0, \tau]$ , the solution of system (3) can be deduced as

$$\begin{aligned} y_\varepsilon(t) = & e^t \left\{ y_\varepsilon(0) + \varepsilon \int_0^t e^{-s} \sum_{i \geq 1} \left(-\frac{1}{4}\right)^i y_\varepsilon(s - i\tau) ds + \varepsilon \int_0^t e^{-s} \sum_{i \geq 0} \left(-\frac{1}{4}\right)^i y_\varepsilon(s - (i+1)\tau) ds \right. \\ & \left. + \varepsilon e^{-t} \frac{1}{\pi} \sum_{j=1}^q (-0.04)y_\varepsilon(t_j) + \sqrt{\varepsilon} \int_0^t e^{-s} \sum_{i \geq 0} \left(-\frac{1}{4}\right)^i y_\varepsilon(s - (i+1)\tau) dB(s) \right\}. \end{aligned} \quad (40)$$

When  $t \in [\tau, 2\tau]$ , the solution of system (3) is deduced as

$$\begin{aligned} y_\varepsilon(t) = & e^{t-\tau} \left\{ y_\varepsilon(\tau) + \varepsilon \int_\tau^t e^{-(s-\tau)} \sum_{i \geq 1} \left(-\frac{1}{4}\right)^i y_\varepsilon(s - i\tau) ds \right. \\ & + \varepsilon \int_\tau^t e^{-(s-\tau)} \sum_{i \geq 0} \left(-\frac{1}{4}\right)^i y_\varepsilon(s - (i+1)\tau) ds + \varepsilon e^{-(t-\tau)} \frac{1}{\pi} \sum_{j=1}^q (-0.04)y_\varepsilon(t_j) \\ & \left. + \sqrt{\varepsilon} \int_\tau^t e^{-(s-\tau)} \sum_{i \geq 0} \left(-\frac{1}{4}\right)^i y_\varepsilon(s - (i+1)\tau) dB(s) \right\}. \end{aligned} \quad (41)$$

Repeat the steps above on  $[2\tau, 3\tau]$ ,  $[3\tau, 4\tau]$ , etc., and we can get the solution  $y_\varepsilon(t)$  on the whole interval  $y_\varepsilon(t)$ . In addition, it is easy to verify that the hypotheses of Theorem 1 and Corollary 1 holds; hence, the solution of the averaged system (3) converges to that of the standard system (1) in the sense of mean square and in probability.

## 5. Conclusion

In this paper, we generalize the periodic averaging principle for neutral stochastic delay differential equations with impulses. The main difficulties in the application of periodic averaging principle for neutral system are caused by the

delay term which is included under the differentiation at the left-hand side of the system. Using the linear operator theory, Theorem 1 and Corollary 1 show that the solutions of neutral stochastic delay differential equations with impulses converge to the solutions of the corresponding averaged stochastic delay differential equations without impulses in the sense of mean square and in probability. We remark that when the noises are Lévy processes other than Brownian motion considered in this paper, and the approach presented in the paper remains valid.

## Data Availability

No data were used to support the findings of the study.

## Conflicts of Interest

The authors declare that they have no conflicts of interest.

## Authors' Contributions

All authors completed the paper together. All authors read and approved the final manuscript.

## Acknowledgments

This work was supported by the National Natural Science Foundation of China (NSFC) under Grant nos. 11771115, 11271106, and 11801128 and Natural Science Foundation of Hebei Province under Grant no. A2018201109.

## References

- [1] R. Z. Khasminskij, "On the principle of averaging the ito's stochastic differential equations," *Kybernetika*, vol. 4, no. 3, pp. 260–279, 1968.
- [2] S. Cerrai and M. Freidlin, "Averaging principle for a class of stochastic reaction–diffusion equations," *Probability Theory and Related Fields*, vol. 144, no. 1–2, pp. 137–177, 2009.
- [3] Y. Xu, J. Duan, and W. Xu, "An averaging principle for stochastic dynamical systems with Lévy noise," *Physica D: Nonlinear Phenomena*, vol. 240, no. 17, pp. 1395–1401, 2011.
- [4] J. Xu, "L-strong convergence of the averaging principle for slow-fast SPDEs with jumps," *Journal of Mathematical Analysis and Applications*, vol. 445, no. 1, pp. 342–373, 2017.
- [5] P. Wei, Y. Chao, and J. Duan, "Hamiltonian systems with Lévy noise: symplecticity, Hamilton's principle and averaging principle," *Physica D: Nonlinear Phenomena*, vol. 398, pp. 69–83, 2019.
- [6] F. Wu and G. Yin, "An averaging principle for two-time-scale stochastic functional differential equations," *Journal of Differential Equations*, vol. 269, no. 1, pp. 1037–1077, 2020.
- [7] W. Mao, S. You, X. Wu, and X. Mao, "On the averaging principle for stochastic delay differential equations with jumps," *Advances in Difference Equations*, vol. 2015, no. 1, pp. 1–19, 2015.
- [8] Y. Xu, B. Pei, and J.-L. Wu, "Stochastic averaging principle for differential equations with non-lipschitz coefficients driven by fractional brownian motion," *Stochastics and Dynamics*, vol. 17, no. 2, Article ID 1750013, 2017.
- [9] S. Ma and Y. Kang, "Periodic averaging method for impulsive stochastic differential equations with Lévy noise," *Applied Mathematics Letters*, vol. 93, pp. 91–97, 2019.
- [10] X. He, S. Han, and J. Tao, "Averaging principle for sdes of neutral type driven by G-brownian motion," *Stochastics and Dynamics*, vol. 19, no. 1, Article ID 1950004, 2019.
- [11] J. B. Conway, *A Course in Functional Analysis*, Vol. 96, Springer Science & Business Media, Berlin, Germany, 2013.
- [12] C. Wang, Y. Li, and Y. Fei, "Three positive periodic solutions to nonlinear neutral functional differential equations with impulses and parameters on time scales," *Mathematical and Computer Modelling*, vol. 52, no. 9–10, pp. 1451–1462, 2010.
- [13] M. Ji, W. Qi, Z. Shen, and Y. Yi, "Existence of periodic probability solutions to fokker-planck equations with applications," *Journal of Functional Analysis*, vol. 277, no. 11, Article ID 108281, 2019.
- [14] T. Taniguchi, "Successive approximations to solutions of stochastic differential equations," *Journal of Differential Equations*, vol. 96, no. 1, pp. 152–169, 1992.

## Research Article

# Fixed-Time Convergent Guidance Law with Impact Angle Control

Zhongtao Cheng <sup>1</sup>, Hao Wu,<sup>2</sup> Bo Wang <sup>1</sup>, Lei Liu <sup>1</sup> and Yongji Wang <sup>1</sup>

<sup>1</sup>National Key Laboratory of Science and Technology on Multispectral Information Processing,  
School of Artificial Intelligence and Automation, Huazhong University of Science and Technology, Wuhan, China

<sup>2</sup>Beijing Aerospace Automatic Control Institute, Beijing, China

Correspondence should be addressed to Bo Wang; [wb8517@hust.edu.cn](mailto:wb8517@hust.edu.cn)

Received 4 April 2020; Accepted 12 May 2020; Published 29 May 2020

Academic Editor: Jianquan Lu

Copyright © 2020 Zhongtao Cheng et al. This is an open access article distributed under the Creative Commons Attribution License, which permits unrestricted use, distribution, and reproduction in any medium, provided the original work is properly cited.

The existing convergence control guidance laws are designed via the Lyapunov asymptotic stability theory or finite-time stability theory. However, guidance law based on the Lyapunov asymptotic stability theory would lead the states to zero only as time approaches infinity, which is imperfect theory. The convergence time for guidance laws based on finite-time stable theory is dependent on the initial states. A fixed-time convergent guidance law with impact angle control is proposed in this paper. The proposed guidance law consists of two parts. One is the heading error angle shaping term, and the other is the bias term to achieve the desired impact angle. The guidance command is continuous during the engagement without utilizing the switching logics. Unlike the existing guidance law in the literature, the fixed-time stability theory is utilized to ensure the impact angle error to converge to zero before the interception. Furthermore, the convergence rate is merely related to control parameters. Simulations are carried out to illustrate the effectiveness of the proposed guidance law.

## 1. Introduction

In the design of the missile guidance system, the primary objective is to reduce the relative range and achieve zero miss-distance attacks. In modern warfare, the mission is more diverse, and the battlefield is more complex [1, 2]. For example, the missile needs to avoid the defensive system by using a detour in certain missions. Also, specific impact angles to the weakest part of the target are effective for anti-tank or anti-ship missiles. Primitive guidance laws that only achieve the primary objective cannot accommodate to modern war. Hence, studies on the impact angle control guidance (IACG) have very high strategic significance [3–5].

Since the first study on impact angle control on a reentry vehicle [6], various guidance and control schemes are applied in the design of IACG, such as the proportional navigation (PN) law and its variants, optimal control theory, nonlinear control theory, and other geometry methods.

Due to the simple structure and optimality, many studies on IACG are based on PN and its variants. Apart from the

terminal position constraint, specific impact angles with high precision are achieved in simple proportional forms with nonlinear adaptive parameters [7]. A two-stage PN impact angle control law was present in [8], the orientation navigation stage leads the missile to certain switching states, which depend on the initial states of the missile and the desired impact angle, and the final stage leads the missile to the target with the desired impact angle. As an extension of the work in [8], both the heading error constraint and the impact angle constraint were considered in the two-stage PN [9]. Switching logic was used in two-stage PN methods; however, this would lead to an accumulated impact angle error because of autopilot dynamics in practice.

After the optimal control theory was utilized in the impact angle constraint research in [6], some other guidance laws in the literature also solved the impact angle control problem via this theory. In [10], considering different missile dynamics, a generalized optimal guidance law was offered in the state feedback form, and its characteristics were also investigated. After obtaining a new time-to-go estimation method, a novel optimal

impact angle control guidance law was proposed for constant velocity missile [11]. A new linear optimal IACG was proposed in [12]; unlike the traditional framework, the linearization was not conducted around the initial LOS angle but around a nominal circular trajectory.

The nonlinear control theories, such as the Lyapunov stability theory and the sliding mode theory, were also adopted in the design of IACG. In [13], to hit the target with a specific angle, the Lyapunov candidate function was augmented with an impact angle error term. A recent Lyapunov stability theory-based guidance law was found in [14], the candidate function was proposed to reduce the heading error angle, and a two-stage IACG was proposed for hitting the target in all aspects. However, the states would converge to zero only as time approached infinitely for the Lyapunov-based guidance law, theoretically. Hence, some other studies involved the finite-time convergence IACG. In [15], an IACG law that insured the convergence of the line of sight (LOS) angle in finite-time was proposed from the sliding mode control theory. In [16], a finite-time convergent IACG based on the non-singular terminal sliding mode control (NTSMT) method was proposed, and the resulting guidance law can hit the target with a desired impact angle. Another finite-time convergent guidance law was found in [17]. However, a guidance law based on the Lyapunov asymptotic stability theory would lead the states to zero only as time approaches infinity, which is imperfect theory. Also, the convergence time for guidance laws based on finite-time stable theory is dependent on the initial states.

In addition to the methods described above, the geometric and polynomial approach has also been adopted to derive the IACG law. The first appearance of the polynomial guidance was found in [18]. After that, an augmented impact angle control polynomial guidance law considering acceleration constraint was proposed in [19]. The guidance command was present in the form with unknown coefficients corresponding to the terminal constraints. To control impact time and angle, the guidance command was proposed as a function of range-to-go in [20]. A very recent research involved the geometric and polynomial approach found in [21], and the resulting guidance law was proposed in the adaptive form.

In this study, to overcome the limitations of the existing studies, a nonswitching fixed-time convergent guidance law with impact angle control is proposed. First, a heading error-shaping method is introduced to ensure the successful impact of the target. Also, the terminal characteristics of this error-shaping method are summarized. Then, the fixed-time stability theory is applied to design a bias term, which can ensure the fixed-time convergence of the impact angle error.

The rest of this paper is organized as follows. Preliminary on fixed-time stability is introduced in Section 2. In Section 3, the heading error shaping and the design of the bias term are offered. In Section 4, the effectiveness of the proposed strategy is verified through different numerical simulations. Finally, the conclusion can be found in Section 5.

## 2. Fixed-Time Stability Theory of a Nonlinear System

Before deriving the guidance law, it is obliged to introduce some basic concepts of fixed-time stability theory [22].

*Definition.* The following nonlinear system is considered:

$$\begin{aligned}\dot{x}(t) &= f(t, x(t)), \\ x(0) &= x_0,\end{aligned}\quad (1)$$

where the state and the upper semicontinuous mapping are denoted by  $x(t) \in R^l$  and  $f: R^+ \times R^n \rightarrow R^n$ , respectively. The state is fixed-time stability if it is globally finite-time stable; meanwhile, the function of the settling time  $T(x_0)$  is restricted by a real positive number  $T_{\max}$ , i.e.,  $T(x_0) \leq T_{\max}, \forall x_0 \in R^l$ . The definition can be stated mathematically as

$$\begin{cases} \lim_{t \rightarrow T(x_0)} x(t, x_0) = 0, & t \in [t_0, T(x_0)), \\ x(t, x_0) = 0, & t \geq T(x_0), T(x_0) < T_{\max}. \end{cases}\quad (2)$$

It should be noted that the settling time in (2) is independent of the initial states. Denote by  $D^* \varphi(t)$  the upper right-hand derivative of a function  $\varphi(t)$ ,  $D^* \varphi(t) = \lim_{h \rightarrow +0} (\varphi(t+h) - \varphi(t))/h$ . Also, the fixed-time stability under the Lyapunov criterion is presented in Lemma 1.

**Lemma 1.** *Suppose a continuous positive definite and radially unbounded function as  $V(x): R^n \rightarrow R^+ \cup \{0\}$ , such that*

$$D^* V(x(t)) \leq -mV^p(x(t)) - nV^q(x(t)), \quad (3)$$

for  $m, n > 0$ ,  $p = 1 - (1/2\gamma)$ ,  $q = 1 + (1/2\gamma)$ ,  $\gamma > 1$ . Then, the origin is fixed-time stable for the system in (1), and the settling time is given by

$$T(x_0) \leq T_{\max} := \frac{\pi\gamma}{\sqrt{mn}} \quad (4)$$

*Remark 1.* Different from finite-time stability theory, the bound of the settling time function for fixed-time stability theory is merely connected with the design parameters.

## 3. Problem Statement and Guidance Law Design

In this section, the two-dimensional kinematic equations that stand for the engagement geometry between the target and the missile are formulated, and the objective of the impact angle control problem is elaborated. Then, the concept of fixed-time convergence of the impact angle error is introduced, and the impact control guidance law is designed.

*3.1. Engagement Geometry and Problem Statement.* The missile-to-target system is denoted in Figure 1, where the planar engagement geometry is considered. In Figure 1,  $r$  denotes the relative range between the missile and target.  $V$

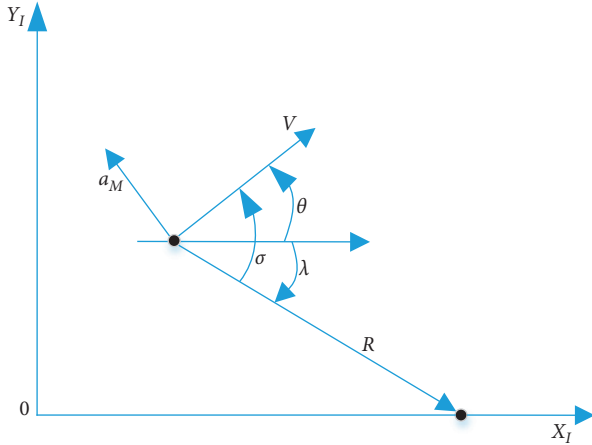


FIGURE 1: Engagement geometry.

and  $a$  represent the missile's speed and later acceleration, respectively.  $\theta$ ,  $\sigma$ , and  $\lambda$  stand for the flight path angle, the heading error angle, and the line of the LOS angle, respectively.

Assume the counterclockwise direction as the positive direction for the aforementioned angles. Under the small angle of attack assumption, the geometry relationship between the angles can be expressed as

$$\sigma = \theta - \lambda. \quad (5)$$

The kinematic equations for the missile to intercept the target can be obtained as

$$\dot{r} = -V \cos \sigma, \quad (6)$$

$$\dot{\lambda} = \frac{-V \sin \sigma}{r}, \quad (7)$$

$$\dot{\theta} = \frac{a_M}{V}. \quad (8)$$

The basic requirement for a guidance law is to lead to missile to hit the target, which is also the primary objective for the guidance law design in this paper. Apart from the primary objective, the additional objective is that the impact angle should converge to the desired value as the engagement proceeds, which can be expressed mathematically as

$$\theta \longrightarrow \theta_d, \text{ as } t \longrightarrow t_s \leq t_f. \quad (9)$$

It should be noted that  $\theta_d$  in (9) refers to the desired value for the impact angle, and  $t_s$  should be smaller than the final impact time.

**3.2. Primary Guidance Law with Zero Miss-Distance.** In this subsection, the primary objective of the guidance law is achieved through the heading error angle shaping method, and the terminal characteristics of this method are briefly summarized.

Since the angle of attack is assumed to be small in the previous subsection, the missile will hit the target with zero miss-distance by zeroing the heading error. Hence, the zero-

miss distance design problem is transformed into the heading error angle control problem. In this regard, the Lyapunov candidate function is proposed as

$$W_1 = \sin^2 \frac{\sigma}{2}. \quad (10)$$

The time derivative of (10) is

$$\dot{W}_1 = \frac{\sin \sigma \cdot \dot{\sigma}}{2}. \quad (11)$$

To meet the asymptotic stability requirement, the candidate function should be positive definite  $W_1$ , and its derivative  $\dot{W}_1$  should be negative definite.

**Theorem 1.** *The asymptotic stability condition can be met if the heading error satisfies*

$$\dot{\sigma} = \frac{cV}{r} \sin \sigma, \quad c \geq 1, \quad (12)$$

where  $c$  controls the speed of the heading error rate.

*Proof.* Combining equations (11) and (12) yields

$$\dot{W}_1 = -\frac{cV}{2r} \sin^2 \sigma. \quad (13)$$

It can be concluded from (10) that  $W$  is positive definite, and (13) denotes that  $\dot{W}_1$  is negative definite. Hence, the Lyapunov asymptotic stability condition is satisfied, and the proof of Theorem 1 is completed.

The Lyapunov asymptotic stability theory-based method only ensures convergence when the time approaches infinity. Obviously, this is imperfect theory. Hence, before prolonging the method to achieve the additional impact angle objective, the terminal characteristics of this guidance strategy are briefly summarized.

Dividing (12) by (6) yields

$$\frac{d\sigma}{\tan \sigma} = \frac{c}{r} dr. \quad (14)$$

By solving a separable differential (15),  $\sigma$  can be expressed as a function of  $r$  as

$$\sin \sigma = \left( \frac{r}{r_0} \right)^c \sin \sigma_0. \quad (15)$$

It can be concluded from (15) that  $\sin \sigma \longrightarrow 0$  as  $r \longrightarrow 0$ , if  $c \geq 1$ . As a result, the heading error can converge to zero at the instant of attack.

The derivative of (5) to time is

$$\dot{\sigma} = \dot{\theta} - \dot{\lambda}. \quad (16)$$

Substituting (7) and (12) into (16) yields

$$\dot{\theta} = -\frac{(c+1)}{c} \dot{\sigma}. \quad (17)$$

In addition, combining (12) and (15) yields

$$\dot{\sigma} = -\frac{cV}{r_0^c}(r)^{c-1} \sin \sigma_0. \quad (18)$$

Hence, the guidance command that leads the missile to the target with zero miss-distance can be acquired as

$$a^L = -\frac{(c+1)V^2}{r_0^c}(r)^{c-1} \sin \sigma_0, \quad (19)$$

where the superscript  $L$  stands for the terminal states of the missile under the heading error-shaping method. By combining (7) and (12), we have

$$\dot{\lambda} = \frac{\dot{\sigma}}{c}. \quad (20)$$

Integrating both sides of (20) from current time  $t$  to final time  $t_f$  yields

$$\lambda_f^L = \lambda + \frac{\sigma_f^L - \sigma}{c}. \quad (21)$$

Substituting (5) into (21) yields

$$\theta_f^L = \theta - \frac{c+1}{c}\sigma. \quad (22) \quad \square$$

*Remark 2.* The heading error-shaping method can ensure the convergence of the guidance command at the instance of interception, and the terminal intercept angle under this method can be calculated from equation (22). Also, the impact angle error can be acquired.

**3.3. Impact Angle Control Guidance Law Design.** In this section, the heading error-shaping method is further investigated. In addition, the impact angle control objective is achieved. The difference between  $\theta_d$  and  $\theta_f^L$  calculated from (22) is regarded as the impact angle error, which can be expressed as follows:

$$e_{\theta f} = \theta_f^L - \theta_d = \theta - \frac{c+1}{c}\sigma - \theta_d. \quad (23)$$

The time derivative of (23) is

$$\dot{e}_{\theta f} = \dot{\theta} - \frac{c+1}{c}\dot{\sigma}. \quad (24)$$

If the impact angle error can converge to zero before the final time, the additional objective expressed in (9) can be achieved. Substituting (8) and (19) into (24) yields

$$\dot{e}_{\theta f} = \frac{a_M}{V} + \frac{(c+1)V \sin \sigma}{r} = \frac{a_M - a^L}{V} = \frac{u}{V}, \quad (25)$$

where  $u$  is defined as the bias term of the guidance command, and the purpose of introducing the bias term  $u$  is illustrated in Figure 2, which aims at governing the dynamics of the impact angle error to zero. Hence, the objective of impact angle control will be achieved through the design of  $u$ . The impact angle control guidance command is constructed as

$$a_M = a^L + u. \quad (26)$$

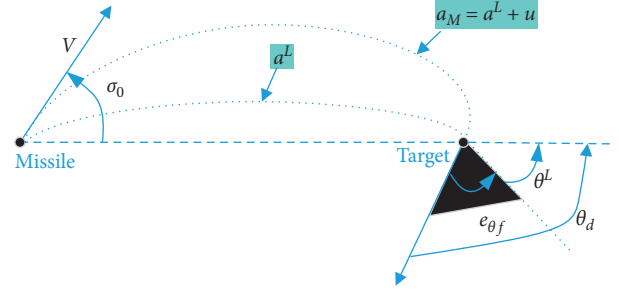


FIGURE 2: The purpose of introducing the bias term  $u$ .

**Theorem 2.** *If the bias term  $u$  can make the impact angle error of the missile satisfying*

$$e_{\theta f} \left[ \dot{e}_{\theta f} + \frac{m}{2} e_{\theta f}^{1-(1/\gamma)} + \frac{n}{2} e_{\theta f}^{1+(1/\gamma)} \right] \leq 0, \quad (27)$$

where  $m = \text{const.} > 0$ ,  $n = \text{const.} > 0$ ,  $\gamma = \text{const.} > 1$ , and then the impact angle error will converge to zero in fixed-time. The convergence rate increases as the values of  $m$  and  $n$  increase, and it will also increase as the value of  $\gamma$  decreases. Besides, different from the finite-time convergence guidance law, the convergence time is independent of the missile's initial states.

*Proof.* The following continuously differential candidate function is considered:

$$W_2 = e_{\theta f}^2. \quad (28)$$

The derivative of (28) to time is

$$\dot{W}_2 = 2e_{\theta f} \dot{e}_{\theta f}. \quad (29)$$

Substituting (28) and (29) into (27) yields

$$\dot{W}_2 \leq -mW_2^{1-(1/2\gamma)} - nW_2^{1+(1/2\gamma)}. \quad (30)$$

According to Lemma 1, the impact angle error will converge to zero in fixed-time, and the fixed-time is given by

$$t_s \leq t_{\max} = \frac{\pi\gamma}{\sqrt{mn}}, \quad (31)$$

where  $t_s$  is the convergence time of the impact angle error and  $t_{\max}$  is the upper bound for the settling time. It can be concluded from (31) that  $t_s$  is independent of the initial states. Define  $t_f$  as the final time of the engagement. To impact the target with a specific direction successfully, the error dynamics of impact angle error of the collision course should be achieved before  $t_f$ . Unlike the finite-time convergence guidance law, the convergence time  $t_s$  is independent of the initial states, which can be adjusted by control parameters. Hence,  $t_s < t_f$  can be guaranteed through proper selection of the control parameters. Figure 3 shows the convergence process of the impact angle error. It is revealed that the impact angle error converges to zero at  $t_s$  and remains there till the end of the engagement.

Substituting (25) into (27) yields

$$e_{\theta f} \left[ \frac{u}{V} + \frac{m}{2} e_{\theta f}^{1-(1/\gamma)} + \frac{n}{2} e_{\theta f}^{1+(1/\gamma)} \right] \leq 0. \quad (32)$$

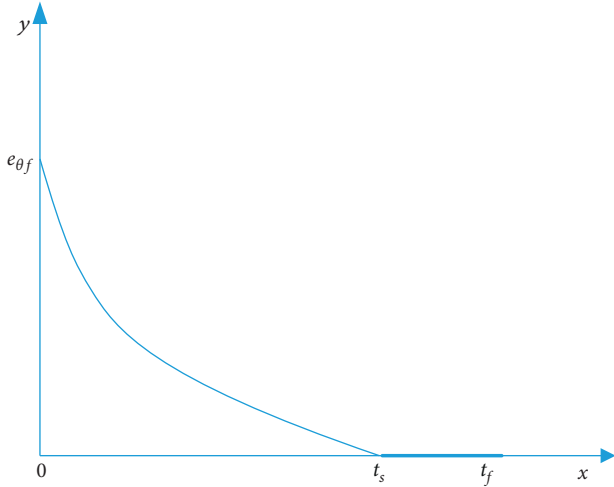


FIGURE 3: Impact angle error variation.

The bias term of the guidance command is chosen as

$$u = V \left( \frac{m}{2} e_{\theta f}^{1-(1/\gamma)} + \frac{n}{2} e_{\theta f}^{1+(1/\gamma)} \right) + kV e_{\theta f}, \quad k > 0. \quad (33)$$

□

**Theorem 3.** *The bias term in equation (33) can achieve fixed-time convergence for the impact angle error.*

*Proof.* Substituting equation (33) into equation (25), we have

$$\dot{e}_{\theta f} = - \left( \frac{m}{2} e_{\theta f}^{1-(1/\gamma)} + \frac{n}{2} e_{\theta f}^{1+(1/\gamma)} \right) - e_{\theta f}. \quad (34)$$

By substituting equation (34) into equation (27), we get

$$-e_{\theta f}^2 \leq 0. \quad (35)$$

According to Theorem 2, the proposed bias term in (33) can lead to fixed-time convergence for the impact angle error, and the convergence rate increases as the values of  $m$  and  $n$  increase or as the value of  $\gamma$  decreases. □

## 4. Simulations

Numerical simulation is performed to show the effectiveness of the proposed method. Three simulations are considered: In Case 1, the comparison between the proposed method and the two-stage impact angle control guidance law is considered. In Case 2, different impact angles are achieved with the same control parameters. In Case 3, three control parameters are considered to achieve the same impact angle.

The initial states for the missile and target used in this simulation are tabulated in Table 1. The simulation step for the second-order Runge–Kutta integral method applied in this study is 0.001 s, and each simulation case will be terminated when the relative range is smaller than 0.5 m. Besides, the maximal value for the acceleration constraint is 15 g.

TABLE 1: Simulation parameters.

Parameter	Value
Initial position for the missile	(0, 0) m
Missile speed	150 m/s
Initial heading angle for the missile	45°
Initial position for the target	(6000, 0) m
Maximal acceleration constraint	15 g

**4.1. Comparison Simulation.** To show the effectiveness of the proposed method, one existing guidance law in Ref. [9] is considered in this comparison study. The guidance command for the comparison law is given by

$$a^{\text{two-stage}} = \begin{cases} V\dot{\lambda}, & \text{first stage,} \\ N^{\text{two-stage}} V\dot{\lambda}, & \text{final stage.} \end{cases} \quad (36)$$

The switching criterion for the comparison law is calculated from the desired impact angle, and the  $N^{\text{two-stage}} = 2$  for the final stage. For the proposed method, the control parameters are  $m = n = 0.05$ ,  $\gamma = 10$ .

The results for this comparison simulation are shown in Figure 4. Dotted lines represent the results of the comparison guidance law, and solid lines represent the results for the proposed method. Figure 4(a) depicts the trajectories for the missile and target. Figure 4(b) shows the acceleration command. Figures 4(c) and 4(d) represent the profile of the impact angle and impact angle rate, respectively.

It can be concluded from Figure 4 that both the proposed method and the comparison law can nullify the impact angle error and impact the target with the desired impact angle successfully. However, the acceleration variation and the convergence of the heading error are significantly different, as shown in Figures 4(b) and 4(d). As for the comparison law, the guidance command will switch to another value once the heading error converges to zero. Due to the switching logic for the comparison law, the guidance command is switched to another value instantaneously; this would lead to an accumulated impact angle error. Besides, the missile cannot achieve this performance in practice with autopilot dynamics.

For the proposed guidance law, there would be no discontinuity. As a result, the proposed guidance law is more applicable and can achieve higher accuracy than the comparison law. Hence, the proposed guidance law has better performance over the comparison law.

**4.2. Various Impact Angles.** In this case, four different desired impact angles selected from the range  $-90^\circ$  to  $90^\circ$  are considered. The control parameters for the proposed guidance law are the same as those of the previous simulation.

The simulation results are shown in Figure 5. Figure 5(a) depicts the trajectories for the missile and target, and it can be concluded from the trajectories that the primary objective can be achieved by the proposed guidance law. Figure 5(b) shows impact angle variation profile, and it can be concluded each desired impact angle can be achieved, which means the

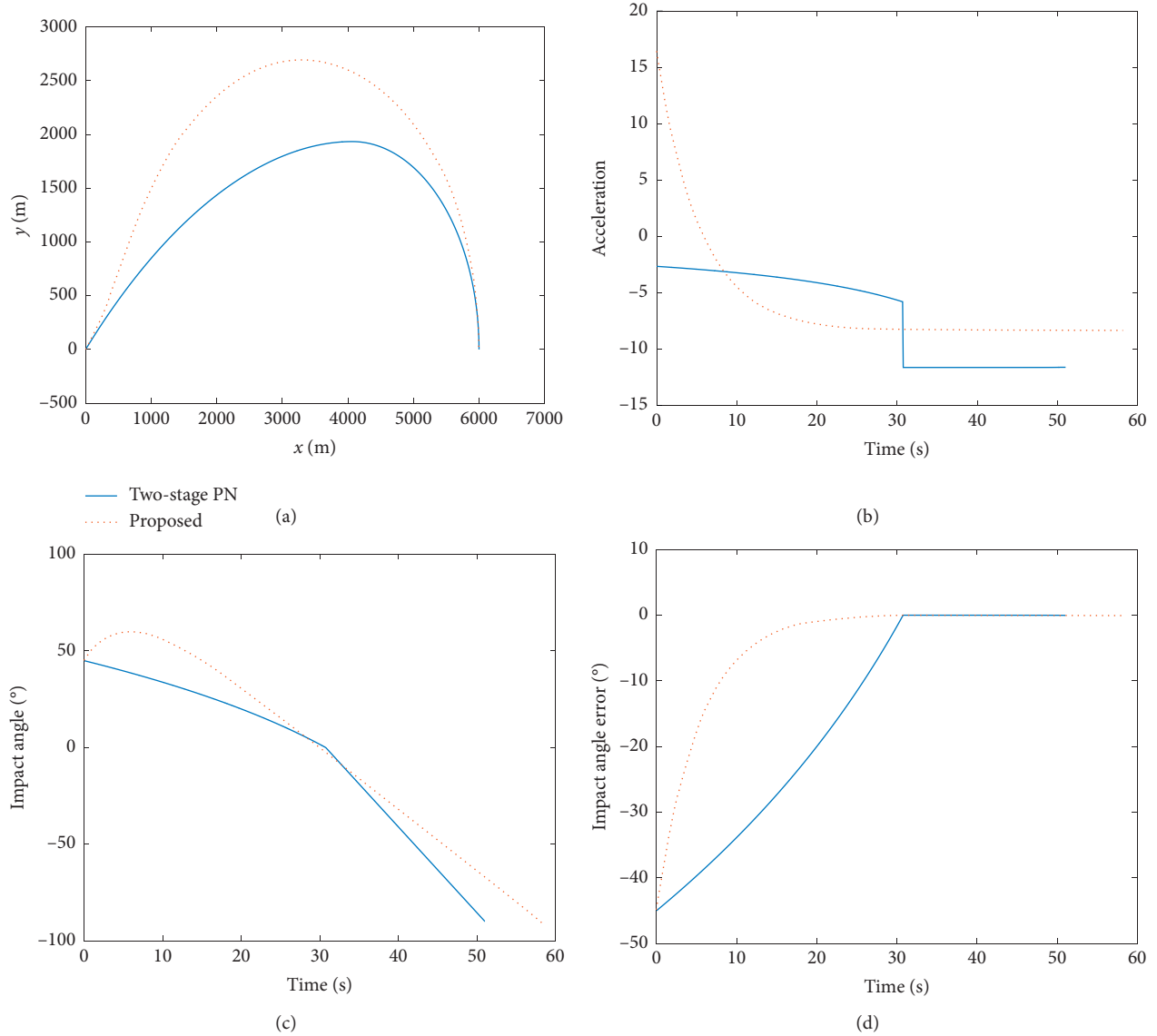


FIGURE 4: Comparison results. (a) Trajectories. (b) Acceleration. (c) Impact angle. (d) Impact angle error.

addition objective can also be fulfilled. Also, Figure 5(c) shows that the impact angle errors can converge to zero in fixed-time, which is in line with Theorem 3. Figure 5(d) represents the profile of the heading angle error, which converges to zero at the instant of attack, corresponding to Theorem 1. Finally, the acceleration profile is demonstrated in Figure 5(e). After the convergence of the impact angle error, the bias term in the acceleration command will be nullified.

**4.3. Various Control Parameters.** In this case, the performance of the proposed guidance law is studied under three different control parameters, which are  $m = n = 0.5$ ,  $m = n = 0.1$ ,  $m = n = 0.05$ ,  $\gamma = 10$ .

The simulation results are shown in Figure 6. Figure 6(a) depicts the trajectories for the missile and target, and it can be concluded from the trajectories that the primary objective can be achieved by the proposed guidance law. Figure 6(b) shows the impact angle variation profile, which means the addition objective can also be fulfilled.

For all the various values of control parameters, the impact angle can converge to zero in fixed-time, as is shown in Figure 6(c), and this is in line with Theorem 3. Figure 5(d) represents the profile of the heading angle error, which converges to zero at the instant of attack, this corresponds to Theorem 1. Finally, the acceleration profile is demonstrated in Figure 5(e). After the convergence of the impact angle error, the bias term in the acceleration command will be nullified. It is obvious that the impact angle error converges



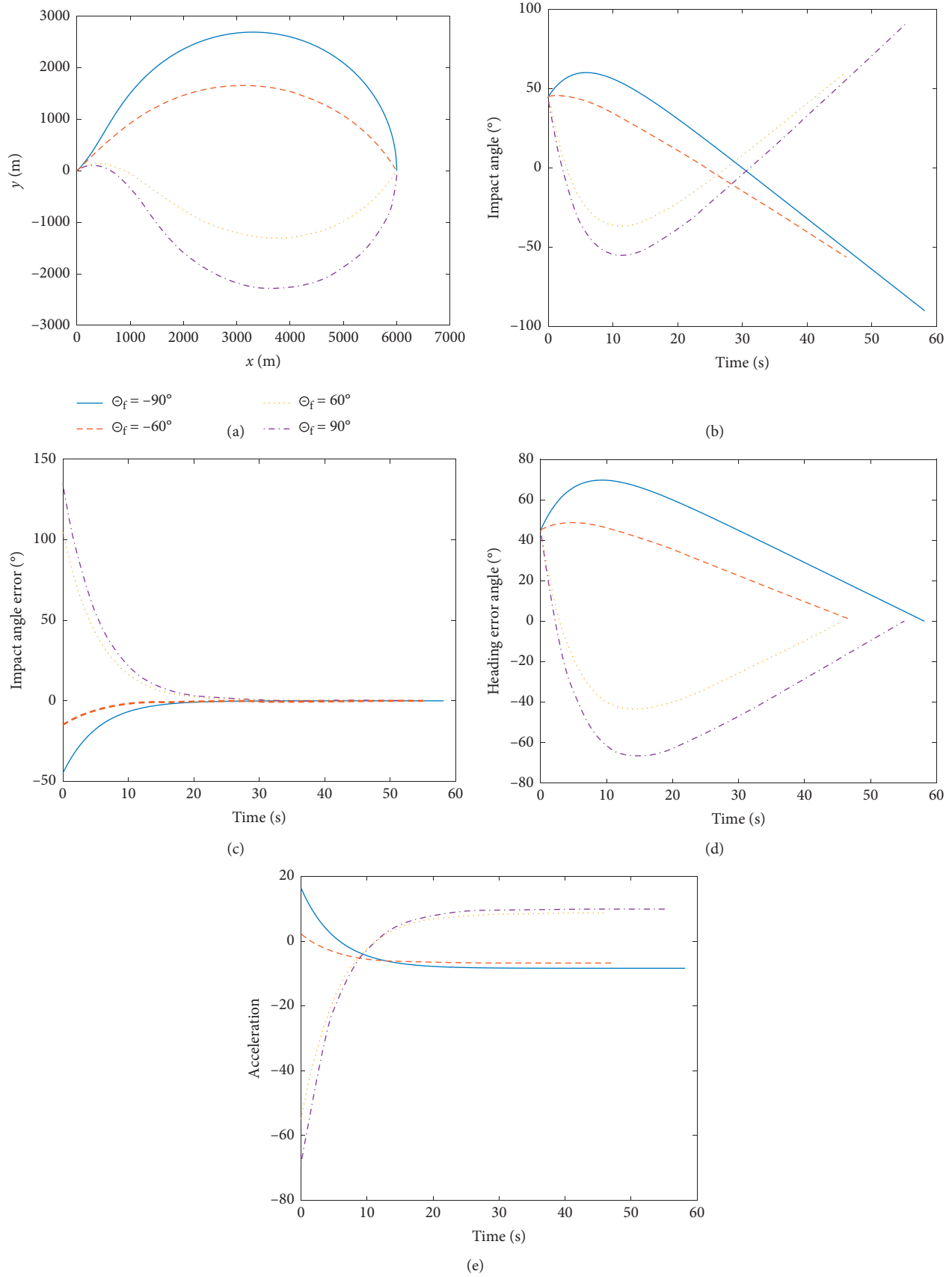


FIGURE 5: Various impact angles under the same control parameters. (a) Trajectories. (b) Impact angle. (c) Impact angle error. (d) Heading error angle. (e) Acceleration.

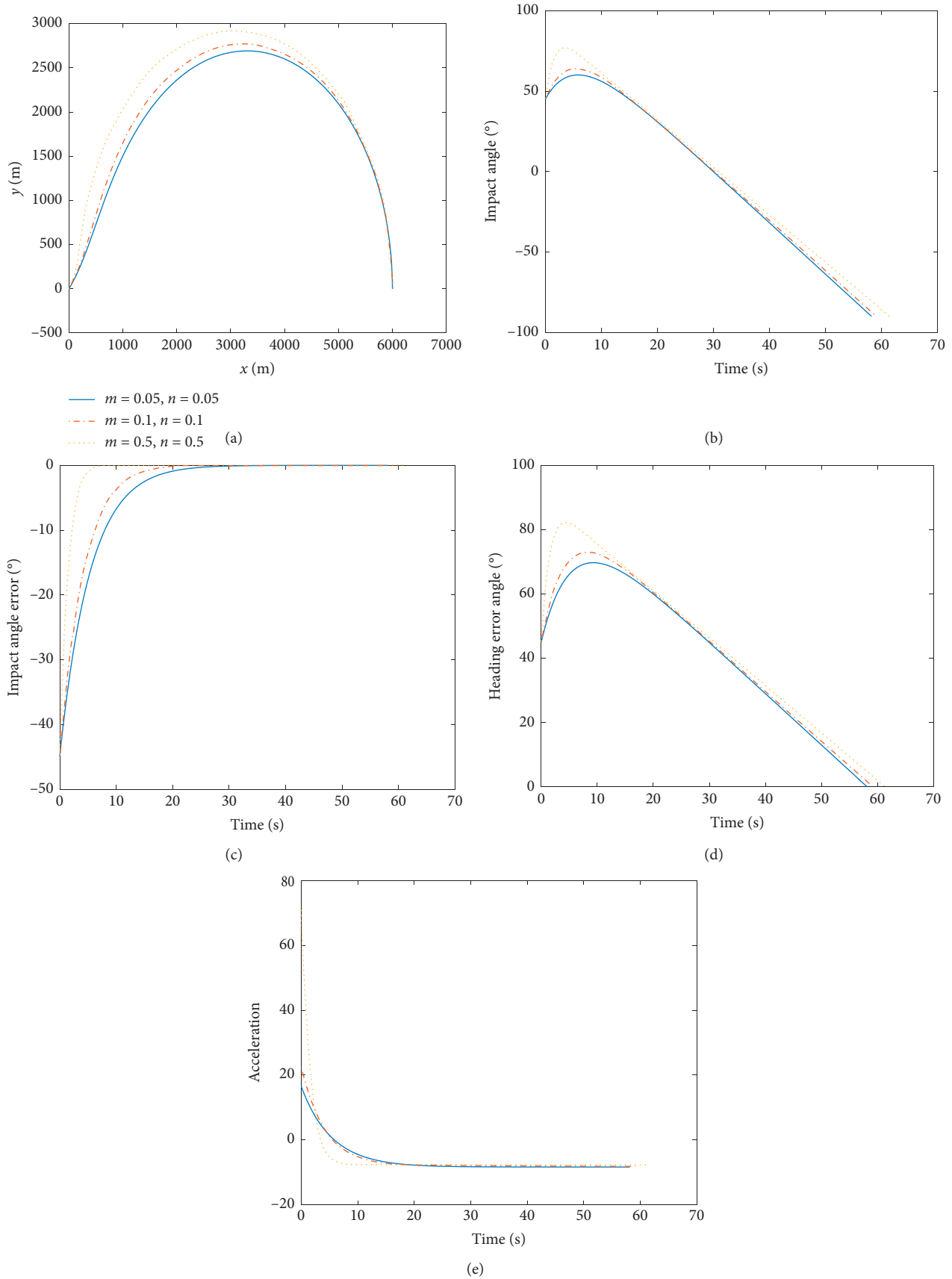


FIGURE 6: Various control parameters with the same impact angle. (a) Trajectories. (b) Impact angle. (c) Impact angle error. (d) Heading error angle. (e) Acceleration.

more quickly with larger control parameters, and this is also in line with Theorem 1.

## 5. Conclusion

Considering the impact course can be achieved with the heading error goes to zero, the heading error shaping is applied to achieve the primary objective of the guidance law. Then, the fixed-time stability theory is utilized to ensure the convergence of the impact angle in fixed-time. The convergence rate is merely related to control parameters, a suitable selection of which can ensure the convergence before the interception. Simulations are carried out to illustrate the properties of the proposed guidance law. In our future related work, more complex scenarios such as 3-D engagement against moving targets and more constraints to improve the missile performance should also be concerned.

## Data Availability

The data used to support the findings of this study are available from the corresponding author upon request.

## Conflicts of Interest

The authors declare that they have no conflicts of interest.

## Acknowledgments

This study was co-supported in part by the National Natural Science Foundation of China (Nos. 61903146, 61873319, and 61803162).

## References

- [1] C. Wei, Y. Han, N. Cui, and H. Xu, "Fifth-degree cubature kalman filter estimation of seeker line-of-sight rate using augmented-dimensional model," *Journal of Guidance, Control, and Dynamics*, vol. 40, no. 9, pp. 2355–2362, 2017.
- [2] J. Zhou and J. Yang, "Guidance law design for impact time attack against moving targets," *IEEE Transactions on Aerospace and Electronic Systems*, vol. 54, no. 5, pp. 2580–2589, 2018.
- [3] Z. Wu, Z. Guan, C. Yang, and J. Li, "Terminal guidance law for UAV based on receding horizon control strategy," *Complexity*, vol. 2017, Article ID 2750172, 19 pages, 2017.
- [4] S. Mao, L. Liu, and Y. Wang, "Integrated estimation/guidance law against exoatmospheric maneuvering targets," *Complexity*, vol. 2018, Article ID 7470823, 19 pages, 2018.
- [5] S. Gao, Z. Peng, D. Wang, and L. Liu, "Extended-state-observer-based collision-free guidance law for target tracking of autonomous surface vehicles with unknown target dynamics," *Complexity*, vol. 2018, Article ID 4154670, 10 pages, 2018.
- [6] M. Kim and K. Grider, "Terminal guidance for impact attitude angle constrained flight trajectories," *IEEE Transactions on Aerospace and Electronic Systems*, vol. AES-9, no. 6, pp. 852–859, 1973.
- [7] P. Lu, D. B. Doman, and J. D. Schierman, "Adaptive terminal guidance for hypervelocity impact in specified direction," *Journal of Guidance, Control, and Dynamics*, vol. 29, no. 2, pp. 269–278, 2006.
- [8] A. Ratnoo and D. Ghose, "Impact angle constrained interception of stationary targets," *Journal of Guidance Control & Dynamics*, vol. 31, no. 6, pp. 1816–1821, 2008.
- [9] A. Ratnoo, "Analysis of two-stage proportional navigation with heading constraints," *Journal of Guidance, Control, and Dynamics*, vol. 39, no. 1, pp. 156–164, 2016.
- [10] C.-K. Ryoo, H. Cho, and M.-J. Tahk, "Optimal guidance laws with terminal impact angle constraint," *Journal of Guidance, Control, and Dynamics*, vol. 28, no. 4, pp. 724–732, 2005.
- [11] C. K. Ryoo, H. Cho, and M. J. Tahk, "Time-to-go weighted optimal guidance with impact angle constraints," *IEEE Transactions on Control Systems Technology*, vol. 14, no. 3, pp. 483–492, 2006.
- [12] R. Tsalik and T. Shima, "Optimal guidance around circular trajectories for impact-angle interception," *Journal of Guidance Control and Dynamics*, vol. 39, no. 6, pp. 1–14, 2016.
- [13] M. Kim and Y. Kim, "Lyapunov-based pursuit guidance law with impact angle constraint," *IFAC Proceedings Volumes*, vol. 47, no. 3, pp. 2509–2514, 2014.
- [14] C. Zhongtao, L. Lei, and W. Yongji, "Lyapunov-based switched-gain impact angle control guidance," *Chinese Journal of Aeronautics*, vol. 31, no. 4, pp. 765–775, 2018.
- [15] Y. Zhang, M. Sun, and Z. Chen, "Finite-time convergent guidance law with impact angle constraint based on sliding-mode control," *Nonlinear Dynamics*, vol. 70, no. 1, pp. 619–625, 2012.
- [16] Z. Hou, L. Liu, Y. Wang, J. Huang, and H. Fan, "Terminal impact angle constraint guidance with dual sliding surfaces and model-free target acceleration estimator," *IEEE Transactions on Control Systems Technology*, vol. 25, no. 1, pp. 85–100, 2017.
- [17] S. He, D. Lin, and J. Wang, "Continuous second-order sliding mode based impact angle guidance law," *Aerospace Science and Technology*, vol. 41, pp. 199–208, 2015.
- [18] B.-M. Min, M.-J. Tahk, H.-C. D. Shim, and H.-C. Bang, "Guidance law for vision-based automatic landing of UAV," *International Journal of Aeronautical and Space Sciences*, vol. 8, no. 1, pp. 46–53, 2007.
- [19] C.-H. Lee, T.-H. Kim, M.-J. Tahk, and I.-H. Whang, "Polynomial guidance laws considering terminal impact angle and acceleration constraints," *IEEE Transactions on Aerospace and Electronic Systems*, vol. 49, no. 1, pp. 74–92, 2013.
- [20] T.-H. Kim, C.-H. Lee, I.-S. Jeon, and M.-J. Tahk, "Augmented polynomial guidance with impact time and angle constraints," *IEEE Transactions on Aerospace and Electronic Systems*, vol. 49, no. 4, pp. 2806–2817, 2013.
- [21] Z. Cheng, B. Wang, L. Liu, and Y. Wang, "Adaptive polynomial guidance with impact angle constraint under varying velocity," *IEEE Access*, vol. 7, pp. 104210–104217, 2019.
- [22] A. Polyakov, "Nonlinear feedback design for fixed-time stabilization of linear control systems," *IEEE Transactions on Automatic Control*, vol. 57, no. 8, pp. 2106–2110, 2012.

## Research Article

# Finite-Time Stability for a Class of Underactuated Systems Subject to Time-Varying Disturbance

Jie Wu,<sup>1</sup> Dan Yang,<sup>1</sup> Xinyi He,<sup>1</sup> and Xiaodi Li <sup>1,2</sup>

<sup>1</sup>School of Mathematics and Statistics, Shandong Normal University, Ji'nan 250014, China

<sup>2</sup>Center for Control and Engineering Computation, Shandong Normal University, Ji'nan 250014, China

Correspondence should be addressed to Xiaodi Li; [sodymath@163.com](mailto:sodymath@163.com)

Received 24 March 2020; Accepted 29 April 2020; Published 12 May 2020

Academic Editor: Sigurdur F. Hafstein

Copyright © 2020 Jie Wu et al. This is an open access article distributed under the Creative Commons Attribution License, which permits unrestricted use, distribution, and reproduction in any medium, provided the original work is properly cited.

Based on the classical finite-time stability theory, the problem of finite-time stability (FTS) for time-varying nonlinear systems is investigated in this paper. Several FTS theorems involving global form and local form are presented, and an estimate of the settling-time of such systems is obtained. As an application, we consider the problem of asymptotic stabilization of the Brockett integrator subject to time-varying disturbance. By the switched finite-time controller design methodology, we establish a sufficient condition to guarantee the relative asymptotic stability. For Brockett-like integrator subject to time-varying disturbance, we achieve better convergence performance. Examples and their simulations are given to demonstrate the applicability of the proposed results.

## 1. Introduction

Over the past decades, many researchers have focused on Lyapunov asymptotic or exponential stability of dynamical systems, see [1–7]. One of the typical features of the asymptotic or exponential stability is that the solution will tend to an equilibrium state as time tends to infinity. Thus, it is difficult to achieve fast transient and high-precision performances. Finite-time stability (FTS) served as a special case of asymptotic stability means that the system reaches an equilibrium state in finite time, which presents an efficient tool for many engineering problems. Lots of interesting results on FTS have been raised from theoretical and practical points of view. Haimo [8] introduced a definition of continuous finite-time differential equations as fast accurate controllers for dynamical systems. Bhat and Bernstein [9] proposed Lyapunov theorem on FTS of continuous autonomous systems. Bhat and Bernstein [10] achieved globally FTS of the double integrator. Yang et al. [11] concerned the stabilization of switched dynamical networks with logarithmic quantization couplings in finite time. Moulay and Perruquetti [12] studied the FTS for a class of continuous systems using Lyapunov function. Furthermore,

Moulay et al. [13] established some FTS theorems for time-delay systems based on Lyapunov functionals and the extension of Artsteins transformation. Polyakov and Hu et al. [14, 15] introduced the concept of fixed-time stability, which means that the system is globally finite-time stable and the settling-time is bounded by some positive constant for any initial values. However, most of existing results, such as [8–13], are based on the framework of time invariant. Recently, Haddad et al. [16] obtained a sufficient condition of FTS for nonlinear time-varying systems. However, it can only be applied to some special cases due to the strict restriction that the derivative of Lyapunov function is less than zero almost everywhere. Moulay and Perruquetti [17] presented the FTS conditions for nonautonomous continuous systems. However, it was simplified to the time-invariant form through the inequality of the Lyapunov function. Hence, more general methods should be established for nonlinear time-varying systems. To avoid confusion, it should be pointed out that the FTS considered in this paper is different from another FTS concept adopted in [18–20], which dealt with the finite-time boundedness.

As stated in Brockett's result [21], Brockett integrator (Nonholonomic integrator), covered in underactuated

systems, was the first example of locally controllable nonlinear system which is not smoothly stabilizable and requires additional constraints. In order to overcome the abovementioned limitations, various methods have been proposed for the problem of asymptotic stabilization of the Brockett integrator [22–26]. Astolfi [22] addressed the problem of almost exponential stabilization with bounded control. Banavar and Sankaranarayanan [23] studied a switched finite-time controller design methodology. Rehman [24] dealt with steering control of nonholonomic systems with drift for the extended nonholonomic double integrator. Rehman and Ahmed [25] presented piecewise constant and state-dependent feedback control for the nonholonomic integrator. Chihchen [26] investigated the time-varying control for globally exponential stabilization of the Brockett integrator. However, the abovementioned works did not take disturbance into account and converged in infinite time domain. Therefore, based on the FTS theorem for time-varying systems, we will explore stability issues of the Brockett integrator subject to time-varying disturbance.

In this paper, we firstly address some essential stability definitions in Section 2. Then, in Section 3, based on the classical finite-time stability theorem [9], the FTS theorem for time-varying nonlinear systems is considered. We apply it to solve the problem of asymptotic stabilization of the Brockett integrator subject to time-varying disturbance, as shown in Section 4. By some examples, we verify the main results in Section 5. In Section 6, conclusions are presented.

## 2. Preliminaries

Notations: let  $\mathbb{R}$  denote the set of real numbers,  $\mathbb{R}_+$  the set of nonnegative numbers,  $\mathbb{R}^n$  the  $n$ -dimensional real spaces equipped with the Euclidean norm  $|\cdot|$ , and  $\mathbb{N}, \mathbb{D} \subset \mathbb{R}^n$  the subspaces of  $\mathbb{R}^n$ .  $a \vee b$  and  $a \wedge b$  are the maximum and minimum of  $a$  and  $b$ , respectively. The notation  $A^T$  denotes the transpose of  $A$ .

Consider the nonlinear system given by

$$\begin{cases} \dot{x}(t) = f(t, x(t)), \\ x(0) = x_0, \end{cases} \quad (1)$$

where  $t \geq 0$ ,  $x \in \mathbb{R}^n$  denotes the state vector,  $f(\cdot): \mathbb{R}_+ \times \mathbb{D} \rightarrow \mathbb{R}^n$  is a continuous function with  $f(t, 0) = 0$  for all  $t \geq 0$ . We assume that  $f(t, x)$  satisfies suitable conditions so the solution  $x(t) = x(t, 0, x_0)$  with initial state  $x_0 \in \mathbb{D}$  uniquely exists in forward time for all initial conditions except possibly the origin (see [9]).

*Definition 1* (see [9]). System (1) is said to be FTS if there exist a function  $T: \mathbb{R}^n \rightarrow \mathbb{R}_+$  and an open neighborhood  $\mathbb{N} \subset \mathbb{D}$  such that the following statements hold:

- (i) Finite-time convergence (FTC): for every  $x_0 \in \mathbb{N} \setminus \{0\}$ ,  $x(t) \in \mathbb{N} \setminus \{0\}$  holds for all  $t \in [0, T(x_0))$  and  $x(t) \rightarrow 0$  as  $t \rightarrow T(x_0)^-$
- (ii) Lyapunov stability (LS): for every  $\varepsilon$  ball  $B_\varepsilon$  around the origin, there exists a  $\delta$  ball  $B_\delta$  around the origin

such that, for every  $x_0 \in B_\delta \setminus \{0\}$ ,  $x(t) \in B_\varepsilon$  for all  $t \in [0, T(x_0))$

*Definition 2* (see [23]). For a given set  $\mathcal{O}$  that contains the origin, system (1) is said to be relatively asymptotically stable (RAS) with respect to the set  $\mathcal{O}$ , if for any  $\varepsilon > 0$ , there exists  $\delta > 0$  such that, for all  $x_0 \in \mathcal{O} \cap B_\delta$ ,  $x(t) \in B_\varepsilon$  holds when  $t \geq 0$ ; moreover,  $x(t) \rightarrow 0$  as  $t \rightarrow \infty$ .  $B_\delta$  and  $B_\varepsilon$  are open balls around the origin of radius  $\delta$  and  $\varepsilon$ , respectively.

## 3. Main Results

In this section, we present a generalization of the classical FTS theorem [9]. Given the following definition

$$\dot{V}(t, x(t)) \triangleq \frac{\partial V}{\partial t}(t, x) + \frac{\partial V}{\partial x}(t, x)f(t, x(t)), \quad (2)$$

for a continuously differentiable function  $V(t, x): \mathbb{R}_+ \times \mathbb{R}^n \rightarrow \mathbb{R}_+$ . With a slight stealing concept,  $V(t, x): \mathbb{R}_+ \times \mathbb{R}^n \rightarrow \mathbb{R}_+$  is said to be positive definite and radially unbounded if there exists a positive definite and radially unbounded continuous function  $W(x): \mathbb{R}^n \rightarrow \mathbb{R}_+$  such that  $V(t, x) \geq W(x)$ , for  $t \geq 0, x \in \mathbb{R}^n$ .

**Theorem 1.** Consider system (1), if there exists a positive definite, continuously differentiable function  $V: \mathbb{R}_+ \times \mathbb{R}^n \rightarrow \mathbb{R}_+$ , an integrable function  $c(t): \mathbb{R}_+ \rightarrow \mathbb{R}_+$ , and two real numbers  $\alpha \in (0, 1)$ ,  $\sigma > 0$ , such that the derivative of  $V$  along the solution  $x(t) = x(t, 0, x_0)$  of system (1) satisfies

$$\dot{V}(t, x(t)) \leq -c(t)V^\alpha(t, x(t)), \quad \forall t \geq 0, \quad (3)$$

where  $c(t)$  satisfies

$$\int_0^{+\infty} c(s)ds \triangleq \beta \geq \frac{\sigma^{1-\alpha}}{1-\alpha}. \quad (4)$$

Then, system (1) is locally FTS with respect to  $x_0$  satisfying  $V_0 < \sigma$ , where  $V_0 \triangleq V(0, x_0)$ . The settling-time function  $T: \mathbb{R}^n \rightarrow \mathbb{R}_+$ , depending on the initial state  $x_0$ , is bounded by

$$T(x_0) \leq \inf \left\{ t > 0: \int_0^t c(s)ds = \frac{V_0^{1-\alpha}}{1-\alpha} \right\}. \quad (5)$$

Moreover, when  $\beta = +\infty$  and  $V$  is radially unbounded, system (1) is globally FTS.

*Proof.* For a given  $x_0 \in \mathbb{R}^n \setminus \{0\}$ , let  $x(t)$  be the solution of system (1) through  $(0, x_0)$ . By transforming (3), we obtain

$$\frac{dV}{V^\alpha} \leq -c(t)dt, \quad \forall t \geq 0. \quad (6)$$

Integrating both sides of the abovementioned inequality, it gives

$$\int_{V_0}^{V(t, x(t))} \frac{1}{V^\alpha} dV \leq \int_0^t -c(s)ds. \quad (7)$$

Since  $V$  is a positive definite function, we can obtain

$$0 \leq \frac{V^{1-\alpha}(t, x(t))}{1-\alpha} \leq \frac{V_0^{1-\alpha}}{1-\alpha} - \int_0^t c(s) ds. \quad (8)$$

When  $\beta < +\infty$  and  $V_0 < \sigma$ , it follows from (4) that there exists a time point  $t^* > 0$  satisfying  $\int_0^{t^*} c(s) ds < \sigma^{1-\alpha}/(1-\alpha)$ , such that  $V_0^{1-\alpha}/(1-\alpha) - \int_0^{t^*} c(s) ds = 0$ . That is to say  $V(t^*, x(t^*)) = 0$ , from which the settling time  $T(x_0)$  can be estimated, namely, (5). When  $t \geq T(x_0)$ ,  $\dot{V}(t, x(t)) \leq 0$ , it follows from [27] that the solution of system (1) through  $(T(x_0), 0)$  is unique in forward time. Therefore,  $V(t, x(t)) \equiv 0$ , for  $t \geq T(x_0)$ , which means system (1) is locally *FTC* with respect to  $x_0$  satisfying  $V_0 < \sigma$ . Noting from (3), it is easy to obtain that system (1) is *LS*. Combining these two aspects, system (1) is locally *FTS* with respect to  $x_0$  satisfying  $V_0 < \sigma$ .

When  $\beta = +\infty$  and  $V$  is radially unbounded, no matter what initial value  $x_0$  it is, there always exists a time point  $t^{**} > 0$ , such that  $V_0^{1-\alpha}/(1-\alpha) - \int_0^{t^{**}} c(s) ds = 0$ , that is,  $V(t^{**}, x(t^{**})) = 0$ . Through a similar procedure, we conclude that system (1) is globally *FTS*.  $\square$

*Remark 1.* The classical *FTS* theorem mentioned in [9] has been widely used in many fields, such as finite-time synchronization of complex networks, finite-time attitude stabilization for spacecraft, and terminal sliding mode method of nonlinear systems, see [10, 23]. However, these theoretical results are applied under the framework of time invariant, that is,  $c(t) \equiv c > 0$ . When  $\inf\{c(t): t \geq 0\} = 0$ , the classical *FTS* theorem is unapplicable. However, in Theorem 1, we can still achieve the *FTS* of system (1), as long as (3) and (4) hold. This assertion can be verified in Section 5.

#### 4. Applications

Consider a class of systems described by equations of the form

$$\dot{x} = G(x)u, \quad (9)$$

where  $x \in \mathbb{R}^n$ ,  $u \in \mathbb{R}^m$ ,  $m < n$ , and  $G(x)$  is a matrix of proper dimension. It has received considerable attention for the asymptotic stabilization of such systems during the past several decades. The reason for such an interest lies in the fact that system (9) cannot be asymptotically stabilized by any continuous differentiable and state feedback control laws (see [22]). The Brockett integrator, as a special case of system (9), has plenty of theoretical results with time-invariant form. However, there are few theoretical results considering the form of time-varying systems. In this paper, we study the Brockett integrator subject to time-varying disturbance, that is,

$$\begin{cases} \dot{x}_1(t) = u_1, \\ \dot{x}_2(t) = u_2, \\ \dot{x}_3(t) = w_1(t)x_1u_2 - w_2(t)x_2u_1, \end{cases} \quad (10)$$

where  $t \geq 0$ ,  $x_i(t): \mathbb{R}_+ \rightarrow \mathbb{R}$ ,  $i = 1, 2, 3$ , denotes the state component,  $u_j(t): \mathbb{R}_+ \rightarrow \mathbb{R}$ ,  $j = 1, 2$ , denotes the control input,  $w_j(t): \mathbb{R}_+ \rightarrow \mathbb{R}$ ,  $j = 1, 2$ , is continuous function

denoting the disturbance term. For any integrable function  $\rho(t): \mathbb{R}_+ \rightarrow \mathbb{R}$ , we introduce a set  $\mathcal{F}$  as follows:

$$\mathcal{F} = \left\{ \rho(t) \in \mathbb{R}: \int_0^t \rho(s) ds \rightarrow +\infty \text{ as } t \rightarrow +\infty \right\}. \quad (11)$$

*Assumption 1.* There exists a continuous function  $\eta(t): \mathbb{R}_+ \rightarrow \mathbb{R}$  such that  $\eta(t)w_1(t) \geq 0$ , for  $t \geq 0$ , and the following inequality holds:

$$\int_0^{+\infty} \eta(s)w_1(s) ds = +\infty. \quad (12)$$

*Assumption 2.* There exist two functions  $\rho_1(t), \rho_2(t) \in F$  such that

$$w_1(t)\rho_2(t) = w_2(t)\rho_1(t). \quad (13)$$

**Theorem 2.** Assume that Assumptions 1 and 2 hold, then the solution of system (10) converges to the origin and system (10) is *RAS* with respect to the set  $\mathcal{O} \triangleq \{x = (x_1, x_2, x_3)^T \in \mathbb{R}^3: x_3 = 0, x_1 \neq 0\}$  under the control input:

$$U = \begin{pmatrix} u_1 \\ u_2 \end{pmatrix} = \begin{pmatrix} -\rho_1(t)x_1 \\ \frac{-\eta(t)x_3^{1/3}}{x_1} - \rho_2(t)x_2 \end{pmatrix}. \quad (14)$$

*Proof.* We firstly show the attractivity of system (10). If  $x_1(0) \neq 0$ , then it follows from (14) that

$$\dot{x}_1(t) = -\rho_1(t)x_1, \quad (15)$$

which implies

$$x_1(t) = x_1(0) \exp \int_0^t -\rho_1(s) ds. \quad (16)$$

Note that  $\rho_1(t) \in F$ ; then, it is easy to see that

$$x_1(t) \rightarrow 0 \text{ as } t \rightarrow +\infty, \quad (17)$$

which shows that  $x_1(t)$  asymptotically tends to zero.

In addition, the third state component of system (10) becomes  $\dot{x}_3(t) = -\eta(t)w_1(t)x_3^{1/3}$  with control input  $u_2$ , which gives that  $x_3(t)$  is *FTS* combining (12) and Theorem 1. Moreover, the settling time  $T$  can be estimated by (5). For the second state component of system (10), when  $t > T$ , it holds  $x_3^{1/3}/x_1 \equiv 0$ ; then, by (13), the derivative of  $x_2$  becomes  $-\rho_2(t)x_2$ . Similar to the above argument, we could conclude that the origin of  $x_2(t)$  asymptotically tends to zero. For the case that  $x_1(0) = 0$ , we can apply any open loop control to steer the system to a nonzero value of  $x_1$ . This completes the proof of attractivity.

Secondly, we show the relative stability of system (10). When  $t > T$ , system (10) is transformed as

$$\begin{aligned}\dot{x}_1(t) &= -\rho_1(t)x_1, \\ \dot{x}_2(t) &= -\rho_2(t)x_2, \\ x_3(t) &= 0,\end{aligned}\quad (18)$$

which implies that  $x(t)$  enters the set  $\mathcal{O}$  from this moment, and  $x_1(t)$  and  $x_2(t)$  will converge to origin. Therefore, when  $x(0) \in \mathcal{O}$ ,  $x_3(t) \equiv 0$ ,  $x_1(t), x_2(t) \rightarrow 0$  as  $t \rightarrow \infty$ , then one can obtain that system (10) is RAS with respect to the set  $\mathcal{O}$ . This completes the proof.

*Remark 2.* Theorem 2 provides a method for the problem of asymptotic stabilization of the Brockett integrator subject to time-varying disturbance. A relatively asymptotical stabilization is achieved by weakening the stability conditions. Besides, in the process of designing controller  $U$ , we apply a switched finite-time controller design methodology. In fact, it is also a discontinuous control. Worth mentioning that it is of vital importance to design functions  $\eta(t), \rho_1(t)$ , and  $\rho_2(t)$ , such that the FTS of  $x_3(t)$  is achieved directly. In Section 5, we will show an example to illustrate our conclusion.

**Corollary 1.** *Under conditions in Theorem 1, when  $w_1(t) = w_2(t)$ , we just need  $\rho_1(t) = \rho_2(t) = p$ , where  $p$  is a positive constant. Then, the solution of system (10) converges to the origin and system (10) is RAS with respect to the set  $\mathcal{O} \triangleq \{x = (x_1, x_2, x_3)^T \in \mathbb{R}^3: x_3 = 0, x_1 \neq 0\}$  under the control input:*

$$U = \begin{pmatrix} u_1 \\ u_2 \end{pmatrix} = \begin{pmatrix} -px_1 \\ \frac{-\eta(t)x_3^{1/3}}{x_1} - px_2 \end{pmatrix}. \quad (19)$$

*Remark 3.* It should be pointed out that, in Theorem 2, the selection of set  $\mathcal{O}$  and control input  $U$  is not unique. In Theorem 2, we only get the FTS of one state component. In order to achieve better performance, we can further consider multiple components to achieve the FTS for the Brockett-like integrator, which is the result we will give in Theorem 3.

Consider the following Brockett-like integrator subject to time-varying disturbance:

$$\begin{cases} \dot{x}_1(t) = u_1, \\ \dot{x}_2(t) = u_2, \\ \dot{x}_3(t) = w_1(t)x_1^k u_2 - w_2(t)x_2 u_1, \end{cases} \quad (20)$$

where  $t \geq 0, x_i(t): \mathbb{R}_+ \rightarrow \mathbb{R}, i = 1, 2, 3$ , denotes the state component,  $u_j(t): \mathbb{R}_+ \rightarrow \mathbb{R}, j = 1, 2$ , denotes the control input,  $w_j(t): \mathbb{R}_+ \rightarrow \mathbb{R}, j = 1, 2$ , is continuous function denoting the disturbance term,  $k = a/b, a < b$ , and  $a$  and  $b$  are positive odd numbers.

*Assumption 3.* There exists a continuous function  $\mu(t): \mathbb{R}_+ \rightarrow \mathbb{R}$  such that  $\mu(t)w_1(t) \geq 0$ , for  $t \geq 0$ , and the following inequality holds:

$$\int_0^{+\infty} \mu(s)w_1(s)ds = +\infty. \quad (21)$$

*Assumption 4.* There exist two functions  $\varphi_1(t), \varphi_2(t) \in \mathcal{F}$  such that

$$w_1(t)\varphi_2(t) = w_2(t)\varphi_1(t). \quad (22)$$

*Assumption 5.* There exist two functions  $T(x_1) = \inf\{t > 0, x_1 \neq 0: \int_0^t \varphi_1(s)ds = (x_1^{1-k}/(1-k))\}$ ,  $T(x_3) = \inf\{t > 0: \int_0^t \mu(s)w_1(s)ds = ((x_3^{2/3})/2/3)\}$  such that the set  $\mathcal{X} \triangleq \{x = (x_1, x_2, x_3)^T \in \mathbb{R}^3: T(x_3) < T(x_1)\}$  is not empty.

**Theorem 3.** *Assume that Assumptions 3, 4, and 5 hold; then, the solution of system (20) converges to the origin, and system (20) is RAS with respect to the set  $\mathcal{X} \triangleq \{x = (x_1, x_2, x_3)^T \in \mathbb{R}^3: \mathcal{X} \cup \{(0, 0, 0)^T\}$  under the control input:*

$$U = \begin{pmatrix} u_1 \\ u_2 \end{pmatrix} = \begin{pmatrix} -\varphi_1(t)x_1^k \\ \frac{-\mu(t)x_3^{1/3}}{x_1^k} - \varphi_2(t)x_2 \end{pmatrix}. \quad (23)$$

*Proof.* If  $x_1(0) \neq 0$ , it follows from (23) that

$$\begin{cases} \dot{x}_1(t) = -\varphi_1(t)x_1^k, \\ \dot{x}_2(t) = \frac{-\mu(t)x_3^{1/3}}{x_1^k} - \varphi_2(t)x_2, \\ \dot{x}_3(t) = -\mu(t)w_1(t)x_3^{1/3}. \end{cases} \quad (24)$$

About the first state component of system (20), we notice that  $\varphi_1(t) \in \mathcal{F}$  and  $k = a/b, a < b$ , and  $a$  and  $b$  are positive odd numbers, so obtained from Theorem 1, the first state component of system (20) is FTS. Meanwhile, combining (21), (22), and Theorem 1, the third state components of system (20) is FTS. Hence, for initial value  $x_1(0)$  and  $x_3(0)$ , the settling time can be established, that is,  $T(x_1(0))$  and  $T(x_3(0))$ . Under the premise of Assumption 5, when  $t > T(x_3(0))$ , system (20) is transformed as

$$\begin{aligned}\dot{x}_1(t) &= -\varphi_1(t)x_1^k, \\ \dot{x}_2(t) &= -\varphi_2(t)x_2, \\ x_3(t) &= 0.\end{aligned}\quad (25)$$

Similar to the proof process of Theorem 2, we can obtain that system (20) is RAS with respect to the set  $\mathcal{X}$ . For the case that  $x_1(0) = 0$ , we can apply any open loop control to steer the system to a nonzero value of  $x_1$ . This completes the proof.

## 5. Numerical Simulations

In this section, we will demonstrate the effectiveness of the proposed results for the above applications through the following simulation examples.

*Example 1.* Consider the following 2D time-varying system:

$$\begin{cases} \dot{x}_1(t) = (\sin t - 1)x_1^{1/3} + \sin t x_2^2 x_1, \\ \dot{x}_2(t) = (\cos t - 1)x_2^{1/3} - x_1^2 x_2, \end{cases} \quad (26)$$

where  $t \geq 0$ . Consider the Lyapunov function  $V(x) = x_1^2 + x_2^2$ , and the derivative along the trajectory of the system (26) is

$$\begin{aligned} \dot{V}(t) &= 2x_1((\sin t - 1)x_1^{1/3} + \sin t x_2^2 x_1) \\ &\quad + 2x_2((\cos t - 1)x_2^{1/3} - x_1^2 x_2) \\ &= 2(\sin t - 1)x_1^{4/3} + 2(\cos t - 1)x_2^{4/3} \\ &\quad + 2(\sin t - 1)x_1^2 x_2^2 \\ &\leq 2(\sin t - 1)x_1^{4/3} + 2(\cos t - 1)x_2^{4/3} \\ &\leq 2((\sin t - 1) \vee (\cos t - 1))(x_1^{4/3} + x_2^{4/3}) \\ &\leq -c(t)V^{2/3}(t), \end{aligned} \quad (27)$$

where  $c(t) = 2 - 2(\sin t \vee \cos t)$  and  $c(t) \geq 0$  on  $\mathbb{R}_+$ . According to Lyapunov's stability theory in [28], system (26) is *LS*. It can be calculated that the lower bound of  $c(t)$  is 0, so the classical *FTS* theorem in [9] is unapplicable. On the contrary, note that  $c(t)$  satisfies (4) with  $\beta = +\infty$ , and it follows from Theorem 1 that system (26) is globally *FTS* and the settling time can be estimated as  $T(x_0) \leq 4.51$ . Figure 1 illustrates the state trajectories of system (26).

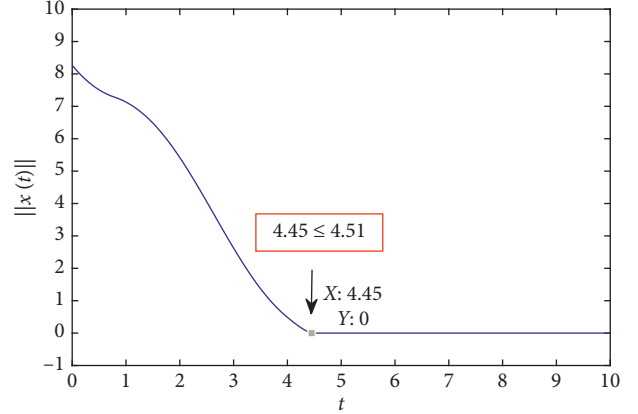


FIGURE 1: Simulation results of states for system (26).

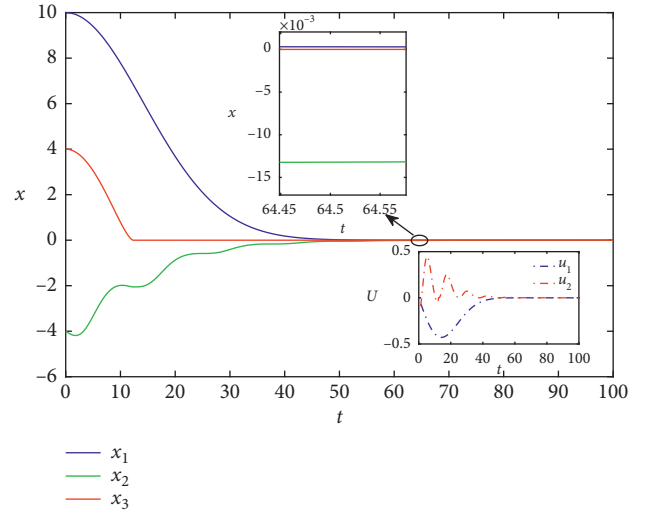


FIGURE 2: Simulation results of states and control inputs for system (10).

*Example 2.* Consider system (10) with  $w_1(t) = t/20$ ,  $w_2(t) = 1 - \cos(t/2)$ ,  $\eta(t) = 1$ ,  $\rho_1(t) = t/200$ , and  $\rho_2(t) = 1/10 - \cos(t/2)/10$ . It is obvious that  $w_1(t), w_2(t) \in \mathcal{F}$ ,  $\eta(t)$  is a continuous function, and  $w_1(t)\rho_2(t) = w_2(t)\rho_1(t)$ . Hence, we can calculate that  $\int_0^{+\infty} \eta(s)w_1(s)ds = +\infty$ . It follows from Theorem 2 that system (10) is *RAS* with respect to the set  $\mathcal{O} \triangleq \{x = (x_1, x_2, x_3)^T \in \mathbb{R}^3: x_3 = 0, x_1 \neq 0\}$ , and the control input could be described by

$$U = \begin{pmatrix} u_1 \\ u_2 \end{pmatrix} = \begin{pmatrix} -\left(\frac{t}{200}\right)x_1 \\ -\frac{x_3^{1/3}}{x_1} - \left(\frac{1}{10} - \frac{\cos(t/2)}{10}\right)x_2 \end{pmatrix}. \quad (28)$$

It is worth pointing out that the classic *FTS* theorem in [9] is not applicable. This is due to the existence of the disturbance term, and the control input will reach infinity within a certain time, which is impractical. The numerical simulations for system (10) are follows.

In Figure 2, it can be clearly seen that  $x_3(t)$  firstly converges to zero, then  $x_1(t)$  and  $x_2(t)$  converge to zero. The control input  $u_1$  and  $u_2$  change over time and turn into 0 when  $x(t)$  converges to zero. In Figure 3, the state vector  $x(t)$  enters the set  $\mathcal{O}$  and finally reaches the origin in finite-time. All of these results are corresponding to the conclusion of Theorem 2, which illustrates the validity of the Theorem 2.

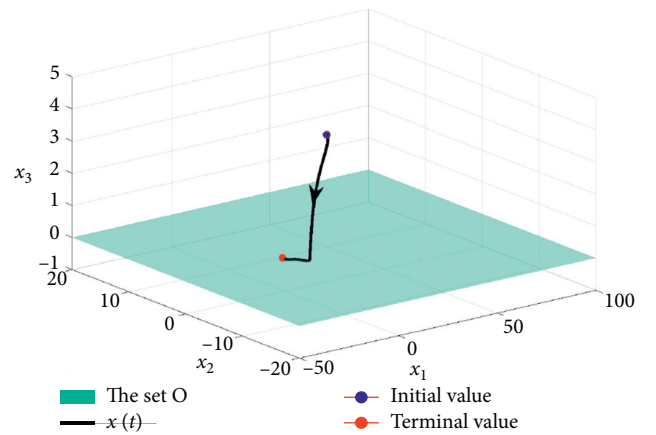


FIGURE 3: Simulation results of states for system (10).

*Example 3.* For convenience, the same parameters as in Example 2 are used. Consider system (2) with  $w_1(t) = t/20$ ,  $w_2(t) = 1 - \cos(t/2)$ ,  $\mu(t) = 1$ ,  $\varphi_1(t) = t/200$ ,



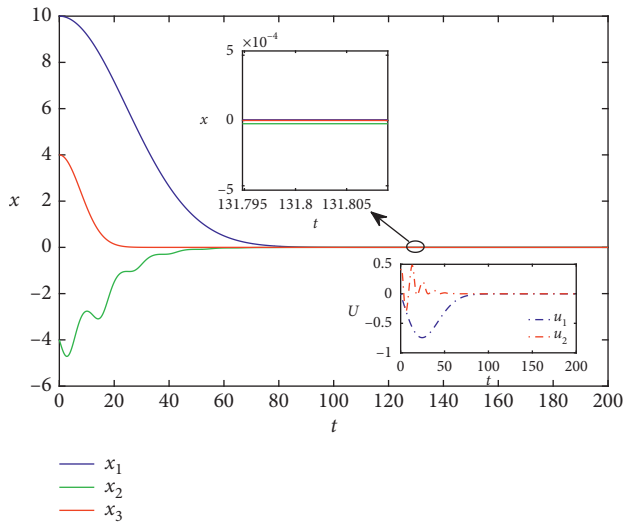


FIGURE 4: Simulation results of states and control inputs for system (20).

$\varphi_2(t) = 1/10, -\cos(t/2)/10$ , and  $k = 1/3$ . It is not difficult to verify that the set  $\mathcal{X}$  is not empty. Therefore, following from (21), (22), and Theorem 3, system (20) is RAS with respect to the set  $\mathcal{X}$  and the control input could be described by

$$U = \begin{pmatrix} u_1 \\ u_2 \end{pmatrix} = \begin{pmatrix} -\left(\frac{t}{200}\right)x_1^{1/3} \\ \frac{-x_3^{1/3}}{x_1^{1/3}} - \left(\frac{1}{10} - \frac{\cos(t/2)}{10}\right)x_2 \end{pmatrix}. \quad (29)$$

It can be seen from Figure 4 that the first and third state components of the system (20) is *F**T**S*, and the second state component of system (20) asymptotically tends to zero, which shows the validity of Theorem 3.

## 6. Conclusion

The problem of *F**T**S* for time-varying nonlinear systems is investigated in this paper, where the results of global *F**T**S* and local *F**T**S* are proposed, respectively. As an application, the stabilization problem of the Brockett integrator subjected to time-varying disturbance is studied. By the switched finite-time controller design methodology, we achieve the *RAS* for the Brockett integrator subject to time-varying disturbance. Further research topics would be considered to extend the main results of this paper to other more complex problems, such as the finite-time stabilization for wheeled mobile robot subject to time-varying disturbance and the *F**T**S* theorem for time-varying nonlinear systems in the sense of Lyapunov.

## Data Availability

No data were used to support this study.

## Conflicts of Interest

The author declares that there are no conflicts of interest.

## Acknowledgments

This work was supported by the National Natural Science Foundation of China (61673247) and Research Fund for Distinguished Young Scholars and Excellent Young Scholars of Shandong Province (JQ201719).

## References

- [1] B. Zhou, "On asymptotic stability of linear time-varying systems," *Automatica*, vol. 68, pp. 266–276, 2016.
- [2] J. Suo and J. Sun, "Asymptotic stability of differential systems with impulsive effects suffered by logic choice," *Automatica*, vol. 51, pp. 302–307, 2015.
- [3] X. Li and J. Wu, "Stability of nonlinear differential systems with state-dependent delayed impulses," *Automatica*, vol. 64, pp. 63–69, 2016.
- [4] C. Aouiti, I. Ben Gharbia, J. Cao, M. Salah M'hamdi, and A. Alsaedi, "Existence and global exponential stability of pseudo almost periodic solution for neutral delay BAM neural networks with time-varying delay in leakage terms," *Chaos, Solitons & Fractals*, vol. 107, pp. 111–127, 2018.
- [5] R. Rakkiyappan, G. Velmurugan, and J. Cao, "Stability analysis of fractional-order complex-valued neural networks with time delays," *Chaos, Solitons & Fractals*, vol. 78, pp. 297–316, 2015.
- [6] Y. Li and X. Meng, "Existence and global exponential stability of pseudo almost periodic solutions for neutral type quaternion-valued neural networks with delays in the leakage term on time scales," *Complexity*, vol. 2017, Article ID 9878369, 15 pages, 2017.
- [7] R. Saravanakumar, M. S. Ali, C. K. Ahn, H. R. Karimi, and P. Shi, "Stability of Markovian jump generalized neural networks with interval time-varying delays," *IEEE Transactions on Neural Networks and Learning Systems*, vol. 28, no. 8, pp. 1840–1850, 2016.
- [8] V. T. Haimo, "Finite time controllers," *SIAM Journal on Control and Optimization*, vol. 24, no. 4, pp. 760–770, 1986.
- [9] S. P. Bhat and D. S. Bernstein, "Finite-time stability of continuous autonomous systems," *SIAM Journal on Control and Optimization*, vol. 38, no. 3, pp. 751–766, 2000.
- [10] S. P. Bhat and D. S. Bernstein, "Continuous finite-time stabilization of the translational and rotational double integrators," *IEEE Transactions on Automatic Control*, vol. 43, no. 5, pp. 678–682, 1998.
- [11] X. Yang, J. Cao, C. Xu, and J. Feng, "Finite-time stabilization of switched dynamical networks with quantized couplings via quantized controller," *Science China Technological Sciences*, vol. 61, no. 2, pp. 299–308, 2018.
- [12] E. Moulay and W. Perruquetti, "Finite time stability and stabilization of a class of continuous systems," *Journal of Mathematical Analysis and Applications*, vol. 323, no. 2, pp. 1430–1443, 2006.
- [13] E. Moulay, M. Dambrine, N. Yeganefar, and W. Perruquetti, "Finite-time stability and stabilization of time-delay systems," *Systems & Control Letters*, vol. 57, no. 7, pp. 561–566, 2008.
- [14] A. Polyakov, "Nonlinear feedback design for fixed-time stabilization of linear control systems," *IEEE Transactions on Automatic Control*, vol. 57, no. 8, pp. 2106–2110, 2012.
- [15] J. Hu, G. Sui, X. Lv, and X. Li, "Fixed-time control of delayed neural networks with impulsive perturbations," *Nonlinear Analysis: Modelling and Control*, vol. 23, no. 6, pp. 904–920, 2018.

- [16] W. M. Haddad, S. G. Nersesov, and L. Du, "Finite-time stability for time-varying nonlinear dynamical systems," in *Proceedings of the American Control Conference*, IEEE, Seattle, WC, USA, pp. 4135–4139, 2008.
- [17] E. Moulay and W. Perruquetti, "Finite time stability conditions for non-autonomous continuous systems," *International Journal of Control*, vol. 81, no. 5, pp. 797–803, 2008.
- [18] F. Amato, R. Ambrosino, M. Ariola, C. Cosentino, and G. D. Tommasi, *Finite-time Stability and Control*, Springer-Verlag, London, UK, 2014.
- [19] M. S. Ali, S. Saravanan, and J. Cao, "Finite-time boundedness, L2-gain analysis and control of Markovian jump switched neural networks with additive time-varying delays," *Nonlinear Analysis: Hybrid Systems*, vol. 23, pp. 27–43, 2017.
- [20] X. Yang, X. Li, Q. Xi et al., "Review of stability and stabilization for impulsive delayed systems," *Mathematical Biosciences & Engineering*, vol. 15, no. 6, pp. 1495–1515, 2018.
- [21] R. W. Brockett, "Asymptotic stability and feedback stabilization," *Differential Geometric Control Theory*, vol. 27, no. 1, pp. 181–191, 1983.
- [22] A. Astolfi, "Discontinuous control of the Brockett integrator," in *Proceedings of the IEEE Conference on Decision & Control*, vol. 4, no. 1, pp. 49–63, IEEE, San Diego, CA, USA, December 1997.
- [23] R. N. Banavar and V. Sankaranarayanan, *Switched Finite Time Control of a Class of Underactuated Systems*, Springer-Verlag, Berlin, Germany, 2006.
- [24] F. Rehman, "Steering control of nonholonomic systems with drift: the extended nonholonomic double integrator example," *Nonlinear Analysis-Theory Methods & Applications*, vol. 62, no. 8, pp. 1498–1515, 2005.
- [25] F. Rehman and N. Ahmed, "Feedback stabilization of non-holonomic integrator (Brockett's system)," *International Journal of Modelling and Simulation*, vol. 26, no. 3, pp. 244–250, 2006.
- [26] Y. Chihchen, "Time-varying control for exponential stabilization of the Brockett integrator," *IET Control Theory & Applications*, vol. 11, no. 12, pp. 1976–1982, 2017.
- [27] T. Yoshizawa, *Stability Theory by Liapunov's Second Method*, The Mathematical Society of Japan, Tokyo, Japan, 1966.
- [28] X. Liao, L. Wang, and P. Yu, *Stability of Dynamical Systems*, Elsevier, Amsterdam, Netherlands, 2007.

## Research Article

# Joint Character-Level Convolutional and Generative Adversarial Networks for Text Classification

Tianshi Wang <sup>1</sup>, Li Liu <sup>1,2</sup>, Huaxiang Zhang <sup>1,2</sup>, Long Zhang <sup>1</sup> and Xiuxiu Chen <sup>1</sup>

<sup>1</sup>School of Information Science and Engineering, Shandong Normal University, Jinan 250014, China

<sup>2</sup>Institute of Data Science and Technology, Shandong Normal University, Jinan 250014, Shandong, China

Correspondence should be addressed to Li Liu; [liuli\\_790209@163.com](mailto:liuli_790209@163.com)

Received 23 March 2020; Accepted 15 April 2020; Published 30 April 2020

Academic Editor: Jianquan Lu

Copyright © 2020 Tianshi Wang et al. This is an open access article distributed under the Creative Commons Attribution License, which permits unrestricted use, distribution, and reproduction in any medium, provided the original work is properly cited.

With the continuous renewal of text classification rules, text classifiers need more powerful generalization ability to process the datasets with new text categories or small training samples. In this paper, we propose a text classification framework under insufficient training sample conditions. In the framework, we first quantify the texts by a character-level convolutional neural network and input the textual features into an adversarial network and a classifier, respectively. Then, we use the real textual features to train a generator and a discriminator so as to make the distribution of generated data consistent with that of real data. Finally, the classifier is cooperatively trained by real data and generated data. Extensive experimental validation on four public datasets demonstrates that our method significantly performs better than the comparative methods.

## 1. Introduction

Machine-learning models have achieved remarkable results in computer vision (CV), automatic speech recognition, and neural language processing (NLP). With the development of artificial neural networks, text classification becomes one of the most intriguing fields of NLP [1, 2]. Text classification refers to the division of texts in the corpus into predefined categories based on its contents and other attributes. It is widely used in many applications [3–9], such as spam filtering, news categorization, sentiment analysis, and digital library.

As typical supervised learning (SL), text classification requires abundant manually labeled samples for training. However, manually adding ground truth to vast amounts of texts is difficult to achieve in practical application, so the number of labeled samples is not enough to meet the requirements. For small training samples, the insufficient depiction leads to the poor generalization ability of classifiers obtained from learning.

To improve the generalization ability of classifiers, the feasible solution is to improve learning algorithms or increase training samples. The method worth mentioning is

support vector machines (SVM), which improves the generalization ability on unknown samples by learning the hyperplane of the maximum interval between different categories. SVM alleviates the problem of small samples to some extent, but the high time complexity leads to the limitation of engineering applications, especially online information processing. Besides, the existence of massive unlabeled samples has gradually drawn the attention of scholars to semisupervised learning (SSL). Most of the semisupervised classification methods train the objective classifier through an initial classifier until it reaches the convergence condition. However, such methods have high-computational complexity and may bring about large-scale sample problems.

Compared with the computationally expensive SSL, generative adversarial nets (GAN) proposed by Goodfellow et al. [10] provides an effective method for generating new data. In this paper, we employ GAN to generate the textual samples according to the data distribution of the input samples and label the generated samples. Furthermore, we use Char-level CNN to extract the text semantics and utilize the textual generative network to increase the training samples. To summarize, our contributions are listed as follows:

- (1) The novel structure of Char-level CNN is designed for small-scale datasets to generate textual features. By optimizing the configuration of the convolutional and pooling layers, the output comprehensively inherits the text semantics. Besides, the dense network is designed deeper because the generated data reduces the risk of its overfitting.
- (2) The data augmentation module based on high-level semantic is proposed. The text semantics are quantified and directly input into the network as real data to obtain various textual features. The module not only avoids the feature extraction of the generated texts and saves the computing resources but also describes the overall distribution characteristics of data to make the classifier perform better on small-scale datasets.

The rest of this paper is structured as follows. Section 2 summarizes the related work of textual feature construction, text generation, and semisupervised learning. Section 3 details our model to solve the small-scale datasets text classification problem. Section 4 presents the experimental setting and results analysis. Section 5 concludes our whole work and gives further research direction.

## 2. Related Work

Compared with other media streams, the most special aspect of texts is that semantic information is difficult to express. For subtasks in NLP, how to quantify abstract semantic information is particularly critical. Therefore, the final performance of text classification is jointly affected by the classification models and feature representation methods [11–13].

The mainstream representation methods for text classification can be roughly divided into three categories. Traditional textual features are mainly generated through methods such as bag of words (BOW) and n-gram. Both are usually combined with term frequency-inverse document frequency (TF-IDF) and other element features as textual features. However, the momentous drawback of these methods is that they ignore the context and order of words. The second language model is based on attention mechanisms, commonly known as hierarchical attention and self-attention, which extracts textual features by scoring input words or sentences differentially. In the third language model, text can be represented by sequence or structured models through the introduction of artificial neural networks. In addition to the above three language models, some pretraining models, such as XLNet and BERT, have also been proposed for NLP. However, these pretrained models require large amounts of labeled textual data and are not suitable for new categories and small samples of textual data.

In the text representation methods based on the sequence or structured models, Bengio et al. [14] first tried to use neural networks to produce dense, low-dimensional vectors for words. Mikolov [15] proposed a language model, called Word2Vec, which can transform each word into vector form according to the context. The model can take the

representative words as the representation of text by working with clustering algorithms. Besides, textual features can be obtained by simply combining the word embeddings to replace sentences or texts, and the linear model FastText [16] is widely used in text classification in this way. Kim [17] applied the convolutional neural network to the classification process and obtained the textual features by processing the matrix formed by word embedding. Kaichbrenner et al. [18] proposed a convolutional architecture and dubbed the dynamic convolutional neural network (DCNN) for sentence modeling. Zhang et al. [19] proposed the use of convolutional networks for text classification at the character level, but their network structures only work well on large-scale datasets. Then, for the structural configuration of convolutional neural networks, Le et al. [20] studied the importance of depth in convolutional models. At the same time, the recurrent neural networks are also applied to the language models due to their memorability and Turing completeness. Chung et al. [21] compared different types of recurrent units, especially gating mechanisms such as long short-term memory (LSTM) and gated recurrent unit (GRU). Zhu et al. [22] attempted to build structured representations using prespecified parsing trees. Recently, Zhang et al. [23] proposed a reinforcement learning (RL) method to get structured sentence vectors. Note that before the abovementioned methods were proposed, some traditional machine-learning algorithms were widely used in text classification. For example, k-nearest neighbor (KNN) for classification by measuring the distance between different features, decision tree combining information entropy and tree structure, and Naive Bayes based on Bayesian theory and characteristic conditional independence hypothesis. However, it is proved that the performance of machine-learning algorithms is lower than that of the methods based on deep learning in the text classification task.

To solve the problem of insufficient training samples, many methods of data augmentation and semisupervised learning can be used to improve the performance of classifiers. Wei and Zou [24] presented an easy data augmentation (EDA) technique for boosting performance on text classification tasks. Although EDA reduces overfitting when training on smaller datasets, the improvement is at times marginal. Wang and Wu [25] proposed a framework that combines variational autoencoder (VAE) and neural networks to deal with text classification and generation tasks. GAN [10, 26] was firstly proposed for continuous data (image generation, inpainting, style transfer, etc.) and has shown excellent performance in computer vision (CV). Yu et al. [27] extended GAN to discrete and sequential data to alleviate the above deficiency. Since then, various text generation methods have been proposed via GAN. Xu et al. [28] proposed a text generation model called DP-GAN, which can encourage the generator to produce diverse and informative text. Li et al. [29] combined reinforcement learning, GAN, and recurrent neural networks to build a category sentence generative adversarial network. Miyato et al. [30] extended adversarial and virtual adversarial training to the text domain. Ahamad [31] also tried to solve the above problem by using Skip-Thought sentence

embeddings in conjunction with GANs. Although the methods utilize text generation and feature reconstruction to alleviate the problem of small-scale datasets, the classification performance is still difficult to further improve due to the large work of feature engineering and the trouble of textual feature extraction.

### 3. Methodology

In the section, the character-level convolutional and generative adversarial networks (CCNN-GAN) are utilized to set up a novel hybrid text classification framework in Figure 1. In contrast to the implementation of continuous data, the textual data is modelled by convolutional networks and character quantization in our model. Char-level CNN embeds the texts in the corpus into fixed-length features, and then the features are input into the generative adversarial network (GAN) and backpropagation network (BP network), respectively. The generated data not only enriches the textual features but also effectively solves the problems of insufficient samples and single information when dealing with small-scale datasets. After that the real samples and generated samples from GAN are mixed into a BP network for training. The design is modular, and the text information is transmitted between modules in the form of processed features.

**3.1. Text Quantization Module.** The acceptable encoding of Char-level CNN includes alphabetic encoding, utf-8 encoding, and pretrained character embedding vector. Since the proposed model is mainly used in the English-dominated alphabetic attachment language, alphabetic encoding is applied to the text quantization process. In the embedding layer, features of encoded characters are used as input. An alphabet of size  $\alpha$  is stipulated; then, an embedded dictionary is created and an embedding matrix is formed based on the alphabet. Null character and characters that do not exist in the alphabet are replaced by an all-zero vector. The quantization length of the character feature is set to  $\beta$ . Assume [19] that  $\beta$  characters in the text can reflect the content of the text and the part that exceeds length  $\beta$  is ignored.

The foundational alphabet ( $\alpha = 45$ ) and elaborate alphabet ( $\alpha = 70 + \alpha_0$ ) are stipulated, where  $\alpha_0$  is the length of the auxiliary characters, and the details are shown in Table 1. The foundational alphabet used in the proposed model consists of 45 characters which are 36 English letters and Arabic numerals, 8 other characters, and the null character. The alphabet is applicable to most documents. For the corpus with high symbol content, the foundational alphabet is supplemented by the elaborate alphabet. The elaborate alphabet consists of 25 symbol characters and auxiliary characters of varying lengths. Char-level CNN consists of 8 convolution layers, 3 pooling layers, and 3/4/5 fully connected layers. The configuration of the convolutional neural network is shown in Table 2 and Figure 2.

The classifier that is composed of fully connected layers is discussed in detail in Section 3.3. The Char-level CNN is

constructed to compute 1D convolution and the weights are initialized using Gaussian distribution. The mean and standard deviation to initialize the model is (0, 0.05). The pooling layers are also applied between the convolutional layers for increasing the area covered with the next receptive fields.

In addition, a rectified linear unit (ReLU) is taken as the activation function in the classifier, and local response normalization (LRN) [32] is added behind each pooling layer. The LRN imitates the biological neural system layer of lateral inhibition mechanism and improves the generalization ability of the model. The function is as follows:

$$L^i = \frac{P^i}{\left(k + a \sum_{j=\max(0,i-n/2)}^{\min(N-1,i+n/2)} (P_j)^2\right)^b}, \quad (1)$$

where  $P$  is the tensor obtained after pooling,  $i$  and  $j$  represent the  $i$ th and  $j$ th kernel,  $k$ ,  $n$ ,  $a$ , and  $b$  are hyperparameters, and  $N$  is the total number of kernels.

**3.2. Data Augmentation Module.** Different from the typical RL setting, the data augmentation module enriches the predetermined corpus at the semantic level. Specifically, the module is an adversarial network, in which the generator can generate directly many textual features with the same distribution of the processed real-world texts and the discriminator takes the convolutional textual data as real data. Thus, given the processed textual features as input, the adversarial network can generate various generated features that contain diverse and informative text semantics.

To optimize the performance of the overall framework, the data augmentation module is simplified. The output of the module is not in the form of sentences or documents but in the form of textual features that contain semantic information. Based on the abovementioned ideas, the adversarial network no longer needs to connect with the structure that converts textual features into sentences or documents. During the network training, the processed features and its category are all input into the adversarial network so that it can output textual features that belong to each category.

More formally, the input data  $X_{1:m} = \{X_1, X_2, X_3, \dots, X_i, \dots, X_m\}$  of  $m$  categories comes from the processed corpus  $\Gamma$ , and the high-level textual features is denoted as  $X_i = x_{i,1:n} = \{x_{i,1}, x_{i,2}, x_{i,3}, \dots, x_{i,i}, \dots, x_{i,n}\}$ , where  $x_{i,j}$  refers to the  $j$ th textual feature of category  $i$ . The generative network outputs multiple categories of labeled textual features  $X_{1:m}^* = \{X_1^*, X_2^*, X_3^*, \dots, X_i^*, \dots, X_m^*\}$ , where  $X_i^* = x_{i,1:n}^* = \{x_{i,1}^*, x_{i,2}^*, x_{i,3}^*, \dots\}$  refers to the generated features of category  $i$ .

The representation of corpus in Section 3.1 show that the data points  $\{x_{i,j}\}$  are independent of each other and identically are taken from real-world distribution  $p_{\text{data}}(x)$ . The generative network is to learn a generator's distribution  $p_g(x)$  that gradually approximates to  $p_{\text{data}}(x)$ . The value function of conditional GAN is defined as follows:

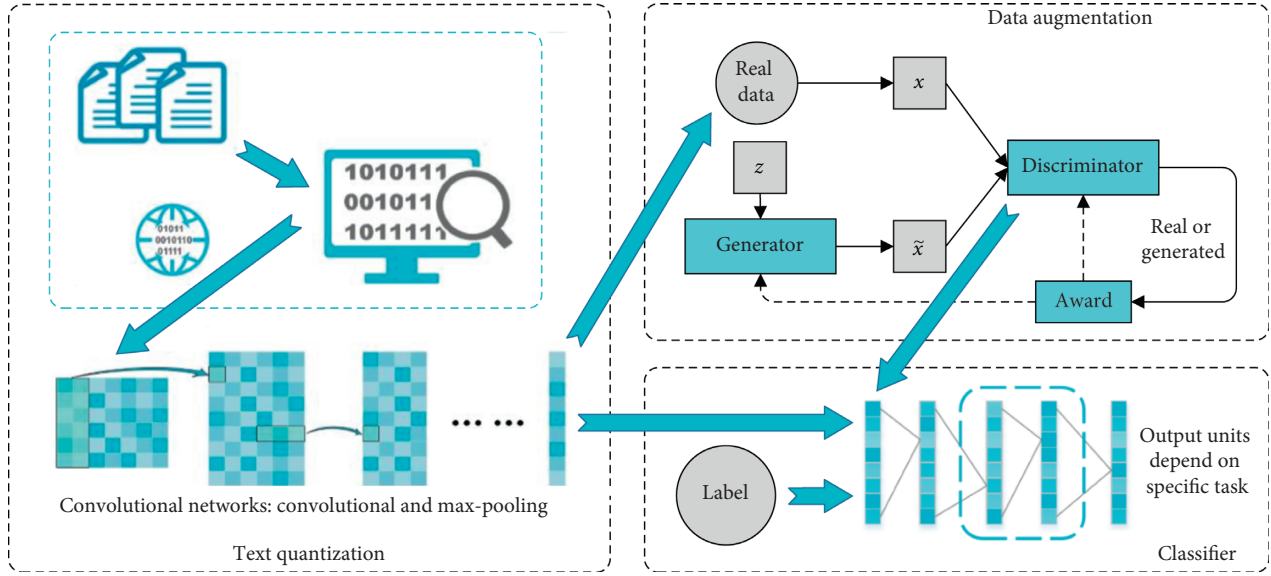


FIGURE 1: The framework of text classification.

TABLE 1: The nonspace characters of alphabets.

Alphabets	Nonspace characters
Foundational	a b c d e f g h i j k l m n o p q r s t u v w x y z 0 1 2 3 4 5 6 7 8 9, ; : ! ? : ( )
Elaborate	- ' " / \   _ @ # \$ % ^ & ? ~ 0 + - = < > [ ] { } ... ..

TABLE 2: The parameter setting of the convolutional neural network.

Layer	Feature	Kernel	Pooling	Stride	
				Conv	Pool
1	256	5	N/A	1	3
2	256	5	3	1	3
3	256	5	N/A	1	3
4	256	5	3	1	3
5	256	3	N/A	1	3
6	256	3	N/A	1	3
7	256	3	N/A	1	3
8	256	3	3	1	3

$$\min_G \max_D V(D, G) = \mathbb{E}_{x \sim p_{\text{data}}(x)} [\log D(x | y)] + \mathbb{E}_{z \sim p_z(z)} [\log(1 - D(G(z | y)))] \quad (2)$$

where  $x$  is the real textual feature,  $y$  is the category label corresponding to feature  $x$ , and  $z$  is random noise. Through the different settings of  $y$ , the textual features of different categories can be obtained in the process of text generation. Note that GAN is designed for continuous data, that is, it can only be constructed by differentiable functions. In the correlation processing of discrete data, it is difficult to transfer the gradient of the discrete outputs to the discriminator, so the discriminator cannot be updated. There are many feasible methods to solve the problem. This paper

uses the policy gradient [27] to improve the application field of the adversarial network. The generator and discriminator are trained alternatively and the detail of the adversarial model is as follows.

**3.2.1. The Generator for Textual Data.** Recurrent neural network (RNN) is designed to solve the vanishing and exploding gradient in backpropagation, and it is widely used in NLP because of the discrete distribution of textual data. The GRU is set as the generative network and the structure is shown in Figure 3. The update gate  $z_t$  is used to control how much the previous state information is brought into the current state. The higher the value of the  $z_t$  is, the more state information is brought at the previous moment. The function of the updated gate is as follows:

$$z_t = \sigma(W_z \cdot [h_{t-1}, x_t]), \quad (3)$$

where  $[h, x]$  is the vector concatenation. The reset gate  $r_t$  controls how much information is written to the current candidate set  $\tilde{h}_t$  from the previous state. The smaller the  $r_t$ , the less information is written from the previous state. The function of the reset gate is as follows:

$$r_t = \sigma(W_r \cdot [h_{t-1}, x_t]). \quad (4)$$

Since each unit has its reset and update gates, each hidden unit learns dependencies on different scales. The units that learn to capture short-term dependencies activate

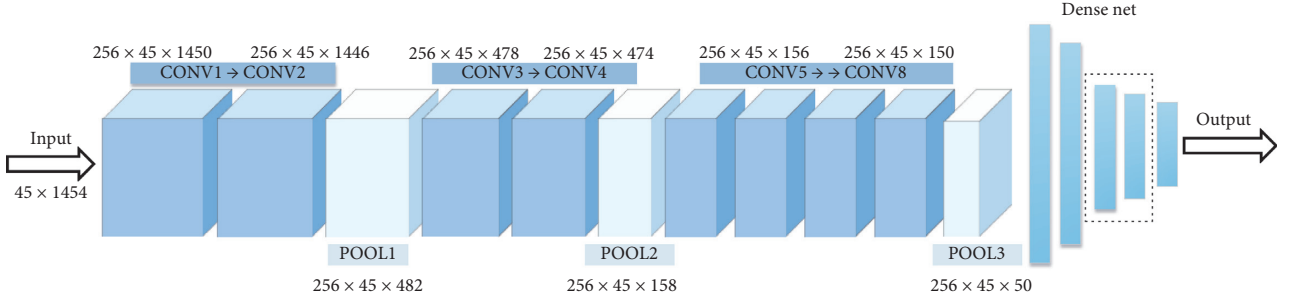
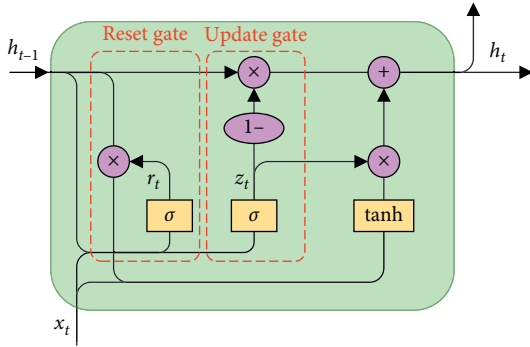


FIGURE 2: The structure diagram of the convolutional neural network.

FIGURE 3: The detailed structure of the gated recurrent unit.  $z_t$  and  $r_t$  are update gate and reset gate, respectively.

the reset gates, while the units that capture long-term dependencies activate the update gates. The update functions are as follows:

$$\begin{aligned} \tilde{h}_t &= \tanh\left(W_h^- \cdot [r_t \odot h_{t-1}, x_t]\right), \\ h_t &= (1 - z_t) \odot h_{t-1} + z_t \odot \tilde{h}_t, \end{aligned} \quad (5)$$

where  $\odot$  is the elementwise product. We use random noise as input into the generator to construct the mapping of noise space to text semantic space.

**3.2.2. The Discriminator for Data Screening.** Since both the real text and the generated text can be quantified as a feature of fixed length, a convolutional network is constructed to discriminate the source of the text. The textual feature  $\{x_1, x_2, \dots, x_n\}$  is processed as follows:

$$s_i = f(x_i \otimes w + b), \quad (6)$$

where  $f(\cdot)$  is a nonlinear function,  $x_i$  is the  $l$ -dim textual features,  $\otimes$  is the convolution operation,  $w \in \mathbb{R}^k$  is a 1D kernel to produce a new feature map, and  $b$  is a bias term. The various numbers of kernels with different window sizes are used to extract different features. Specifically, the textual feature extracted by the kernel  $w$  with window size  $k$  is represented as follows:

$$s_i = [s_{i,1}, s_{i,2}, \dots, s_{i,l-k+1}]. \quad (7)$$

Finally, the max-pooling operation is performed on the feature map  $\tilde{s} = \max\{s\}$  and all pooling features from

different kernels are transferred to a fully connected softmax layer to get the probability that a given feature is real. When optimizing discriminative models, supervised training is applied to minimize the crossentropy, and the objective function is as follows:

$$\mathcal{H}(x, q) = -p(x)\log(q(x)) - (1 - p(x))\log(1 - q(x)), \quad (8)$$

where  $p(x)$  is the real label of the textual features and  $q(x)$  is the predicted probability from the discriminator.

**3.3. Classifier Module.** The classifier constructed by dense networks is a multilayer-feedforward network based on error backward propagation algorithm. The principle is to calculate the difference between the actual output and the expected output recursively, and the network adjusts the weights according to the difference.

The real features  $X_{1:m}$  and generated features  $X_{1:m}^*$  are input to the network for training. Here, ReLU is used as the activation. To explore the optimal network structure, the dense network consisting of three to five fully connected layers is constructed, as shown in Figure 4. Besides, the dropout modules are inserted between the fully connected layers to prevent overfitting, and the dropout probability is 0.5. The real semantics  $X_{1:m}$  and generated semantics  $X_{1:m}^*$  are input to the network for training. The activation function and its derivative are as follows:

$$\begin{aligned} f(x) &= \max(0, x) = \begin{cases} 0, & x < 0, \\ 1, & x \geq 0, \end{cases} \\ f'(x) &= \begin{cases} 0, & x < 0, \\ 1, & x \geq 0. \end{cases} \end{aligned} \quad (9)$$

## 4. Experiments

In this section, we detail the experimental content and related setting, involving the datasets, the baselines, parameter setting, and experimental result analysis. To effectively demonstrate the advantages of the proposed method, we not only compare different text classification methods but also make the comparison of influence factors of our method. In this way, we further study the feasibility of the method through comparative experiments.

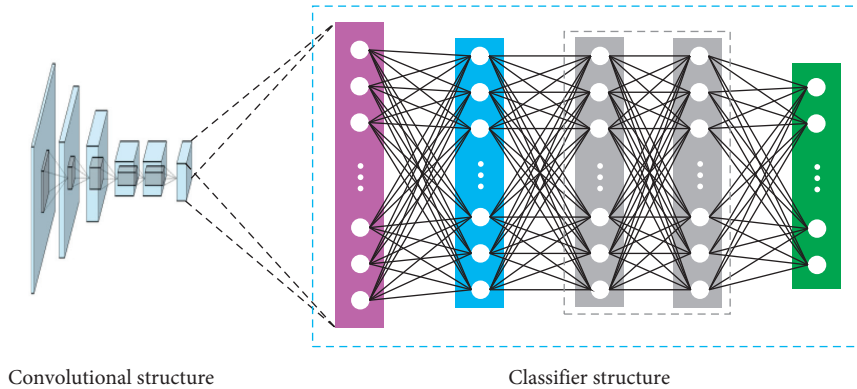


FIGURE 4: The diagram of the classifier structure.

4.1. *Datasets.* We use four corpora to evaluate the proposed framework. These datasets are

AG-News: original AG-News has over one million news articles collected from over 2,000 different news sources. We extract the data from the four largest categories in the original dataset, including world, environment, sport, and business news, and each category contains 30,000 for training and 1,900 for testing. The dataset can be downloaded from [http://www.di.unipi.it/~gulli/AG\\_corpus\\_of\\_news\\_articles.html](http://www.di.unipi.it/~gulli/AG_corpus_of_news_articles.html).

DBPedia [33]: DBPedia ontology dataset is composed of 14 nonoverlapping categories from Wikipedia. In the experiment, we adopt the updated corpus by Zhang et al. Each category contains 40,000 training samples and 5,000 testing samples.

20NG: 20 newsgroup dataset is one of the international standard datasets for text classification, text mining, and information retrieval research. The dataset collects about 20,000 newsgroup documents that are evenly divided into newsgroup collections of 20 topics. Some newsgroups are dedicated to similar subjects, and some are completely unrelated. The dataset can be downloaded from <http://qwone.com/~jason/20Newsgroups>.

IMDB: the dataset is widely used for binary sentiment classification of movie reviews. It provides 25,000 highly polar movie reviews for training, 25,000 for testing, and additional unlabeled data. The dataset comes from <http://ai.stanford.edu/~amaas/data/sentiment>.

Note that most open datasets for text classification consumed huge resources to artificially tag it. To simulate the real-world small-scale datasets, we randomly extract parts of these datasets in the experiment. The details of the datasets are shown in Table 3.

4.2. *Baselines.* To make the experimental comparison more comprehensive and objective, we reproduce the mainstream text classification method, such as FastText, DPCNN,

TABLE 3: Dataset statistics.

Dataset	Before extracting			$L$	$K$	$\alpha$
	Train	Test	Unlabeled			
AG-News	120 k	7.6 k	—	46	4	5
DBPedia	560 k	70 k	—	56	14	5
20NG	11314	7532	—	221	20	10
IMDB	25 k	25 k	50 k	239	2	10

$K$  is the number of categories,  $L$  is the average length of a document, and  $\alpha$  is the extracting times of the sample sets.

LEAM, and Virtual Adversarial. The details of these methods are as follows:

Tree-LSTM [34]: the model proposed by Tai et al. extends the LSTM of sequence to the tree structure, that is, it can skip (or ignore) the whole subtree that has little effect on the result through the forgetting gate mechanism of LSTM, rather than just some subsequences that may have no linguistic significance.

Self-Attentive [35]: a model for extracting an interpretable sentence embedding by introducing self-attention. The method uses a 2D matrix to represent the embedding and proposes a self-attention mechanism and a special regularization term for the model.

Emb-CNN [17]: the model is a slight variant of the CNN architecture of Collobert et al. It shows that a simple CNN with little hyperparameter tuning and static vectors achieves excellent results on multiple benchmarks. Learning task-specific vectors through fine-tuning offers further gains in performance. Kim additionally proposes a simple modification to the architecture to allow for the use of both task-specific and static vectors.

Char-CNN [19]: the method treats text as a kind of raw signal at character level and applies temporal ConvNets to it. The most important conclusion from the method is that character-level ConvNets can work for text classification without the need for word embedding.



Char-CRNN [36]: a architecture that utilizes both convolution and recurrent layers to efficiently encode character inputs. Compared with character-level convolution-only models, it can achieve comparable performances with much fewer parameters.

FastText [16]: the linear models with a rank constraint and fast loss approximation are often on par with deep-learning classifiers in terms of accuracy, and many orders of magnitude can be improved in evaluation.

L-MIXED [37]: a training strategy, even a simple BiLSTM model with crossentropy loss, can achieve competitive results compared with more complex methods. In addition to crossentropy loss, by using a combination of entropy minimization, adversarial, and virtual adversarial losses for both labeled and unlabeled data, the method can also perform very well.

DPCNN [38]: a low-complexity word-level deep convolutional neural network architecture for text classification that can efficiently represent long-range associations in text. Johnson et al. studied deepening of word-level CNNs to capture global representations of text and found a simple network architecture with which the best accuracy can be obtained by increasing the network depth without increasing computational cost by much.

LEAM [39]: the method of considering text classification as a label-word joint embedding in which each label is embedded in the same space with the word vectors. It maintains the interpretability of word embedding and has a built-in ability to leverage alternative sources of information, in addition to input text sequences.

Ad-Training [30]: the framework extends adversarial and virtual adversarial training to the text domain. The method applies perturbations to the word embedding in recurrent neural networks rather than to the original input itself.

Text GCN [40]: the model is initialized with one-hot representation for word and document, and it then jointly learns the embeddings for both words and documents, as supervised by the known class labels for documents.

**4.3. Implementation Details.** The 5/10-fold crossvalidation is applied to each dataset. The reduced training sets are marked as a part-dataset part- $i$  ( $i = 1, 2, 3, \dots, 8$ ), where the amount of text in the dataset is, respectively, 200, 400, 800, 1,500, 2,500, 4,000, 6,000, and 10,000. To reduce the occasionality brought by sample selection, we use the same test set for multisize training sets. The total test sets are used to evaluate the performance on the 20NG dataset, and the other datasets are tested with 10,000 samples, respectively. Note that, on the IMDB, entire unlabeled samples are always provided for the semisupervised methods.

The baseline used in this paper replicates and sets parameters basically according to the original literature. The special cases are as follows: L-MIXED has two objective

functions, the crossentropy loss  $\mathcal{L}_{ML}$  is adopted on the supervised datasets, and the mix function  $\mathcal{L}_{MIXED}$  is adopted on the IMDB. The unsupervised embeddings obtained by  $tv$ -embedding training in DPCNN. Adversarial Training has several training strategies, the virtual adversarial method based on unidirectional LSTM is utilized on the supervised datasets, and the bidirectional LSTM with virtual adversarial training on the IMDB.

In the details of our method, the elaborate alphabet length is set to 25, the convolution operation is set to “valid” and the pooling operation is the max-pooling,  $\beta = 1454$ . The number of output units for the last layer is determined by the problem in the classifier, that is, for the DBPedia it is 14. Besides, the other fully connected layers, all have 4096 units. During the training process, CCNN-GAN without the data augmentation module is first trained. Then, the parameters of the Char-level CNN are fixed and the data augmentation module is introduced to conduct incremental training of the classifier.

**4.4. Results and Analysis.** We analyze in detail the effect of different model settings, including the size of the alphabet, the number of generated features, and the structure of the classifier network. Besides, we compare the performance of the proposed method with those of the representative methods on the benchmark datasets.

**4.4.1. Model Parameter Analysis.** We use AG-News to analyze the impact of different settings. The alphabet size directly affects the time and efficiency of the classification method. We employ the foundational alphabet and the elaborate alphabet with the auxiliary symbols, respectively. As shown in Figure 5, the classification accuracy of the proposed method significantly improves with the growth of the dataset. When the scale increases to Part-6, the growth of the classification accuracy tends to be flat, which indicates that the dataset has a similar representational ability to the complete dataset.

However, the classification accuracy of the synthetic alphabet (the foundational alphabet and the elaborate alphabet) is similar to that of the foundational alphabet. Although the elaborate alphabet increases the representativeness of textual features, the improvement is negligible. Besides, with the alphabet increase, the network training time significantly increases.

To get the optimal network settings, we adjust the classifier structure and the amounts of samples by the generative network, respectively. Firstly, the number of fully connected layers and neurons in each layer is adjusted continuously to find the optimal configuration. Then, we adjust the quantity of generated texts and analyze the impact of generated samples on the accuracy. We compare the effects of the abovementioned variables on AG-News. As shown in Figure 6, the increase of the fully connected layers improves the accuracy of the classifier, but its change is not obvious.

When the number of real-world samples is small, the proposed framework can improve the performance of the

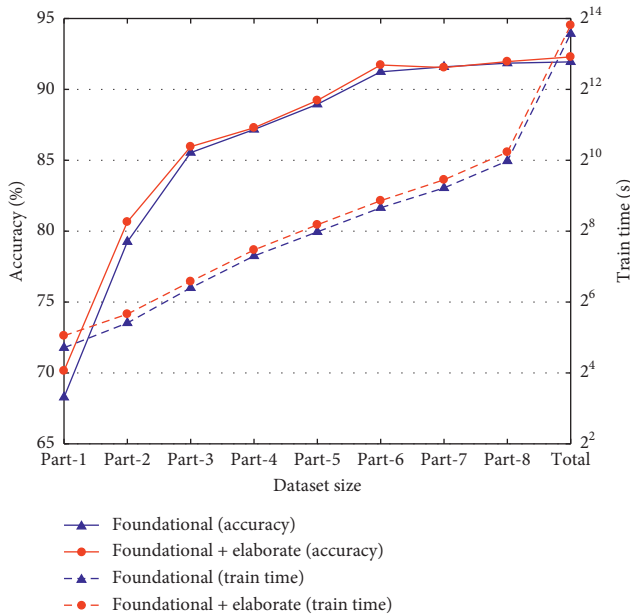


FIGURE 5: The impact of the alphabet size in CCNN-GAN.

classifier. However, when the number of generated samples continues to increase after reaching a certain level, the classifier is not significantly improved, which may be because the scale of original data limits the performance of the generative network, further limits the generation space of text, and finally affects the abstract semantic space of samples.

**4.4.2. Comparison of Different Methods.** We test different methods on the datasets mentioned in Section 4.1. To improve the efficiency on the premise of better accuracy, the structure setting of CCNN-GAN is as follows: the alphabet is foundational, the number of fully connected layers is three, and the number of generated textual features is the same as the number of real samples.

CCNN-GAN is superior to all the comparison methods when dealing with small-scale datasets, especially compared to the state-of-the-art methods, which indicates that the generated texts greatly optimize the training of the classifier. We can see classification methods that perform well on large-scale datasets lose their advantages on small-scale datasets such as L-MIXED and DPCNN. The reason is that fewer samples lead to the overfitting of the deeper network. The unlabeled data provide useful information for semisupervised learning, so the semisupervised methods show good results on IMDB. As shown in Figure 7, the classification accuracy of various semisupervised models is similar, our method performs better than these semisupervised models on small-scale datasets. Note that, on the Part-1 dataset, the classification accuracy of Ad-training is slightly higher than that of the proposed

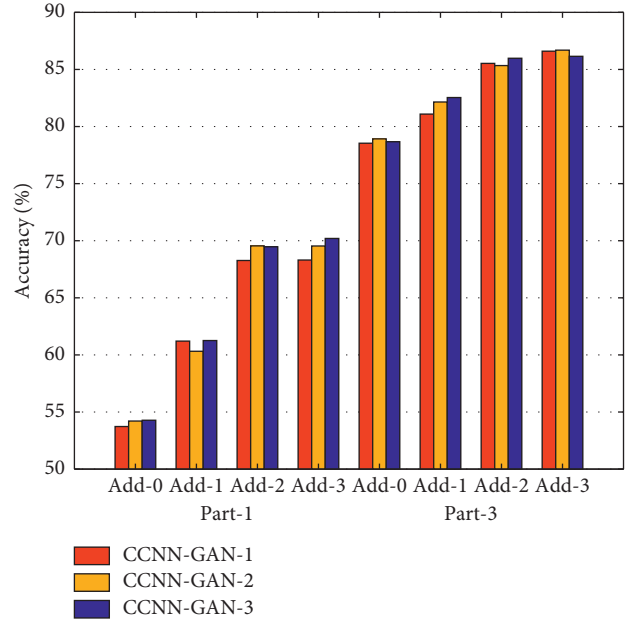


FIGURE 6: The impact of the number of generated features and the structure of the classifier network. Add- $i$  ( $i = 0, 1, 2, 3$ ) represents the number of samples generated by GAN, and the quantity of generated samples is 0, 0.5, 1, and 2 times of the real text quantity, respectively. CCNN-GAN- $j$  ( $j = 1, 2, 3$ ) represents the layers of dense networks, and the layers are 3, 4, 5, respectively.

method, but it uses a large amount of unlabeled real data in the training process. Besides, CCNN-GAN has the optimal or suboptimal performance on datasets of various sizes, which indicates that the method has a strong generalization ability.

To observe the experimental effect more conveniently, we bold the optimal experimental data. As shown in Tables 4 and 5, experimental results indicate that the accuracy of the classifier improves with the increase of training data. When the dataset is small, our method has better performance than other methods, but its accuracy improves more slowly as the dataset size increases. The reason is that the generation of textual features further enriches the dataset, which indirectly expands the dataset and reduces the importance of the original dataset. Besides, the classification accuracy is close to a saturation state when the dataset expands to a certain extent.

Overall, the experimental results show that the classifier based on deep neural networks achieves excellent performance in multiclass text classification. Although the proposed method is less competitive than the state-of-the-art methods on some large-scale datasets, CCNN-GAN is better than all the comparison methods in various small-scale datasets. Besides, our method inherits the advantages of the previous character-level convolutional network and makes it easier to adapt to multiple languages by updating the alphabet freely.

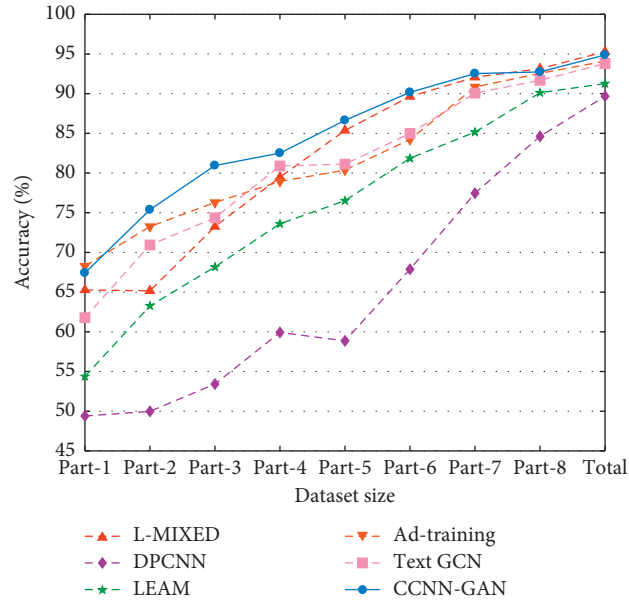


FIGURE 7: The performance on IMDB semisupervised classification task.

TABLE 4: Test performance on the AG-news classification task.

Method	Dataset size								
	Part-1	Part-2	Part-3	Part-4	Part-5	Part-6	Part-7	Part-8	Total
Tree-LSTM	37.96	58.13	68.33	76.20	87.12	90.75	91.56	91.80	91.83
Self-Attentive	30.81	54.89	72.26	85.47	86.37	90.83	91.28	92.03	91.17
Emb-CNN	48.83	68.38	79.74	84.11	83.85	85.94	87.93	89.36	90.08
Char-CNN	52.97	72.14	78.93	84.46	85.85	88.02	87.36	87.75	87.28
Char-CRNN	52.47	68.36	75.29	85.17	84.78	90.26	91.53	91.26	91.44
FastText	53.36	68.48	75.48	80.83	85.37	91.05	91.25	91.54	91.51
L-MIXED	24.68	25.45	66.21	79.25	84.20	90.27	<b>93.82</b>	<b>93.90</b>	<b>94.38</b>
DPCNN	25.94	25.62	69.85	77.29	82.44	86.71	90.89	91.12	93.13
LEAM	33.24	49.13	61.85	70.21	80.97	87.38	91.75	91.82	92.45
Ad-Training	47.29	57.63	69.15	76.21	82.37	87.83	90.89	90.22	91.37
Text GCN	57.32	68.96	77.83	84.54	87.62	89.35	90.74	91.32	92.56
CCNN-GAN	<b>66.47</b>	<b>77.53</b>	<b>85.37</b>	<b>86.93</b>	<b>88.34</b>	<b>91.48</b>	91.25	91.79	91.94

TABLE 5: Test performance on the DBPedia and 20NG classification task.

Method	DBPedia				20NG			
	Part-1	Part-4	Part-7	Total	Part-1	Part-4	Part-7	Total
Tree-LSTM	74.56	94.17	98.39	98.24	46.27	63.81	79.66	81.68
Self-Attentive	73.58	93.24	97.24	98.13	35.57	57.85	82.94	86.57
Emb-CNN	80.28	96.38	98.24	98.56	54.02	67.85	82.17	83.29
Char-CNN	76.86	<b>97.38</b>	98.24	98.37	52.53	73.19	81.28	82.61
Char-CRNN	80.12	96.27	<b>98.50</b>	98.67	53.95	67.38	81.72	83.78
FastText	82.68	95.98	98.45	98.63	44.32	67.29	<b>85.64</b>	87.26
L-MIXED	7.61	75.24	93.28	99.09	5.24	72.18	85.34	86.94
DPCNN	7.24	77.72	91.25	99.12	5.27	63.55	76.51	82.42
LEAM	79.65	95.26	97.38	99.02	49.16	64.81	83.67	87.13
Ad-Training	82.34	97.32	98.37	<b>99.24</b>	43.70	68.27	64.85	86.29
Text GCN	81.76	96.85	98.30	99.07	53.74	74.32	83.35	87.15
CCNN-GAN	<b>84.84</b>	97.35	98.47	98.64	<b>56.79</b>	<b>76.28</b>	84.32	<b>88.14</b>

## 5. Conclusion

In this paper, we propose a hybrid neural network framework for text classification. Our framework introduces generative networks to enrich corpus and utilizes a character-level convolutional network to extract latent semantic. Experimental results show that the performance of the framework on large-scale datasets outperforms other mainstream methods, and it performs significantly better than other methods on small-scale datasets. In the future, we intend to improve the output of the generative network and further enrich the generated text semantics.

## Data Availability

The data supporting this paper are from the reported studies and datasets in the cited references.

## Conflicts of Interest

The authors declare that there are no conflicts of interest regarding the publication of this paper.

## Acknowledgments

The work was partially supported by the National Natural Science Foundation of China (nos. 61702310 and 61772322) Major Fundamental Research Project of Shandong, China (no. ZR2019ZD03), and Taishan Scholar Project of Shandong, China (no. ts20190924).

## References

- [1] Z. Wu, H. Zhu, G. Li et al., "An efficient wikipedia semantic matching approach to text document classification," *Information Sciences*, vol. 393, pp. 15–28, 2017.
- [2] T. Wang, L. Liu, N. Liu, H. Zhang, L. Zhang, and S. Feng, "A multi-label text classification method via dynamic semantic representation model and deep neural network," *Applied Intelligence*, pp. 1–13, 2020.
- [3] F. Shang, H. Zhang, L. Zhu, and J. Sun, "Adversarial cross-modal retrieval based on dictionary learning," *Neurocomputing*, vol. 355, pp. 93–104, 2019.
- [4] F. Shang, H. Zhang, J. Sun, and L. Liu, "Semantic consistency cross-modal dictionary learning with rank constraint," *Journal of Visual Communication and Image Representation*, vol. 62, pp. 259–266, 2019.
- [5] M.-F. Ge, C.-D. Liang, X.-S. Zhan, C.-Y. Chen, G. Xu, and J. Chen, "Multiple time-varying formation of networked heterogeneous robotic systems via estimator-based hierarchical cooperative algorithms," *Complexity*, vol. 2020, Article ID 8357428, 18 pages, 2020.
- [6] X. Chen, D. Li, P. Wang, X. Yang, and H. Li, "Model-free adaptive sliding mode robust control with neural network estimator for the multi-degree-of-freedom robotic exoskeleton," *Complexity*, vol. 2020, Article ID 8327456, 10 pages, 2020.
- [7] X. Li, "Further analysis on uniform stability of impulsive infinite delay differential equations," *Applied Mathematics Letters*, vol. 25, no. 2, pp. 133–137, 2012.
- [8] X. Li, T. Caraballo, R. Rakkiyappan, and X. Han, "On the stability of impulsive functional differential equations with infinite delays," *Mathematical Methods in the Applied Sciences*, vol. 38, no. 14, pp. 3130–3140, 2015.
- [9] X. Li, J. Shen, H. Akca, and R. Rakkiyappan, "LMI-based stability for singularly perturbed nonlinear impulsive differential systems with delays of small parameter," *Applied Mathematics and Computation*, vol. 250, pp. 798–804, 2015.
- [10] I. Goodfellow, J. Pouget-Abadie, M. Mirza et al., "Generative adversarial nets," in *International Conference on Neural Information Processing Systems*, pp. 2672–2680, Montreal, Canada, December 2014.
- [11] M. Zhang, J. Li, H. Zhang, and L. Liu, "Deep semantic cross modal hashing with correlation alignment," *Neurocomputing*, vol. 381, pp. 240–251, 2020.
- [12] L. Liu, B. Zhang, H. Zhang, and N. Zhang, "Graph steered discriminative projections based on collaborative representation for Image recognition," *Multimedia Tools and Applications*, vol. 78, no. 17, pp. 24501–24518, 2019.
- [13] L. Liu, S. Chen, X. Chen, T. Wang, and L. Zhang, "Fuzzy weighted sparse reconstruction error-steered semi-supervised learning for face recognition," *The Visual Computer*, pp. 1–14, 2019.
- [14] Y. Bengio, R. Ducharme, P. Vincent, and C. Jauvin, "A neural probabilistic language model," *Journal of Machine Learning Research*, vol. 3, pp. 1137–1155, 2003.
- [15] T. Mikolov, *Statistical Language Models Based on Neural Networks*, vol. 80, Brno University of Technology, Brno, Czechia, 2012.
- [16] A. Joulin, E. Grave, P. Bojanowski, and T. Mikolov, "Bag of tricks for efficient text classification," 2016, <https://arxiv.org/abs/1607.01759>.
- [17] Y. Kim, "Convolutional neural networks for sentence classification," 2014, <https://arxiv.org/abs/1408.5882>.
- [18] N. Kalchbrenner, E. Grefenstette, and P. Blunsom, "A convolutional neural network for modelling sentences," 2014, <https://arxiv.org/abs/1404.2188>.
- [19] X. Zhang, J. Zhao, and Y. LeCun, "Character-level convolutional networks for text classification," in *Proceedings of the Advances in Neural Information Processing Systems*, pp. 649–657, Montreal, Canada, 2015.
- [20] H. T. Le, C. Cerisara, and A. Denis, "Do convolutional networks need to be deep for text classification?" in *Proceedings of the Workshops at the Thirty-Second AAAI Conference on Artificial Intelligence*, New Orleans, LA, USA, February 2018.
- [21] J. Chung, C. Gulcehre, K. Cho, and Y. Bengio, "Empirical evaluation of gated recurrent neural networks on sequence modelling," 2014, <https://arxiv.org/abs/1412.3555>.
- [22] X. Zhu, P. Sobihani, and H. Guo, "Long short-term memory over recursive structures," in *Proceedings of the International Conference on Machine Learning*, pp. 1604–1612, Lille, France, July 2015.
- [23] T. Zhang, M. Huang, and L. Zhao, "Learning structured representation for text classification via reinforcement learning," in *Proceedings of the Thirty-Second AAAI Conference on Artificial Intelligence*, New Orleans, LA, USA, February 2018.
- [24] J. Wei and K. Zou, "Eda: easy data augmentation techniques for boosting performance on text classification tasks," 2019, <https://arxiv.org/abs/1901.11196>.
- [25] Z. Wang and Q. Wu, "An integrated deep generative model for text classification and generation," *Mathematical Problems in Engineering*, vol. 2018, Article ID 7529286, 8 pages, 2018.
- [26] M. Mirza and S. Osindero, "Conditional generative adversarial nets," 2014, <https://arxiv.org/abs/1411.1784>.
- [27] L. Yu, W. Zhang, J. Wang, and Y. Yu, "Seqgan: sequence generative adversarial nets with policy gradient," in

- Proceedings of the Thirty-First AAAI Conference on Artificial Intelligence*, San Francisco, CA, USA, February 2017.
- [28] J. Xu, X. Ren, J. Lin, and X. Sun, “DP-GAN: diversity-promoting generative adversarial network for generating informative and diversified text,” 2018, <https://arxiv.org/abs/1802.01345>.
  - [29] Y. Li, Q. Pan, S. Wang, T. Yang, and E. Cambria, “A generative model for category text generation,” *Information Sciences*, vol. 450, pp. 301–315, 2018.
  - [30] T. Miyato, A. M. Dai, and I. Goodfellow, “Adversarial training methods for semi-supervised text classification,” 2016, <https://arxiv.org/abs/1605.07725>.
  - [31] A. Ahamad, “Generating text through adversarial training using skip-thought vectors,” 2018, <https://arxiv.org/abs/1808.08703>.
  - [32] A. Krizhevsky, I. Sutskever, and G. E. Hinton, “Imagenet classification with deep convolutional neural networks,” in *Proceedings of the Advances in Neural Information Processing Systems*, pp. 1097–1105, Lake Tahoe, CA, USA, 2012.
  - [33] J. Lehmann, R. Isele, M. Jakob et al., “DBpedia—a large-scale, multilingual knowledge base extracted from wikipedia,” *Semantic Web*, vol. 6, no. 2, pp. 167–195, 2015.
  - [34] K. S. Tai, R. Socher, and C. D. Manning, “Improved semantic representations from tree-structured long short-term memory networks,” 2015, <https://arxiv.org/abs/1503.00075>.
  - [35] Z. Lin, M. Feng, and C. N. d. Santos, “A structured self-attentive sentence embedding,” 2017, <https://arxiv.org/abs/1703.03130>.
  - [36] Y. Xiao and K. Cho, “Efficient character-level document classification by combining convolution and recurrent layers,” 2016, <https://arxiv.org/abs/1602.00367>.
  - [37] D. S. Sachan, M. Zaheer, and R. Salakhutdinov, “Revisiting LSTM networks for semi-supervised text classification via mixed objective function,” *Proceedings of the AAAI Conference on Artificial Intelligence*, vol. 33, pp. 6940–6948, 2019.
  - [38] R. Johnson and T. Zhang, “Deep pyramid convolutional neural networks for text categorization,” in *Proceedings of the 55th Annual Meeting of the Association for Computational Linguistics*, pp. 562–570, Vancouver, Canada, July 2017.
  - [39] G. Wang, C. Li, W. Wang et al., “Joint embedding of words and labels for text classification,” 2018, <https://arxiv.org/abs/1805.04174>.
  - [40] L. Yao, C. Mao, and Y. Luo, “Graph convolutional networks for text classification,” *Proceedings of the AAAI Conference on Artificial Intelligence*, vol. 33, pp. 7370–7377, 2019.